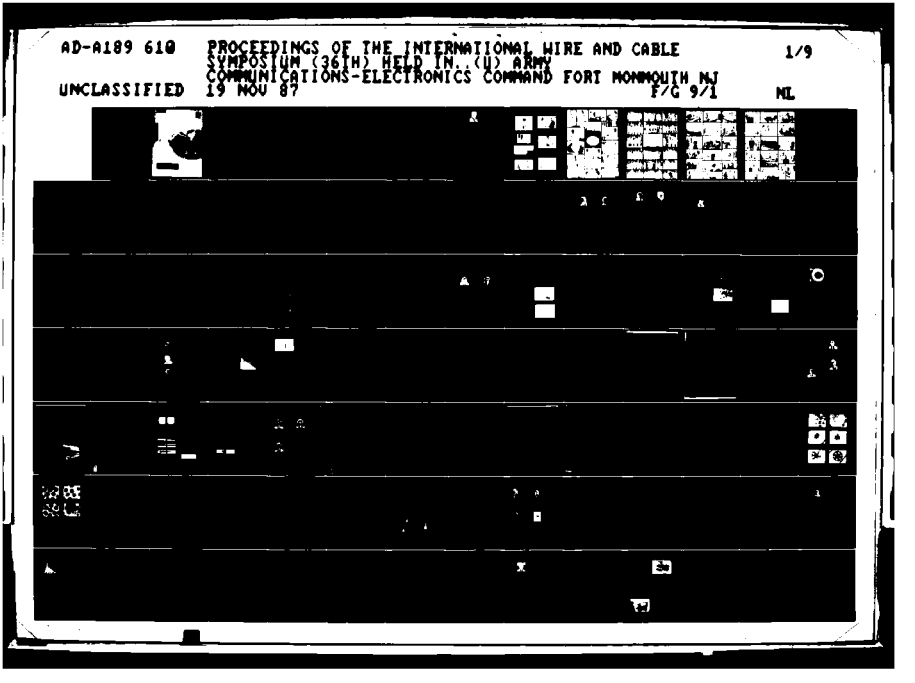
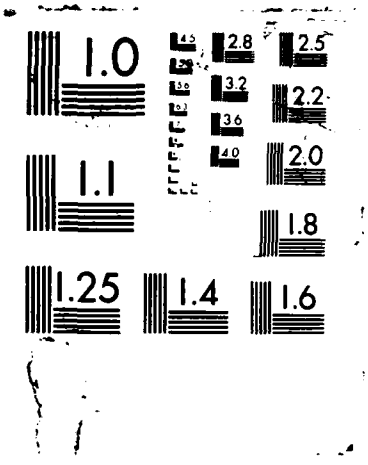
AD-A189 610 PROCEEDINGS OF THE INTERNATIONAL WIRE AND CABLE SYMPOSIUM (36TH) HELD IN..(U) ARMY COMMUNICATIONS-ELECTRONICS COMMAND FORT MONMOUTH NJ 1/9

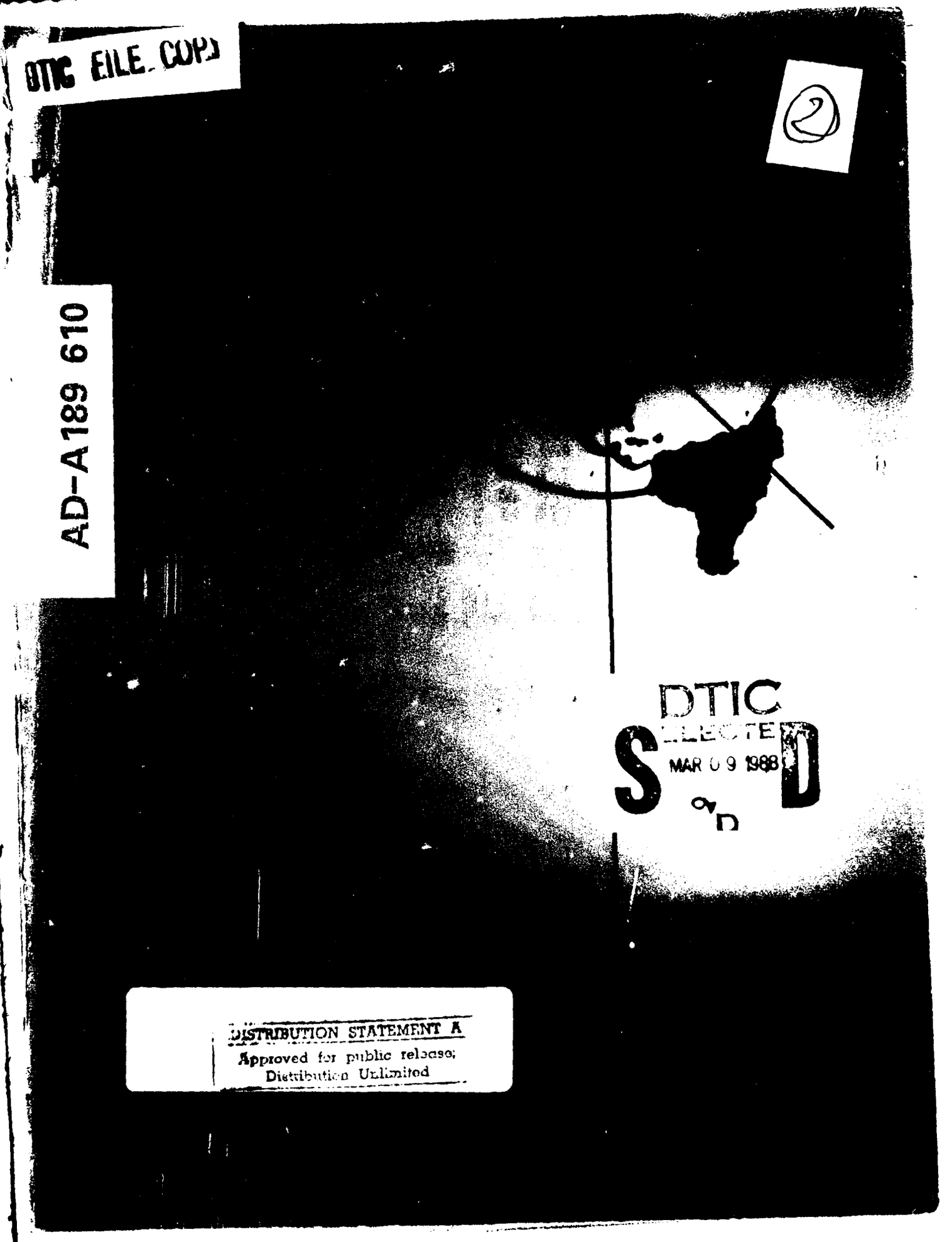
UNCLASSIFIED 19 NOV 87 F/G 9/1 NL




1.0
1.1
1.25
1.4
1.6
1.8
2.0
2.2
2.5
2.8
3.2
3.6
4.0

DTIC FILE COPY

AD-A189 610



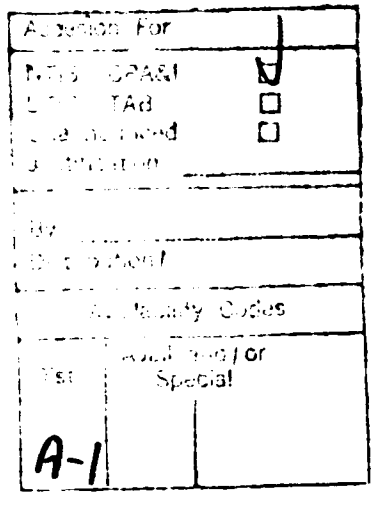
DTIC
ELECTE
MAR 09 1988
S D

DISTRIBUTION STATEMENT A
Approved for public release;
Distribution Unlimited

PROCEEDINGS OF 36TH INTERNATIONAL WIRE AND CABLE SYMPOSIUM

Sponsored by
US Army Communications-Electronics Command
(CECOM)
Fort Monmouth, New Jersey





CRYSTAL GATEWAY MARRIOTT HOTEL
ARLINGTON, VIRGINIA
NOVEMBER 17, 18 and 19, 1987

APPROVED FOR PUBLIC RELEASE: DISTRIBUTION UNLIMITED

88 3 7 075

36TH INTERNATIONAL WIRE AND CABLE SYMPOSIUM

SYMPOSIUM COMMITTEE

Elmer F. Godwin, *Director*
GEF Associates
3A Buttonwood Drive
Shrewsbury, NJ 07701
(201) 741-8864

Susan Burgher, *Assistant*
US Army CECOM
ATTN: AMSEL-RD-C^3-PB
Fort Monmouth, NJ 07703-5202
(201) 544-2770

Peter R. Bark
Siecor Corporation
489 Siecor Park
Hickory, NC 28603

Reiner J. Gerdes
Contel Laboratories
270 Scientific Drive—Suite 10
Technology Park/Atlanta
Norcross, GA 30092

Edward A. Gurney
GTE Service Corporation
3050 Harrodsburg Road
Lexington, KY 40503

L. G. "Les" Hewitt
Pacific Bell
2600 Camino Ramon
Room 3N954
San Ramon, CA 94583

Raymond E. Jaeger
SpecTran
50 Hall Road
Sturbridge, MA 01566

Tom Jones
Wyrough & Loser, Inc.
P.O. Box 5047
Trenton, NJ 08638

Vieney Mascarenhas
Canada Wire & Cable Ltd.
22 Commercial Road
Toronto, Ontario
Canada M4G 1Z4

C. Ronald Simpkins
E. I. DuPont de Nemours & Co., Inc.
Polymer Products Dept.
P-182212
Wilmington, DE 19898

Robert Streich
AT&T Network Systems
505 North 51st Avenue
P.O. Box 13369
Phoenix, AZ 85043

Keiji Tachikawa
NTT
200 Park Avenue
New York, NY 10017

George Webster
AT&T Bell Laboratories
2000 Northeast Expressway
Norcross, GA 30071

SYMPOSIUM ADVISORY GROUP

Leo Chattler
DCM Industries, Inc.
13666 East 14th Street
San Leandro, CA 94578

Michael A. DeLucia
David Taylor Naval Ship R&D Center
Energy R&D Office, Code 2759
Annapolis, MD 21402-5067

Marta Farago
Northern Telecom Canada Ltd.
P.O. Box 6122, Station A
Montreal, Quebec
Canada H3C 3J4

Irving Kolodny
Consultant
80-56 230th Street
Bellerose Manor, NY 11427

Frank Short
Consultant
1821 Howard Street
Saint Charles, IL 60174

MISSION

The International Wire and Cable Symposium provides a forum for the exchange of technical information amongst suppliers, manufacturers, and users on technological advancements in materials, processes, and products used for voice, data and video signal transmission systems.

TECHNICAL SESSIONS

Tuesday, 17 November 1987

10:00 a.m.	SESSION 1	Tutorial—Future Network Architecture
1:30 p.m.	SESSION 2	Material & Processing
1:30 p.m.	SESSION 3	Testing of Optical Fibers and Cables
1:30 p.m.	SESSION 4	Fiber Optic Cable Design for Special Applications I
1:30 p.m.	SESSION 5	Tutorial on Combustion Toxicology of Polymeric Materials Used in Cables
3:30 p.m.	SESSION 6	Poster Session

Wednesday, 18 November 1987

8:30 a.m.	SESSION 7	Coatings for Optical Fiber
8:30 a.m.	SESSION 8	Fire, Smoke & Toxicity Technology
8:30 a.m.	SESSION 9	Fiber Optic Cable Design for Special Applications II
2:00 p.m.	SESSION 10	Materials and Processing II
2:00 p.m.	SESSION 11	Fiber Optic Cable Design I
2:00 p.m.	SESSION 12	Optical Splices and Connectors
4:00 p.m.	SESSION 13	Superconductivity and the Telephone Network

Thursday, 19 November 1987

8:30 a.m.	SESSION 14	Aerial Fiber Optic Cables
8:30 a.m.	SESSION 15	Copper Cable Design I
8:30 a.m.	SESSION 16	Fiber Optic Installation & Systems
8:30 a.m.	SESSION 17	Topical Seminar Materials
1:30 p.m.	SESSION 18	Characteristics of Optical Fiber
1:30 p.m.	SESSION 19	Fiber Optic Cable Design II
1:30 p.m.	SESSION 20	Closures and Encapsulates
1:30 p.m.	SESSION 21	Copper Cable Design II

PAPERS

The papers in this volume were printed directly from unedited reproducible copies prepared by the authors. Responsibility for contents rests upon the authors and not the symposium committee or its members. After the syposium, all the publication rights of each paper are reserved by their authors, and requests for republication of a paper should be addressed to the appropriate author. Abstracting is permitted, and it would be appreciated if the symposium is credited when abstracts or papers are republished. Requests for individual copies of papers should be addressed to the authors.

PROCEEDINGS
INTERNATIONAL WIRE AND CABLE SYMPOSIUM

Bound—Available at Fort Monmouth

30th International Wire & Cable Symposium Proceedings—1981— $8.00
31st International Wire & Cable Symposium Proceedings—1982— $8.00
32nd International Wire & Cable Symposium Proceedings—1983— $8.00
33rd International Wire & Cable Symposium Proceedings—1984—$10.00
34th International Wire & Cable Symposium Proceedings—1985—$15.00
35th International Wire & Cable Symposium Proceedings—1986—$20.00
*36th International Wire & Cable Symposium Proceedings—1987—$25.00

*Extra copies: 1-3 $25.00; next 4-10 $20.00; next 11 & above $15.00 each

Make check or bank draft payable in US dollars to the INTERNATIONAL WIRE & CABLE SYMPOSIUM and forward request to:

International Wire & Cable Symposium
P.O. Box 7597
Shrewsbury, NJ 07702

Telephone inquiries may be directed to Susan Burgher at (201) 544-2770.

NOTE: Overseas air mail will be an additional $20.00 per copy.

Photocopies are available for complete sets of papers for 1964 thru 1986. Information on prices and shipping charges should be requested from the:

US Department of Commerce
National Technical Information Service
Springfield, Virginia 22151
USA

Include Title, Year and "AD" Number

13th Annual Wire & Cable Symposium (1964)	—AD 787164
15th Annual Wire & Cable Symposium (1966)	—AD A006601
16th International Wire & Cable Symposium (1967)	—AD 787165
17th International Wire & Cable Symposium (1968)	—AD 787166
18th International Wire & Cable Symposium (1969)	—AD 787167
19th International Wire & Cable Symposium Proceedings 1970	—AD 714985
20th International Wire & Cable Symposium Proceedings 1971	—AD 733399
21st International Wire & Cable Symposium Proceedings 1972	—AD 752908
22nd International Wire & Cable Symposium Proceedings 1973	—AD 772914
23rd International Wire & Cable Symposium Proceedings 1974	—AD A003251
24th International Wire & Cable Symposium Proceedings 1975	—AD A017787
25th International Wire & Cable Symposium Proceedings 1976	—AD A032801
26th International Wire & Cable Symposium Proceedings 1977	—AD A047609
27th International Wire & Cable Symposium Proceedings 1978	—AD A062322
28th International Wire & Cable Symposium Proceedings 1979	—AD A081428
29th International Wire & Cable Symposium Proceedings 1980	—AD A096308
30th International Wire & Cable Symposium Proceedings 1981	—AD A110859
31st International Wire & Cable Symposium Proceedings 1982	—AD A125662
32nd International Wire & Cable Symposium Proceedings 1983	—AD A136749
33rd International Wire & Cable Symposium Proceedings 1984	—AD A152119
34th International Wire & Cable Symposium Proceedings 1985	—AD A164384
35th International Wire & Cable Symposium Proceedings 1986	—AD A180828
Kwic Index of Technical Papers, International Wire & Cable Symposium (1952-1975)	—AD A027558



Message from the Director

The sponsor, U.S. Army Communications-Electronics Command (CECOM), Fort Monmouth, New Jersey and the symposium committee, welcomes each contributor and attendee to the 36th International Wire and Cable Symposium (IWCS). The symposium continues to attract a large segment of the wire and cable community worldwide. Foreign participation in the presentation of technical papers and overall attendance continues to be outstanding.

The committee is extremely excited over this years technical program. The tutorial on "Future Network Architecture" and the 106 additional excellent papers scheduled for presentation represent the largest and most extensive program to date. The special sessions on Superconductivity, Combustion Toxicology and Materials, in addition to the Poster Session which represents a new innovation by the committee, should provide the interest and enthusiasm for a successful symposium. Furthermore, it is hoped that the excellent facilities and convenient location of the Crystal Gateway Marriott Hotel will provide all attendees with the comfort and conveniences essential for an enjoyable meeting.

I wish to express my appreciation to all committee members for their dedication and support in planning and organizing the activities for the symposium, especially the technical program which is considered outstanding. On behalf of the committee, I take this opportunity to express their appreciation to all members of the wire and cable industry for their support and contributions. The future success of the symposium and the mutually beneficial rewards derived there from, depends on the continued support of the industrial companies and governmental agencies that participates each year.

The 1988 symposium (37th) will return to the Bally's Grand Hotel in Reno, Nevada and the 1989 symposium (38th) will be at the Hyatt Regency in Atlanta, Georgia.

Elmer F. Godwin
Director, IWCS

Highlights of the 35th International Wire and Cable Symposium November 18, 19, and 20, 1986 Bally's MGM Grand Hotel, Reno, Nevada



Greetings by Mr. Theodore A. Pfeiffer, Technical Director, U.S. Army Communications-Electronics Command, Fort Monmouth, New Jersey.



Committee Member Vieney Mascarenhas (right), Canada Wire & Cable presenting the award for best technical presentation to Mr. Stephen Hornung, British Telephone Research Laboratories.



Luncheon Guest Speaker—Mr. R. I. Epifani, Director of Marketing and External Affairs, Nevada Bell.



COL Merton Chun (left), Deputy Director of Center for Command, Control and Communication (C^3) Systems, Fort Monmouth, New Jersey presenting a Retirement Certificate to Committee Member Kazuo Nomura, Sumitomo Electric, USA Inc.



Panel Members—Tutorial Session: (left to right) Mr. Joseph F. Urich, Bell Communications Research (Bellcore), Morristown, New Jersey; Mr. Stephen P. Welsh, Contel Laboratories, Norcross, Georgia; Mr. Thomas J. Herr, AT&T Network Systems, Morristown, New Jersey; Mr. Dean C. Swanson, Standard Telephone Company, Cornelia, Georgia.



Committee Member Vieney Mascarenhas (left), Canada Wire & Cable presenting the award for outstanding technical paper to Mr. John W. Kincaid, Belden Technical Research Center.



Committee Member Frank Short (right), Consultant presenting Retirement Certificate to Advisory Committee Member Joe Neigh, AMP, Inc. With Joe is his wife, Dee.


HIGHLIGHTS
of the
35th IWCS





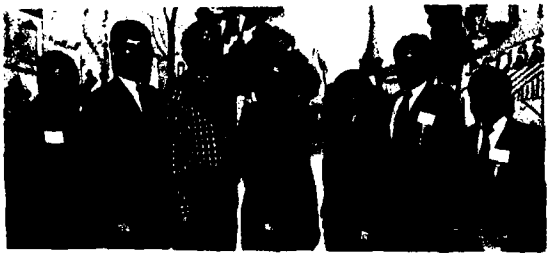



INTERNATIONAL
WIRE AND CABLE
SYMPOSIUM

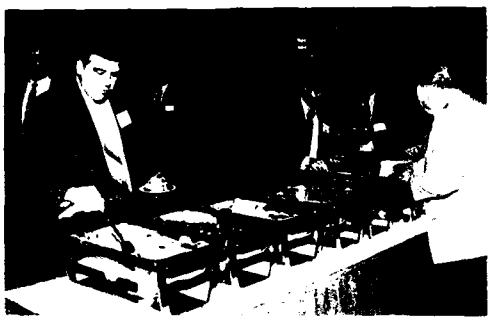
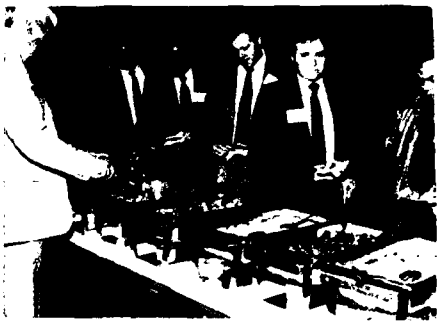
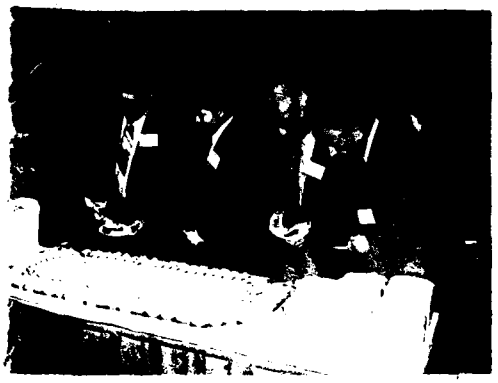




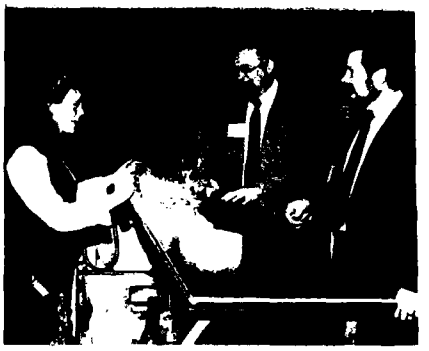












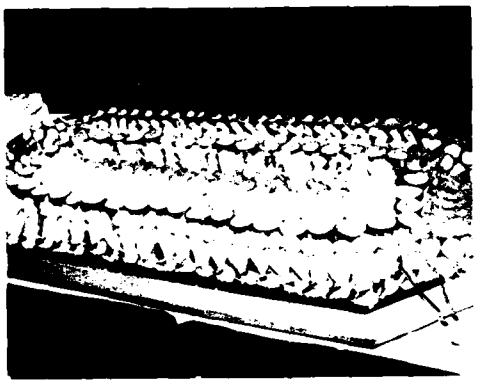






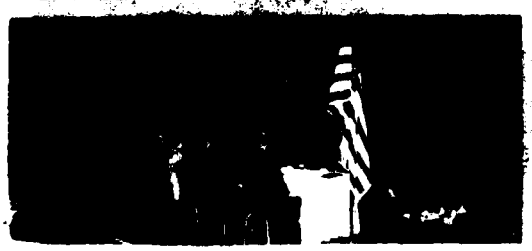











CASINO





AWARDS

Outstanding Technical Paper		*Best Presentation*
H. Lubars and J. A. Olszewski, General Cable Corp.—"Analysis of Structural Return Loss in CATV Coaxial Cable"	1968	N. Dean, B.I.C.C.—"The Development of Fully Filled Cables for Distribution Network"
J. P. McCann, R. Sabia and B. Wargotz, Bell Laboratories—"Characterization of Filler and Insulation in Waterproof Cable"	1969	J. D. Kirk, Alberta Government Telephones—"Progress and Pitfalls of Rural Buried Cable"
D. E. Setzer and A. S. Windeler, Bell Laboratories—"A Low Capacitance Cable for the T2 Digital Transmission Line"	1970	Dr. O. Leuchs, Kable and Metalwerke—"A New Self-Extinguishing Hydrogen Chloride Binding PVC Jacketing Compound for Cables"
R. Lyenger, R. McClean and T. McManus, Bell Northern Research—"An Advanced Multi-Unit Coaxial Cable for Toll PCM Systems"	1971	S. Nordblad, Telefonaktiebolaget L. M. Ericsson—"Multi-Paired Cable of Nonlayer Design for Low Capacitance Unbalance Telecommunications Network N. Kojima, Nippon Telegraph and Telephone—"New Type Paired Cable for High Speed PCM Transmission"
J. B. Howard, Bell Laboratories—"Stabilization Problems with Low Density Polyethylene Insulations"	1972	S. Kaufman, Bell Laboratories—"Reclamation of Water-Logged Buried PIC Telephone Cable"
Dr. H. Margin, Kabelmetal—"High Power Radio Frequency Coaxial Cables, Their Design and Rating"	1973	R. J. Oakley, Northern Electric Co., Ltd.—"A Study Into Paired Cable Crosstalk"
D. Doty, AMP Inc.—"Mass Wire Insulation Displacing Termination of Flat Cable"	1974	G. H. Webster, Bell Laboratories—"Material Savings by Design in Exchange and Trunk Telephone Cable"
T. S. Choo, Dow Chemical U.S.A.—"Corrosion Studies on Shielding Materials for Underground Telephone Cables"	1975	J. E. Wimsey, United States Air Force—"The Bare Base Electrical Systems"
N. J. Cogelia, Bell Telephone Laboratories and G. K. Lavoie and J. F. Glahn, US Department of Interior—"Rodent Biting Pressure and Chemical Action and Their Effects on Wire and Cable Sheath"	1976	Michael DeLucia, Naval Ship Research and Development—"Highly Fire-Retardant Navy Shipboard Cable"
Thomas K. McManus, Northern Telecom Canada Ltd. and R. Beveridge, Saskatchewan Telecommunications, Canada—"A New Generation of Filled Core Cable"	1977	William L. Schmacher, AMP Inc.—"Design Considerations for Single Fiber Connector"
Fumio Suzuki, Shizuyoshi Sato, Akinori Mori and Yoichi Suzuki; Sumitomo Electric Industries, Ltd., Japan—"Microcoaxial Cables Insulated with Highly Expanded Polyethylene By Chemical Blowing Method"	1978	Richard C. Mondello, Bell Labs.—"Design and Manufacture of an Experimental Lightguide Cable For Undersea Transmission Systems"
S. Masaki, Y. Yamazaki and T. Ideguchi, Nippon Telegraph and Telephone Public Corporation, Japan—"New Aluminum Sheath Cable Used for Electromagnetic Shielding"	1979	I. Wadehra, IBM Corporation—"Performance of Polyvinyl Chloride Communication Cables in Modified Steiner Tunnel Test"
P. Kish and Y. BeBorgne, Northern Telecom Canada Limited, Montreal, Canada—"General Crosstalk Model For Paired Communication Cables"	1980	J. J. Refi, Bell Laboratories—"Mean Power Sum Far-End Crosstalk of PIC Cables as a Function of Average Twist Helix Angle"
C. J. Arroyo, N. J. Cogelia, Bell Laboratories, and B. J. Darsey, Western Electric—"Thermal Behavior of Experimental Plenum Cable Sheaths Determined in a Radiant Heat Chamber"	1981	G. S. Anderson, Belden Corporation—"Installation of Fiber Optic Cable on 457 Meter Tower"
R. H. Whiteley, Raychem Ltd.—"A Comprehensive Small Scale Smoke Test"	1982	A. Yoshizawa, The Furukawa Electric Co., Ltd.—"Structure and Characteristics of Cables for Robots"
V. A. Fentress, Raychem Corp. and D. V. Nelson, Stanford University—"Fracture Mechanics Evaluation of the Static Fatigue Life of Optical Fibers in Bending"	1983	J. R. Bury, Standard Telecommunication Laboratories, Ltd., Hailow, England—"Development of Flame Retardant, Low Aggressivity Cables"
M. Fujise and Y. Iwamoto, KDD Research & Development Laboratories, 1-23 Nakameguro, 2-Chrome, Meguro-Ku, Tokyo, Japan—"Self-Core-Alignment Arc-Fusion Splicer Based on a Simple Local Monitoring Method"	1984	William E. Dennis, Dow Corning Corporation, Midland, Michigan—"Hydrogen Evolving Tendencies of Cable Fillers and Optical Fiber Coatings"
James A. Krabec and John W. Kincaid, Jr., Belden Technical Research Center—"Advances in the Optimization of Multi-Layer Shield Design"	1985	Stephen Hornung, British Telecom Research Laboratories—"Manufacture and Performance of Fibre Units for Installation by The Viscous Drag of Air"
Simon D. Dadakarides and Bruce B. Lusignam, Stanford University—"Magnetically Loaded Cables"	1986	Dave Fischer, Superior Cable Corp.—"Progress Towards the Development of Lightning Test for Telecommunication Cables" John C. Chamberlain, Siecor Corp.—"Zero Halogen Fire Retardant Fiber Optic Shipboard Cable"

CONTRIBUTORS

AEG KABEL Aktiengesellschaft
Monchengladbach 2, Germany
AFA Industries
Garfield, NJ
Alambres Y Cables Venezolanos C.A. "ALCAVE"
Caracas, Venezuela
Alcatel Cable Systems Defense Fiber Optics Group
Roanoke, VA
Alcatel NA
Claremont, NC
Allied Engineered Materials
Morristown, NJ
Allied-Signal Inc.
Morristown, NJ
Allied-Signal, Inc., Engineered Plastics
Morristown, NJ
Amoco Chemicals Company
Chicago, IL
AMP Incorporated
Harrisburg, PA
Ampacet Corporation
Mount Vernon, NY
Arvey Corporation
Cedar Grove, NJ
AT&T
New York, NY
AT&T Bell Laboratories
Norcross, GA
Ausimont
Morristown, NJ
Austral Standard Cables Pty. Limited
Clayton, Victoria, Australia
Barcel Wire and Cable Corp.
Irvine, CA
BASF Corporation
Parsippany, NJ
Beacon Reel Co.
New Milford, CT
Belden Technical Research Center
Geneva, IL
Bell Canada
Montreal, Quebec, Canada
Bell Communications Research, Inc.
Morristown, NJ
Berkshire Electric Cable Co.
Leeds, MA
BICC Cables Limited
Helsby, Warrington, England
BP Performance Polymers Inc.
Hackettstown, NJ
Brand-Rex Cable Systems Division
Willimantic, CT
Breen Color Concentrates, Inc.
Lambertville, NJ
Burgess Pigment Company
Sandersville, GA
Cabot Corporation
Billerica, MA
Canada Wire and Cable Limited
Don Mills, Ontario, Canada
Carlew Inc.
Quebec, Canada
Carris Reel Inc.
Rutland, VT
R.E. Carroll, Inc.
Trenton, NJ
Cary Chemicals, Inc.
Farmingdale, NJ
Chase & Sons, Inc.
Randolph, MA
Chengdu Cable Plant
Chengdu, P.R. China
Ciba-Geigy Corporation
Hawthorne, NY
CIL Inc.
North York, Ontario, Canada
Condumex Telecommunications Division
San Juan Del Rio, Qro., Mexico
Contel Corporation
Atlanta, GA
Copperthorne Industries 86 Ltd.
Vancouver, B.C., Canada
Crellin, Inc.
Chatham, NY
Davis-Standard
Pawcatuck, CT
Dow Chemical U.S.A.
Midland, MI
DuPont Canada Inc., Plastics Division
Mississauga, Ontario, Canada
E.I. du Pont de Nemours & Company
Wilmington, DE
Dussek Campbell Limited
Belleville, Ontario, Canada
Dussek Campbell Ltd.
Crayford, Kent, England
EMS-CHEMIE AG
Domat/EMS, Switzerland
Essex Group, Inc.
Decatur, IL
Excelsior Wire Corporation
Los Angeles, CA
Exxon Chemical Co.
Baton Rouge, LA
FACILE Technologies
Patterson, NJ
FIRET bv
Veenendaal, Holland
FITEL Corporation
Carrollton, GA
Fujikura Ltd.
Tokyo, Japan
The Furukawa Electric Co., Ltd.
Tokyo, Japan
Gavitt Wire & Cable Company
Brookfield, MA
GEM Gravure Company, Inc.
Leeds, MA
General Cable Company
Woodbridge, NJ
Global Products Corporation
Leominster, MA
Goldstar Cable Co., Ltd.
Seoul, Korea
BF Goodrich—Geon Vinyl Division
Cleveland, OH
W.L. Gore & Associates, Inc.
Newark, DE
Great Lakes Chemical Corporation
West Lafayette, IN
Harbour Industries, Inc.
Shelburne, VT

Hong Kong Telephone Co., Ltd.
Hong Kong
ICI Americas Inc.
Wilmington, DE
ITT Cannon—Fiber Optics Group
Fountain Valley, CA
ITT Europe, Inc.
Brussels, Belgium
Kabelmetal Electro North America Inc.
c/o Cable Consultants Corporation
Larchmont, NY
Kroschu-Kabelwerke Kromberg & Schubert GmbH u. Co.
Wuppertal, West Germany
KT Industries, Ltd.
Winnipeg, Manitoba, Canada
Lamart Corporation
Clifton, NJ
Laribee Wire Manufacturing Co., Inc.
Jordan, NY
Lindsay & Williams Limited
Manchester, United Kingdom
LNP Engineering Plastics
Malvern, PA
Lonza Inc.
Fair Lawn, NJ
Lynn Plastics Corporation
Lynn, MA
M&T Chemicals Inc.
Woodbridge, NJ
Mach-1 Compounding Division
Macedonia, OH
Manuli Cavi SPA
Milan, Italy
Mobay Corporation
Pittsburgh, PA
National Electric Cable Company
Portland, OR
NEK Cable, Inc.
Ronkonkoma, NY
Nesor Alloy Corporation
West Caldwell, NJ
The New Brunswick Telephone Co., Ltd.
New Brunswick, Canada
Nippon Telegraph and Telephone Corp.
New York, NY
NKF Kabel B.V.
Waddinxveen, The Netherlands
NKT Elektronik
Copenhagen, Denmark
Nokia Machinery, Inc.
Atlanta, GA
Northern Telecom Canada Limited
Lachine, Quebec, Canada
Northern Telecom Canada Ltd.
Saskatoon, Canada
NTT (Nippon Telegraph and Telephone Corp.)
Tokai Ibraraki-ken 319-11, Japan
Occidental Chemical Corporation
Niagara Falls, NY
Ocean Cable Co., Ltd.
Yokohama, Japan
Olex Cables
Melbourne, Australia
Omega Wire Inc.
Camden, NY
Pacific Bell
San Ramon, CA
Pantasote, Inc.
Passaic, NJ
Pennwalt Corporation
Philadelphia, PA
Penreco
Butler, PA
Philips Kommunikations Industrie AG
Koln, West Germany
Philips Telecom Equipment Corporation
Brookfield, CT
Phillips Cables Limited
Vancouver, B.C., Canada
Pirelli Cables Inc.
Surrey, BC
PPG Industries, Inc.
Pittsburgh, PA
Rea Magnet Wire Co., Inc.
Fort Wayne, IN
Riken Electric Wire Co., Ltd.
Tokyo, Japan
Ruffhead & Vaufrouard
Kent, England
RXS Schrumpftechnik-Garnituren GmbH
Hagen, West Germany
Santech Inc.
Toronto, Ontario, Canada
S.A.T. (Societe Anonyme de Telecomm.)
Paris, France
Shell Chemical Co.
Houston, TX
Siecor Corporation
Hickory, NC
Siemens
Munich, West Germany
S.I.P.
Rome, Italy
Soc. Cavi Pirelli
Milano, Italy
Soltex Polymer Corporation
Houston, TX
Sterling Davis Electric
Wallingford, CT
Sumitomo Electric
Research Triangle Park, NC
Sumitomo Electric Industries Ltd.
Yokohama, Japan
Superior Cable Corp.
Atlanta, GA
The Swiss Insulating Works, Ltd.
Switzerland
Syarikat Telekom Malaysia Berhad
Kuala Lumpur, Malaysia
Syncro Machine Company—Ceeco Group
Perth Amboy, NJ
Tamaqua Cable Products Corporation
Schuylkill Haven, PA
Tasuta Electric Wire & Cable Co., Ltd.
Osaka, Japan
Teknor Apex Company
Pawtucket, RI
Telecom Australia
Melbourne Vic., Australia
Teledyne Thermatics
Elm City, NC
Tensolite Company
Buchanan, NY
Texas Instruments Incorporated
Attleboro, MA

3M Company
Austin, TX
Times Microwave Systems Inc.
Wallingford, CT
Torpedo Wire & Strip, Inc.
Pittsfield, PA
Trea Industries Inc.
North Kingstown, RI
UBE Industries (America), Inc.
New York, NY
Union Carbide Corporation
Danbury, CT
USI Chemicals Co.
Cincinnati, OH

R.T. Vanderbilt Company, Inc.
Norwalk, CT
Weber & Scher Manufacturing Co., Inc.
Newark, NJ
Wilson-Fiberfil International
Neshanic Station, NJ
Wire Industry
Oxted, Surrey, England
Witco Corporation
New York, NY
Wyre Wynd
Jewett City, CT
Wyrough and Loser, Inc.
Trenton, NJ

TABLE OF CONTENTS

TUESDAY, NOVEMBER 17, 1987—9:30 AM-12:00 Noon

Arlington Ballroom, Salons III and IV

Greetings: Mr. Eugene Famolari, Jr., Director, Center for Command, Control and Communications (C^3) Systems, U.S. Army CECOM, Fort Monmouth, NJ

SESSION I: TUTORIAL—"FUTURE NETWORK ARCHITECTURE"

Chairperson: Les Hewitt, Pacific Bell

Panelists:

Michael L. Bandler, Vice President Network Engineering and Planning—Pacific Bell, San Ramon, CA 1

Clark Barlow, Vice President Operations Support—GTE Services Corp., Stanford, CT 1

Gary Handler, Vice President Network Planning—Bell Communications Research, Livingston, NJ 2

William J. Noll, Vice President Network Technology—Bell Northern Research, Ottawa, Canada 2

TUESDAY, NOVEMBER 17, 1987—1:30 PM-4:30 PM

Grand Ballroom, Salons, F, G, H and J

SESSION II: MATERIALS AND PROCESSING I

Chairperson: Marta Farago, Northern Telecom Canada Ltd.

Embrittlement of Crosslinked Polyvinylchloride Insulation—*T. N. Bowmer* and *P. C. Warren*, Bell Communications Research, Red Bank, NJ 5

Extrusion Foaming of ETFE Fluoropolymer Resin—*S. K. Randa, C. R. Fyrwald*, and *D. P. Reifschneider*, E. I. du Pont de Nemours & Co., Inc., Wilmington, DE 14

Processing of Thin Wall Flame Retardant, Non-Halogenated Insulation for Indoor Telephone Exchange Wiring—*E. Buczma, H. A. Mayer*, and *A. C. Day*, Olex Cables, A Division of Pacific Dunlop Ltd., Victoria, Australia 23

Analysis of and Countermeasures to Peculiar Phenomena of Halogen-Free Flame-Retardant Cables in Cable Tunnels: Growh of Mold and Deposition of Metal Carbonate—*K. Tanaka, F. Kozono*, and *F. Takaesu*, Nippon Telegraph and Telephone Corporation, Tokyo, Japan 34

Temperature Rating of Nickel Plated Copper as a Function of Plate Thickness—*T. Eng* and *T. Inagaki*, Hudson Wire Company, Ossining, NY 39

Arlington Ballroom, Salon III

SESSION III: TESTING OF OPTICAL FIBERS AND CABLES

Chairperson: George Webster, AT&T Bell Laboratories

Cabling Dependence of Optical Fiber Cutoff Wavelengths—*J. P. Kilmer, W. T. Anderson, R. M. Kanen* and *C. M. Conner Davenport*, Bell Communications Research, Inc., Morristown, NJ 49

A Probability Model for Obtaining the Splice Loss in SM Optical Fibers from One-Way OTDR Measurements—*L. Bjerkan*, EB Cables, Asker, Norway 57

Continuous Monitoring of the Loss of Large Numbers of Fiber Optic Splices—*R. Raman*, Contel Laboratories, Norcross, Georgia 63

High Resolution OTDR-Measurement for Quality Control of Long Fiber Optic Cables—*R. Klar* and *H. Schoenfeld*, Kabelmetal Electro GmbH, Hannover, West Germany 71

Heterodyne-OTDR: The Long Wavelength, Long Range Solution—*J. Rybach, S. Heckmann*, Philips Kommunikations Industrie AG, Koln, Germany; *M. Fuchs*, Philips Forschungslaboratorium, Hamburg, West Germany; and *E. Brinkmeyer*, Technische Universitat Hamburg-Harburg, West Germany 77

OTDR Automation—Methodology and Results—*L. Bird* and *W. Miller*, Corning Glass Works, Wilmington, NC; and *S. Saikkonen*, Corning Glass Works, Corning, NY 85

Interferometric Measurement of Cable Thermal Expansion—*M. S. O'Sullivan, R. S. Lowe*, and *C. Saravanos*, Northern Telecom Optical Cable Division, Saskatoon, Saskatchewan 91

Arlington Ballroom, Salon IV

SESSION IV: FIBER OPTIC CABLE DESIGN FOR SPECIAL APPLICATIONS I

Chairperson: Peter R. Bark, Siecor Corporation

Mathematically Modelled Fully Filled Strandless Optical Cable Designs—*S. T. Spedding*, BICC Optical Cables Unit, Merseyside, England; *J. E. Taylor*, BICC Research and Engineering Limited, London, England 94

A New Concept for Fiber Optic LAN Cables—*P. Rohner* and *G. Ziemek*, Kabelmetal Electro GmbH, Hannover, West Germany 102

Single-Mode Tactical Fiber Optic Cable Assemblies—*B. V. Darden, K. Kathiresan*, AT&T Bell Laboratories, Norcross, GA; and *V. E. Kalomiris*, US Army Communications-Electronics Command, Ft. Monmouth, NJ 108

Field Deployable Fiber Optic Cables—*T. R. Ulijasz* and *R. L. Ohlhaber*, Belden Wire & Cable, Technical Research Center, Geneva, IL 116

Fibre Optics in Dynamic Strain Cables—*T. R. Smith*, STC Defence Systems, Newport, Gwent, United Kingdom; and *D. R. Carter*, Ministry of Defence, Admiralty Research Establishment, Portland, Dorset, United Kingdom 122

Characteristics and Long-Term Stability of Mass Produced Optical Fiber Submarine Cables—*H. Abe, Y. Yamazaki, H. Yamamoto* and *Y. Niiro*, Kokusai Denshin Denwa Co., Ltd. (KDD), Tokyo, Japan 135

Grand Ballroom, Salons B, C, D and E

SESSION V: TUTORIAL ON COMBUSTION TOXICOLOGY OF POLYMERIC MATERIALS USED IN CABLES

Chairperson: Vieney Mascharenhas, Canada Wire & Cable Ltd.

Combustion Toxicology: Principles, Methods and Regulations—*S. C. Packham*; and Hazard Analysis Using Toxic Potency and Other Material Property Data—*R. W. Bukowski*, National Bureau of Standards, Gaithersburg, MD 143

Principal Test Methods for the Evaluation of the Combustion Toxicity of Materials and Products—*H. W. Stacy*, Southwest Research Institute, San Antonio, TX 144

Question period and summation, *Steven C. Packham*, NFACT

TUESDAY, NOVEMBER 17, 1987—3:30 PM-5:30 PM

Arlington Ballroom, Salons V and VI

SESSION VI: POSTER PAPERS

Chairperson: Reiner J. Gerdes, Contel Laboratories

Development of a Compound Flow Test Method for Predicting Drip Performance of Filling Compounds in Finished Cables—*G. J. Hughes*, United Technologies/Essex, Decatur, IL 148

Performance Analysis of Optical Fiber Cleavers—*W. W. Wood*, Bell Communications Research, Morristown, NJ 155

A Method of Determining the Percent Expansion of Cellular Insulations—*N. J. Baer*, United Technologies/Essex Group Inc., Decatur, IL 160

A Test for Optical Fiber Coating Strippability—*J. Moses* and *M. Sigmon*, Siecor Corporation, Hickory, NC 163

Distribution of Fiber Optic Facilities in Commercial Buildings—*J. P. Varachi* and *C. H. Hasz*, Bell Communications Research, Morristown, NJ 169

A Device for Measuring Excess Fiber Length in Buffer Tubes—*J. S. Barker*, Siecor Corporation, Hickory, NC 175

Effective Handling of Aramid Reduces Cable Cost—*W. H. Allfather* and *A. V. Youngblood*, E. I. du Pont de Nemours & Co., Inc., Wilmington, DE 179

Understanding the Stress-Strain Properties of Aramid Fiber—*A. V. Youngblood*, E. I. du Pont de Nemours & Co., Inc., Wilmington, DE 183

Technology of Installation and Repair of Submarine Cable—*F. Y. Tsai, G. T. Tzeng, S. F. Lin* and *H. K. Peng*, Telecommunications Laboratories, Taiwan, Republic of China 188

Interferometric Characterization of Biconic Fiber Optic Connector Sleeve—*M. J. Saunders* and *B. V. Darden*, AT&T Bell Laboratories, Norcross, GA 193

An Efficient Method of Jointing Foam Skin STP and Paper Insulated STP Cables—*P. Lung Yu, R. Chou, S. Chong Chen, L. Mean Shiea* and *Yiang I*, Telecommunications Laboratories, Taiwan, Republic of China 198

Comparison of Single-Mode Splice Loss Measurement Methods—*A. F. Judy, G. F. DeVeau* and *K. M. Yasinski*, AT&T Bell Laboratories, Norcross, GA 202

Accelerated Cable Shield Corrosion Testing—*C. Kinder, R. O'Brien* and *J. D. Lawler*, General Cable Company, Edison, NJ 205

Compartmentalized Splice Case—*A. L. Gittle* and *J. D. Lawler*, General Cable Company, Edison, NJ 209

Improvements in Efficiency of UV Curing Systems for Optical Fiber Buffer Coatings and Fiber Coloring—*R. W. Stowe*, Fusion UV Curing Systems, Rockville, MD 212

WEDNESDAY, NOVEMBER 18, 1987—8:30 AM-11:30 AM

Grand Ballroom, Salons F, G, H and J

SESSION VII: COATINGS FOR OPTICAL FIBERS

Chairperson: Raymond E. Jaeger, SpecTran

Study on Transmission Characteristics of UV Curable Resin-Coated Optical Fibers at Low Temperatures—*H. Kuzushita, T. Zushi, T. Watanabe, K. Imamura* and *H. Tanaka*, Mitsubishi Cable Industries, Ltd., Hyogo, Japan 217

Tight Buffering for Optical Fibres Using Multiple Coatings—*S. R. Barnes, A. T. Summers*, STC Telecommunications; *B. A. Eales, M. M. Ramsey* and *M. K. R. Vyas*, STC Technology, Cable Products Division, South Wales, United Kingdom ... 223

An Improved Composite Coating for Tight Buffer Cable Design—*G. Kar, C. K. Chien, R. Kannabiran L. G. Amos* and *D. J. Eccleston*, Corning Glass Works, Corning, NY ... 228

LCP Coated Fiber with Zero Thermal Coefficient of Transmission Delay Time—*T. Kakuta* and *S. Tanaka*, Sumitomo Electric Industries, Ltd., Yokohama, Japan ... 234

Hermetically Coated Optical Fibers—*K. E. Lu, G. S. Glaesemann*, and *G. Kar*, Corning Glass Works, Corning, NY ... 241

Grand Ballroom, Salons B, C, D and E

SESSION VIII: FIRE, SMOKE & TOXICITY TECHNOLOGY

Chairperson: Michael A. DeLucia, David W. Taylor Naval Ship Research & Development Center

A New High Efficient Flame Retardant Plasticizer for PVC Wire and Cable Coatings—*T. P. Fidelle*, Great Lakes Chemical Corp., West Lafayette, IN ... 245

Fire Parameters and Combustion Properties of Cable Pulling Compound Residues—*J. M. Fee* and *D. J. Quist*, American Polywater Corporation, Stillwater, MN ... 248

Recent Advances in Thermoplastic, Zero Halogen, Low Smoke, Fire Retardant Cable Compound Technology—*S. Artingstall, J. Taylor* and *A. J. Pyle*, Lindsay & Williams Limited, Manchester, England ... 254

Fiber Optic Intrabuilding Cables—*H. R. McDowell* and *M. A. Sigmon*, Siecor Corporation, Hickory, NC ... 265

Evolution of a Small Scale Test Device Which Simulates the UL 910 Flammability Test—*N. I. Patel*, Siecor Corporation, Hickory, NC ... 272

Experimental Design for Full-Scale Evaluation of the Toxicity of the Products of Combustion from Cables—*F. B. Clarke* and *H. J. van Kuijk*, Benjamin/Clarke Assoc., Inc.; *J. E. Bonesteel, J. G. DiPinto* and *R. Valentine*, E. I. du Pont de Nemours and Co., Inc.; *M. Janssens* and *P. Vandevelde*, State Univ. of Ghent, Belgium ... 276

Arlington Ballroom, Salons V and VI

SESSION IX: FIBER OPTIC CABLE DESIGN FOR SPECIAL APPLICATIONS II

Chairperson: C. Ronald Simpkins, E. I. Du Pont de Nemours & Company

Optical Fiber Cable with Submersion Sensor Fiber—*H. Sawano, M. Akiyama, O. Kojima, T. Tsujita, H. Suzuki, Y. Sugawara* and *N. Misono*, Fujikura Ltd., Telecommunication Department, R&D Division, Chiba-Ken, Japan ... 284

Optical Fibre Cable for Mobile Application in Brown Coal Mining Area—*H. G. Haag, G. Hög* and *P. E. Zamzow*, AEG KABEL AG, Monchengladbach, Federal Repubic of Germany ... 291

Intra-Aircraft Fiber Optic Communication System—*C. E. Polczynski*, Lockheed California Co., Burbank, CA ... 297

Applications of all Plastic Optical Fiber Cord for Consumer Electronics Equipment—*T. Yano, K. Sugawara* and *H. Saen*, Sumitomo Electric Industries, Ltd., Tochigi-ken, Japan ... 306

Field Performance of Fiber-Optic Elevator Traveling Cable—*R. Laney, F. Davidson* and *W. McCallum*, Siecor Corporation, Hickory, NC 311

Development of Composite Fiber-Optic Traveling Cable for Elevator—*A. Hasemi, T. Akagawa, H. Hawsegawa*, Riken Electric Wire Co., Ltd.; Tokyo, Japan and *S. Hiraiwa*, The Furukawa Electric Co., Ltd., Tokyo, Japan 316

Arlington Ballroom, Salons I, II, III and IV

AWARD LUNCHEON

11:30 AM–2:00 PM

Guest Speaker: Dr. C. Kumar N. Patel, Executive Director, Research, Materials Science, Engineering and Academic Affairs Division, AT&T Laboratories, Murray Hill, NJ 3

WEDNESDAY, NOVEMBER 18, 1987—2:00 PM–3:45 PM

Arlington Ballroom, Salons V and VI

SESSION X: MATERIALS AND PROCESSING II

Chairperson: Robert Streich, AT&T Network Systems

A Comparative Stability Study Related to the Performance of PE/PJ and ETPR Filling Compounds—*A. W. Stratton, T. J. Roessing* and *J. D. Burkhard*, Witco, Petrolia, PA ... 322

Cable Sheathing Systems Design and Performance Criteria—*C. V. Maguire* and *R. Rossi*, General Cable Company, Woodbridge, NJ 327

Performance of High Density Polyethylene Insulation Antioxidants in Filled Telephone Cable Applications—*G. D. Brown*, Union Carbide Corporation, Somerset, NJ 337

Grand Ballroom, Salons B, C, D, and E

SESSION XI: FIBER OPTIC CABLE DESIGN I

Chairperson: Irving Kolodny, Consultant, Telecommunications

A High Performance Nonmetallic Sheath for Lightguide Cables—*C. J. Arroyo, A. C. Jenkins* and *P. D. Patel*, AT&T Bell Laboratories, Norcross, GA 344

Dry Type Water-Blocking Optical Fiber-Tape Cable With Slotted Rod—*M. Fukuma, N. Akasaka* and *S. Suzuki*, Sumitomo Electric Industries, Ltd., Yokohama, Japan 350

A New Nonmetallic and Waterproof Optical Fiber Cable with Absorbent Polymer Ribbon—*S. Kukita, T. Nakai, A. Hayashi* and *H. Koga*, NTT Electrical Communications Laboratories, Ibaraki-ken, Japan 357

Grand Ballroom, Salons F, G, H and J

SESSION XII: OPTICAL SPLICES AND CONNECTORS

Chairperson: Keiji Tachikawa, Nippon Telegraph and Telephone Corp.

A Study of Multi Channel Optical Rotary Joint with Ring-Shaped Photo Diode—*K. Nemoto* and *M. Inoue*, Ocean Cable Company, Ltd., Research & Development Division, Yokohama, Japan 372

Design and Performance of the New Single-Mode Fiber Connector with MP Ferrule in the Subscriber Network—*K. Kashihara, T. Kakii, S. Suzuki* and *M. Fukuma*, Sumitomo Electric Industries, Ltd., Yokohama, Japan 379

Single-Mode Optical Fiber Ribbon Splicer—*Y. Kato* and *A. Ishikura*, NTT Electrical Communications Laboratories, Ibaraki-ken, Japan; *T. Sano* and *S. Takashima*, Engineering Dept., Nippon Telegraph and Telephone Corporation, Tokyo, Japan 386

Study on Arc-Fusion Splicing Ge-Doped Silica Single-Mode Fibers Manufactured by Outside and Inside Vapor Deposition Processes—*M. Hopiavuori* and *J. E. Matthews III*, Corning Glass Works, Corning, NY; *A. DeVito*, BellSouth Services, Birmingham, AL 392

WEDNESDAY, NOVEMBER 18, 1987—4:00 PM-6:00 PM

Arlington Ballroom, Salon III and IV

SESSION XIII: SUPERCONDUCTIVITY AND THE TELEPHONE NETWORK

Chairperson: Leo Chattler, DCM Industries, Inc.

What is Superconductivity? Fundamentals and State of the Art—*P. H. Hor*, University of Houston, Department of Physics, Houston, TX 399

Processing of Superconductive Materials and High Frequency—*J. L. Smith*, Los Alamos Laboratories, Los Alamos, NM 402

High-T_c Superconducting Wire Fabrication and Testing—*D. W. Capone II, J. T. Dusek* and *K. C. Goretta*, Argonne National Laboratory, Argonne, IL 404

Transmission Parameters on Superconductive Communication Cables—*P. Kish*, Northern Telecom Canada Limited, Montreal, Canada 410

THURSDAY, NOVEMBER 19, 1987—8:30 AM-12:00 Noon

Arlington Ballroom, Salon III

SESSION XIV: AERIAL FIBER OPTIC CABLES

Chairperson: Frank Short, Consultant

Figure-8 Fiber Optic Cable—*P. S. Keith, E. L. Buckland* and *S. K. Hovis*, Sumitomo Electric Fiber Optics Corporation, Research Triangle Park, NC 419

Practical Experience with the Metal-Free Self-Supporting Aerial Optical Fibre Cable in High Voltage Networks—*A. T. M. Grooten, E. J. Bresser* and A. G. W. M. Berkers, NKF Kabel B. V., Telecommunication Cable Systems, AB Waddinxveen, The Netherlands 426

Pre-Stranded Self-Supporting Aerial Cable Design—*D. Wong* and *S. Lyons*, Siecor Corporation, Hickory, NC 438

Withstanding High-Voltage Characteristics of Non-Metallic Self-Supporting Optical Cable—*H. Takehara, Y. Ishihata* and *K. Saito*, Tohoku Electric Power Co., Inc., Sendai, Japan; *K. Niikura* and *H. Horima*, Sumitomo Electric Industries, Ltd., Yokohama, Japan; *A. Kurosawa, T. Takeda* and *T. Ohmori*, Kitanihon Electric Wire Co., Ltd., Sendai, Japan 441

The Development of a Metal-Free, Self-Supporting Optical Cable for Use on Long Span, High Voltage Overhead Power Lines—*S. Rowland*, STC Technology, Essex, England; *D. Delme Jones, I. Houghton* and *K. Craddock*, STC Telecommunications, Newport, Gwent, South Wales; and *C. N. Carter*, Central Electricity Research Laboratories, Surrey, England 449

Development of Optical Ground Wire for 1.55 μm Wavelength—*B. Lin, Y. Kitayama* and *Y. Masuda*, Sumitomo Electric Industries, Ltd., Yokohama, Japan 457

Optical Fiber Ground Wire—*G. Bianchi* and *D. Rota*, Societa Cavi Pirelli, Milan, Italy and *M. Rohman*, Pirelli Cable Corp., Lexington, SC 464

Grand Ballroom, Salons F, G, H and J

SESSION XV: COPPER CABLE DESIGN I

Chairperson: Robert Streich, AT&T Network Systems

A Global Test Method for Long Term Stability of Solid and Foam Skin Insulation—*L. E. Davis*, Superior Cable Corporation, Atlanta, GA 475

High Speed Coaxial Cables for Electronic Computers—*K. Sakamoto, S. Yamamoto, T. Kato, K. Negishi* and *K. Akimoto*, The Furukawa Electric Co., Ltd., Chiba, Japan 483

A Compact Cable for within Building 1.544 Mb/s Digital Transmission—*M. L. Fuller*, AT&T Bell Laboratories, Norcross, GA 492

High Speed Miniature Coaxial Ribbon Cable (Rectangular Jacket Type)—*K. Kadoya, K. Tanaka, A. Mori, T. Komura* and *T. Abe*, Sumitomo Electric Industries, Ltd., Tochigi-ken, Japan 499

Error Correction of Characteristic Impedance Measurement of Twisted Pair Cables—*R. Hoffman* and *E. Stremme*, Philips Kommunikations Industrie AG, Koln, West Germany 504

Ultrafine Coaxial Cable for High-Speed Transmission—*K. Yokoi, S. Satoh* and *A. Mori*, Sumitomo Electric Industries, Ltd., Tochigi-ken, Japan 509

Crosstalk and Shield Performance Specifications for Aluminum Foil Shielded Twisted Pair Cable (MIL-C-49285)—*J. A. Krabec*, Belden Wire & Cable, Technical Research Center, Geneva, IL 517

Arlington Ballroom, Salon IV

SESSION XVI: FIBER OPTIC INSTALLATIONS AND SYSTEMS

Chairperson: Reiner J. Gerdes, Contel Laboratories

Operating History of Lightwave Systems in the REA Telephone Program—*W. O. Grant*, TB, TSD, REA, US Department of Agriculture, Washington, D.C. 526

Fiber Optic Subscripter Networks Using 85/125 Fibers—*J. P. Boinet* and *M. de Vecchis*, Les Cables DeLyon, Clichy Cedex, France; *J. P. Bonicel*, Les Cables DeLyon, Lyon Cedex France; and *J. P. Bregeon*, Direction Generale Des Telecommunications, Montpellier, France 534

Provision of Wideband Optical Fibre Cable Networks for Central Business Districts—*L. deValle, W. I. Harry* and *M. McKiterick*, Telecom Australia, Melbourne, Australia 540

Production and Installation of Single-Mode Optical Cable on a 39 Km Route Without Repeaters Under EMI Conditions at Mexico City Area—*G. Chávez Diaz, J. C. Salazar Cerda* and *E. Goddard Moore*, Condumex, San Juan Del Rio, Qro., Mexico 546

Procedure for the Experimental Determination of Friction Coefficient Between a Cable and Duct—*H. M. Kemp*, AT&T Bell Laboratories, Whippany, NJ 557

Development of the Pipe Camera for Telephone Cable Installation and Piping Maintenance—*M. Nakano, Y. Kajio* and *H. Hino*, Nippon Telegraph and Telephone Corporation, Ibaraki, Japan; *T. Shimizu* and *M. Wakagi*, The Furukawa Electric Co., Ltd., Tokyo, Japan 564

Fiber/Metallic Distribution Plant Concept—*F. J. Mullin, W. C. Reed* and *C. Scholly*, AT&T Bell Laboratories, Norcross, GA 567

Grand Ballroom, Salons B, C, D and E

SESSION XVII: TOPICAL SEMINAR-MATERIALS

Chairperson: Thomas Jones, Wyrough & Loser, Inc.

Methods of Differentiating Among PTFE Fine Powder Resins—*J. J. Bednarczyk* and *P. M. Mehta*, E. I. Du Pont Company, Wilmington, DE 575

Characterization of Polyolefin Materials Used as Telecommunication Cable Jackets Based on Their Toughness Related Properties—*V. B. Mascarenhas* and *W. H. Englehart*, Insulated Cable Engineers Association, South Yarmouth, MA 581

Reduced Emissions Plenum Cable Telephone Jacket Compounds—*M. J. Keogh*, Union Carbide Corp., Somerset, NJ 592

Reduction of Fire Hazards Due to the Cables Fitted to Warships—*J. A. Pownall*, Ministry of Defence, United Kingdom 598

THURSDAY, NOVEMBER 19, 1987—1:30 PM-4:30 PM

Arlington Ballroom, Salon III

SESSION XVIII: CHARACTERISTICS OF OPTICAL FIBER

Chairperson: Peter R. Bark, Siecor Corporation

Optical Fibers Irradiated with 3800 Rads X- or Gamma-Rays Show Large Attenuation Differences—*B. H. W. S. de Jong*, Corning Glass Works, Corning, NY 604

Radiation Resistant Optical GI Cables—*A. Iino, M. Niijima, H. Hayashi, S. Sentsui* and *H. Yoshino*, The Furukawa Electric Co., Ltd., Chiba Research Laboratory, Chiba-ken, Japan 611

Evaluation of Hydrogen Generation From Optical Fiber Cable—*I. M. Plitz* and *P. C. Warren*, Bell Communications Research, Red Bank, NJ 616

Modal Noise Due to Second Mode Interference in Singlemode Fiber Systems—*M. J. Brandtner, D. W. Schicketanz* and *C. K. Eoll*, Siecor Corporation, Hickory, NC 622

Loss Spread in Single-Mode Fibers Due to Ohlon Concentration and Transmitter-Wavelength Fluctuations—*R. Díaz de la Iglesia*, D. J. Lao Soriano, *E. Tobias Azpitarte* and *J. Rueda García*, Telefonica—P. T. (Sistemas), Madrid, Spain 629

A Novel Evaluation Technique and Refractive Index Profile Control in the VAD Method—*S. Okubo, S. Asari*, and *W. Nakagawa*, Tatsuta Electric Wire & Cable Co., Ltd., Osaka, Japan 640

Arlington Ballroom, Salon IV

SESSION XIX: FIBER OPTIC CABLE DESIGN II

Chairperson: Irving Kolodny, Consultant-Telecommunications

Fiber/Metallic Service and Distribution Media—*E. R. Campbell, W. C. Reed* and *F. J. Mullin*, AT&T Bell Laboratories, Norcross, GA 645

A Study on the Design of Composite Cable Containing Optical Fiber and Multi Pairs—*S. Hisano, S. Shimada, Y. Tokumaru* and *Y. Amano*, Sumitomo Electric Industries, Ltd., Yokohama, Japan 651

Designing Compression Resistance in Loose Tube Cables—*P. E. Neveux, Jr.* and *W. H. Hatton*, Sumitomo Electric Fiber Optic Corporation, Research Triangle Park, NC 656

An Analysis of Loose Tube Cable Design Theory, Compatible with Physical Measurement—*I. Houghton, A. Summers* and *S. R. Barnes*, STC Telecommunications, Newport, Gwent, United Kingdom 662

Performance Characteristics of Enhanced Buffer Tube Cable—*R. J. Williams* and *J. Rowe*, Northern Telecom, Saskatchewan, Canada; *M. Plouffe*, Bell Canada, Montreal, Canada and *B. Hurtig*, Bell Canada, Toronto, Canada 667

Grand Ballroom, Salons F, G, H and J

SESSION XX: CLOSURES AND ENCAPSULATES

Chairperson: Edward A. Gurney, GTE Service Corporation

A Novel Non-Polyurethane Re-enterable Encapsulant Compatible with Both Filled Cable and Polycarbonate Connectors—*T. S. Croft, H. A. Haugen, S. P. Hays, T. I. Chen* and *G. J. Swampillai*, TelComm Products Division Laboratory/3M, Austin, Texas 676

A Novel Adhesive Closure System for Heat Recoverable Sleeves—*L. P. Beltz, T. J. Bonk, T. I. Chen, P. M. Olson, J. I. Zeller-Pendrey* and *D. E. Weiss*, TelComm Products Division Laboratory/3M, Austin, Texas 685

The Highly Reliable Mechanical Splice Closure—*S. Ota, S. Tachigami, H. Miyazawa* and *E. Tanabe*, The Furukawa Electric Co., Ltd., Chiba-ken, Japan 693

New Universal Splice Closure System—*D. Kunze, E. Bachel* and *J. Rost*, Siemens AG, West Germany; *L. Mendat*, AMP Netcon, Valley Force, PA; *G. Boscher*, RXS Schrumpftechnik-Garnituren GmbH, West Germany 699

Grand Ballroom, Salons B, C, D and E

SESSION XXI: COPPER CABLE DESIGN II

Chairperson: Leo Chattler, DCM Industries, Inc.

Voltage Gradient Considerations in Communication Cables—*J. W. Levengood*, AT&T Technologies, Inc., Norcross, GA 705

Comparison of One Second and Three Second Dielectric Withstand Test—*J. A. Isley*, AT&T Technologies, Inc., Omaha, Nebraska 712

Digital Transmission on Customer Premises Wiring—*S. B. Pierce*, Contel Laboratories, Norcross, GA 716

Geometric Calculation of Longitudinal Wrapping Tooling Used in Telecommunication Cable Manufacture—*Yuan Zhang*, Chengdu Cable Plant, Sichuan, People's Republic of China 723

Evaluation of Materials for Improved Life Expectancy of Foam Skin Insulation—*G. D. Brown*, Union Carbide Corporation, Bound Brook, NJ; *L. E. Davis*, Superior Cable Corp., Atlanta, GA 734

Active Transceiver Cable for Local Area Networks—*H. Yokosuka, Y. Kobayashi, K. Arai, O. Watanabe* and *K. Karai*, Fujikura Ltd., Telecommunication Cable R&D Dept., Chiba-ken, Japan 744

TUTORIAL PANEL

Future Network Architecture

PANELISTS



MICHAEL L. BANDLER

Mr. Michael L. Bandler is Vice President-Network Engineering & Planning for Pacific Bell.

Mr. Bandler began his Bell System career with the New York Telephone Company in 1961, as an Engineering Assistant. In 1971 he became a District Traffic Supervisor and in 1973 a Division Network Manager. Two years later he was appointed Chief Engineer for New York City. The next year he was named Assistant Vice President in Marketing. In 1981, he transferred to AT&T, Basking Ridge, as a Director in Marketing and then assumed his present position with Pacific Bell in 1982.

Mr. Bandler received a B.E.E. degree from Cornell University in 1960 and his MBA from New York University in 1968. He is past President of the Cornell Society of Engineers and is currently President of the California Engineering Foundation.

A partial listing of his other present affiliations include: Cornell Council, Cornell Engineering Council, Board and Executive Committee of the exchange Carriers Standards Association, President's Council of Cal Poly, Engineering Board of Visitors U.C. Davis and President of the Board of Directors San Francisco Bay Area Science Fair. In addition to being a tournament bridge player, he is an avid runner, with many Boston and New York marathons in his background.



CLARK W. BARLOW

Mr. Clark W. Barlow was named Vice President-Operations Support for the GTE Telephone Operating Group in March 1987. Mr. Barlow was formerly Vice President-Customer Service for General Telephone Company of the Southwest in San Angelo, Texas.

In his new position, Mr. Barlow is responsible for the existing network and service groups along with evaluation and support functions within telephone operations.

He began his career with General Telephone Company of Florida in 1956. After serving in various management functions, he was named Director-Toll Operations in 1975, General Manager-Switching Services in 1977 and Vice President-Service in 1978. In June 1984, he was named to his most recent position with the Southwest company.



GARY J. HANDLER

Mr. Gary J. Handler is Vice President of Network Planning at Bell Communications Research, Livingston, NJ. He is responsible for conceiving, defining, developing and implementing technical plans for profitable Network of the 90's for the Bell Operating Companies. His responsibilities range from developing an infrastructure of research, analyses, planning guidelines, and standards for Bellcore clients to build and deploy leading edge technology in a cost effective manner, to providing vertically integrated support to Bellcore clients from initial design to implementation of new profitable network architectures and services.

Mr. Handler started with Bell Telephone Laboratories in 1965 in Local Switching Systems Engineering. In 1970 he was promoted to Technical Supervisor and worked on a variety of traffic, inventory and economic modeling problems. In 1978 he assumed responsibility for the first implementation planning of new PBX/CO based private network offerings. In 1980 he transferred to AT&T as Division Manager responsible for managing voice and data services implementation projects. In 1983 he became Assistant Vice President of the New Services Planning and Implementation Center at Bell Communications Research. He assumed his current position in 1985.

Mr. Handler has a BS in Electrical Engineering from Columbia University, an MS in Electrical Engineering from the Massachusetts Institute of Technology, and a Ph.D. in Operations Research from New York University. His publications have appeared in various Operations Research magazines, IEEE conference proceedings, and the ICCC. He is a member of the ICCC Board of Governors and of the University of Illinois, College of Engineering Advisory Board. He is the Deputy Chairman of the Exchange Telephone Group Committee of the Exchange Carrier Standards Association. He is also a senior member of the IEEE.



WILLIAM J. NOLL

Mr. William J. Noll of Ottawa is Vice-President, Networks Technology Division, BNR. Mr. Noll assumed his present position on June 8, 1987. Prior to this position, Mr. Noll was Assistant Vice-President, Engineering and Networks Technology, Bell Canada.

Mr. Noll joined Bell Canada on May 10, 1965 upon obtaining an Electrical Technology diploma from Ryerson Polytechnical Institute in that same year.

In his early career, Mr. Noll worked with the engineering family at Bell Canada and has held several positions in that family in Toronto, Montreal and Ottawa. He was also on loan to Newfoundland Telephone for approximately two years.

In the late seventies, Mr. Noll was transferred to the Marketing Department and has held several positions within the Marketing family in Toronto and Ottawa.

Mr. Noll is a member of the Association of Professional Engineers of Ontario and a member of the IEEE.

AWARD LUNCHEON

Guest Speaker
Dr. C. Kumar N. Patel
AT&T Laboratories
Murray Hill, NJ



C. KUMAR N. PATEL

Dr. C. Kumar N. Patel is Executive Director, Research, Materials Science, Engineering and Academic Affairs Division at AT&T Bell Laboratories, Murray Hill, New Jersey. He joined Bell Laboratories in 1961 where he began his career by carrying out research in the field of gas lasers. He has made numerous seminal contributions in several fields, including gas lasers, nonlinear optics, molecular spectroscopy, pollution detection, and laser surgery.

In 1963 he discovered the laser action on the vibrational-rotational transitions of carbon dioxide. This discovery and his invention of efficient vibrational energy transfer between molecules, in 1964, led to his series of experiments which demonstrated that the carbon dioxide laser was capable of very high cw and pulsed power output at very high conversion efficiencies. The carbon dioxide lasers have now become work horses in at least four major fields of applications of lasers. These are: (1) Industrial applications which include cutting, drilling, and welding; (2) Scientific applications which include spectroscopy, nonlinear optics, and optical pumping to create newer lasers such as far infrared lasers and x-ray lasers; (3) Medical applications which include laser surgery in the areas of otolaryngology, gynecology, tumor removal, and general surgery; and (4) Remote probing applications which, among others, include pollution detection, ranging and Doppler radar, as well as a multitude of military uses. No other laser has made a greater impact on the society than the carbon dioxide laser. His discovery of laser action on vibrational-rotational transitions of molecules has directly led to many other infrared high power laser systems.

In 1966, Dr. Patel carried out the first infrared nonlinear optics experiments by discovering the second harmonic generation in tellurium. These pioneering studies created new field of infrared nonlinear optics. In 1967, Dr. Patel and his colleagues discovered an entirely new mechanism for nonlinear interactions - the third order nonlinearities of free electrons. In 1969, he invented the spin-flip Raman lasers which are a class of tunable infrared lasers. This was the first tunable Raman laser in any wavelength region. Using the tunable spin-flip Raman lasers Dr. Patel carried out very high resolution spectroscopy of both ground as well as vibrationally excited states of molecular gases. A direct outgrowth of these studies is his unique contribution to the problem of pollution detection. In 1970, he developed a tunable laser opto-acoustic measurement technique for detection of extremely small concentrations (1 part in trillion at atmospheric pressure) of pollutant gases. The opto-acoustic detection technique, also some times called the photo-acoustic technique, is now a standard method for measuring very small absorptions in gases. In 1973, he carried out the first measurements of the temporal variation of concentration of nitric oxide in the stratosphere. These measurements provided crucial data which bear on the problem of ozone depletion by man-made nitrogen oxide emission from sources such as the SST. Starting in 1975, Dr. Patel and his colleagues have carried out elegant laser-based measurements of Lamb Shift in heavy hydrogenic atoms; these measurements provide some of the most stringent tests of QED calculations.

In the last few years, Dr. Patel has invented and perfected an opto-acoustic detection technique which has now been shown to be capable of measuring very small optical absorptions in liquids, solids, thin films, and powders. Of special interest is the application of this technique to measurements of submonolayers of adsorbed molecules on technologically important materials such as silicon. In 1980, he started opto-acoustic spectroscopy studies of cryogenic liquids and solids. These studies are

providing crucial data of scientific interest of understanding these materials and for practical applications to the spectroscopic studies of the atmospheres of outer giant planets. These studies have now culminated in the first observations of high vibrational overtone absorption of molecular hydrogen in solid hydrogen.

Dr. Patel's current research interests include spectroscopy of highly transparent liquids and solids, and surgical and medical applications of carbon dioxide lasers.

Son of a Civil Engineer in India, Dr. Patel received his B.E. in Telecommunications from the College of Engineering in Poona, India. He received his M.S. and Ph.D. in Electrical Engineering from Stanford University in 1957 and 1961, respectively.

At Bell Laboratories in 1967 he became head of the Infrared Physics and Electronics Research Department and in 1970 he assumed the position of the Director of the Electronics Research Laboratory. In 1976 he became Director of the Physical Research Laboratory. In 1981 he became Executive Director, Research, Physics and Academic Affairs Division. He assumed his present position in 1987. Since his election in 1979, he has served as a member of the Board of Trustees of the Aerospace Corporation, El Segundo, California. In January 1986, he was elected to the Board of Directors of the Newport Corporation, Fountain Valley, California.

For his discovery of the laser action on the vibrational-rotational transitions of molecules, for his invention of the high power carbon dioxide lasers, for his nonlinear optical studies leading to the invention of the spin-flip Raman lasers and for molecular spectroscopy and pollution detection studies, Dr. Patel has received numerous honors. These include the Optical Society of America's Adolph Lomb Medal (1966); the Franklin Institute's Stuart Ballantine Medal (1968); Coblentz Society's (of the American Chemical Society) Coblentz Prize (1974); the Association of Indians in America's Honor Award (1975); the Institute of Electrical and Electronic Engineer's Lamme Medal (1976); National Academy of Engineering's Zworykin Award (1976); Texas Instrument Foundation's Founders Prize (1978); the Optical Society of America's Townes Medal (1982); the Society of Applied Spectroscopy's N.Y. Section Award (1982); the Schawlow Award of the Laser Institute of America (1984); and the New Jersey Governor's Thomas Alva Edison Science Award (1987).

Dr. Patel is a member of the National Academy of Sciences and the National Academy of Engineering. He is a Foreign Fellow of the Indian National Science Academy and The Institution of Electronics and Telecommunication Engineers (INDIA). He is an Associate Fellow of the Third World Academy of Sciences. He is a fellow of the Institute of Electrical and Electronic Engineers, the American Physical Society, the Optical Society of America, the American Academy of Arts and Sciences, and the Association for Advancement of Arts and Sciences. In 1980 Dr. Patel was elected an Honorary Member of the Gynecologic Laser Surgery Society, and in 1985 he was elected an Honorary Member of the American Society for Laser Medicine and Surgery.

EMBRITTLEMENT OF CROSSLINKED POLY(VINYL CHLORIDE) INSULATION

T. N. Bowmer and P. C. Warren

Bell Communications Research, Inc.
Red Bank, NJ 07701-7020

ABSTRACT

Crosslinked poly(vinyl chloride), XPVC, has been used since the 1970's as an abrasion resistant, solder heat stable, fire retardant wire insulation on main distributing frames in telephone central offices. Recently, field reports were received of XPVC insulations that cracked after only a few years in service. Laboratory exposures of the material to heat and or medium wavelength UV light (300 nm) resulted in the usual discoloration, crosslinking and or plasticizer loss, but no cracking. When irradiated with ordinary "cool white" fluorescent tubes, however, the field embrittlement was reproduced exactly. Ordinary plasticized poly(vinyl chloride), PVC, insulation did not fail in this manner. It is proposed that when the XPVC material was originally crosslinked by electron beam irradiation at the factory, reaction of oxygen with stable free radicals produced peroxides and or hydroperoxides that subsequently photooxidized to give weak, low molecular material on the surface. An accelerated test was devised to screen out those insulations that would not stand fluorescent illuminated environments for at least ten years.

INTRODUCTION

An individual subscriber of a local telephone company is connected to the central office switch through the main distributing frame. The copper wire connections between points on the frame are insulated with crosslinked poly(vinyl chloride), XPVC, an innovation developed in the mid-1970's to replace an archaic, expensive PVC textile lacquer composite construction. The XPVC material consists of poly(vinyl chloride), PVC, a multi-functional methacrylate monomer and a dialkyl phthalate plasticizer, along with small quantities of additional additives to provide thermal stability, lubrication and pigmentation.[1-6] Irradiation with an electron beam after extrusion crosslinks the PVC through the methacrylate linkages into a plasticized, three-dimensional network. The result is a material that can be processed on conventional wire equipment yet gives extraordinary resistance to crushing, abrasion, heat from soldering irons, fire and friction, all highly desirable for the distributing frame application.[6]

In the mid-1980's, isolated reports were received of cracked XPVC insulation in central offices around the country, but particularly from California, Texas and New York. The failed insulation showed no apparent signs of damage, but when even slightly moved or jostled would crack axially around the wire. Although embrittled wire was found at all positions on the frame, it seemed to be concentrated several inches from the terminations, on horizontal runs and along the higher racks. Failed insulations never actually fell off the wire, but the many connections in close proximity caused some shorts to ground or neighboring lines, resulting in complaints of service disruption. In a related instance, the insulation on several unused 3000 ft spools of distributing frame wire that had been stored on a repair van for an unknown length of time were also found to be embrittled, but only on the outside, exposed portions; the interior XPVC insulation displayed no signs of damage.

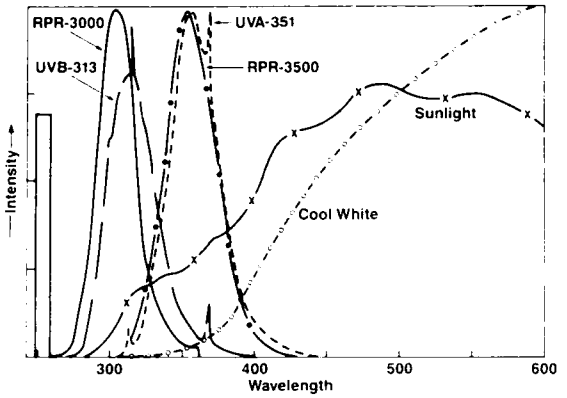
Our concern was to determine if the failure was the result of a simple batch error in manufacturing, either in the material formulation or in the subsequent electron beam irradiation step, or whether there was a fundamental defect in the XPVC technology. The latter problem was far more serious since tens of billions of conductor feet of XPVC insulated wire were in service in ten thousand or so central offices around the country; conceivably, this failure mode could eventually involve a significant fraction of this installed plant.

EXPERIMENTAL

Failed XPVC insulated, 24 AWG distributing frame wire samples were removed from frames in New York and California. Brand new product was obtained from three different manufacturers, the insulations consisting of (i) XPVC, (ii) two additional versions of XPVC (XPVC-1 and XPVC-2), and (iii) conventional plasticized PVC.

Also, two laboratory formulations were prepared from (iv) PVC containing 25 phr phthalate plasticizer and (v) PVC containing 25 phr of the same plasticizer and 26 phr methacrylate monomer. These latter two materials, whose chemistry and properties have been detailed elsewhere,[1-4] duplicate conventional PVC and XPVC insulation materials, respectively.

Fig.1 SPECTRAL DISTRIBUTIONS.



Photodegradation studies were carried out in a QUV Accelerated Weathering Tester[7] that operated at 45-50 C, which used either UVA-351 or UVB-313 light sources with a measured power of 4500 μW cm^2. In addition, a Rayonet Model RPR-100 Photochemical Reactor, with eight fluorescent RPR-3000 or RPR-3500 lights, provided total intensities of 3500 μW cm^2 at room temperature. Finally, an ad-hoc reactor made up of four commercial indoor fluorescent fixtures and eight "cool white" bulbs gave a radiant power of 200 μW cm^2 at the center. These intensities can be compared to 10-40 μW cm^2 measured over a typical main frame in a central office and 3000 μW cm^2 found outside in direct sunlight, as shown in Table 1. Radiant energies were measured with the same International Light IL700A Radiometer that was sensitive between 300-400 nm. The spectral distributions of all of the above sources are summarized in Figure 1. The UVB-313 and RPR-3000 lights simulated outside sunlight while the UVA-351, RPR-3500 and "cool white" sources duplicated the longer wavelength indoor lighting.

Table 1. UV-Exposure Measurements.

Position	Distance from source (feet)	UV-exposure μWatts/cm^2	Temp. range (°C)
Mahopac Office:			
Top of Frame	1.5	40	15-50
Middle of Frame	3.0	24	15-48
Bottom of Frame	7.5	12	15-45
Center of Aisle	6.5	16	15-40
Desk under lights with diffuser present	4.0	0.35	15-35
Outside - direct sun	$5x10^{11}$	3000	0-50
Testing Chambers:			
Ad-hoc 8-bulb Chamber	0.2	200	28-32
Rayonet Reactor (3500 lamps)	0.25	3500	25-27
QUV Tester (UVA-351 lamps)	0.3	4500	46-50

Thermal properties were measured using calorimetric, thermogravimetric and thermomechanical methods on the Perkin-Elmer DSC-4, TGS-2 and TMS-2 instruments, respectively. Soxhlet extractions with cold ether and or hot tetrahydrofuran provided information on plasticizer and or gel contents. A chromatographic technique (described elsewhere)[5] was used to quantify sol and gel fractions. Infrared spectral analyses were done on a Nicolet10-DX Fourier Transform IR Spectrophotometer in both transmission and reflectance modes. Tensile measurements were carried out on insulations stripped from conductor and as well as on Type V cut specimens (as per ASTM D-638)[8] of the laboratory blends. The electron-beam curing process used in the manufacture of XPVC was simulated by exposure to ionizing radiation from a Cobalt-60 Gammacell.

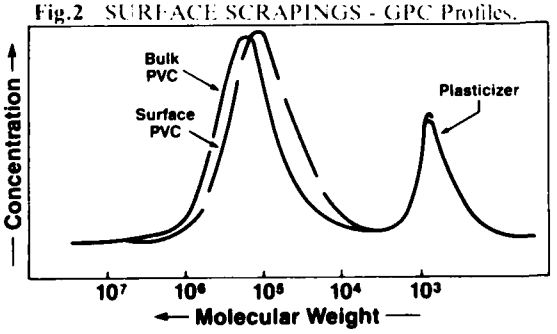
RESULTS & DISCUSSION

Visits to central offices in rural Mahopac (New York) and urban San Francisco both confirmed that cracking predominantly occurred near the top of the frame, along horizontal runs and very close to the termination points. In the small rural office, the wire in a representative section of the frame was purposefully stressed and fully 25% of the insulation cracked. Usually, the embrittled insulation was visually similar to brand new or

undamaged material, i.e., there was no discoloration of the white or fading of colors. Further, there was no obvious color dependence; cracked areas more often than not involved both wires of a twisted pair. The tensile elongation-to-break numbers were 150-200% for new or unaffected insulations, but only 0-10% for the failed ones. Values of 100% were often found for material only inches from a crack site.

Initial attempts to identify differences in the bulk properties of brand new and failed XPVC insulations were largely unsuccessful. Densities of 1.30-1.35 were measured for all samples. The linear expansion coefficients were determined to be $3 \pm 1 \times 10^{-4}$ for the insulations and blends. Differential scanning calorimetric measurements indicated no changes in glass transition temperatures of $50 \pm 5°C$ or in stress relaxation peaks at 50-60°C. Reflectance infrared spectra obtained from the surface and inside of cracked and uncracked insulations revealed the same characteristic resonances of the plasticized PVC-methacrylate system assigned to C-Cl, C=O, C=C and aryl moieties.[1-3] There was only a minor (~5%) increase in the relative magnitude of the 1720 cm^{-1} peak for the embrittled material, which was interpreted as evidence of oxidation products on the surface. Extraction with cold ether showed that plasticizer made up about 15% of the compounds, and an additional 25% of material (chiefly unincorporated PVC) could be withdrawn using hot tetrahydrofuran (THF). The rest of the PVC and all of the methacrylate monomer were left behind as an insoluble, crosslinked residue, a fact which hampered complete analysis. All the field samples, both cracked and uncracked, as well as brand new XPVC insulated product, showed the same composition within ±3%. Clearly any simple onetime formulation or curing errors would not explain the field embrittled XPVC insulations.

Fig.2 SURFACE SCRAPINGS - GPC Profiles.



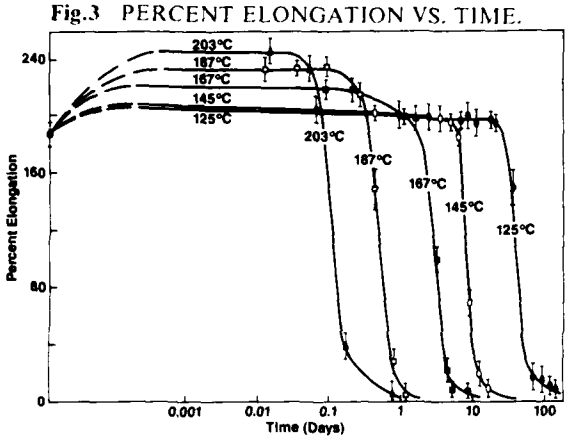
The surfaces of both the cracked exterior and undamaged interior portions of XPVC insulated wire from the unused spools (that were stored on a van) were carefully scraped and these scrapings were then extracted with THF. Figure 2 compares the gel permeation chromatograms (GPC) of the soluble fraction (M_n = 80,000), revealing a small but definite (25-30%) reduction in molecular weight of the embrittled sample. Unfortunately, a similar experiment was not possible for the intractable portion of surface material. Oxidation, initiated by heat and or radiation, is the most prevalent mechanism for the gradual deterioration and ultimate failure of plastics materials.[9] Inside the central office, heat is generated by switching equipment and mild ultraviolet (UV) radiation is produced by overhead fluorescent tubes, typically banks of 40 watt "cool white" fluorescent tubes without diffusers. In order to try to duplicate the field failure that occurred over several years time in a central office, several accelerated aging experiments were carried out, including (1) thermal aging experiments in forced air ovens, (2) exposures to medium wavelength UV light (270-330 nm) and (3) exposures to long wavelength UV light (320-380 nm).

Thermal Experiments

Thermal degradation studies of XPVC insulations were carried out between 125 and 215 C in forced air ovens. The XPVC discolored to a deep brown and eventually black after long aging times and or high temperatures. The discoloration is indicative of polyene formation that results from dehydrochlorination of the PVC component, which for the virgin polymer is reported to have an activation energy of 100 and 120-135 KJ-$mole^{-1}$ in air and vacuum, respectively.[10-12]

Tensile elongation-to-break measurements were carried out on aged XPVC samples and are graphed in Figure 3 as a function of time. The initial increase in elongations is probably due to thermal relaxation of stresses introduced during the extrusion or later electron beam irradiation; the length of the plateau region is related to the volatility of the plasticizer and the concentration and activity of thermal stabilizers. Using the times to the catastrophic drop in elongation at several temperatures, an Arrhenius activation energy was determined to be 106 KJ-$mole^{-1}$. Since the retention of elongation is a composite of plasticizer loss, stabilizer activity and the inherent thermal stability of the crosslinked network, this activation energy cannot be compared directly with the literature values quoted above. Nevertheless,

Fig.3 PERCENT ELONGATION VS. TIME.



extrapolation of the time to 0-10% elongation at room temperature reveals that the insulated wire should not crack for many years, entirely inconsistent with the field embrittlement failure. In addition, all of the laboratory aged samples were highly discolored at low elongations. Finally, since cracking was *independent of the type* of termination, overheating during soldering was eliminated as a contribution to deterioration. The overwhelming conclusion is that a thermal degradation mechanism could not possibly describe the observed failure.

Medium Wavelength UV Experiments

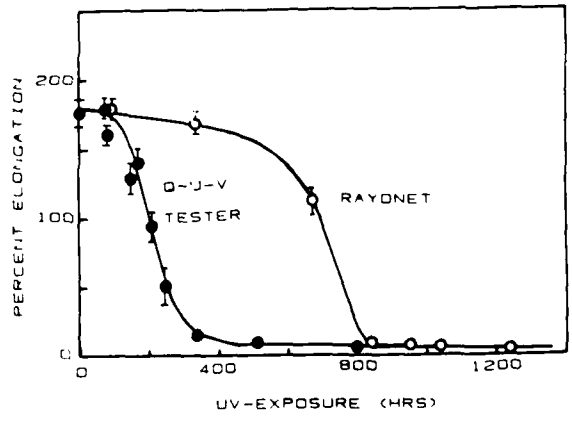
Circumstantial evidence indicated that the embrittled XPVC was, at least in part, related to indoor light. The horizontal orientation and upper frame involvement of failed wire, as well as non-involvement of shaded areas, seemed to indicate that overhead fluorescents (or sunlight through a nearby window) might have catalyzed oxidation of the material. The cracks themselves seemed to initiate from only one side of the insulation. In the Mahopac office, for instance, a particularly brightly lit aisle made this mode of action highly suspect. At the top of the frame, about 1.5 feet from the fluorescent tubes, 40 $\mu W\ cm^2$ were measured with a light meter sensitive in the 300-400 nm range. Lower portions of the frame showed values in the range of 10-25 $\mu W\ cm^2$. Even the cardboard cores of the reels stored in the van showed evidence of bleaching where sunlight apparently streamed in through a window.

In an attempt to compress time, laboratory experiments were initiated using UV sources that simulated sunlight rather than the weaker indoor light. Various XPVC insulated wires were irradiated in a Rayonet Reactor as well as in a QUV Weathering Tester, using RPR-3000 and UVB-313 lamps, respectively. A relatively rapid deterioration of the insulation was noted under these conditions, but never did it result in embrittlement. Instead, the samples showed the usual PVC outdoor weathering behavior, namely, gross discoloration and loss in elongation. These observations, along with the lack of embrittlement, again ruled out this explanation for the central office failure.

Long Wavelength UV Experiments

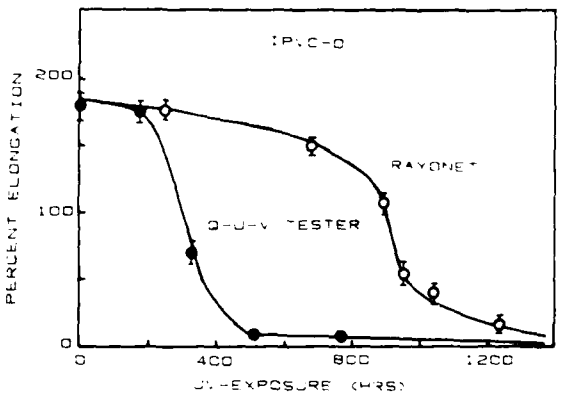
An ad-hoc apparatus was constructed by bolting together four 4 foot, double "cool white" fluorescent fixtures to form a vertical, circular, chamber, intended to accelerate the experiment by intensifying weak UV light rather than by shortening its wavelength. A small fan was attached to the bottom which maintained the inside temperature at about 30°C. White, new production XPVC insulated wires, as well as similar undamaged ones recovered from the field, were hung vertically inside the chamber and periodically checked for embrittlement. After approximately 2000 hours, the insulations cracked under slight mechanical stress yet showed no signs of discoloration. The embrittlement phenomena had been reproduced in the laboratory using the identical light source as that found in the central office.

Fig.4 320-380nm DEGRADATION OF SPOOL SAMPLE.



Long wavelength UV sources (RPR-3500 and UVA-351 lamps) were then substituted into the respective Rayonet photochemical reactor and QUV weathering tester and entirely different results were noted relative to the medium wavelength UV experiments. For instance, Figure 4 shows the %elongation versus time for undamaged, interior wire from the spool stored on a van; Figure 5 is the result of an identical experiment for brand new XPVC insulated wire. In both cases, a catastrophic reduction in elongation with no discoloration was observed; cracking correlated with elongations that were ~ 30%. The differences in times to failure of the two samples are explained by their relative thermal histories, the former having been in storage for five years or so. The difference in failure times in the two test chambers is explained by the relative severity of conditions. The Rayonet Reactor had a measured intensity of 3500 $\mu W\ cm^{-2}$ while that of the QUV apparatus was 30% greater. In addition, the latter unit operated at a temperature about 20 C higher.

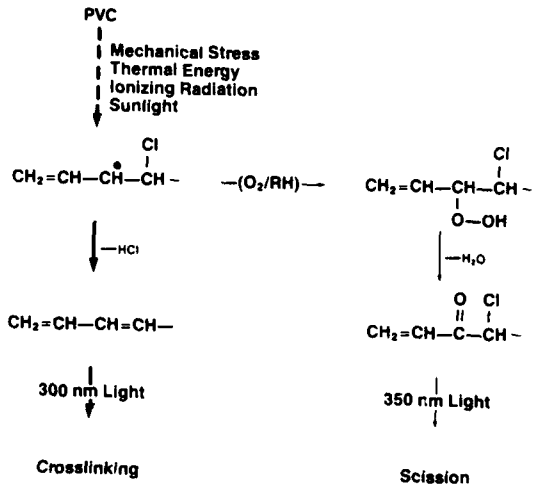
Fig.5 320-380nm DEGRADATION OF BRAND NEW XPVC.



monitored with time and all increased during the first minute of processing at 170 and 210 C. Subsequent irradiation with UV light (>290 nm) revealed that photooxidation now occurred rapidly compared to the unprocessed material. Scott[13] proposed a mechanism based on two alternative reactions available to free radicals produced during processing, namely, (1) reaction with oxygen to give alkyl peroxy radicals, and ultimately hydroperoxides, or (2) initiation of dehydrochlorination by loss of a chlorine atom, resulting in a conjugated polyene. The photoactivation effect apparently depended on the presence of species from both competitive reactions.

We postulate that the embrittlement of XPVC occurs in a fashion analogous to that proposed by Scott[13], summarized in the schematic in Figure 6.

Fig.6 REACTION SCHEME.



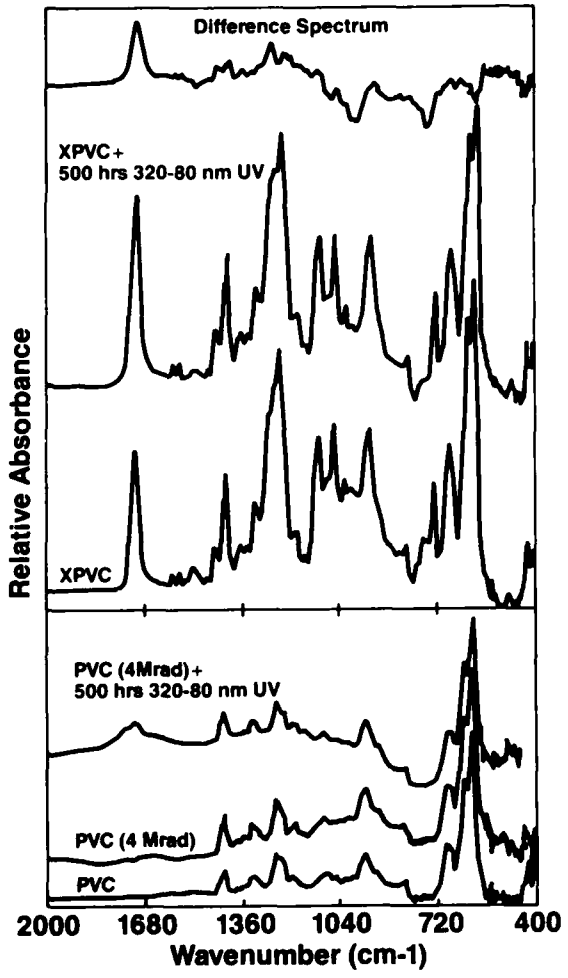
Mechanism

Scott[13] has reported enhanced photooxidation rates of PVC after the polymer was mechanically processed at high shear rates. After mechanically working the polymer in a small laboratory mixer at 170 and 210°C, the olefin, peroxide and carbonyl contents of the base resin were

The ionizing radiation used to crosslink the XPVC coating produces not only grafted crosslinked products but also stable free radicals. For instance, an electron paramagnetic resonance (EPR) study of radiation-cured XPVC revealed that methacrylate radicals persisted up to two months after exposure to the electron beam.[1] It is

proposed that the oxygenated intermediates are formed on the surface that ultimately cause scission and initiation of cracking. The yields from such reactions are small as can be seen in a comparison of the infrared spectra of photolyzed and unphotolyzed samples of gamma irradiated PVC and XPVC laboratory preparations in Figure 7. PVC exposed to 320-380 nm UV light showed no oxidation product peak at 1720cm^{-1}. Gamma-irradiated PVC and XPVC showed growth in the 1720cm^{-1} peak upon photolysis with UV light, confirming the synergistic effect of pre-irradiation on UV degradation.

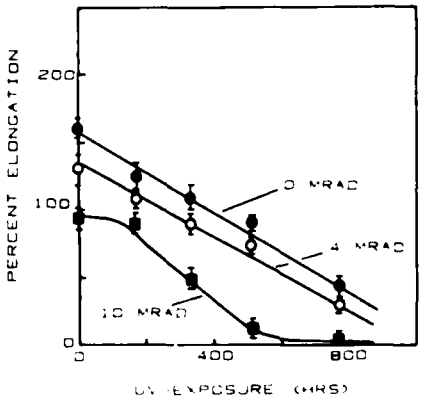
Fig.7 REFLECTANCE INFRARED SPECTRA.



The importance of these intermediates is that they are labile chromophores,which act as initiation and catalytic sites for degradation by low energy radiation that emanates from "cool white" fluorescents over several years time.

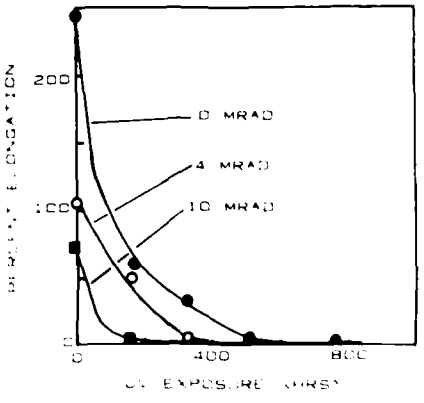
Figures 8 and 9 compare the reductions in elongation of conventional plasticized PVC and plasticized XPVC when irradiated with the indoor UVB-351 lights. The rates of elongation loss were clearly enhanced when they were exposed to ionizing radiation prior to photolysis. Higher amounts of cure lowered the times to deterioration, and indeed the original dose of ionizing radiation may determine the sensitivity of the insulation to later ultraviolet irradiation. Normally, doses of 3-6 Mrad are used to achieve 90% cure for XPVC materials.[1-4] Our laboratory samples decayed more rapidly than field materials because they did not contain the stabilizers usually found in commercial materials.

Fig.8
DEGRADATION OF PVC PHTHALATE BLEND UNDER 320-380nm LIGHT. Samples were pre-irradiated with γ-rays for 0(●), 4(○) & 10(■) Mrad.



It is now obvious that the photolytic degradation of XPVC insulation is wavelength dependent. Medium wavelength UV light is chiefly absorbed by unsaturated chromophores in the polymer, resulting in classical outdoor weathering of the material, as evidenced by dehydrochlorination, substantial discoloration and gel

Fig.9
DEGRADATION OF PVC-METHACRYLATE--PHTHALATE BLEND UNDER 320-380nm LIGHT. Samples were pre-irradiated with γ-rays for 0(●), 4(○) & 10(■) Mrad.



formation[13-15] Apparently, crosslinking is the dominant surface process because there is no tendency for the material to crack under these conditions. Any contribution by the oxidation pathway is overwhelmed by the dehydrochlorination route. Long wavelength UV light, on the other hand, is not readily absorbed by the unsaturated portion of the polymer and the photooxidation described by Scott[13], while relatively slow and inefficient, becomes the major degradative pathway. The surface reactions now exhibit no discoloration and lead predominantly to scission products.

Accelerated Testing

A major goal of this work was to develop a measurement that would predict whether or not a given XPVC-insulated product would endure the fluorescent illuminated environment for some minimum period of time. To that end, the QUV Weathering Tester was equipped with UVB-351 lamps resulting in an intensity that was approximately 200 times the maximum found in the measured Mahopac central office. A sample XPVC that was known to fail in the field in about five years was found to crack in this laboratory test in about 400 hours. If a typical installed lifetime field were 10-15 years, then a 1000 hour survival time in the above apparatus might be a reasonable minimum. Table 2 lists the results of five different samples tested under these conditions; only three of the five passed the 1000 hour mark.

Stabilization from weak indoor UV light-catalyzed oxidation is not normally a concern with inside wire insulations, but electron beam-cured XPVC insulation is now known to be an exception. While we did not undertake the task of incorporating different types and concentrations of UV stabilizers into the XPVC formulation, we assume that this would be a viable solution to the above problem. For current installed, presumably vulnerable plant, the fluorescent bulbs themselves might be equipped with diffusers or filters to respectively scatter or remove the UV portion of the visible spectrum; such aftermarket fixes are available and it remains an economic decision to decide whether such action is warranted or not.

Table 2. Screening Test in QUV-Tester.

Insulation (*)	%Elongation after T hrs		
	T = 0	T = 400	T = 1800
Unused undamaged spool XPVC	180	< 10	< 3
(i)Brand new XPVC	180	40	< 3
(ii) XPVC-1	200	200	100
(ii) XPVC-2	200	190	74
(iii) Plasticized PVC	200	200	114

* see experimental section.

SUMMARY

The photodegradation behavior of electron-beam cured XPVC wire insulation has been shown to be extremely wavelength sensitive. Exposure to heat or medium wavelength UV light (300nm) gives the usual dehydrochlorination, polyene formation, discoloration and loss of elongation associated with PVC deterioration, but no embrittlement. Because crosslinking reactions predominate, the material remains tough and useful for long periods of time. Exposure to UV light of lower energy (350nm), however, will initiate a very slow loss in elongation and eventual embrittlement. In this case, oxidative scission reactions occur on the surface, forming weak material that ultimately leads to cracks. The latter

pathway is apparently associated with the failure of XPVC distributing frame wire near fluorescent lighting in telephone central offices. An 1000 hour accelerated test was devised that will screen out those XPVC insulations that will not endure fluorescent lighting for at least ten years.

ACKNOWLEDGEMENTS

The authors wish to thank I.M. Plitz for Gel Permeation Chromatography experiments, C.C. Chang for microscopy results, R.L. Decker for supplying samples of XPVC insulated wire and R.J. Miner for mechanical testing. Messers. F. Rogers, F. Febre, B. Gesner and F. Szipsky all provided timely advice and or samples from the field. Finally, thanks are due to B. Gesner for making the original suggestion that light played a significant role in XPVC degradation.

REFERENCES

1. I.N.Bowmer, D.D.Davis, T.K.Kwei & W.I.Vroom; *J. Appl. Polym. Sci.*, **26,** 3669 (1981).
2. I.N.Bowmer, M.Y.Hellman & W.I.Vroom; *J. Appl. Polym. Sci.*, **28,** 2083 (1983).
3. I.N.Bowmer, W.I.Vroom & M.Y.Hellman; *J. Appl. Polym. Sci.*, **28,** 2553 (1983).
4. I.N.Bowmer & W.I.Vroom; *J. Appl. Polym. Sci.*, **28,** 3527 (1983).
5. M.Y.Hellman, I.N.Bowmer & G.N.Taylor; *Macromolecules*, **16,** 34 (1983).
6. E.Scalco & W.F.Moore; *Proceedings of the Plastics and Rubber Institute International Conference on radiation Processing for Plastics and Rubbers*, Brighton, June 1981, p34.
7. **ASTM G53-83,** *Standard Test Method for Exposure Testing of Plastics Materials* (1983).
8. **ASTM D638-77a,** *Standard Test Method for Tensile Properties of Plastics*, (1977).
9. N.Grassie & G.Scott; "Polymer Degradation and Stabilization", (Cambridge Uni. Press) 1985.
10. J.Brandrup & E.H.Immergut (Eds.); *"Polymer Handbook"*, (2nd Ed.) Wiley pII-468 (1975).
11. R.R.Stromberg, S.Straus & B.G.Achhammer; *J. Polym. Sci.*, **35,** 355 (1959).
12. G.Talamini & G.Pezzin; *Makrol.Mol.Chem.*, **39,** 26 (1960).
13. G.Scott; *Advances in Chemistry Series* **169,** 30 (1978) and ref. 9, pages 87-118 (1985) .
14. W.H.Starnes,Jr.; *ACS Symposium Series* **No. 151,** p197 (1981) and references cited therein.
15. E.D.Owen; *ACS Symposium Series* **No. 25,** p208 (1975).
16. B.A.Khalifa, S.E.Morsi, W.M.Khalifa & S.Barsoum; *Brit. Polym. J.*, **11,** 13 (1979).
17. V.P.Gupta & L.E.St.Pierre; *J. Polym. Sci., Polym. Chem. Ed.*; **17,** 931 (1979).
18. T.A.Skowronski, J.F.Rabek & B.Ranby; *Polym. Degrad. Stab.*, **8,** 37 (1979).



Trevor N. Bowmer is a member of the Polymer Chemistry and Engineering Research group in Bell Communications Research, Inc., Red Bank, N.J. He received his Ph.D. in chemistry from University of Queensland, Australia, where he specialized in radiation chemistry of polymers. Joining Bell Laboratories in 1980, he studied radiation cured systems and lithographic materials. In 1984, he came to his present position and is studying degradation mechanisms and characterization of polymeric materials used in telecommunications applications.



Paul C. Warren is District manager of the Polymer Chemistry and Engineering Research group in Bell Communications Research, Inc., Red Bank, N.J. After receiving a Ph.D. in organic chemistry from Cornell University in 1969, he joined Bell Laboratories where he pursued research in polymer flammability, test methods and PVC technology. He attained his present position in January, 1984 and his interests now center on the use and reliability of polymeric materials in telecommunications products.

EXTRUSION FOAMING OF ETFE FLUOROPOLYMER RESIN

Stuart K. Randa, Carl R. Fyrwald and David P. Reifschneider

E.I. du Pont de Nemours & Co. (Inc.)

Abstract

Continuous gas foaming of "Tefzel" ETFE fluoropolymer resin, as presented in this paper, is a practical process for producing foam primaries. Thin-wall foam and foam-skin constructions, with void contents as high as 70 percent, have been made at high speed using this technique. Foam primaries are generally used in twisted pair, computer network cables.

I. Introduction

With the continued growth of computer networks, the use of twisted pair and coaxial cables has increased significantly. These cables provide the low capacitance required for high-speed data transmission. Twisted pair primaries insulated with foamed ETFE resin, a co-polymer of tetrafluoroethylene and ethylene marketed under the trademark "Tefzel" ETFE fluoropolymer by Du Pont, provide the enhanced properties necessary for today's demanding data transmission requirements.

ETFE cables are physically tough, highly resistant to chemicals and able to withstand high temperatures. What's more, through foaming, the excellent electrical properties of ETFE cables are greatly enhanced.

ETFE foamed cables can be designed to meet the flame and smoke requirements of the National Electrical Code for plenum cable applications. Cables meeting these requirements can be installed in the air plenums above suspended ceilings without the use of metal conduit - saving both time and money.

Foamed "Tefzel" is a very versatile insulating material. It has been used to make thin insulations for small diameter wires in twisted pair cable constructions and for heavier industrial cables. Foam/skin extrusions permit the combination of many materials to achieve specific properties in the most cost-effective constructions. Cables made of foam "Tefzel" could be used for telecommunication and computer applications, as well as control cables for utilities. Two twisted pair ETFE foam cables are shown below.

Figure 1
FOAMED ETFE CABLE OF SHIELDED PAIRS

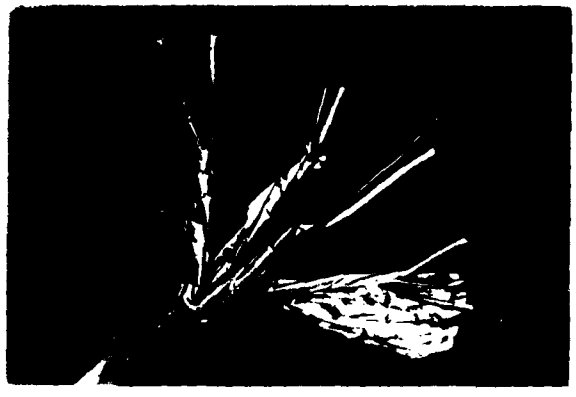


Figure 2
FOAMED ETFE CABLE OF UNSHIELDED PAIRS



The foaming process requires injection of a gas into an extruder. The ETFE resin used in this process contains a nucleant that has been compounded into the resin. The nucleant provides sites for foam cell growth. Final cell size is 1 to 3 mils in diameter. Void contents as high as 70 percent have been demonstrated.

These foams can be either a single uniform layer or a single layer surrounded by a thin, solid skin. The skin provides added dielectric strength and an easy way to color the insulation.

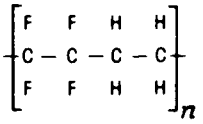
Foaming is an excellent way to achieve low mutual capacitance in twisted pair cables. In comparison to solid insulation, foam can be made much thinner, while still providing the desired impedance. In addition, foam insulation offers a weight savings and can allow the use of a larger conductor to achieve even lower cable attenuation.

II. PROCESS

A. Resin Characteristics

"Tefzel" ETFE fluoropolymer resin has the general polymeric repeat structure shown below.

Figure 3
ETFE MOLECULAR STRUCTURE



"Tefzel" ETFE possesses some of the toughness of nylon, almost the same inertness as "Teflon" and much of the radiation resistance of polyethylene.

The base resin used for foaming is "Tefzel" 220. Three grades are supplied in cube form: 220 for solid skin, 220F for foaming and 220CC color concentrates.

The ETFE resin used in foaming is one of the most fluid ETFE resins available. The standard melt flow of this resin is greater than 20 grams/10 minutes at 298°C (568°F). This resin has been specially designed to meet the melt flow requirements of high-speed processing through dies having small orifices, while still retaining adequate mechanical properties for use as thin-wall foam.

The critical shear rate of this resin (the point prior to that rate where rough-surfaced extrudates are encountered), at 305°C and 340°C, is listed in Table I.

Table I
ETFE RESIN RHEOLOGY

TEMPERATURE	MAXIMUM CRITICAL SHEAR RATE (Reciprocal Seconds)
305°C (581°F)	100,000
340°C (645°F)	500,000

The shear rate formula for pressure extrusion is shown in reference 1. This formula can be used to estimate possible production speeds for specific foamed wire constructions.

"Tefzel" resins for foaming have an approximate melting point of 270°C (518°F); a room temperature specific gravity of 1.7; and a specific gravity of 1.3 at 300°C (572°F).

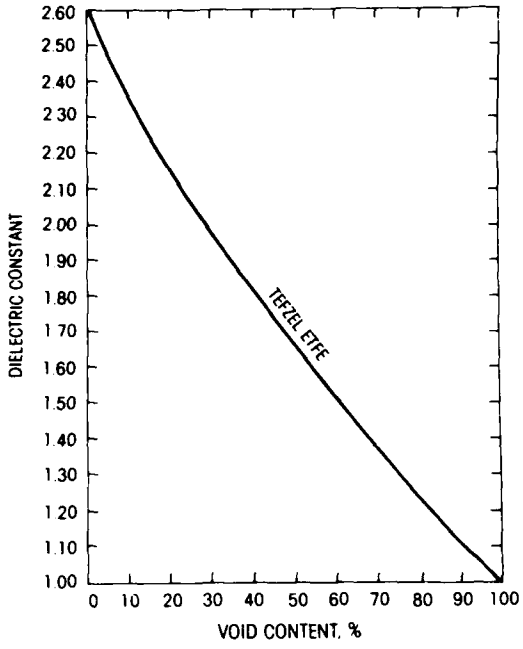
The relatively low dielectric constant and dissipation factor make ETFE resin an attractive electrical insulating material, even as a solid. Table II shows these values at various frequencies.

Table II
ELECTRICAL PROPERTIES OF ETFE 220 RESIN

FREQUENCY	DIELECTRIC CONSTANT	DISSIPATION FACTOR
1 KHz	2.58	0.001
1 MHz	2.56	0.006
100 MHz	2.45	0.020

Foaming reduces the dielectric constant from 2.6 for a solid material toward the 1.0 value of air. Lower dissipation factors, necessary to achieve low cable attenuation, also accompany foaming. For example, an ETFE foam having 70 percent voids would possess a dielectric constant and a dissipation factor nearly half that of solid material. The relationship between dielectric constant and foam level is shown in figure 4.

Figure 4
ETFE DIELECTRIC CONSTANT VS. VOID CONTENT

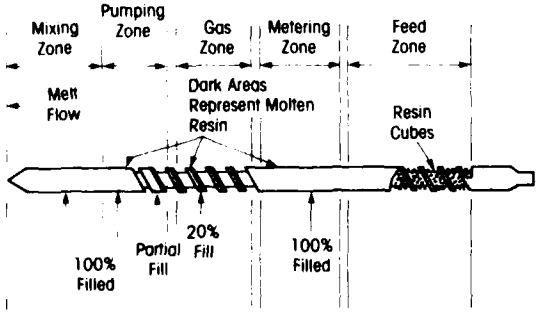


B. Equipment for Extrusion

1. Extruder

A special extruder screw is used. Five zones comprise the design of this screw: feed, meter, gas injection, pumping and mixing, as shown in figure 5. The partially filled zone is where the gas is injected and dissolves into the molten resin.

Figure 5
SCHEMATIC DRAWING OF A MELT-FILLED EXTRUSION FOAMING SCREW FOR ETFE RESIN



Details of the design of a 1.25-in. diameter ETFE foam extruder screw are shown in Table III. This design differs from that used for the foaming process of FEP resin (2). The main difference is that the channel depths are shallower.

Table III
EXTRUDER SCREW DETAILS (1.25 in./31.75 mm diameter) SQUARE PITCHED SCREW

EXTRUDER SCREW ZONES	NUMBER OF FLIGHTS	CHANNEL DEPTH (in./mm)
Feed	8.0	0.160/4.06
Transition	3.0	–
Metering	4.0	0.035/0.89
Transition	0.5	–
F-22 Injection	3.5	0.200/5.08
Transition	0.5	–
Pumping	6.8	0.054/1.37
Mixing Head and Tip	3.7	0.155/3.26
Total	30.0	

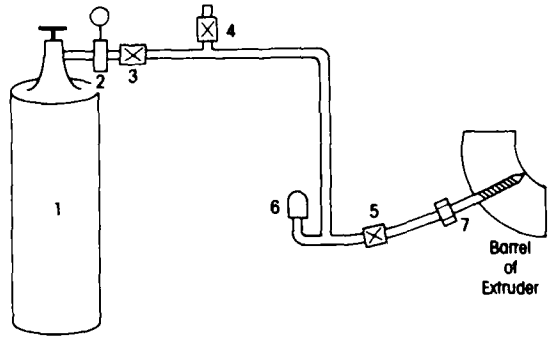
Screw diameters range from 1.25 to 2.35 inches. Standard length to diameter (L/D) ratios range from 28 to 35:1.

To obtain precision control of melt temperature, PID temperature controllers should be used. Motor control for wire conveying and screw melt delivery must also be precise (i.e., 0.1 to 0.5 percent D.C. control). Such equipment should result in acceptable capacitance and diameter control.

2. Gas Injection System

The gas injection system, shown in figure 6, is comprised of a gas cylinder (1), a gas regulator (2), manual valves (3, 4 and 5), a pressure relief valve (6) and a gas injection probe (7).

Figure 6
GAS INJECTION SYSTEM

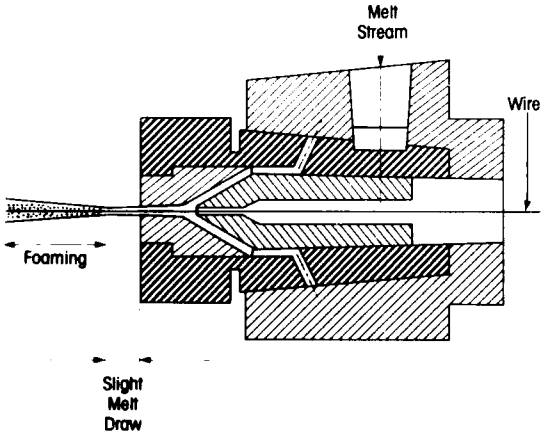


Gas pressure is adjusted with the regulator. The gas flows into the extruder barrel through the injection probe. For a given screw speed, void content is adjusted by varying the gas pressure. This type of gas injection is a simple process setup because no pumps or automatic control valves are required. In addition, the process allows the use of either nitrogen or "Freon" 22 as the foaming gas. The latter is preferred.

3. Crosshead

The 4/6F fixed center crosshead used in our ETFE foam development studies was made by the Maillefer Corporation of South Hadley, Massachusetts. Use of different center cartridges within the Maillefer crosshead allows simple foam extrusion or a foam-skin duplex extrusion. Cross-sectional views of this crosshead during both types of extrusion are shown in figures 7 and 8. The information in these figures is presented courtesy of the Maillefer Company.

Figure 7
MAILLEFER 4/6F WIRE COATING CROSSHEAD SINGLE EXTRUSION



In the foam-skin extrusion set-up, a smaller auxiliary extruder with a conventional type screw provides the molten ETFE resin for the outer skin coating of solid ETFE resin. The two extruders should be positioned head to head, as shown in figure 9, to best accomplish the foam-skin extrusion.

Figure 8
MAILLEFER 4/6F WIRE COATING CROSSHEAD FOAM-SKIN EXTRUSION

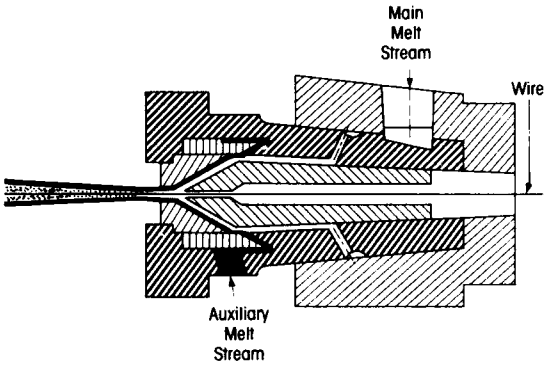
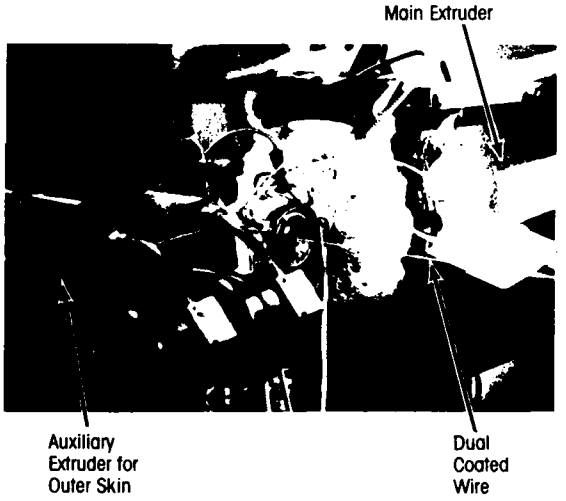


Figure 9
DUAL EXTRUSION FOR FOAM-SKIN PRODUCTION



ETFE resin extrusion foaming normally requires a pressure extrusion. With insulation thicknesses greater than 20 mils, a low melt draw extrusion (less than 5:1) may be used. However, in each type of extrusion, a slight melt draw is applied prior to foaming.

Pressure extrusion is preferred for foaming ETFE resin because this technique minimizes the occurrence of elongated foam cells.

Each of these extrusion techniques is shown schematically in the following figures.

Figure 10
PRESSURE EXTRUSION FOAMING

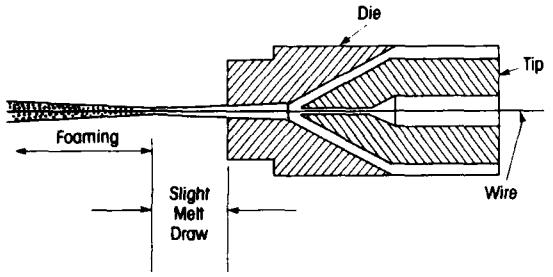
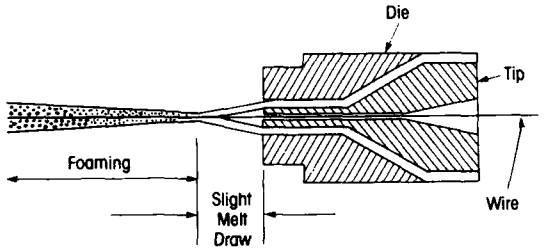


Figure 11
MELT DRAW EXTRUSION FOAMING



C. Extrusion Conditions

Extrusion conditions for production of a 6-mil foam on solid AWG 24 wire, which includes a 1-mil colored skin, are reviewed here. The production speed of the wire coating was 1,000 ft/min. Table IV lists the details of the extrusion equipment used; Table V lists the operational settings for this equipment; and Table VI shows the properties of the foamed primary wire.

Table IV
EQUIPMENT FOR FOAM-SKIN EXTRUSION

- 2-in. Diameter Foam Extruder
- 1-in. Diameter Extruder (Skin Coating)
- Dual Coating Maillefer Crosshead
- Die: 0.033-in. (0.88-mm) orifice
- Electronic Wire Preheater

Table V
OPERATIONAL SETTINGS AT 1,000 FT/MIN WIRE SPEED

	2-in. EXTRUDER	1-in. EXTRUDER
Extruder	315°C (600°F)	315°F (600°F)
Crosshead and Die	332°C (630°F)	
Screw RPM	25	7
Melt Pressure (psi)	700	1,000
F-22 Gas (psi)	60	none
Melt Temperature	323°C (615°F)	
Shear Rate	107,000 sec^{-1}	
Wire Speed	1,000 ft/min (304 m/min)	

Table VI
PROPERTIES OF THE FOAMED PRIMARY WIRE CONSTRUCTION

Construction Diameter	33 mil (0.84 mm)
Foam Thickness	6 mil (0.15 mm)
Skin Thickness	1 mil (0.025 mm)
Capacitance	56 pf/ft
Dielectric Constant	1.79
Resin Weight/1,000 ft	0.2 lb (0.09 kg/304 m)

At a shear rate of 100,000 reciprocal seconds, extrusion rates of 1,000 ft/min (304 m/min) have been demonstrated with a 7.5-mil (0.19-mm) foam coating on AWG 24 wire. The pressure die used had a 0.033-in. (0.84-mm) orifice. The melt temperature was 315°C (600°F) and the melt draw was 1.6:1.

III. WIRE PROPERTIES

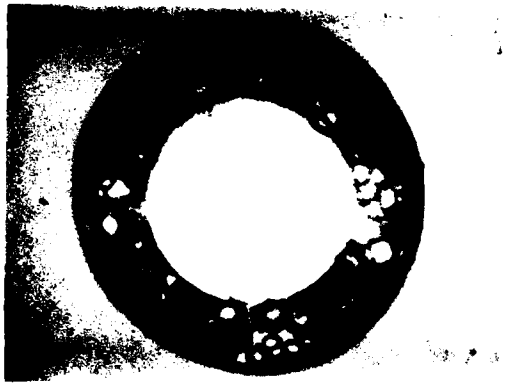
A. Foam Structure

Figures 12 and 13 show the foam structure of this insulation magnified at 30X and 75X. Figure 12 shows a cutaway view from the side of the construction. Figure 13 shows an end view of the insulation. The presence of the black exterior skin can be seen in each photograph. Note the excellent uniformity of the insulation wall in figure 13. This concentricity is a direct result of using the fixed centered crosshead.

Figure 12
FOAM-SKIN ETFE INSULATION, TOP VIEW @ 30X



Figure 13
FOAM-SKIN ETFE INSULATION, END VIEW @ 75X



To obtain a foam without an outer skin, use the same approximate extrusion conditions with the crosshead in its single coating mode and without the auxiliary extruder.

B. Mechanical Properties

As foam-skin constructions, the ETFE resin could have an upper service temperature of 150°C (302°F). This temperature was established by Du Pont as a result of a study where the primaries were tested according to the Mil-22759 procedure, modified to a 1,000 volt breakdown.

Table VII shows a comparison of the mechanical properties of ETFE resin as solid and as foam.

Table VII
ETFE RESIN MECHANICAL PROPERTIES: SOLID VERSUS FOAM MEASURED AT 23 C (73 F) (2-in./min.)

PROPERTY	UNFOAMED	FOAMED 45% voids*
Yield Strength	4,450 psi (30.7 x 10^6 pascal)	–
Tensile Strength	6,060 psi (41.8 x 10^6 pascal)	1,200 psi (8.3 x 10^6 pascal)
Elongation at Break	300%	125%
Flexural Modulus	170,000 psi	35,000 psi
GTE Crush Test, 5-mil Insulation (600 lb minimum)	>1,000 lb passes	>900 lb passes

*Five-mil thick foams, with or without the solid exterior skin

C. Electrical Properties

The electrical properties of extruded wire coatings can be predicted using standard formulas. These formulas are also applicable to foamed ETFE.

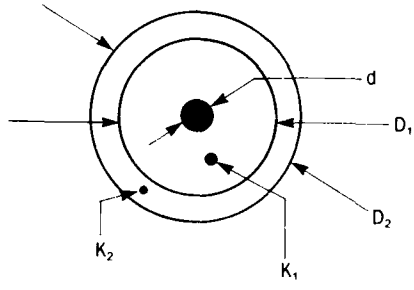
Coaxial capacitance, the capacitance measured in-line with the extrusion process, decreases with either increasing wall thickness or increasing void content.

For foam/skin combinations (layers of materials of differing dielectric constants) the coaxial capacitance is obtained by the following formula.

$$C = \frac{7.354}{\log \left[\left(\frac{D_1}{d}\right)^{\frac{1}{K_1}} \left(\frac{D_2}{D_1}\right)^{\frac{1}{K_2}} \right]}$$

where: C is in picofarads per foot
D_2 is the diameter over the outer layer
D_1 is the diameter over the inner layer
K_2 is the dielectric constant of the outer layer
K_1 is the dielectric constant of the inner layer
d is the conductor diameter

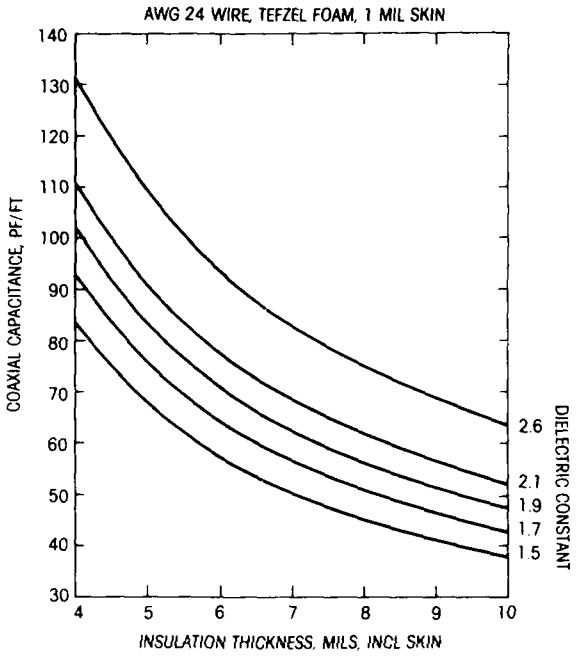
Refer to the schematic diagram below.



For an ETFE skin/foam construction, K_2 would be 2.6 and K_1 would be the dielectric constant of the foam. If no skin is used, K_2 would be 1.0, D_2 would equal D_1 and the formula would be the same as for a single layer of insulation.

Figure 14 is a graph of the coaxial capacitance of an AWG 24 wire where the insulation has an outer 1-mil skin of solid "Tefzel."

Figure 14
COAXIAL CAPACITANCE



The dielectric strength of a foam is typically lower than that of solid insulation, and ETFE foam is no exception. ETFE with 45 percent voids in a 5-mil wall would have a dielectric breakdown voltage of 1,000 volts. Adding a thin outer skin coating and/or increasing the foam thickness improves this breakdown voltage. A 10-mil foam having a 2-mil outer solid skin has a breakdown voltage of more than 3,000 volts.

Some telephone cable specifications require that the insulation withstand 2,500 volts D.C. for three seconds between paired conductors. Foams typically will not meet this specification. However, a 6-mil ETFE foam has withstood voltages of 1,500 to 2,000 volts D.C., and foam/skin constructions have far exceeded the 2,500 volts D.C. test.

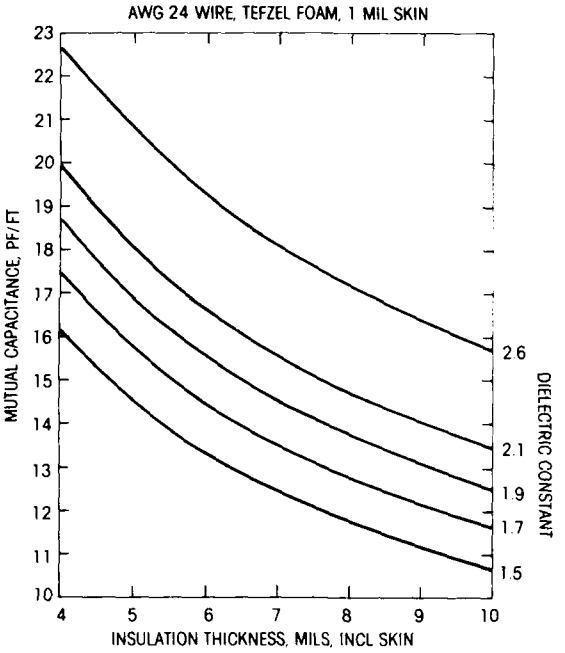
IV. Cable Products and Applications

Typical cables that can be fabricated using primary wires insulated with foamed "Tefzel" include: inside telephone cables for plenum use; computer interconnection cables, such as RS-232 types; and other instrumentation and control cables for Class 2 and 3 power-limited applications.

In scouting tests, foamed ETFE passed the flame and smoke requirements of the Underwriters' Laboratories 910 test. The cables tested were 4 and 12 1/2 pairs with jackets of "Teflon" FEP. The AWG 24 primaries had 5-mil coatings each containing 50 percent voids.

In telephone cables, the mutual capacitance can be determined using traditional formulas with a value for the dielectric constant of the composite insulation(3). Figure 15 shows mutual capacitance as a function of insulation wall thickness.

Figure 15
MUTUAL CAPACITANCE



As previously discussed, an outer skin provides several important benefits. It can enable color coding without blending color into the foam concentrate and it gives greater electrical and mechanical durability to the wire coating. It may also contribute to easier stripping and termination.

Foamed ETFE for telephone cables has been made in a 5.5-mil coating on AWG 24 wire. The insulation was made up of a 4.5-mil foam of 55 percent voids and a 1-mil colored skin. The insulation weight was 0.16 lb/1,000 ft of primary wire. The mutual capacitance was less than 15 pf/ft, which is a significant improvement when compared to the 22 pf/ft industry norm.

The current trend in office automation is more cabling from a central wiring hub to individual offices. These computer cables must meet stringent controlled impedance requirements. One such requirement for telephone-type wiring is 100 ohms at 1 MHz; a requirement that can easily be met using foamed "Tefzel."

The foam extrusion process lends itself to meeting controlled impedance requirements because the foam level can be matched to wall thickness combinations. The specific combination of wall thickness and dielectric constant, as determined by foam level, can be chosen by design; however, it should be verified by actual cable tests since variations in manufacturing and shielding can significantly change the impedance.

During our study, we fabricated three cable constructions with the goal of having each cable exhibit 100 ohm impedance. Although this impedance level was not precisely achieved, each cable possessed a balanced combination of excellent properties.

The cables we fabricated were a 4-pair individually shielded, a 4-pair overall shielded and a 4-pair unshielded. Construction details, as well as measured data, are listed in Table VIII.

Table VIII
FOUR PAIR CABLE DATA

INDIVIDUALLY SHIELDED

24 AWG conductor, 11-mil wall, foamed 50%
Inline coaxial capacitance 37.2 pf/ft
Resin weight, ~.40 lb/1,000 ft of conductor

Frequency	256k	1M	10M	20M
Attenuation db/100 ft	.48	1.3	3.8	5.6
Impedance, ohms	102	87	77	76

OVERALL SHIELD

24 AWG conductor, 7-mil wall, foamed 60%
Inline coaxial capacitance 49 pf/ft
Resin weight, ~.20 lb/1,000 ft of conductor

Frequency	256k	1M	10M	20M
Attenuation db/100 ft	.41	.87	2.7	3.9
Impedance, ohms	93	88	83	83

UNSHIELDED

24 AWG conductor, 7-mil wall, foamed 60%
Inline coaxial capacitance 49 pf/ft
Resin weight, ~.20 lb/1,000 ft of conductor

Frequency	256k	1M	10M	20M
Attenuation db/100 ft	.29	.59	2.1	3.2
Impedance, ohms	116	109	106	105

Coax cables are not likely candidates for the use of foamed "Tefzel." That's because coax cables require low attenuation values and the use of materials with low dissipation factors, such as "Teflon" FEP or polyethylene. "Tefzel" has dissipation factor values an order of magnitude higher than FEP or polyethylene. Thus, cable attenuation would be significantly higher.

If the higher attenuation can be tolerated, or shorter cable lengths used, a possible application area for ETFE coax cable might be in the nuclear power industry in radiation areas.

Cables of foamed "Tefzel" are currently being evaluated for use in aerospace, military electronics, transit, automotive and industrial applications.

References

1. "Equipment and Design Changes in the Extrusion of Foamed Fluoropolymer Resins," 32nd Wire and Cable Symposium 11/20/83, E-85784.

2. "Extrusion Foaming of Coaxial Cables of Melt Fabricable Fluorocarbon Resins," 30th Wire and Cable Symposium 11/18/81, E-90839.

3. "Lee's abc of the Telephone", Riley & Acuna, Volume 7.

Acknowledgements

Daniel Kennifick, E.I. du Pont de Nemours & Co. (Inc.): Assistance with MIL-22759 tests for temperature rating.



Stuart K. Randa

Stuart K. Randa, Technical consultant with Du Pont's Specialty Polymers Division, joined Du Pont in 1956 after earning a B.S. in Chemical Engineering from the University of Wisconsin. He has held positions in the Research, Sales and Manufacturing Divisions of the Polymer Products Department. His current responsibilities include process development and product application for TEFLON® FEP, PFA and TEFZEL® fluoropolymers.



Carl R. Fyrwald

Carl R. Fyrwald, Development Programs Manager with Du Pont's Specialty Polymers Division, joined Du Pont in 1953 after earning a master's degree in mechanical engineering from the Technical University of Denmark. He has held positions in the Research, Sales and Manufacturing Divisions of the Polymer Products Department. His current responsibilities include market development for TEFLON® FEP, PFA and TEFZEL® fluoropolymers.



David P. Reifschneider

David P. Reifschneider, Senior Technical Specialist with Du Pont's Specialty Polymers Division, joined Du Pont in 1970 after earning a Bachelor of Electrical Engineering degree at the University of Delaware. He has held positions in the Design and Construction Divisions of the Engineering Department and in Sales, Market Development and Marketing with the Polymer Products Department. He is presently responsible for electrical product applications for TEFLON® FEP, PFA and TEFZEL® fluoropolymers.

PROCESSING OF THIN WALL FLAME RETARDANT NON HALOGENATED INSULATION FOR INDOOR TELEPHONE EXCHANGE WIRING

E. Buczma, H. A. Mayer, A. C. Day

Olex Cables a Division of Pacific Dunlop Limited
Melbourne, Victoria, Australia.

ABSTRACT

A cable for indoor exchange wiring requires the use of a very thin insulation 0.1mm (3-4 mils). For such thin wall higher strength materials are required. Other material properties such as electrical, flame retardance and absence of halogens limit the possible materials. A modified polyphenylene oxide compound has been used for this application. The processing parameters have been outlined and results presented which show that good insulation properties can be achieved. The cable sheath materials are to be flame retardant and halogen free. Two such materials are evaluated for their behaviour in a fire. In a cable the use of these materials restricts the smoke generation of the modified PPO material in a fire thus improving the overall cable performance.

INTRODUCTION

A particular telecommunications cable is used in Australia and in Sweden for the indoor wiring of telephone exchanges. The cable core consists of insulated conductors in a unit twin construction made up of 0.4mm diameter plain copper conductor with a very thin radial thickness of insulation in the range 0.07-0.10mm (3-4 mils).

The overall diameter of the insulated conductor is required to be nominally 0.60mm but not greater than 0.64mm. One common type of this cable is made up of a 32 wire core with an outer sheath of PVC but this is to be changed to a highly flame retardant non halogenated type sheath.

Figure 1 shows a 16 wire and 32 wire cable of this type of construction.

The cable specification[1] requires the insulation material to be flame retardant and non halogenated.

These properties are required to prevent in case of a fire the propagation of the flame front and the formation of highly corrosive gases which can destroy delicate equipment. With the above material and dimensional constraints it is also a requirement that the insulated conductors have good electrical and mechanical properties and adequate ageing properties. The insulation material must also have the ability to be processed on standard processing equipment at economical line speeds and be of low to moderate cost.



Figure 1 - 16 and 32 Wire Cables for Indoor Exchange Wiring

The low insulation thickness is required to allow the necessary number of insulated wires to enter the particular connector housing used. Figure 2 shows a connector used in exchanges for this application and an insulation stripping tool.

INSULATION REQUIREMENTS

The insulant material for the application is required to be non halogenated, flame retardant and has to achieve all the test requirements of the insulated conductor such as mechanical and electrical properties. These latter properties are required to be at least as good as those of PVC.

The insulation also has to meet the tests as set out in Table 1.

The modified polyphenylene oxide

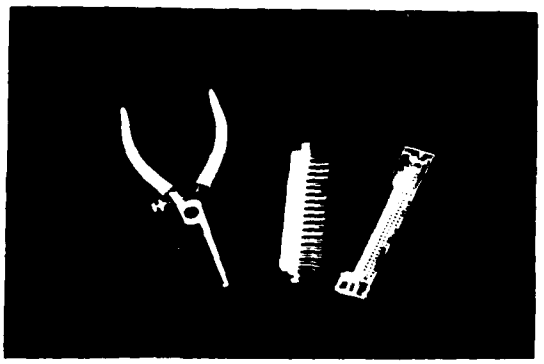


Figure 2 - Telephone Exchange Connector Housing

material discussed later meets the requirements of Table 1.

INSULATION PROPERTIES

The latest Telecom Australia specification requirements for the modified polyphenylene oxide insulation material are listed in Table 2.

Some short notes on the more critical tests related to the modified polyphenylene oxide insulation material are as follows.

Tensile Properties

Test specimens of 150mm length were used. The insulation was removed from the conductor by elongating the conductor 10% on a tensile machine. The crosshead speed used for the test was 50mm/min and the initial jaw separation distance 50mm.

For the ageing test the insulated conductor samples were placed in an oven at 100°C for 120 hours. A recent amendment[2] to the specification has allowed a 10% conductor elongation prior to the ageing test if conditions of the specification cannot be met with samples with no conductor elongation.

Table 1 - Insulation Type Approval Tests

Test	Requirement
Oxygen Index	Insulated conductor samples not to burn for a distance more than 50mm and to cease burning 180 sec. after removal of ignition source when gases in the tube contain not less than 30% oxygen.
Temperature Index	Critical temp. index to be 300°C when tested to NES 715.
Corrosivity Tests	Measured to DIN 57472 Part 813.

Volume Resistivity

To measure the volume resistivity a 10m length of insulated conductor was immersed in water at 23±1°C for approximately 20 hours. The measurement was then repeated at 60°C.

Volume resistivity was determined from the relationship.

$$\text{Volume resistivity} = \frac{2.73RL}{\log_{10}\frac{D}{d}} \quad (G\Omega\,m)$$

R - insulation resistance of the sample (GΩ)
L - length of sample (m)
D - diameter over the insulation (mm)
d - diameter of copper wire (mm).

Table 2 - Modified Polyphenylene Oxide Insulation Requirements

Property	Value
Unaged Properties	
Tensile stress at break,min	35.0 MPa
Elongation at break,min	130%
Aged Properties (100°C for 120 hours)	
% Retention of Elongation	60%
Stripping Force	2-12 N
Volume Resistivity	
At 23°C, min	$1x10^4$ GΩm
At 60°C, min	$1x10^3$ GΩm
Volatile loss, max	$10g/m^2$
Shrinkback, % max	2%
Cold bend test No cracking at	-15°C

The dielectric strength test was carried out at 2.8kV DC for 1 min after immersion of the sample in water for 20 hours at 23±1°C. Voltage breakdown was determined on the same sample by uniformly increasing the voltage to failure.

Stripping Force

Samples of 100mm length were prepared by removing 50mm of insulation from one end and 25mm from the other end. The longer end of the bare wire was threaded through a hole in a metal fixture the hole diameter being approximately 10% greater than the diameter of the wire. The fixture and the threaded end of the conductor were clamped in the tensile testing machine used and the maximum force at a crosshead speed of 250-350mm/min recorded.

COMPARISON OF SOME INSULATION MATERIALS

Table 3 presents typical properties obtained for 0.1mm (4 mil) radial thickness insulation on 0.4mm diameter copper wire for some insulation materials.

The abrasion resistance was determined using the apparatus[2] shown in figure 3. The number of completed up and down movements of the wire before a circuit occurred between the wire under test and the abrading insert was recorded.

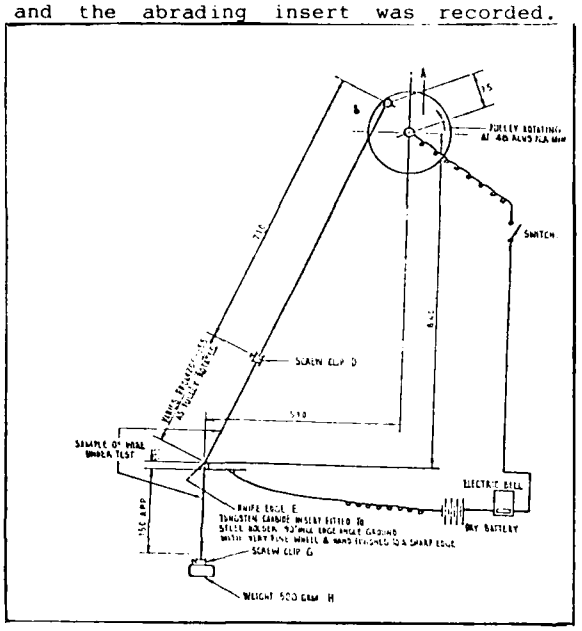


Figure 3 - Wire Abrasion Testing Apparatus[2]

Table 3 illustrates the higher strength of the engineering plastic type of material like the Nylon 12 and the modified polyphenylene oxide (PPO) compound compared to the traditional materials like the PVC and polyethylene.

This becomes particularly apparent at the low insulation thickness of 0.1mm (4 mil) where the tensile properties are lower than the values obtained when these materials are processed at their usual radial dimensions of 0.18mm for PVC and 0.22mm for polyethylene.

Table 4 shows the properties of PVC and polyethylene processed at their more common radial thicknesses.

The ageing performance for the insulation materials at the radial wall thickness of 0.1mm is shown in Figure 4. The results are for insulated conductor samples aged at 100°C in an air oven to the specification[1] with the conductor not being pre-stretched prior to ageing.

The ageing of polyethylene and PVC at a radial wall thickness of 0.1mm is more rapid than that of the nylon and the modified PPO compound. The same polyethylene and PVC was used for the results obtained in Tables 3 and 4 and figures 4 and 5. The performance of the PVC may be improved by changing the formulation but the

Table 3 - Insulation Properties of some Materials Processed as 0.1/0.4mm Wires

Property \ Insulation Material	PVC	Poly-ethylene		
Unaged				
Tensile stress at Yield MPa	21.8	[illegible]	9.0	[illegible]
Tensile stress at Break MPa	19.1	[illegible]	[illegible]	[illegible]
Elongation at Break %	92	412	20%	[illegible]
Aged 120 hrs, 100°C				
Tensile strength MPa	48.3	[illegible]	[illegible]	[illegible]
Elongation at Break %	Very low	220	20%	170
Stripping Force, N	2.2	[illegible]	[illegible]	[illegible]
Volume Resistivity GΩm				
23°C	6x10[illegible]	[illegible]	1x10[illegible]	[illegible]
60°C	12	6x10[illegible]	-	[illegible]
Dielectric Strength				
2.8 kV 1 min	Fail	Pass	Pass	Pass
Breakdown Voltage	-	[illegible]	6kV	9kV
Abrasion Resistance (scrapes to failure)				
250 g Weight	48	8	144	53
500 g Weight	3	1	20	7
Flame Test on Single Wire, IEC 332-2 Draft	Pass	Fail	Fail	Pass
Corrosivity, BS6724 Draft.				
pH	[illegible]	4.1	7.5	4.2
Conductivity μS/cm[-1]	9150	93	107	22

Table 4 - Typical Properties of PVC and Polyethylene at 0.18 and 0.22mm Radial Thickness

Property \ Insulation Material	PVC	Poly-ethylene
Radial thickness of insulation	0.18mm	0.22mm
Unaged		
Tensile Stress at Yield MPa	15.5	10.0
Tensile Stress at Break MPa	22.7	17.0
Elongation at Break %	180	412
Aged 120 hrs at 100°C		
Tensile Strength MPa	25.6	14.9
Elongation at Break %	140	365
Volume Resistivity GΩm		
23°C	$1x10^4$	$8x10^6$
60°C	37	$1x10^6$
Dielectric strength 2,8 kV 1 min	Pass	Pass
Breakdown Voltage	>10kV	>10kV

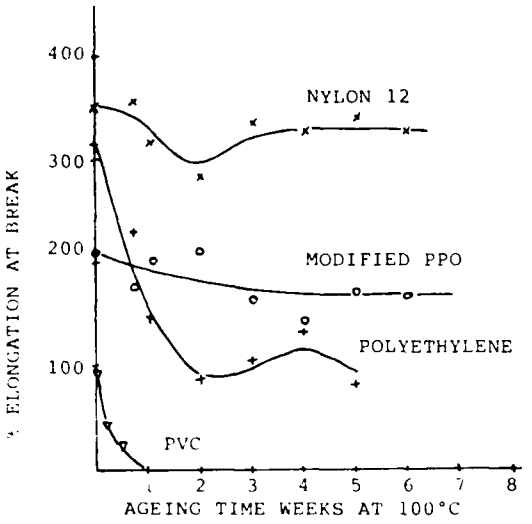


Figure 4 - Ageing Performance of the Insulation at 100°C

PVC material has other drawbacks in the requirements for this product as outlined in an earlier section.

Over the duration of the ageing tests presented in Figure 4 the modified PPO compound insulation could be stripped from the conductor using the method described earlier.

Table 3 shows that generally the stripping force is higher for the modified PPO compound insulation compared to that of the other materials.

Polyethylene insulation at 0.1mm radial thickness has very good electrical properties but very poor abrasion properties.

Nylon 12 has excellent abrasion resistance but inferior electrical properties compared to polyethylene and PVC. The PVC insulation at 0.1mm radial thickness has a low breakdown voltage. For the modified PPO insulation the electrical properties are good and only slightly inferior to polyethylene.

Both the PVC and Nylon 12 insulations undergo a large drop in volume resistivity when measured at 23°C and 60°C. This is illustrated in Table 3 and Figure 5.

Comparing the flammability characteristics, the PVC compound on ignition produces copious amounts of black smoke and releases corrosive gases even if it can be flame retarded sufficiently to reduce flame propagation. Polyethylene burns very freely with low smoke evolution and produces droplets of molten burning material which on falling can initiate secondary ignition points. The nylon insulation material used is not flame retardant.

Thus the modified PPO insulation material offers some promise for this application because at the insulation radial thickness of 0.1mm it has good strength characteristics, good electrical properties, is flame retardant and does not contain halogens.

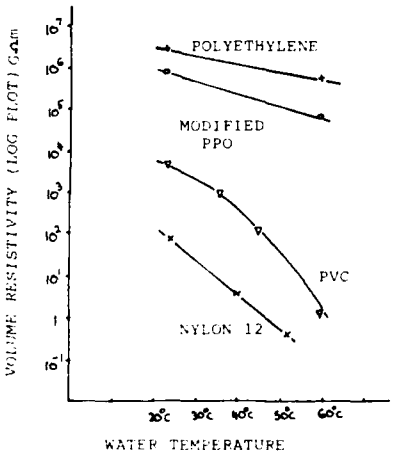


Figure 5 - Volume Resistivity as a Function of Temperature

THE MODIFIED PPO MATERIAL

A modified polyphenylene oxide compound for wire and cable applications was introduced by E. de Munck et al at the 1980 IWCS[3]. The material was proposed as having a high degree of flame retardance, low evolution of aggressive fumes on burning, good mechanical and electrical properties over a broad temperature range and the ability to be processed into thin wall insulation on high speed insulation lines.

H. A. Mayer et al[4] discussed the use of non halogenated flame retardant materials in cable designs and the use of a modified PPO compound as an insulation material for telecommunication cables[5].

In 1983 a new grade based on the above material was introduced for which a better ageing performance was claimed. The material properties for this new grade of modified PPO material named Noryl PX1766 are listed in Table 5.

Typical processing data for the modified PPO material has been described [3,6,7]. These also present data on insulated conductor, of the mechanical, electrical and ageing properties.

Table 5 - Material Properties of Modified PPO Material [7]

Property	Test Method	PX1766
Specific Gravity, g/cm^3	ASTM D792	1.04
Limiting Oxygen Index, %	ASTM D2863	32
Temperature Index, °C	NES 715	310
Smoke generation		
-Flaming mode D max, 4 min.	ASTM E662	490
-Smouldering mode D max, 16 min.		120
Combustion Gas Corrosion (Limit 20%), %	UTE C20453	1.5
Combustion Gas Corrosion		
-pH value (limit>4.0)	VDE 0472	4.1
-Conductivity (limit<100), $\mu S cm^{-1}$	PART 813	12
Dissipation factor, 1 MHz		0.0045
Relative permittivity: 50 Hz	ASTM D150	2.7
1MHz		2.6

However, all the above discuss the use of the modified PPO material at larger wall thicknesses of 0.2-0.3mm and above. When the material is processed down to the very low radial wall thicknesses covered in this paper the application becomes more critical and several other parameters have to be taken into account for successful processing.

The modified PPO compound is a complex polymer alloy or blend consisting of a number of components. These components include the polyphenylene oxide, elastomeric deformation modifier, flame retardant, processing aids and stabiliser. The components of the material are dealt with in [3] where the use of deformation modifiers is discussed.

Examples of the use of thermoplastic rubbers based on styrene of the S-EB-S type for modification of engineering plastics of the PPO type are covered in [8,9].

PROCESSING OF THE MODIFIED PPO MATERIAL AT 0.1mm RADIAL WALL THICKNESS

Extrusion Equipment

The extruder used for the processing of the modified PPO material at 0.1mm radial wall thickness onto 0.4mm conductor was a standard 60mm 20:1 L/D machine of common use in the wire and cable industry. The extrusion line was suitably equipped with standard equipment for high speed insulating.

Heating/cooling systems on the extruder barrel and die need to be accurately controlled for this type of product. Control of insulation diameter is also a prerequisite at the high line speeds used. A suitable wire preheater of adequate capacity at high line speeds is an essential requirement of this line, together with some means of altering the temperature of the first stage of the cooling trough.

Extruder Temperature Profile

The extruder temperature profiles used have been in the range from 200°C to 275°C with melt temperatures in the range 250°C to 275°C.

Reports received have indicated that extruder barrel temperatures in the range 220°C (back zones) to 280°C (extruder head) with melt temperatures in the range 284°C-294°C have been used for the extrusion of the modified PPO material at a 0.1mm radial thickness.

The following results show that processing at a higher extruder temperature profile may lead to higher insulation elongation but also could result in a higher insulation stripping force.

Melt Temperature	Radial Thickness (mm)	Insulation Elongation %	Stripping Force (N)
265°C	0.10	172	6.2
273°C	0.10	206	8.9

Conductor Preheat Temperature

For the extrusion of the modified PPO material at the low radial wall thicknesses discussed in this paper the conductor preheat temperature used is important in obtaining good insulation mechanical properties.

The wire preheat temperature affects the adhesion of the melt to the copper wire thus influencing the stripping force and the elongation obtained.

For the extrusion of the modified PPO material at 0.1mm radial wall thickness conductor preheat temperatures in the range 50-90°C have been used for the results obtained in this paper.

The following results show the effect of conductor preheat temperature on the elongation (unaged) and stripping force of the insulation, processed at the same line speed and insulation cooling conditions.

Conductor Preheat Temperature °C	Insulation Elongation %	Stripping Force (N)
30	162	7.4
50	220	5.7
70	240	6.5

With an increase in the wire preheat temperature the elongation increases but the stripping force appears to pass through a minimum value.

In achieving the stripping force values no treatment of the conductor with any release agents was used. The use of a particular conductor preheat temperature may also not be optimum in terms of the insulation elongation retention value after ageing.

This may in part be due to the ageing process and in part to the very thin coating on the hot wire undergoing orientation, shrinkage and cooling effects immediately after exit from the die.

Line Speed

Line speeds used for processing have ranged from 500-1500m/min.

An increase in line speed generally leads to a slight increase in insulation elongation at a particular preheat temperature.

Line Speed	% Elongation (Unaged)
500 m/min	212
1000 m/min	227

Line speed can also increase the insulation stripping force.

Line Speed m/min	Conductor Preheat Temp. °C	Stripping Force (N)
1000	50	5.7
1300	50	7.4

Insulation Cooling Conditions

The insulation cooling conditions can be modified by the temperature of the water in the first cooling trough and by altering the distance of the die to the quench point. For the particular die design used these factors can affect the insulation stripping force obtained.

The effect of the water temperature on the stripping force is shown by the following result.

Water Temperature of First Cooling Zone °C	Stripping Force (N)
60	8.3
80	7.4

Bringing the first cooling trough closer to the die increases the stripping force.

Position of First Cooling Trough	Stripping Force (N)
0.02m to Die	8.0
1m to Die	6.8

Die Design

For the thin wall insulation of the modified PPO compound, pressure type extrusion dies have been used. In pressure die designs the design criteria include:

1. the die internal angles
2. land length of the die
3. size of die opening.

Four pressure extrusion dies each with some change in the above parameters were evaluated for the surface appearance of the insulation on extrusion. The results obtained were:

Die	Insulation surface appearance
A	Slightly rough at the higher line speeds.
B	Good - smooth
C	Good - smooth
D	Rough at all line speeds.

Both dies B and C produced insulations with smooth surfaces.

The die design used also has an effect on the stripping force of the insulation. The following results were obtained from various trials on 0.1mm radial thickness insulation at the same conductor preheat temperature.

Trial No.	Die Type	Stripping Force (N)
1	B	6.1
	C	5.7
2 (high line speed)	B	18.0
	C	8.0

With die design B the stripping force required to remove the insulation from the conductor tends to be higher. Both dies B and C produced insulation of high elongation.

However, the use of a particular die may affect the ability to remove the insulation from the conductor after ageing the insulated conductor at 100°C for 5 days. Thus with die B in some cases the insulation could not be removed from the conductor after ageing. Of course if the conductor is prestretched 10% prior to ageing the insulation can be removed easily. This procedure may not be required if the appropriate die is used.

Screw Type

Two different barrier type screws have been trialled with the extruder described above, the essential difference between the two screws being the channel depth. Both the screws produced insulation with good properties at similar processing conditions.

Screen Packs

For the successful processing of a thin radial wall thickness of 0.1mm the modified PPO material requires a screen pack to give a minimal spark test fault result. The product is usually run under 2kV DC spark fault test conditions. For the processing conditions used the screen pack selected gives relatively fault free results.

The screen pack arrangement normally used has the finest screen size larger than 200 mesh.

The use of very fine screen packs may affect the properties of the insulation.

Screen Pack Arrangement	Insulation Elongation Unaged %	Stripping Force (N)
1	180	7.8
2	160	10.3

Screen pack 2 is a finer mesh than screen pack 1. For these results the other extrusion parameters were kept constant.

Masterbatches

For identification in the cable the individual insulated conductors need to be coloured. For colouring the modified PPO compound colour masterbatches were used at a level up to 3% wt/wt. The type of masterbatches used can have an effect on the insulation properties as the following results show:

Masterbatch	Insulation Elongation Unaged %	Aged 5 Days at 100°C, %
Polyolefin Type	200	130
Polystyrene Type	200	40

Material Cleanliness

In order to obtain good mechanical and electrical properties from the 0.1mm radial thickness insulation of the modified PPO compound the material must be free from contamination. If there is any contamination present this can have severe effects especially because the radial thickness is so small. The affected properties are volume resistivity, dielectric strength and aging properties.

Table 6 shows the effect of line speed on volume resistivity and dielectric strength when contamination is present in a batch of the raw material.

The presence of foreign material causes a drop in volume resistivity values as line speed is increased and poor dielectric strength figures.

RESULTS OBTAINED

Optimising all the parameters discussed in the previous section Table 7 presents typical results that can be achieved in processing the 0.1mm radial thickness modified PPO compound on 0.4mm copper wire.

Table 6 - Effect of Contamination on Electrical Properties

Line Speed	Volume Resistivity GΩ m 23°C	60°C	Dielectric Strength, 23°C
500 m/min	$1x10^6$	$2x10^5$	Passed 2.8kV 1min
750 m/min	$6x10^4$	$3x10^4$	Failed at 2kV
1000 m/min	$1x10^3$	$7x10^3$	Failed at 2kV

Table 7 - Results at Different Line Speeds (standard batch)

Property \ Line Speed	1000m/min	1500m/min
Unaged Values		
Tensile Stress at Break MPa	53.8	53.7
Elongation at Break %	227	213
Aged Values (Aged 120 hrs.at 100°C)		
Elongation at Break %	175	172
% Retention	77	81
Stripping Force N	5.2	3.9
Volume Resistivity		
At 23°C GΩ m	$7x10^5$	$7x10^5$
At 60°C GΩ m	$7x10^4$	$1x10^5$
Dielectric Strength		
2 kV for 1 min	Pass	Pass
Breakdown Voltage	5 kV	5.5 kV

For the above no spark test faults were obtained at 2kV DC, the extruder RPM was in the range 15-25 and the extruder amps in the range 45-55. The masterbatch level was 2.5 wt/wt.

Table 8 shows results achieved during a cable production run together with the electrical properties of the completed cable. The electrical property requirements of the cable are covered in references [1,2].

BEHAVIOUR UNDER FIRE CONDITIONS

As mentioned in the introduction, for these type of cables a highly flame retardant thermoplastic non halogenated material is to replace PVC as the sheath material.

The use of these flame retardant non halogenated materials has been described [4,5] and over the last few years more of these type of materials have appeared. Two of these materials were used to sheath 32 wire laid up cores of the 0.1mm radial thickness modified PPO material insulation to

Table 8 - Results Achieved on a Cable Production Run

PROPERTY	SPECIFICATION VALUE	MODIFIED PPO INSULATION								
		RED	YELLOW	ORANGE	BLUE	WHITE	BLACK	BROWN	GREEN	AVERAGE OF 8 COLOURS
Unaged										
Tensile Stress at Break MPa	35.0MPa min	44.3	43.8	45.0	44.9	42.1	43.7	42.0	41.4	43.4
Elongation at Break %	130% min	240	238	230	235	215	210	208	210	223
Aged 100°C for 120 Hrs.										
Elongation at Break %	Min.	225	191	220	250	219	191	172	206	209
% Retention	60% of Unaged	94	80	96	106	102	91	83	98	94
Stripping Force , N	2 - 12 N	9.0	6.5	6.0	6.5	7.0	4.0	6.0	8.5	6.7
Volume Resistivity										
At 23°C GΩ mx10^5	Min. 1x10^4 GΩ m	17	17	10	6	5	2	7	15	10
At 60°C GΩ mx10^4	Min. 1x10^3 GΩ m	17	4	5	12	15	3	17	5	10
Average Radial Thickness mm		0.091	0.090	0.096	0.101	0.091	0.096	0.091	0.101	0.095
Minimum Radial Thickness mm		0.08	0.07	0.08	0.07	0.08	0.07	0.08	0.08	0.08
Spark Fault Level at 2.0kV DC 1 Fault / - km		8	6	8	6	6	22	8	15	8 (Length) / (Faults)

Conductor Size = 0.400 mm
Insulated Conductor OD = 0.58 mm
Total Run of Insulated Conductor 2000 km

ELECTRICAL PROPERTIES OF COMPLETED CABLE

PROPERTY	SPECIFICATION VALUE	RESULT
Mutual Capacitance nF/km	60-80 nF/km	Mean 72-73
Insulation Resistance MΩ km	Min. 1x10^3 MΩ km at 20 °C	Lowest Value 1.4x10^4
Capacitance Unbalance pair to pair pF	Corrected to 500m length Max. 150 pF	Mean 7-17 Max 121 pF

a wall thickness of min. 0.6mm and a cable OD of 6.5mm.

The properties of the two materials have been detailed [10,11] while Table 9 shows the on cable results obtained. Comparison is made with a PVC sheath of the same dimensions used for this application.

Table 9 - Comparison of Sheath Materials

Property \ Material	Sheath Material 1 SM-1	Sheath Material 2 SM-2	PVC
Tensile Properties			
Unaged			
Tensile Stress at Break MPa	9.3	16.7	18.3
Elongation at Break %	330	165	245
Aged 120 hrs 100°C			
Elongation at Break %	220	140	260
Combustion test at 28% Oxygen	Pass	Pass	Pass
Oxygen Index	48	40	30
Corrosivity BS 6724 Draft			
pH -1	4.0	4.1	2.0
Conductivity μS.cm^{-1}	40	20	4500

The test procedure for the above tests are outlined in [1].

To evaluate the behaviour of the insulations and sheathing materials in a fire situation the insulated conductors and completed cables were subjected to fire tests.

The fire test in Australian Standard AS1530.3 "Test for Early Fire Hazard Properties of Materials" was developed for the assessment of building materials but in this instance was adapted to assess cable behaviour in a fire.

The test classifies the samples under test in terms of index numbers for ignitability, spread of flame, heat evolved and smoke developed.

In the test, cable samples covering an area 600 x 450mm in a panel form were held in a vertical plane parallel to a radiant heater and moved towards the heater in steps, from an initial distance of 850mm, over a 20 min. period or until ignition induced by a pilot flame occurred.

For the cable size used 50 lengths were required to cover the surface of the sample panel. When insulations were tested, again 50 lengths of 32 wire cores of insulation were used. The apparatus is shown in Figure 6.

Table 10 shows the samples tested while Table 11 gives the results obtained.

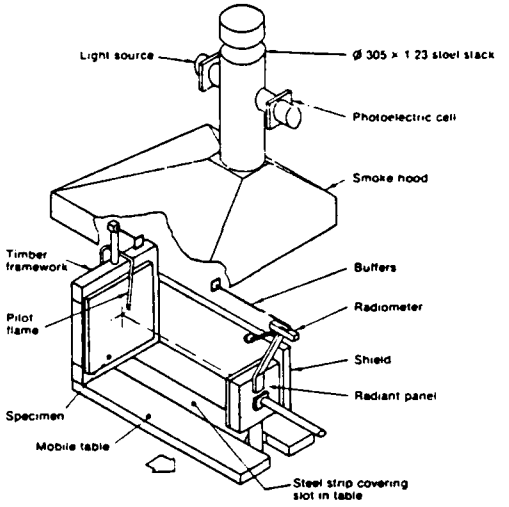


Figure 6 - Apparatus for AS1530.3 Fire Test

The radiant panel is 300mm square in size and is calibrated to give an intensity of radiant heat of 2.4kW/m^2 as measured by the radiometer at a distance of 850mm in front of the panel.

The test is terminated after 20 mins. if no ignition occurs, 120 secs after ignition if during this period the radiometer records a rise of 1.4kW/m^2 or any time up to 203 secs max after ignition when a rise of 1.4kW/m^2 occurs.

Table 10 - Samples Tested

Sample	Composition					
	Core	Conductor Diameter	Radial Thick.	Insulation	Sheath	Cable OD
1	32 Wire	0.4mm	0.1mm	PVC	PVC	6.5mm
2	32 Wire	0.4mm	0.1mm	PPO	SM-2	6.5mm
3	32 Wire	0.4mm	0.1mm	PPO	SM-1	6.5mm
4	32 Wire	0.4mm	0.1mm	PVC	-	-
5	32 Wire	0.4mm	0.1mm	PPO	-	-
6	32 Wire	0.4mm	0.1mm	PE	-	-

The indices in Table 11 are defined as follows:
ignitability index = 20 - TIME for ignition (mins), from 0-20.
spread of flame index = 1.33 x TIME from ignition point for 1.4kW/m^2 to be reached (secs), from 0-10.
heat evolved index = heat evolved integral for 2 mins after ignition KJ/m^2 from 0-10.
smoke developed index = max. smoke developed (optical density/metre)in 1 min. period during the test, from 0-10.

Table 11 gives the indices and the actual values obtained. The relationships

between the two can be found in AS1530.3.

The modified PPO compound insulation did not ignite under the conditions of the test but it had a higher smoke level than the polyethylene insulation which even as a 0.1/0.4 construction burnt very fiercely evolving the most heat much more than the cable constructions and had the fastest rate of flame spread. During the test the polyethylene insulation formed a burning pool at the base of the test chamber.

Table 11 - AS1530.3 Results

Sample	Ignitability		Spread of Flame		Heat Evolved		Smoke Developed		Test Duration
	I	Time Mins	I	Time Secs	I	KJ/m^2	I	% Obs	Mins
1	15	5.2	0	>270	0	23	8	54	8.2
2	13	6.6	0	>270	2	69	5	12	10.5
3	13	6.8	0	>270	2	54	4	7	10.3
4	12	7.9	0	>270	1	34	7	50	11.4
5	0	Did not Ignite	0	-	0	0	5	15	20
6	10	9.4	8	48	7	180	5	12	11.4

NOTE: % Obs = % Obscuration, I = Index.

If the test simulates a fire front approaching a bank of cables it can be seen that the PVC cables will ignite first developing the highest smoke density, although the heat evolved is lower than for the flame retardant halogen free sheathing materials. However, in the latter case the smoke developed is very low and no corrosive gases are present.

To determine the smoke level produced when the sample is burnt by a flame as distinct from a radiant panel two pieces of each sample in Table 10 120mm long were burnt in a chamber $0.7m^3$ volume described in NES 713[12]. The samples were burnt with a bunsen burner fitted with a fan shaped cone to spread the flame.

Flame temperature was measured at between 750-800°C. This ensured the whole sample was burnt. The chamber was fitted with a light source and detector. Table 12 shows the obscuration results obtained when the samples in Table 10 were tested.

Table 12 - Smoke Obscuration Results

Sample	Obscuration
1	84
2	8
3	1*
4	32
5	10
6	20

The results in Table 12 show that the modified PPO insulation material when subjected to a flame burns with high smoke evolution but this can be overcome in a cable construction by using a sheath of the type SM-1, SM-2. The low smoke level of these sheath materials is again apparent.

To test the fire behaviour of the samples in bunched cable arrangements IEEE 383 was used. A flame temperature of approximately 800-850°C was used and 6x8 ft. lengths of samples 1-5 in Table 10 were tested. One half of the cable diameter was the spacing distance between the individual lengths.

All samples passed the test.

To increase the volume of combustible materials 5 layers of 11 cables each layer were tied to the ladder. Cable samples 1, 2 and 3 of Table 10 were tested. This number of cables make up 1.5 litres/metre of combustible material which is the volume specified in IEC 332 Pt. 3 Category C. On testing with this volume all the cables passed the IEEE 383 test.

CONCLUSION

For thin wall extrusion 0.1mm (3-4 mil) higher strength materials are required. The material requirements of mechanical, electrical, flame retardance and non halogen severely limits the number of possible materials for this application. The modified PPO which although more difficult to process possesses many of the desired properties. Processing parameters required for successful extrusion have been outlined. Together with a halogen free highly flame retardant sheath a suitable cable for indoor telephone exchange wiring can be produced.

REFERENCES

1. Telecom Australia Specification Schedule C 6344 Appendix C.
2. Telecom Australia Correspondence.
3. De Munck, Bury, Simpson, Devoldere. "A New Non Halogenated Flame Retardant Wire Insulation Based on Polyphenylene Oxide" 29th IWCS 1980.
4. Mayer, H. A., Hog. G. "A New Generation of Non Halogenated Flame Retardant Compounds and Cables" 29th IWCS 1980.
5. Dageforde H. G., Berchem. W., Mayer H. A. - "Flame Retardant Halogen Free Thermoplastic Telecom Indoor Wiring" 31st IWCS 1982.

6. Wire Insulation PX1766, Communication ID Meeting, Canterbury, England 29-30th March, 1983.

7. Technical Data, GEP, Noryl PX1766 Non Halogenated, Self Extinguishing Wire Insulation.

8. Masuko N. "Thermoplastic Rubbers Based on Styrene" International Polymer Science and Technology Vol. 12, 3, 1985, T/41.

9. Yoshimura D. K., Richards. "Gaging The Rheological Behaviour of Triblock Polymer Blends" Modern Plastics International 4, 1987, 56.

10. Taylor J. "Halogen Free Cable Compounds" Wire Industry, April, 1987.

11. Technical Data, Megolon, Lindsay and Williams, Manchester, England.

12. NES 713 Naval Engineering Standard Ministry of Defence, U.K.

Acknowledgements:

The support of the Olex Telecommunications Division, in particular M. Stretton for help in conducting the trials and other colleagues for assistance at various stages, is gratefully acknowledged.

Authors



Arthur C. Day obtained a Graduate Diploma of Applied Chemistry from the Royal Melbourne Institute of Technology in 1959. He joined Olex Cables in 1959, working initially on PVC, and then elastomer formulation. In 1968 he took over the control of the Central Laboratory and in 1976, was appointed Chief Chemist. Experience prior to joining Olex Cables, was gained in research work on pulp and paper technology, followed by two years in the printing industry. Special interests at Olex Cables are development of materials and tests for halogen-free cables.



Eugene Buczma, graduated from the Department of Industrial Science, Melbourne University in 1971. From 1971 to 1979 he was employed at Austral Standard Cables in the Materials Development Section. In 1980 he received his Masters Degree from Melbourne University with a thesis on the extrusion of cellular polyethylene. In 1979 he joined Hoechst Australia in the Plastics Technical Service Section. He has extensive experience in polymer processing technology in injection moulding, blow moulding and extrusion. In 1985 he joined Olex Cables as a Senior Development Engineer.



Hans A. Mayer, 1951-1956 studied Chemical Engineering at Technical University, obtained Dipl.-Ing. degree in Engineering. 1956-1961 Plastics & Rubber Industry, 1961-1964 Chemical Industry, mainly as Manager Technical Q.C. & Central Laboratories. 1965-1983 AEG-TELEFUNKEN Kabelwerke AG, West-Germany in various factories, mainly as Manager Central R & D Materials & Process Engineering and Chief Engineer. 1983 Hans joined Olex Cables, as Technical Operations Manager. Hans is author/co-author of various patents. Member of the Institution of Engineers Australia.

Address:

Olex Cables, Melbourne,
A Division of Pacific Dunlop Limited,
207 Sunshine Road, Tottenham, 3012,
Victoria, Australia.

ANALYSIS OF AND COUNTERMEASURES TO PECULIAR PHENOMENA OF HALOGEN-FREE FLAME-RETARDANT CABLES IN CABLE TUNNELS: GROWTH OF MOLD AND DEPOSITION OF METAL CARBONATE

Kazuhiko Tanaka, Fumio Takaesu and Fuminori Kozono

NTT Network Systems Developmert Center
Nippon Telegraph and Telephone Corporation
Chiyoda-ku, Tokyo, JAPAN

INTRODUCTION

NTT has developed halogen-free flame-retardant telecommunication cables, which use metal hydroxide-filled sheath material. These were installed in cable tunnels in a commercial test.

This test revealed a peculiar phenomenon, the turning white of cable sheath in deep cable tunnel. After careful inspection it was discovered that there were two phenomena involved, the growth of mold and the deposition of metal carbonate.

Tests showed the mold to be a kind of trichoderma. It was found that certain agents have a tendency to grow mold, and that the deposition was a result of reaction with carbon dioxide and water in the air.

These phenomena are suppressed by elimination of susceptible agents and by careful selection of the base polymer and extruding agents.

BACKGROUND

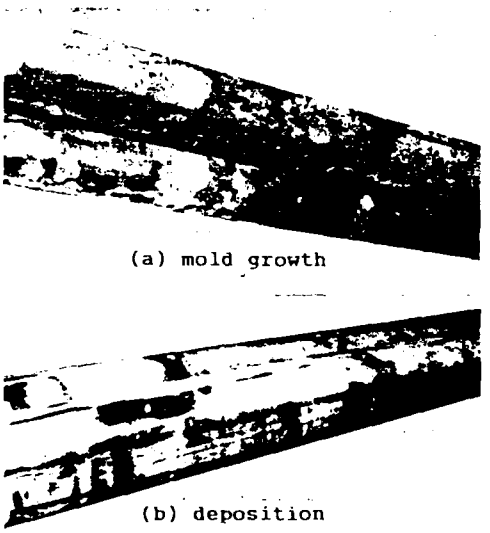
NTT has developed halogen-free flame-retardant telecommunication cables, and has been installing them in cable tunnels since August 1985. They now extend over 2,400 km.

The occasion for this development was a serious cable fire in front of a Tokyo telephone office in November 16, 1984. The fire damaged the whole subscriber loop of the telephone office, damaging more than 89,000 lines. Restoration of services required up to ten days. The social effects of this fire were so serious that NTT has changed the cable joint method from lead-tube to mechanical closures. Moreover, the halogen-free flame-retardant cables are now being installed in cable tunnels rather than non-flame-retardant cables as formerly.

REPORT AND ANALYSIS OF PHENOMENA

In early autumn of 1986, about one year after the first installation of halogen-free flame-retardant cable, reports appeared of a peculiar phenomenon, the turning white of cable sheath, occurring with halogen-free flame-retardant cable in deep cable tunnels in central Tokyo. After this report, careful inspection of the cable sheath was made in Tokyo and other big cities, Sapporo, Nagoya and Osaka, and surface samples were collected from the sheath.

Biological and chemical analyses were carried out to ascertain the mechanism of this phenomenon, and the temperature and humidity were measured continuously to gauge the conditions in the cable tunnel. As a result, we found that the humidity in the cable tunnel is very high, and discovered that two phenomena are actually involved: the growth of mold and the deposition of metal carbonate (Figure 1).



(a) mold growth

(b) deposition

Figure 1 Appearance of mold and deposition phenomena

CONDITION OF CABLE TUNNEL

Temperature and humidity in the cable tunnel were measured so that the phenomena could be reproduced in the laboratory (Figure 2). The temperature is almost constant, about 19°C, but the humidity is very high and shows an up-and-down curve. This change of humidity is caused by the air ventilation. The ventilation system is activated when a cable installation crew enters the tunnel or by timer operation, and the humidity is decreased. Sometimes water accumulates on the cable surface because of the condensation of water in the air, and sometimes this water is dried by the flow of air.

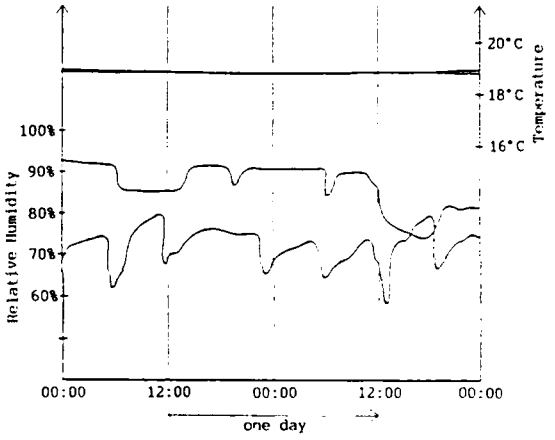


Figure 2 Temperature/Humidity in cable tunnel

MOLD GROWTH

Two analyses were conducted regarding mold. First, the kinds of mold were examined to determine the effects of the mold on cable sheath and on the human body. Second, research was undertaken to find the material in the sheath compound responsible for mold growth.

Separation and incubation tests showed the mold to be a kind of trichoderma, a common fungus normally found in soil. There are no reports about the harm to cable sheath or to human health (Figure 3).

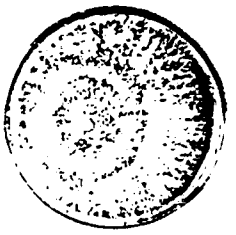


Figure 3 Mold incubation test

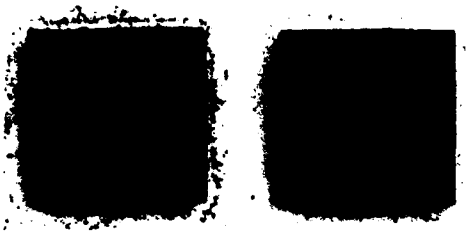
Incubation tests in the laboratory, using several sample sheets of halogen-free flame-retardant compound having different combinations of materials, showed that a certain extruding agent is closely related with the growth of mold on the surface of the sheet (Table 1; Figure 4). Next, two sample cable pieces, one containing a suspect extruding agent and the other containing no such agent, were installed in deep cable tunnels. Observations were taken after 13 days, 45 days and 280 days. Observation after 13 days showed light mold growth. After 45 days and 280 days mold growth was evident on the first sample cable piece, but none on the second piece (Figure 5).

These experiments indicate that it is possible to eliminate agents tending to grow mold by testing sample sheets in the laboratory, without the need to perform tests in cable tunnel.

Table 1 Incubation test using different combination of agents

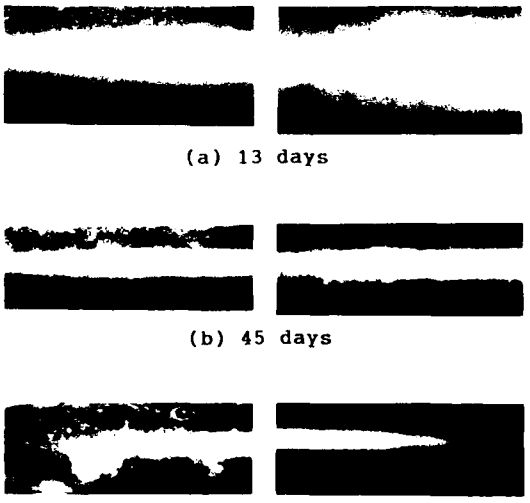
		Test 1			Test 2				
		Polyethylene	Compound A	Compound B	Comparing retardant		Comparing extruding agents		
					B	C	None	Add	Add more
Retardant	A			○					
	B		○		○		○		
	C		○			○	○		
Carbon		○	○	○	○	○	○	○	○
Antioxidant		○	○	○			○		
Extruding agent	A			○					
	B		○					○	◎
Result		+	− 2	+	+	+	+	− 3	− 3

(+:no growth ←→ −:growth)



(a) compound A (b) compound B

Figure 4 Mold growth in incubation test using different combination of agents



(a) 13 days

(b) 45 days

(c) 280 days

Figure 5 Mold growth observation in cable tunnel

DEPOSITION OF METAL CARBONATE

Deposition samples were analyzed by infrared spectrophotometry, X-ray diffraction and lumination analysis. These showed the samples to be a deposition of basic metal carbonate. Such deposition was found in high-humidity locations in cable tunnels. Thus temperature/humidity cycle tests of sample sheets under carbon dioxide conditions were conducted in an attempt to duplicate this deposition in the laboratory (Figure 6). After four test cycles, over a period of 24 hours, the sample sheets turned white (Figure 7). The deposition material was determined to be the same as that noted on cables in cable tunnels. This test shows that the deposition is a result of the reaction with carbonic acid gas and water in the air (Figure 8).

Several sample sheets were tested under high-humidity and carbon dioxide conditions to evaluate the deposition tendency. The amount of deposition was determined by measuring the mass of the sheets, since the deposition increase the mass of sheets by reaction. Importantly, some sheets had less deposition than others, depending on the selection of the base polymer and extruding agents (Figure 9). The difference was confirmed visually in the temperature/humidity cycle test (Figure 10).

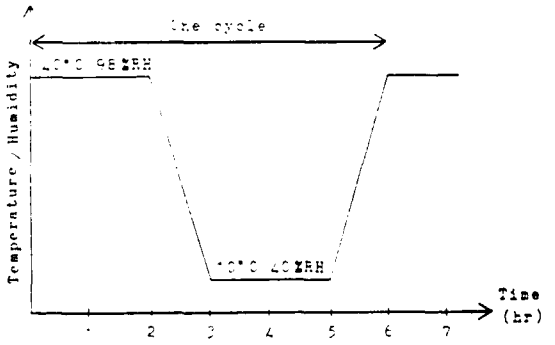


Figure 6 Temperature/Humidity cycle test



Figure 7 Reproduced deposition

$$H_2O + CO_2 \rightarrow H_2CO_3 \quad \cdots(1)$$

$$2 \cdot M(OH)_n + n \cdot H_2CO_3 \rightarrow M_2(CO_3)_n + 2n \cdot H_2O \quad \cdots(2)$$

Figure 8 Reaction with carbon dioxide and water

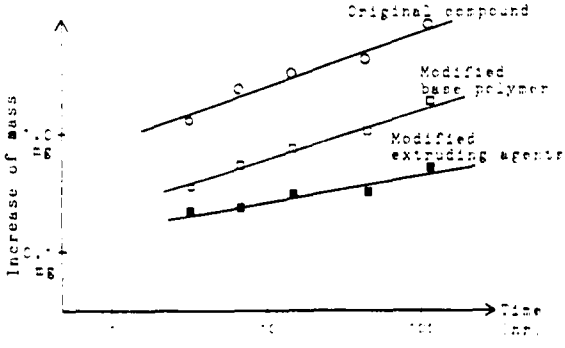


Figure 9 Deposition vs material combination selection



(a) original (b) improved

Figure 10 Difference in result based on material combination selection

FURTHER STUDY

The halogen-free flame-retardant sheath material is a recent development. We are therefore continuing with the following studies:

(1) estimation of long-term reliability,
(2) increasing mechanical strength and
(3) application to aerial cables.

CONCLUSION

Halogen-free flame-retardant compounds which have certain extruding agents are easily susceptible to mold growth under the high-humidity conditions found in cable tunnels. Laboratory tests confirmed that it is possible to eliminate these agents by testing sample sheets.

In addition, metal hydroxide in halogen-free compounds can cause the deposition of basic metal carbonate as a result of the reaction with carbon dioxide and water in the air. This deposition appears as a bright white deposit on the black cable sheath. This deposition can be suppressed by careful selection of the base polymer and extruding agents.

ACKNOWLEDGEMENTS

The authors wish to thank Seiji Takashima, general maneger of our project, Mr. Hiroshi Oshima and his staffs in the Technical Assistance & Support Center in the NTT Telecommunications Service Supprt Headquarters. In addition, we greatly appreciate the assistance of Furukawa Electric Co, Ltd., Sumitomo Electric Industries, Ltd. and Fujikura Ltd. in preparation of this paper.



Kazuhiko Tanaka

NTT Network Systems
Development Center

2-1 Uchisaiwai-cho 1-Chome
Chiyoda-ku, Tokyo 100 Japan

Kazuhiko Tanaka received his M.S degree in information science from Kyoto University in 1983. He joined NTT in 1983 and has been engaged in development of metallic conductor communication cable and indoor wiring systems. He is an engineer in the Telecommunication Cable Systems & Outside Plant Project in the NTT Network Systems Development Center. He is a member of the Institute of Electronics, Information and Communication Engineers of Japan.

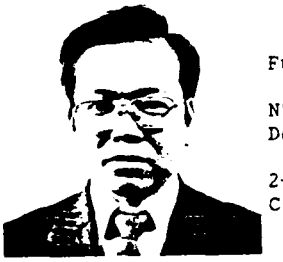


Fuminori Kozono

NTT Tokyo-Minato
District Headquarters

12-3 Sibuya 2-Chome
Sibuya-ku, Tokyo 150 Japan

Fuminori Kozono received his B.S degree in electrical engineering from Kyushu University in 1975. He joined NTT in 1975. After gaining experience in outside plant management in the Tochigi telecommunications division, he had been engaged in development of metallic conductor cable in the NTT Engineering Department. He is an assistant manager in the NTT Tokyo-Minato district headquarters. He is a member of the Institute of Electronics, Information and Communication Engineers of Japan.



Fumio Takaesu

NTT Network Systems
Development Center

2-1 Uchisaiwai-cho 1-Chome
Chiyoda-ku, Tokyo 100 Japan

Fumio Takaesu received his B.S degree in communication engineering from Kyushu Univ. in 1973. He joined NTT in 1973. After gaining experience in outside plant management in the Kyoto urban telecommunications division and Kyushu telecommunications bureau, he has been engaged in development of metallic conductor cable and optical fiber cable systems. He is an exective engineer in the Fiber Optics Network Systems Project Group in the NTT Network Systems Development Center. He is a member of the Institute of Electronics, Information and Communication Engineers of Japan.

TEMPERATURE RATING OF NICKEL PLATED COPPER AS A FUNCTION OF PLATE THICKNESS

Thomas Eng
Tsutomu Inagaki

Hudson Wire Company
62 Water Street, Ossining NY 10562

ABSTRACT

Elevated temperature (400-600°C) life-time performance data of nickel plated copper conductors were obtained under the conditions of (1) continuous elevated temperature (Thermal Aging) and (2) cycled heating and cooling, current load and vibration (HCV). Under Thermal Aging conditions, conductor life as a function of temperature was inversely proportional to plating thickness up to a transition range of 500-600 °C, and at higher temperatures became directly proportional. This behavior is believed to be the combined effects of diffusion and oxidation each being predominant at different temperatures. Under HCV conditions, conductor life as a function of temperature was directly proportional to plating thickness.

1.0 INTRODUCTION

Historically, nickel plated copper conductors, due to their inherent physical stability, have been widely used in elevated temperature applications. Despite such long term industrial usage, relatively little data has been accumulated relating nickel plate thickness to conductor performance at elevated temperatures. This lack of information has led the end user, in many instances to specify a 27% by weight nickel coating on copper conductors for utilization at temperatures above 260 °C. As a result, they may be sacrificing substantial cost savings as well as other properties such as conductivity in applications where the use of a conductor with a lower nickel coating thickness could have satisfied their performance criteria. Further, the difficulty in producing a clad or electroplated 27% nickel coated copper has traditionally led to procurement problems.

The purpose of this investigation is to generate data which can relate elevated temperature performance to nickel plate thickness on copper conductors. The benefits of the investigation are threefold:

1. The generation of quantitative elevated temperature performance data for nickel coated copper conductors from which the end user can base product design;

2. Substantial cost saving to the end user if lower coating thicknesses can be shown to satisfy design requirements; and

3. The potential for greater availability of nickel coated conductors for high temperature applications.

2.0 EXPERIMENTAL PROCEDURE

2.1 Material

Conductors of 22 AWG (19/34) CDA 107 with nickel plates of 6%, 11%, 15%, 20%, and 24% by weight (2.54, 4.44, 6.35, 8.25, and 10.16 um thicknesses, respectively) were used for all testing in this investigation. Silver bearing copper CDA 107 was chosen for its thermal stability. Prior tests involving oxygen free copper CDA 102 have revealed adverse thermal effects due to annealing above 250 °C [1]. All conductors were insulated with a ceramic braid rated at 1000°C.

2.2 Experimental Procedure

Samples of each nickel plating thickness were monitored for resistivity changes at elevated temperatures under test conditions of (1) continuous elevated temperature exposure (Thermal Aging) and (2) simultaneously imposed ambient heating, current load and vibrational stress in a repeated on/off cycle (HCV Simulation).

The comparison between the conductors' performance in these test conditions were used as an indication of the additional effects of applied stress and current loading in conjunction with elevated temperatures on the conductors' life span.

2.2.1. Thermal Aging

In the Thermal Aging test, the samples were exposed to a continuous temperature of 475 °C, 575 °C, and 650 °C through ambient heating. A minimal current of 0.2 amps was continuously applied to obtain voltage drop readings on the samples without current heating.

The experimental set up consisted of a furnace, DC power supply, and sample support (Fig. 1a). Three 15" long specimens of each plate thickness were placed in the tube furnace in a series circuit. The terminals of each wire and the ring tongue crimp contacts were outside the furnace. Thus only the insulated conductor was exposed to the Thermal Aging test. The voltage drop of each specimen was continuously recorded on a 30 channel hybrid data logger.

Tests were run until the samples exhibited a 100% increase in voltage drop at which point the specimen was considered to have failed.

2.2.2. HCV Simulation

In HCV Simulation, the nickel plated samples were tested under conditions of elevated temperature, current load, and mechanical vibrational stress. These factors were simultaneously imposed and continuously cycled on a repeated ten hour "on" period followed by a two hour "off" period. Test temperatures of 400 °C, 525 °C and 650 °C were employed in the investigation. The temperatures were a result of ambient heating and Joule heating due to a direct current load of 4.5 amps. A 55 Hz vibration was applied to the sample support to supply the vibrational stress.

Specimens (8" long) with pure nickel crimp-type ring tongue terminals (rated at 650 °C) attached at each end were mounted on a stainless steel tube specimen chamber. The external end supports of the tube were mounted on grommet-type vibration isolators and the specimen area was placed inside a tube furnace (Fig. 1b). The entire connector assembly (wires and crimp contacts) was exposed to HCV Simulation conditions. To facilitate cooling, air was circulated inside the steel tube during the "off" cycle. An electromagnetic vibrator was mounted to the specimen support to provide the mechanical stress.

Three specimens of each sample type were employed. They were connected in series and energized with a constant current. The voltage drop was measured across each specimen and continuously recorded on a 30 channel hybrid data logger. The conductor test temperature was monitored utilizing a 0.005" diameter, glass braid insulated, chromel-alumel thermocouple bonded to the surface of the conductor with an electrically insulating thermally conductive epoxy.

The voltage drop across each sample was continuously recorded until a mechanical failure or a 100% increase in voltage drop (100% increase in resistance) was observed.

2.3 Sample Analysis

Wire samples were stripped of their insulation, then mounted and polished using standard metallographic techniques for evaluation of transverse cross sections.

Samples were also macroscopically observed to note the general condition of the specimens after conditioning.

3.0 EXPERIMENTAL RESULTS

All experimental data were statistically analyzed using linear and non-linear regression techniques.

Arrhenius expected life equations as a function of time and temperature were developed for each plate thickness. These equations were used to extrapolate expected life up to 50,000 hours. This data was then used to determine the temperature rating of the conductors as a function of plate thickness based on the end of life criteria of mechanical failure or an increase in voltage drop of 100%.

3.1 Thermal Aging

The percentage voltage drop increase of the samples with respect to time for each plate thickness at the three test temperatures (475 °C, 575 °C and 650 °C) are shown in Figures 2a-c. The points graphed are averages of the values extracted from the raw data for the three samples. Samples aged at 475 °C did not fail after 4800 hours and therefore were extrapolated using best-fit regression analysis. Table 1a summarizes the times to failure at each test temperature.

The values in Table 1a were used to extrapolate the expected life for each of the plating thicknesses. Regression analysis suggested an Arrhenius type behavior, with correlation coefficients of 0.986 to 0.998 as shown in Figure 3a.

Data from the Arrhenius expected life curves were also used to develop the extrapolated temperature rating curves up to 50,000 hours shown in Figure 4a.

The results of the Thermal Aging experiment indicate three types of behavior depending on the temperature range. At low temperatures, time to failure is inversely proportional to plate thickness, at higher temperatures the relationship is directly proportional, and at intermediate temperatures the relationship depends upon the plating thickness.

Microscopic examination of thermally aged samples at 475 °C as seen in Figures 5a and 5b revealed diffusion layers at the copper-nickel interface.

Oxide layers were also observed on all conductors tested at 575 °C and 650 °C. Samples with lower nickel coating thicknesses, showed relatively thicker oxide layers as shown in Figures 6a thru 6d.

3.2 HCV Simulation

The percentage voltage drop increase with respect to time for each of the plate thicknesses at the three test temperatures (400 °C, 525 °C and 650 °C) are shown in Figures 2d-f. The points graphed are the averages of the values from the three samples. In HCV Simulation, exposure to high temperatures caused mechanical failures to occur with more instances at lower plate thicknesses. At the 400 °C temperature, the highest plate (10.16um) samples did not fail. These results were extrapolated to end of life using regression analysis.

The test data appears to initially follow a logarithmic behavior which then changes to exponential with increased time. Table 1b contains the times to failure at each test temperature.

Assuming an Arrhenius expected life behavior, the extrapolations of expected life are graphed in Figure 3b with correlation coefficients of 0.887 to 0.997. Figure 4b indicates the extrapolated temperature rating of the conductors up to 50,000 hours as a function of plate thickness and temperature.

The results have a common trend that times to failure are directly proportional to plate thickness at any temperature.

Visual examination of the conductors revealed that higher nickel plating yielded relatively less oxidation at each test temperature. On the surface of the samples having 8.25 and 10.16 um plating thicknesses, yellow-red regions were observed. Thick oxide layers were observed on all conductor surfaces tested at 650 °C.

Metallographical examination of the copper conductors with 2.54 um plating thickness tested at 400 °C and 525 °C revealed a diffusion layer with no free nickel as shown in Figures 7a and 7b. The conductors with 10.16 um nickel plating thickness, exposed at the same temperatures, revealed an intermediate diffusion layer with free nickel as shown in Figures 7c and 7d.

3.3 Comparative Test Results

Examination of the data reveals that all the samples subjected to HCV Simulation failed sooner than samples subjected only to Thermal Aging. The rate at which the voltage drop changed in the samples Thermally Aged decreased in the later stages of life. This is radically different for the HCV samples which exhibited a rapid rise in the rate of voltage drop increase just prior to sample failure.

4.0 DISCUSSION

Figures 2a thru 2f indicates that an increase in test temperature results in a decrease of the time to failure at all nickel plating thickness for both the Thermal Aging and HCV Simulation tests. Voltage drop increases under these experimental conditions can be attributed to diffusion or alloying of the nickel coating with the copper base metal as well as oxidation of the nickel coating.

As seen in Figures 4 and 6, all samples exhibit a diffusion layer after exposure to elevated temperatures. The thickness of the diffusion layer was directly proportional to the test temperature and thickness of the nickel plating.

Oxidation is also a contributing factor with more intense oxidation causing a higher resistivity increase and lower time to failure. Oxidation was observed to be more intense with less nickel plating thickness and at higher temperatures.

4.1 Thermal Aging

Figures 2a thru 2c show the results of the percent voltage drop increase with respect to time for each of the plating thicknesses. At the 475 °C test temperature, the lowest nickel plating thickness samples exhibited the longest time to failure. At the 650 °C temperature, the highest nickel plated samples had the longest time to failure. At the 575 °C temperature, the longest time to failure was exhibited by the samples with intermediate nickel platings. Both the lowest

(2.54um) and highest (10.16um) nickel plated samples had shorter times to failure at this temperature.

The expected life and temperature rating curves in Figures 3a and 4a illustrate that expected life of nickel plated conductors is very dependent upon plate thickness and temperature. This is shown by the intersection of the curves in Figure 3a, and the change in slope of the curves in Figure 4a, which shows the reversal from the direct relationship of plate thickness and expected life at high temperatures to an inverse relationship at lower temperatures.

These results lead to the hypothesis that there are two mechanisms affecting the nickel plated samples at elevated temperatures. One failure mode operates predominantly at the lower temperatures, and the second mode becomes predominant at higher temperatures. At intermediate temperatures, both mechanisms operate simultaneously with neither being very predominant over the other.

Observing the photomicrographs in Figures 5 and 6 which are from the samples Thermally Aged at 475 °C and 650 °C respectively, and from the visual observations, the samples tested at 650 °C exhibit large amounts of oxide on the surface of the conductor. The samples aged at 475 °C have much less oxide on the surface. It can be concluded that oxidation is predominant at 650 °C and has less of an effect at 475 °C. Diffusion occurs at both temperatures and is much more rapid at higher temperatures. Since there is less oxidation at 475 °C and the samples with more nickel plating failed sooner, diffusion is probably more predominant at this temperature and is the main cause of failure.

These hypotheses could explain the reaction and the results. At high temperatures, nickel oxidation is the overriding mechanism to failure. When oxidation occurs, the degradation rate is much higher than the diffusion related failure mechanism. Therefore times to failure are directly related to plating thickness due to nickel's resistance to oxidation. At low temperatures, when the nickel oxidation rate is very low, diffusion is the predominant failure mechanism. The diffusion rate is dependent upon the concentration gradient of the two constituents which is dependent on the availability of the constituents (i.e. when the nickel plating is completely diffused into the copper, the reaction approaches equilibrium and the diffusion rate decreases). The maximum effect of diffusion causing the resistivity increase is limited by the maximum concentration of the plating on the conductor. The oxidation rate of the nickel-copper surface eventually becomes the only mechanism of degradation. Higher plating percentages would therefore be degraded more rapidly by diffusion than the lower percentages assuming the oxidation rate of the surface is not significant at low temperatures.

These hypotheses could also explain the behavior observed at the 575 °C temperature. At this higher temperature, oxidation rates increase as well as diffusion rates. A possible explanation for the results showing shorter times to failure in the thinner (2.54um) and thicker (10.16) platings with the longest times by the intermediate plating could be the result of another mechanism in effect. The oxidation of the nickel depleted surface could now be affecting the thinner plated conductors.

The nickel oxidation rate is still not predominant over the diffusion rate, therefore for the higher platings, time to failure is inversely proportional to plating thickness. However, at the lower plate thicknesses, the nickel depleted surface may become subject to oxidation at a failure rate greater than the nickel-copper diffusion reaction. Lower plate thickness samples now fail sooner due to consumption of nickel from the surface and time to failure becomes directly proportional to plate thickness (similar to the reactions observed at 650 °C).

There appears to be a transition temperature in the 500 °C and 600 °C range in which the three possible failure mechanisms become predominant. Nickel-copper diffusion is probably predominant below this range and nickel oxidation becomes predominant above this range. A combination of diffusion, nickel-copper oxidation and nickel oxidation seems to control the reaction within the range.

4.2 HCV Simulation

Figures 2d thru 2e show the results of the percent voltage drop increase with respect to time for each of the plating thicknesses. The results indicate that time to failure was a direct function of the plating thickness. The curves follow a logarithmic behavior then in later life the trend appears exponential.

The direct relationship of life to plating thickness correlates to the behavior observed in Thermal Aging at 650 °C which is predominantly an oxidation mechanism of failure. But the direct relationship exists for all the test temperatures. Visual examination revealed that similar conductors tested at 525 °C in HCV had less oxidation than the con-

ductors Thermally Aged at a lower temperature (475 °C). The HCV samples failed at an earlier time, allowing less time for oxidation to occur, which means that another failure mechanism is in effect. This behavior may suggest that not only the conductor, but the entire connector assembly including the crimp terminations, also exposed to HCV conditions, must be considered. Weddle Marchese and Inagaki [2] also observed the importance of ring tongue crimp connections under similar experimental conditions. As oxidation proceeds with a vibrational stress, the brittle oxide layer breaks, forming voids which separate the conductor strands from the terminal barrels. Such voids expose unoxidized material causing the conductor to be more susceptible to further oxidation. Therefore, crimping defects due to oxidation appear to have significantly increased the contact resistance resulting in premature failure. The net effect is accelerated oxidation and conceivably results in the observed exponential failure rate.

The expected life and temperature rating curves in Figures 3b and 4b illustrate that expected life is dependent upon plate thickness and temperature. This is shown by the intersection of the expected life curves in Figure 3b. The resultant curve also suggests that the direct relationship of plate thickness and time to failure will also become inversely related, but at lower temperatures (approx. 300 °C) than was tested in this investigation. The extrapolated temperature rating curves (Figure 4b) indicate this by the change in slopes of the different life curves.

4.3 Comparative Test Performance

The results indicated in all cases that times to failure of samples subjected to HCV were always shorter than those subjected to Thermal Aging at "similar" temperatures. This is probably attributable to the additional effects of the supplementary applied current load and vibrational stress. The applied stress contributes to the increase of the conductors' resistivity by creating new defects, even if the temperature is high enough to constantly anneal the material. Current heating at 4.5 amps can also increase the temperature in localized higher resistance areas where small defects exist or form by the applied stress, accelerating the reaction. In addition to this and more importantly, the entire conductor assembly was exposed to HCV Simulation conditions. The vibrational stress caused defects in the crimps resulting in an increase in contact resistance.

These two investigations basically result in similar conclusions that the mechanism to thermal failures is the same for Thermal Aging alone as well as with mechanical stress. Mechanical stress will greatly accelerate failure, but the mechanism for both conditions is mass diffusion and oxidation controlled. The dependency is not only on temperature but it is equally as important to consider the plate thickness of the conductor when extended life times are required.

5.0 CONCLUSIONS

1. Under Thermal Aging conditions conductor life changed from an inverse relationship with plate thickness at lower temperatures to a direct relationship at higher temperatures. This behavior may be due to diffusion as the predominant failure mechanism at low temperatures and oxidation at higher temperatures.

2. Under HCV conditions conductor life was directly proportional to plate thickness. This behavior appears to be the result of oxidation as the controlling mechanism at the wire and crimp contact interface.

3. Conductor life under HCV conditions were consistently less than under Thermal Aging conditions over similar temperature ranges. This behavior appears to be a function of the accelerating affects of current loadiing and vibrational stress.

4. The extended life extrapolations indicate that the mechanism to failure under Thermal Aging and HCV conditions are similar. Due to the acceleration of failure by the mechanical stress, the transition from a diffusion controlled failure to an oxidation controlled failure in HCV occurs at a temperature lower than tested in this investigation.

References

1. T. Inagaki, "Effect of Thermal Aging on the Flexibility and Conductivity of Plated and Unplated Copper Conductors", 28th IWCS, Nov. 1979

2. L. Weddle Marchese, T. Inagaki, "An Evaluation of the Effects of Simulated Operating Conditions on Tin-, Silver-, and Nickel-Plated and Unplated Copper Conductors for Aerospace Applications", 3rd Conf. Proc SAE AE-8 Aerospace Electrical Interconnect System Conf., Sept. 1985

3. Handbook of Chemistry and Physics, 62nd Edition, CRC Press, 1981-82, F-57

4. R. E. Reed Hill, Physical Metallurgy Principles, New York, NY, D.Van Nostrand Co., 1973.

5. D. B. Butrymowick, J. R. Manning, M. E. Read, "Diffusion in Copper and Copper Alloys . Part IV. Diffusion in Systems Involving Elements of Group VIII" J. Phys. Chem. Ref. Data 5 1, 103-200 (1976).

6. H. H.Uhlig, Corrosion and Corrosion Control, J. Wiley and Sons, New York 1967

7. Copper. The Science and Technology of the Metal, Its Alloys and Compounds, ed.by A. Butts, Reinhold Publ. Corp., New York 1954

ACKNOWLEDGEMENTS

The authors would like to thank Joana Groza, Lisa N. Weddle Marchese and Joel Meyers for their extensive time and effort put forth to conduct this investigation.

BIOGRAPHY

Mr. THOMAS ENG is the Manager of Product Development and Technical Services for the Hudson Wire Company. Since joining the company in 1986 he has been actively involved in research and development of new and existing conductor systems. He was previously employed as a Senior Engineer by Westinghouse Electric Company, Bettis Atomic Power Laboratory. Mr. Eng holds both B.S. and M.S. degrees in Metallurgical Engineering from the Polytechnic Institute of Brooklyn, is a member of ASM and is an active participant in the SAE-AE8D technical committee.

Mr. TSUTOMU INAGAKI is Vice President of Planning and Development for the Hudson Wire Company and President of Camden Hudson Conductors Inc. Since 1977 he has been involved in development of new conductor systems and holds patents in high strength alloy wire products. He has also published several technical reports on conductor testing and design. Mr. Inagaki holds both B.S. and M.S. degrees in Metallurgical Engineering from the Polytechnic Institute of Brooklyn, is a member of AAAS, AES, ASM and Sigma XI and is an active participant of SAE-AE8D, NEMA and ASTM B-1 technical committees.

TABLE 1A

TIMES TO FAILURE (hours) - THERMAL AGING

PLATING THICKNESS	TEMPERATURE (°C) 475	575	650
2.54 um	26,038	1,168	390
4.44 um	19,167	1,800	541
6.35 um	13,067	1,808	632
8.25 um	12,180	1,489	846
10.16 um	9,992	1,350	862

TABLE 1B

TIMES TO FAILURE (hours) - HCV

PLATING THICKNESS	TEMPERATURE (°C) 400	525	650
2.54 um	2056	495	127
4.44 um	2334	1676	353
6.35 um	2690	2049	440
8.25 um	2869	2312	640
10.16 um	3753	2530	829

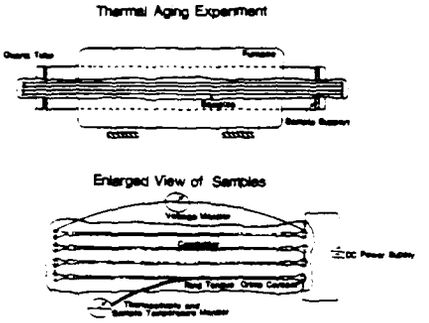


Figure 1

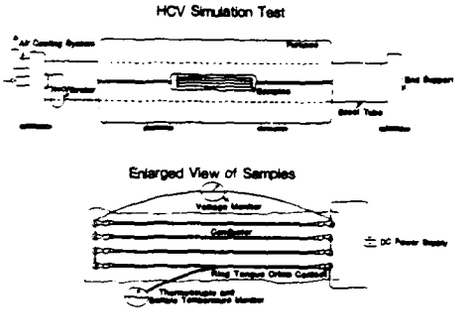


Figure 2

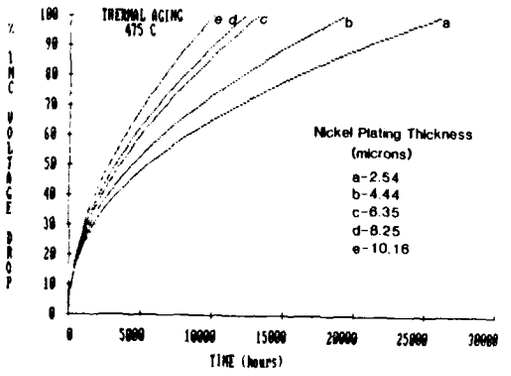


Figure 3

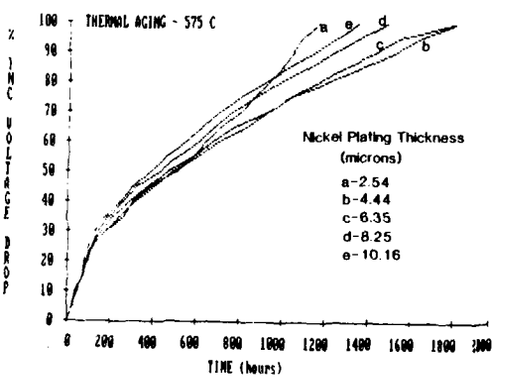


Figure 4

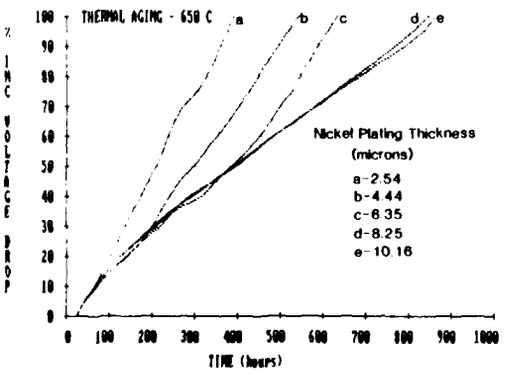


Figure 5

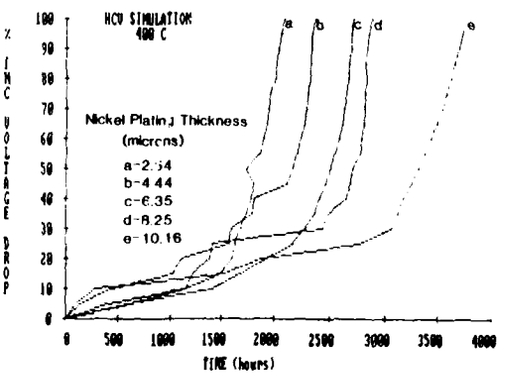


Figure 6

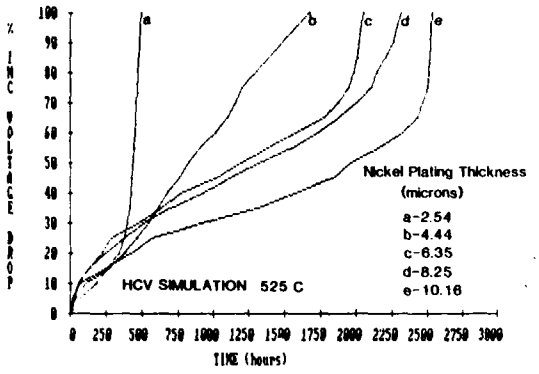


Figure 2c

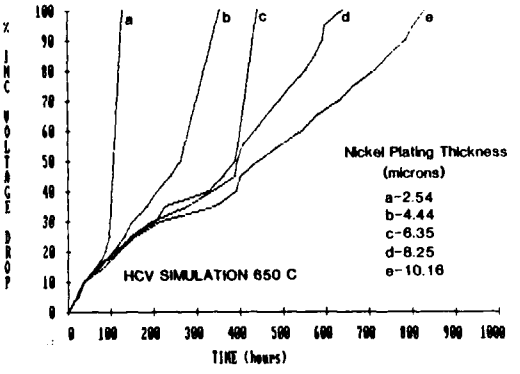


Figure 2f

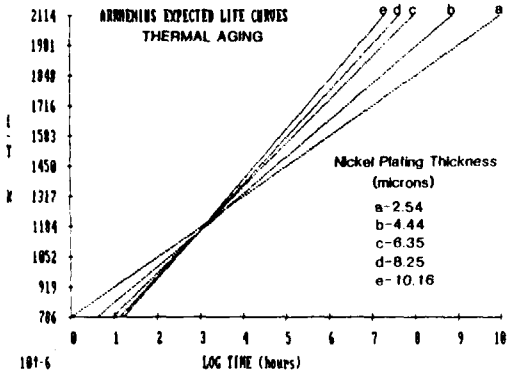


Figure 3a

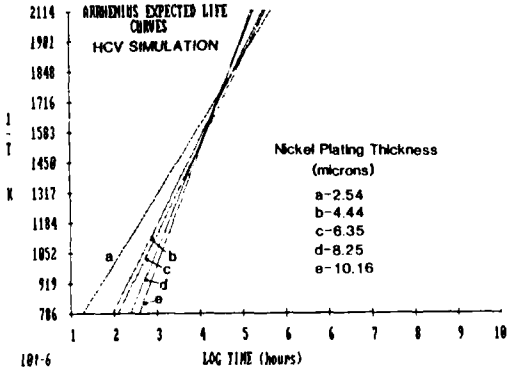


Figure 3b

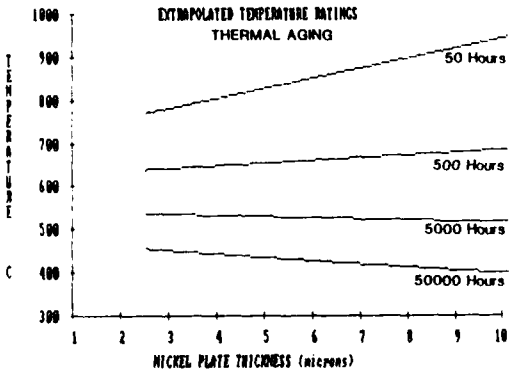


Figure 4a

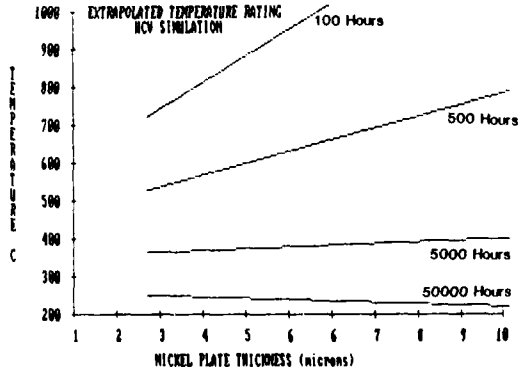


Figure 4b

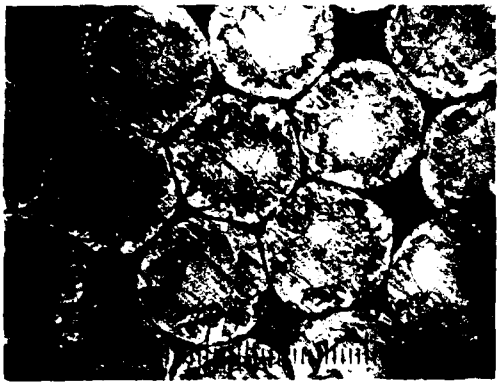


Figure 5a. 6% Nickel plated conductor Thermally Aged at 475 C. Magnification 150X (2.54 micron Nickel plate thickness)

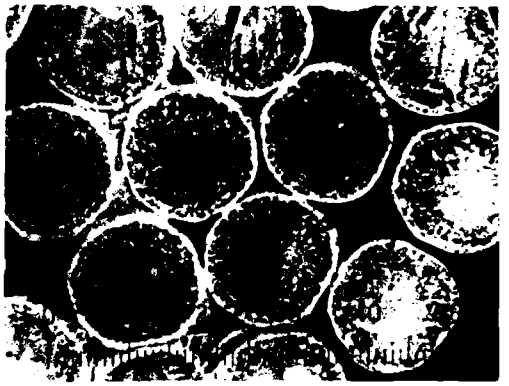


Figure 5b. 24% Nickel plated conductor Thermally Aged at 475 C. Magnification 150X (10.16 micron Nickel plate thickness)



Figure 6a. 6% Nickel plated conductor Thermally Aged at 650 C. Magnification 75X (2.54 micron Nickel plate thickness)

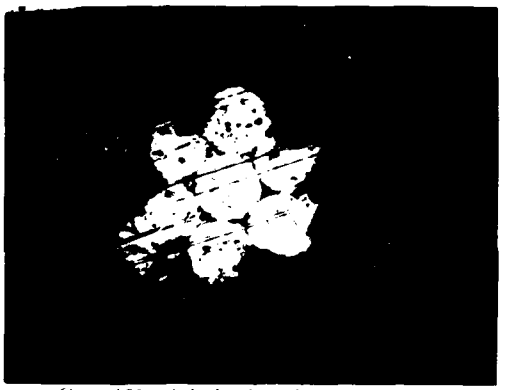


Figure 6b. 15% Nickel plated conductor Thermally Aged at 650 C. Magnification 75X (6.35 micron Nickel plate thickness)

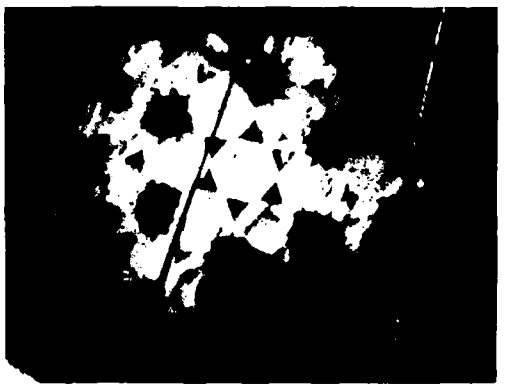


Figure 6c. 20% Nickel plated conductor Thermally Aged at 650 C. Magnification 75X (8.25 micron Nickel plate thickness)

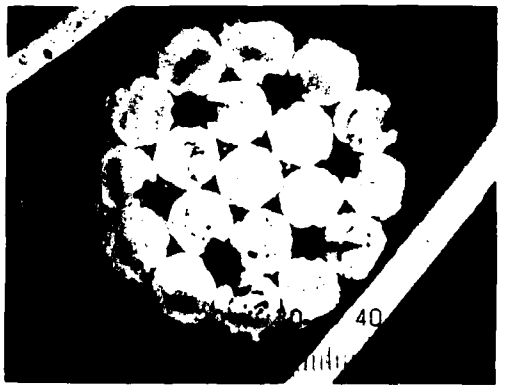
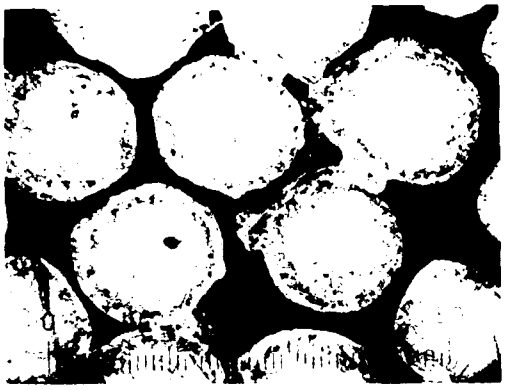
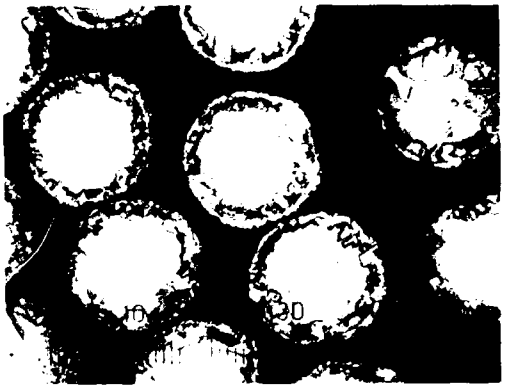
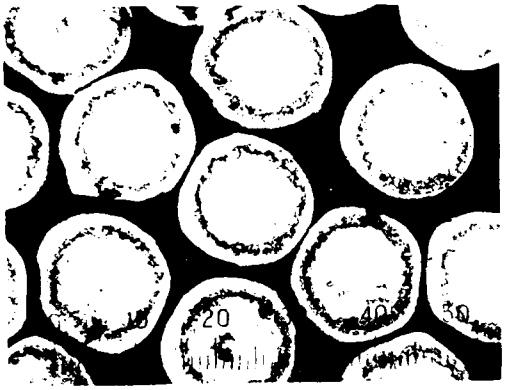
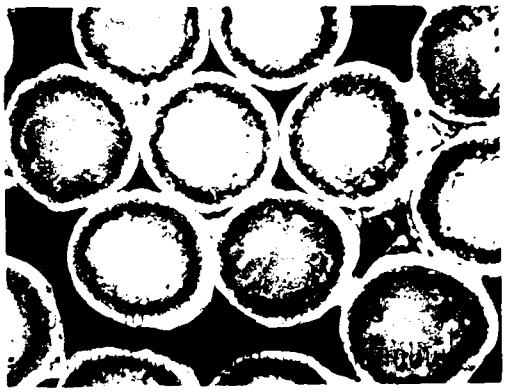


Figure 6d. 24% Nickel plated conductor Thermally Aged at 650 C. Magnification 75X (10.16 micron Nickel plate thickness)









CABLING DEPENDENCE OF OPTICAL FIBER CUTOFF WAVELENGTHS

J. P. Kilmer, W. T. Anderson, R. M. Kanen, and C. M. Connor Davenport†

Bell Communications Research
435 South Street, Morristown, NJ 07960-1961

1. *Abstract*

From a user's perspective, the specification of a cabled fiber's cutoff wavelength, λ_{cc}, measured from a cabled fiber sample whose deployment conditions simulate worst-case field conditions, provides a more functional value for cutoff wavelength than the uncabled fiber cutoff wavelength, λ_{cf}, of a fiber sample deployed in a fashion which is never found in the field. Samples of a variety of fiber designs in different cable constructions were measured to determine the relationship, or mapping function, between λ_{cc} and λ_{cf}. It was found a simple two coefficient linear mapping function can be used to confidently predict λ_{cc}'s from measured λ_{cf}'s. However, the coefficients of the linear mapping function differ for different fiber types in different cable designs. Cabled fiber cutoff wavelengths provide a more fundamental basis for optical cable cutoff wavelength specifications since a maximum cabled fiber cutoff wavelength specification directly reflects the user's requirements.

2. *Introduction*

In the short distance intra-LATA trunk and loop networks, the future use of multiple high bit-rate WDM systems around 1300 nm may make the neglected 1250 to 1300 nm region more attractive than the 1550 nm region where there is greater chromatic dispersion. The primary limitation on the lower edge of the 1300 nm window is cutoff wavelength to prevent single-mode system operation in the fiber's multimode region. The highest cutoff wavelengths are found on the shortest sections of cabled fiber deployed in the system. To address this concern, a second definition for an optical fiber's cutoff wavelength, the cabled fiber cutoff wavelength was adopted by the Electronic Industries Association (EIA) in 1984. The second definition gives a value for cutoff wavelength closer to what a user may expect in installed cables. In addition, cabled fiber cutoff wavelength measurements give a value for cutoff wavelength which can be directly used in system design to help ensure a single-mode optical link is free from the problems associated with operation in the fiber's multimode region [1-3]. Some fiber manufacturers have raised cutoff wavelengths to reduce bend sensitivity and allow more predictable performance in the 1550 nm wavelength range. This results in a reduction in usable 1300 nm window width in return for improved 1550 nm performance. In the short distance intra-LATA trunk and loop networks, where deployment of conventional dispersion unshifted single-mode fiber prevails, the 1550 nm window with its lower attenuation may not be as important as a broad window at 1300 nm.

Cutoff wavelength exhibits a length, bend, and consequent cabling dependence which makes it very difficult to specify generically. Until standards groups adopted this second definition of cutoff wavelength, the only standard method for cutoff wavelength measurement was EIA FOTP 80 [4] which is consistent with the method prescribed in CCITT Recommendation G.652. In FOTP 80, the cutoff wavelength of an uncabled fiber, λ_{cf}, is measured on a 2 meter fiber sample with a single 28 cm diameter loop (see Figure 1) to improve reproducibility. Since fiber is never deployed in this fashion in the field, this procedure gives a value for cutoff wavelength which is not directly applicable to the user. Consequently, users must interpret these λ_{cf} values and map them into functional cutoff wavelength values which are more likely to be found in field applications. A more direct method for measuring functional cutoff wavelength values is described in EIA FOTP 170 [5]. In FOTP 170, a cabled fiber's cutoff wavelength, λ_{cc}, is measured on a cabled fiber sample whose deployment conditions are specified by the user or manufacturer in a detailed specification. By using FOTP 170, the user can develop a more generic cutoff wavelength specification. However, routine testing of λ_{cc} is generally impractical for fiber suppliers. Consequently, as an alternative, a supplier may establish a mapping function which translates a λ_{cc} specification into an internal cutoff wavelength specification for use in process control. Establishment of mapping functions by suppliers for each fiber and cable combination, with periodic reverification of the mapping, will ensure a single-mode fiber optic system is free from the problems associated with operation in the fiber's multimode regime. These mapping functions for various fiber and cable designs were investigated and are reported.

3. *Experimental Details*

Seven 25 meter samples of optical cable were obtained. The mix of fiber types and cable constructions is listed in the following table.

Fiber Type and Cable Construction			
Cable	Fiber		Cable Construction
	Type	Process	
A	DCF	IVD	Mylar wrapped 12 fiber array
B	DCF	IVD	Loose tube -- continuous helix
C	MCF	OVD	Loose tube -- continuous helix
D	DCF	IVD	Loose tube -- continuous helix
E	MCF	OVD	Loose tube -- reversing helix
F	MCF	IVD	Slotted core
G	DCF	IVD	Slotted core
H	MCF	VAD	Loose tube -- continuous helix
I	MCF	OVD	Loose tube -- reversing helix
J	EMCF	OVD	Loose tube -- reversing helix

DCF and MCF refer to depressed and matched cladding fiber types respectively, while IVD and OVD refer to inside outside vapor deposition processes. VAD refers to vapor axial deposition process. EMCF refers to (as described by the supplier) an "enhanced" matched clad fiber which has larger specified cutoff wavelength than the MCF fiber. The three common outside plant cable constructions: ribbon, loose tube, and slotted core, are represented. From each 25 meter cable section, a two meter cable section was cut and the fibers were removed for λ_{cf} measurements. Each fiber sample was measured under strict adherence to FOTP 80 (Method B). In FOTP 80, either

† A Bell Communications Research fellowship summer employee

a single-mode fiber with a single loop of small radius (Method A) or a multimode fiber (Method B) may be used as a reference. Careful record of fiber color and buffer tube or slot location was kept such that a direct comparison could be made between λ_{cf} and λ_{cc} on a fiber by fiber basis.

For the cabled fiber cutoff wavelength measurements, the cable sample's sheaths were cut to a 20 meter (65.6 ft.) length with one meter of exposed fiber at each cable end. One 76 mm (3 in.) loop was inserted in each end of the one meter of exposed fiber to simulate a splice organizer as shown in Figure 2. Since the highest cable cutoff wavelengths will be found on the shortest cable sections, λ_{cc} should be measured on the shortest cable lengths likely to be deployed in the field, typically repair sections or stubs. A twenty meter repair length is considered a worst-case minimum repair length for a short patch restoration.

In a field environment, fiber splices are always placed in splice organizer trays housed in splice cases or fiber distribution frames. These trays provide space to coil slack fiber typically into 3 in. loops. Each fiber deployed in the field will typically have one or more 3 in. loops at each end of the short cable section. Matched cladding fibers exhibit the strongest cutoff wavelength bend dependence [6]. The effect of multiple 3 in. loops on λ_{cf} for a matched cladding fiber is shown in Figure 3. As can be discerned from the figure, the first loop dominates the reduction of cutoff wavelength.

For cable samples greater than 10 meters, the bend reference technique cannot be used for measuring cutoff wavelength. For long cable sections the cutoff wavelength is often shorter than the wavelength region where the small diameter loop acts as an effective mode filter [7]. Consequently, in FOTP 170, only the multimode reference method can be used. Typical data from the λ_{cf} and λ_{cc} measurements are shown in Figures 4 and 5.

4. *Results*

For each cable the histograms of the distributions of measured λ_{cf}'s, λ_{cc}'s, and fiber by fiber differences between λ_{cf} and λ_{cc} were plotted. A typical group of histograms for one manufacturer's cable is shown in Figure 6. N is the number of measured fibers in each cable. Pertinent data from these distributions is tabulated below.

Fiber and Cable Cutoff Wavelength Comparisons (in nm)

Cable	N	FOTP 80		FOTP 170		Differences			
		mean	sigma	mean	sigma	mean	sigma	min	max
A	16	1269	33	1193	36	76	15	43	96
B	15	1256	48	1182	43	74	9	57	91
C	23	1206	24	1109	19	96	10	80	114
D	18	1205	31	1102	27	103	17	67	134
E	14	1194	35	1085	33	109	9	97	128
F	19	1195	43	1129	45	66	20	39	132
G	18	1190	39	1121	40	69	12	48	98
H	18	1262	87	1165	67	97	30	50	159
I	14	1214	21	1087	19	127	5	119	138
J	6	1230	15	1124	11	106	7	97	116

The wide distribution of λ_{cf}'s is indicative of the manufacturer's process control. The narrow distribution of the differences is indicative of how well λ_{cf} and λ_{cc} track on a fiber by fiber basis. While the actual cutoff wavelengths show large variations, the differences show small variations such that the mean difference constitute the bias between FOTP 80 and FOTP 170 for a specific cable product. Consequently, the mapping functions are simply systematic negative biases with magnitudes that vary according to cable design and fiber type.

There is considerable variability among the mean differences between λ_{cf} and λ_{cc} which range from 66 to 109 nm. The three loose tube design cables (excluding Cable B) closely group around an average reduction of 103 nm while the other four cables closely group around an average reduction of 71 nm. This is curious as both groups contain both DCF and MCF fibers. Evidently, a consistent single-valued mapping of FOTP 80 into FOTP 170, generic for all fiber and cable combinations, does not exist. However, the two extreme fiber designs, the DCF and the MCF, do behave predictably. Cables A and B show a consistent cutoff reduction of 75 nm regardless of cable design. This is explained by evidence that the depressed cladding fiber design exhibits a cutoff wavelength that is length dependence-dominated [7]. The following equation can be used to determine cutoff wavelength reduction due to increase in fiber length alone.

$$\left[\lambda_c\right]_{actual} = \left[\lambda_c\right]_{2m} - A \log\left[\frac{L}{2}\right] \qquad (1)$$

with A = 65 nm per decade of length for Cable A and B fiber designs [7], 65 nm of the cutoff wavelength reduction is expected from the L = 20 meters of cable length. The 3 in. loops must account for the small residual reduction. Conversely, for matched cladding fibers (such as those in cables C and E), A is closer to 18 nm per decade of length and accounts for only approximately 20% of the cutoff wavelength reduction. Here the 3 in. loops dominate and account for the other 80% of the cutoff wavelength reduction as was verified in Figure 3.

5. *Mapping Functions and Confidence Levels*

To further investigate the mapping functions, the λ_{cc}'s were plotted as a function of λ_{cf}'s. A typical plot is shown in Figure 7. A linear least squares fit to the data, $\lambda_{cc}(\lambda_{cf}) = m\lambda_{cf} + b$, is plotted as the solid diagonal line in Figure 7. The dashed parallel lines drawn on either side of solid line shows the standard error of the estimate (SEE) of the linear fit [8, p.297], and provides a convenient measure of the probable error of the mapping. The results of the linear fitting to all the measured data for each cable is tabulated below:

Linear Fitting Statistics

Cable	N	m		b		SEE
		mean	sigma	mean	sigma	
A	16	0.973	0.121	-41.6	153.2	16
B	15	0.882	0.037	73.8	46.9	7
C	23	0.718	0.063	243.1	75.8	7
D	18	0.723	0.122	230.7	147.0	16
E	14	0.908	0.068	0.9	81.7	9
F	19	0.946	0.112	-1.7	133.6	21
G	18	0.988	0.074	-54.9	88.2	12
H	18	0.735	0.053	237.4	67.5	20
I	14	0.850	0.064	54.4	77.5	5
J	6	0.676	0.192	292.6	236.7	7

where m is the dimensionless slope and b is the λ_{cc} axis intercept (in nm). For statistical analysis of a small cluster of points distant from the origin, such as the case here, the SEE provides a more meaningful measure of the quality of the fit, than monitoring the standard deviations (sigmas) of the slope and λ_{cc} axis intercept. In general, the mapping of λ_{cf} into λ_{cc} is sublinear (i.e. $m < 1$). This implies that a wide specification tolerance for λ_{cf} will map into a narrower specification tolerance for λ_{cc}. Such sublinearity has the advantage of ensuring the user's tight functional requirements (i.e., tolerances on λ_{cc}) can be met with more relaxed process control requirements (i.e., tolerances on λ_{cf}) for the manufacturer.

For the purposes of system design, to ensure a single-mode system will not operate in the fiber's multimode regime, considering the possible range of laser operating wavelengths, the quantity of interest to be provided by the cable supplier is $(\lambda_{cc})_{max}$ [9]. In order for a supplier to guarantee a customer that a cable will meet a specified $(\lambda_{cc})_{max}$, the supplier can use the mapping function to establish a confidence interval and avoid measuring λ_{cc} directly on a routine basis. By using the mapping function and establishing a confidence interval the

supplier can guarantee (to whatever percent the confidence interval is established) a $(\lambda_{cc})_{max}$ will be met by monitoring λ_{cf} values. As an example, lets look at the statistical probability or certainty that an arbitrary $(\lambda_{cf})_{max}$ = 1330 nm will map into a $(\lambda_{cc})_{max}$ = 1250 nm requirement [10]. This is shown on Figure 7 by the horizontal and vertical dashed lines. Determining the certainty or confidence of an extrapolated value of λ_{cc} corresponding to value of λ_{cf} outside the range of observation, is statistically handled by considering a certain percentage confidence interval. The uncertainty of an extrapolated λ_{cc} value will be denoted by σ_x, where x=95 or 99% corresponding to a 95 or 99% confidence interval. Extrapolated λ_{cc} values corresponding to a λ_{cf} = 1215 nm,, λ_{cc}(1330), and the associated σ_x's have been calculated [8, p. 301] for the cables we measured and the results are tabulated below.

Extrapolated λ_{cc}'s and confidence intervals				
Cable	N	λ_{cc} (1330)	$\sigma_{95\%}$	$\sigma_{99\%}$
A	16	1252	39	54
B	15	1247	17	23
C	23	1198	22	30
D	18	1192	47	65
E	14	1208	29	40
F	19	1257	55	76
G	18	1259	35	48
H	18	1215	44	60
I	14	1185	20	28
J	6	1192	57	95

To determine if a cable can meet a $(\lambda_{cc})_{max}$ = 1250 nm the following inequality is employed.

$$\lambda_{cc}(1330) + \sigma_x < 1250nm \qquad 2$$

From the data of the above table it can be seen cables C, E, and I can meet a $(\lambda_{cc})_{max}$ = 1250 nm specification with a 99% confidence. Cable D can meet a 95% confidence but not a 99%. Cable J is close to meeting a 95% confidence but the few data points makes an extrapolation very difficult. Cables A, B, F, G, and H will not be able to meet the requirements as defined in this example with such a limited data base. A general trend is a reduction in σ_x as N is increased and as more data near the extrapolation point is included.

6. *Conclusions*

User requirements are reflected in a λ_{cc} specification. The data shows a generic single-valued mapping function of λ_{cf} into λ_{cc} does not exist. For generic cable requirements, the λ_{cf} is less appropriate as its specified value must vary from manufacturer to manufacturer to meet a specific user requirement. However, when λ_{cc} is used as a basis for specification a singular value can be specified which is generic to all cable products. Using a mapping function of λ_{cf} values into λ_{cc} values and establishing a confidence level was shown to be a viable means of ensuring user's λ_{cc} requirements are met without routine testing of cables for λ_{cc}. However, if specifications based on λ_{cf} are to be used, specified λ_{cf}'s should be more conservative as these values should map into the λ_{cc} requirement considering worst-case length scaling and bend sensitivity. The fundamental basis for cutoff wavelength specification is ultimately the cable cutoff wavelength as this reflects actual cutoff wavelengths observed in cabled fibers deployed in typical field situations.

References

[1] F. T Stone, "Modal Noise in Single-Mode Fiber Communication Systems," *SPIE Proceedings 500-04*, San Diego, (1984).

[2] R. W. Tarwater, M. J. Maslaney, D. L. Philen, F. T. Stone and D. G. Duff, "Bandwidth and Cutoff Wavelength of Single-mode Lightguide System Considerations," *IWC Symposium Proceedings*, pp. 261-265, Reno, Nevada, (1984).

[3] N. K. Cheung and P. Kaiser, "Cutoff Wavelength and Modal Noise in Single-Mode Fiber Systems," *NBS Special Publication 683*, pp.15-18, (1984).

[4] EIA-455-80, "Cutoff Wavelength of Uncabled Single-Mode Fiber by Transmitted Power," Electronic Industries Association, Engineering Dept., 2001 Eye St., N.W., Washington, D.C.

[5] EIA-455-170, "Cutoff Wavelength of Single-Mode Fiber Cable by Transmitted Power," Electronic Industries Association, Engineering Dept., 2001 Eye St., N.W., Washington, D.C.

[6] V. Shah, "Effective Cutoff Wavelength for Single-Mode Fibers," Symposium on Optical Fiber Measurements, *NBS Special Publication 683*, pp. 7-9, (1984).

[7] W. T. Anderson and T. A. Lenahan, "Length Dependence of the Effective Cutoff Wavelength in Single-Mode Fibers," *IEEE Journal of Lightwave Technology*, Vol. *LT-3*, No. 3, pp. 238-242, (1984).

[8] I. Miller and J. E. Freund, *Probability and Statistics for Engineers*, Prentice Hall, 1977.

[9] "Single-Mode Fiber Optic System Transmission Design," EIA Special Bulletin Electronic Industries Association, Engineering Dept., 2001 Eye St., N.W., Washington, D.C.

[10] Bellcore TR-TSY-000020 "Generic Requirements for Optical Fiber and Optical Fiber Cable," Issue 3, December, 1987.

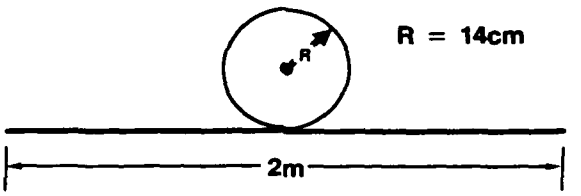


Figure 1. Uncabled Fiber Cutoff Wavelength (FOTP 80) Deployment Condition

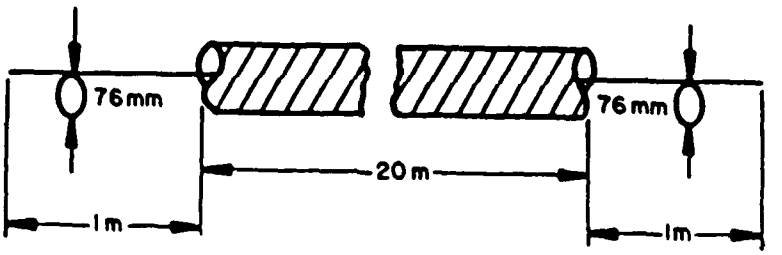


Figure 2. Cabled Fiber Cutoff Wavelength (FOTP 170) Deployment Condition

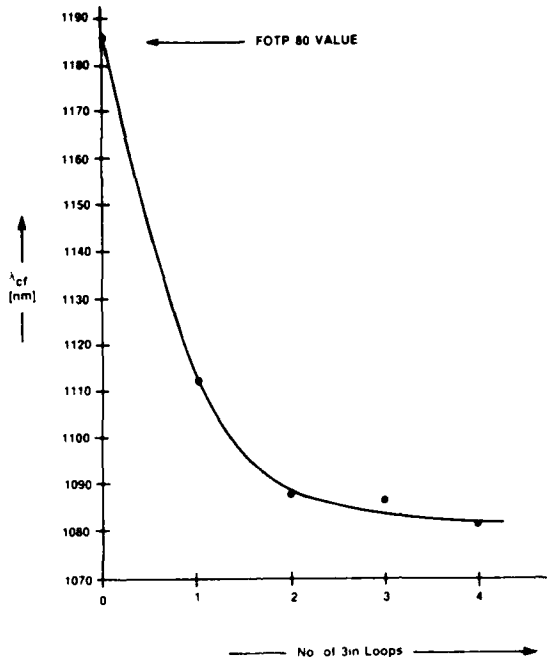


Figure 3. Effect of Multiple 3 in. Loops on a Matched-Clad Fiber's Uncabled Fiber Cutoff Wavelength

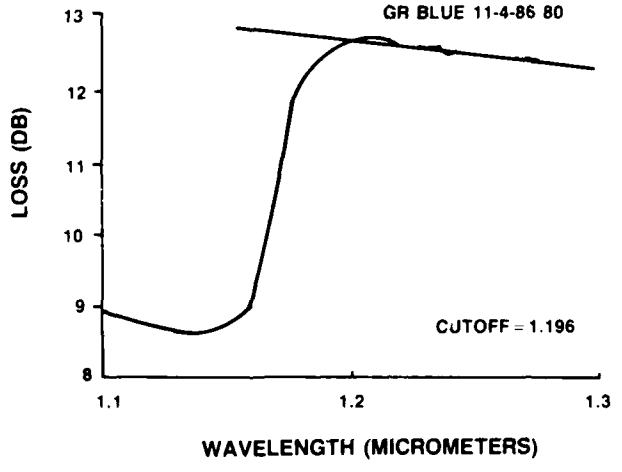


Figure 4. Typical FOTP 80 Cutoff Wavelength Measurement Data

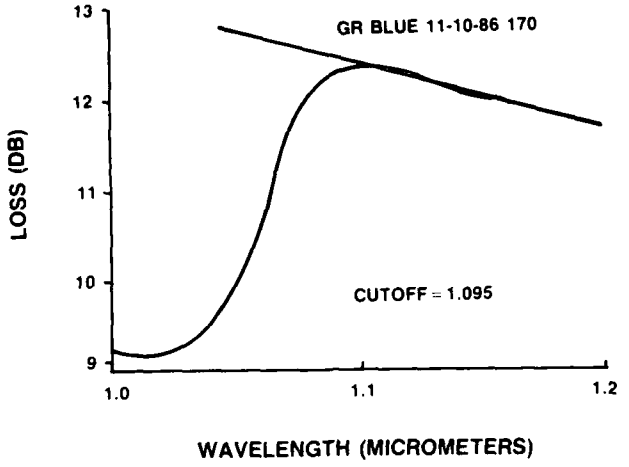


Figure 5. Typical FOTP 170 Cutoff Wavelength Measurement Data

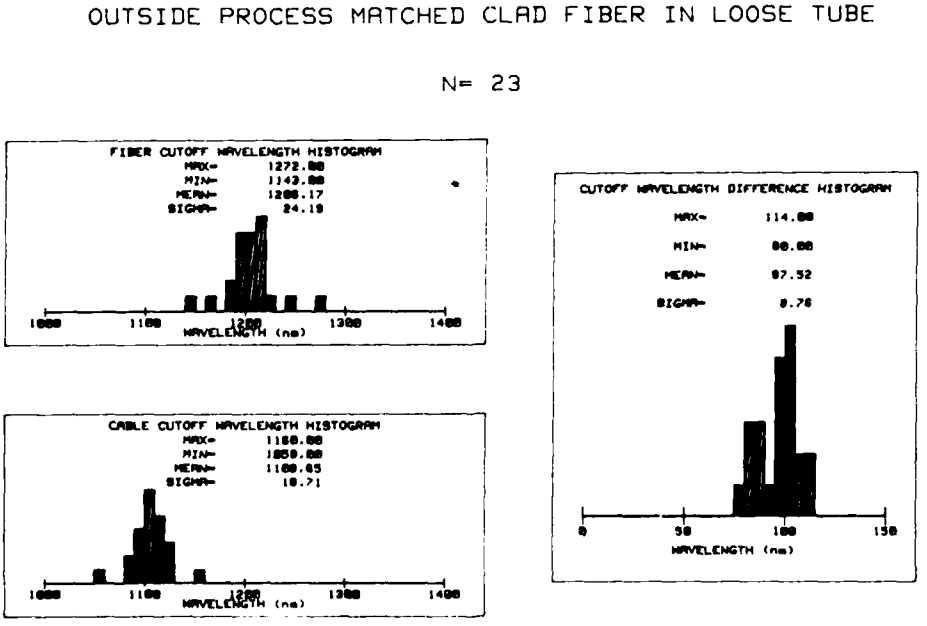


Figure 6. Examples of λ_{cf}, λ_{cc}, and $\lambda_{cf} - \lambda_{cc}$ Histograms

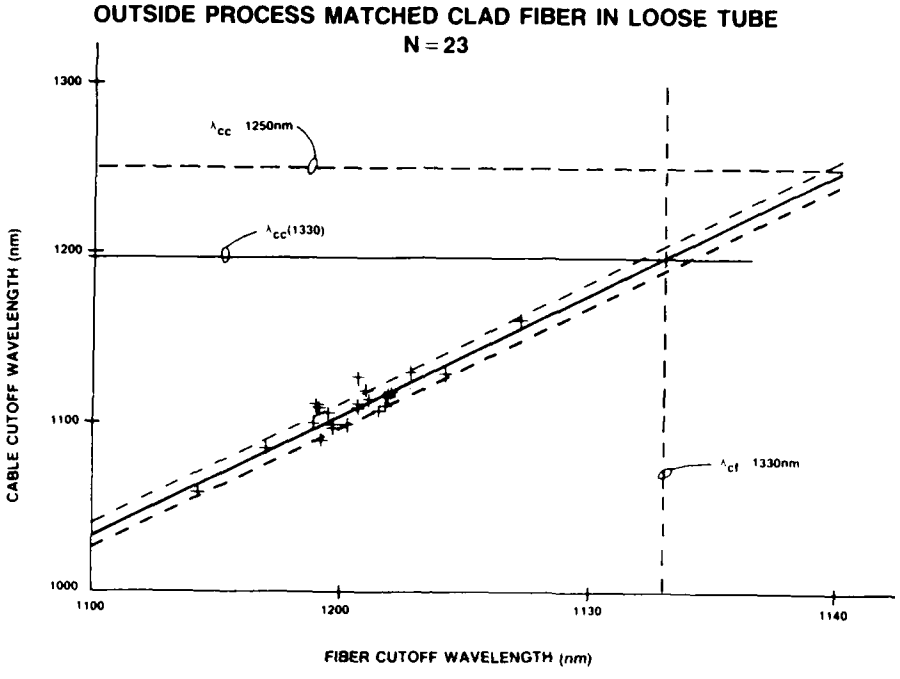


Figure 7. Typical Example of Measured λ_{cc}'s Plotted as a Function of λ_{cf}'s



Joyce Kilmer was born in Pittsburgh, PA, in 1958. He worked in the Noise Research Laboratory in the Electrical Engineering Department of the University of Florida for four years studying $1/f$ noise in solid-state devices before receiving the Ph.D. degree in electrical engineering in 1984.

He joined Bell Communications Research in 1984 as the optical requirements engineer of the optical cables district. Since then he has been involved in developing criteria and measurement methods for optical fibers and active in industry standards organizations.

Dr. Kilmer is a member of the Optical Society of America.



William T. Anderson was born in Buckhannon, WV, on November 30, 1948. He received the B.S.E.E. degree with highest honors from Georgia Institute of Technology, Atlanta, in 1970, the M.S. degree from Stanford University, Stanford, CA, in 1971, and the Ph.D. degree from Georgia Institute of Technology in 1979.

At Bell Laboratories, he worked in the area of transmission and crosstalk in multipair telephone cable from 1970 to 1979. From 1979 to 1983, he was involved in the design and measurement of single-mode optical fibers. In 1983, he joined Bell Communications Research, Morristown, NJ, where he is responsible for optical fiber and cable requirements and analysis.



Robert M. Kanen came to work for Bell Communications Research in 1986.

He attended Champlain College and Worcester Polytechnic Institute.

Prior to Bellcore, he had been employed by ITT-Federal Electric, HRP-Singer, Singer Co., R. H. Wagner Co., as well as 4 years of Naval Electronics.



Carolyn M. Connor Davenport was born in Denver, Colorado on June 23, 1963. She received the B.S. in electrical engineering from New Mexico State University in 1985 and the M.S.E.E. from the Georgia Institute of Technology in 1987. She is the recipient of a Bell Communications Research Graduate Fellowship and is beginning work toward the Ph.D. at the University of Arizona Optical Sciences Center.

A PROBABILITY MODEL FOR OBTAINING THE SPLICE LOSS IN SM OPTICAL FIBERS FROM ONE-WAY OTDR MEASUREMENTS

L. Bjerkan

EB Cables
P.O. Box 419, N-1371 Asker
NORWAY

SUMMARY

A statistical analysis has been carried out on some hundred bidirectionally measured splices between match clad SM optical fibers using OTDR at 1300 nm. The variations in the measured discontinuities at a splice and actual splice losses are described using a bivariate probability distribution function. From this distribution one can obtain the probability of keeping the splice loss below a certain maximum value given a one-way measured OTDR discontinuity. Satisfactory agreement between the theoretical model and the experimental data is obtained. In the case where the splice in question does not reach the desired probability a model for enhancing this probability by repeated splicing is finally presented.

INTRODUCTION

Optical time-domain reflectometry (OTDR) is now commonly used in the characterization of attenuation, faults and splices in optical fibers both in manufacturing processes and field installations. For the latter purpose it is very convenient since current OTDR's are lightweight, portable and most of the needed information can be obtained by measuring from one end. However, it is well known that one-way measurements of splices between optical fibers by the OTDR technique gives rise to difficulties in the interpretation of splice loss due to statistical variations in the magnitude of backscattered light among fibers[1-3]. This controversy can be resolved by measuring from both ends and defining the splice loss as the bidirectionally measured average. In practical field installations, however, a two-way measurement may become very inconvenient. In addition to the generation of additional labour and cost, while carrying out a one-way measurement is usually a reasonable task. An operator is usually concerned about keeping the sum of the splice losses below a certain maximum value determined by system considerations. For installations involving match clad SM fibers typical values of the mean loss can be 0.1 dB/splice.

Since the one way measured OTDR discontinuity cannot yield the accurate splice loss directly, the question of extracting a satisfactory estimation of the splice loss from the measured discontinuity arises. In other words one can ask for the probability of finding the splice loss below a certain maximum value based on the one-way OTDR reading.

Installations on SM fiber systems are now common practice and a lot of measured data on splices exists. We have collected data from some hundred splices measured bidirectionally from recent fiber installations and carried out a statistical analysis. Based on the empirical data a probability model will be described from which the splice loss may be estimated.

STATISTICAL ANALYSYS

In OTDR measurements of splices between optical fibers three quantities are involved; the observed discontinuity G, the actual splice loss L and the scattering factor ratio S. On the dB scale they are related by:

$$G = L + S \qquad (1)$$

where $S = 10\log S_1/S_2$ with S_1, S_2 being the scattering factors of the two fibers in question[4]. The quantity S is determined by statistical variations among basic fiber parameters (geometry and doping concentration). S as defined above may be positive or negative and since the succession of two spliced fibers is equally probable, it is a symmetric statistical distribution with zero mean. L contains two contributions, intrinsic splice losses which again are attributed to basic fiber variations and extrinsic loss contributions which mainly originate in geometrical mismatches, nonperfect cleave ends and profile slurring for fusion splices[5]. The three quantities G,

L and S will not be independent statistical variables.

A bivariate probability density function f(G,L) will describe the simultaneous variations of the quantities G and L. From this function marginal probability densities for the actual splice loss and OTDR reading $f_1(L)$ and $f_2(G)$ respectively may be obtained straightforwardly by integrating out the other variable. When these functions are defined one can calculate the probability of obtaining the splice loss below a certain maximum L_1 when the observed OTDR reading is in the region $G\in(G_1,G_2)$ by the conditional probability:

$$p(L<L_1 \mid G\in(G_1,G_2)) = \int_{G_1}^{G_2}\int_{0}^{L_1} f(G,L)\,dG\,dL \Big/ \int_{G_1}^{G_2} f_2(G)\,dG \qquad (2)$$

In a practical situation the G scale may be divided in 0.05 or 0.1 dB steps (i.e. $G_2-G_1=0.05$ or 0.1 dB) while typical values for L_1 may be 0.1 or 0.2 dB.

As a model for f(G,L) the well described bivariate normal distribution is suggested. In this distribution both variables take on values in the region $(-\infty,\infty)$. Splice losses can only take on positive values so the distribution must be truncated for L<0. For simplicity it is assumed that the OTDR discontinuity extends to infinity in both directions while the splice loss is defined in the region from zero to infinity. By defining the relative quantities:

$$x=(L-\mu_L)/\sigma_L \qquad y=(G-\mu_G)/\sigma_G \qquad (3)$$

where μ_L, μ_G, σ_L and σ_G are parameters of the bivariate distribution we can write:

$$f(G,L) = k/\pi\sigma_L\sigma_G\sqrt{1-\rho^2} \cdot \exp(-(x^2-2\rho xy+y^2)/2(1-\rho^2)) \qquad (4)$$

where $|\rho|<1$ and is a measure of the correlation between the variables L and G which are not statistically independent. The normalization k is obtained by

$$\int_{-\infty}^{\infty} dG \int_{0}^{\infty} dL f(G,L) = 1$$

yielding

$$k=(1+\mathrm{erf}(\alpha))^{-1}$$

where erf is the error function and $\alpha=\mu_L/\sqrt{2}\sigma_L$.

The marginal probability densities $f_1(L)$ and $f_2(G)$ are obtained as:

$$f_1(L)=\sqrt{2/\pi}/\sigma_L\,(1+\mathrm{erf}(\alpha))\cdot\exp(-.5x^2) \qquad (5)$$

$$f_2(G)=1/\sqrt{2\pi}\sigma_G(1+\mathrm{erf}(\alpha))\cdot\exp(-.5y^2)\cdot (1+\mathrm{erf}((\mu_L/\sigma_L+\rho y)/\sqrt{2(1-\rho^2)})) \qquad (6)$$

Since S is defined to have zero mean one can easily show from (1) that G and L have the same means $\bar{L}=\bar{G}$. This quantity together with the standard deviations s_L and s_G are obtained straightforwardly from the measured data. However, since the distribution defined in (2) is truncated for L<0 the parameters μ_L and σ_L are not direct estimates of the means and standard deviations of G and L. However, they can be calculated straightforwardly from the marginal distributions defined in (5) and (6) as:

$$\bar{L} = \int_{0}^{\infty} L f_1(L)\,dL = \mu_L+\sigma_L R \qquad (7)$$

$$s_L^2 = \int_{0}^{\infty} L^2 f_1(L)\,dL - \bar{L}^2 = \sigma_L\sqrt{1-(\mu_L/\sigma_L R+R^2)} \qquad (8)$$

Similarly:

$$\bar{G} = \mu_G+\rho\sigma_G R \qquad (9)$$

$$s_G = \sigma_G\sqrt{1-\rho^2(\mu_L/\sigma_L R+R^2)} \qquad (10)$$

where $R=\sqrt{2/\pi}\exp(-\alpha^2)/(1+\mathrm{erf}(\alpha))$ and $\alpha=\mu_L/\sqrt{2}\sigma_L$. The parameters μ_L and σ_L are obtained numerically from (7) and (8) when $\bar{L}$ and s_L are obtained experimentally from a given set of data. From (9) and (10) μ_G and σ_G are obtained as functions of the correlation coefficient ρ. This parameter is finally obtained by fitting the experimental data to (4) by a least squares method. Hence all parameters of the bivariate distribution are obtained. The conditional probabilities can then be

determined by performing numerical integrations of (2).

EXPERIMENTAL DATA

We have collected data from 482 splices between SM fibers measured bidirectionally by OTDR. All splices were made using an Ericsson FSU 850 automatic fusion splicer without any local monitoring. The fibers were cleaved with a simple commercial handheld cleaver. All data are obtained from splices between similar fibers (match clad step index SM fibers from the same manufacturer) using commercial SM reflectometers at 1300 nm. A handful of trained operators were involved in the splicing process. The estimated measurement accuracy is ±0.02 dB. All data are taken from recent field installations.

RESULTS

Figure 1 shows the distribution of the three quantities G, L and S as obtained from all 482 splices at 1300 nm. The fitted marginal densities defined by (5) and (6) are included in figs. 1a and 1b respectively. Figure 2 shows the corresponding two-dimensional distribution in G and L. Table I lists values of minimum and maximum values, means and standard deviations of the three quantities G, L and S for the 482 splices. Table II lists the fitted parameters of the bivariate distribution.

The conditional probabilities are calculated from (2) using numerical integration by a gaussian method". Figure 3 shows results of this calculation where the smooth curves indicate the probability of obtaining splice losses <0.1 and 0.2 dB respectively as a function of the measured OTDR reading. Calculations from the corresponding measured data are also indicated. For the integration over G in (2) intervals of $G_i - G_{i-1} = 0.05$ dB were chosen. When the integration interval becomes infinitesimally small a perfectly smooth curve appears. At the low and high end of the G scale there are few observations and the uncertainty in the measured data becomes large while around the center of the G distribution where the number of observations are high the match between theory and experiments is good.

PRACTICAL CONSIDERATIONS

Fiberoptic links are designed with a certain loss budget where the sum of the splice losses or the average loss per splice is to be maintained below a given value L_{max}. As long as the sum of the splice losses only matters the actual loss in each splice becomes less important. Therefore the method outlined here may be advantageously employed in predicting the splice losses below L_{max} with a chosen probability determined from one-way OTDR measurements. As an example we may choose $L_{max} = 0.2$ dB/splice and accept the splice if the probability is greater than 75% that the splice loss is less than 0.2 dB. From fig. 3 this is obtained from OTDR discontinuity readings <0.25 dB. If the observed discontinuity reading exceeds 0.7 dB, the highest value encountered, the splice must be rejected.

In between there is an uncertainty range. However, by resplicing one can enhance the probability of having obtained an acceptable splice. This can be visualized as follows: Suppose the OTDR reading for the first attempt yields a probability p_1 of an acceptable splice (event A) and similarly p_2 for the repeated splice (event B). From basic probability theory the union of these two events is $p(A \cup B) = p(A) + p(B) - p(A \cap B)$. Since these two events can be considered independent the resulting probability can be written:

$$p_{1,2} = p_1 + p_2 - p_1 p_2 \qquad (11)$$

By using this principle it can further be shown that for n repetitions one obtains:

$$p_{1,n} = 1 - \prod_{i=1}^{n} (1 - p_i) \qquad (12)$$

where p_i is the probability for each repetition. If for example the first reading yields a 50% probability of an acceptable splice, and the repeated splice also yields 50% then (11) predicts a 75% probability for the acceptance of the repeated splice. In practice one or two repetitions will be sufficient in assuring the quality of the splice.

Table I

Minimum, maximum, mean and standard deviation encountered from bidirectionally measured OTDR data (G), splice loss (L) and scattering factor ratios (S) from 482 splices at 1300 nm.

Quantity	Minimum (dB)	Maximum (dB)	Mean (dB)	Standard dev. (dB)
G	-0.33	0.70	0.113	0.174
L	0	0.49	0.113	0.085
S	0	0.90	0	0.303

Table II

Fitted parameters to the bivariate distribution defined in (3) and (4)

Parameter	Value
μ_1 (dB)	0.004
μ_2 (dB)	-0.06
σ_1 (dB)	0.14
σ_2 (dB)	0.25
ρ	0.92

CONCLUDING REMARKS

Although a one-way OTDR measurement of a splice between matched clad SM fibers cannot yield the splice loss directly it has been demonstrated that one can predict the probability of keeping the splice loss below a certain maximum value based on the measured one-way splice discontinuity. By fitting experimental data to a bivariate probability distribution function a theoretical model with satisfactory agreement with the experiments was obtained. Based on information such as given in fig. 3 it will be easier for an operator to decide whether a splice is acceptable or not. In the case of an unacceptable splice a model to enhance the acceptance probability by repeated splicing has also been outlined.

ACKNOWLEDGEMENT

The author wishes to thank the Norwegian Telecommunications Administration and the Icelandic Telecommunications Administration for providing some of the data used in this analysis.

REFERENCES

1. S. Heckman, E. Brinkmeyer and J. Streckert, Opt. Lett. 6, 634-635 (1981)

2. M. P. Gold, A. H. Hartog, Electron. Lett. 17, 965-966 (1981)

3. P. DiVita, U. Rossi, Electron. Lett. 15, 467-469 (1979)

4. J. Lidh, Lightwave 3, no. 6, 43- 47 (1986)

5. R. Engel, E. McNair, Tech. Dig: Symp. on Opt. Fiber Measurements, Boulder Co., 43-48 (1986)

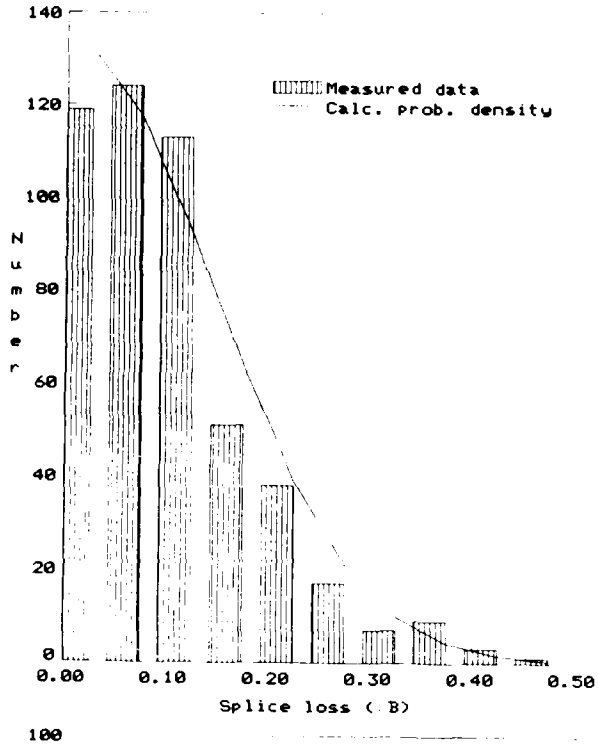
6. F. Kapron, C. Kozikowski, R. Crotts, Tech: Dig; Symp. on Opt. Fiber Measurements, Boulder Co., 81-84 (1986)

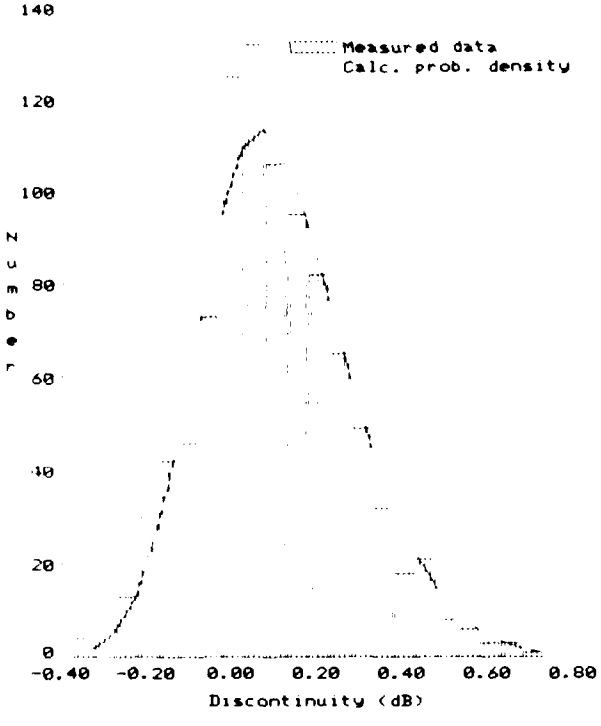
7. R. Engel, Proc. 12th ECOC, Barcelona, 145-148 (1986)

8. M. Abramowitz, I. A. Stegun, Handbook of mathematical functions, ch. 25 New York, Dover (1972)



Leif Bjerkan graduated from the University of Trondheim with a Ph. D. in physics in 1978. He has been involved in research on optical fibers and lasers since that time. He joined EB Cables in 1985 where he is presently a senior research engineer.





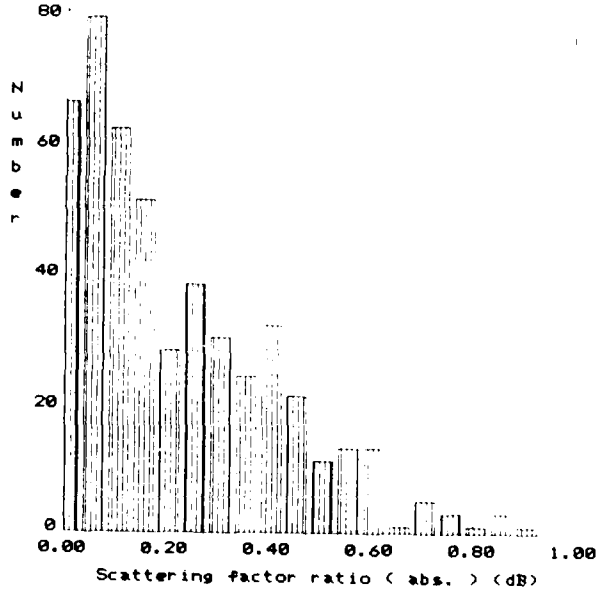


Figure 1.
Distribution of a: Measured OTDR discontinuities, b: Splice losses and c: Scattering factor ratios from 482 spliced SM fibers. Fitted probability density curves are shown as solid lines in a. and b.

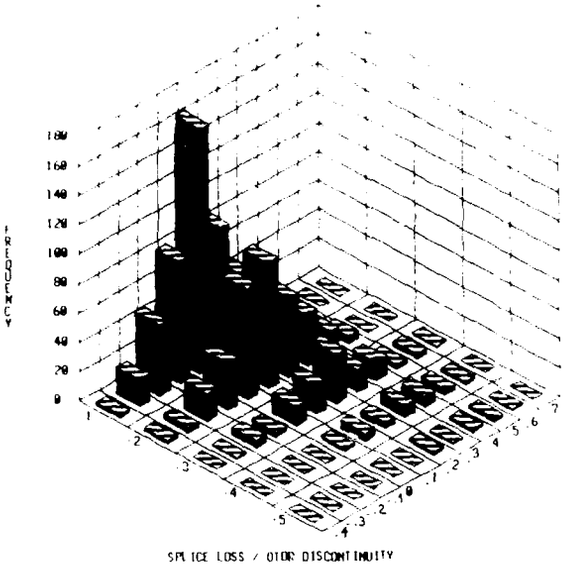


Figure 2.
Two-dimensional plot of measured OTDR discontinuity and actual splice loss from 482 spliced SM fibers

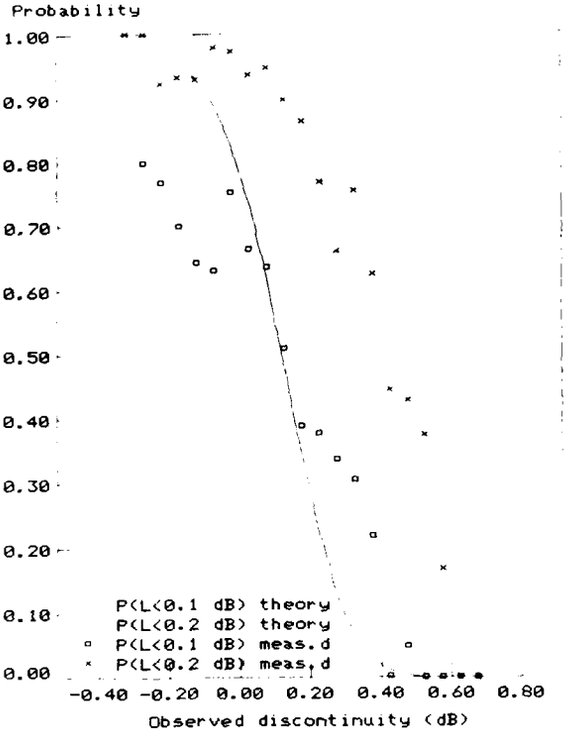


Figure 3.
Probability of obtaining splice losses <0.1 dB and <0.2 dB vs. measured OTDR reading (theory and experimental data)

CONTINUOUS MONITORING OF THE LOSS OF LARGE NUMBERS OF FIBER OPTIC SPLICES

R. Raman

Contel Laboratories
Norcross, GA 30092

ABSTRACT

A new experimental procedure developed to reduce uncertainties due to mating and unmating of fiber ends at test points is described. It combines a cutback step and substitution and offers a number of advantages.

The method consists of first determining a reference loss value of a launch fiber, introducing a splice with a precisely known loss, and finally substituting the test sample between this splice and the detector. Prior to the test, the errors resulting from mating and unmating of the fiber ends of the sample are accurately determined. Data show that the error can be reduced to as little as 0.003 dB.

The technique permits measurement in both directions, loss when dissimilar fibers are spliced, or when the test fiber is short. Environmental testing of splices is demonstrated.

INTRODUCTION

General

In order to establish the performance of a fiber optic splice or a connector, it is vital to determine not only its absolute loss value but also its stability in various environmental exposures. When a single sample is considered, the procedure is straightforward and simple. The method is illustrated in Figure 1. The power transmitted in a reference fiber section is first measured using a suitable source and a power meter under appropriate light launch and receive conditions. The fiber is cut, the splice inserted, and the change in power level is measured.

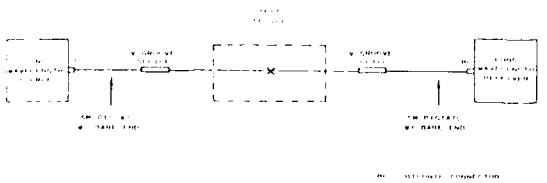


FIGURE 1. MEASUREMENT OF LOSS
TRANSMISSION METHOD

A cutback technique shown in Figure 2 is used when dissimilar fibers are involved. In this method, the near end of fiber A is first connected to the source and the far end to the detector. This represents the reference measurement, P_0. Next, the far end is removed and connected to fiber B using the test splice. The splice loss is the difference between a second reading (P_1) and the initial power value.

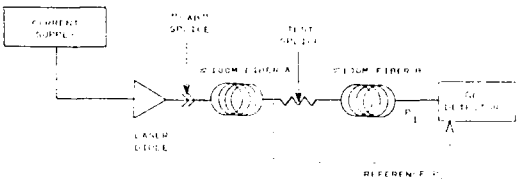


FIGURE 2. MEASUREMENT OF LOSS
CUTBACK METHOD
SOURCE GTE
LOSS = $P_0 - P_1$

Continuous monitoring of the splice loss or change in optical transmittance is possible, provided the launch and receive conditions remain undisturbed. This implies that the optimized fiber alignment at the sample connectorization points is constant. However, when several samples are being tested, the measurements become complicated due to the need to uncouple the end connections for each sample. The removal of the terminations will introduce uncertainties and errors. Testing one sample at a time is laborious and time-consuming.

The development of a new experimental procedure is described in this paper. In this method the errors and uncertainties are reduced. It also enables continuous measurements on a large number of samples. Although the method is applicable to both multimode and single mode splices, the emphasis in the discussion will be single mode splices.

Multiple Splice Tests

In the industry, there are a number of methods suggested to avoid the errors of mating and unmating the sample fiber ends at the test points. In one case, an array of sources and detectors is proposed[1]. This can be very expensive, especially if lasers are used. A schematic of a measurement system is shown in Figure 3. One difficulty with this is that the sample fiber ends should be preterminated with connectors. Otherwise, samples must be prepared using pigtails rather than fibers. If it is desired to test 200 samples, the cost of the sample preparation itself can be prohibitive.

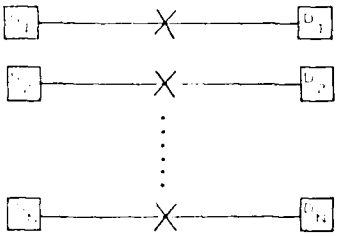


FIGURE 3. MULTIPLE SOURCE/DETECTOR MEASUREMENT ARRANGEMENT

In a second method, a single source/detector combination is used in conjunction with splitters and couplers as indicated in Figure 4. This also entails some problems. First, the signal level is attenuated considerably. Second, the splitting and coupling ratios may vary from sample to sample. In the particular example[2] cited, the experiment is performed using a short wavelength source (632 nm), which makes alignment easy. When long wavelength sources are employed, the air-gaps at the launch and receive stations will be undesirably large.

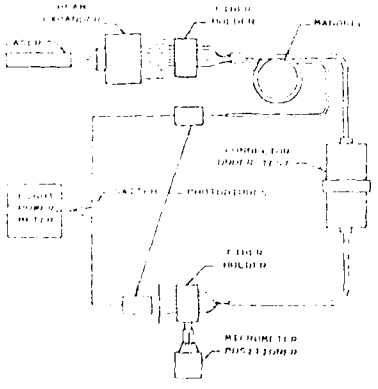


FIGURE 4. INSERTION LOSS MEASUREMENT SPLITTER-COUPLER METHOD (REF. IWCS 1980)

A third alternative is to prepare a chain sample consisting of a series of several splices and connectors, and join them to a single source and detector. This certainly can provide an enhanced signal-to-noise ratio. In addition, the link will simulate a span in the field. However, it is difficult to pinpoint defective splices if failure occurs.

Experimental Conditions - Background

Before the absolute loss value of a splice can be established, it is first necessary to avoid experimental conditions that adversely affect the results. In this regard there has been considerable debate and confusion in the industry; techniques designed for multimode fibers are often applied to single mode systems. A case in point is the concept of equilibrium mode power distribution. Splice measurements under equilibrium (steady state) conditions are expected to yield results that are definitive and representative of transmission line environments.

For multimode fibers the splice loss depends on the mode distribution. Equilibrium is achieved either by using a very long fiber section, by means of a mandrel wrap of a short section, or by controlling the spot size and numerical aperture of the beam. In contrast, most single mode fibers do not require a long length or a mandrel wrap because only one mode is present. This approach is well-recognized now and contained in the Fiber Optic Test Procedure (FOTP) 171 recently drafted by the EIA.

The factors that affect insertion loss are: nature of the source, light launch conditions, nonequilibrium modal state, presence of cladding modes, fiber type, and the test fiber interface at both ends. Detailed analysis of many of these parameters, specifically relating to multimode fibers, have appeared in several publications[3-5]. It is appropriate to review this with reference to single mode fibers.

Source: Selection of a light source depends on the output and the range of values desired. Traditionally, an LED is preferred. Because it provides a wide beam angle, it is easy to overfill the fiber core. Also, it is unaffected by temperature fluctuations and back-scattered light. However, its spectrum is somewhat wide.

A laser has a narrow spectrum, but it is sensitive to temperature. Back-scattered light is also a feature. Although white light can be used, it would need an optical filter to control wavelength and a chopper with associated electronics for signal processing. One difficulty with white light is that its output is comparatively low.

Most experimentalists tend to build their own source and detector assemblies. This has resulted in much discussion about the specifics involved. One problem with coherent laser light is the generation of modal noise at misaligned connections.

Launch: For multimode fibers, the numerical aperture is important. On the other hand, for single mode fibers, the correct alignment and air-gap at the source are the factors that should be considered.

As stated earlier, there is no need for a mandrel wrap when single mode fiber is involved. If the fiber coating has an index lower than that of the cladding, cladding mode strippers (CMS) must be placed both after the source and ahead of the detector. However, the present-day coatings are well standardized, the CMS may not be required.

For single mode, the source must be chosen so that the spectral output is above the cutoff wavelength of the test fiber. Otherwise, undesirable secondary modes will be generated.

One point of importance is the length of the launch fiber. This is not a problem with matched cladding fibers which are insensitive to length. When depressed cladding fibers are used, the length is considered to be critical.

Interconnection Points

To conduct splice testing, the fiber ends must be connected to the equipment by appropriate means, and the alignment should be optimized if necessary. Care must be exercised to eliminate errors that may arise at these points. The same power losses that can occur at the test splice are also possible at the two interconnection points.

The variables consist of both fiber intrinsic parameters as well as extrinsic mechanical parameters. The fiber intrinsic parameters are mode field radius (spot size), core ellipticity, fiber diameter, and core-cladding eccentricity. The extrinsic parameters consist of transverse offset, end separation, tilt angle, and fiber end angle.

Industry experience shows that fiber diameter variations and core-cladding offset are negligible with lightguides that represent current technology. According to the literature[5], changes in spot size in combination with a 5-percent core ellipticity will result in only a maximum loss of 0.015 dB. At Contel Labs, losses less than 0.01 dB have been achieved using a simple V-groove splice. This confirms that the intrinsic parameters of currently manufactured fibers have no effect on the real splice loss. Furthermore, extrinsic mechanical alignment factors are usually well controlled. Fiber end angles also appear to be less critical because of the use of index matching gel. Therefore, the real concerns are the errors due to mating and unmating at the interconnection points.

Mating/Unmating Errors

Tables I and II show the variability of reference power levels due to mating and unmating the test fiber ends inherent in the method illustrated in Figure 1.

TABLE I
VARIABILITY OF REFERENCE POWER LEVELS
10-FOOT MATCHED CLADDING FIBER
Instrument - Siecor M81/M82 Optical Test Set
Output Stability - 0.15 dB
Multimode Pigtails at Both Ends

FIBER	MEASUREMENT								MEAN	SIGMA
	1	2	3	4	5	6	7	8		
1	11.3	11.6	9.4	9.9	9.4	9.1	9.3	9.5	9.9	1.0
2	10.0	10.2	10.1	9.6	9.5	11.5	8.9	9.2	9.9	0.8
3	11.0	10.6	10.0	8.6	9.2	11.6	9.3	9.2	9.9	1.0
4	11.6	10.8	9.2	8.6	9.0	9.2	9.5	9.0	9.6	1.0
5	9.7	9.9	9.4	10.0	9.4	10.1	10.5	9.9	9.8	0.4
6	10.0	10.4	9.4	9.2	10.1	10.6	8.6	8.5	9.6	0.8
7	-	-	9.7	9.4	10.2	9.1	9.1	9.4	9.5	0.4
8	9.2	10.2	10.2	10.2	9.6	8.8	8.6	8.2	9.4	0.8
9	10.0	10.0	10.7	9.2	9.5	9.0	8.9	8.6	9.5	0.7
10	10.1	10.5	10.9	8.8	10.1	9.4	11.0	11.3	10.3	0.8

TABLE II
VARIABILITY OF REFERENCE POWER LEVELS
10-FOOT MATCHED CLADDING FIBER
Instrument - Anritsu MG921A/ML93A
Output Stability - 0.2 dB
Single Mode Pigtails at Both Ends

FIBER	MEASUREMENTS								MEAN	SIGMA
	1	2	3	4	5	6	7	8		
1	10.36	9.68	9.94	10.40	8.95	10.65	10.43	10.21	10.08	0.55
2	10.94	10.30	9.31	8.84	11.23	9.44	9.63	10.07	9.97	0.82
3	10.16	10.57	10.84	10.79	11.32	11.07	9.65	11.09	10.69	0.55
4	8.86	9.01	8.79	8.78	9.67	9.87	8.98	8.74	9.09	0.44
5	9.17	8.88	8.80	9.20	9.91	9.39	8.72	9.00	9.20	0.43
7[1]	8.75	8.90	8.95	8.57	8.67	9.26	9.16	8.91	8.90	0.23
6	8.72	8.39	8.67	8.50	8.66	8.58	8.65	8.66	8.60	0.11
7	8.77	8.82	8.63	8.74	8.91	8.75	8.72	8.76	8.76	0.09
8	8.96	9.20	9.11	9.07	9.28	8.96	9.15	9.03	9.10	0.11
9	8.66	8.51	8.49	8.37	8.62	8.48	8.48	8.39	8.50	0.10

Note 1: Using a different set of pigtails.

Table I represents experiments conducted using multimode pigtails to obtain maximum power transfer at the connection points. To ensure that the variabilities remained within acceptable limits, the V-groove splices were disassembled, cleaned, and refilled with index matching gel at the completion of each set of measurements. Because of the absence of a coating, care had to be taken to ensure that the bare fiber ends originating from the pigtails were held rigidly at the interconnection points. Sometimes some movement is unavoidable.

The standard deviation ranges from 0.4 dB to 1.0 dB. This reflects a standard error (Sigma/$n^{\frac{1}{2}}$) of 0.14 to 0.35 dB, which is substantial. The high standard error is attributable to random insertions of the fiber ends at the splice points as well as the limitation of the meter resolution (0.1 dB).

Smaller standard deviations are observed when single mode pigtails are used in conjunction with a power meter of better resolution (0.01 dB). As indicated in Table II, the standard deviation varies from 0.09 dB to 0.82 dB. The corresponding standard error varies from 0.04 dB to 0.29 dB, depending on the pigtail used. An error of 0.29 dB is still high.

Bare Fiber Adaptors (BFA)

One quick way to avoid the mating/unmating error is to use bare fiber adaptors at both the source and detector recepticles. However, it will be very difficult to reproduce the original launch and receive conditions due to the variations in the fiber end quality.

LID

The Local Injection and Detection (LID) system is another method to circumvent the connection problems relating to the test fiber ends.

This method is based on the fact that bending a fiber creates "leaky modes" which can transfer power from a fiber core into the cladding and coating. Conversely, light can be injected at a bend.

A lens focuses light into the core on one side of the splice. The radiation ejected from the core on the other side of the splice is detected by means of a photodetector. The alignment is optimized by measuring the output at the second bend. This technique is ideal to optimize fiber alignment at the splice point, but provides only an estimate of the splice loss.

PROPOSED PROCEDURE

The method is illustrated in Figure 5. An initial loss reading is taken by connecting fiber No. 1 between M_1 and M_2. The fiber end on the detector side is removed, and the test splice contained in fiber No. 2 is measured by coupling it with M_2 and M_3.

The loss of M_3 and its variability can be determined. Knowing this, B, representing the deviation due to mating and unmating at the splice points M_3 and M_2, is calculated. An assumption implied in this procedure is that the coupling at M_1 and M_2 are precise.

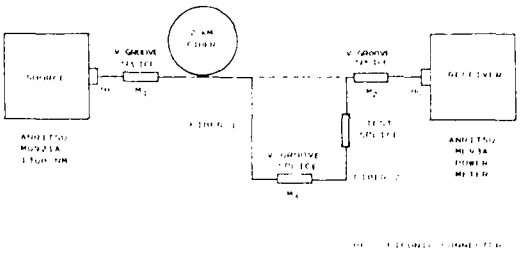


FIGURE 5. METHOD FOR CONTINUOUS MONITORING OF LOSS

The loss is composed of three components:

$$\text{Loss} = L_T + L_3 + B$$

where

L_T = Loss of test splice
L_3 = Loss of M_3 splice
B = Error

During the experiment, splice M_1 is not disturbed so that the light launch conditions are constant. However, the splices at M_3 and M_2 are disturbed each time the test splice fiber ends are inserted or removed. Therefore, it is essential that the alignment is restored to its original optimized state as best as possible. This means that the devices used at these two points are required to be precisely controlled.

Several commercially available mechanical splices were investigated to select a splice suitable for use as the interconnection point. Attention was focused on the elastomeric splice (GTE) and a V-groove splice (Mekconlite).

The elastomeric splice consists of two half-hexagonal pieces, one with a V-groove. The triangular interstitial space formed by the two pieces is smaller than the fiber size. This enables equal distortion of all three sides so that the fibers are concentric to one another. To minimize the losses due to variations in the fiber end quality, an index matching gel is contained in the core.

The second splice features an anodized aluminum barrel with a V-groove and a flat alumi-

num leaf on top. The groove is filled with an index matching fluid. The fibers are placed in the end caps so that the ends make contact at the midsection of the barrel. The leaf is squeezed to press the fibers into the groove prior to locking it in place. To optimize, the leaf is unlocked and one fiber rotated. The fiber rotation and the compression of the leaf are performed alternately until maximum power transfer is achieved.

Repeated insertions of the fibers in the elastic core tended to break the fibers. In contrast, the V-groove splice was less cumbersome and more reproducible when repeated insertion and removal of the fibers were considered. For this reason, the latter device was selected for use in the experiments.

SAMPLES

The initial measurements were conducted using fibers manufactured by different vendors and fused with a variety of fusion splicers including the Siecor M67 and the Fujikura FSM-20. The fiber ends were cleaved using either a GTE or Thomas & Betts tool. The end angles were checked using a Newport Corporation Model F-IM1 micro-interferometer. A total of 23 splices, 8 of which represented chain samples, were prepared. The fiber section utilized was 10 to 15 feet in length.

Tests to check the correlation between the true value and the measured value involved both mechanical splices as well as fusion splices prepared using a Northern Telecom splicer. The following number of splices were prepared:

Optasplice (TRW)	9
Elastomeric (GTE)	7
Rotary Mechanical Splice (AT&T)	2
Fusion	17

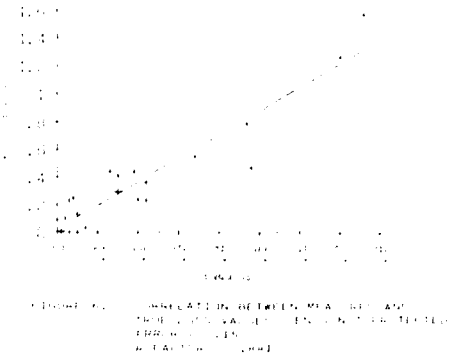
The true loss values were determined using either the method shown in Figure 1 (uncut fiber) or a profile alignment system (cut fiber).

The splice loss values were adjusted to include the entire range from 0.01 to 2 dB.

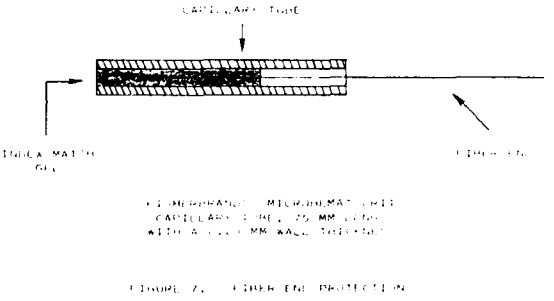
RESULTS

Figure 6 illustrates the correlation between measured and actual splice loss values for several splices consisting of both mechanical and fusion splices, including a few chain samples. The error (0.15 dB) was determined using only one control splice. Not only is the term B high, but the points are scattered. The R factor of 0.881 is low and is not quite satisfactory. The fiber ends were handled carefully, but the ends were left exposed to air.

In order to improve the correlation factor, a method to protect the fiber ends was devised. This is shown in Figure 7.



The measurements were repeated with additional samples. The error term was determined based on seven control splices. The term was 0.01 dB, which represents considerable improvement. It shows the importance of the end protection step.



The results summarized in Figures 8 and 9 demonstrate that very good correlation is achieved. The R factor ranges from 0.954 to 0.998. The data are reproducible even when the measurements were repeated after storing the samples at room temperature for two months. As indicated in Table III, the error is reduced to as little as 0.003 dB, which is below the accuracy of the measuring instrument.

Table III demonstrates the experimental capability for bidirectional measurements as well as the determination of losses for splices formed using dissimilar fibers. With two exceptions, good agreement and repeatability are observed in most of the measurements. In the case of the V-groove splice, for some unknown reason, the delta is considerably high (0.11 dB). Splices identified as 47 and 41 also evidence a slightly larger difference than nominal 0.01 to 0.02 dB. This is probably due to the fact that the true loss values were estimated.

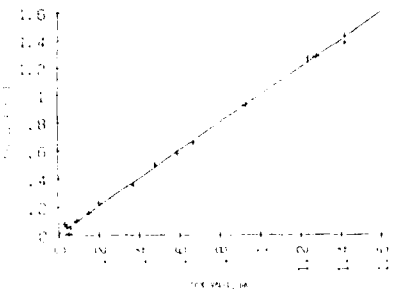


FIGURE 5. CORRELATION BETWEEN MEASURED AND TRUE LOSS VALUES - ENDS PROTECTED MECHANICAL SPLICES
ERROR = 0.01
R FACTOR = 0.998

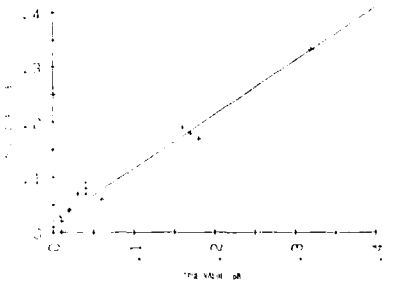


FIGURE 6. CORRELATION BETWEEN MEASURED AND TRUE LOSS VALUES - ENDS PROTECTED FUSION SPLICES
ERROR = 0.01
R FACTOR = 1.454

TABLE III
BIDIRECTIONAL MEASUREMENTS
Instrument - Anritsu[1]
Correction Term = +0.003
Standard Deviation = 0.01, Standard Error = 0.004

FIBER	SPLICE TYPE	SAMPLE I.D.	MEASURED VALUE, dB			CORRECTED VALUE, dB	TRUE VALUE, dB	Δ
			A	B	Avg.			
Matched Cladding	Fusion	3	0.01	0.01	0.01	0.013	0.010	+0.003
	Elastomeric	1	0.49	0.51	0.50	0.503	0.480	+0.023
	V-Groove	1	0.79	0.77	0.78	0.783	0.890	-0.107
	Elastomeric	2	1.27	1.24	1.26	1.263	1.240	+0.023
	Elastomeric	3	0.62	0.69	0.68	0.683	0.670	+0.013
Depressed Cladding	Fusion	27	0.02	0.01	0.015	0.018	0.010	+0.008
	Fusion[2]	43	+0.02	-0.02	0	0.003	0.016[3]	-0.013
Matched Cladding/ Depressed Cladding	Fusion	47	0.05	0.05	0.05	0.053	0.026[3]	+0.027
	Fusion	41	0.01	0.01	0.01	0.013	0.056[3]	-0.043

Notes: 1. See Figure 6.
2. Fiber from two different sources.
3. True value based on estimates using Profile Alignment System (Fujikura).

Additional tests were performed to determine whether or not the length of the launch fiber section adversely affected the accuracy of the measurements. The loss value of selected splices were remeasured after introducing a minor modification of the experimental arrangement.

In the first two tests, the 2-km test fiber was replaced with 1-meter fiber sections representing both matched cladding and depressed cladding types. In the final two tests, the 2 meters of the fiber were connected directly to the source by means of a bare fiber adaptor (BFA). This eliminated both the M_1 splice and the 2-km fiber contained in the experimental arrangement.

TABLE IV
SPLICE LOSS MEASUREMENTS
EFFECT OF FIBER LENGTH

SPLICE NO.	TEST CONDITION	PIGTAIL FIBER	LAUNCH FIBER	SPLICE LOSS, dB		Δ
				MEASURED	TRUE	
1	Initial with M_1	Matched Cladding	2 km Matched Cladding	0.57	0.56	+0.01
2				0.63	0.62	+0.01
1	With M_1	Matched Cladding	2 m Matched Cladding	0.61	0.58	+0.03
2				0.04	0.02	+0.02
1	w th M_1	Depressed Cladding	2 m Matched Cladding	0.60	0.58	+0.02
2				0.03	0.02	+0.01
1	No M_1	Not Applicable[1]	2 m Matched Cladding	0.61	0.59	+0.03
2				0.04	0.02	+0.02
1	No M_1	Not Applicable[1]	2 m Depressed Cladding	0.58	0.58	0.00
2				0.01	0.02	-0.01

Note 1. Bare fiber adaptor used.

The results are contained in Table IV. The data confirm that the test is insensitive to the length of the launch fiber section irrespective of the cladding type used. Therefore, single mode fibers can be tested using launch fibers as short as 2 meters. There was also no variability when the length of the fiber section containing the test splice was reduced to 3 feet.

Having established the technique, the next step was to verify its application. A large number of samples was prepared and the loss changes due to environmental exposures were monitored. The samples represented a variety of mechanical splices and several fusion splices. The results shown in Tables V and VI confirm that the method is very satisfactory.

TABLE V

LIGHTGUIDE SPLICES - TEMPERATURE CYCLING[1]

FIBER	SPLICE	INITIAL SPLICE LOSS, dB	LOSS CHANGE IN dB			
			CYCLE 1	CYCLE 25	CYCLE 50	CYCLE 100
Matched Cladding	1	0.20	-0.10	0	+0.17	-0.20
	2	0.02	-0.06	+0.13	+0.12	+0.13
	3	0.13	-0.12	+0.03	+0.01	+0.86
	4	0.09	-0.09	-	-0.03	-0.09
	5	0.03	+0.34	-	+0.03	+0.15
	6	<0.01	+0.22	+0.10	+0.04	+0.05
	7	0.22	+0.18	+0.06	-0.01	+0.13
	8	0.01	-0.01	+0.07	+0.03	+0.03
	9	0.11	-	-0.11	-0.04	-0.02
	10	0.01	-	-0.01	+0.13	+0.01
	11	0.21	-0.13	-0.01	-0.21	+0.04
Depressed Cladding	12	0.05	-0.05	-0.05	+0.13	+0.21
	13	0.19	-0.18	-0.19	+0.20	+0.31
	14	0.07	+0.08	+0.06	-0.07	-0.07
	15	0.01	+0.18	+0.01	+0.08	+0.03
	16	0.01	+0.18	+0.01	+0.08	+0.05
	17	0.05	-0.02	+0.11	-0.04	+0.01
	18	0.22	-0.03	-0.07	-0.10	+0.19
	19	0.04	+0.22	+0.01	+0.07	+0.05
	20	0.31	-0.08	+0.02	-0.31	-0.31
	21	0.02	-0.02	+0.07	+0.04	0
	22	0.12	-	+0.09	+0.10	-0.09
	23	0.22	-0.06	-0.09	-0.47	-0.46

Note: 1. -40°F to +140°F, 6 cycles per day.

TABLE VI

LIGHTGUIDE SPLICES - ENVIRONMENTAL TESTING

SPLICE	INITIAL SPLICE LOSS, dB	SPLICE LOSS CHANGE IN dB			
		-40°F	+140°F	VIBRATION[1]	WATER SOAK[2]
1	0.20	-0.03	+0.12	-0.16	-0.20
2	0.02	+0.10	+0.09	+0.20	+0.30
3	0.13	+0.25	+0.34	+1.35	+0.04
4	0.01	0	0	-0.10	+0.10
5	0.03	+0.19	+0.38	+0.43	-0.02
6	<0.01	+0.11	+0.08	+0.05	0
7	0.22	+0.11	-0.07	-0.03	+0.02
8	0.01	0	-0.01	0	+0.03
9	0.31	-0.11	-0.31	+0.04	+0.07
10	0.02	-0.01	-0.11	+0.04	+0.07
11	0.12	+0.02	+0.20	-0.09	-0.11
12	0.21	-0.02	-0.01	-0.05	+0.03

Notes: 1. 10 Hz to 45 Hz with a displacement of 0.04 inch and a cycling time of 2 minutes; duration 30 minutes in each direction.

2. At room temperature, 7 days.

CONCLUSIONS

An experimental method that permits continuous monitoring of single mode splice loss has been developed. The procedure is a modified version of the traditional transmission measurement which includes a cutback and substitution steps.

The errors introduced when the fiber ends of a test splice are removed and reinserted at the interconnection points are calculated based on the known values of control splices. It is shown that the correction term for these errors can be determined precisely. By protecting the fiber ends during handling, it is possible to reduce the error to as little as 0.003 dB, which is below the accuracy of the measuring equipment.

A comparison of the measured loss values and the true values shows that a correlation factor R of 0.954 to 0.998 is achieved. It is also demonstrated that bidirectional tests, as well as the determination of losses of splices formed using dissimilar fibers, can be made. Another advantage of the method is that measurements can be performed using fiber sections as short as 2 meters.

ACKNOWLEDGMENTS

The author wishes to thank Dr. R. Gerdes for helpful suggestions, Dr. O. Szentesi (Siecor) for valuable discussions, J. Boyles and G. Dockery for performing numerous measurements, and Corning and AT&T for furnishing the fiber.

REFERENCES

1. J.D. Fridman, F. Gomes, L. Jon, and G.W. Styskal, "Instrumentation for Multichannel Hermaphroditic Connector Evaluation", SPIE, Fiber Optic Technology '82, **326**, 66-73 (1982).

2. J.G. Woods, M.H. Hodge, and J.F. Ryley, Jr., "A Military Six-Fiber Hermaphroditic Connector", Proceedings of the 29th IWCS, (1980), pp. 229-235.

3. F.L. Thiel and R.M. Hawk, "Optical Waveguide Cable Connection", Applied Optics, **15**, 2785-2791 (Nov. 1976).

4. R. Cooper, "Fiber Optic Connector Splice Loss Measurements: The Laboratory Versus the Real World", FOC '81, San Francisco, CA, Sept. 1-3, 1981.

5. T.C. Cannon and T.L. Williford, "High Technology at the Submicron Level", Telephony, pp. 72-79, Nov. 18, 1985.



R. Raman
Contel Laboratories
270 Scientific Drive, Suite 10
Technology Park/Atlanta
Norcross, GA 30092

R. Raman joined Contel Laboratories in 1978. He is currently Senior Materials Evaluation Engineer.

He holds two Ph.D. degrees, one from the Indian Institute of Science, Bangalore, India, and the second from the University of Nottingham, England, specializing in dielectric materials, photoconductivity, and polymer applications. He is engaged in the evaluation of cables and cable components, lightguide splices and connectors, fiber optic closures, organizers, and terminals.

HIGH RESOLUTION OTDR-MEASUREMENT FOR THE QUALITY CONTROL OF LONG FIBER OPTIC CABLES

R. Klar and H. Schoenfeld

Kabelmetal Electro GmbH, 3000 Hannover, West Germany

Summary.

This paper will show that routine quality testing of optical fiber cables is, in our opinion, best done through the well known OTDR technique. A computer-assisted system has been developed for this purpose. It has been in use since 1983 and it represents an essential part of cable testing during and after production. During that time, several improvements have been implemented to match the massive technical progress in the fiber optic cable field. Improved production methods now enable fiber manufacturers to supply fibers with lengths up to 12 km or more on a regular basis. To take full advantage of this development, it is not only necessary to process these fibers as one unit but also to measure them as one single cable production length in such manner that, after dividing into individual sections, these do not need further measurement.

Advantages of the OTDR Measurement.

Although they are well known, it may be useful to summarize the prominent advantages offered by this technique which is specific to optical fibers. No other comparable measurement technique yields so many simultaneous data as does the OTDR.

First of all, it provides information on the spatial distribution of defects and imperfections along the fiber in a manner very similar to the TDR measurements performed on copper cables. Furthermore, we also obtain a picture of the distribution of the attenuation along the fiber and this is perhaps the most exciting property of this technique. However, this applies strictly speaking only if some boundary conditions are considered. For example, we have to take into account the possibility of inhomogeneities and directional dependence of the measurement. One therefore has to recognize that the OTDR measurement is not a true attenuation measurement when compared to the traditional transmission attenuation method like the cut-back procedure. The experience gained during the past years, however, has confirmed the reliability of OTDR-based attenuation values.

A third and very important property is that the OTDR measurement needs to be performed from one end of the fiber only. Everybody involved with fiber optic cables knows how time-consuming it can be to prepare the end of a cable for measurement and to align the fibers for connection to the test equipment. In fact, this point is of fundamental importance to the cable testing department when it comes to savings of cost and time.

State-of-the-Art.

In the field of OTDR measurement, today's market offers the so-called third generation of equipment. A variety of OTDRs with different properties for virtually all imaginable applications are now available. Sophisticated signal conditioning and evaluation, a choice of two selectable wavelengths (1,300 and 1,550 nm), computer interface and a very convenient selection of pulse widths, attenuation, distance and resolution ranges can be considered standard.

Significant improvements have been achieved with regard to distance range, measurement time, signal conditioning and reproducibility.[1] It is no longer surprising to observe a variation of less than 0.01 dB/km in a group of consecutive measurements carried out on the same single mode fiber in either the second or third window.

As far as the fiber properties are concerned, we can record nowadays a high degree of uniformity and homogeneity. The problems encountered in the early days of fiber technology are, as a rule, no longer of any concern.

A particular problem source for the measurement of attenuation, namely the definition and observance of suitable launching conditions, is eliminated as single mode fibers have replaced graded index fibers in most applications. One can also see a remarkable evolution toward longer fiber cable delivery lengths. This fact has an impact on the cable manufacturing process which leads to new technical solutions like the one described in this paper.

Cable Testing.

The quality control of fiber optic cables in our company was based, from the beginning, on OTDR measurements. This is the only measurement carried out on a 100% basis after each production step, starting with 100% inspection of each arriving fiber shipment. The adopted procedures have been described earlier.[1] It should be pointed out, however, that the final testing of the cable also consists of an OTDR measurement, usually performed only from one end of the cable. This could, of course, have been complemented by the measurement from the other end, before jacketing. The tests are made at both wavelengths of interest, in the same operation, if necessary. The results are recorded by a Personal Computer (PC) associated with each OTDR and stored on a diskette. These results comprise not only a complete digital record of the OTDR screen trace with all related parameters, but also the calculated attenuation coefficient. The corresponding diskette file contains the complete records of all fibers in the cable, the applicable cable identification data and also the measurement parameters, such as pulse width and wavelength. The configuration of the test sets and their associated software have been developed in our laboratory. A view of such a test set is illustrated in Fig. 1.



Fig. 1. OTDR test equipment with PC.

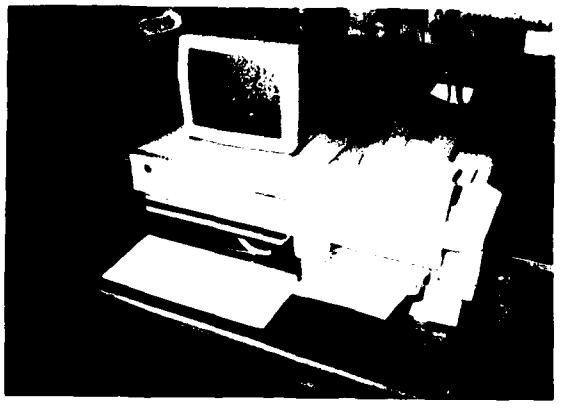


Fig. 2. PC and printer for data analysis of OTDR measurements.

The software guides the operator during the test so as to avoid erroneous fiber selection. The data analysis is, again, done with the help of a Personal Computer, associated with a dot-matrix printer, as shown in Fig. 2.

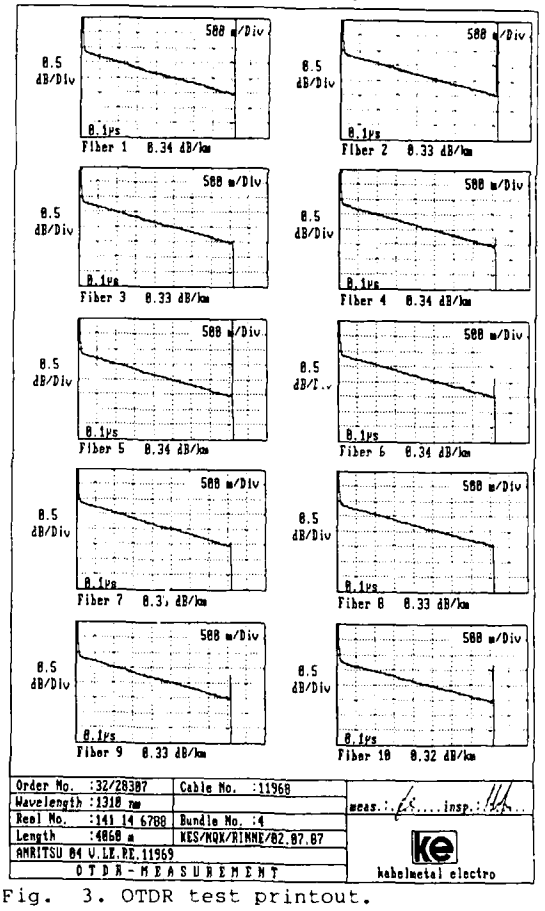


Fig. 3. OTDR test printout.

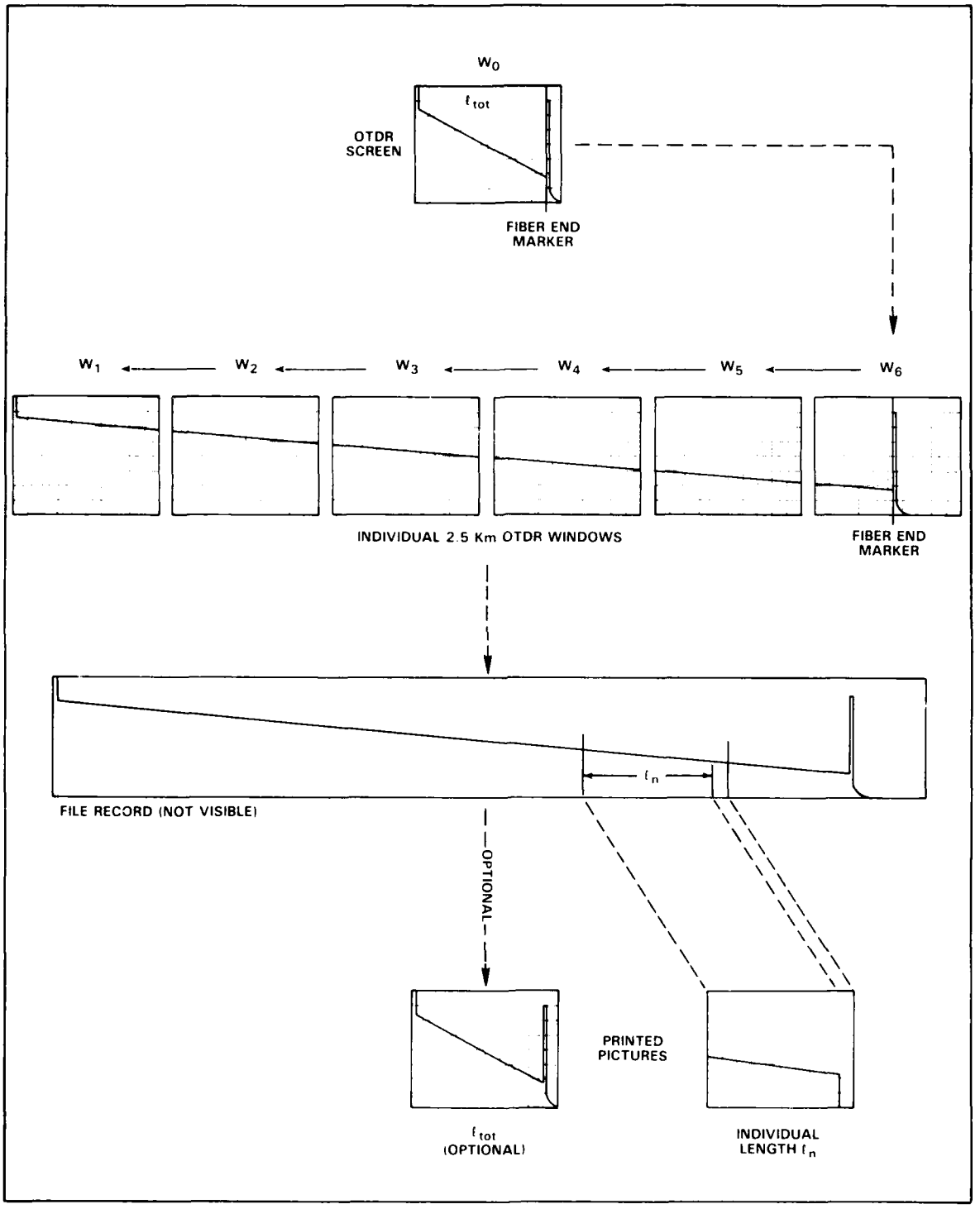


Fig. 4. OTDR measurement sequence.

Ten OTDR screen pictures, making up one page, are printed out together with the corresponding attenuation values and all relevant data pertaining to the order, as shown in Fig. 3. If the screen pictures are not needed, it is possible to print out only the attenuation values. This system has proven itself to be very reliable during the last five years. It had to be adapted, of course, to newer equipment generations and it was improved along with the increased requirements of the test department.

New Requirements.

As already mentioned, present deliverable optical fiber manufacturing lengths are on the order of 12 km. This value is expected to be exceeded in the near future. To take full advantage of this impending development it is necessary to prepare a process, during cable manufacture, that can accommodate the long, uncut cable. On the other hand, cables of shorter length (i.e.: 2 km) will continue to be delivered, depending on installation requirements. In these cases it becomes necessary to cut the long production length into individual delivery lengths.

The great number of expensive and time-consuming tests to ensure quality represents a substantial portion in the overall cost of cable manufacture. One must therefore keep in mind the advantages arising from longer production lengths without sacrificing reliability.

Measurement of Long Cables.

This problem is solved by a measurement performed on the long production cable, using adequately high resolution. After cutting the long cable into individual sections, the corresponding portion of the recorded backscattering trace is identified and printed out separately for each section. This procedure relies on the assumption that cutting does not affect the cable properties. This process obviates the need for measuring each individual cable before shipment. Regardless of the length of the individual sections, we are now able to supply a reliable backscattering record - at least for the majority of the cables - without the uncertainties associated with saturation of the detector at the beginning of the cable. Obviously, the main advantage offered is the substantial reduction of measuring time and resulting increase in throughput which reduces the need for additional measuring capacity. A diagram of the adopted solution is illustrated in Fig. 4.

Basic Considerations.

Until now, the common delivery length was about 2 km or less. Therefore, the measurements were carried out with a 2.5 km OTDR window. The digital resolution of the x-axis is 500 points, which corresponds to 5 m increments. The pulse width has to be selected depending on the needs of the measurements and the capabilities of the OTDR. A commonly used value for factory measurements is 100 ns. This provides adequate digital resolution.

If one has to make a measurement on a 12-km cable with a 20-km window for example, this leads to a 40 m digital resolution. This resolution seems to be unacceptably low because the quality of the backscattering pictures would be degraded by a factor of eight. To solve this problem, a different approach was adopted, whereby the long cable is measured in 2.5-km sections by shifting the OTDR window in successive incremental steps. The individual records are then linked together and stored as a single data file. This method ensures that the required resolution is maintained.

Another important factor is the data analysis after the long cable is cut. One has to carefully read the metering marks at both ends of the delivery length. Both of these values determine the limits for the required portion of backscattering trace and only this part will be printed. It should be mentioned that a part of the responsibility is now shifted from the test team to the supervisor.

Carrying out the Measurement.

The outer end (on the reel) of the long production cable length is prepared for the measurement and then connected, fiber by fiber, to the OTDR as usual. Preparation of the inner end (on the reel) is limited to permit testing the end reflection, so as to ensure the continuity of the fibers. At the same time, the metered readings from both ends are delivered to the input of the Personal Computer.

In the operational mode which allows the viewing of the whole cable length, the fiber is tuned to maximum signal response and the trace is checked for imperfections. At the same time, an overall attenuation coefficient is obtained and stored and the approximate length of the fiber is set manually with a marker. Once this step is accomplished, the 2.5 km OTDR window containing the end of the fiber is set.

The marker is again set to the end of the fiber, thus enabling the computer to calculate the effective apparent index of refraction of the cable.

We have developed the process to the point where, once the procedure is started, the whole measurement sequence is performed automatically. In order to ensure the shortest measuring time for the required signal quality, the software has been optimized to stop the averaging process at the proper time, depending on signal amplitude.

To ascertain that the measurement is transmitted accurately to the PC, each OTDR screen picture is displayed again as a copy on the PC monitor. Small imperfections can be seen at this time. Another point of interest is that the backscattering signal has to be recorded on an absolute scale to get a continuous trace across all windows. Once the process is completed, the OTDR is switched back in 2.5 km window increments and the procedure is automatically repeated until the first section is completed.

All measurements of a fiber at one wavelength are stored as a single record on the diskette and all records of the same cable constitute a single file. It is our practice to treat the measurements of the same cable at different wavelengths as measurements of different cables. Once the measurements are completed, the diskette is sent to the office for analysis.

Data Analysis.

Once the diskette is copied into the files of the data analysis computer, it is stored in the office as a document. The first part of the data analysis is the certification of compliance of the measured attenuation with the customer's specifications. At this point acceptance of the cable by the customer should take place. Depending on the customer's order, the cable may later be cut into individual sections. If this occurs, the analysis continues and the required backscattering records are printed out. For this purpose each part of the printout is first assembled as a graphic display on the computer monitor and then simply printed out as text using standard commands. This significantly simplifies the

The data analysis

advisable to use a Personal Computer with higher speed and a laser printer. For laboratory use, however, simpler equipment may be satisfactory. The software developed for this purpose is compatible for both types of processing.

Future Developments.

The described system has been installed in our test department and has shown itself to be a great improvement. For good vendor-customer relations it is important now to establish that this system is state-of-the-art by proving its reliability day after day. Based on our encouraging experience, we are confident that this will be possible in the near future.

Several future developments are now being investigated. Among these is the integration of this system into the general factory computerization and the replacement of the Personal Computer and diskette attached to the OTDR by a direct link to a central computer. Another interesting development will be an automatic fiber feeding and connecting device suitable for speeding up the measurement and simplifying the work of the operators. A remaining task is the adaptation to newer equipment emerging with technical progress.

Conclusion.

The reasons for selecting the OTDR measurement as the principal measurement technique during and after optical fiber cable production have been explained. A system based on computerized measurement of long cable lengths for final testing is presented. This system

need for the measurement of lengths cut from a

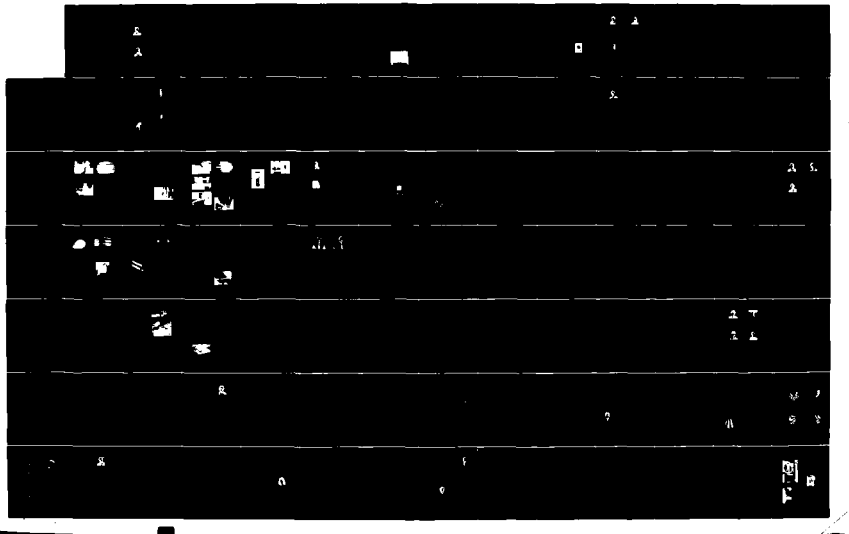
of the procedure have

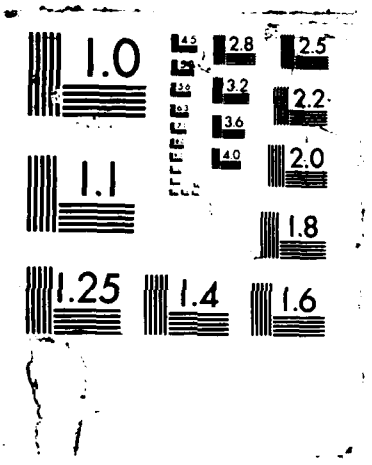
some of the

consideration

AD-A189 610 PROCEEDINGS OF THE INTERNATIONAL WIRE AND CABLE SYMPOSIUM (36TH) HELD IN..(U) ARMY COMMUNICATIONS-ELECTRONICS COMMAND FORT MONMOUTH NJ 2/9

UNCLASSIFIED 19 NOV 87 F/G 9/1 NL




1.0
1.1
1.25
1.4
1.6
1.8
2.0
2.2
2.5
2.8
3.2
3.6
4.0

References.

1. G. Shinn, "Practical Application of OTDR for Cable Measurements", EFOC/LAN 87, Basel, Switzerland, June 1987
2. R.Klar and H. Schoenfeld, "Die Rueckstreumessung als begleitendes Messverfahren bei der Herstellung und Montage von LWL-Kabeln". NTG-Conference on Fiber Optic Cables, Bad Nauheim, FRG, October 1985



Ruediger Klar
Kabelmetal
Electro GmbH
Kabelkamp 20
3000 Hannover 1
West Germany

Ruediger Klar was born in 1941 in Eberswalde (Germany). He graduated in 1969 as a telecommunications engineer from the Hamburg Engineering School. After a 2-year engagement at Siemens in the department of computer-controlled telecommunication exchange systems, he joined Kabelmetal Electro GmbH in 1971 as a software development engineer in the production data systems group. Since 1982 he is responsible for the software of test- and measurement systems in the development of fiber optic cables.



Hans Schoenfeld
Kabelmetal
Electro GmbH
Dept. NKEM
Kabelkamp 20
3000 Hannover 1
West Germany

Hans Schoenfeld was born in 1941 in Madrid (Spain). After graduating from the Ohm Polytechnikum in Nuernberg he joined Kabelmetal Electro GmbH in 1966, where he has been engaged in the field of telecommunication cables development. As a group leader he is currently responsible for fiber optic measurement techniques and systems considerations. He is a member of several German standardization working groups.

HETERODYNE-OTDR: THE LONG WAVELENGTH, LONG RANGE SOLUTION

JOHANNES RYBACH
Philips Kommunikations Industrie AG
Cologne, West Germany

SIEGFRIED HECKMANN
Philips Kommunikations Industrie AG
Cologne, West Germany

MANFRED FUCHS
Philips GmbH Forschungslaboratorium
Hamburg, West Germany

ERNST BRINKMEYER
Technische Universität
Hamburg-Harburg, West Germany

Abstract

By means of heterodyne detection the sensitivity of OTDRs can be increased considerably. Problems concerning source bandwidth, optical system attenuation and long-period fading effects could be solved. The newly developed field-portable HOTDR opens ultra long measurement range.

Introduction

The first Optical Time Domain Reflectometer was demonstrated just in 1976[1] and the first commercial OTDR was available only ten years ago[2]. Nevertheless this fiberoptic instrument has proved to be extremely valuable for simple and quick measurements of optical cable transmission characteristics (e.g. attenuation, splice loss, fault location).

Its basic idea is to launch a short light pulse into one end of the fiber under test. The fiber response, composed of reflections and backscatter, is measured, time-resolved, and then analysed until the signal is buried in noise. OTDR measurement range, that means optical one-way dynamic range, is usually specified for SNR=1.

Nowadays the "second window" of silica fibers at 1300 nm is widely used for long haul communication. This has been a challenge for OTDRs, because - compared to the "first window" at 850 nm -

- Rayleigh backscatter level decreases by the forth power,
- detector sensitivity is inferior by at least 10 dB,
- semiconductor laser power is lower by at least 20 dB,
- coupling to single-mode fibers mostly used at long wavelengths causes additional losses.

Technological progress, especially computer-based fast averaging, has helped compensating for these physical difficulties in part. However, with the general introduction of the "third window" at 1550 nm, the sensitivity requirement for OTDRs will be increased further.

Heterodyne Detection

In a previous paper[3] we demonstrated that the best way to overcome the noise limitation of current instruments is coherent detection.

Up to now OTDR detectors resembled radio

receivers from the early days of radio engineering: the first stage of technical development was based on direct detection.

Thereafter the so-called superhet receiver improved radio sensitivity considerably.
The essence of all coherent detection schemes is to mix the weak received signal wave with a higher power locally generated wave from the local oscillator (LO). Applying a nonlinear detector causes a cross-product term in the detector output which contains the phase and the amplitude of the signal.

Most attempts to create a coherent OTDR were made by using the heterodyne technique[4,5,6]. A general block diagram of a Heterodyne OTDR (HOTDR) is shown in fig. 1.

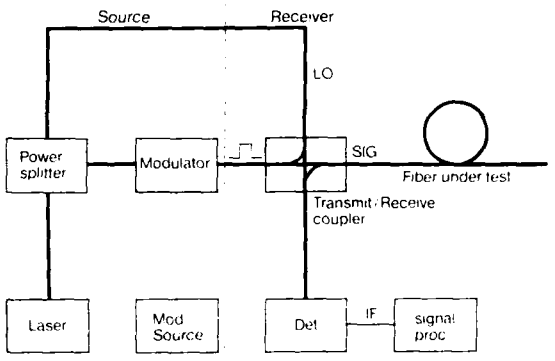


Fig. 1. Schematic of Heterodyne OTDR

The probing wave and the LO wave are derived from the same continuous wave laser.A probing pulse can be sent into the fiber by light gating with the help of an acoustooptical modulator (AOM). Thereby the excitation wave is additionally frequency shifted. When mixing the backscatter signal with the LO a cross-product term corresponding to the modulators acoustical frequency (e.g. 100 MHz) will be produced by the photodiode [3]:

$$I_{PD} \sim \frac{1}{2} P_{LO} + \frac{1}{2} P_{SIG} + \sqrt{P_{LO} \cdot P_{SIG}} \cos(\omega_{IF} t - \phi_{IF})$$

with P: Power of LO and signal wave, respectively,

ω, ϕ: frequency and phase of the beat or intermediate frequency term.

This IF-signal carries the complete backscatter information.

The main advantages of the heterodyne principle can be concluded straight from the formula:

- The backscatter signal is amplified by the LO.
- The backscatter signal is proportional to the square root of optical power only, so that the electrical dynamic range is compressed to the half.

On the other hand some complications arise which are typical for coherent detection schemes:

- The optical waves must have sufficient coherence properties in order to get a stable IF signal with narrow bandwidth. Therefore the HOTDR source must have an extremely narrow spectrum during measurements.
- Heterodyne detection is polarization and phase-sensitive. In worst case the beat signal even vanishes.
- The optical system configuration is comparatively complicated. Moreover bulk optical components are inevitable. The additional loss must be minimized in order not to compensate the heterodyne sensitivity advantage.

HOTDR Optical System

Our solutions concerning these principal HOTDR difficulties are schematically summarized in Fig. 2 and will be discussed in detail hereafter.

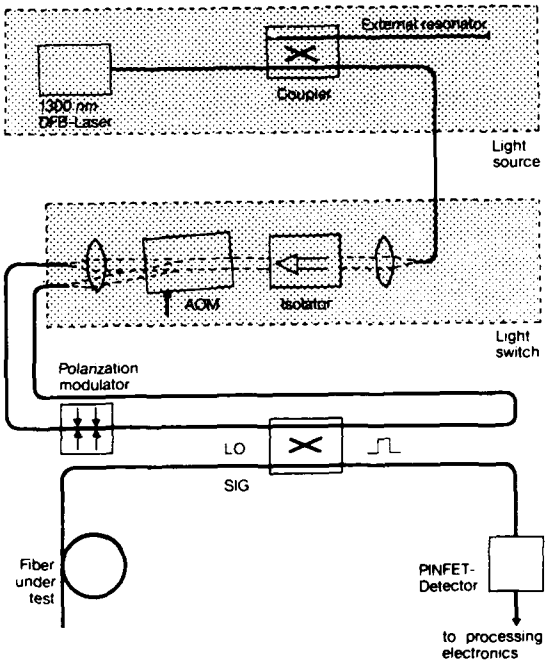


Fig. 2. HOTDR optical system

1. Source

To meet the essential HOTDR requirement (bandwidth < 1 MHz) a line-narrowed laser was developed based on a semiconductor DFB-LD. For that purpose an external resonator was built including a fiber coupler and a short length of fiber with an integrated mirror. Variations of the mirror reflectivity and the coupling ratio yielded minimal linewidth ranges as shown in fig. 3.

2. Light switch

For pumping the detector and excitating the test fiber with the same light source a fast switch is necessary. This was realized by means of an acoustooptical modulator (AOM). Light radiated upon the AOM and meeting the bragg condition is deviated from straight passing when the acoustic wave is activated. Simultaneously light frequency is shifted amounting to the acoustic frequency due to the doppler effect.

In this manner probing pulses in the microsecond-range can be produced and sent into the fiber under test (see fig. 2). When the AOM is deactivated the laser light passes to the detector. Fig. 4 shows a schematic of the newly developed light switch.

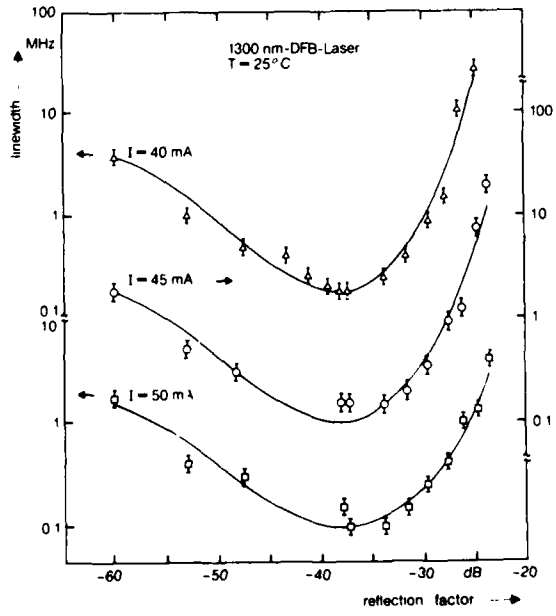


Fig. 3. Laser linewidth as a function of reflection factor

The construction of such a device designed for single mode fibers is rather sophisticated because:

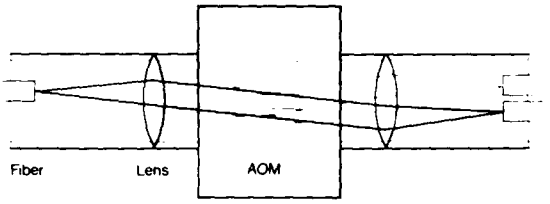


Fig. 4. Schematic of the light switch

- coupling of the bulk AOM crystal to the fibers must be done by lenses although typical bragg angles amount to only 1 degree. This complicates beam separation in a compact instrument component.

- In production and adjustment sub-micrometer precision is required. Coupling loss has to remain minimal even under field conditions.

- Both internal reflections and strong optical signals out of the test fiber may disturb the source spectral purity. Therefore special precautions including an optical isolator are taken.

In spite of these complications the entire attenuation of the light switch - including coupling and insertion losses, AOM diffraction efficiency etc. - is only about 5 dB.

3. Phase- and Polarization Scramblers

The scattered light returning from the fiber under test contains all states of phase and polarization. Moreover, certain fiber sections, e.g. in buried cables, may be "frozen in" concerning phase and polarization. This results in bad or even missing beat signals.

A typical heterodyne backscatter trace from one single measurement is shown in fig. 5. The coherent backscatter signal behaves like an inhomogeneous noise signal [8], each pulse response having such a speckle-like appearance.

Thus signal averaging is essential for the HOTDR. To achieve reasonable measuring times in spite of long-period coherent fading [7] active scrambling of phase and polarization is necessary.

Statistical phase variations between signal and LO wave are achieved by small and slow chirps of the laser frequency. These must carefully be tuned to preserve short-term coherence, but, on the other hand, to attain smooth backscatter traces after short average time.

Polarization scrambling is done by means of a mechanical fiber squeezing device. Theoretical studies and experimental investigations proved only two linear polarization retarders being able to regulate any state of polarization (SOP). Accurate timing with averaging periods results in nearly complete elimination of polarization fading. Insertion loss of such an device is only 0.05 dB.

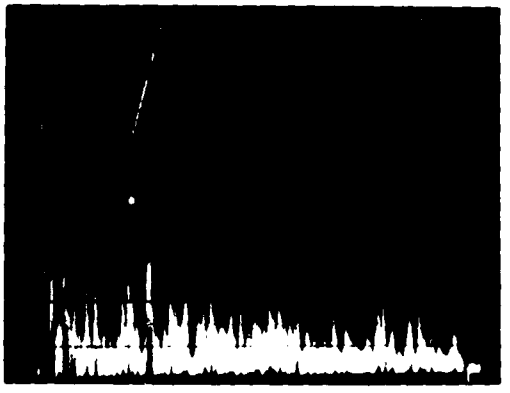


Fig. 5. Typical HOTDR backscatter signal without averaging

Heterodyne Signal Processing

Signal processing in an HOTDR comprises first and second detection of the heterodyne beat signal, fast averaging and data preparation for waveform evaluation.

First detection, that means beat signal optical to electrical conversion, is done by a PINFET receiver adapted to the IF bandwidth. After filtering, the IF signal is demodulated at the second detector. The squared demodulator output is processed in conventional manner.

To gain full advantage from heterodyne detection it is necessary to fit the data processing unit to the ultra long range feasibilities. Therefore a real-time averager was developed capable of accumulating unlimited numbers of backscatter traces.

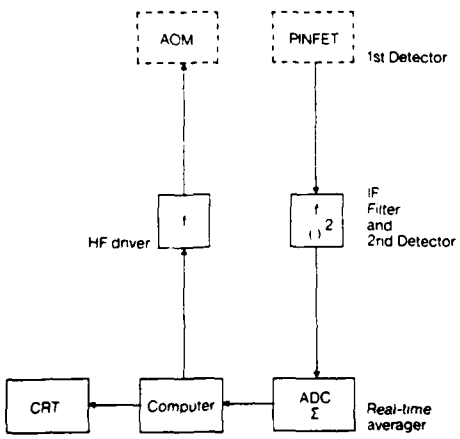


Fig. 6. HOTDR signal processing unit

In fig. 6 the system configuration is schematically shown. Distance ranges up to 400 km can be processed in 40% parallel channels with cycles up to some MHz. Extension of optical one-way dynamic range through improvement of SNR amounts to 2,5 log (m) dB with m: Measurement repetition number.

With an HOTDR measurement range can be extented further, if necessary, through ultra long pulses. Optical gating allows optional puls width, limited only by distance resolution decrease.

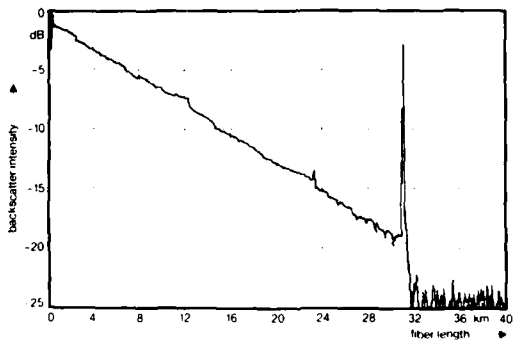


Fig. 7. Typical averaged HOTDR backscatter trace measured with 1 us pulswidth

In fig. 7 a preliminary result of an HOTDR measurement is demonstrated. Though pulse width was only 1 µs corresponding to a distance resolution of 100 m, more than 30 km of single-mode fiber could be analysed without limiting noise.

Gain-Loss Analysis

The principal HOTDR advantage can be calculated from the heterodyne receiver sensitivity compared to direct detecting receivers, but must be contrasted against additional losses due to the more complicated optical system.

Conventional detectors sensitivity at long wavelengths is limited by shot noise owing to photodiode dark current. Therefore the minimal directly detectable power P_{min} is given by:

$$P_{min} = \sqrt{2 \cdot e \cdot I_d \cdot B / r}$$

With e: atomic charge
I_D: detector dark current (1...10 nA)
B: receiver bandwidth (typ. 1 MHz)
r: detector conversion factor (typ. 0.7 A/W)

P_{min} theoretically amounts to -71 ... -76 dBm, depending on dark current. Best experimental result for an uncooled receiver was -73 dBm [9].

However, for a coherent receiver pumped with sufficient LO power all internal noise sources are insignificant. This leads to a performance only limited by the signal noise itself. Thus P_{min} is given by [10]:

$$P_{min} = h \cdot \nu \cdot B / \eta$$

With h: Plancks constant
ν: optical frequency
η: quantum efficiency (typ. 0.7)

For 1300 nm the minimum detectable power of heterodyne signals is -97 dBm, leading to a gain of 24 dB.

The one-way dynamic range L of an OTDR can be estimated by summation of all limiting quantities, resulting in SNR = 1 or 0 dB [8]. These are: Laser power P, backscatter coefficient R [11], receiver sensitivity P_{min}, instrument internal attenuation C and SNR-improvement by averaging SNRI:

$$L = \frac{1}{2} (P + C + R - P_{min} + SNRI)$$

The internal losses are composed of launching losses C_l and detection losses C_d. Table 1 shows a comparison of OTDR and HOTDR one-way ranges.

The HOTDR suffers from extra launching losses due to the light switch. As a detection loss, a mixing penalty of 3 dB appears due to the random polarized backscatter signal.

		OTDR	HOTDR
C_l	: launching loss	- 4 dB	- 9 dB
R	: backscatt. coeff.	- 55 dB	- 55 dB
C_d	: detection loss	- 4 dB	- 7 dB
P_{min}	: detection limit	- 73 dB	- 97 dB
L	: one-way range	$\frac{1}{2}$ (P + 10)	$\frac{1}{2}$ (P + 26)

Table 1: Comparison of conventional and heterodyne OTDR one-way dynamic ranges

Nevertheless, assuming equal laser power, pulswidth and SNR improvement, the heterodyne net gain for our system leads to an 8 dB better one-way measurement range.

At present investigations are in progress concerning the optical system. When using the light switch as a four-fiber coupler, another 2 or 3 dB advantage seems to be within reach.

Conclusion

Though research on heterodyne detection in OTDR started as early as 1982, fundamental problems concerning source bandwidth, system attenuation and backscatter trace smoothing remained up to now.

Our solutions presented in this paper are completely integratable into a ruggedized and field-portable instrument. The net advantage of heterodyne detection amounts to 16 dB.

The better HOTDR dynamic range can be even more increased by specially adapted real-time averaging. Furthermore pulswidth is principally unlimited. Thus measurement ranges better then 30 dB are possible.

Acknowledgement

This work has been supported under the technological program of the Federal Department of Research and Technology of the FRG. The authors alone are responsible for the contents.

References

1.)..M.K. Barnoski and S.M. Jensen, "Fiber waveguides: A novel technique for investigating attenuation characteristics", Appl. Opt., vol. 15, pp. 2112-2115, 1976

2.) Typ OFBM-2000, for example, was presented in 1977 by F & G Carlswerk AG, one of the predecessors of Philips Kommunikations Industrie AG

3.) S. Heckmann, J. Rybach, E. Brinkmeyer, R. Knöchel, "The future of optical time domain reflectometry: utilization of the coherent detection technique", Proc. Int. Wire & Cable Symp., 1985, pp. 125-134

4.) P. Healey and D. J. Malyon, "OTDR in single-mode fibre at 1.5 µm using heterodyne detection," Electron. Lett., vol. 18, pp. 862-863, 1982.

5.) S. Wright, K. Richards, S.K. Salt, and E. Wallbank, "High dynamic range coherent reflectometer for fault location in monomode and multimode fibres," in Proc. 9th Eur. Conf. on Optical Communication, 1983, pp. 177-180.

6.) E. Bodtker, B. Tromberg, "Heterodyne OTDR at 0,82 µm", Electron. Lett., vol. 19, pp. 361-362, 1983.

7.) P. Healey, "Fading in heterodyne OTDR", Electron. Lett., vol. 20, pp. 30-32, 1984.

8.) P. Healey, "Review of long wavelength single-mode optical fiber reflectometry techniques", J. Lightw. Technol., Vol. LT-3, No. 4, pp. 876-886, 1985.

9.) P. Healey and D. R. Smith, "OTDR in single-mode fibre at 1.55 µm using a semiconductor laser and p-i-n FET", Electron. Lett., vol. 18, pp. 959-961, 1982.

10.).R. Knöchel, S. Heckmann, J. Rybach, E. Brinkmeyer, "Optical time domain reflectometry using the heterodyne principle", Proc. Laser / Opto-Elektronik, 1985.

11.) E. Brinkmeyer, "Backscattering in single-mode fibres," Electron. Lett. vol. 16, pp. 329-330, 1980.



Johannes Rybach studied at the Universities of Cologne and Düsseldorf and received the Diplom degree in 1976, the Dr. rer. nat. degree in 1982, both in physics. From 1976 to 1984 he was a Research and Teaching Assistent at the Physikalisches Institut in Düsseldorf where he worked on lasers and optical diagnostic methods. Since 1984 he has been with Philips Kommunikations Industrie AG, where he is engaged in R&D on line-narrowed lasers and optical measuring equipment.



Siegfried Heckmann studied at the University of Bochum and graduated in 1978 in electrical engineering. 1983 he obtained his doctorate at the University of Wuppertal on the basis of his thesis on a subject taken from the field of communication engineering. Since 1983 he has been active as group leader with Philips Kommunikations Industrie AG, where he is responsible for the development of optical measuring equipment.



Manfred Fuchs studied at the Universities of Clausthal-Zellerfeld and Göttingen where he received the Diplom degree in physics in 1981 and the Dr. rer. nat. degree in 1985. From 1979 to 1985 he worked at the Max-Planck-Institut für Strömungsforschung in Göttingen on problems concerning laser excitation of molecular beams. He joined the Philips Forschungslaboratorium Hamburg in 1986 where he is involved in research on Optical Time Domain Reflectometry and Optical Sensors.



Ernst Brinkmeyer received the Diplomphysiker and the PhD-degree from the Faculty of Physics of the University of Göttingen, Germany, in 1973 and 1976, respectively. Up to that time he worked on problems concerning shock waves and cavitation. Subsequently, he joined the Electrical Engineering Department of the University of Wuppertal, where he was involved in experimental and theoretical work on optical waveguides. Since 1983 he is a Professor for Technical Optics at the Technische Universität Hamburg- Harburg.

OTDR AUTOMATION - METHODOLOGY AND RESULTS

Lindwood Bird
Wesley Miller

Corning Glass Works
Wilmington, North Carolina

Stuart Saikkonen

Corning Glass Works
Corning, New York

Abstract

Computer automation of an Optical Time Domain Reflectometer (OTDR) for the detection and quantification of point defects and for optical length measurements has been done and is being used in a fiber manufacturing environment. Experiments were done to ensure that the measurement results from the computer automated methods were at least comparable to those using pre-existing manual methods.

This paper details the results and benefits of this automation and the general measurement logic and algorithms that were used. This automation was designed to meet the exact needs of a fiber manufacturing facility using specific equipment, but similar benefits could be realized if implemented on different equipment and for cabling or field applications.

Background

For an accurate and precise measurement of point defects, the techniques that must be used for standard OTDR measurements require that the operator do many specific operations and make judgments. These include peaking of the OTDR fiber trace, inspection of the fiber on the appropriate scale and placing of cursors. Additionally, they include pulse width selection, end cut preparation, connecting the correct end of the fiber to the OTDR, ensuring correct end reflection height and so on.

Because this measurement is critical to fiber inspection, it was decided to computer automate this measurement to make it more user-friendly with operator prompts and self-checking to ensure proper OTDR setup. The automation was also done to remove operator judgment and simplify repetitive operator procedures when using an OTDR.

Equipment

The automation results presented in this paper were from an OTDR having a pulse width of 2500 nanoseconds (250 meters), an approximate data spacing of 50 meters and a recommended minimum end reflection height of 3 dB. With minor software changes, another OTDR was successfully tested that had a pulse width of 50 meters, a data spacing of 12.5 meters and no recommended end reflection height. Both OTDR's communicated by an IEEE-488 interface bus to the computer.

Measurement Methods

The following measurement methods were used in this experiment to quantify the magnitude of point defects:

Delta Method (manual): This is a manual method of measuring attenuation across a point defect and requires that an operator position the cursors at the two "break" points (A and B in Figure 1) of the defect. Because the OTDR will show a point defect on the trace as having a length at least equal to the OTDR pulse width, a loss measurement using this technique will include the intrinsic fiber loss between the two cursors. This will exaggerate the apparent loss measured for a point defect. For example, a 250 meter OTDR pulse width would add 0.1 dB on a 0.4 dB/km fiber.

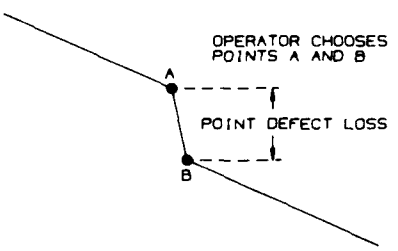


FIGURE 1. DELTA METHOD

Auto-Splice Method (manual): This method is internal to the specific OTDR used. The operator positions the cursor in the approximate middle of the point defect. The internal OTDR software then determines the "break" points of the defect and fits straight line segments to the trace segments both before and after the point defect. The OTDR uses the vertical drop between these two line segments to determine point defect or splice loss. This method is shown in Figure 2. This method does not include the fiber's intrinsic loss, and is a more accurate representation of the loss due to a point defect than the Delta Method.

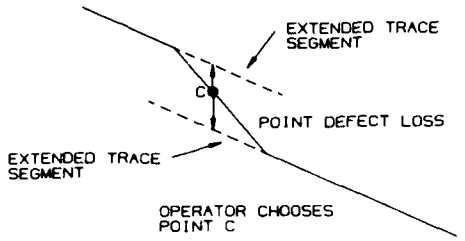


FIGURE 2. AUTO-SPLICE METHOD

Automated Method: This method is similar to the Auto-Splice Method except that the point defect loss measurement algorithm is stored in an external computer and point defects are located and measured automatically. This computer algorithm will be detailed later.

Experiment Design and Results

An experiment was run to compare all three methods of point defect loss measurement. Also, length measurements were compared between operator and computer controlled methods. All manual measurement methods were performed by one technician to reduce operator dependence for these measurement techniques. Fifty fibers were selected so that all possible fiber lengths and point defect sizes and locations were represented. All measurements were done bi-directionally. Twenty of the fibers were measured for point defects an additional two times to determine measurement repeatability.

Fifty fibers were used to compare measurement methods and to ensure that the Automated Method of point defect detection and quantification was equivalent or better than the manual measurement methods. In all cases, the automated algorithm was able to detect and quantify the point defects.

All three point defect loss measurement methods are capable of reliably discerning large point defects (equal to or greater than 0.4 dB); however, the detection of small point defects is of the greatest interest to a fiber manufacturing facility. Because the inclusion of the large defects in the analysis tended to hide meaningful results as applied to the smaller point defects, the following comparison analysis between measurement methods was only done for small point defects. (Small point defects being arbitrarily defined as less than 0.4 dB.) Table 1 details the results of this comparison for point defects of less than 0.4 dB.

Table 1

(N=28)

Method	|Δ Loss| (End-to-end) [dB]		Δ Loss (Manual-Automated) [dB]	
	Average	Sigma	Average	Sigma
Delta	0.037	0.036	0.087	0.044
Auto-Splice	0.016	0.015	-0.014	0.024
Automated	0.022	0.018	N.A.	N.A.

The first two columns of Table 1 represent the absolute differences between the point defect loss values as measured from one, then the opposite fiber end. There was no significant statistical difference end-to-end between the Auto-Splice and Automated Method. The Delta Method of measurement showed the greatest end-to-end difference and sigma. This was attributed to operator judgment in the positioning of the two cursors as required for this method.

The third and fourth columns in Table 1 show the differences of the point defect loss values between the Delta and Auto-Splice (manual) Methods versus the Automated Method. The difference between the Delta Method and the Automated Method is explained by the intrinsic loss of the fiber. Most defects appeared to be about 250 meters long because of the OTDR pulse width, and the average fiber attenuation was about 0.35 dB/km giving an average calculated intrinsic loss of 0.085 dB between the two cursors using the Delta Method. Although the Automated Method appears to measure point defects slightly larger than the Auto-Splice Method, this difference was not considered statistically significant.

The measurement repeatability of measuring point defects was checked by measuring 20 fibers three times each. Each individual measurement was bi-directionally averaged. The Delta Method was used for comparison because it was considered to be the most operator dependent and potentially the least repeatable. Table 2 shows that the measurement repeatability of the Automated Method is almost twice as good as that of the Delta Method. The better measurement repeatability is attributed to the automatic checks that are done for each fiber setup to ensure proper fiber peaking and to the consistency of cursor placement that occurs when the point defect measurement was automated.

Table 2

Method	(N=20) Sigma [dB] (All fibers)	(N=12) Sigma [dB] (Fibers with point defects <= .4 dB)
Delta	0.052	0.019
Automated	0.025	0.011

Both, the operator controlled and computer controlled method of optical length measurement, were performed using the OTDR manufacture's recommendations for cursor placement and end reflection height. The results using these two methods are shown in Table 3.

Table 3

(N=50)

Method	Δ length [m] (End-to-end)		Δ length [m] (OTDR-mechanical)	
	Average	Sigma	Average	Sigma
Operator Controlled	2.76	3.33	-2.50	9.92
Computer Controlled	0.93	1.04	2.45	8.17

The first two columns in Table 3 show the absolute difference in meters (m) of fiber length as measured in each direction. This shows that the repeatability for the computer controlled length measurements is better than for operator controlled length measurements. The last two columns show the difference in length measurement between the two OTDR measurement methods and a mechanically metered length as obtained by a winding machine. As the average fiber length was 8 km for this experiment, the average OTDR versus mechanically measured length difference represents a total measurement error, for either OTDR method, of about 0.03 percent. Therefore, there were considered to be no practical differences between the operator and computer controlled methods of measuring fibers for optical length.

Automation

General

The OTDR was made user-friendly by adding operator prompts, automated setup checks and defect and length determination automatically performed by the computer. The general outline of the computer and operator interface is:

I. The computer prompts for operator inputs of:

- A. Identification of fiber.
- B. Effective Index of Refraction
- C. Mechanically metered fiber length.
- D. Type of Measurement (Standard bi-directional or single-ended)

II. The computer prompts the operator to load the proper fiber end and to power peak the fiber trace.

III. The operator:

- A. Cuts fiber ends.
- B. Connects the proper fiber end to the OTDR
- C. Optimizes the fiber connection for the highest noise-free trace on the OTDR screen. (Defined as peaking the fiber).
- D. Confirms that the far end reflection is greater than a minimum value.
- E. Lets the computer know when the previous four steps are completed.

IV. The computer:

- A. Automatically measures the fiber for length and point defect sizes and locations. (This will be detailed later.)
- B. Notifies the operator on the CRT if a point defect is found or the optically measured length does not agree with the mechanically measured length.

C. Prompts the operator to request a plot if a point defect is found.

D. Prompts for measurement of the other end of the fiber when required.

The following details the steps that the computer follows in making a automated check of a fiber for length and point defects.

I. Premeasurement check

This check is done by the computer to confirm that the optical connection is sufficiently optimized by checking that the fiber trace is properly power peaked. The power trace is checked at a position about 2000 meters from the measurement end of the fiber to see that the power level is greater than a predetermined minimum value. This distance is past the non-linear region of the OTDR trace that is caused by connector reflection and detector saturation. This check shows that the fiber connection to the OTDR is correctly optimized and the fiber end cut is good.

II. Data Collection

Because all calculations for length and point defects are done external to the OTDR, the data array must be transferred to the computer. This array is a two dimensional (X,Y) array describing the OTDR trace. The X coordinate contains the distance along the fiber corrected for the fiber's effective index of refraction and the Y coordinate contains the OTDR measured power expressed in dB.

III. Location of the fiber end and determination of optical length

The fiber is checked for an end reflection by testing successive 250 meter sections of the trace from right to left, starting in the noise floor of the OTDR trace beyond the fiber end position. This is shown in Figure 3. When the average power of two adjacent 250 meter sections differs by more than 7 dB, a search area of +/- 500 meters around the last section checked is defined. Each individual data point in this search interval is then checked and the data point having maximum power is chosen to be the local maximum.

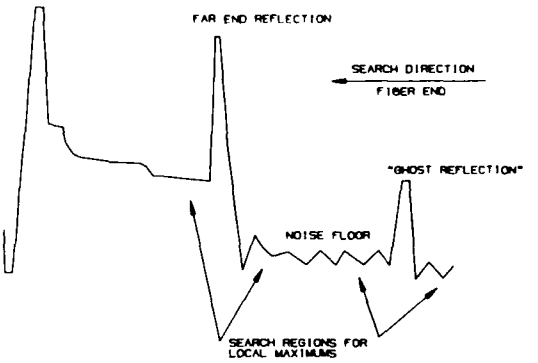


FIGURE 3. LOCATION OF FIBER END

An OTDR trace can have a "ghost" reflection if the end reflection pulse is echoed from the measurement end of the fiber. This "ghost" reflection is found at twice the fiber length. The local maximum is checked to see that it is not a "ghost" end reflection by dividing the distance to the local maximum by two and searching for another local maximum in an analogous manner to the technique stated above.

A predetermined position on the OTDR trace, relative to the local maximum, is used to calculate fiber length. This position is usually recommended by the particular OTDR manufacturer.

IV. Determination of the fiber inspection region for point defects

The OTDR trace is inspected for point defects in a search region bounded by a search start and a search end position as shown in Figure 4. This search region excludes the end reflection and the beginning non-linear region of the trace. The beginning non-linear region of the OTDR trace is excluded from the search region because the detector saturation obscures point defects in this section of the trace. Even if a point defect can be seen in this region, the detector saturation precludes accurate measurement of that defect. It is for this reason that fibers are normally measured for point defects in both directions in a fiber manufacturing environment.

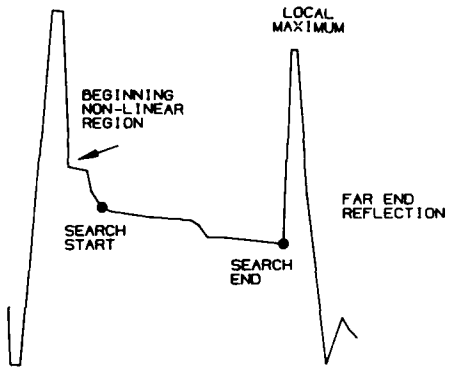


FIGURE 4. DETERMINATION OF FIBER INSPECTION REGION

The trace search end position is determined by searching a 500 meter section to the left of the local maximum for the minimum power point. At this time the computer checks for a proper fiber endcut. The difference between the power at the local maximum and the power at the trace search end position must be a specified minimum value. If it is less than that required value, the operator is prompted to re-cut the fiber far end and restart the fiber measurement.

The trace search start position for point defect detection is chosen by comparison of the slopes of five consecutive trace segments, as shown in Figure 5. The initial starting point to test for linearity is chosen at 1200 meters. Each trace segment is 250 meters long and is separated by 50 meters. Comparing the slope of the first line segment to the other four slopes and stepwise testing either backwards or forward in 50 meter increments, the first linear starting point is determined that ensures the maximum amount of fiber is inspected for each measurement.

V. Calculation of the error array and location of point defects

A normalized error is defined as:

$$E(I)=Y(I)-YN(I)$$

Where Y(I) is the measured power and YN(I) is the normalized power along the OTDR trace at the I'th data point. In addition, a three-point smoothing is done on the error array before defect location, to reduce the OTDR trace noise.

The filtered error array is then used to calculate slopes along a 250 meter line segment, each segment separated by 50 meters. Consecutive slopes are compared and when three consecutive slopes are found that met a minimum criteria, the location is then checked for inflection points. If starting and ending inflection points are found, then that location is marked as having a point defect and the defect start and end positions are defined.

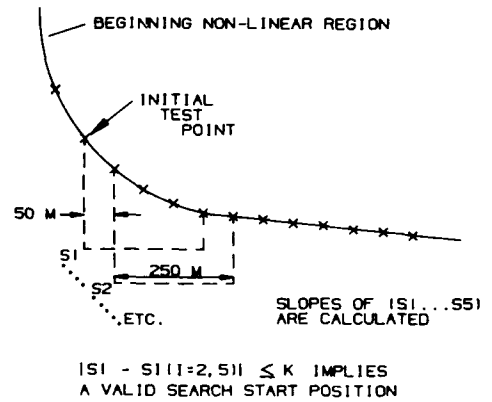


FIGURE 5. SEARCH START POSITION DETERMINATION

VI. Quantification of point defects

Each point defect that has been detected has a start of defect and end of defect location defined. This information plus the trace search start and end locations is used to determine the point defect size as shown in Figure 6. Between the search start or the previous defect end and the defect start, a least squares fit line is calculated. A similar least squares fit line is calculated between the defect end and the next defect start or the search end position. The point defect size is determined by the vertical distance as measured between these two extended lines. All calculations are done on the (X,Y) data array without data smoothing.

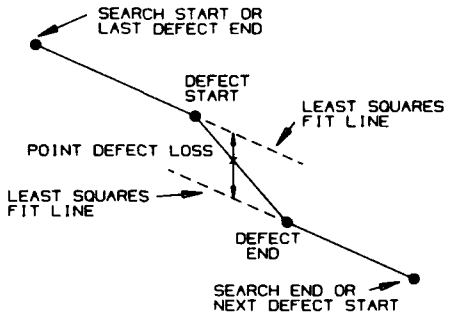


FIGURE 6. AUTOMATED METHOD

Summary

The user-friendly OTDR automation has proven itself in a fiber manufacturing environment with nine months of operation. Because each measurement is computer prompted and checked for proper fiber setup, the OTDR is a more controlled measurement station. Measurement repeatability is a factor of two better with OTDR automation. Measurement accuracy and precision is no longer operator dependent for scaling, cursor positioning and fiber setup.

Authors



Lindwood Bird is the Quality Engineering Supervisor at Corning Glass Works' optical fiber manufacturing facility in Wilmington, North Carolina. His current responsibilities include the design of quality systems and quality enhancement projects. Previous responsibilities have been the development of optical fiber manufacturing equipment and processes. Mr. Bird received a M.S.E.E. from Renssalaer Polytechnic Institute in Troy, New York, in 1974.



Wesley Miller is a Quality Statistical Technician at Corning Glass Works' optical fiber manufacturing facility in Wilmington, North Carolina. His current responsibilities include data analysis, experimentation, and quality enhancement projects. Since joining Corning in 1980, his responsibilities have included troubleshooting and maintenance of optical fiber measurement equipment. Mr. Miller received a A.A.S. degree in Specialized Electronics Technology BMET from United Electronics Institute in Louisville, Kentucky, in 1980.



Stuart Saikkonen currently is a Senior Product Engineer with Corning's Telecommunications Products Division in Corning, New York. His responsibilites include the specification, qualification, and certification of Corning's dispersion non-shifted single-mode fiber and fiber measurements Prior to his current position, he was responsible for process development, equipment design, and product testing for optical fiber fusion splicing. Mr. Saikkonen received a B.M.E. degree from Rochester Institute of Technology in 1981.

Acknowledgments

The authors would like to thank Carson Benson, Steve Friedl, and Jerry Nease for their technical contributions, time, and support for this project and paper.

INTERFEROMETRIC MEASUREMENT OF CABLE THERMAL EXPANSION

M.S. O'Sullivan
R.S. Lowe
C. Saravanos

Northern Telecom Optical Cable Division
Saskatoon, Saskatchewan

ABSTRACT

In order to optimize the design of a fiber optic cable, knowledge of its thermal expansion characteristics is essential. In the past, these were predicted from the thermal expansion of the individual cable components, rather than the finished product, either at room temperature or over a wide temperature range. Since the thermal characteristic of these components can be affected by processing, such a prediction is prone to error. In this paper, we present a direct measurement of the thermal expansion characteristics of composite optical cable by using a Fabry-Perot interferometer. With this technique, the cable elongation can be measured to within $\pm$ 0.005% for a 30 cm long cable sample. Results will be presented which show that the thermal expansion coefficient can be as much as 2.5 times larger at low temperature than at room temperature.

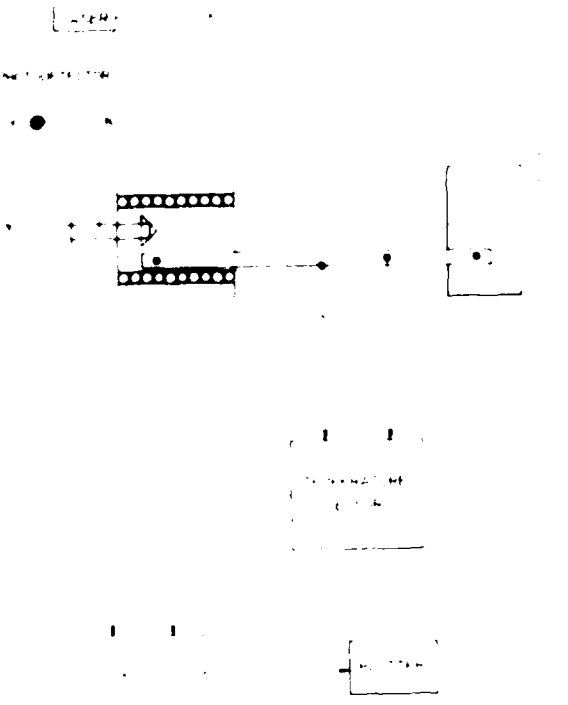
INTRODUCTION

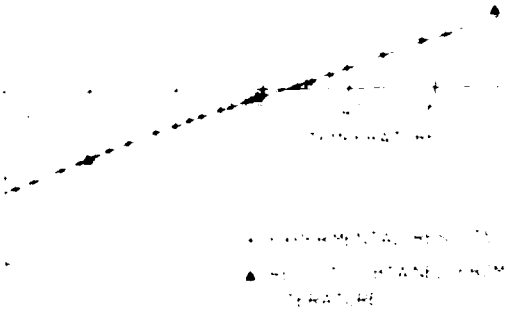
The attenuation characteristics of optical fibers can be strongly influenced by the contraction or expansion of the fiber optic cable materials that surround them. These effects can degrade the optical characteristics of the fibers, if the length change of the cable due to temperature variations is larger than the allowable strain window. To a certain extent, consideration of these thermal expansion effects can be incorporated during the design stage, both through appropriate material selection and by choosing a cable structure with geometrical characteristics that permit the fiber to remain relatively unaffected by either expansion or contraction of the cable. However, to fully characterize the completed product, it is important to develop an accurate and simple technique to measure the thermal expansion characteristics of the optical cable itself that does not rely on indirect measurements of the individual components whose temperature performance may be quite sensitive to the conditions under which the cable was manufactured.

EXPERIMENTAL APPARATUS

Elongation measurements on short cable lengths can be determined accurately with the use of interferometric metrology. The cable elongation as a function of temperature is measured using a Fabry-Perot interferometer, and from it its thermal expansion coefficient is determined. The experimental apparatus is shown in Fig. 1 and consists of a casing with an access window and a translation stage on its one end. A 30 cm long cable sample is mounted to the casing on one end and to the translation stage on the other. The translation stage allows freedom of motion along the cable axis. A corner cube, also fixed to the translation stage, can be illuminated through the access window and serves as part of the Fabry-Perot interferometer. Thermocouples are placed inside and outside the cable sample to monitor its temperature. A 30% reflecting mirror, fixed to the bench just outside the access window, completes the interferometer. Hence laser light, directed through the mirror and normal to its plane, is retroreflected by the corner cube and returns to a silicon photodetector after reflecting from the mirror. Thus, the mirror serves as both an entrance and exit port to the interferometer whose length varies with changes in the corner cube position.

In order to determine the thermal expansion properties of the cable, the sample and its casing are placed in an environmental chamber and taken to a low or high temperature (either -60 degrees Celsius or +70 degrees Celsius). The unit is then removed from the chamber and fixed to an optical bench at the location of the cable's fixed end. The output of the photodiode and the thermocouple are monitored by a computer. For a given temperature variation, changes in the cable length alter the Fabry-Perot length and hence, the condition of interference sensed by the photodiode. Since each fringe corresponds to a variation of 0.14 or 0.15 um in cable length, elongations as small as 0.00005% can be measured for 30 cm cable sample.





American Institute of Physics handbook (McGraw-Hill, Inc., 1963), 2-[illegible].

Fig. [illegible]: Elongation of copper wire versus temperature.

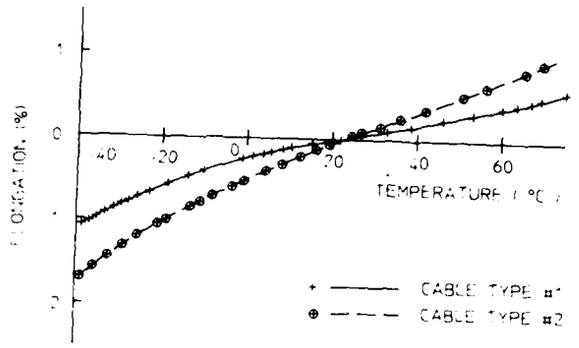


Fig. 3: Cable elongation versus temperature for two cable types.

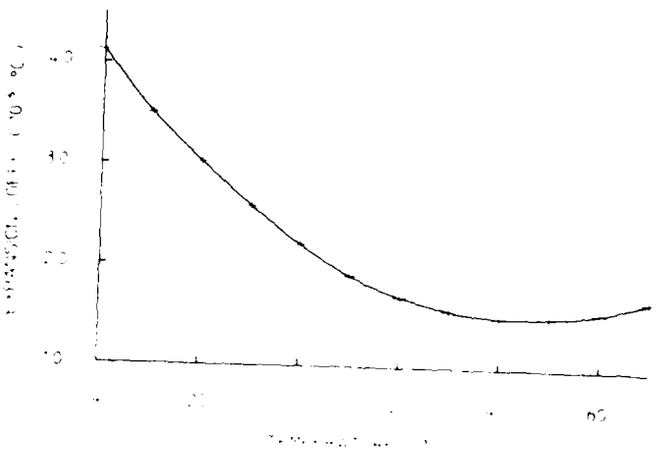


Fig. 4: Cable thermal expansion coefficient versus temperature.

MATHEMATICALLY MODELLED FULLY FILLED STRANDLESS OPTICAL CABLE DESIGNS

S.T. SPEDDING * J.E. TAYLOR **

* BICC OPTICAL CABLES, WHISTON MERSEYSIDE, ENGLAND
** BICC RESEARCH AND ENGINEERING, LONDON, ENGLAND

SUMMARY

An all linear manufacturing process was devised to produce a novel cable design based on ribbon. Speed limitations associated with heavy rotating plant are thus avoided. Long length manufacture and tandem running become possible. The novel cable structure requires special filling techniques, and was subject to mathematical modelling at the design stage to predict its performance under real, as opposed to ideal conditions.

BACKGROUND

Used in conjunction with multi-fibre splicers, ribbon cables offer user advantages in economy of jointing. The cable maker can also realize advantages in production speed by questioning the traditional approaches to cable design, and by eliminating all rotating operations from the production cycle.

We set out to devise a production cycle for duct installed cables, based on linear operations only. In particular, stranding, which is a slow, cumbersome process, had to be eliminated. The resulting process is speed limited by process factors only, and not by the mechanical safe working speed limits of rotating machines. It is therefore much easier to achieve higher speeds, and the present three operations are matched in speed and type for tandem running. Long length cable manufacture is greatly simplified.

BASIC DESIGN PRINCIPLES

Eight optical fibres, each colour coded on line, are encapsulated into a ribbon element with acrylate resin. In the second operation, one or more of these ribbons is incorporated into a cavity within an essentially rectangular extrusion. Two copper wires are bonded within the walls of the section. The free space within the cavity is filled with a tube filling compound. In the final operation, a strong, high modulus sheath is formed by embedding bundles of glass yarn into the wall of a polyethylene tube. The sheath is heat bonded to precoated aluminium tape formed and sealed into a tube. A hollow, moisture barrier sheath with integral longitudinal strength results. One or more ruggedised ribbon units is fed into the bore of the sheath, after being formed into a semi circular wave. Arrangements are made to fill all free space with a low density water blocking filling compound. A cross sectional drawing of a 16 fibre version of the design is shown in figure 1.

The extension of the glass yarn reinforced sheath under load is greater than would be expected in designs with a central strength member. This arises from a low modulus "pre extension" region before all yarns in the sheath wall take load. Working to the boundary condition that fibres shall not strain (other than bending strain) under all conditions, necessitates the incorporation of significant excess fibre length, by means of the corrugation of the ruggedised ribbon units. However, too much excess length within a certain bore size will need too small a radius of curvature. Decisions have to be made as to the required bore, radius of curvature and strain margin. Once this is done, forming techniques have to be devised to achieve the calculated parameters. Finally, allowances must be made to accommodate the full spectrum of fibre bend sensitivities.

THEORY

Bending Radii

Existing bending loss theory was modified to take into account the skewing effect on refractive index profile under bending conditions. The predicted losses under different bending radii are shown in figure 2, for a fibre with a cut off wavelength of 1130 nm. Although much of the theory had previously been developed, it was expressed in terms of the variables which were of least usefulness to us, such as delta. We recast them in terms of cut off wavelength and mode field radius. We corrugated ruggedised ribbon units and proved our theory to our satisfaction.

Representing the same equations at a fixed bending radius of 50 mm, for different cut off wavelengths, results in figure 3. We kept in mind all through the subsequent mathematical modelling phase that it would be necessary to find the window of acceptance for the most bend sensitive fibre, and under the least advantageous combination of process variations.

We chose an attenuation increase of 0.05 dB Km above intrinsic fibre loss, at 1550 nm as the maximum acceptable under worst case conditions. Assuming a doubling of bending loss for each 25 nm, this would result in 0.5 dB/Km increase at 1650 nm. Figure 3 shows that for a bending radius of 50 mm, all in-specification fibres will suffer less than 0.05 dB Km additional loss due to macrobending at 1550 nm. We chose 55mm as the design minimum radius of curvature.

Corrugation

Figures 5 and 6 represent the semi-circularly corrugated ruggedised ribbon element as it would appear within the confines of the sheath. Figure 5 is a side view and figure 6 is an "end on" cross section. P is the pitch length and Q is the path length for one wavelength of the element. Then:

$$P = 4R\sqrt{1 - (1 - A/2R)^2} \quad \ldots\ldots\ldots\ldots\ldots\ldots (1)$$

$$Q = 4R \sin^{-1}\sqrt{1 - (1 - A/2R)^2}$$

$$Q/P = \frac{\sin^{-1}\sqrt{1 - (1 - A/2R)^2}}{\sqrt{1 - (1 - A/2R)^2}}$$

and $Q/P = 1 + e$ where e = excess fibre length (strain margin)

So

$$1 + e = \frac{\sin^{-1}\sqrt{1 - (1 - A/2R)^2}}{\sqrt{1 - (1 - A/2R)^2}} \quad \ldots\ldots\ldots (2)$$

By using an expansion for $\frac{\sin^{-1} x}{x}$, an approximate formula results:

$$e = A/6R$$

This approximation is useful in providing a simple insight into the interplay of radius of curvature and strain margin. It shows with devastating simplicity the inescapable conclusion that for a given bore size, strain margin will be increased at the expense of bending radius and vice versa.

From figure 6,

$$Db = \sqrt{(A + (n-1)T)^2 + (W - T)^2} + T \quad \ldots\ldots\ldots (3)$$

(n = number of stacked flat units)

Considering the same flat element at the actual point of corrugation, see figure 7, where it is apparent that the path length per wavelength is laid down. This is Q and unlike P, it remains constant during the subsequent relaxation and sizing operation and on incorporation into the sheath bore.

$$Q = \pi (Db + T)$$

When inserted into a cable,

$$P + (P \cdot e) = \pi (Ds + T) + (\pi \cdot e)$$

From this and equation (3) the following formula results;

$$Ds + T = 4R/\pi \sqrt{2e - (1 + e)} \quad \ldots\ldots\ldots\ldots (4)$$

From equations 1, 2 and 4, values for A, P and e can be worked out for each set of values for W, T, Db and Ds.

PRACTICE

The above theory supposes that an infinitely variable selection exists for corrugation radii of curvature and for glass yarn reinforced sheath bore sizes. In reality, our corrugating machine is simply a number of round formers carried on a pair of drive chains. These chains have only two pitch possibilities of 9.5 mm and 12.7 mm, and formers can be fastened only an integral number of links apart. Also, we had available to us a number of tooling sets for the glass yarn reinforced sheath, and other sets are costly.

We had chosen 55mm as our minimum bending radius in finished cable, and we had chosen our outside dimensions for the ruggedised ribbon units, as 5.5 mm by 2.6 mm. Figure 4 shows the strain margins theoretically achieved with these dimensions, for three different radii of curvature. Plotted on the same graph, the lines A through D represent possible

solutions for corrugator designs. Intersections between lines A through D with the curves give theoretical sheath bores and strain margins. This plot clearly demonstrates the interplay of radius of curvature and strain margin.

Experience and practical verification taught us that we needed to design for a strain margin of 1.5% when using glass yarn reinforced sheath for duct installation. This will allow for a pull of 3W, where W is the cable weight per kilometre. This would seem to permit the choice of corrugator design A or B and would point to a sheath bore of around 12 mm. It was now necessary to take into account the variations in dimensions which were likely to occur.

ROBUSTNESS OF DESIGN

We next set out to quantify the effect of inevitable process variations on strain margin, and radius of curvature. The intention was to devise a design that the manufacturing process was not excessively critical, and thus to ensure a saleable product with at most only attention to close tolerances.

For this, we set three levels for four parameters as follows:

- Nominal cable weight per unit length W
- Nominal wall thickness T
- Glass yarn reinforced sheath internal dia. DE
- Corrugator former diameter Dc

We employed the effect of variations of W, T, DE and Dc by using a fractional array of the Taguchi type orthogonal array.

By reference to Figure 4 you can see that it would be expected that corrugator design A, with a sheath bore of 12.0 mm, corrugator design B, with a sheath bore of 11.4 mm would be adequate in both terms of strain margin and radius of curvature. Accordingly we set three levels which we designated 1, 2 and 3, for each of our parameters and used a micro computer to analyse nine combinations in the Taguchi orthogonal array. The levels 1, 2 and 3 chosen for the four variables represent target values, maxima and minima envisaged for each variable, taking into account the known or expected difficulty in holding close tolerance on that variable.

Design A - Mathematical Modelling Analysis

e = Strain margin % ; R = Radius of curvature (mm).

Run No.	W	T	DE	Dc	e	R
	-level number-					
1	1	1	1	1	2.01	57.9
2	1	2	2	2	1.85	59.9
3	1	3	3	3	1.19	77.8
4	2	1	2	3	1.74	63.4
5	2	2	3	1	1.71	61.7
6	2	3	1	2	1.85	61.8
7	3	1	3	2	1.23	74.4
8	3	2	1	3	1.99	58.3
9	3	3	2	1	1.38	70.7
	Average				1.66	65.1
	Standard Deviation				0.30	6.9
	3 sigma point				0.76	44.4

For a normal distribution, more than 99% of results will lie within three standard deviations of the average, so for a near zero rejection rate, it is necessary to cater for the extreme case of three standard deviations from the mean. For corrugator design A, note the "3 sigma points". Since these are outside the permitted values for both e and R, corrugator design A will not ensure adequate insensitivity to dimensional variations.

Design B - Mathematical Modelling Analysis

Similarly, we ran the analysis on corrugator design B. The results emerging were:

	e	R
Average	2.35	66.5
Standard Deviation	0.33	4.07
3 sigma point	1.36	45.9

Therefore corrugator design B also fails in both radius of curvature and strain margin.

Design C - Mathematical Modelling Analysis

	e	R
Average	2.15	64.51
Standard Deviation	0.30	4.06
3 sigma point	1.25	52.42

Even corrugator design C cannot guarantee the required strain margin, although it would have been acceptably close to be admitted on the 3 sigma point for R.

Design D - Mathematical Modelling Analysis

	e	R
Average	2.00	72.87
Standard Deviation	0.15	3.16
3 sigma point	1.55	63.39

We conclude that corrugator design D is the first solution capable of meeting the twin requirements of strain margin and radius of curvature. The solution dictates the bore of the glass yarn reinforced sheath as 11.5 mm and the amplitude of corrugation as 0.5 mm.

Novel Aspects of the Process

The choice of polymer from which to form the ruggedised ribbon units had to be based on all the usual criteria, plus one more; **corrugation behaviour.** The flat ruggedised ribbon units contain two copper wires, whose sole purpose is to retain the corrugation form against the tendency of the polymer to relax. A thermoplastic elastomer based on an SEBS block copolymer was chosen after rigorous testing. The internal filling compound is a hot melt devised by ourselves for our loose tube work.

At the sheathing stage, two versions of this cable type are offered. One is left dry, and one is fully filled. The cavity is large, and so precautions have to be taken to reduce weight penalties for fully filled cables. For this reason, a microsphere loaded filling compound was chosen. This has a thixotropic base, with the addition of PVDC microspheres to reduce density to less than 0.5 g/cc. There was a need to work very closely with filling compound manufacturers to make successive alterations to the compound formulation until the correct pumping and water blocking properties were found.

Since the cable has no stranded core over which to apply the filling compound, an alternative approach is needed. It is necessary to ensure that:

- Filling compound delivery rate is metered to match line speed,
- Filling compound is formed into a circular cross section of the same diameter as the internal diameter as the glass yarn reinforced sheath.
- Because of the aluminium foil water barrier, filling must take place before the formation of the foil into a tube.

We designed a filling compound applicator which is fed by a metering pump, run at a speed proportional to line speed. The applicator has a double walled tube, the innermost tube having a spiral cut in its wall. The undulating ribbon unit passes through the innermost tube and the filling compound is metered into the outer tube and flows through the spiral slot to fill the spaces above and below the waveform. A bead of filling compound emerges from the applicator, with the flat unit embedded within.

The applicator is fixed at the foil forming station, just prior to the closing of the foil into a tube. Thus the foil effectively wraps around the compound bead and the overlap is then glued.

CABLE PERFORMANCE

Examples of fully filled and dry cable of this format have been fully tested. There is, as predicted, no fibre strain at the maximum rated tension of 8W. Attenuation levels at 1550 nm are well within the intrinsic level plus the allowance of 0.05 dB Km which we set ourselves.

To probe the width of the third window, we have looked at spectral analyses of the cables and found a wide operating region, which remains open even at high and low operating temperatures. We submitted the measured attenuation values at 1650 nm in addition to those at 1300 amd 1550 nm as indication of the width of the third window. The performance of the cable at -40° Celsius was especially encouraging, as the tube filling compound is not intended for use at this level. We believe that the facts are explained by the resistance of the ribbon to buckling as compared to individual fibres.

Typical Attenuation Measurements - Ambient Temperature.

Attenuation at (nm)---		1300	1550
Fibre Number	1	.36	.19
	2	.34	.21
	3	.37	.20
	4	.35	.21
	5	.35	.20
	6	.34	.20
	7	.37	.21
	8	.34	.19
	9	.35	.20
	10	.35	.19
	11	.35	.19
	12	.36	.22
	13	.35	.20
	14	.34	.19
	15	.35	.21
	16	.35	.19

MANUFACTURING EXPERIENCES

Production of principally the dry version of this design has been substantial over the last three months, and we have not seen failures attributable to high attenuations of the type associated with poorly controlled bonding ribbon or local fibre buckling.

We eliminated the stranding stage completely, and have replaced it with a process already running at least three times as fast. Future plans include the optimisation of the [illegible] of the bedding, which will include investigation of the process variables and the drawdown ratios at which it is optimally applied. The ideal bedding is to be determined by mathematical modeling analysis.

ACKNOWLEDGEMENTS

The authors wish to express their gratitude to several people who have helped develop this technique. Those people concerned will immediately realise that this acknowledgement refers to themselves.

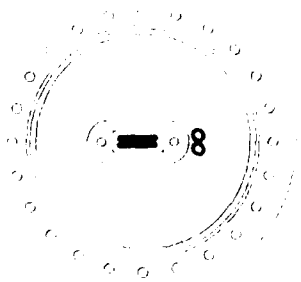
Our thanks also to BICC plc for allowing the work to be published.



Stephen Spedding graduated from Imperial College, London in 1973, with a BSc degree in Physics.

He joined BICC in the same year, and entered the field of Optical Cables in 1980, as Head of the Pilot Manufacturing Unit. As the business expanded, the Pilot Plant became a full scale manufacturing facility and Mr. Spedding became its Production Manager.

In 1985, he took on a project within the framework of the RACE programme. Mr. Spedding is currently Technical Manager - Design and Development at the newly purpose built optical cables factory at Whiston.



CABLE ELEMENT DESCRIPTION

Corrugated flat unit containing optical fibre ribbons, and copper corrugation elements. Ribbon arrays coated with a water repellent gel

One pair of twisted copper conductors

Tape

Cavity filled with low density water repellent compound

Polymer coated aluminium tape

Black polyethylene sheath incorporating tension relief elements

FIGURE 1

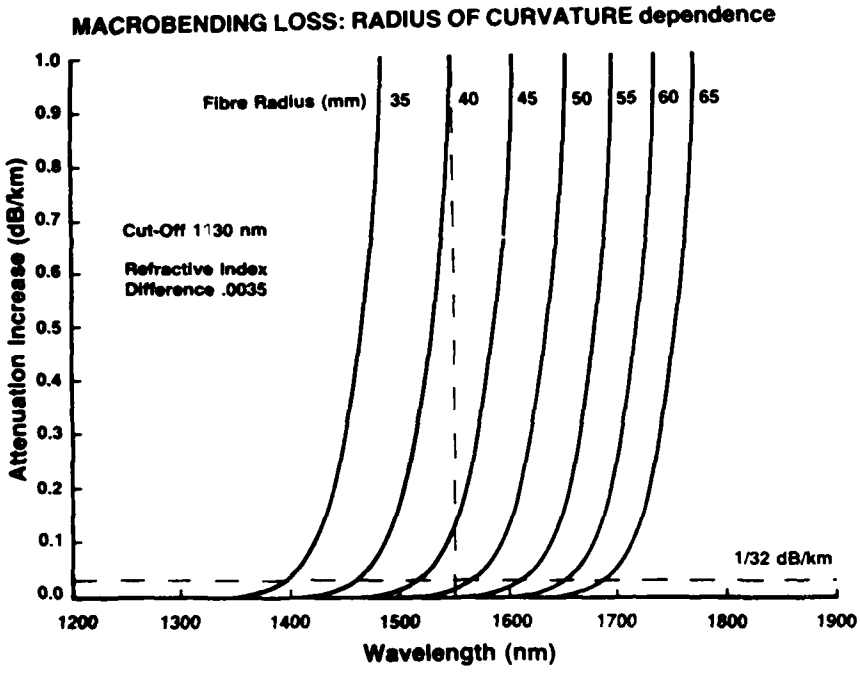


FIGURE 2

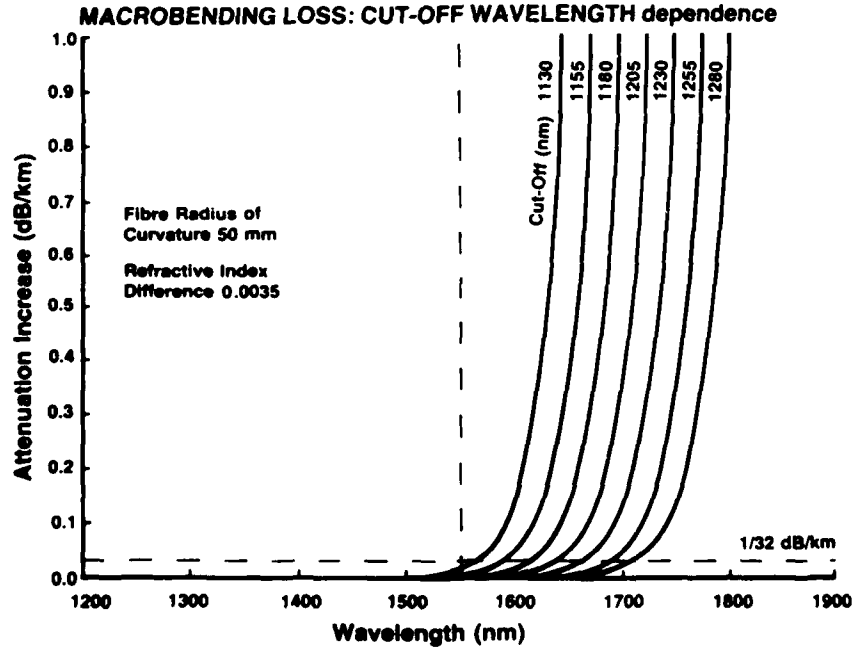


FIGURE 3

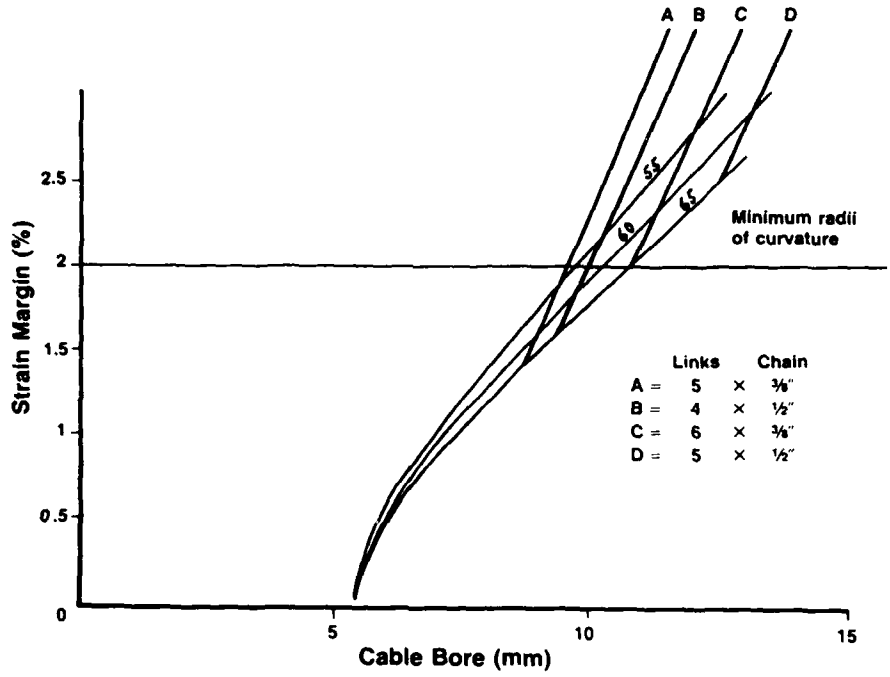


FIGURE 4

FIGURES 5 AND 6 : CORRUGATED UNIT WITHIN SHEATH BORE

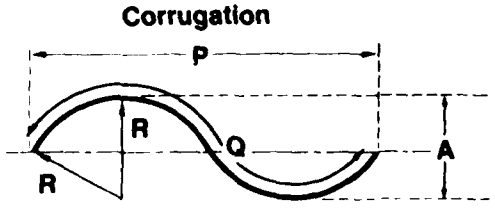


FIGURE 5: SIDE ASPECT

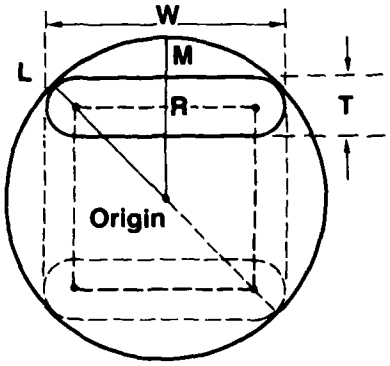


FIGURE 6: "END-ON" ASPECT

CORRUGATOR

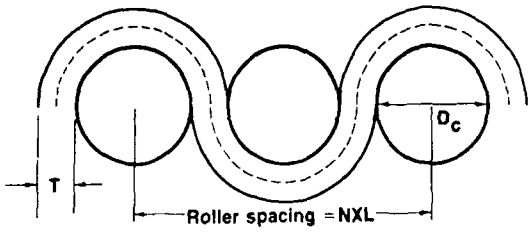


FIGURE 7: FLAT UNIT AT POINT OF CORRUGATION

A NEW CONCEPT FOR FIBER OPTIC LAN CABLES

P. Rohner and G. Ziemek

Kabelmetal Electro GmbH, 3000 Hannover, West Germany

Summary.

A new concept for fiber optic LAN cables which shows promising results in manufacture as well as in on-site splicing has been developed. The basic building block of this new cable consists of a ribbon-type sub-unit which contains ten optical fibers sandwiched between two fiberglass-reinforced tapes. These tapes are bonded to each other and to the fibers, thus providing perfect fiber alignment . A stack of ten ribbons is fed into a metallic corrugated tube fabricated on a UNIWEMA® machine. The UNIWEMA® is designed to process a metallic strip into a longitudinally welded and corrugated tube. The stack of ten sub-units is twisted with a reverse lay (lay length: 500 mm) prior to being fed into the metal sheath. The tube can be made watertight by filling jelly in the space between the core and the sheath or by introducing a hygroscopic powder. The corrugated tube is covered with a corrosion protection and a polyethylene jacket.

General Considerations.

Optical fibers for long distance signal transmission are known to be sensitive to increases in attenuation resulting from mechanical stresses in the fiber. These stresses can be caused by mechanical forces or by temperature gradients. Consequently, a considerable amount of time and effort has been devoted in the design of a hollow tube construction which will prevent stresses in the fiber.

Our new concept represents a different approach to the design of a stress-free optical fiber cable. Instead of leaving the fibers to move freely whenever outside forces are applied, a member which absorbs all stresses is bonded to them. This is accomplished by means of a pair of fiberglass-reinforced plastic tapes which have the same coefficient of thermal expansion as the fibers. These tapes can absorb a considerable amount of mechanical stress before they elongate and start transferring the stress to the embedded fiber. This paper describes the design of a LAN cable based on this new concept.

Manufacture of the Sub-Unit.

The availability of optical fibers and glass-reinforced tapes called for the design of a line capable of processing measurable lengths of sub-units . Special care had to be taken to preserve the fiber properties during the bonding operation.

A schematic representation of the line, which is 20 m long, is shown in Fig. 1. The fibers are fed into the line from individual payoffs. Two coils of fiberglass-reinforced tape are paid off from top and from bottom with the bonding side adjacent to the fibers. A special drive was developed to ensure that the tapes are dispensed to the bonding station without sticking or slippage. Special attention had to be given to ensure that the strips are handled with great care to avoid spoiling the bonding surface.

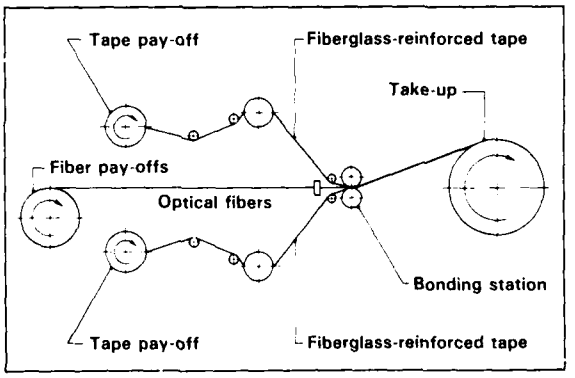


Fig. 1. Production line of the sub-unit.

Fig. 2 illustrates the fibers and tapes entering the bonding station. Single-mode 9/125 µm optical fibers were used throughout. The positioning of the fibers between the tapes is assured by a guide which permits perfect alignment. This feature is especially helpful in on-site splicing.

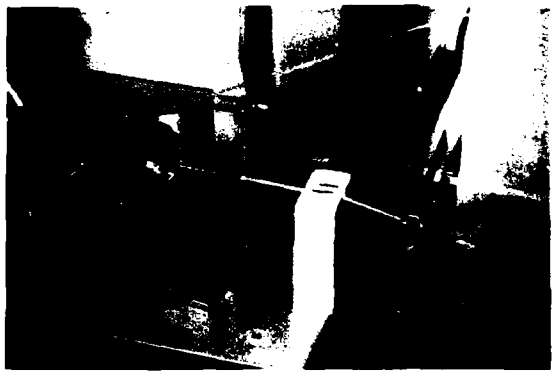


Fig. 2. Guidance of sub-units

The actual bonding is illustrated in Fig. 3. Again, everything is done to ensure that the fibers are handled with care and that the least amount of pressure is applied to the sandwich by two soft plastic rolls. The sandwich sub-unit is then taken up on a reel, ready for testing.

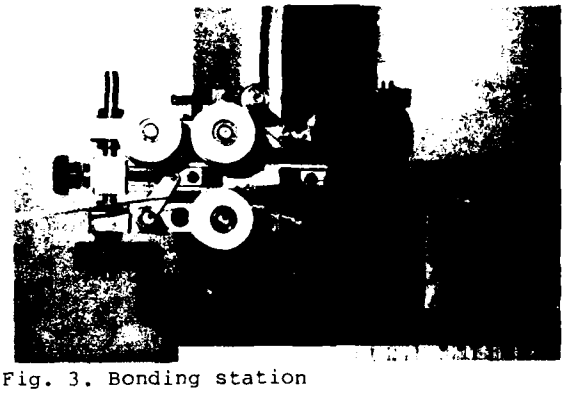


Fig. 3. Bonding station

As can be seen, the line allows for any number of fibers to be sandwiched. The manufacturing speed can reach up to 30 m min^{-1}. The fiberglass tapes are 6 mm wide, which is adequate to accommodate ten fibers in a sub-unit. Several sub-units which have been manufactured and tested are shown in Fig.4.

Fiber Properties in the Sub-Unit.

Testing.

Sandwiching. As a first step we had to investigate any possible impact by the manufacturing of the sub-unit on the fiber properties. All tests on the individual fibers before and after sandwiching revealed, in the worst case, an attenuation increase of 0.1 dB km^{-1}. Most fibers in the same sub-unit did not exhibit any relative difference.

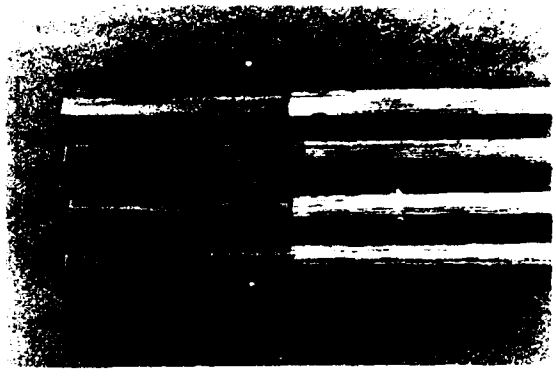


Fig. 4. Typical sub-units.

Tension test. The purpose of the second test was to determine the tension forces that could be applied to the sub-units without an increase in attenuation. The length of the samples for this test was 600 m.

Tension (N)	α (dB)	ε (°/oo)
100	0	2.5
200	0	5.0
300	0	7.5
400	0.02	10.0
500	0.02	13.8

Table 1

Table 1 illustrates the dependency of strain and attenuation on the applied forces. As can be seen, while there is an increase in strain, there is no increase in attenuation up to 300 N of applied tensile force. Assuming that the pulling force on the sub-unit will be less than 100 N during its life time, this leaves a perfectly safe margin for handling the sub-unit during testing, further processing and, above all, during on-site splicing.

Temperature cycling. In order to investigate the effect of temperature variations, the sub-units were measured between -20°C (-4°F) and +60°C (140°F). The tests were conducted at the 1,300 nm wavelength. The test consisted of two consecutive temperature cycles. Table 2 shows the results of the temperature cycling tests: there is almost no deviation in the attenuation within the given temperature range at this wavelength. Tests conducted at the 1,550 nm wavelength showed a considerable increase in attenuation at -20°C(-4°F).

This condition will have to be improved in the event that this wavelength should be used in the local area network.

Attenuation at 1,300 nm							
0	-20	+60	0	-20	+60	+20	(°C)
0	-4	+140	32	-4	+140	+52	(°F)
0.39	0.39	0.37	0.36	0.38	0.35	0.33	dB km^{-1}

Table 2

Twisting. For the bending properties of a complete cable having a stack of sub-units as a core, it was interesting to determine whether the sub-unit could be twisted and, if so, how often over a given length without having an impact on the attenuation.

The tests revealed that a 10-fiber sub-unit could be twisted five times on its axis over a one-meter unit length without a noticeable increase in attenuation. It was therefore decided to twist the stack two to three times per meter during manufacture.

Manufacture of a Cable with Ribbon Sub-Units.

The ribbon type design of the flat sub-unit was meant to be a part of a LAN cable where a multitude of closely packed optical fibers is required, along with protection against outside mechanical damage.

As a first step, a cable with ten sub-units, each containing ten fibers, was produced. This made for a total of 100 fibers which are carefully protected by a strong corrugated steel sheath.

The UNIWEMA® system is illustrated in Fig. 5. It shows that the metal strip is cleaned, trimmed along both edges and formed into a smooth tube, longitudinally welded and, finally, corrugated. The stack of ten sub-units is fed into the formed smooth tube prior to welding. Feeding the stack into the tube in a straight line would, in all likelihood, affect the bending properties of the final cable along its two perpendicular axes. This is the reason for applying a reverse lay to the stack prior to feeding it into the tube, ensuring identical bending behavior in all directions. The fact that the sub-units are free to move with respect to each other, enables them to absorb outside bending forces without affecting the optical fibers.

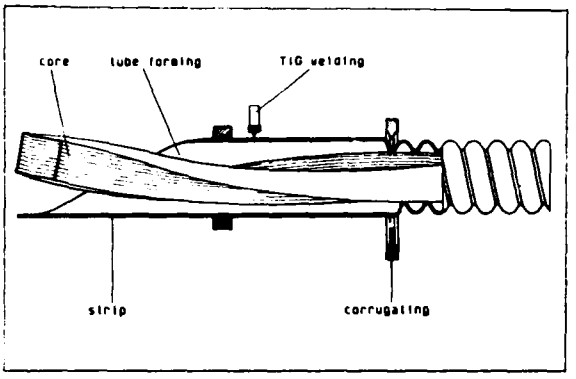


Fig. 5. UNIWEMA® System

The corrugation process shortens the smooth tube between 10% and 20%. Therefore, the stack speed is slower than the speed of the smooth tube. Their relative speed can be adjusted depending on the desired restraint one wishes to apply to the stack within the tube.

Fig. 6 shows the stack entering the UNIWEMA® machine. The reverse lay is imparted to the stack by means of a mechanical device driven by a reversing electrical motor.



Fig. 6. Manufacture of a LAN cable

During strip forming, a hygroscopic powder is introduced to provide a humidity-absorbing substance. Petrojelly can be substituted for the powder, if preferred (Fig.7).

Fig. 8 illustrates the argon-arc welding head in the process of seam-welding the strip. A split-clamp caterpillar pulls the strip through the forming and welding stations and pushes the tube through the corrugator (Fig. 9).

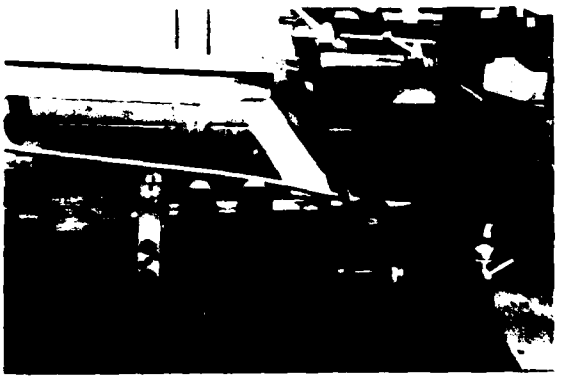


Fig. 7. Feeding the hygroscopic powder into the tube

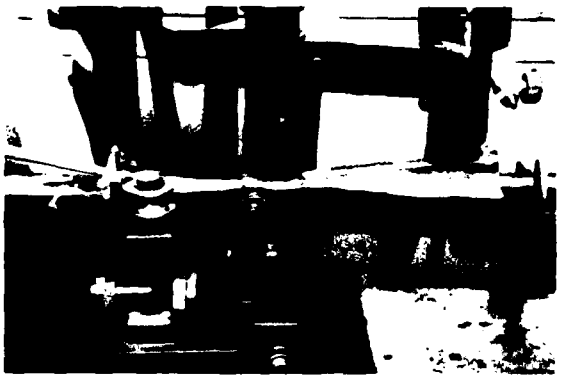


Fig. 8. Welding the sheath

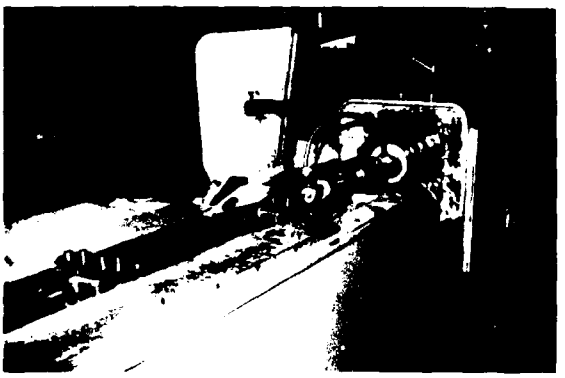


Fig. 9. Split-clamp caterpillar and corrugator

Fig. 10 shows the corrugated tube with the open stack. Corrosion protection is applied over the corrugated sheath and, finally, a polyethylene jacket is extruded over the cable.

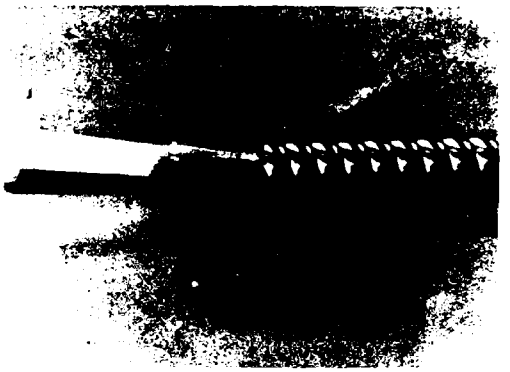


Fig. 10. LAN cable

Splicing.

In the eyes of a cable manufacturer, an adequate splicing technique is one of the foremost imperatives. Therefore, considerable effort was placed on developing a splicing technique. One of the conditions was the ability to splice a 10-fiber sub-unit in the shortest possible time, with the smallest increase in attenuation and with the highest probability for successful splicing at all times. Numerous techniques were tested. It was concluded that welding the fibers would yield the best results. As is usual for successful welding, strict cleanliness and proper preparation of the edges are pre-conditions.

Fig. 11 illustrates how the two fiberglass-reinforced strips can be peeled off. The coating is removed from the fibers, ten fibers at a time, using the conventional methylene chloride process. The fibers are now clean and ready for cutting.



Fig. 11. Peeling off the fiberglass reinforcements

A special cutter was developed for the correct cutting of all ten fibers. Studies were made on high-speed film to ensure that the cuts are properly made, even in the event that the ten fibers are not of exactly the same diameter. A special tool, consisting of a spring-loaded diamond blade jumping from fiber to fiber while all fibers are under tension, was developed for this purpose (Fig. 12).

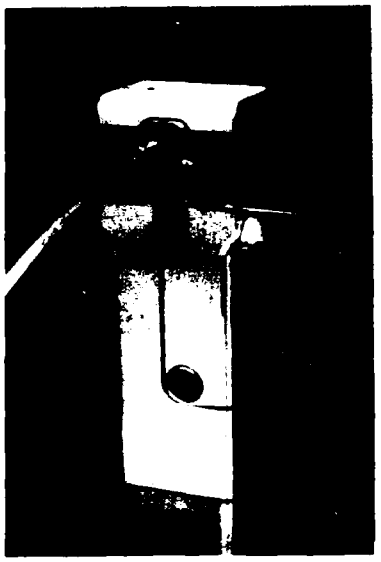


Fig. 12. Spring-loaded diamond cutter for the simultaneous processing of ten fibers

The splicing was performed on a modified, commercially available welding unit. This device (Fig. 13) is microprocessor-controlled, with an electric arc having a voltage range between 3 kV and 10 kV and a current range between 7 mA and 30 mA. Prior to welding, the fibers are positioned automatically with respect to each other by a light alignment and measuring system. The modified fusion splicer enabled us to position all ten fibers at once and to weld each fiber following an automatic adjustment. The alignment of each individual fiber to the arc is made by the operator. After splicing is completed, the joint is covered with fiberglass-reinforced tape, which renders it as sturdy as the rest of the sub-unit.



Fig. 13. Semi-automatic splicing of ten fibers

Conclusion.

The newly developed multi-fiber cable offers new possibilities for LAN cables due to its simple design and easy handling properties of its sub-units. These sub-units can be fabricated with one to twenty optical fibers which are easily identifiable by numbering or color-coding. By defining the direction of counting within a sub-unit, any individual fiber can be traced within seconds in a stack of 100 or more fibers. For safety reasons and with the enormous amount of information flowing through such a stack of fibers, a strong corrugated steel sheath should be applied to protect this valuable core.

Acknowledgments.

The authors wish to express their thanks to Mr. G. Verdenhalven for providing the extensive test data and to Mr. H. Hofheimer of Cable Consultants Corporation, Larchmont NY for his valuable assistance in preparing this paper.



Peter Rohner
Kabelmetal
Electro GmbH
Kabelkamp 20
3000 Hannover 1
West Germany

Peter Rohner obtained his Ph. D. from the Technical University, Berlin, West Germany, in 1968, where he remained as Assistant Professor for Theoretical Physics. He joined Kabelmetal Electro GmbH in 1974. After holding several development and marketing functions, he became Head of Kabelmetal's Telecommunication Department. He is presently a member of the Executive Board.



Gerhard Ziemek
Kabelmetal
Electro GmbH
Kabelkamp 20
3000 Hannover 1
West Germany

Gerhard Ziemek received his engineering degree in 1961 from the Technical University at Hannover, West Germany and earned his engineering doctorate while engaged as a research engineer at the German Iron & Steel Institute. He joined Kabelmetal in 1965 and assumed his present position as Head of Kabelmetal's Department for Licences and Production Machinery in 1981.

SINGLE-MODE TACTICAL FIBER OPTIC CABLE ASSEMBLIES

B. V. Darden and K. Kathiresan
V. E. Kalomiris

AT&T Bell Laboratories, Norcross, Georgia 30071
U.S. Army Communications - Electronics Command, Ft. Monmouth, New Jersey 00703-5202

Abstract

The design and development of a single-mode fiber optic tactical cable assembly for use in the Single-Mode Fiber Optic Communications System (SIMFOCS) have been completed. Development effort was guided by the detailed design criteria as required by the contracting organization, the U. S. Army CECOM. A completed cable assembly consists of a 1-km cable containing two tightly-buffered single-mode optical fibers terminated with duplex, hermaphroditic connectors. Fiber utilized in the cable assembly is a standard AT&T single-mode fiber. The cable design is based on the earlier multimode Tactical Fiber Optic Cable Assembly (TFOCA) design. The connector design is also an adaptation of the multimode TFOCA design. However, due to the smaller core diameter of the single-mode fiber, further design improvements were incorporated to attain the required low loss performance.

Introduction

AT&T Bell Laboratories has completed the development of the single-mode tactical cable assembly for the Single-Mode Fiber Optic Communications System (SIMFOCS) program. This development program was funded by the U.S. Army Communications - Electronics Command (CECOM).[1] The cable assembly was designed to meet stringent specifications imposed by the contracting agency. The design is basically a single-mode adaptation of the Tactical Fiber Optic Cable Assembly (TFOCA) which uses 50/125 micron multimode fiber and was developed by AT&T for CECOM.[2] Like its multimode counterpart, the single-mode unit is ruggedized for use in tactical environments and it offers additional advantages of longer unrepeated transmission distances, higher bandwidth, and the potential for further performance improvements. This paper describes the design and development of this cable assembly and enumerates performance test results for the assembly as well as its components.

Cable Assembly Design

A completed cable assembly consists of a 1-km cable terminated with hermaphroditic connectors at both ends as illustrated in Figure 1. A cross-sectional view of the cable and an illustration of the connector are given in Figures 2 and 3, respectively.

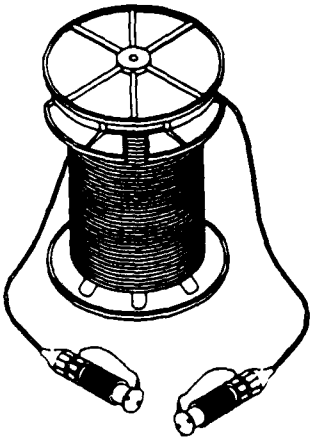


Figure 1. SIMFOCS Cable Assembly

The single-mode fiber used in the cable assembly is the standard AT&T depressed cladding design which has been shown to have exceptional microbending and macrobending performance. For this application, the fibers were prooftested to 700 MPa (100 ksi). These fibers can operate at both 1310 nm and 1550 nm wavelengths. However, tests were conducted and the results are presented only at 1310 nm wavelength. The fiber is coated with dual acrylate coatings which are mechanically strippable. These fibers are then tight-buffered to 1 mm (.039 inch) diameter with a polyester elastomer. The buffering material is also mechanically strippable in order to facilitate termination and repair in the field. The buffering material was chosen to minimize microbend-

ing losses induced by exposure of the cable to temperature extremes of -40°C to 71°C as required by the design criteria.

The core of the cable contains two buffered fibers which are color coded for identification purposes. Aramid yarns, which are the main tensile load-carrying members, are stranded around the buffered fibers in two opposing layers. The sheath over the aramid yarns is a composite of a flame-retardant polyurethane and four epoxy-glass reinforcement rods. The outer diameter of the cable is 5.0 mm (0.234 inch). The cable design is the same as the TFOCA cable design[3] except for the fiber.

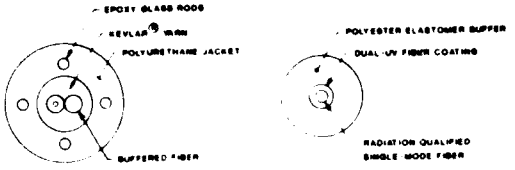


Figure 2. SIMFOCS Cable Cross Section

The connector is a single-mode adaptation of the TFOCA duplex connector.[3] It meets the mechanical and environmental requirements supplied by CECOM in the contractual statement of work. The connector, shown in Figure 3, is less than 4 cm (1.57 inch) in diameter, and a mated pair weighs under 0.6 kg (1.3 lb). A companion bulkhead receptacle was developed for the system and shares a common hermaphroditic interface.

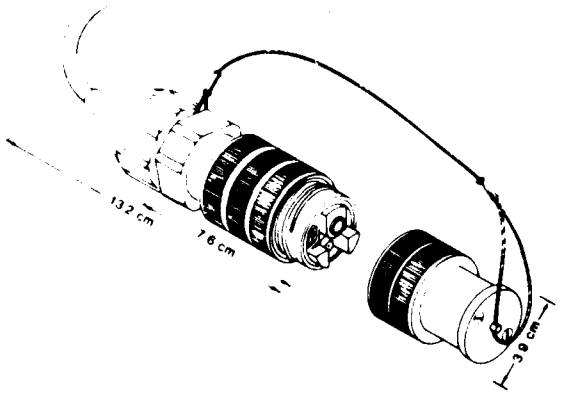


Figure 3. SIMFOCS Connector

One of the two fibers in the connector terminates with a plug and the other with a biconic sleeve. A sealed connector-insert subassembly contains the biconic components. Special features prevent water ingress and allow the plug and sleeve to float radially and axially to properly align when two connectors are mated. The front portion of the subassembly, called the sleeve retainer, houses the sleeve and provides the connector's hermaphroditic profile.

A die-cast aluminum shell houses the connector insert and retains the cable-termination hardware. It also provides storage space for slack fiber. A threaded aluminum nut couples two connectors or a connector and bulkhead receptacle. The shell and coupling nut are designed to elastically withstand 1780 N (400 lb) tension across mated connectors.

All possible water leak paths into the connector are blocked by elastomeric seals, and a hermaphroditic dust cover prevents water or dust entry into an unmated connector.

The dust-cover shell and end cap of the SIMFOCS unit are gold anodized to visually distinguish it from the all-black TFOCA connector. The SIMFOCS sleeve retainer differs intentionally from the corresponding TFOCA part to mechanically prevent the inadvertent mating of single-mode and multimode connectors.

Except for the sleeve retainer and the two gold-anodized parts mentioned above, all hardware is common between the TFOCA and SIMFOCS designs. This common parts usage reduces SIMFOCS costs by reducing the development effort, and by increasing the volume of the common parts.

Another crucial but somewhat imperceptible difference between the designs is the increased precision of the biconic components required for the single-mode application.

Performance

The whole cable assembly and individual components (fiber, buffered fiber, cable, and connector) were subjected to the required optical, environmental, and mechanical performance tests. The results for individual components and the assembly are enumerated in the following paragraphs.

Fiber Performance

All the fibers were tested for their optical and dimensional requirements before being used in the cable. These tests include attenuation, attenuation uniformity, cut-off wavelength, mode-field radius, clad and coating diameters, core eccentricity, etc. Though not required under the development program, the fibers were tested for response to environmental temperature cycling. The temperature cycle used was:

- baseline the loss measurements through multiple measurements at room temperature, 25°C,
- reduce the temperature to -40°C and dwell at least 24 hours before measurement,
- reduce the temperature to -55°C and dwell at least 12 hours before measurement,
- return to room temperature, 25°C, and dwell at least 12 hours before measurement,
- increase the temperature to 71°C and dwell at least 12 hours before measurement,
- increase the temperature to 85°C and dwell at least 24 hours before measurement,
- return to room temperature, 25°C, and dwell at least 12 hours before measurement.

The contract required that the assemblies and components be subjected to three temperature cycles described above. Instead, five cycles were run. The design requirement of temperature extremes is from -40°C to 71°C. The temperature range was extended to -55°C and 85°C to investigate the performance at these temperatures. The performance of the SIMFOCS single-mode fibers for the temperature cycles is presented in Figure 4. The fibers show excellent performance with a maximum added loss of 0.05 dB/km.

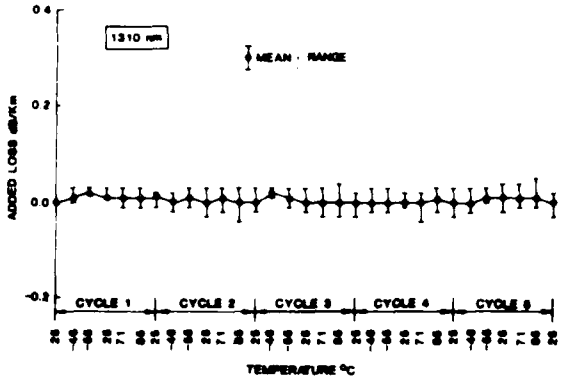


Figure 4. SIMFOCS Fiber Temperature Cycling Test Results

Buffered Fiber Performance

There were no specific requirements for buffered fibers, other than the dimensional requirements on the outer diameter and concentricity of the fiber. Every buffered fiber used in the cables was screened for these dimensional requirements. Though not required, the buffered fibers were also tested for response to temperature cycling. The results of this test, which uses the same cycle described in the fiber section, are given in Figure 5. The buffered fibers were also subjected to an accelerated-aging test which basically simulates the use of this buffered fiber (and the cable in general) at 85°C for the design life of 25 years. The accelerated aging test consists of exposure of the materials to 110°C for 14 days. This time-temperature relationship was arrived at by using viscoelastic principles. The excellent accelerated-aging performance of the buffered fibers is illustrated in Figure 6. After the completion of the accelerated-aging test, further testing was continued with temperature cycling between -75°C and 100°C. The results of this temperature cycling are also presented in Figure 5 and again show the excellent performance of the buffered fibers.

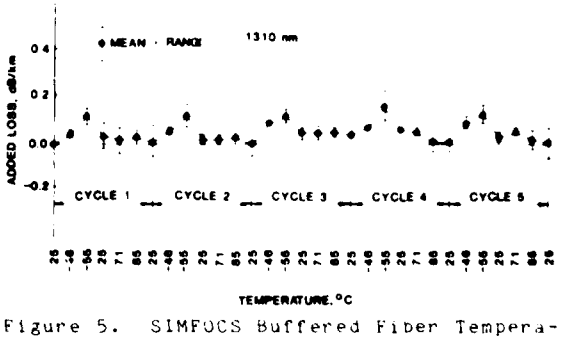


Figure 5. SIMFOCS Buffered Fiber Temperature Cycling Test Results

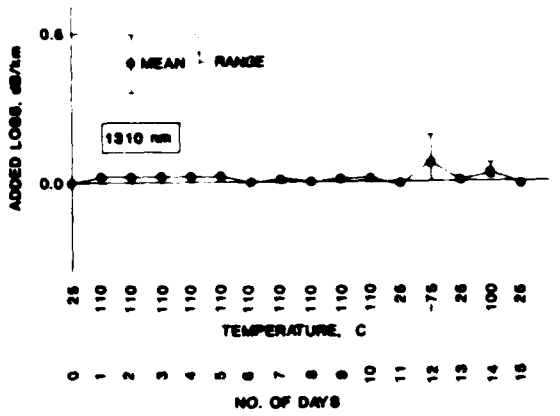


Figure 6. SIMFOCS Buffered Fiber Accelerated Aging Test Results

Cable Performance

The SIMFOCS cables, as a component of the assembly, were subjected to a battery of optical, environmental, and mechanical tests. The mean optical loss was [illegible] dB/km at 1310 nm, showing that there was basically no added loss due to the buffering and cabling processes for these cables. The cable was designed for a temperature range of -40°C to 71°C, and the evaluation was extended to -75°C and 85°C as mentioned before. The results of temperature cycling of three samples of 1-km lengths are presented in Figure 7. The stars (*) in Figure 7 are worst case data points which represent one out of six test fibers. The plotted means given also include these worst case data.

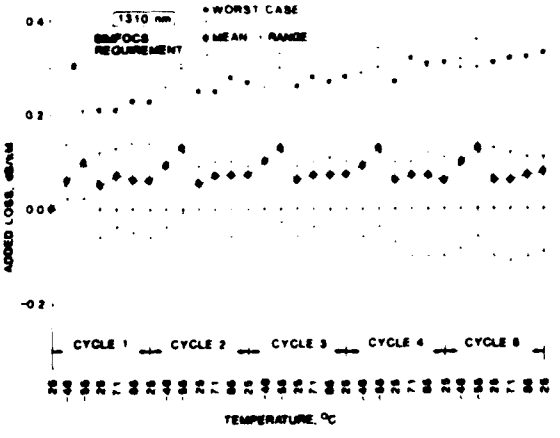


Figure 7. SIMFOCS Cable Temperature Cycling Test Results

The cables pass the requirement of 0.5 dB/km maximum added loss for three temperature cycles between -40°C and 71°C. The cable also passes the requirement for five temperature cycles between -55°C and 85°C, accounting for the accuracy of the measurement system of ± .05 dB/km. The maximum of mean added loss was at -55°C and was less than 0.15 dB/km. As a comparison, the multimode TFOCA cable had an added mean loss of less than 0.2 dB/km as opposed to the requirement of 0.5 dB/km between -55°C and 85°C. This establishes that the basic cable design is applicable for both multimode and single-mode fibers.

The results of accelerated aging testing of three 0.5 km lengths are presented in Figure 8. This figure, again, shows excellent performance of the cable not only for the accelerated aging test, but also for the unrequired temperature cycling between -75°C and 100°C. The temperature cycling between -75°C and 100°C was added to this aging test just to study the performance beyond the cable's design limits. During the temperature cycling, at -75°C, one fiber had an added loss of about 1.0 dB/km, whereas the remaining five fibers were far below the requirement.

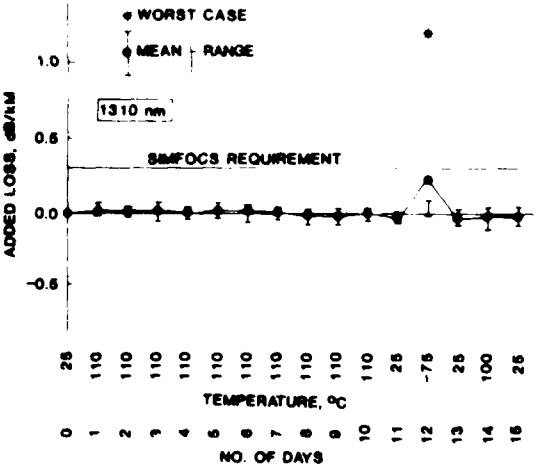


Figure 8. SIMFOCS Cable Accelerated Aging Test Results

The cables were also subjected to a long list of mechanical tests. The results of these tests are summarized in tabular form. Table I presents these tests, test procedures, test requirements, and the SIMFOCS cable's performance. Figures 7 and 8 and Table I clearly show the SIMFOCS cables meet and surpass all the optical, environmental and mechanical requirements.

TABLE 1.

SIMFOCS CABLES MECHANICAL REQUIREMENTS AND PERFORMANCE

NO.	TEST DESCRIPTION	PROCEDURE AND REQUIREMENTS	SIMFOCS CABLE PERFORMANCE
1	OPERATING TENSILE LOAD	EIA-455-FOTP-33 300N (66lbf), 5 MINS ADDED LOSS, $\Delta \leq$ 0.2 dB	300N (66lbf), 5 MINS $\Delta \leq$ 0.1 dB
2	TENSILE STRENGTH	EIA-455-FOTP-33 1780N (400lbf), ELONGATION $\leq$ 2.0% Δ -NOT SPECIFIED	1780N (400lbf), ELONGATION = 0.67% $\Delta \leq$ 0.1
3	COLD BEND	DOD-STD-1678, 2020 MANDREL DIA. = 30mm -46°C, 10 kg, 1 TURN $\Delta \leq$ 0.2	3 TURNS, $\Delta \leq$ 0.1
4	IMPACT	DOD-STD-1678, 2030 1.5 kg, 15 cm, 100 CYCLES $\Delta \leq$ 0.2	2.0kg, 15 cm, 200 CYCLES $\Delta \leq$ 0.1
5	KNOT	AT&T BELL LABORATORIES DIAMETER = 30 mm $\Delta \leq$ 0.2	$\Delta \leq$ 0.2
6	COMPRESSION	DOD-STD-1678, 2040 10.1 cm DIA., 2110N (475lbf), $\Delta \leq$ 0.2	8450N (1900lbf), $\Delta \leq$ 0.2
7	CYCLIC FLEXING	EIA-455-FOTP-104 MANDREL DIA = 30mm 4 kg, 2000 CYCLES $\Delta \leq$ 0.2	10 kg, 4000 CYCLES $\Delta \leq$ 0.1
8	FREEZING WATER IMMERSION	DOD-STD-1678,4050 -10°C, 8 HOURS -2°C, 1 HOUR $\Delta \leq$ 0.2dB	$\Delta \leq$ 0.1
9	TWIST BEND	NOT RFQUIRED	DOD-STD-1678, 2060 MANDREL DIA = 30mm 10 kg, 4000 CYCLES $\Delta \leq$ 0.1
10	CORNER BEND	NOT REQUIRED	AT&T BELL LABORATORIES 1 mm RADIUS, 900N (200lbf) $\Delta \leq$ 0.2
11	FLAMMABILITY	DOD-STD-1678, 5010 60 ANGLE TEST, EXTINGUISH $\leq$ 30 SEC	$\leq$ 6 SEC

Connector Performance

The primary design objectives of the duplex connector are low coupling loss and field ruggedness. The unit is required to remain optically and mechanically functional under environmental and mechanical exposures typical of tactical field applications. Tests were conducted to evaluate performance with respect to the requirements listed in Table II. Some of the tests are reviewed and the results summarized in the following paragraphs.

TABLE 2

CONNECTOR REQUIREMENTS

- INSERTION LOSS : 0.8dB MAXIMUM AVERAGE
- MATING DURABILITY : 1000 COMPLETE CYCLES
- COUPLING TORQUE : 0.75 INCH-POUND MAXIMUM
- SHOCK DROP : 10FT. DROP 6 TIMES
- SHOCK : 40G SAWTOOTH PULSE. 11ms DURATION
- VIBRATION : 5-500-5Hz. 15 MINUTE SWEEP. 4.2g
- CABLE RETENTION : 1780N (400LB.)
- FLEX LIFE : 2000 CYCLES AT 20°C. 1000 CYCLES AT -55°C
- TWIST LIFE : 1000 CYCLES AT +20°C
- HIGH TEMPERATURE : MIL-STD-810D, METHOD 501.1 (71°C)
- LOW TEMPERATURE : MIL-STD-801D, METHOD 502.1 (-57°C)
- WATER IMMERSION : 2-METER DEPTH, 24 HOURS
- HUMIDITY : MIL-STD-810D, METHOD 507.1
- SALT FOG : MIL-STD-810D, METHOD 509.1
- DUST : MIL-STD-810D, METHOD 510.1

Coupling Loss: Coupling loss measurements were made by concatenating pairs of plug-terminated 1-km cables randomly selected from a group of 16. The coupling loss was derived by subtracting the cabled-fiber attenuation from that of the measured assembly. For 60 couplings (120 channels) the mean loss and standard deviation were 0.67 and 0.24 dB, respectively, as shown in Figure 9.

Connector-loss measurements were also made using the cut-and-insert method per EIA Fiber Optic Test Procedure No. 34 on four 12-m long cables. Average loss was 0.55 dB with standard deviation of 0.11 dB.

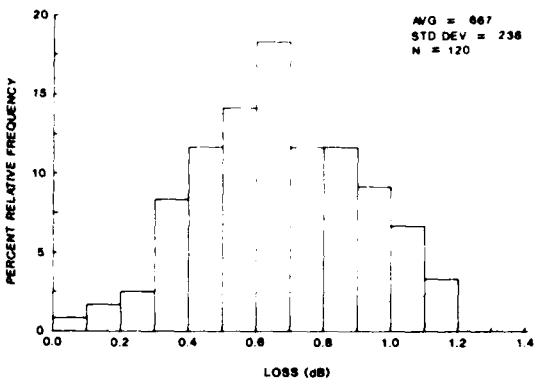


Figure 9. SIMFOCS Connector Coupling Loss

Mating Durability: This test was conducted to determine the mechanical durability of the connector assemblies as a result of 1000 coupling cycles. The failure criteria includes visible physical damage as well as optical malfunction. Loss readings were made at increments of 50 matings. At the conclusion of the test, the loss in each channel was within 0.09 dB of the initial baseline readings. The maximum loss increase observed during the test was 0.24 dB. The connectors were cleaned once after 750 matings.

Mud Immersion: The connector was designed to allow quick access to the biconic components so they can be easily cleaned after mud immersion. This aspect of the design was evaluated by subjecting a connector pair to 10 cycles of the following sequence:

a. decouple and immerse each end in a mud bath for 5 minutes;

b. water rinse, wipe clean, and air dry;

c. recouple and measure loss.

The maximum observed loss change was 0.13 dB.

Cable Assembly Performance

The 1-km long cable assemblies, including connectors, are required to be subjected to a battery of environmental and mechanical tests to insure reliable performance in the tactical field environment. Table III lists the tests. Some of the results are summarized below.

TABLE 3.
BATTERY OF CABLE ASSEMBLY TESTS

ATTENUATION
STORAGE/TRANSIT TEMPERATURE
HUMIDITY
SALT FOG
IMMERSION
TEMPERATURE CYCLING
VIBRATION
SHOCK

Attenuation: Attenuation measurements were made by concatenating pairs of plug-terminated 1-km cables randomly selected from a group of 16. For 64 couplings (128 channels) the mean loss and standard deviation were 1.08 and 0.23 dB, respectively, as shown in Figure 10.

Storage and Transit Temperature: The cable assembly was exposed to temperature extremes from -55°C to +85°C to determine whether adverse effects would result from storage and transit environments. Maximum loss increase observed was 0.09 dB.

Immersion: The cable assembly was immersed in a tank with one meter of water covering the unit for two hours. No evidence of leakage was observed.

Conclusions

The single-mode duplex tactical cable assembly described herein meets the requirements prescribed by the project sponsor, the U. S. Army CECOM. The average cable-assembly loss of 1.08 dB is well within the system transmission loss target of 1.4 dB for cables. Low-loss fiber, cable, and connector designs have been integrated successfully into the assembly.

By adapting the basic TFOCA design and AT&T's single-mode fiber technology, considerable development effort, time, and expense was conserved.

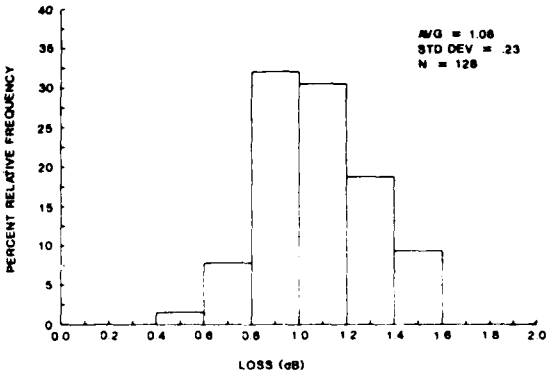


Figure 10. SIMFOCS Cable Assembly Loss

Acknowledgements

This development and testing was supported by a number of people from AT&T Bell Laboratories and AT&T Network Systems. The authors gratefully acknowledge their contributions.

References

1. U. S. Army CECOM Contract No: DAAB07-85-C-K565.

2. U. S. Army CECOM Contract No: DAAB07-84-C-K551.

3. A. C. Jenkins, C. R. Lovelace, M. R. Reynolds and V. E. Kalomiris, "A Tactical Fiber Optic Cable", International Wire and Cable Symposium Proceedings, 1985, pp. 82-87.

4. J. M. Anderson, B. V. Darden, B. G. LeFevre, V. E. Kalomiris, "A Two-Fiber Tactical Fiber-Optic Connector," International Wire and Cable Symposium Proceedings, 1985, pp. 286-292.



Bruce V. Darden is a Member of Technical Staff at AT&T Bell Laboratories, Norcross, Georgia. He received a B.S. degree in Engineering from North Carolina State University in 1951, and held engineering positions with Western Electric until 1960 when he joined AT&T Bell Laboratories. He is currently a member of the Connector Systems Development Group.



K. Kathiresan is a Member of Technical Staff in the Lightguide Technology Department at AT&T Bell Laboratories in Norcross, Georgia. He is responsible for design and development of specialty fiber optic cables, including military applications.

Dr. Kathiresan joined AT&T Bell Laboratories in 1985 at Norcross, Georgia. He has a B.E. Hons degree in Mechanical Engineering from University of Madras, India, M.E. in Aerospace Engineering from Indian Institute of Science, India, and Ph.D. in Engineering Science and Mechanics from Georgia Institute of Technology, Atlanta, Georgia.

Dr. Kathiresan is a Senior Member of American Institute of Aeronautics and Astronautics and a Member of American Society of Mechanical Engineers. He is a Registered Professional Mechanical Engineer in States of Georgia and Florida.



V. E. Kalomiris is currently a project leader responsible for fiber optic cables, connectors, and fiber optic system development. He received the 3rd annual Engineering Excellence Award for 1986 from CECOM; served for three years as chairman of the Tri-Service Group on fibers, cables and connectors; and as a member of EIA FO.7 Working Group on Fiber Optic Cables. Most recently, he worked for ITT-EOPD as a project engineer for the air layable cable which he designed. Prior to joining ITT-EOPD, Mr. Kalomiris was associated with General Cable Corp. R&D as a research engineer for 6 years. While at General Cable he was involved with the design, development and manufacture of the prototype super-conductive power cable with flexible core. He is a member of IEEE and the Technical Chamber of Greece (Society of Professional Engineers). Education: B.A. in Mathematics, B.S. in Electrical Engineering, and an M.S. in Electrical Engineering, all from the New York University.

FIELD DEPLOYABLE FIBER OPTIC CABLES

Thaddeus R. Vlijasz and Ronald L. Ohlhaber

Belden Wire and Cable - Cooper Industries
Technical Research Center, Geneva Illinois

Summary

Fiber optic field deployable cables have been used for many years in a wide variety of applications not necessarily associated with the military tactical environment. These include transmission of video signals for electronic news gathering, at major sports events, and as data busses for signals from transducers in geophysical testing. For these applications, the survival requirements of a cable can be more demanding than in a military environment.

Experience with early field deployable cables containing two to six optical fibers in a tight buffer design indicated the potential for improvements in their mechanical properties. Some cables exhibited major changes in transmission between on-reel and service conditions.

Experimental data will be presented on various secondary buffer coatings and the trade-offs possible with this component. Consideration will also be given to strength members such as aramid fiber and how options such as the braid helical lay can affect tensile elongation.

Introduction

Field deployable cables must meet two contradictory sets of requirements. First, they must be rugged enough to withstand rigors of an unprotected outdoor environment which contains temperature extremes and various forms of physical abuse. Second, they must be light weight and very flexible. In addition, the cable test requirements must be commensurate with the intended application. For example, early military cable impact test requirements were excessively severe while a knot test was not required.

Field Experience

Initial field cable designs were driven by the need for excellent optical performance over a wide temperature range such as -55 to +85°C. This was due in part to the system optical power budget required for 850 nm electro-optic devices available at that time. Consequently, many of the first generation cable designs contained a rather large 1.1 mm fiberglass epoxy (FGE) rod as a central core. This produced a cable that provided stable transmission over the temperature range, however, other difficulties occurred in actual field applications. These field problems can be grouped in three categories.

1) Method of deployment and take-up. Although most cables are paid-out and recovered by using a reel without too much difficulty, alternate methods can result in major problems. Some of these other methods are the following:

   a) The cable is recovered by a mechanically powered take-up. Such equipment can often generate huge elongation forces when the cable is restrained by a snag. A monitoring device and slip clutch are needed on the take-up to limit tension on the cable. Another alternative is the use of safety shear pins which fracture when an overload is applied.

   b) The cable is pulled over the reel end or from a storage barrel. This method causes a 360° longitudinal twist in the cable for each turn removed. The result is a cable that probably won't lay flat. It will also tend to get knotted, kinked and snagged. Replacing the cable in its storage container can increase the twists and result in worse problems during the next deployment.

   c) The cable is paid-out and recovered one loop at a time while being carried on the shoulder. This method places low force on the cable. However, repeated deployment and recovery using the same direction winding will again place longitudinal twists in the cable. This again causes problems identical to the prior case.

It should be noted that all these methods are successful with non-fiber optic cables. Additionally, the prior methods can leave residual strains in the cable when stored. This may lead to a failure after one deployment. Figure 1 shows a cable that passed its required



Figure 1. Fiber Optic Cable in Storage Drum.



Figure 2. Cables After a Rodent Attack.

attenuation performance while on the shipping reel, however, it later failed in the drum container. This can be attributed to fiber microbending losses at the cable kinks and bends.

2) Animal attack. Many accounts of animal attack have been reported. Some were anticipated, but the severity of this problem in some parts of the world was not expected. For example, in Egypt it was reported, "The rats here are as large as cats and eat absolutely anything." In Sumatra, "Can you deliver a cable with a much thicker jacket? The rodents here chew anything they can get their mouths over." And in the Western U.S.A., "The cable cannot always withstand the action of cattle hoofs." The weight applied by a cattle hoof doesn't seem to be the problem. Instead, it appears that the wiping action of the hoof movement causes internal damage.

   There have been many attempts to make a rodent-proof cable. However, the most effective cables have passed Rural Electrification Association (REA) testing with the use of a metallic armoring system. The result of an attack on a double-jacketed cable with a stainless steel braid by a pocket gopher is shown in Figure 2. This cable passed the test, but the armor added considerable weight to the construction.

3) Other field problems. This category contains human errors which probably are the major cause of cable failures. Such things as accidental machete slash, vehicle attachments, crushing in doors and numerous other unforeseen events lead to the damage or disruption of deployed cables.

The one method of handling cable breaks in the field is to have additional cables available for substitution. However, the economics of cable repair make eventual splicing very attractive for the damaged cable. Figure 3 shows a cable that has been repaired for various reasons at six locations over a 600 m length. To date, some field cable applications have seen three generations of improvement in cable repair techniques.



Figure 3. Repairs on a Fiber Optic Cable.

Based on these experiences, fiber optic field deployable cable must be considered expendable in that it cannot withstand every environmental hazard and can only be repaired a limited number of times. Also, customer and manufacturer coordination on methods of cable handling can alleviate potential problems.

The preceding experiences indicated that many properties of cable design could be examined for improvement. The following areas were selected to improve physical performance:

1) Impact resistance and the fiber secondary coating.
2) Microbend resistance for reduced localized loss.
3) Flexibility via suitable strength members.

Fiber Secondary Coating

An early cable design employed a soft, conformal secondary buffer coating with a Young's modulus of only 800 PSI. This cushioned the fiber in a construction, however, it did not offer much aid in physically protecting the fiber. A tougher, harder material with a modulus of 30,000 PSI was also investigated. A comparison was made by performing impact testing on both types of fiber coatings in a cable construction.

These fiber coatings were tested in two styles of fiber cable, see Figure 4. The first had a single thick 1.75 mm wall jacket and the other a dual jacket with a 0.5 mm wall inner jacket and 1.0 mm wall outer jacket. All four cables had a 6.0 mm O.D.

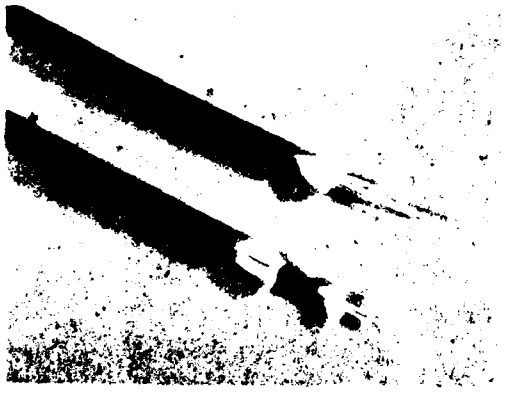


Figure 4. Single - and Dual-Jacketed Two Fiber Field Cables.

The results of impact tests on the four cables revealed that the higher modulus fiber secondary buffer coating produced significantly better protection. Also, the double jacketed cables produced a higher level of impact resistance.

During impact testing, initial data seemed inconsistent until it was determined that the exact point of impact was very important. If the lay of the fibers in the cable were over each other at the impact point, as shown in Figure 5, they broke much sooner than if they were side by side.



Figure 5. Cable Configuration During Impact Testing.

Other tests such as twist bend and flex were performed. However, these tests revealed no distinct advantage to any of the four constructions. All constructions passed these tests.

Microbend Resistance

In addition to improved impact resistance, it is also possible to improve the microbend resistance. This makes the cable less sensitive to the bending losses.

It is extremely difficult to account for all the forces creating increased attenuation in a cable construction on a theoretical basis. One goal is to have a fiber buffer coating with a high modulus that offers maximum lateral protection while causing minimum microbending. This topic has been the subject of an intense industry-wide investigation (Ref. 1 to 9).

Many different fiber coating schemes were examined including one which had five coating layers (9). Again, a single overcoat of a harder material was selected on the basis of simplicity and the belief that the fiber would still achieve acceptable temperature performance.

Microbend testing of various secondary coating materials was performed by pressing the fiber between plates containing sand paper surfaces as described in the current draft of EIA FOTP-68. The results are shown in Figure 6.

Strength Member

In order to improve cable elongation properties, a careful evaluation of strength member configuration is necessary. Both braids and serves can be considered with particular attention to the braid helical lay. The popular method of describing a braid is in picks per inch (PPI) with a "pick" referring to each crossover in the braid.

When comparing a braid to a served strength member, there are significant differences. A braid is a balanced construction while a serve is not. Axial loading a served cable results in the core tending to wrap around the serve. On

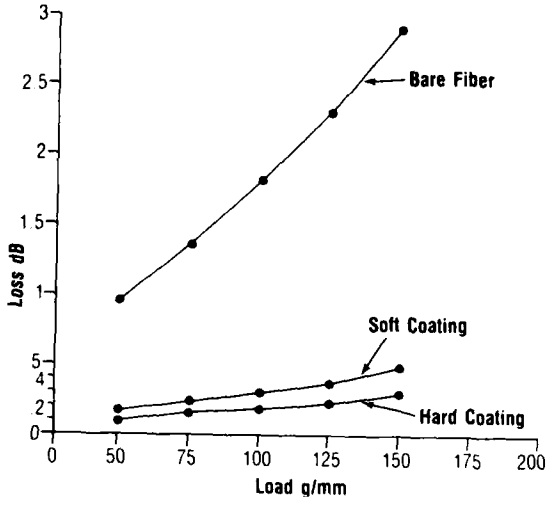


Figure 6. Fiber Microbend Resistance Tests.

the other hand, a braid tends to compress the core when under strain. This can be significantly reduced by selecting the proper PPI or braid helical lay for a given core size. The pressure exerted on the cable core can be modeled by:

$$P = \frac{Aa\,(2\pi)^2}{WL\,[(2\pi a)^2 + L^2]^{\frac{1}{2}}}$$

where P = pressure
A = tension along cable axis
a = radius of helix
W = width of strength elements
L = lay length.

To calculate the pressure, the effective "W" must be determined. It depends on the following factors:

1) The width of each strength member end wrapped on the cable.
2) The number of strength member ends.
3) Voids, coverage and crossover area of the braid.

As an example, let's assume the area of double coverage at crossover equals the area of voids. Then the prior equation becomes:

$$P = \frac{A\,(2\pi)}{L\,[(2\pi a)^2 + L^2]^{\frac{1}{2}}}$$

Figure 7 is a graph of this expression which shows that the pressure on the cable core for a large radius braid is greatly influenced by a lay length of less than two inches. The lay length and core radius also determine the helical lay angle or the PPI. A low PPI or helical lay angle applies the major contribution of the strength member toward elongation instead of core compression.

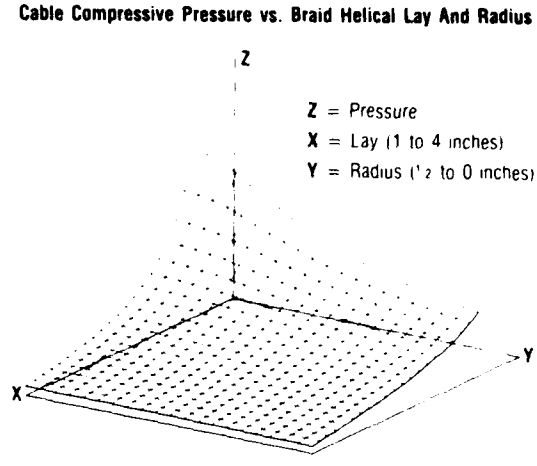


Figure 7. Cable Compressive Pressure Versus Braid Lay Length and Center Radius.

However, if the PPI is too low, there is a risk of unacceptable braid movement during a twist-bend test. This can result in movement of the core through the braid as shown in Figure 8. Here, the core element has been exposed due to friction between the outer jacket and the braid. This results in eventual increased fiber attenuation and possible damage. A served strength member also has this potential problem.

Central Stabilizing Member

For cables with more than two fibers, a central member made of fiberglass epoxy (FGE) can be employed to improve temperature stability. The thickness of this rod determines cable rigidity. It can be rather small to make the cable more flexible and allow it to pass a knot test. The trade-off for doing this is a larger net thermal coefficient of expansion for the cable. A



Figure 8. Braid Movement Resulting From Cable Flexing.

simple comparison of the net thermal coefficient of expansion for a 1.1 mm vs. 0.5 mm FGE rod was made using a 6.4 mm O.D. cable construction. The calculated result was a 33 percent increase in the net expansion coefficient.

Overall Cable Structure

Combining the prior components leads to cables which have a higher modulus buffer coated fiber, the proper braid or serve and an appropriate central core. The resulting cables provide performance properties listed in Table 1. Here, an early cable is compared with a current design. The result is conformance to all the desired test requirements.

Conclusions

Based on information from field experience, cable structures were redesigned to optimize their performance. It was found that harder secondary buffer coatings on the fiber, smaller stabilizing elements, double jackets and an improved strength member configuration could substantially improve performance.

References

1. D. Marcuse, "Bent Optical Waveguide With Lossy Jacket," The Bell System Technical Journal, July-Aug., 1974.

2. D. Gloge, "Optical-Fiber Packaging and Its Influence on Fiber Straightness and Loss." The Bell System Technical Journal, Feb., 1975.

3. G. S. Brockway and M. R. Santan, "Analysis of Thermally Induced Loss in Fiber-Optic Ribbons." The Bell System Technical Journal, April 1983.

4. Yutaka Katsuyama, et al, "Transmission Loss of Coated Single-Mode Fiber at Low Temperatures." Applied Optics/Vol. 19, No. 24/ 15 Dec. 1980.

5. Fumio Yamamoto, et al, "High-Modulus Low-Linear-Expansion Coefficient Loose-Jacket Optical Fibers." Journal of Lightwave Technology, Vol. LT-2, No. 2, April 1984.

6. Tetsuro Yabuta, et al. "Excess Loss of Single-Mode Jacketed Optical Fiber at Low Temperature." Applied Optics/Vol. 22, No. 15/1 August 1983.

7. K. Masuno, et al. "Optimum Design of Coated Optical Fiber Considering Excess Loss at Low Temperatures." Journal of Optical Communications, 1982.

8. L. L. Blyler, Jr., et al. "Buckling of Optical Fibers Within Elastomers Used in an Embedded-Core Cable Structure." International Wire & Cable Symposium Proceedings 1983.

9. Antonio Portinari, et al, "Metal Free, Fully Filled Optical Cable for Telecommunication Use." International Wire & Cable Symposium Proceedings 1981.

Table 1 Mechanical Testing of Six Fiber Cables.

Mechanical Parameter and Requirements	Maximum Change in dB/km	Test Methods DOD Std. 1678	Early Cable	Current Cable
Impact, 200 Impacts at 4.4 N-m	0.5	2030	Fail	Pass
Tensile Load, 600 lbs.	1.0	3010	Pass	Pass
Cycle Flex, 2000 Cycles	0.5	2010	Pass	Pass
Cold Bend	0.5	2020	Pass	Pass
Temperature Cycling, (-55 to +85°C)	1.0	4010	Pass	Pass
Compressive Strength, 600 lb. Load, 4 inch Plates	0.5	2040	Fail	Pass
Ice Crush	0.5	4050	Pass	Pass
Twist Bend 2000 Cycles	0.5	2060	Pass	Pass
Knot Test	0.5	-	Fail	Pass





About The Authors

Ronald Ohlhaber received a B.S. Degree in Physics from Loyola University and an M.S. Degree, also in Physics, from DePaul University. He is presently Product Development Manager for the Fiber Optics Group located at Belden's Technical Research Center in Geneva, Illinois. Prior to joining Belden, he was engaged in fiber optic and electro-opic research as a staff member at IIT Research Institute and also worked in similar areas for the government and industry.

Ted Ulijasz received a B.S. Degree in Physics (1969) and an M.S. Degree in Electronics Engineering Technology from Northern Illinois University. He is a Belden Product Development Engineer with responsibility for fiber optic cables. Before joining Belden, he worked in Engineering for Fermilab.

FIBRE OPTICS IN DYNAMIC STRAIN CABLES

DR. TREVOR R. SMITH - STC DEFENCE SYSTEMS (UK)
MR. DENNIS R. CARTER - MINISTRY OF DEFENCE A.R.E.(S) (UK)

SUMMARY

The paper examines the development of a load carrying electro-optic cable assembly typically used for naval towed applications. As a full scale research and development exercise, different arrangements and positions of fibre optics were incorporated into the design to allow the evaluation of manufacturing parameters to be undertaken in order to determine suitability for long term operational use.

Coupled with the design and manufacturing programme was an extensive series of land based and sea trials, which have proven that an adequately ruggedised fibre optic element, if correctly positioned within the structure, is capable of withstanding all the rigours of operational service.

FIBRE OPTICS IN DYNAMIC STRAIN CABLES

Introduction

Copper cored cables have been extensively used for many applications in Naval and offshore applications, in which the cable is continuously exposed to stressing both static and dynamic. Over the past 30 years considerable expertise has been built up in the design and application of the cable technology. Specialist techniques have evolved to give high performance and high reliability.

Over the past decade considerable development has taken place in the development of optical fibres, methods of buffering, reinforcement and nuclear hardening, but most of this technology has been directed towards mainly static systems land telecommunications, pylon mounted data links, fixed installations, etc. However, there was little data or experience of fibre optic cable systems in dynamically strained environments. The only experience available applied to bundles of optical fibres being included in umbilicals for ROV where bandwidth was the major requirement, but this was not considered relevant to dynamically strained cables in the context discussed in this paper.

Perceiving the obvious advantages of the properties of optical fibres, STC Defence Systems and the Ministry of Defence, Admiralty Research Establishment, Southwell, Portland, jointly set out to develop the technology for introducing fibre optics in dynamically strained cables. A tow cable design was selected as a suitable study. This paper describes the background to the design and evaluation of such a cable. In many cases we have had to relearn the obvious. Hindsight is always helpful when you have a track record, but is no use without knowledge of the full limitations. Foresight when extending the boundaries of knowledge, without the base data, may lead you into uneconomic or too conservative designs.

Strain Cable Design

A dynamically strained cable consists of a series of cores helically laid up in a manner to give long term performance, all contained within a plastic sheath. Two or more layers of contrahelically wound high strength galvanised steel wire is wrapped around this sheath to take the dynamically imposed operating loads and provide torque balance. The optical fibre units had to be designed to withstand not only the projected operating loads, but also the handling and manufacturing loads, since these are far more demanding than for conventional loose tube telecommunication cable designs. A cable was designed which satisfied the need to investigate different positions for optical fibre cores in an electro-optic centre. It contained both reinforced single fibre units and a reinforced quad. Whilst the former was a well tested design, a sub programme of mechanical tests was necessary to prove the suitability of the quad unit in the dynamic mode prior to its inclusion in the cable. Also contained within the development tow cable were electrical power conductors necessary to energise wet end instrumentation in future sea trials.

Two lengths of electro-optic cable were produced with particular attention paid to the performance of the optical fibres during cabling. For each production stage, process development was undertaken to provide the fibres maximum chance of survival and ensure minimal deterioration of optical transmission properties.

In parallel with the development of the tow cable, STC and A.R.E.(S) organised the design and construction of an optical transmitter/receiver pod for use in the planned sea trial. This contained a loss monitoring system for the requisite number of fibre channels and utilised one channel for transmission of depth information.

Upon completion of the cable development, one cable length was submitted for land simulation tests whilst the other was prepared with mechanical, electrical and optical terminations in readiness for the towing trials.

TOW CABLE DESIGN

Fibre Optic Units

The basic fibre used was 50/125 micron graded index type, designed for multimode transmission at 850 nm. Each fibre had a thermoplastic secondary coat of polyether-ester elastomer, and had been subjected to a proof strain test of 1% elongation.

Two types of unit were included in the tow cable design; a reinforced single fibre and a reinforced quad. The former was an existing design which had been developed by STL Harlow for use in single fibre dispenser applications. It included Kevlar reinforcement over the fibre and an outer jacket of polyether-ester to 1.5 mm diameter. Three such units were produced for each cable length with an over-extrusion of polyethylene bedding compound applied to the fibre forming the cable centre.

The quad unit was purpose designed for the tow cable. It was originally intended that two fibres should be combined with two insulated constantan wires although the design was later changed in favour of four fibres. This was because it was found that the constantan cores could not be used for strain evaluation during cabling due to the process length losses. The four cores were twisted together at an appropriate helix lay angle and with Kevlar reinforcement members laid in the outer interstitial spaces. The reinforced quad was then oversheathed with a solid extrusion of high density polyethylene giving the finished unit a diameter of 3.62 mm.

Constantan Units

Two Kevlar reinforced, insulated constantan wires were included in the design with the intention of evaluating the strain changes in the reinforced optical units during cabling. For reasons described above these units became redundant although they were cabled as intended to preserve symmetry.

Power Cores

Three 19 strand copper conductors functioned as the power link to energise wet end electronics. The diameter over the high density polyethylene insulation was identical to the optical quad unit (3.62 mm) to obtain a regular formation.

Cable Lay Up

As shown in Figure 1, the three power cores and the optical quad were laid around a reinforced single fibre. The remaining two reinforced single fibres plus the two reinforced constantan wires were laid into the outer interstices formed by the major units.

The whole formation provided a means to investigate the effects of cabling fibres with no helix (centre), a single helix (outer interstitials) and a double helix (quad).

Cable Sheath

A solid extrusion of low density polyethylene functioned as external protection and an overall water barrier for the electro-optic centre. This material is widely used in conventional electrical towed array cables for its flexibility and resiliance to marine degradation and can be easily moulded to form pressure tight terminations.

Armour

Particular attention was paid to the design and processing of the double layered external strain member to avoid excessive twisting of the cable at any stage. Its helix lay angles and wire sizes were chosen to give torsional balance between the inner and outer layers. In addition, special techniques were employed during application of the high tensile steel wires to minimise rotation of the centre.

The diameter of the completed tow cable was 20.3 mm and its theoretical minimum breaking load was 20 tonnes.

Cable Development

The cable described above was produced in two lengths 368 and 573 m, the former being for land testing and the latter for extensive sea trialling. The difference between the two cables existed only in the design of the optical quad unit. This contained two fibres plus two constantan wires in the land test lengths whilst the quad for the sea trials contained four fibres.

During the manufacturing process it was noted that the central and interstitial fibres suffered high attenuation increments rendering them unsuitable for evaluation. The design of the reinforced quad was however successful and in both the land and the sea trial cables, all fibres withstood quadding and subsequent cabling operations, with attenuation below 6 dB/km in all but one fibre. This other fibre at 12.7 dB/km was considered unsuitable for trialling.

CABLE LAND TESTS

Cyclic Tension Test

Under the influence of ship motion, a towed cable will be subjected to repeated axial loading above and below the nominal system drag forces. Using the loads measured during sea trialling of a towed drogue and known periods typical for ship motion, a land simulation of this towing condition was produced.

One 220 metre length of armoured tow cable was prepared with resin cone strain terminations contained within suitable armour blocks. Optical/electrical pigtails extended beyond the mechanical terminations at each end to enable performance monitoring during the test.

The test sample was fitted to the tension rig by means of anchorage ropes at both ends. This enabled the cable to be held completely straight and avoided standing turns on the tensioning winches at either end of the test bed. The general arrangement was shown in Figure 2.

Prior to testing, the three available fibres (two from the quad unit and one from the centre position) were examined using an O.T.D.R. (Optical Time Domain Reflectometer) at zero load, 500 kgf, 1000 kgf and 1500 kgf with the loads being sustained for at least five minutes in each case.

There followed a low load cycling phase intended to settle the armour construction. This consisted of 100 loading cycles of sinusoidal waveform having a ten second period and maximum and minimum load levels of 1000 kgf and 500 kgf respectively.

Upon completion of these preliminary trials, the cable sample was subjected to the desired test conditions. For this, the period was again ten seconds but the maximum load was increased to 1500 kgf and the minimum to 1000 kgf. The cycling proceeded with three fibres continuously monitored by O.T.D.R. analysis. This enabled estimates of changes in fibre attenuation to be made over the 1000 tension cycles completed.

Using two channels of optical monitoring, loss estimates were obtained for one quad fibre and a loop path formed by the other quad fibre and the central core spliced together at the far end. The use of O.T.D.R. equipment for this application enabled a constant visual display of localised effects along each fibre. Also obtained from this analysis was the net loss for each optical path. Since this figure also contained splice losses, only the changes have been listed in Table 1. These are assumed to be derived from the fibres only.

It was apparent that small increases in attenuation resulted when the cable was loaded. The distribution of these increments inferred that they were caused by compression of the armour on the sheathed cable centre. From the magnitude of the changes, it can be concluded that the microbending induced in the central position was significantly higher than within the quad unit. This was expected since the external polyethylene sheath over the quad offered additional mechanical buffering to the fibres.

It was also demonstrated that partial recovery of the fibre states occurred upon tension release. Some residual attenuation increases were noted, but these were small compared with the values at maximum applied load.

Flexing Under Load

For the optical tow cable to function satisfactorily at sea it must have the capability to be reeled and flexed. This follows from the winches, pulleys and guides which facilitate deployment and recovery of the towed system. Simulation of this action was obtained using a cable reeling machine which had been fitted with a pulley of appropriate diameter. The load applied to the cable corresponded to the maximum predicted for the experimental towed system.

One test sample, approximately 15 metres in length was fitted with resin cone strain terminations and armour blocks at both ends. The sheathed cable centre was brought through the mechanical termination to allow optical monitoring during reeling. For this purpose, a series link was made of the three functional fibre cores using two splices.

In order that the fibres in the test sample could be monitored clearly on a O.T.D.R. screen, a tail was spliced onto one end to accommodate the input pulse launch signature.

The fully prepared test piece was subsequently fitted to the reeling equipment as shown in Figure 3. This had been prepared with a test pulley of similar size to the guide pulleys intended for the sea trial i.e.

0.75 metres radius. The stroke of the machine was adjusted so that at least one metre of cable passed from a straight position around the pulley and to the opposite straight position. Each machine cycle consisted of this movement and the return.

The test proceeded in two stages. First, the cable was reeled under relatively low tension (500 kgf) to confirm its bending capability. Second, a load corresponding to the maximum expected in service (1500 kgf) was applied and reeling undertaken again. In each case, the reeling rate was approximately 25 metres/minute; similar to the speed of the winch on the trials vessel.

Having reached 5000 cycles under these conditions, a small number of reeling cycles under a higher tension were included for investigative purposes. The maximum load applied in this analysis was 3200 kgf which corresponded to the theoretical maximum working strain of 0.25 .

Since the total length of the three tow cable fibres in series was not sufficient to produce a satisfactory backscatter trace on a O.T.D.R., their combined attenuation performance could not be monitored with an acceptable degree of accuracy. However, the O.T.D.R. pattern was used to confirm optical continuity and in the event of a break would have been able to identify the optical path at fault.

At intervals throughout the reeling programme, the backscatter trace was regenerated to check the integrity of the fibre link. At no time during the 100 low tension cycles, 5000 towing tension cycles or 160 cycles at 3200 kgf did this pattern undergo significant change. Reproductions of the O.T.D.R. outputs obtained before and after the 5000 cycles at 1500 kgf are provided in Figure 4. These demonstrate that no measurable deterioration occurred in any of the fibre cores.

The absence of any optical failures suggested that the fibres were adequately protected from crushing forces within the tow cable. Further, it confirmed that the radius of curvature of the helically laid fibres was appropriate for this mode of operation.

Other than consolidating the fundamental design principles used for construction of the tow cable, no further information (such as performance) could be gained from the results of the test, due to the restriction on sample length which prevented accurate loss measurement.

Load Versus Elongation and Ultimate Breaking Strength

The tensile characteristics of the tow cable needed to be fully understood prior to the sea trials to determine the strain which would be induced during towing. In addition it was necessary to confirm the theoretical value for breaking load to ensure adequate safety over the proposed maximum working load.

To suit the tensile test equipment, a seven metre sample was fitted with resin cone strain terminations. These were identical in design to the wet end strain terminations for the sea trials cable. The chosen dimensions of the armour blocks enabled interface between the strain termination and the standard shackles of the test equipment.

The sample was tensioned slowly up to 6.1 tonnes with measurements of diameter and a marked reference length taken at 1 tonne intervals. The results from the latter were compared to the value at 0.5 tonnes to obtain reliable extension figures.

At the 3 and 6 tonne levels, the sample was relaxed and retensioned twenty times to test the operation of the strain terminations. Above 6 tonnes no physical measurements were allowed for safety reasons. The tension was gradually increased up until ultimate tensile failure occurred.

The measured load-strain characteristics, are plotted in figure 5.

Ultimate tensile breakage for the sample was instantaneous (i.e. all wires failing together) at 20 tonnes. The cable break was located at the entry of one strain termination at the apex of the resin cone.

The load-elongation results inferred that the 0.25 maximum working strain would occur at approximately 3 tonnes cable tension. This was also verified as a safe working level compared with the ultimate breaking strength of the cable (the theoretically predicted value of 20 tonnes).

SEA TRIALS REPORT

Background Information

Trials Period:	20th January to 5th February 1986
Location:	Mediterranean Sea (off Gibraltar)
Trials Vessel:	R.M.A.S. Auricula

System Description

The towed system consisted of an optical signal transmitter contained within a protective metal pod connected mechanically to the experimental tow cable. The cable carried electrical power to the transmitter

and optical signals back to the shipboard receiver. The optical power levels sensed at the receiver were converted into voltage outputs which were fed to a laboratory via a multicore deck cable. In this way the losses introduced by the optical cores within the tow cable could be monitored during towing. Diagrams of this arrangement are shown in Figure 6 and 7.

The Fibre Optic Cable

A 573 metre length of armoured tow cable, as described above, was used for the sea trial. It contained three operational fibres within the quad unit plus one fibre displaying high attenuation (>10 dB/km). This was assumed to be an operational element for investigative purposes, but was not expected to endure the towing trials.

Cable Terminations/The Towed Pod

The Fibre Optic Tow Cable was mechanically, electrically and optically terminated within the cylindrical instrumentation pod, seen in Figure 8. Its steel wire armour was terminated using the potted resin cone technique which had previously been validated by tensile testing. A proof load of 6.6 tonnes was applied to the strain termination within its housing as part of the assembly procedure.

Exterior to the strain termination housing was the moulded urethane bend restrictor. This reduced the bending radius about the strain cone and protected the cable in this region.

Water penetration into the instrumentation pod was prevented by the use of double 'O' seals on all metal metal surfaces and a moulded collar on the cable's inner sheath. This collar was sealed in a watertight housing and thus prevented the ingress of water into the inner sheath.

Inside the watertight compartment of the pod was the optical transmitter unit. This contained the butt joint connectors which accepted the terminated fibres. The whole transmitter was clamped against the inside surface of the pod to prevent movement whilst towing.

Also contained within the pod was the wiring from the depth transducer which was connected to the transmitter by a standard circular plug and socket. The transducer itself was screwed and sealed into the nose at the towing eye end of the pod and was exposed to water pressure through two ducts drilled in the nose section.

Transmitter/Receiver Pair

The transmitter and receiver pair were designed and built for the towing trial. Their primary function was to enable continuous monitoring of optical losses within the tow cable. The system also included circuitry to transmit and decode information on the depth of the cable termination.

The wet end transmitter, powered via the tow cable contained five LED's producing amplitude-modulated light at 850 nm wavelength. The modulation frequency was fixed for the four channels involved by simple power monitoring and controlled by the pressure transducer output in the fifth channel.

The receiver, mounted on the shipboard winch, contained five PIN diodes which sensed optical signal outputs from the operational fibre cores. The outputs from these devices were amplified and their peak levels measured to obtain voltages which were proportional to the maximum power levels received. The receiver also included circuitry to decode the depth information. An analogue voltage output represented this parameter in addition to the four digit display visible on the outside of the receiver casement.

Towed Drogue and Tail

Since safety legislation had precluded the use of a weighted towed body to generate the required back tension, it was necessary for A.R.E.(S) to supply a drogue which would radically increase the drag forces on the system. During separate trials on the drogue to test its stability, back tensions of 1500 kgf had been recorded. However, this analysis had only been undertaken with a short length of steel wire rope so it was expected that speed/tension characteristics would be different when used with the optic tow cable.

To aid steady passage of the pod and drogue whilst towing, approximately 100 metres of rope tail was attached to the towing eye on the pod and threaded through the centre of the drogue. This not only improved stability whilst towing, but also created a small back-tension on the system prior to immersion of the transmitter pod. This helped to keep the pod and cable in line during deployment.

The Cable Handling System

The tow cable was contained on the shipboard winch drum occupying approximately one and a half layers when fully recovered. Its inner end was passed through an exit in the drum's flange and clamped into a convenient position for connection to the optical receiver (Figure 9).

In the outboard passage of the cable from the drum, the cable first rounded the guide pulley to the rear of the winch. The force on this pulley was sensed by pressure transducers attached to its framework. This provided a means of monitoring cable tension at any time during deployment, towing or

recovery.

The cable was then deployed from an elevated guide pulley which was supported by an A frame at the stern of the trials vessel (Figure 10). This could be pivoted seaward to facilitate safe immersion of the towed system. The guide pulley was suspended from the framework by an arrangement of orthogonally pivoted sub-frames which allowed free movement in all planes. A counter-weight positioned above this arrangement ensured that the pulley's weight would not dictate the cable position.

Instrumentation

The electrical outputs from the winch-mounted optical receiver were carried to the trials laboratory via a multicore deck cable. These were monitored using calibrated chart recorders provided by A.R.E.(S).

In a similar way, outputs from the ship's winch and a towed log allowed cable tension and ship speed to be recorded alongside pod depth and optical losses.

Since all unfaired cables strum when towed due to vortex shedding, the amplitude and frequency were measured by accelerometers attached to the cable in the x, y and z axis. This information was recorded on magnetic tape to allow subsequent computational analysis.

The Trials Programme

Since no previous sea trial had been undertaken by the Royal Navy using a dynamic fibre optic strain cable, the proposed towing programme reflected the need to gain performance data over a wide range of conditions. It was agreed between A.R.E.(S) and STC Defence Systems that trialling should consist of a series of confidence winning exercises applying slightly more stringent conditions each time.

For this reason, initial work consisted of straight line towing under relatively low loads. Speeds were gradually increased thereafter to monitor the effects of higher tensions in the cable. This was continued up to the cable's maximum working load.

After consolidating the cable's performance at high speeds and its recovery upon return to lower speeds, ship turns were attempted. These were designed to test the ability of the cable to be detensionsed and retensioned over a relatively short time. First 90° course changes were implemented at various speeds, then the more severe 180° turns were undertaken.

As a consequence of the cable's ability to survive this treatment, the provisional Towing Trials Plan was exceeded in cable tensions and ship manoeuvres.

Straight Line Towing

Preliminary Trial

Before immersion of the transmitter or movement of the cable, the system was activated on deck. This confirmed satisfactory operation of the three active optical channels and a very low output from the defective fibre (the gain of the receiver amplification had been maximised for this channel).

The deck cable was then disconnected to allow approximately 200 metres of cable to be deployed. Using this short tow mode, the operation of all monitoring systems was checked. It was noted that after energising the system a stabilisation period was necessary. This was believed to be a result of change in ambient temperature of the transmitter from the deck stowage position to the towing mode.

There followed an increase in ship speed from 4 to 6 knots under gentle acceleration and then a return to 4 knots. This was repeated to qualify the output from the towed log and to compare its value with the display of ships speed obtained from propellar rotation and pitch. The equipment was shown to be functioning reliably.

During this sequence of speed changes, it was first noted that instantaneous changes in optical power output accompanied the change in cable tension. This occurred on all channels. Also a feature of this first towing run was the intermittent output level changes from the defective fibre, suggesting a flaw or discontinuity in the optical path.

Upon recovery of the cable, pod and drogue, the system was re-activated to check the fibre outputs. These returned as before, but were again subject to a stabilisation period.

Operation Verification Exercises

To further test the performance capabilities of the towed system, the above procedure was repeated with the maximum towing length. This corresponded to approximately 430 metres of submerged cable, approximately 40 metres through the cable handling system and 100 metres remaining on the winch was standing turns (this number was reduced for subsequent towing runs to change the tow-off position).

Speeds were changed over the range 2.8 to 8.0 knots with particular interest paid to the recovery of optical power outputs upon return to the lower speeds. The changes were again shown to be coincidental with tension change and appeared to have no net degradational effects on fibre perfor-

mance. Also accompanying the speed changes were the predictable variations in pod depth. Reproducible values were obtained for similar ship speeds.

Towards the latter part of this phase of work, the sea conditions deteriorated. Accompanying the ship movement in 3 - 3.5 m (10 - 12 ft.) swell were oscillations in cable tension. As an analogous effect to the speed change this phenomenon also produced cyclic variations in optical power outputs. The peak tension reached by the compounded effect of high speed and large swell was 2.5 tonnes.

The inclement conditions also made recovery of the towed pod considerably more hazardous. Note was made that upon breaking the surface of the sea, the pod tended to pivot about a point beyond the cable bend restrictor. This suggested that a longer, telescoped sectioned bend restrictor would have been more protective.

O.T.D.R. Analysis

Although the loss levels measured by the system's receiver did not predict significant deterioration in any of the fibres, it was considered advisable to analyse their backscatter characteristics at this point. Using a O.T.D.R. traces were obtained for all three operational fibres. None contained any point defects or discontinuities which would infer the onset of damage through towing.

A list of the attenuation predictions derived from O.T.D.R. traces at this and subsequent stages is given in Table 2.

Extended Straight Line Towing

An extensive series of straight line tows at various speeds was undertaken. The effects of changing the towing speed relating to cable tension, pod depth and optical power output are presented graphically in Figure 11 - 12, and correspond to the three operational fibres.

It can be seen from these results that the values of relative attenuation ($= 10 \log P_T / P_0$ dB) where P_T = receiver output at any time T and P_0 = receiver output at the reference speed) followed closely the changes in cable tension and returned to approximately 0 dB upon return to the reference conditions.

Also noted, was the higher attenuation changes in Fibre No. 2 suggesting a greater sensitivity to internal compression. The fact that this fibre displayed the highest absolute attenuation (Table 2) is not thought coincidental.

During this prolonged period of straight line towing, an analysis of cable strumming was made. An accelerometer was attached to the cable above the water line and positioned on a nodal point of the observed oscillation (Figure 11). Lightweight instrumentation wire was used to carry voltage outputs from the sensor to the laboratory chart recorders. The three outputs corresponding to amplitude in three axis were displayed next to the recordings of optical outputs.

Whilst there appeared no common trends, the magnitude of oscillation was slightly less than that expected for deep surface towed systems. This was a consequence of the shallow towing angle.

Straight Line Towing with Additional Towed Weight

In an effort to induce strumming with a greater amplitude, a 50 kg "bomb" was shackled to the pod towing eye and the system deployed for further straight towing. Although the bomb did not have a significant effect upon the towing depth, it seemed to increase the amplitude of vibration at the slower speeds.

Data was again recorded by A.R.E.(S) personnel and stored on magnetic tape for future analysis.

During this investigation, the optical power outputs of all channels were again monitored. The results obtained followed similar patterns to those obtained without the towed weight i.e. attenuation increasing with speed but recovering upon return to the reference conditions.

90° Ship Turns

Sufficient confidence of the cable's durability had been gained to allow 90° ship turns using the full towing length. The nature of the turns was varied by selection of different speeds and rates of turn. However, it was soon established that a combination at low speed and wide turn was undesirable because of the stiffness in the guide pulley's orientation system. Under these conditions the cable had a tendency to ride up over the pulley's flange. Conversely, the limitation of the sharp turns was the lateral deflection of the pulley within the A frame.

A consistent pattern emerged for all turns regardless of severity. From the moment the ship commenced a change of course, the cable tension would start to relax. This would cause an increase in received optical power (i.e. a reduction in relative attenuation) on all three channels. The effect would continue until the end of the turn when the return to a fixed course would

cause the cable tension to recover. Optical power outputs would then return to their steady state values.

The relaxation of cable tension through the turn also caused the tow cable to sink in the water. Since the depth gauge was located at the extreme end of the cable the depth changes recorded by the receiver always lagged the changes in tension and optical attenuation.

The cumulative effect of a series of 90° turns to port and starboard with up to 20° of helm is recorded in Figure 15. It should be noted that Fibre No. 2 has been chosen since it represented the most extreme case. Also, the time axis, has been used to represent the order in which the turns were made and not the duration of each turn. An important feature to note in Figure 15 is the peak tension recorded during high speed towing. The 3.7 tonnes reached represents a cable strain in excess of 0.3% (as predicted from the Land Testing).

180° Ship Turns

Following a similar procedure to the above, the towed system was subjected to 180° turns under a range of speeds and rates of turn. Predictably, the longer turns were accompanied by greater changes in cable tension, fibre losses and pod depth although optical power outputs of all three channels returned to their starting values upon return to the steady state reference conditions.

To illustrate the effect of a severe 180° turn (at knots and with 15° of helm) the relevant parameters have been plotted with reference to time in minutes from the start of the manoeuvre. Figures 16 - 18 show the sequence for all three fibres.

O.T.D.R. Analysis During Towing

Having completed an extensive set of ship manoeuvres whilst loss measuring on all channels, the final phase of the allotted trials period was dedicated to O.T.D.R. analysis during towing. This endeavoured to determine the distribution of attenuation increase over each fibre in the towed cable and to make certain that the measured increases derived from the fibres.

From this analysis, it was necessary to disconnect the optical inputs from the receiver in order to access one end of each fibre with the O.T.D.R. test set. Traces were then obtained for each fibre while the cable was in a steady, straight line towing state. The procedure was repeated for different speeds to further investigate previously observed trends.

In each of the backscatter patterns it was apparent that an increase in attenuation was occurring within the fibre link and was distributed over the whole of the towed length. The attenuation estimates obtained are listed for the various speeds in Table 2. This also shows the values of attenuation estimated with the cable recovered onto the winch. Care must be taken in comparing this information with the earlier values since the cable tension was subject to variation during recovery. This was a consequence of the ship motion in rough sea.

Conclusions

The sea trial demonstrated that optical fibre components can be included in steel armoured multimore dynamic strain cables and function satisfactorily in the towing mode environment. The ability of the fibres to survive load cycling and flexing follows from the measures taken during cabling to provide adequate protection and to minimise the strains induced by each process.

By monitoring the levels of optical power output from the towed cable, it was possible to detect changes of fibre state corresponding with different towing conditions. The measured increase in attenuation followed directly increases in cable tension and are thought to be caused by the additional compression of the armour on the opto-electric centre. Upon release of the higher tensions back to a reference level, it was found that the fibre outputs generally recovered to their original values, inferring minimal net deterioration. As the converse of this condition, it was discovered that the reduction in cable tension during ship turns caused a temporary recovery in the optical power received i.e. the microbending was reducing by removing the compression forces.

Further verification of the nature of the loss changes was provided by the backscatter patterns of each fibre during towing. These indicated distributed increements along the towed length and did not suggest the presence of localised defects. O.T.D.R. analysis made after the sea trials confirms that loss increases measured during towing were fully recoverable upon relaxation of the cable.

Regarding the effects of low frequency strumming upon fibres, no certain conclusions can be drawn from the data obtained since the amplitude of vibration was not representative of standard towed array systems.

Overall Review

The design and manufacturing evaluation established that optical fibres can be laid up in a tow cable provided they are ruggedised and laid up in a manner to resist crusing forces (i.e. quadding or

with good bedding).

The land trials proved that the suitable optic fibre elements in the cable should be able to withstand all the rigours of sea deployment and operation, and this was confirmed by the extensive sea trials. The success of the trials reported have encouraged further demanding sea trials to be carried out during Summer 1987 with the existing cable and a programme of work to design and manufacture a more advanced cable has been commenced.

Acknowledgement

The programme of work described has been carried out with the support of the Procurement Executive of the Ministry of Defence.

The authors' wish to acknowledge the assistance of Mr. G. Lawrence and Mr. C.N. Davies for invaluable assistance in preparing this paper.

AUTHORS

Dr. Trevor R. Smith

Dr. Smith graduated as a Mechanical Engineer and stayed at the University of Nottingham to undertake research into glass reinforced plastics for which he was subsequently awarded his Ph.D.

He started his industrial career in 1968 with British Gas where he was responsible for the development of plastic gas distribution systems. He subsequently jointed Stanton & Staveley, an international pipe and fitting manufacturer, where he was Manager, Sales Technical Services. His career lead him in 1982 to become Engineering Director of valve manufacturer Battersley Heaton Limited. In 1984 he joined STC Defence Systems where he now holds the post of Technical Manager, Cable Systems Division.

Mailing Address:
STC Defence Systems,
Cable Systems Division,
Wednesbury Street,
Newport,
Gwent.
NP9 0WS

Tel: 0633 52131 Ext. 2229

Dennis R. Carter

On leaving the Royal Airforce in 1952, after completion of two years national service, he spent two years as a Design Draughtsman with Elliott Brothers working on Naval Gunnery Projects. He joined Her Majestys Underwater Detection Establishment in November, 1958 and spent the next seven years in design of hull outfit domes, directing gears, etc., for various ship and submarine sonars. With the advent of Admiralty Underwater Weapons Establishment in 1965 he started work on the Joint U.S./U.K. HMS Matapan Sonar Project, until culminating in the early trials in 1973. From 1973 to 1979 he led a design team working on various Sonar Projects from Butec Range Work, Sonar Buoys, Shock Effects, etc. From 1979 to present, he is responsible for strain cable research and cable handling systems involving design test and sea trials.

Mailing Address:

Admiralty Research Establishment,
(Southwell),
Portland,
Dorset.
DT5 2JS

Tel: 0305 820381 Ext. 3993

TABLE 1

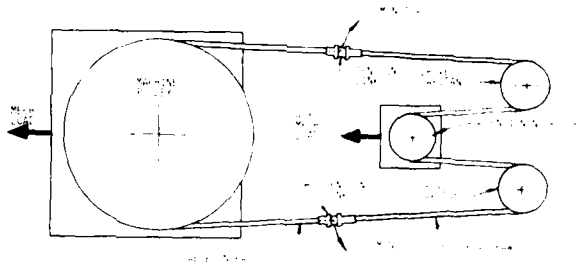
CYCLIC TENSION TEST: ATTENUATION CHANGES

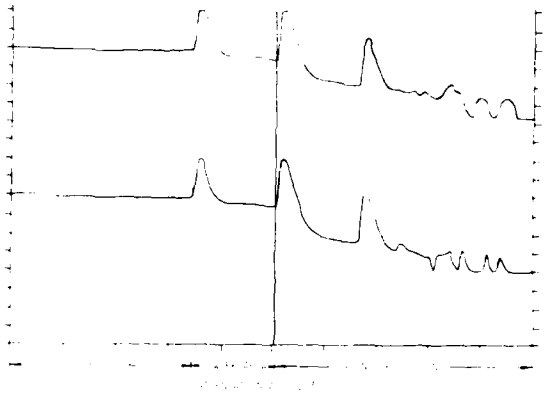
TEST STAGE			NET ATTENUATION CHANGE (dB/220 M)	
NO. CYCLES	LOAD (kgf) MAX.	LOAD (kgf) MIN.	QUAD NATURAL FIBRE PLUS CENTRE FIBRE	QUAD RED FIBRE ONLY
-	-	-	-	-
-	[illegible]	-	+ [illegible]	+ .1
-			- [illegible]	+ [illegible]
-	[illegible]	-	+ [illegible]	+ [illegible]
-		-	- .3	+ 0.1
-	[illegible]	-	+ [illegible]	+ .2
-		-	- [illegible]	+ [illegible]
[illegible]	[illegible]	[illegible]	+ [illegible]	-
[illegible]	[illegible]	[illegible]	+ [illegible]	+ 0.1
[illegible]	[illegible]	[illegible]	+ [illegible]	+ 0.1
[illegible]	[illegible]	[illegible]	+ [illegible]	-
[illegible]	[illegible]	[illegible]	-	+ 0.1
[illegible]	[illegible]	[illegible]	+ [illegible]	+ 0.2
[illegible]	[illegible]	-	+ [illegible]	+ 0.1

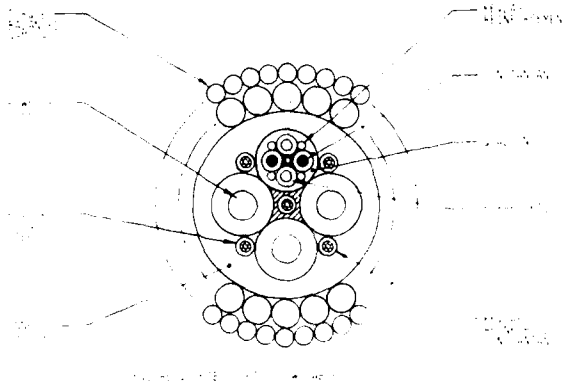
TABLE 2

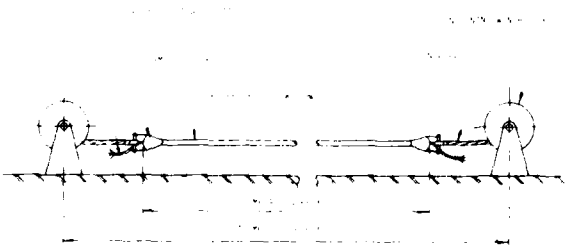
STRAIGHT LINE TOWING @ FULL SCOPE
T.D.R. ATTENUATION ESTIMATES

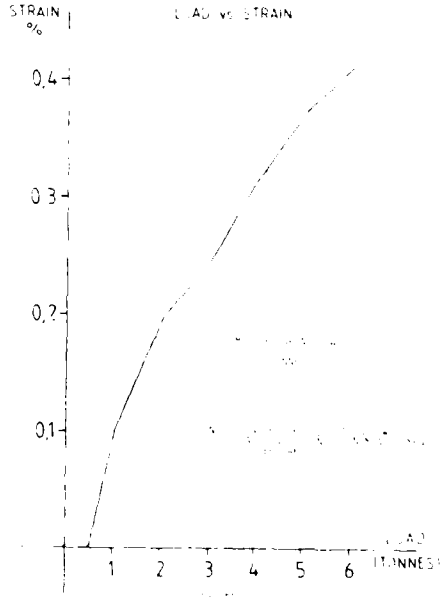
SPEED (KNOTS)	ATTENUATION (dB @ 850 nm)			TENSION (TONNES)
	CHANNEL 1	CHANNEL 2	CHANNEL 4	
0	3.47	4.89	3.22	0.2
4.4	3.96	5.15	4.48	1.0 - 1.2
6.4	3.93	4.75	4.84	1.3 - 1.6
8.0	4.55	5.92	4.86	1.7 - 2.0
10.0	4.67	6.46	5.22	2.1 - 2.5
6.4	4.25	5.78	4.71	1.2 - 1.4
4.7	4.11	5.62	4.72	0.9 - 1.1
0	3.90	5.16	4.31	0.2 - 1.0

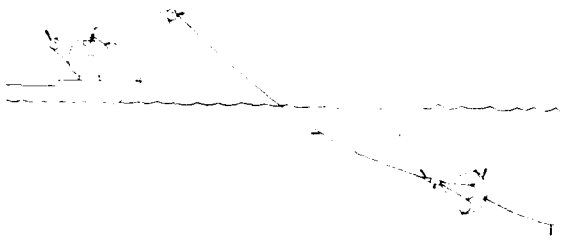


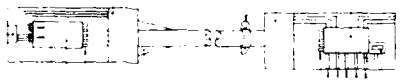


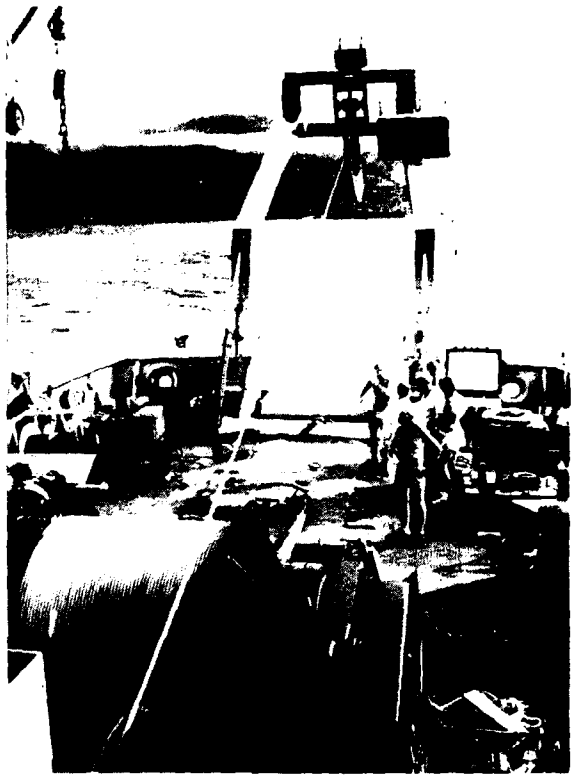




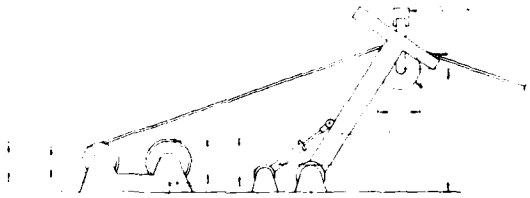


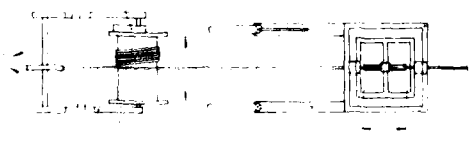


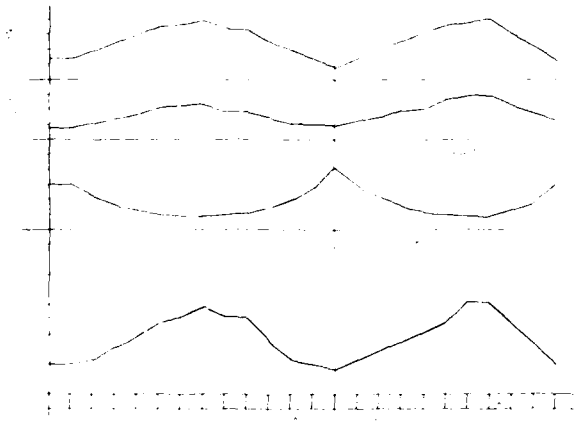


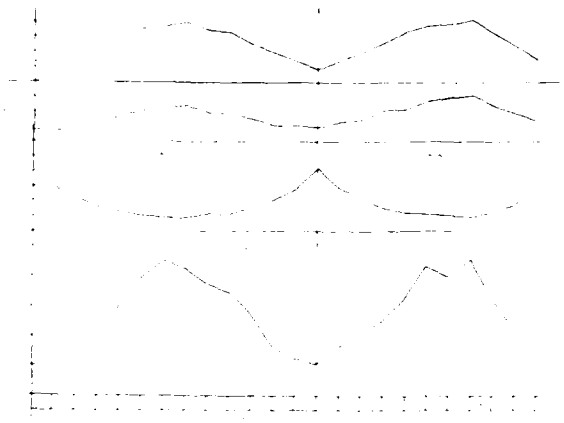


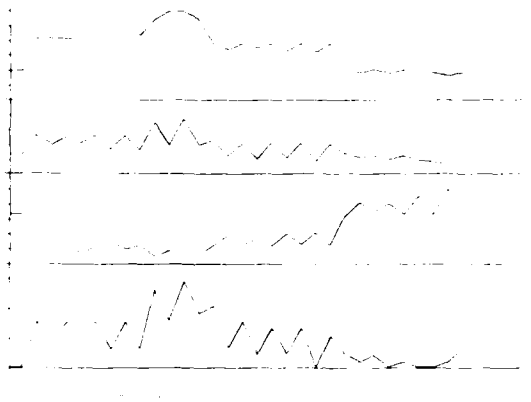


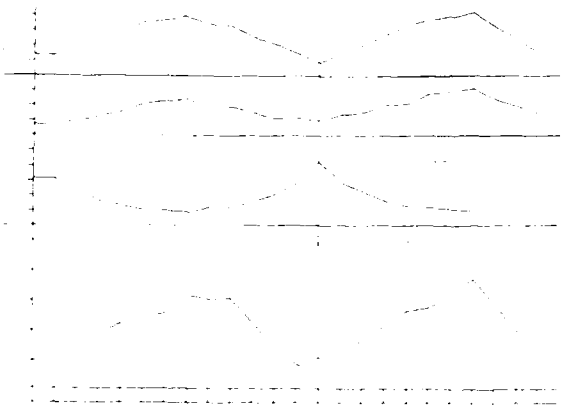


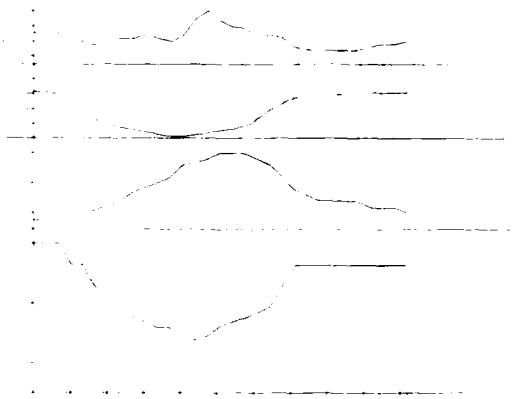




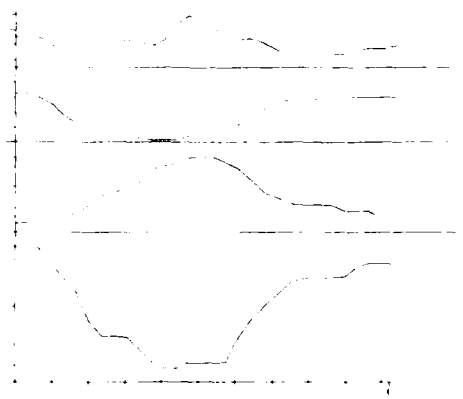


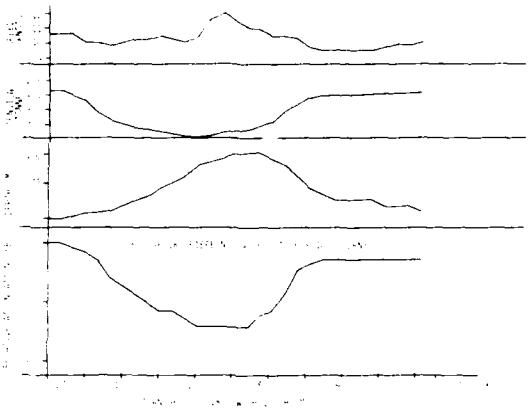












CHARACTERISTICS AND LONG-TERM STABILITY OF MASS PRODUCED OPTICAL FIBER SUBMARINE CABLES

Haruo Abe Yoshihiko Yamazaki Hitoshi Yamamoto Yasuhiko Niiro

KOKUSAI DENSHIN DENWA CO.,LTD. (KDD)
2-3-2 Nishi-shinjuku, Shinjuku-ku, Tokyo 163, JAPAN

Summary

Long-haul optical fiber submarine cable systems are expected to perform a major role as large-capacity international digital transmission lines. To realize these systems, it is essential and has to be verified that the cables have high reliability and long-term loss stability of more than 25 years.

In this paper, the high reliability and long-term loss stability of mass produced optical fiber submarine cables were confirmed through temperature variation and mechanical stress tests, transmission loss measurements during and after the manufacturing process, and one-year high-temperature loss change test and loss stability test. Measurements after a trial lay of a short haul cable system on the sea floor of 8,200 m depth was also performed. The maximum transmission loss increase of the cables after 25 years was estimated to be less than 0.5 dB per repeater spacing of 53 km.

1 Introduction

KDD has developed OS-280M optical fiber submarine cable system using 1.3 μm wavelength. [1, 2] This OS-280M cable system is scheduled to be used as part of the Third Transpacific Submarine Cable (TPC-3) which is to be ready for 1988. Prior to the installation of TPC-3, KDD performed a commercialization test of the system of about 300 km in total system length with 6 repeaters in order to verify mass producibility, characteristics, high reliability of the cables, repeaters and other plants, and overall system performance. In 1986, the system was laid in the Pacific Ocean including the Japan Trench of 8,200 m depth and was landed at Chikura Cable Landing Station. It was the first time in the world that optical fiber submarine cable was laid in sea depth of 8,200 m. The performance of the system and transmission losses of the cables have been measured and good results have been obtained.

This paper verifies the high reliability and long-term stability, as well as mass producibility and characteristics, of manufactured optical submarine cables about 350 km in total length.

To verify the high reliability and long-term stability of the cable, the following measurements and tests were performed;

1. Optical characteristic measurements of each cable at each manufacturing process from the beginning of the manufacturing.
2. Temperature variation and mechanical stress tests.
3. One-year optical transmission loss change tests
   (1) High-temperature test; cable was put in high-temperature (60°C) bath.
   (2) Loss stability test; cable was set in an environment of temperature of 3°C and water pressure of 800 kg/cm^2.
4. Optical transmission loss measurements after the trial lay of the OS-280M system of about 300 km in total cable length. The trial lay included lay at the Japan Trench of 8,200 m in depth.

2 Structure

The following ten pieces of optical submarine cables were manufactured for the commercialization test of the OS-280M system; 4 pieces of 53km cable, 2 pieces of 40km cable, 3 pieces of 15km cable and one 13km cable. All the cables were manufactured in single cable lengths without jointing box. Table 1 shows the principal design parameters of the OS cable.

2.1 Optical Fiber

The optical fiber is a high-strength mono-mode MCF manufactured by the VAD process. The fiber has a mode field diameter of approximately 10 um and a specific refractive index difference of approximately 0.3. To protect the optical fiber and to suppress the generation of micro-bending due to temperature variations and mechanical distortions, the fiber is coated with ultraviolet (UV) cured and nylon resins. The outside diameter of the coated optical fiber is approximately 0.6 mm.

Taken into consideration the mechanical strength reliability over 25 years, the optical fibers had 2% elongation screening. Optical fiber splicing was performed by high-strength arc-fusion splicing. For the splicing point, 2.5% elongation screening was performed.

Table 1 Deep Water Cable Parameters

Item		Parameter
Maximum Sea Depth		8,000m
Diameter		22mm
Weight	In Air	0.9ton/km
	In Water	0.5ton/km
Cable Tensile Strength		More than 10 tons
Strength/Weight in Water		More than 20km
Minimum Bending Radius		1m
Water Ingress at each sea depth		Less than 2km/2 Weeks, at 7,500m Less than 1 km/2 Weeks, at 5,500m Less than 0.25km/2 Weeks, at 1,000m
D.C.Resistance		Less than 0.72Ω/km
Insulation Resistance		More than 2×10⁶MΩ-km
Maximum Voltage		12kV
Number of Optical Fibers		4(Maximum6)
Optical Fiber Loss		Less than 0.45 dB/km at 1.31±0.01μm
Zero Dispersion Wavelength		1.31μm
Dispersion		±2ps/km/nm at 1.31±0.01μm
Cut Off Wavelength		Less than 1.29μm

2.2 Fiber Unit

Fig.1 shows the fiber unit cross section and the cable cross section. The fiber unit has a center tensile strength member in its center; it is stranded with six coated optical fibers around it in fixed pitches. This structure is filled and covered with UV resin. The copper plated center tensile strength member was covered with a UV resin. Thus, the coated fibers do not contact the surface of the center tensile strength member directly in order to inhibit the generation of fiber micro-bending. The outside diameter of the fiber unit is slightly less than 3 mm.

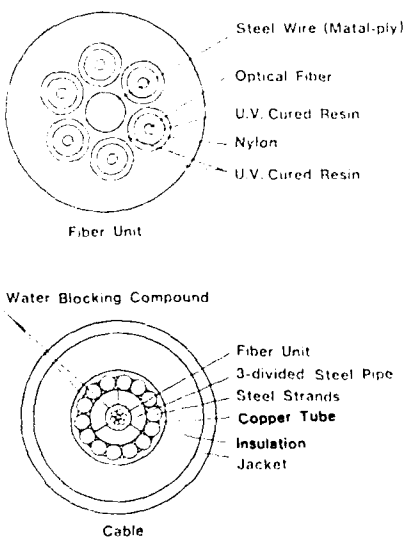


Fig.1 Optical Fiber Submarine Cable

2.3 Cable

The cable has the fiber unit in its center; the fiber unit is surrounded by a 3-divided steel anti-pressure pipe, over which tensile strength wires are stranded in fixed pitches. The structure is tightened by a copper tube layer around it and covered with a low-density polyethylene insulation layer and high-density polyethylene jacket layer. The outside diameter is 22 mm. The composite metal structure consisting of the 3-divided pipe, tensile strength wires, and copper tube layer functions as an anti-water pressure structure, as a tensile strength structure, and as a power feed conductor line to the repeaters. A anti-water compound is filled intermittently in the longitudinal direction of the cable to prevent water from ingress in the gap inside the cable in case of a cable break, and it fixes the fiber unit to the 3-divided steel pipe.

2.4 Single Fiber Lengths and Splicing Losses

The maximum single fiber length after 2% screening was approximately 27 km; single fiber lengths averaged 10.5 km and standard deviation was 5.0 km.

The maximum and average splicing losses were 0.29 dB and 0.14 dB, and the standard deviation was 0.08 dB.

3 Characteristics

3.1 Optical loss

Fig.2 shows the distribution of the optical transmission losses at 1.30 and 1.55 μm. The maximum and minimum loss values at 1.3 μm were 0.411 and 0.348 dB/km, and the mean loss value was 0.373 dB/km. The maximum and minimum loss values at 1.55 μm were 0.246 and 0.201 dB/km, and the mean loss value was 0.233 dB/km. The 53km cables had an average of five splices per optical fiber, and the optical transmission loss values include the splicing losses at these splices.

3.2 Dispersion

The dispersions were within -1.75 ~ 1.50 ps/km/nm in the wavelength region of 1.3 ~ 1.32 μm. The dispersion values' variation of 40 optical fibers at each wavelength was within approximately +/-0.7 ps/km/nm. The mean value of the zero-dispersion wavelengths was 1.313 μm, and the standard deviation was 0.004 μm. Thus the dispersions' deviation was very small; this indicates that manufacturing deviation of the dimensions and refractive indexes of the optical fibers was very small.

3.3 Optical Loss Variations in Manufacturing Processes

Fig.3 shows optical transmission loss change in the manufacturing process. The average optical loss increased approximately 0.003 and 0.007 dB/km at 1.3 and 1.55 μm after the insulation

layer process, respectively. This loss increase can be attributed to micro-bending generated in the fibers due to heat applied during the insulation layer process, and to pressure caused by the heat.

Except for this loss increase, optical loss change in the manufacturing process was hardly recognizeable.

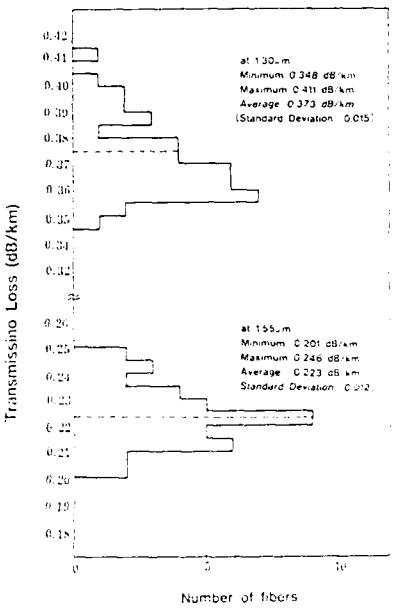


Fig.2 Transmission Loss Distributions

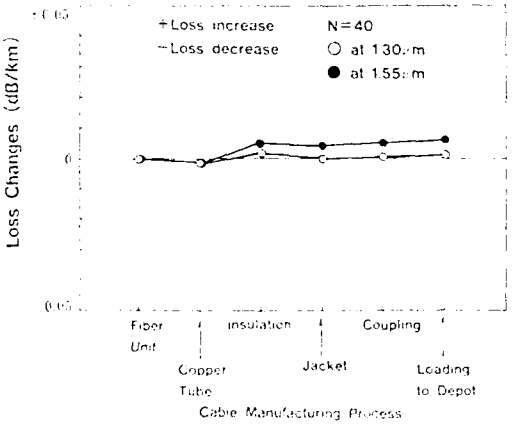


Fig. 3 Average Loss Characteristics during Cable Manufacturing

3.4 Temperature Characteristic

Fig.4 shows the temperature-optical loss characteristics between -20 and 50°C. The loss measurement was made by looping the four optical fibers of each 500m sample cable to form a loss measurement length of 2 km. Although temperature characteristics would differ depending on individual cables, losses varied within +/-0.007 dB/km at -20°C and +/-0.004 dB/km at 50°C from the loss values at the reference temperature of 15°C. The optical losses returned to the original levels when the temperature was returned to the reference temperature. On the average, the optical loss decreased 0.002 dB/km at -20°C and increased 0.002 dB/km at 50°C.

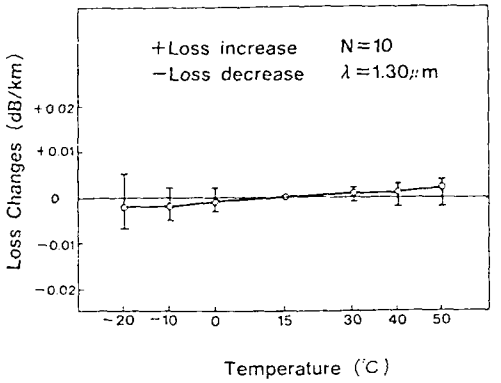


Fig.4 Temperature-Loss Characteristic

3.5 Tensile Strength Characteristic

Fig.5 shows tension-optical loss characteristics to the tension of 7 metric tons. From sea trials, the tension of 7 metric tons was assumed to be the maximum tention applied during laying and recovery from 8,000 m depth with enough margin. The losses were measured by looping four optical fibers in each 200m sample cable to obtain a loss measurement length of 800 m. Although the tension-optical loss characteristics would differ depending on individual cables, the losses varied within +/-0.004 dB/km when 7 metric tons were applied. The loss values returned to the original level when the tension was reduced to zero. The loss increased an average of 0.002 dB/km when 7 metric tons were applied.

The elongation distortion was an average of 0.65% when 7 metric tons was applied. The residual elongation distortion when the tension was returned to zero was less than 0.1%.

The breaking tensile strength was more than 10.2 metric tons (100 kN), averaging 10.5 metric tons, indicating that a sufficient under-water cable strength/cable weight ratio (more than 20 km) could be obtained.

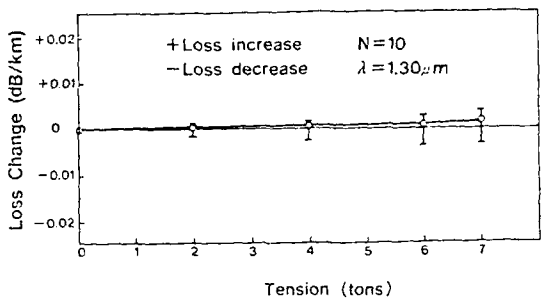


Fig. 5 Tension-Loss Characteristic

3.6 Water Pressure Characteristics

Fig.6 shows the water pressure-optical transmission loss characteristics to 850kg/cm^2 at 1.5°C. The loss was measured by looping four optical fibers of each cable sample to obtain a loss measurement length of 800 m. The deviation of the measured values was within the measurement accuracy of +/-0.001 dB/km in all cases; the optical losses did not change the pressure to 850 kg/cm^2.

The cables were found to be free of mechanical deterioration, such as deformation, after the tests.

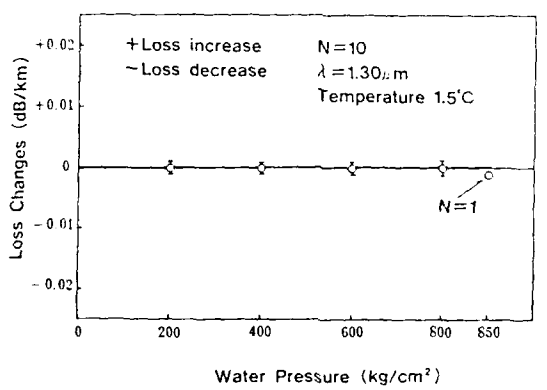


Fig. 6 Water Pressure-Loss Characteristic

3.7 Anti-water Ingress Characteristics (Time-Water Ingress Distance Characteristics)

The anti-water ingress characteristics tests were performed by measuring the water ingress time through 200m sample cables under water pressure of 100, 550, and 750 kg/cm^2 at a test temperature of 3°C. The following is an experimental formula between the water ingress distance "L", and water pressure application time "t".[3]

$$L = A\, t^{a} \qquad (1)$$

where "A" is a proportional constant at each water pressure and "a" is 0.3 ~ 0.4. The water ingress distances under each water pressures in two weeks were estimated using the test results and experimental formula. The average water ingress distances two weeks later under water pressures of 100, 550, 750 kg/cm^2 calculated based on the test results were approximately 80, 360, and 530 m, respectively. These values fully meet the design objective with enough margin.

3.8 Summary of Characteristics

In addition to the above mentioned tests, bending, bending tension, repetitive tension, jerks and squeezes, and lateral stress tests were performed. All the tests were made with presumptions of temperature variations, external mechanical stress and others which would be applied to the cable in submarine environments during and after laying and during recovery with considerable margins. Deviation of optical and mechanical characteristics of each manufactured cable was very small and prominent optical transmission loss changes or cable mechanical deterioration could not be found.

It was confirmed that the mass produced optical fiber submarine cables have sufficient strength and that optical transmission losses were also quite stable. These results show the high reliability of the OS-280M optical fiber cable.

4 Long-Term Transmission Loss Variation (Long-Term Loss Stability)

The following are considered to be the main factors for long-term aging changes (loss increase) of the transmission loss of the optical fiber submarine cable.

1) Loss increase by hydrogen generated inside the cable.[4,5]
   (1) Hydrogen generation from non-metallic materials of the cable such as optical fiber unit and anti-water compound.
   (2) Hydrogen generation by electric-chemical reaction on the surface of metallic materials of the cable, which may involve moisture in the cable.
2) Loss increase by optical fiber's microbending caused by aging and deterioration of optical fiber coating materials.

The cable structure was designed and materials were selected during the cable design so that the optical transmission loss increase in 25 years would present absolutely no problems in the above mentioned items in addition to the reliability of mechanical characteristics. Verification tests on each material including optical fiber were performed. In addition to the above tests, long-term loss stability tests were made to verify overall long-term stability of the cable for more than 25 years.

4.1 Hydrogen Generation from the optical fiber unit

Measurement on temperature dependency of the hydrogen gas generated from the optical fiber unit was made. Fig.7 shows the amount of hydrogen gas generated from the fiber unit at 60°C, 80°C and 100°C. The length of each fiber unit used in the measurement was 20 m.

Assuming the hydrogen was generated through the thermal activation process, and using Arrhenius formula, the amount of generated hydrogen gas "V" is expressed as follows;

$$V = A \exp(-E/RT)\ t^{k} \qquad (2)$$

where "A" is a proportional constant, "R" is the molar gas constant, "T" is an absolute temperature, "t" is time (hours), and k = 0.36 from Fig.7. According to the Arrhenius plot of the test result, $E/R \cdot k = 9.14 \times 10^{3}$ was obtained. Using R = 1.987 cal/mol·K, the activation energy of the hydrogen generation process becomes E = 6.53 Kcal/mol. Then the amount of generated hydrogen gas is expressed as follows;

$$V\ (\mu l/m) = 1.9 \times 10^{4} \exp(-3.3 \times 10^{3}/T)\ t^{0.36} \qquad (3)$$

Fig.8 shows the estimated amount of hydrogen gas generation at 3°C. The measured values at each temperature in Fig.7 were converted to the values at 3°C using Eq.(3) and plotted on Fig.8.

From Fig.8, the amount of hydrogen gas generation from the fiber unit at 3°C in 25 years is estimated to be about 10 µl/ m. This corresponds to hydrogen gas pressure of 1.4×10^{-3} atm inside the cable.

The transmission loss increase of optical fiber at 1.30 (L(1.3)) and 1.55 µm (L(1.55)) due to hydrogen gas is approximately given by the following formulae (the optical fibers were measured to have an O-H absorption peak at 1.39 um.); [5]

$$L(1.3) = 0.033\ L(1.24) + 0.6\ L(1.39)\ \ dB/km \qquad (4)$$

$$L(1.55) = 0.083\ L(1.24) + 0.5\ L(1.39)\ \ dB/km \qquad (5)$$

$$L(1.24) = 0.56\ P_{H2} \exp(1.55 \times 10^{3}/RT)\ \ dB/km \qquad (6)$$

$$L(1.39) = \sqrt{P_{H2}}\ (M \log(t) - N)\ \ dB/km \qquad (7)$$

$$M = 1.90 \times 10^{5} \exp(-9.61 \times 10^{3}/RT) \qquad (8)$$

$$N = 8.88 \times 10^{4} \exp(-8.32 \times 10^{3}/RT) \qquad (9)$$

where "L(1.24)" is loss increase at 1.24 µm due to H_2 absorption and "L(1.39)" is loss increase at 1.39 µm due to O-H absorption, "P_{H_2}" is the hydrogen gas pressure (atm), "R" is the molar gas constant, "T" is an absolute temperature and "t" is time (hours).

Then loss increase at 1.3 µm and 1.55 µm due to hydrogen generation from the fiber unit at 3°C in 25 years is estimated to be 4.3×10^{-4} dB/km and 1.1×10^{-3} dB/km, respectively.

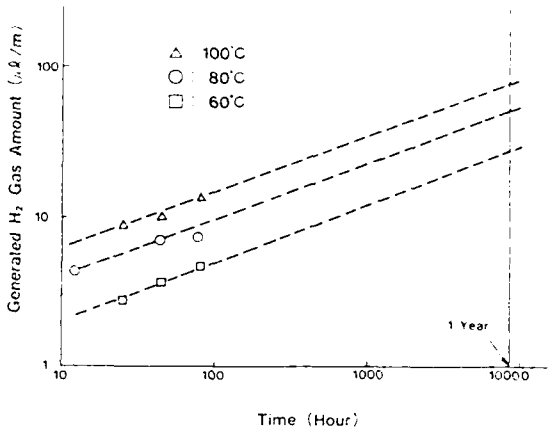


Fig.7 Temperature Dependency of H_2 gas from Optical Fiber Unit

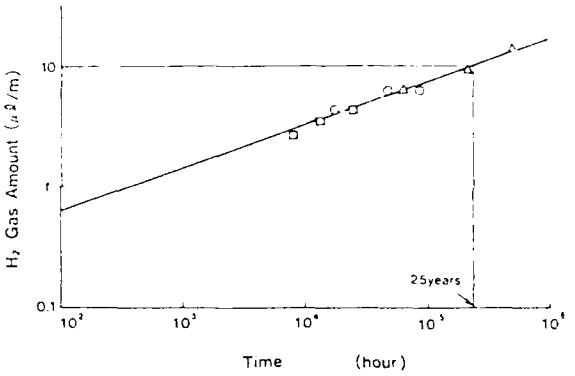


Fig.8 Estimated H_2 gas Amount at 3°C

The amount of hydrogen gas generated from anti-water compound was measured to be less than 7×10^{-2} µl/g at 100°C for one hour. When converted to the value per 1 m cable length, it corresponds to much less than 1/10 of hydrogen generation from the fiber unit.

4.2 Long-Term Loss Change at 80°C

To observe transmission loss change of the cable at a high temperature, the following test was performed. A 500m sample cable was put into high temperature bath of 80°C and loss change was measured through wavelength-loss measurement. Six fibers were looped to form a measurement length of 3 km. To observe effects of power feed current such as electrical corrosion, an electric current of 10 A was feeded through the composite metal structure and center tensile strength member of the fiber unit.

Fig.9 shows the temperature loss changes at 1.24, 1.3, 1.32, and 1.55 μm for one year. Measurement accuracy is about 0.01 dB/km.

The dotted curve in Fig.9 shows estimated loss increase at 1.24 μm due to hydrogen gas generation from the fiber unit, calculated by Eq.(5) to (6). Measured loss increase at 1.24 μm in Fig.9 seems to be approximately consistent with the dotted curve. Then it is considered that the hydrogen generation due to metallic materials and electric current is negligible and hydrogen generation from the fiber unit mainly attributes the loss increase of the cable.

Estimated loss increase at 80°C after one year is calculated to be approximately 0.01 dB/km at both 1.3 μm and 1.55 μm by Eq.(5) to (6). Measured loss increase at 1.3 μm and at 1.55 μm in Fig.9 seems to be consistent with this value. No prominent loss increase was observed at higher wavelength region such as 1.6 and 1.7 μm.

As for acceleration of loss increase by high temperature, further tests would be needed to analyze the loss change more quantitatively.

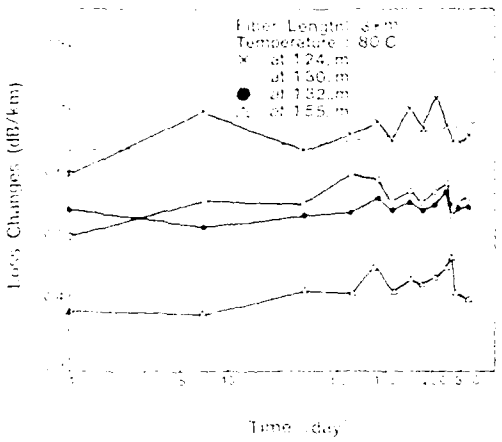


Fig. 9 Temperature Accelerated Loss Changes

4.3 Long-Term Loss Change at a temperature of 3°C and water pressure of 800 kg/cm²

To observe loss change of the cable in environment of 8,000 m sea depth, the following test was performed. Four 200m sample cables were put into the ocean simulator. Fibers were looped to form a measurement length of 3.2 km. The temperature and water pressure in the ocean simulator was set to be 3°C and 800 kg/cm², respectively, and the loss change was measured for one year.

Fig.10 shows the test result. The loss changes for one year was within +/-0.002dB/km and no loss increase tendency was observed. It is considered that there would be little generation of micro-bending of the optical fibers due to low temperature and high water pressure.

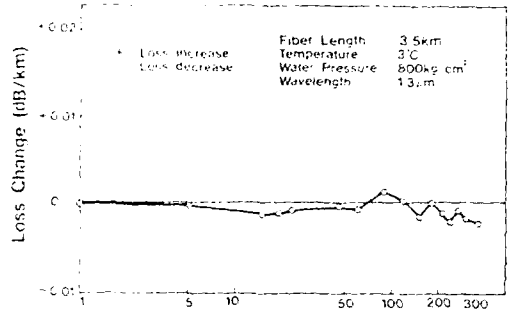


Fig.10 Long-term Loss Change under water Pressure of 800kg/cm²

4.4 Loss Changes of the manufactured cables during storage

Fig.11 shows the loss changes of the ten manufactured cables during storage. No prominent loss increases at 1.3 and 1.55 μm were observed. Wavelength-loss characteristics of 15km and 13km cables were measured and loss increases at 1.24 μm and longer wavelength region such as 1.6 and 1.7 μm were not observed. It is considered that hydrogen gas generation and optical fiber micro-bending is also negligible in this case.

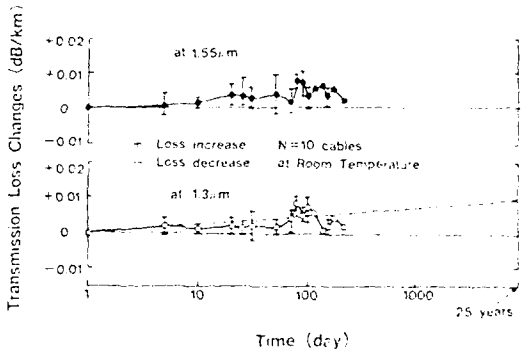


Fig.11 Transmission Loss Changes during Storage

Loss changes in Fig.11 is considered to be due to measurement accuracy of short length cables because estimated loss increase due to hydrogen at 23°C for one year is less than 0.001 dB/km at both 1.3 and 1.55 μm. Even if the worst case is assumed; loss variation will transit proportional to log(t) as the dotted line in Fig.10, the loss increase at 1.3 μm at room temperature after 25 years is estimated to be less than 0.01 dB/km. This value corresponds to loss increase of less than 0.5 dB per repeater

spacing of 53 km. According to the tendency of loss change at 80°C in Fig.9 and at 3°C under water pressure of 800 kg/cm^2 in Fig.10, it would be the worst case to assume that loss increase is proportional to log(t).

4.5 Summary of the Long-Term Stability

It was estimated that hydrogen generation from the fiber unit mainly attributes the long-term loss increase of the cable and hydrogen generation from other materials such as anti-water compound and metallic materials' surfaces (corrosion etc.) can be negligible. The loss increase at 1.30 and 1.55 μm due to hydrogen generation inside the cable at 3°C in 25 years is estimated to be less than 0.001 dB/km and 0.002 dB/km, respectively.

No obvious micro-bending generation of optical fibers has been observed at 80°C and at 3°C under water pressure of 800 kg/cm^2 for one year.

Every long-term loss change test including the long-term loss measurements of all the manufactured cables showed that the OS-280 cable had quite stable long-term optical transmission loss characteristics, and maximum transmission loss increase after 25 years was estimated to be less than 0.01 dB/km even if the worst data were used.

5 Conclusion

Measurements and tests of optical transmission loss and mechanical characteristics of ten manufactured OS-280M optical fiber cables were performed. The total length of the manufactured cables was about 350 km. Deviations of these optical transmission loss and mechanical characteristics between the cables were very small and the test results showed that the cables have quite stable optical and mechanical characteristics. From these results, mass producibility and high reliability of the OS-280 optical fiber submarine cable was confirmed.

One year transmission loss changes at 80°C, and at 3°C under water pressure of 800 km/cm^2 were measured. Loss measurements of all the manufactured cables during storage at a room temperature were also performed. No prominent loss changes was observed in these measurements. It was estimated that hydrogen generation from materials other than the fiber unit could be negligible and that micro-bending generation of the fibers could be also negligible. Maximum transmission loss increase at a lower temperature such as 23°C or 3°C after 25 years was estimated to be less than 0.01 dB/km (0.5 dB/53km repeater spacing) at 1.3 μm.

Loss change measurements of the cables which actually laid in Pacific Ocean including the Japan Trench of 8,200 m have been performed. The manufactured cables were spliced with repeaters to form the short haul OS-280M optical fiber submarine cable system of 300 km in length. The system was laid in the Pacific Ocean in December of 1986. The system has been fed a current of 1.6 A. Fig.12 shows long-term loss changes of the 53km cable laid on the Japan Trench of 8,200 m sea depth. Loss changes of the other laid cables have also been quite stable. This result verifies that transmission losses of the cables are very stable even in the actual sea bottom of up to 8,200m depth, and supports the above mentioned conclusions; high reliability and long-term stability of the OS-280M optical submarine cable.

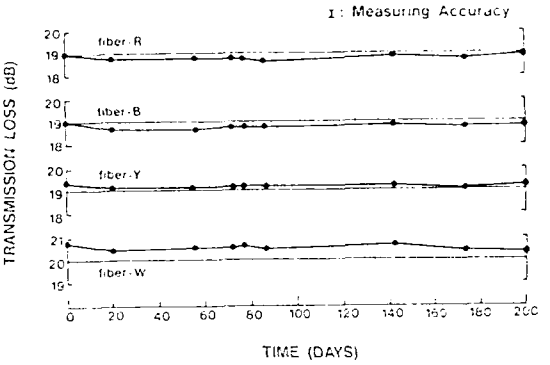


Fig.12 Transmission Loss Changes of Cable Laid on Japan Trench (8,200m sea depth)

Acknowledgement

The authors would like to thank Managing Director Mr K.Kobayashi for his encouragement. They also wish to acknowledge NTT for their cooperation and wish to thank Fujikura Co.Ltd, Sumitomo Industries Ltd., Furukawa Electric Co.Ltd. and Ocean Cable Co.Ltd for their manufacturing of optical fiber units and cables.

Reference

(1) Y.Niiro, H.Yamamoto,"The international long-haul optical-fiber submarine cable system in Japan", IEEE Communication Magazine, Vol.24, No.5, May 1986.

(2) Y.Niiro,"The OS-280M optical-fiber submarine cable", IEEE Jour. Lightwave Tech., Vol. LT-2, No.6, pp 767-772, 1894.

(3) Y.Yamazaki, Y.Niiro, H.Yamamoto, H.Nishikawa, M.Mochizuki," The OS-280M optical fiber submarine cable", International Conference on Optical Fiber Submarine Telecommunication Systems '86.

(4) K.Mochizuki, Y.Namihira, M.Kuwazuru, M.Nunokawa," Influence of hydrogen on optical fiber loss in submarine cables", Jour. Lightwave Tech., Vol. LT-2, No.6, December 1984.

(5) M.Kuwazuru, Y.Namihira, K.Mochizuki, N.Nunokawa," Effects of hydrogen on optical fiber transmission loss", IEICE Technical Report, OQE86-89, 1986.



Haruo Abe received his B.S. degree in 1977 and M.S. degree in 1979 in Electrical Engineering from Keio University, Japan. He joined KDD in 1979. He received M.S. degree in 1984 in E.E. (Applied Physics) from U.C.San Diego. He has been engaged in the development and construction of optical-fiber submarine cable system in KDD Head Office since 1984.



Yoshihiko Yamazaki received his B.S. degree in 1974 and M.S. degree in 1976 in Electrical Engineering from Tohoku University, Japan. He joined KDD Research and Development Labs. in 1976 , and has been engaged in research and development of optical-fiber cable system. He was transferred to KDD Head Office in 1983, and has been engaged in the development and construction of optical-fiber submarine cable system.



Hitoshi Yamamoto received his B.S. degree in 1971 and M.S. degree in 1973 in Communication Engineering from Osaka University, Japan. He joined KDD Research and Development Labs. in 1973 , and has been engaged in the research and development of optical-fiber submarine cable system since 1977. He was transferred to KDD Head Office in 1983, and has been responsible for the development and construction of optical-fiber cable, repeaters and terminal equipment.



Yasuhiko Niiro received his B.S. degree in 1964 from Musashi Institute of Technology, Japan. He joined KDD in 1964. He has been engaged in the development of coaxial submarine cable systems since 1971 and responsible for research on optical-fiber submarine cable systems since 1977 in KDD Research and Development Laboratories. He is presently manager of system engineering division, Submarine Cable Systems Department in KDD Head Office.

Submarine Cable Systems Department
Kokusai Denshin Denwa Co.Ltd. (KDD)
2-3-2 Nishi-Shinjuku, Shinjuku-ku, Tokyo 163, Japan

Combustion Toxicology: Principles, Methods and Regulations

by Steven C. Packham, Ph.D.

The science of combustion toxicology will be discussed from three perspectives:

(1) basic principles of toxicology,

(2) methods which have been used to test the toxicity of smoke from burning materials, and

(3) the future of combustion toxicology in materials regulations.

The fundamental principles of combustion toxicology will be discussed including the definition and quantification of dose in smoke inhalation testing and research. In addition, rationals for selection of specific animal models will be presented including the usefulness of different kinds of endpoints, e.g., lethality, blood chemistry, etc.

There are five different test procedures currently being reviewed by the International Standardization Organization (ISO), one from Japan, one from West Germany and three from the United States. The author will compare and contrast these methods on the basis of the type of furnaces they use to burn test specimens. Also, a new test method being developed through the National Institute of Building Sciences will be discussed.

Finally, the author will speculate about the possible significance of combustion toxicity testing in current and future regulations. A plan for encouraging international uniformity in combustion toxicity testing specifications will be presented.

Hazard Analysis Using Toxic Potency and Other Material Property Data

by Richard W. Bukowski, P.E., Head
Hazard Analysis Center for
Fire Research
National Bureau of Standards
Gaithersburg, Maryland

Abstract: Over the past few years, the Center for Fire Research (CFR) has been developing a method for predicting the hazard to building occupants from fires. This method, based on numerical fire modeling technology, is soon to be released as a software package called HAZARD I which is intended for use on personal computers. It includes programs and procedures for predicting the time-dependent environment (e.g., temperature, smoke density, and concentration of a number of gas species) in multiple rooms on multiple floors of any building of interest. Also, the evacuation progress of a user-specified group of occupants is traced through the building as influenced by the smoke encountered along the way, and by "normal" behavior under such circumstances. Finally, the predicted impact of exposure of these occupants to the fire-induced environment is determined and fatalities along with the time, location, and cause of death are assigned.

The capabilities and limitations of these programs will be presented in the context of their use in evaluating the potential hazards associated with wire and cable products. A previously published analysis (using a "pencil and paper" calculation) of plenum cables will be reviewed. Finally, the use of these techniques for the calculation of product risk for the case of wire and cable in concealed spaces of office occupancies will be outlined.

PRINCIPAL TEST METHODS FOR THE EVALUATION OF THE COMBUSTION TOXICITY OF MATERIALS AND PRODUCTS*

Howard W. Stacy

Southwest Research Institute, 6220 Culebra Road
San Antonio, Texas 78284

ABSTRACT

Several test methods have been developed over the last several years for the evaluation of the acute inhalation toxicity of the combustion products released from materials and products during thermal decomposition. Principal test methods in this country include the University of Pittsburgh (UPitt) test, the National Bureau of Standards (NBS) protocol (Cup Furnace method) and the Radiant Furnace test method ("Packham" method). Two other test methods worthy of mention are the German DIN Method (based on DIN 53 436) and the Japanese Government Building Regulation (JGBR) test. This paper provides a general review of the following: 1) the basic components of the principal test protocols, including descriptions of the combustion apparatus and the operational procedures for generation of combustion atmospheres, the animal exposure system and the mode of operation (static or dynamic), the toxicological measurements (primary endpoint) and the chemical analyses of combustion atmospheres; and 2) the respective advantages and disadvantages of the test procedures.

INTRODUCTION

The mounting concern over the contribution of materials to the life hazard of smoke has resulted in an accelerated development of the field of combustion toxicology over the past ten years. During this time, several test methods have been developed for the evaluation of smoke toxicity, each with its own combustion device (fire model), exposure chamber and method of exposing animals. The primary purpose of this discussion is to review the major test methods either in use or under consideration today, and at the same time outline the general principles of combustion toxicity testing.

There are at least five major test methods for assessing the performance of materials with regard to toxicity of smoke produced during combustion. Several additional methods have also been used to some extent. The test procedures referred to as the National Bureau of Standards (NBS), Radiant (Packham), University of Pittsburgh (UPitt), DIN (German) and JGBR (Japanese) have received a significant level of attention either as proposed standards (ASTM, ISO) or as regulatory tools.

* Text abstracted in part from Kaplan, H. L., A. F. Grand, and G. E. Hartzell, Combustion Toxicology: Principles and Test Methods, Technomic Publishing Company, Incorporated, Lancaster, Pennsylvania (1983).

REQUIREMENTS FOR COMBUSTION TOXICITY TESTS

For the purpose of evaluating materials, economic factors dictate the use of small-scale tests. Control of exposure temperature (or heat flux) and the precise measure of the sample size and quality also make laboratory experiments desirable.

Laboratory experiments in combustion toxicology generally comprise the following:

1) a combustion device for controlled combustion (either temperature or heat flux) of a single material;

2) an exposure chamber for exposure of test animals to the smoke;

3) a method for measurement of toxicity;

4) chemical analysis of the combustion atmosphere.

Combustion Devices

In order to develop practical and reproducible laboratory combustion toxicology experiments, certain choices must be made. One must consider radiant vs. conductive heating, smoldering (nonflaming) vs. flaming combustion, and the physical configuration of material that represents its actual use. The rate at which samples decompose is also an important consideration, since the release of toxicants is proportional to the burning rate of the material. It is important to recognize that the chemical composition, and therefore the toxicity, of the combustion or pyrolysis products of a given material can be highly dependent on the decomposition conditions.

The more common combustion devices which have been used in the studies of combustion toxicology can be characterized by the following parameters:

1) the use of radiant vs. conductive heating;

2) the available air supply and freedom of convective flow of air around the test specimen;

3) the capabilities for accommodating various sample configurations.

The common combustion devices in use include the cup (Potts) furnace of the NBS test, the quartz radiant furnace of the "Packham" test, the UPitt muffle furnace,

the combustion tube (radiant) furnace of the DIN apparatus and a radiant furnace used by the Japanese Ministry of Buildings test.

With regard to the laboratory fire model, it has been recognized that no laboratory apparatus is perfectly adequate for reproducing the changing conditions of a real fire.[1, 2] This is an important limitation of **all** fire test methods. For example, ASTM tests E119 and E84 make no attempt to duplicate the wide variety of conditions that are found in real fires. These tests only endeavor to assess material performance under standardized laboratory fire conditions.

Exposure Conditions

The chambers that have been used for exposure of animals to smoke are as diverse as the devices used for generating the smoke. Both dynamic chambers, which are continuously supplied with smoke diluted with fresh air, and static chambers have been used in laboratory combustion toxicity tests. The proponents of each type can identify similarities of the dynamic or static chamber to certain real fire scenarios or to some phases of real fires. Exposure chambers also differ in size, configuration and construction materials.

Toxicity Measurements

The traditional toxicity index in laboratory combustion tests has been the LC_{50} which, in general toxicological usage, is defined as the concentration of a gas or vapor that results in death of 50 percent of the test animals. Because the smoke produced by materials is a mixture of particulates and several gases, this index of toxicity must be related to the material or to the smoke mixture. The LC_{50} value is determined by measuring the response of the animals to different concentrations of the smoke. This may be accomplished by conducting a series of experiments in which the quantity of material combusted is varied in order to produce different concentrations of smoke. Obviously, the number of animals showing a response (death) will increase as the exposure concentration is increased. When the percent of animal responding within a specified time is graphed as a function of the logarithm of the concentration, a straight line may be approximated. Statistical methods are then employed for the calculation of the LC_{50}. It must be emphasized that differences in data among materials must be evaluated both for statistical significance and practicality before concluding that one material differs from another in the toxicity of the smoke produced. This is due to the inherent variability in biological response of animals and by the difficulty in generating reproducible combustion atmospheres.

Time-to-effect (incapacitation and lethality) has also been considered an important concept in combustion toxicity testing and has been used as an endpoint in some test procedures.[1, 2]

Chemical Analyses

Chemical analyses serve a number of important purposes in laboratory combustion toxicity tests. The first and most important purpose of these measurements is to enable the determination of whether observed toxic effects are produced by carbon monoxide or by other toxic decomposition products. Another function of these analyses is to provide an indication of the reproducibility and validity of the combustion of the material. Measurements of CO and CO_2 generation can provide evidence of an improper combustion condition and the necessity to repeat an experiment. Analyses are also needed to insure that excessive oxygen depletion does not occur during the exposure of animals. Other analyses that may be useful in support of the toxicity experiment include those for the following species:

1) Hydrogen cyanide;

2) Halogen acid gases;

3) Acrolein, formaldehyde or other specific chemical species.

REVIEW OF PRINCIPAL TEST METHODS

National Bureau of Standards (NBS) Protocol

This test method, under development since about 1976 at the U.S. National Bureau of Standards, has been described in detail in a Bureau report entitled "Further Development of a Test Method for the Assessment of the Acute Inhalation Toxicity of Combustion Products."[3] According to the NBS report, the test method ". . . provides a means of assessing the acute inhalation toxicity of the combustion products of materials under specified laboratory conditions and is primarily intended for research and preliminary screening purposes."

The basic components of the NBS test method consist of the following:

1) A combustion device, commonly referred to as the Potts furnace, consisting of a 9-in. cubical stainless steel box containing an insulated stainless steel cylindrical cup surrounded by a ceramic sleeve and resting on a ceramic disk. Nichrome wire wound about the sleeve and below the disk constitutes the heating element. A 1,000-mL quartz beaker, to which the material for evaluation will be added, is placed into the stainless steel cup. The combustion furnace is interfaced with the floor of the exposure chamber. For flaming combustion, an electrically heated wire or other electrical ignition source is used to ignite the products as they exit from the furnace.

2) A nominal 200-L animal exposure chamber with interior dimensions of 122 x 36 x 46 cm and constructed of clear polymethylmethacrylate or polycarbonate. Animal ports constructed of polymethylmethacrylate tubing permit exposure of six rats in the head-only mode to the smoke generated within the chamber. Exposure is conducted in the static mode.

3) Toxicological measurements of lethality as the primary end point, exposure and post-exposure observations of toxic signs and animal body weight determinations during the 14-day postexposure period.

4) Chemical analyses consisting of continuous or frequent measurements of O_2, CO_2 and CO in the chamber atmosphere during exposure and of blood determinations of COHb in two of the six animals immediately after termination of the 30-minute exposure.

The test protocol evaluates a material under flaming combustion (at 25°C above the autoignition temperature) and nonflaming combustion (at 25°C below the autoignition temperature).

Radiant Furnace Toxicity Test ("Packham Protocol")

This test method, which utilizes radiant heat energy in the combustion device, has recently been proposed for evaluating the toxicity of smoke by S.C. Packham.[4] The method utilizes the same 200-L animal exposure chamber as the National Bureau of Standards procedure. However, both the combustion furnace and the experimental protocol are considerably different. The combustion chamber has an elongated trapezoidal shape with quartz windows forming the nonparallel sides. The radiant heat source consists of tubular quartz, tungsten-filament lamps housed in parabolic reflectors and positioned on each side of the combustion chamber. Using lamps with a 2,000-Watt power rating (i.e. 200 W/linear in.), heat fluxes up to 7.5 W/cm^2 can be obtained. A sample holding tray is suspended from a load cell into the combustion zone of the furnace. The furnace configuration allows testing based on exposed surface area for many materials such as composites, laminates, tiles, fabrics and coatings. The procedure is intended to determine if the toxic potency of smoke from the test material exceeds prespecified values based on the performance of natural polymers (wool and Douglas fir).

University of Pittsburgh (UPitt) Method

This test method, developed by Dr. Yves Alarie and coworkers at the University of Pittsburgh, exposes mice to smoke produced from the ramped heating of materials.[5] Weighed samples are heated, starting from room temperature, at the rate of 20°C/min. in a box furnace, and an airflow is maintained through the furnace for the entire heating period. Thermal decomposition products are conducted to the animal exposure chamber via a 60-cm quartz tube. The furnace effluent is cooled and diluted with cold dried air, resulting in a total airflow of 20 L/min through the animal exposure chamber. Progressive sample weight change is recorded from a weight sensor, allowing thermogravimetric analysis (TGA) for each exposure. The four male Swiss-Webster mice are contained in holders and are exposed in the head-only mode to the smoke produced by materials. For all experiments, the animal exposure is initiated at the temperature at which 1.0-percent weight loss is recorded and continues for 30 minutes. A 10-minute recovery period follows each exposure. The LC_{50}, defined as the sample weight which causes death of half of the exposed animals within the exposure period is the lethality end point. Any animal which dies during the exposure or the recovery period is counted in the LC_{50} calculation. The New York State Uniform Fire Prevention and Building Code currently requires that certain types of materials are to be tested by this method and placed on file before being used in regulated buildings under its jurisdiction.

DIN Method

The DIN 53 436 method is at this time only a combustion apparatus and operating procedure, with an animal response model not yet actually designated a standard.[6] The method is characterized by the use of a moving annular tube furnace operated at a constant temperature, with smoke being diluted with air before rats are exposed. Smoke is generated dynamically. Dose-response relationships are normally obtained, with dose being varied by dilution of the smoke.

Japanese Government Building Regulation (JGBR) Toxicity Test

The JGBR toxicity test includes a radiant heat furnace (modified UK BS 476 Part 6 - Fire Propagation Test) and exposes mice in a whole body configuration to smoke which is generated dynamically.[7] Eight mice are placed in rotary cages and incapacitation times are assessed. Incapacitation times are compared with those of a reference material.

LIMITATIONS OF LABORATORY SMOKE TOXICITY TESTS

The **ultimate** objective of laboratory combustion toxicity tests may be stated as the assessment of the potential of smoke to impair escape and to cause lethality in order to provide input data for an overall hazard assessment of materials in real fires. This objective is difficult to attain because of two major limitations: 1) the inability to reproduce, in the laboratory, the changing conditions found in fire environments; and 2) the relevancy and validity of presently used animal models and toxicological endpoints.

It is unrealistic to expect a single laboratory test to be relevant to all stages of all fires because of the rapidly changing conditions in a real fire involving the dynamics of fuel, heat and air interactions. However, all the tests would be expected to be relatable to at least some stages of actual fires. This has been shown in certain cases.[8,9] Most laboratory combustion devices also present certain physical limitations with regard to specimen size, shape, assembly or material thermal decomposition characteristics. The NBS cup furnace is, for example, admitted to be inappropriate for composites, laminates, etc.[3] The UPitt box furnace has some difficulty with materials which decompose rapidly and generate smoke faster than the test system is able to clear it from the combustion chamber (personal observation).

With regard to animal models and toxicological endpoints, all of toxicology is plagued with the question of the relevance of test animals to exposure of humans. In the case of asphyxiant gases such as carbon monoxide and hydrogen cyanide, mice and rats are considered reasonable models, with animal responses fairly predictive of toxicological effects in humans. With other toxicants commonly found in smoke such as irritant gases, use of the rodent as a model is highly questionable. Until further definitive studies are made, caution must be exercised in extrapolation of laboratory data obtained with rodents to predict effects in humans exposed to irritants.

Because of their obvious limitations, laboratory tests should not be used to compare and rank materials solely on the basis of toxicity. Such toxicity comparisons and

rankings are influenced by test methodology and experimental conditions and may vary considerably when these parameters are changed in a test. Other parameters of the material, including flame spread, ignitability, heat release, smoke obscuration and decomposition temperature, may contribute more or less than toxicity to the hazard of material and must be included in evaluating the potential hazard of a material in a fire. Any one laboratory scale toxicity test method is going to ignore several important aspects of a fire exposure. Toxicity test information, when placed in perspective along with essential combustibility properties of a material, can be of value to a producer for purposes of research information and guidance relative to produce development.



REFERENCES

1. Alarie, Y., "The Toxicity of Smoke from Polymeric Materials During Thermal Decomposition," Ann. Rev. Pharmacol. Toxicol., Volume 25, pp. 325-347 (1985).

2. Kaplan, H. L., A. F. Grand, and G. E. Hartzell, Combustion Toxicology: Principles and Test Methods, Technomic Publishing Company, Incorporated, Lancaster, Pennsylvania (1983).

3. Levin, B. C., A. J. Fowell, M. M. Birky, M. Paabo, A. Stolte, and D. Malek, "Further Development of a Test Method for the Assessment of the Acute Inhalation Toxicity of Combustion Products, NBSIR 82-2532, National Bureau of Standards, Washington, D.C. (1982).

4. Alexeeff, G. V. and S. C. Packham, "Use of a Radiant Furnace Fire Model to Evaluate Acute Toxicity of Smoke," J. Fire Sciences, Volume 2, No. 4, pp. 306-320 (July/August 1984).

5. Alarie, Y. C. and R. C. Anderson, "Toxicologic and Acute Lethal Hazard Evaluation of Thermal Decomposition Products of Synthetic and Natural Polymers," Toxicol. Appl. Pharm., Volume 51, pp. 341-362 (1979).

6. German Standards Institution, DIN 53 436, "Erzeugung Thermischer Zersetzungsprodukte von Werkstoffen unter Luftzufuhr und ihre Toxikologisch Prufung. Part 1, Zersetzungsgerat and Bestimmung der Versuchstemperatur. Part 2, Verhahren zur Thermischen Zersetzung" (January 1979).

7. Tsuchiya, Y., "New Japanese Standard Test for Combustion Gas Toxicity," J. Combustion Toxicology, Volume 4, pp. 5-7 (February 1977).

8. Huggett, C., "Combustion Conditions and Exposure Conditions for Combustion Product Toxicity Testing," J. Fire Sciences, Volume 2, pp. 328-347 (September/October 1984).

9. Woolley, W. D. and M. M. Raferty, "Smoke and Toxicity," INTERFLAM '82, Conference Workbook, University of Surrey, Guildford, England, pp. 93-95 (March 30 - April 1, 1982).

DEVELOPMENT OF A COMPOUND FLOW TEST METHOD FOR PREDICTING DRIP PERFORMANCE OF FILLING COMPOUNDS IN FINISHED CABLES

GREGORY J. HUGHES

ESSEX GROUP, INC., 800 EAST GARFIELD AVENUE, DECATUR, ILLINOIS 62525

ABSTRACT

Since the introduction of the filled cable design, many efforts have been made to improve performance of the filling compound. One characteristic of the compound which has received considerable attention is high temperature flow. This characteristic is currently evaluated in terms of oven drip performance in the finished cable. Oven drip performance can be affected not only by the chemical composition of the compound but also by processing conditions encountered during filling. Current raw material testing of compounds does not adequately relate these processing conditions to oven drip performance of the cable. Without this relationship, complete evaluations of newly developed filling compounds can not be made without actual cable production. This step can cause disruption in production schedules and slow the evaluation process. To eliminate this constraint, a test method has been developed which can relate raw material performance in the laboratory to oven drip performance in finished cable.

INTRODUCTION

In development of filling compounds for filled cable systems, there are several key characteristics which must be considered. These characteristics include:[1]

1. Dielectric constant and dissipation factor.
2. Compatibility with insulating materials.
3. Stability over service life of cable.
4. Flexibility at installation temperatures.
5. Resistance to flow at elevated temperatures.

There exists for all these characteristics, raw material test methods which attempt to predict performance in finished cable. For those characteristics which are not sensitive to processing conditions, these test methods are adequate. However, for those which are sensitive to processing conditions, these methods are not sufficient. One characteristic, which has been identified as being process sensitive, is resistance to flow at elevated temperatures. The raw material test method used to screen this parameter is the compound flow or slump test. This test consists of pouring melted compound into aluminum containers, allowing the compound to cool, and placing the containers vertically in an air circulating at an elevated temperature. The compound is then observed for movement in the form of flow or "slumping". This test is an attempt to predict oven drip performances of the finished cable. The oven drip test relates directly to resistance to flow at elevated temperatures.

The compound flow test, however, does not correlate to oven drip performance. This is because it does not simulate actual processing conditions encountered during the filling operations. During these operations, the filling compound is subjected to mechanical shearing which can in some cases cause actual separation of the compound components. Since most compounds contain some amounts of low melting point materials (i.e. oils), oven drip performance could be affected. Most of these materials also develop some degree of crystallinity. Depending on time, temperature, and conditions during filling, the degree of crystallinity and hence stability can be greatly affected. Additionally, the geometry of the test specimen used for compound flow is significantly different than that used for oven drip testing. For these reasons, resistance to flow in the finished cable could be lower even though raw material results would indicate resistance should be high. Because of this possible discrepancy, a development program was initiated to identify a test method which would simulate process conditions and therefore relate raw material performance to oven drip performance.

DEVELOPMENT OF METHOD

The initial investigation focused on established industry test methods. A review of the ASTM procedures revealed a test method which could be modified for use. This test method was D-1742, OIL SEPARATION FROM LUBRICATING GREASE DURING STORAGE.[2] The procedure outlines a method of applying pressure, at room temperature, to a container holding a sieve strainer full of compound. A small beaker under the container collects any oil which flows from the sieve strainer. The beaker is weighed before and after testing to determine the amount of oil separated.

Since this procedure was not specifically written

for cable filling compounds, modifications to the procedure were necessary. These modifications were based on an evaluation of the major contributing factors which were considered influencial on the rate and amount of compound that could be separated. These factors were selected on the basis of simulating process conditions as well as variations in the current test method and sample preparation. Ten factors were identified which could affect the rate and amount of compound that could be separated. These factors and a description of each are as follows:

1. Test Temperature - The test had to be conducted at an elevated temperature due to the viscosity difference between filling compound and lubricating grease at room temperature.

2. Test Pressure - The test pressure would be similar to that specified in D-1742 due to the limitations of the test fixture.

3. Type of Compound - Two different types of compounds were evaluated. These represent compounds commonly used in the telephone cable industry today.

4. Type of Insulation Mixed with Compound - Two different types of insulating materials were mixed with the compound prior to placement in the sieve strainer. This factor was included in an attempt to simulate the actual cable core environment.

5. Amount of Insulation Material Mixed with Compound - This relates to previous factor. The amount was based on a percentage of the compound weight.

6. Temperature of Compound During Mixing of Insulation Material - The temperature at which the insulating material was added to the compound was controlled. This relates to application temperature of the compound in a cable core.

7. Amount of Agitation of Compound During Mixing of Insulation Material - The amount of mixing was controlled by means of mechanical stirring or hand stirring. This relates to possible shearing of the compound immediately after filling.

8. Rate of Cool Down of Compound/Insulation Mixture - This factor relates to cooling rate of the cable core.

9. Amount of Working (mechanical shearing) of Cooled Compound/Insulation Mixture - The compound/insulation mixture was physically worked prior to placement in the sieve strainer. This relates to the additional mechanical shearing which may occur in winding of a cable on a reel.

10. Addition of Hot Compound to Cooled Compound/Insulation Mixture Prior to Test - This factor relates to subsequent filling operations which may occur in multi-unit cables. Initial layers of compound have solidified prior to final filling.

Due to the large number of factors, the analysis was conducted using a concept known as "Design of Experiments (DOE)". DOE is a statistical method for setting up and executing experiments. It is based on a method developed by Dr. Genichi Taguchi and Professor Yu-In Wu. The main benefit of this method is that a number of variables can be evaluated at the same time using a limited number of tests. The statistical analysis of the results allows determination of those variables (factors) which have the most influence on the evaluation.

With the factors established, it was necessary to determine the number of levels within each factor. Two levels for each factor were assigned. These levels, in most cases, reflected a more is better or less is better condition. The factors with assigned levels are shown in Table 1. In addition to the assignment of levels, possible interactions between factors were identified. These interactions are outlined as follows:

1. Test temperature and pressure (A & B).
2. Mixing temperature and amount of agitation (F & G).
3. Mixing temperature and rate of cool down (F & H).
4. Mixing temperature and amount of working (F & I).

After the factors and interactions were established, the selection of a best fit orthoginal table and corresponding linear graph was done. Since there were ten (10) factors at two (2) levels and four (4) interactions, an L_{16} (2^{15}) orthoginal table was chosen. The orthoginal table with the factors assigned to each column is located in Table 2. The corresponding linear graph used to assign columns to each factor and interaction in the orthoginal table is shown in Figure 1. The interaction columns shown in the linear graph between 5 and 14, 5 and 6, and 6 and 4 were not used. Because of this, the results assigned to factors C (type of compound), D (addition of hot compound), and e (error term) may be influenced by those interactions if they are strong. From the orthoginal table, sixteen (16) experiments were established.

TABLE 1

FACTORS AND LEVELS

A. Test Temperature
   1. 65 °C
   2. 80 °C

B. Test Pressure
   1. 0.44 psi
   2. 0.88 psi

C. Type of Compound (Petrolatum-based)
   1. Compound A
   2. Compound B

D. Addition of Hot Compound to Cooled Compound/Insulation Mixture
   1. No addition
   2. Addition at 225°F (85% solid, 15% liquid, by weight)

E. Percentage by Weight, of Pellets Added to Compound
   1. 25%
   2. 50%

F. Temperature of Compound During Mixing of Insulation
   1. 190°F
   2. 225°F

G. Amount of Agitation of Compound During Mixing of Pellets
   1. Light (hand stirring - 6 minutes)
   2. Heavy (mechanical stirring - 15 minutes)

H. Rate of Cool Down of Compound/Insulation Mixture
   1. Slow (room temp. 72°F constant)
   2. Fast (methanol bath - 20°C constant)

I. Working of Cooled Compound/Insulation Mixture
   1. No working
   2. Working (hand kneading - 10 minutes)

J. Type of Insulation (Pellets)
   1. High density polyethylene
   2. Polypropylene

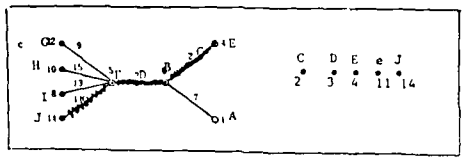
TABLE 2

ORTHOGINAL TABLE

Run No. \ Column	1 A	2 C	3 D	4 E	5 F	6 B	7 AB	8 J	9 FJG	10 H	11 H	12 G	13 FGI	14 J	15 FJH
1	1	1	1	1	1	1	1	1	1	1	1	1	1	1	1
2	1	1	1	1	1	1	1	2	2	2	2	2	2	2	2
3	1	1	1	2	2	2	2	1	1	1	1	2	2	2	2
4	1	1	1	2	2	2	2	2	2	2	2	1	1	1	1
5	1	2	2	1	1	2	2	1	1	2	2	1	1	2	2
6	1	2	2	1	1	2	2	2	2	1	1	2	2	1	1
7	1	2	2	2	2	1	1	1	1	2	2	2	2	1	1
8	1	2	2	2	2	1	1	2	2	1	1	1	1	2	2
9	2	1	2	1	2	1	2	1	2	1	2	1	2	1	2
10	2	1	2	1	2	1	2	2	1	2	1	2	1	2	1
11	2	1	2	2	1	2	1	1	2	1	2	2	1	2	1
12	2	1	2	2	1	2	1	2	1	2	1	1	2	1	2
13	2	2	1	1	2	2	1	1	2	2	1	1	2	2	1
14	2	2	1	1	2	2	1	2	1	1	2	2	1	1	2
15	2	2	1	2	1	1	2	1	2	2	1	2	1	2	1
16	2	2	1	2	1	1	2	2	1	2	1	1	2	1	2
Groups	1	2		3				4							

FIGURE 1

LINEAR GRAPH



Samples were prepared and conditioned as required per the orthoginal table. Sample quantities were 220 grams. This allowed two identical experiments to be conducted per preparation and condition sequence. The compound/insulation mixture was then placed in the sieve strainer. The sieve strainer was placed in the base of the oil separator apparatus and weighed. This weight was subtracted from the weight of the empty sieve strainer and base. This was to insure uniformity in compound/insulation mixture weights between experiments. The entire oil separator apparatus was then assembled. A complete break down of the oil separator apparatus is found in Figure 2. This oil separator apparatus was then placed in an air circulation oven maintained at the specified temperature (±2°C). Pressure through the apparatus was generated by an air compressor and regulated by the use of a mercury U-tube manometer. Pressure was regulated to ± 0.05 psi. Figure 3 provides a complete description of the test set-up. The experiments were conducted over a time interval of seven hours. The catch pan was removed each hour and any compound found was weighed. After the seven hour test period, total compound accumulation was recorded.

FIGURE 2

OIL SEPARATOR APPARATUS

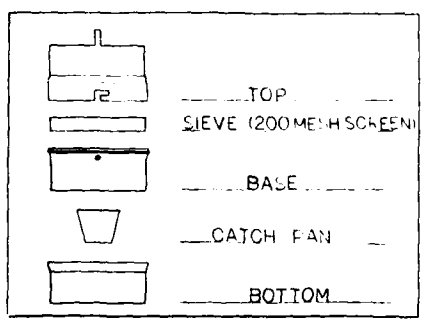
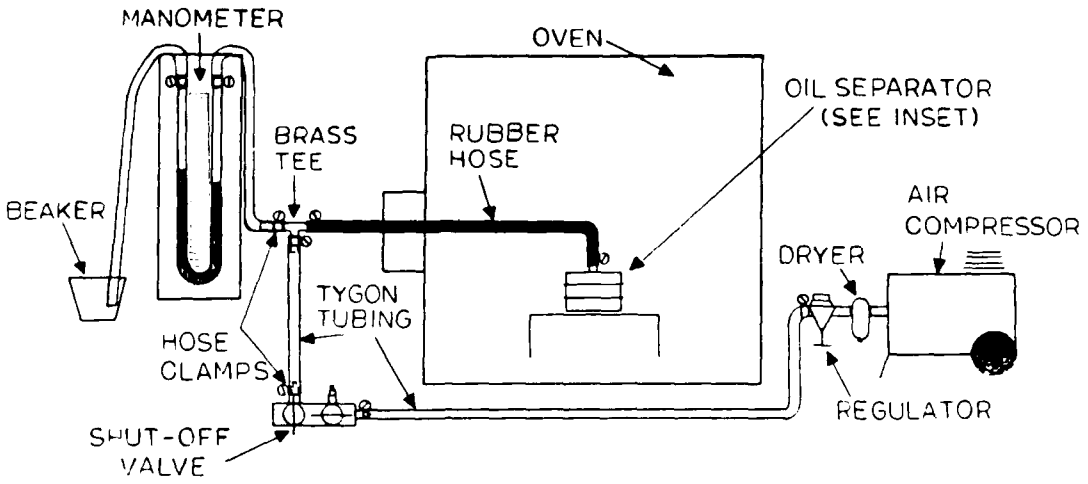


FIGURE 3

TEST SET-UP



RESULTS OF COMPOUND SEPARATION TESTING

The total compound accumulation for both runs of each experiment was determined and is summarized in Table 3. The statistical analysis as outlined in the Taguchi Method was then performed. The main part of this analysis is to construct an ANOVA (analysis of variance) table. The key parts of the ANOVA table are the variance due to each function (V), the variance ratio due to each function (F) and the degree of contribution of each function (ρ). The variance (V) gives an indication of what factors influence variation in results. The greater the number the more variability its factor has on the results. The variance ratio (F) provides a test to determine the significance of the factor's variation in comparison to the correction factor and error variance. This test is sometimes referred to as the F-test and uses a table developed by R.A. Fisher to show corresponding numbers at 5% and 1% significances. By comparing the calculated variance ratio numbers to values located in the table, the degree of significance of each factor can be determined. The degree of contribution (ρ) allows the experimenter to express the significant factors in order by assigning a percentage of contribution to the total variation. Table 4 represents a summary of the compiled ANOVA for these experiments.

From the ANOVA table it is clear that the most significant factor is the rate of cool down on the compound after mixing in the insulation material (Factor H). Its contribution accounts for 35% of the total variation in the results.

The next significant factor is the test temperature (Factor A) which contributed 20% to the

TABLE 3

COMPOUND SEPARATION RESULTS

Experiment Number	Run #1 Total Accum(g)	Run #2 Total Accum(g)
1	2.0877	2.5885
2	1.3232	0.5669
3	2.4568	1.4958
4	0.1941	0.4418
5	0.3127	0.3932
6	1.5150	0.9393
7	0.7031	0.7513
8	0.5485	0.6941
9	2.9151	3.0241
10	0.7290	0.7193
11	2.7335	2.8065
12	1.0095	0.6633
13	2.3299	1.8976
14	2.0980	1.2982
15	1.1663	0.8139
16	2.4383	1.9025

TABLE 4

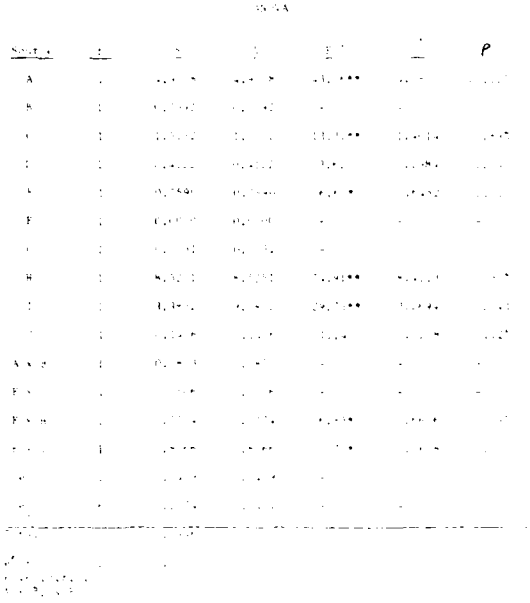
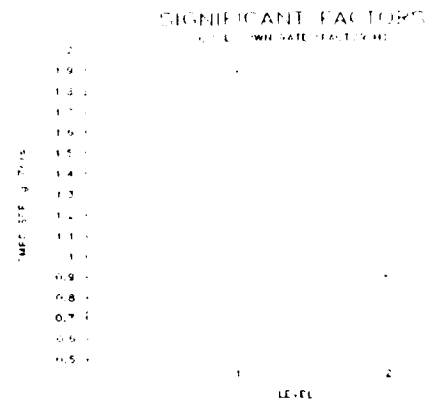
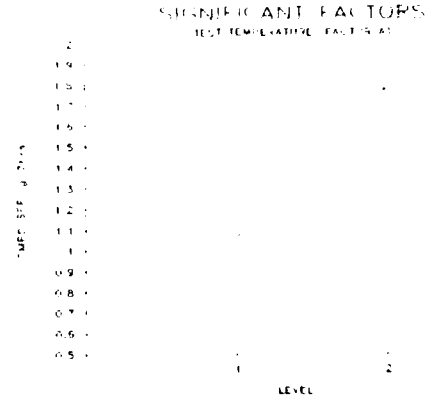
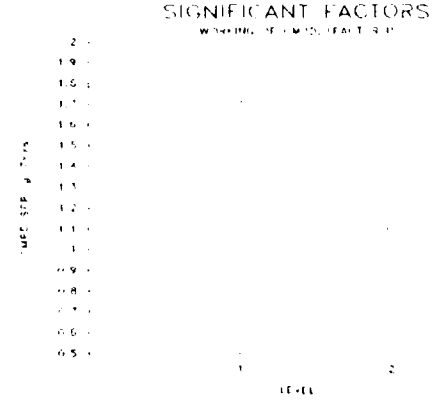


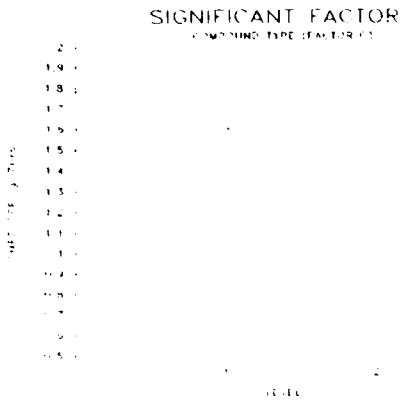
FIGURE 4







total variation. These are followed by the factor on working the compound (I) and the type of compound (C). Each of these four significant factors was then analyzed as to which level caused the greatest amount of compound accumulation. This was done by finding the average compound accumulation where column A=1 experiments and comparing that to the average compound accumulation where column A=2. A graph of this factor for each level was then constructed. This procedure was repeated for the other three factors, These graphs can be found in Figure 4. In the case of test temperature, the higher the temperature, the greater the amount of compound separation. For rate of cooling, the slower the rate the greater the amount of compound separation. Of surprise, was the factor that no working of the compound actually created more compound separation than working did. Practical experience has proven that shearing forces encountered during the manufacturing process can indeed cause compound separation. The shearing forces generated during this evaluation were not of the magnitude or duration necessary to cause this situation to occur. In regard to type of compound, compound B was found to have less accumulation of residue than compound A.



ESTABLISHMENT OF TEST PROCEDURE

Based on the results obtained during this evaluation of compound separation, the following sample preparation and testing environment was established:

1. Test temperature - 80°C.
2. Test pressure - 0.44 psi.
3. Type of insulation mixed with compound - high density polyethylene.
4. Amount of insulation material mixed with compound-25% by weight.
5. Temperature of compound during mixing - 225°F.
6. Amount of Agitation - hand mixing.
7. Rate of cool down - slow.
8. Working-none.
9. Addition of hot compound - none.

To this point, all testing had focused exclusively on petrolatum-based compounds. Gel-type compounds were then included in the evaluation. During this screening process, it was discovered that the procedure established above yielded results which were very inconsistent. This inconsistency was traced back to the filling of the sieve strainer. Filling of the sieve strainer was conducted after the compound had cooled to room temperature. Due to the consistency of the petrolatum component at room temperature, this filling could be accomplished with no difficulty. However, with gel-type compounds, the rubber component of these formulations caused the material to flake or crumble at room temperature. This made filling the sieve strainer at room temperature extremely difficult. Therefore, a modification based on compound type was necessary. For gel type compounds, following addition of the polyethylene pellets, the mixture was poured into the sieve strainer. The mixture was then allowed to slowly cool back to room temperature. Testing was conducted as described previously. Results obtained this time were much more consistent with similar variations as observed with the petrolatum - based compounds.

CORRELATION TO OVEN DRIP

With the test procedure established for both petrolatum-based and gel-type compounds, correlation of these results to actual oven drip performance in finished cables was conducted. A total of five different filling compounds were evaluated. These included three petrolatum-based compounds and two gel-type compounds. The first two petrolatum-based compounds (Compound A and Compound B) were those used in the original DOE testing. Several experimental cable runs were then made with each of the five compounds. These cables were tested for oven drip performance at 80°C per ASTM D4565[3]. Table 5 and table 6 represent a summarization of the oven drip performance with corresponding compound flow data. The data shows that compounds which exhibit high amounts of compound flow also have poor oven drip performance. In addition, those compounds which show little or no compound separation, exhibit good oven drip performance.

TABLE 5

OVEN DRIP PERFORMANCE
PETROLATUM-BASED COMPOUNDS

COMPOUND A	COMPOUND FLOW - 2.16 g/ 7 hrs.		
100/26	foam skin	polyethylene	5/6 failures
400/24	foam skin	polyethylene	6/6 failures
1500/24	solid	polypropylene	3/6 failures
25/24	solid	polypropylene	6/6 failures
COMPOUND B	COMPOUND FLOW - 0.73 g/ 7 hrs.		
50/22	foam skin	polyethylene	1/6 failures
400/26	foam skin	polyethylene	1/6 failures
25/22	solid	polypropylene	1/6 failures
COMPOUND C	COMPOUND FLOW - 0.02 g/ 7 hrs.		
400/24	foam skin	polyethylene	0/6 failures
200/22	foam skin	polyethylene	0/6 failures
100/24	solid	polypropylene	0/6 failures

TABLE 6
OVEN DRIP PERFORMANCE
GEL-TYPE COMPOUNDS

COMPOUND A	COMPOUND FLOW - 3.56 g/ 7 hrs.		
100/24	foam skin	polyethylene	6/6 failures
600/26	foam skin	polyethylene	6/6 failures
200/22	foam skin	polyethylene	6/6 failures
COMPOUND B	COMPOUND FLOW - 0.02 g/ 7 hrs.		
100/24	foam skin	polyethylene	0/6 failures
100/24	foam skin	polyethylene	0/6 failures
100/24	foam skin	polyethylene	0/6 failures

CONCLUSIONS

Both petrolatum-based and gel-type filling compounds can be evaluated in terms of compound flow performance using a modified version of ASTM D-1742. Additional modification in sample preparation is necessary in testing gel-type compounds versus petrolatum-based compounds. This compound flow performance can be directly related to oven drip performance in the finished cable. Those compounds which exhibit low resistance to compound separation, demonstrate poor oven drip performance in finished cable. Those compounds which exhibit high resistance to compound separation, demonstrate good oven drip performance in finished cable.

Additionally, some correlation between compound flow of the raw material and resistance to oil separation in the finished cable may be possible. This would be of significant importance regarding the evaluation of ETPR (Extended Thermoplastic Rubber) compounds which contain high amounts of oil. Further evaluation is necessary, however, before this correlation can be substantiated.

REFERENCES

1. F.W. Horn, "ABC of the Telephone, Volume 5 - Cable, Inside and Out" revised 1977, pp. 40-44.

2. ASTM D-1742 - 64 (1978).

3. ASTM D-4565 - 86, Section 35.



Gregory J. Hughes
800 E. Garfield Ave.
Decatur, IL 62525

Gregory J. Hughes obtained a B.S. degree from Illinois State University in 1982. He joined Essex Group, Inc. after graduating in 1982 and currently holds the position of Materials Engineer.

PERFORMANCE ANALYSIS OF OPTIC FIBER CLEAVERS

W. W. Wood

Bell Communications Research
Morristown, N. J.

ABSTRACT

Many of the optical fiber splices that are being used for splicing telephone cables require cleaved fiber ends. The performance of these splices greatly depends on the quality of the cleaves that are used in the splices. The performance of cleaving tools that are on the market varies, and even the best tools do not always produce excellent results.

A program for analyzing cleaving tools has been developed by, and is being used by, Bell Communications Research. In this program the tools are subjected to tests that simulate usage by telephone company personnel, and the quality of the cleaves produced by the tool is classified. An analysis program for a cleaver requires the classification of 200 cleaves.

The classification is based on observation of cleaved fiber ends under an interferometric microscope. The angle of the cleave is measured, defects are identified and measured, and a classification is assigned to each cleave.

INTRODUCTION

Most of the splicing procedures for optical fibers require that the ends of the fibers be cleaved. The power loss in splices that use cleaved fibers depends largely on the quality of the cleaves that are used in the splice. The cleaving tool is therefore an important factor in splicing optical fibers. Poor cleaves result in a low yield of splices that have acceptable loss. Splices with unacceptable loss must be removed and the splice remade. The time required for refabricating splices is lost to production. Furthermore, when a splice crew is faced with a series of splices with high loss, they will tend to accept splices with higher loss than would otherwise have been acceptable.

Fiber ends that are to be spliced must be flat, smooth, and perpendicular to the axis of the fiber. Cleaving is a quick and simple method for preparing fiber ends for splicing. Glass is a brittle material, and under controlled conditions glass fibers can be made to fracture in such a way that the end surfaces are suitable for use in splices. There are two steps in cleaving a fiber: score it, then stress it. Cleaving tools for optical fibers perform both steps. The quality of the cleave depends on the score that the tool makes on the fiber and on the stress distribution that the tool establishes in the fiber at the instant that the fracture occurs.

The ideal cleaver will, even in the hands of an inexperienced operator, produce nearly perfect cleaves every time it is operated. The performance of the tools currently on the market varies, and even the best tools do not produce excellent cleaves all the time.

PROGRAM FOR ANALYZING OPTICAL FIBER CLEAVERS

A Technical Reference (TR) which outlines the criteria for cleavers in a telephone company environment has been developed by Bell Communications Research.* Included in this TR is a program for testing the compatibility of the individual cleaver tool with the criteria. This program has three phases which are conducted in the following order:

1. Initial Performance Analysis
2. Simulation of Field Usage of the Cleaver
3. Final Performance Analysis

In the Initial Performance Analysis, five operators who have had no previous experience with the tool that is being analyzed are selected to produce the cleaves for the analysis. Each operator is instructed in the use of the tool and is then asked to make 20 cleaves with the tool for the Initial Performance Analysis. Fibers from four different vendors are used. Each of the five operators makes five cleaves with each of the four types of fiber, and the quality of each of the resulting 100 cleaves is then measured.

During the Simulation of Field Usage, the tool is exposed to a series of tests that simulate use of cleaving tools in a telephone company environment. The tool is exposed to vibration, mechanical shock, thermal shock, and temperature and humidity cycling, and is used to produce 900 additional cleaves.

In the Final Performance Analysis, the original five operators produce a second set of 100 cleaves, and the quality of these cleaves is measured.

This paper presents the procedures used in this program for classifying the quality of cleaves produced by the cleaving tools.

CLEAVED SURFACE ANGLE

The single feature most frequently used to characterize the quality of a cleave is the end angle of the fiber. This is the angle that the cleaved surface makes with a plane perpendicular to the axis of the fiber. The angle is measured with an interferometric microscope. Fringe patterns observed in the microscope serve as contour line that graphically illustrate the topology of the cleaved surface. The cleave angle as well as other information needed to analyze a cleave is contained in this fringe pattern. This information can be easily observed, and the fringe pattern can be recorded for future reference.

---

* TR-TSY-000264, Optical Fiber Cleaving Tools, Issue 1, December 1986, Bell Communications Research.

The operation of an interferometric microscope is illustrated in Figure 1.

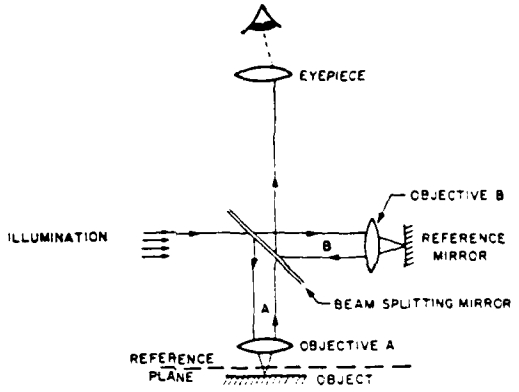


Figure 1. Interferometer

If the object being viewed has a smooth reflecting surface fringe patterns will be seen through the microscope that represent contour lines of constant distance from the reference plane. The contour lines will appear on the surface of the object at intervals that correspond to differences in distance from the reference plane of 1/2 the wavelength of the light being used to illuminate the object. Green light with a wavelength of 0.546 microns is generally used in interferometric microscopes. With this light the distance between contour lines corresponds to differences in distance from the reference plane of 0.273 microns.

For these measurements, the cleaved end of a fiber is mounted in the field of view of the microscope with the axis of the fiber perpendicular to the reference plane. If the end of the fiber is flat a pattern of straight, parallel, evenly spaced fringes will be observed, and the angle of the cleave may be measured by counting the number of fringes. If the fiber has a diameter of 125 microns, there will be eight fringes per degree. The image of the end of a cleaved fiber, as displayed on a video monitor, is illustrated in Figure 2. There are three fringes in this image which indicates that this cleave has an angle of about 0.4 degree.



Figure 2. Interferometer End Angle 0.4°, No Defects

Angular measurements of the end of a fiber in these analyses are accurate to within 0.2°. Resolution is better than one fringe (0.125°), and the perpendicularity between the fiber and the reference plane is maintained to within 0.05°.

Cleaved surfaces however are generally not flat, and there may be areas that are too rough to produce interference patterns. Therefore, an algorithm was developed to define the end angle for these cases. This algorithm is illustrated in Figure 3.

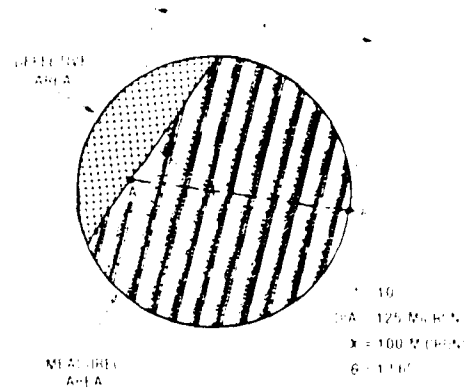


Figure 3. Method For Measuring Fiber Ends

The first step in the algorithm is to divide the end of the fiber into two areas: defective areas and measured areas. Defective areas are areas that are too rough to produce interference patterns or that have a slope of more than 10°. Measured areas are areas that are smooth enough to produce interference patterns and have a slope of less than 10°.

The second step in the algorithm is to pass line A-B through the measured area of the fiber. Line A-B is positioned so that it intersects the greatest density of fringes and passes through the center of the fiber. Points A and B lie on the boundary of the measured area.

The third step is to count the number of fringes that intersect line A-B and to measure the length of line A-B. This length is determined relative to the diameter of the fiber (125 microns). For a fiber that is 125 microns in diameter, the cleave angle is calculated as follows:

$$\theta = \frac{\frac{I}{8}}{\frac{X}{125}}$$

where I is the number of fringes between A and B, and
X is the length of line A-B.

CLEAVED SURFACE DEFECTS

The defective areas over which measurements for angle cannot be made must also be considered in the analysis of a cleave.

The procedure for analyzing defects is based on the interferometric patterns associated with the defective areas. Eight distinct patterns have been identified in the course of examining several hundred cleaves. These patterns provide the basis for the system for classifying defective areas. The eight defects used in the classification are: score, hp, rolloff, chip, spiral, step, hackle-mist, and shattered. During the analysis the size of each defect other than "shattered" is recorded.

Descriptions of each of these defects follow, along with a line drawing and a photograph of the fringe patterns for seven of the defects (Figures 4 through 10). The size ("y") of each of type of defect is also defined in Figures 4 through 10. The eighth defect is defined but not illustrated because the entire surface is defective and no fringe patterns are developed.

- Score: A score is the area that is damaged when the fiber is scored preparatory to being cleaved. The score area is generally small (Figure 4).

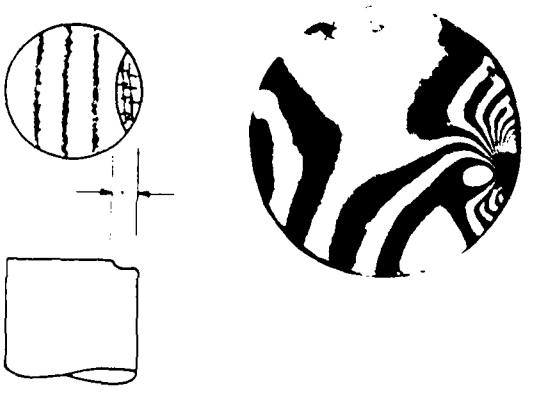


Figure 4. Score Defect

- Lip: A lip is a raised portion of glass at the edge of the cleave (Figure 5).

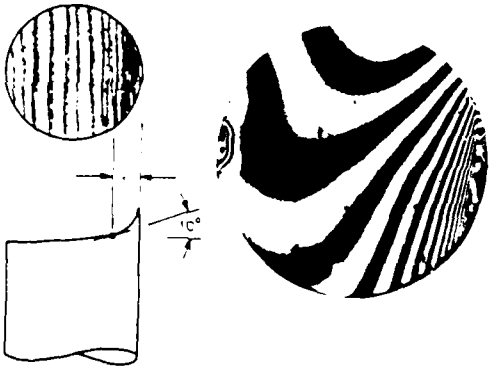


Figure 5. Lip Defect

- Rolloff: A rolloff is the mirror image of a lip (Figure 6).

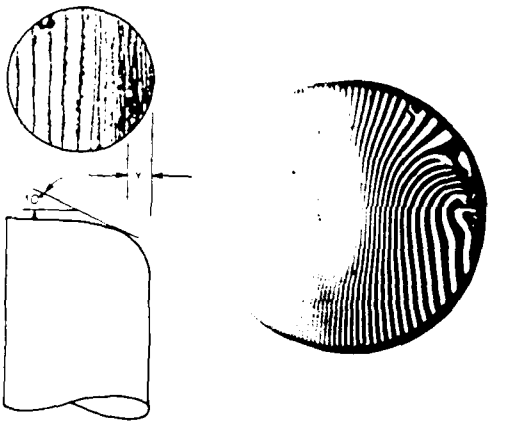


Figure 6. Rolloff Defect

- Chip: A chip is similar to a rolloff except that it has a sharp edge where the chip begins (Figure 7).

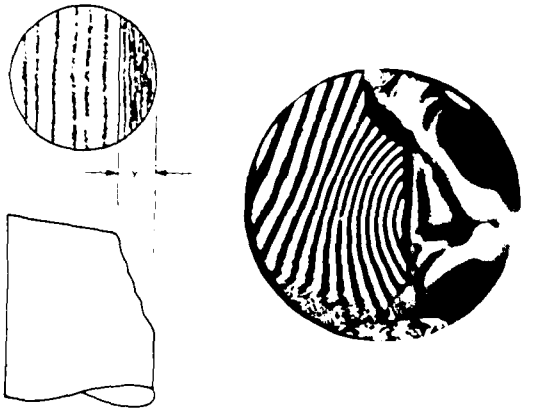


Figure 7. Chip Defect

- Spiral — A spiral has a discontinuity at the edge of the fiber where there is a change in elevation in which fringe patterns are not distinguishable. Fringes radiate out from this point (Figure 8).

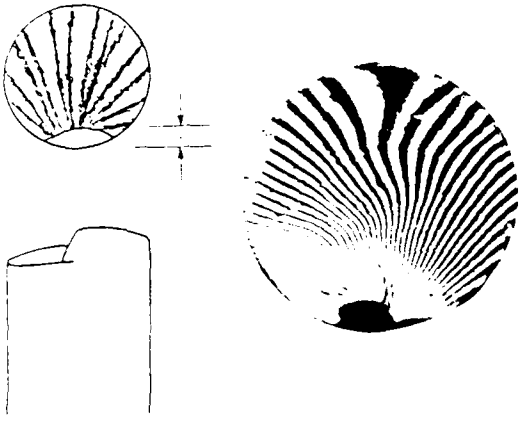


Figure 8. Spiral Defect

- Step — A step is similar to a spiral except that the point of discontinuity extends further into the fiber, and the fringes do not in general radiate evenly (Figure 9).

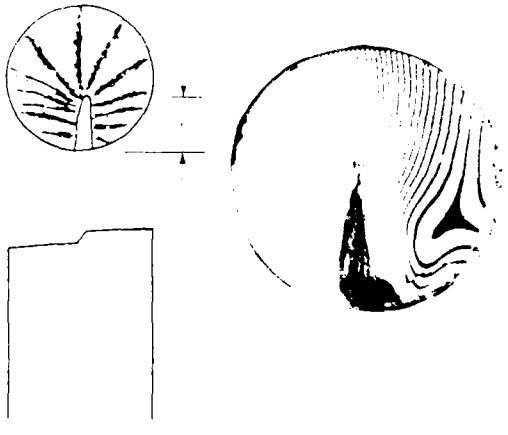


Figure 9. Step Defect

- Hackle-Mist — Hackle and mist are rough areas that do not develop smooth continuous fringes (Figure 10).

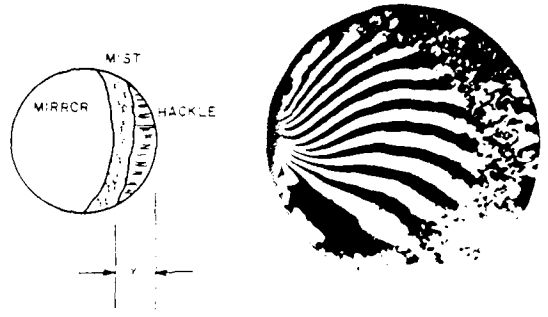


Figure 10. Hackle-Mist Defect

- Shattered — A shattered end is a broken sliver of glass. There are no flat areas, and only a small area can be brought into focus at any one time. (Not illustrated.)

CLASSIFICATION OF CLEAVES

The classification system assigns to each cleave a rating of A, B, or C on the basis of the end angle, the defects that are present, and the size of the defects. The classifications and their definitions are:

A — The cleave surface is flat with a mirror finish and has an angle of less than 1 degree.

B — The cleave surface has at most only minor defects, and the angle is less than 2 degrees.

C — The cleave surface has major defects and or an angle of more than 2 degrees. (Cleaves in this category are not considered to be satisfactory for telephone company splicing.)

To classify a cleave, the end angle is determined and the defects are identified and measured. A classification from Table I is assigned to the angle and to each of the defects. The classification for the cleave is the lowest of these classifications.

The overall objective of this classification system is to rank-order cleaves on the basis of their expected performance in a splice. The classification system was developed on the basis of experience in making splices and a review of the requirements for a good splice.

The three requirements for a good splice are:

1. The core areas of the two fibers should be in contact.
2. The core areas should be mirror smooth.
3. There should be no gaps or cavities in the interface between the two fibers.

Table 1. Cleave Classification System

Defect Type	Cleave Quality Rating		
	A	B	C
	Defect Distance in Microns (fiber edge to core)		
Score	< 12	12-20	> 20
Lip	0	0	> 0
Rolloff	0	< 15	> 15
Chip	0	< 20	> 20
Spiral	0	< 15	> 15
Step	0	< 20	> 20
Hackle Mist	< 10	10-20	> 20
Shattered			(Note 1)
End Angle	< 1°	1° – 2°	> 2°

Note 1. The quality rating for all shattered ends is C.

The weighting to be to given to each of the defects was based on the effect they would have on producing a low-loss splice. For example, a lip is a rather serious defect in that it separates the fiber ends, whereas with a chip the core and most of the fiber end can be in contact. Consequently, a cleave with a lip of any size is classified as C, whereas a cleave with a chip of 19 microns may be classified as B.

RESULTS

The data in Bellcore product analysis reports are proprietary and are released only to the former Bell Operating Companies sponsoring the analysis and to the manufacturer of the particular tool. However, a few general conclusions can be presented from the tests that have been conducted so far.

Eight tools have been tested. The results of these tests showed large variations between tools. The best tools had only 60% of their cleaves in the A or B classification. The poorest cleavers had no cleaves in the A classification and 50% of their cleaves in the C classification.

Most of the tools showed no significant change in performance as a result of the simulated field usage. Some tools however show a significant variation in performance with different operators. This is important since it indicates that the performance of these tools is sensitive to the technique used by the operator. It may indicate a need for additional procedures for training in the use of these tools and/or redesign to reduce operator sensitivity.



William W. Wood
Bell Communications Research
435 South Street
Morristown New Jersey 07960

Mr. Wood is a Member of the Technical Staff at Bell Communications Research, Morristown N. J. His current responsibilities include the analysis of fiber optic splices. Mr. Wood received a Bachelor of Science degree in Mechanical Engineering from Newark College of Engineering in 1955, and a Master of Science Degree in Engineering Mechanics from Columbia University in 1960. He joined Bell Telephone Laboratories in 1957 where he worked on the development of tools and equipment for use in the telephone system. He joined Bell Communications Research in 1984.

A METHOD OF DETERMINING THE PERCENT EXPANSION OF CELLULAR INSULATIONS

N. JEAN BAER

ESSEX GROUP, INC., 800 EAST GARFIELD AVENUE, DECATUR, ILLINOIS 62525

ABSTRACT

The percent expansion of cellular insulations, defined as the ratio of the volume of gaseous cells or voids in the insulation to the total volume of the insulation, is of prime interest to the cable design engineer. It allows the material usage required for a particular insulation design to be calculated.

A detailed analytical method for measuring the percent expansion of cellular insulations based on the determination of the insulation density using a liquid displacement technique is presented. Direct measurement of the percent expansion of foam insulation and of the apparent percent expansion of foam/skin insulation is possible with this technique. No assumptions or measurements of dimensions are required for these determinations.

A mathematic calculation, based on the dimensions of the copper diameter, insulation diameter, and skin thickness, allows the percent expansion of the foamed portion of the foam/skin insulation to be determined.

INTRODUCTION

Percent expansion, the ratio of the volume of gaseous cells or voids in cellular insulation to the total insulation volume, is a necessary design parameter. It is necessary for calculating the material usage in a cable construction and is a consideration in cable design since the parameter may influence the electrical and/or physical properties of the insulation. The dielectric strength of the insulation and hence its ability to meet the conductor to conductor High Voltage Tests of various cable specifications, and the tensile strength and compression strength of the insulation are all properties which are directly affected by the percent expansion of the insulation. In addition, while insulation diameter and coaxial capacitance are used as process parameters to control the cellular extrusion process, measurement of percent expansion provides a relative quality control check of the cellular insulation, independent of process conditions, temperature, or line speed.

Cellular insulation as it was first introduced in the United States in 1973 was in the form of foam insulation. This design distributes small gaseous cells uniformly throughout the cross-section of the insulation and lends itself more easily to exact measurement of the percent of expansion.

Today, however, foam insulated conductors have been augmented in the cable industry with foam/-skin insulation, a design which still incorporates the concept of foam insulation, but which was further refined by the addition of a thin layer of solid material over the foamed portion. Determining the actual percent expansion, and thereby knowing the exact amount of material usage, is more difficult with this combination of solid material and foamed material on the same insulated conductor.

The term percent expansion is used here to mean the amount of gas present in the insulation and can be calculated as the ratio of the volume of air present in the insulation to the total volume of the insulation expressed as a percent. While theoretically it is possible to approach 100% expansion, physically it is not practical. Evaluation of physical properties of the resulting insulation as a function of percent expansion have shown that these physical properties decrease gradually with increased percent expansion. As the volume of the gas approaches and exceeds the volume of solid material, the cells tend to become interconnecting, severely reducing the mechanical and dielectric strength of the insulation.

In order to produce the smallest and therefore the least costly cellular product, the cable design engineer must know what is the maximum percent of expansion that can be utilized without sacrificing physical or electrical properties.

By manufacturing cables with different percentages of expansion and measuring the expansion of cables that have known values of various physical and electrical characteristics, the designer can achieve an optimum design.

It was for that reason that the following test method was established.

TEST METHOD

Determination of percent expansion is based on first measuring the density of the insulation. Density is measured using Archimedes' Principle which consists of weighing the material in air and in water. However, because the density of the cellular insulation is less than that of water, it will float in the water. For this reason, the measurements are made using an insulated conductor and the effects of the conductor subtracted from the results to obtain the appropriate weights of only the insulation. Once the density of the insulation is determined, the percent expansion is obtained by dividing the measured density by the density of the solid material and subtracting this value from 1.

Detailed test methodology and formulae for calculating density and percent expansion are as follows.

1. SCOPE

This method describes the procedure for determining the degree of expansion of cellular polyolefin insulations based on their density, using a water displacement technique.

2. EQUIPMENT

2.1 Analytical Balance capable of measuring to 0.1 mg.

2.2 Beaker: 250 ml

2.3 Beaker Support: A stationary platform to support the beaker above the balance weighing pan.

2.4 Sample Support Wire: 22-26 AWG wire, approximately 4 inches long for suspending the test specimen from the specific gravity hook of the balance into the beaker.

2.5 Thermometer: Graduated in increments of 1°F.

3. PROCEDURE

3.1 Cut two (2) cellular insulated conductor specimens approximately 10 inches long. Wind each into an individual coil having a diameter of 1 to 1.5 inches. Test each specimen individually.

3.2 Weigh the coiled sample in air on the analytical balance to the nearest 0.0001 g. Record this weight as W_1.

3.3 Fill the beaker with water. Position the support and filled beaker over the balance pan.

3.4 Attach the support wire to the specific gravity hook, positioning directly above the filled beaker.

3.5 Suspend the coiled specimen on the freely hanging support wire, immersing the coil into water. Make sure the coil is completely immersed, that it is not touching the side or bottom of the beaker and there are no air bubbles adhering to the support wire or test specimen. Gentle shaking of the support wire should usually remove any bubbles.

3.6 Determine the weight of the support wire plus the totally immersed coiled specimen in water to the nearest 0.0001 g. Record this weight as W_2.

3.7 Carefully uncoil the specimen and strip the insulation from the entire length of conductor. Recoil the wire and weigh the bare conductor in air to the nearest 0.0001 g. Record this weight as W_3.

3.8 Suspend the bare conductor from the support wire in water as previously described in Step 3.5. Weight to the nearest 0.0001 g and record as W_4.

3.9 Measure the temperature of the water in the beaker to the nearest 1°F.

3.10 Following the calculations in Section 4, determine the percent expansion for each cellular polyolefin insulation specimen.

4. CALCULATIONS

4.1 Calculate the specific gravity of the cellular insulation as follows:

$$S.G. = \frac{(W_1-W_3)}{(W_1-W_3) + (W_4-W_2)}$$

Where:
- S.G. = Specific gravity of test specimen
- W_1 = Weight of insulated conductor in air (grams)
- W_2 = Weight of insulated conductor and support wire in water (grams)
- W_3 = Weight of bare conductor in air (grams)
- W_4 = Weight of bare conductor and support wire in water (grams)

4.2 Calculate density of the cellular insulation as follows:

$$D_c = (S.G.)\ (D_w)$$

Where:
- D_c = Density of cellular insulation (grams/cm^3)
- D_w = Density of water at test temperature (grams/cm^3)
- D_w = 1.00 g/cm^3 at 70°F; consult handbook for D_w at other temperatures.

4.3 Calculate the degree of expansion of the cellular insulation to 2 significant figures as follows:

$$E = \frac{(D_s - D_c)}{D_s} \times 100$$

Where E = Percent expansion, %
D_s = Density of solid material corresponding to the insulation (grams/cm^3)
0.905 g/cm^3 for polypropylene
0.948 g/cm^3 for high density polyethylene

If the insulation is foam, the percent expansion calculated in 4.3 is the actual percent expansion of the insulation. If the insulation is foam/-skin, 4.3 only gives the apparent percent expansion, that is as if the cells were uniformly distributed over the entire cross-section rather than being concentrated in the inner foam portion with solid material as the skin.

To determine the actual percent expansion of the foam portion of foam/skin insulation, the following information must be obtained from actual or design measurements of the sample being tested:

DOD = Overall diameter of insulated conductor, inches
t = Skin thickness, inches

DOF = Diameter over the foamed portion of the insulated conductor = DOD - 2t, inches
d = Conductor diameter, inches

Then, the density of the composite cellular insulation, D_c, measured above can be related to the density of the foamed portion only, D_f, by the equation:

$$D_c = \frac{V_s D_s + V_f D_f}{V}$$

Where: V_s = Volume of skin, inches
V_f = Volume of foamed portion, inches
V = Volume of overall insulation, inches

or $$D_c = \frac{(DOD^2 - DOF^2)\, D_s + (DOF^2 - d^2)\, D_f}{(DOD^2 - d^2)}$$

Rearranging and solving for D_f yields.

$$D_f = \frac{(DOD^2 - d^2)\, D_c - (DOD^2 - DOF^2)\, D_s}{(DOF^2 - d^2)}$$

Since D_s is a known for a given material, D_c is known from the previous measurement, and DOD, DOF, and d are known from design parameters or actual measurements on the specimen being tested, D_f can be calculated.

Percent Expansion, E_f, of the foamed portion only can then be calculated from:

$$E_f = \frac{D_s - D_f}{D_s} \times 100$$

The reproducibility of the above test has been shown through extensive laboratory testing to be within ± 2-3% for foam insulation and within ± 5% for foam/skin insulation.

CONCLUSION

This paper outlines a method for determining the actual percent expansion of foam insulation and the apparent percent expansion of foam/skin insulation. This methodology has been extended, through mathematical calculations, to determine the actual percent expansion of the foamed portion of foam/skin insulation.

REFERENCES

1. The Universal Cable Design For The Outside Plant, 1980, Dr. James S. Tyler.



N. Jean Baer
800 East Garfield Avenue
Decatur, Illinois 62525

N. Jean Baer attended Lake Land College. She joined Essex Group, Telecommunication Products Division in 1981 in the Quality Assurance Department. She currently holds the position of Manager of Product Engineering.

A TEST FOR OPTICAL FIBER COATING STRIPPABILITY

James Moses and Mark Sigmon

Siecor Corporation
Hickory, North Carolina

ABSTRACT

In the practical use of optical fibers it is necessary to mechanically strip the protective coating off the fiber in order to splice or connectorize it. It is desirable to strip the required length of coating in one step. Therefore the stripping force cannot be too high. At the same time some adhesion of the coating to the glass is required for environmental reasons. Until recently this force has not been quantified. In this paper a test for strippability of optical fiber coatings is described. The testing apparatus and procedure are presented, and the results of this strippability test are discussed. A correlation is made between the strippability profile and the environmental stability of the coating system.

THE STRIPPABILITY TESTER

A device for accurately measuring the mechanical force required for stripping the coating from a fiber is now in use. The test apparatus consists of five main components, and is sketched in Figure 1.

1. Load cell
2. Translating stage
3. Fiber optic strippers
4. Control panel
5. Chart recorder

The heart of the strippability tester is the load cell. Physical stripping force is measured electronically by the load cell. One end of the fiber is secured to the load cell by wrapping it around the cylindrical holder. The other end of the fiber is threaded through the fiber optic strippers and clamped. The strippers are mounted on a translating stage. By setting the stage in motion the coating is automatically removed from the fiber. The stripping end of the fiber is fed into a tube that keeps the coated fiber in position as the stripping occurs. The depth of the tube can be used to control the strip length. Stripping force is digitally displayed on the force transducer indicator located in the control panel. The transducer indicator features a peak hold mode displaying maximum force measured during the strip. A continuous force readout is also possible by locking out the peak hold. Also housed in the control panel is the stripping speed adjustment with digital readout. A chart recorder graphs the stripping force profile versus time.

Capabilities of this test equipment include a force range of 0 to 45 Newtons. Stripping speed may be varied from 0 to 9 cm/min. In addition, a wide range of stripping tools may be used by simply changing holders for the desired stripper and mounting it on the translating stage.

TESTING PARAMETERS

It is important to choose the correct testing parameters to provide comparable measurements among a wide range of coating systems. Coatings with high levels of adhesion should not be tested by stripping a long length of coating from the glass. When this strip length is too long, the coating does not slide away from the glass. Rather it exhibits a buckling, twisting effect, making the results difficult to analyze. The pure sliding mechanism of strippability testing is easier to analyze.

From experience, the best testing parameters are as follows:

Strip length: 1 cm from fiber end
Stripping speed: 1.5 cm/min (0.6 in./min.)

This allows a wide range of coatings to be tested under the same conditions.

The Seiko stripping tool was chosen for this test. The Seiko tool is effective for coated fibers in the 500 micron and 900 micron geometries. The Seiko tool with the .3 mm blades cuts down to 300 microns. When a pulling force is applied, the remaining coating is stretched and torn away from the 125 micron glass. Then this coating sleeve slides away from the glass. For 250 micron fiber, a different tool must be used, since this fiber size would simply slide through the 300 micron blades. Please note that this paper will present data for 900-micron coated fiber only.

STRIPPABILITY RESULTS AND ANALYSIS

Table 1 lists the peak stripping force for a variety of coating systems. The coatings have been identified by ranking them in order of decreasing peak strip force. Each of these coatings is a dual-acrylate buffered out to 900 microns with a thermoplastic tight buffer.

TABLE 1

COATING	AVERAGE PEAK FORCE (Newtons)	STANDARD DEVIATION OF THE SAMPLE (n=10)
1.	28.1	1.0
2.	14.0	0.6
3.	12.5	0.5
4.	12.2	0.4
5.	10.2	0.9
6.	7.2	0.6
7.	6.6	0.7

Figure 2 shows a representative strippability profile for a 900 micron coated fiber. This behavior is analogous to that shown in a previous study of the adhesion between coated fibers and slabs of elastomeric material. (*) The ordinate is force in Newtons. The abscissa, reading right to left, is time. Since a constant speed of 1.5 cm/min is maintained, the abscissa can also be converted to distance. The strippability profile is divided into two regions. Region I is that part of the stripping process where the stripping tool is tearing the remaining coating from the glass. The peak stripping force is encountered here. This force is dependent on the ultimate tensile strength of the coating material and the force that it takes to overcome the static coefficient of friction between the glass and coating. Region II is that part of the stripping process where the coating is sliding along the glass at the 125 micron interface. The force taken to accomplish this stripping is solely a function of the (dynamic) friction coefficient between glass and primary coating. The slope of the Region II portion of the strippability profile gives an indication of the magnitude of the adhesion between coating and glass.

Figures 3a through 3g illustrate the strippability profiles characteristic of coatings 1 through 7, respectively. Coating 1 has the highest stripping force, and the adhesion is so high that there is no apparent second region. This is an example of the tested strip length of 1 cm being too long for this well-adhered coating. The dual force peaks seen in Figure 2a are characteristic of the buckling or twisting mechanism of stripping. At the other extreme, Coating 7 has almost no measurable adhesion between glass and coating once the initial break is made. Note that Coatings 3 and 4 have very similar strip profiles and peak force values. In fact, it is known that these two coatings are composed of the same materials.

ENVIRONMENTAL STABILITY: "FIBER PISTONING"

While it is desirable to keep the peak stripping force low in order to make the strippability process craft-friendly, some level of adhesion is required for reasons of environmental stability. Since there is a mismatch of the thermal expansion coefficients of the glass and the coating materials, it is possible that the coating system will shrink away from the glass fiber. This problem has been referred to as "fiber pistoning," since the glass moves independently of the coating. This presents a problem with connectorization, in some cases leading to fiber breaks.

The susceptibility of a coating system to fiber pistoning can now be predicted by analyzing its strippability profile. Coating 1 has the highest stripping force, and the friction coefficient is so high that there is no apparent second region. No fiber pistoning is expected, due to the large adhesion value. On the other hand, Coating 7 is a likely candidate for fiber pistoning.

A check for fiber pistoning has been devised. Coated fibers are cut into 1-meter lengths and exposed to 65 degrees C and 70% relative humidity for a period of 3 days. The results can be seen in Table 2:

TABLE 2

COATING	OBSERVED PISTONING
1.	none
2.	none
3.	almost imperceptible, < 1 mm
4.	none
5.	none
6.	6 mm glass exposed each end
7.	6 mm glass exposed each end

As expected, the well-adhered Coating 1 showed absolutely no pistoning effects. Coatings 6 and 7 pistoned greatly. This low adhesion was predicted by their strippability profiles, Figures 6 and 7. The only other coating to exhibit any pistoning was Coating 3. It is surprising that Coating 3 would piston and Coating 4 would not, since their strippability profiles are virtually the same. It must be recognized that the level of pistoning in Coating 3 is so slight that there may not be any meaningful difference between the pistoning performance of Coating 3 and those coatings that exhibited no pistoning at all.

Although the coatings with the lowest peak strip force from Table 1 also were the most susceptible to pistoning, the peak force value alone is not enough to predict the environmental stability of the coating system. This is because the peak strip force includes the force required to completely break the coating after the stripping tool clamps down. It is felt that the

complete strippability profiles seen in Figures 2a-g are a better indication of the glass/coating adhesion. The Region II portion of the profile is a direct measure of the force required to slide the coating from the glass, and hence is a good indicator of pistoning performance.

CONCLUSION

The use of this optical fiber coating strippability tester now allows one to accurately measure the mechanical force required to strip the coating from a fiber. The critical test parameters are the strip length and the stripping speed, with recommended values of 1 cm and 1.5 cm/min. respectively. The strippability tester produces chart records of stripping force profile versus time. These strippability profiles indicate the peak stripping force that will be required by craftspeople in the field, and also provide a prediction of the environmental stability of a coating system by measuring its adhesion to the glass.

REFERENCE

(*) L.L. Blyer, Jr., C.Gieniewski, X. Quan, and H. Ghoneim, "Buckling of Optical Fibers Within Elastomers Used in an Embedded-Core Cable Structure," Proceedings of the 32nd International Wire and Cable Symposium (CORADCOM, Fort Monmouth, NJ), Cherry Hill NJ, November 15-17, 1983, p.146.

James A. Moses
489 Siecor Park
Hickory, NC 28603



James A. Moses was born in Huntsville, Alabama in 1963. He received his Bachelor's degree in Mechanical Engineering from Vanderbilt University in 1985. He is currently employed as a Process Specialist in the Research, Development and Engineering division of Siecor Corporation.

Mark A. Sigmon
489 Siecor Park
Hickory, NC 28603



Mark A. Sigmon was born in Newton, North Carolina in 1962. He received his Bachelor's Degree in Mechanical Engineering from North Carolina State University in 1985. Since then, he has worked as a Process Engineer for Siecor Corporation - Research, Development and Engineering Department, and is currently Supervisor of the Process Lab.

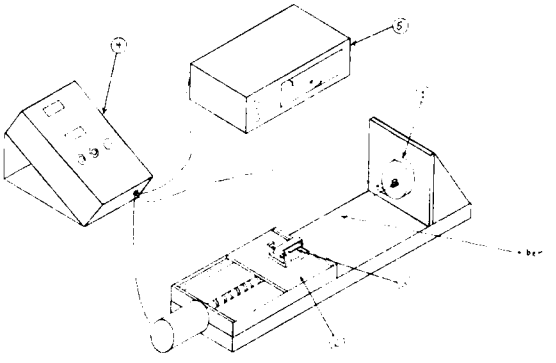


FIG. 1

Figure 2

Representative Strippability Profile

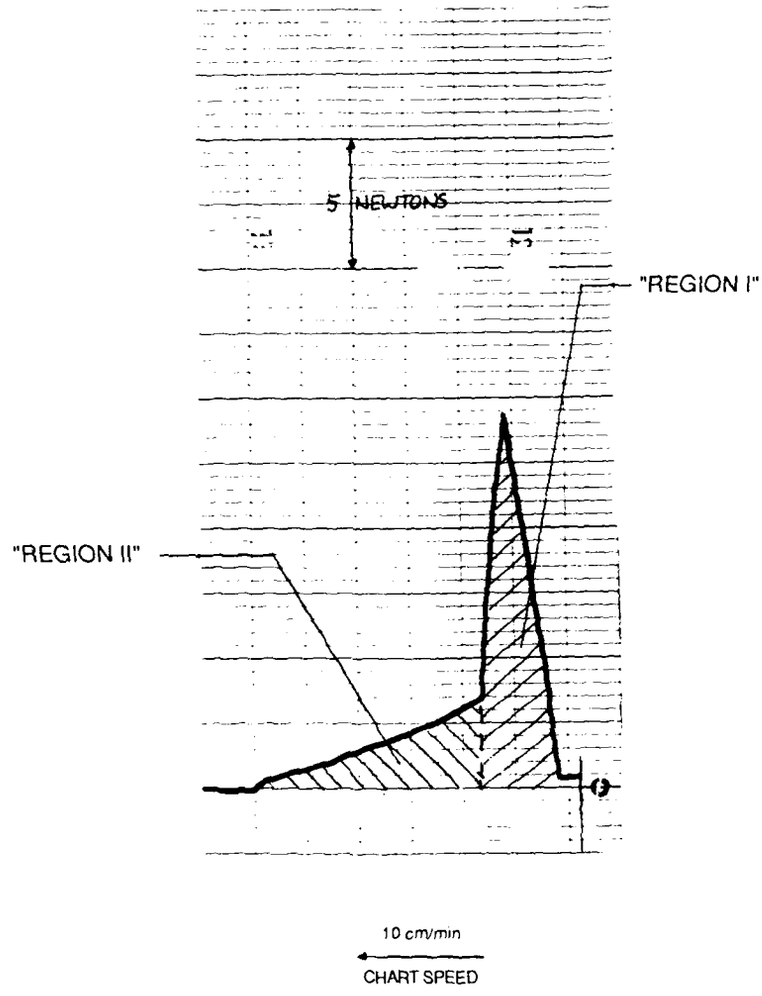
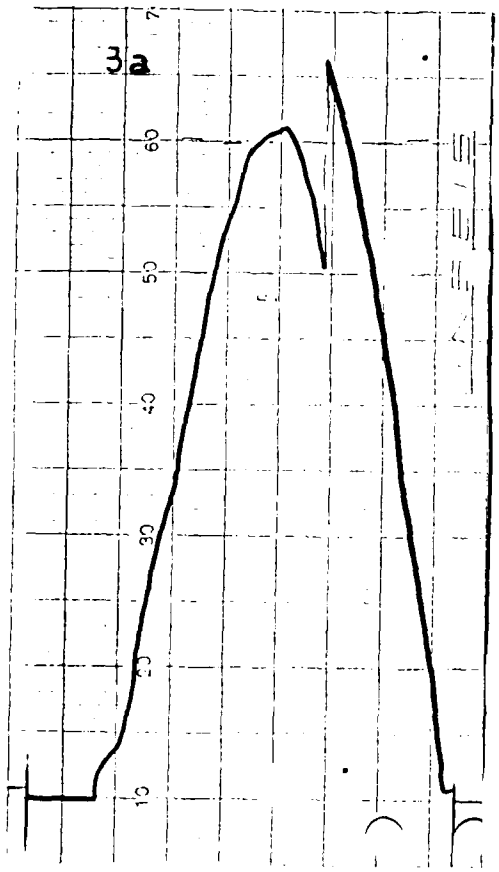
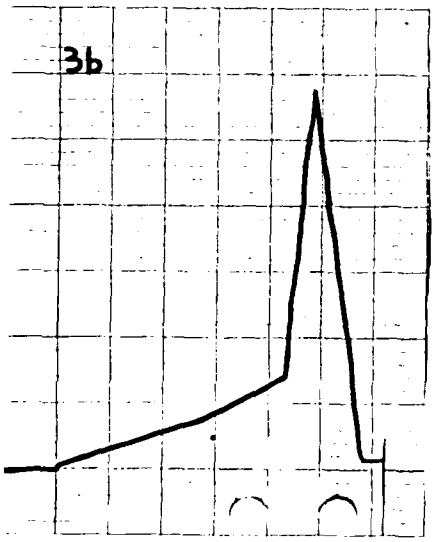
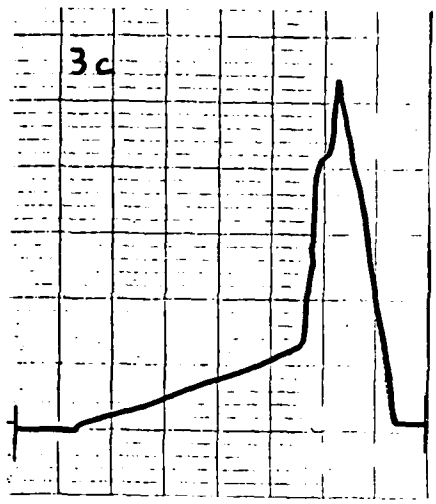


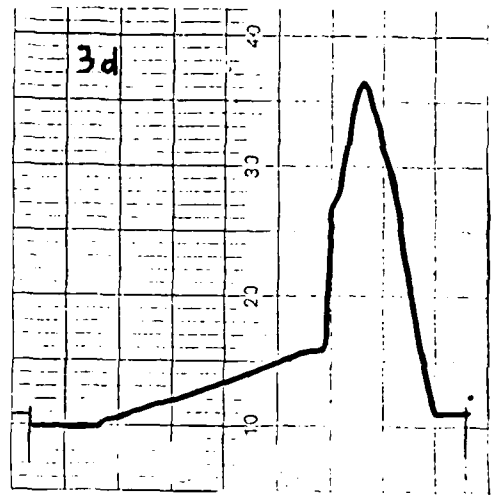
Figure 3

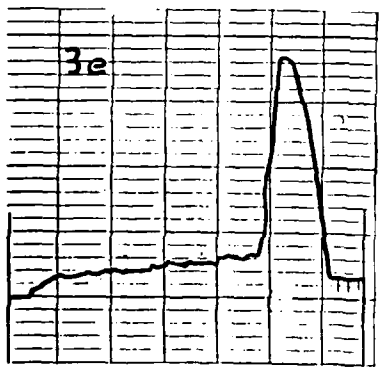


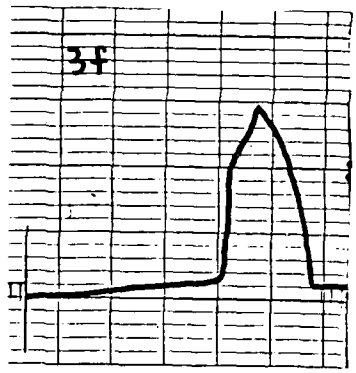
Strippability Profiles for Seven Fiber Coatings

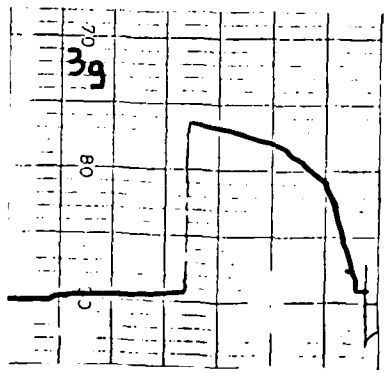



3c


3d
40
30
20
10


3e


3f


3g
90
80

DISTRIBUTION OF FIBER OPTIC FACILITIES IN COMMERCIAL BUILDINGS

John P. Varachi and Charles H. Hasz
Bell Communications Research
435 South Street
Morristown, New Jersey 07960

ABSTRACT

As new wideband services become available, their first applications will undoubtedly be in the business community. The need for packet data, low and high speed video will require, in many cases, a fiber network overlay to the copper risers and distribution cables in existing commercial buildings. The need to overlay this copper plant with fiber presents a challenge to telco engineers and installers and to the manufacturers of the cables and apparatus they will use. This paper will review the experience and insight gained from the design and installation of an experimental fiber optic network at Bell Communications Research in Morristown, NJ. Special emphasis will be placed on the significant effect cable and apparatus design have on efficiency, ease of installation and reliability of the installed network. Design requirements for manufacturers' products, increasingly, must emphasize the customers' ability to install, maintain and repair them because this cost can far outweigh the original purchase price.

Introduction

Unlike the residential market, where the cost of deploying "the last mile" of a fiber optic network must compare with existing technology costs for basic service with incremental increases for services generally entertainment or convenience in nature, the business community will take advantage of new broadband services to generate new revenues or reduce the cost of generating the current revenue stream. Dollars to pay for these broadband services and the network to deliver them will therefore be more readily available and fiber optic overlays of existing copper facilities will be common in downtown commercial centers. This presents a unique and early challenge to the telco engineer, the installer, and the equipment vendor to engineer, develop and install fiber optic facilities in spaces that, in general, are already overcrowded by copper facilities and equipment.

Commercial Building Environment

Traditionally, telephone facilities in commercial buildings have been located in space provided by the landlord. It is generally a combination of a room located in the basement, riser shafts, telephone closets on each floor and floor distribution raceways as shown in Figure 1. Basement areas may be poorly lighted, damp or subject to flooding, common to other building facilities, unsecured, and poorly ventilated. Small distributing frames, crossconnect panels, splice cases, and multiplexing/demultiplexing electronics, PBXs, power supplies and batteries can all be found there. Riser space will be partially if not fully occupied by the existing copper network. Telephone closets, located in building core areas, are usually very small (4' x 6' in some cases) providing only enough floor area for entry and exit. Virtually all telephone apparatus is wall mounted including crossconnects, cable racking, riser tie points and occasionally telephone equipment serving lines in the surrounding space. Any unoccupied wall space may have limited usefulness due to its height off the floor or inaccessibility because of the volume of existing cable being routed and dressed within the closet.

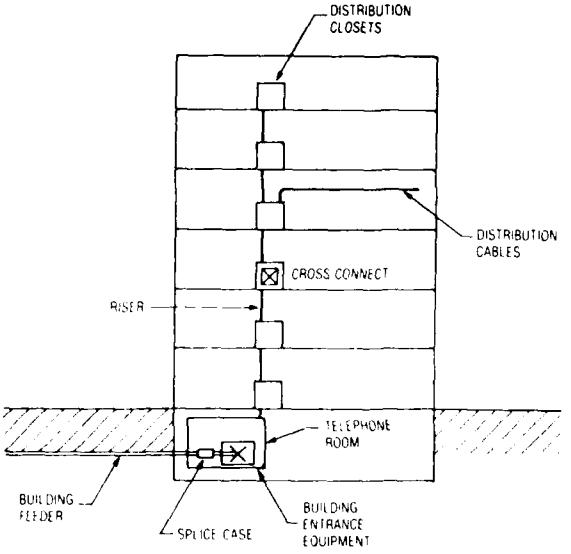


FIGURE 1. COMMERCIAL BUILDING DISTRIBUTION

Distribution cables, terminated in each closet, are run to the telephone equipment on the floor in one of several ways. (See Figure 2). Some buildings are designed with an under-floor distribution system, ducts that are set within the concrete slab of the building. This is a reasonable solution except that these ducts may already be crowded in critical crossing areas. Raised floors and suspended ceilings provide usable space, but are shared with computer or other equipment or building service cables and conduits and place additional requirements on cable sheath materials because these spaces are generally used as return air plenums for the building ventilation system.

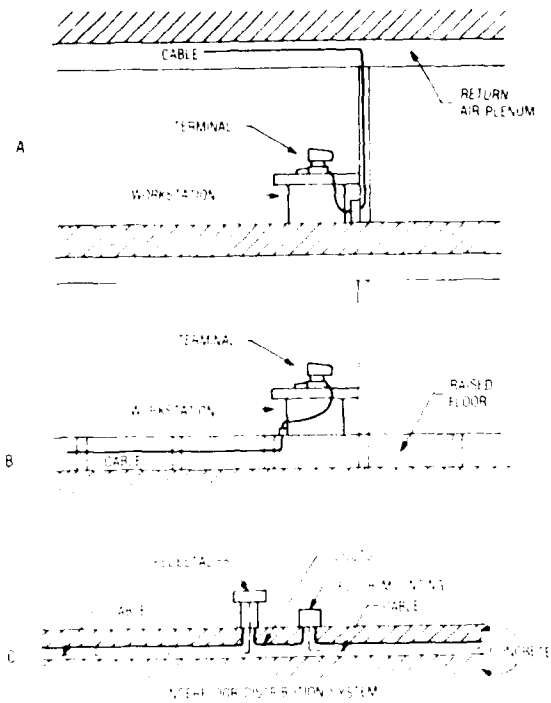


FIGURE 2. CABLE DISTRIBUTION METHODS

Finally, record keeping is done by labeling the terminals or marking the backboards at each successive fan-out point in the building and is therefore dependent on the craftsperson for accuracy.

In summary, the extensive copper telephone plant that exists in commercial buildings today heavily taxes the allocated real estate, exists in places that may not be well suited for apparatus and equipment that may be environmentally sensitive, locally powered and requires ventilation and protection from local hazards. And, of course, it has been deployed without consideration for the fiber optic network that we would now like to introduce.

Experimental Network

The Bellcore Fibernet is an interlocation fiber optic network employing both single mode and multimode technology to provide a research test bed for fiber network deployment, optical transmission and systems and services experiments. Sixteen single mode fibers connect two corporate locations, a distance of about 20 kilometers, and some 500 fiber drops have been deployed in offices and laboratories.

A major benefit has been the experience gained on the deployment of fiber optic networks in commercial buildings including installation methods, available apparatus, and the training of craft personnel in the handling and termination of optical fibers.

The design and implementation strategy for this network differs in several ways from other early fiber network deployments. Typical installations have been based on available apparatus and cable assembled in the most cost effective way to meet a service availability deadline. Although this makes good business sense right now, it does not address the most cost effective way to deploy fiber networks long term given the existence of all the necessary technology, apparatus and expertise. By taking this approach, attention could be brought to the missing elements and, hopefully, stimulate their development before they are needed by the operating telephone companies.

As an example, most if not all, current fiber deployments use either factory pre-terminated cables or factory connectorized pigtails spliced to cable ends in the field. Clearly, this is not optimum from a network provider's point of view. Factory pre-terminated cables cause extra pre-engineering of run lengths and inevitably result in the storage of coils of excess cable at termination points (Figure 3) creating significant housekeeping problems and are less rugged and difficult to pull into building raceways because of the bundled terminations at each end. Factory connectorized pigtails carry the combined cost of connectorization and splicing on a per-fiber basis and require extra splice organizers. The long range view is to deploy building fiber cable at the site from large reels, cut to length as installed and apply a low cost, quick splice, connector or connecting block as required, similar to the way copper cables are handled today.

The experimental intra-building network is a composite of both single mode and multimode technology to meet the needs of the user community. Several different vendors' cables and connectors were used to obtain experience with as large a cross-section of hardware as possible. Apparatus choices were severely limited or nonexistent particularly for large and small crossconnect panels and user interfaces. Some wall mounted

network access ports were fabricated in house (Figure 4). In fact, in the early planning, even plenum rated fiber cables were not available although there are several sources now.

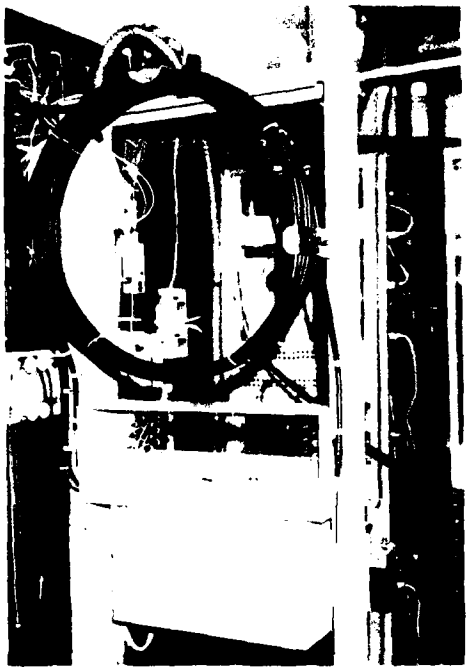


FIGURE 3. Excess Cable Storage Results From The Use of Pre-Terminated Cable

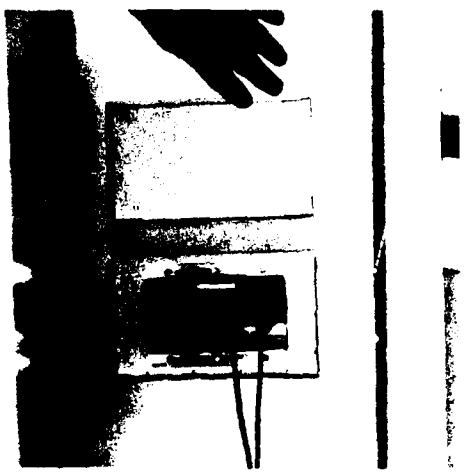


FIGURE 4. Fiber Network User Access Port

In this experimental network, offices and laboratories are connected by either single or duplex fiber cables to telephone (fiber) closets on each floor. These cables are crossconnected to riser cables as shown in figure 5 that connect all closets to a main distribution frame in the basement. Cables from the outside world also appear on this frame and cross connections can be made in any combination. Maximum flexibility was provided in this network due to its experimental nature by the use of connectorized jumpers in both the closet and the basement although it is anticipated that splices will be used to create "home run" fibers from the user interface to the location of the multiplexing electronics. Although re-arrangability is important this close to the customer end, it is expected that one higher loss crossconnect facility per building is sufficient. User access to the network is through a wall mounted outlet where an optical equipment cord can be connected.

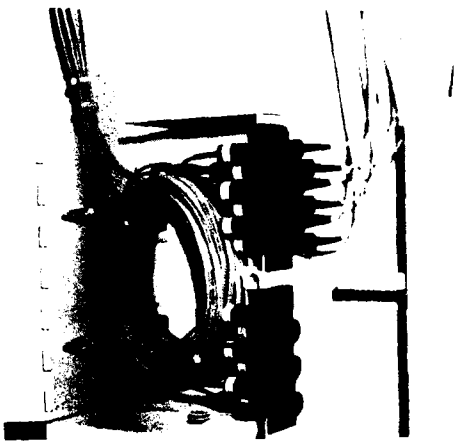


FIGURE 5. Optical Fiber Interconnection Hardware

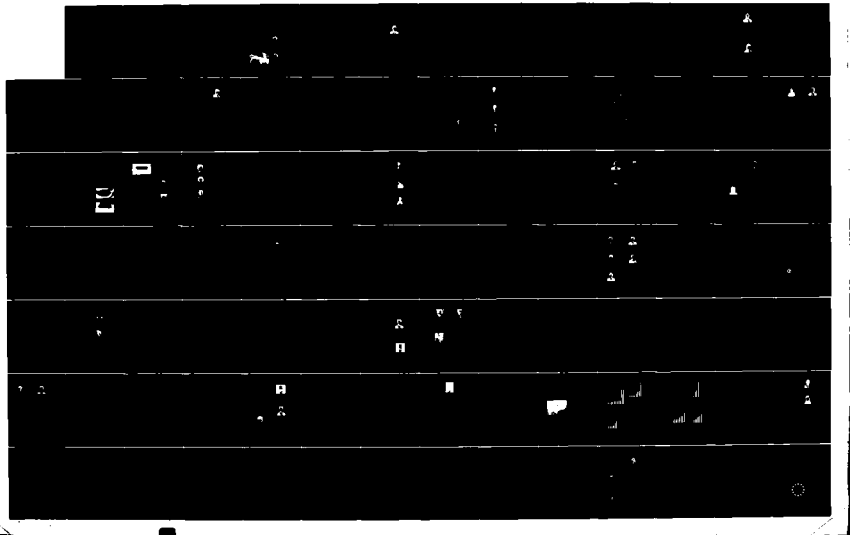
Experimental fiber based equipment in any office or laboratory can be connected to any other location within or outside the building by appropriate placement of fiber jumpers in the closet and/or basement interconnection [illegible]. Examples of interoffice, intrabuilding and interlocation network configurations [illegible] at this time.

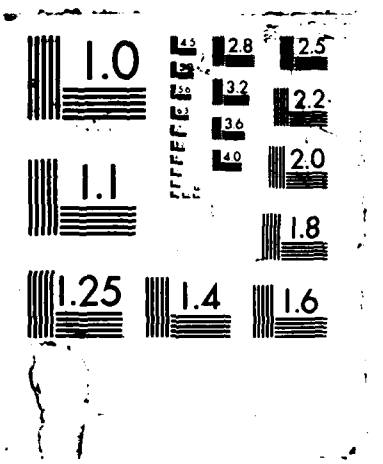
Installation Considerations

Fiber network deployment [illegible] by fiber cable [illegible] raceways, conduits [illegible] connectorization [illegible]. The mounting [illegible] and [illegible] straightness [illegible] apply [illegible] Fiber [illegible]

AD-A189 610 PROCEEDINGS OF THE INTERNATIONAL WIRE AND CABLE SYMPOSIUM (36TH) HELD IN..(U) ARMY COMMUNICATIONS-ELECTRONICS COMMAND FORT MONMOUTH NJ 3/9

UNCLASSIFIED 19 NOV 87 F/G 9/1 NL




1.0
1.1
1.25
1.4
1.6
1.8
2.0
2.2
2.5
2.8
3.2
3.6
4.0
4.5
5.0
5.6
6.3
7.1
8.0
9.0
10.0
11.2
12.5
14.0
16.0
18.0
20.0
22.4
25.0
28.0
32.0
36.0
40.0
45.0
50.0
56.0
63.0
71.0
80.0
90.0
100.0
112.0
125.0
140.0
160.0
180.0
200.0
224.0
250.0
280.0
320.0
360.0
400.0
450.0
500.0
560.0
630.0
710.0
800.0
900.0
1000.0
1120.0
1250.0
1400.0
1600.0
1800.0
2000.0
2240.0
2500.0
2800.0
3200.0
3600.0
4000.0
4500.0
5000.0
5600.0
6300.0
7100.0
8000.0
9000.0
10000.0
11200.0
12500.0
14000.0
16000.0
18000.0
20000.0
22400.0
25000.0
28000.0
32000.0
36000.0
40000.0
45000.0
50000.0
56000.0
63000.0
71000.0
80000.0
90000.0
100000.0
112000.0
125000.0
140000.0
160000.0
180000.0
200000.0
224000.0
250000.0
280000.0
320000.0
360000.0
400000.0
450000.0
500000.0
560000.0
630000.0
710000.0
800000.0
900000.0
1000000.0
1120000.0
1250000.0
1400000.0
1600000.0
1800000.0
2000000.0
2240000.0
2500000.0
2800000.0
3200000.0
3600000.0
4000000.0
4500000.0
5000000.0
5600000.0
6300000.0
7100000.0
8000000.0
9000000.0
10000000.0
11200000.0
12500000.0
14000000.0
16000000.0
18000000.0
20000000.0
22400000.0
25000000.0
28000000.0
32000000.0
36000000.0
40000000.0
45000000.0
50000000.0
56000000.0
63000000.0
71000000.0
80000000.0
90000000.0
100000000.0
112000000.0
125000000.0
140000000.0
160000000.0
180000000.0
200000000.0
224000000.0
250000000.0
280000000.0
320000000.0
360000000.0
400000000.0
450000000.0
500000000.0
560000000.0
630000000.0
710000000.0
800000000.0
900000000.0
1000000000.0
1120000000.0
1250000000.0
1400000000.0
1600000000.0
1800000000.0
2000000000.0
2240000000.0
2500000000.0
2800000000.0
3200000000.0
3600000000.0
4000000000.0
4500000000.0
5000000000.0
5600000000.0
6300000000.0
7100000000.0
8000000000.0
9000000000.0
10000000000.0
11200000000.0
12500000000.0
14000000000.0
16000000000.0
18000000000.0
20000000000.0
22400000000.0
25000000000.0
28000000000.0
32000000000.0
36000000000.0
40000000000.0
45000000000.0
50000000000.0
56000000000.0
63000000000.0
71000000000.0
80000000000.0
90000000000.0
100000000000.0
112000000000.0
125000000000.0
140000000000.0
160000000000.0
180000000000.0
200000000000.0
224000000000.0
250000000000.0
280000000000.0
320000000000.0
360000000000.0
400000000000.0
450000000000.0
500000000000.0
560000000000.0
630000000000.0
710000000000.0
800000000000.0
900000000000.0
1000000000000.0
1120000000000.0
1250000000000.0
1400000000000.0
1600000000000.0
1800000000000.0
2000000000000.0
2240000000000.0
2500000000000.0
2800000000000.0
3200000000000.0
3600000000000.0
4000000000000.0
4500000000000.0
5000000000000.0
5600000000000.0
6300000000000.0
7100000000000.0
8000000000000.0
9000000000000.0
10000000000000.0
11200000000000.0
12500000000000.0
14000000000000.0
16000000000000.0
18000000000000.0
20000000000000.0
22400000000000.0
25000000000000.0
28000000000000.0
32000000000000.0
36000000000000.0
40000000000000.0
45000000000000.0
50000000000000.0
56000000000000.0
63000000000000.0
71000000000000.0
80000000000000.0
90000000000000.0
100000000000000.0
112000000000000.0
125000000000000.0
140000000000000.0
160000000000000.0
180000000000000.0
200000000000000.0
224000000000000.0
250000000000000.0
280000000000000.0
320000000000000.0
360000000000000.0
400000000000000.0
450000000000000.0
500000000000000.0
560000000000000.0
630000000000000.0
710000000000000.0
800000000000000.0
900000000000000.0
1000000000000000.0
1120000000000000.0
1250000000000000.0
1400000000000000.0
1600000000000000.0
1800000000000000.0
2000000000000000.0
2240000000000000.0
2500000000000000.0
2800000000000000.0
3200000000000000.0
3600000000000000.0
4000000000000000.0
4500000000000000.0
5000000000000000.0
5600000000000000.0
6300000000000000.0
7100000000000000.0
8000000000000000.0
9000000000000000.0
10000000000000000.0
11200000000000000.0
12500000000000000.0
14000000000000000.0
16000000000000000.0
18000000000000000.0
20000000000000000.0
22400000000000000.0
25000000000000000.0
28000000000000000.0
32000000000000000.0
36000000000000000.0
40000000000000000.0
45000000000000000.0
50000000000000000.0
56000000000000000.0
63000000000000000.0
71000000000000000.0
80000000000000000.0
90000000000000000.0
100000000000000000.0
112000000000000000.0
125000000000000000.0
140000000000000000.0
160000000000000000.0
180000000000000000.0
200000000000000000.0
224000000000000000.0
250000000000000000.0
280000000000000000.0
320000000000000000.0
360000000000000000.0
400000000000000000.0
450000000000000000.0
500000000000000000.0
560000000000000000.0
630000000000000000.0
710000000000000000.0
800000000000000000.0
900000000000000000.0
1000000000000000000.0
1120000000000000000.0
1250000000000000000.0
1400000000000000000.0
1600000000000000000.0
1800000000000000000.0
2000000000000000000.0
2240000000000000000.0
2500000000000000000.0
2800000000000000000.0
3200000000000000000.0
3600000000000000000.0
4000000000000000000.0
4500000000000000000.0
5000000000000000000.0
5600000000000000000.0
6300000000000000000.0
7100000000000000000.0
8000000000000000000.0
9000000000000000000.0
10000000000000000000.0
11200000000000000000.0
12500000000000000000.0
14000000000000000000.0
16000000000000000000.0
18000000000000000000.0
20000000000000000000.0
22400000000000000000.0
25000000000000000000.0
28000000000000000000.0
32000000000000000000.0
36000000000000000000.0
40000000000000000000.0
45000000000000000000.0
50000000000000000000.0
56000000000000000000.0
63000000000000000000.0
71000000000000000000.0
80000000000000000000.0
90000000000000000000.0
100000000000000000000.0
112000000000000000000.0
125000000000000000000.0
140000000000000000000.0
160000000000000000000.0
180000000000000000000.0
200000000000000000000.0
224000000000000000000.0
250000000000000000000.0
280000000000000000000.0
320000000000000000000.0
360000000000000000000.0
400000000000000000000.0
450000000000000000000.0
500000000000000000000.0
560000000000000000000.0
630000000000000000000.0
710000000000000000000.0
800000000000000000000.0
900000000000000000000.0
1000000000000000000000.0
1120000000000000000000.0
1250000000000000000000.0
1400000000000000000000.0
1600000000000000000000.0
1800000000000000000000.0
2000000000000000000000.0
2240000000000000000000.0
2500000000000000000000.0
2800000000000000000000.0
3200000000000000000000.0
3600000000000000000000.0
4000000000000000000000.0
4500000000000000000000.0
5000000000000000000000.0
5600000000000000000000.0
6300000000000000000000.0
7100000000000000000000.0
8000000000000000000000.0
9000000000000000000000.0
10000000000000000000000.0
11200000000000000000000.0
12500000000000000000000.0
14000000000000000000000.0
16000000000000000000000.0
18000000000000000000000.0
20000000000000000000000.0
22400000000000000000000.0
25000000000000000000000.0
28000000000000000000000.0
32000000000000000000000.0
36000000000000000000000.0
40000000000000000000000.0
45000000000000000000000.0
50000000000000000000000.0
56000000000000000000000.0
63000000000000000000000.0
71000000000000000000000.0
80000000000000000000000.0
90000000000000000000000.0
100000000000000000000000.0
112000000000000000000000.0
125000000000000000000000.0
140000000000000000000000.0
160000000000000000000000.0
180000000000000000000000.0
200000000000000000000000.0
224000000000000000000000.0
250000000000000000000000.0
280000000000000000000000.0
320000000000000000000000.0
360000000000000000000000.0
400000000000000000000000.0
450000000000000000000000.0
500000000000000000000000.0
560000000000000000000000.0
630000000000000000000000.0
710000000000000000000000.0
800000000000000000000000.0
900000000000000000000000.0
1000000000000000000000000.0
1120000000000000000000000.0
1250000000000000000000000.0
1400000000000000000000000.0
1600000000000000000000000.0
1800000000000000000000000.0
2000000000000000000000000.0
2240000000000000000000000.0
2500000000000000000000000.0
2800000000000000000000000.0
3200000000000000000000000.0
3600000000000000000000000.0
4000000000000000000000000.0
4500000000000000000000000.0
5000000000000000000000000.0
5600000000000000000000000.0
6300000000000000000000000.0
7100000000000000000000000.0
8000000000000000000000000.0
9000000000000000000000000.0
10000000000000000000000000.0
11200000000000000000000000.0
12500000000000000000000000.0
14000000000000000000000000.0
16000000000000000000000000.0
18000000000000000000000000.0
20000000000000000000000000.0
22400000000000000000000000.0
25000000000000000000000000.0
28000000000000000000000000.0
32000000000000000000000000.0
36000000000000000000000000.0
40000000000000000000000000.0
45000000000000000000000000.0
50000000000000000000000000.0
56000000000000000000000000.0
63000000000000000000000000.0
71000000000000000000000000.0
80000000000000000000000000.0
90000000000000000000000000.0
100000000000000000000000000.0
112000000000000000000000000.0
125000000000000000000000000.0
140000000000000000000000000.0
160000000000000000000000000.0
180000000000000000000000000.0
200000000000000000000000000.0
224000000000000000000000000.0
250000000000000000000000000.0
280000000000000000000000000.0
320000000000000000000000000.0
360000000000000000000000000.0
400000000000000000000000000.0
450000000000000000000000000.0
500000000000000000000000000.0
560000000000000000000000000.0
630000000000000000000000000.0
710000000000000000000000000.0
800000000000000000000000000.0
900000000000000000000000000.0
1000000000000000000000000000.0
1120000000000000000000000000.0
1250000000000000000000000000.0
1400000000000000000000000000.0
1600000000000000000000000000.0
1800000000000000000000000000.0
2000000000000000000000000000.0
2240000000000000000000000000.0
2500000000000000000000000000.0
2800000000000000000000000000.0
3200000000000000000000000000.0
3600000000000000000000000000.0
4000000000000000000000000000.0
4500000000000000000000000000.0
5000000000000000000000000000.0
5600000000000000000000000000.0
6300000000000000000000000000.0
7100000000000000000000000000.0
8000000000000000000000000000.0
9000000000000000000000000000.0
10000000000000000000000000000.0
11200000000000000000000000000.0
12500000000000000000000000000.0
14000000000000000000000000000.0
16000000000000000000000000000.0
18000000000000000000000000000.0
20000000000000000000000000000.0
22400000000000000000000000000.0
25000000000000000000000000000.0
28000000000000000000000000000.0
32000000000000000000000000000.0
36000000000000000000000000000.0
40000000000000000000000000000.0
45000000000000000000000000000.0
50000000000000000000000000000.0
56000000000000000000000000000.0
63000000000000000000000000000.0
71000000000000000000000000000.0
80000000000000000000000000000.0
90000000000000000000000000000.0
100000000000000000000000000000.0
112000000000000000000000000000.0
125000000000000000000000000000.0
140000000000000000000000000000.0
160000000000000000000000000000.0
180000000000000000000000000000.0
200000000000000000000000000000.0
224000000000000000000000000000.0
250000000000000000000000000000.0
280000000000000000000000000000.0
320000000000000000000000000000.0
360000000000000000000000000000.0
400000000000000000000000000000.0
450000000000000000000000000000.0
500000000000000000000000000000.0
560000000000000000000000000000.0
630000000000000000000000000000.0
710000000000000000000000000000.0
800000000000000000000000000000.0
900000000000000000000000000000.0
1000000000000000000000000000000.0
1120000000000000000000000000000.0
1250000000000000000000000000000.0
1400000000000000000000000000000.0
1600000000000000000000000000000.0
1800000000000000000000000000000.0
2000000000000000000000000000000.0
2240000000000000000000000000000.0
2500000000000000000000000000000.0
2800000000000000000000000000000.0
3200000000000000000000000000000.0
3600000000000000000000000000000.0
4000000000000000000000000000000.0
4500000000000000000000000000000.0
5000000000000000000000000000000.0
5600000000000000000000000000000.0
6300000000000000000000000000000.0
7100000000000000000000000000000.0
8000000000000000000000000000000.0
9000000000000000000000000000000.0
10000000000000000000000000000000.0
11200000000000000000000000000000.0
12500000000000000000000000000000.0
14000000000000000000000000000000.0
16000000000000000000000000000000.0
18000000000000000000000000000000.0
20000000000000000000000000000000.0
22400000000000000000000000000000.0
25000000000000000000000000000000.0
28000000000000000000000000000000.0
32000000000000000000000000000000.0
36000000000000000000000000000000.0
40000000000000000000000000000000.0
45000000000000000000000000000000.0
50000000000000000000000000000000.0
56000000000000000000000000000000.0
63000000000000000000000000000000.0
71000000000000000000000000000000.0
80000000000000000000000000000000.0
90000000000000000000000000000000.0
100000000000000000000000000000000.0
112000000000000000000000000000000.0
125000000000000000000000000000000.0
140000000000000000000000000000000.0
160000000000000000000000000000000.0
180000000000000000000000000000000.0
200000000000000000000000000000000.0
224000000000000000000000000000000.0
250000000000000000000000000000000.0
280000000000000000000000000000000.0
320000000000000000000000000000000.0
360000000000000000000000000000000.0
400000000000000000000000000000000.0
450000000000000000000000000000000.0
500000000000000000000000000000000.0
560000000000000000000000000000000.0
630000000000000000000000000000000.0
710000000000000000000000000000000.0
800000000000000000000000000000000.0
900000000000000000000000000000000.0
1000000000000000000000000000000000.0
1120000000000000000000000000000000.0
1250000000000000000000000000000000.0
1400000000000000000000000000000000.0
1600000000000000000000000000000000.0
1800000000000000000000000000000000.0
2000000000000000000000000000000000.0
2240000000000000000000000000000000.0
2500000000000000000000000000000000.0
2800000000000000000000000000000000.0
3200000000000000000000000000000000.0
3600000000000000000000000000000000.0
4000000000000000000000000000000000.0
4500000000000000000000000000000000.0
5000000000000000000000000000000000.0
5600000000000000000000000000000000.0
6300000000000000000000000000000000.0
7100000000000000000000000000000000.0
8000000000000000000000000000000000.0
9000000000000000000000000000000000.0
10000000000000000000000000000000000.0
11200000000000000000000000000000000.0
12500000000000000000000000000000000.0
14000000000000000000000000000000000.0
16000000000000000000000000000000000.0
18000000000000000000000000000000000.0
20000000000000000000000000000000000.0
22400000000000000000000000000000000.0
25000000000000000000000000000000000.0
28000000000000000000000000000000000.0
32000000000000000000000000000000000.0
36000000000000000000000000000000000.0
40000000000000000000000000000000000.0
45000000000000000000000000000000000.0
50000000000000000000000000000000000.0
56000000000000000000000000000000000.0
63000000000000000000000000000000000.0
71000000000000000000000000000000000.0
80000000000000000000000000000000000.0
90000000000000000000000000000000000.0
100000000000000000000000000000000000.0
112000000000000000000000000000000000.0
125000000000000000000000000000000000.0
140000000000000000000000000000000000.0
160000000000000000000000000000000000.0
180000000000000000000000000000000000.0
200000000000000000000000000000000000.0
224000000000000000000000000000000000.0
250000000000000000000000000000000000.0
280000000000000000000000000000000000.0
320000000000000000000000000000000000.0
360000000000000000000000000000000000.0
400000000000000000000000000000000000.0
450000000000000000000000000000000000.0
500000000000000000000000000000000000.0
560000000000000000000000000000000000.0
630000000000000000000000000000000000.0
710000000000000000000000000000000000.0
800000000000000000000000000000000000.0
900000000000000000000000000000000000.0
1000000000000000000000000000000000000.0
1120000000000000000000000000000000000.0
1250000000000000000000000000000000000.0
1400000000000000000000000000000000000.0
1600000000000000000000000000000000000.0
1800000000000000000000000000000000000.0
2000000000000000000000000000000000000.0
2240000000000000000000000000000000000.0
2500000000000000000000000000000000000.0
2800000000000000000000000000000000000.0
3200000000000000000000000000000000000.0
3600000000000000000000000000000000000.0
4000000000000000000000000000000000000.0
4500000000000000000000000000000000000.0
5000000000000000000000000000000000000.0
5600000000000000000000000000000000000.0
6300000000000000000000000000000000000.0
7100000000000000000000000000000000000.0
8000000000000000000000000000000000000.0
9000000000000000000000000000000000000.0
10000000000000000000000000000000000000.0
11200000000000000000000000000000000000.0
12500000000000000000000000000000000000.0
14000000000000000000000000000000000000.0
16000000000000000000000000000000000000.0
18000000000000000000000000000000000000.0
20000000000000000000000000000000000000.0
22400000000000000000000000000000000000.0
25000000000000000000000000000000000000.0
28000000000000000000000000000000000000.0
32000000000000000000000000000000000000.0
36000000000000000000000000000000000000.0
40000000000000000000000000000000000000.0
45000000000000000000000000000000000000.0
50000000000000000000000000000000000000.0
56000000000000000000000000000000000000.0
63000000000000000000000000000000000000.0
71000000000000000000000000000000000000.0
80000000000000000000000000000000000000.0
90000000000000000000000000000000000000.0
100000000000000000000000000000000000000.0
112000000000000000000000000000000000000.0
125000000000000000000000000000000000000.0
140000000000000000000000000000000000000.0
160000000000000000000000000000000000000.0
180000000000000000000000000000000000000.0
200000000000000000000000000000000000000.0
224000000000000000000000000000000000000.0
250000000000000000000000000000000000000.0
280000000000000000000000000000000000000.0
320000000000000000000000000000000000000.0
360000000000000000000000000000000000000.0
400000000000000000000000000000000000000.0
450000000000000000000000000000000000000.0
500000000000000000000000000000000000000.0
560000000000000000000000000000000000000.0
630000000000000000000000000000000000000.0
710000000000000000000000000000000000000.0
800000000000000000000000000000000000000.0
900000000000000000000000000000000000000.0
1000000000000000000000000000000000000000.0
1120000000000000000000000000000000000000.0
1250000000000000000000000000000000000000.0
1400000000000000000000000000000000000000.0
1600000000000000000000000000000000000000.0
1800000000000000000000000000000000000000.0
2000000000000000000000000000000000000000.0
2240000000000000000000000000000000000000.0
2500000000000000000000000000000000000000.0
2800000000000000000000000000000000000000.0
3200000000000000000000000000000000000000.0
3600000000000000000000000000000000000000.0
4000000000000000000000000000000000000000.0
4500000000000000000000000000000000000000.0
5000000000000000000000000000000000000000.0
5600000000000000000000000000000000000000.0
6300000000000000000000000000000000000000.0
7100000000000000000000000000000000000000.0
8000000000000000000000000000000000000000.0
9000000000000000000000000000000000000000.0
10000000000000000000000000000000000000000.0
11200000000000000000000000000000000000000.0
12500000000000000000000000000000000000000.0
14000000000000000000000000000000000000000.0
16000000000000000000000000000000000000000.0
18000000000000000000000000000000000000000.0
20000000000000000000000000000000000000000.0
22400000000000000000000000000000000000000.0
25000000000000000000000000000000000000000.0
28000000000000000000000000000000000000000.0
32000000000000000000000000000000000000000.0
36000000000000000000000000000000000000000.0
40000000000000000000000000000000000000000.0
45000000000000000000000000000000000000000.0
50000000000000000000000000000000000000000.0
56000000000000000000000000000000000000000.0
63000000000000000000000000000000000000000.0
71000000000000000000000000000000000000000.0
80000000000000000000000000000000000000000.0
90000000000000000000000000000000000000000.0
100000000000000000000000000000000000000000.0
112000000000000000000000000000000000000000.0
125000000000000000000000000000000000000000.0
140000000000000000000000000000000000000000.0
160000000000000000000000000000000000000000.0
180000000000000000000000000000000000000000.0
200000000000000000000000000000000000000000.0
224000000000000000000000000000000000000000.0
250000000000000000000000000000000000000000.0
280000000000000000000000000000000000000000.0
320000000000000000000000000000000000000000.0
360000000000000000000000000000000000000000.0
400000000000000000000000000000000000000000.0
450000000000000000000000000000000000000000.0
500000000000000000000000000000000000000000.0
560000000000000000000000000000000000000000.0
630000000000000000000000000000000000000000.0
710000000000000000000000000000000000000000.0
800000000000000000000000000000000000000000.0
900000000000000000000000000000000000000000.0
1000000000000000000000000000000000000000000.0
1120000000000000000000000000000000000000000.0
1250000000000000000000000000000000000000000.0
1400000000000000000000000000000000000000000.0
1600000000000000000000000000000000000000000.0
1800000000000000000000000000000000000000000.0
2000000000000000000000000000000000000000000.0
2240000000000000000000000000000000000000000.0
2500000000000000000000000000000000000000000.0
2800000000000000000000000000000000000000000.0
3200000000000000000000000000000000000000000.0
3600000000000000000000000000000000000000000.0
4000000000000000000000000000000000000000000.0
4500000000000000000000000000000000000000000.0
5000000000000000000000000000000000000000000.0
5600000000000000000000000000000000000000000.0
6300000000000000000000000000000000000000000.0
7100000000000000000000000000000000000000000.0
8000000000000000000000000000000000000000000.0
9000000000000000000000000000000000000000000.0
10000000000000000000000000000000000000000000.0
11200000000000000000000000000000000000000000.0
12500000000000000000000000000000000000000000.0
14000000000000000000000000000000000000000000.0
16000000000000000000000000000000000000000000.0
18000000000000000000000000000000000000000000.0
20000000000000000000000000000000000000000000.0
22400000000000000000000000000000000000000000.0
25000000000000000000000000000000000000000000.0
28000000000000000000000000000000000000000000.0
32000000000000000000000000000000000000000000.0
36000000000000000000000000000000000000000000.0
40000000000000000000000000000000000000000000.0
45000000000000000000000000000000000000000000.0
50000000000000000000000000000000000000000000.0
56000000000000000000000000000000000000000000.0
63000000000000000000000000000000000000000000.0
71000000000000000000000000000000000000000000.0
80000000000000000000000000000000000000000000.0
90000000000000000000000000000000000000000000.0
100000000000000000000000000000000000000000000.0
112000000000000000000000000000000000000000000.0
125000000000000000000000000000000000000000000.0
140000000000000000000000000000000000000000000.0
160000000000000000000000000000000000000000000.0
180000000000000000000000000000000000000000000.0
200000000000000000000000000000000000000000000.0
224000000000000000000000000000000000000000000.0
250000000000000000000000000000000000000000000.0
280000000000000000000000000000000000000000000.0
320000000000000000000000000000000000000000000.0
360000000000000000000000000000000000000000000.0
400000000000000000000000000000000000000000000.0
450000000000000000000000000000000000000000000.0
500000000000000000000000000000000000000000000.0
560000000000000000000000000000000000000000000.0
630000000000000000000000000000000000000000000.0
710000000000000000000000000000000000000000000.0
800000000000000000000000000000000000000000000.0
900000000000000000000000000000000000000000000.0
1000000000000000000000000000000000000000000000.0
1120000000000000000000000000000000000000000000.0
1250000000000000000000000000000000000000000000.0
1400000000000000000000000000000000000000000000.0
1600000000000000000000000000000000000000000000.0
1800000000000000000000000000000000000000000000.0
2000000000000000000000000000000000000000000000.0
2240000000000000000000000000000000000000000000.0
2500000000000000000000000000000000000000000000.0
2800000000000000000000000000000000000000000000.0
3200000000000000000000000000000000000000000000.0
3600000000000000000000000000000000000000000000.0
4000000000000000000000000000000000000000000000.0
4500000000000000000000000000000000000000000000.0
5000000000000000000000000000000000000000000000.0
5600000000000000000000000000000000000000000000.0
6300000000000000000000000000000000000000000000.0
7100000000000000000000000000000000000000000000.0
8000000000000000000000000000000000000000000000.0
9000000000000000000000000000000000000000000000.0
10000000000000000000000000000000000000000000000.0
11200000000000000000000000000000000000000000000.0
12500000000000000000000000000000000000000000000.0
14000000000000000000000000000000000000000000000.0
16000000000000000000000000000000000000000000000.0
18000000000000000000000000000000000000000000000.0
20000000000000000000000000000000000000000000000.0
22400000000000000000000000000000000000000000000.0
25000000000000000000000000000000000000000000000.0
28000000000000000000000000000000000000000000000.0
32000000000000000000000000000000000000000000000.0
36000000000000000000000000000000000000000000000.0
40000000000000000000000000000000000000000000000.0
45000000000000000000000000000000000000000000000.0
50000000000000000000000000000000000000000000000.0
56000000000000000000000000000000000000000000000.0
63000000000000000000000000000000000000000000000.0
71000000000000000000000000000000000000000000000.0
80000000000000000000000000000000000000000000000.0
90000000000000000000000000000000000000000000000.0
100000000000000000000000000000000000000000000000.0
112000000000000000000000000000000000000000000000.0
125000000000000000000000000000000000000000000000.0
140000000000000000000000000000000000000000000000.0
160000000000000000000000000000000000000000000000.0
180000000000000000000000000000000000000000000000.0
200000000000000000000000000000000000000000000000.0
224000000000000000000000000000000000000000000000.0
250000000000000000000000000000000000000000000000.0
280000000000000000000000000000000000000000000000.0
320000000000000000000000000000000000000000000000.0
360000000000000000000000000000000000000000000000.0
400000000000000000000000000000000000000000000000.0
450000000000000000000000000000000000000000000000.0
500000000000000000000000000000000000000000000000.0
560000000000000000000000000000000000000000000000.0
630000000000000000000000000000000000000000000000.0
710000000000000000000000000000000000000000000000.0
800000000000000000000000000000000000000000000000.0
900000000000000000000000000000000000000000000000.0
1000000000000000000000000000000000000000000000000.0
1120000000000000000000000000000000000000000000000.0
1250000000000000000000000000000000000000000000000.0
1400000000000000000000000000000000000000000000000.0
1600000000000000000000000000000000000000000000000.0
1800000000000000000000000000000000000000000000000.0
2000000000000000000000000000000000000000000000000.0
2240000000000000000000000000000000000000000000000.0
2500000000000000000000000000000000000000000000000.0
2800000000000000000000000000000000000000000000000.0
3200000000000000000000000000000000000000000000000.0
3600000000000000000000000000000000000000000000000.0
4000000000000000000000000000000000000000000000000.0
4500000000000000000000000000000000000000000000000.0
5000000000000000000000000000000000000000000000000.0
5600000000000000000000000000000000000000000000000.0
6300000000000000000000000000000000000000000000000.0
7100000000000000000000000000000000000000000000000.0
8000000000000000000000000000000000000000000000000.0
9000000000000000000000000000000000000000000000000.0
10000000000000000000000000000000000000000000000000.0
11200000000000000000000000000000000000000000000000.0
12500000000000000000000000000000000000000000000000.0
14000000000000000000000000000000000000000000000000.0
16000000000000000000000000000000000000000000000000.0
18000000000000000000000000000000000000000000000000.0
20000000000000000000000000000000000000000000000000.0
22400000000000000000000000000000000000000000000000.0
25000000000000000000000000000000000000000000000000.0
28000000000000000000000000000000000000000000000000.0
32000000000000000000000000000000000000000000000000.0
36000000000000000000000000000000000000000000000000.0
40000000000000000000000000000000000000000000000000.0
45000000000000000000000000000000000000000000000000.0
50000000000000000000000000000000000000000000000000.0
56000000000000000000000000000000000000000000000000.0
63000000000000000000000000000000000000000000000000.0
71000000000000000000000000000000000000000000000000.0
80000000000000000000000000000000000000000000000000.0
90000000000000000000000000000000000000000000000000.0
100000000000000000000000000000000000000000000000000.0
112000000000000000000000000000000000000000000000000.0
125000000000000000000000000000000000000000000000000.0
140000000000000000000000000000000000000000000000000.0
160000000000000000000000000000000000000000000000000.0
180000000000000000000000000000000000000000000000000.0
200000000000000000000000000000000000000000000000000.0
224000000000000000000000000000000000000000000000000.0
250000000000000000000000000000000000000000000000000.0
280000000000000000000000000000000000000000000000000.0
320000000000000000000000000000000000000000000000000.0
360000000000000000000000000000000000000000000000000.0
400000000000000000000000000000000000000000000000000.0
450000000000000000000000000000000000000000000000000.0
500000000000000000000000000000000000000000000000000.0
560000000000000000000000000000000000000000000000000.0
630000000000000000000000000000000000000000000000000.0
710000000000000000000000000000000000000000000000000.0
800000000000000000000000000000000000000000000000000.0
900000000000000000000000000000000000000000000000000.0
1000000000000000000000000000000000000000000000000000.0
1120000000000000000000000000000000000000000000000000.0
1250000000000000000000000000000000000000000000000000.0
1400000000000000000000000000000000000000000000000000.0
1600000000000000000000000000000000000000000000000000.0
1800000000000000000000000000000000000000000000000000.0
2000000000000000000000000000000000000000000000000000.0
2240000000000000000000000000000000000000000000000000.0
2500000000000000000000000000000000000000000000000000.0
2800000000000000000000000000000000000000000000000000.0
3200000000000000000000000000000000000000000000000000.0
3600000000000000000000000000000000000000000000000000.0
4000000000000000000000000000000000000000000000000000.0
4500000000000000000000000000000000000000000000000000.0
5000000000000000000000000000000000000000000000000000.0
5600000000000000000000000000000000000000000000000000.0
6300000000000000000000000000000000000000000000000000.0
7100000000000000000000000000000000000000000000000000.0
8000000000000000000000000000000000000000000000000000.0
9000000000000000000000000000000000000000000000000000.0
10000000000000000000000000000000000000000000000000000.0
11200000000000000000000000000000000000000000000000000.0
12500000000000000000000000000000000000000000000000000.0
14000000000000000000000000000000000000000000000000000.0
16000000000000000000000000000000000000000000000000000.0
18000000000000000000000000000000000000000000000000000.0
20000000000000000000000000000000000000000000000000000.0
22400000000000000000000000000000000000000000000000000.0
25000000000000000000000000000000000000000000000000000.0
28000000000000000000000000000000000000000000000000000.0
32000000000000000000000000000000000000000000000000000.0
36000000000000000000000000000000000000000000000000000.0
40000000000000000000000000000000000000000000000000000.0
45000000000000000000000000000000000000000000000000000.0
50000000000000000000000000000000000000000000000000000.0
56000000000000000000000000000000000000000000000000000.0
63000000000000000000000000000000000000000000000000000.0
71000000000000000000000000000000000000000000000000000.0
80000000000000000000000000000000000000000000000000000.0
90000000000000000000000000000000000000000000000000000.0
100000000000000000000000000000000000000000000000000000.0
112000000000000000000000000000000000000000000000000000.0
125000000000000000000000000000000000000000000000000000.0
140000000000000000000000000000000000000000000000000000.0
160000000000000000000000000000000000000000000000000000.0
180000000000000000000000000000000000000000000000000000.0
200000000000000000000000000000000000000000000000000000.0
224000000000000000000000000000000000000000000000000000.0
250000000000000000000000000000000000000000000000000000.0
280000000000000000000000000000000000000000000000000000.0
320000000000000000000000000000000000000000000000000000.0
360000000000000000000000000000000000000000000000000000.0
400000000000000000000000000000000000000000000000000000.0
450000000000000000000000000000000000000000000000000000.0
500000000000000000000000000000000000000000000000000000.0
560000000000000000000000000000000000000000000000000000.0
630000000000000000000000000000000000000000000000000000.0
710000000000000000000000000000000000000000000000000000.0
800000000000000000000000000000000000000000000000000000.0
900000000000000000000000000000000000000000000000000000.0
1000000000000000000000000000000000000000000000000000000.0
1120000000000000000000000000000000000000000000000000000.0
1250000000000000000000000000000000000000000000000000000.0
1400000000000000000000000000000000000000000000000000000.0
1600000000000000000000000000000000000000000000000000000.0
1800000000000000000000000000000000000000000000000000000.0
2000000000000000000000000000000000000000000000000000000.0
2240000000000000000000000000000000000000000000000000000.0
2500000000000000000000000000000000000000000000000000000.0
2800000000000000000000000000000000000000000000000000000.0
3200000000000000000000000000000000000000000000000000000.0
3600000000000000000000000000000000000000000000000000000.0
4000000000000000000000000000000000000000000000000000000.0
4500000000000000000000000000000000000000000000000000000.0
5000000000000000000000000000000000000000000000000000000.0
5600000000000000000000000000000000000000000000000000000.0
6300000000000000000000000000000000000000000000000000000.0
7100000000000000000000000000000000000000000000000000000.0
8000000000000000000000000000000000000000000000000000000.0
9000000000000000000000000000000000000000000000000000000.0
10000000000000000000000000000000000000000000000000000000.0
11200000000000000000000000000000000000000000000000000000.0
12500000000000000000000000000000000000000000000000000000.0
14000000000000000000000000000000000000000000000000000000.0
16000000000000000000000000000000000000000000000000000000.0
18000000000000000000000000000000000000000000000000000000.0
20000000000000000000000000000000000000000000000000000000.0
22400000000000000000000000000000000000000000000000000000.0
25000000000000000000000000000000000000000000000000000000.0
28000000000000000000000000000000000000000000000000000000.0
32000000000000000000000000000000000000000000000000000000.0
36000000000000000000000000000000000000000000000000000000.0
40000000000000000000000000000000000000000000000000000000.0
45000000000000000000000000000000000000000000000000000000.0
50000000000000000000000000000000000000000000000000000000.0
56000000000000000000000000000000000000000000000000000000.0
63000000000000000000000000000000000000000000000000000000.0
71000000000000000000000000000000000000000000000000000000.0
80000000000000000000000000000000000000000000000000000000.0
90000000000000000000000000000000000000000000000000000000.0
100000000000000000000000000000000000000000000000000000000.0
112000000000000000000000000000000000000000000000000000000.0
125000000000000000000000000000000000000000000000000000000.0
140000000000000000000000000000000000000000000000000000000.0
160000000000000000000000000000000000000000000000000000000.0
180000000000000000000000000000000000000000000000000000000.0
200000000000000000000000000000000000000000000000000000000.0
224000000000000000000000000000000000000000000000000000000.0
250000000000000000000000000000000000000000000000000000000.0
280000000000000000000000000000000000000000000000000000000.0
320000000000000000000000000000000000000000000000000000000.0
360000000000000000000000000000000000000000000000000000000.0
400000000000000000000000000000000000000000000000000000000.0
450000000000000000000000000000000000000000000000000000000.0
500000000000000000000000000000000000000000000000000000000.0
560000000000000000000000000000000000000000000000000000000.0
630000000000000000000000000000000000000000000000000000000.0
710000000000000000000000000000000000000000000000000000000.0
800000000000000000000000000000000000000000000000000000000.0
900000000000000000000000000000000000000000000000000000000.0
1000000000000000000000000000000000000000000000000000000000.0
1120000000000000000000000000000000000000000000000000000000.0
1250000000000000000000000000000000000000000000000000000000.0
1400000000000000000000000000000000000000000000000000000000.0
1600000000000000000000000000000000000000000000000000000000.0
1800000000000000000000000000000000000000000000000000000000.0
2000000000000000000000000000000000000000000000000000000000.0
2240000000000000000000000000000000000000000000000000000000.0
2500000000000000000000000000000000000000000000000000000000.0
2800000000000000000000000000000000000000000000000000000000.0
3200000000000000000000000000000000000000000000000000000000.0
3600000000000000000000000000000000000000000000000000000000.0
4000000000000000000000000000000000000000000000000000000000.0
4500000000000000000000000000000000000000000000000000000000.0
5000000000000000000000000000000000000000000000000000000000.0
5600000000000000000000000000000000000000000000000000000000.0
6300000000000000000000000000000000000000000000000000000000.0
7100000000000000000000000000000000000000000000000000000000.0
8000000000000000000000000000000000000000000000000000000000.0
9000000000000000000000000000000000000000000000000000000000.0
10000000000000000000000000000000000000000000000000000000000.0
11200000000000000000000000000000000000000000000000000000000.0
12500000000000000000000000000000000000000000000000000000000.0
14000000000000000000000000000000000000000000000000000000000.0
16000000000000000000000000000000000000000000000000000000000.0
18000000000000000000000000000000000000000000000000000000000.0
20000000000000000000000000000000000000000000000000000000000.0
22400000000000000000000000000000000000000000000000000000000.0
25000000000000000000000000000000000000000000000000000000000.0
28000000000000000000000000000000000000000000000000000000000.0
32000000000000000000000000000000000000000000000000000000000.0
36000000000000000000000000000000000000000000000000000000000.0
40000000000000000000000000000000000000000000000000000000000.0
45000000000000000000000000000000000000000000000000000000000.0
50000000000000000000000000000000000000000000000000000000000.0
56000000000000000000000000000000000000000000000000000000000.0
63000000000000000000000000000000000000000000000000000000000.0
71000000000000000000000000000000000000000000000000000000000.0
80000000000000000000000000000000000000000000000000000000000.0
90000000000000000000000000000000000000000000000000000000000.0
100000000000000000000000000000000000000000000000000000000000.0
112000000000000000000000000000000000000000000000000000000000.0
125000000000000000000000000000000000000000000000000000000000.0
140000000000000000000000000000000000000000000000000000000000.0
160000000000000000000000000000000000000000000000000000000000.0
180000000000000000000000000000000000000000000000000000000000.0
200000000000000000000000000000000000000000000000000000000000.0
224000000000000000000000000000000000000000000000000000000000.0
250000000000000000000000000000000000000000000000000000000000.

Installation of fiber from the users' receptacle to the fiber closet was done via the return air plenum using single and duplex fiber cables. Fiber drop-off points at offices and labs occurred at 10 or 20 foot intervals in the long corridors making large count cables impractical. Therefore, many small diameter, light and flexible cables were bundled and pulled into 2½" square electrical wireways with removable covers and knockouts available at drop-off points. This assembly met air plenum requirements although the fiber cables alone did not. Flexible conduit was used from the wireway to the user receptacle. This conduit not only continued the integrity of the air plenum design, but also protected the fiber in ceiling and wall areas, and provided control of bending radii along the run. Wireway sweeps were also necessary to control bend radii, particularly where they emerge in the closets. A total of 25 miles of building distribution fiber was deployed.

A major problem was encountered in pulling some of the cable designs through the wireway. The cable jacketing material must be selected to meet a number of requirements set by the cable vendor regarding fiber protection, strength and durability, fire and toxicity, cost and ease of manufacture. But the deployed cost of the cable, a telco concern, is also affected by other properties. The two most notable properties among the cables used were cable memory and surface friction.

Cable memory affects the installer's ability to dress many cables into manageable bundles without their springing back when released. This is important since damage and snagging can occur if the cables do not lay along the intended route, for example, in a rack above a suspended ceiling. Cable jacket friction against a wireway or rack can make it impossible to pull cables into place without copious amounts of lubricant and extra personnel. Some cables, in runs of 25 to 200 feet, not only required large amounts of lubricant (undesirable in buildings), but also required extra personnel, one at each end and one at each bend to coax it through. This makes installation very costly and time consuming and is an excellent example of the need for vendors to design cables with ease of installation in mind. Also, wireways and conduits are very costly. A more suitable building distribution cable might provide built-in durability and bend control so that no additional precaution is necessary.

Connectorization and Testing

Again, an assortment of available hardware was used to gain the broadest experience. Five different designs of single and multimode connectors from seven different vendors were used for a total of more than 1000 fibers terminated. All connectors were of the epoxy/polish construction (see figure 6) to minimize losses in this connector intensive network. As previously mentioned, field installable connectors are envisioned as the method of choice long term although all of the connectors we used were more easily applied at a lab bench. All of the connectors required some skill and a lot of practice to install as concluded after training and observing fourteen experienced craftsmen who had no previous fiber optics training. Special care was taken to follow each vendor's instructions precisely when applying their connector.

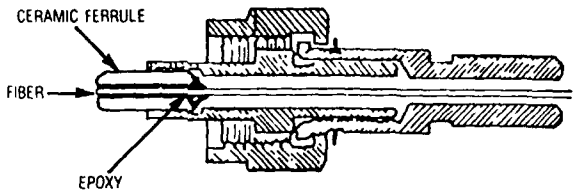


FIGURE 6. CROSS-SECTION OF TYPICAL FIBER OPTIC CONNECTOR

There are five basic steps in applying any of these connectors:

1. Strip the cable jacket and coating from the fiber.
2. Position the fiber within the connector.
3. Secure the fiber within the connector body.
4. Strain relieve the cable.
5. Polish the fiber end.

Several of these steps may lead to problems. Stripping the cable jacket mechanically may cause nicks or scratches on the surface of the glass fiber which may result in subsequent failure due to stress free aging or static fatigue and securing the fiber within the connector body using highly exothermic epoxies and heat guns may produce significant thermal stresses. More on these two later. Polishing the fiber end requires practice and seemed to require a "touch" that some craftsmen never developed during their training. Positioning the fiber within the connector body is not a problem assuming reasonable dexterity and eyesight and strain relieving the cable generally requires nothing more than the use of a properly set crimping tool.

A significant number of badly applied connectors were discovered using a white light source at the far end to back light the fiber and examining the polished connector end with a 400X scope. Even though initial measured losses were within the manufacturer's specs, this back light technique revealed cracks in the glass fibers within the region of the precision ferrule. This could be disastrous in a telco installation where connectors test good on installation, but fail sometime later due to crack propagation. The

accompanying diagram (Figure 7) shows how a sample lot of 48 connectors degraded over time. Also, some connectors remained dark when back lit. Micro-sectioning revealed large cracks in the glass in the region of accumulated epoxy at the back end of the precision ferrule.

Two conditions may have caused or contributed to these fiber cracks. First, as previously mentioned, mechanical stripping tools use precisely aligned and sharp blades to separate a length of coating and slide it off the fiber. Normal wear or misuse of the tool may have caused one or both blades to contact the glass causing a surface flaw. Second, the selection of a highly exothermic epoxy and/or the use of a hand held heat gun may have caused significant thermal stress during cure and residual "locked-in" stress post cure. The magnitude of these stresses are affected by thermal expansion coefficient, epoxy curing temperature, shear modules and thickness between the fiber and ferrule, and analysis has shown that stresses high enough to cause short term failure can occur. Also, the temperature to which a connector is heated using a heat gun is heavily dependent on the distance it is held from the nozzle. A quick lab measurement showed a range from 180°C to 125°C corresponded to a distance of 4" to 6". Better control of cure temperature was achieved using an oven. The use of a slow curing room temperature epoxy greatly improved connector yield giving good support to this theory but would clearly be less convenient for field installations.

On average, field connectorization takes 20 minutes per fiber assuming a work station is set up and many connectors are to be done for both single and multimode regardless of vendor. The combined cost of these connectors and labor seems too high for widespread use even with a very low reject rate. New connector designs are needed that are low cost, low loss, easily applied and not dependent on a high degree of skill.

Testing of the fiber cables was accomplished

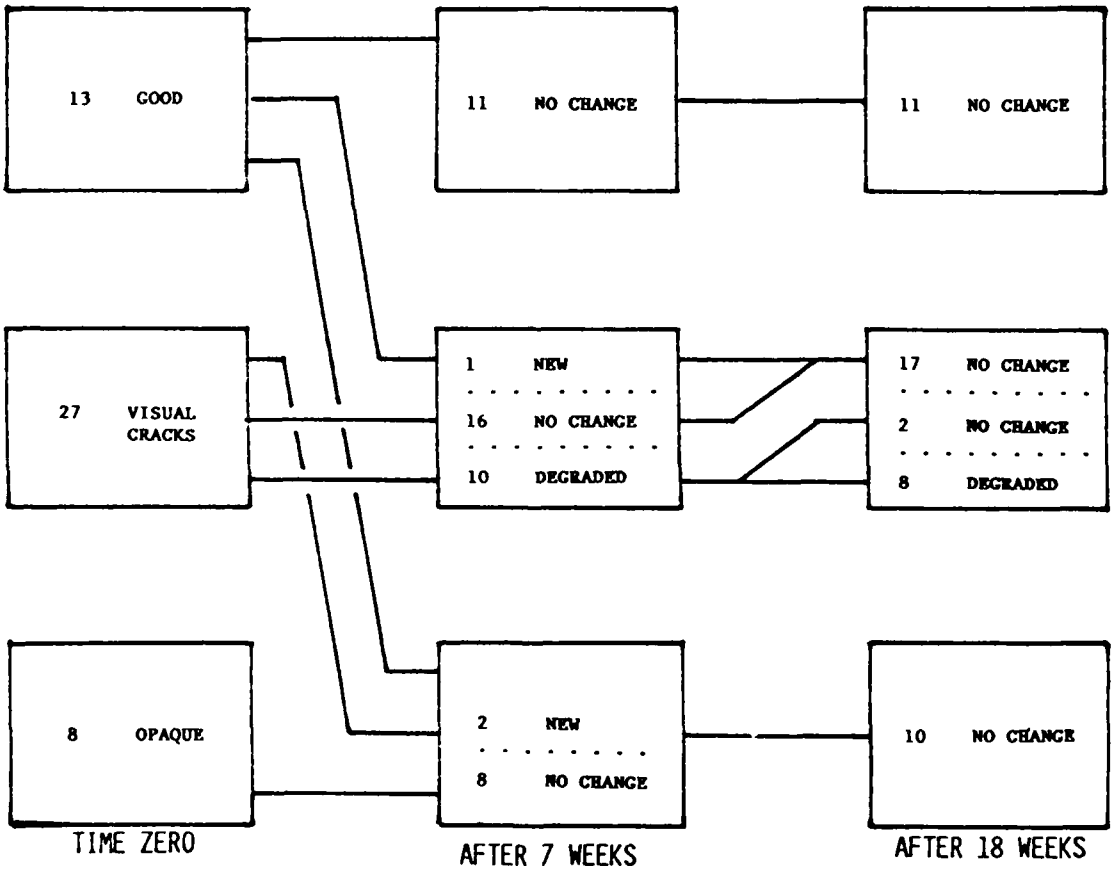


FIG. 7 DEGRADATION OVER TIME FOR A SAMPLE OF 48 CONNECTORS BY VISUAL INSPECTION

relatively easily using hand held test sets. The loss attributed to the fiber was insignificant due to the short distances involved and only the more significant losses of multiple connectors or splices were measured. Some variability was noted during testing and appeared to be due to an inability to reproduce the loss associated with connections to the test sets. A simple continuity check may prove to be most cost effective and sufficient once confidence is gained in field connectorization.

Apparatus

The most important point regarding apparatus is that it is virtually nonexistent. Significant work is needed on interconnection hardware for the building entrance, riser/distribution interface and network terminal outlets. Less obvious, but just as important are the piece parts necessary to anchor route and dress fiber cables. Much of what was used in the experimental network was homemade.

The design of building cables both riser and plenum, and distribution/termination apparatus requires an understanding of the application and consideration to the installation process and problems. Figure 8 shows fiber cables bundled and routed over standard cable rings. Although the importance of adequate bending radii was emphasized, the apparatus did not assure they were maintained. Human factors engineering must be emphasized to enable and encourage installers to perform their duties in a workmanlike way and to meet the special requirements of fiber to assure long term reliability. And, the special demands of terminal equipment users, untrained in handling fiber optics, must be recognized in designing the user interface to the building network. This presents an important challenge to vendors because the availability of suitably designed cables and apparatus will significantly affect the cost effective deployment of fiber optic networks.

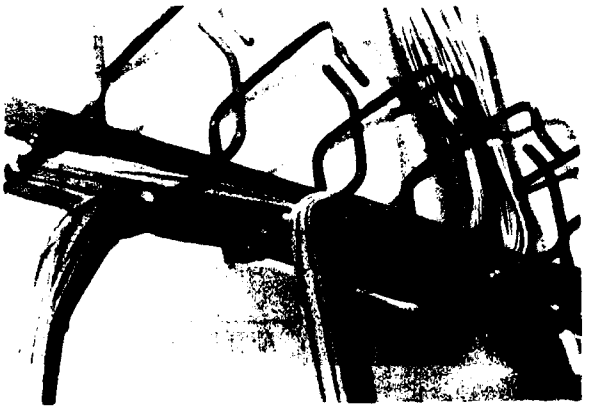


FIGURE 8. Sharp Bends In Fiber Cables Result From Using Apparatus Intended For Copper Cables

Conclusions

Cable and apparatus design will have a significant effect on the efficiency, ease of installation and reliability of the installed fiber optic network. A major benefit of the implementation of the Bellcore Fibernet has been the experience gained in its deployment at a time when the attention of the vendor community could be called to recognize the importance of the installer's and user's ability to get the most from product designs.

Demand for new services and the network to support them will surely be dependent on the cost/value ratio to the communications customer. Efficiency of installation and reliability are key ingredients in that cost and cable, and apparatus designed to optimize them will greatly help to improve that ratio.

Acknowledgements

The authors would like to thank Chris Stoveken of New Jersey Bell Telephone Company and Phil Grimado of Bell Communications Research for their work in data collection and analysis of optical fiber cracking in field installable connectors.



John P. Varachi
Rm. 2Q184
435 South Street
Morristown, NJ 07960

John Varachi received the B.S.M.E. degree from Fairleigh Dickinson Univ. Rutherford, NJ in 1976 and the M.S.M.E. degree from the Polytechnic Institute of New York, Brooklyn, NY in 1978. He is currently District Mgr. of the Lightwave Analysis & Mechanics Research Group at Bellcore. From 1969 through 1983 he was engaged in exploratory development at Bell Labs in mechanical design and analysis for telephone central office and outside plant apparatus. He also did physical design and systems engineering for copper and fiber-based digital loop electronic carrier systems for the outside plant and customer premises.



Charles H. Hasz
Rm. 2Q172
435 South Street
Morristown, NJ 07960

Charles Hasz attended RCA Institutes and Newark College of Engineering, and joined Bell Labs in 1956. He has worked in acoustic research, submarine cable, voice frequency devices and in-band signalling. In 1983 he joined Bellcore where he is involved with procedures for deploying fiber optic systems in commercial buildings.

A DEVICE FOR MEASURING EXCESS FIBER LENGTH IN BUFFER TUBES

Jeff S. Barker

Siecor Corporation
Hickory, North Carolina

ABSTRACT

The amount of excess fiber length (EFL) in buffer tubes is a critical parameter in ensuring the proper operation of loose tube fiber optic cables. For this reason, a device to accurately measure EFL during cable manufacturing was designed and fabricated. This device uses a basic mechanical approach where a tube sample is placed in a precision V-groove and cut to a length of 10 meters. Permanently mounted pneumatic cutters allow for repeatable sample lengths. After the tube sample is cut, the fibers are removed and placed one at a time into a second precision V-groove. At each end of the device is a digital micrometer, the summation of which measures the EFL relative to the tube length. The error associated with this measurement technique was determined to be less than ±1 mm. Given the standard sample length, this corresponds to a measurement error of less than 0.01% EFL.

INTRODUCTION

The amount of EFL present in buffer tubes has long been recognized as a critical parameter when producing loose tube fiber optic cables. As illustrated in Figure 1, EFL is the condition where the length of fiber within a buffer tube is greater than the buffer tube length itself. In many instances, accurate EFL data has been obtainable only through long length tensile testing after the buffer tubes are cabled. In such testing, EFL is determined through making time-of-flight measurements on the fiber for increasing levels of cable strain.

The capability to accurately measure EFL in a buffer tube prior to cabling was needed to expedite product development efforts focusing on buffer tube processing. The costs and time involved made it impractical to cable buffer tubes in order to determine if the buffer tube process yielded EFL values in the proper range. To address this need, a device was designed to measure EFL directly after the buffer tube process. In addition to expediting product development efforts, this device also offered an additional quality control measure for plant production.

DEVICE DESCRIPTION

This device uses a simple mechanical approach to directly measure excess fiber length for a 10 meter sample of buffer tube. The fundamental principle of the device is that a buffer tube sample is cut to a repeatable standard length and the lengths of the fibers within the tube are then measured relative to the tube length. Key to the success of this device is the high precision achieved both in cutting of the tube and fiber measurement.

As shown in Figure 2, the device consists of a table which is 10 meters in length, 0.1 meters wide with a height of 1.1 meters. Permanently mounted to each end of the table is a pneumatic cutter and a digital micrometer head. The micrometer head is located such that the zero reading position is adjacent to the blade of the cutters. Two parallel V-grooves run the length of the table surface for placement of the tube and fiber, respectively. The micrometers are aligned with the small groove for fiber measurement while the cutters are aligned with the large groove for cutting of the tube samples. At the bottom of the fiber groove is a small slit to allow vacuum to secure the fiber. Spring clips located every 10 cm along the large groove secure the tube for cutting. A solenoid switch located at the midpoint of the device enables the pneumatic cutters to be actuated simultaneously.

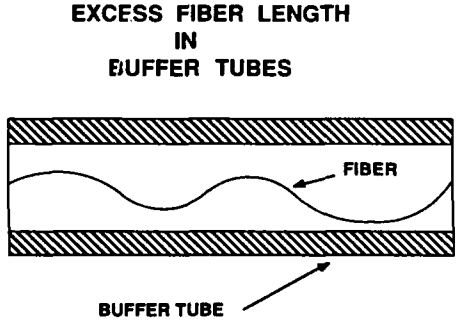


FIGURE 1

MEASUREMENT PROCEDURE

Operation of the device is as follows: A 30 meter sample of buffer tube is placed such that 10 meters of tube lies in the larger of the two V-grooves and 10 meters extends through each cutter to eliminate end effects. Once the tube sample is placed into the groove, the pneumatic cutters are actuated, cutting the sample length to 10.0 meters. The tube is then removed from the groove and slit with a fiber access tool[1] such that the fibers may be obtained. The fibers are cleaned and placed one at a time into the fiber V-groove to be measured. At each end of the device, the micrometer is adjusted until contact is made with the end of the fiber. Using the summation of the micrometer readings, the EFL expressed as a percentage of tube length is calculated from the equation:

$$\% \text{ EFL} = \frac{(\text{Fiber length} - \text{Tube length})}{\text{Tube Length}} * 100\%$$

$$= \frac{(\text{Sum of micrometer readings, mm})}{10000\ mm} * 100\%$$

Shown in Figure 3 are EFL data generated from this device for a typical 6 fiber maxi-tube with an inner diameter of 3.1 mm and an outer diameter of 4.5 mm. Also shown on the graph is a EFL measurement for fiber number 6 which was obtained from a long length tensile test. Note, the EFL values are comparable for both measurement techniques, ranging from 0.63% EFL to 0.69% EFL, respectively.

DEVICE MEASUREMENT ERROR

Small buffer tubes containing no fiber were used to quantify the measurement error of the device. Two sets of twenty samples of tube were cut, placed in the fiber groove and measured. From this data, the total measurement error at three standard deviations was determined to be 0.82 mm for the device. Given the 10 meter sample length, this corresponds to a total measurement error of 0.008% EFL. The significance of this error obviously decreases as the amount of EFL increases.

The measurement error components were identified as the error associated with cutting the sample tube length and the error associated with measuring the fiber length. To determine the error associated with measuring the fiber, 22 samples of fiber were measured three times each. From this data, it was determined that the error associated with measurement of the fiber (at three standard deviations) was 0.47 mm. Subtracting the fiber measurement error from the total measurement error (each expressed as variances), the resulting tube cutting error at three standard deviations was 0.67 mm.

CONCLUSION

A device has been developed which will accurately measure excess fiber length in loose buffer tubes. Though simple in design, this device offers an effective means for evaluating buffer tubes without having to manufacture a cable.

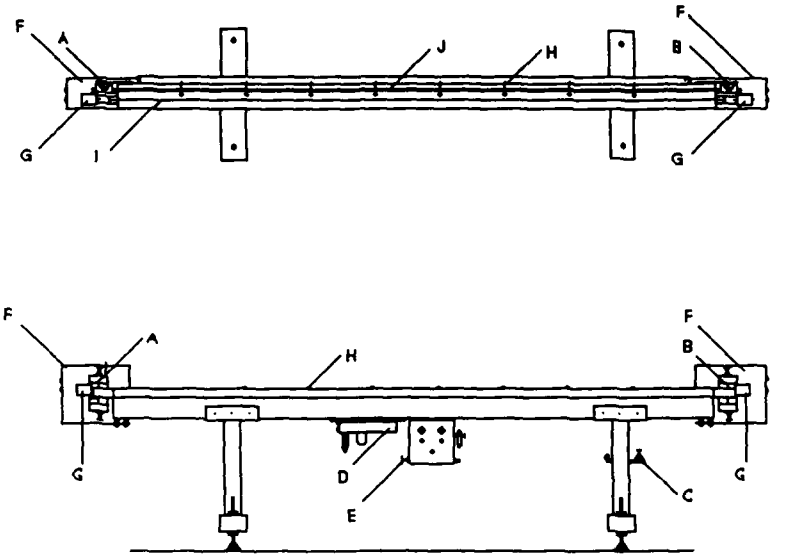
References

[1] Patent Pending.



Jeff S. Barker
489 Siecor Park
Hickory, NC 28603

Jeff S. Barker was born in Statesville, North Carolina in 1961. He received his Bachelor's Degree in Mechanical Engineering from North Carolina State University in 1984. Upon graduation, he was employed as a Process Engineer in the Research, Development and Engineering division of Siecor Corporation and is currently the Supervisor of the R,D&E Mechanical Lab.

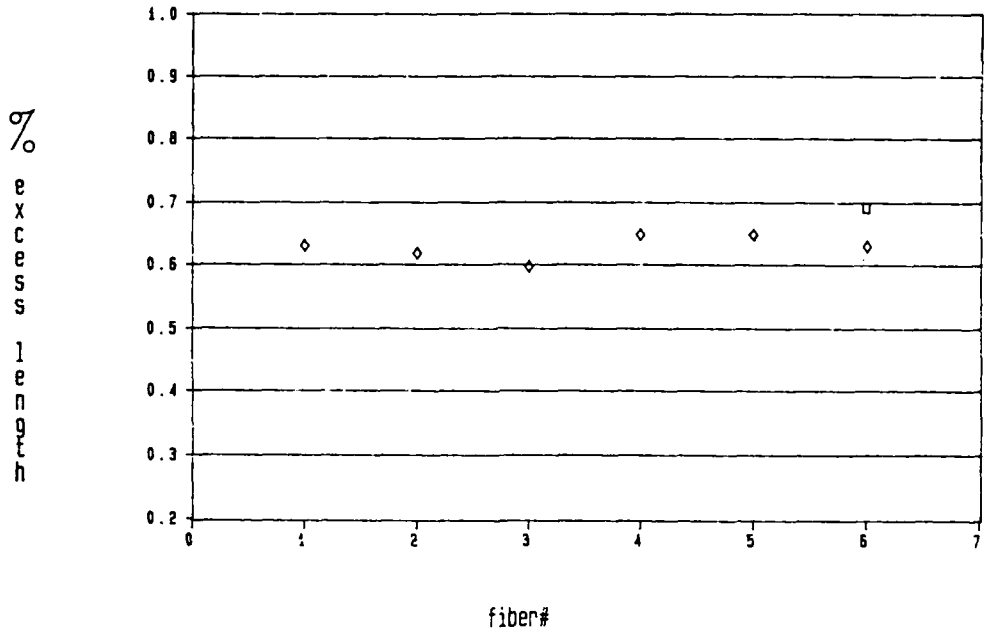


ITEM	DESCRIPTION
A	LEFT CUTTER
B	RIGHT CUTTER
C	FIBER ACCESS TOOL
D	VACUUM PUMP
E	CUTTER SOLENOID SWITCH
F	GUARD
G	MICROMETER
H	SPRING CLIPS
I	FIBER GROOVE
J	BUFFER TUBE GROOVE

FIGURE 2. EXCESS LENGTH MEASUREMENT DEVICE

FIGURE 3. EFL DATA FOR A SIX FIBER MAXI-TUBE

TUBE DIMENSIONS - 3.1 mm Inner diameter
4.5 mm Outer diameter



◊ - DATA FROM EFL MEASUREMENT DEVICE

□ - DATA FROM LONG LENGTH TENSILE TESTING

EFFECTIVE HANDLING OF ARAMID REDUCES CABLE COST

W. H. Allfather and A. V. Youngblood

E. I. du Pont de Nemours & Company, Incorporated
Wilmington, Delaware 19898

Abstract

Cable designers and manufacturers can continue to offer competitively priced para-aramid reinforced cables without compromising or sacrificing cable quality and mechanical properties. Using p-aramid yarn effectively requires proper handling and processing techniques as well as selection of the proper yarn product and size. The p-aramid products now available to meet the unique needs of fiber optic cable designers are described. Suggested design, manufacturing and storage procedures are discussed. Many cable manufacturers can increase the value of their products or reduce cable costs by taking advantages of the knowledge available in these areas.

Introduction

Para-aramid yarn, such as Kevlar* aramid, can provide cost-effective fiber optic cable reinforcement if properly used in cable design and manufacturing. P-aramid yarn provides very high modulus per unit cross-sectional area while at the same time being flexible, nonconductive, thermally stable, and creep resistant. Representative properties are shown in Table I. Although many cable designers and manufacturers believe that p-aramid reinforcement is expensive to use, it typically represents less than 10% of the total cost of an all-dielectric fiber optic cable (Table II). To allow cable designers and manufacturers to reduce further the cost of using p-aramid yarn as a cable reinforcement, several product changes have been made in the past year. By taking advantage of these product changes and by following the design, manufacturing, and storage suggestions discussed below, cable designers and manufacturers can reduce waste, improve the translation of p-aramid yarn properties into cable properties, and maximize the effectiveness of p-aramid cable reinforcement.

*Du Pont registered trademark

Aramid Products for Fiber Optics

In response to the unique needs of fiber optic cable designers and manufacturers, new versions* of p-aramid yarn are available, the yarn size range has been expanded, and tailored length packages have been developed. The addition of the new yarn versions gives designers added flexibility in the selection of yarn stress-strain properties. The addition of new yarn deniers provides an even progression in yarn size so that cable designers can meet cable stress-strain design requirements using the least amount of yarn. Table III shows typical properties for a range of version 49 p-aramid yarns.

Tailored length yarn can be obtained in lengths which closely match available optical waveguide lengths. The use of tailored length yarn significantly reduces yarn waste caused by large amounts of random length, leftover yarn on used bobbins. Packages with tailored length yarn may contain a short section of spliced yarn. These splices are extremely small and are hard to spot in the yarn unless one knows where to look. The stress-strain curves for spliced and continuous yarn are very similar (Figure 1) and spliced yarn has been shown not to adversely affect cable performance.

Design Considerations

Most cable designers calculate the amount of p-aramid yarn required in a particular cable design using the maximum cable force expected and the quoted yarn modulus. Initial modulus figures are obtained on yarn twisted to 1.1 twist multiplier and are determined at elongations greater than 0.5% using a tangent modulus method. Since the stress-strain area of interest for fiber optic cable is between 0 and 0.5% elongation, it is suggested that modulus values used in cable design calculations be recalculated at the elongation where the fiber optic waveguide is expected to demonstrate reduced performance using data obtained from zero-twist yarns (Reference 1).

*Kevlar® p-aramid yarn comes in four different versions as denoted by the product number (e.g., Kevlar® 29, 49, 68 and 149). Each version has unique stress-strain, moisture regain, and tensile creep properties.

TABLE I

PROPERTY COMPARISON FOR FIBER OPTIC CABLE REINFORCEMENT

	P-Aramid	E-Glass	Steel Wire[2]
Tenacity, gpd[1]	23	4.8	2.9
, 10^3 psi	425	160	285
, MPa	2,930	1,103	1,965
Modulus, gpd	890	318	200
, 10^6 psi	16.5	10.5	29
, MPa	113,768	72,398	199,955
Elongation to Break, %	2.5	2.1	2.0
Density, gm/cc	1.44	2.5	7.86
Coefficient of Thermal Expansion per °C	− 5 ppm	+ 2.8 ppm	+ 6.6 ppm
Conductive	No	No	Yes
Flexibility	Yes	Yes	No

(1) gpd = grams per denier. Denier is the weight in grams of 9,000 meters of yarn. gpd is a unit for specific strength or specific modulus.

(2) Improved plow steel.

TABLE II

FIBER OPTIC CABLE RAW MATERIAL COSTS

	% of Total
Waveguide (18 guides)	83%
Buffer Tubes (6 tubes)	2%
Pultruded Glass Core	4%
Jacketing (½" diameter cable)	3%
p-aramid (22 ends, 2160 denier, version 68)	6%

FIGURE 1

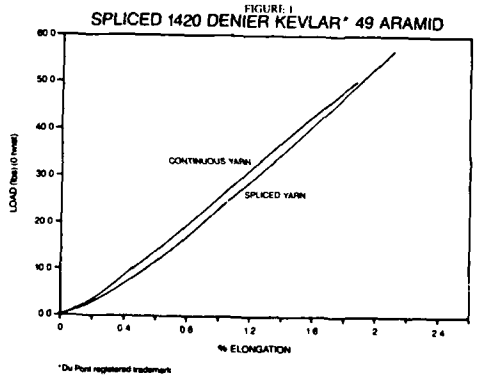


TABLE III

ARAMID PRODUCTS FOR FIBER OPTICS

Yarn Denier[1]	Twist	Yarn Diam.[2]	Yarn Cross-Sect. Area[2]	Number of Filaments	Filament Diam.	Yield Per Pound
		(10^{-3} in)	(10^{-4} sq in)		(10^{-4} in)	(meter/lb)
380	0	8.6	0.6	267	4.7	10,784
1,420	0	16.5	2.1	1,000	4.7	2,875
2,160	0	20.4	3.3	1,000	5.7	1,891
2,840	0	23.3	4.3	1,333	5.7	1,437
4,320	Roving	28.8	6.5	2,000	5.7	945
5,680	Roving	32.9	8.5	2,666	5.7	718
7,100	Roving	37.1	10.8	5,000	4.7	576

(1) Denier is the weight in grams of 9,000 meters of yarn

(2) Assumed 80% packing factor

Yarn twisting should be avoided when cabling p-aramid yarn into a cable since twist levels above 0.5 twist multiplier negatively impact the load-carrying capacity of the yarn at an elongation of 0.5%. P-aramid yarn lays flat and assumes a ribbon-like shape when applied to a cable because the yarn is flexible and pliable.

Nonroved yarns are more cost-effective to use as cable reinforcement than roved ones. The roving process plies together several ends of yarn which increases the cost, adds twist, causes yarn catenary, and lowers the yarn modulus. In addition, roved yarn properties translate less efficiently into cable properties.

Manufacturing Considerations

To assure maximum translation efficiency of all the yarns served in a cable, uniform and accurate tension control is required for each end of yarn being cabled. A tension of 0.05 grams per denier is recommended. Spring loaded tensioners, ball and cone tensioners, or electromagnetic brake rolls are most often used. Yarn rewinding should be avoided since rewinding can add additional yarn catenary (especially if the yarn being rewound is a roved yarn) and since the extra handling step can reduce the mechanical quality of the yarn.

Frictional drag should be eliminated as much as possible by using rolling takeoffs, rolling guides, and as few contact surfaces as possible. Where contact surfaces are absolutely necessary, clean, nick-free, matte-finished chrome oxide or "Alsimag"* guide surfaces are suggested since they give the lowest coefficient of friction with p-aramid yarn (Table IV). Polished chrome, steel, brass, and glass surfaces cause problems. If deposits build up on guides or on contact surfaces, they should be cleaned frequently. Sharp yarn angles should be avoided. Conditioning the yarn at 75°F and 60-68% R.H. for 28 to 48 hours before processing helps to reduce static. Static eliminators can also solve static problems. For safety reasons, never touch running yarn or measure yarn tension with fingers or hands.

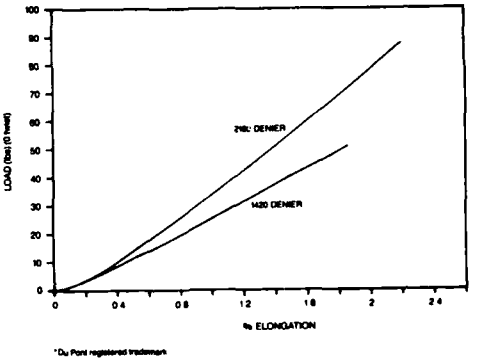
TABLE IV

COEFFICIENT OF FRICTION OF ARAMID WITH VARIOUS CONTACT SURFACES

Surface	Coefficient of Friction
Yarn/Yarn	0.33
Matte Chrome	0.18
Alsimag** Ceramic	0.37
Polished Chrome	0.45

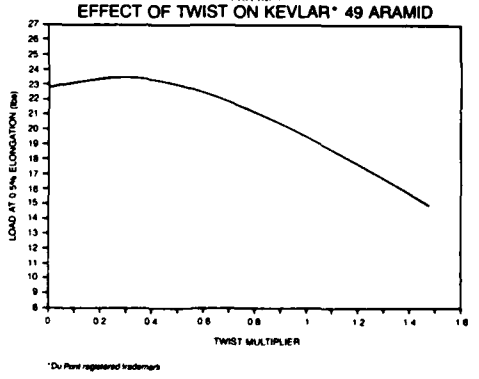
**3M registered trademark

FIGURE 2
KEVLAR* 49 ARAMID STRESS–STRAIN CURVES



*Du Pont registered trademark

FIGURE 3
EFFECT OF TWIST ON KEVLAR* 49 ARAMID



*Du Pont registered trademark

Storage and Handling Considerations

The handling of yarn tubes should be minimized to reduce the risk of degrading the yarn mechanical quality and yarn properties. Cartons should be stored in areas of relatively constant temperature and humidity. The plastic wrapping on each bobbin which inhibits yarn moisture change should be removed just prior to use. Any partial bobbins should be tightly rewrapped with the plastic wrap upon storage. Yarn should be used in the order received and merge numbers should not be mixed.

Conclusions

Used properly, p-aramid yarn is a cost-effective fiber optic cable reinforcement. The proper selection of yarn denier and tailored length along with thoughtful cable design and careful cable manufacturing can reduce p-aramid reinforcement costs significantly. By reducing reinforcement costs, cable designers and

*3M registered trademark.

manufacturers can continue to offer competitively priced cables without compromising or sacrificing the cable quality and mechanical properties provided by p-aramid reinforcement.

Acknowledgements

The authors wish to express thanks to Ellis Dunlap and to Sandy McKinney for their valuable assistance in the preparation of this paper.

References

Youngblood, A. V., "Understanding the Stress-Strain Properties of Aramid Fiber," International Wire and Cable Symposium Proceedings, Crystal City, Virginia, November 1987.



William H. Allfather

E. I. du Pont de Nemours & Company, Inc.
Textile Fibers Department
Wilmington, Delaware 19898

William H. Allfather joined Du Pont in 1965 as a supervisor in manufacturing at the Martinsville, VA, nylon plant. From 1968-74 he was involved in various fiber development programs for apparel yarns. Market development activities since 1974 have centered on industrial nylon, polyester, and Kevlar® aramid fibers. Mr. Allfather currently has responsibility for sales and development of Kevlar® aramid yarns used by the fiber optic cable industry. He holds a B.S. degree from Lynchburg College in biology/chemistry.



A. Virginia Youngblood

E. I. du Pont de Nemours & Company, Inc.
Textile Fibers Department
Wilmington, Delaware 19898

A. Virginia Youngblood is a Senior Research Chemist at Du Pont working on research and development of Kevlar® aramid yarn for use in the fiber optic cable industry. Dr. Youngblood has been with Du Pont since 1982 and areas of interest have included ropes and cables as well as fiber optic cable reinforcement. She holds a B.S. in Chemistry from the College of William and Mary and a Ph.D. in Chemistry from Yale University.

UNDERSTANDING THE STRESS-STRAIN PROPERTIES OF ARAMID FIBER

A. V. Youngblood

E. I. du Pont de Nemours & Company, Incorporated
Wilmington, Delaware 19898

Abstract

Property data for p-aramid yarn fiber optic cable reinforcement is often misunderstood and misused by cable designers and manufacturers. The stress of p-aramid yarn at a particular elongation is dependent on yarn twist, yarn denier and yarn type. Since the stress-strain curve of p-aramid yarn is nonlinear, the use of modulus values rather than stress values can be misleading, can reduce design accuracy, and can increase raw materials costs. This paper discusses the proper measurement of p-aramid yarn stress-strain properties and the use of such properties in the design and manufacture of fiber optic cables.

Introduction

Para-aramid continuous-length fiber such as Kevlar* is now widely used as a tensile reinforcement or load-bearing member in all types of fiber optic cables. However, much confusion still exists among fiber optic cable designers and manufacturers concerning interpretation of modulus and stress-strain data for p-aramid fiber. Even though p-aramid fibers are highly oriented, crystalline, organic polymers with very high specific modulus, the yarn made from these fibers still exhibits a nonlinear stress-strain curve. The yarn version[+], yarn denier, and yarn twist all affect the nonlinearity of the stress-strain curve, particularly at low elongations where fiber optic cables are designed to be used. Many cable manufacturers and designers are unaware of this nonlinearity or do not account for it when designing with p-aramid yarn. Understanding the position and magnitude of this nonlinearity can prevent serious design errors, reduce cable raw materials costs, and shorten proveout time.

Most cable designs use a reinforcement, such as p-aramid yarn to avoid treating the sensitive optical fibers as the principal cable load-bearing member. Under these design conditions, the amount of p-aramid which should be used in the cable is often calculated by dividing the final cable load by the final cable elongation and the initial modulus of the reinforcing material (Reference 1). While this method seems straightforward enough, yarn initial modulus is a calculated value, defined at a certain place on the yarn stress-strain curve. Since p-aramid stress-strain curves are nonlinear, the initial modulus quoted by a manufacturer may not be suitable for a particular fiber optic cable design, particularly if the cable is being designed to operate at elongations different from that used to determine the initial modulus quoted in p-aramid literature. Table I shows how the p-aramid yarn modulus can change as a function of the elongation where the modulus is defined.

TABLE I

EFFECT OF ELONGATION ON ARAMID YARN MODULUS

(2160 denier, Kevlar* 49 aramid, zero-twist yarn)

Elongation Range	Modulus Value Calculated (Million psi)	(MPa)
0.0% - 0.1%	5.9	40,680
0.1% - 0.2%	9.8	67,571
0.2% - 0.3%	11.4	78,603
0.3% - 0.4%	14.1	97,220
0.4% - 0.5%	16.5	113,768
0.5% - 0.6%	16.5	113,768
0.6% - 0.7%	16.1	111,010
0.7% - 0.8%	16.1	111,010
0.8% - 0.9%	17.2	118,594
Initial Modulus	15.5	106,872

*Du Pont registered trademark

[+]Kevlar® p-aramid yarn comes in four different versions as denoted by the product number (e.g., Kevlar® 29, 49, 68 and 149). Each version has unique stress-strain, moisture regain, and tensile creep properties.

Determining Modulus

Modulus is determined by picking two points on the stress-strain curve, drawing a secant line between the points, obtaining the slope of the secant line, and dividing by the yarn cross-sectional area. The yarn cross-sectional area is calculated by multiplying the number of filaments in the yarn by the filament area.

To generate a stress-strain curve for p-aramid yarn, dry yarns are tested in a tensile tester equipped with air-actuated 4C yarn clamps. The test method itself is an adaptation of ASTM D885, "Method of Test for Tire Cords, Tire Cord Fabrics, and Industrial Filaments, made from Man-Made Organic-Base Fibers". Test samples are conditioned for a minimum of 16 hours at 55% relative humidity and 75°F. One out of every five specimens is monitored for denier (weight in grams of 9000 meters) by accurately weighing a 90 cm length. Every specimen is twisted to 1.1 twist multiplier where

$$\text{Twist Multiplier} = \frac{\text{Turns/inch} \times \sqrt{\text{denier}}}{73}$$

Tests are conducted on specimens of 10-inch gage length at a 10% per minute strain rate. Calculations for strength and modulus are made on a grams per denier basis which can be converted to psi by multiplying by 18,540 or to MPa by multiplying by 127.8.

The denier is measured after drying the yarn for a minimum of 3 hours at 105°C (220°F). The denier must be obtained promptly after removing the yarn from the oven because p-aramid has a rapid moisture regain. The value reported for denier is an average of two specimens.

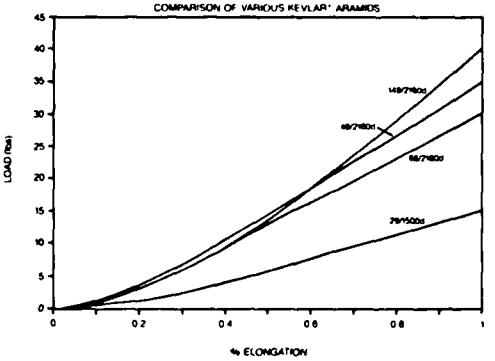
Once the yarn stress-strain curve has been generated and the operating elongation area for the cable has been identified, an appropriate value for the modulus can then be easily calculated.

Selection of Aramid Yarn Version

Figure 1 compares the stress-strain curves of various zero-twist p-aramid yarns. There are currently four versions of Kevlar® p-aramid yarn available. The version 68 and version 149 yarns are new additions recently made commercially available to give designers added flexibility in the selection of yarn stress-strain properties.

The stress-strain curve of 149 yarn is more nonlinear than that of 49 yarn. Although 149 yarn has a higher modulus when calculated at 1.0% elongation, at elongation ranges of 0.2%-0.5%, the load-carrying capacity of 149 yarn equals that of 49 yarn. Since 149 yarn is more expensive than 49 yarn, 149 yarn is not recommended for general use as a fiber optic cable reinforcement.

FIGURE 1
STRESS-STRAIN CURVES
COMPARISON OF VARIOUS KEVLAR® ARAMIDS



®Du Pont registered trademark

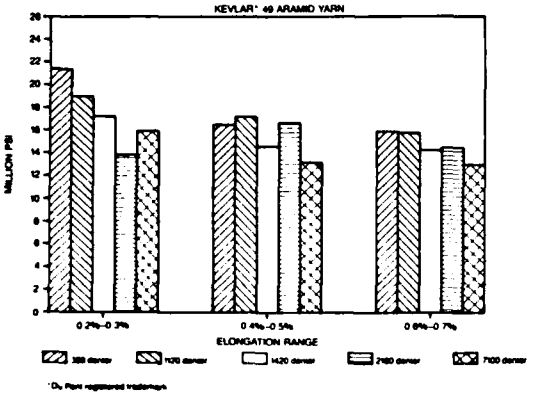
The load-carrying capacity of 68 yarn at any given elongation is approximately 10% lower than for 49 yarn. Although 68 yarn has a lower modulus than 49 yarn, it is also priced to reflect this difference for fiber optic end uses. Version 68 yarn is therefore recommended for fiber optic reinforcement applications where an increase in cable diameter is of little design concern. The nonlinearity in the stress-strain curve for 68 yarn is about the same as for 49 yarn.

The load-carrying capacity of 29 yarn is much lower than for 49 yarn at any given elongation. The use of 29 as a fiber optic cable reinforcement is cost effective only when strength, rather than modulus, is of primary importance in the cable design.

Effect of Yarn Denier

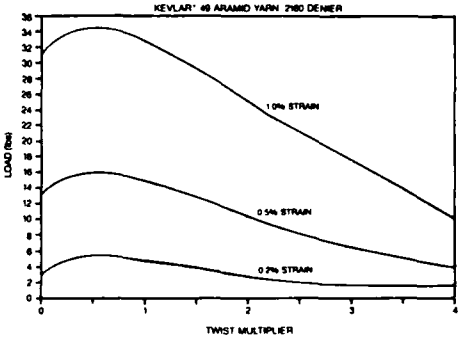
P-aramid yarn can be obtained in different yarn sizes. The yarn sizes are denoted by denier (the weight in grams of 9000 meters of yarn). As Figure 2 shows, p-aramid yarn can change as a function of denier with lower denier yarns exhibiting higher modulus. For 49 yarn, the modulus is highest when determined in the 0.2%-0.3% elongation range and drops off by roughly 20% when determined for the 0.6%-0.7% elongation range. One exception to this behavior pattern is the 2160 denier 49 yarn which has a higher modulus when calculated at 0.4%-0.5% elongation than when calculated at either of the other two elongation ranges. It can be important when planning the reinforcement of a fiber optic cable to consider the effect on cable construction of the tradeoff between the larger number of ends required with smaller denier yarns versus the higher modulus of these yarns.

FIGURE 2
EFFECT OF DENIER ON MODULUS



®Du Pont registered trademark

FIGURE 4
INFLUENCE OF TWIST ON LOAD

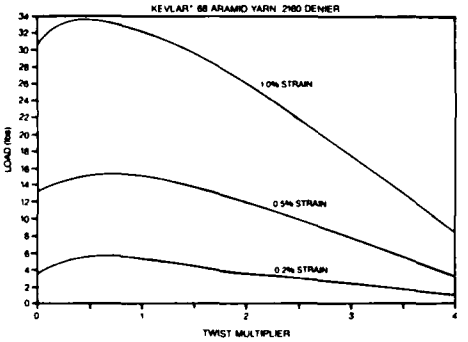


®Du Pont registered trademark

Effect of Yarn Twist

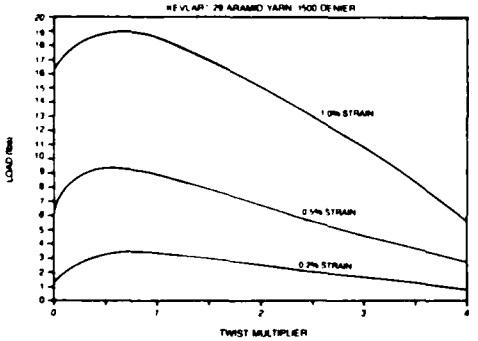
The yarn twist significantly influences the determined modulus of p-aramid yarn. Figures 3, 4, 5 and 6 show the effects of twist multiplier (defined above) on the load-carrying capacity of various versions of p-aramid yarn. For all yarn versions, adding twist up to 0.5 twist multiplier increases the yarn load-carrying capacity. The addition of more twist, particularly at levels beyond 1.5 twist multiplier decreases the yarn load-carrying capacity, especially at elongations of 0.5% or more.

FIGURE 5
INFLUENCE OF TWIST ON LOAD



®Du Pont registered trademark

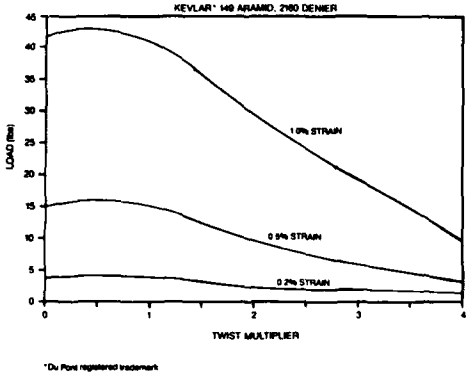
FIGURE 3
INFLUENCE OF TWIST ON LOAD



®Du Pont registered trademark

Modulus values for p-aramid yarns are generally quoted in the literature for yarn twisted to 1.1 twist multiplier. For fiber optic applications higher modulus can be realized at lower yarn twist level and should be accounted for when designing with p-aramid yarn for fiber optic cable reinforcement.

FIGURE 6
INFLUENCE OF TWIST ON LOAD



*Du Pont registered trademark

Conclusions

Determining modulus values for p-aramid yarn at the elongation range and the twist level for the desired fiber optic cable application can make a large difference in the amount of p-aramid needed to meet performance criteria. Table II shows a comparison for 2160 denier yarn for version 49 p-aramid. Using modulus values determined for zero-twist, 2160 denier yarn at the elongation range of 0.4%-0.5% can make as much as 20% difference in the amount of yarn, and therefore the raw materials costs, required to reinforce a typical cable rated for 600 lbs. at 0.5% elongation.

By understanding the stress-strain behavior of p-aramid cable reinforcement, better cable designs which use the minimum raw materials necessary can be realized. In addition, unnecessary proveout time will be reduced and higher product confidence will be achieved.

TABLE II

EFFECT OF ARAMID MODULUS VALUE IN CABLE DESIGN

ASSUMPTIONS:

- 600 lbs rated
- @ 0.5% elongation
- 2160 denier, Kevlar* 49 yarn

CALCULATIONS:

Modulus Value		Modulus Calc. Conditions		Number Yarn
(Million psi)	(MPa)	Elongation Range	Twist	Ends Needed
16.5	2,109	0.4%-0.5%	Zero-twist	22
15.5	2,982	Initial modulus	1.1TM	24
14.0	1,790	0.4%-0.5%	1.1TM	27

CONCLUSIONS:

As much as 20% lower yarn needed for design when proper modulus selected.

*Du Pont registered trademark

Acknowledgment

The author wishes to express thanks to Ellis Dunlap and to Sandy McKinney for their valuable assistance in the preparation of this paper.

References

Miller, Stewart E. and Cynoweth, Alan G., Optical Fiber Telecommunications, Academic Press, 1979, p. 440.



A. Virginia Youngblood
E. I. du Pont de Nemours & Company, Inc.
Textile Fibers Department
Wilmington, Delaware 19898

A. Virginia Youngblood is a Senior Research Chemist at Du Pont working on research and development of Kevlar® aramid yarn for use in the fiber optic cable industry. Dr. Youngblood has been with Du Pont since 1982 and areas of interest have included ropes and cables as well as fiber optic cable reinforcement. She holds a B.S. in Chemistry from the College of William and Mary and a Ph.D. in Chemistry from Yale University.

TECHNOLOGY OF INSTALLATION AND REPAIR OF SUBMARINE CABLE

F. Y. TSAI G. T. TZENG S. F. LIN H. K. PENG

Telecomunication Laboratories, Directorate General of Telecomunication
P. O. Box 71. Chung-Li, Taiwan Republic of China

ABSTRACT

The paper describes detail technology of repairing submarine cable and some installation approaches which includes (1)Setting up equipments for repairing ship such as hauling machine, winch and cable tank etc., (2) Submarine cable recovery, which includes processes of searching, grapnelling and picking up, (3) The splice of coaxial cable, (4) The sweeping assignment and investigation of installation: By using searching equipment for removing obstacles of submarine cable route and sediment sampling as for burying reterance, (5) Submarine cable installation process, which covers the cautionary detail items and explanation of burying machines.

1. Introduction

The TM submarine coaxial cable system is damaged when the anchors are hooking and trawling, because the fault area is full of fishing activities. This paper describes the methods and processes of repairing and burying submarine cable.

The cable was buried at a depth deeper than 1 m for about 55 km of the whole route, but the repeater is buried at a depth of about 60 cm deep by the divers assistance. The processes of whole operation is shown as flow chart. (see figure 1.)

2. Cable ship for repairing work

The cable ship is equipped with facilities for the installation and maintenance of submarine cable and is designed to provide safety, large working space and ease of operation to withstand the severe enviroment, so the ship is unnecessary a large body, only the fish boat, tugboat, barge is remade as following condition.

(1) Gross tonnage ranging from 100 to 200 tons, main engine horsepower about 100 hp.
(2) The central partion of ship can accomodate spare cable, recovery cable and materials for repairing.
(3) With suitable place to set the instrumental equipment and machine on the deck.
(4) Have adequate space to splice the cable on the deck.
(5) The level difference between the front and back deck is small.
(6) Locate ship position is accurate.
(7) It is easy to operation for the ship.

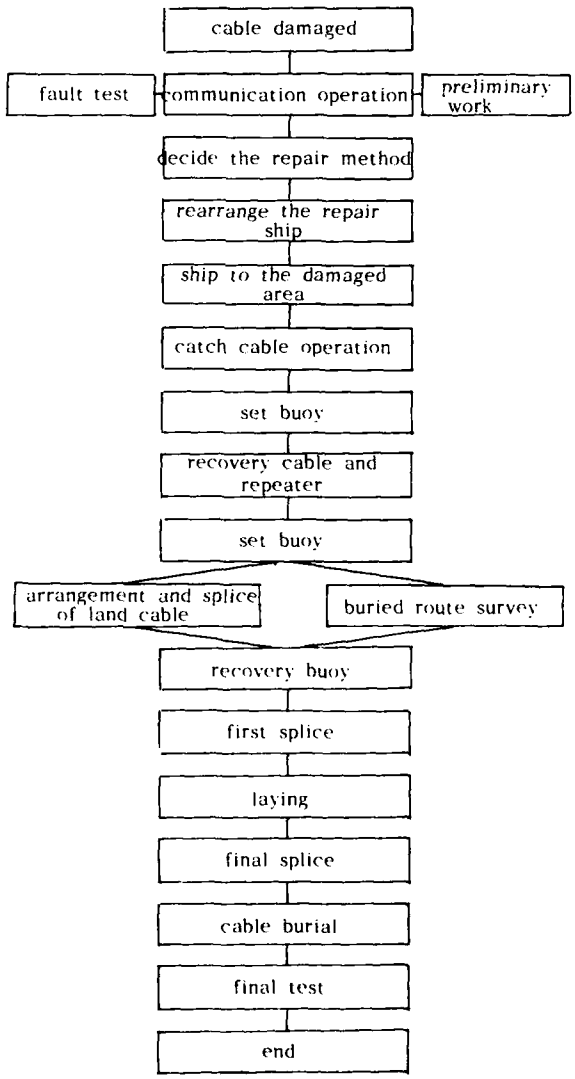


Fig 1. Flow chart of repairing submarine cable

3. Equipment of cable ship for repairing work.

The layout of equipment is shown as in figure 2 & 3 from the fish boat and platform ship were remade. The cable ship's equipment included (1) Bow sheave and shooter (2) stern sheave (3) crane (4) tension meter (5) Bow cable engine (6) hold back gear (7) cable tank (8) cable through (9) taut wire gear (10) hauling machine (11) radar (12) satellite navigation system (13) cable drum engine (14) winch (15) echosounder (16) current meter (17) buoy set (18) bottom sampler (19) burying machine etc.

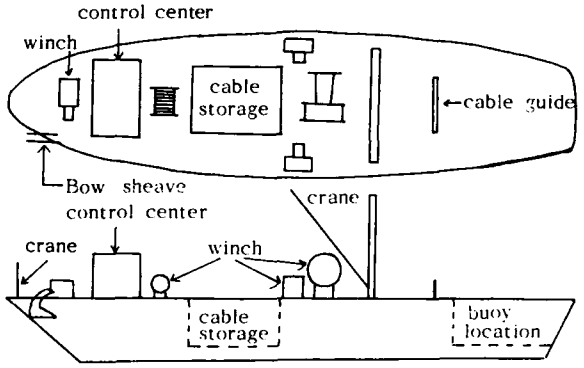
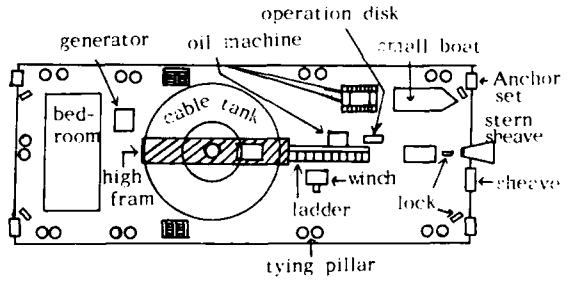


Fig 2. The layout of repairing ship (from fish boat)



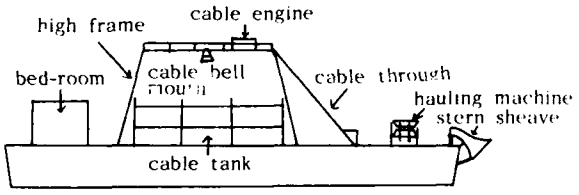


Fig 3. The layout of repairing ship (from platform ship)

4. Cable repair

When a submarine cable is damaged, the fault point can be found by the testing of the landing station. After the fault point is located, a cable ship goes to the fault area and then is ready for repairing the cable. The processes of cable repair included the following discriptions.

4.1 Grabbing cable

For casting a grapnel on the seabed from the bow-sheave for grabbing a cable, Its processes are listed as follows.

(1) decides the direction, location and range of grabbing cable, then marks on the sea chart.
(2) linking the Grapnel, Grapnel chain, Grapnel rope in sequence, and set the Grapnel under the bow, Grapnel rope encicles on the winch.
(3) laying the Grapnel into the sea bottom slowly from the Bow sheave, and utilize winch to control the laying speed.
(4) Grapnel's location must be controlled far from the fault point about 200 to 500 m, and the Grapnel rope's length is about twice of the water depth of fault point.
(5) During the grabbing cable is processing, conditions of the wind, tide, current and water depth etc, need to be considered.
(6) Operational direction of grabbing cable must be perpendicular to cable, and go forward in zigzag.
(7) The velocity of grabbing cable is about two knots.
(8) When the grapnel rope's tension goes up gradually, it means that the cable have been grabbed.

4.2 Picking up the cable

After finishing the operation of grabbing cable, then picking up the cable on board finally cutting down the cable and testing, the whole processes are described as follow.

(1) After the Grapnel grabbing the cable, untilizing the winch to pull up the Grapnel rope, at the moment, the tension of Grapnel rope, need be controlled and maintained with a suitable tension value.
(2) when the submarine cable is pulled near the Bow shooter, the Grapnel chain on the deck is then fixed. By utilizing another steel wire to lock the cable and loose the Grapnel, then the cable is received by winch.
(3) Utilizing crane to life the Grapnel, then cutting it down and testing the cable. The cable without fault is attached to a buoy and is cast into water. The other cable end with fault is repaired.

4.3 Splicing operation

First, cleaning the surface of recovery cable, setting the working frame and necessarily equipment, taking out the spare cable, then starting the working of cable splicing, the processes shown as flow chart in figure 4.

4.4 Cable laying

It is important to lay cable with the proper amount of slack on a route. Excess or shortage of this slack causes kinks or suspensions which will cause damage, theofore adjusting the slack accurately is the main working in laying cable. On the other hand, and the other important point in laying cable is how to locate ship poition and ship velocity accurately, now the processes of laying cable are described as follow.

(1) to control the ship velocity and laying velocity, the ship velocity about 3 knots (one knot equal to 1.85 km/hr) at this operation.
(2) to control the slack which can be inspected by the cable horizontal angle into the sea. This working must be finished by the experienced technician, to control and to adjust it at any time.

(3) during the cable laying, when the repeater is laid, it will be very careful, because the repeater is very large and heavy, it can't be laid the same as that of the cable, utilizing the crane to lift the repeater through into the cable bell mouth carefully, then adjust the width of hauling machine and utilize the cable engine to pull the cable, let the repeater through the hauling machine into the sea.

(4) laying near the buoy of another end, at the moment, the laying speed must reduce slowly for stopping then reovering the buoy set and cable, loosing the buoy set, arranging the cable and commencing the final splice of cable, when the splice is finished, working of laying cable is finished too.

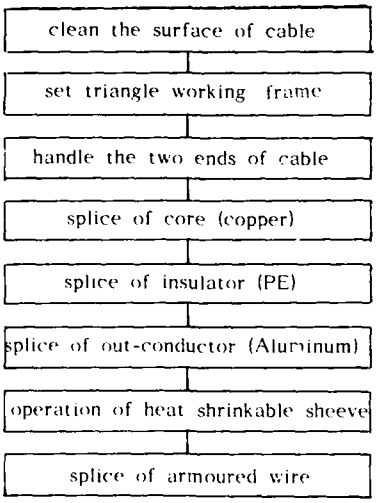


Fig 4. The flow chart of splicing operation

5. Cable burial

5.1 Sea-bottom sweep

Before commencing cable laying and burying, final confirmation of the route where the cable was to be buried was made with the assistance of a tugboat to check hardness of seabed undulation and obstacles.

The depth measuring, seabed sampler, tide current measuring and an anchor towing were performed before the cable was buried, and a sea-bottom sweep, bottom hardness check, sea-bottom undulation reconfirmation were also made.

5.2 Methods of cable burial

At present, methods of cable burial can be split broadly into two groups.

(1) buried as laid (simultaneously).
The method applied to new systems under construction and it consists of the simultaneous laying and burying.

(2) burial after laying.
The method involves the burial of cable that has previously been laid on the seabed, it is usually applicable to maintenance of existing systems, but can also be used for burying new systems shortly after they have been laid.

Because the TM submarine cable is the existing system, recovery cable from seabed, then repairing, laying and burying, so the method of burial after laying is adopted.

Early Burial after laying systems are based on jetting techniques (water). They are generally high-flow medium-pressure systems and range from jetting tools directed by divers through to purpose built jetting structures that straddle the pipe or cable and extend into the seabed to the required depth of burial, water jets break up the seabed and the water lifts the soil out of the trench allowing the cable to sink to the bottom. Motive effort along the route is provided by surface tow. Generally, it is limited to shallow water because of the fluid resistance of hoses used for delivery of air and water from pumps, which are located on the surface barge or support ship. They are also limited by current speed and water depth, Therefore it is necessary to have divers in attendance to supervise the operation.

5.3 Burying machine

(1) Outline

This waterjet-type burying machine (it is 4.5 tons, 4.7 m long, 3.7 m wide and 2.6 m high) consists of a burryer, skies and supporting frame, and is provided with a cable depth sensor and angle sensor of side level. The buryer moves up and down with C on the drawing as its axis, when setting a bolt at point A on the guide bar, the cable burying depth is set at 2 M max, when installing a bolt at point B, the cable can be buried down to 1 M max. For instance when setting maximan burying depth at 2 m for the cable, the buryer can move between 0 and 2 m, so a cable depth detector aboard the ship must be monitored while burying the cable. The buryer is provided with 12 waterjet nozzles, which are arranged on both sides of the cable guide ditch. Each nozzle is connected to 280 ps pump (transport water pressure is 12 kg/cm^2, water quantity is 6000 m^3/min for one set) with 3" hose. The weight should be adjusted between 20 and 30 kg according to the sea bed soil quality etc.

(2) Installation

When installing the waterjet type 2 m burying machine on the beach, a trench, about 3 m long, 50 cm wide and 1 m to 2 m deep, should be digged, after laying the cable in the trench, the waterjet type 2 m burying machine should be hoisted, then installed along the trench. During the installation, It needs to confirm that the cable is certainly placed along the cable guide ditch of the buryer. When the waterjet-type burying machine has been installed, hose and cable should be installed according to the specified procedure for 280 ps pump, pipe line of small ship, then, start buryer.

(3) Cable depth detector

The sensor of cable depth detector is interlocked with shaft C on the drawing. When the angle between the buryer and the skis bottom is changed, output of the variable resistor will be changed. This, in turn, the voltage is changed for enabling direct reading of the cable burying depth on the meter aboard the ship. It is also possible to set an automatic recorder.

(4) detector of side level

It is designed so that the incline from side

to side of the waterjet type 2 m burying machine is sensed by an angle sensor, thereby enabling monitoring it aboard the ship.

5.4 methods and processes of cable burial

(1) first inspecting the burying machine's equipment, hose, wire and buoy is set or not, and starting the crane, pump (tran-port water pressure display 7-8 kg/cm^2) before burial.

(2) after the burying machine lauched the water, two wire, one is towing wire and the other is a control cable, are used to tow the cable burier. The main tensile power is supported by the towing wire which is connected with the cable burier.

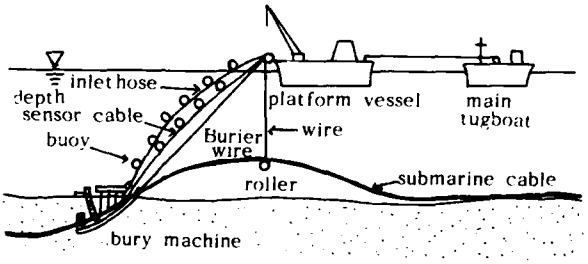
(3) Burying cable speed is about 0.5-1.5 knots, according to the sea bottom's hardness.

(4) A towing angle about 10°-30° is suitable for the vertical angle, outside this range, the cable burier becomes unstable and either of the length of the towing wire, or the speed of ship need to be adjusted.

(5) This operation describes the method of buring after laying, when the burying machine proceed near the repeater (about distance of 600 to 800 m), because the repeater can't through the Burying machine's cable quide, so the main tugboat must stop towing, then proceed slowly and is changed to barge towing anchors. When the roller touch the repeater, the tension value of tensionmeter will be enlarged, at the moment, the operation must stop and the divers loose the lock between cable guide and cable into the sea, then take the cable to hang on the roller, Burier continue going foward. At last, loosing the roller, let the repeater be through the Burier and then finish the operation of cable burial.

(6) Burial of the repeater by the divers who hold the water-jet into the seabed, and jet water into the soft mud, the repeatr was merged slowly, the depth of burial is about 0.6 m.

(7) the layout of Burying operation is shown as figure 5.



Burier wire length: about double water depth
Inlet hose length: burier wire length + 10M-20M
depth sensor cable length: inlet hose longth + 10M
roller wire length: about 10M above the seebed

Fig 5. Burying operation

6. Conclusion

Submarine cable transmission systems have played an important role in the telecommunication network, the inevitable expansion of global communications will increase the demand for submarine cable systems in the future. In order to ensure that the best protection is provided against envirionmental hazad from the increase in size of fishing boats, dreadgers and other ships. At present, burying submarine cable in the seabed is still an effective method to ensure the reliabilty of submarrine cable systems.

It is a trend and necessity for the cable burial exfuipment and technique need to be developed and be suitable for any different enviornment, in the future.

References

1. E. E. EATAC, "Dynamics and Kinematics of the Laying and Recovery of Submarine Cable", B.S. T. J, 36, Sept, 1957. pp1129-1207.
2. R. W. GRETTCY, "Cable payout System", B. S. T. J, July, 1964, pp1395-1433.
3. Toshio Sekine, "Submarine Cable Activities in NTT", J. T. R. April 1979, pp90-97.
4. Hideo Uematsu, Norio Abe, ichiro Ono and Mitsuo Iida, "Asean Submarine Cable system (Malaysia-Singapor-Thailand)", FUjitsu Sci, Tech, J. 19, 2, June, 1983, pp199-238.
5. Yasuji Murakami, "Seabed Surveying and Cable Burying Equipment (SEAB) for the new Cable ship Koyo Maru", J. T. R. Octor. 1984, pp258-263.



Fwu-Yuan Tsai
P.O. BOX 71. Chung-Li
Taiwan, Republic of China

He received a M. S degree in Harbor and River engineering in 1982 from National Taiwan college of Marine science and Technology. He joined Telecomunication Laboratories D. G. T. in 1985 and now is a member of out-side plant department.



Gwo-Tay Tzeng
P.O. BOX 71. Chung-Li
Taiwan, Republic of China

He received a M. S. degree in Harbor and River engineering in 1982 from National Taiwan college of Marine Science and Technology. he joined Telecomunication Laboratories D. G. T. in 1985 and now is a member of out-side plant department.



Shing-Fwu Lin
P.O. BOX 71. Chung-Li
Taiwan, Republic of China

He received a M. S. degree in Hydraulics and ocean Engineering in 1983 from National Cheng-Kung university. He joined telecomunication Laboratories D. G. T. In 1985 and now is a member of out-side plant department.



Hai-Kuen Peng
P.O. BOX 71. Chung-Li
Taiwan, Republic of China

He received a M. S. degree in oceanography in 1985 from National Taiwan university. He joined telecomunication Laboratories D. G. T. In 1985 and now is a member of out-side plant department.

INTERFEROMETRIC CHARACTERIZATION OF A BICONIC FIBER OPTIC CONNECTOR SLEEVE

M. J. Saunders and B. V. Darden

AT&T Bell Laboratories
Norcross, Georgia

Abstract

An interferometric method is described for measuring the absolute value of the biconic sleeve end separation of the master sleeve used to determine the suitability of plastic product sleeves. The end separation, g_2, is defined as the outermost distance between two truncated balls of a particular diameter inserted with a particular force into both openings of a biconic connector sleeve. Previously, the absolute value of end separation was not measured so that one never knew whether or not wear of the master sleeve contributed to the product sleeves being out of tolerance. Sources of error are discussed and the result of ten measurements of the master sleeve end separation is $g_2 = (7.5659 \pm 0.0008)$ mm.

Introduction

In a biconic connector assembly, the precise alignment of the fiber plugs within the connector is greatly affected by the mechanical precision of the biconic components. In particular, the biconic sleeve end separation, g_2, (see Figure 1) is a quantity of paramount importance. Currently, g_2 is measured by inserting with a particular force, F, a truncated precision steel ball into each end of the plastic product sleeve and comparing the separation between the gage balls with the separation when they are inserted into a precision reference steel sleeve. Thus, the measurement is relative and only the deviation with respect to the reference steel sleeve is measured. Consequently, any undetected wear of the reference sleeve will result in a shortening of the product sleeve end separation, leading to instability of fiber connections and, in the worst case, broken fibers. In this paper we describe an interferometric method for determining the end separation of the master sleeve. This method could also be used to measure plastic product sleeves.

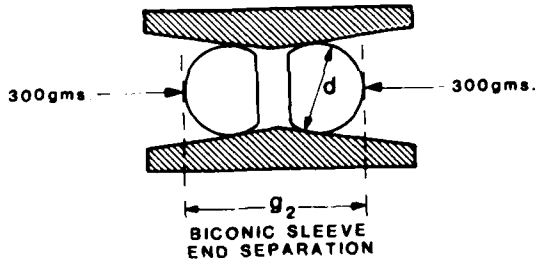


Figure 1. Biconic Sleeve End Separation Using Two Truncated Spheres.

The method described here uses another approach to determine g_2, shown in Figure 2. An untruncated ball of diameter d is inserted under a force F in the upper cone of the biconic sleeve and the location of the upper pole of the ball is determined. The ball is then removed from the upper cone and inserted in the lower cone under a force F. Again, the location of the upper pole of the ball is determined. The difference between these locations is g_1. A measurement of the diameter, d, of the ball then gives $g_2 = g_1 + d$, the biconic sleeve end separation.

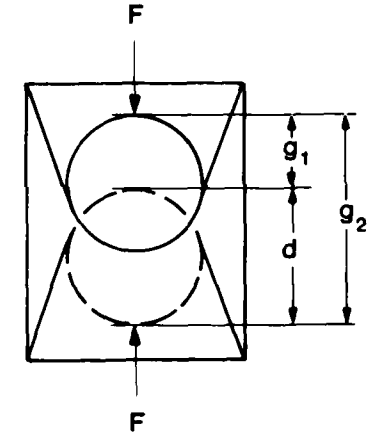


Figure 2. Biconic Sleeve End Separation Using One Sphere.

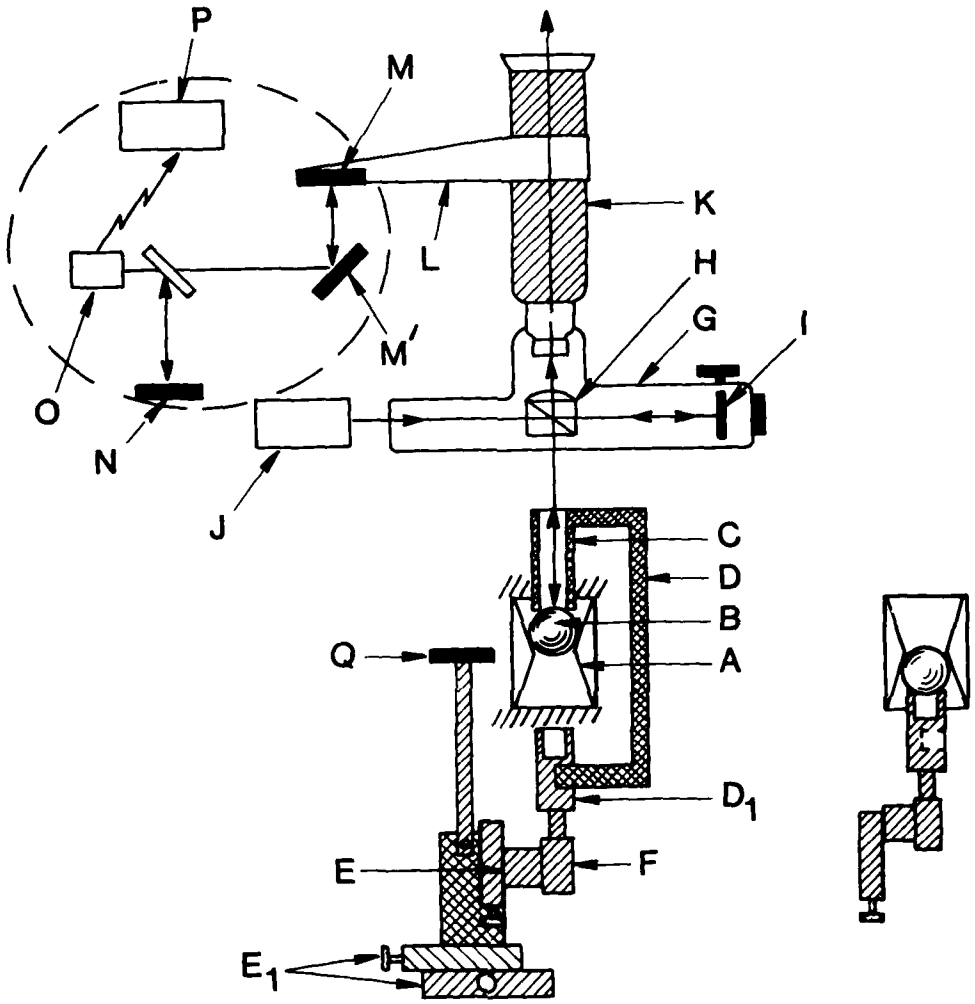


Figure 3. Schematic of Experimental Apparatus.

Experimental

The interferometric method of determining g_2 can be understood by means of Figure 3. A precision ball (the diameter to be determined) is placed in the upper cone of biconic sleeve, A. The ball is loaded to 300 grams against the upper cone by means of hollow tube, C, connected to cross-slide, E, through fixtures D, D_1, and load cell, F. Slide E is attached to two orthogonal, horizontally-acting cross-slides, E_1.

The interferometer, G, is a commercially available Michelson interferometer attached to body tube, K, of a microscope that has a precision fine focus control with a least count of 1 μm. This microscope is firmly attached to a vertically-acting cross-slide that serves as a fast-acting coarse focus control. The beamsplitter cube, H, in combination with other optical elements, is a 10X microscope objective. Therefore, when the microscope is focussed on an object, the interferometer can be adjusted so that the object is crossed with interference fringes.

A white light source, J, is used to illuminate the interferometer and, by means of the coarse and fine focus controls of the microscope, the interferometer is adjusted until the distance between the center of the beam splitter, H, and the uppermost point on the surface of the ball is equal to the distance between the center of H and I, the reference mirror of the interferometer (equal distance condition). When this condition obtains, circular concentric, high contrast interference fringes appear around the uppermost point on the ball. The fringe contrast decreases as the interferometer is moved so as to upset the equal distance condition. For the interference fringes to disappear, the interferometer must be moved on the order of the coherence length of the source, $\frac{\lambda^2}{\Delta\lambda}$, where λ is the mean wavelength and $\Delta\lambda$ is the wavelength range. For the white light source, J, λ and $\Delta\lambda$ are approximately 0.6 μm and 0.4 μm, respectively, so that $\frac{\lambda^2}{\Delta\lambda} \approx 0.9\ \mu m$ so that, if the interferometer is moved about 0.9 μm from the equal distance condition, the fringes disappear. However, the contrast of the fringes varies from a maximum value at the equal distance condition to a value of zero at $\frac{\lambda^2}{\Delta\lambda}$ and if the equal distance condition is upset by 0.3 μm, the contrast decrease is discernible by the human eye. Therefore, the location of the uppermost surface of the ball when loaded into the upper cone can be determined with an uncertainty of about $\pm$ 0.3 μm.

Bracket L, attached to the microscope body tube, supports a retroreflector, M, that is the movable mirror of another Michelson interferometer contained within the dashed circle on Figure 3. In this interferometer, N and M' are fixed mirrors, O is a helium-neon laser and detector and P is a bidirectional fringe counter that is used to determine the motion of M, the same motion as that of the interferometer, G. The interferometer within the dashed circle is a Hewlett Packard 5501A Laser Transducer System, the least count of which is $\lambda/4 \approx 0.16\ \mu m$.

After the equal distance condition has been obtained with the ball in the upper cone of the biconic sleeve, the counter, P, is zeroed, the load is removed from the ball and the tube, C, and fixture, D, are removed from D_1. The ball is removed from the upper cone and transferred to the tubular top of D_1. Cross-slide, E, is then advanced until the ball is seated in the lower cone under a load of 300 grams. The loading of the ball in the lower cone is shown on the right of Figure 3. A tube connected to a vacuum line is used for transferring the ball.

Interferometer, G, is then driven down by means of the coarse focus cross-slide and the fine focus control until the equal distance condition is restored.

As the interferometer is moved from the equal distance condition for the ball in the top cone, the bidirectional counter, P, counts the passage of monochromatic interference fringes, and when the equal distance condition is reached with the ball in the lower cone, the distance between these two equal distance conditions (g_1 in Figure 2) is known. However, the biconic sleeve end separation is the sum of g_1 and of the ball diameter.

To determine the ball diameter, we proceed as follows: The biconic sleeve is moved, by means of the horizontally-acting cross-slides, E_1, so that an optical flat, Q, placed on a levelling plate, is intersected by the optical axis of the microscope. The microscope and interferometer are positioned so that the equal distance condition is obtained, with respect to the optical flat, whereupon a few straight line, colored interference fringes will be seen superimposed on the flat. The levelling plate is then adjusted so that the optical axis of the microscope is perpendicular to the optical flat. This condition means that the fringe spacing is infinite so that one fringe covers the entire optical flat. The equal distance condition is manifested by a white field, the central fringe. The field is colored (one color over the entire flat) when the equal distance condition is upset. The fringe counter is reset to zero and the ball to be measured is placed on the optical flat and held there by two magnetic strips glued to the flat. The microscope and interferometer are raised until the equal distance condition is satisfied with respect to the uppermost point of the ball. The diameter of the ball is given by the fringe counter reading. Since g_1 and d have been measured, the biconic sleeve end separation is known.

Error Considerations

There are a number of possible error sources that must be considered if the biconic sleeve end separation is to be accurately determined. These sources can be reduced to negligible values by properly aligning the apparatus and by working in a clean environment.

The central ray of the beam reflected toward the ball by the beamsplitter, H, must be directed along a diameter of the ball. If the central ray of the downward directed beam is displaced from coincidence with a diameter of the ball by the amount, δ, the ball diameter, d, will be in error by $d-d' \approx \delta^2/d$, where d' is the apparent ball diameter. Since, for $\delta \neq 0$, the measured diameter, d', is too small, the quantity g_2 will be too small. When the central ray is parallel and colinear with a diameter of the ball, the interference fringes are concentric circles, the luminance of a fringe being constant along the fringe. However, if the central ray is parallel to a diameter of the ball, but is displaced by an amount, δ, the fringes are ellipses, the ellipticity increasing with δ, and the luminance of a fringe is dependent upon position along the fringe. The minimum value of δ for which a change in the luminance along one of the white light fringes can be visually detected is about 0.051 mm for a steel ball of diameter about 4.8 mm, so that the uncertainty in diameter is $d-d' \approx 0.5\ \mu m$.

Another important consideration is the presence of foreign matter on the ball, the biconic sleeve and the optical flat used in the ball diameter measurements. Foreign matter on the optical flat causes a shift in the interference fringes as the fringes cross the foreign matter, or when a fringe is spread over the entire flat, by a color change at the location of the foreign matter. Foreign matter of diameter 0.5 μm can be detected in this manner.

Foreign matter between the ball and the biconic sleeve would cause the value of g_1 to be too large. A group of particles of mean diameter, p, between the ball and the cone will cause the ball to move away from the apex of the cone by an amount $\Delta h \approx \frac{p}{\sin\Theta}$, where Θ is the half-angle of the cone. For $\Theta = 9.75°$, $\Delta h \approx 6p$. If these particles are present along the line of contact for both cones, g_1 will be increased by $2\Delta h \approx 12p$. If, however, only one particle is between the ball and the cone, $\Delta h = 3p$, and if this obtains for both cones, g_1 will be increased by $\Delta h = 6p$. We think that a single particle between the ball and cone, for both cones, is the more realistic case. We determined g_1 ten times with $\sigma = 2.0\ \mu m$. Equating this to $\Delta h = 6p$, we obtain $p = 0.3\ \mu m$, a reasonable value for the size of a particle of foreign matter. This discussion shows the importance of cleanliness in these measurements.

Another source of error is the motion of the biconic sleeve when the ball is subjected to the loading force of 300 grams due to bending and displacement of components S, T, U, V and W, Figure 4, that support and connect the biconic sleeve to the vertically-acting cross-slide, E. This motion, in the direction of the applied load, causes the distance g_1 to be too small. To investigate this motion, a steel ball was placed on top of S, and the motion of the ball was measured interferometerically as the loading force on a ball placed first in the upper, and then in the lower cone, was varied. If, due to loading, the biconic sleeve moves down by y_1 and up by y_2 when the ball is in the upper and lower cones, respectively, then $(g_1)_{true} = (g_1)_{meas} + (y_1 + y_2)$. For F = 300 grams, $y_1 + y_2 = 0.5$ μm, while for F < 200 grams, $y_1 + y_2$ is negligible.

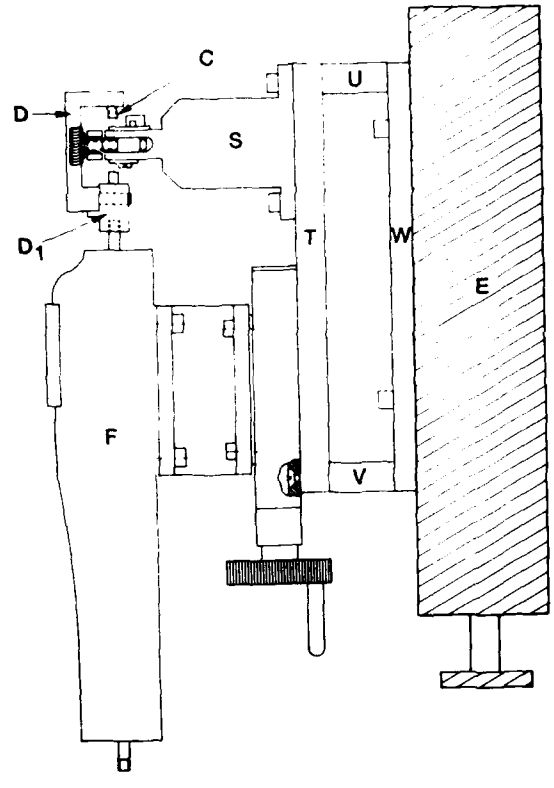


Figure 4. Diagram of Ball Loading Apparatus

The last error to be discussed is the so-called "cosine error", that arises when the motion of the retroreflector, M, Figure 3, is not parallel to the direction of the laser beam. A lateral displacement of the laser beam at M is observed if M moves at an angle to the laser beam. This lateral displacement can be effectively reduced to zero by adjusting the tilt of the plane mirror, M', Figure 3, below the retroreflector.

Results

The ball used to obtain g_1 is a master grade tungsten carbide ball manufactured by Industrial Tectonics, Inc. of Ann Arbor, Michigan. The manufacturer reports an average diameter of 4.7625 mm and, for 10 measurements, the sphericity, the difference between the maximum and minimum diameters, of 0.025 μm. Using the procedure described in this paper, d = 4.7622 mm for 12 measurements, with a standard deviation $\sigma = 0.8$ μm. The standard deviation of the average is $\sigma_{\bar{d}} = 0.2$ μm. Consequently, there is no significant difference between the two diameter determinations. The value of sphericity obtained by the manufacturer implies a standard deviation less than 0.025 μm, or about 30 times less than the value obtained using the procedure of this paper. We attribute the difference primarily to the presence of foreign matter, since the interferometric apparatus is not located in a clean room and since we have estimated from the standard deviation of the g_1 measurements that the mean diameter of a foreign particle is about 0.3 μm.

The quantity g_1 was measured ten times, using the tungsten carbide ball, and g_1 = 2.8032 mm, with $\sigma = 2.0$ μm and $\sigma_{\bar{g}_1} = 0.6$ μm. Since we have indicated that, for F = 300 grams, $y_1 + y_2 = 0.5$ μm, the true value is g_1 = (2.8032 + 0.0005) mm, or g_1 = 2.8037 mm. Consequently, adding to g_1 the average diameter of the ball, d, we obtain, for the biconic sleeve end separation, g_2 = 7.5659 mm.

The standard deviation of g_2 is $\sigma_{g_2} = (\sigma_d^2 + \sigma_{g_1}^2)^{1/2}$ and $\sigma_d = [(0.2)^2 + (0.5)^2]^{1/2} = 0.54$ μm, where the 0.5 μm is due to the uncertainty in knowing whether or not the central ray of the beam is coincident with a diameter of the ball. Using $\sigma_d = 0.54$ μm and $\sigma_{g_1} = 0.6$ μm, $\sigma_{g_2} \approx 0.8$ μm so that, g_2 = (7.5659 ± 0.0008) mm.



M. J. Saunders received the BA and MS degrees in Physics from the University of Virginia in 1950 and 1952, respectively, and the PhD. degree in Physics in 1956 from the University of Florida. He joined Bell Laboratories in 1956 and spent 15 years in the Whippany, NJ laboratory working on a variety of optical problems. For the past 15 years, he has been working in the field of Fiber Optics in the Norcross, Georgia Laboratory. In 1982 he received the Distinguished Member of Technical Staff Award. He is a member of the Optical Society of America and the New York Academy of Sciences.



Bruce V. Darden is a Member of Technical Staff at AT&T Bell Laboratories, Norcross, Georgia. He received a B.S. degree in Engineering from North Carolina State University in 1951, and held engineering positions with Western Electric until 1960 when he joined AT&T Bell Laboratories. He is currently a member of the Connector Systems Development Group.

AN EFFICIENT METHOD OF JOINTING FOAM SKIN STP AND PAPER INSULATED STP CABLES

Po Lung Yu, Rex Chou, Si Chong Chen, Lei Mean Shiea, Yiang I

Telecommunication Laboratories, DGT, MOC.
P.O. Box 71, Chung-Li, Taiwan, ROC 32617

ABSTRACT

In this paper, a new procedure for jointing air-core foam-skin STP and paper insulated STP cables was developed and field tested. Instead of a previous by-pass set up, silica gel powder was packed in a chain envelope of non-woven fiber and wrapped around splices core. The detailed procedure and practical evaluation of different desiccants is discussed. This method has been proved efficient and can be applied to either mechanical closure or lead sleeve.

Introduction

It was decided in 1985 to phase out the paper STP cables previously used in Taiwan, and to replace it with the new foam-skin STP cables. However, the number of paper STP cables installed in Taiwan was so large in quantity that it would take several years before a complete conversion is possible. At the same time, connection between these two types of cable would be unavoidable. Previous experiences on the connection of PEF and paper STP cable indicated that the transfer of moisture from the plastic insulated cable to the paper insulated cable would cause problems in the latter case. Therefore a method to prevent the transfer of moisture in such junctions was needed.

Foam-skin cable, or plastic insulated cable in general, has a higher resistance to the moisture than the paper insulated cable. Moisture usually has limited influence on the insulating resistance of the plastic insulated cables unless the cable is filled with condensed water. On the other hand, the insulating resistance of the paper insulated cables decreases, while its conductance and capacitance increase exponentially with the moisture content in the cable. Friesen and Windeler (1) studied the effect of moisture on paper cable and plastic insulated cable (PIC). They found that when air core pulp cable is pressurized via a PIC cable, the relative humidity of the air will build up to a point where it can degrade the electric properties of the pulp cable. They also suggested that the PIC-pulp cable junction should be plugged and another air source should be used for the pulp cable, in order to avoid the moisture problem.

In this study, a method of eliminating moisture from the foam skin pulp cable junction was proposed and field tested in experimental route. This method was able to remove the moisture blow out of the plastic cable, and keep the paper STP cable under a very low relative humidity for a long time.

Problem specification:

The FS STP cable used locally has a core thickness of 0.11mm, with about 0.0275 mm of skin(2,3). The radius of the pores in the foamed part was under 50A as determined by mercury penetration(4). Although the purchasing specification required that the dew point of the filling gas in the cable be below -4°C, the relative small pores of the foam skin could adsorb a large amount of water. Moreover, the core wires were so tightly packed in the cable that it became a difficult process to purge the moisture out of the cable. For example, when a one meter cut of a fresh cable was purged with 0.5 l/min of dry nitrogen, the dew point took seven days to drop from -4°C to -20°C There was an amount of 580 mg of water collected at the exit for this one meter cable.

It has been set that the compressed air used as air core for the paper STP cable must meet a dew point specification of below -20°C. Therefore, even without foreign water from outside the cable, 580 mg of moisture must be removed per each meter of foam skin cable ahead of the junction before the compressed air can be passed into the paper insulated cable.

Purging the FS cable with dry air

before connection would be impossible as it was found that it took almost a week just to dry ten meters of FS cable. Using another air source for the paper insulated cable as suggested by Friesen and Windeler was also impractical since extra air source would not be conveniently available at the junction site. We were therefore forced to consider a direct way of removing the moisture at the junction.

A desiccant unit was first proposed and subjected to field test at some experimental junctions. The junction was plugged at the center, and air nozzles were made at both side of the plug. Air was bypassed through a drier before entering the paper cable side. Dew point measurement on the paper cable side indicated that the moisture was effectively removed. However, there were other problems associated with this practice found in the field test. For example, local manhole are typically crowded with cables and junctions. They are mostly filled with water or at best very humid. A desiccant unit occupied too much space in the manhole. Making gas nozzles on junction was a difficult work in such a environment. The bypass tubing as well as the desiccant unit corroded quickly in the wet condition of the manhole, which cause additional problems.

The proposed solution

The desiccant unit was finially replaced with a direct approach of encapsulation of the moisture adsorbent in the junction body itself. The new approach occupied less space and was easier to work with. No gas nozzle was needed which means less corrosion problem. It can be used with any existing cable junction structure without much trouble.

There were two possible choice of desiccant(5) materials, molecular sieve and silica gel. Molecular sieve has a strong affinity toward moisture, and saturated at a very low humidity in a short time. It require a very high temperature to regenerate, which is impossible to attend on site. Silica gel, on the other hand, has a lower regeneration temperature. It change color on the adsorption of moisture. This would be a very indicative sign of the residual desiccant ability.

It was found that small silica gel packages were commercially used in many food and drag container. These packages were made of about 5 grams of silica gel in a non-woven fibber envelope. It could be purchased as a chain of 50 continuous envelopes. This form of packaging is very suitable for our purpose. Based on the sorption capacity of silica gel and the amount of moisture in the FS cable, it was determined that four of this 50 envelope chain were needed for drying each kilometer of FS cable.

These chain of desiccant packages were used to wrapped around the core body of the cable junction after the copper wires were cornected. Other than this step, all the other procedures of making a cable junction were the same as usual. The desiccant packages were regenerated at the hot air blowing step, which was commonly used to dry the core body in the convensional procedure. Only in this case, a longer purge time of one and half hours was needed.

The envelopes chain of desiccant was showed in photo 1. They were about 5 cm in width, and could be mananged easily. A half assembled junction was showed in photo 2,3. The desiccant packages did not increase the junction size by too much. Since there was very little change made to the conventional junction method, this proposed procedure need practically no training at all.

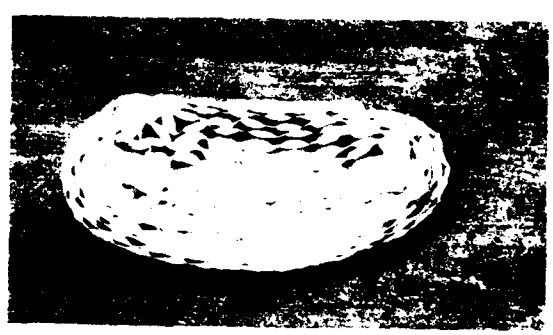


Photo 1 The envelopes chain of silica gel



Photo 2 A half assembled lead sleeve closure with desiccant envelopes



Photo 3 A half assembled mechanical closure with desiccant envelopes

Field test result

Three test routes each with a 1.1 Km long FS cable were connected with paper STP cables. The supply air was kept at 0.5 l/min with a dew point of -53°C. The dew point on the paper cable side was constantly monitored. It was -20°C when the junction was first completed. it gradually raised to -10°C a month latter. At which instance, the junctions were reopened, and hot air purge was again applied for another hour. The dew point at the paper side quickly dropped to -20°C after this regeneration. This value of dew point last for more than half year without much increase since then.

Conclusion

A method of applying desiccant material directly at the junction of foam-skin to paper cable was proposed. It was easy to use and made very little change to the original procedure of cable junction. No extra training was needed. If it is combined with a mechanical closure, regular regeneration could be conveniently made to ensure the dryness of the air going from the foam skin cable side to the paper cable side. The problems associated with the moisture in the paper STP cable could thus be eliminated

Acknowledgements

The authors wish to thank the president of Telecommunication Laboratories for permission to publish this paper and to acknowledge the contribution of Dr. A.S.T. Chiang for his helpful discussion and assistance in the prepration of this paper.

References

1 Friesen H. W., Windeler A. S.; Bell Telephone Laboratories, P148-180, IWCS, 1966.

2 Jitsukawa M., etc. " A method for manufacturing polyfin insulated communucation cable by solvent injection foaming process", IWCS 1970.

3 D.G.T. "FS-STP cable specification", ML 1021-0, July, 1985.

4 Akira Tsujikawa, "A comparison of PEF and Foam-Skin cores", p9, IWCS.

5 Hillar M, Rootare, "Advanced experimental technique in powder metallurgy", p225-252, Plenum Press, New York, 1970.



Mr. Po Lung Yu received his M.S.in Chemistry in 1972 from National Taiwan University. He joined Telecommunication Laboratories (T.L) in 1983 and now is the vice leader of out-side plant group in out-side plant department.



Mr. Rex Chou received his B.S. in electrical engineering in 1970 from Chung-Yuan University and joined Telecommunication Laboratories in 1978. He is the group leader of optical fiber cable implementation.



Mr. Si Chong Chen graduated from Chung-Yuan University in 1968 with a B.S. in Chemistry. He joined T.L. in 1984 and is a member of out-side plant department.



Mr. Lei Mean Shiea graduated from Kun-Shan Technical Institute in 1974. He is now a staff engineer of optical fiber cable implementation group, T.L.



Mrs. Yiang I received her M.S. in Chemistry in 1979 from Rutgers University, Piscataway (U.S.). She is currently the group leader of out-side plant in T.L.

COMPARISON OF SINGLE-MODE SPLICE LOSS MEASUREMENT METHODS

A. F. Judy, J. F. DeVeau, K. M. Yasinski

AT&T Bell Laboratories
Norcross, Georgia 30071

Abstract

Laboratory and field measurements on single-mode splices verify that the OTDR, the Local Splice Alignment and Measurement method and the two-point transmission measurement are in good agreement. The ability to construct low loss mechanical splices in the lab and field is verified.

Introduction

The easiest and most common methods for measuring splice losses in the field are: (1) local detection' and (2) Optical Time Domain Reflectometry (OTDR). Both are 'secondary' measurements that detect scattered power and infer splice loss. A 'primary' splice measurement method is the two-point, cut-back (2PCB) transmission loss measurement. However, it is a destructive test and cannot be performed on installed splices. This paper presents experimental data that verify that the secondary methods agree with the primary one when a variety of single-mode fibers are randomly spliced. The approach will be to establish the repeatability of each method and then to make comparisons between them.

Measurement Methods

The three measurement methods to be compared are shown schematically in Figure 1. They are described below along with the procedures used to determine the repeatability of each method.

2 Point Cut-Back

The 2PCB method measures all the power in the fiber immediately after and immediately before the splice. In each case the fiber is broken and the power measured with an InGaAs detector and lock-in amplifier. The 2PCB repeatability is determined by sequentially rebreaking the fiber and remeasuring the power.

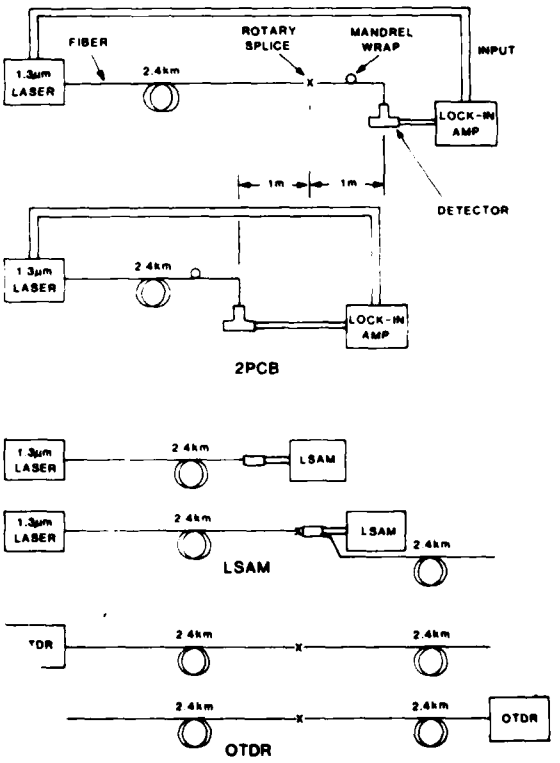


FIGURE 1. SCHEMATIC OF TEST METHODS

Local Splice Alignment and Measurement Method (LSAM)

The model 935A LSAM is designed to locally tune or optimize the Rotary Mechanical Splice.[2] The LSAM detects a portion of the light that is scattered or lost due to core misalignment. Since the amount of scattered light is proportional to the amount of misalignment, the LSAM is easily calibrated to measure splice loss.

The LSAM's repeatability is estimated two different ways: (1) by measuring the same splice 20 different times on the same LSAM and (2) by measuring 20 different splices on two different LSAMs.

OTDR

The OTDR repeatability is determined by measuring 30 different splices on two different Anritsu MW95A OTDRs. Each splice is measured in both directions resulting in 60 uni-directional measurements or 30 bi-directional ones.

TABLE 1. REPEATABILITY OF TEST METHODS

Test Method	No. Samples	$\bar{X}$ (dB)	CI (dB)	σ (dB)	CI (dB)	Evaluation Procedure
2PCB	20	na		.013	(+.005,+.004)	Repeated Meas.
LSAM	20	.001±.004		.006	(+.003,+.002)	2 Units Compared
LSAM	20	na		.006	(+.003,+.002)	Repeated Meas.
OTDR (Field)	60	.004±.003		.010	(+.002,+.002)	2 Units Compared
OTDR (Field)	30	.004±.004		.008	(+.003,+.002)	2 Units Compared

Repeatabilities

Table 1 summarizes the repeatability results. Each line in the table corresponds to one of the five procedures described above. The principle metric of repeatability is the standard deviation (σ). It is shown with its 95% confidence interval (CI) as determined by the minimum-interval Chi-square test. The repeatability of a single measurement is approximately 2.58σ.

When two test sets are compared, Table 1 lists the mean difference ($\bar{X}$) between the two. Its CI is calculated from a "Student's t" test. The σ shown is that of a single measurement, i.e., the σ of the difference divided by √2.

All three methods exhibited acceptably low σ's indicating good repeatability. Since the bi-directional OTDR is the average of two uni-directional readings, its σ should be the uni-directional σ divided by √2. This is close to the ratio obtained.

Comparison Between Methods - Lab Results

To compare the three test methods we assembled 15 splices between 30 unmatched 2.4-km single-mode fibers (8.5/125 μm, AT&T's standard depressed cladding design). Some of the rotary splices were purposely detuned to yield a variety of splice losses. Each splice was measured with an LSAM during assembly, then bi-directionally with two OTDRs, and then by the 2PCB method. All measurements were made at 1.3 μm. Table 2 summarizes the results.

TABLE 2. COMPARISON OF THREE TEST METHODS

Test Method Compared	No. Samples	$\bar{X}$ (dB)	CI (dB)	σ (dB)	CI (dB)
OTDR1-OTDR2	15	.007±.006		.011	(+.008,-.005)
OTDR1-2PCB	15	.013±.007		.012	(+.008,-.005)
OTDR2-2PCB	15	.005±.010		.018	(+.012,-.007)
LSAM -2PCB	15	.032±.034		.062	(+.030,-.020)
2PCB-LSAM(<.15 dB)	10	.005±.009		.013	(+.009,-.005)
OTDR1-LSAM(<.15 dB)	10	.019±.011		.015	(+.010,-.006)
OTDR2-LSAM(<.15 dB)	10	.007±.012		.016	(+.010,-.006)
OTDR3-LSAM(Field)	32	.020±.012		.034	(+.010,-.008)
OTDR3	32	.046±.011		.033	(+.010,-.008)

Several conclusions are apparent. OTDR1 and the 2PCB agreed very well for all splices. OTDR1 averaged about 0.01 dB higher than OTDR2 and the 2PCB. The LSAM, OTDR2 and 2PCB all agreed to better than 0.01 dB for splice losses below 0.15 dB. (Normally the LSAM is tuned well below this level.) For larger losses associated with very misaligned splices (Figure 2), the LSAM tended to read high.

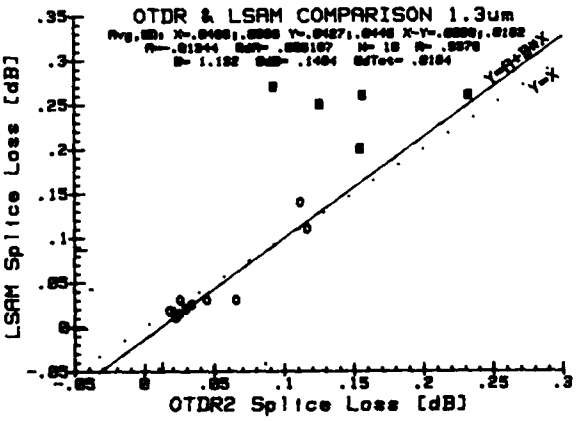


Figure 2. LSAM vs Bi-directional OTDR

Field Results

The last two lines in Table 2 shows the results of measuring 32 splices in the field with an LSAM and bi-directionally with a third OTDR. These splices were assembled by AT&T Communications' splicers using normal craft procedures. The results verified the good agreement seen in the lab. Note the low mean loss obtainable in the field.

Splices with large differences between OTDR readings taken in opposite directions tended to result in larger LSAM values (Figure 3). This has two causes. The principal one is that the OTDR differences are primarily caused by spot size mismatch between the fibers. This mismatch causes larger intrinsic splice losses. For example, the curve in Figure 3 shows the splice loss resulting from 0.02 dB of extrinsic loss and the theoretical intrinsic loss due to spot size mismatch.[3] A secondary reason is that spot size mismatch causes more power to be launched into symmetrical higher order modes than does a transverse offset. These modes will scatter out more quickly, thereby increasing the LSAM reading somewhat.[4]

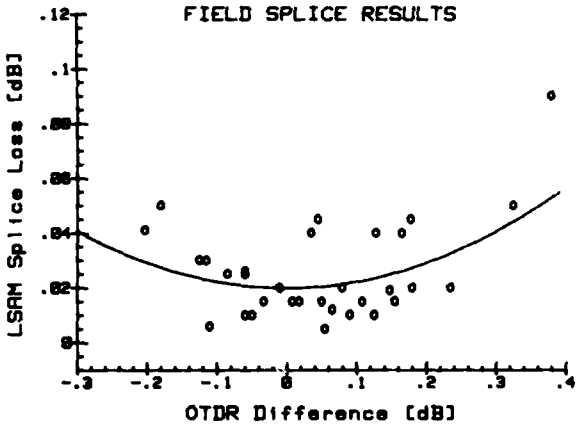


Figure 3. Effect of Spot Size Mismatch

References

1. C. M. Miller, OFC '82 Proceedings, THAA2, Apr. 1982.

2. C. M. Miller and G. F. DeVeau, OFC '85, MI2, Feb. 1985.

3. F. Kapron, et al, NBS Symposium on Optical Fiber Measurements, pp. 81-84, Sept. 1986.

4. I. A. White, Private Communications.



Arthur F. Judy is a Distinguished Member of Technical Staff in the Lightguide Systems and Applications Engineering Group. In his 20 years at AT&T Bell Laboratories he has worked on the theory, modeling and measurement of various transmission media including coaxial, multi-pair and lightguide cable. He has BSEE and MSEE degrees from the Universities of Maryland and Michigan.



Mr. DeVeau is a Member of Technical Staff at AT&T Bell Laboratories, Norcross, Georgia. After joining Bell Laboratories in 1957 he was involved with multipair cable design and development. Since 1980 Mr. DeVeau has been engaged in the development of fiber optic splicing systems.



Kenneth M. Yasinski is a Senior Technical Associate at AT&T Bell Laboratories in Norcross, Georgia. After joining AT&T Bell Laboratories in 1981, his main area of responsibility has been in the development of fiber splicing hardware and tools. Mr. Yasinski received his BMET degree from the Southern College of Technology in Marietta, Georgia.

ACCELERATED CABLE SHIELD CORROSION TESTING

Claus Kinder, John Lawler, Raymond O'Brien

General Cable Company, Edison, New Jersey

SUMMARY

The purpose of this study was to determine the corrosion rate for coated and uncoated metallic tapes using four different flooding compounds. Typically, field testing was required for this type of analysis. This method was time consuming and costly. Therefore, an accelerated aging process which simulates typical environmental conditions was developed to determine the corrosion behavior of tapes in a laboratory environment. The procedure involved the coating of tapes with flooding compound and then immersing them in an electrolytic solution with an applied AC voltage for seventy hours. The results of the flooding compounds tested revealed that the PE/PJ Type I and II based compounds showed the best overall protection, followed by polybutene and amorphous polypropylene.

SAMPLES

Specimens consisting of 2" x 6" strips as described below were prepared for evaluation.

1) Electrolytically Chrome Coated Steel (ECCS) - A 6 mil chrome coated steel protected on both sides with an ethylene acrylic acid copolymer.

2) Electrolytically Chrome Coated Steel (ECCS) - A 6 mil chrome coated steel protected on one side with an ethylene acrylic acid copolymer.

3) Tin plated steel - 6 mils thick.

4) Black Carbon Steel - 6 mils thick.

5) Fused Polyethylene Aluminum (FPA) - An 8 mil aluminum coated on both sides with an ethylene acrylic acid copolymer.

6) Aluminum - An 8 mil uncoated aluminum.

7) Electrolytically Chrome Coated Steel (ECCS) - A 6 mil chrome coated steel (see No. 2) but with an "X" scratched through the coating to simulate mechanical damage.

8) Fused Polyethylene Aluminum (FPA) - An 8 mil aluminum coated on both sides (see No. 5) but with an "X" scratched through the coating to simulate mechanical damage.

EQUIPMENT USED

1) Regulated Power Supply
2) Digital Multimeter

CHEMICAL SOLUTIONS

To represent typical field environments, the following 0.1N chemical solutions were used as electrolytes:

1. Sulphuric Acid, H_2SO_4 of ph 1.16 (Industrial Fill)
2. Ammonium Hydroxide, NH_4OH of pH 11.55 (Sand)
3. Acetic Acid, CH_3COOH of pH 2.5 (Clay)
4. Sodium Chloride, NaCl of pH 5.0 (Loam)

FLOODING COMPOUNDS

1. PE/PJ Type I
2. PE/PJ Type II with increased polyethylene percentage
3. Amorphous Polypropylene
4. Polybutene

BACKGROUND

The corrosion of a subsurface metallic component will occur if the following four conditions are present at the same time. These are:

- anodic state metal
- cathodic state metal
- electrical bond between anode and cathode
- common electrolyte environment

Current will flow in a complete cell from the anodic metal through the electrolyte to the cathodic metal. The current returns from the cathode to the anode by way of a metallic connection completing a circuit through the cell.

The study provides a comparison of coated and uncoated metallic tapes using four different flooding compounds. The rate of corrosion is based on their resistance to current flow.

A seventy hour test was performed and its results indicate the PE/PJ I and PE/PJ II show the best overall resistance to corrosion followed by polybutene and finally amorphous polypropylene.

TEST ENVIRONMENT

All the samples were placed in an air hood at room temperature for 70 hours. The electrolyte in all cases was 750 milliliters under a current of 1.5 volts. Additional testing was performed at elevated temperatures of 60°C, 70°C and 80°C using Black Carbon Steel. These samples were set up similarly using air ovens for a period of 24 hours.

SAMPLE PREPARATION

The above specimens were arranged as shown in Figure 1. A spacer made of polypropylene was used to prevent electrical contact and to keep the electrodes equidistant and equally immersed in the solutions throughout the experiment. Each beaker contained two anodes (positive electrode) and two cathodes (negative electrode). Four samples of each category were prepared for testing and evaluation.

PE/PJ I and PE/PJ II compounds were applied at 121°C (250°F). Samples were immersed in hot flooding compound and immediately allowed to cool at room temperature while being held upright.

The polybutene compound was applied at 138°C (280°F) similarly and the amorphous polypropylene was applied at 188°C (370°F).

Uncoated tapes were used as a control in each case.

The flooding compounds were also applied to Black Carbon Steel for testing at the elevated temperatures of 60°C, 70°C and 80°C in 0.1N Sulphuric Acid electrolyte. Black Carbon Steel was chosen because of its accelerated aging characteristics with the highest degree of corrosion in sulphuric acid. The samples were put in air ovens and examined after 24 hours.

DISCUSSION

The test results indicate that the application of flooding compounds does mitigate corrosion attach on the metal tape substrates. The best illustrated individual protection was achieved on the black carbon steel using PE/PJ I and PE/PJ II as hot coated flooding compounds. This was followed by polybutene and then the amorphous polypropylene. The Black Carbon Steel was used as an example because the differences can be seen most significantly, especially when Sulphuric Acid was being used as the electrolyte.

In all cases when the FPA tape was used, regardless of which flooding compound was applied, protection was outstanding. The bare aluminum had excellent protection as well with the flooding compounds. Actual test results were determined by the degree of corrosion when measured along the edges.

The tin coated steel resisted corrosion attack more than the black carbon steel. When the flooding compounds were applied under these same conditions, the polybutene performed better than the PE/PJ I and PE/PJ II in the acidic solutions.

ECCS with both sides polymer coated and coated with amorphous polypropylene is clearly superior to PE/PJ I, PE/PJ II and finally polybutene in that order.

The single sided polymer coating of the ECCS material showed us that PE/PJ I had the best protection followed by amorphous polypropylene. PE/PJ II and the polybutene showed similar results, just slightly less protection.

Tin plated steel indicated the polybutene had the best resistance to corrosion followed closely by the amorphous polypropylene, PE/PJ II and PE/PJ I respectively.

The accelerated aging at 60, 70 and 80°C showed that the polybutene created the best protection while amorphous polypropylene had a significant amount of discoloration. The PE/PJ II and PE/PJ I lost about 30 percent of the tape on the (+) electrode at 80°C while at the lower temperatures the corrosion was not as intense.

The 6 mil ECCS samples with both sides polymer coated had the best of the steel protection followed by the ECCS single-sided polymer coated, the 6 mil tin plate steel, and, finally, the black carbon steel.

CONCLUSIONS:

1. The application of polybutene, amorphous polypropylene, PE/PJ I and PE/PJ II on black carbon or tin plated steel tapes mitigates the corrosion attack and is most effective under acidic conditions.

2. The application of the subject flooding compounds on black carbon steel shows the worst scenerio using the four electrolytes with PE/PJ I and PE/PJ II having the best protection.

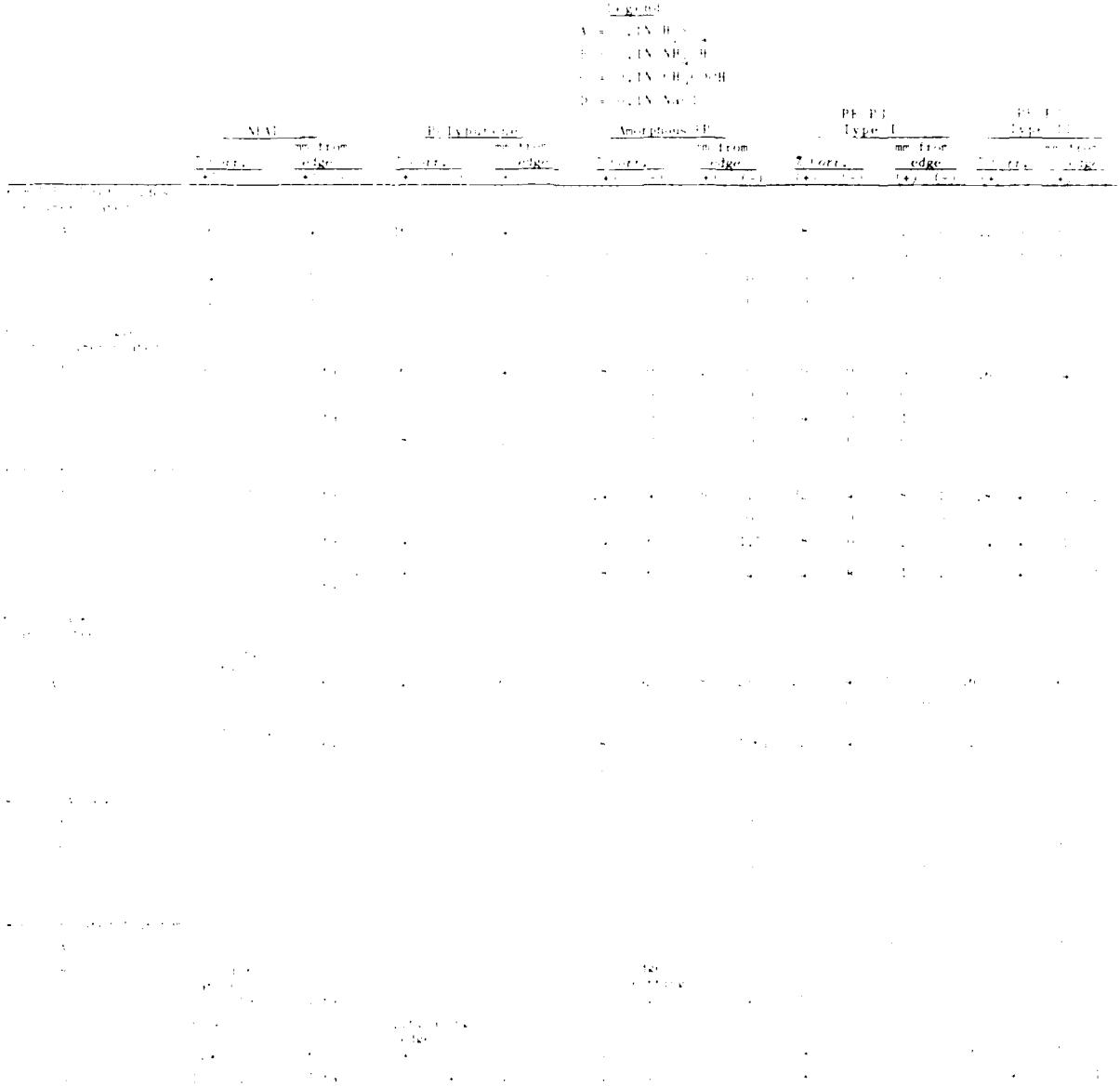
3. Bare aluminum had a very good protection using all four flooding compounds.

4. When flooding compounds are used for corrosion protection, their effectiveness is dependent on two factors:

   1 - type of metal
   2 - type of environment (electrolyte)

TABLE I

Percent Corrosion and Distance from Edge Corrosion





Claus P. Kinder, Manager of Research and Development, General Cable Company, a division of Penn Central Telecommunications, is a graduate of Fairleigh Dickinson University MBA 1984 and New Jersey Institute of Technology BSEE 1975. He is an active member in Research and Development Council of New Jersey and Director of Professional Affairs with the North Jersey Chapter of the Project Management Institute.



Raymond O'Brien has been with General Cable's Research and Development Center since his hire in 1981. Ray received his B.A. degree in Chemistry from Rutgers University in New Jersey. He has concentrated his efforts in the development of new materials for inside and outside plant cables and, more recently, new product development. He is a member of ASTM and ACS.



John D. Lawler joined General Cable in 1967. John was educated at Fairleigh Dickinson University in New Jersey. His present assignment is Manager of the New Products and Materials Research section of General Cable's Research Center in Edison, New Jersey. John has been deeply involved in the concept of "value added" products for both inside and outside plant cables. John holds several patents and has written various technical papers and articles.

COMPARTMENTALIZED SPLICE CASE

Alan L. Gittle, John D. Lawler

General Cable Company, Edison, New Jersey

SUMMARY

A splice case is featured which permits the joining of dissimilar copper cables (e.g. paper insulated pressurized to plastic insulated filled) within a single closure. Complete separation of the dissimilar cables is achieved by means of a dividing panel, establishing two individual compartments. Re-entry into either compartment for maintenance is easily accomplished without disturbing the integrity of the other compartment. Additionally, either or both compartments may be filled with encapsulate or pressurized.

BACKGROUND

In the Outside Plant Network, the use of paper insulated pressurized feeder cable is widespread. These cables feed a distribution network that is made up largely of filled plastic cables. A problem arises when splicing these two designs to one another. To do so requires an air core stubbing cable to block pressurization of the paper cable and make available a re-enterable splice at the junction with the filled cable. Figure 1 is a diagram showing the conventional method used when splicing pressurized paper to filled PIC cable. The amount of material and labor required is excessive, i.e. two splices and a stubbing cable. A section of stubbing cable remains unpressurized and, therefore, unprotected in the event of sheath damage. A major problem area in the Outside Plant Network is the splice point, here two splices are used to effect one. Additionally, an inventory of stubbing cables of different pair counts, copper gauges, lengths and sheath designs must be maintained. All of this translates into high installation and maintenance costs. Figure 2 depicts the proposed method for joining incompatible cable designs utilizing only one splice case.

DESCRIPTION

The novelty is the development of a "pass-through" module which mounts into a rigid membrane, dividing the closure into two individual compartments. Each module has a 100 pair tail extending from oppposite sides, providing a means for securing electrical connections of pairs between compartments. Each membrane contains one or more openings to accommodate either modules or blanks. If a module is not needed, a blank may be used in its place. Once mounted into the membrane an air tight seal is effected. Additionally, the method of assembling the closure allows re-entry into either compartment without disturbing the integrity of the other compartment. Figure 3 is an exploded view of a splice case with the separator panel dividing the splice case into two compartments. Figure 4 is a cut-away side view of the splice case showing the "pass-through" module and how it connects cable from one compartment to the other compartment. For example, let's assume we have an 1800 pair paper insulated pressurized feeder cable and we would like to splice into a 200 pair plastic insulated filled feeder cable. Straight, "pass-through" or butt splices are possible. The paper cable would enter one compartment where it would be pressurized and the plastic cable would enter the other compartment where it would be encapsulated. If the splice closure contains a membrane with three positions to accommodate either modules or blanks', two 100 pair modules and one blank would be used.

The "pass-through" module, although simple in appearance, performs the very difficult task of maintaining electrical continuity of paired conductors while sustaining a pressure tight seal about them under harsh environmental conditions.

This is accomplished through a combination of wire-wrapping and potting within the module. Effected is a moisture proof, gas tight seal capable of performing through 100 temperature cycles of -40°C to +60°C. The materials used have proven to be resistant to cable filling compounds and the harsh environmental conditions seen in the field.

The membrane is constructed to be a light-weight, rigid panel equally resistant to cable filling compounds and the environment. Its stainless steel core is coated with neoprene, allowing an easy means of sealing to the outer case of the closure and to the "pass-through" module.

CONCLUSION

It is feasible to join a pressurized paper cable and a filled cable in a single splice closure. The closure consists of physically and pneumatically isolated compartments with a means for electrically joining copper circuits from one compartment to the other. Additionally, each compartment may be pressurized or filled with an encapsulate and re-entered without disturbing the integrity of the other compartment.



Alan Gittle was graduated in 1981 from Rutgers University, College of Engineering, with a Bachelor of Science in Ceramic Engineering and joined General Cable in 1982 as a Research Engineer in the Value Added Products group. After two years he was promoted to Senior Research Engineer. During this time he developed splicing and pressure blocking procedures and ancillary products for telecommunications cables. He also trained craftsmen at Kennedy Space Center on installation techniques of fiber optic cable. Currently he has a patent pending on a compartmentalized splice case, the topic of this IWCS paper. In 1986 he was transferred to the Fiber Optic Division as Senior Product Development Engineer. Here he assisted in development of fiber optic cable and maintaining the technical documentation necessary for its manufacture. Additionally, he has lectured on fiber optic cable design, manufacture and installation.



John D. Lawler joined General Cable in 1967. John was educated at Fairleigh Dickinson University in New Jersey. His present assignment is Manager of the New Products and Materials Research section of General Cable's Research Center in Edison, New Jersey. John has been deeply involved in the concept of "value added" products for both inside and outside plant cables. John holds several patents and has written various technical papers and articles.

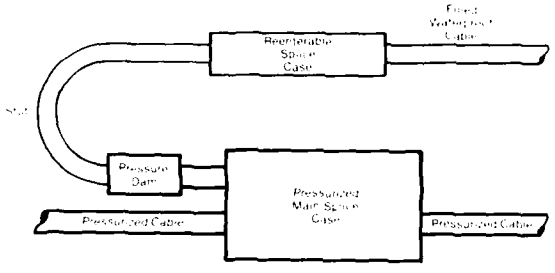


Figure 1. Present Day Method

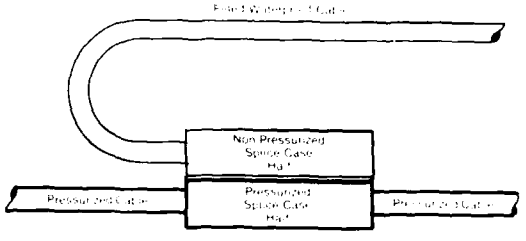


Figure 2. Proposed Method

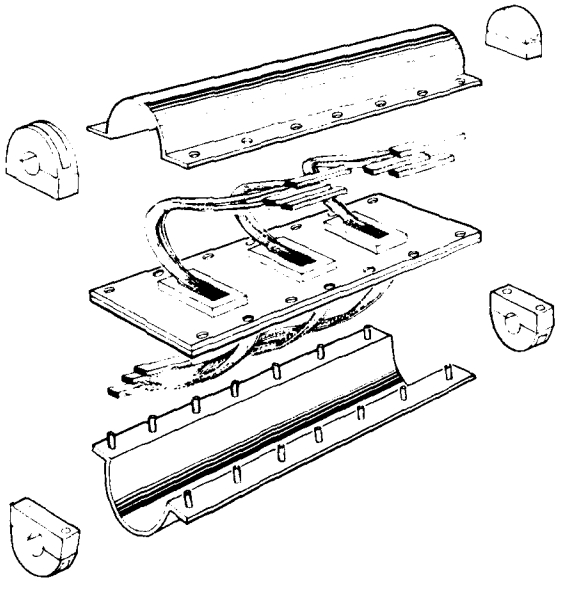


Figure 3. Compartmentalized Splice Case-Exploded View

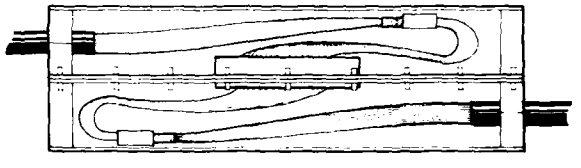


Figure 4. Compartmentalized Splice Case-Cut-away Side View

IMPROVEMENTS IN EFFICIENCY OF UV CURING SYSTEMS FOR OPTICAL FIBER BUFFER COATINGS AND FIBER COLORING

R W Stowe

Fusion UV Curing Systems
Rockville, Maryland

ABSTRACT

A major performance improvement in optical fiber curing systems offers a significant increase in the productivity of UV curing of buffer coatings in optical fiber production and for UV curable inks for fiber marking and identification. The small diameter electrodeless bulb is ideal for the full focused, elliptical reflector system in which the bulb is located at one focus and the fiber at the opposing focus. The performance improvements derive from design and construction changes which concentrate more light on the fiber coating. The most significant increase is achieved by concentrating the same amount of light power on a smaller target zone, this results in an increase of irradiance (light flux density) at the fiber line.

Background

UV materials and curing technology as applied to coatings on optical fibers has become well established over recent years. Advances in fiber draw technology and in coatings have been combined into fiber production systems capable of operating at draw speeds not achievable 5 years ago.

The requirements of a fiber coating are essentially mechanical: low modulus, high yield, low coefficient of friction, and high abrasion resistance. A coating also provides permanent environmental protection of the fiber from gas or liquid contaminants. Coatings need resiliency to reduce microbending in the fiber, high tensile strength to withstand forces which could be encountered in cabling operations, and hardness to facilitate spooling and handling.

UV curable formulations are available and being improved which can achieve the necessary physical characteristics required of the finished coating systems. Further, methods of control and precise application of the resin systems for single or dual composite coatings are well developed. Finally, UV curing systems which provide the correct quality and amount of UV energy in order to reliably develop the required physical properties of the polymerized coating are in widespread use. The curing system must deliver sufficient energy to the fiber to

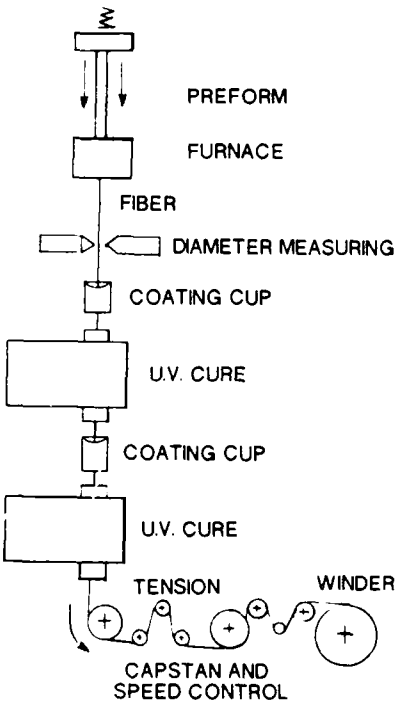


FIGURE 1
SIMPLIFIED DRAW TOWER ORGANIZATION

Reprinted courtesy of the author and the Society of Manufacturing Engineers. Copyright 1986, from Radcure '86 Conference Proceedings.

"keep up" with draw and coating speeds. Figure 1 illustrates a draw tower arrangement in which draw, coating and curing steps are carried out entirely in one vertical operation. Typically, faster draws require more individual lamps to provide the necessary UV energy, but space on high production rate towers is at a premium. As draw speeds increase with improved designs and materials, simply adding more lamps becomes less practical. As the advance to higher production speeds continues, UV sources will have to become more effective.

Situation

The most generally accepted arramgement for exposing the fiber to light from a UV source is the use of a full elliptical reflector, in which the UV bulb is at one focus of the ellipse and the fiber positioned at the other. In theory, the light is focused on the fiber. However, that theory works only when the source is an infinitely thin line. In fact, the light source has a necessary diameter, as small as 9 mm, but always much larger than we would wish. The laws of physics allow only a fraction of the radiant energy to be focused exactly at the target, because light originating at a distance from the centerline of the source will be focused at a similar distance from the centerline of the target. The target, of course, is the coated fiber. The combination of a relatively large diameter source and a small diameter target is not an ideal optical plan, and has a relatively low optical efficiency.

Approach

It becomes clear that the key to improving the performance of the curing system is to improve its optical efficiency and so increase the light striking the fiber surface. There are many factors affecting the optical efficiency, including geometry, surface area, source size and reflector shape, among them. If nominal improvements in each can be accomplished, then a significant improvement in overall performance can be achieved by compounding their effects.

Reflector

With an elliptical reflector, virtually all of the energy arriving at the target has been reflected at least once by a reflector surface. The incidence/reflection angle of a light ray at the reflector surface controls the travel of that ray to the target. See Figure 2. Small errors in the "purity" of the elliptical shape will have a serious effect on efficiency; the ray will be misdirected and not reach the target.

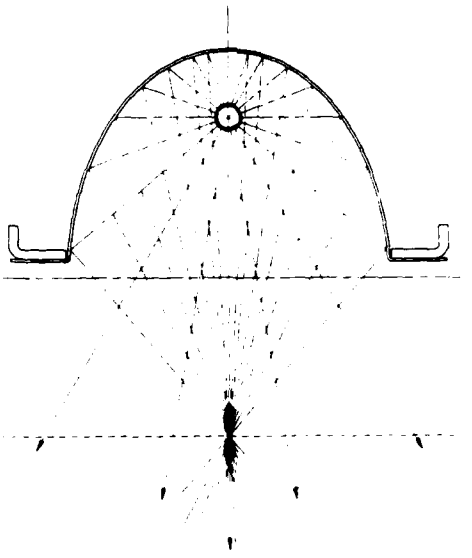


FIGURE 2
LIGHT RAY REFLECTION

The reflector is usually made from sheet material and bent or rolled into an approximately elliptical shape. This kind of reflector is easily removed for replacement. Upon assembly into a lamp housing, it conforms to the elliptical shape of the holder into which it is fastened. We found that this fabrication and assembly method caused small variations in "ellipticity" of the final surface. A change in method of forming the reflector produced the desired result: by carefully slip-roll forming of the reflector to a more exact "free" shape, the reflector is not subjected to bending and deforming when subsequently installed in its mounting. A substantially more pure elliptical shape is preserved.

The benefit of more exact shaping is illustrated by the dashed curve in Figure 3, a scan of intensity observed at a flat surface in the plane of the focus of the primary reflector. An increase in intensity at the focal area is accompanied by a narrowing of the width of the "focus." The same amount of energy has been concentrated in a narrower zone. With the primary reflector alone the peak intensity increase is about 15 percent; when the effect is combined with other portions of the complete reflector in the final system, the composite increase is nearly 30 percent.

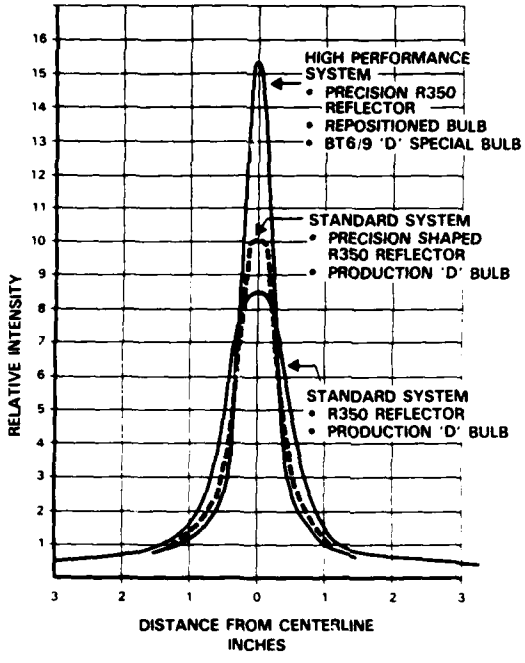


FIGURE 3
CENTER PEAK INTENSITY

A bulb position error of .040 inch can have an effect on the peak intensity of as much as twenty percent. The design of the tips of bulbs was changed so that the bulb sits more accurately in its supports, and the end supports were repositioned so that the bulb is exactly at the geometric focus. The benefit of repositioning the bulb (in conjunction with a modified bulb shape) is also shown in Figure 3.

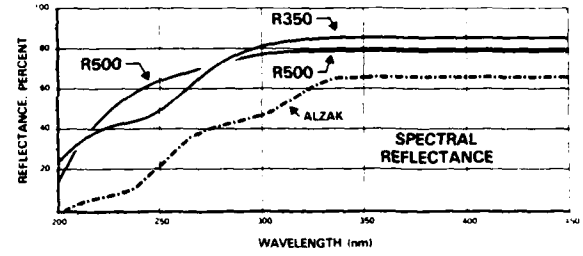


FIGURE 4
SPECTRAL REFLECTANCE

Reflector Coating

The spectral energy distribution which has generally found to be most effective in curing of buffer coatings is richest in the 350 to 400 nm wavelength range. The reflector should be its most effective in that same range. To achieve this, the reflector has a spectral enhancement hardcoat applied to increase its reflectivity in the region of 350 nm by approximately 8 percent. See Figure 4. The improved method of forming reflectors and the resulting reduction in metal stress in localized areas of the reflector when assembled further helps to avoid any microcracking or reduction of the specularity and high reflectivity of the coated reflector.

Bulb Positioning

As light will be transmitted from one focus of the full ellipse to the other, the bulb (source) must be positioned precisely at the primary elliptical focus. By comparison, this is not so critical for a lamp with only a primary reflector such as used for flat curing, in which a positioning error is hardly noticed. With less precise elliptical reflectors, the effects of variation in position are less detectable at the plane of focus.

Bulb

Reducing the effective diameter of the bulb and thus compacting the source has a direct effect on concentration of flux at the fiber. One design of an experimental electrodeless bulb, whose average effective diameter (8 mm) is slightly smaller than a standard model (9 mm) is compared to the standard in Figure 5 and its effect can be seen in Figure 3. A 15 percent increase in intensity is attributable to the smaller bulb diameter.

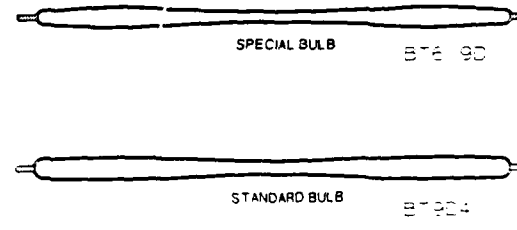


FIGURE 5
STANDARD BULBS

These changes to primary reflector, bulb position, reflector coatings and bulb are all on the lamp side of the UV system. Accordingly, these changes may have some benefit in flat curing especially in applications which respond to higher peak intensity. The benefits in 360 degree curing, as required for optical fiber, are considerably more dramatic.

Secondary Reflector, End Reflectors, and Back Reflector

On the fiber (target) side of the ellipse, the same precision is applied to the fabrication of the secondary reflector and positioning of the quartz tube (required for atmospheric isolation of the fiber). The quartz tube must be accurately located and be concentric with the fiber to avoid distortion by effects of refraction by the quartz.

End reflectors added at both ends of the elliptical cavity, collect a significant amount of light energy which would otherwise be lost. Their addition increased light to the fiber by approximately ten per cent.

One of the most novel reflector changes is shown in Figure 6. Upon examination of the light which "nearly misses" the fiber as it is directed toward the target, we realize that this light would normally strike the secondary elliptical reflector and be returned toward the source, not to the fiber! This light passes close by the fiber and toward the reflector as though it came from the region of the fiber. Returning it to the fiber requires a reflector of circular shape* rather than elliptical. This back reflector, when extended the length of the secondary reflector, is semi-cylindrical in shape. It is extremely important and effective in delivery of light to the "back" of the fiber; it increases the return of light to the far side of the fiber by over 50 percent, for a 25 percent contribution to the total increase.

Results

In order to evaluate what has been achieved in optical efficiency, a method of a measuring light at the fiber is necessary. Measuring light delivered to the fiber is a particularly difficult problem. As we have demonstrated, a significant increase of light impinging on the fiber can be effected without any increase of the light generated at the source. A radiometer placed at some location away from the fiber line will

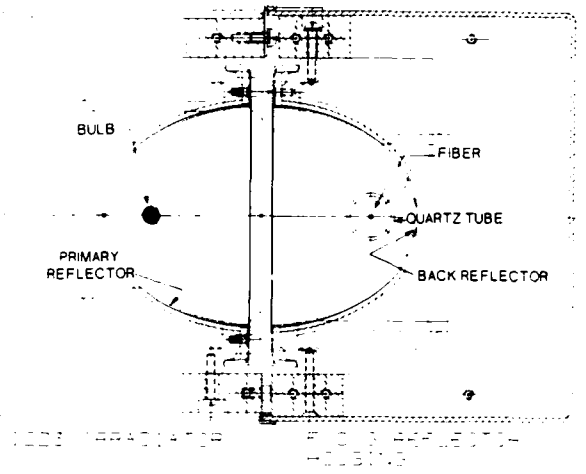


FIGURE 6
REFLECTOR SYSTEM

give information about the source and reflectors but not about optical efficiency. This requires a radiometer which, as closely as possible, approximates the size of the fiber and can be placed in the fiber position.

An instrument** was developed for this evaluation. It is a microradiometer consisting of a quartz "light pipe" probe (resembling a knitting needle) which has a small diameter (.060 inch) diffusing receptor at its tip and a UV sensor at the other. Light radially striking the probe tip is transmitted to the sensor. The tip can be freely moved about within the quartz tube and, owing to its rigid stem, can be accurately located. This instrument was used to probe the space in which the fiber travels. Measurements with this instrument permit important observations: 1) the comparative target irradiance from any one lamp system to another; and 2) the irradiance at the various positions in a plane perpendicular to the fiber. By plotting the points of equal irradiance, we can produce a map of the interior of the focal zone. These comparisons are shown in Figure 7.

The measured relative irradiance of experimental lamps which incorporated all of the changes discussed was increased by an average of 100 percent in comparison to the standard production lamp systems. The irradiance pattern is also more concentric with the quartz tube center. Concentricity is essential to the ability to mechanically locate the fiber in the "bright zone". The standard system, by comparison, is somewhat more forgiving of

* Patent pending by Fusion UV Curing Systems, Inc.

** Patent pending by Fusion UV Curing Systems, Inc.

fiber misalignment; more precise alignment on a tower will be required with the more highly focused system. The benefit of this precision, as can be seen, is substantially more light flux on the fiber.

Testing on production towers has indicated a general correlation between irradiance, as measured with the micro-radiometer described in this work, and increase of cure speed achieved. Not all physical properties of the coating will show the same degree of change with higher cure speed. In practice, factors such as accuracy of lamp alignment on a tower and production repeatability from assembly to assembly will affect the benefits.

Conclusion

The performance of a curing system for optical fiber can be increased substantially by increasing its optical efficiency. By concentrating on the unique geometry of curing systems, small variations in design have produced large effects. Significant cumulative effects were achieved by improvements in: reflector shaping enabled by tooling and methods changes, accurate positioning of optical components, reflector coating, reduction of bulb diameter, the addition of end reflectors and a special back reflector.

The need to evaluate the results in these studies of optical efficiency required an advance in the sophistication of measurement. For this, radiometers were devised to interpret the effective light at the fiber. Refinement of these instruments has led to new tools for quality control and has contributed to better understanding of requirements of instrumentation for process control monitoring. Variations will certainly result in new instruments for production on-line measurement and control.

The methods explored for improving these curing systems are expected to offer similar benefits in other applications such as optical fiber color coding, and wire marking.

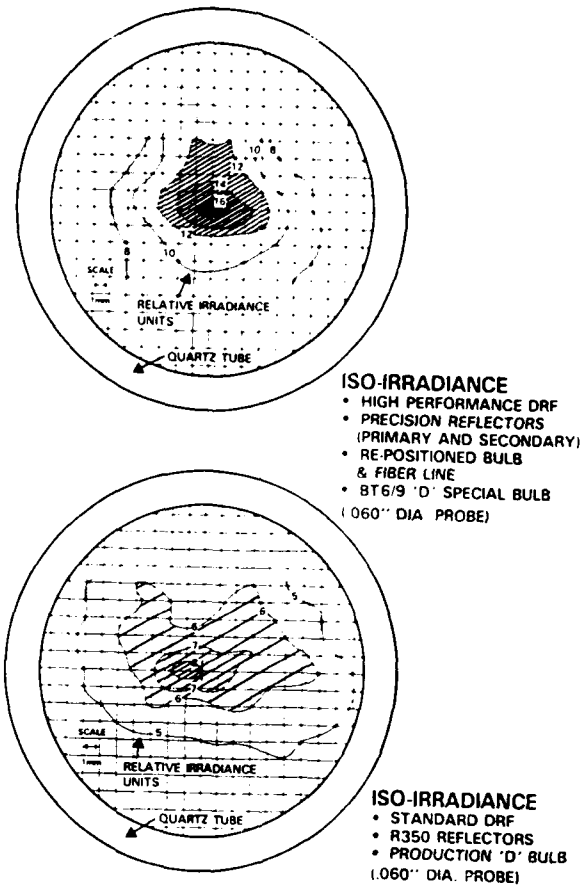


FIGURE 7
RELATIVE IRRADIANCE IN CURING ZONE SHOWING COMPARATIVE EFFECTS OF IMPROVEMENTS

STUDY ON TRANSMISSION CHARACTERISTICS OF UV CURABLE RESIN-COATED OPTICAL FIBERS AT LOW TEMPERATURES

H.Kuzushita , T.Zushi , T.Watanabe*, K.Imamura*, H.Tanaka*

MITSUBISHI CABLE INDUSTRIES, LTD
8 Nishinocho , Higashimukaijima , Amagasaki , Hyogo , 660 Japan
* 4-3 Ikejiri , Itami , Hyogo , 664 Japan

Summary

The low temperature excess loss of UV resin-coated optical fiber was studied systematically and statistically in order to clarify the mechanism and to design the optical fiber having low loss both under high lateral pressures and at low temperatures.

The experimental results using the experimental planning method showed that the primary coating material is the most important factor to affect the low temperature excess loss significantly. From the results of the study on various primary coating UV resins, it was revealed that the primary coating material having larger modulus at low temperatures prevents the excess loss caused by buckling. Dual-coated optical fibers with the new primary coating UV resin of which modulus is small at room temperature and gradually increases as temperature lowers, showed very low excess loss both under high lateral pressures and at low temperatures.

1. Introduction

It has been desired for resin-coated optical fibers to have low transmission loss both under high lateral pressures and at low temperatures. In order to prevent the excess loss caused by lateral pressure, widely used is the dual coating structure with a soft primary layer which enhances buffering effect and a hard secondery layer which enhances shell effect. The optical fiber dual-coated with organic polymers, however, shows excess loss at low temperatures by the excess contraction of coating materials.

Two opposing theories have been reported to prevent the excess loss at low temperatures. One is called Buffering Effect Theory that a softer primary coating meterial prevents microbending loss at low temperatures by its buffering effect.[1]-[3] An UV resin-coated optical fiber is considered to have large loss increase at low temperatures because UV resins have much larger moduli at low temperatures than silicones.[2][3] The other theory is called Buckling Theory that the contraction of coating resins in the direction of fiber axis incurs fiber buckling in the soft primary layer leading to loss increase,[4]-[6] and the primary coating material having larger modulus at low temperatures prevents excess loss caused by buckling.[6]

While the excess loss cased by lateral pressure can be prevented by designing the fiber structure so as to enhance buffering effect and shell effect, the two opposing theories on low temperature excess loss has made it complicated to design a dual-coated fiber having low loss both under high lateral pressures and at low temperatures.

This paper reports the experimental results of systematic and statistical study on the loss increase at low temperatures and the optimum design of the optical fiber coated with UV curable resins.

2. Factors of Low Temperature Excess Loss

The factors of low temperature excess loss of UV resin-coated optical fibers were investigated in detail using the statistical experimental planning method. The fibers for the experiments were a dual-coated fiber shown in Fig.1(a) and a fiber ribbon shown in Fig.1(b). Used was a standard GI type fiber with core diameter of 50μm, fiber diameter of 125μm, and relative refractive index of 1 %. The dual-coated fiber had the primary coating layer of a soft UV resin 0.25 mm$^{\phi}$ in diameter, and the secondary coating layer of a hard UV resin 0.3 mm$^{\phi}$ in diameter. The fiber ribbon was made by aligning five dual-coated fibers (shown in Fig.1(a)) in parallel and coating with a hard UV resin.

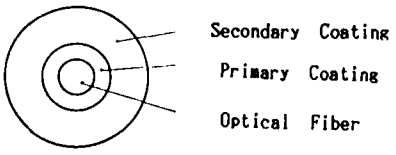
Nine factors in the fiber drawing and the ribbon coating processes, which may affect the temperature characteristics, and their interactions were arranged in L_{16} (2^{15}) type orthogonal arrangement table with two levels of conditions. Table 1 lists the factors and the conditions for experiments. Table 2 shows the moduli of UV resins used.

Sixteen types each of dual- coated fiber and fiber ribbon were prepared with varied coating materials and under varied production conditions based on the orthogonal arrangement table. Temperature dependence was measured by monitoring the loss change (λ=0.85μm) of a 500m long dual-coated (or fiber ribbon) coiled to approximately 300mm diameter under the temperature

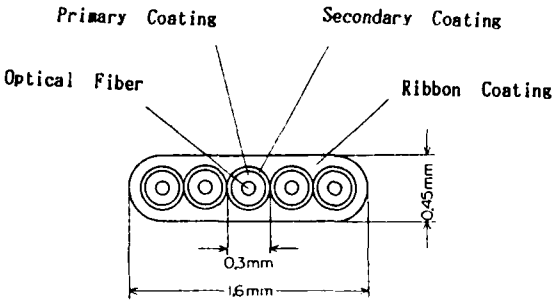
ranging from -50℃ to +60℃.

The results of measured excess loss at -50℃ were subjected to the analysis of variance. Table 1 shows the results, where V is the unbiased estimate of population variance and F_0 is the ratio of variance. As F_0 of factor B (primary coating material) is larger than $F_{0.05}$ on both the dual-coated fiber and the fiber ribbon, this factor is found to be significant at the level of 5%, showing that the use of resin I having larger moduli at low temperatures than resin II will result in lower excess loss. The other factors and interactions, whose F_0 values were smaller than the values of $F_{0.05}$, showed no significant difference between these conditions.

It was found that the primary coating material is the most important factor to affect the low temperature characteristics of both the dual-coated fibers and the fiber ribbons.



(a) Dual-coated fiber



(b) Fiber ribbon

Fig.1 Fiber structure

3. Excess Loss and Modulus of Primary Coating Material at Low Temperatures

In order to obtain the optimum primary coating material, investigated was the relationship between the moduli at low temperatures of various primary coating materials and the low temperature excess loss of the dual-coated fibers. Nine grades of soft UV resins shown in Table 3 were evaluated for the resin type and for the modulus temperature dependence.

Table 2 Young's modulus of UV resins

Resin	Young's modulus (Kg/mm^2)		
	25℃	-30℃	-40℃
I	0.75	22	35
II	0.39	0.53	0.90
III	60	140	160
IV	50	85	120
V	70	130	150

Table. 1 The factors and the analysis of variance of the low temperature excess loss (at -50℃)

	Factor	Condition		Dual-coated fiber		Fiber ribbon	
		1	2	V (*1)	F_0 (*2)	V (*1)	F_0 (*3)
A	Drawing speed (m/min.)	50	100	(1) 178	2.7	(1) 111	1.2
B	Primary coating material	I	II	(1) 657	10.1	(1) 4862	52.0
C	No. of UV lamps for primary	2	1	(1) 21	<1	(1) 581	6.2
D	Oxygen concentration for primary	20%	< 1%	(1) 83	1.3	(2) 10	<1
E	Secondary coating material	III	IV	(2) 15	<1	(1) 159	1.7
F	No. of UV lamps for secondary	2	1	(1) 6	<1	(2) 851	9.1
G	Oxygen concentration for secondary	20%	< 1%	(2) 206	3.2	(2) 30	<1
H	Ribbon coating material	V	III	−	−	(1) 850	9.1
I	No. of UV lamps for ribbon	2	1	−	−	(1) 52	<1
AXB	Interaction			180	2.8	94	1.0
AXE	Interaction			14	<1	47	<1
BXC	Interaction			19	<1	589	6.3
HXI	Interaction			−	−	27	<1
e	Error			65	−	94	−

(*1) (1) shows the better result was obtained under condition 1. (*2) $F_{0.05}$=6.61 (*3) $F_{0.05}$=18.51
(2) shows the better result was obtained under condition 2. $F_{0.01}$=16.26 $F_{0.01}$=98.49

Prepared were GI type optical fibers 125 μm^{ϕ} in fiber diameter coated with the UV resins shown in Table 3 as the primary coating layer 0.3 mm^{ϕ} in diameter and a hard UV resin (50 Kg/mm^2 and 85 Kg/mm^2 in modulus at 25℃ and -30℃ respectively) as the secondary coating layer 0.9 mm^{ϕ} in diameter. The excess loss of these fibers (λ=0.85μm) at low temperatures were measured. The experimental results at -30℃ are shown in Table 3.

The relation between the modulus of the primary coating resins and the excess loss of the fibers at -30℃ is plotted in Fig. 2 . Shown is a tendency that the larger the modulus of the primary coating material at a low temperature is, the smaller the excess loss is.

These experimental results are cosistent with the results of T.A.Lenahan[6] obtained from Buckling Theory. That is, the contraction of resin in the direction of fiber axis incurs fiber buckling within the soft primary coating layer and leads to higher loss and the primary coating material having larger modulus at low temperatures prevents loss increase by buckling. Too large modulus of a primary coating, however, may give microbending loss. The optimum modulus of primary coating material at low temperatures is considered to exist.

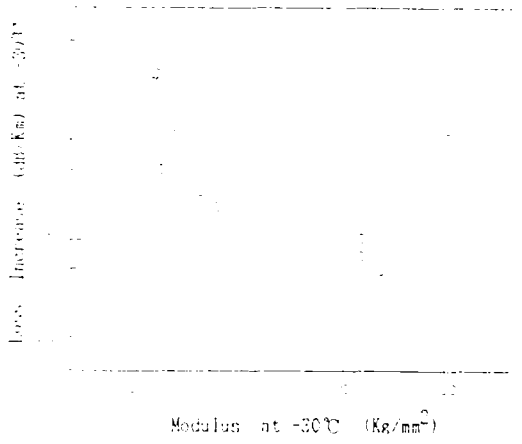


Fig. 2 Dependence of the excess loss on the modulus of primary coating at a low temperature

4. The Effect of Coating Dimensions

The experiments to study the effects of coating dimensions were made by measuring loss increse of a dual-coated fiber at low temperatures and under high lateral pressures. Used was the standard GI type optical fiber and a soft urethane acrylate for primary coating whose modulus is 0.30 Kg/mm^2 at R.T. and 5.4 Kg/mm^2 at -40℃, and a hard urethane acrylate for secondary coating whose modulus is 50 Kg/mm^2 at R.T. and 120 Kg/mm^2 at -40℃.

With regard to lateral pressure characteristics, loss increase ($\Delta\alpha_P$) was monitored when the fiber 1m in length placed between flat plates (500mm x 500 mm) was squeezed by applying load at a compression speed of 10mm/min.. Temperature dependence was measured by monitoring the loss change ($\Delta\alpha_T$) in the test fiber under the temperature (T) ranging from -50℃ to +60℃.

Fig.3 plots $\Delta\alpha_P$ (P=500Kg/m) and $\Delta\alpha_T$ (T=-40℃), where the diameter of the primary coating (d_1) was constant and the diameter of the secondary coating (d_2) was varied. Fig.4 plots $\Delta\alpha_P$ (P=500 Kg/m) and $\Delta\alpha_T$ (T= -40℃), where d_2 was constant and d_1 was varied.

Under a high lateral pressure, loss increase is smaller as d_1 and d_2 increase. This is because the buffering effect of the soft primary coating is enhanced as d_1 decomes larger, and the shell effect of the secondary coating is enhanced as d_2 increases. In view of temperature characteristics, on the contrary, loss increase is small when both d_1 and d_2 are small. These results are consistent with the result of T.A.Lenahan[6] obtained from Buckling Theory that thinner primaries and thinner secondaries prevent the excess loss caused by buckling.

Table 3 Properties of UV resins for primary coating and excess loss at a low temperature

Fiber No.	1	2	3	4	5	6	7	8	9
UV resins for primary Resin type(*)	a	c	b	a	b	b	b	b	d
Modulus (at 25℃)	0.75	0.39	0.38	0.50	0.57	0.25	0.14	0.16	0.10
(at -30℃)	22	0.53	0.38	15	15	110	0.15	0.16	0.12
Excess loss (at -30℃)	0.05	0.20	0.25	0.10	0.07	1.05	4.45	0.53	3.72

(*) a: polyesterpolyol type urethane acrylate
b: polyetherpolyol type urethane acrylate
c: polybutadiene acrylate
d: UV curable silicone

Since the conclusions to improve lateral pressure resistance and to prevent the low temperature excess loss are contrary, it is necessary to select the optimum coating dimensions which balance both the lateral pressure and the low temperature characteristics. The optimum coating dimensions were concluded as 0.25/0.50 mm^{ϕ} (primary/secondary) from Fig.3 and Fig.4.

5. Development of Optical Fiber Coated with New UV Resins

In order to obtain a dual-coated optical fiber with both better lateral pressure resistance and lower excess loss at low temperatures, new coating materials were designed. According to the above-mentioned experimental results, the desiable primary coating material is not only soft enough to prevent microbending loss incurred by lateral pressure but also stiff enough at low temperatures to prevent excess loss by buckling. The newly designed UV resin for primary coating is in modulus in the range from 0.1 to 0.3 Kg/mm^2 at R.T., but the modulus gradually increases as the temperature lowers down from 0℃ where the contraction of the hard secondary coating material becomes large, up to the range from 20 to 50 Kg/mm^2 at -40℃ . Table 4 shows the temperature dependence of modulus of a newly developed resin (UV resin A) for primary coating.

The desirable secondary coating material has a modulus large enough to prevent the excess loss by lataral pressures and its modulus is as little dependent on temperature as possible. The temperature dependence of the modulus of UV resin B developed as the secondary coating is also shown in Table 4.

A dual-coated optical fiber (125 μm^{ϕ} in fiber diameter, GI type) coated with th UV resins A and B in the optimum dimensions (pri./sec.=0.25/0.50mm^{ϕ}) was prepared and evaluated.

Temperature dependence of loss of the fiber is shown in Fig.5 and lateral pressure characteristics is shown in Fig.6. This dual-coated optical fiber demonstrated very low excess loss both at low temperatures (<0.05 dB/Km at -40℃) and under high lateral pressures (<0.02 dB under 500 Kg/m) .

Also prepared was a fiber ribbon coated with UV resins A (for primary layer) and B (for secondary and ribbon coating layer) in the dimensions as Fig.1 (b). The fiber ribbon has a good temperature dependence as shown in Fig.7.

Table 4 Temperature dependence of modulus of newly developed UV resins (Kg/mm^2)

Resin	60℃	25℃	0℃	-30℃	-40℃
A	0.16	0.15	0.50	10	25
B	30	65	–	105	120

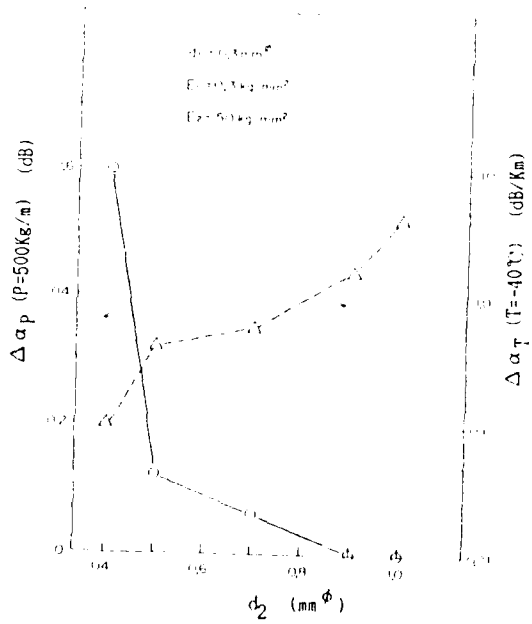


Fig. 3 Dependence of the loss increase on the secondary coating diameter

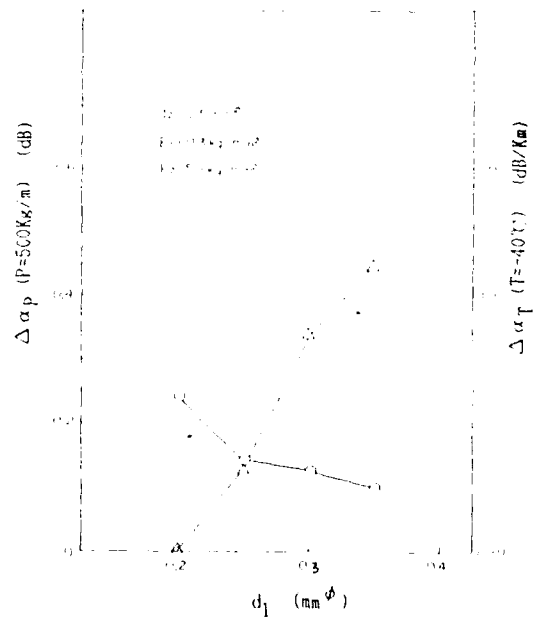
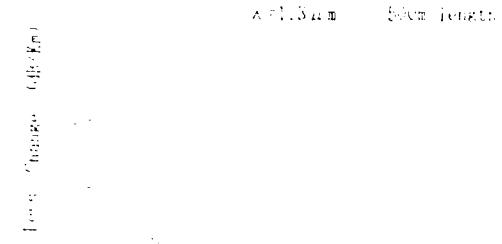
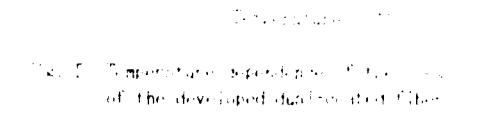
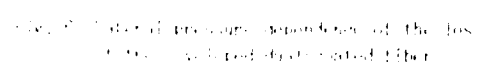


Fig. 4 Dependence of the loss increase on the primary coating diameter









6. Conclusion

1. The experimental results using the statistical experimental planning method revealed that primary coating material is the most important factor to affect low temperature characteristics of both the dual-coated optical fibers and the fiber ribbons.
2. From the results of the study on various UV resins for primary coating, it was clarified that the primary coating material having large modulus at low temperatures prevents the excess loss, caused by buckling.
3. The optimum coating dimensions of a dual-coated fiber which balance both the lateral pressure and the low temperature characteristics are 0.25~0.50 mm$^{\phi}$ (primary secondary).
4. Dual-coated optical fibers with the new primary coating UV resin of which modulus is small at room temperature and gradually increases as the temperature lowers, exhibited very low loss both under high lateral pressures and at low temperatures.

7. References

(1) D.Gloge, Bell Syst. Tech. J., 54, p.245 (1975)
(2) L.L.Blyler Jr. and A.C.Hart, Proc. 4th ECOC, Genoa, p.245 (1978)
(3) T.Kimura and S.Yamakawa, Electron. Lett., 20, p.207 (1984)
(4) Y.Katsuyama et al., Appl. Opt., 19, No.24, p.4200 (1980)
(5) T.Yabuta et al., Appl. Opt., 22, No.15, p.2356 (1983)
(6) T.Suzaki et al., AT&T Tech. J., 64, No.7, p.1565 (1985)



Hirokazu Kazushita
Mitsubishi Cable
Industries, Ltd.
6 Nishinocho,
Higashimukaijima, Amagasaki,
Hyogo, 660 Japan

H.Kazushita joined Mitsubishi Cable Industries,Ltd. after received a M.E. Degree in Applied Chemistry from Kyoto University in 1973. He is a assistant senior chemist of Materials Research Department and is engaged in development of coating materials for optical fibers. He is a member of the Institute of Electronics and Communication Engineers of Japan and the Society of Polymer Science,Japan.



Kazuo Imamura
Mitsubishi Cable
Industries, Ltd.
1-3, Ikejiri, Itami,
Hyogo, 664 Japan

Mr. Imamura, staff engineer of Telecommunication Engineering Department, is engaged in development of optical fiber cables. He received his M.S. degree in Electrical Engineering from Osaka University in 1983. He is a member of the Institute of Electrical Engineers of Japan.



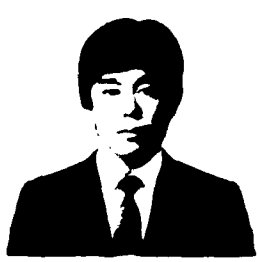
Toshihiro Ishii
Mitsubishi Cable
Industries, Ltd.
6 Nishinocho,
Higashimukaijima, Amagasaki,
Hyogo, 660 Japan

T.Ishii joined Mitsubishi Cable Industries, Ltd. after received a B.E. Degree in Synthetic Chemistry from Kyushu University in 1985. He is engaged in development of coating fibers for communication cables. He is chemist of Electronics & Communication Research Department and a member of the Institute of Electronic and Communication Engineers of Japan.



Mr. Tanaka
Mitsubishi Cable
Industries, Ltd.
1-3, Ikejiri, Itami,
Hyogo, 664 Japan

Mr. Tanaka, [illegible] engineer [illegible] Research Department, [illegible] coating materials of optical fiber cables. He received [illegible] degree in Electrical Engineering from Osaka University in 1971. He is a member of the Institute of Electronics and Communication Engineers of Japan.



Kunihiro Watanabe
Mitsubishi Cable
Industries, Ltd.
1-3, Ikejiri, Itami,
Hyogo, 664 Japan

Mr. Watanabe, engineer of Telecommunication Department, is engaged in development of optical fiber cables. He received his M.S. degree in Engineering from Kyoto University in 1985. He is a member of the Institute of Electronics & Communication Engineers of Japan.

TIGHT BUFFERING FOR OPTICAL FIBRES USING MULTIPLE COATINGS.

S.R. Barnes *, B.A. Eales **, M.M. Ramsey **, A. Summers *, M.K.R. Vyas **

* STC Telecommunications, Newport, Gwent U.K.

** STC Technology Limited, Harlow, U.K.

ABSTRACT

Over recent years acrylate coated fibre has dominated the market for external cables, in preference to the more traditional tight jacketed fibre which has poorer tensile properties and is much more bulky. There is still a need in specific applications for high performance tight jacketed fibre cables. A fibre coating system has been developed which combines the higher performance of acrylate fibres with the advantages of tight jacketing.

1. INTRODUCTION

In some situations, notably military and internal applications where cables must survive harsh environments and rough handling, tight buffer fibres provide the most superior opto-mechanical characteristics. These situations have been met using a fibre with a polydimethyl siloxane coating applied on-line with fibre pulling, and a second jacket of polyamide, polyester or fluoropolymer extrudate, chosen to meet the particular environmental conditions.

However, recently there has been a strong trend towards the use of single or multiple acrylate coatings applied on-line with fibre pulling, since their use can lead to considerable improvements in fibre production economics and provide a stronger fibre. Unfortunately, direct substitution of acrylate for siloxane coatings seldom leads to a satisfactory buffer, and acrylate is an unsatisfactory coating for some severe applications.

Frequently, these problems can be overcome by using an intermediate buffer layer, but if optimum buffering is to be achieved the moduli of all the coatings and their relationship must be considered. It is also necessary to consider the effects of subsequent extrusion on the layers already deposited, as well as the chemical compatibility of the layers. Such considerations exclude some coating systems, but solutions are possible that offer superior buffering to polydimethyl siloxane and higher modulus extrudates. STC has developed a multiple layer construction that has been successfully tested in a typical range of common cables.

2. FIBRE DESIGN

The choice of fibre encapsulation is also important in terms of improvement in macro- and microbending performance. Following the work of Lenahan, one can show that if a fibre is treated as a beam in an elastic medium, a force and movement balance yields the differential equation:

$$E_f I \frac{d^4y}{dz^4} + F \frac{d^2y}{dz^2} + Ky = 0$$

where

E_f is the fibre modulus

I is the moment of inertia of the fibre

F is the longitudinal compressive force

and K is the spring constant of the fibre

By calculating the longitudinal compressive force at a given temperature from the material properties of the fibre and coatings, the temperature at which the minimum bunching force arises can be determined:

$$F \text{ min.} = (E_f IK)$$

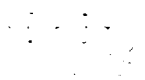
These calculations describe the performance of different coating designs accurately. Secondary parameters, such as coating concentricity, interlayer adhesion and fibre uniformity, make accurate prediction impossible.

The nylon/silicone design was always a leading design where consistent low temperature and general bend performance were essential; for instance, ruggedised constructions, patch cords, single fibre cables. However, a major problem with such two-layer constructions has been fibre strength. It has long been known that the nature of the fibre primary coat has influenced the resultant fibre strength. The use of methane acrylate coatings has allowed proof strain levels to rise consistently over recent years.

Further consideration of Lenahan's work would suggest that a hard/soft/hard structure could give improved thermomechanical characteristics over the standard hard/soft configuration of nylon sylgard. A further advantage of this approach is that one can utilise the strength advantages of methacrylate primary coatings if one used this as the first coating.

3. FIBRE MANUFACTURE

The fibre fabrication route is illustrated below:



4. FIBRE PROPERTIES

4.1 Properties of Multiple Coated Fibre

Multiple coating with primary acrylate and secondary nylon could improve fibre performance in several respects:-

- Very low environmental losses
- Lower temperature onset of fibre buckling
- Higher tensile strength
- Improved microbend protection

The very low environmental losses introduced by the primary multiple coating process can be judged from the fact that packaged fibres can often give an attenuation at 1.55 μm which is 0.1 dB/km lower than that measured at the cable factory. Presumably, this is because the multiple coatings introduce local microbends in areas other than that contributed by the drum on which the fibre was wound for measurement.

Because the fibre is locally supported by a hard acrylate coating within the soft buffer layer, the applied pressure represents a stiffer beam in compression and this lowers the temperature at which fibre buckling occurs. This critical temperature can be lowered further by the reduction in thickness of the low modulus layer or layers which is possible because of the improved microbend protection. Table 1 illustrates how this can lead to an extremely stable performance with temperature.

One of the major problems with fibres coated with standard silicone/nylon is additional to the fibre strengths. Yields of both fibre manufacture and cabling stages have tended to be unacceptable. With multiple coatings the strength of the acrylate coated fibres is preserved. Both the Weibull plot of the probability of failure of tensile tests on lengths of the acrylate and multiple coated fibres.

Microbend performance can be seen from the remarks above on attenuation and from tests in which, after winding twenty single mode fibre samples (on 75 mm, 50 mm and 25 mm mandrel), the mean increase in attenuation was less than 0.01 dB at a maximum of 0.1 dB. Also, when a weight was applied to a 10 mm strip of fabric with 1 mm pitch, the incremental loss could be observed.

5. CABLE PROPERTIES

5.1 Cabling

This fibre has applications from single-fibre ruggedised tails through to high-fibre-count internal cable.

Cable performance is identical to that of acrylate coated fibres so that the advantages of low tail cable and the improved survivability of similar fibres can be realised.

5. Performance

Fibre

Stripping	Mechanical
Proof test	> 1% possible
Dynamic strength	> 5 g/mm²
Microbend resistance	< 0.1 dB/m/kg/m
Environmental post cabling	< 0.1 dB/Km @ 1.55 μm
	< 0.5 dB/Km @ 1.55 μm
Attenuation	< 0.5 dB/Km @ 1.55 μm
	< 0.5 dB/Km @ 1.55 μm

6. MULTIPLE COATED FIBRE IN CABLES

The multiple coated fibre has now replaced the secondary coated fibre in a number of standard cables. In all cases the cable has shown comparable performance to its secondary coated counterpart. In the case of the FOCA tactical cable, however, the performance is significantly better than that demonstrated by the original FOCA cables.

A summary of the environmental characteristics at 1300 nm is shown in Table 1.

7. CONCLUSIONS

The technique provides a means of producing a tight buffered package from the standard 250 micron acrylate fibres for both single-mode and multimode applications.

The performance is a considerable improvement on standard nylon-silicone packages in the key areas of strength and temperature performance. Intrinsic fibre parameters can be selected at the acrylate coated stage with the confidence that there will be zero attenuation increment due to processing.

The fibre shows excellent characteristics in a range of standard cables; in particular, Internal PTT Cables or Ruggedised Cables (including the FOCA Tactical Cable).

TABLE 1

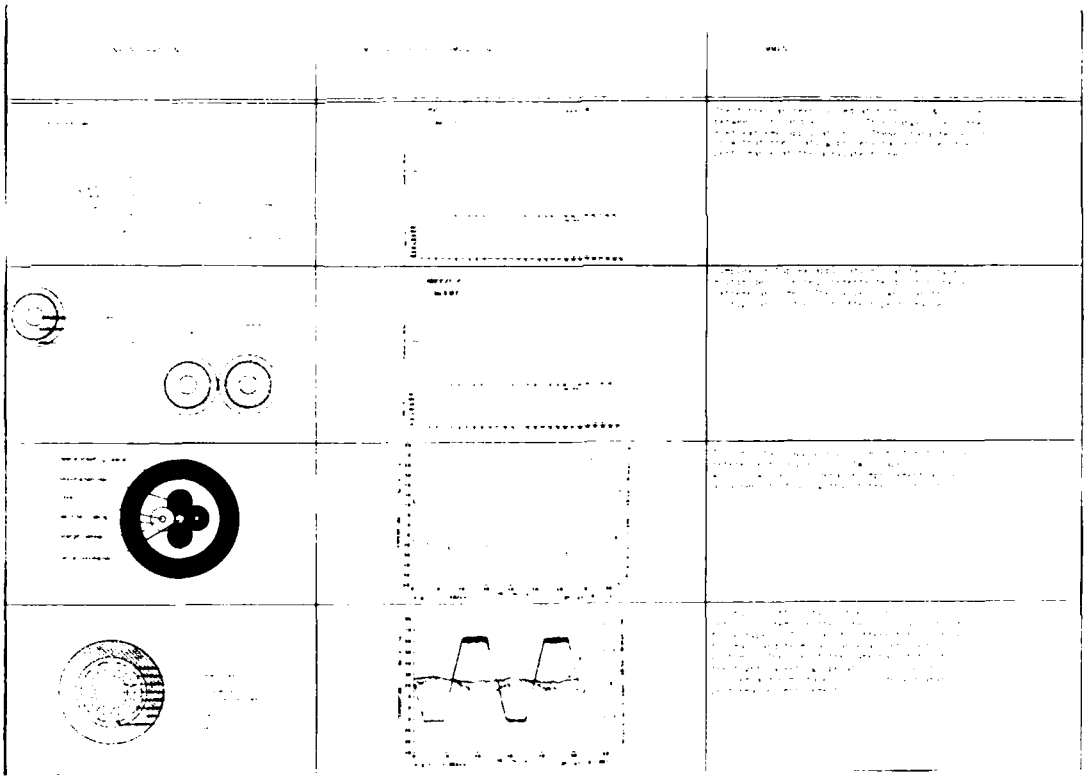


TABLE 2

Weibull statistics for polydimethyl siloxane coated fibres.

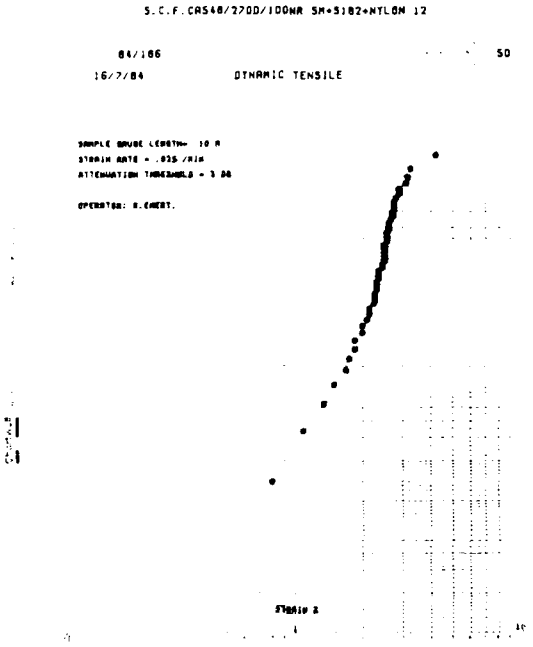
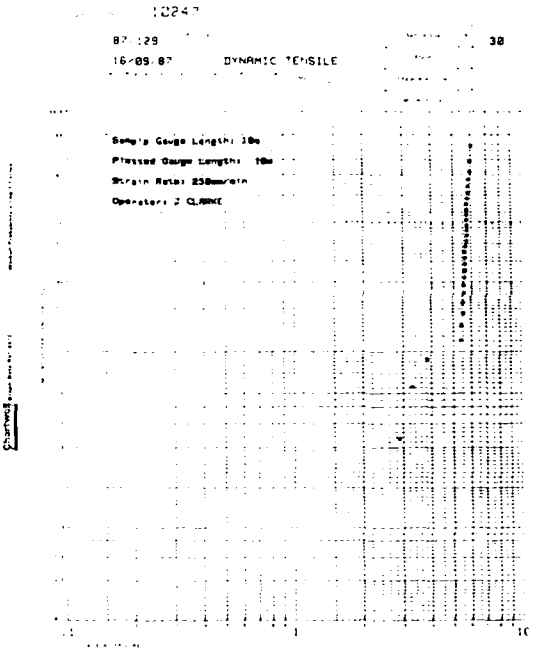


TABLE 3

Weibull statistics for multiple coated fibres.





Dr. J.E. Bowen,
STC Telecommunications,
Cable Products Division,
Wednesbury Street,
Newport,
Gwent,
NP9 0AG
U.K.

Dr. J.E. Bowen was born in Newport, England, and received a B.Sc.(Eng.) and Ph.D from Queen Mary College, University of London. After this he joined STL where he was involved in many aspects of cable design and development; in particular, cables for submarine applications. Later he concentrated on all aspects of the manufacture of optical fibre cables. Currently he is Technical Manager of STC Cable Products Limited, Newport.



K. Murray Ramsay,
STC Technology Limited,
Harlow,
U.K.

K. Murray Ramsay obtained a B.Sc. from University College, London in 1964. He is a Chartered Physicist and Fellow of the Institute of Physics. He joined STL after graduating in 1964 and was a member of the team setting up the first optical communication systems. He acted as Technical Manager for the TAT-7 Project in 1979 when optical communication systems were started there. He later returned to STL and is currently Chief Research Engineer for STC Cables Laboratory.

Mahesh Kumar R. Vyas,
STC Technology Limited,
Harlow,
U.K.

Mahesh Kumar R. Vyas graduated with an Honours Degree in electrical engineering from Queen Mary College, University of London in 1979. He joined STL in July, 1979, and whilst working on High Pressure Interband Carrier Transfer in Semiconductors, he did an external postgraduate course and gained an M.Sc. in Solid State Physics from the Imperial College of Technology, University of London in 1981. He has worked on various aspects of optical fibres and cables and is currently a Senior Research Engineer in the Optical Cable Technology Laboratory.



Brian A. Fisher,
STC Technology Limited,
Harlow,
U.K.

Brian A. Fisher graduated with an Honours Certificate in Physics from the Queen Mary College, London University in 1961. His career has so far been mainly involved in the development of semi-conductor lasers and associated systems technology for military and telecommunications use, in particular and responsible for the development of the first high reliability 1.3 μm single mode laser package used in Undersea and submarine systems use. He is currently a Senior Principal Research Engineer working in the Optical Cable Technology Laboratory.



Andy Simmons,
STC Telecommunications Ltd.,
Cable Products Division,
Wednesbury Road,
Dyfed,
Gwent,
NP9 0AG.

Andy Simmons was born in Rhoose, Wales, England, in 1961. He graduated from Aston University in 1982 with a B.Sc. in Electrical and Electronics. After this he joined STL as Commissioning Engineer, to develop and perform acceptance test methods for optical cable manufacture. In 1986 he became Quality Manager for the Optical Fibre and Cable Manufacturing Unit, from where he became Development Manager for optical cables, based at Newport.

AN IMPROVED COMPOSITE COATING FOR TIGHT BUFFER CABLE DESIGN

G. Kar C. K. Chien R. Kannabiran L. Amos D. Eccleston

Corning Glass Works
Corning, New York

A variety of UV cured acrylate coatings were evaluated to identify an improved composite coating for tight buffer cable design. The coatings were buffered with extruded nylon to 900 μm O.D. and evaluated for ease of mechanical stripping, lateral load resistance, and environmental stability. Results of this study are reported in this paper.

INTRODUCTION

Tight buffer fiber optic cable design is primarily used for pigtails, jumper cables, and other short length applications in data and telecommunication transmission systems. The cable design may contain single or multiple fibers; these fibers are either unstranded or stranded directly around a central strength member. The 900 μm OD nylon/silicone (Room Temperature Vulcanized) tight buffer coating has been extensively used in Japan for these, as well as long haul applications. Because of high material cost and slow processing speeds, one alternative approach in the United States has been the use of a 500 μm, composite, UV cured acrylate coating which is subsequently buffered to 900 μm with materials such as nylon, Hytrel®, or Polyvinyl Chloride. The important requirements for these acrylate coatings are:

a. Compatibility with the extrusion overcoating material and process.

b. Ease of mechanical strippability once buffered to 900 μm.

c. Zero shrink-back for trouble-free connectorization and for use as laser pigtails.

d. Resistance to lateral loading.

e. Stability of optical performance in the use environment.

A composite coating structure for optical fibers with at least two layers of coatings, a soft primary (inner) layer and a hard secondary (outer) layer, was first proposed by Gloge[1] based on a lateral load microbending model and has since become the preferred design for most applications. It has been shown that microbending can also arise from buckling of the fiber.[2] Most coating materials used today have thermal expansion coefficients two to three orders of magnitude higher than that of the glass fiber. If the thermally induced strain exceeds a critical limit at low temperatures, the coatings can exert a compressive stress on the fiber and buckle the fiber inside the primary coating. In order to protect the fiber from both lateral pressure and thermally induced buckling at low temperatures, the coating geometry, coefficient of thermal expansion, as well as the modulus versus temperature, play important roles. Also, for stable environmental performance, the coatings must exhibit low water absorption characteristics. In addition to the modulus, coefficient of thermal expansion and water absorption properties, other coating properties that are important to satisfy the requirements stated above are refractive index, controlled adhesion to the fiber for the primary coating, and coefficient of friction for the secondary coating. The primary coating refractive index should be higher than that of the silica cladding to facilitate mode stripping during cut back attenuation measurements on the fiber. Controlled adhesion of the primary coating to the glass fiber is desirable for ease of mechanical stripping of the coating, both under dry and humid environments. Lower

self-coefficient of friction for the secondary coating minimizes pay out difficulties during rewinding and overcoating process.

This paper reports the results of a recent study at Corning Glass Works to identify improved UV cured coating(s) suitable for tight buffer cable designs.

EXPERIMENTS

A variety of UV curable, urethane acrylate coatings were evaluated with respect to their rheological, mechanical, environmental, and other relevant properties. Based on the initial screening of nearly a dozen coatings, one primary coating and three secondary coatings, designated as A, B, and C respectively, were selected for detailed evaluation. Their properties are shown in Table 1. The dynamic modulus of each of these coatings was determined as a function of temperature using an Autovibron (Model DDV-2, I-Mass Corporation) and are shown in Figure 1. For ease of discerning coating induced microbending loss, 50/125 μm, graded index fiber was chosen for this study. The fiber was coated with the chosen primary and three secondary coatings using the conventional manufacturing process. The diameter of the primary coating layer was approximately 325 μm and that of the secondary coating layer was approximately 500 μm. Optical attenuation for each of these fibers was well within the specification for this type of fiber. These fibers were subsequently overcoated with Nylon 12 - ELY60, a commonly used thermoplastic jacketing material for optical fibers, by an extrusion process. The process conditions for fiber draw, coating, and extrusion were held constant for the three types of coatings under investigation. Care was taken to keep any excess loss due to overcoating to less than 0.2 dB/km at 1300 nm.

TABLE 1: CURED FILM PROPERTIES

	PRIMARY	SECONDARY A	SECONDARY B	SECONDARY C
Modulus (by Autovibron)	← See Figure 1 →			
Elongation %	120.0	16.0	30.0	15.0
Tg (From tan δ by Autovibron), °C	-49.0	68.0	87.0	55.0
Water Absorption, %	2.6	4.3	3.8	2.7
Self-Coefficient Of Friction	-	3.9	0.5	0.9

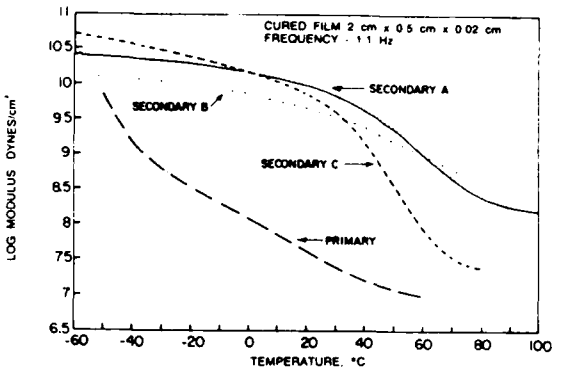


FIGURE 1 DYNAMIC MODULUS VERSUS TEMPERATURE FOR VARIOUS COATINGS

The performance of each coating combination was assessed through a series of tests. The standard cutback optical attenuation method was used to determine any coating induced loss. The lateral load microbending test was carried out using Instron 4202 from I-Mass Corporation. A 1.080 mm length of fiber was placed between two flat plates (surface finish ≈3 μm) and a load from zero to 1.000 Kg was applied. Optical loss increase at 1300 nm was monitored as a function of increased load.

Temperature dependence was determined between -60°C to +85°C on a 1 km length of fiber. The fiber was tested in a 12 inch diameter, loose coil configuration, and placed in an environmental chamber (Model 3471, Thermal Dynamic Engineering Company). Attenuation increase over that at room temperature was measured at 1300 nm after the fiber reached equilibration at the measurement temperatures.

The strip force was measured by measuring the force required to strip 1 inch of the coating from the end of a fiber. A motor driven Clauss No-Nik™ Stripper was used for this purpose. The force was detected by a Lebow Force Transducer (Model 7530). The pulling rate was 1 inch/minute.

To examine the coating shrink-back, one meter fiber samples were placed in a Blue-M Environmental Chamber (Model CFR-7652C) at 65°C and 70% relative humidity. The samples were removed after three days and measured for coating shrink-back.

The water soak test was conduced on 1 km long, 12 inch diameter loose coils of fiber. Attenuation change was measured as a function of time up to 14 days.

The tests conducted on both acrylate coated and nylon jacketed fibers were optical attenuation, lateral load microbending, temperature dependence, and strip force, while coating shrink-back and the excess attenuation due to water soak were measured on nylon jacketed fibers only. It should also be noted that all measurements involving optical attenuation were carried out at 1300 nm using a full flood launch condition in order to capture the worst case macrobending and microbending scenario.

RESULTS AND DISCUSSION

Lateral Load Resistance

Figures 2 and 3 show the lateral load microbending behavior of the three types of coatings with and without the nylon jacket. In both cases, coating C provides the best lateral load resistance followed by Coatings B and A, in that order. As expected, the nylon jacketing provides additional buffering against lateral pressure and increases the load required to produce any loss increase by a factor of approximately two. As a reference point, Figure 3 includes the data on a 50/125 μm, graded index fiber with RTV silicone and nylon coating to 900 μm O.D.. The acrylate coated fibers B and C compare quite favorably with silicone-nylon coating in this regard.

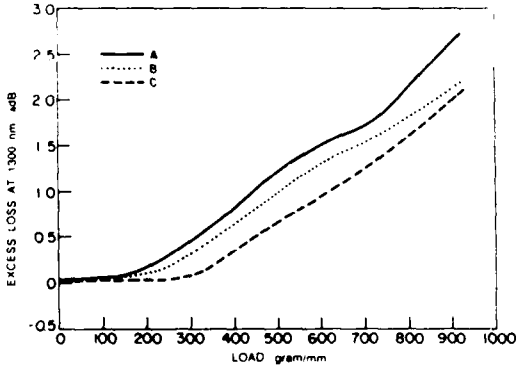


FIGURE 2 LATERAL LOAD RESISTANCE OF COATED FIBERS (500 μm O.D.)

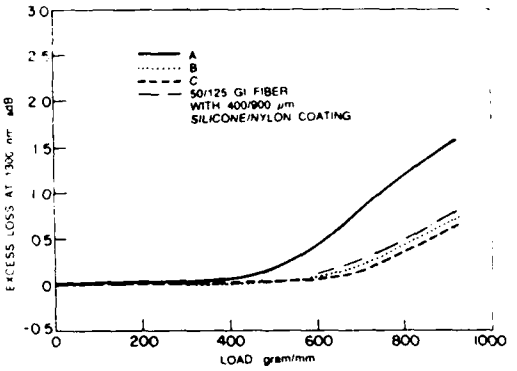


FIGURE 3 LATERAL LOAD RESISTANCE OF FIBERS AFTER NYLON JACKETING (900 μm OD)

Temperature Dependence

Figures 4 and 5 demonstrate the temperature dependence of these three coatings with and without the nylon jacket. On the as-coated samples, all three types of coatings performed adequately down to -60°C with the excess loss at 1300 nm less than 0.2 dB/km, suggesting very little thermal strain and buckling of the fiber due to coating modulus changes at lower temperatures. When these fibers were jacketed with nylon, the temperature dependence at lower temperatures increased. This is an expected result since the additional mass of the jacketing layer (combined with the fact that the polymers have coefficient of thermal expansion several orders of magnitude higher relative to the glass fiber) accentuate the thermal strain on the fiber at low temperatures.[2,3,4] It should be mentioned that the choice of a low modulus primary coating that remains soft at lower temperatures (i.e., low glass transition temperature, Tg), along with a higher modulus secondary coating, provide excellent resistance to lateral pressure while such a combination is more susceptible to thermal buckling at lower temperatures. Relatively speaking, Coatings B and C show reasonable temperature dependence ($\leq$ 1 dB/km) at -60°C, under full flood launch conditions. Coating A, on the other hand, shows higher losses at low temperatures. This cannot be explained purely by the modulus versus temperature behavior alone. The other factors that may be contributing to the observed behavior are the coefficient of thermal expansion[2] and the degree of slip between the acrylate and nylon coatings.[5] It was hypothesized[5] that low frictional force between the two layers could lower the compressive stress from the nylon buffer at low temperature and reduce buckling. The self-coefficient of friction

of Coating A is several times higher than those for Coatings B and C (Table 1). Assuming a similar trend in the frictional force between nylon and the various coatings, one would expect Coating A to exhibit higher losses at low temperatures. Again, as a reference point, data is included for a 900 μm O.D., RTV silicone-nylon buffered fiber which also shows high loss in a single fiber loose coil format. Since the silicone-nylon design typically yields high attenuation at low temperatures due to thermally induced buckling, it is a common practice to strand it directly around a central strength member to reduce buckling induced loss.[6]

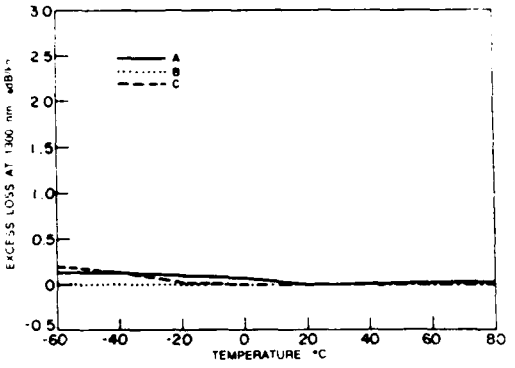


FIGURE 4 TEMPERATURE DEPENDENCE OF COATED FIBERS (500 μm OD)

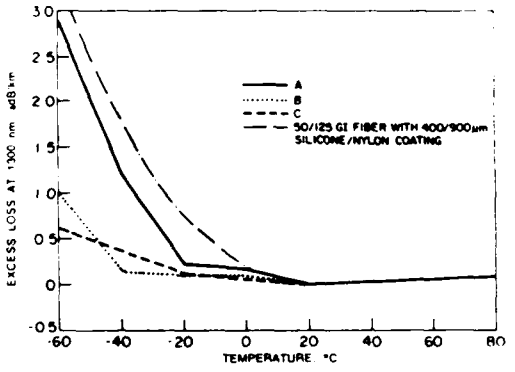


FIGURE 5 TEMPERATURE DEPENDENCE OF FIBERS AFTER NYLON JACKETING (900 μm OD)

From our study it appears that either Coating B or C can be successfully overcoated with nylon and be used in both stranded or unstranded cable designs without any concern for low temperature performance. While not a subject of discussion in this paper, it has been previously demonstrated[7,8] and confirmed in our experimental work that the extrusion process conditions such as melt temperature, line speed, cooling rate, and tension have significant impact on the excess loss due to jacketing, as well as the low temperature performance of the jacketed fibers. Based on this it can be concluded that optimal extrusion parameters may be different for different composite coating selections and overcoating materials.

Water Soak Test

Based on the lateral load resistance and temperature dependence results, the water soak test was performed at room temperature on B and C coating samples only, and the results are shown in Figure 6. The data indicate ≤ 0.1 dB/km loss increase for both coatings after 14 days, considered sufficient time to show any microbending or macrobending effect due to coating property changes.

In addition to the above tests, the ability to mechanically strip the coating was determined and the strip force data are presented in Table 2. All three coatings could be stripped without difficulty when dry. Compared to dry strip forces, the wet strip forces were lower. After a 24 hour water soak, the strip forces for these coatings dropped by 20% to 30% only, suggesting that reasonable control of adhesion in both dry and wet environments was achieved. None of the coatings exhibited any coating shrink-back after three days of exposure at 65°C and 70% RH.

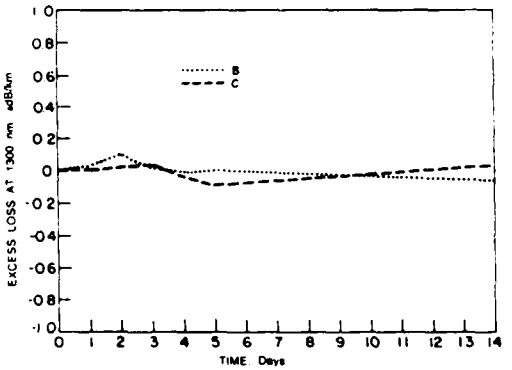


FIGURE 6 ATTENUATION CHANGE DUE TO WATER SOAK OF NYLON JACKETED FIBER

TABLE 2: PROPERTIES OF NYLON JACKETED FIBERS

	COATING A	COATING B	COATING C
Strip Force, Kg			
. Dry	1.37	1.35	1.52
. Wet (24 Hour Water Soak)	0.98	1.07	[illegible]
[illegible]-Back, mm	0	0	

SUMMARY

Based on this study, both Coatings B and C appear to be suitable candidates for tight buffer applications. These coatings are expected to perform well in indoor, as well as outdoor environments. Before either coating B or C is chosen as the next coating to pursue, further investigation in cabling studies are warranted. Additionally, it should be recognized in any event that the optimum overcoating conditions need to be determined with other commercially used overcoating materials, such as Hytrel® and PVC.

ACKNOWLEDGMENT

The authors wish to acknowledge David Shucavage for providing the coated fiber samples, Clint Hauber, Edwin Francis, and Kelly Jo Disbrow for experimental support.

REFERENCES

1. G. Gloge, Bell System Tech. J. 54, p. 245, 1975.

2. T. A. Lenahan, AT&T Tech. J. 64 (7), p. 1565, 1985.

3. A. Portinari and G. Grasso, 13th Int. Wire and Cable Symp. Proc., Fort Monmouth, NJ, p. 161, 1981.

4. K. Masuno and K. Ishihara, J. Opt. Communications, 1982.

5. H. Itoh, T. Kimura, and S. Yaurakawa, Electronic Letters, 20 (21), p. 879, 1984.

6. M. Komachi, H. Kashimoto, O. Ichikawa, and Y. Saitoh, Proc. ECOC, 1983, p. 235.

7. B. Hillerich, D. S. Parmar, and P. Schlang, 16th Int. Wire and Cable Symp. Proc., p. 367, 1977.

8. S. R. Barnes, P. G. Hale, J. N. Russel, S. V. Wolfe, Plastics in Telecommunication III, Plastics and Rubber Institute, London, p. 15, 1982.



Gitimoy Kar received his PhD in Materials Science and Engineering from the University of California, Berkeley, California in 1972. In 1973 he joined Corning Glass Works where he has worked in high temperature corrosion and electrochemistry, precious and refractory metals for glass melting and forming, glass ceramic finishing processes, and optical waveguide. Currently he is the Manager of Draw and Coating Development, Optical Waveguide Technology, in the Research and Development Division.



Ching-Kee Chien received his PhD in Polymer Chemistry from the College of Environmental Science and Forestry, SUNY in 1980. He joined Corning Glass Works in 1985 and is currently working on the development of polymeric coatings for optical fiber.



Rengan Kannabiran received his MS degree from the Indian Institute of Technology, Madras, India in 1971 and a PhD in Materials Engineering from the University of Pittsburgh in 1982. He was a Scientific Officer in the Department of Atomic Energy, India and Senior Research Engineer in Gencorp, Akron, Ohio before joining Corning Glass Works in 1985 as Senior Development Scientist. His main interests are in the area of rheology and processing of polymers and composites, and has six publications in this area.



Lynn G. Amos received his BS degree in Mechanical Engineering from the University of Tennessee in 1963. Prior to joining Corning, he worked for IBM and did part-time Graduate work at the University of Kentucky and North Carolina State University. He has been with Corning for 20 years and has 20 issued patents in the areas of Fluid Flow Devices, Medical Instrumentation, Optical Devices, and Optical Waveguides. Presently he is the Supervisor of Draw and Coating Development in Corning's Optical Fiber Plant in Wilmington, North Carolina.



Douglas Eccleston graduated from the United States Military Academy in 1971 with a BS degree in Electrical Engineering. After a six year tour in the Army, in 1977 he joined Corning Glass Works as a Process Engineer in the Harrodsburg, Kentucky Opthalmic Glass Plant. Between 1980 and 1987 he has held positions of Senior Applications Engineer, Supervisor and, most recently, the Manager of North American Application Engineering in the Telecommunications Products Division.

LCP coated optical fiber with zero thermal coefficient of transmission delay time

T. Kakuta, S. Tanaka

Sumitomo Electric Industries, Ltd.
1, Taya-cho, Sakae-ku, Yokohama, 244, Japan

Abstract

Thermal coefficient of transmission delay time (TCD) for an optical fiber was first reduced to zero at about 0°C. The optical fiber in this paper was coated with liquid crystal polymer (LCP) having a negative value of thermal expansion coefficient. In this optical fiber, the change in transmission delay time in the temperature range from -40°C to +40°C was also as small as 100 ps/km, which is only 4 % of the intrinsic TCD of silica glass fiber. The characteristic of the optical fiber became to be stabilized after passing through the high temperature condition and it was considered no degradation occurred under the ambient temperature range below +40°C for 20 years.

1. Introduction

For the applications of some synchronized networks such as phased array antenna systems, telemetry systems, and high bit-rate transmission networks, transmission line with high thermal stability in transmission delay time is strongly required. Many papers have been reported about the optical fibers with various dopants [1], cabled fibers [2][3], and an optical fiber coated with an oriented polymer [4]. The TCD of the optical fiber coated with Kevlar FRP was reported by us, and it showed the smaller TCD than that of intrinsic glass material [5]. Although, these optical fibers and cables whose thermal coefficient of transmission delay time is more than 30 ps/km/°C, failed to meet the requirement for the above purpose. The thermal coefficient of transmission delay time less than 10 ps/km/°C, is required from the optical fiber sensor area and high speed data transmission systems. The excellent optical fiber having zero thermal coefficient of transmission delay time at about 0°C is reported in this paper.

2. Theory

2.1 Transmission delay time

The thermal coefficient of transmission delay time for an optical fiber is given by the following equation (1),

$$\frac{d\tau}{dT} = \tau\left[\frac{1}{N}\frac{dN}{dT} + \frac{1}{L}\frac{dL}{dT}\right] \quad \text{——— (1)}$$

The first term indicates the temperature dependence of refractive index of silica glass, which is intrinsic value in the optical fiber. The value of this term is approximately +30 ps/km/°C, or 6 ppm/°C of total transmission delay time. In order to reduce and finally eliminate the TCD of the optical fiber, the second term, the thermal expansion coefficient of the coated fiber,must be of a negative value and cancel the first term as well.

The thermal expansion coefficient α of a coated fiber is given by,

$$\alpha = \frac{1}{L}\frac{dL}{dT} = \frac{\sum_i k_i E_i S_i}{\sum_i E_i S_i} \quad \text{——— (2)}$$

where k_i, E_i, and S_i represent the thermal expansion coefficient, Young's modulus and cross section ofi-th material, respectively. From the above disscussion, a new coating material having the negative thermal expansion coefficient which can be applied to the optical fiber without any degradation in the optical performance, was endeavored to develop.

2.2 Design for the tight coated optical fiber

Generally, the tight coated optical fibers are doubly coated with soft resins (primary coating resins: silicone, UV curable resin) and thermoplastic resin (secondary coating resins: nylon, elastmer etc,). When the product of Young's modulus and the cross section of primary coating resin (Epri × Spri) is much smaller than the others in equation (2), we may neglect this term. Then equation (2) is given by,

$$\alpha = \frac{\sum_i k_i E_i S_i}{\sum_i E_i S_i} \simeq \frac{k_g E_g S_g + k_{sec} E_{sec} S_{sec}}{E_g S_g + E_{sec} S_{sec}} \quad \text{——— (3)}$$

g: glass fiber
sec: secondary coating resin

In order to give zero thermal coefficient of transmission delay time, the following equation is required (4).

$$\left(1 + \frac{1}{N}\frac{dN}{d\varepsilon}\right)\left(\frac{d\varepsilon}{dT}\right)_{\frac{dL}{dT}=0} = -\frac{1}{N}\frac{dN}{dT} + \frac{1}{N}\frac{dN}{d\varepsilon}\alpha g \qquad \text{——— (4)}$$

where, $\frac{1}{N}\frac{dN}{d\varepsilon}$ represents the stress dependence of refractive index of silica glass. Using equations (3) and (4), the relation of k_{sec} versus E_{sec} and S_{sec} can be given by,

$$k_{sec}^{\frac{dT}{dT}=0} = \left(\frac{d\varepsilon}{dT}\right)_{\frac{dL}{dT}=0} - \frac{\left(\left(\frac{d\varepsilon}{dT}\right)_{\frac{dL}{dT}=0} - \alpha g\right)E_g S_g}{E_{sec}S_{sec}} \qquad \text{——— (5)}$$

where $\left(\frac{d\varepsilon}{dT}\right)_{\frac{dL}{dT}=0} = \dfrac{-\frac{1}{N}\frac{dN}{dT} + \frac{1}{N}\frac{dN}{d\varepsilon}\alpha g}{1 + \frac{1}{N}\frac{dN}{d\varepsilon}}$

When we put each typical value for equation (5) shown in Table 1, the equation (6) is given,

$$k_{sec}^{\frac{dT}{dT}=0} = -8.28\times10^{-6} - 7.73\times10^{-6}(E_{sec}S_{sec}) \qquad \text{——— (6)}$$

Fig.1 shows the relation of k_{sec} versus sencondary coat diameter d_{sec} which is required to give the zero thermal coefficient of transmission delay time when primary coat diameter d_{pri} is 0.4mm. For example, when an optical fiber is coated with a material whose Young's modulus is 2000 kg/mm² and its coating diameter is 0.8 mm, theoretical value of $\left(\frac{d\varepsilon}{dT}\right)_{k_{sec}}$ is caluculated as $-9.31\times10^{-7}\,°C^{-1}$.

3. Experimental

3.1 LCP coated optical fiber

A secondary coating resin having a negative thermal expansion coefficient is required in tight coated optical fibers based on the above theory. Thermotropic hard liquid crystal polymer (LCP) that had a negative thermal coefficient ($-7\sim-9\times10^{-6}\,°C^{-1}$) as the secondary coating resin was selected. Fig.2 shows the cross section of an LCP coated optical fiber. The glass fiber was doubly coated with soft silicone resin and hard LCP. Table.2 shows the typical condition of LCP coating by extrusion.

3.2 Measuring system of transmission delay time

The measuring system of transmission delay time is shown in Fig.3. A sinusoidal curve (λ=1.30μm) of 800 MHz was continuously transmitted through the test fiber, and the modulation phase at the output was measured by the vector voltmeter. The change in transmission delay time $\Delta\tau$ was caluculated by equation (7) using the value of change in output phase $\Delta\phi$, mudualation frequency f, and fiber length L.

$$\Delta\tau = \frac{\Delta\phi}{2\pi fL} \qquad \text{——— (7)}$$

The temperature of the fiber was changed by 10 degrees with a sufficient time interval to realize the local equilibrium. Typical time period for the whole thermal cycle from -40°C to +80°C was 24 hours for the LCP coated optical fiber.

4. Results and Discussions

4.1 Transmission delay time of the LCP coated optical fiber

Fig.4 shows the temperature dependence in transmission delay time of the LCP coated optical fiber under heat cycle condition from -40°C to +80°C. The temperature dependence of transmission delay time under the first cycle (from -40°C to +80°C) was different from those under the second and the third cycles. At the first cycle, the change in transmission delay time was small from -40°C to +40°C, however, the characteristic of the LCP coated optical fiber began to turn back to that of a bare fiber over +40°C. Although, the change in transmission delay time at the second cycle was small in the range of temperature from -40°C to +80°C, and the characteristic of transmission delay time at the third cycle was the same as that at the second cycle and stabilized.

TCD takes zero value at about 0°C under the second and the third heat cycle condition. Also, in the wide range from -40°C to +40°C, the change in transmission delay time was as small as 100 ps/km. Compared with the performance of conventional fiber cables shown by the dotted line in Fig.4, drastic improvement was recognized and it was observed that the characteristic of the LCP coated optical fiber was stabilized after passing through the annealing condition.

4.2 The relations of Young's modulus and the thermal expansion coefficient of LCP for the characteristic of transmission delay time

The temperature dependences of Young's modulus and the thermal expansion behavior of LCP were examined. Fig.5 shows the temperature dependence of Young's modulus of LCP in the range from -40°C to +80°C and after the annealing at +80°C. It was recognized that Young's modulus of LCP did not change after the annealing at +80°C for 100 hours.

Fig.6 shows the thermal expansion behavior of LCP tube under the heat cycle in the range of the temperature from -80°C to +80°C. It was good agreement to the characteristic of transmission delay time in the LCP coated optical fiber that the thermal expansion behavior of LCP tube was stabilized after it passed through the high temperature condition. Fig.8 shows the temperature dependence of the thermal expansion coefficient k_{LCP} of LCP. Before and after LCP was attained to the high temperature condition, the thermal expansion behaviors differed from each other.

Before LCP passed through the high temperature condition, the thermal expansion coefficient began to rise rapidly from $-7 \sim -9 \times 10^{-6}°C^{-1}$ to a positive value starting from the temperature of +20°C. After the high temperature condition, k_{LCP} was stabilized with a high negative value ($-8 \sim -9 \times 10^{-6}°C^{-1}$) in the range from -40°C to +80°C. These behaviors were similar to those of the temperature dependence of the thermal expansion coefficient caluculated from the characteristic of transmission delay time and the temperature dependence of Young's modulus of LCP.

From the above results, it is obvious that the stabilization of the characteristic of transmission delay time in an LCP coated optical fiber after passing through high temperature condition is caused by the stabilization of the thermal expansion coefficient with a high negative value.

4.3 Thermal stability

The degradation characteristic of transmission delay time under high temperature was examined for LCP coated optical fibers. Fig.8 shows the change in transmission delay time of LCP coated optical fibers after heat aging at +80°C, +100°C, and +150°C for 120 hrs. After heat aging at +80°C for 120 hrs, the change in transmission delay time was almost the same as the initial one, however the increase of the change in transmission delay time was observed after heat agirg at +100°C and +150°C, especially below the temperature of 0°C.

Fig.9 shows the relative change in transmission delay time at -40°C of LCP coated optical fibers for the aging time. The increase of the relative change in transmission delay time at -40°C for the aging time and the aging temperature was roughly given by,

$$\Delta\tau_{-40°C} = \Delta\tau_0 e^{-\frac{Ea}{RT}} \cdot t^{\alpha} \qquad \text{---- (8)}$$

And the activation energy Ea for the degradation was obtained as 14 kcal/mol. Using the equation (8), $\Delta\tau_{-40°C}$ for 20 years at +40°C was eliminated as 10 ps/km. It was so minute increase that the stability of characteristic of transmission delay time in an LCP coated optical fiber was considered no degradation occurred under using the LCP coated optical fiber in the ambient temperature range below +40°C.

5. Conclusion

Zero thermal coefficient of transmission delay time was achieved at about 0°C with LCP coated optical fiber. The change in transmission delay time in the temperature range from -40°C to +40°C was also as small as 100 ps/km, which is only 4 % of the intrinsic TCD of silica glass fiber. The characteristic of transmission delay time in the LCP coated optical fiber was stabilized after passing through the heat aging condition, and it is also assumed that no degradation may not occurred in using this optical fiber for 20 years in the ambient temperature range below +40°C. Using this fiber, it will be possible to construct a larger array antimma system than the present one which uses a special coaxial transmission line.

References

[1] L.G. Cohen and J.W. Fleming, "Effect of temperature on transmission in lightguides", BSTJ. Vol. 58, (1979) pp. 945-951.

[2] E.F. Andersen, "Differential propagation delay in optical multifibre cables", Electron Lett. Vol. 16 No. 10, (1980) pp. 389-391.

[3] L.A. Bergman, S.T. Eng, and A.R. Jhonston, "Temperature stability of transit time delay for a single-mode fiber in a loose tube cable", Electron Lett. Vol. 19 No.21, (1983) pp. 865-866.

[4] R. Kashyap, S. Hornung, M.H. Reeve, and S.A. Cassidy, "Temperature desensitisation of delay in optical fibres for sensor applications", Electron Lett. Vol. 19 No. 24, (1983) pp. 1039-1040

[5] S. Tanaka, T. Ono, "Reduced thermal coefficient of transmission delay time in optical fiber", ECOC '84 Conference proceedings, pp 284-285.

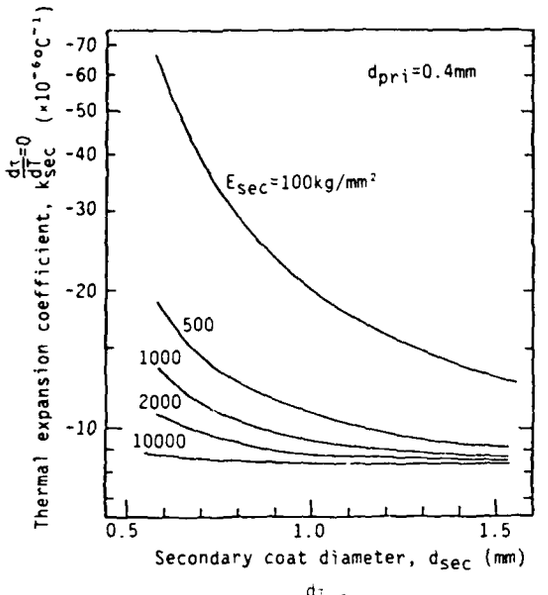


Fig.1 Relation of k_{sec} ($\frac{d\tau}{dT}=0$) versus d_{sec}

Table 1 Typical values for equation(5)

Eg (kg/mm²)	7100
Sg (mm²)	0.123 fiber diameter=125μm
kg (°C⁻¹)	6×10^{-7}
$\frac{1}{N}\frac{dN}{dT}$	6.5×10^{-6}
$\frac{1}{N}\frac{dN}{d\varepsilon}$	0.2

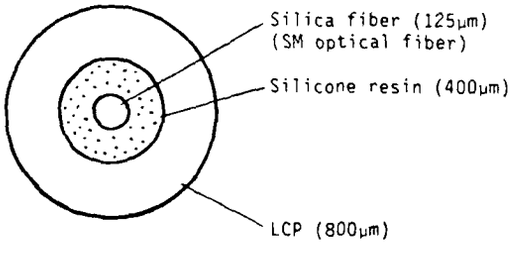


Fig.2 Cross section of LCP coated fiber

Table 2 LCP coating conditions

Extrusion Temperature (°C)	280
Draw Down Ratio (-)	7.9
Coating Velocity (m/min)	30
Cooling Condition	water bath

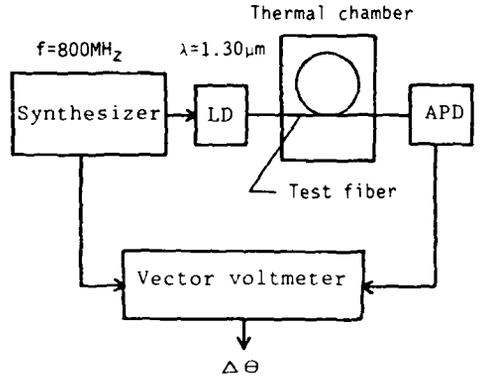


Fig.3 Measuring system of transmission delay time

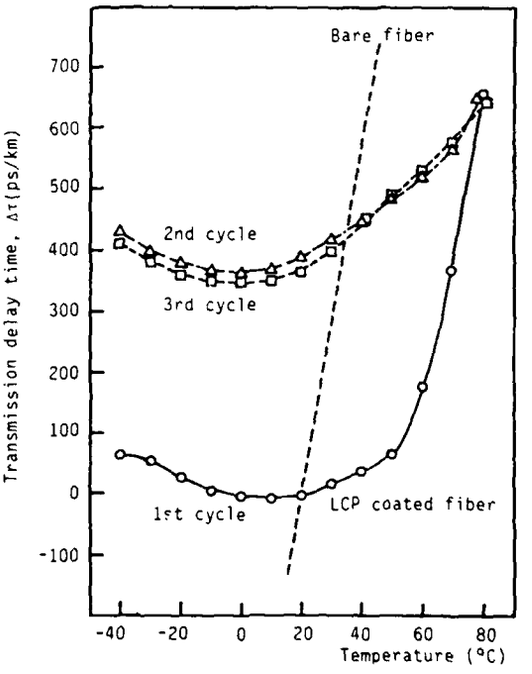


Fig.4 Temperature dependence of transmission delay time

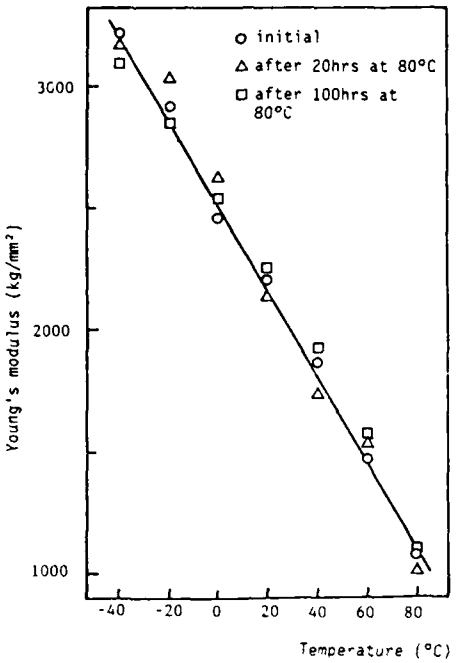


Fig.5 Temperature dependence of Young's modulus of LCP

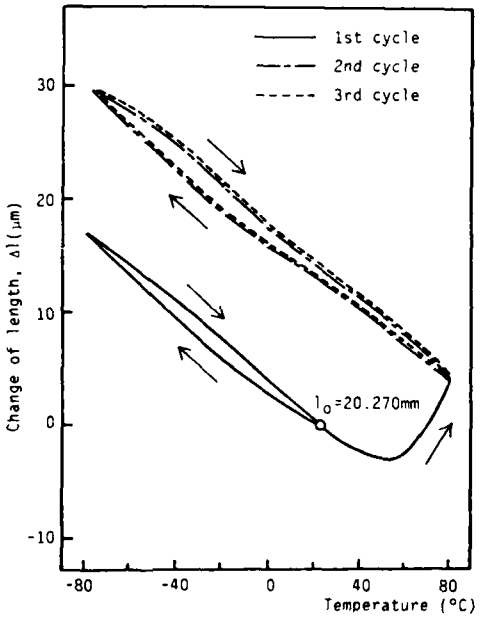


Fig.6 Thermal expansion behavior of LCP tube

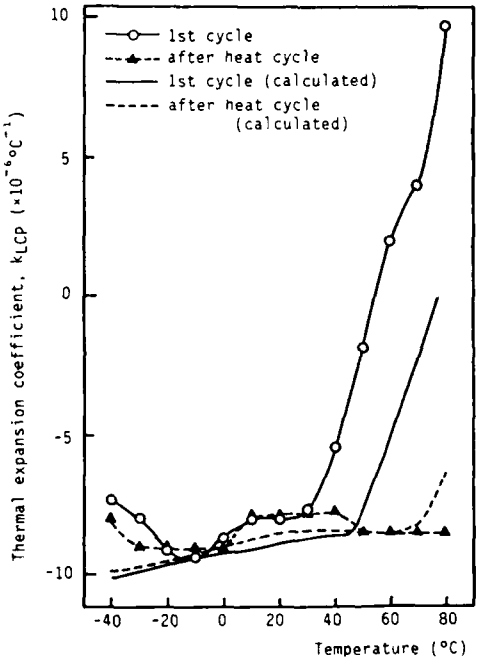


Fig.7 Temperature dependence of thermal expansion coefficient of LCP

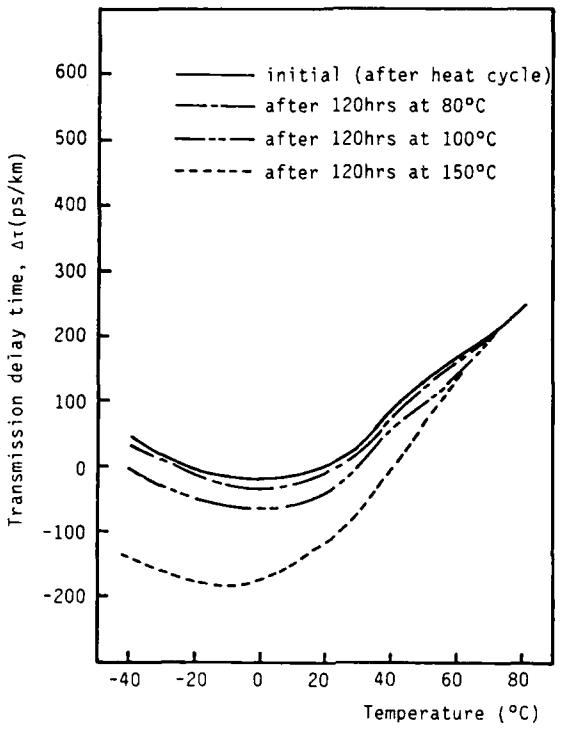


Fig.8 Degradation characteristics of Δτ in LCP coated optical fiber

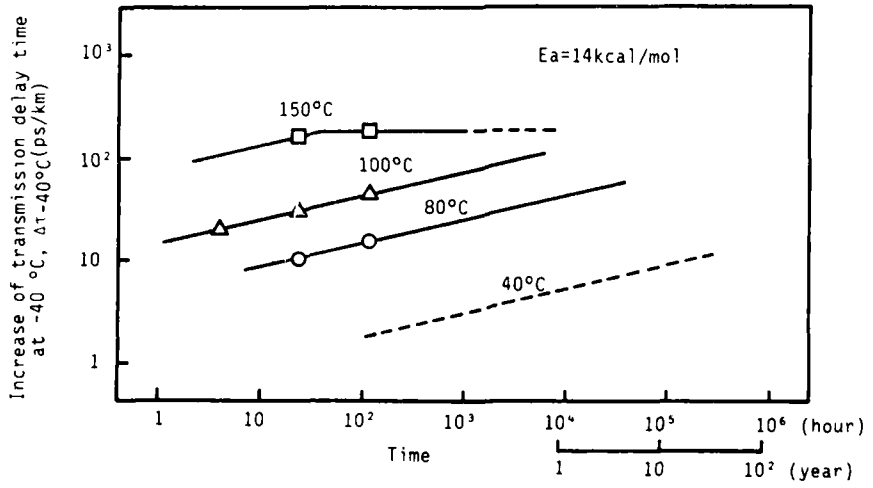


Fig.9 Degradation characteristics of $\Delta\tau_{-40^{\circ}C}$ under heat aging



Tatsuya Kakuta

Sumitomo Electric
Industries, Ltd.

1, Taya-cho, Sakae-ku
Yokohama, Japan

Tatsuya Kakuta was born in Osaka, Japan, on February 17, 1960. He received the B.S. and M.S. degrees in Applied Chemistry from Osaka University in 1983 and 1985, respectively. He joined Sumitomo Electric Industries, Ltd. in 1985, and has been engaged in research and development of optical fibers and cables. Mr. Kakuta is a member of Transmission Media R & D Department in Yokohama Research Laboratories.



Shigeru Tanaka

Sumitomo Electric
Industries, Ltd.

1, Taya-cho, Sakae-ku
Yokohama, Japan

Shigeru Tanaka was born in Tokyo, Japan, on December 2, 1951. He received the B.S. and M.S. degrees in Electrical Engineering from Tokyo University in 1974 and 1976, respectively. He joined Sumitomo Electric Industries, Ltd. in 1976, and has been engaged in the design and characterization of optical fibers and fiber cables. Mr. Tanaka is a member of Communication R & D Department in Yokohama Research Laboratories and of Institute Electronics and Comunication Engineers of Japan.

HERMETICALLY COATED OPTICAL FIBERS

K. E. Lu G. S. Glaesemann G. Kar

Corning Glass Works
Corning, New York

Corning's hermetically coated fiber exhibited a uniform strength distribution over 4 kilometers of fiber with an overall Weibull modulus of 40. The fatigue resistance of the fiber tested in long lengths is summarized by the high fatigue parameter, n, of 110 compared to 21 for standard fiber. In addition, the coating was found to resist hydrogen induced attenuation at room temperature and chemical corrosion. These attributes make this hermetically coated fiber an excellent candidate for use in undersea cables, many military applications, and other applications where a harsh environment is prevalent.

INTRODUCTION

Low loss optical fibers are being considered for use in tethered missiles, undersea cables, as well as various other harsh environments.[1,2] These new applications require that fibers be exposed to high stress for extended periods of time. This implies proof testing at very high levels (several hundred thousand psi) or the development of coatings which prevent strength loss from static fatigue. For extreme applications, both may be required. In addition, requirements for resistance to hydrogen permeation and chemical corrosion are becoming increasingly important.

Metals such as aluminum, tin, and lead[3-6] have been used to make hermetic coatings to minimize fatigue; however, metals tend to form polycrystalline solids which can themselves be rapidly corroded via grain boundary diffusion. Processing complexities and slow application speeds also make metallic hermetic coatings less practical. Inorganic and ceramic coatings have recently been found to improve fiber fatigue resistance, as well as reduce attenuation increases from hydrogen permeation.[7,8] Corning has pursued a hermetic coating technology in this area that would provide a moisture barrier, limit hydrogen diffusion, chemical corrosion, and meet the necessary strength requirements.

The purpose of this paper is to review the performance of Corning's hermetic coating in light of the above mechanical and chemical requirements and to compare these results with those of typical standard fibers.

HERMETIC COATING

Corning's hermetic coating technology is compatible with the existing fiber drawing process.[9] The coating consists of an ultra thin (<500 Å) layer of an inorganic material deposited directly on the surface of a freshly-drawn optical fiber through a chemical vapor deposition technique.[9] After applying the hermetic coating the fiber can then be coated with any number of polymer coatings. However, for the purposes of this paper all test results are for acrylate coated fiber.

STRENGTH

The mechanical performance of fibers should be based on strength data from a sample representative of the application. Therefore, for long length applications, the strength of 4 kilometers of hermetically coated fiber proof tested at 200 kpsi was measured using a rotating capstan fiber tester (RCFT)[10] with a 20 meter gauge length. All strength tests were performed in air at a strain rate of 4%/minute. The strength distribution is given in a Weibull[11] fashion in Figure 1 along with similar data for a standard fiber also proof tested at 200 kpsi.

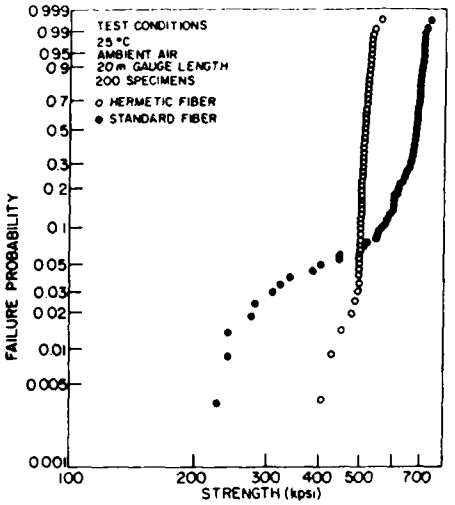


FIGURE 1 Weibull Strength Distribution Plots For Hermetically Coated And Standard Fibers

The two distributions in Figure 1 are quite different with the standard fiber being tri-modal in shape with an upper region with a Weibull modulus, m, of 15 extending above the failure probability of 7%, a middle region with a Weibull modulus of only 3 and a low region near the proof stress with a modulus similar to that of the upper region extending below a failure probability of 2%. The hermetically coated fiber has a more uniform distribution than the standard fiber. The Weibull modulus of all the hermetically coated fiber strength data in Figure 1 is approximately 40, which is a significant improvement over the standard fiber. The uniform strength of the hermetically coated fiber over the entire 4 kilometers is attributed to the hermetic coating process. It is believed that this process covers or heals large underlying flaws on the glass surface with a material having flaws of a uniform size, the largest of which has a strength of approximately 400 kpsi.

DYNAMIC FATIGUE

It is well known that standard glass fibers exhibit subcritical crack growth (fatigue) when subjected to stress in the presence of moisture.[10] A hermetic coating is, therefore, desirable simply because it limits the availability of moisture to the the crack tip, thereby, retarding subcritical crack growth. To characterize the fatigue resistance of the hermetically coated fiber, fiber strength was measured under dynamic fatigue conditions; whereby, fibers are loaded slowly to failure over a range of strain rates.[12] The principle behind this test is that strength degradation increases with increasing time to failure, i.e., decreasing strain rate. Little change in strength with strain rate indicates excellent fatigue resistance.

Fibers proof tested at 200 kpsi were loaded to failure at strain rates of 4, 0.4, 0.04, and 0.004%/minute using a 10 meter gauge length RCFT apparatus. The tests were performed at 25°C in 100% relative humidity with a minimum of 75 specimens per rate. The strength and stressing rate results for the hermetically coated fiber were analyzed in terms of a power law crack velocity relationship[13,14] and are plotted in a logarithmic fashion in Figure 2. Included in Figure 2 are similar results for a standard fiber also proof tested at 200 kpsi. The lines in Figure 2 represent a best fit of all the data.

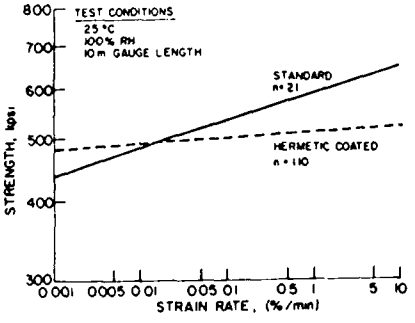


FIGURE 2 Dynamic Fatigue Of Hermetically Coated And Standard Fibers In 10 Meter Gauge Lengths

The strength of the hermetically coated fiber in Figure 2 shows little change with strain rate giving a power law crack velocity parameter, n, of 110. This high value for n indicates minimal fatigue with time. The strength of the standard fiber, on the other hand, decreases more readily with decreasing strain rate as indicated by the n value of 21. In practical terms, for a 40 year lifetime, it is believed that the hermetically coated fiber could withstand a stress equal to 80% of the proof stress; whereas, an allowable stress equal to 30% of the proof stress is more appropriate for the standard fiber for the same lifetime.[12] It is important to note that a recent study has shown similar fatigue behavior for the hermetically coated fiber tested in water at 90°C using short gauge length specimens.[9]

HYDROGEN PERMEABILITY

Recent studies have demonstrated that resistance to hydrogen induced attenuation is of particular importance, especially for undersea cables.[1,2] The resistance of a single-mode hermetically coated fiber to hydrogen permeation was measured by placing the fiber in 100% H_2 at room temperature for 200 days. No attenuation increase was observed at the operating wavelengths of 1300 and 1550 nm. Penetration of H_2 to the fiber core was observed, however, by the growth of the interstitial peak at 1240 nm. Figure 3 shows the attenuation change with time, at 1240 nm, for the hermetically coated fiber and a standard fiber. As can be seen in Figure 3, the attenuation increase at this wavelength for the hermetically coated fiber was less than 0.4 dB/km after 200 days under this condition, whereas, the standard fiber showed an increase of ~8 dB/km in two weeks. This data suggests that the hermetically coated fiber can significantly retard hydrogen permeation.

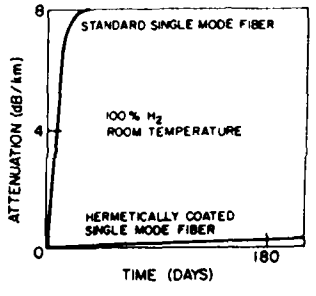


FIGURE 3 Attenuation Change At 1240 As A Function Of Time (Linear Scale)

A study of induced attenuation as a function of hydrogen partial pressure, total pressure, and environmental temperature on hermetically coated fibers is forthcoming.

CHEMICAL DURABILITY

Some applications may subject fibers to environments which are particularly corrosive to silica glass and, therefore, require a long-term protective coating. The chemical durability of the hermetically coated fiber was determined by stressing the fiber to 250 kpsi by wrapping specimens on 0.25 inch diameter mandrels and exposing them to chemicals known to be corrosive to silica glass, such as hydrofluoric acid and hot sodium hydroxide (5% concentration at 95°C). Similar experiments were performed on standard fibers for comparison purposes. The standard fibers failed in 20 seconds in HF and 2 hours in hot NaOH solutions, whereas the hermetically coated fibers lasted >4 hours in these solutions and failed only when acrylate coating degradation allowed the bare fiber to touch the mandrel.

SUMMARY

Corning's hermetically coated fiber exhibited a uniform strength distribution over 4 kilometers of fiber with an overall Weibull modulus of 40. The fatigue resistance of the fiber tested in long lengths is summarized by the high fatigue parameter, n, of 110 compared to 21 for standard fiber. In addition, the coating is resistant to hydrogen induced attenuation at room temperature and chemical corrosion. These attributes make this hermetically coated fiber an excellent candidate for use in undersea cables, various military applications and situations where a harsh environment is prevalent.

REFERENCES

1. R. Hiskes, et al., "High Performance Hermetic Optical Fibers", Post Deadline Paper, OFC, 1984.

2. K. J. Beales, et al., "Practical Barrier To Hydrogen Diffusion Into Optical Fibers", OFC, 1984.

3. J. Wysocki, "Reduction In Static Fatigue of Silica Fibers By Hermetic Jacketing", App. Phys. Ltr., vol. 34 p. 17, January, 1979.

4. P. G. Hale, J. B. Almedia, and C. J. R. Sheppard, "On-line Metal Coating of Silica Fiber Using Magnetron Sputter," in Physics of Fiber Optics, vol. 2 p. 115, The American Ceramic Society, Inc., 1981.

5. J. C. Williams, et al., "Method of An Arrangement For Coating Optical Fibers With Metallic Materials", U.S. Patent 4,485,122, November, 1984.

6. S. Tanaka, T. Siota, R. Yamauchi, and K. Inada, "Low Loss Hermetically Coated Optical Fibers," OFC Proceedings, p. 104, 1984.

7. D. R. Biswas and S. Raychaudhuri, "Hermetic Coating For Optical Fiber and Method of Forming the Same," European Patent 0 166649 A2, December, 1985.

8. P. C. Schultz and R. S. Chaudhuri, "Hermetic Coating on Optical Fibers", Proc. SPIE, 1986.

9. K. E. Lu, G. S. Glaesemann, R. V. VanDewoestine, and G. Kar, "Recent Developments In Hermetically Coated Optical Fiber," to be published J. Lightwave Tech., December, 1987.

10. J. D. Helfinstine and F. Quan, "Optical Fiber Strength/Fatigue Experiments," Optics and Laser Tech., pp. 133-6, June, 1982.

11. W. Weibull, "A Statistical Distribution Function Of Wide Applicability," J. Appl. Mech., vol. 18, pp. 293-7, March, 1951.

12. S. T. Gulati, "Crack Kinetics During Static and Dynamic Loading", J. Non-Crys. Solids, vol. 38, pp. 475-80, 1980.

13. A. G. Evans, "Slow Crack Growth in Brittle Materials Under Dynamic Loading Conditions," Int. J. Frac. vol. 10, pp. 251-9, February, 1974.

14. J. E. Ritter, Jr., "Engineering Design And Fatigue Failure Of Brittle Materials," in Fracture Mechanics of Ceramics, vol. 4; ed. R. C. Bradt et al. Plenum Press, New York, pp. 667-86, 1978.



Kun-Er (Rebecca) Lu joined Corning Glass Works' Research and Development Division in 1976 after completing her PhD in Chemistry from Cornell University. She has worked on several projects related to glass and glass-ceramic surfaces and has several publications and patents in these areas. Currently she is Supervisor of Optical Fiber Draw Process Development.



G. Scott Glaesemann received his B.S. degree in Mechanical Engineering from North Dakota State University, Fargo, North Dakota in 1981, a Masters and PhD in Mechanical Engineering from the University of Massachusetts, Amherst, Massachusetts in 1983 and 1986 respectively. He joined Corning Glass Works in 1986 and has been engaged in researching the strength and fatigue behavior of optical glass fibers.



Gitimoy Kar received his PhD in Materials Science and Engineering from the University of California, Berkeley, California in 1972. In 1973 he joined Corning Glass Works where he has worked in high temperature corrosion and electrochemistry, precious and refractory metals for glass melting and forming, glass ceramic finishing processes, and optical waveguide. Currently he is the Manager of Draw and Coating Development, Optical Waveguide Technology, in the Research and Development Division.

A NEW HIGH EFFICIENT FLAME RETARDANT PLASTICIZER FOR PVC WIRE AND CABLE COMPOUNDS

T. T. TIDELLE

Great Lakes Chemical Corporation
West Lafayette, IN 47906

Abstract

A newly developed brominated aromatic flame retardant plasticizer, BZ-54, overcomes two limitations of phosphate esters in PVC applications; low flame retardant efficiency and marginal thermal stability. In experimental studies involving typical wire and cable coating formulations, comparisons were made between several phosphate esters and BZ-54. Effects on [illegible] of the primary plasticizers were made and compositions evaluated for flame retardant efficiency, low temperature properties, thermal stability, oil extraction and other properties. [illegible] which will result in improved flame retardant PVC compounds.

Introduction

[illegible] flame retardant plasticizers [illegible] were introduced [illegible] primarily [illegible] phosphate esters [illegible] limitations, [illegible] limitations. Due to the demand [illegible] flame retardancy that can be achieved. Another limitation is thermal stability, the phosphate ester permits relatively poor [illegible] exposure. A new chemical, BZ-54, has been developed which overcomes these deficiencies, creating new opportunities for highly flame retardant, primary stable flexible PVC compositions. The product is a clear, light amber liquid containing 54% bromine and having a density of 1.61 g/cc and a room temperature viscosity of 1400 cps. Its FAA [illegible] weight loss point is about 220°C.

Procedure

All experimental studies involved the [illegible]

[illegible]

[illegible] P. O. Box 1200, West Lafayette, IN 47906.
[illegible] Great Lakes Chemical Corp.
[illegible] Mobay Corp.
[illegible] CPC Int'l.
[illegible] Great Lakes Chemical Corp.
[illegible] Mobay Chemical Co.
[illegible] Stauffer Chemical Co.

[illegible] flame retardant plasticizer was [illegible] a primary plasticizer, either a phosphate ester or a phthalate, in the [illegible] was used [illegible] Brabender Plastograph [illegible] Specimens were [illegible] ASTM [illegible] tests.

[illegible]

[illegible] a series of experiments [illegible] where a standard [illegible] was [illegible] with [illegible] flame retardant plasticizer. At the [illegible] level, [illegible] BZ-54 [illegible] of the primary plasticizer, [illegible] and [illegible] only 1 and 2, respectively, were [illegible] the [illegible] BZ-54 was [illegible]

Plasticization Effects

When used in a range of up to about 75% replacement of the primary plasticizer, DP-45 functions as a typical phthalate ester plasticizer. Table 2 shows tensile and elongation values for selected compositions of Table 1. At greater than 75% substitution, tensile strength increases significantly as the composition becomes more rigid. If increased stiffness can be tolerated, one can formulate to very high levels of oxygen index.

Table 2

[illegible]

[illegible]	[illegible]	[illegible]	[illegible]	[illegible]
[illegible]	[illegible]	[illegible]	[illegible]	[illegible]
[illegible]	[illegible]	[illegible]	[illegible]	[illegible]
[illegible]	[illegible]	[illegible]	[illegible]	[illegible]
[illegible]	[illegible]	[illegible]	[illegible]	[illegible]

UL Jbol Evaluations

Specimens were evaluated using the Class 4[illegible] 105°C rating test requirements. Minimum requirements of this test are:

[illegible]	[illegible]	[illegible]
[illegible]	[illegible]	[illegible]
[illegible]	[illegible]	[illegible]
[illegible]	[illegible]	[illegible]

Table [illegible] lists typical tensile data from the respective explosion and shows that DP-45 meets both explosive and optimum criteria. Compared to the phthalate ester samples evaluated, DP-45 showed the least change compared to the [illegible] for [illegible]. Only DP-45 was evaluated in [illegible] immersion, a much less severe exposure.

Table

[illegible]

[illegible]	[illegible]	[illegible]	[illegible]
[illegible]	[illegible]	[illegible]	[illegible]
[illegible]	[illegible]	[illegible]	[illegible]
[illegible]	[illegible]	[illegible]	[illegible]
[illegible]	[illegible]	[illegible]	[illegible]

Low Temperature Brittleness

Depending on the formulation, specimens containing DP-45 give low temperature brittleness number [illegible] approximately [illegible]. This level may be lowered further by addition [illegible] of parts of polymeric plasticizers such as di-2-ethylhexyl or di-n-hexyl azelates.

Smoke Evolution

A wire and cable formulation containing varying levels of DP-45 was subjected to ASTM E662 NBS smoke chamber testing, utilizing both smoldering and flaming modes. Sample thickness was 25-30 mils. Results in Table 4 show flaming mode values to be higher than smoldering mode values, which is typical. Specimen thickness also is a factor for DP-45 smoke values. A composition rated at about 200 (smoldering) at 30 mils will yield a value of about 275 when thickness is increased to 100 mils. Significant reduction of smoke is possible by adding any one of a number of commercially available molybdenum-based smoke suppressants. Unlike many flame retardants, smoke values with DP-45 do not significantly increase with increasing concentration.

Table [illegible]

[illegible]

[illegible]	[illegible]	[illegible]
[illegible]	[illegible]	[illegible]
[illegible]	[illegible]	[illegible]
[illegible]	[illegible]	[illegible]
[illegible]	[illegible]	[illegible]

Electrical Properties

A typical wire and cable insulation containing 40 phr DP-45 was evaluated for electrical properties. Values in Table 5 indicate excellent insulative properties of DP-45.

Table

[illegible]

[illegible]	[illegible]
[illegible]	[illegible]
[illegible]	[illegible]
[illegible]	[illegible]
[illegible]	[illegible]

Conclusion

DP-45 is a new flame retardant plasticizer that will meet UL VW-1, which offers better [illegible] flame retardancy and thermal stability than previously available [illegible] phosphate ester additives. When utilized as a diluent for PVC or other primary plasticizers, oxygen indexes above 40 are attainable without adversely affecting [illegible] properties. The product offers high thermal stability, all with a UL [illegible] temperature index of 105°C. Be attained. Other [illegible] properties include minimal effects on electrical properties and smoke evolution. Availability of this product offers the wire and cable industry formulation new opportunities for high performance products.



AUTHOR/PRESENTOR

Biographical Sketch, Dir. T. F. Fidelle

Dr. Fidelle is Director of Research for Great Lakes Chemical Corporation, a producer of flame retardants for thermoplastic and thermoset resins.

He holds a PhD from the University of Massachusetts and has fifteen years of industrial experience in product applications including fibers, films, extruded and molded plastics, and water soluble polymers. He has several papers and patents to his credit.

Address: Dr. T. F. Fidelle
Director - Research
Great Lakes Chemical Corp.
Box 2200
West Lafayette, IN 47906

FIRE PARAMETERS AND COMBUSTION PROPERTIES OF CABLE PULLING COMPOUND RESIDUES

J. M. Fee and D. J. Quist
American Polywater Corporation
Stillwater, Minnesota 55082

SUMMARY

Fire parameters of cable lubricant residues have been determined using a specially designed device. The device simulates field conditions by heating lubricant contained in a conduit. The heating rate (heat flux) can be varied to develop various fire parameters.

Significant combustion differences are found among commercially available lubricants. These differences include, critical heat flux, ignition energies, ignition temperature, time of burn and tendency to spread (propagate) or extinguish fire.

The most combustible of residues are from lubricants based on Hydrocarbon Waxes or combination Wax Soaps. These residues have critical heat fluxes well under 40 KW m^{-2}, ignition energy of 15,000-20,000 KJ m^{-3} and ignition temperatures of 230 -330 C. They burn vigorously for lengthy periods (5-15 minutes) and spread flame along a conduit whether or not the combustion is supported by an outside heat source.

Certain Polymer, Polymer Teflon and Bentonite Glycol Lubricants show higher ignition energies and shorter burn times than the Wax-based materials. However, these lubricants still sustain and spread flame once ignited.

One lubricant, a High-performance Gel Polymer, was found to be considerably less combustible than fire-retardant cables. In the High-performance Gel Polymer, ignition was very difficult to induce, burn times were nil and flame spread did not occur.

INTRODUCTION

Cable pulling compunds are specialty lubricants which lower the force or tension on a cable as it is pulled into conduit. As field installers know, the use of such lubricants can often mean the difference between a successfully installed cable or one damaged by excessive mechanical stress.

Cable lubricants reduce pulling tension by reducing the frictional force between the cable jacket and the conduit wall. Low cable lubricant coefficient of friction is an important characteristic, and has been the subject of much study and measurement.

A second factor considered when choosing a cable pulling lubricant is its compatibility with the cable jacket. The lubricant should not affect the jacket's physical properties or performance. Testing usually consists of determining the lubricant's effect on jacket tensile strength, elongation, dielectric strength, volume resistivity and stress cracking.

A great variety of performance requirements for pulling lubricants come from end users. Such practical issues as pulling through water, adhesion to cable jacket, temperature stability and even odor are considered important by end users.

Surprisingly, an area of cable lubricant performance that has not been discussed much or measured until now is combustibility. Cable pulling lubricants, or, actually, their residues, are as real a part of a conduit system as the cable or conduit itself. The combustion character of the cable and conduit has been the subject of numerous studies and standards designed to minimize their contribution to the intensity or spread of a fire.

The nuclear industry has made some attempts to measure fire parameters of lubricant residues. A number of conventional cable flame tests have been adapted to lubricants. The approach has been to put typical amounts of lubricant on a fire retardant cable. The lubricant is allowed to dry. Then the lubricated cable and a non-lubricated control are subjected to the flame test to determine any lubricant effect.

When tested in this fashion, many of the Hydrocarbon Wax lubricant residues simply melt and drop into the flame. This does not duplicate the real conditions under which these residues would be exposed to fire. Such testing does not show the very significant differences in the combustibility of lubricants.

The purpose of this research was to develop a more realistic fire performance testing procedure for cable lubricant residues. Additionally, we wanted to quantify flame propagation and combustion differences among lubricant residues.

TEST METHOD AND SAMPLES

Cable Lubricant Types and Their Residues

A wide variety of cable pulling lubricants are used throughout the world. A number of these lubricants are manufactured and marketed specifically for cable pulling. Occasionally, automotive grease or even dish soap is used.

With high-performance plastic and rubber cable jackets becoming more and more common, the worldwide trend is to use lubricants proven to be compatible with these materials. These lubricants can be generally categorized as follows.

1) Polymer Water Solutions: Low solids materials (< 5% residue by weight) which have extremely low friction based on high molecular weight polymers dissolved in water.

2) Wax Emulsions: Various types of hydrocarbon waxes emulsified in water. Solids content (residue) is 15-30% by weight.

3) Soaps: Salts of various fats or oils, often dissolved in water. Solid residue can vary significantly (20-80% by weight).

4) Bentonite Clay Slurries: Finely divided, inorganic, bentonite clay slurried in water glycol solutions. Residue is 12-25% by weight.

5) Dry Powders: Talc or other inorganic powder base. 100% solids with no evaporating component.

How Lubricants are Used — Fire Exposure

Cable pulling lubricants are applied to cable jackets or coated on conduit walls in sufficient quantity to lower the friction and tension on the cable as it is pulled. The lubricant ends up distributed (perhaps unevenly) throughout the conduit.

The amount of lubricant in the conduit varies. Typically, the more difficult the pull (the higher the expected tension), the more lubricant is used. Experienced cable pullers know that length of run, cable weight, conduit fill, jacket conduit type, and number degree of conduit bends are all factors that determine the appropriate amount of lubricant to use. In industrial pulling, lubricant usage can vary from .3 to as much as 6 gallons per 100 feet of conduit. At typical lubricant densities, this is 10 to 200

grams of lubricant per foot of conduit.

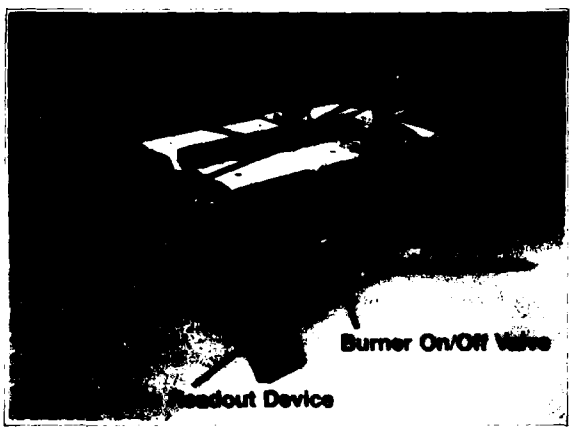
After use, the volatiles in the lubricant (water, glycerine, glycol) evaporate leaving only the residue in the conduit. In the case of a fire, this residue is heated but **contained** by the conduit system. Depending on the residue combustion character, it can ignite and spread fire through the conduit.

Fire spreading through conduit systems is not new. Non-flammable conduit, fire retardant jackets, fire stops, etc., are used to prevent such spread. How do cable lubricant residues perform relative to these better known cable and conduit materials?

Test Apparatus

To simulate field exposure, and to evaluate the performance of lubricant residues under fire conditions, the device shown in Figure 1 was built.

Figure 1



The device generates heat from a gas burner roughly one foot in length, which is contained in a non-combustible box. The burner heats a rigid steel conduit split in half with welded end caps to retain the lubricant. Specifically, 2" rigid conduit was placed over a 2" x 12" slot in the box to yield an area for heat impingement of 24 square inches (.01548m²).

A flow meter was used to control the gas burn rate and the heat flux from the burner. 2.25 cubic feet per hour (cfh) was the lowest gas flow rate which would maintain a continuous burner flame. This converted to a minimum heat flux of 42 KW m², which was focused on the split conduit residue sample.

An iron constantan thermocouple was inserted **into** the residue (when possible) to measure its temperature. Finally, a pilot light (also gas) was devised which could be brought in from above the conduit to direct a flame onto the contents to attempt ignition.

Lubricants Evaluated

Commercially available cable lubricants were evaluated. No powder lubricants (talc type) were represented. Inorganic powders are poor friction reducers and thus are not commonly used or available commercially for cable lubrication.

The lubricants selected are in Table 1.

TABLE 1

Lubricants Used in Combustion Testing

Lubricant Designation	Color	Appearance	%Solids*
High-performance Gel Polymer Lube	Off-white	Thick translucent gel	3.3
Wax Lube #1	Yellow	Particulate paste	14.0
Wax Lube #2	Yellow	Smooth pearly appearance flowable	14.1
Wax Lube #3	Yellow-beige	Chunky paste	10.4
Wax Lube #4	Yellow	Smooth pearly appearance flowable	13.7
Fluffed (air filled) Wax Soap Lube	Cream-tan	Low density paste	15.4
Polymer Teflon Lube	Red	Thick pourable liquid	2.2
Wax Soap Lube	Light green	Very thick flowable	12.3
Bentonite Slurry Lube	Tan-brown	Thick paste	13.4
Polymer Lube	Colorless	Clear thick gel	1.1

*The percent solid residue was determined for 4 samples by oven drying at 105 C (221° F) oven for 24 hours. This period of 24 hours was used to ensure that all lube residue samples were dry. Actual testing

Test Sample Preparation

The test samples were prepared by evenly distributing 200 grams of wet lubricant in the foot-long, split conduit. The lubricant was dried (typically one day at 105 C) and percent solids determined to ensure drying.

This procedure duplicated the field situation of dried lubricant dispersed throughout a conduit system. While 200 grams per foot is a high lubricant usage, it is not unrealistic. As data shows later, the use of smaller quantities of lube somewhat shortens burn times, but does not affect ignition or flame propagation character.

There were, of course, significant differences in the amount and appearance of the residue after drying. The conduit containing each residue sample was put on the heating device described earlier to conduct the tests.

To provide a control for the test results, 20 gms. of Hypalon Cable Jacket were tested using the same methods, but without lubricant. This jacket was taken from a Class 1E nuclear qualified cable that was fire retardant. The jacket was stripped from the cable and cut into 1" squares for the test.

COMBUSTION DATA

Ignition Measurements

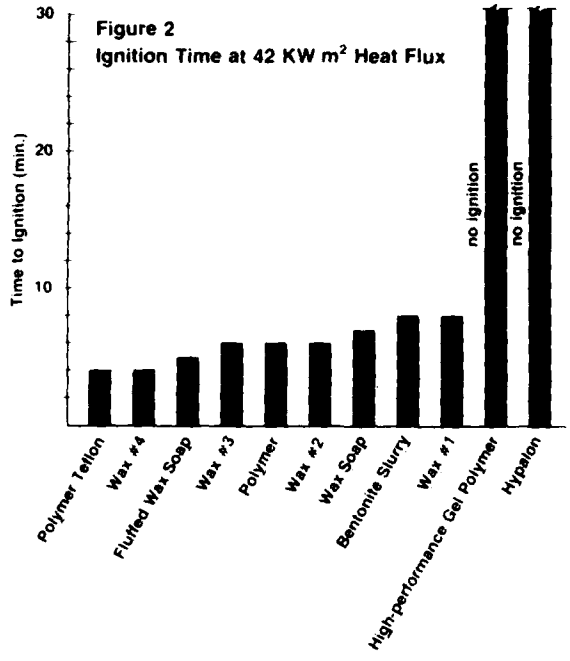
These measurements were made to determine the ease of ignition of each residue. None of the residues would ignite with only a match and no outside heat source. Therefore, none are "flammable" in the common sense of the word. Many, however, are "combustible" as will be shown.

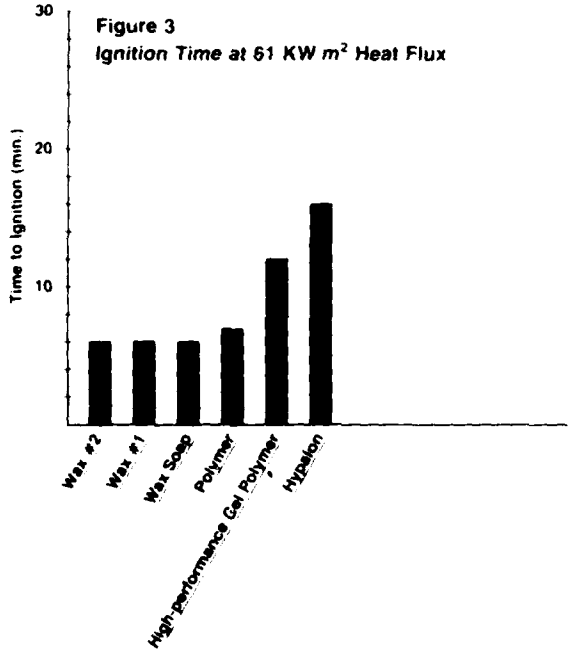
Using an approach described by Factory Mutual Research, several heat fluxes (heating levels) were focussed on the split conduit lubricant residue by varying the gas burn. The purpose was to determine the size of the fire source, if any, needed to ignite the lubricant residue. Based on Factory Mutual work with cable jackets, three different heat fluxes (gas burn rate) were chosen. These were 2.25 cfh (42 KW m²), 3.25 cfh (61 KW m²) and 4.5 cfh (85 KW m²).

At a given flame setting (heat flux), the split conduit with dried lube was placed over the flame and time to ignition was measured. The thermocouple was inserted into the residue and temperature was also monitored. Ignition was induced by briefly impinging the pilot flame on the residue sample at 30-second intervals. Ignition was defined as a sustained flame for at least 5 seconds after removal of the pilot light. With most of the samples, the pilot produced the ignition. Occasionally, at the

high heat fluxes, the Hydrocarbon Wax Lubricants would spontaneously ignite (without the pilot).

The heating was continued for 30 minutes. If a sample ignited, burned for a short while and then self-extinguished, the pilot was again applied at 30-second intervals to try to ignite a different area of the sample. Data from these ignition tests are presented in Figures 2, 3 and 4 and Table 2 below.





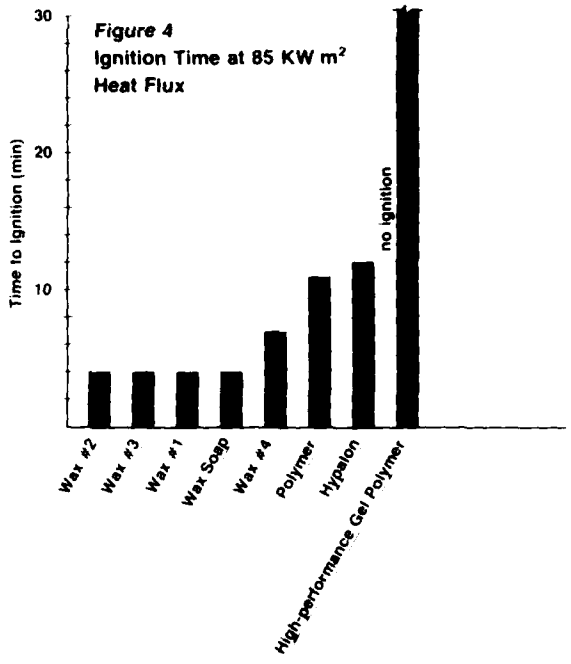


TABLE 2

Temperature at Ignition and Ignition Energy (Calculated) for Various Heat Fluxes

Lubricant	42 KW m² Flux		61 KW m² Flux		85 KW m² Flux	
	Temp (°C)	Ignition Energy (KJ m²)	Temp (°C)	Ignition Energy (KJ m²)	Temp (°C)	Ignition Energy (KJ m²)
High-Performance Gel Polymer	No Ignition	No Ignition >74,000	285	44,000	No Ignition	No Ignition >150,000
Wax #1	260	20,000	260	18,000	230	20,000
Wax #2	290	15,000	230	18,000	250	20,000
Wax #3	250	15,000			350	27,000
Wax #4	200	9,800			340	36,000
Fluffed Wax Soap	200	12,000				
Polymer Teflon	200	9,800				
Wax Soap	280	11,000	290	18,000	260	20,000
Bentonite Slurry	240	20,000				
Polymer	320	15,000	300	27,000	380	56,000
Hypalon	No Ignition	No Ignition >74,000	280	58,000	280	61,000

To understand this data, we must review a few concepts. Critical heat flux is defined as the heat flux (in KW m^2) below which samples will not ignite. In a fire, heat flux represents the intensity of the outside fire source. The gas burner would not function at gas flows under 2.25 cfh, which limited our minimum heat flux to 42 KW m^2. As Figure 2 shows, all samples could be ignited at 42 KW m^2 except the High-performance Gel Polymer Lube and the Hypalon Jacket control.

Ignition energy, shown in Table 2, is defined as the heat flux multiplied by the time to ignition. It is expressed in KJ m^2 and represents the amount of energy required to heat the lubric-

ant residue to ignition temperature. This, in turn, is related to the quantity, specific heat and thermal conductivity properties of the lubricant residue.

The data show significant differences in the ignition properties of the lubricant residues. The Wax and Wax Soap Lubes have critical heat fluxes well under 40 KW m^2 and ignition energies under 20,000 KJ m^2. They ignite at temperatures between 200 and 300 C.

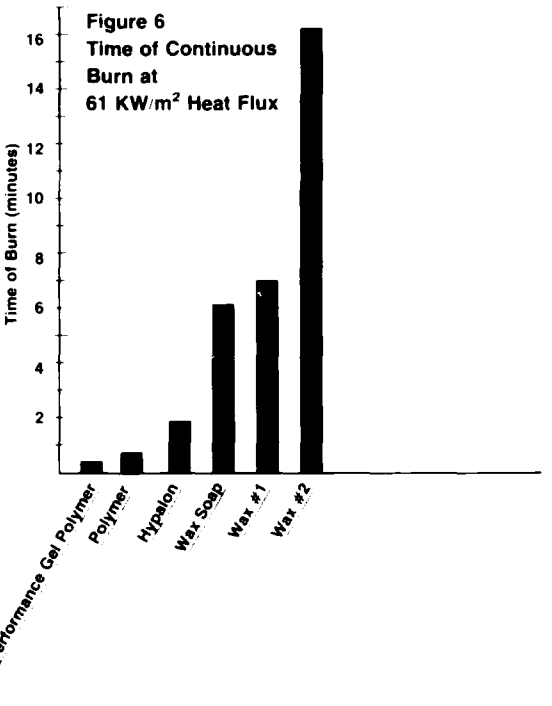
The Hypalon Cable Jacket and the High-performance Gel Polymer Lube have critical heat fluxes above 40 KW m^2 and ignition energies above 50,000 KJ m^2. We could not determine a consistent critical heat flux for the High-performance Gel Polymer since it ignited briefly at 61 KW m^2, but would not ignite at 85 KW m^2. Regardless, the Hypalon Jacket control and High-performance Gel Polymer were clearly much harder to ignite than the other lubricants tested.

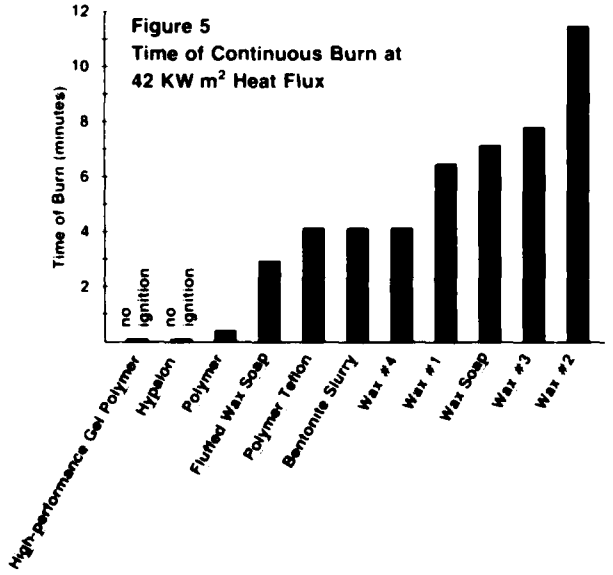
We should note that the Bentonite Clay Lubricant ignition seems illogical. However, these lubes contain ethylene glycol, which is what burned.

Flame Propagation & Burn Times — Continued Outside Heat Source

Once a residue had ignited (greater than five seconds burn), several additional measurements and observations were made. First, the burn was timed until the flame extinguished. If the flame **spread** through the conduit from the initial ignited area, this was noted. If the flame went out, additional attempts were made to ignite other areas of the residue with the pilot for the full 30 minutes of the test.

Data on burn times and flame propagation are presented in Figures 5, 6, 7 and Table 3 below.





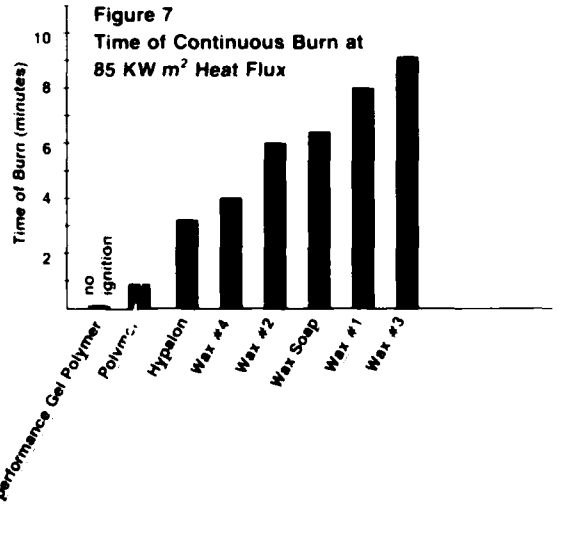


TABLE 3

Flame Propagation at Various Heat Fluxes

Lubricant	Flame Spread @ 42 KW m²?	Flame Spread @ 61 KW m²?	Flame Spread @ 85 KW m²?
High-performance Gel Polymer	No	No	No
Wax #1	Yes	Yes	Yes
Wax #2	Yes	Yes	Yes
Wax #3	Yes		Yes
Wax #4	Yes		Yes
Fluffed Wax Soap	Yes		
Polymer Teflon	Yes		
Wax Soap	Yes	Yes	Yes
Bentonite Slurry	Yes		
Polymer	No	No	No
Hypalon	No	No	No

The lubricant residues fall into several categories. The Hydrocarbon Wax and Combination Wax Lubes, once ignited, burn freely and at length, allowing the flame to spread throughout the conduit.

The Clay Slurries and Teflon-containing Lube also burn continuously, and spread the flame, although not with such vigor.

Finally, while the Hypalon Jacket, High-performance Gel Polymer and plain Polymer can sometimes be ignited for short time periods at the higher heat flux, they self-extinguish and do not spread flame. The High-performance Gel Polymer Lubricant shows very short, if any, burn times and quick self-extinguishment. The High-performance Gel Polymer Lubricant is, in fact, considerably more fire resistant than the Hypalon Cable Jacket.

Flame Propagation & Burn Time — Discontinued Outside Heat Source

Tests were done where the burner was turned off once the sample had ignited. The lowest heat flux which had previously resulted in ignition was used for these tests. The burning sample was then observed to see if the flame spread throughout the conduit from the point of ignition. Total time of burn was also measured.

This test determines whether the heat produced by combustion of the lubricant residue is sufficient to sustain the flame without any additional outside heat source. In a fire situation, this could result in the spread of the fire into a non-burning area (through a firewall).

The data on burn times and flame propagation are presented in Table 4 below.

TABLE 4

Fire Parameters with Burner Turned Off *on Lubricant Ignition*

Lubricant	Heat Flux	Time of Burn (Minutes & Seconds)	Spread on Propagation Through Conduit?
High-performance Gel Polymer Lube	61 KW m²	No Ignition	No
Wax Lube #1	42 KW m²	10:9	Yes
Polymer Teflon Lube	42 KW m²	2:0	Yes
Wax Soap Lube	42 KW m²	14:0	Yes
Hypalon Jacket	61 KW m²	3:40	No

Results show that the Hydrocarbon Wax, Combination Wax and Polymer Teflon Lubricants burn vigorously even when the outside heat source is removed. The combustion of these lubricants produces enough heat to self-sustain and propagate flame.

The High-performance Gel Polymer Lube would not burn for more than five seconds, barely enough time to turn off the burner. The Hypalon Jacket material did burn for several minutes after the heat flux was removed. The flame did not spread, however.

Residue Quantity

To see how combustion properties changed with a smaller quantity of residue, several of the combustible lubricants were tested with one-half the amount in the test conduit (100 gms.). Results are presented in Table 5.

TABLE 5

Fire Parameters with 100 gram Sample Size

Lubricant	Heat Flux (KW m²)	Ignition Time	Temperature At Ignition (°C)	Time of Burn (Minutes & Seconds)	Flame Spread Throughout Conduit?
Wax Lube #1	42	[illegible]	220	6:47	Yes
Wax Soap Lube	42	[illegible]	275	6:33	Yes

With half the residue, the results did not differ significantly from before. Ignition times and temperature are similar. Surprisingly, even with the significant decrease in fuel, burn times are down only slightly.

Residue Mobility

It was noted earlier that the Hydrocarbon Wax Lubes melted on heating. Melting data on the lubes are presented in Table 6.

TABLE 6

Melting Data on Lubricant Residues

Lubricant	Liquifies When Heated Above 300°C?
High-performance Gel Polymer Lube	No
Wax Lube #1	Yes
Wax Lube #2	Yes
Wax Lube #3	Yes
Wax Lube #4	Yes
Fluffed Wax Soap Lube	Yes
Polymer Teflon Lube	No
Wax Soap Lube	Yes
Bentonite Slurry Lube	No
Polymer Lube	No
Hypalon Jacket	No

To see if melted lubricant residue would flow and spread flame, a test was run on Wax Lube #1. The residue from 200 grams of Wax Lube #1 was placed in half the length of conduit. The same device and heating procedure (42 KW m⁻²) was used as before. As expected, the lubricant residue melted (at about 120 C) and flowed through the conduit. The flowing residue ignited at 240 C. The flame was then spread by the mobile fluid through the entire length of the conduit.

CONCLUSIONS:

Significant differences can be observed in the combustibility of lubricant residues.

The Wax and Combination Wax Soap Lubricant residues are combustible. They ignite at heat fluxes below 40 KW m^2 and temperatures of 200 -300 C. Once the wax residue is ignited, the flame sustains itself without any outside heat source. Flame will also spread along these residues. This flame movement is accelerated if the residue melts and flows.

There are a number of other lubricants — Polymer Teflon, Bentonite Clay Glycol Slurries — which can also be ignited but do not burn as vigorously nor as long (lower solids). These also spread flame once ignited.

Finally, there was one lubricant which showed little tendency to ignite or burn; in fact, less tendency than fire retardant cable jacket. This was the High-performance Gel Polymer Lube.

The ignition behavior of the lubricant residues is specific to the residue, rather than its quantity. Some residues were quite combustible, with only one demonstrating outstanding fire resistance.

A secondary factor is the quantity of the residue remaining. This quantity is directly proportional to the percent non-volatiles (% solids) of the lubricant. Lubricants with **very low solids** (<1%) don't seem to have enough residue to propagate or spread flame, even if their residues can be ignited.

In applications where the spread of fire is of concern, and particularly where fire-retardant cables are used in conduit, care should be used in selecting a lubricant. One approach is to select lubricants which are less combustible than the cable itself. Based on this approach, suggested performance criteria for such a lubricant (residue) would be:

1) Will not ignite for more than 10 seconds at a 40 KW m^2 heat flux or at a 315 C temperature (200 gm. sample).

2) At a heat flux of 60 KW m^2, will not burn for more than 60 seconds after removal of heat source (200 gm. sample).

3) Will not melt or flow when heated to 350 C.

REFERENCES

[1] Friction Theory and Lubrication Techniques for Improved Cable Pulling. Weitz, Gene C., American Polywater Corporation, Stillwater, Minnesota. 1985, IEEE Industrial and Commercial Power Systems Conference, Denver, Colorado.

[2] A Laboratory-Scale Test Method for the Measurement of Flammability Parameters. Tewarson, A. and Pion, R., Factory Mutual Research, Norwood, Massachusetts. Technical Report 22524 (October 1977).

[3] IEEE Standard for Qualifying Class 1E Electric Cables and Field Splices for Nuclear Power Generating Stations. IEEE Standard 383 (1974). Institute of Electrical and Electronics Engineers, Inc., New York, New York.

[4] Cable Flammability Testing at Factory Mutual Insurance Research Facilities. Tewarson, A., Factory Mutual Research, Norwood, Massachusetts. Insulated Conductors Committee of the IEEE Power Engineering Society, 78th Meeting, Knoxville, Tennessee, April 1986.

[5] Overall Fire Safety of Cable and Wiring Materials. Clark, III, Frederick B., Benjamin, Irwin A., DiNerro, Philip J., Benjamin Clark Associates, Kensington, Maryland. 32nd International Wire & Cable Symposium, Cherry Hill, New Jersey (November 1983).



John M. Fee
American Polywater Corporation
P.O. Box 53
Stillwater, Minnesota 55082
U.S.A.

John M. Fee graduated from Massachusetts Institute of Technology in 1968 with a degree in Chemistry. He has worked at 3M and American Polywater on the development of a variety of specialty chemical products. Mr. Fee is currently President of American Polywater Corporation, a manufacturing firm specializing in cable installation products.



Deborah J. Quist
American Polywater Corporation
P.O. Box 53
Stillwater, Minnesota 55082
U.S.A.

Deborah J. Quist has an associate degree as a laboratory technician from Hennepin Technical Center. She is currently employed by American Polywater as a Research and Development Technician. Ms. Quist's current work includes the development and evaluation of cable pulling lubricants.

RECENT ADVANCES IN THERMOPLASTIC, ZERO HALOGEN, LOW SMOKE, FIRE RETARDANT CABLE COMPOUND TECHNOLOGY

Mr.S.Artingstall, Mr.A.J.Pyle, Dr.J.A.Taylor

LINDSAY AND WILLIAMS LTD
COLUMBINE STREET
MANCHESTER M11 2LH
ENGLAND

ABSTRACT

The development of a thermoplastic, halogen free, low smoke, fire retardant compound which is suitable for use in the manufacture of both power and telecommunication cables is described. Results are presented to show that the compound possesses similar mechanical properties to a typical PVC jacketing compound. The low smoke, low acid gas, and low toxic gas emission characteristics of the material are discussed. The effect of prolonged immersion in water on the electrical properties of the compound has also been studied, and results presented which show that after an initial drop in insulation resistance constant, an equilibrium value is achieved, which is higher than that specified for a PVC jacketing material. The processing characteristics of the compound have been investigated, and results presented to show that extrusion speeds similar to those of typical PVC jacketing compounds can be achieved. Cables jacketed with the compound have passed a severe vertical fire test.

INTRODUCTION

For many years, many halogen containing polymers have been used in the manufacture of electrical cables. Compounds based on these polymers, which include polyvinylchloride(PVC), polychloroprene(PCP) etc; have provided the cable manufacturer with robust, inexpensive, easy processing materials, which have given good service in practice. There has in recent times however, been a recognition that some of the conventionally used cable compounds based on halogen containing polymers, can present problems in the event of a fire.

These problems can be classified into three main categories. Firstly, some conventionally used compounds can propagate a fire along a cable run, or, by generating drips of burning material, can transmit the fire to a lower level of an installation. Secondly, the formation of large amounts of dense black smoke and acidic and/or toxic fumes is a major concern where large numbers of people gather in a confined area eg Underground railway systems, Hotels, Exhibition Halls, [illegible] Finally, the formation of highly acidic fumes can damage expensive equipment eg. Telephone Exchanges, Computer Suites, Military Electronic Systems etc. In response to these problems, "zero halogen" or "halogen free" compounds have been developed.

The general requirements for thermoplastic, zero halogen compounds have been described previously[4,5]. This has led to the development of thermoplastic compounds which possess excellent fire retardant characteristics, thus making possible the manufacture of cables which generate only very low amounts of smoke and acidic fumes[6,7,8].

Many cable manufacturers, however, prefer to offer cables manufactured using compounds of their own design, which has led in certain cases to zero halogen cables possessing adequate fire and smoke properties but exhibiting a number of drawbacks. These drawbacks can be summarised as poor mechanical properties (in some cases, cable jackets with tensile strengths of less than 5 MPa, 725 psi, have been offered), poor electrical properties (especially when immersed in water), poor abrasion resistance and processing difficulties.

Furthermore, as most of the applications into which zero halogen cables are now being installed would, in previous years, have used PVC jacketed cables, it would seem reasonable to attempt to develop materials which possess the desirable attributes of zero halogen compounds, coupled with the mechanical and electrical properties normally associated with PVC jacketing compounds.

DISCUSSION

Laboratory Evaluations

It is beyond the scope of this paper to discuss in detail all of the compound formulation philosophies which were examined in the present work. A broad classification can be made however, based on the types of polymers eg. EEA, EBA, EVA, EPR, EPDM etc. used in each class of formulation. A programme of experiments was executed in which only the important properties were evaluated. The general conclusions from these experiments is given in Figure 1.

Base Polymer Type	I		II	III	IV	V		
Lab Formulation No.	19	38	67Q	DR1	51	72R	62E	40
Tensile Strength	**	**	*	*	*	***	***	**
Elongation	***	***	**	*	*	***	***	***
Cold Elongation	*	*	**	**	*	***	**	*
Dimensional Stability at 100°C	*	*	*	*	*	**	*	*
Electricals after immersion in water	*	*	**	**	*	***	***	*
Manufacture	**	**	**	**	**	***	*	*
Scuff Resistance	*	*	*	*	*	**	*	*
Processability	*	*	*	*	**	***	*	**

* = poor, ** = moderate, *** = good

Figure 1.

General Conclusions from Screening Programme

Property	Result
Tensile Strength	15 MPa(2175psi)
Elongation	150 %
Elongation at -25°C(-13°F)	50 %
Insulation Resistance Constant (K value)	345 Megohm Km
Oxygen Index	35
Specific Gravity	1.57

Figure 2.

Properties of Laboratory Formulation 72R Extrudate

Laboratory formulation 72R stood out as the only compound which gave a good or moderate performance in most of the areas initially under consideration. Some of the actual results obtained from laboratory extrudate are reproduced in Figure 2.

Following these initial results, formulation 72R was renumbered as compound 300 for production manufacturing trials, customer evaluation and further detailed study. Several cables were manufactured in the factories of different customers using standard production quality compound. The results obtained from these trials, along with supporting laboratory tests, are presented in the remainder of this paper.

PROPERTIES	CABLE A[9]	CABLE B[10]	CABLE C[11]
Tensile Strength	14.5 MPa (2100 psi)	14.0 MPa (2030 psi)	15.1 MPa (2620 psi)
Elongn. at Break	158 %	148 %	164 %
After Ageing 10 days at 100°C (212°F)			
Tensile Strength	18.3 MPa (2650 psi)	16.4 MPa (2375 psi)	17.2 MPa (2180 psi)
Elongation	134 %	132 %	134 %
After Ageing 7 days at 121°C(250°F)			
Tensile Strength	-	17.6 MPa (2550 psi)	-
Elongation	-	114 %	-

Figure 3.

Mechanical Properties of Cable Jackets

MECHANICAL PROPERTIES

As can be seen in Figure 3, similar results have been obtained from cables produced by different manufacturers and which are in broad agreement with the laboratory results demonstrated in Figure 2. Furthermore, the absolute values obtained, and the retention values after ageing, exceed the minimum values required for a general purpose PVC jacketing compound[12], as well as those for zero halogen cable jacketing compounds[13,28].

THERMOMECHANICAL PROPERTIES

Hot Pressure and Hot Deformation

For a single cable jacketing compound to be suitable for use in the manufacture of both power and telecommunication cables, it is essential that the compound possess adequate hot pressure and/or hot deformation characteristics. These tests were carried out on extruded samples and the results are presented in Figures 4 and 5. As can be seen,

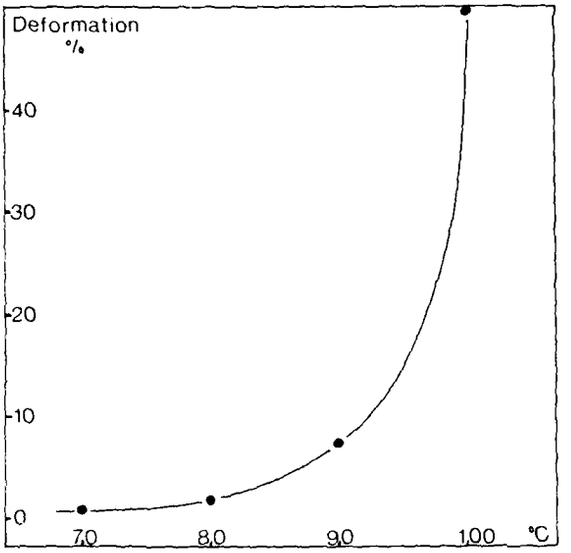


Figure 4.

Hot Deformation Test BS 6469:1984

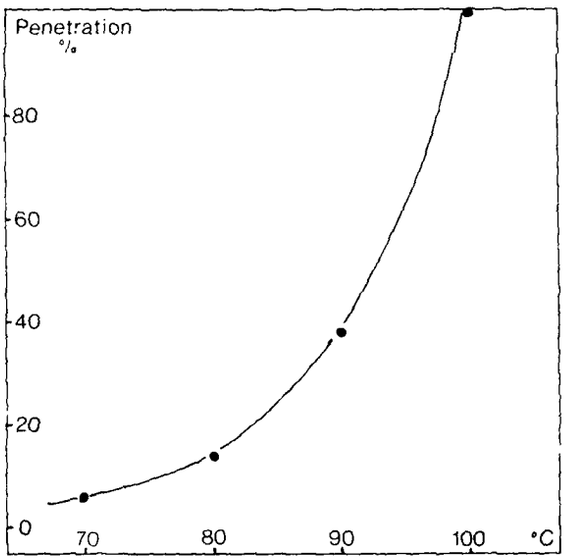


Figure 5.

Hot Pressure Test BS 6469:1984

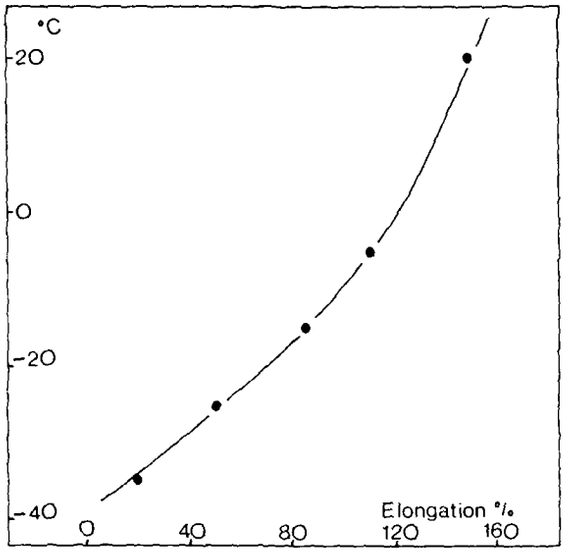


Figure 6.

Elongation at Break vs Temperature

compound 300 easily exceeds the requirements of 50% penetration at 80°C(176°F) which are specified for a PVC jacketing compound[12]. The results would indicate that in this respect, the compound is suitable for use on cables with rated conductor temperatures up to 90°C(194°F).

Low Temperature Properties

Having investigated the high temperture thermomechanical properties of the compound, it is important to establish the lower practical temperature at which the cable may be handled without cracking. Figure 6 shows the measured elongation at break over a range of sub zero temperatures. Applying the criteria of 20% minimum elongation which is specified for a hard PVC jacket[12], the minimum practical installation temperature would be expected to be approximately -35°C (-31°F).

Finished cables jacketed with compound 300 have also passed Cold Bend and Cold Impact tests at -25°C(-13°F)which lends practical support to the above data.

ELECTRICAL PROPERTIES

Many European cable constructions rely on the use of galvanised steel wire armour or other metallic tapes as protective members,and often to act as electrical screening or as an earth conductor/fault

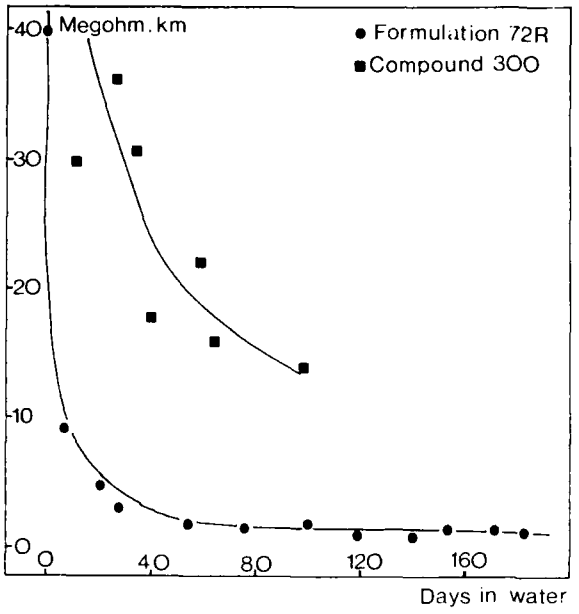


Figure 7.

Insulation Resistance Constant vs Time

path. There is a concern in some cases, when a halogen free cable has been immersed in water for even a short period, the insulation characteristics of the sheath rapidly deteriorate, leading to the possibility of accelerated corrosion of the armour due to electrochemical processes. Because of this concern there has been an attempt, in a recent zero halogen cable specification[13] to address this problem by specifying a minimum insulation resistance constant. The test method specified, however, only considers the effects of immersion in water for a relatively short period (12 hours). In practice, cables may come into contact with water for longer periods than this and so it is of interest to examine the electrical properties after prolonged immersion. The insulation resistance of Formulation 72R has been monitored for a period of 182 days at the time of writing utilising the method specified for a PVC jacketing compound[12]. The insulation resistance is measured on an approximately 1mm(0.040inch) thick plaque, and the insulation resistance constant or K value is calculated using the following formula.

$$K = \frac{3.66 \times 10^{-7} \times R \times A}{t}$$

R = measured resistance in Megohm
A = area of electrode in mm^2
t = sheet thichness in mm

The results are presented in Figure 7.

TEST	VALUE
Limiting Oxygen Index	35
Temperature Index	270°C
BS4066 Part 1 (on cable A)	Pass

Figure 8.

Small Scale Fire Tests on Compound 300

The minimum permitted K value of a PVC jacketing compound and that of a zero halogen compound has been specified as 0.0035 Megohm Km [12,13]. The value obtained for the insulation resistance constant of Formulation 72R when tested by the specified procedure (ie after 12 hours immersion) was 345 Megohm Km. At that point however, the sample was not at equilibrium, and the insulation resistance continued to fall, until an equilibrium value was attained; which for Formulation 72R, appeared to be equivalent to 2 megohm Km: still considerably higher than the permitted minimum value of 0.0035 Megohm km.

The insulation resistance of Compound 300 has also been monitored for an extended period, although somewhat shorter than for Formulation 72R, and shows a better performance than that of its laboratory predecessor. This apparent improvement in electrical properties is known to be due to the higher degree of dispersion of the inorganic ingredients obtainable from the production plant which was used to manufacture compound 300.

FIRE TEST PROPERTIES

Several small scale laboratory fire tests have been performed on compound 300, and the results are given in Figure 8. The Limiting Oxygen Index of a typical PVC jacketing compound would be expected to be in the order of 28-32, whilst that of compound 300 is somewhat higher at 35. The Temperature Index of compound 300 is higher than the minimum value of 260°C required for a zero halogen jacketing compound for Metro (subway) cables[15].

Most fire retardant cable specifications however, do not refer to the fire performance of individual elements within the construction of a cable but to the performance of the finished cable, although there are several notable exceptions[14,15] where minimum values of limiting oxygen index and temperature index are specified.

In order to test the effectiveness of compound 300, as a fire retardant cable jacketing compound, it was therefore necessary to test a finished cable to



Figure 9.

Schematic Drawing of BS 4066 Part 3 Vertical Fire Test

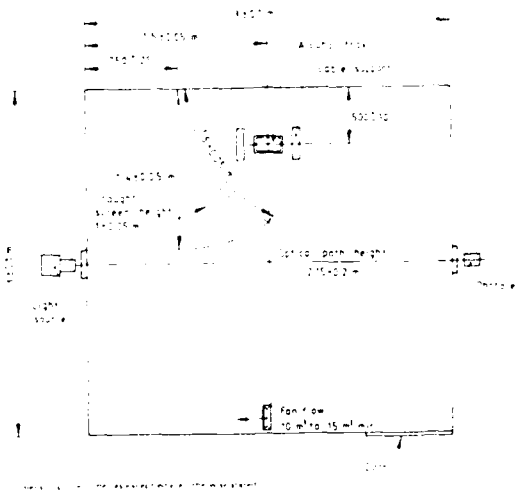


Figure 10.

Schematic Drawing of the 3 Metre Cube Smoke Test

a recognised fire test procedure. There are several vertical fire test procedures which possess similar general characteristics[16,17,18,19] and the test method selected was the relevant British Standard[17] which is refered to in a specification for halogen free, low smoke cables[13]. This test method has three categories dependent on the amount of combustible material on the ladder. For this test, the highest loading of 7 litres per metre was selected (category NMV 7). The cables are subjected to a 70,000 Btu burner for 40 minutes and damage should not exceed 2.5 metres (8.2 ft) from the burner.The general layout of the test chamber is shown in Figure 9.

A zero halogen, fire retardant cable[10] jacketed with compound 300 and constructed according to an appropriate British Standard[13] which incorporates standard XLPE low voltage insulation material,was tested in this manner. Lengths of this cable were wired on the ladder in a staggered formation. This is the more severe method of bunching the cables as the igniting flame can penetrate around the cables on the front of the ladder, to those at the rear, and the relative positions of the cables on the ladder can produce a 'chimney' effect. Following the test, damage to the cable jacket was limited to 1.05 metres(3.5 ft) from the burner,ie. the cable had achieved a 'pass' rating to Category NMV 7 in the BS4066 Part3 vertical fire test. The cable self extinguished at the end of the test, and no burning drips were observed throughout the duration of the test.

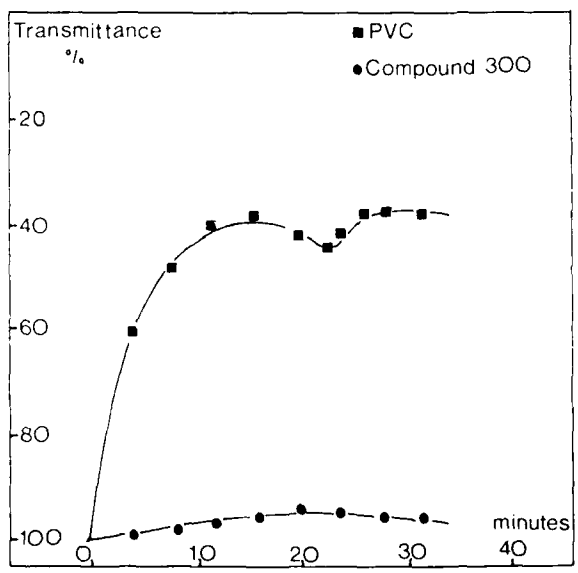


Figure 11.

Results From 3 Metre Cube Smoke Test

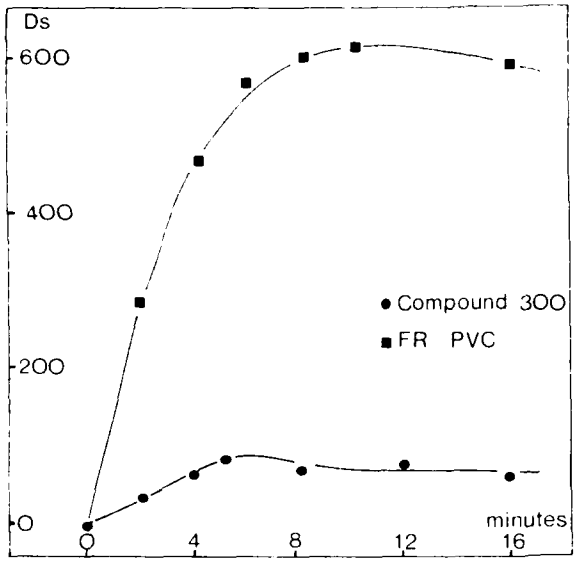


Figure 12.

NBS Smoke Chamber Results

SMOKE TESTS

The "3 Metre Cube" or 27m³ smoke test is gaining in popularity and is specified in a number of cable specifications[3,4,25]. The test was originally developed to assess the formation of smoke arising in a Metro(Subway) application, and in this respect, the 27 m³ test chamber approximates to a tunnel section. The basic layout of the test chamber is shown in Figure 10. A burning alcohol fire source is used and the smoke generation is monitored continuously by a horizontal light source/photcell assembly. The chamber may also be modified to include pilot lights or EXIT signs in order to obtain a subjective assessment of smoke generation.

Figure 11 shows the trace obtained from Cable C[11], along with the equivalent data for a similar PVC jacketed cable. This result clearly shows the dramatic improvement in the degree of smoke generation of compound 300 over the PVC equivalent.

Other data supporting this result has been found from smaller scale tests carried out in the NBS Smoke chamber, where a maximum specific optical density(Ds max) of 89 has been obtained for tests carried out in the flaming mode. The equivalent results for a typical PVC compound would be approximately 600. The results of this work are presented in figure 12.

Gas	Concentration ppm	Index
Carbon dioxide	3050	0.255
Carbon monoxide	9	0.045
Formaldehyde	0	0
Hydrogen fluoride	0	0
Hydrogen chloride	0	0
Hydrogen bromide	0	0
Hydrogen cyanide	0	0
Nitrous oxides	2.2	0.145
Acrylonitrile	0.15	0.02
Ammonia	0	0
Hydrogen sulphide	0	0
Phosgene	0	0
Phenol	0	0
Toxicity Index		0.465

Figure 13.

NES 713 - Toxicity Index for Compound 300

TOXICITY

The question of toxicity is one which is highly emotive and is bedevilled by the lack of meaningful test methods. The concept of a "Toxicity Index" has been adopted in a number of areas, particularly by the military[21,22]. This method involves completely burning the organic content of a small sample in a chamber of specified volume, then measuring the concentration of a number of specific gases during the combustion. These concentrations are then processed mathematically using factors based on the exposure levels of each gas considered fatal to man for a 30 minute exposure time, and using correction factors for background concentration to produce a single figure known as the toxicity index.

The mean of duplicate results of tests carried out to NES 713[21] are presented in Figure 13. As can be seen, the absence of halogenated or sulphurous gases confirm the halogen and sulphur free nature of the compound. Other potentially toxic gases were present in only trace amounts.

The observed toxicity index value of 0.465 is significantly lower than the maximum value of 5 allowed by the U.K. Naval Specification NES 518[24].

ACID GAS EVOLUTION

There are several methods which can be used to evaluate the evolution of acidic gases from burning polymeric materials[23,24]. Most of these methods involve the combustion of a small sample of compound in a current of air. The fire gases are collected in wash bottles and the resulting

	Compound 300	PVC
BS 6425		
Hydrogen chloride	less than 0.5%	28.5
VDE 0472 part 813		
Conductivity us cm^{-1}	14	4500
pH	5.0	2.4

Figure 14.

Acid Gas Evolution Results

solutions examined, either by chemical methods[23] or by measurment of pH and conductivity[24]. The results obtained for compound 300 using both of these procedures are presented in Figure 14, along with the equivalent results for a typical PVC jacketing compound.

The British Standard method is only accurate for hydrogen chloride contents greater than 0.5% and hence, only this lower detection limit can be assigned to compound 300 despite its zero halogen nature. With the VDE method, the low pH and high conductivity of the solution obtained from the PVC jacketing compound demonstrates the highly acidic nature of the fire gases. As anticipated, compound 300 produced only a weakly acidic solution, which also possessed a low conductivity, thus confirming the low level of acid gases.

PROCESSING CHARACTERISTICS

A pre-requisite of any cable jacketing compound is that it can be processed efficiently within a cable factory, with the minimum of ancillary processes, such as pre-drying etc. Furthermore, as the object of this work was to develop a halogen free material which possessed similar properties to a PVC cable jacketing compound, it is not unreasonable to attempt to achieve similar processing speeds.

A 60mm(2.36 inch), 24 L/D extruder was used[25], fitted with a 16/30 head, into which was installed 13.3 mm(0.524 inch) point and 14.9 mm(0.589 inch) die. No breaker plate or screen pack was used. The same simple temperature profile was adopted throughout the series of experiments and is reproduced in Figure 15. The processing characteristics of compound 300 were examined on three different designs of screw.

Screw design A, known as "Constance" design, is a proprietary design[26], incorporating a barrier flight. This design is commonly used to process PVC jacketing compounds.

Zone 1	140°C (284°F)
Zone 2	140°C (284°F)
Zone 3	140°C (284°F)
Zone 4	140°C (284°F)
Zone 5	140°C (284°F)
Head 1	150°C (302°F)
Head 2	150°C (302°F)
Die	160°C (320°F)

Figure 15.

Temperature Profile for Extrusion of Compound 300

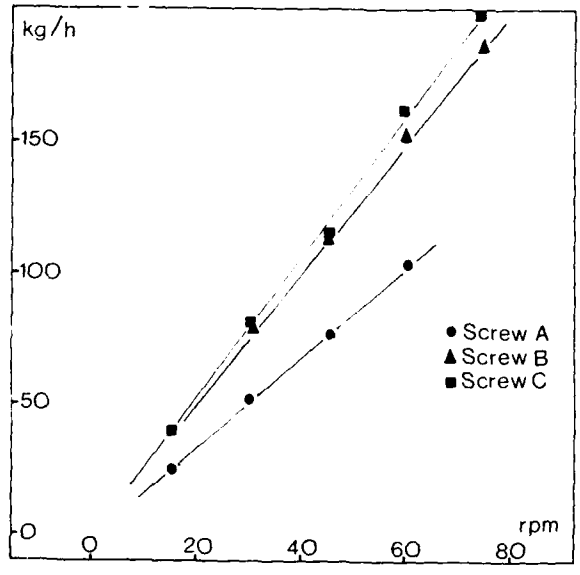


Figure 16.

Output Versus Screw Speed

Screw design B is a low compression, low shear screw and is highly effective for processing low smoke, fire retardant compounds[27].

Screw design C is a developmental design[26] which combines the barrier flight technology of screw design A with the low compression and shear characteristics of screw design B.

Compound 300 was used without any pretreatment such as drying etc., and was extruded at several screw speeds with each of the screws. The output, melt temperature, head pressure and screw torque were measured at each speed. The results of these experiments are presented in figures 16 - 19.

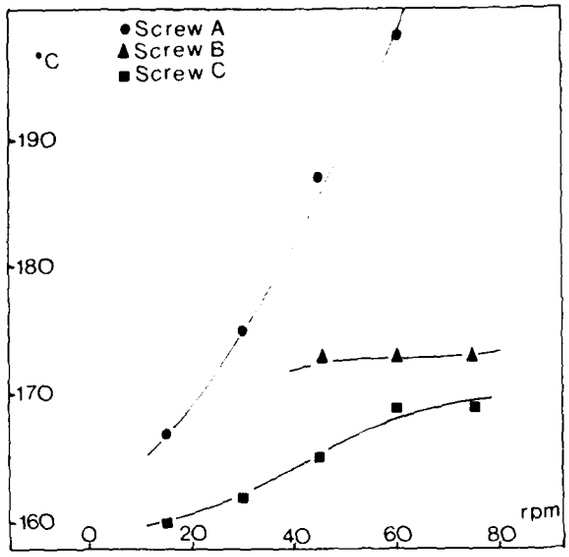


Figure 17.

Melt Temperature Versus Screw Speed

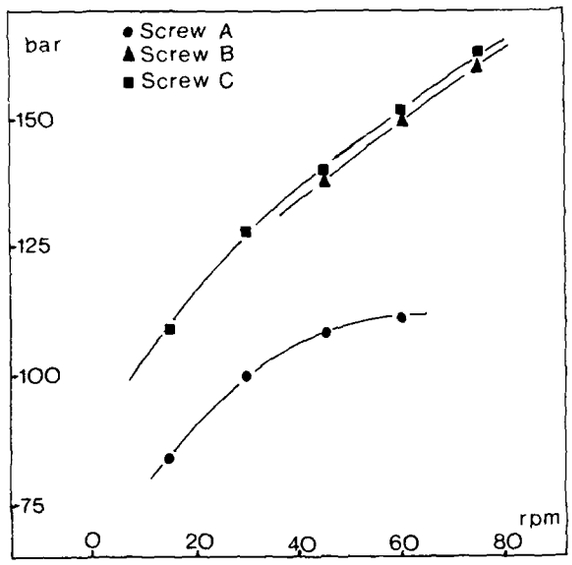


Figure 18.

Head Pressure Versus Screw Speed

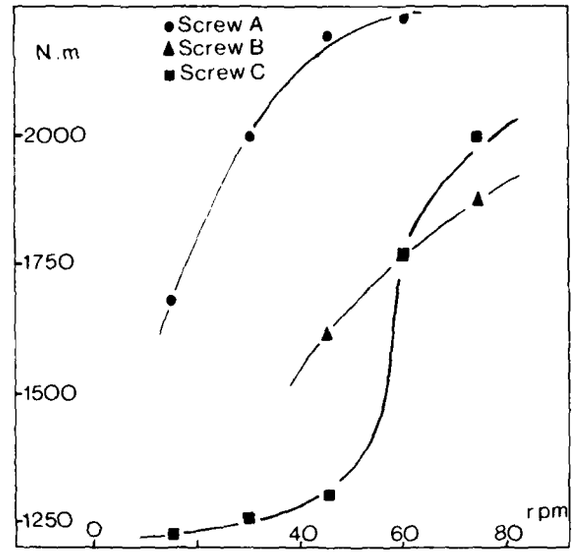


Figure 19.

Screw Torque Versus Screw Speed

The barrier flight of screw A, imparts a relatively high degree of shear, which results in a higher screw torque and more rapid rise in melt temperature. The maximum practical volumetric output of compound 300 obtained from screw A was 49 litre/hour (77 kg/hour; 170 lb/hr) which is significantly lower than the 115 litre/hour(160 kg/hour; 352 ib/hour) which would be typical for a PVC jacketing compound processed on this screw at 140 rpm.

A significantly higher output was obtained from screw B as anticipated, although at high screw speeds (90 r.p.m.) the extrudate was lumpy and contained occasional isolated single blisters. This lumpy appearance was ascribed to poor thermal homogenisation and the blisters are believed to be due to the entrapment of air within the melt. These phenomena are not surprising since the screw channels are relatively deep and the compression ratio is very low (approximately 1.2 : 1).

The developmental screw (designated Q15 by the manufacturer) has a deep flight similar to screw B but has a relatively low barrier flight throughout a short section of the screw length. This barrier flight imparts sufficient compression within the screw to ensure that no air is entrapped and that good thermal homogenisation is achieved. Good quality extrudate was obtained at high output rates. Indeed, at 75 rpm, a volumetric output of 127 litre/hour (200 kg/hour; 440 lb/hour), which compares favourably with the 115 litres/hour, typically expected from a PVC compound being processed on a screw designed to process PVC.

Property	Pressure Extrusion	Tubing Extrusion DDR 1.5:1	Bleed
Unaged			
Tensile Strength MPa (psi)	12.9 (1870)	15.9 (2305)	12.8 (1860)
Elongation %	168	148	163
After 7 days at 80°C(176°F)			
Tensile Strength MPa (psi)	15.7 (2275)	16.3 (2360)	15.9 (2305)
Elongation %	144	146	135
After 7 days at 100°C(212°F)			
Tensile Strength MPa (psi)	16.7 (2420)	19.6 (2840)	16.6 (2410)
Elongation %	135	112	130
After 10 days at 100°C(212°F)			
Tensile Strength MPa (psi)	17.1 (2480)	20.1 (2910)	17.2 (2490)
Elongation %	126	126	122

Figure 20.

Effect of Extrusion on Properties

THE EFFECT OF PROCESSING ON PROPERTIES

The effect of different types of extrusion processing techniques commonly used were examined. A 60mm(2.36inch), 20 L/D extruder equipped with a screw of type B above was fitted with a 20 mm(0.79 inch) point and a 23 mm(0.91 inch) die. the positions of the point and die relative to each other was varied, to enable both pressure and tubing style extrusion (draw down ratio 1.5:1) to be performed. Additionally, extrudate was allowed to 'bleed' from the extruder in an unsupported manner. The extrudate so produced was aged under various test regimes and the results are presented in Figure 20. As can be seen, the hignest tensile strength is obtained from a tubing style extrusion, in which the orientation within the jacket would be expected to be the greatest.

In a second series of tubing extrusion experiments, the effects of different drawdown ratios on dimensional stability was examined. For this work, two sets of tools were employed : the first set of tools gave drawdown ratios in the range 1.7:1 to 2.2:1 whilst jacketing a 19mm(0.748 inch) core; and

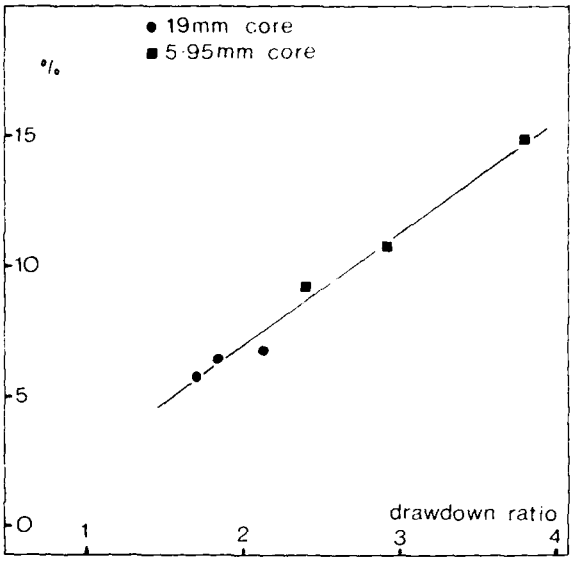


Figure 21.

Dumbell Shrinkage vs Drawdown Ratio

the second set of tools gave drawdown ratios in the range 2.4:1 to 3.8:1 whilst jacketing a 5.95mm(0.234 inch) core. Dumbell samples taken from the jackets so produced were aged at 100°C(212°F) for 2 hours. Previous thermal ageing work had shown that any dimensional changes taking place in these materials occurs in the first few hours of the ageing procedure. The results of these experiments are presented in Figure 21. As can be seen, a reasonably direct relationship exists between the drawdown ratio used in the tubing extrusion and the shrinkage obtained with the dumbell samples.

In practice, cables A and B (see Figure 3) were manufactured using a tubing technique with a draw down ratio of approximately 1.5 : 1, and dumbells taken from the jackets exhibited shrinkage values of 3.5 % and 4 % respectively after ageing for 7 days at 100°C (212°F). The retraction of the sheath on an experimental cable which had previously showed a dumbell shrinkage of approximately 10 %, was found to be 2 % after ageing the cable for 7 days at 100°C (212°F).

The above results would suggest that compound 300 is suitable for either pressure or tubing style extrusion techriques. In the latter case however, the drawdown ratio should be preferably below 2 : 1 in order to prevent excessive dumbell shrinkage, although, in practice, high dumbell shrinkage values may not lead to high sheath retraction.

It is gratifying to discover that the laboratory results obtained with Formulation 72R have been generally reproduced with Compound 300 in practical manufacturing environments (cf. Figures 2, 3, and

20) despite the operational differences found within these seperate factories.

CONCLUSIONS

The object of this work has been to develop a halogen free, thermoplastic material with similar performance characteristics to a PVC jacketing compound, yet provide improved performance in a fire.

To this end it has been demonstrated that compound 300 is a thermoplastic, halogen free, fire retardant compound which is suitable for use as a cable jacketing.

Compound 300 possesses tensile strength and elongation properties which enable the material to satisfy the requirments expected from a jacketing grade of PVC.

The excellent thermomechanical properties of compound 300 make it suitable for use in the manufacture of both power and telecommunication cables.

Cables jacketed with Compound 300 exhibit very low fire propagation characteristics as evidenced by results from BS 4066 Part 3 fire tests.

Generation of smoke, acidic and toxic fumes from compound 300 is minimal.

By utilising modern screw design technology, compound 300 may be extruded at similar rates to typical PVC jacketing compounds.

Compound 300 may be processed using various conventional extrusion techniques, and in each case can comply with the specification for a hard PVC jacketing compound[12].

It is the view of the authors therefore, that compound 300 provides a viable alternative to a PVC cable jacketing material for use in environments where smoke, acidic and toxic fumes may present special problems in the event of a fire.

It is envisaged that cables utilising compound 300, will be installed in areas either where people need to be evacuated safely and quickly in an emergency, or in areas containing expensive or sensitive equipment. These areas include hotels, high rise buildings, exhibition centres, hospitals, telephone exchanges, metro(subway) systems, airports, offshore platforms, military applications, power generation facilities, oil and petrochemical installations and many others.

ACKNOWLEDGMENTS

The authors would like to express their thanks to friends and collegues within the industry for their help and assistance in aquiring and compiling the data contained in this paper.

REFERENCES

1. T. Weardon ,Electronics Times, 8 January 1987,page 12.
2. S.E.Philbrick, BSI News, May 1987, page 11.
3. A.Kynaston, Electrical Equipment, November 1984, page 5.
4. H.A.Mayer, G.Hoeg,"A New Generation of Nonhalogenated, Flame Retardant Compounds and Cables",29th IWCS, Cherry Hill, November 1980
5. J.A.Taylor, Wire Industry, April,1987, page 259.
6. H.G.Dagefoerd, W.Berchem, H.A.Mayer, "Flame Retardant Halogenfree,Thermoplastic Telecom Indoor Wiring",31st IWCS, Cherry Hill, 1982
7. H.A.Mayer, Wire Industry,July,1985.
8. H.A.Mayer, Fireworld, Winter 1986, page 31.
9. Steel Wire Armoured Signalling Cable, Bedding and Jacket in Compound 300, compliant with London Underground Ltd Specification SE 569.
10. Steel Wire Armoured Power Cable, Bedding and Jacket in Compound 300, compliant with BS 6724: 1986
11. Mineral Insulated Cable jacketed with Compound 300
12. BS 6746:1984 "PVC insulation and Sheath of electric cables."
13. BS 6724:1986 "Armoured Cables for electricity supply having thermosetting insulation with low emission of smoke and corrosive gases when affected by fire".
14. Naval Engineering Standard 518, 1985, MOD UK.
15. "Specification for Low Smoke, Zero Halogen Cables for Electicity Supply", Specification Number SE569, 1985, London Underground Ltd.
16. DIN VDE 0472, Part 804
17. BS 4066 part 3;1986 "Tests on Electric Cables Under Fire Conditions: Part 3 : Method for classification of flame propagation characteristics of bunched cables"
18. IEC 332 part 3
19. IEEE 383
20. UITP Test Method E4; October 1981
21. Naval Engineering Standard 713, MOD, UK.
22. MIL-C-24640, MIL-C-24643; 1984; US NAVY
23. BS 6425:Part1:1983; "Method for determination of amount of halogen acid gas evolved during

combustion of polymeric materials taken from cables"

24. DIN VDE 0472, part 813

25. Joint Programme of experiments carried out at Maillefer SA in Ecublens, Switzerland. The Authors acknowledge the help and assistance of Mr. U. Hochstrasser.

26. Maillefer SA, Ecublens, Switzerland.

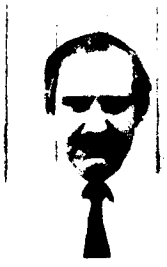
27. European Patent 0054424, 1986

28. VDE 0207; part 24; 1986: "Isolier- und Mantelmischungen Fur Kabel und isolierte Leitungen".

AUTOBIOGRAPHICAL NOTES



Simon Artingstall joined Lindsay and Williams Ltd in 1980 as a Quality Control assistant. He studied Polymer Technology at the John Dalton Faculty of the Manchester Polytechnic. For the past three years Mr. Artingstall has worked as a Development Technologist engaged solely in the design, testing and production of the MEGOLON range of Halogen Free, Low Smoke Fire Retardant cable jacketing compounds.



Mr. A. J. (Tony) Pyle studied both Electrical and Mechanical Engineering at the North West Kent College of Technology, and the Polytechnic of the South Bank in London. He joined AEI Cables Ltd in the mid 60's where he worked in the QC Dept., High Voltage Laboratories and finally as the Factory Liason Engineer. In 1975 he joined Lindsay and Williams Ltd as the Cable Product Manager and subsequently became the Technical Director responsible for the Cable Tape and Halogen Free Compound Development sections in addition to the Quality Control function.



Jack Taylor began his working life as a laboratory technician examining fibre reinforced polymers. He gained his BSc Hons. and PhD degrees in Chemistry at the University of Salford, subsequently joining Akzo Chemie UK where he worked on the synthesis of novel halogenated flame retardants and evaluation of PVC stabiliser systems. Dr. Taylor is currently the Product Manager for the MEGOLON range of halogen free, fire retardant cable compounds supplied by Lindsay and Williams Ltd.

FIBER OPTIC INTRABUILDING CABLES

Harvey R. McDowell, III and Mark A. Sigmon

Siecor Corporation
Hickory, NC 28603

ABSTRACT

A family of intrabuilding fiber optic cables was developed to meet Bellcore TR-TSY-000409 Riser and Plenum Requirements. The specifications require that cables installed within buildings must comply with the requirements of the National Electrical Code Article 770-6; cables for plenum applications pass the UL 910 Fire and Smoke Test and cables for riser applications pass the UL 1666 Flame Test.[1] The Multi-Fiber Intrabuilding Cable, used in riser applications, and Fan-Out Intrabuilding Cable, used in plenum applications, are rugged, high performance communication cables. Attenuation change is less than 0.50 dB/km over the cable's operating range of various indoor distribution environments.

These cables consist of 6 - 36 fibers tightly buffered with a mechanically strippable protective thermoplastic coating. The fibers are stranded around an all dielectric central member and then wrapped with a high strength aramid yarn for further mechanical protection and strength. An outer jacket with required flame retardant and low smoke properties completes the design.

This paper will discuss in detail design parameters, material selection, and performance data of both plenum and riser intrabuilding cables.

INTRODUCTION

Point-to-point communication between buildings (campus links) has proven to be a cost-effective application for fiber in the premises market. As users' needs increase, along with the upgradeability of fiber to provide the capacity for higher data rate services such as video and voice, fiber has become very attractive for indoor applications within the premises wiring system. Areas such as distribution runs in the plenum, (eg. interconnecting the wiring closet with the work station), and floor-to-floor runs in the riser shaft, (eg. connecting the entrance terminal with the wiring closet), are two intrabuilding applications where fiber optic cables have become cost effective and usage is increasing significantly.[2]

The growth for voice, data, and video services stimulated a demand for a set of guidelines for the industry to follow. Bell Communications Research, Inc. (Bellcore) published a Technical Reference detailing Bellcore's position on generic requirements for optical fibers and cables.[1] This Technical Reference was targeted at Fiber Optic Intrabuilding Cables and has since become a leading industry standard.

Discussed within are the plenum and riser product lines developed and tested to meet Bellcore's TR-409 specifications. In all cases the cables tested met or exceeded the test criteria specified.

CABLE DESIGN REQUIREMENTS

Bellcore's Technical Reference (TR-409) is written as a performance specification as opposed to a design specification. However, areas such as jacket thickness and fiber requirements are mentioned to assist the manufacturer in designing a cable meeting the performance requirements. The most critical and design dependent of these specifications are the environmental (temperature cycling and fire resistance) and mechanical requirements. These requirements are listed in Table 1.[1]

Except for the fire resistance requirements, the test procedures follow the EIA-455 Fiber Optic Test Procedures. The fire resistance requirements of the cables are dictated by the intended installation site of the cable. These cables must comply with the requirements of the National Electrical Code (NEC) Article 770 and meet one of three levels of fire safety (plenum, riser, or general purpose).

For plenum applications, where a cable is used in any space for handling environmental air, the optical cable must have "adequate fire-resistant and low-smoke producing characteristics".[3] This is measured by satisfying Standard UL 910 Test Procedure. This test is the most stringent because it measures both flame propagation and smoke generation while being burned within a Steiner Tunnel.[4] For riser applications, any opening at which point the cable passes from floor-to-floor, the cable must have "fire-resistance characteristics capable of preventing the carrying of fire from floor to floor".[3] These cables must pass the UL 1666 simulated riser shaft test where the cable is subjected to a burner flame for 30 minutes. The cable passes UL 1666 if flame propagation is less than 12 feet. General purpose is simply the applications where intrabuilding cables are used in areas which are neither riser nor plenum. When used in general purpose applications the optical cable must pass the UL 1581 Vertical Tray Flame Test.

The 1987 NEC allows substitutions for the three levels of fire safety. A plenum cable can be used for plenum, riser, and general purpose applications. A riser cable can be used for riser and general purpose applications. Table 2 lists cable description, designator, application, and substitution for the three levels of fire safety.[5]

Table 1

CABLE REQUIREMENTS	RISER	PLENUM
Impact Resistance [1]	20 impacts	10 impacts
Compressive Strength [1]	20 N/mm	10 N/mm
Tensile Strength [1]	1330 N	665 N
Cable Cyclic Flexing [1]	25 cycles	100 cycles
Fire Resistance	UL 1666	UL 910
Operating Temperature [2]	-20 C to +60 C	0 C to +50 C
Storage Temperature	-40 C to +70 C	-40 C to +70 C

1 max. increase in attenuation: 0.20 dB singlemode; 0.40 multimode

2 max. increase in attenuation: 0.30 dB/km singlemode; 0.60 multimode

Table 2

UL TYPE DESIGNATIONS FOR ARTICLE 770 OPTICAL FIBER CABLE

Cable Description	Designator	Application/Test	Substitution
Conductive Optical Fiber Cable	OFC	General Purpose/ UL 1581 Vertical Tray Flame	OFCR/OFNR, OFCP/OFNP
NonConductive Optical Fiber Cable	OFN		
Conductive Riser	OFCR	Riser/UL 1666	OFCP/OFNP
Nonconductive Riser	OFNR		
Conductive Plenum	OFCP	Plenum/UL 910	
Nonconductive Plenum	OFNP		

CABLE DESIGN

Both plenum and riser cables consist of fibers coated out to 500 microns. The fibers are 100 kpsi proof stressed, twice the proof stress of standard outdoor cables, and tightly buffered out to a diameter of 900 microns with a mechanically strippable thermoplastic coating for protection. Multimode fibers with a core of 50 microns, a cladding of 125 microns, and a NA of 0.20 are used in the designs discussed because of their relatively high micro-bend sensitivity.[6] Because of different cable requirements for plenum and riser applications, the cable designs differ in overall construction.

The Multi-Fiber Intrabuilding Cable (MIC) is used for riser applications. Within the MIC, fibers are individually color-coded and directly stranded around an all dielectric central member. High strength aramid yarn is then spun around the fibers providing tensile strength for the cable. The yarn also acts as a cushion in absorbing impacts and protecting the fibers from compression. An outer jacket of flame retardant PVC completes the design. Because of high fiber density, small size, low weight, and cost effectiveness, the MIC is the best solution for point-to-point links in riser systems. A final cable cross section is shown in Figure 1.

The Fan-Out Intrabuilding Cable is used where small size is not as critical and the requirement for fanning out fibers at more than one location is much greater, (eg. plenum applications). As a result, the 900 micron buffered fibers have aramid yarn spun around them and an individual fluoropolymer jacket for added protection and stand alone use. The individual cables are stranded around an all dielectric central member. A flame retardant, low smoke fluoropolymer outer jacket completes the cable design. A final cable cross section is shown in Figure 2.

Although the plastic materials of the riser and plenum cables differ, the same design parameters were used to determine the size of the antibuckling dielectric central member (GRP). By knowing the modulus and coefficient of thermal expansion of the plastics and the desired temperature range, the central member size is calculated for a particular contraction. Ideally, to avoid microbends that result in an increase in attenuation, the fiber should see no strain throughout the temperature range. Consequently, there should be virtually no contraction of the cable as not to induce any fiber strain. A calculated compression of 0.30% for each cable's low operating temperature has proven to show little increase in attenuation and was used to determine the required size of the GRP rod.

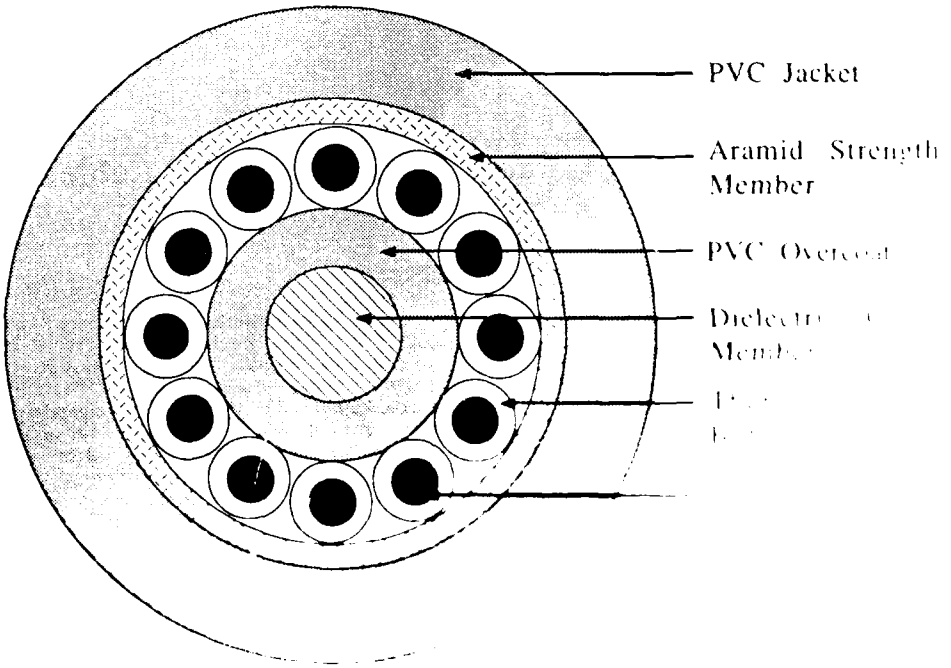
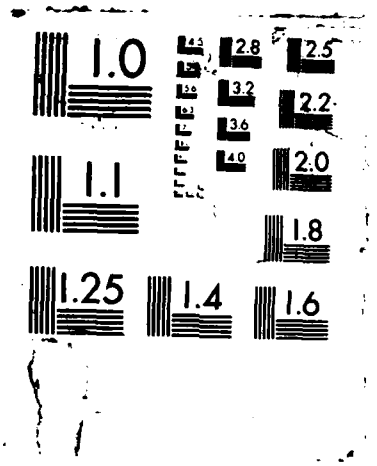


Figure 1

AD-A189 610 PROCEEDINGS OF THE INTERNATIONAL WIRE AND CABLE SYMPOSIUM (36TH) HELD IN..(U) ARMY COMMUNICATIONS-ELECTRONICS COMMAND FORT MONMOUTH NJ 4/9

UNCLASSIFIED 19 NOV 87 F/G 9/1 NL




1.0
1.1
1.25
1.4
1.6
1.8
2.0
2.2
2.5
2.8
3.2
3.6
4.0

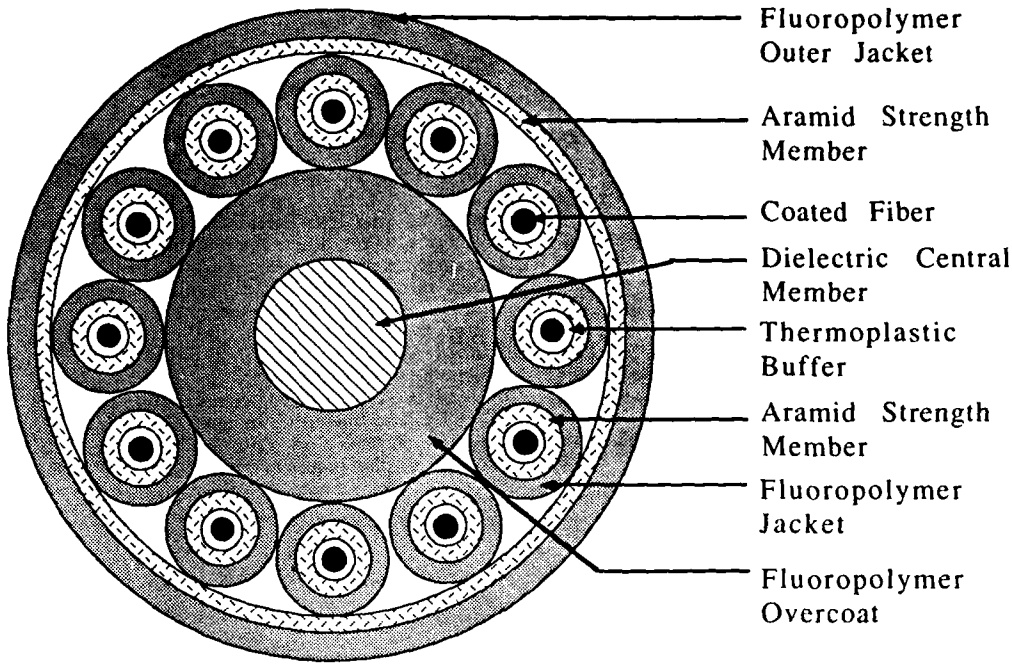


Figure 2: Siecor Fan-Out Intrabuilding Cable

CABLE PERFORMANCE

The final designs of both cables were tested to the Bellcore TR-409 specification. Mechanical tests and results for both riser and plenum cables are listed in Table 3. The riser and plenum cables passed the flame tests according to UL 1666 and UL 910 respectively. All of the test results exceed the stringent requirements of Table 1. Each mechanical test was performed several times on different cable samples. The result for each test is an average of the gathered data.

Temperature cycling results are shown in Figures 3 and 4 for the riser and plenum cables respectively. Each cable met and exceeded the required specifications listed in Table 1. Both the riser and the plenum cable had no irreversible attenuation increases within the specified storage temperature. The riser cable increased less than 0.15 dB/km within its operating range. The plenum cable increased less than 0.40 dB/km within its operating range.

CONCLUSION

We have designed, manufactured and tested a family of riser cables (Multi-Fiber Intrabuilding Cables) and plenum cables (Fan-out Intrabuilding Cables) that meet current Bellcore TR-409 Specifications. The families are comprised of 6 - 36 fibers and designed for high performance optical transport of voice, data, and video communications with less than 0.50 dB/km increase in attenuation within the cable's operating temperature range and exceed all mechanical performance requirements.

Table 3

CABLE RESULTS

TEST	RISER	PLENUM
Impact Resistance	1000 impacts	1500 impacts
Compressive Strength	1500 N/cm	2000 N/cm
Tensile Strength	2000 N	4700 N
Cable Cyclic Flexing	2000 cycles	1000 cycles
Fire Resistance	UL 1666 Listed	UL 910 Listed
Operating Temperature	< 0.15 dB/km (-20 C to +70 C)	< 0.40 dB/km (0 C to +70 C)
Storage Temperature	No residual.	No residual.

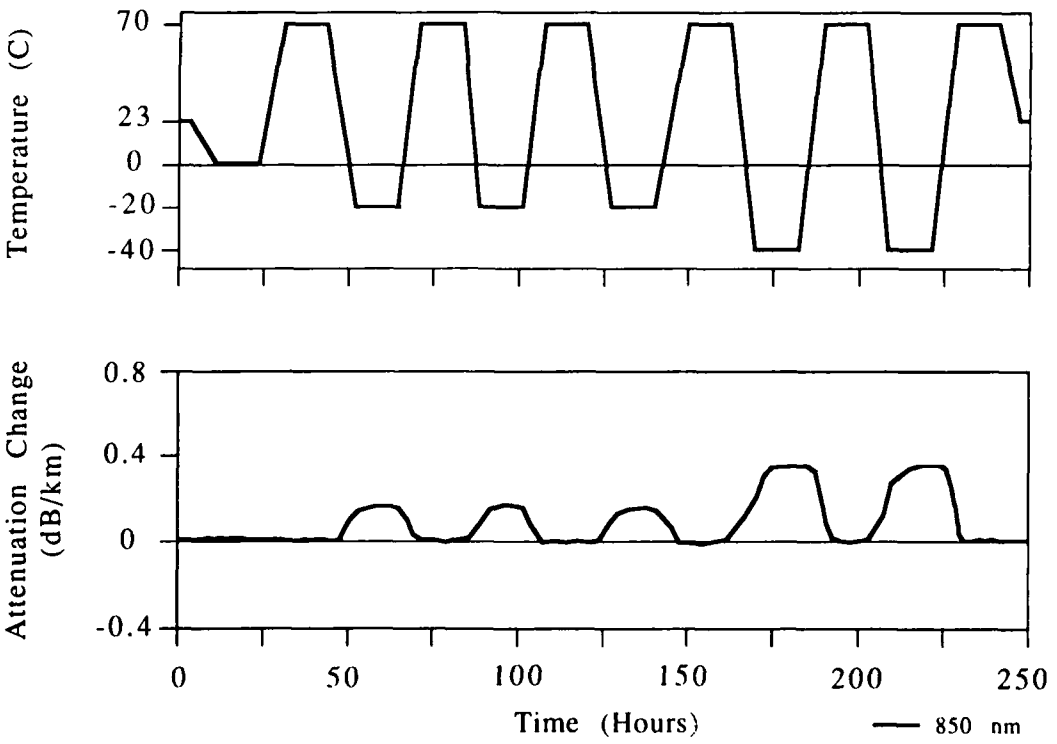


Figure 3: MIC Temperature Cycling Results

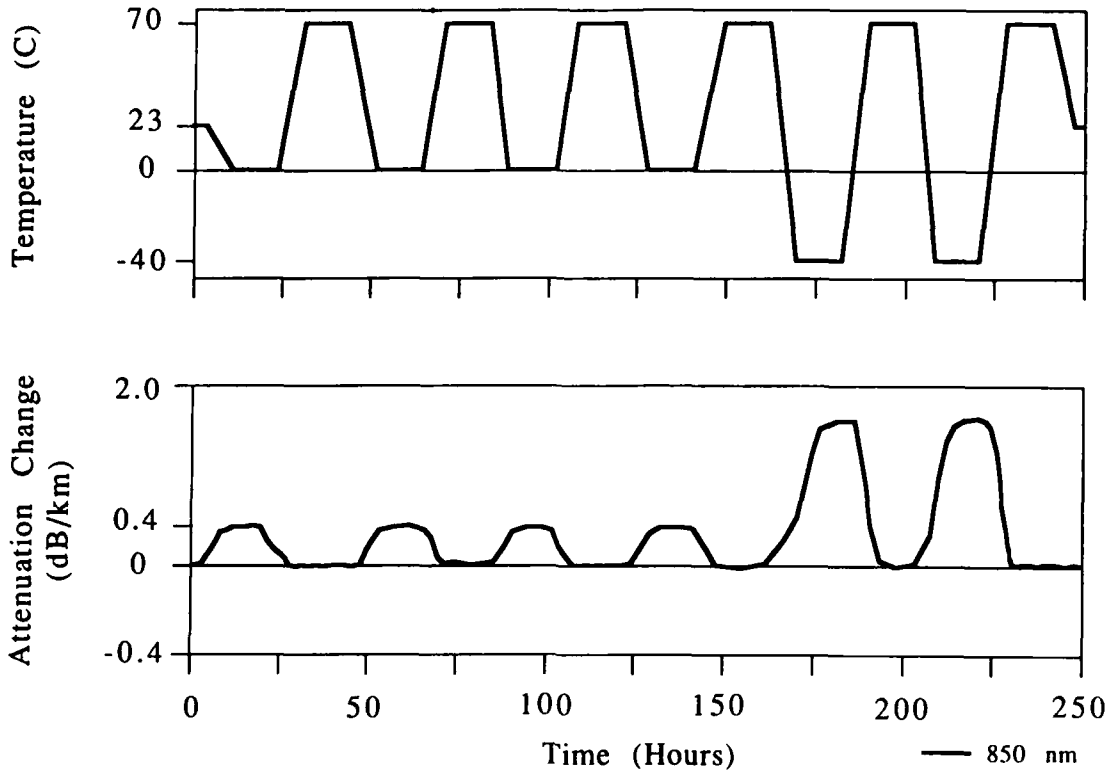


Figure 4: Fan-Out Temperature Cycling Results

REFERENCES

1 Bell Communications Research, Inc., "Generic Requirements for Intrabuilding Optical Fiber Cable", Technical Reference, TR-TSY-000409, June 1987 Edition.

2 K. Koehn, "Product Development Methodology for Premises Fiber Optic Products", International Fiber Optic Communications and Local Area Network Exposition 1986, pp. 33-38.

3 National Electrical Code, 1987 Edition (Quincy, Mass.:NFPA).

4 N. Patel, "Evolution of a Small Scale Test Device which Simulates the UL 910 Flammability Test", International Wire and Cable Symposium *Proceedings* 1987.

5 C. Peffley, "The 1987 National Electrical Code and Fiber Optic Cable", Pamphlet, Siecor Corporation.

6 G. Stilwell, L. Hass, M. See, Optical Fiber *Dimensional Optimization for LAN Systems* Operating at 1300nm, May 27, 1983, EIA P6.6 Meeting, Boston, June 15-16, 1983.

ACKNOWLEDGMENTS

Special thanks are due to K. Koehn and T. Huegrich for their valuable help and input. We also thank L. Miller for her valuable help in the preparation of this manuscript.

Harvey R. McDowell, III
489 Siecor Park
Hickory, NC 28603



Harvey R. McDowell, III was born in Hickory, North Carolina in 1963. He received his B.S. Degree in Electrical Engineering from North Carolina State University in 1985. Since graduation, he has been employed by Siecor Corporation as a Product Development Engineer in the Research, Development and Engineering Department.

Mark A. Sigmon was born in Newton, North Carolina in 1962. He received his Bachelor's Degree in Mechanical Engineering from North Carolina State University in 1985. Since then, he has worked as a Process Engineer for Siecor Corporation - Research, Development and Engineering Department, and is currently Supervisor of the Process Lab.



Mark A. Sigmon
489 Siecor Park
Hickory, NC 28603

EVOLUTION OF A SMALL SCALE TEST DEVICE WHICH SIMULATES THE UL 910 FLAMMABILITY TEST

Naren I. Patel

Siecor Corporation
Hickory, North Carolina

ABSTRACT

The Underwriters' Laboratories Standard 910 (UL 910) is the test method for determining values of flame propagation distance and optical smoke density for electrical and optical fiber cables that are to be installed in ducts, plenums, and other spaces used for environmental air without the cables being enclosed in raceways. The method uses a 25-foot-long fire chamber, generally referred to as the UL 910 Tunnel or the Steiner Tunnel.

This paper discusses the design and construction of a small scale device or test apparatus, called the Mini-Tunnel. The fire chamber of the Mini-Tunnel is approximately 10 (ten) feet long, and it adequately simulates the results of the longer UL 910 Tunnel. General features of the Mini-Tunnel, and a comparison of the results of tests conducted on cable samples from the same reel in the Mini-Tunnel and the UL 910 Tunnel are presented. A discussion of advantages and limitations of the Mini-Tunnel is also included.

INTRODUCTION

Unintended and uncontrolled fires cause damage to life and property. Various fire safety tests, commonly referred to as "flammability tests", are designed to reduce occurrence of such fires, and to minimize the damage caused by them. The 1987 National Electrical Code[1] has established four levels of fire-resistance for communications cables. The highest level is required for plenum cables; these cables are tested per the UL 910 tunnel test. [2]

The UL 910 test is used to determine whether the flame propagation and smoke generation characteristics of cables installed without raceways in air handling plenums are in accordance with the provisions of the National Electrical Code (NEC), ANSI/NFPA 70-1987.

In this test, cables are exposed to a fire of considerable severity and of a precise flame length, for a certain length of time. During that period, the maximum length of flame spread, and the maximum value of optical smoke density or smoke obscuration are measured. From these experimental data, contribution to flame propagation and smoke generation by the test cable are calculated.

DISADVANTAGES OF THE UL 910 TEST

In the development phase of new cables, one has only an intermittent need for testing cables per UL 910; therefore, erecting a full-scale UL 910 Tunnel to conduct tests in-house is not very practical for the following reasons:

The full scale tunnel occupies a large space, the test requires long lengths of cables for burning, and the fuel and labor costs for running the test are high.

DEVELOPMENT OF THE MINI-TUNNEL

To make rapid iterations in developmental cable design work, it is desirable to have in-house testing capability. But the results of small scale flammability tests such as measurement of Oxygen Index (LOI), vertical or horizontal burn tests, smoke-box tests for measuring smoke generation values, etc., are not reliable indicators for predicting the results of UL 910 tests. Hence, a small scale device which can be installed in-house, and which can simulate the results of the UL 910 test is very desirable. The Mini-Tunnel is one such device. (Table 1, Figure 1)

Table 1

COMPARISON OF THE SET UP FOR UL STANDARD 910 AND MINI TUNNEL TESTS

CRITERIA	UL STANDARD 910	MINI-TUNNEL
Floor space, area	50' X 3'6"	24' X 3'6"
Horizontal duct, length	28'6"	12'
Fire chamber, length	25'	10'
Cable rack, length	24'	9'8"
width	11 1/4"	5 1/4"
Cable sample, length	24'	9'6"
Flame spread distance, max.	19'6"	5'

5. The Mini-Tunnel is mobile. It can be moved from one place to another if necessary.

LIMITATIONS

Associated with the advantages of the Mini-Tunnel test are certain limitations. They generally arise due to the shorter length of the tunnel. They may be summarized as follows:

1. The Mini-Tunnel test can measure whether the flame propagation distance for a cable sample is five feet or less, and thus indicate whether the cable passes or fails the test. But for those cables that fail the test, the test will not indicate whether the same cable sample will have a flame propagation distance of six, seven, or even nineteen feet when tested according to the full scale UL 910 test.

2. As mentioned earlier, the length of cable samples tested in the Mini-Tunnel is nine feet six inches. Thus the extent of cable damage that would occur beyond that distance in the UL 910 test would not be known by conducting the test in the Mini-Tunnel. Again this applies only to the cables that fail the test.

3. Furthermore, due to the shorter length of the Mini-Tunnel, the exhaust gases will leave the tunnel at a higher temperature than the gases from a full scale tunnel test. For this reason, the smoke detection device needs to be cooled during the test and for some time after the test.

4. The Mini-Tunnel has not been calibrated yet to generate the same value for the average smoke density obtained by conducting the UL 910 test.

5. The Mini-Tunnel test can only be used for screening the cables prior to testing them per UL 910. For approval purposes, they must pass the UL Standard 910 test carried out by an independent laboratory

Nevertheless, the experience of conducting tests in the Mini-Tunnel and the UL 910 Tunnel would lead one to the conclusion that the advantages of using the Mini-Tunnel far outweigh its limitations.

CONCLUSIONS

The Mini-Tunnel is a useful device to screen communications cables before testing them in the UL 910 Tunnel. The results for the maximum flame spread distance and the peak optical density obtained using the Mini-Tunnel test are reproducible. The test data satisfactorily simulates the data obtained using the UL Standard 910 test.

The Mini-Tunnel is smaller than the UL 910 Tunnel. Due to its smaller size, it is suitable for in-house installation for companies interested in conducting similar tests. By using it in-house, it is possible to do as many iterations, as often as necessary, for cable design and development work. Furthermore, the Mini-Tunnel test requires less cable for testing purposes. This is a boon for the research and development work. Also, it is less expensive and less cumbersome to conduct tests in the Mini-Tunnel than in the UL 910 Tunnel.

ACKNOWLEDGEMENTS

Many employees of Siecor Corporation have contributed to the design and construction of the Mini-Tunnel, and they have helped in conducting the flammability tests. I am grateful to all of them. My special thanks to Kitty Tedder for her valuable assistance in conducting the tests, and to Diane Kerley for preparing this manuscript.

REFERENCES

[1] National Electrical Code, 1987 Edition (National Fire Protection Association, Quincy, MA.)

[2] Kaufman S.: "The 1987 National Electrical Code Requirements for Cables", Proceedings of the 35th International Wire and Cable Symposium, 1986.



Naren I. Patel

Siecor Corporation
489 Siecor Park
Hickory, NC 28603-0489

Naren Ishwarbhai Patel is the Staff Materials Specialist for the R,D&E Division of Siecor Corporation. Previously he had served as a Materials Engineer, the Supervisor of Polymer Chemistry, and the Supervisor of Materials Engineers in the same Division. He received a B.S. degree in Chemistry from the Gujarat University, India; a B.Sc. (Technology) degree in Textile Chemistry from the University of Bombay, India; and was awarded a Ph.D. degree by the University of Leeds, England. Prior to joining Siecor Corporation, he had served as the Director of Quality Control, and as the Director of Research and Development in the Textile Industry.

The first section is a 12-foot-long horizontal duct with approximately square lateral dimensions. Within this duct is a test chamber or tunnel lined with heat-resistant bricks at the bottom and two sides. The front side of the tunnel is provided with a row of double-pane pressure-tight glass windows through which the entire length of the cable being tested can be observed for the distance of flame propagation. A single burner acts as the flame and heat flux source. A horizontal ladder-type tray with adjustable height supports is provided for placing cable samples during the test. The top of the tunnel is effectively sealed whenever desired, by placing removable, high-temperature-resistant, mineral composition boards over the entire length of the tunnel, and by closing a heavy metal lid over them. Thermocouples are installed in the tunnel to measure temperature 1/8-inch below the floor surface, and temperature of the air exiting the fire-chamber. Devices to regulate the pressure and the flow of natural gas, and the electronic ignition system for the gas burner, are placed close to the first section.

The second section of the Mini-Tunnel consists of a square-to-round tubular section, provided with smoke detection and manual air flow control devices. The smoke detection device feeds the test data to a computer for continuous recording and analysis. As for the UL 910 test, the computer samples data points at 15 second intervals, and computes the maximum and the average smoke density values from these points. The test report is issued by the computer through a printer within a few seconds after the test is completed.

The third section of the Mini-Tunnel has a draft-inducing system, an exhaust system and a static pressure indicator device.

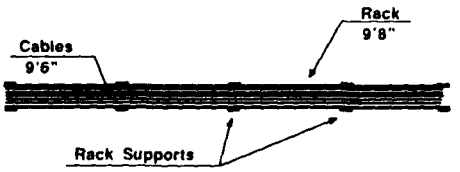
The three sections of the Mini-Tunnel are assembled as a single unit by making all connections pressure tight. The total length of the Mini-Tunnel is less than 24 feet.

TEST METHOD

To check the validity of the data that are obtained by testing cables in the Mini-Tunnel, frequent calibration of the tunnel by burning cables that were tested per UL Standard 910 by an independent laboratory is necessary.

The tunnel is cleaned and pre-heated until the floor surface reaches at least 150 °F. Then it is allowed to cool. When the surface temperature reaches 110 °F ± 5 °F, the tunnel is opened to introduce the calibration cables or the test cable samples. Nine and 1/2-foot-long cable samples are laid parallel and close to each other to fill the 5-1/4 inch wide tray. (Figure 3) In order to minimize the movement of cables during the test, they are fastened in place to three or four rungs using No.22 AWG Copper wires. Then the tunnel is properly closed, and the smoke detection device is adjusted to the zero reading. The air flow through the tunnel is also adjusted to the proper level.

Figure 3: Installation of Cable Samples For Testing



To start the test, the natural gas is ignited and the computer is switched on to begin collecting data points for smoke density values. The air flow through the tunnel is maintained constantly at the initial level throughout the 20 minute duration of the test. The flame propagation distance is measured visually through the observation windows described earlier. Only the maximum value for the flame propagation distance is recorded. The temperature of the air within the tunnel is also monitored. The maximum value of the temperature is recorded on the test report print-out issued by the computer.

If the temperature of air within the tunnel rises above 1100 °F during the test, or if the cable sample produces excessive smoke, the test is terminated. This is done to prevent damage by high temperatures to the tunnel and the measuring devices, and to stop unnecessary pollution of the environment with high levels of smoke.

ADVANTAGES

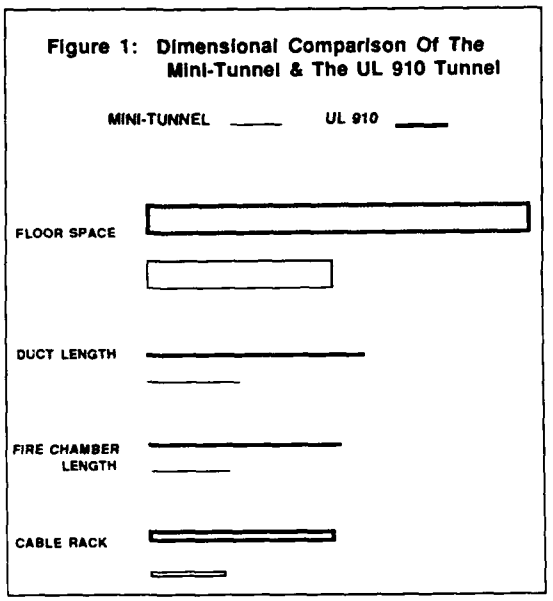
The Mini-Tunnel offers several advantages over the UL 910 test. They are:

1. The Mini-Tunnel test can be conducted in-house. One can conduct as many tests as often as needed, even on short notice. It enhances one's ability to do as many iterations, as often as necessary, for cable design and development work.

2. The Mini-Tunnel can be used first to screen or proof-test experimental cables, and then send to the independent laboratories for testing in the UL 910 tunnel only those cables which have the potential of passing the test.

3. In the Mini-Tunnel test, approximately one-fifth as much cable is burned per test as in the UL 910 test. For some experimental cables this is of great value.

4. Less fuel is required to pre-heat the tunnel and to conduct the test, and less time is needed to cool the tunnel after the test. The fuel used is natural gas.



For developing the Mini-Tunnel, the following objectives were established:

1. To design a reduced-scale test that gives flame propagation and maximum optical density values approximately the same as those obtained by testing per UL Standard 910.
2. To design a test for in-house use so that as many developmental cables as necessary can be tested within short notice.
3. To design a test which would use less cable for testing.
4. To design a test which would use a smaller laboratory floor space.
5. To design a test which could be conducted by two people.
6. To design a test which would consume less fuel.
7. To design a test which would reduce environmental pollution.

After many trials and errors, satisfactory correlation between the results of Mini-Tunnel and UL 910 tests was established. (Table 2)

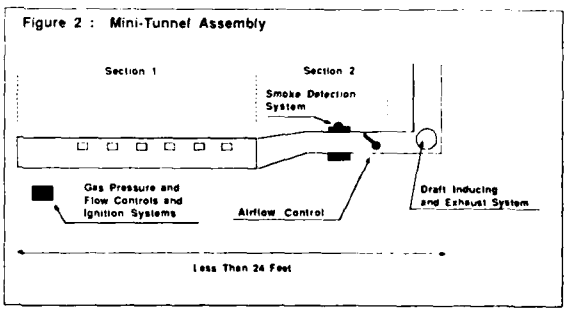
Table 2

COMPARISON OF THE RESULTS OF
UL STANDARD 910 AND MINI-TUNNEL TESTS

CABLE	CRITERIA	UL STANDARD 910	MINI-TUNNEL
A	Maximum Flame Spread	3' 3'	3.5' 3'
	Optical Density, Peak	0.08 0.05	0.05 0.04
B	Maximum Flame Spread	3 1/2' 3'	4' 4 1/2'
	Optical Density, Peak	0.18 0.15	0.20 0.17
C	Maximum Flame Spread	3'	3' 3'
	Optical Density, Peak	0.29	0.30 0.35
D	Maximum Flame Spread	3'	3' 3' 3'
	Optical Density, Peak	0.30	0.35 0.39 0.30
E	Maximum Flame Spread	3 1/2' 4'	3 1/2' 3 1/2'
	Optical Density, Peak	0.40 0.35	0.36 0.38
F	Maximum Flame Spread	3' 3.5'	4 1/2' 4'
	Optical Density, Peak	0.53 0.60	0.58 0.55
G	Maximum Flame Spread Optical Density, Peak	6.7' 1.878	5'+ 1.8
H	Maximum Flame Spread Optical Density, Peak	6.1' 2.0	5'+ 1.8

MINI-TUNNEL DESIGN

The Mini-Tunnel is assembled from three sections (Figure 2):



Experimental Design for Full-Scale Evaluation of the Toxicity of the Products of Combustion from Cables

1. Frederic B. Clarke and Henri J. van Kuijk
2. J.E. Bonesteel, J.G. DiPinto and R. Valentine
3. Marc Janssens and Paul Vandevelde

1. Benjamin/Clarke Associates, Inc.
2. E.I. du Pont de Nemours and Company, Inc.
3. State University of Ghent, Belgium

Summary

An evaluation of cable smoke toxicity under actual fire conditions has been undertaken in an attempt to provide a basis for comparison of cable smoke toxicity, as measured in the laboratory, with that of smoke generated by actual cable fires. A versatile and rugged system has been designed and demonstrated, in a series of full scale fire experiments, to provide an effective method for the exposure of a significant quantity (up to 30kg, or 66 lbs.) of cable to a large developing (1 megawatt) room fire, sampling the fire environment for chemical analysis of combustion generated fire gases, and then cooling the smoke to a temperature suitable for assessing its toxic affects on laboratory animals. By varying the amount of cable burned and dilution rates of the smoke into the chambers, this procedure allows the estimation of the lethal smoke dose for cable insulation materials.

I. Introduction

In the past few years, attention has increasingly been focused upon the fire properties of wire and cables, as these materials find new and specialized uses and as the demand for electronically based control and communication systems continues to proliferate. Ironically, as the fire properties of modern cables improve, there is a reduced likelihood of encountering a fire where the cable alone is the principle fuel. For that reason, modern fire hazard analysis must address the contribution of the cable in the real-fire scenarios in which it is likely to be involved. This concern has prompted the publication of several papers dealing with the overall fire hazard of cables (1). Hazard assessment is often concerned with identifying and quantifying all the cable flammability factors which go into producing smoke, but also relies upon appropriate measures of the toxic potency of the smoke in order to determine the actual hazard posed under in-use conditions. As a rule, one of several small scale tests is used to measure the toxic potency of the smoke in the laboratory (2); this measurement is always assumed to reflect the toxicity of the smoke from the same product when burned under actual fire conditions.

A real fire is likely to encounter a variety of fuel sources, ventilation conditions, and heat transfer parameters during the course of burning. Small scale tests necessarily fix all of these parameters, so the best that can be expected of such results is an indication of the smoke toxicity at full scale. Earlier work has shown that, for some materials, the burning conditions themselves can have a profound effect upon the toxicity of the smoke (3,4). These observations, as well as the increasing recognition that smoke toxicity is often an important, but seldom the controlling, component of fire hazard, have prompted us to attempt to measure the toxicity of smoke from cables when the cables are burned under something approximating real, full-scale conditions.

The barriers to such an undertaking are formidable, since a number of difficulties are encountered at full scale which are not encountered in small-scale laboratory tests. Chief among these are: 1) the intense heat generated by a large fire must be removed from the smoke before its exposure to laboratory animals, otherwise the heat effects will mask any toxic affect of the smoke; 2) traditional methods of heat exchange to cool the smoke are usually inappropriate because the smoke contains gases, solids, and aerosols, the latter two of which are subject to condensation or removal from the smoke

stream if it is cooled by conductive methods; 3) methods must be found to control the dosage of smoke reaching the animals, since toxicity measurements require that dose-response relationship be determined; 4) the usual problems of measuring temperature, ventilation, mass loss, and smoke components are more in full scale fire experiments.

This paper reports the design, construction and employment of a full scale experimental regimen to measure the toxic potency of smoke from cables. How each of these barriers was dealt with is described in the following sections.

II. Design of the Full Scale Test System

A diagram of the overall test setup is presented in Figure 1. It consists of three main elements.

1. Burn Room

The room in which the fire took place, and the cable bed was exposed, was a 4 x 5 x 3m compartment, lined with Type X gypsum 1.25cm [1/2 inch] thick. The floor was concrete. The doorway to the room, centered upon one wall was of normal (2m) height; the width could be varied to obtain various ventilation conditions. The source fire, either a wood crib or pans of diesel fuel, were placed in the middle of the room on the platform of a large load cell, which permitted the weight loss of the fuel to be followed during the course of the fire. The cable, in 2m lengths, was contained in an open steel pan, suspended from the ceiling of the room, approximately 1/2m below the ceiling, directly over the source fire. The cable pan was connected to a separate load cell, so that its weight loss could be followed as well during the course of the fire. The cable pan differed from conventional cable trays in that its bottom was a solid sheet, which allowed any cable insulation which melted away from the wires to be contained, rather than dripping down onto the fire or the floor. This ensured that the cable insulation and jacket would continue to be subjected to the fire's heat flux during the experiment and that observed weight loss of the cables was due to burning, not melting. The work undertaken to date has been on high performance, low combustibility, cables and a relatively large fire was therefore required in order to produce the high temperatures necessary to decompose the cable insulation. In the studies to date, approximately 100 kg (220 lbs.) of wood, or a pan containing an energetically equivalent amount of diesel fuel, was used.

2. The Smoke Corridor

A corridor approximately 10m long and 1.5m wide was connected to the burn room as shown in Figure 1. Because of space limitations, this corridor was not a straight run, but bent back upon itself at 180° to give it two legs of approximately 5m each. The ceiling and the walls of the corridor were also faced with Type X gypsum board to a distance of approximately 3m from the door of the room. The remaining length of the corridor was surfaced with concrete masonry blocks. A partition, approximately 2m in height, was installed at the end of the corridor just prior to its exit into the smoke collection hood. This was done to eliminate bidirectional flow in the corridor, which would dilute the smoke by air entrainment and reduce the concentration of the smoke which could be introduced into the animal exposure chambers. Ventilation for the fire was supplied by a 1m x 2m opening at the end of the corridor adjacent to the door of the burn room. Preliminary experiments showed that a vent of this height was low enough to prevent smoke escape through the vent, yet high enough to provide acceptable ventilation to the fire.

3. Smoke Collection and Animal Exposure System

Smoke to which the animals were to be exposed was withdrawn from the corridor just prior to its exit into the smoke collection system, as shown in Figure 1. The smoke collection system consisted of a 5cm stainless steel pipe, which protruded through the side of the corridor wall into the corridor, and to which was connected a manifold containing three animal exposure chambers. After removal from the corridor, the smoke was cooled by the introduction of a stream of chilled air (0-5°C). The amount of air blended into the smoke was determined by that required to lower the smoke temperature in the upper part of the manifold to below 60°C.

The smoke was then pulled through one of three animal exposure chambers, each of which was equipped with additional air bleeds. These air bleeds served two purposes: first, to cool the smoke further to maintain

continually temperatures of 40°C or less in the animal exposure chambers; second, to permit further dilution, thus providing control over the smoke concentration. As a rule, two chambers were used. One of them was maintained as close as possible to the original diluted smoke concentration as it came from the manifold.

The second chamber was operated at approximately 1/2 the smoke concentration of the first. The third chamber could be operated either at greater dilution or could be sealed off during the course of the experiment so that the smoke it contained could be trapped. This permitted one to carry out a "static" exposure of the animals for comparison to the other two chambers in which a "dynamic", or continuous flow, mode of exposure was followed. A schematic of the smoke manifold and dilution system is presented in Figure 2.

The animal exposure chambers themselves were constructed of stainless steel, which had been coated on the inside with polytetrafluoro-ethylene. The chamber volume was 175 liters. A drawing of the animal chambers used is presented as Figure 3. Each chamber contained 10 exposure ports, into which were introduced holders suitable for the confinement of a Sprague-Dawley rat. The laboratory animals were exposed to the smoke in a nose-only position, in accord with most small scale smoke toxicity test protocols. Each animal chamber was monitored for temperature, and fitted with a collection port from which samples of the atmosphere in the chamber could be withdrawn. Finally, the oxygen, carbon dioxide, and carbon monoxide concentrations in the chambers were monitored continuously. Flow from the manifold through the chambers was driven by a large high capacity fan which maintained the system at a slight negative pressure relative to that of the core. The exhaust from the fan was returned to the smoke collection system.

4. Instrumentation

Temperature and flow measurements were made throughout the system. Table 1 describes the smoke analysis which was carried out both in the corridor and in the chamber. Each chamber, and one collection port in the corridor itself, was fitted with a standard stainless steel taper joint to which could be attached a gas sample collection flask. These flasks had a volume of approximately 0.5 liters and were evacuated prior to the start of the experiment. Each flask contained 50ml of 0.1 molar sodium hydroxide. At appropriate intervals during the fire, a smoke collection flask was attached to the standard taper port, a volume of smoke was drawn into the flask, and the flask was shaken. The aqueous phase in the flask contained the smoke components which were either water soluble or hydrolyzable, and the gas phase above contained the other gaseous components. This procedure, in conjunction with the instrumental analyses of carbon oxides and oxygen in the chambers and the corridor, provided the means for a relatively complete accounting of the smoke and mass balance coming from the fire.

5. Animal Studies

Animals were exposed to the smoke for approximately 30 minutes. Temperature in the animal chambers was maintained at or below 40°C, as previously described. Animals were observed during the course of the fire for any anomalous affects. Following exposure, four of the animals were sacrificed for carboxyhemoglobin determinations on their blood and the remaining six were used as a basis for mortality studies. Animals which had survived the smoke exposure itself were retained for fourteen days of observation. Their appearance, pathology, and weight gain were monitored over that time.

III. Results and Discussion

A typical weight loss curve for the wood crib and the cable bed is presented in Figure 4. As can be seen, cable decomposition lags initial fire buildup by several minutes and did not become significant until 10 to 15 minutes into the burn. For the cables tested, weight loss was relatively rapid and proceeded smoothly once high temperatures in the burn room had been reached.

Other workers have shown that, where halogenated cable materials are burned, a sizable fraction of the expected hydrogen halides can be lost on the walls of the burn room and the smoke corridor (5). In the experiments carried out here, approximately 40% of the cable mass, as determined by analysis of the smoke, was transported down the corridor to the vicinity of the manifold to the animal exposure chamber. Some material was then lost in the sojourn from the corridor

through the exposure chambers, but overall approximately 30% of the smoke produced in the room, as measured by the weight loss of the cable tray, is accounted for in the animal exposure chambers.

One might expect that, as the walls of the corridor are heated during the course of the burn, material initially deposited on the relatively cool walls would be revolatilized into the smoke stream. This does not seem to be an important mechanism in the present studies, however, as can be seen by examination of Figure 5 in which the maximum amount of material detected in the chambers occurs within a few minutes of the time when the maximum rate of weight loss is observed in the burn room. Allowing for a sojourn time of several minutes down the corridor, revolatilization of the smoke components collected in the corridor does not seem to be significant.

This experimental arrangement has now been used to obtain the toxic potency (LC50 or L(Ct)50) of cable materials under full scale conditions. The actual results of these studies will be presented elsewhere (6). Experiments to date have focused upon fluoropolymer materials, which contain large amounts of halogens and are therefore subject to losses in the burn room and corridor as discussed above. This replicates what will occur in an actual fire incident, and the approach therefore characterizes what really happens to the smoke of such materials. The methodology will be equally suitable to the study of cable smoke from other kinds of constructions and for a wide range of end-use scenarios.

Although the focus of this presentation has been on an experimental system and design to determine the toxic potency of smoke from full-scale fires it is not a hazard assessment because it does not take into account the other fire threats, such as temperature, oxygen depletion, and the toxic effects of the wood fire. Because of the large fire source required to involve the cable used in these tests, even locales distant from the room of fire origin were untenable because of temperature and depleted oxygen.

The test facility and the test regimen are well-suited to the determination of a detailed fire hazard assessment, which will be the subject of subsequent presentations.

References

1. c.f. Clarke, F., and DiNenno, P., "Fire Safety of Wire and Cable Materials, Part III: An Approach to Estimating Fire Hazard," 33rd International Wire and Cable Symposium Proceedings, p. 40-49 (1984).

2. a.)Levin, B., et al, "Further Development of a Test Method for the Assessment of Acute Toxicity of Combustion Products," NBSIR 82-2532, U.S. Department of Commerce, National Bureau of Standards, June, 1982.
   b.) "Determination of the Toxicity Index of the Products of Combustion from Small Samples of Materials," Naval Engineering Standard 713, Ministry of Defense (United Kingdom), 1983.
   c.) Alarie, Y., and Anderson, R., "Toxicologic and Acute Lethal Hazard Evaluation of Thermal Decomposition Products of Synthetic and Natural Polymers," Toxicology and Applied Pharmacology, 51, 341-362 (1979).

3. Williams, S., and Clarke, F., "Combustion Product Toxicity: Dependence on the Mode of Product Generation," Fire and Materials, 1, 96 (1983).

4. Williams, S., Baker, B., and Lee, K., "Formation of Acute Pulmonary Toxicants Following the Thermal Degradation of Perfluorinated Polymers: Evidence of a Critical Atmospheric Reaction," 25, 177 (1987).

5. Beitel, J., Bertelo, C., Carroll, W., Grand, A., Hirschler, M., and Smith, G., "Hydrogen Chloride Transport and Decay in a Large Apparatus: II. Variables Affecting Hydrogen Chloride Decay," Journal of Fire Science, 5, pp. 105-145 (1987).

6. Clarke, F., van Kuijk, H., Valentine, R., Baker, B., Kasprszak, A., Janssens, M., "Full-Scale Fire Experiments on Cables with Fluoropolymer Insulation," Combustion Institute, Eastern Section Fall Meeting,

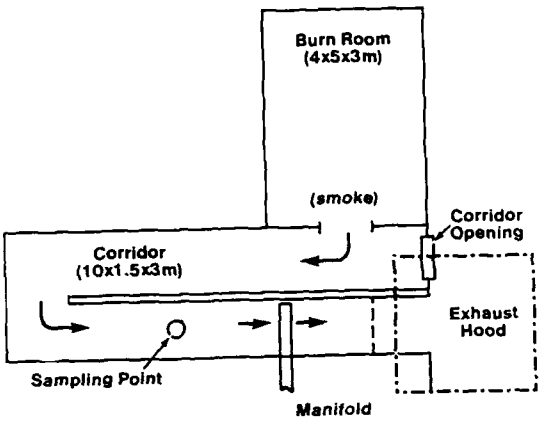


Figure 1. Burn Facility Layout

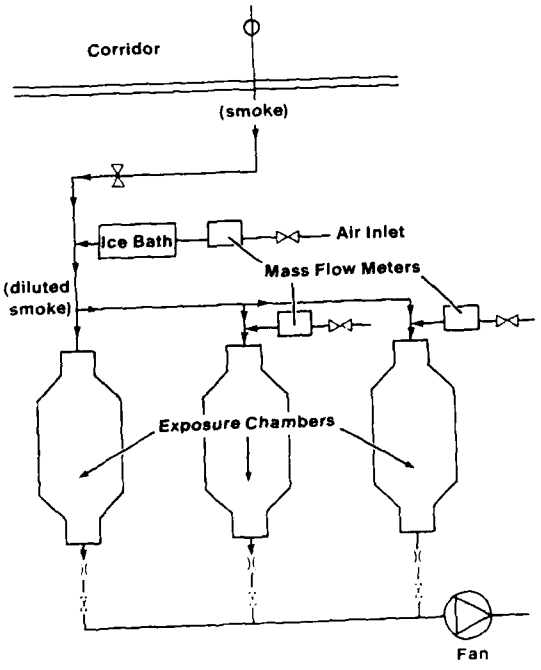


Figure 2 Smoke Dilution System

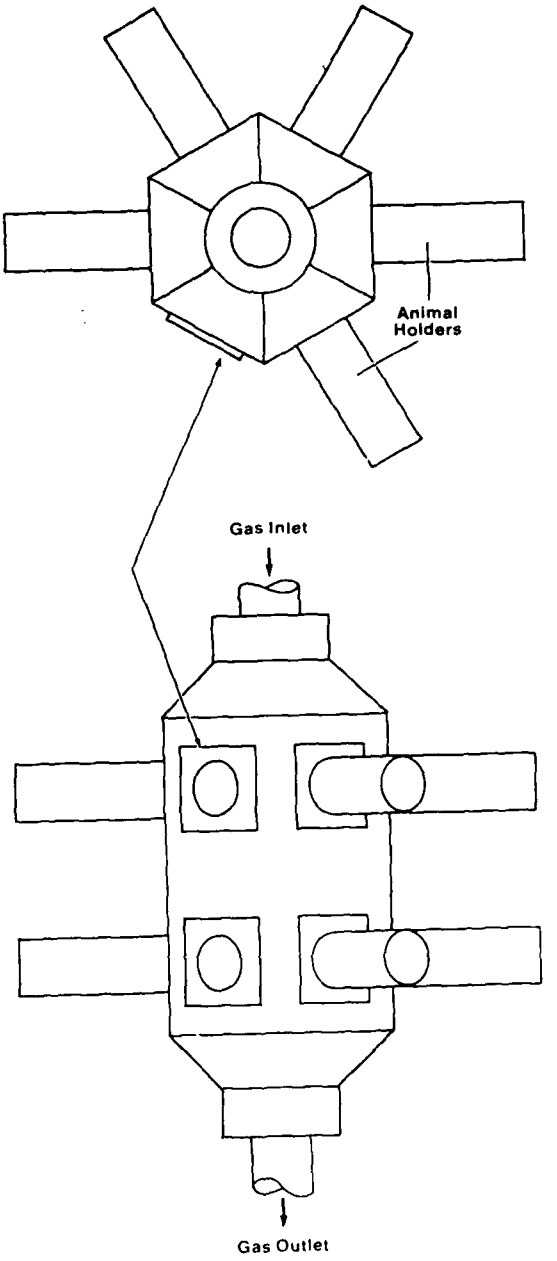


Figure 3 Detail of an Exposure Chamber

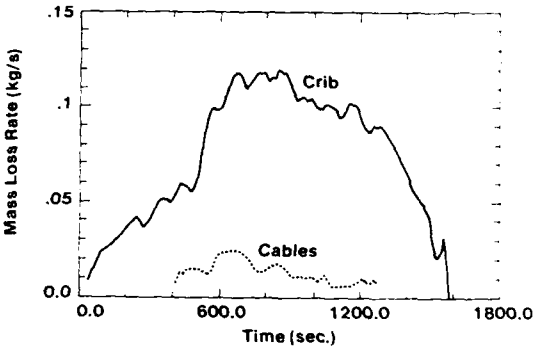


Figure 4. Mass Loss Rates of Crib and Cables

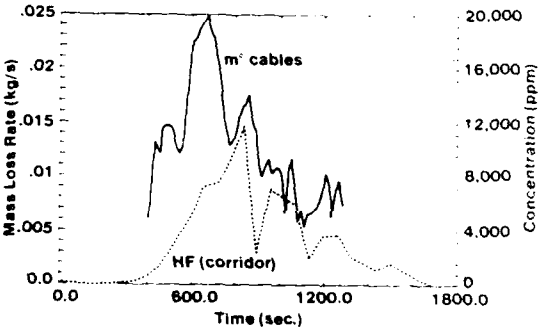


Figure 5. Mass Loss Rate of Cables vs. HF Concentration

Table 1
Analytical Measurements on Smoke

Measurement	Location		
	Corridor	Animal Chamber #1	Animal Chamber #2
CO_2	Infared, 15 sec. intervals	Infared, 15 sec. intervals	Infared, 15 sec. intervals
CO	Infared, 15 sec. intervals	Infared, 15 sec. intervals	Infared, 15 sec. intervals
Oxygen	Paramagnetic, 15 sec. intervals	Paramagnetic, 15 sec. intervals	None
Chemical Analysis	Gas Collection Bottles, 1 min. intervals	Gas Collection Bottles, 2 min. intervals	Gas Collection Bottles, 2 min. intervals
Temperature	Bank of Four Thermocouples	Thermometer	Thermometer



Frederic B. Clarke, III, Ph.D.

Frederic Clarke is President of Benjamin/Clarke Associates, Inc., a firm specializing in the characterization and analysis of fire safety problems. Until fall, 1981 he was director of the National Bureau of Standards' Center for Fire Research, the Nation's principal Federal fire laboratory. He was a member of the National Academy of Sciences Committee on Fire Toxicity, 1985-86 and is currently Technical Director of the National Fire Protection Association Risk Analysis Project.

He holds a Ph.D. in chemistry from Harvard University.



Henri J. van Kuijk

Henri van Kuijk is an Engineering Associates at Benjamin/Clarke Associates, Inc. with responsibilities in computer modeling of fire and smoke behavior in buildings. He has expanded the Harvard Computer Fire Code, and developed a user friendly graphic package written in Fortran to include on-line calculations.

He holds a M.S. from the University of California, Berkeley.

Jo-Anne Bonesteel, Ph.D.

Dr. Bonesteel has been affiliated with the Polymer Products Department of the E.I. du Pont de Nemours and Company, Inc. since 1982. She is responsible for the Nuclear Magnetic Resonance Department.

She holds a Ph.D. in physical chemistry from Georgetown University and a B.S. in chemistry from Siena College, Loundonville, New York.

Joseph G. DiPinto

Mr. DiPinto is Manager of Product Technology in the research and Development Division of the Polymer Products Department of the E.I. du Pont de Nemours and Company, Inc. He is presently assigned to the Wire & Cable Division as coordinator of combustibility - related issues.

He received a B.S. degree in Chemical Engineering from the University of Notre Dome in 1954. He has been employed by the Du Pont Company since that time, involved in research, development and marketing of elastomers and plastic products. He is active in ASTM and the National Fire Protection Association.

Active in elective politics, he completed 14 years as a Wilmington (Delaware) City Councilman and is serving in his first term in the Delaware State House of Representatives.



Rudolph Valentine

Dr. Rudolph Valentine is presently a Research Toxicologist at the Haskell Laboratory for Toxicology and Industrial Medicine of the E.I. du Pont de Nemours and Company, Inc. Dr. Valentine received a B.S. degree in Chemistry and Physics from California State College at Sonoma in 1975 and a Ph.D. in Pharmacology and Toxicology from the University of California at Davis in 1982. Since joining Du Pont in 1984, Dr. Valentine has been a study director for short-term inhalation toxicity studies for the Acute and Developmental Toxicology Section. Dr. Valentine has ongoing research interests on the mechanisms of Teflon decomposition product toxicity, combustion toxicity test method development, and the pulmonary toxicity of particulates. Dr. Valentine has authored several papers on pulmonary biochemistry and toxicology.



Marc Janssens

B.S. and M.S. in Mechanical Engineering at the University of Ghent, Belgium (1974-1980). Affiliated with the University of Ghent, Laboratory of Heat Transfer, Combustion and Fire (1980-1980). Experimental experience: Full scale room fire tests, bench scale Rate of Heat Release (cone calorimeter) and other flammability tests, mathematical pre-flashover fire modeling. Since 1983, chairman of ISO/TC92/SC1/WGS dealing with Rate of Heat Release Testing. Currently a research associate at Center for Fire Research, National Bureau of Standards.

Paul Vandevelde, Ph.D.

Dr. Vandevelde is Senior Scientist at the Laboratory for Fuel Technology and Heat Transfer, State University of Ghent, Belgium. He holds a doctorate in Applied Science from the same institution. He is active in international fire standards work, particularly ISO TC92.

Optical fiber cable with submersion sensor fiber

H. Sawano T. Tsujita O. Kojima H. Akiyama N. Hisono H. Suzuki Y. Sugawara

Fujikura Ltd. 1440 Mutsuzaki, Sakura, Chiba, Japan

ABSTRACT

A cable monitoring system, which uses an optical fiber, has been developed. The feature of this system is to monitor an attenuation distribution of an optical fiber all along a transmission network. An attenuation change of a network is detected by an optical time domain reflectometry (OTDR) to locate fault points of a network. This system uses optical fiber as a sensor, so this system can be applied to also non-metallic optical fiber cable network.

1. Introduction

It is necessary to protect elements of a transmission network, such as cable, splice closure, from water penetration to keep high reliability of a transmission network.1) Generally, a transmission network is maintained by gas pressurized system or fully filled system. However, an optical fiber cable is often required to be free from an electromagnetic influence, so that this type of optical cable is designed as the metal free cable. By the way, gas pressurized system is hard to be applied to metal free cable system. So in this case, there was no way to locate the fault points.

To solve this problem, a new cable monitoring system in which optical fiber works itself as the submersion sensor is proposed. The characteristics of the equipments and the system is discussed.

2. Design concept

As well known, a cable monitoring system is composed of sensors, analyzing equipments and alarm system. In the newly developed system, the fundamental system configuration is similar to conventional one. The different point is that the optical fiber is used as a sensor. The attenuation of the optical fiber in the network is continuously monitored by OTDR. Therefore if the network is damaged at somewhere, the fault points can be located by analyzing the attenuation data from OTDR. Generally, the network is composed of many transmission lines. In this case the optical line selector is useful to monitor many transmission lines by one monitoring system.

Fig.1 shows the typical scheme of the system. In this system, a submersion sensor fiber is stranded in a cable and a submersion sensor is equipped in every splice closure. Scanning all the transmission lines, the attenuation data from each line are collected and analyzed to inform the line status to the control center.

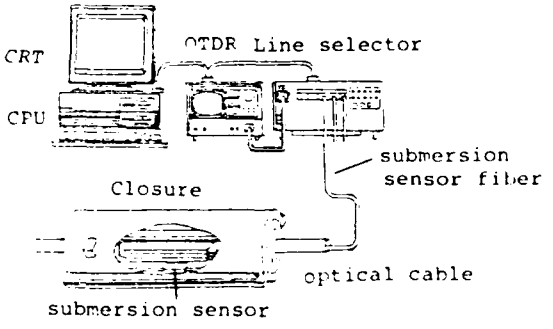


Fig.1 Scheme of the system

3. Sensors

3-1. Submersion sensor

A type of submersion sensor is illustrated in Fig.2. This sensor is composed of four essential elements. These are two fixed mandrel with small diameter, free piston with small mandrel at one side and water swellable material at the other side, and an optical fiber fed through three small mandrels. This submersion sensor is equipped in a splice closure. When water breaks into a splice closure, the water swellable material in

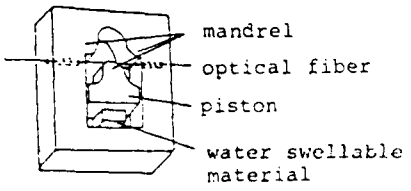


Fig.2 Sketch of the submersion sensor

the sensor reacts on water to expand and free piston with a mandrel moves toward two fixed mandrels. As a result, the optical attenuation of the fiber, which is fed through three mandrels, increases. In designing the sensor, the attenuation increase is an important factor. Because small attenuation increase makes it difficult to detect a water immersion. But also large attenuation increase makes it difficult to detect another water immersion beyond it due to restriction of dynamic range of OTDR. The attenuation increase is determined by the radius of the two mandrels in the sensor. Fig.3 shows the relation between the attenuation increase and the radius of mandrel.

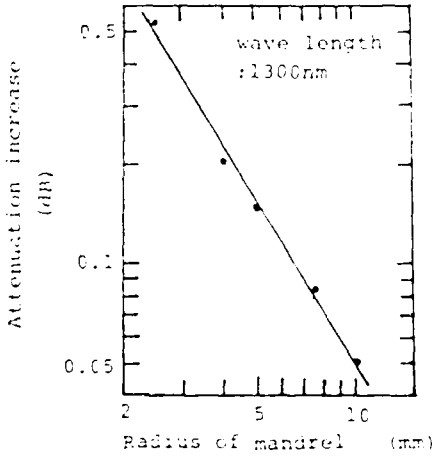


Fig.3 Relation between attenuation increase and radius of mandrel

3-2.Submersion sensor fiber

Fig.4 shows the submersion fiber sensor. This sensor fiber is composed of a standard multi-mode fiber, a FRP rod coated with water swellable material and a string with high Young's modulus. The optical fiber is wound on a coated FRP rod and a string is cross-wound on it. The

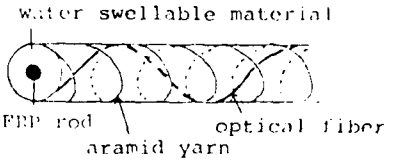


Fig.4 Sketch of the submersion fiber sensor

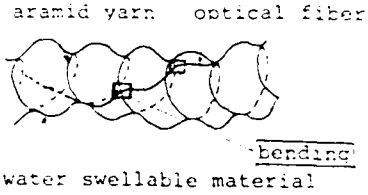


Fig.5 Mechanism of attenuation increase of sensor fiber

mechanism of attenuation increase of this fiber is illustrated in Fig.5. If this fiber sensor is subjected to water, the water swellable material coated on FRP rod intends to expand three-dimensionally, as a result, big undulation happens on this fiber and the optical attenuation increases at the cross points of the fiber and the string. This attenuation increase depends on the lay length of the high modulus string. The relation between the attenuation increase and the lay length of the high modulus string is shown in Fig.6.

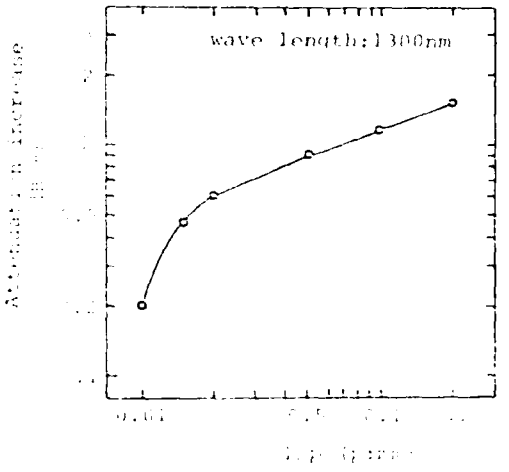


Fig.6 Relation between attenuation and stranding lay length of string

3-3.Water swellable material

The water swellable material, which is used in sensors, is composed of thermoplastic rubber, water swellable polymer and others. Table 1 shows the water absorptive power and tensile properties of the water swellable material. It was confirmed that the water swellable material was stable against temperature and humidity.

4.Reliability of the system

The followings are the investigation results of the attenuation stability and the operation reliability of the system under various environmental conditions.

4-1.Attenuation in cable manufacturing process

Fig.7 shows the cross-section of the examined cable. This cable is a non-metallic slot type cable using optical fiber ribbons. A submersion sensor fiber is stranded in a slot. At each cable manufacturing process, the attenuation was measured. The result is shown in Fig.8. The attenuation changes of each manufacturing process were less than 0.1 dB/km.

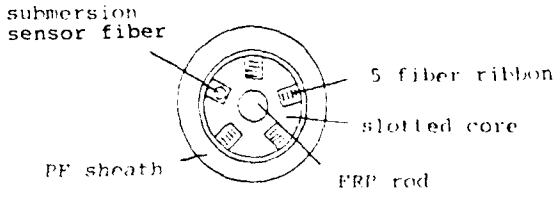


Fig.7 Cross-sectional structure of cable

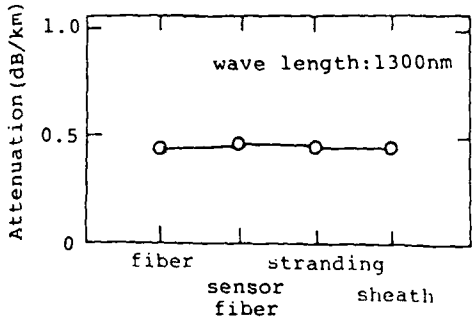


Fig.8 Attenuation of submersion fiber sensor in cable manufacturing

4-2.Mechanical properties of the submersion sensor fiber in the cable

The mechanical properties of the submersion sensor fiber in the cable was investigated. The test conditions and the results are shown in Table 2.

The attenuation change was within 0.01 dB/l (l is the length of the cable under test) in each mechanical condition.

Table 2 Mechanical properties of the submersion sensor fiber in optical cable

Item	Condition	Result
Bending	R=200mm, 180 , 1 turn	less than 0.01dB/turn
Stretching	up to 0.2% elongation 100m	less than 0.01dB/100m
Crush	up to 2500N/50mm of lateral force	less than 0.01dB/50mm
Vibration	10Hz, 5mm of amplitude and 1 million times	less than 0.01dB/m
Impact	1kg, 1m height	less than 0.01dB
Squeezing	R=200mm, up to 0.2 % elongation, 100m	less than 0.01dB/100m

Table 1 Characteristics of the water swellable material

Item	Unit	Typical value	After 80C,1000hr treatment	After 60C,95RH 1000hr treatment	Test procedure
Water absorption	%	4500	4200	4300	Specimen 1g in 300ml pure water at 20C
Tensile strength	kg/cm	400	320	330	ASTM D638
Elongation at break	%	650	620	600	ASTM D638

4-3.Stability of the submersion sensor fiber under high humidity and temperature change

A installed cable is affected by humidity and temperature change. It is known that the strength of the optical fiber become weak under high humidity. The tensile characteristics of the fiber was investigated compared to standard fiber. Fig.9 shows the results of failure probability distributions for tensile strength. The degradation of fiber strength arose after humidity treatment. But the difference of strength degradation between the fiber used in sensor and standard fiber was scarcely observed.

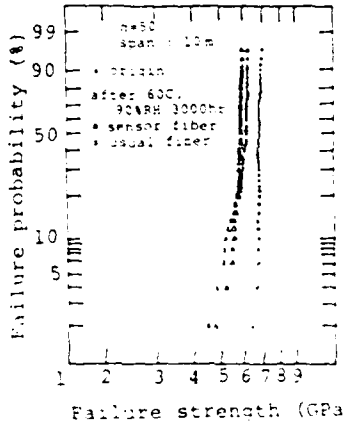


Fig.9 Weibull probability plot of fibers

Fig.10 shows the temperature characteristics of the fiber. The attenuation change was less than 0.1dB/km for the temperature change of -30C to +60C.

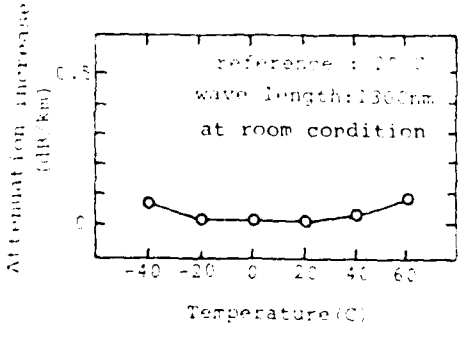


Fig.10 Temperature dependence of submersion sensor fiber

5.Operation characteristics of the submersion sensor and sensor fiber

5-1.Temperature dependence of the operation characteristics

Fig.11 shows the relations between the attenuation increase and water temperature. The water temperature was between 4C and 60C. The attenuations began to increase in 30 to 45 minutes for both the submersion sensor and the fiber sensor. The rising times of the attenuation increases do not depend upon water temperature so much. The saturated attenuation increase becomes smaller as temperature becomes higher for the fiber sensor (see Fig.11). This is because the modulus of the water swellable material becomes low at higher temperature. OTDR detection limit (about 0.2dB) is guaranteed even for the lowest attenuation increase of 60C.

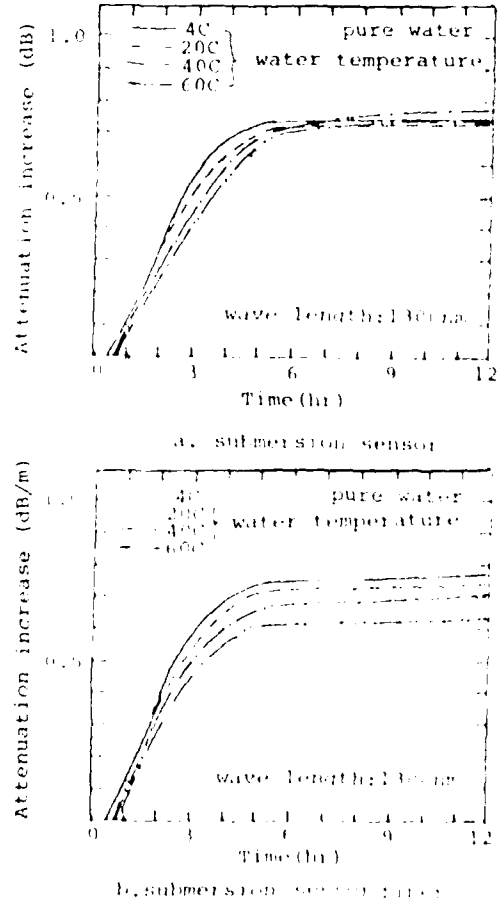


Fig.11 Temperature dependence of attenuation increase

5-2. Effect of the water nature

The operation characteristics of the submersion sensor and sensor fiber were examined in five different natures of water, e.g., pure water, pH3 HCl aq., pH11 NaOH aq., 1% surface active agent aq. and practical manhole water. Fig.12 shows the results. The attenuation increases reach the sufficient level to be detected in ionized water.

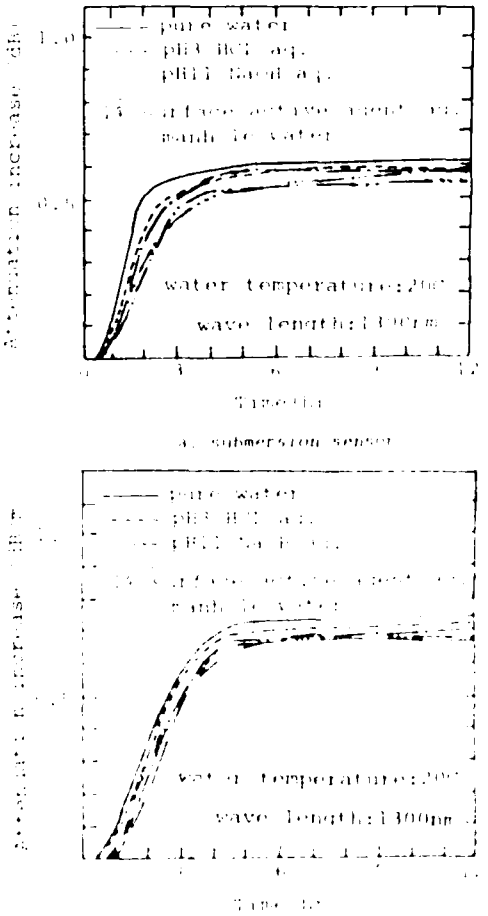


Fig.12 Water nature dependence of attenuation increase

6. Application test of the cable monitoring system

Based on above results, a cable monitoring system was experimentally constructed (See Fig.1) and the operation characteristics was investigated. This system was constructed with a CPU, CRT, OTDR, line selector and two optical fiber lines. Table 3 shows the performance of the equipments. Line 1 is 21,100, meter long concatenated multi-mode 50/125 submersion fiber sensor in which a submersion sensor B is installed at 16,600 meter point. Line 2 is 5,800 meter long, which is for the experimental purpose of the line selector. The lines were alternatively monitored by using the line selector. The test water is actual manhole water and the temperature is 18C. Fig.13 shows the attenuation shape of line 1 before and after immersed in water, respectively. At points A, B and C, water submersions were obviously detected. As a result, it is found that the submersion fiber sensor has an ability to sense the damage along a cable and that the submersion sensor senses the damage of cable splice closures.

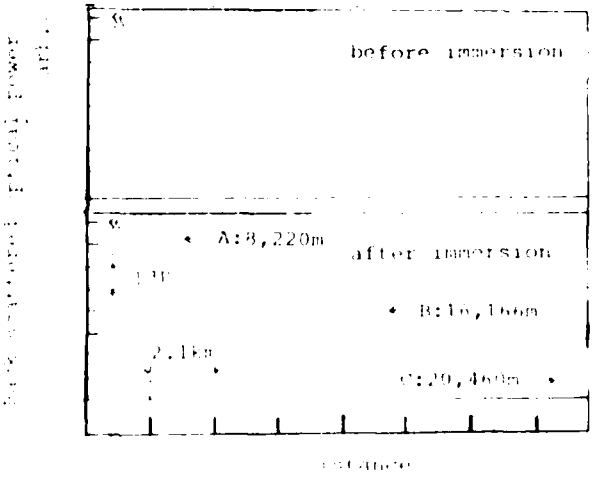


Fig.13 Attenuation shape of line 1 before and after water immersion

Table 3 Equipments of the system

Equipment	Performance
Submersion sensor	Designed saturation loss ; [illegible] dB Equipped in cable splice closure
Submersion sensor fiber	Designed saturation loss ; [illegible] dB Stranded in cable
OTDR	Minimum distance resolution ; 4m Minimum detection limit; 0.2dB at 30km distance, 1310nm
Line selector	Maximum line number ; 16 lines Joining loss ; less than 0.2dB

7.Conclusion

A new cable monitoring system was proposed. In this system the fault points in a transmission network are located by monitoring the bending loss of the optical fiber. The attenuation loss increase was designed based on experimental result and the reliability of the system was assured in various tests.

The newly developed cable monitoring system is available not only for ordinary optical cables but also non-metallic optical cables. The introduction of this system will make change the concept of the maintenance of non-metallic optical fiber cable network.

8.Acknowledgment

The authors would like to express the great appreciation for the useful advice and encouragement from Dr. K. Inada and Mr. K. Sato.

reference

1) F. Jontai and A. Joss, "A FIBER OPTIC CABLE MONITORING SYSTEM", 35th IWCS, USA, 1986.

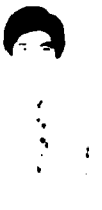


Hiroyuki Sawano

Fujikura Ltd.

1440 Mutsuzaki,
Sakura, Chiba, 285
Japan

Mr. Sawano received the M.S. degree in Polymer Science from Hokkaido University in 1983 and joined Fujikura Ltd.. He has been engaged in the develop of optical cable. He is now an engineer of Telecommunication Cable Section in Research and Development Division and a member of IEICE of Japan.



Teruyuki Tsujita

Fujikura Ltd.

1440 Mutsuzaki,
Sakura, Chiba, 285,
Japan

Mr. Tsujita received the M.E. degree in Applied Chemistry from Niigata University in 1980 and joined Fujikura Ltd.. He has been engaged in the study of plastic materials and optical cable. He is now an engineer of Telecommunication Cable Material section in Research and Development Division and a member of IEICE of Japan.



Osamu Kojima

FUjikura Ltd.

1440 Mutsuzaki
Sakura, Chiba, 285
Japan

Mr. Kojima received the B.E. degree in Electrical Engineering from Chiba University in 1982 and joined Fujikura Ltd. in 1987. He has been engaged in the study of telecommunication system. He is now an engineer of Optical Cable Section in Research and Development Division and a member of IEICE of Japan.



Michio Akiyama

Fujikura Ltd.

1440 Mutsuzaki,
Sakura, Chiba, 285
Japan

Mr. Akiyama received the M.E. degree in Electrical Engineering from Yokohama National University in 1975 and joined Fujikura Ltd.. He has been engaged in the development of optical fiber and optical cable. He is now a senior engineer of Telecommunication Cable Section in Research and Development Division and a member of IEICE of Japan.



Nobuyuku Misono

Fujikura Ltd.

1440 Mutsuzaki
Sakura, Chiba, 285
Japan

Mr. Misono received the B.E. degree in Electrical Engineering from Chiba University in 1972 and joined Fujikura Ltd.. He has been engaged in the development and design of telecommunication cable and optical cable. He is now a senior engineer of Telecommunication Cable Section in Research and Development Division and a member of IEICE of Japan.



Hideo Suzuki

Fujikura Ltd.

1440 Mutsuzaki,
Sakura, Chiba, 285,
Japan

Mr. Suzuki received the B.E. degree in Polymer Chemistry from Gunma University in 1971 and joined Fujikura Ltd.. He has been engaged in the study of plastic materials, polymer processing and the development of optical cables. He is now a chief of Telecommunication Cable Material Section in Research and Development Division and a member of IEICE of Japan and the Society of Polymer Science, Japan.



Yasuyuki Sugawara

Fujikura Ltd.

1440 Mutsuzaki,
Sakura, Chiba, 285
Japan

Mr. Sugawara received the B.E. degree in Telecommunication Engineering from Tohoku University and joined Fujikura Ltd.. He has been engaged in the development and design of telecommunication cable and optical cable. He is now a chief of Telecommunication Cable Section in Research and Development Division and a member of IEICE of Japan.

OPTICAL FIBRE CABLE FOR MOBILE APPLICATION IN BROWN COAL MINING AREA

by Helmut G. Haag, Georg Hog and Peter E. Zamzow

AEG KABEL Aktiengesellschaft
Monchengladbach, Federal Republic of Germany

Abstract

In the brown coal mining area there exists a large requirement for information transmission for steering and supervision of machinery and transportation controlled from a central station. The transmission with copper pairs and power line carrier telephony used up to now becomes more and more problematic by the increase of distances, electromagnetic interference and transmission rates by the increasing complexity of the equipment. Therefore an optical transmission system for telephone, steering and video controlling will be the future. The contribution describes the single components like drag cable, rotary transfer coupler, conveyor road cable and closures as well as line equipment together with the relevant requirements. First experiences are reported.

Introduction

Up to now, optical fibres and optical fibre systems have been put extensively in telecommunication networks where they replace by their high digital transmission capacity existing copper lines /1/, /2/. But now also industrial areas are penetrated by optical fibre transmission systems. Here the large bandwidth and low attenuation is only of marginal interest, but the characteristic of optical fibres being immune against electromagnetic interference is the main advantage of optical fibres in comparison to copper systems or open wire systems in industrial areas. In order to avoid human danger by induced voltages from neighboured power systems optical fibre cables must be dielectric if they are used separately. This means that all mechanical protection like steel wire braid or steel tape armouring must be achieved by dielectric materials. On the other hand where optical fibre cables are incorporated in power cables e. g. drag cables they must not restrict the behaviour of the hospitality cable.

In this contribution we describe optical fibre cables which will be necessary for a transmission system which connects in a brown coal area the digger with the supervision station. The use of optical fibre systems in coal mining areas, steel mills or with power electric utilities are described elsewhere /3/, /4/, /5/.

Total System

In the brown coal mining area the different moving digging equipment and boom stacker with their conveyor roads must be connected with the supervision end steering centre. It is desired to transmit telephone signals from the team on the digger to the control station. Moreover relevant data like location, capacity and surveillance conditions must be transmitted to the central station automatically. In some cases it may also be desireable to transmit a video picture from the off-side to the control monitors.

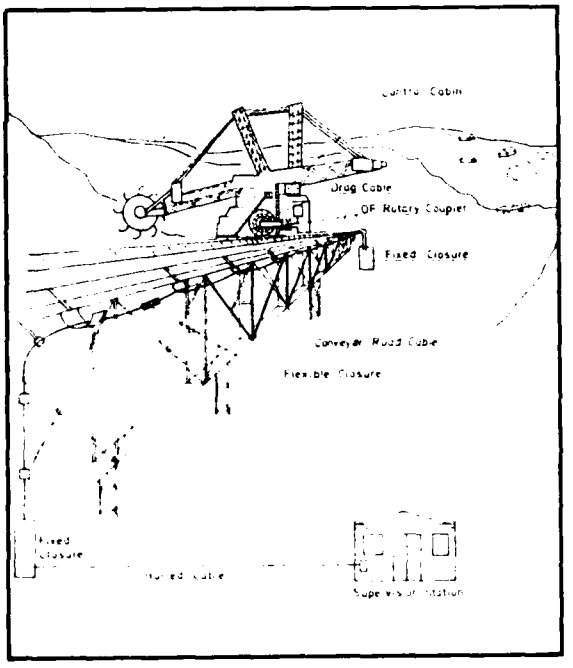


Fig. 1: Optical fibre link in a brown coal mining area

Transmission systems used nowadays on symmetric copper pairs, coaxial cables and power line carrier telephony can only transmit few

datas. Higher transmission rates can only be transmitted in using extended screening measures.

In cases where a distance of about 1 or 2 kilometers must me bridged optical fibre transmission systems can give the required transmission capacity on an economic basis. Such an optical fibre transmission system in a brown coal mine (Fig. 1, 2) consists of the electrooptical transceivers on both sides of the link and the cables and closures between them. Coming from the control cabin on the digger, a mobile cable must be installed to the drag cable which connects the digger with its power supply. Because the control cabin is installed on moving parts of the digging equipment not a fixed installation of optical fibre cable is possible. Then in the path of the optical light to the mining control station an optical fibre cable must be incorporated in the drag cable. Because

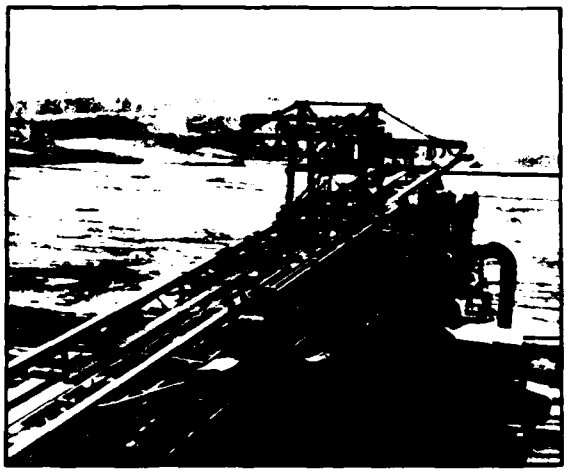


Fig. 2: Bridge from the digger to the conveyor road

of the fact that communication must also work on a moving digging equipment the connection between the mobile cable on the digger to the drag cable must be a rotary transfer coupler. On the further path of the light an optical fibre conveyor road cable must be installed. Because the conveyor road will be moved from time to time depending on the digging progress, the optical fibre conveyer road cable must withstand these severe conditions, where in moving the cables remain on the conveyer road. At the end of the conveyor road the light can draw a deep breath. The further path guides through a conventional buried cable and indoor cable to the mining control.

The following chapters describe the optical fibre drag cable together with the rotary transfer coupler, the conveyor road cable with its special closures and the required transmission systems.

Drag cable

The drag cable with a length of about 500 m has incorporated under a common sheath an element with 6 optical fibres besides the power conductor. The geometrical dimensions of this optical fibre element are chosen in such a way that it fits into the outer interstices of the 3 phase conductors of the drag cable. The ground conductor's cross section of 70 mm^2 were divided in 2 single conductors instead of 3 in the case where no optical fibre element is in the cable. The phase conductors are copper conductors with 120 mm^2 cross section (Fig. 3).

In order to withstand the mechanical and temperature induced loadings of the optical fibre element during the stranding and the extrusion and cross linking of the rubber sheath, the optical fibre element itself has to be especially designed. The 6 optical fibres are incorporated in a common loose buffer which is

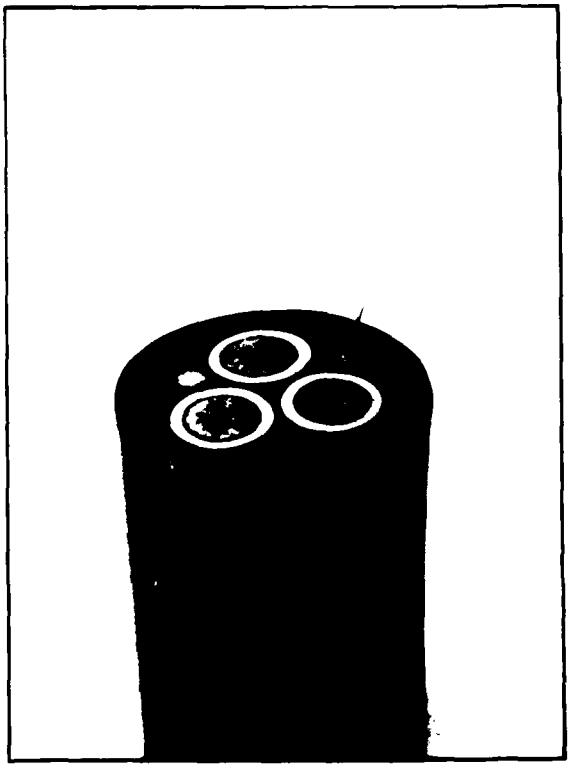


Fig. 3: Drag Cable 3x120 + 2x35 with 6 optical fibres

filled with high-temperature resistant jelly. Over this buffer fibre-reinforced plastic elements were stranded and over this a braid of glass elements was applied. This construction gives the robust armour for the followed extrusion of the rubber sheath. This so produced optical fibre element was stranded together with the other elements of the drag cable. This optical fibre element was strong enough to be stranded on the normal stranding machine which normally strands the high voltage power cables. After finishing the cable the optical fibres were measured. No change in attenuation between the bare fibres and the fibres in the drag cable was observed.

Also after the exposure of the drag cable to the different environmental conditions like temperature changes between -30 °C and +60 °C, maximum tensile force of 25,000 N only small but fully reversible changes in attenuation were observed. Only after 2,000 bendings an increase in attenuation of 0.1 dB for the 500 m length in maximum is due to ageing effects. The characteristics of the optical fibre drag cable are shown in figure 4.

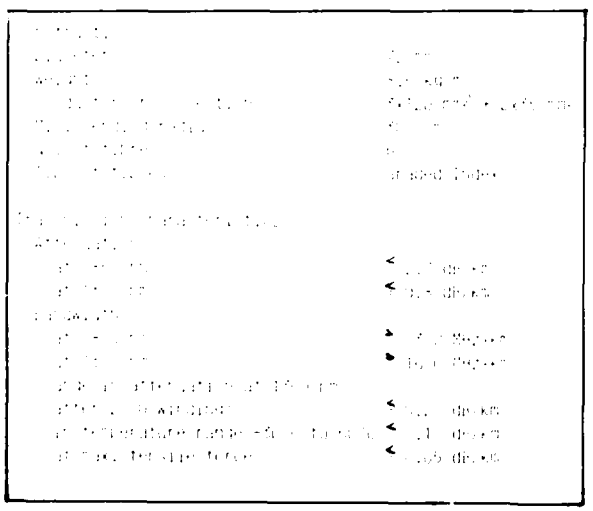


Fig. 4: Data of the optical fibre drag cable

In order to put such a drag cable into operation it is necessary to apply at the inner side of the drag's cable reel a rotary transfer coupler for the 6 optical fibres. Figure 4 shows such a rotary transfer coupler. The coupler is designed following the principle, that the required turns of the reel are put into the transfer coupler in winding it on 2 reels building an "8". Depending on the construction it is not possible to have an endless rotary transfer coupler. The coupler designed for the 500 m drag cable requires the possibility to make about 25 turns. By this principle it is not necessary to have a rotation part between the fibres to be coupled. Therefore the coupling loss of this rotary transfer coupler is only 2 times the connector loss. This means about 1.5 dB.

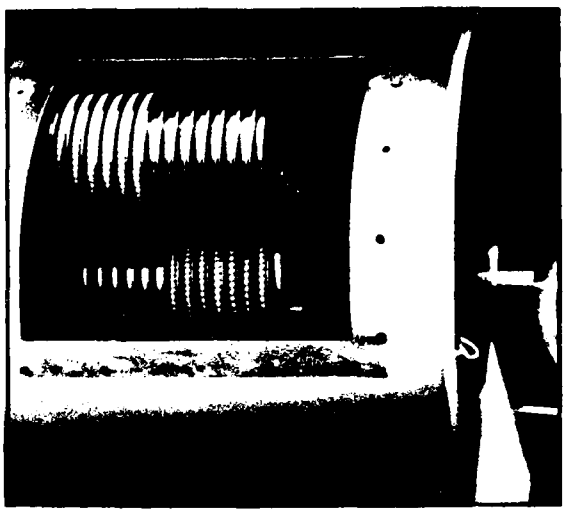


Fig. 5: Rotary Transfer Coupler for 6 optical fibres (by GKL, Elsdorf, FRG)

Conveyor Road Cable

The optical fibre conveyor road cable is intended to be used along moveable conveyor roads, whereas normally the telecommunication cables as well as the power cables are metall-armoured, the optical fibre cable was designed to be fully dielectric. This allows much easier installation and termination at the end points where no care must be taken for human safety in case of induced voltages.

The designed cable consists of a central strength element around which a maximum of 8 fibres can be stranded. The cable core is then petrojelly filled and a glass fibre reinforcement is stranded around the filled cable core in two layers. The cable is finalized by a Polyurethane sheath of 2 mm thickness which results in a total cable diameter of about 11 mm (Fig. 6).

For the test single mode fibres as well as graded index fibres with 50 and 62.5 µm core diameter were used. The fibre buffer was chosen to be a tight buffer to allow in case of repair and also primary installation a direct mounting of connectors on the buffered fibre.

The attenuation of the optical fibres (graded index as well as single mode fibres) show no change in attenuation during the production process from the bare fibre to the

finalized cable. The cable was then tested with respect to all specified parameters like tensile strength, bending, torsion and change in attenuation with respect to temperature change. The results of these measurements are shown in Fig. 7. The results show that this cable is well designed with respect to the requirements.

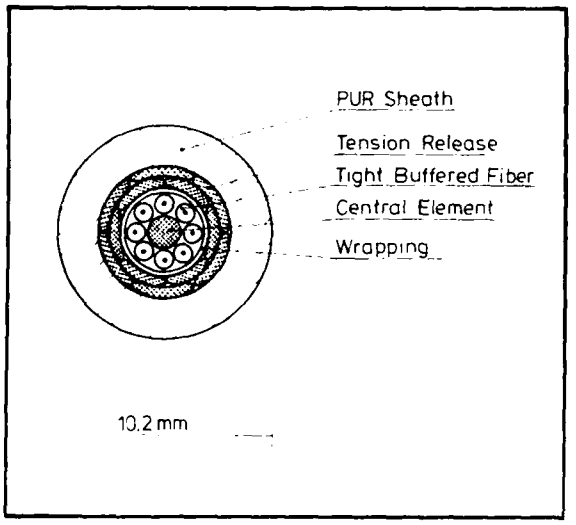


Fig. 6: Cross-Section of the optical fibre conveyor road cable

If in a new installation the cable length is shorter than the required link length it is necessary to mount a closure. Such a closure is also necessary in case of repair. By the installation condition this means the conveyor road cable is hanging besides the conveyor road, the closure must be approximately equal in diameter to the cable and moreover must withstand the same requirements as the cable itself and the closure may not hinder in excess the flexibility of the cable.

The closure developed for this purpose fullfils the requirement on flexibility and strength and has an outer diameter of about 40 mm. It consists of 2 concentric hollow tubes. The inner tube has a diameter in the range of the cable diameter and a length of about 500 mm. In the inside of this tube the central strength element of the cable to be jointed is connected and on the outside of the tube the spliced fibres are helically wound in order to give the required spare fibre length for splicing. The bare fibres and splices are protected by soft tapes to avoid damage and microbending. The outer tube is a flexible corrugated tube with a slightly larger diameter than the protected inner tube. Over the outer tube the strength elements of both cables are applied. These strength elements are fixed by a shrinkable tube and gives a strength to the closure which is at least the strength of a single cable. Moreover this closure is flexible by the usage of soft

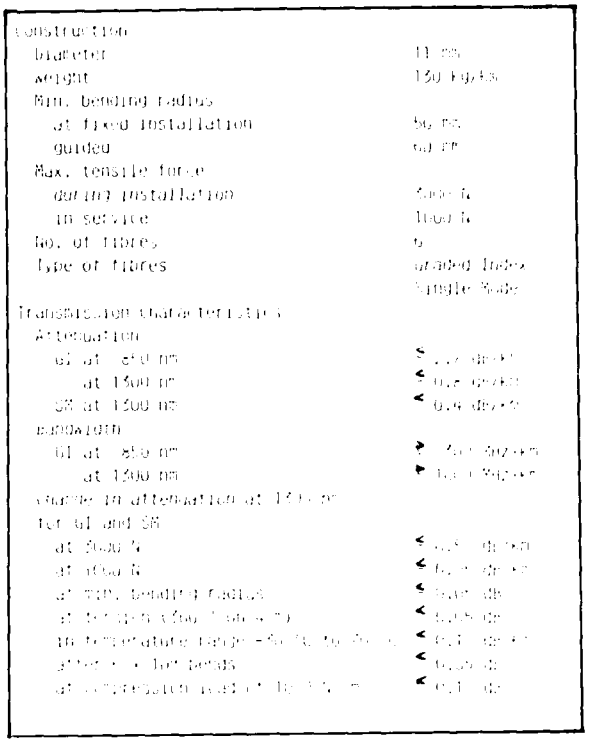


Fig. 7: Data of optical fibre conveyor road cable

inner tube material and corrugated outer tube. Fig. 8 shows such a bended conveyor road cable with the closure.

Besides this closure which fullfils the general requirement for a conveyor road cable

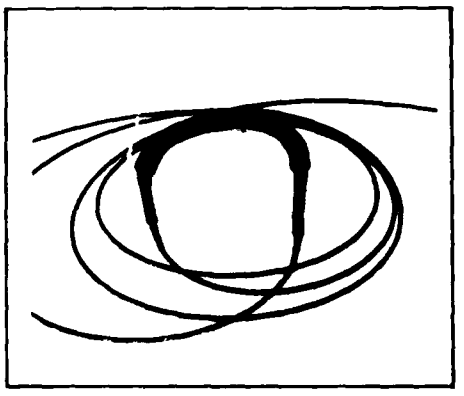


Fig. 8: Conveyor road cable closure with high flexibility and strength

closure also the possibility of a fast repair splice by the maintenance people of the brown coal mining itself is required. This can be done by adhesive splices which are protected in a small splice box. In order to get a sufficient strength of repair splice it is necessary to overlap the both cable ends and fix them together by a shrinkable tube. The cable ends are then fed into the provisional splice box from the rear.

Transmission System

In the brown coal mining area it is desirable to transmit between the digger and the supervision station telephony and remote control signals. These are both narrow band signals. But by the different structure of the signal coding it is adviseable to use for shorter distances 2 fibre pairs, one for each type of signals. For longer links one can choose between a 2-way-wavelength multiplex or electronical multiplexing of the telephone and the remote control signals to one data stream in order to reduce the number of fibres from 4 to 2.

If additional broad band services like video controlling or video communication should be transmitted one respectively two additional fibres are necessary.

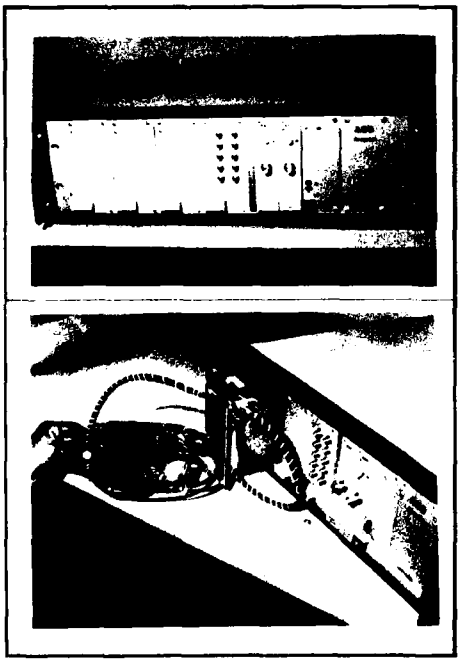


Fig. 9: Line termination equipment for fast data transmission in 19" rack

For distances of up to 15 km for all the above mentioned systems LED's on graded index fibres will be the economical solution. In this, for distances of up to 6 km LED's in the 850 nm region are preferred. For longer link lengths the 1,300 nm region should be used. Only for system lengths of more than 15 km the use of single mode fibres together with lasers may be considered. Fig. 9 shows some hardware of the line termination equipment.

Summary

In the contribution the different components of an optical fibre transmission system connecting the control cabin of a digger with the supervision station are described in detail. It is shown that the drag cable, the conveyor road cable and the required rotary transfer couplers and closures are well designed for this rough environment. Systems with LED's in the first or second window gives the required availability for the transmission system with respect to the distances and required signal structure.

By the progressing control technique using digital coding it is obvious that optical fibre systems fullfil the requirements for troublefree and reliable transmission path without exorbitant effort on screening and redundancies.

The experience up to now shows the usability of optical fibre systems in brown coal mining area and the further experience will give advise for the ongoing development.

Literature

/1/ Kanzow J., Activities of the Deutsche Bundespost towards the introduction of optical fibres in the subscriber line network. Proc 10th ECOC 1984, Stuttgart, pp. 26 - 27.

/2/ Haag H. G., Hög G., Zamzow P. E.; Optical Fibre and System Considerations for a Broadband Subscriber Network, Proc. 34th IWCS 1985, pp. 355 - 363

/3/ Gregor P., Hög G., Gläsel W., Haag H. G.; Optical Fibre/Copper Conductor Composite LAN Cable for Mining Application

/4/ Haag H. G., Zamzow P. E.; Luftkabel mit Lichtwellenleitern, etz 106(1985)4, pp. 154 - 160

/5/ Haag H. G., Lichtwellenleiter-Phasenseil-luftkabel, etz 108(1987), pp. 170 - 176



Helmut G. Haag (Speaker)
AEG KABEL AG
Manager Communication System Techniques
Mönchengladbach, West Germany

Helmut G. Haag (39) is head of the Technical Sales Division for Telecommunications. After reaching his Dipl.-Physiker-degree from the University of Stuttgart he joined AEG KABEL AG in 1975 for the development of coaxial cables. Later he has been also responsible for the development of optical fibre cables. From 1980 to 1983 he built up the production plant for these cables. In autumn 1983 he took his present position.



Georg F. Hög
AEG KABEL AG
Telecommunications Development
Mönchengladbach, West Germany

Georg F. Hög (37) is head of the Development Group for Optical Fibre Cables. He reached his Dipl.-Ing.-degree from the University of Aachen and joined AEG KABEL AG in 1977. After being engaged in the development of symmetrical telecommunications cables he got the responsibility for this group in 1980. Since spring 1985 he covers his present position.



Peter E. Zamzow
AEG KABEL AG
Telecommunications Development
Mönchengladbach, West Germany

Peter E. Zamzow (47) is director of the Telecommunications Development Division. After finishing his postgraduate studies in telecommunications at Munich and Graz as Dipl.-Ing. he joined AEG KABEL AG in 1970. He has been engaged in development and production of telecommunications cables. In 1980 he became head of the fibre optic division in AEG KABEL and in 1982 he was nominated as a senior engineer. Since 1985 he has covered his present position.

INTRA-AIRCRAFT FIBER OPTIC COMMUNICATION SYSTEM

Christopher E. Polczynski

Lockheed California Company
Burbank, California

Abstract

A fiber optic system replacing 12 twisted, shielded pairs with a single fiber, electronics and optics is described. The system transmits 12 command/ data signals from wing to wing equipment pods. Of the 12 signals, five propagate right-to-left and seven left-to-right. System components in each wing include a Time Division Multi-demultiplexer, a Laser Transmitter (1300 nm in one wing 1550 nm in the other), a Wavelength Division Multi-demultiplexer, and a PIN-FET Receiver. Most of the transmitted signals are asynchronous. Therefore, a supersampling approach to time division multiplexing was required resulting in quite high serial data transmission rates-300MBPS left-to-right and 294.912 MBP, right-to-left. The wavelength division multi-demultiplexer allowed for simultaneous, bidirectional transmission of two independent serial data streams over a fiber. The fiber cable from wing to wing required six bulkhead connectors. A laboratory prototype of the fiber system was successfully tested with the aircraft system. Flight qualified hardware is now being developed. Upon successful completion of flight tests, existing Lockheed aircraft will be retrofitted. The system will also be used as a test bed for advance fiber optic applications on existing and future Lockheed aircraft.

Introduction

Optical fiber technology, together with rapid advances in high-speed integrated circuits, is laying the foundation for new interconnect systems replacing conventional wire cabling on aircraft.

Initially, fiber was used as a one-for-one replacement for copper wire. In the near future, multiple twisted shielded pairs (TSP) and coaxial cables will be replaced by a fiber optic interconnect system containing a single fiber.

The major incentives for "fiberizing" existing aircraft are weight and volume savings, and elimination of EMI problems due to cabling. It is estimated that the use of fiber instead of conventional wire cabling could reduce the weight of a small military plane by hundreds of pounds, and a large plane by at least a ton. The volume reduction of cabling and connectors can be 90%. Weight and volume reductions which can be realized by multiplexing and then transmitting over metallic cables are not as great. For many existing aircraft, the weight and volume reduction potential offered by fiber optic retrofit is very attractive.

Future electronic systems for aircraft will be based on components resulting from the VHSIC (Very High Speed Integrated Circuits) program. This program will provide IC's orders of magnitude faster and more powerful than the current devices. VHSIC will be mandatory on the new tactical fighter programs, such as the Air Force Advanced Tactical Fighter, the Navy's Advanced Tactical Aircraft, as well as on other programs. Fiber optic technology is required to interconnect VHSIC based equipment.

Thus, developments in technology are quickly forcing fiber optics to be used for aircraft retrofit, new systems,and next generation aircraft applications.

This paper describes a laboratory version of a fiber optic interconnect system which replaces 12 existing TSP with a single optical fiber, electronics, and optics. The system was successfully tested,and flight qualified hardware is now being developed. Upon successful completion of flight tests, existing aircraft will be retrofitted. The system will also be used as a test bed for advanced fiber optic applications on existing and future Lockheed aircraft.

Existing Wire System Parameters

Twelve command/data signals are now transmitted over 12 TSP from wing to wing equipment pods for a distance of approximately 30 meters. In that length, six bulkhead connectors are required. The cables run in non-pressured areas of the aircraft. The operating altitude is 0 to 70,000 feet. The operating temperature range is -65°C

to +65°C degrees.

Transmitted signal characteristics are shown in Table 1. All signals are differential, TTL levels. Signaling frequencies range from 1.5 KHZ for an alarm signal to 6.25 MHZ for a clock signal. Referring to Table 1, note that there are four groups of signals that contain synchronous signals within each group. However, signals in any one group are not synchronous to signals in any other group. The first group contains signals A, C, D; the second group-Z, E; the third-T, U; and the fourth-V, W. The remaining three signals are asynchronous.

Furthermore, five signals occur in bursts. The 6.25 MHZ clock and its data occur in bursts of 22 clock periods duration. The duration of the gap between bursts is random. The duration of the three alarm signals (B,X,Y,)is also unpredictable. The remaining signals are continuous.

Of the 12 signals, seven flow from left to right, and five flow from right to left. Note that the 1.152 MHZ clock is transmitted in the opposite direction of the 1.152 MHZ data.

The lack of a common clock and the need for bidirectional transmission were the key requirements which drove the design of this fiber optic system. Details of how this was accomplished will be discussed later.

Fiber Optic System Description

The fiber optic system block diagram is shown in Figure 1. The subsystem components in each wing are the same with the exception of a 1300 nm transmitter on one side, and a 1500 nm transmitter on the other. Each subsystem consists of a Time Division Multi-demultiplexer (TDM), Laser Transmitter (TX), PIN-FET Receiver (RX), and Wavelength Division Multi-demultiplexer (WDM). A fiber optic cable with six bulkhead connectors provides an optical interface between the subsystems. Two wavelengths propagate in opposite directions over the fiber cable allowing for independent, simultaneous, and bidirectional transmission of data.

For either direction of transmission, parallel differential TTL level input signals to the TDM are multiplexed into a high speed serial data stream. The ECL-level differential TDM outputs drive a laser transmitter. It's output is coupled into the WDM, and the output of the WDM is coupled into the fiber cable. After propagating through 30 meters of cable with six in-line connectors, the optical signal is coupled to the second WDM from which it is coupled into the PIN-FET receiver. The receiver converts the optical signal into a differential ECL elvel serial bit stream which then drives the second TDM. The TDM demultiplexes that data into parallel differential TTL level outputs corresponding to the input TTL level signals at the first TDM.

Figure 2 shows the laboratory prototype of the fiber optic system. Electronic system components are now being hybridized for flight tests. The anticipated sizes of components and their packaging configuration, for one side, are shown in Figure 3. Packaging dimensions are 5" X 5" X 1.5" and were determined primarily by the bend radius of the fiber pigtails.

The laboratory prototype was ground tested successfully with the aircraft system. The aircraft system operated equally well over fiber or over wire. Acutally, the wire system causes some signal distortion at the output compared to the input, the fiber system does not. Description of the fiber system components follows.

Time Division Multi-Demultiplexer

The TDM multiplexes the signals in a manner suitable for optical transmission. Since, as discussed above, most of the signals are asynchronous to each other, a supersampling approach to multiplexing is required. This results in very high serial data rates. In the left to right direction the data rate is 300 MBPS, and 294.912 MBPS in the right to left direction.

The serial word transmitted by a multiplexer is 16 bits long. A unique bit sequence is transmitted for achieving word synchronization. It requires six data bits and is assembled by transmitting three consecutive logic levels followed by three consecutive complementary logic levels. The first six bits also signify the state of one input data channel. (Referring to Table 1, signal D for left to right, signal Z for right to left.) When the first three bits are logic level high, then that input channel is in logic level high, and vice-verse. The last ten bits are assigned to the remaining five data channels as follows. Each data channel occupies two bit times. A bit is directly followed by it's complement. If the it is logic level high, then the input hannel is logic level high, and vice se. Figure 4 shows one word with all a channels at logic level high. The advar ges of this coding scheme are: (1) high ansition density for reliable clock recov , and (2) 50 percent duty cycle for ease o fiber optic transmission.

Since ly five signals are transmitted in the left-to-right direction, one of the six data channels is reserved for future use. In the other direction, signals U and W are premultiplexed into one channel prior to

the mux section of the TDM thus reducing the number of signals to 6.

The 300 MBPS output bit stream from the left-to-right mutiplexer is synchronized with an additional available 6.25 MHZ continuous clock from the aircraft system. The 6.25 MHZ burst clock, the 6.25 MBPS burst data, and the 320 nS pulses (signal A) are all synchronized to the continuous 6.25 MHZ clock. All these signals, therefore, are sampled synchronously. The other signals are sampled asynchronously at a rate of 18.75 MHZ. Sampling error on the 1.152 MBPS data is removed by retiming it with its own clock originating at the destination of the data. Sampling error on the 1.5 KHZ alarm signal is insignificant for system operation.

The 294.912 MBPS output bit stream from the right-to-left multiplexer is synchronized with the 1.152 MBPS clock. The other signals are sampled asynchronously at a rate of 18.432 MHZ. Sampling errors on the asynchronously sampled signals are insignificant for system operation.

The demultiplexers feature error resistance to word sync detection. Three consecutive word sync errors need to be detected before the demultiplexer assumes that sync was lost, and starts to reaquire it.

The TDM devices were designed around commercially available GaAs time-division multi-demultiplexer chips. The laboratory prototype was constructed using surface mount device (SMD) packaging technology. The flyable units will be hybridized.

Transmitter and Receiver

The transmitter uses a bipolar differential amplifier to modulate the laser. Average power feedback loop keeps the optical power constant over time. Temperature control of the laser is required primarily to keep the lasing wavelength within the bandpass of the WDM devices. A cooler is used both as a cooler and as a heater to keep the laser chip at room temperature as the ambient varies over the range of +65°C to -65°C.

Laboratory prototypes were built with commercially available lasers in DIP packages. Typical measured optical rise time of a transmitter was 700 pS. A hybrid version will have the laser chip mounted closer to the modulator. As a result, the optical rise time should decrease to about 400 pS. The peak output power for a hybrid transmitter will be 0 dBM for either 1300 nM or 1550 nM lasers.

The receiver uses a commercially available PIN-FET front end followed by linear gain stages and limiting amplifiers. Differential, ECL-compatable outputs are provided. The receiver sensitivity was tested at higher than the required 300 MBPS data rate. The measured sensitivity for 10E-9 bit error rate (BER) with a 350 MBPS pseudo-random data was -35dBM (average).

Hybrid versions of the receiver or transmitter will be housed in a 1" X 1" X .38" high DIP package, as shown in Figure 3. Optical interface will be via a fiber pigtail.

Wavelength Division Multi-Demultiplexer (MUX/DEMUX)

The WDM couplers allow for bidirectional transmission over a single fiber. The couplers used for this program are filter based. One coupler consists of 1.3 MUX/ 1.5 DEMUX, the other is 1.3 DEMUX/ 1.5 MUX.

Back reflections into the laser cavity generate noise and degrade performance characteristics of laser diodes. In order to eliminate back reflections from the junction of the laser to the WDM, the laser pigtail was fusion spliced to the WDM input fiber. To eliminate back reflection from the six inline bulkhead connectors in the fiber optic cable, the couplers contain absorbing attenuators. Reflections reaching the laser from the connectors were reduced by 24 dB which was sufficient to eliminate noise generation and the degradation of laser properties.

The MUX and DEMUX loss without the attenuator was less than 0.6 dB total. With the attenuator, the MUX loss was 12.0 dB and the DEMUX loss was 6.5 dB for a total loss of 18.5 dB.

The couplers were temperature stabilized to minimize loss variations. To verify their performance over temperature, they were subjected to two types of testing: (1) Temperature cycling where the couplers were cycled over the range of + 65°C for ten equal cycles for a total time of 75 hours. (2) Temperature shock test where the couplers were brought to one or the other extreme (+65°C or -65°C) and then rapidly cooled/heated to +25°C. For both tests, the maximum variation in attenuation was no more than 0.1 dB with full recovery at the end of the tests. Measured resolution of the tester was 0.1 dB. Figure 5 shows typical temperature cycling test results. It should be added that the couplers were also temperature cycled to +125°C. No change was observed from the results obtained at +65°C.

Fiber and Connectors

The 62.5/125 fiber and ST-type connectors were chosen for this program. Typical measured attenuation with a laser source for 30 meters of fiber and six inline connectors was 1.2 dB total.

Optical Power Budget

The summary of the optical power budget for the system is presented in Table 2. As shown, the optical margin for the system is 12.1 dB. Typically, a margin of six dB is required for systems of the type described here. The extra 6.1 dB of margin guarantees reliable performance in aircraft environments.

Two BER tests were performed on the optical portion of the system. One test was with a 300 MBPS pseudo-random data pattern. For the second test, the BER tester was programmed to simulate data patterns corresponding to those supplied by the TDM. The measured BER was 0 X 10E-11 for both tests. Also, the system was checked end to end (TTL in to TTL out) for each of the 12 channels. Again, no errors were detected during 12 hours of testing per channel. These excellent test results have proven the feasibility of the system.

Summary

An aircraft fiber optic system designed to replace 12 twisted, shielded pairs was described. System testing has proven the feasibility of the system. Flight qualified hardware is now being developed. Upon successful completion of flight tests, existing aircraft will be retrofitted with the fiber optic system. The system will also be used as a test bed for advanced fiber optic applications on existing and future Lockheed aircraft.

TABLE 1 TRANSMITTED SIGNALS

LEFT TO RIGHT

Signal	Data Rate	Description	Comments
A	320ns pulses at 40 HZ	sync. signal	synchronous to signal D
B	zero or 1.5 KHz	alarm signal	gated square wave
C	6.25Mbps	NRZ data burst	synchronous to signal D
D	6.25MHz	data burst clock	
E	1.152Mbps	NRZ data	unrestricted transition density

RIGHT TO LEFT

Signal	Data Rate	Description	Comments
T	50Kbps	NRZ data	unrestricted transition density
U	50KHz	data clock	synchronous to signal T
V	5Kbps	NRZ data	unrestricted transition density
W	5KHz	data clock	synchronous to signal V
X	zero or 75KHz	alarm signal	gated square wave
Y	zero or 10KHz	alarm signal	gated square wave
Z	1.152MHz	data clock for signal E	synchronous to signal E

TABLE 2 OPTICAL POWER BUDGET

		LOSS	COMMENTS
A)	Splices	0.2 DB	[illegible]
B)	Connectors	1.2 DB	[illegible]
C)	WDM	18.5 DB	
D)	Total Loss	19.9 DB	A + B + C
E)	Laser Coupled Power	[illegible] DB	Average [illegible]
F)	Power At Receiver	-22.9 DB	E - D
G)	Receiver Sensitivity	-35.0 DB	10E-9 BER, Average Power, 90 MBit
	Optical Margin	12.1 DB	G - F

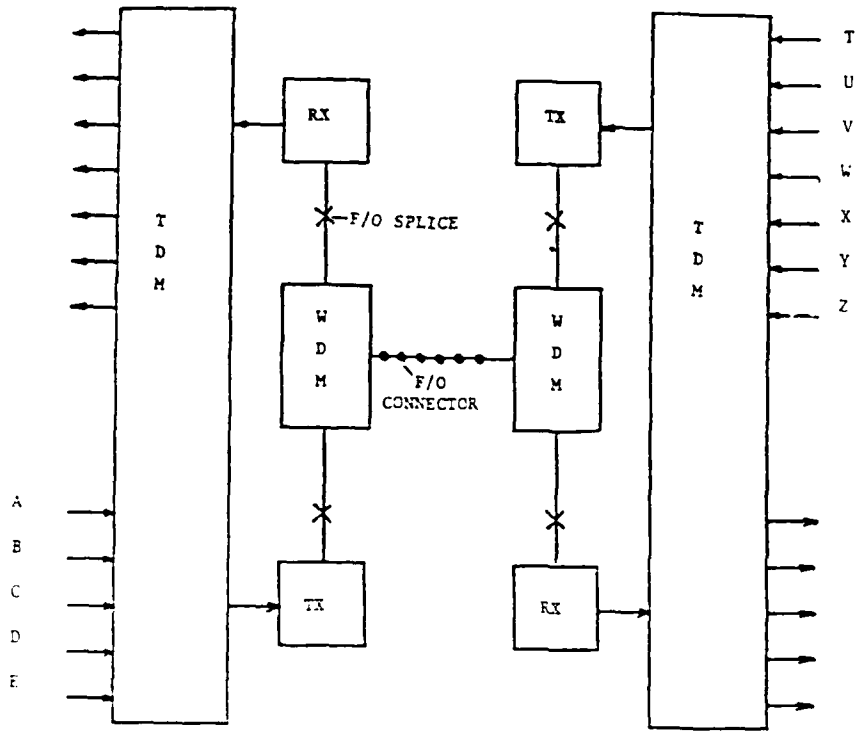
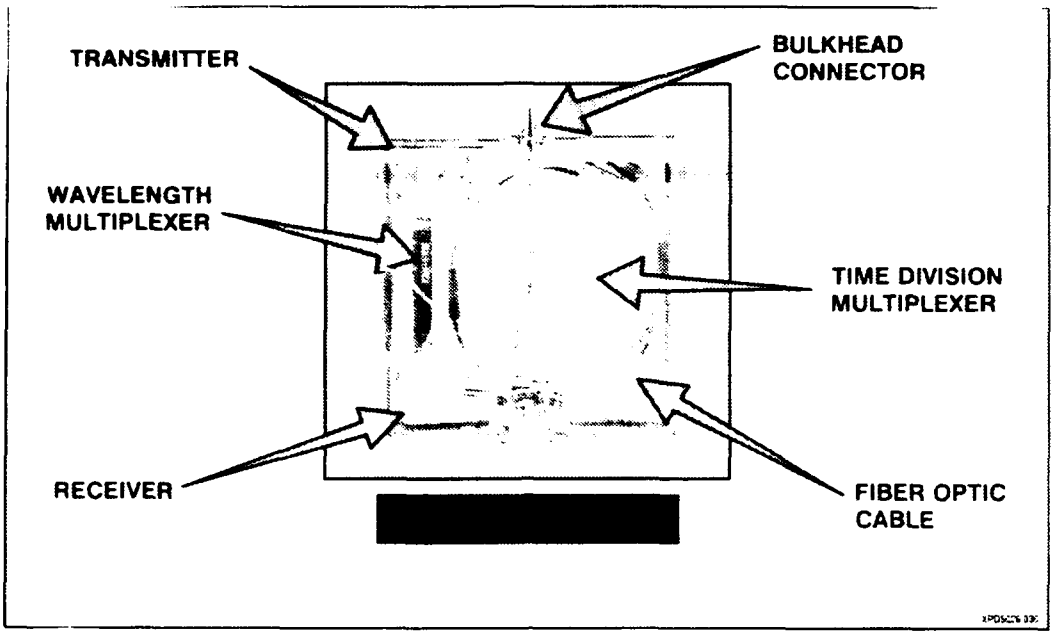


FIG. 1 FIBER OPTIC SYSTEM BLOCK DIAGRAM
(Refer to Table 1 for signal description)



Figure 2 - Laboratory Prototype
(Note size of TSP vs Fiber Cable)



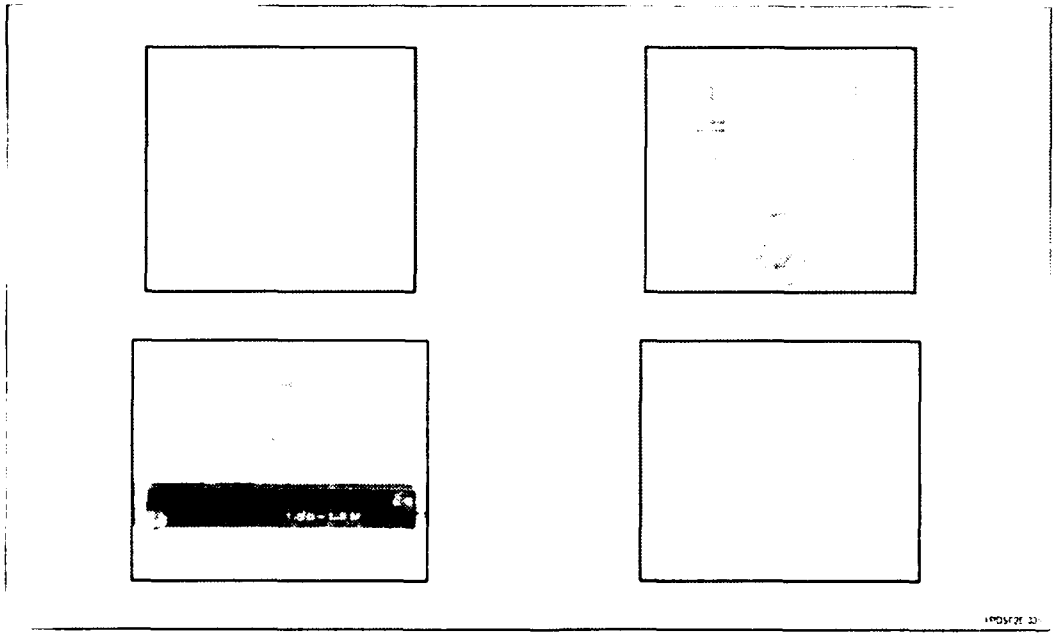


Figure 3 - Packaging Configuration For Flyable Units

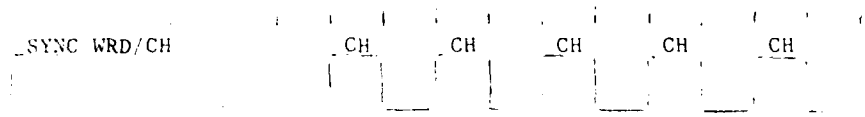


Figure 4 - Serial Word With All Data Channels At Logic Level 1

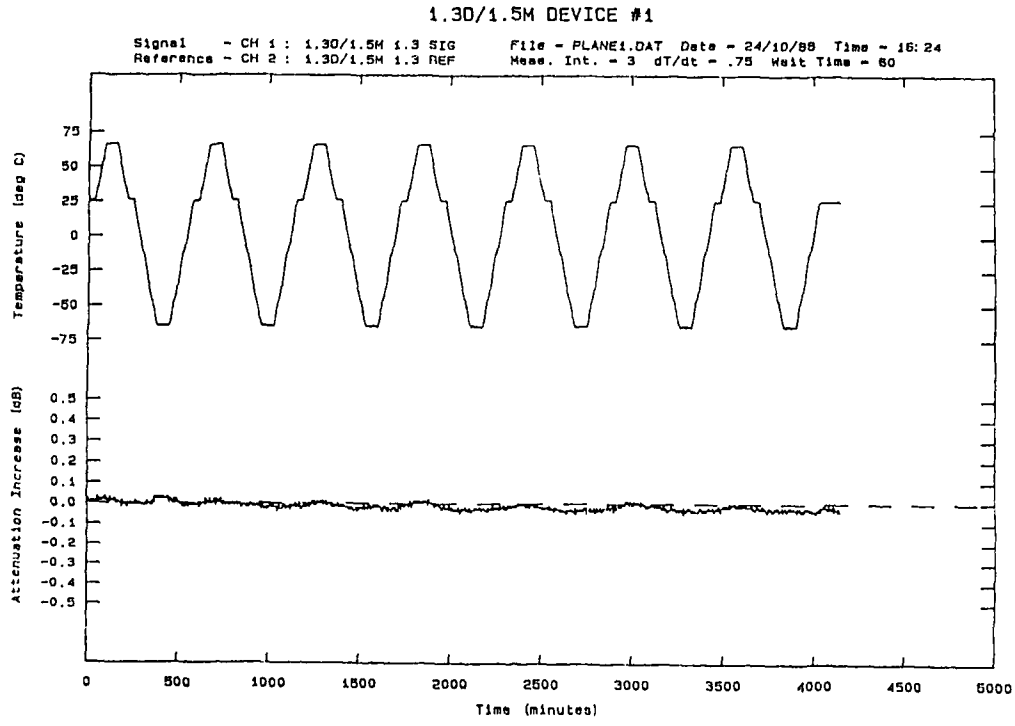


Figure 5 - WDM Temperature Test Results

Applications of all plastic optical fiber cord for consumer electronics equipment

T. Yano H. Saen K. Sugawara

Sumitomo Electric Industries, Ltd.
3-3 Satuki-cho, Kanuma-shi, Tochigi-ken 322 Japan

Abstract

All plastic optical fiber (APOF) was developed about twenty years ago in the U.S.A and now, many companies in several countries are manufacturing many sizes of APOF. APOF has several good characteristics and has been considered for internal or external wiring for consumer electronic equipment. However actual applications of APOF for consumer electrronics equipment are very few. Appliance wiring material or APOF for consumer electronics equipment has several special requirements. We have developed APOF cords which meet the requirements of consumer electronics equipment. We present three types of APOF cords which have been used in consumer electronics equipment. The first one is an APOF cord UL AWM 5234, recognized as appliance wiring material by UL. The second one is extendable curl form APOF cord. The third one is heat resistant APOF. The above two types of APOF cords are use the same APOF material is PMMA plastic. However this heat resistant APOF material is not PMMA. It is silicone.

1.APOF cord recognized as appliance wiring material category by UL. (UL AWM 5234)

1 1 Introduction

Appliance wiring material for electronics equipment is required to have the recognition of UL as a safety requirement. We have developed UL recognized APOF cord. The UL AWM style number of this cord is 5234. Following is the construction, material and basic properties.

1-2 Construction and Material

Construction and material are shown in Fig 1 and Table 1 respectively.

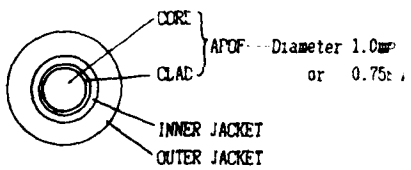


Fig 1 Construction of UL AWM 5234

Table 1 Material of UL AWM 5234

ITEM	MATERIAL
CORE	PMMA
CLAD	Fluoropolymer
INNER JACKET	PURE PLASTIC
OUTER JACKET	PVC

The APOF itself is very flammable. Oxgen index of PMMA is about 18. We extrude a two layer jacket over the APOF. The purpose of the outer jacket is to meet the flame retar dant requirements of UL subject 758 and to prevent mechan ical damage of the APOF. The purpose of inner jacket between the APOF and the outer jacket is prevention for inversion of annexes of outer jacket PVC into APOF. Inversion of annexes into APOF would decrease the transpar ency of APOF.

1 3 Properties

1-3 1 Flame retardant properties

Almost all safety requirements specify flame resist ance. The vertical flame test requirments described in Electrical Bulletin No. 1371 of CSA and the Japanese law controlling appliances and materials are almost the same as the VW-1 test of UL subject 758. VW 1 test results are given in Table 2.

Table 2 VW-1 test results

Number of specimen	Burning time application of flame					Indicator Burning	Surgical cotton Burning	Result
	1	2	3	4	5			
1	2	0	0	0	0	0 %	none	Passed
2	2	0	0	0	0	0 %	none	Passed
3	1	0	0	0	0	0 %	none	Passed
4	1	0	0	0	0	0 %	none	Passed
5	1	0	0	0	0	0 %	none	Passed

1-3-2 Optical loss (un aged)

Optical loss of UL AWM 5234 APOF cord is the same as bare (un-jacketed) APOF. Optical loss measurement results of UL AWM 5234 are given in Fig 2

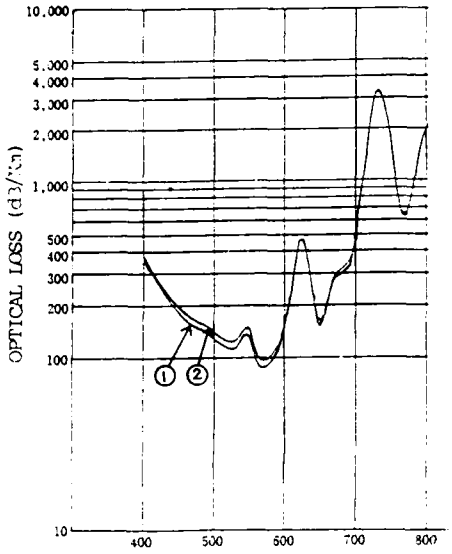


Fig 2

①Specimen

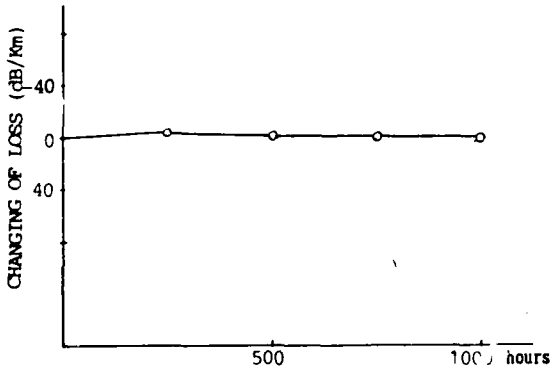
UL AWM 5234 with 1.0mm dia. APOF

②Specimen

UL AWM 5234 with 0.75mm dia. APOF.

1-3-3 Optical loss after aging at 80 degrees c

We tested the optical loss of UL AWM 5234 APOF cord after aging 1000 hours at 80 degrees c. The test results are given in Fig 3.

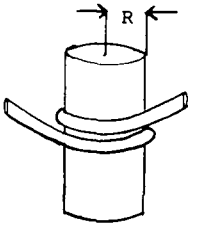


There is no change up to 1000 hours.

Fig 3 Changing of optical loss at 80 degrees c

1-3-4 Optical loss by bending

We show the test method and results of optical loss by bending UL AWM 5234 in Fig 4 and Fig 5.



Specimen is wrapped one turn one the mandrel and optical loss is measured.

Specimen:UL AWM 5234 with 1.0mm dia APOF.

R :Radius of mandrel (mm)

Fig 4 Test method of bending

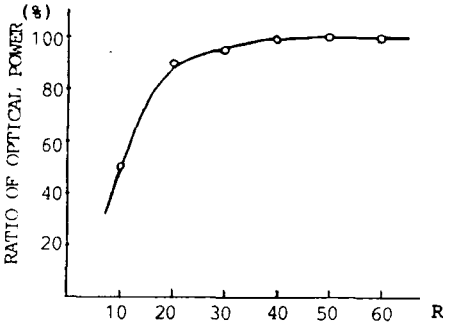


Fig 5 Test results of bending

1-4 Application of UL AWM 5234

UL AWM 5234 APOF cord has been used as the lead wire for indicator lights in compact video tape cameras in Japan.

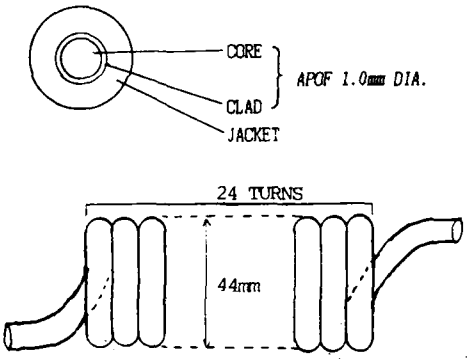
2.Extendable curl form APOF cord

2-1 Introduction

This APOF cord is covered with a sunlight-resistant polyethylene jacket and is formed into a curl form by heating. This curl form is just like a spring form. This curl form is compact and saves space although the actual length of the cord is long. When the cord is not being used, it is compact. When the cord is used, it can stretch. This APOF cord is useful as the external lead wire for equipment. The ratio of optical properties between un-formed straight APOF cord and curl formed cord is very small. Following are the construction and basic properties of extendable curl form APOF cord.

2 2 Construction and Material

Construction and materials are shown in Fig 6 and Table 3.



3.5 meter length cord is formed into curl form.

Fig 6

Table 3 Material

ITEM	Material	Diameter
CORE	PMMA	
CLAD	Fluoropolymer	1.0 mm
JACKET	Polyethylene	2.0 mm

2 3 Properties

2 3-1 Extension force

The test method and results of extension force of curl form are shown in Fig 7 and Table 4.

Test method.

The specimen should be set vertically and the length (L1) measured as shown in Fig 7. 25 grams weight is hung at the end of the cord and held 10 seconds. Then the length (L2) is measured as shown in Fig 7.

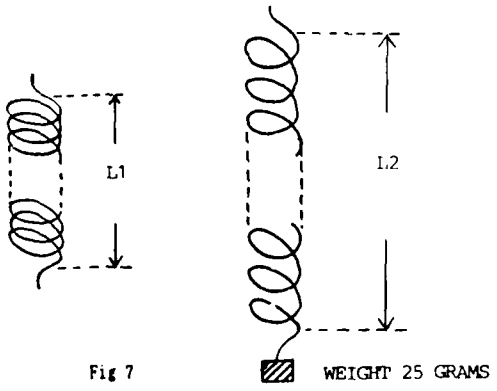


Fig 7

Table 4 Test results at room temp.

L1 (mm)	L2 (mm)
49.0 ~ 50.3	165 ~ 168

Minimum and maximum data among three specimens is shown Table 4.

2-3-2 Entension and retraction

Following are the test method and results of extension and retraction testing.

Test method.

Specimen is extended to 2.7 meter length and allowed to retract. This extension and allowed to retract. This extension and retraction should be repeated one hundred times at room temperature. Then the length of the curl form part and optical loss are measured.

Test results.

Minimum and maximum data among three specimens is shown in Table 5.

Table 5

ITEM	Before test	After 100 times
Length (mm)	49.0 ~ 50.5	55.0 ~ 55.8
Optical loss(dB)	18.2 ~ 18.7	18.0 ~ 19.0

2 3-3 Properties after twisting

Following are the test method and results after twisting.

Test method.

Fix one end of the specimen and twist the other end ten turns in the clockwise derection, retract, twist ten turns in the counterclockwise direction and retract. This is one cycle. The length of the curl form part and optical loss are measured after 50 cycles at room temperature.

Test results.

Minimum and maximum data of specimens is shown in Table 6.

Table 6

ITEM	Before test	After 50 cycles
Length (mm)	49.0 ~ 50.2	48.5 ~ 52.8
Optical loss(dB)	18.4 ~ 18.7	18.3 ~ 18.6

2-3-4 High temperature, low temperature and heat cycle test

Following are the test conditions and results of high temperature, low temperature and heat cycle tests.

Conditions:

High temperature test : 80°C, 1000 hours
Low temperature test :-30°C, 1000 hours
Heat cycle test : one cycle is,
-30°C 30 minutes, 25°C 5 minutes, 80°C 30 minutes, 25°C 5 minutes.

Test results.

We measured the optical loss of three specimens. Minumum and maximum deta is shown in Table 7.

Table 7 Test results

TEST ITEM	Before test (dB)	After test (dB)
High temp.	18.7 ~ 19.4	16.8 ~ 17.7
Low temp.	18.6 ~ 18.9	18.2 ~ 18.5
Heat cycle	18.7 ~ 18.9	17.6 ~ 17.8

2-4 Application of extendable curl form APOF cord

This extendable curl form APOF cord has been used as the external lead wire in the previous program booking system of home video tape recorders.

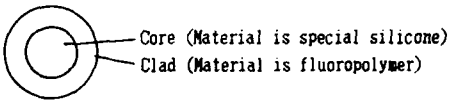
3.Heat-resistant all plastic optical fiber

3-1 Introduction

APOF of the UL AWM 5234 cord and extendable curl form cords is the same. The material of this APOF is PMMA core and fluoropolymer clad. This PMMA APOF is very clear and has good optical properties. However this APOF does not have heat-resistant properties. The maximum operating temperature is about 80 degrees c. We have developed heat-resistant all plastic optical fibers rated at 150 degrees c. The optical loss of heat-resistance APOF is larger than PMMA APOF. But it has been used in short lengths in electronics equipment.

3-2 Construction and material

Construction and material are shown in Fig 8.



Diameter of core is 1.0 mm
Fig 8 Diameter of clad is 1.8 mm

3 3 Properties

3-3-1 Optical loss

Optical loss of heat-resistant APOF is shown in Table 8. We measured 3.1 meter length specimens with wave length 660 nm light. Measurment is by the cut back method.

Table 8

Number of specimens	Loss (dB/m)
1	2.85
2	2.46
3	2.30
4	2.61
5	2.82

3-3-2 Properties for lateral pressure

Optical loss of a two meter specimen is measured by the method described in Fig 9.

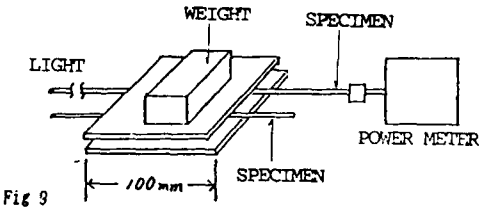


Fig 9

Optical loss is measured with weights 0 Kg to 140 Kg and 0 Kg at 660 nm wave length.

Test results are shown in Fig 10.

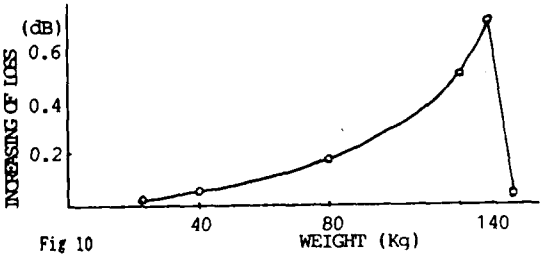


Fig 10

3-3-3 Optical loss after bending

Test method is the same as 1-3-4 Fig 4.

Test results after bending are given in Fig 11.

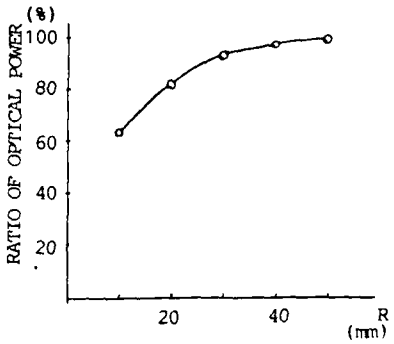


Fig 11 Optical loss after bending

3 3 4 Heat resistance

Optical loss of one meter specimens is measured after exposure at 150 degrees c for 100 hours, 200 hours, 300 hours, 400 hours and 500 hours. Test results are givin in Fig 12. Number of test specimens was three. Increase of loss is within about plus or minus 1.0 dB.

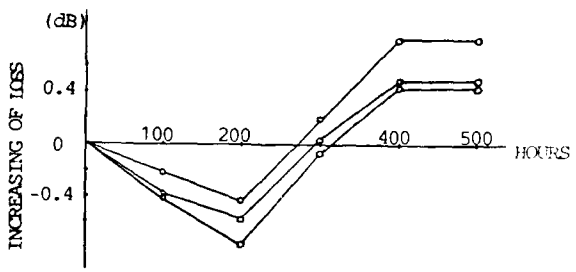


Fig 12 Optical loss at 150 degrees c

3 4 Application

This heat-resistance all plastic optical fiber has been used as the sensor lead wire of micro-wave ovens. Conditions of cooking food in micro-wave ovens is monitored with this optical fiber.

Conclusion

PMMA APOF itself does not meet the requirement of consumer equipment. We have developed PMMA APOF cords and silicon APOF which meet the requirement of consumer equipment. These cords will be used in consumer field widely.



Tomizo Yano is a senior engineer of Electronics Wire Division of Sumitomo Electric Industries Ltd.
He was received a B.S. degree in electrical engineering from Hokkaido University in 1975. And he joined Sumitomo Electric Industries Ltd. in the same year.
He has been engaged in design of wire used in electric equipment.



Haruo Saen

Haruo Saen is a manager of Flat components Section of Electronics Wire Division of Sumitomo Electric Industries Ltd.
He was received a B.S. degree in electrical engineering from Fukui University in 1972. And he joined Sumitomo Electric Industries Ltd. in the same year.
He has been engaged in design of wire and flat component used in electric equipment.



Kiyoto Sugawara

Kiyoto Sugawara is a senior engineer of Electronics Wire Division of Sumitomo Electric Industries Ltd.
He was received a B.S. degree in mechanical engineering from Tohoku University in 1975. And he joined Sumitomo Electric Industries Ltd. in the same year.
He has been engaged in manufacturing of wire used in electronic equipment.

FIELD PERFORMANCE OF FIBER OPTIC ELEVATOR TRAVELING CABLE

Richard Laney, Frank Davidson, and William McCallum

Siecor Corporation
489 Siecor Park
Hickory, NC 28603

ABSTRACT

The increasing sophistication of elevator systems requires precise transmission and increased information carrying capacity.

This report describes the development of a composite elevator traveling cable containing optical fiber subunits and the results of testing and field performance. Optical fiber units were introduced into the conventional manufacturing processes required to produce elevator traveling cables. The cable design itself is consistent with designs which have functioned in the elevator environment for the past twenty years.

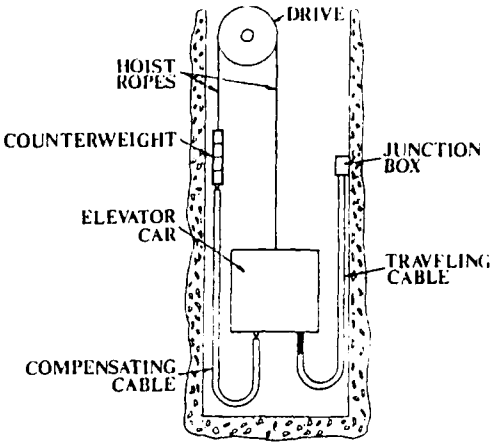
This cable is currently in service with the optical fibers providing video transmission from an elevator car to a security command post.

INTRODUCTION

Elevator traveling cables provide the power, control, and communication link to the elevator car. With increasing demand and sophistication of elevator systems, improved signal quality and greater information carrying capacity of traveling cables has become necessary. An optical fiber's immunity to electrical and electromagnetic interference allows for the transmission of high quality signals to and from the elevator car. In addition, an optical fiber's bandwidth is significantly greater than a coaxial cable which enables higher bit rates and longer repeater spacings. Optical fibers in elevator traveling cables could provide a higher quality transmission link with the elevator car. This project's objective was to manufacture and field test an elevator traveling cable containing optical fibers.

BASIC ELEVATOR DESCRIPTION

The basic elements of a typical elevator system are: drive, counter-weight, elevator car, compensating cable or counterweight rope, hoisting ropes, junction box, and traveling cable. (See Figure 1)



TYPICAL ELEVATOR
Figure 1

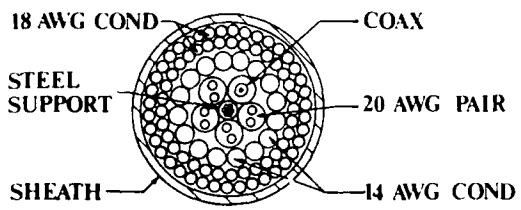
As a general rule, the elevator car is connected to a counterweight by hoist ropes threaded over one or more sheaves or pulleys located in the upper reaches of the elevator hoistway. The traveling cable provides a connection between the car and junction box. Signals are sent via the traveling cable between the elevator car and the controller. The compensating cable with one end connected to the counterweight and the other to the bottom of the car, provides dynamic balance.

The elevator traveling cable is suspended in a U shape between the bottom of the car and the junction box at the middle or upper part of the elevator hoistway. Multiple cables may be necessary to supply the required electrical circuits. The cables must be flexible and torsion free in order to travel within the limited space in the hoistway as the car ascends and descends in rapid vertical motion.

High rise buildings necessitated the development of high-speed, high-utilization elevator cars. This demanded more sophisticated traveling cables with respect to electrical and mechanical performance. Traveling cable performance considerations include minimal deflection during travel, constant loop diameter, and long term flex life.

The elevator hoistway is subject to significant environmental conditions such as temperature, wind, and undesirable physical contamination. Traveling cables are required to conform to UL, CSA, NEC and other regional and local building codes.

State of the art traveling cables contain 18 AWG conductors for control circuits, 14 AWG conductors for constant current circuits, shielded 20 AWG conductor pairs for telecommunications and electrostatically protected circuits, and coax for video and data requirements. Figure 2 shows a representative cross section.

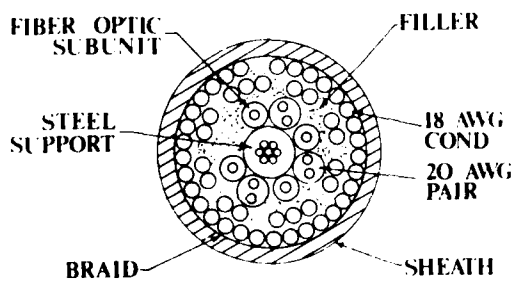


ELEVATOR
TRAVELING CABLE

Figure 2

CABLE SPECIFICATIONS

A prototype traveling cable was built to evaluate construction and field performance. The components chosen for the prototype cable were 18 gauge conductors, 20 gauge shielded pairs, and fiber optic subunits. (See Figure 3)



ELEVATOR TRAVELING CABLE
CONTAINING OPTICAL FIBER

Figure 3

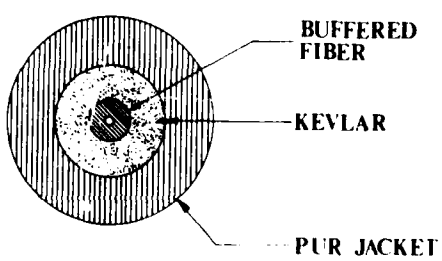
These components were successfully incorporated into a traveling cable that is consistent with the design integrity that has been in use for over 20 years. The cable weight and outer diameter had to be sufficient to provide protection to the optical fibers yet allow for optimum traveling performance and operating characteristics.

The optical subunits were manufactured using 100/140 μm fiber. This fiber type is typical for short distance applications where attenuation and bandwidth requirements are not critical. (See Table I)

TABLE I

FIBER SPECIFICATIONS	
Fiber Type	Multimode Graded Index
Core Diameter	100 μm
Clad Diameter	140 μm
Coated Outside Diameter	900 μm
Numerical Aperture	0.29 ± .015

Ten strands of Kevlar 49 and a polyurethane jacket were used to increase the optical subunit's strength. This produced a component compatible with the copper components in the prototype cable as well as created a rugged subunit that could withstand the rigors of cable assembly and field operation. (See Figure 4 & Table II)



FIBER OPTIC
SUBUNIT

Figure 4

TABLE II

SUBUNIT SPECIFICATIONS	
Number of Fibers	1
Attenuation (850 nm)	6.0 dB/km
Bandwidth (850 nm)	100 MHz·km
10 Strands of Kevlar 49-1420 Denier	
Flame Retardent PUR Jacket	.8 mm
Subunit OD	3.6 mm
Subunit Weight	12 kg/km
Crush Resistance (between parallel plates, minimum value for negligible attenuation increase after force removed)	550 N/cm
Storage Temperature Range	-40 to +70°C
Operating Temperature Range	-20 to +70°C
Max. Tensile Load for Installation	300 N
Max. Tensile Load Long Term	50 N
Min. Bend Radius for Installation	8 cm
Min. Bend Radius Long Term	4 cm

The cable was composed of a steel central member for vertical support, copper conductors, shielded twisted pairs, the fiber optic subunits, electrical grade jute fillers, rayon braid over the core, and an overall sheath of flame retardant polyvinyl chloride. The cable was designed to comply with UL and CSA regulatory specifications for flexible cords and cables with an exception made for the optical fibers. The cable's natural loop diameter and flexibility was to be similar to that of comparable designs not containing optical fibers. (See Table III)

TABLE III

CABLE SPECIFICATIONS	
Construction:	49 conductors 18 gauge + 3 shielded pairs 20 gauge + 4 optical fibers + steel core
Outer Diameter:	34.3 mm
Weight:	1266 kg/km
Voltage Rating:	300 volts
Operating Temperature Range:	20 to +60°C
Natural Cable Loop Diameter:	1.0 meter
Traveling Speed:	Up to 450 meter/min.

IN-HOUSE TESTING

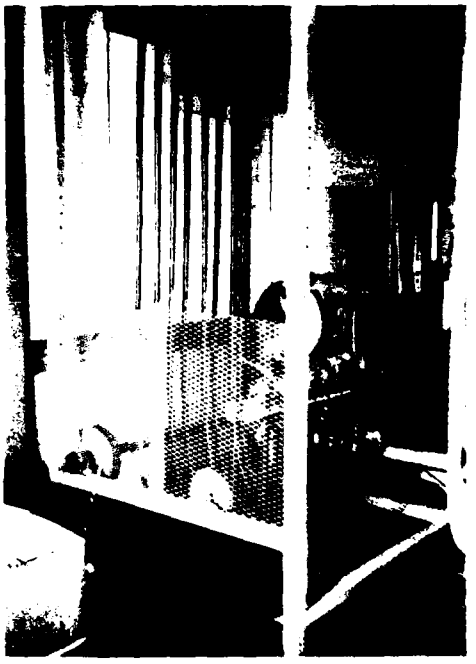
The tensions and centrifugal forces encountered in conventional cabling equipment for elevator cable were a concern during cable assembly. The cable was assembled on conventional planetary cabling equipment with no special precautions taken for the fiber subunits. The optical fiber subunits were tested with an OTDR prior to and after the cabling process to ensure performance was not compromised. The fibers showed a slight average increase in attenuation of .14 dB/km possibly due to microbending from stresses encountered during cable manufacturing. (See Table IV)

TABLE IV

FIBER SUBUNIT	ATTENUATION (dB/km) @ 850 nm	
	BEFORE CABLING PROCESS	AFTER CABLING PROCESS
1	3.14	3.29
2	3.20	3.34
3	3.19	3.29
4	3.31	3.51

NOTE: OTDR used for Attenuation Measurements

After the cable was assembled and jacketed, physical tests were performed to determine if the cable could withstand cyclic flexing. A flexing apparatus simulating the vertical motion of an elevator traveling cable was used for in-house testing. The test apparatus was specifically designed to duplicate the actual motion an elevator traveling cable would see during normal operation. The equipment develops cable speeds of 70 meters/min. and passes a sufficient length of cable through a 92 cm loop to simulate an elevator car in an upper and lower position in the hoistway. (See Figures 5A and B)



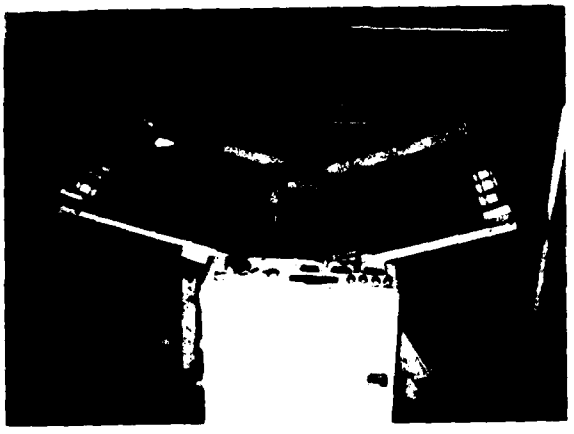
VERTICAL CABLE FLEXER
Figure 5A



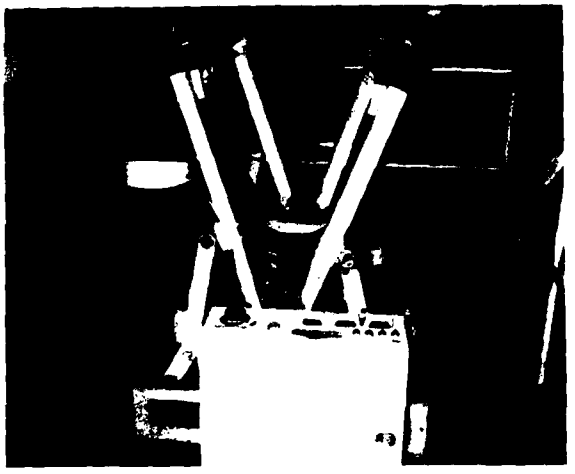
VERTICAL CABLE FLEXER
Figure 5B

Three 6 meter lengths of cable were attached to the flexer for evaluation. The copper conductors were connected in series and a voltage was applied to monitor conductor performance. The optical fiber was checked for continuity every 75,000 cycles. Because of the short test length, other performance characteristics of the fiber were not evaluated. All conductors and fibers remained continuous over a 1.6 million cycle test period.

A horizontal test simulating U-bending and straightening of elevator traveling cable was performed to determine if failure would occur. (See Figures 6A and B)



HORIZONTAL CABLE FLEXER
Figure 6A



HORIZONTAL CABLE FLEXER
Figure 6B

This test is similar to the test required by Underwriters Laboratories for endurance flexing of elevator traveling cable. Two 2-meter lengths of cable were continuously flexed for over 3 million cycles. The fibers were checked for continuity every 200,000 cycles. Because of the short length of the cable, optical tests were not performed. All fibers remained continuous throughout the test period.

FIELD INSTALLATION

The building selected for field testing has a rise of 40 floors, cable traveling length of 80 meters, and car speed of 150 meters/minute. This car completes 60,000 to 100,000 cycles of travel annually. The traveling cable was installed in April 1985 by elevator mechanics using standard installation procedures. In August 1985, the fibers in the traveling cable were fusion spliced to fibers in an interconnecting cable at the junction box. The interconnecting fiber optic cable completed the connection between the junction box and the security center. Splice loss was measured with an OTDR at 850 nm and averaged 0.5 dB. OTDR traces on all fibers were linear with no signs of localized attenuation.

The fibers were checked in August, 1986 using an OTDR with similar results. All fiber traces were linear with no localized attenuation nor apparent change.

In October 1986 one of the fibers was put into service transmitting video signals from the elevator car to a video recorder/monitor at the security center. The transmitter/receiver require a system bandwidth of 15 MHz and allow for a loss budget of 15 dB. Actual loss for this particular system is approximately 6 dB. Signal reception from the fiber was clearly superior to that on the coaxial cable. No changes in OTDR traces were detected while the car was in use.

The three spare fibers were checked with an OTDR on August 18, 1987. There were no signs of degradation in the fibers and no increase in loss at the splice points. Video reception from the working fiber remained at its high level of quality.

CONCLUSION

Optical fibers have been successfully incorporated in a conventional elevator traveling cable utilizing standard manufacturing techniques. More than 3 million horizontal and 1.6 million vertical cycles of in-house testing have been conducted with no failures. The traveling cable with optical fibers has been performing in the field since April 1985 with the fibers transmitting video signals since October 1986. Periodic testing with an OTDR indicated linear traces with no localized attenuation. The electronics company responsible for the system reports excellent results with the fiber without typical coaxial associated concerns such as ground loops or spikes and interference from AC motors and radio frequencies.

Considering the success to date with video transmission, the future requirements of more sophisticated and advanced elevator systems could be met through the incorporation of fiber optics in elevator traveling cables.

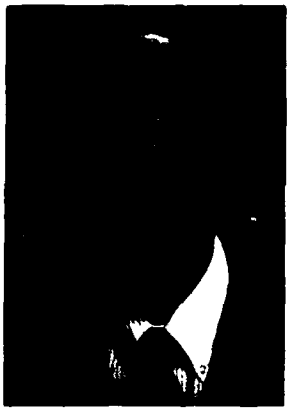
ACKNOWLEDGEMENTS

Many colleagues assisted with design, assembly, and experimentation of this cable and their help is gratefully acknowledged. Special thanks is given to Henry Brothers, Otis Elevator, and Republic Wire and Cable for their contributions to this paper.



Frank Davidson
Siecor Corporation
489 Siecor Park
Hickory, NC 28603

Frank Davidson graduated in Electronics Engineering from the Nova Scotia Institute of Technology, Canada in 1974. He was employed by the Bell Telephone System as an Outside Plant Engineer prior to joining Siecor in 1981. He has held various engineering positions in the copper cable field and is currently an Applications Engineer in the optical cable division.



Richard Laney
Siecor Corporation
P.O. Box 1237
Rocky Mount, NC
27801

Richard Laney is the Rocky Mount Plant Engineering/Production Manager with Republic Wire and Cable, Siecor Corporation, Hickory, N.C. He has held various engineering positions with Siecor during the past 17 years and has been actively involved with the manufacture of elevator cable products for the last ten years. Mr. Laney graduated from The Citadel in 1968 with a B.S. degree in Electrical Engineering.



William McCallum
Siecor Corporation
P.O. Box 1237
Rocky Mount, NC
27801

William McCallum is the Rocky Mount Plant Product Engineer and Engineering Supervisor with Republic Wire and Cable, Siecor Corporation, Hickory, N.C. He has been involved in the development of elevator cables and is currently responsible for the design and engineering of elevator traveling cable and related products. Mr. McCallum graduated from the University of North Carolina at Charlotte in 1982 with a B.S. degree in Engineering Analysis and Design.

DEVELOPMENT OF COMPOSITE FIBER-OPTIC TRAVELING CABLE FOR ELEVATOR

Akio Hasemi*, Takehiro Akagawa*, Hideya Hasegawa*, Shoji Hiraiwa**

*Riken Electric Wire Co.,Ltd.
1-12-22, Tsukiji, Chuo-ku,
Tokyo, 104 Japan

**The Furukawa Electric Co.,Ltd.
2-6-1, Marunouchi, Chiyoda-ku,
Tokyo, 100 Japan

ABSTRACT

We have successfully developed a composite fiber-optic traveling cable for elevators to which a new cable design was applied taking the special requirements into consideration. Various tests were performed to check its electrical, mechanical and environmental characteristics, and the satisfactory results were obtained in these tests.

The number of elevator cables can be decreased by utilizing this new elevator cable because of its large trasmission capacity and electromagnetic interference immunity. Furthermore, the use of this cable makes it possible to provide new services such as transmission of video signals and integrated elevator control systems.

INTRODUCTION

Elevator cables are installed between elevator control room on the top of a building and elevator-cage. Generally 4 to 8 cables are used in one elevator system and their lengths are about 100m as shown in Figure 1.

With the increase of high-rise buildings and improvement of elevator, precise elevator control and providing of new services such as transmission of video signals and integrated elevator control systems are demanded. Conventional cables for elevator are unable to satisfy these needs, because they have problems such as susceptibility to electromagnetic interference from power lines and increasing total cable weight.

The point of our development is how to achieve the mechanical properties comparable to conventional metallic cables. The number of cables can be reduced by half by exploiting large transmission capacity characteristics of an optical fiber, so the total cable weight can be decreased.

We have developed a new elevator cable based on the accumulated knowhow of elevator cable design and manufacturing. In order to evaluate the mechanical characteristics, tests of tensile, bending, compression, impact, heat-cycle and so on were made. During these tests, transmission loss increase of optical fibers were scarcely observed under practical use conditions.

As shown in Figure 1, the elevator cable must follow the movement of elevator-cage in the shape of U-bending.

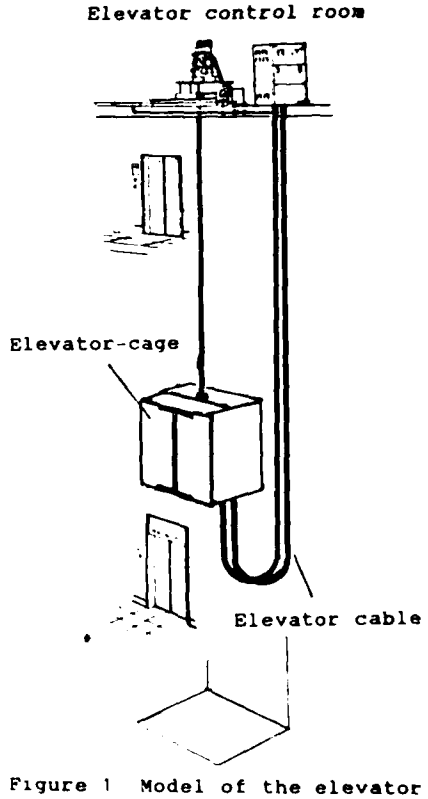


Figure 1 Model of the elevator cable system

We have obtained good results in the 5,000,000 time continuous U bending test, which is most important among the mechanical properties for practical use. Transmission loss fluctuation during U bending test was less than 0.1 dB.

CABLE DESIGN

Design Requirements

Basic design requirements on the new elevator cable are as follows.

(a) The cable should be easily handled and installed in the same manner as conventional elevator cables.
(b) Under practical use conditions, it should have good transmission characteristics.
(c) Maximum suspending length of the cable is 200m.
(d) In case of the cable suspending, the cable should not be twisted.

Cable Structure

The structure of the new cable is shown in Figure 2 and Table 1. 50 PVC-insulated wires and 2 optical fiber cords are stranded around a central tension member. The cable diameter is about 33 mm and the weight is about 1.17 kg/m, but it is very flexible. Loop diameter set in the static flexibility test is about 700 mm, as shown in Figure 3.

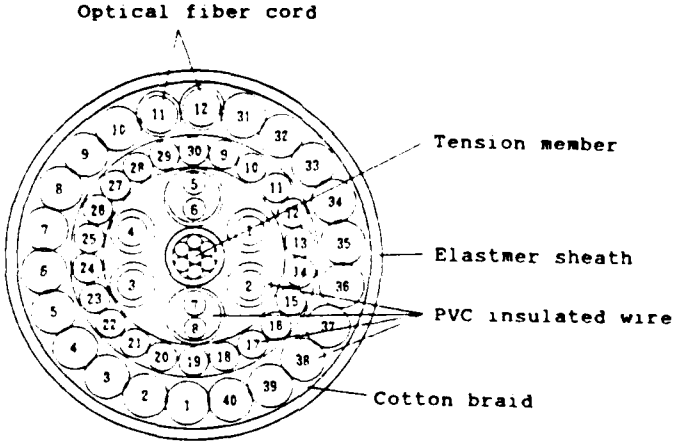
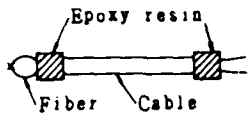
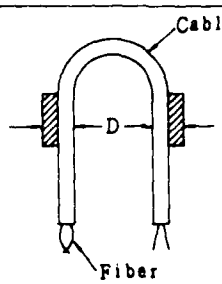
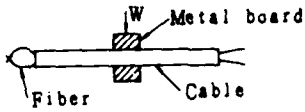
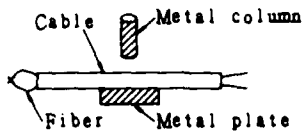
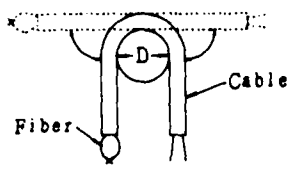
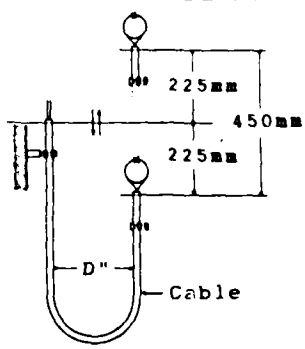


Figure 2 Structure of composite fiber-optic traveling cable for elevator

Table 1 Construction of the cable

Fiber	Type	Silica type multi mode fiber
	Core	50μm in dia.
	Cladding	125μm in dia.
	Buffer	Silicone resin 400μm in dia.
	Jacket	Nylon 0.9mm in dia.
Cable	No.of fiber	2
	No.of PVC insulated wire	50
	Tension member	Steel wire rope 4.0mm in dia.
	Sheath	Elastmer sheath 31mm in dia.
	Weight	1.17 kg/m

Table 2 Test methods and target values of various cable characteristics

Item	Testing method	Target value
Tensile test	Measuring length ; 2m Tensile speed ; 100m/min Cable temp. ; 30,25,60° 	Breaking load > 1,000kgf
Bending test	Bending dia. ; 700mm - minimum Cable temp. ; 30,25,60° 	No loss increase up to 300mm
Compression test	Metal board length ; 50mm Compression load ; 0 - 1000kg 	No breaking
Impact test	Column dia. ; 25mm Column weight ; 1.5,3.0kg Impact time ; 10 times/1.5kg, 5 times/3.0kg Impact height ; 1m 	No breaking
Flexure test	Mandrel dia. ; 60mm Bending time ; 50 times 	No breaking
U-bending test	Bending dia ; D" 230mm Bending time ; 5,000,000 times (30 cycle/min) 	No breaking

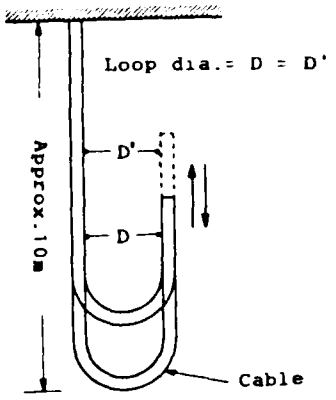


Figure 3 Situation of static flexibility test

CHARACTERISTICS OF CABLE

The mechanical and thermal tests were performed to simulate external forces that the cable is expected to encounter during installation. Table 2 shows the testing methods for various mechanical and thermal characteristics and their target values.

Two fibers in the fabricated cable were spliced to form a loop and the loss variation during a test was measured using a LED light source of 0.85 μm wavelength.

(1) Tensile test

The test results are shown in Table 3. Load at breakage was more than 2000kgf and elongation at breakage was about 2.9%. Fluctuation in transmission loss was hardly observed up to just before the breakage.

Table 3 Tensile characteristics of the cable

Temp. (°)	No	Load (kgf)	Elongation (%)	Δα (dB)
-30	1	2,840	2.9	0
	2	2,850	3.1	0
	3	2,850	2.8	0
+25	1	2,470	2.9	0
	2	2,270	2.8	0
	3	2,310	2.9	0
+60	1	2,210	2.9	0
	2	2,160	2.9	0
	3	2,200	2.7	0

(2) Bending test

The test results are shown in Figure 4. Transmission loss increase was observed when the cable is bent by hand. The minimum bending diameters were 100mm at -30°, 60mm at room temperature and 20mm at 60°.

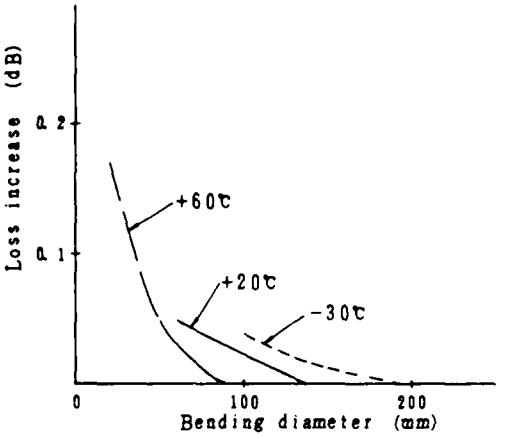


Figure 4 Bending characteristics of the cable

(3) Compression test

The test results are shown in Figure 5. Tansmission loss fluctuation was observed when the pressure was applied via a board of 50mm length. The loss fluctuation was less than 0.2dB under 1000kgf load and residual transmission loss change was not observed after the load was removed.

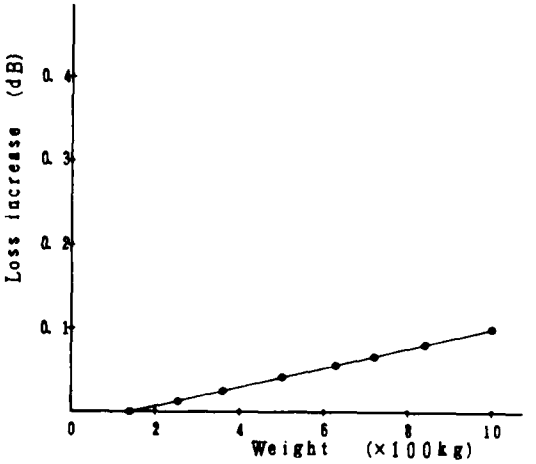


Figure 5 Compression characteristics of the cable

(4) Impact test

The test was carried out using a metal column of 25mm diameter and the results are shown in Table 4. Loss variation was less than 0.1dB even when metallic core was broken.

Table 4 Impact characteristics of the cable

Weight of column	No.of times at metallic core broken	Δα (dB)
1.5 kgf	39	0.06
	26	0.04
	30	0.02
	25	0.03
	38	0.02
3.0 kgf	7	0.04
	7	0.04
	5	0.01
	8	0.03
	9	0.01

(5) Flexure test

There was no breakage of fiber observed after the cable was bent repeatedly 50 times, and significant loss fluctuation was scarcely observed.

(6) U bending test

The test results are shown in Figure 6. The loss fluctuation was less than 0.1dB during 5,000,000 time continuous U bending.

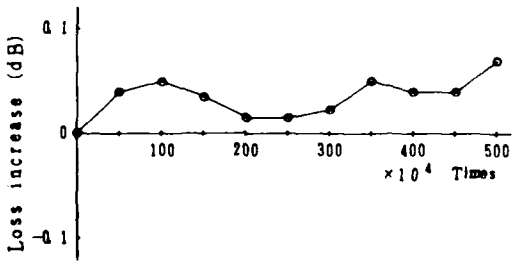


Figure 6 U-bending characteristics of the cable

(7) Temperature cycling test

The test results are shown in Figure 7. The loss fluctuation was less than 0.05dB in the temperature range of -30℃ ~ +60℃. In the practical temperature range, this cable was confirmed to be quite stable.

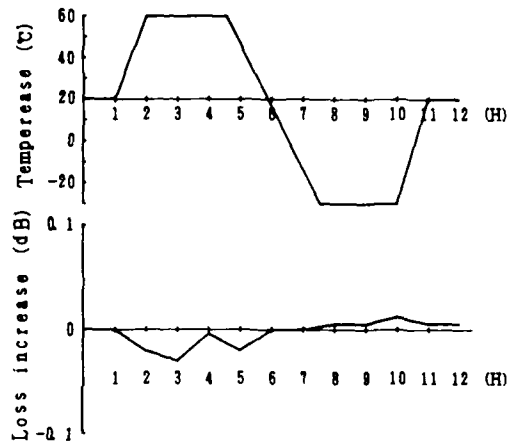


Figure 7 Temperature characteristics of the cable

CONCLUSION

A composite fiber-optic traveling cable for elevator has been developed. This new cable design has been applied to actual elevator cables on the field. So far 40 elevators have been running with new elevator cables without any trouble. It is found that optical fibers can be applied to very flexible cables as well as rigid type cables.



Akio Hasemi

Riken Electric
Wire Co., Ltd.
1-12-22, Tsukiji,
Chuo-ku,
Tokyo 104, Japan

Mr.Hasemi was born in 1955. He joined Riken Electric Wire Co., Ltd. after graduation from Chiba University in 1979, and has been engaged in research and development of flexible cables. He is now a sales engineer of cable section.



Takehiro Akagawa

Riken Electric
Wire Co., Ltd.
3-7-12, Shiohama,
Ichikawa-city,
Chiba, Japan

Mr.Akagawa was born in 1943. He joined Riken Electric Wire Co., Ltd. after graduation from Ichikawa Daiichi junior high school in 1959, and has been engaged in manufacturing of flexible cables. He is now a staff of Engineering Section.



Hideya Hasegawa

Riken Electric
Wire Co., Ltd.
3-7-12, Shiohama,
Ichikawa-city,
Chiba, Japan

Mr.Hasegawa was born in 1959. He joined Riken Electric Wire Co., Ltd. after graduation from Chiba Institute of Technology in 1982. and has been engaged in research and development of flexible cables. He is now an engineer of Research & Development Section.



Shoji Hiraiwa

The Furukawa
Electric Co.,Ltd.
4-13-14,Higashi-
Shinagawa,
Shinagawa-ku,
Tokyo 140, Japan

Mr.Hiraiwa graduated from Tokyo Physical College 1950 and joined The Furukawa Electric Co., Ltd. and has been engaged in Planning & Equipment for wire and cable. He is now Depty General Manager of The Engineering Department Power Cable Division at The Furukawa Electric Co., Ltd.

A Comparative Stability Study Related to the Performance of PE/PJ and ETPR Filling Compounds

A. W. Stratton T. J. Roessing J. D. Burkhard

Witco Corporation
Petrolia, PA

Abstract

A six year study was conducted to compare the performance of cellular insulations when exposed to a high oil content Extended Thermoplastic Rubber (ETPR) filling compound and when exposed to a PE/PJ filling compound. A performance property, namely capacitance, was used to monitor the test cells. As expected, at ambient the PE/PJ compound did not cause any significant increase in capacitance. However, at ambient the ETPR compound caused a significant increase in capacitance.

Introduction

Various mechanisms have been proposed to explain the cell filling phenomena that occurs when cellular insulation is exposed to filling compounds under certain conditions.[1-3] A detailed description of the cell filling process is beyond the scope of this paper. In this study, we accepted that cell filling can occur via some mechanism and would result in the replacement of air in the cellular insulation with the mobile fraction of the filling compound. This increased dielectric would cause an increase in the capacitance of the test system.

The effect of petrolatum based filling compounds (e.g. PE/PJ) upon cellular insulations has been studied by several investigators.[4-5] Most are in agreement that while petrolatum based compounds will have a tendency to fill cells at elevated temperatures, under ambient conditions no significant cell filling will occur. Last year, Englehart and Bayes[5] reported that after ten years of service, cable filled with a petrolatum based compound showed no significant increase in capacitance.

In 1980, Mitchell and Sabia introduced a new type of filling compound to the industry.[6] This compound was an oil based material containing a styrene block copolymer and polyethylene. Today, this type of filling compound is being referred to as an Extended Thermoplastic Rubber or ETPR compound. Mitchell and Sabia studied the impact of various oils, unmodified petrolatum, and the high oil content ETPR compound on various insulations at 70°C(158°F).

The objective of our study was to compare the cell filling tendencies of a PE/PJ compound with that of an ETPR compound at elevated temperatures and at ambient conditions.

Test Cell Description

In this study, it was decided to utilize a *functional property, namely capacitance, to monitor* the affect of the filling compounds upon the insulation. To accomplish this in our laboratory, our study used a test cell that was designed by J. J. Kaufman.[7] A diagram of the test cell is presented in Figure 1.

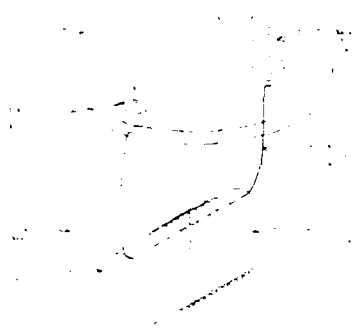


FIG. 1

The test cells were constructed by first soldering the No. 14 copper wire inside the copper pipe. Then, ten feet of the conductor

to be tested was coiled around the pipe with three inches of conductor extending tangentially at each end. The conductor was taped to the pipe at each end to hold it in place. One end of the conductor to be tested and one end of the No. 14 copper wire were soldered to the bottom contacts of a banana jack which was mounted in a plexiglas disc. The other end of the conductor to be tested was not connected and was long enough to extend above the surface of the cable filler being evaluated. The second end of the No. 14 copper wire was connected to a brass bolt mounted in and extending above the plexiglas disc. Test cells were constructed in duplicate for five sets of conductors, with two different filling compounds, and two test temperatures. In addition, test cells were constructed that were not exposed to filling compound and were used as controls.

The cable filler to be tested was heated to 127°C (260°F) and then 300 grams of material were poured into a 600 ml beaker. The beaker was conditioned in an oven at 104°C (220°F) overnight. The assembled test cells were placed in the cable filler and the assembly was allowed to come to the test temperature (70°C or ambient). This procedure was carried out for each conductor and both filling compounds.

After five hours at the test temperature, the capacitance of each cell was measured using a Doric C-Meter Model 130A. The brass bolt of the test cell was connected to a ground wire. The connection between the test cell and the C-Meter was a patch cord with double banana plugs at each end. The capacitance of the patch cord connector was subtracted from the total capacitance to give the capacitance of the test coil.

Conductors Tested

Test conductors were provided by two cable manufacturers. These materials consisted of a foamed polypropylene, a skin-foam medium density polyethylene, and a skin-foam high density polyethylene. The test conductors are described in Table 1.

Table 1

Description of Conductors Tested

Set No.	Gauge	Description	Expansion %
1	22	Foamed Polypropylene	32
2	19	Foamed MDPE-White	28
3	19	Foamed MDPE-Yellow	44
4	24	Skin-Foam HDPE-Black	45
5	24	Skin-Foam HDPE-Coral	38

Filling Compounds Tested

Two types of filling compounds were used in this study. One was a PE/PJ compound and the other was an ETPR compound. The properties of the two compounds are presented in Table 2.

Table 2

Properties of Filling Compounds Studied

	ETPR	PE/PJ
D127 Drop M.P., °C	95.5	96.3
D3236 Apparent Vis. @ 130°C, cps	28.7	12.9
D445 Vis. @ 130°C, SUS	162	81
D937 Consistency, dmm	119	56
D150 Diss. Factor @ 1 MHz	0.0003	0.0005
D150 Dielectric Constant @ 1 MHz	2.13	2.17
D257 Volume Resistivity, ohm-cm	9×10^{14}	2.2×10^{16}
Slump @ 65°C	Pass	Pass

Data and Discussion

The capacitance of each test cell was measured on a weekly basis for the first three years of the study. At that point in time, evaluation of the test cells at 70°C was concluded. Testing continued on the ambient test cells for a total time period of six years, however, during the last three years of the study measurements were made on a monthly instead of weekly basis. The capacitance of the control cells changed less than 1% during the study (312 weeks). Figures 2-7 present the per cent gain in capacitance versus time for the various test cells.

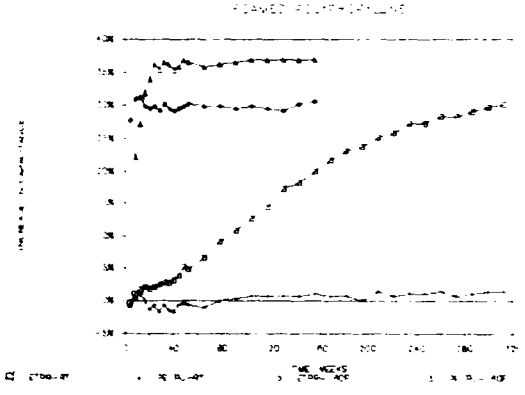


FIG. 2

Figure 2 shows that for the foamed polypropylene the PE/PJ compound and the ETPR compound have similar cell filling tendencies at 70°C. However, under ambient conditions there

is a significant difference. The increase in capacitance with the ETPR compound at ambient approaches that of the ETPR compound at 70°C, approximately 30%. This value compares with an increase of approximately 1% for the PE/PJ material at ambient.

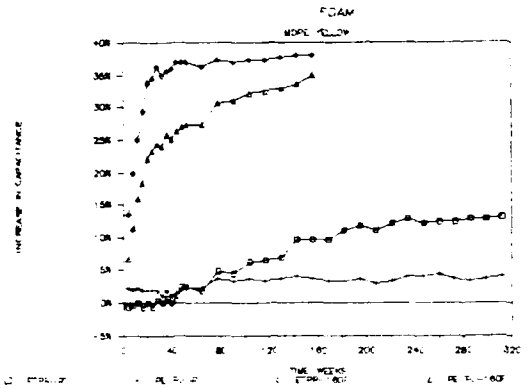


FIG. 3

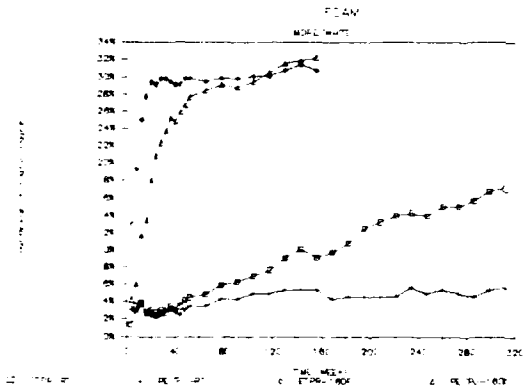


FIG. 4

Figures 3 and 4 present similar data for the samples of white and yellow foamed medium density polyethylene. Again, the PE/PJ and the ETPR compounds showed similar cell filling tendencies at 70°C. Under ambient conditions the ETPR compound caused an approximate 15% increase (average of white and yellow) in capacitance. This compares to an approximate 4% increase (average of white and yellow), for the PE/PJ compound. It should be noted that the foamed MDPE showed the highest per cent increase in capacitance for the PE/PJ compounds at ambient. Figure 5 presents the capacitance increases at ambient for the white and yellow foamed MDPE in ETPR and PE/PJ compounds. There is an approximate 10% difference in capacitance increase between the PE/PJ compound and the ETPR compound.

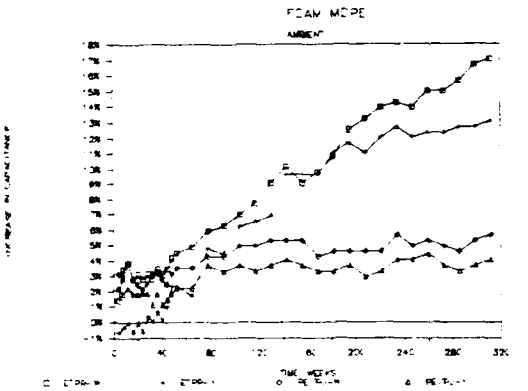


FIG. 5

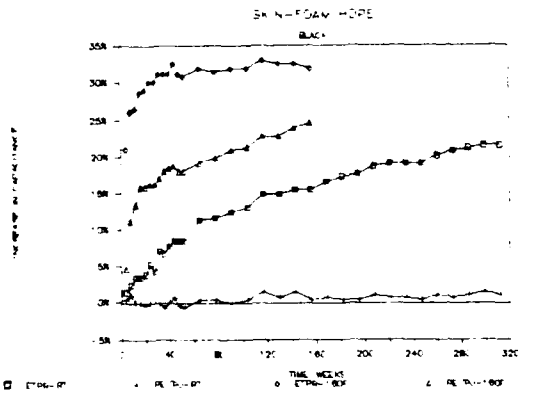


FIG. 6

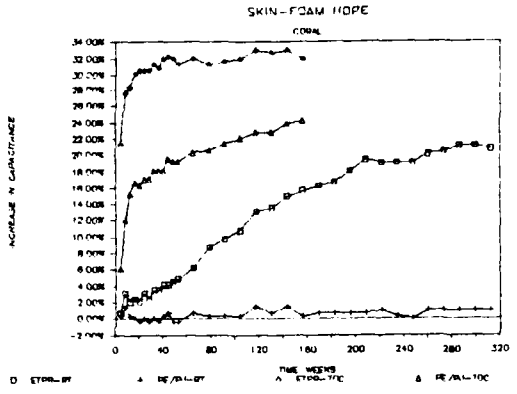


FIG. 7

Figures 6 and 7 present the capacitance increase versus time curves for the samples of skin-foam HDPE conductors. As in the previous cases, the ETPR and PE/PJ compounds both caused significant capacitance increases at 70°C. The cell filling tendencies of the two compounds at ambient are significantly different. At ambient the conductors exposed to the ETPR compound showed an approximate 20% capacitance increase as compared to the 1% increase for the PE/PJ material.

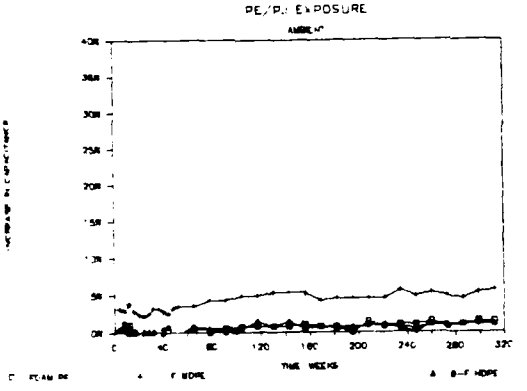


FIG. 8

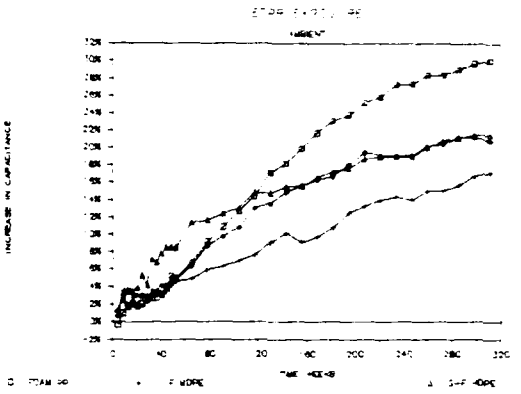


FIG. 9

Figures 8 and 9 present a comparison of the different conductors when exposed to PE/PJ (Figure 8) or ETPR (Figure 9) filling compounds at ambient. Figure 8 shows that of the three types of conductors exposed to PE/PJ at ambient, the skin-foam MDPE showed the highest capacitance increase (~ 5%). Figure 9 shows that of the three types of conductors exposed to ETPR at ambient, the skin-foam MDPE showed the lowest capacitance increase (~ 15%) which was significantly higher than that obtained with the PE/PJ compound.

Conclusions

Test conductors exposed to an ETPR filling compound at ambient showed a significant increase in capacitance over a six year period. Test conductors exposed to PE/PJ filling compound at ambient showed very little gain in capacitance. This indicates that the high oil content ETPR filling compounds cause significantly higher cell filling of cellular insulation than do PE/PJ compounds.

Acknowledgments

We would like to acknowledge the contributions of the following groups and individuals.

1) Essex Group Inc. for determining the properties of the cellular insulations studied.

2) Dr. M. C. Biskeborn for early discussions with John Kaufman and encouragement regarding the design of the test cell.

3) Mr. Barry McHenry and Mr. Robert Lipnichan for their help with setting up the computer programs for doing the calculations and graphics.

References

1. D. Mangaraj, M. C. Biskeborn, and K. D. Kiss, "The Effect of Filling Compound Migration on Cellular Insulation, 27th International Wire and Cable Symposium, 1978.

2. C. K. Eoll, "The Aging of Filled Cable with Cellular Insulation", 27th International Wire and Cable Symposium, 1978.

3. C. J. Aloisio and E. D. Nelson, "The Effect of Water and Petroleum Jelly Migration on Capacitance of Plastic Insulated Cables, 22nd International Wire and Cable Symposium, 1973.

4. S. Verne, R. T. Puckoswki, and A.A. Pinching, "Long Term Stability of Polyethylene Insulating Fully-Filled Telephone Distribution Cables, 20th International Wire and Cable Symposium, 1971.

5. W. Englehart and R. Hayes, "An Analysis of Field Performance of Cellular Insulated Filled Telephone Cable After a Decade of Service", 35th International Wire and Cable Symposium, 1986.

6. D. M. Mitchell and R. Sabia, "Development, Characterization, and Performance of an Improved Cable Filling Compound", 29th International Wire and Cable Symposium, 1980.

7. Manager Quality Assurance and FDA Regulatory Affairs, Sonneborn Division, Witco Corp., Petrolia, PA 16050.



A. W. Stratton received a B.A. in Chemistry from Clarion University of Pennsylvania. Al joined Witco's Technical staff in 1975 and is located at the Petrolia, PA plant. His present position is R & D Group Leader for Wax, Petrolatum, and Cable Compounds. He is a member of the American Chemical Society, A.S.T.M., and the North American Thermal Analysis Society. He presently serves as Chairman of ASTM Committee E-37 on Thermal Measurements.



T. J. Roessing received a B.S. in Chemistry from Gannon College and a M.S. in Fuel Science from Penn State University. Tom joined Witco's Technical staff in 1971 and is located at the Petrolia, PA plant. As a cable filler research chemist, his areas of responsibility include new product development, technical service, and plant process support. Tom is a member of ASTM and TAPPI. Tom serves as Secretary for the Wax Subcommittee 10 of ASTM Committee D-2 on Petroleum Products.



J. D. Burkhard is a Research Technician at Witco's Petrolia, PA plant. He has been a member of the Technical staff since 1969. Joe has participated in the development and testing of cable filling compounds since 1969, when Witco became involved in this area. In addition to his laboratory responsibilities, Joe is involved in pilot plant operations and plant process support.

CABLE SHEATHING DESIGN AND PERFORMANCE CRITERIA

C. V. Maguire, R. Rossi

General Cable Company
Woodbridge, New Jersey

ABSTRACT

The telephone network is evolving at an ever increasing pace into a very sophisticated communication and data transmission facility. Cables employed as the backbone of this network must be extremely reliable and designed in a manner to provide many years of trouble-free service life.

As cable designs change and advances are made in material technology it become increasingly important to review the field performance of these design changes and the test procedures used to predict field behaviour.

In this paper we will discuss some further modifications to design changes to further improve overall performance and we shall comment on some specification requirements and testing procedures presently in use. Correlation of laboratory sheath evaluation tests with large scale installation simulations provide data relative to the usefulness of these tests.

INTRODUCTION

The primary function of a cable sheath is to electrically and mechanically protect the transmission conductors against conditions which would jeopardize their function. This function must be accomplished during installation, splicing and throughout the service life of the cable.

With regard to splicing, the cable components must certainly be compatible with all other components of the splice closure. The cable must lend itself to joining to the closure in a manner that is consistent with the environment, installation conditions and the service application of the cable. This may be to merely provide protection from the weather or to be leak-tight under a head of water.

During the service life of the cable, the sheath must protect the core from moisture and other contaminants to the degree necessary for proper circuit performance. Much has been written about the effects of moisture in telephone cable. In paper insulated cable, the catastrophic effects are obvious. Plastic insulated cable, while generally able to tolerate a less moisture resistant sheath, can suffer severe impairment of transmission properties if an excessive amount of moisture is permitted to enter the cable core. This has been sufficiently covered in previous papers, such as by Metcalf[1],Cox et al[2] and Olszewski et al[3]. Many service requirements also necessitate an extra degree of mechanical protection from attack by gophers or insects, or to provide resistance to crushing or penetration by rocks, hard digging operations or other hazards. This has also been adequately treated in prior literature.

It is during installation tnat the cable sheath many times undergoes its most severe test. The rigors of placing a cable can result in sheath damage far greater than may be encountered during the service life of the cable. The damage, in some cases, may manifest itself only after the cable circuits are put in service.

This paper will deal primarily with sheath designs and their relationship to the rigors encountered during installation including jacket slippage of filled cables, sheath buckling, low temperature cable stiffness and jacket zippering on bonded sheath. We will briefly consolidate data from previous experience and discuss solutions to some problems encountered during installation. We will also discuss how some of these solutions gave rise to some unanticipated problems.

Finally, this paper will center on a few key parameters for sheath components as well as some design techniques that will maximize the ability of the sheath to perform its function. We will present the rationale for selecting tensile yield as well as flexular modulus as two significant properties of the cable jacket. The effects of a adhesive polyolefin bridging tape will provide the design engineer with an option that can significantly reduce the risk of damage during installation.

CABLE INSTALLATION AND BACKGROUND

Outside plant cable is installed in three different manners - aerially, directly buried, or in duct. The most predominant design for aerial application is still unfilled plastic cable either in a Figure 8 configuration supported by special clamps or in a round configuration lashed to a support strand. No significant problems have been encountered in the installation of plastic cable in an aerial plant.

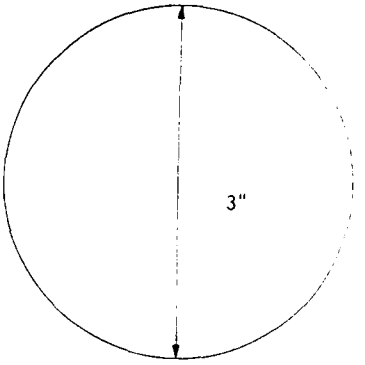
Direct Burial

For direct burial, the chief method of installation is by cable plowing. During the years when the predominant design for direct burial was Aircore PIC, no installation problems of major consequence were encountered. The polyethylene jacket is a fairly tough, abrasion-resistant material well able to withstand the rigors of plowing. The introduction of filled cable in the early 1970's added variables to the plowing process which resulted in a significant increase in the incidence of sheath damage problems. The reasons for this were discussed by Pehrson[4], and measures to minimize the impact of these new variables were discussed. One of the chief properties of a filled cable is the virtual incompressibility of the cable cross section. We repeat the illustration of this phenomenon in Figures 1 and 2 below for easy reference.

The problems of added weight and resultant increased friction were further discussed by Lawler et al[5]. In some cases cable plowing, particularly during hot weather, resulted in jacket slippage. This was attributed to the ease with which sheath components moved relative to one another when subjected to the tensions of cable plowing especially in ASP designs where there was no bonding between jacket and shield such as with the FPA sheath design.

This problem was solved by the use of heavier jackets and by use of jacket materials with higher tensile yield than that afforded by Low Density Polyethylene (LDPE).

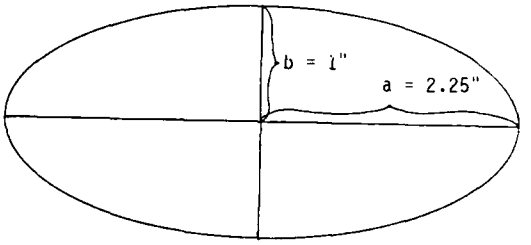
Linear Low Density Polyethylene (LLDPE) which was introduced for a different purpose, nonetheless afforded higher protection against sheath slippage by virture of its higher yield strength. Mid-to-Medium Density compounds afforded a higher level of protection but suffered from the disadvantage that they were stiffer and therefore more difficult to handle, particularly at lower temperatures.



Circumference = πd = 9.43 inch

Area = $\frac{\pi d^2}{4}$ = 7.07 sq. in.

FIGURE 1



Assume a 3 inch diameter circle is deformed to an ellipse with a 2 inch minor diameter but maintaining the same area.

Area = πab = 7.07 sq. in.

If b = 1 inch

Then a = $\frac{7.07}{\pi}$ = 2.25 inches

Circumference = $2\pi \sqrt{\frac{a^2 + b^2}{2}}$

= $2\pi \sqrt{\frac{2.25^2 + 1^2}{2}}$

= 10.94 inches

The circumference is 1.51 inches or 16% greater than the circle.

FIGURE 2

Duct Installation

For duct installation, problems surfaced when more and more large cables were introduced into the underground plant. In the years prior to World War II lead sheathed cable was extensively employed. For installation in underground duct, much care was required to ensure that the cable was straight and properly aligned at the entrance to the duct since lead was a relatively unforgiving material. After the war, polyethylene was increasingly used for both underground and direct buried plant. The relatively small pair sizes coupled with the fact that polyethylene is much more flexible eliminated the need for extraordinary care during duct installation. Whereas the C-bend configuration was extensively employed for lead sheathed cable, S-bend and side payout configurations come into increased use for plastic sheaths. These were more severe than the C-bend configuration.

Yanizeski et al[6] discussed the problems of buckling, kinking and torsion damage as cable pair sizes increased. In that paper, the use of a bonded stalpeth sheath was proposed to eliminate the problems. While this was a significant step in reducing the incidence of sheath buckling this solution gave rise to jacket zippering problems. The concept of a bonded steel sheath was extended to filled PIC cable in 1984 by Mitchell et al[7].

FORCES ON THE CABLE SHEATH

We have identified direct burial cable plowing and pulling cable into duct as the more rigorous of the installation methods.

Many of the forces encountered in both installation techniques are similar. Where differences are encountered they will be treated separately.

Cable plowing is basically as represented in the diagram of Figure 3. At points 1, 2, and 3 the forces are primarily compressive, resulting in stresses at the shield overlap as depicted in Figure 4. In an unbonded sheath, the force due to the increase in sheath circumference is distributed evenly around the cable. If a notch, or step, is introduced at the shield overlap, greater stresses are concentrated at that point increasing the probability of jacket separation.

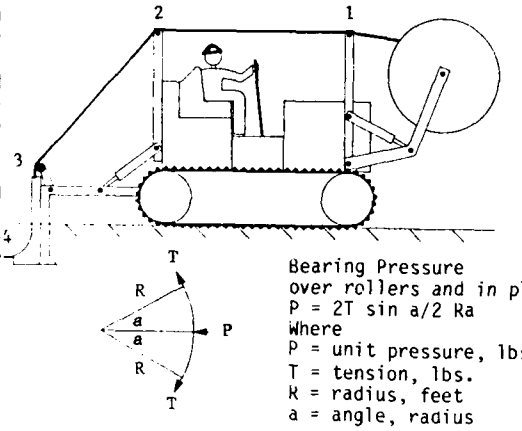
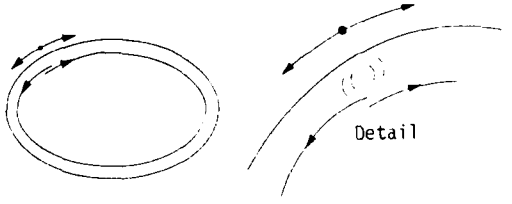


FIGURE 3

When the sheath stretches



If the bonding of the shield to the jacket is incomplete, stresses are concentrated at that point.

FIGURE 4

If the jacket is bonded to the shield, all jacket movement, to accommodate the changing circumference due to cable deformation, is confined to the area of steel overlap, creating very high stresses in the jacket. Any step or notch in the jacket, particularly where a steel edge is presented, will be prone to zippering. As illustrated in Figure 2, the circumferential increase for a 3" diameter cable may be as much as 1.5". If the bonding is uniform around the circumference of the sheath, this may represent no large problems. If, however, a 1/4" portion is unbonded, then the elongation of the sheath would be:

$$\frac{1.5" - .25"}{.25"} \times 100 = 500\%$$

In most cases, this figure is well within the elongation limits for polyethylene jacket. Any step, or notch at that point will significantly impair the ability of the jacket to withstand rupturing.

At point 4 of the plowing process, significant friction forces are introduced. As discussed in Ref. 4 the friction on the sheath could result in longitudinal force as great as 700 lbs. This force may be sufficient to cause jacket slippage.

Duct installation can be roughly represented by the diagrams in Figure 5. As discussed by Yanizeski[6], the C-bending method is the least punishing on the cable, resulting mainly in reverse bending forces within the duct. For the S-bend method additional compressive and friction forces are generated. In most cases these are quite similar to the forces seen in cable plowing.

It is in the side payout method that forces not encountered in plowing are introduced. Here, the cable is subjected to bending and torsion as it is payed off the reel and turned into the entrance to the duct. Torsional buckling may quite often result under these conditions.

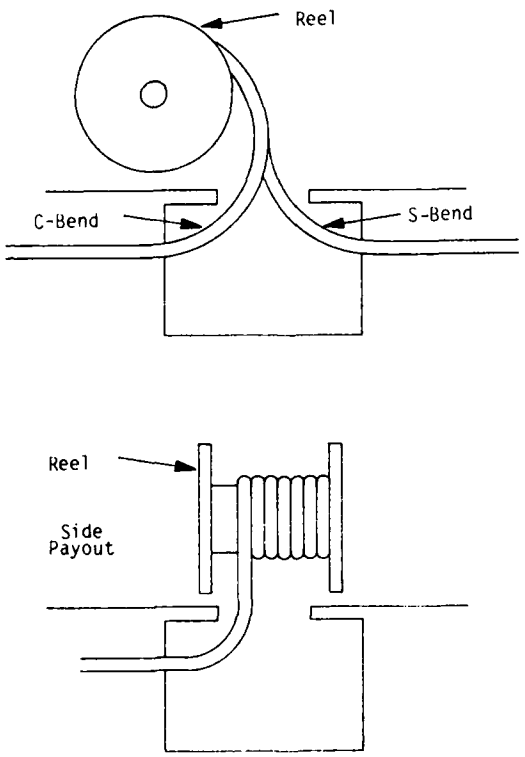


FIGURE 5

PROBLEM SOLUTIONS

The response by the wire and cable community to the problems generated by new cable designs and by increased use of larger size cables was comprehensive. Table I provides a quick overview:

TABLE I

INSTALLATION PROBLEMS AND SOLUTIONS

Problem	Solutions
1) Filled cable jacket slippage during plowing.	a) Mid-density polyethylene jacket. b) Thicker low-density polyethylene jacket. c) Bonded sheath. d) Cable temperature control
2) Sheath buckling during duct installation.	a) Bonded sheath.

As we discussed previously, the solutions to the original problems resulted in significant reductions in the incidence of those problems. The Medium Density jacket provided an excellent solution to the jacket slippage problem but suffered from the drawback that it increased cable stiffness, particularly at lower installation temperatures. Clearly, cable stiffness needed to be addressed.

General Cable Company has taken a step in that direction by defining additional parameters for polyethylene sheath. In a previous paper[5], we proposed that tensile yield be selected as a key parameter for the polyethylene jacket. The adoption of this proposal by the wire and cable community is evidenced by its inclusion in currently available specifications[8]. It is, however, debatable whether specifying different tensile yield limits for different densities of compound is the proper course. It is our opinion that tensile yield should be a single design limit regardless of jacket compound density.

At the time General Cable Company originally proposed the use of tensile yield as a design parameter, choice of jacket material was limited. The need for materials with higher tensile yield necessitated the selection of mid-density jacket material. Attendant to that selection was the fact that cable stiffness increased, particularly during cold temperature months. This was due to the high flexular modulus of these higher density compounds. Flexular modulus of 140,000 psi was a normal reading for some of these materials.

Today, we have a much wider choice of polyethylene jacket materials and it is not necessary to select stiff cable jackets in order to provide more rugged cable sheathing. Compounds are available today with tensile yield above 2000 psi

yet with flexular modulus readings as low as 60,000 psi at room temperatures.

The Linear Low Density jacket compounds, while not going as far as the mid-densities, provide additional toughness vis-a-vis Low Density jackets.

Table II summarizes the proposed solutions and the new problems which surfaced.

TABLE II

SOLUTIONS AND NEW PROBLEMS

Solution	New Problem
1) Mid-density polyethylene jacket.	a) Somewhat stiffer cable, particularly at cold temperature.
2) Thicker jacket.	b) Somewhat stiffer cable, particularly at cold temperature.
3) Bonded sheath.	c) Increased jacket zippering at shield overlap.

Jacket zippering is a problem that appears to have increased with the use of bonded sheath. Certainly, the stresses introduced by the transverse forces due to compression play a significant role. Coupled with the "sawing" action of the shield overlap edge as the cable is being subjected to tension and torsional forces, they provide a formidable reason for sheath failure. The proper forming of the shield overlap minimizes the probabilities of shield penetration into the jacket wall but occasional abberations in the shield forming process can occur. Jacket zippering occurs frequently enough to warrant the effort for further improvements.

In order to address the zippering problem, jacket material selection alone does not provide a complete solution. The underlying shield plays a very significant role. This has been recognized by specifying acceptable and unacceptable steel tape overlaps[8]. Figure 6, taken from Reference 8 is an example. While proper forming is a key factor, there may still be instances where penetration of the shield into the jacket occurs. To eliminate any possibility of jacket "injury" by the shield, General Cable has adopted the use of a polyolefin, chemically modified to impart high levels of adhesive properties. The adhesion eliminates the possible slipping of tape from the overlap area. The use of this bridging tape has virtually eliminated jacket notching even if the shield is poorly formed. This, then, provides an extra measure of safety to prevent sheath splitting as a result of compressive and torsional stresses.

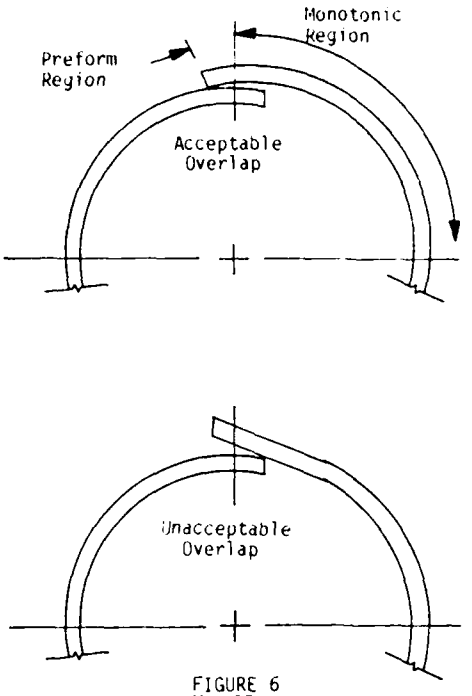


FIGURE 6

EVALUATION TECHNIQUES

As a result of the problems encountered during plowing and duct installation, the wire and cable industry developed means to evaluate not only material parameters of the polyethylene jacket, but also completed cable tests to enable prediction of cable performance during installation. Some of these tests are:

Material

- Yield Strength

Cable

- Sheath Adherence
- Torsion Test
- Cable bend
- Impact Test
- Jacket Notch Test
- Sheath Slip Test
- Column Strength Test

For this paper, General Cable Company performed the cable tests shown as well as a large scale test to simulate the rigors of plowing and duct installation. We also determined the flexular modulus of each jacketing compound as an additional correlating factor.

The test methods employed were as follows:

Tensile Yield - ASTM D-638

Flexular Modulus - ASTM D-790 Method I, Procedure A

Sheath Adherence - TR-TSY-000421[8]

Torsion Test - TR-TSY-000421[8]

Jacket Notch Test- TR-TSY-000421[8]

Cable Bend - Cable is bent 90° around a radius and the pounds force measured and recorded

Sheath Slip Test - REA Specification PE-89, Appendix II

EVALUATION SAMPLES

We selected cable measuring roughly 2 inches in diameter, or slightly less. To assess the various sheathing options, we also selected cables with bonded and unbonded sheath as well as cables with mid-density and low density polyethylene jackets. For the bonded sheath designs we also added other variations such as the adhesive bridging tape and also steel tape overlaps ranging from poor forming to good forming as previously shown in Figure 6. Table III will illustrate all of the designs and variations employed.

TABLE III

Sample	Cable Description	Jacket	Shield
1	600/26 Bonded PIC ASP	Mid-Density	No edge curl Good forming No bridging tape
2	900/26 Bonded PIC ASP	Linear Low Density	Good edge curl No bridging tape
3	600/24 Bonded PIC ASP	Mid-Density	a) Good edge curl; No bridging tape b) Good edge curl with bridging tape c) No edge curl - good forming; No bridging tape d) No edge curl - good forming with bridging tape e) No edge curl - poor forming; No bridging tape f) No edge curl - poor forming with bridging tape
4	900/26 PIC ASP	Linear Low Density	Good edge curl; No bridging tape
5	900/26 PIC ASP	Mid-Density	Good edge curl; No bridging tape
6	600/24 PIC ASP	Linear Low Density	Good edge curl; No bridging tape
7	900/26 PIC Alpeth	Linear Low Density	Std. sheath No bridging

TEST RESULTS

TABLE IV

Sample	Jkt. Dens.	Flex. Mod.	Shield Type	Cable Bend (Lbs./In^2) 0°F	R.T.
1	.94	74,700	Bonded Steel	9	4
2	.93	40,000	Bonded Steel	8.9	4.3
3a	.94	74,700	Bonded Steel	-- *	--
3b	.94	74,700	Bonded Steel	10.8	4.5
3c	.94	74,700	Bonded Steel	-- *	--
3d	.94	74,700	Bonded Steel	-- *	--
3e	.94	74,700	Bonded Steel	9.0	3.8
3f	.94	74,700	Bonded Steel	-- *	--
4	.93	40,000	Steel	7.7	4.5
5	.94	74,700	Steel	5.0	3.6
6	.94	63,800	Steel	4.2	2.1
7	.93	40,000	Aluminum	4.9	2.5

* Not tested for this characteristic.

TABLE V

Sample	Jacket Density	Tensile Yield	Notch Test	Sheath Adherence
1	.94	2100 psi	205%	*
2	.93	1700 psi	325%	*
3a	.94	2100 psi	515%	*
3b	.94	2100 psi	905%	*
3c	.94	2100 psi	970%	*
3d	.94	2100 psi	485%	*
3e	.94	2100 psi	170%	*
3f	.94	2100 psi	120%	*
4	.93	1700 psi	450%	17.4 lb/in
5	.94	2100 psi	850%	42.6 lb/in
6	.94	2100 psi	380%	64.3 lb/in
7	.93	1700 psi	715%	23.6 lb/in

Sample	Sheath Slip	Torsion 0°F	Torsion R.T.	Plowing Test
1	*	1080°	1080°	Good
2	*	720°	720°	Good
3a	*	--	720°	Good
3b	*	720°	720°	Good
3c	*	--	540°	Good
3d	*	--	720°	Good
3e	*	270°	90°	Zippered
3f	*	--	720°	Good
4	100 lb	720°	720°	Jacket Slip
5	115 lb	720°	720°	Good
6	130 lb	720°	720°	Rippled
7	70 lb	720°	720°	Good

* These test were not performed on bonded constructions.

DISCUSSION OF RESULTS

The results of the material and cable tests are illustrated in Tables IV and V. Table IV shows data that would relate to the bending property or flexibility of the cable. In an effort to provide a basis of comparison, the lbs force to bend the cable 90° was equated to cable cross sectional area. Readily apparent are the following:

1. Bonded constructions are less flexible than the unbonded sheath designs.
2. Within any sheath design category flexibility does not appear to be a function of density.
3. For cables with flexular modulus of 75,000 psi or less, flexibility is less a function of jacket compound than sheath design.

While field experience has certainly verified that cables with mid-density jackets have been stiffer, particularly at cold temperatures, this has been true mainly where jacket flexular modulus has been in the area of 120,000 psi or greater. Our results suggest that flexular modulus, rather than density, is the parameter of choice when cable flexibility is of concern. In addition, an upper limit of 80,000 psi is indicated.

Table V exhibits data with regard to sheath performance when the sheath is subjected to excessive stresses as might be encountered during plowing or duct installation. A number of points are brought to the readers attention:

a. Jacket zippering occurred only in the bonded sheath design with no bridging tape.

b. Jacket slippage occurred only on unbonded sheaths with low density polyethylene jackets.

c. Compliance with Sheath Slip Test and Sheath Adherence does not assure against jacket slippage during plowing.

d. The Notch Test does not appear to be a reliable indicator of sheath zippering.

e. The Torsion Test appears to be an accurate indicator of sheath zippering.

f. Sheath Adherence and Sheath Slip testing appear to have no value as an indicator of cable performance during installation.

Figure 7 shows a typical zippering failure that occurred as a result of plowing stresses. This is sample 3e which was deliberately produced to simulate a poor shield overlap. Without a bridging tape, the sheath zippered both during the Torsion Test and during the simulated plowing duct installation test. When a bridging tape was placed over the same poor overlap, the sheath withstood a severe Torsion Test as well as the large scale simulation.

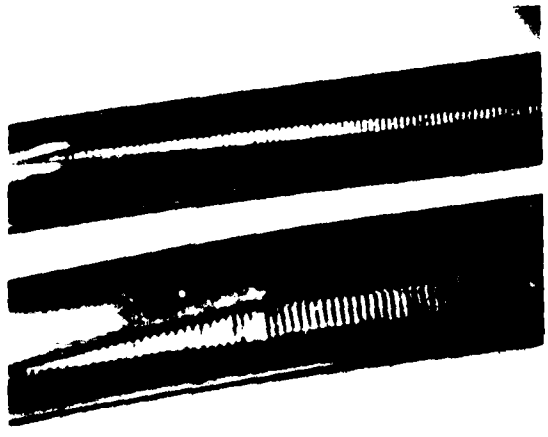


FIGURE 7

Of interest to note is a phenomenon we experienced on a number of samples. In these cases the samples were subjected to the Torsion Test and exhibited no apparent sheath failure. After a number of days, however, separation of the sheath along the edge of the overlap was evident. It appears that zippering, in some cases, may be a slow action, starting at the inner surface of the jacket at the point of "injury" and slowly progressing through the jacket wall to the outer surface. This is illustrated in Figure 8. The zippering phenomenon can be further illustrated by examining the displacement of a point on the shield overlap along the longitudinal axis of the cable. Depending on the degree of torsion, the displacement can be significant.



FIGURE 8

In our apparatus for simulating plowing and duct installation, the cable is passed through a guide sheave, after which it is passed over and through a series of sheaves which may be locked into position to increase the stress on the cable. Pulling tension is controlled by means of adjusting the back-tension at the pay-out reel. Sheath buckling, as shown in Figure 9, is produced in the same fashion as in actual field conditions. As shown in Table V, sheath damage was produced when the following conditions existed:

1. Shield edge "injury" to the inner surface of the jacket was evident.

2. Low density jacket on an unbonded sheath.



FIGURE 9

CONCLUSION

From the data developed, a number of points are readily apparent:

1. Cable stiffness is more a function of sheath make-up and bonding than of jacket density.

2. To minimize the effect of the jacket on cable flexibility, material with flexular modulus of 80,000 psi or less should be selected.

3. Polyethylene jacket density should not be a parameter employed to select or reject a candidate material.

4. To minimize the tendency of the jacket to slip during plowing, polyethylene jacketing material with tensile yield of 2000 psi and greater are preferable.

5. Where a bonded sheath design is employed to provide a more rugged cable, the use of a bridging tape at the overlap will provide a significant measure of protection against jacket zippering.

6. Sheath Adherence and Sheath Slip testing to have no value as an indicator of cable performance during installation.

7. Based on our observations, a torsion test limit of 180° minimum should provide adequate assurance that zippering will not be encountered during field installation.

SUMMARY

In this paper, we have attempted to show that good cable sheathing, particularly for protection during installation, is a function not only of the materials selected, but how these materials are made to act together to result in improved performance. This is certainly evidenced by the contribution of bonded sheath design and the significance of a bridging tape in the performance of the sheath.

Also, it is evident that plastics technology has progressed beyond the point of using density as a barometer of sheath performance. The contribution of tensile yield strength and flexular modulus to sheath ruggedness and cable flexibility is clear.

The results of our evaluation, reported in this paper, are consistent with observations made in our own facilities, and in the field over a period of several years.

ACKNOWLEDGEMENTS

The authors wish to acknowledge the valuable contributions of J. Justiss and C. Darwin of Bonham, Texas in bringing this paper to a successful conclusion. Their many long hours spent in performing the tests were invaluable. We thank them for their time and dedicated efforts.

REFERENCES

1. Metcalf, E. D., "A Bonded, Non-Corrugated Aluminum/Polyethylene Sheathing System for Telephone Cable", Proceedings of the Twenty-First International Wire and Cable Symposium, 1972.

2. Cox, C. L., Tingley, T. E. and Webster, H. A., "Problems of Water in PIC Cable", Proceedings of the Twenty-First International Wire and Cable Symposium, 1972.

3. Olszewski, J. A., Pehrson, V. W. and Simon, H., "Effects of Water in Plastic Insulated Telephone Cable", Proceedings of the Twenty-First International Wire and Cable Symposium, 1972.

4. Pehrson, V. W., "Engineering for Cable Installation", Proceedings of the Twenty-Fourth International Wire and Cable Symposium, 1975.

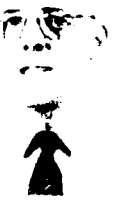
5. Lawler, J. D., Rossi, R. and Virkus, K. J., "More Rigorous Sheathing for Outside Plant Cables", Proceedings of the Twenty-Seventh International Wire and Cable Symposium, 1978.

REFERENCES (Cont'd.)

6. Yanizeski, G. M., Johnson, E. L. and Schneider, R. G., "Cable Sheath Buckling Studies and the Development of a Bonded Stalpeth Sheath", Proceedings of the Twenty-Ninth International Wire and Cable Symposium, 1980.

7. Mitchell, D. M., Collins, R. P., West, D. E., and Kinard, M. D., "Bonded ASP: A Superior Sheath for Buried and Underground Filled Cables", Proceedings of the Thirty-Third International Wire and Cable Symposium, 1984.

8. Bell Communications Research, Technical Reference TR-TSY-000421, Issue 1, December 1986.



Mr. C. V. Maguire joined General Cable Company in 1962. Since that time he has worked extensively in the areas of Manufacturing, Product Engineering and Development and Quality Control. A graduate Electrical Engineer, he is currently Vice President and Technical Director, General Cable Company-U.S.



Mr. R. Rossi joined General Cable Company in 1963. Since that time he has worked in Product Engineering, Quality Control, Quality Assurance and Application Engineering. With a B.S. Degree in Engineering Sciences, he is currently Application Engineering Manager, Technical Operations, General Cable Company-U.S.

PERFORMANCE OF HDPE INSULATION ANTIOXIDANTS IN FILLED TELEPHONE CABLE APPLICATIONS

GEOFFREY D. BROWN

UNION CARBIDE CORPORATION, WESTON CANAL CENTER, SOMERSET, NEW JERSEY

Abstract

A material testing procedure has been used to evaluate high density polyethylene insulation antioxidant performance for filled telephone cables. To simulate the filled cable application, the testing includes aggressive conditioning of high density polyethylene samples in filling compound prior to oven aging. This filler conditioning greatly reduces the antioxidant functionality of existing commercial formulations.

Alternative antioxidant formulations are reviewed and antioxidant system optimization to achieve substantially improved performance is demonstrated. The test method is relatively simple and shows good repeatability. The test is most useful when used as a screening technique in conjunction with long term cable aging studies. Good correlation with improvements demonstrated with foam/skin insulation samples in a filled test cable confirms the utility of this approach.

Introduction

An accelerated aging cable testing procedure has been developed which simulates commercial applications for insulations in filled telephone cables. The requirements of the commercial application and details of the test method are summerized in the companion paper "A Global Test Method for Long Term Stability of Solid and Foam Skin Insulation". A distinctive feature of this cable test is a substantial preaging requirement. The filled cable sample is conditioned for four weeks at 70°C prior to removal of insulation samples for pigtail testing in air ovens. Comparison to field samples of commercial cable indicate that the 70°C preaging simulates the commercial application. A broad sampling of commercial cable exhibited unexpectedly rapid oven aging insulation cracking failures when evaluated with this new testing procedure.

This cable testing procedure was used in a study of insulating materials with the goal of identifying and commercializing products with substantially improved performance. The cable study is summarized in the companion paper "Evaluation of Materials for Improved Life Expectancy of Foam Skin Insulation." As the work evolved, testing of insulations revealed that there was a dramatic decrease in 190°C Oxygen Induction Time associated with the 70°C cable preaging. As a result, this bench study was undertaken to identify an antioxidant formulation providing improved functionality after filler exposure.

Test Method

The test method is detailed in the appendix. The sample aging procedure parallels the cable aging study. Film samples of selected product formulations are prepared and are preaged by immersion in cable filling compounds for 4 weeks at 70°C. After preaging, the samples are removed and wiped thoroughly and suspended in a circulating air oven at 80°C. Antioxidant functionality is measured by 190°C copper pan Oxygen Induction Time at selected intervals during the test cycle. Sample testing includes an initial measurement before filler exposure and testing of wiped samples after 14 and 28 days of 70°C filler immersion. During the 80°C oven aging, samples are tested at 2 week intervals for 6 to 10 weeks and then the test series is ended.

The filler preaging/oven aging sequence is an accelerated simulation of the commercial application. Insulations are initially exposed to molten cable fillers above 100°C in the cable jacketing process. Finished cable may then experience a substantial time/temperature history with direct sunlight exposure in warm climates as it is tested and stored by the manufacturer, transported, and stored by the user. The four week 70°C immersion in cable filler simulates this cable history and allows sufficient insulation filler interaction. Subsequently, the cable is installed with sections of the cable sheathing removed and cable filler wiped away to allow insulated wire interconnections at pedestals and other junctures. Internal temperatures in pedestals are often substantially hotter then ambient conditions, with maximum internal pedestal temperatures ranging from 50°C to 70°C for southwestern United States locations cited in the literature[1,2]. This pedestal exposure provides a severe thermal-oxidative environment for the exposed insulations. Accelerated aging temperatures ranging from 70° to 130°C have typically been used[3,4] to simulate the pedestal environment, with the relatively moderate temperature of 80°C being

used in this study.

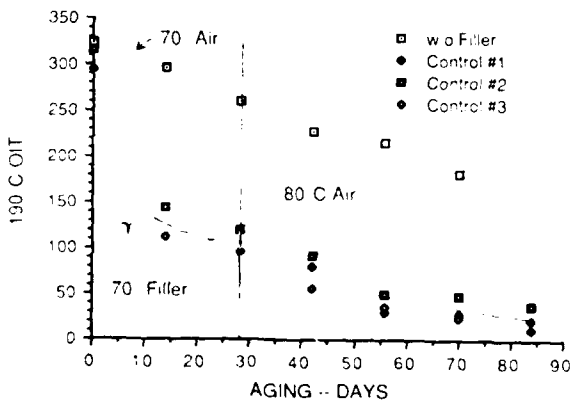
A Dupont Model 990 Thermal Analyzer with a Differential Scanning Calorimeter cell is utilized to measure Oxygen Induction Time. The 190°C copper pan induction time condition selected provides good resolution among samples. Use of oxidized copper pans is consistent with a copper conductor insulating application. A 0.25 millimeter thick film specimen was selected to approximate insulation thicknesses.

The preparation of material test samples is consistent with commercial practice. Low melt temperatures are usually desirable in melt processes to minimize product degradation and antioxidant consumption. In addition, high melt temperature is unacceptable for cellular materials production.

Experimental Results

The performance of the existing commercial HDPE antioxidant systems was investigated first. A two component system (antioxidants are listed in Table 1) composed of a primary antioxidant, AO-1, and a metal deactivator, MD-1, was developed and is used commercially for both HDPE solid and cellular insulations. Figure 1 shows test data on a standard commercial formulation.

Figure 1
Cable Filler Conditioning



1 0 Days OIT measured before filler exposure
2 All samples formulated with 0.18% AO 1.0 15% MD 1 in Ethylene-Hexene Base Resin (.945 density HDPE)
3 Control samples aged 4 weeks at 70 C in PE/PJ filler

A sample aged without filler exposure for four weeks at 70°C and subsequently at 80°C shows a gradual decrease in induction time. In contrast, there is a large decrease in induction time associated with four week 70°C filler immersion. For the preaged samples, the subsequent depletion of the residual functionality in 80°C oven aging results in induction time dropping to marginal values of less then 5 minutes. Several mechanisms could contribute to the rapid decrease in induction time of filler preaged samples including:

- Migration of the antioxidant from the insulation into the cable filler.
- Migration of filler into the insulation where it would serve to catalyze degradation during the subsequent 80°C oven aging and during the 190°C induction time test.
- Swelling of the polyethylene and the presence of absorbed filler might increase antioxidant migration losses during subsequent oven aging.

Table 1
Antioxidants Used in This Study

AO-1 Tetrakis [methylene 3-(3',5'-di-tert-butyl-4-hydroxyphenyl) propionate] methane; Trade name: Irganox 1010; Ciba Giegy.

AO-2 1,3,5-tris(4'-tert-butyl,5'-hydroxy-2,6'-dimethylbenzyl)isocyanurate; Trade Name: Cyanox 1790; American Cyanamid

AO-3 2,2'-methylene-bis(4-methyl-6-tert-butylphenol); Trade Name: Cyanox 2246; American Cyanamid

AO-4 2,2'-methylenebis(4-methyl-6-(1'-methyl-cyclohexyl)phenol)); Trade Name: Nonox WSP; ICI Americas

MD-1 N,N'-bis[3-(3',5'-di-tert-butyl-4'-hydroxyphenyl) propionyl] hydrazine; Trade Name: Irganox 1024, Ciba Giegy.

MD-2 N,N'-bis(salicylal) oxalyldihydrazide; Trade Name: CDH; Eastman Chemical

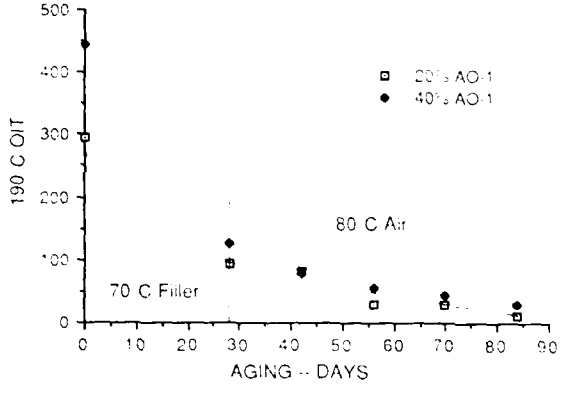
MD-3 2,2'-oxamido-bis-ethyl-3-(3,5-di-t-butyl-4-hydroxyphenyl) propionate; Trade name: XL-1; Uniroyal

Figure 2 shows test data generated at increasing levels of the AO-1 primary antioxidant. The data shows that substantial increases in AO-1 concentration provide relatively minor improvement after 4 week filler immersion. When compared to the substantial improvements in the initial induction times for no filler exposure, this result suggests that filler related losses greatly limit the AO effectiveness.

The MD-1 component has primary antioxidant functionality and has been commercially promoted as an oil extraction resistant antioxidant. This is consistent with test data presented in Figure 3 which shows increasing the MD-1 component to provide substantial improvements in retained

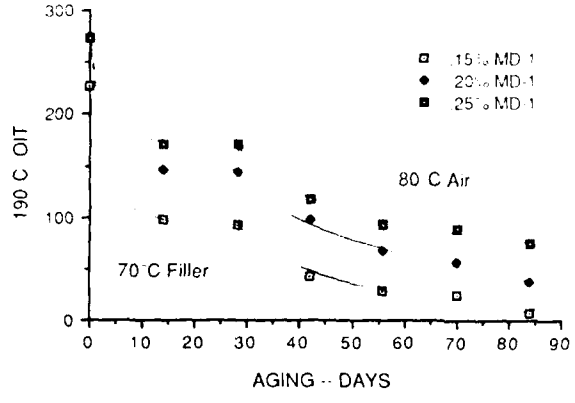
stabilization after the 4 week filler immersion. The good performance of the MD-1 is consistent with past studies [1] incorporating filler conditioning of insulation samples prior to oven aging. Comparison of the MD-1 and AO-1 data reinforces the observation that AO-1 may be unsuitable for applications involving extended contact with cable filling compounds. The likely explanation is leaching of the AO-1 by the cable filler and good permanence of the MD-1.

Figure 2
AO-1 Performance



1. 0 Days OIT measured before filler exposure
2. PE/PJ type filler
3. Samples formulated with ethylene-hexene base resin and 0.15% MD-1

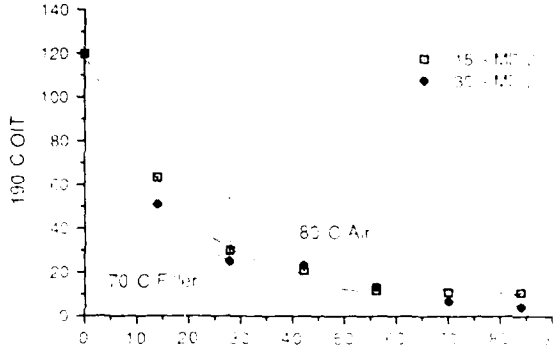
Figure 3
MD-1 Performance



1. 0 Days OIT measured before filler exposure
2. PE/PJ type filler
3. Samples formulated with ethylene-hexene base resin and 0.08% AO-1

MD-2, an alternate metal deactivator, was [illegible] prior years combined with AO-1 [illegible] insulation in filled cables. As shown in Figure 4, an MD-2 AO-1 system showed [illegible] oxygen barrier [illegible] immersion properties. Since the MD-2 [illegible] doesn't provide primary anti-oxidant functionality, the presence of AO-1 [illegible] but should not render the system inert. [illegible] the observed trend. [illegible] It can act as a primary anti-oxidant [illegible] a [illegible] after filler [illegible] [illegible] identify a [illegible] system such as [illegible] MD-2 could be beneficial.

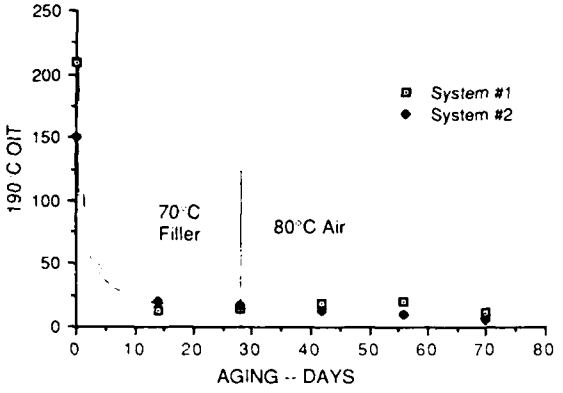
Figure 4
MD-2 Performance



1. 0 Days OIT measured before filler exposure
2. PE/PJ type filler
3. Samples formulated with ethylene-hexene base resin and 0.18% AO-1

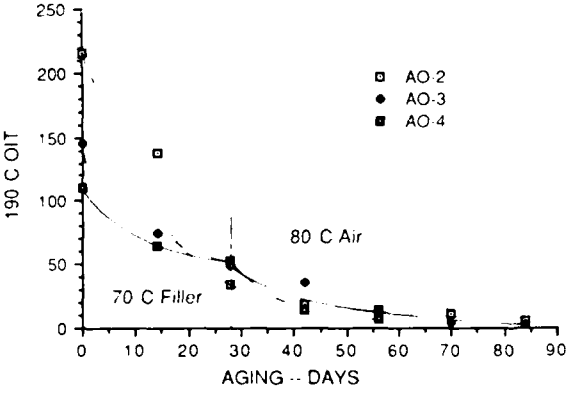
[illegible] alternative metal deactivator [illegible] anti-oxidant [illegible] primary [illegible] [illegible] The data suggests that [illegible] [illegible] [illegible]

Figure 5
MD-3 Performance



1. 0 Days OIT measured before filler exposure
2. PE/PJ type filler
3. Formulated with ethylene-hexene base resin
   System #1: 0.15% MD-3/0.18% AO-1
   System #2: 0.30% MD-3

Figure 6
Alternate Primary Antioxidants



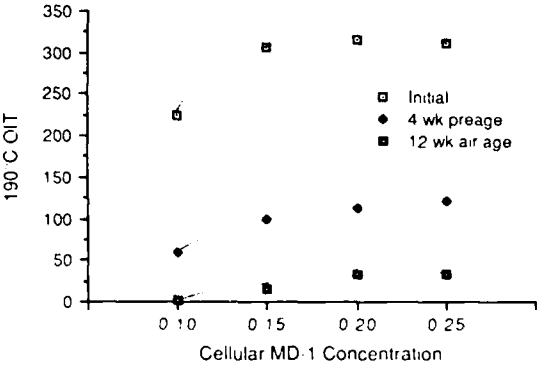
1. 0 Days OIT measured before filler exposure
2. PE/PJ type filler
3. Samples formulated with ethylene-hexene HDPE base resin and 0.15% MD-1

Cable Aging Study Insulations

The findings of this study were incorporated into the accelerated aging cable studies on an ongoing basis. As a result, experimental ethylene-hexene HDPE cellular materials were formulated with increased MD-1 antioxidant. Foam/skin insulations incorporating this foam showed dramatically increased accelerated aging life. There was uncertainty about whether to attribute the improvement to the optimization of stabilizer or the use of ethylene-hexene HDPE instead of ethylene-butene HDPE feedstocks.

The most recent test cable series includes ethylene-butene HDPE cellular materials incorporating a range of MD-1 concentrations. Preliminary results suggest that increasing MD-1 concentration provides the most or all of the performance improvement, as the foam/skin insulations incorporating ethylene-butene cellular appear to rival ethylene-hexene cellulars when both incorporate the same increased MD-1 concentrations. Samples of insulations from this test cable were tested for 190°C oxygen induction time and the data is presented in Figure 7. Samples including foam containing lower concentrations of MD-1 appear to show the fastest deterioration in OIT performance. Samples containing lower concentration of MD-1 are also are showing the most rapid cracking failure trends in the oven aging studies.

Figure 7
Foam/Skin Insulation Aging Stability



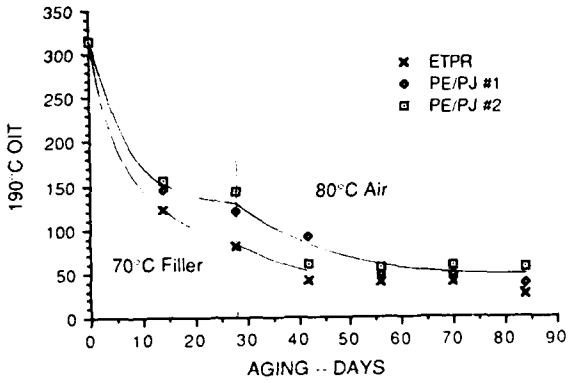
1. Aluminum pan Oxygen Induction Time
2. Initial - insulation without filler exposure
3. Preage - oven age cable for 4 weeks at 70°C
4. Air age - 4 week preage in cable and then air oven age insulated wire for 12 weeks at 80°C
5. Samples are 24AWG foam-skin, ethylene-butene cellular product

Cable Filler Interactions

Testing confirmed that the decrease in antioxidant system functionality wasn't specific to the filler sample or filler type being evaluated. Figure 8 shows data the same film sample tested with two PE/PJ based compounds plus an extended thermoplastic rubber (ETPR) type filler. There is basic similarity in the severe drop in induction time during filler immersion followed by gradual depletion of the remaining functionality during oven aging. A major study of cable filler interactions with insulations established that ETPR type (Flexgel) fillers exhibit higher diffusion rates (faster absorption to equilibrium) into HDPE than PE/PJ type fillers. If antioxidant leaching is a

significant mechanism for loss of stabilizer functionality, this diffusion rate data might explain the observed differences in antioxidant functionality.

Figure 8
Cable Filler Comparison



1. 0 Days OIT measured before filler exposure
2. Samples formulated with ethylene-hexene HDPE and 0.15% AO-1/0.15% MD-1

Discussion

Pedestal field cracking failures of low density polyethylene solid insulations were first observed in the mid 1960's. Investigation revealed that the low molecular weight phenolics used at the time migrated to the insulation surface and diffused into the air. Replacement with a higher weight phenolic counteracted this tendency and improved performance. In the late 60's, additional cracking failures were observed and after study were attributed to copper conductor catalyzed degradation. Addition of metal deactivator stabilizers[1] to minimize the copper catalytic effect corrected this deficiency. Additional factors complicated the commercial situation with the development of filled cables for buried plant and the introduction of cellular and foam/skin insulations. Use of chemical blowing agents in cellular products to produce foam and foam/skin insulations significantly increased the stabilization requirements.[2,3] The tendency for contact with cable fillers to significantly detract from the long term aging performance of insulations was also well documented.[4] Nevertheless, overall good performance and economics of foam and foam/skin insulations led to widespread commercialization.

The generally favorable ten year plus commercial history of foam/skin insulations decreases the likelihood of widespread systematic failures. This most recent study suggests that minor antioxidant optimization should provide a considerable safety margin over and above the existing commercial experience.

The experimental method exhibits good repeatability with control samples providing similar results and performance trends repeating among the experimental series. High air turnover of the vented air convection ovens utilized minimizes the potential for sample cross-contamination observed with more static tests and this allows higher productivity with limited equipment resources. The ovens were tested via the ASTM D 2436-68 procedure and were vented to provide about 200 air changes per hour.

It is believed that the 4 week 70°C filler immersion and the 80°C oven aging simulate the requirements for oxidative stability of filled cable insulations. Use of the 190°C copper pan oxygen induction time to measure antioxidant functionality is more controversial. Pedestal aging involves stabilization considerations associated with oxidation of a solid polyethylene while the oxygen induction test measures melt stability. Indeed, past studies have shown that extreme miscalculation can result from Arrhenius extrapolation of melt induction time data to service conditions. However, in this study, this concern is largely circumvented because there is no attempt to quantitatively extrapolate induction time to service conditions. Rather, induction time is used as a rough measure of antioxidant functionality changes resulting from filler conditioning and oven aging at moderate temperatures. Specifically, good retention of induction time during filler immersion and oven aging is very favorable and reflects good antioxidant permanence in the HDPE with filler contact. Conversely, a dramatic decrease in induction time probably reflects poor permanence of a given antioxidant system. Accelerated cable aging studies are then used to more precisely evaluate promising systems. In addition, it should be noted that the 190°C oxygen induction time measurement is appropriate to measure stabilization for melt processing. Good melt stabilization is necessary to minimize polyethylene degradation in the product compounding and wire insulating melt processes.

It is recognized that the 190°C oxygen induction time testing would be inappropriate for antioxidants that exhibit poor melt stabilization but which have good filler permanence and provide good stabilization at the lower temperatures of the commercial application. Antioxidants having this characteristic would consistently exhibit low induction times. Stabilization systems incorporating such antioxidants would need to include a melt processing stabilizer for the product compounding and insulating processes, but permanence of this component would be less important.

The bench test eliminates many variables associated with evaluating antioxidants in long term cable aging studies and this provided good experimental repeatability. Cabling study variables that were either not a factor or less of a factor in this bench study include:

- Insulation Materials Production
- Insulating Process
  - Extrusion Conditions
  - Equipment
- Cabling Process
- Additives
  - Blowing Agent
  - Colorant Masterbatch
- Test Sample Variability
  - Cell Structure
  - Skin Thickness

Many of these variables are interactive and encompass more then one factor. For example, additive variables include concentration, particle size and dispersion, and composition and impurities. The bench test also improves control of cable filler composition, age, and quality. Using this test to help design cabling trials increases the likelihood that clear performance trends can be demonstrated.

Both colorants and especially chemical blowing agent are known to detract from oxidative stability; but while the stabilization requirement is increased, the need for good polyethylene antioxidant functionality after filler exposure remains. With minor refinement, the bench techniques could be adapted to study the interaction of blowing agent or colorant variants on oxidative stability of polyethylenes with filler exposure.

Conclusions

A test method having good utility for evaluation of insulation antioxidant system after exposure to cable fillers has been presented. The method is low cost and simple and provides good repeatability. In addition, the relatively fast test allows iterative experiments leading to better materials refinement prior to the major expense and delay of cabling trials and insulation aging studies.

Testing of a commercial HDPE formulation reveals that the primary antioxidant, AO-1, exhibits a high loss of functionality after cable filler exposure. It is thought that the AO-1 is lost to filler extraction. Attempts to identify a primary antioxidant having substantially better permanence after filler immersion were unsuccessful, and this need remains outstanding. The metal deactivator component, MD-1, appears to have much better permanence after filler immersion. The MD-1 has primary antioxidant functionality and appears to assume the major stabilization burden after loss of the AO-1. Retention of oxygen induction time after filler exposure is enhanced by antioxidant system reformulation to favor increased concentrations of MD-1. Foam/skin insulation aging studies described in a companion paper confirm that increased MD-1 concentrations lead to substantial increases in life performance.

Also observed in this study was significant variability among various samples of cable fillers. This confirms that cable manufacturers need to utilize a systems approach; specifying and testing specific combinations of insulations and cable fillers to insure good aging performance. Fortunately, the testing method described herein provides a reasonable capability to optimize cable filler materials as well as insulations prior to the major cost and delay of long term aging studies.

As an outcome of this antioxidant study and the ongoing cabling studies, commercial high density polyethylene solid and cellular product formulations have been optimized to provide increased concentration of the MD-1 antioxidant. The stabilization of the cellular products was identified as the weakest link in current high density insulations and the MD-1 concentration increase in the cellular products was on the order of 100%. This increase should provide a suitable safety margin as compared to the satisfactory 10 year commercial history of prior formulations. It is recommended that the AO-1 antioxidant be retained in the insulation product formulations at reduced concentration as a cost/effective melt processing stabilizer. Primary antioxidants will continue to be investigated since the identification of a cost/effective alternative to AO-1 with good filler permanence would further improve performance and economics.

Acknowledgements

The author wishes to thank the suppliers who provided antioxidants and technical guidance for this study. The support of Witco Corporation in providing experimental and commercial cable filler samples was also appreciated.

Peter J. Dellatore performed the experiments in a dedicated and competent manner. Bob Turbett was a mentor providing invaluable support and guidance.

References

1. Howard, J.B., "Stabilization Problems with Low Density Polyethylene Insulations," 21st International Wire and Cable Symposium, 1972, pp. 329-341.
2. Schmidt, G.A., "Methods for Life Prediction of Insulations of Air Core Cables and Filled Cables," 22nd International Wire and Cable Symposium, 1973, pp. 11-22.
3. Pusey, B. B., Chen, M. T., and Roberts, W. L., "Evaluation of Thermal Degradation in Polyethylene Telephone Cable Insulation," 20th International Wire and Cable Symposium, 1971, pp. 209-217.
4. Gesner, B.D., Shea, J.W., and Wight, F.R., "Establishing Longevity Criteria From Thermo-Oxidative Cracking Measurements on

Polyolefin Insulations," 22nd International Wire and Cable Symposium, 1973, pp. 7-10.
5. Gilroy, H. M., "Thermal Oxidative Cracking of Polyethylene Insulation on Telephone Conductors," 23rd International Wire and Cable Symposium, 1974, pp. 42-45.
6. Turbett, R. J., Canadian Patent 988642
7. Chan, M.G., and Powers, R.A., "Stabilization Systems for Waterproof Cable Insulation," 33rd Annual Technical Conference, Society of Plastics Engineers, 1975
8. DiBattista, A., Farber, J. M., Trainor, M. A., and Klemchuk, P. P., "New Antioxidant/Metal Deactivator System for Polyolefins Used in Wire and Cable Applications," 33rd Annual Technical Conference, Society of Plastics Engineers, 1975
9. Patel, A., "A Bifunctional Antioxidant/Metal Deactivator for Polyolefin Wire Insulation", 26th International Wire and Cable Symposium, 1977, pp. 83-88.
10. Ruddell, H.J., Adams, D.J., Latoszynski, E., and deBour, B. T., "Behavior of Four Non-Migratory Antioxidants in Solid Polyethylene Insulation,", 32nd International Wire and Cable Symposium, 1982, pp. 104-110.
11. L. L. Blyler and C. Gieniewski, "Effects of Waterproofing Cable Fille[illegible] on Some Physical Properties of Polyethylene Cable Materials", 30th IWCS, 1981,
pp. 270-279.
12. O'Rell, D.D., and Patel, A., "Oxidative Stability Studies on Cellular High Density Polyolefin Insulation for Communications Wire", 24th International Wire and Cable Symposium, 1975, pp. 231-236.
13. Kiss, K.D., and Malaver, E. G., "Oxidative Stability of High Density Polyethylene, 26th International Wire and Cable Symposium, 1977, pg. 68-82.
14. Schmidt, G.A., "Life Prediction of Insulations for Filled Cable," 26th Annual International Wire and Cable Symposium, Cherry Hill, N.J., November 1977, pg 161-181.

Appendix

Test Method

1. Insulation Materials Preparation
Weigh antioxidants on high resolution laboratory balance. Use a 300 gram Brabender laboratory melt mixer or equivalent. Add a 230 gram charge of high density polyethylene base resin and flux at low RPM's. Reduce mixer speed to 5 RPM and carefully add the antioxidant. Increase the mixer RPM to 120 RPM's and hold this condition for 5 minutes. Melt temperature should stabilize at 170 ± 10°C.

2. Test Sample Preparation
Use a window frame mold with a 15 x 15 cm opening and two stainless steel backing plates covered with Mylar sheets to mold the film samples. Place a 15 gram charge of high density polyethylene into mold and place into compression press with 180°C platen temperatures. Close press at low pressure for 4 minutes and then increase to maximum pressure for 2 minutes. Quench cool and remove samples. Cut 25mm thick sheet into specimens approximately 2 mm square.

3. Filler Conditioning of Samples
Obtain a representative sample of cable filler to be used. Melt and mix cable filler at 110°C for 5 minutes. Add approximately 17 grams of cable filler to a #6 dram glass vial (approximate internal dimensions: 25 mm diameter x 45 mm high) and let these bottles cool to 70°C. Place 10 specimens of a sample in each bottle. Prepare caps on bottles and put 15 mm rubber disk in caps. Place sample bottles in 70°C circulating air oven (Blue M Model MF-6160C-1 or equivalent). When samples are removed for testing or oven aging, wipe off surface jelly thoroughly with paper tissue towels.

4. Oven Aging of Samples
After surface filler has been thoroughly wiped from specimens, place specimens on heap of stainless steel wire. Use stainless steel beads between each specimen to hold them apart and ensure good air circulation. Allow Blue M Model MF-6160C-1 or equivalent circulating air oven to equilize at 80±1°C with venting to provide approximately 200 air changes per hour. Hang stainless steel wires to suspend specimens in circulating air oven.

5. Oxygen Induction Time Testing
Use a Dupont Model 990 Thermal Analyzer with a Module II Cell Base and a Differential Scanning Calorimeter module or equivalent apparatus to measure oxygen induction time. Cut an approximately 8 milligram test specimen and place specimen in precoxidized copper test pan and into test chamber. Purge with Nitrogen at 100 cc/minute and increase temperature to 190°C using isothermal control mode. After reaching 190°C, continue purging with Nitrogen for approximately 2 minutes and then switch to 100cc/minute Oxygen flow to start induction time period.

6. Miscellaneous Notes
- Always include set of control specimens in each experimental series.
- Secure adequate supply (10 liters) of each cable filler material to avoid changing filler samples midway through a study.



Geoffrey D. Brown received a MSME degree from Bucknell University in 1977. He joined Union Carbide in 1977 and specialized in polymer melt process development in the Polyolefin Specialties R&D Department. Since 1983, he has been involved in product development for telecommunications.

A HIGH PERFORMANCE NONMETALLIC SHEATH FOR LIGHTGUIDE CABLES

C. J. Arroyo, A. C. Jenkins, P. D. Patel

AT&T Bell Laboratories, Norcross, Georgia 30071

A. J. Panuska

AT&T Network Systems, Norcross, Georgia 30071

ABSTRACT

A flexible yet rugged nonmetallic lightguide sheath has been developed for AT&T's ribbon and Lightpack® cables. In this design two types of nonmetallic strength members are employed. They are rigid epoxy-impregnated glass rods and flexible polymer-impregnated glass rovings. The new sheath consists of two layers of these strength members helically applied over a core tube followed by a single high density polyethylene jacket. A computer simulation, based on an analytical model, is used to optimize the placement and combination of the nonmetallic strength members. The design offers excellent optical performance over the temperature range of -40 to 88°C. Results of qualification tests performed in accordance with EIA standard show that the design meets or exceeds both the AT&T as well as Bellcore requirements. This new design provides easy handling during installation and is craft friendly, especially during express entry. A UL classified fire-resistant riser cable that provides distribution between two or more floors in a building is also available.

1. INTRODUCTION

Historically, outside plant cables have employed metallic strength members to withstand first the rigors of cable placement, such as tensile loads, crushing, bending, and abrasion, and then the environmental hazards over the life of the cable. The metallic crossply sheath[1] is available for the AT&T's Lightpack® cables[2] and ribbon cables.[3] However, metallic sheath components are susceptible to lightning and power crosses such that metallic sheath is not suitable in certain applications. A nonmetallic sheath provides the best deterrent to lightning and may be successfully used in lightning prone areas[4] where gnawing rodents are not a threat. For areas where both rodent and lightning protection is desired, AT&T's primary RL sheath[5] is recommended. Nonmetallic cables are also preferred for long span aerial applications near overhead power lines.[6][7][8][9]

In a typical nonmetallic sheath design, metallic strength members are replaced with nonmetallic ones, as shown in Figure 1. Although comparable in performance, nonmetallic strength members are generally more expensive. Therefore design optimization is crucial to achieve an economical design. A nonmetallic sheath offers other advantages too. In addition to being lighter in weight, the nonmetallic sheath is particularly attractive for environmental stability. Furthermore, the need for the grounding of metallic strength members and metallic shields is eliminated in a nonmetallic design.

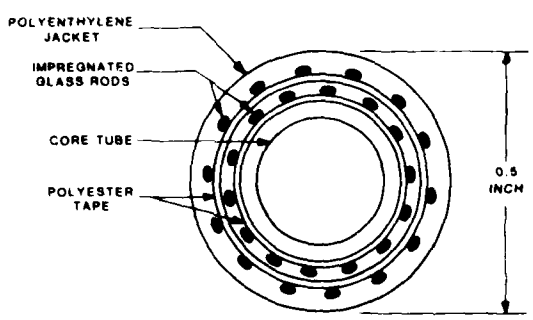


FIGURE 1. CROSSPLY NONMETALLIC SHEATH

In military applications, electromagnetic pulse (EMP)[10] survivability is not an issue with a nonmetallic cable. This EMP consists of a broad spectrum of energies delivered to earth by a nuclear explosion and occurs in a fraction of a second. Peak field strengths can reach tens of kilovolts per meter within nanoseconds. This intense pulse will induce extremely high voltages and currents in communications cables containing metals. Therefore, nonmetallic designs can be very attractive for military applications.

® Lightpack is a Registered Trademark of AT&T.

For riser cable applications, to serve the upper floors of buildings, a nonmetallic design is preferred for its grounding free installation. For this application, however, a stringent fire resistance requirement specified by the National Electrical Code (NEC) must be met. A sheath to meet this need was developed and will be discussed later in this paper.

In order to capitalize on these features, while providing a cost effective design, a high performance nonmetallic lightguide cable using a combination of epoxy-glass rods and impregnated glass rovings was designed. This paper will describe this new sheath design, and its mechanical and optical performance.

2. SHEATH DESIGN

The most convenient approach for a nonmetallic sheath design is to directly replace the steel strength members with appropriate nonmetallic ones. A continuous filament fiber glass roving is economical and thermally compatible with optical fibers thus making it an excellent choice. Furthermore, these rovings are impregnated with a polymer to improve their mechanical properties. At the present time the impregnated glass rovings are available in two suitable forms: rigid epoxy-impregnated rods and flexible polymer-impregnated rovings.[1] Because of low processing speeds the rods are inherently more expensive than the impregnated rovings. This factor is considered in optimizing the new sheath design.

A nonmetallic cable must meet the same optical and mechanical requirements as its metallic counterpart. A partial list of industry approved requirements that the cable must meet is shown in Table I. The strength member selection is based on the tensile load rating requirement. For example, according to the tensile requirement, the sheath must be designed for a minimum of a 2,700 N (600 lb) load rating.

During cable manufacture a hot polymer jacket is extruded directly over the strength members. The hot polymer wants to undergo a large volume change (shrinkage) during cooling. Typically the metallic strength members or rigid epoxy-impregnated rods which are used to provide tensile strength also control polymer shrinkage during processing. The completed cable then provides an ideal elastic (linear) load-strain behavior. Flexible impregnated fiber glass rovings are more economical and easier to process; however, they alone do not have adequate compressive stiffness to resist the polymer shrinkage. A suitable combination of rods and rovings is needed to obtain a desired tensile behavior of the sheath.

AT&T Bell Laboratories has developed an optimized nonmetallic sheath that has excellent optical and mechanical characteristics. A developed view of this new design is shown in Figure 2. This design effectively combines the desired properties of rigid rods and flexible rovings. Both rods and rovings are designed to give necessary tensile stiffness to meet the load rating. Furthermore, the rods minimize polymer shrinkage and the rovings offer flexibility and ease of processing. A computer simulation is used to choose the desired combination of rods and rovings so that the load-strain response is optimized.

In addition to meeting the tensile load rating, the optimized sheath design has to be rugged and environmentally stable. A good measure of environmental performance is the sheath's effective coefficient of thermal expansion. Since the flexible

Table I. EIA Test Requirements

Test	Conditions
Tensile loading and bending (FOTP-33)*	Tensile load = 600 lb Bend radius = 20 x cable OD
Compressive loading (FOTP-41)	Linear load = 1000 lb 4-inch length
Twist (FOTP-85)	± 180° twist 13-ft length 10 cycles
Low- and high-temperature bending (FOTP-37)	Bend radius = 10 x cable OD‡ Four wraps -20° F and 140° F
Cycle flex (FOTP-104)	Bend radius = 10 x cable OD‡ 180° arc 25 cycles
Cycle impact (FOTP-25)	Impact = 52 in-lb 25 impacts
Water penetration (FOTP-82)	Sample length = 3.3 ft Water head = 3.3 ft Test duration = 1 hr

* EIA Test procedures

‡ 10 x cable OD for nonmetallic and lightning protected sheath

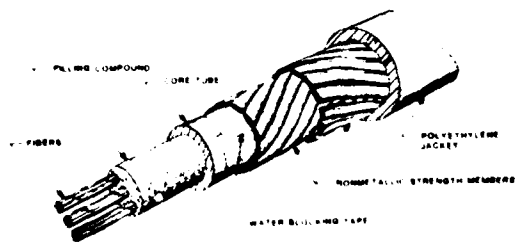


FIGURE 2. NEW NONMETALLIC CABLE

rovings have very low compressive stiffness, the sheath containing them may produce a high coefficient of thermal contraction as the temperature drops. Therefore, a suitable combination of rods and rovings is chosen to limit the thermal contraction and hence the compressive fiber strain at low temperatures.

This cable has been designed to pass the AT&T and Bellcore water penetration requirements. Water blocking in the core is provided by the conventional method of a filling compound. A water blocking tape is used over the core tube to prevent water ingress along the sheath. The tape swells upon contact with water and fills the interstices among all the strength members of both layers of crossply sheath.

A single jacket extrusion over the two layers of reinforcement completes the new sheath design. The jacket is sufficiently coupled to the core to provide desired mechanical characteristics, yet isolated from the core to prevent bonding. This feature along with the flexible rovings makes sheath entry extremely easy and fast, particularly, in mid-span.

Furthermore, this construction allows for easy torque balancing since the two layers are in direct contact with each other and have the same lay length in opposite directions. A compact, flexible and torque free design is very easy to install and simple to handle by the craftperson in the field.

3. FIRE RESISTANT RISER CABLE

The nonmetallic riser cable has been designed to meet the Underwriters Laboratories (UL), UL 1666, Riser Cable Fire test[12] requirements and it is UL classified. This test requires that the cables do not propagate fire up to the second floor opening (12 feet), when ignited by a 450,000 Btu/hr propane flame for a one-half hour duration.

The National Electrical Code (NEC) impacts on the design of riser cables by recommending practices that apply to residential and commercial buildings and structures. Specifically, since 1984, NEC article 770-6 and 800-3b permit riser cables to be installed outside of noncombustible conduit or tubing if they demonstrate fire-resistant characteristics capable of preventing the spread of fire from floor-to-floor. Underwriters Laboratories (UL) classifies products that meet the intent of the NEC.

Riser cables connect outside plant to building distribution cables. In downtown central offices they also connect interoffice and intercity trunks and, as their name implies, they provide riser distribution between two or more floors. One major difference between this design and the outside plant cables is that this design must meet stringent fire test requirements discussed above. Therefore, the high density polyethylene jacket is replaced by a fire resistant PVC jacket. Furthermore, since there is no water hazard, riser cables do not contain filling compound to minimize fuel load. These cables are generally of air-core design, and a thermal wrap is placed around the fibers for protection during core tube extrusion and against heat from fire.

4. OPTICAL PERFORMANCE

Nonmetallic cables containing up to 96 fibers have been manufactured and optically characterized. AT&T Technologies depressed-cladding single-mode fibers with core and cladding diameters of 8.3 and 125 μm, respectively, were employed. The dual-coated fibers have an outside diameter of 250 μm. Figure 3 shows histograms of fiber loss after cabling for 236 fibers at ambient temperature. This

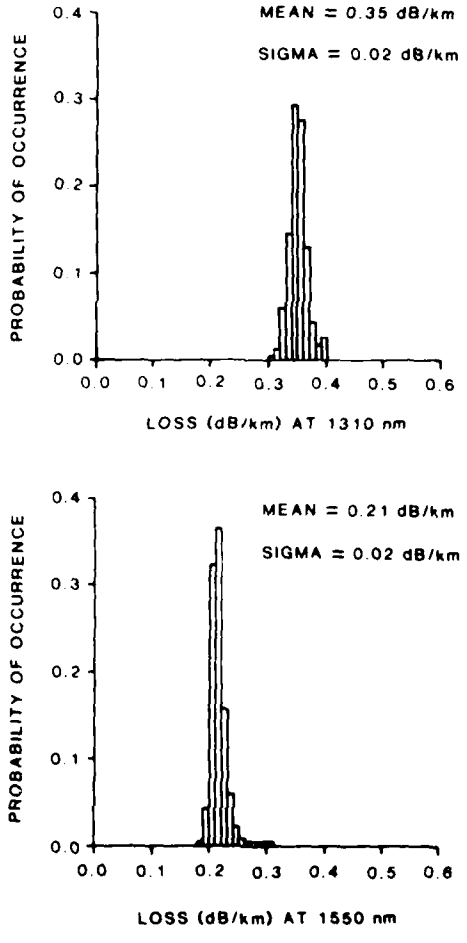


FIGURE 3. NEW NONMETALLIC CABLE PRODUCTION RESULTS

represents production data for AT&T's Lightpack cable cores with customer specified losses less than 0.40 dB/km. The mean loss is 0.35 dB/km at 1310 nm and 0.21 dB/km at 1550 nm with a standard deviation of 0.02 dB/km at both wavelengths. In addition, a Lightpack cable with 84 fibers was environmentally tested and loss measurements were made at a number of critical points during the temperature cycle. Specifically, loss measurements were made at a critical aging point of -40 C (-40 F) temperature after a five day exposure to 88 C (190 F). The mean added loss at 1310 and 1550 nm was less than 0.03 dB/km over the entire temperature range as shown in Figure 4. The added loss, however, was seen only at extreme cold temperatures. These results demonstrate excellent thermal stability between -40 C (-40 F) and 88 C (190 F).

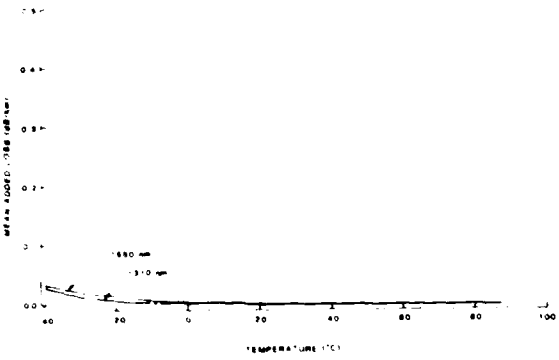


FIGURE 4. ENVIRONMENTAL PERFORMANCE

5. MECHANICAL PERFORMANCE

This new nonmetallic sheath design with both the Lightpack and ribbon fiber cable cores has been subjected to the industry standard EIA tests as well as two plow simulation tests developed by AT&T Bell Laboratories. The results show that the new sheath design passes these requirements. The EIA tests included: combined tension and bending, cyclic flex, cyclic impact, twist, compressive loading and bending at hot and cold temperatures. These tests are summarized in Table I and also comply with Bellcore requirements. In the tension and bend test, a 150-meter (490 feet) length of a one kilometer (3280 feet) test cable is looped around sheaves and subjected to a 2,700 N (600 lb) load for a minimum of 30 minutes. The sheave diameter is equal to 20 times the cable diameter. In the cyclic bend test, the cable sample is bent around a mandrel with a diameter equal to 10 times the cable diameter. The test is performed at a rate of 30 cycles per minute for a total of 25 cycles. The impact test is performed on a cable sample at the rate of 30 impacts per minute with a total of 25 impacts. In the compression test, a 4,450-Newton (1000 lb) force is applied over a 100 mm (4 inch) cable length for ten minutes. During the twist test, a cable sample is rotated ± 180° about its axis for a minimum of ten cycles. The capability of the cable to endure bending at various temperatures is evaluated during the hot and cold bend test. A cable sample is wrapped four times around a mandrel whose radius is ten times the diameter of the cable at -29 C (-20 F) and 60 C (140 F). All of these EIA tests require that there is no sheath damage and a maximum added loss of less than 0.2 dB after testing. In addition to the required EIA tensile test, load-strain behavior was measured for several nonmetallic sheath samples. The results show that the samples met the 2,700 N (600 lb) load rating.

The two specialized tests developed to simulate plowing are described by P.D. Patel and C.H. Gartside, III.[2] In the first test, a cable sample is tensioned around a 17.8-cm (7 inch) diameter pulley with a sharp 3 mm (0.12 inch) radius discontinuity. Cable tension and fiber continuity are recorded throughout the test. This test is intentionally destructive and it is terminated when all the fibers are broken or when the sheath had failed. The results show that the performance of the new sheath is equivalent to the metallic sheath.

In the second test, a cable sample is repeatedly squeezed through a series of three rollers over a ten-foot test length. This test simulates abuses of the cable encountered in certain aerial as well as plowing installation. Cable pulling tension and fiber continuity are recorded throughout the test. This also is a destructive test and it is terminated when all the fibers are broken or when the sheath had failed. A 84-fiber Lightpack cable of the new nonmetallic design was tested. Figure 5 shows the percentage of broken fibers as a function of cumulative squeeze. Since the flexible rovings are softer than the metallic wires, they act as a buffer and enhance the mechanical performance as shown by this test.

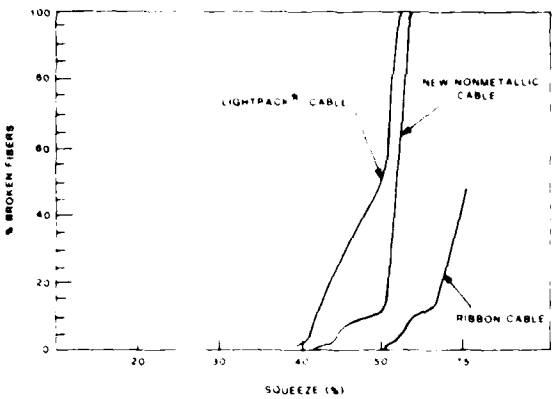


FIGURE 5. SQUEEZE TEST RESULTS

6. CONCLUSIONS

A high performance nonmetallic sheath has been developed for both the ribbon and Lightpack cables and many kilometers have been commercially deployed. The new design is flexible yet rugged and passes stringent mechanical testing. The design is optimized using an analytical model and computer simulation. The design offers excellent optical performance at ambient temperature and superior thermal stability between -40 C (-40 F) and 88 C (190 F). A UL classified fire-resistant riser cable is also available that provides floor to floor distribution in a building. The new design is very easy to handle and simplifies mid-span entry.

7. ACKNOWLEDGEMENTS

The authors would like to thank all members of AT&T Technologies and AT&T Bell Laboratories who have contributed to this development. Our special thanks to G. H. Webster for assistance in the development of the riser cable and L.C. Hotchkiss for coordinating the optical loss measurements.

REFERENCES

1. P. F. Gagen and M. R. Santana, "Design and Performance of a Crossply Lightguide Cable Sheath," IWCS 1979.

2. P.D. Patel and C.H. Gartside, III, "Compact Lightguide Cable Design",IWCS 1985.

3. C. H. Gartside, III and J. L. Baden, "Single-Mode Ribbon Cable and Array Splicing," Telephony, p. 80, June 17, 1985.

4. C. H. Gartside III, A. J. Panuska, and P. D. Patel, "Single-mode Cable for Longhaul,Trunk, and Loop," AT&T Technical Journal, Vol. 66, Issue 1, January-February 1987.

5. M. R. Reynolds, C. J. Arroyo, and M. D. Kinard, "Primary Rodent and Lightning Protective Sheath for Lightguide Cable," IWCS 1986.

6. W. Schmidt, K. Kimmich, and S. Metz, "Self-Supporting Metal Free Optical Fiber Cable for Large Span Length," IWCS 1982.

7. O. Ichikawa, K. Sakamoto, and Y. saitoh, "Development of Nonmetallic, Loose-Groove Spacer-Type Optical Fiber Cable," IWCS 1982.

8. E. Hayasaka, F. Ohtsuka, M. Monma, S. Ohira, H. Horima, K. Yamashita, M. Dazai, and N. Abe, "Non-Metallic Optical Cable with Optical Fiber Catenary for Long Span Aerial Application," IWCS 1983.

9. H. G. Haag and P. E. Zamzo, "Non-Metallic Long Span Aerial Cable with Optical Fibres for the Use at 1.3 μm," IWCS 1983.

10. Tippe Anthony P. , "The Threat of Electromagnetic Pulse," American Defense Preparedness Association (APDA) National Defense, December 1984.

11. M. M. Girgis and M. G. Decker, "Impregnated Fiber Glass Yarn for Reinforcing Fiber Optic Cables," IWCS 1986.

12. Underwriters Laboratory (UL) 1666 "Standard Flame Test for Cable Run Vertically in Shafts."



C. John Arroyo is a Member of Technical Staff at AT&T Bell Laboratories, Norcross, GA. He joined Bell Laboratories in 1969 after receiving his AAS degree in Mechanical Technology from New York City Community College. Since 1972 he has worked in Fire Research Technology and is currently a member of the Lightguide Cable Group engaged in sheath design, rodent-lightning protection and standardization of cable specifications.



P. D. Patel is a Distinguished Member of Technical Staff at AT&T Bell Laboratories, Norcross, Georgia. He joined Bell Laboratories in North Andover, Massachusetts in 1969 after receiving degrees in Mechanical Engineering, including a B. E. from Maharaja Sayajirao University, India, and Engr. Sc. D. degrees from Columbia University. Since 1979 he has worked in the Lightguide Technology Department at Norcross and is currently working in the Exploratory Lightguide Cable Group. He is a member of the American Society of Mechanical Engineers.



Artis C. Jenkins joined AT&T Bell Laboratories in Norcross, Georgia in 1980. Prior to 1986, his responsibilities included military cable design, nonmetallic sheath design, cable testing and cable termination. Currently, he is the supervisor of the Lightguide Building and LAN Cable Group. He received his BSME degree in 1976 and worked as a design engineer at Eastman Kodak in Kingsport, Tennessee from 1976 through 1978. He received his MS and Ph.D. from Georgia Institute of Technology in 1980 and 1984 respectively from the School of Mechanical Engineering. He is an associate member of the American Society of Mechanical Engineers.



Andrew J. Panuska is a Senior Development Engineer with AT&T Network System in Norcross, Georgia. He joined AT&T in 1963 after receiving B. S. degree in Mechanical Engineering and Civil Engineering, both from Johns Hopkins University. He is responsible for the development of lightguide cable products and processes.

Dry Type Water-Blocking Optical Fiber Tape Cable with Slotted Rod

Masumi Fukuma, Nobuhiro Akasaka, Shuzo Suzuki

Sumitomo Electric Industries, Ltd.
1, Taya-cho, Sakae-ku, Yokohama, 244, Japan

Abstract

A novel water-blocking optical fiber cable which used water-absorbing material has been developed. This cable has a central slotted rod with six slots in each of which two 4 count-fiber-tapes and a water-absorbing tape are accomodated. The cable joining operation has become easier compared with jelly filled cables. In this paper, the design criteria for accomodating water-absorbing tapes and experimental results concerning water-blocking properties, thermal properties and mechanical properties are described.

1. Introduction

When an optical fiber cable is inundated with a water, the strength of the optical fiber is degradated and the optical fiber transmission loss may be increased by hydrogen which is generated by a chemical reaction between water and components of the cable [1]. Therefore, the performance of water-blocking is needed for an optical fiber cables.

There are two water-blocking methods, one method is gas-pressurizing maintenance which uses air-core cables which are filled with dry-air after installation. The other method uses water-blocking cables which are filled with water-proof materials in the cable. The air-core cable has a maintenance cost during operation of this communication system. However, water-blocking cables have no maintenance cost. Therefore, when the optical fiber cable is applied to the field without gass-pressuring maintenance system, water-blocking cable must be used.

Recently, the water-blocking cable is attractive from the viewpoint of maintenance free cable systems [2]. However conventional water-blocking cables which are jelly filled cables and water-absorbing powder filled cables have some problems in the cable joining operation, such as degradation of workability due to the viscosity of jelly [illegible] on the human body resulting from [illegible] of water-absorbing powder.

[illegible] present a new type of water-[illegible] is free from these problems.

2. Requirements

The water-blocking optical fiber cable can be used for trunk and subscriber transmission line systems. Design of the water-blocking cable was done with taking the following considerations *in mind*;

1) The water-blocking properties should be excellent in order to keep longterm reliability of optical transmission lines. We set the permissible water-penetration length which was less than 0.5 m at 1 m water-head pressure from the viewpoint of thermal properties of water penetrated cable portion.

2) The dielectric optical fiber cable is necessary to the system in which an optical fiber cable is used in the serious electromagnetic influence.

3) A compactness, light weight, and easy operation of cable joining are required for the cable structure when optical fiber cable is used by subscribers. The cable diameter should be minimized.

4) The water-blocking optical fiber cable should have sufficient stability for temperature cycling, and be able to withstand various mechanical forces. These properties should be as good as those of air-core optical fiber cable.

With these factors in mind, our water-blocking optical fiber cable has been designed.

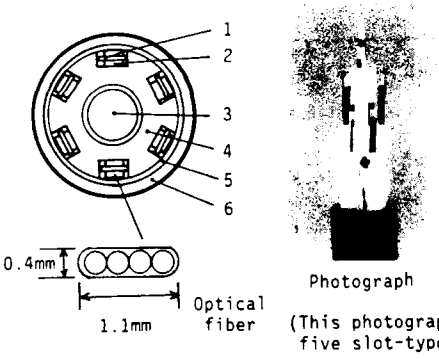
3. Cable design

3.1 Structural design

The cross-sectional structure and the side view photograph of the newly developed water-blocking optical fiber cable are shown in Figure 1. The structure of cable was based on the tape-slot type cable [3]. An optical fiber tape is composed of four single mode fibers which are individually coated up to 250 μm in diameter with UV-curable resin, and these fibers are further coated by UV-curable resin. The thickness and width of the fiber tape are 0.4 and 1.1 mm, respectively. A

Slotted rod is made of polyethlene, and six rectangular slots are provided hellically on the rod. The strength member in the center of the slotted rod is selected as FRP (Fiberglass-Reinforced Plastics), which has the advantages of low weight and being free from electromagnetic influence. The diameter of tne slotted rod is designed to be 8.0 mm. Two fiber-tapes and a water-absorbing tape are tightly embedded in each slots with a residual tensile strain of about 0.05 %. The acrylic-acid water-absorbing material was selected concerning the material of water-absorbing tape, water-absorbing materials which are not selected with regard to the appropriate tests may generate hydrogen in the cable when it is exposed to muddy water containing a large number of microorganisms. It has been confirmed that our acrylic-acid water-absorbing material passed the appropriate decomposition test[4].

Water-absorbing tapes are wound around a slotted rod. An outer-sheath is coated up to 11 mm in diameter by extruding low density polyethylene. The cable is able to accomodate 48 fibers and its weight is 105 kg/km. The structure of this cable can provide a compact water-blocking optical fiber cable when it is applied to a high-fiber count optical fiber cable.



4 count-fiber-tape

1. Water-absorbing tape
2. Fiber-tape
3. FRP strength member of 3.4 mmφ
4. Slotted rod
5. Water-absorbing tape
6. Outer sheath

Figure 1 Cable structure of water-blocking optical fiber cable

3.2 Design of water-blocking performance

A water-absorbing material blocks the water penetration by swlling up the penetrated water and rapidly expanding those volume inside the cable. Therefore, the water penetration length depends on the filling density of water-absorbing materials in the cable [5]. When the water-absorbing materials are applied to a tape-slot type cable, the optimum filling density of water-absorbing material should be determined in order to achieve both good water-blocking properties and transmission characteristics of the cable, because optimum space in the slot is necessary to get the mechanical and thermal stability of the cable.

In order to determine the minimum filling density of water-absorbing materials in the slot, the relationship between the water-penetration length and the filling density was measured by the experimental set up as shown in the inset of Fig. 2 Figure 2 shows the experimental results where M is the ratio of the cross-sectional area of water-absorbing materials and that of the inner cross section of the glass tube, and R is the water-absorbing ability which is defined as the ratio of the weight of the saturated swelled water-absorbing material and that of dry water-absorbing material. In the experiment, water-absorbing material was filled in a glass tube having an inner diameter of 9 mm with the filling density as a parameter, and the tube was applied to 1 meter water head pressure with salt water (NaCl 0.75g + $CaCl_2$ 0.5g in the liter water) was applied to the tube [6]. The experimental results show that the water-penetration length was reduced by increasing the filling density M·R. The measured penetration length l can be expressed by the following equation

$$l = a\left(\frac{1}{M \cdot R}\right)^{\alpha} + l_{\infty} \quad [m] \qquad (1)$$

, where a and α are constants which are determined from the experiment, and l_{∞} is the water-penetration length expected for the infinite filling density of M·R. The values of a, α, and l_{∞} of our absorbing materials are determined to be 2.89, 2.18 and 0.12, respectively.

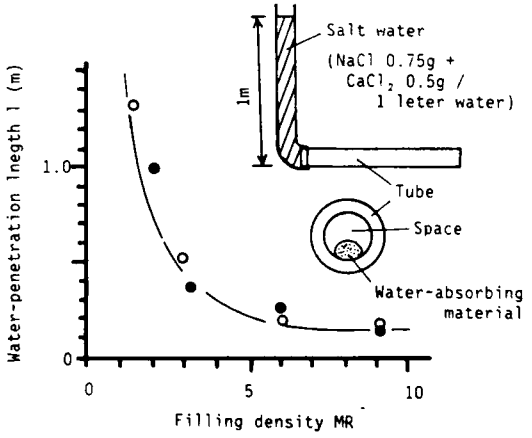


Figure 2 Relationship between water-penetration length and filling density

On the other hand, the optimum space design of the slot must be considered to realize mechanical and thermal stability. The value of the accommodating ratio Ms is required to be in the range of 0.45 to 0.55 from the experimental results of tape-slot type cable. Where, Ms is defined as the ratio of cross-sectional area of contents, that is, two fiber tapes and water-absorbing materials in a slot and that of a slot. The accomodating ratio Ms is expressed by the following equation

$$Ms = \frac{S_T + Sa}{Ss + S_T + Sa} \qquad (2)$$

, where Ss is the cross-sectional area of space in the slot, S_T is the total cross-sectional area of two fiber tapes, and Sa is the cross-sectional area of a water-absorbing tape in the slot.

In the design of a water-blocking cable, M = Mo is determined by equation (1) when the required penetration length l is given to be lo and R is determined by the selection of water-absorbing material. On the other hand, Mo is already defined as

$$Mo = \frac{Sa}{Sa + Ss} \qquad (3)$$

The equations (2) and (3) can be transformed to equations (4) and (5)

$$Sa = \frac{Ms}{1 - Ms} Ss - S_f \qquad (4)$$

$$Sa = \frac{Mo}{1 - Mo} Ss \qquad (5)$$

The solutions of equations (4) and (5) give the dimensions of required cross-sectional area Ss of space in the slot and cross-sectional area Sa of water-absorbing tape. From equations (4) and (5), the design deagram for Sa and Ss is obtained as shown in Figure 3. Sa and Ss are determined to be 0.18 mm^2 and 1.0 mm^2, respectively considering the following:

(1) Water-penetration length is less than 0.5 m

(2) Cross-sectional area of water-absorbing tape should be minimized

(3) Considering manufacturing of error of slot dimension is around 0.1 mm.

4. Cable performance

The arrangement of two optical fiber tapes and a water-absorbing tape in the slot is determined through trial manufacturing and the finally designed cable is shown in Figure 1. The wave-absorbing tape is sandwiched between two optical fiber tapes. The single mode fibers have the mode field diameter of 10 μm and the cut-off wavelength of 1.1 ∿ 1.3 μm .

4.1 Transmission loss

The transmission losses at each stage of the manufacturing process were measured. The average transmission losses at the two wavelengths of 1.3 μm and 1.55 μm are shown in Figure 4 for each process. The changes in transmission loss were within 0.03 dB/km during each process and the average losses at 1.3 μm and 1.55 μm were 0.36 and 0.23 dB/km, respectively. It can be concluded that there is no excess loss during manufacturing processes.

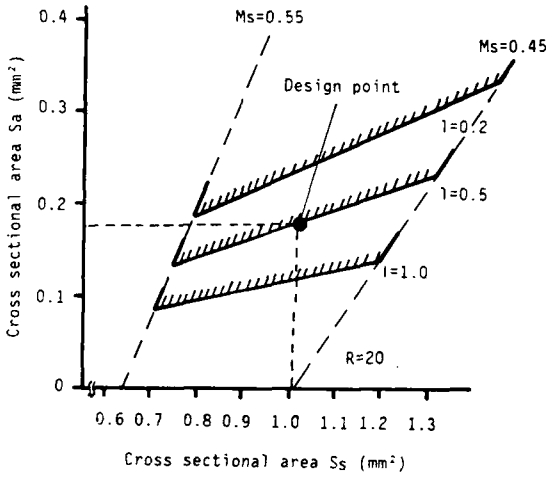
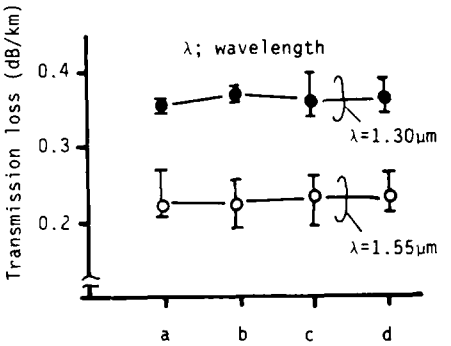


Figure 3 Design diagram for cross sectional area of space in a slot and that of water-absorbing tape which ahs the water-absorbing ability (R=20)



a: Optical fiber
b: Fiber-tape
c: Cable core
d: Cable

Figure 4 Transmission loss in cabling process

4.2 Water-blocking properties

The water-blocking cable will be penetrated by many kinds of water in practical application. The water-blocking properties of this cable for a salt water and alkaline water are shown in Figures 5 and 6. In Figure 5, a salt water which contains 0.75g NaCl and 0.5g $CaCl_2$ in a liter of water is used. The penetration length was 0.5 ∿ 0.6 m at 1 m water head pressure. It is indicated that the manufactured cable has the water-blocking performance as expected from Figure 3. The time dependence of water-penetration length was very small for all conditions of 1.0 to 5.0 m water head pressure. The water head pressure dependence was saturated in the pressure region higher than around 3 m water head pressure. The water penetration length was less than 1.3 m even at 5 m water head pressure which corresponds to the maximum depth of a manhole.

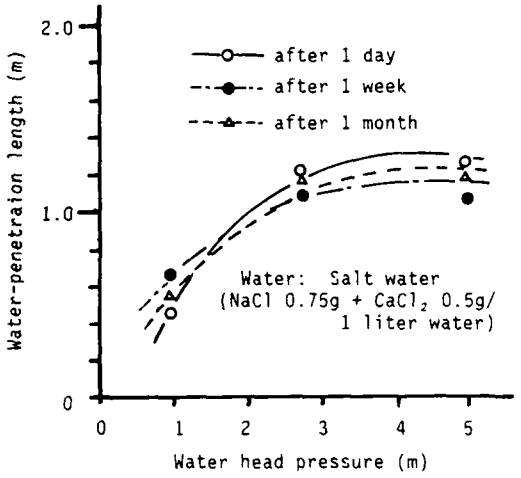


Figure 5 Water head pressure dependence of water-penetration length

(Different samples were used for 1 day, 1 week and 1 month measurement)

Figure 6 shows the pH dependence of the water-penetration length for alkaline water. The water-penetration length was slightly increased by increase in pH, and the penetration length for pH 11 alkaline water was less than 0.8 m after one week. The value of pH 11 corresponds to the largest pH of alkaline water in a Japanese manhole.

In order to investigate the thermal properties of the water penetrated cable portion, the water penetrated cable was manufactured as follows. The cable core all of which was immersed in water was made and then, the cable core was wond by rubber tape to protect evaporation of penetrated water. Figure 7 shows the thermal properties of this intentionally water immersed cable. The transmission loss increase was observed in low temperature region from 0 to -40 °C. It will be the microbending loss which is caused by freeze of the water which penetrated the cable. The maximum excess loss was 0.5 dB/km at -40 °C. Therefore, the excess loss of 0.5 m water penetrated cable portion at -40 °C was 2.5 x 10^{-4} dB. This experimental result confirms us that the water-blocking properties of the newly developed cable is sufficient for practical application.

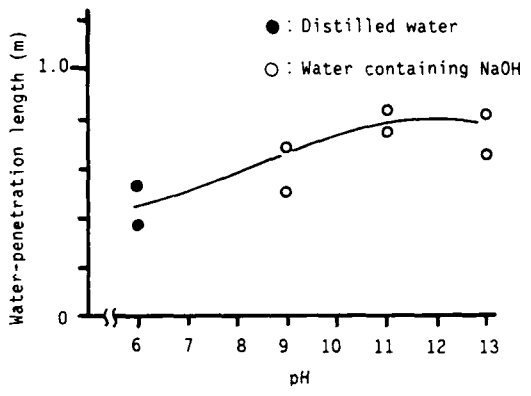


Figure 6 pH dependence of water-penetration length

(Water head pressure was 1 m)

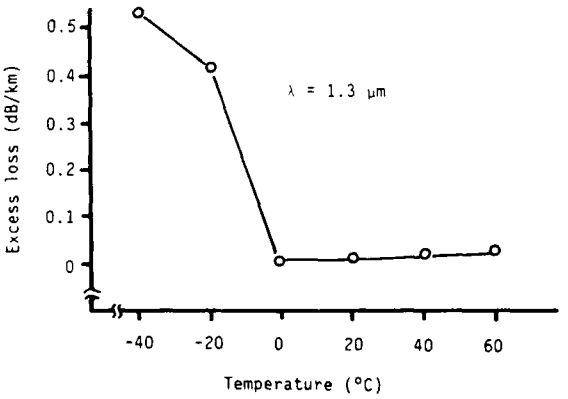


Figure 7 Thermal properties of water-penetrated cable

4.3 Thermal properties

Figure 8 shows the transmission loss change of the water-blocking cable in the range from -40 to 60 °C for two cycles (1 cycle takes 60 hours). The transmission loss was measured with on LED light source of 1.3 μm wavelength. The transmission loss change was within 0.04 dB/km. The experimental results indicate there was no significant degradation.

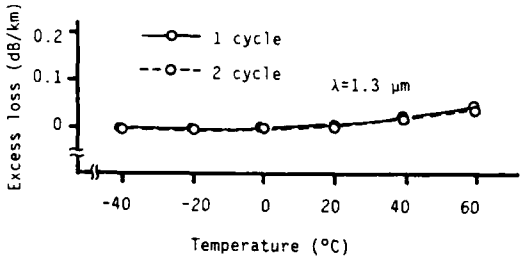


Figure 8 Thermal properties of water-blocking cable

4.4 Mechanical properties

Mechanical characteristics were examined against lateral force, tensile strength, bending, impact, twist and squeezing. Table 1 shows methods of mechanical test and results for various mechanical tests. Mechanical characteristics of both the water-blocking cable and water penetrated cable portion were measured. The transmission loss change was measured by on LED light source of 1.3 μm wavelength.

(A) Lateral force test
A lateral force was applied to a 50 mm length of cable. The excess loss was not observed up to 500 kg. These results are as good as those of an air-core cable. The excess loss by a lateral force applied to a water penetrated portion was not also observed up to 500 kg.

(B) Tensile test
The relationship between strength and elongation which were measured for optical fiber and cable is shown in Figure 9 involving excess loss changes. No significant excess loss was obsorved up to the fiber elongation of 0.48 %, and the elongation of optical fiber is almost the same as the elongation of the cable. These results show that the optical fiber are tightly embedded in the slots. No excess loss was also observed for water penetrated cable against tensile strength.

(C) Bending test
The cable was bent by ±180 degrees to the right and left repeatedly around various mandrels. The minimum permissible bending diameter which corresponds to the diameter of 0.01 dB loss increase was 120 mm. The minimum permissible bending diameter for a water penetrated portion was also 120 mm.

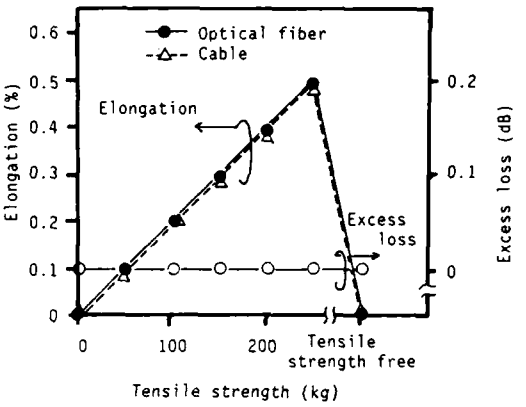


Figure 9 Relationship between tensile strength and elongation of optical fiber and cable (involving excess loss)

(D) Impact test
A hammer was dropped 5 times on the same position of the cable for a given impact energy which are 1.2 and 3 kg·m. No significant transmission loss increase was observed even at 3 kg·m of impact energy.

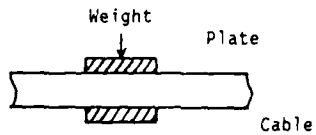
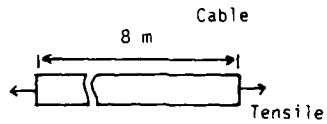
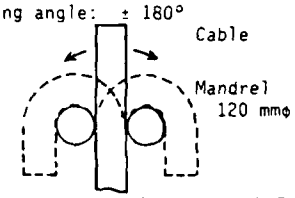
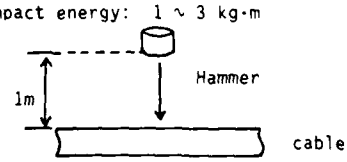
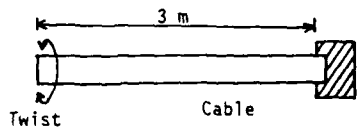
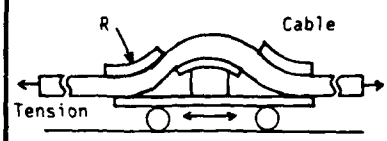
(E) Twist test
The cable of 3 m length was twisted by ±720 degrees. No significant transmission loss increase was observed.

(F) Squeezing test
The Table 1 shows sketch of squeezing test set up. There are 3 squeezing wheels which radii are 250 mm. The cable was squeezed under a tension of 50, 100 and 200 kg respectively. Each tension was chosen as a designed elongation of optical fiber of 0.1, 0.2 and 0.4 %. The squeezing length of water blocking cable and water penetrated cable portion are 100 m and 8 m. During the squeezing, no change in the transmission loss was observed including impulsive flactuation.

5. Conclusion

A novel dry-type water-blocking optical fiber cable has been developed which uses water-absorbing tapes. The cable joining operation becomes easier compared with jelly filled cables. The design criteria of accommodating water-absorbing tape is also clarified, and it is confirmed that the cable has excellent water-blocking, mechanical and thermal properties under adverse conditions. This cable will contribute to the construction of a maintenance free cable system.

Table 1 Mechanical test methods and results

Test items	Test methods	Results
Lateral force test	Plate length: 50 mm 	No loss increase at 500 kg/50mm.
Tensile test	Tensile speed: 10 mm/min 	No loss increase up to the tensile strength of 250 kg.
Bending test	Bending angle: ± 180° 	No loss increase at the bending diameter of 120 mmφ after 10 cycle.
Impact test	Hammer dia.: 25 mm Impact energy: 1 ∿ 3 kg·m 	No loss increase up to the impact energy 3 kg·m.
Twist test	Twist angle: ± 720° 	No loss increase within the twist angle of ± 720°.
Squeezing test	Squeezing wheel radius R: 250 mm. 	No loss increase up to the tensile strength of 250 kg.

References

[1] Y. Mitsunaga, T. Kuwabara, T. Abe and Y. Ishida, "Molecular Hydrogen Behaviour for Loss Increase of Silica Fiber in Cable Filled with Water", Electron. Lett., 20, pp. 76 ~ 78 (1984).

[2] Y. Kameo, H. Horima, S. Tanaka, Y. Ishida and Y. Koyamada," Jelly-filled Optical Fiber Cables", IWCS, 30, pp. 236 ~ 243 (1981).

[3] S. Hatano, Y. Katsuyama, Y. Kokubun and K. Hogari, "Multi-hundred-fiber Cable Composed of Optical Fiber Ribbons Inserted Tightly into Slots", IWCS, 35, pp. 17 ~ 23 (1985).

[4] H. Koga, Y. Mitsunaga and T. Kuwabara, "Hydrogen Generation due to Decomposition of Carboxymethyl-Cellulose in muddy Water", Electron. Lett., 26, pp. 902 ~ 903 (1985).

[5] S. Kukita, M. Kawase and F. Nihei, "Novel Waterproof Optical Fiber Cable with Absorbent Polymer Yarn", Trans. IECE, Japan (Section E), E69, 2, pp. 89 ~ 91 (February 1986).

[6] S. Kukita, Y. Nakai, A. Hayashi and H. Koga, "A New Nonmetallic and Water Proof Optical Fiber Cable with Absorbent Polymer Ribbon", IWCS, 36 (1986).



Nobuhiro Akasaka

Sumitomo Electric Industries, Ltd.

1, Taya-cho, Sakae-ku
Yokohama, Japan

Nobuhiro Akasaka received a M.S. degree in Chemical Engineering from Tokyo University in 1983. He joined Sumitomo Electric Industries, Ltd. in 1983, and has been engaged in research and development of optical fiber and cables. Mr. Akasaka is a member of Transmission Media R & D Department, Yokohama Research Laboratories.



Shuzo Suzuki

Sumitomo Electric Industries, Ltd.

1, Taya-cho, Sakai-ku
Yokohama, Japan

Shuzo Suzuki received a M.S. in 1972 from Tokyo University. He joined Sumitomo Electric Industries, Ltd. in 1972, and has been engaged in research and development of optical fiber, cable and jointing technologies. He is a member of the Institute of Electronics and Communication Engineers of Japan.



Masumi Fukuma

Sumitomo Electric Industries, Ltd.

1, Taya-cho, Sakae-ku
Yokohama, Japan

Masumi Fukuma received a M.S. degree in Electrical and Electronic Engineering from Toyohashi University of Technology in 1985. He joined Sumitomo Electric Industries, Ltd. in 1985, and has been engaged in research and development of optical fiber and cables. Mr. Fukuma is a member of Communication R & D Department in Yokohama Research Laboratories.

A New Nonmetallic and Waterproof Optical Fiber Cable with Absorbent Polymer Ribbon

Shigezou KUKITA, Takashi NAKAI, Akira HAYASHI, and Hiroaki KOGA

NTT Transmission Systems Laboratories,
Nippon Telegraph and Telephone Corporation,
Tokai-mura, Ibaraki-ken, 319-11, Japan

Abstract

This paper proposes a new, nonmetallic, optical fiber cable waterproofed with absorbent polymer. The cable can construct the transmission line at low cost and does not require maintenance. This paper describes design methods and evaluation methods to achieve the proposed cable.

A waterproofing technique is investigated based on the selection of absorbent polymer for its long-term stability. Also studied is the waterproof structure design with absorbent polymer ribbon. As a nonmetallic technique, a sheath design for the suppression of shrinkage and moisture permeation, and a strength member design to endure a long-term fatigue, are clarified. A nonmetallic water penetration sensor, composed of a fiber and a shrinkable thread, is also proposed.

Cables manufactured using these new designs showed performance sufficient for practical application.

1. Introduction

The demand for broad-band telecommunication networks has been increasing. To comply with the demand, it is becoming necessary to construct and maintain the network which is composed of optical fiber cables at low cost. To make the construction cost lower, a cable is desired which is small in diameter and light-weight, and which has easy operation in jointing. As for maintenance cost, a maintenance-free cable is necessary.

Conventional optical fiber cables are grouped into two classes from the view point of maintenance techniques. One is a gas-pressurized cable, and the other is a jelly-filled cable.

The gas-pressurized cable exhibits high reliability, though it has some demerits. These are its excessive weight due to the usage of metallic material, such as its LAP (Aluminum Laminated PE) sheath and copper wire for monitoring gas leaks. Also, its diameter is large, because of the assembled gas-pipe to supply gas into the space of the cable. Additionally, the gas-pressurized cable can not be applied in areas subject to electro-magnetic interference because it uses metallic materials. This means that it cannot make full use of the distinctive features of the fiber.

The jelly-filled cable, on the other hand, is inherently waterproof, making such a maintenance system unnecessary. The tack of jelly-compound, however, degrades the efficiency of manufacturing, fiber inspection, and cable jointing. To improve the operation efficiency of jelly-filled cables, a few waterproof cables filled with powder (composed of calcium carbonate and polymeric resin[1], or stearate-coated chalk and polyacrylamide[2]) have been proposed. However, it was pointed out that these cables have a problem in that the powder negatively influences the manufacturing and operating circumstances. They also have a bad influence on the health of operators, as the powder diffuses into the air[3].

As mentioned above, conventional cables are not suitable for lowering the construction and maintenance costs. Also, they can not make full use of the distinctive features of fibers.

To solve these subjects, this paper proposes a new optical fiber cable which is nonmetallic and waterproofed with absorbent polymer ribbon instead of jelly-compound. This paper describes the development process of this cable, and discusses the following concerns.

(1) The selection method of the absorbent polymer.
(2) The waterproofing design with the absorbent polymer.
(3) The nonmetallic sheath design.
(4) The nonmetallic strength member design.
(5) The nonmetallic water penetration sensor design.
(6) The manufactured cable characteristics.

2. Investigations regarding design

To make the cable waterproof and nonmetallic, it is necessary to study the following.

A. Waterproofing technique.
(1) Absorbent material selection, and long-term reliability checks, as applied to waterproofing material.
(2) Determination of allowable penetration length and the design of waterproofing structure with absorbent material to satisfy the allowable values.
(3) Waterproofing test method to precisely evaluate the waterproof ability of the cable.

B. Nonmetallic technique.
(1) Nonmetallic sheath design to suppress shrinkage of the sheath and to resist moisture permeation.
(2) Nonmetallic material selection for the strength member, and an appropriate method to suppress the long-term fatigue of the material.
(3) Design of a nonmetallic water penetration sensor, using an optical fiber and a shrinkable thread.

C. Manufactured cable evaluations.
Evaluations of a manufactured cable, conducted in the field.

3. Waterproofing technique

It should be emphasized that the waterblocking mechanism of an absorbent polymer is completely different from that of a conventional jelly-compound. The jelly-compound is designed to keep water out of the cable. However, the absorbent polymer first absorbs the penetrated water, and then swells up, constructing a waterblocking dam in the cable space. Therefore, a new waterproofing structure should be designed, and a waterproofing test method should be established to precisely evaluate the waterproofing ability.

3.1 Selection of absorbent material

Many kinds of absorbent polymers, such as synthetic polymers (e.g., poly-acrylic-acid, isobutylene, and PVA) and natural polymers (e.g., cellulose and starch), have been developed. However, most of these are for short-term sanitary use, rather than industrial use.

Requirements to apply an absorbent polymer to the waterproofing material of a cable are as follows.
(1) Superior waterblocking ability.
(2) No negative effect on the material constructing the cable.
(3) Long-term stability.
(4) Fit for the manufacture as well as the jointing efficiency of the cable.

Here, evaluating methods which meet these requirements are proposed. Also, one type of poly-acrylic-acid absorbent polymer is selected, with special consideration given to its long-term stability.

1. Long-term stability evaluation of absorbent polymers

An absorbent polymer applied as a waterproofing material should satisfy the following stability requirements. It should provide:
(1) Resistance against decomposition by microorganisms contained in soil water.
(2) Stability when subjected to long-term temperature fluctuations.

1.1 Decomposition by microorganisms

Several tests are currently used to evaluate a material's resistance to microorganism decomposition. These include the MIL-E-5272C test, and the AATCC Test Method 90. However, these tests evaluate resistance only with respect to specific kinds of microorganisms. They are not suitable for evaluating resistance to the broad spectrum of microorganisms contained in soil water. Thus, the following simple and practical method, is proposed taking into account the actual conditions under which waterproofing materials are applied.

A. Method for evaluating microorganism decomposition

Two samples (in flasks) were used to evaluate the extent of decomposition due to microorganisms. Sample A contained soil water which had been poured through filter paper, an absorbent polymer, and ammonium dihydrogenphosphate ($NH_4H_2PO_4$). The $NH_4H_2PO_4$ is a kind of manure. Many decomposition test results have shown that $NH_4H_2PO_4$ accelerates the growth of microorganisms. Sample B contained absorbent polymer and filtered soil water to which sodium azide (NaN_3) was added, instead of $NH_4H_2PO_4$. The NaN_3 is a germicide. Both flasks (containing air at 1 atm) were sealed by teflon cocks and stored at 30 °C, which is an ideal temperature for microorganism growth.

The following evaluations were carried out using these samples:
(a) The gases generated in the flasks, as well as their partial pressures, were examined by gas-chromatography.
(b) The viscosity of the solutions was measured.
(c) The external appearance of the solutions was examined.

B. Evaluation results

The results of the gas analysis for a typical natural absorbent polymer in Sample A are shown in Fig.1. The nitrogen and oxygen gas pressures gradually decreased, and hydrogen gas began to appear after 3 days. This is a typical decomposition phenomenon associated with the activity and growth of microorganisms.

Furthermore, the measured viscosity of Sample A decreased rapidly from 5 poise to 0.02 poise after 15 days. This value is almost equivalent to the viscosity of water. On the other hand, the viscosity of Sample B remained almost constant over 20 days. The viscosity change in Sample A is also indicative of microorganism decomposition.

These phenomena, which indicate microorganism decomposition, occur with almost all natural absorbent polymers. Some synthetic absorbent polymers are even decomposed by microorganisms. Therefore, before selecting an absorbent polymer for use in an optical fiber cable, it is essential that the above tests be carried out.

C. Effect of microorganisms on optical fibers

The effect of microorganisms on the wavelength loss characteristics of optical fibers was measured using a 300-meter-long graded-index fiber. The fiber was soaked in soil water at 30°C for 20 days. The soil water consisted of filtered soil water,

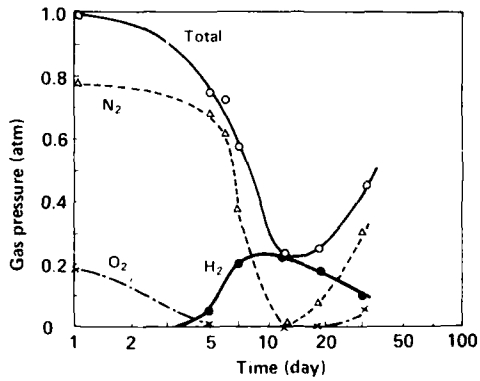


Fig.1 Gas pressure in a flask (in which absorbent polymer and soil water were mixed) as a function of time

absorbent polymer, and $NH_4H_2PO_4$. The results are shown in Fig.2. Fiber loss increased markedly at 1.24 μm, 1.70 μm, and 1.88 μm. This result indicates that the hydrogen gas generation, due to microorganism decomposition, causes changes in wavelength characteristics.

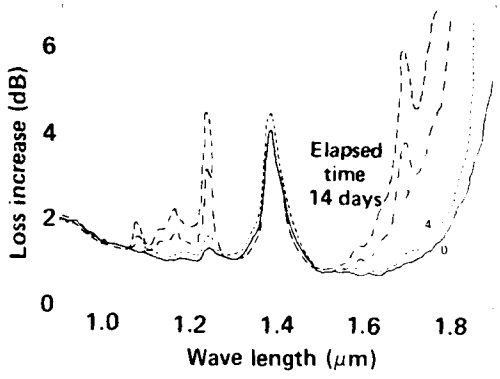


Fig.2 Change in wave-length characteristics due to microorganism decomposition

2. Thermal stability

Absorbent polymers with water (wet condition) and without water (dry condition) must maintain their absorptive and waterblocking performance for more than ten years.

2.1 Degradation of absorption characteristics (dry condition)

The aging characteristics of dry absorbent polymers were evaluated by examining the water absorbing ability after the absorbent polymer had been stored at temperatures of 90℃, 150℃, and 200℃. The absorption ratio is defined as the maximum water volume that a unit weight of absorbent polymer can absorb. The relationship between time and temperature, when the absorption ratio degrades to 80% or 50% of the initial value, is shown in Fig.3. The fact that the absorption ratio degrades with both time and temperature indicates that cross-linking in the absorbent polymer is destroyed by heat, resulting in an altered absorption performance. From interpolating these results, it can be stated that Synthetic polymer A maintains an absorption ratio greater than 80% of its initial value, and exhibits sufficient absorptive characteristics, even after 10 years. However, Synthetic polymer B can be expected to lose its absorbing ability after about 2 years.

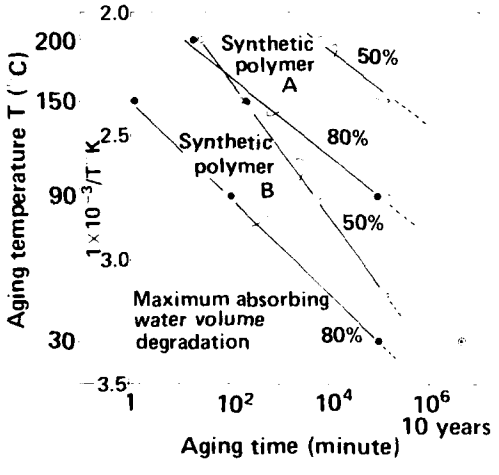


Fig.3 Degradation in absorbing characteristics of absorbent polymers due to temperature variation over time

2.2. Degradation of waterblocking characteristics (wet condition)

When water penetrates a cable, the absorbent polymer swells and changes into a gel, which forms a waterblocking dam.

The long-term waterblocking ability was evaluated by measuring the viscosity of the gel. The results are shown in Fig.4. After 240 hours (10 days) at 60℃, the viscosity of Synthetic polymer B decreased markedly. It fell to less than 0.03 poise, which is almost equal to the value of water. Meanwhile, the viscosity of Synthetic polymer A remained almost the same as its initial value.

The reduced viscosity results in a greater water penetration length. Glass pipes filled with absorbent polymer were set at 60℃, and a water pressure level at 1 meter was applied through the cross-section of the pipe. Then the penetration

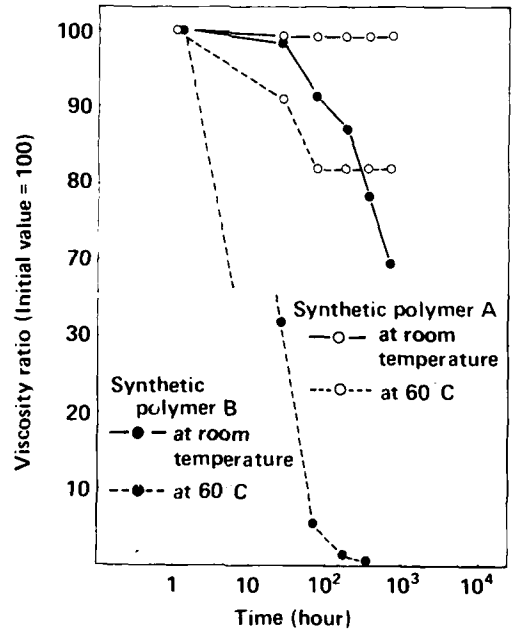


Fig.4 Viscosity changes in absorbent polymer gel due to thermal degradation as a function of time

length was measured. The results are shown in Fig.5. It is clear that the viscosity change results in degradation of the waterblocking ability.

These results show that microorganism decomposition and thermal stability must be evaluated in order to properly select the absorbent polymer. The evaluations demonstrated that the Synthetic polymer A, that is, the poly-acrylic-acid, is suitable for use as a waterproofing material.

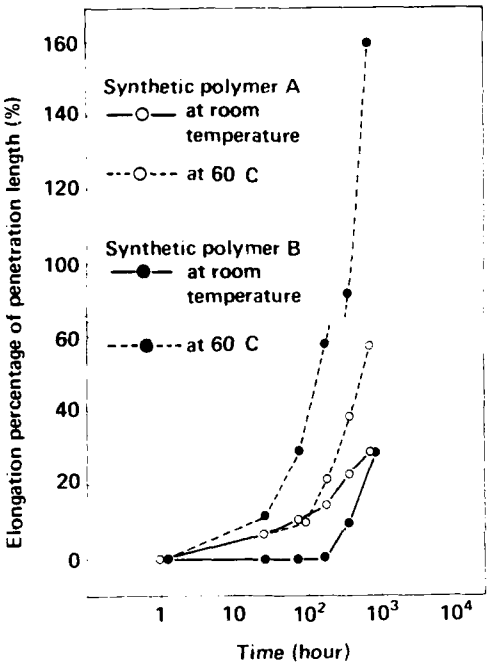


Fig.5 Increase in penetration length due to thermal degradation of absorbent gel as a function of time

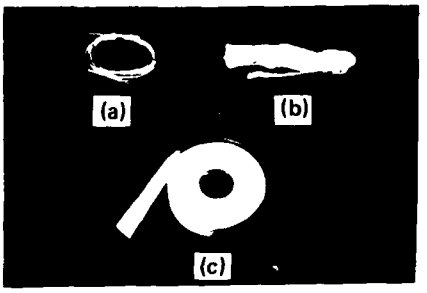
3. Processing of absorbent polymer

The absorbent polymer which was selected contained two kinds of source material, fiber and powder. To apply these absorbent polymers to cables, form processing of the source material is important to permit efficient manufacturing and operation. Especially with regard to powder, form processing is indispensable to prevent its scattering in the air.

The absorbent polymers which are powders are thinly painted onto the plastic ribbon with adhesives. The absorbent polymers which are fibers are processed into the forms of a yarn and a tape. The appearance of the forms of the absorbent material processed for the cable are shown in Fig.6.

3.2 Waterproofing structure design

Absorbent polymers allow water to penetrate to a certain length before forming a waterblocking dam. A short penetration is desirable, since penetrated water degrades the fiber characteristics. The following discusses an allowable penetration length so that the cable characteristics can be maintained. A waterproofing design using an absorbent polymer based on this allowable value is also discussed.



(a) Absorbent powder painted ribbon
(b) Absorbent polymer yarn
(c) Absorbent polymer tape

Fig.6 Appearance of absorbent materials processed for the cable

1. Allowable penetration length

In nonmetallic cables which have suffered from penetration, the problem was suspected to result in fiber loss increase due to freezing, and fiber strength degradation over long time periods. The allowable penetration length should be determined to resolve these problems.

1.1 Loss increase due to freezing

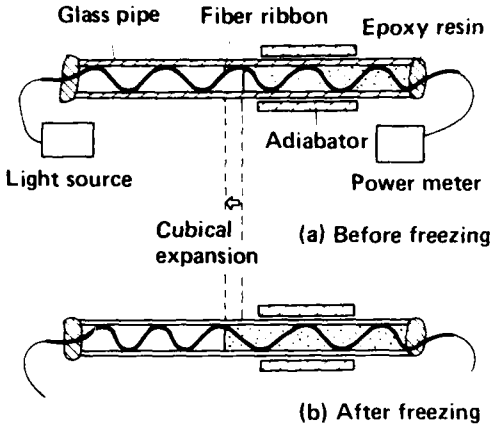
It was pointed out that the freezing of water which has penetrated an optical fiber cable induces a large loss increase[2,4]. To determine the allowable penetration length, it is essential to understand the mechanism responsible for increasing loss, and to determine the amount of loss increase.

A. Mechanism responsible for loss increase due to freezing

The cause of loss increase due to freezing has been presumed to be the lateral pressure associated with cubical expansion[4]. To confirm the validity of this presumption, experiments using stainless-steel pipe models were carried out. Stainless-steel pipes were filled with water. In one sample, a fiber ribbon was inserted straight into the pipe, whereas in the other sample, the fiber ribbon was inserted with bending. These samples were set in a thermostat of -20℃, and the loss change was monitored.

A resulting loss increase was observed with the bent fiber ribbon sample, but not with the straight one. Also, during freezing, expansion of the stainless-steel pipe was observed. The expansion ratio of the pipe diameter indicated that a lateral pressure of 120 MPa was generated in the pipe. This value was almost the same as that measured in the freezing of a closed water pipe[5]. These results suggests that the fiber bending, rather than the lateral pressure, is the cause of loss increase.

To confirm the above suggestion, freezing experiments with glass pipe models, as shown in Fig.7(a), were carried out. A fiber ribbon was inserted in the glass pipe with bending, and an adiabator was wrapped around the pipe to control



Glass pipe length = 20 cm
Water part length = 10 cm
Adiabator length of sample 1 = 0 cm
sample 2 = 5 cm
sample 3 = 9 cm

Fig.7 Glass pipe model configuration to investigate the loss increasing mechanism due to freezing

the freezing speed. The change in appearance of the model during the freezing process was observed and recorded by a video tape recorder. The loss change was also monitored.

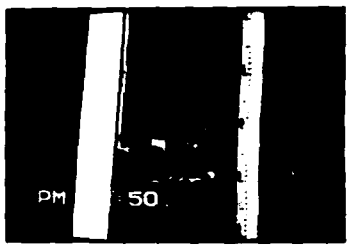
The change in appearance and the change in fiber loss during the freezing process are shown in Fig.8 and Fig.9, respectively. Figure 8 shows that the curvature radius of the fiber in the air-filled part of the pipe becomes small with the cubical expansion during the freezing as illustrated in Fig.7(b). At the same time, a steep loss increase was measured with the cubical expansion.

These results and the recorded video tape reveal the following to be the loss increasing mechanism.

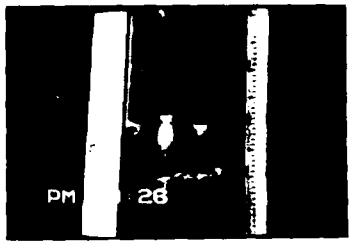
(1) Some portions of the water, for example, the place where the water meets an air bubble, freezes first.
(2) The frozen part attaches to the coated fiber.
(3) Other parts freeze gradually, and large cubical expansion occurs.
(4) The first frozen part moves by attaching to the coated fiber, due to the cubical expansion of other parts.
(5) The coated fiber becomes more steeply bent, and fiber loss increases.

B. Loss increase estimation

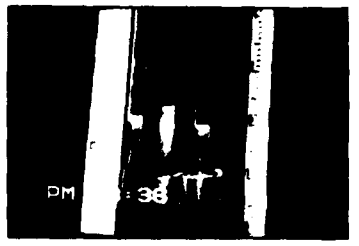
On the basis of the above mechanism, the amount of loss increase was estimated experimentally. A single-mode fiber ribbon was inserted into glass pipes with inner diameters of 2, 4, and 6 mm. The fibers were given a sinusoidal curvature, and the fiber loss change was measured. The results are shown in Fig.10. Regardless of the pipe's inner diameter, the fiber loss was inversely and exponentially proportional to the increase in the minimum curvature radius. The relationship between the loss increase α and the minimum curvature radius R_{min} is given as follows:



(a) Before freezing (+10C)



(b) In freezing (-15C)



Sample No. 3 2 1

(c) After freezing (-23C)

Fig.8 Appearance change of the glass pipe model

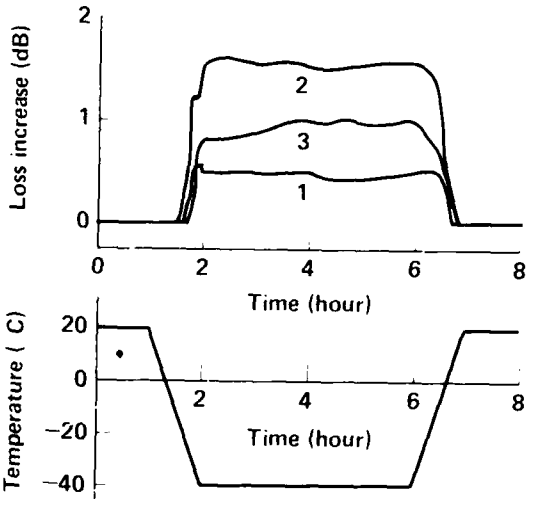


Fig.9 Loss increase of fiber in glass pipe model due to freezing

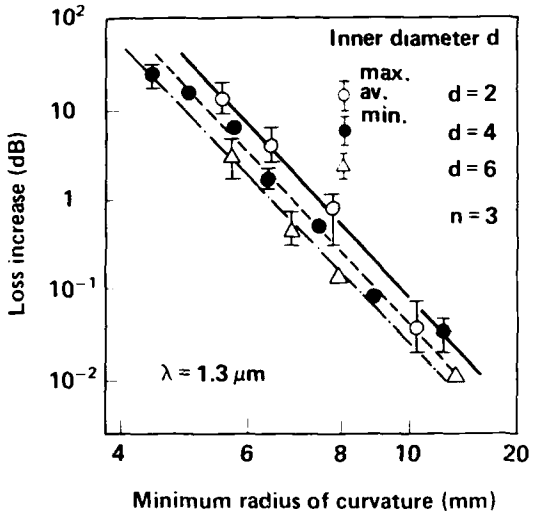


Fig.10 Loss increase as a function of the minimum radius of curvature for fibers bent into a sinusoidal shape

$$\alpha = 10^{-8} \quad (1)$$

In general, during manufacture, fiber ribbons are assembled in slotted cores having 27-30 mm R_{min}. In this condition, a cubical expansion of 9‰ during the freezing brings a R_{min} change of 1 mm. This R_{min} change causes a 2-5 dB/km loss increase, as is clear from Eq.(1).

The measured loss increase with a slotted core cable due to freezing is shown in Fig.11. The lengths of the frozen cable and the frozen coated fiber were 50 meters and 200 meters, respectively. The measurement loss increase was 2.5 dB/km at -10℃. This value agrees well with the estimated value. This agreement indicates that the amount of loss increase can be estimated from Eq.(1) by using the actual R_{min} value in manufacturing.

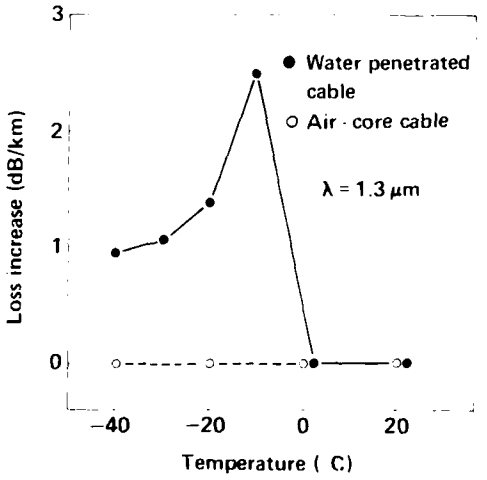


Fig.11 Increase in optical fiber loss of water-penetrated cable due to freezing

For example, if the loss increase is assumed to be 5 dB/km, which is the estimated maximum value, and the allowable loss increase of the cable is assumed to be at 0.02 dB/km, the allowable *penetration* length will be less than 4 meters.

1.2 Strength degradation of the fiber in water

In water, fiber strength degrades gradually over a long time. Therefore, the shorter the penetration distance, the better.

Miyajima et al.[6] guaranteed the long-term reliability of fibers by using the proof test condition in manufacturing, as follows:

$$\varepsilon_p^{\,n} \cdot t_p = \varepsilon_f^{\,n} \cdot t_f \cdot \ln(1/(1-F)), \quad (2)$$

where ε_p is the strain in the proof test, ε_f is the strain in the field, t_f is the period of time in service, and F is the failure probability per 5000 km. Under the conditions of ε_f = 0.5 %, strength fatigue index n = 17 (in water), and t_f = 10 years, the allowable length a fiber may be submerged in water becomes 487 meters. For a 40-fiber cable, the allowable submerged cable length is approximately 12 meters.

2. Penetration length design

Many waterproofing tests show that water penetrates into cables filled with absorbent polymer according to two modes. One is the initial penetration mode, which corresponds to the first 20-30 minutes of penetration. In this mode, the *penetration length increases rapidly.* The other mode is a long-term penetration mode, which occurs continuously after the initial penetration mode. In this mode, *the penetration length hardly increases.*

The waterproofing structure should be designed in consideration of each penetration mode, so as to restrict the penetration to an allowable value.

2.1 Initial penetration mode

In the initial penetration mode, the penetration length varies with the water pressure, and the cross-sectional area and the shape of the space in the cable.

The penetration length, L(t), at time t is given by the following equation, taking into considering the reduction in the cross-sectional area of the watercourse due to absorbent polymer swelling:

$$L(t) = \int_0^t \frac{2gH}{\left(\frac{\lambda L(t)}{d_e} + \zeta + 1\right) v(t)}\, dt, \quad (3)$$

where $\lambda = 64 / R_e$,

$d_e = 4A / U$,

R_e = Reynolds number,
d_e = equivalent diameter,
A = cross-sectional area of watercourse,
U = wetted perimeter of watercourse,
ζ = loss coefficient at the entrance of watercourse, and
g = acceleration due to gravity.

To determine whether this equation is valid, watercourse model of the cable space were

constructed, as shown in Fig.12. The absorption ratio and the absorbing speed of the absorbent ribbon were 120 cc/g and 0.3 cc/gsec, respectively. For the absorbing powder, the values were 480 cc/g and 5.8 cc/gsec, respectively. Figure 12 shows the penetration length calculated from Eq.(3), as well as the experimental values. The calculated results are in good agreement with the experimental values. These results indicate that the initial penetration length can be estimated using Eq.(3).

The relationship, calculated by using Eq.(3), between the initial penetration length and the filling condition of the absorbent polymer in a 2 mmø pipe is shown in Fig.13. In this model, a fiber ribbon and two absorbent ribbons were inserted into the pipe. Here, the filling conditions of the absorbent polymer were determined by two parameters. One is the normalized filling density of the absorbent polymer, which is defined by:

$$D_n = D \cdot S \quad , \qquad (4)$$

where D_n = normalized filling density of the absorbent,
D = filling density of the absorbent (g/cm^3), and
S = absorption ratio (cm^3/g).

The other parameter is the wetted perimeter ratio, which indicates the degree of uniformity of the filling for the absorbent polymer in the watercourse. This is defined as:

$$R = P_a / P_t \quad , \qquad (5)$$

where R = wetted perimeter ratio,
P_a = wetted perimeter of absorbent (cm),
P_t = total wetted perimeter of the watercourse (cm).

Figure 13 shows that a large D_n and large R combine to yield a short penetration length. Therefore, to achieve a short penetration length, the absorbent polymer must be filled densely and *uniformly*.

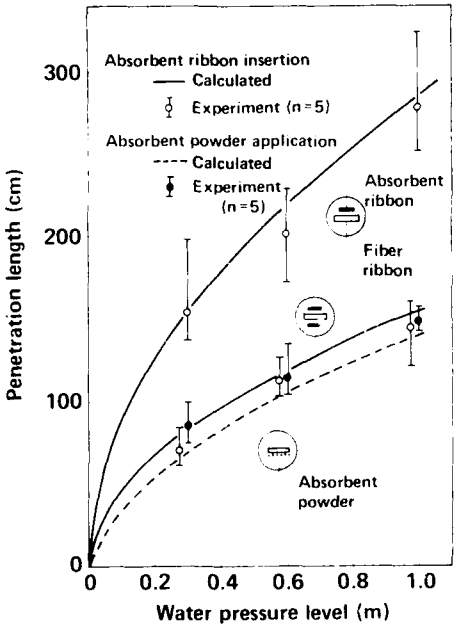


Fig.12 Initial penetration length in watercourse model

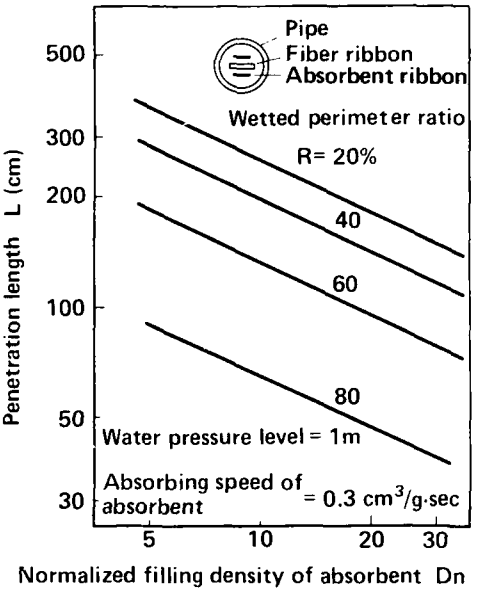


Fig.13 Example of penetration length computed for absorbent ribbons

2.2 Long-term penetration mode

A glass pipe was filled with the absorbent polymer, and the long-term increase in penetration length was examined under the conditions of 1.2 meters water pressure level at D_n of 10-16. The results are shown in Fig.14. The penetration length increased proportionally to about the 1/2 power of time T, as given by the following equation, regardless of the water pressure level and the filling density of the absorbent polymer.

$$L = L_0 + \alpha T^{1/2} \quad ,$$

This indicates that long-term elongation of the penetration length is caused by water diffusion in the absorbent polymer, which can be estimated by Eq.(6). The estimated increase in penetration length is approximately 50 cm over a 10-year

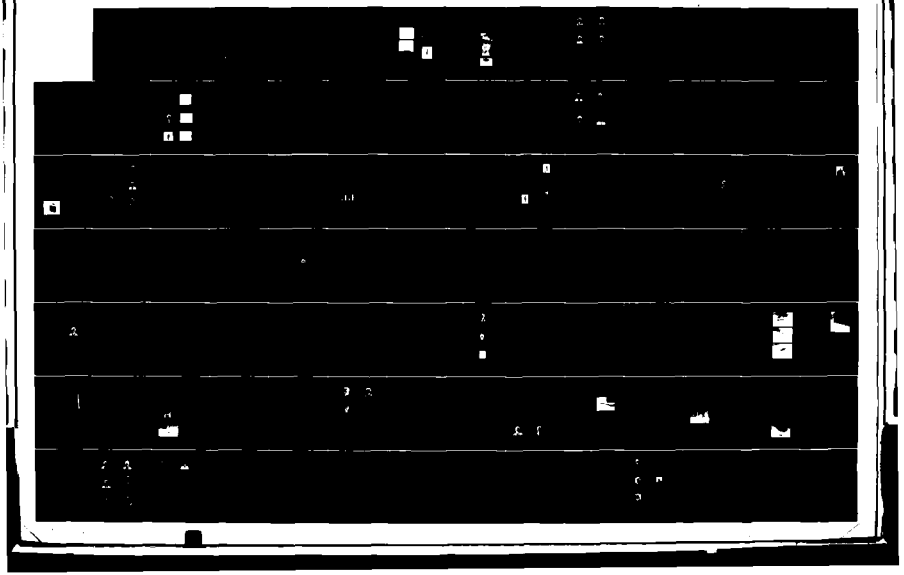
The waterproofing structure is designed to suppress the initial penetration length in accordance with the results in Fig.13. This means that the long-term penetration length is controlled as a function of the filling condition of the absorbent polymer.

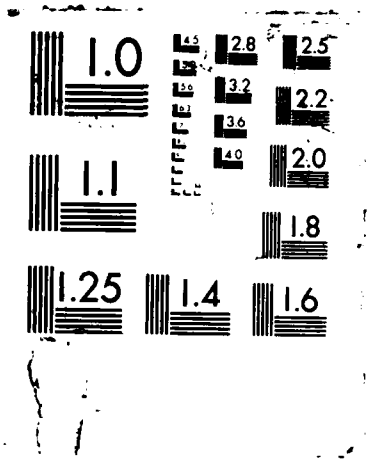
3. Waterproof test method

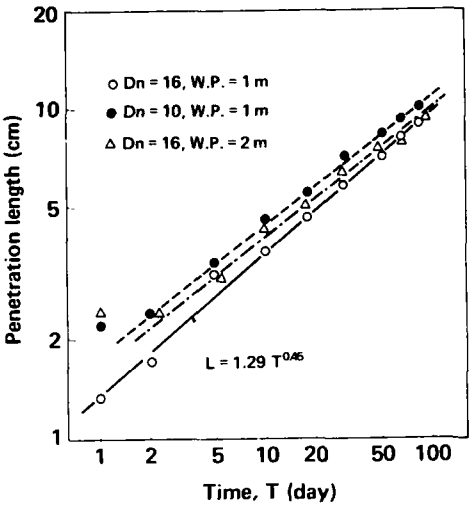
As mentioned above, the [illegible] for an absorbent-polymer [illegible] different from that [illegible] cable. Therefore, [illegible] waterproofing test [illegible] precisely evaluate [illegible]

AD-A189 610 PROCEEDINGS OF THE INTERNATIONAL WIRE AND CABLE SYMPOSIUM (36TH) HELD IN..(U) ARMY COMMUNICATIONS-ELECTRONICS COMMAND FORT MONMOUTH NJ 5/9

UNCLASSIFIED 19 NOV 87 F/G 9/1 NL




1.0
1.1
1.25
1.4
1.6
1.8
2.0
2.2
2.5
2.8
3.2
3.6
4.0
4.5
5.0



Dn : Normalized filling density
W.P. : Water pressure level

Fig.14 Long-term elongation of penetration length

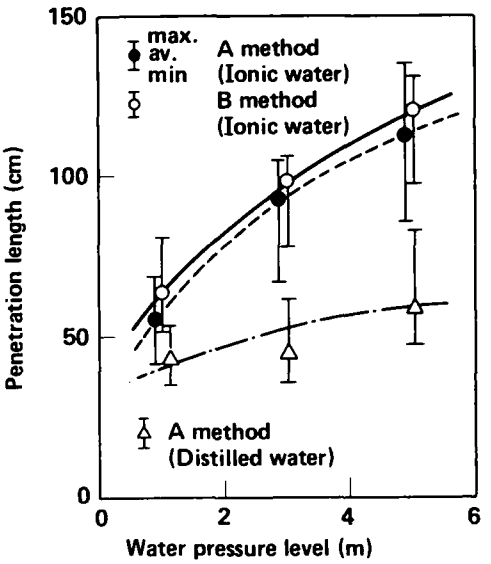


Fig.15 Penetration length as a function of water pressure level, using the waterproof test method as a parameter

3.1 Quality of water

Underground water contains many kinds of ions and microorganisms. The waterproofing ability of absorbent polymers varies with the kinds and amounts of ions in the water. Therefore, for precise evaluation, it is necessary to determine what these are.

Water in manholes is considered to contain most kinds and amounts of ions. This is because not only soil water pours into manholes, but also many kinds of ions seep out from the concrete or metallic materials in the manhole.

Ion analysis results of water tested from 46 manholes in Japan[7] showed that the water in 99% of the manholes contained 300 mg/l of Na^+, 200 mg/l of Ca^{2+}, and 100 mg/l of K^+, at maximum. Therefore, a cable which has waterproofing ability against such water can be applied to 99% of all manholes.

3.2 Water supplying method

Conventionally, there are two water supplying methods. One is to supply it through a cross-section of the cable (the A method), and the other is to supply it through the lateral face of the cable from which the sheath is removed (the B method).

To confirm the dependency of penetration length on the water supplying method and the quality of water, waterproofing tests were carried out for a 40-fiber slotted-core cable. The number of samples was 10. The penetration length was measured after 24 hours. The results are shown in Fig.15.

The penetration length tested with ion water was about twice that tested with distilled water. There was no difference between the two water supplying methods.

These results indicate that for waterproof testing of cables filled with absorbent polymer, water containing the aforesaid ions should be used, and either water supplying methods can be applied.

4. Nonmetallic sheath design

To make the sheath nonmetallic, the following two subjects need to be studied.

(1) Sheath shrinkage.
(2) Moisture permeation through the sheath.

Here, these subjects and the nonmetallic sheath design are discussed.

1. Design in consideration of sheath shrinkage

Large sheath shrinkage is feared to induce the displacement of coated fibers in cable cores, and is feared to result in fiber loss increase. Therefore, a design to suppress the sheath shrinkage as much as possible is necessary.

1.1 Sheath shrinking mechanism and the amount of shrinkage

In a plastic sheath, the shrinking force due to the residual strain in manufacturing is always acting, as shown in Fig.16. Furthermore, a shrinking force caused by temperature variation also operates on the sheath.

In a nonmetallic sheath, only the friction force between the sheath and cable core resists this shrinking force. In the region where the shrinking force is larger than the friction force, sheath shrinkage occurs.

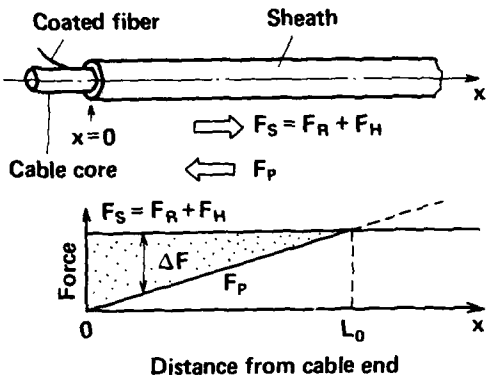
The sheath displacement, $\delta(t)$, at the cable end is given by the following equation:

$$\delta(t) = \int_0^t \int_0^{l_0} K_s \varepsilon_s(x,t)\,dx\,dt \quad , \qquad (7)$$

$$\varepsilon_s = (F_s - F_p)/EA \quad ,$$

where E and A are the Young's modulus and cross sectional area of sheath, respectively, and K_s is the strain releasing ratio per unit time.

A waterproof optical fiber cable (shown in Fig.17) which has comparatively small friction force was installed in a thermostat, and a heat-cycle test



F_S=Total shrinking force
F_R=Shrinking force due to residual strain
F_H=Shrinking force due to temperature variation
F_P=Friction force between the sheath and the cable core
L_0=Region where the sheath is displaced

Fig.16 Sheath shrinking mechanism

in the temperature range of -20℃ to +80℃ was carried out. The cable length was 200 meters. The amount of shrinkage at the cable end was measured, and the results are shown in Fig.17. They accord with the results calculated from Eq.(7).

The amount of shrinkage increases with the heat cycles, at first. However, after about 10 cycles, it shows a tendency to saturate, due to the release of residual strain. Thus only the shrink variation caused by temperature change is left.

Experimental values agree well with the calculated results and it is clarified that the amount of shrinkage can be estimated by Eq.(7).

By setting the allowable amount of shrinkage to suppress the loss increase, the maximum sheath thickness and the minimum friction can be determined by using Eq.(7).

1.2 Loss increase due to sheath shrinkage

Sheath shrinkage induces coated fiber displacement with an interaction between the sheath and the coated fiber. The fiber displacement causes a steep bend in the fiber, as well as large loss increase.

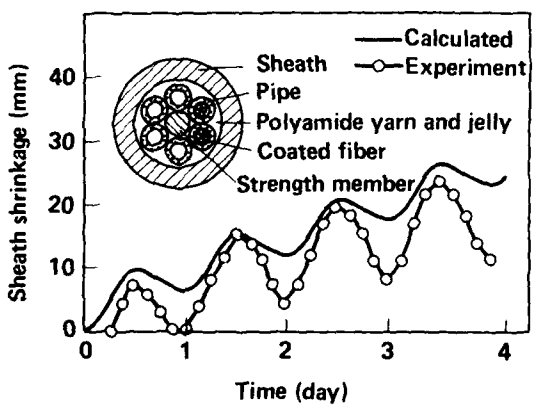


Fig.17 Sheath shrinkage during heat-cycle test

The displacement of the coated fiber, δ_f, due to the sheath shrinkage, $\delta(t)$ is given by following equation:

$$\delta_f(t) = K\delta(t) \quad , \quad (8)$$

where K is the transfer coefficient of displacement between the sheath and the coated fiber. As R_{min} caused by $\delta_f(t)$ is obtained geometrically, the loss increase $\Delta\alpha$ due to the sheath shrinkage is obtained from Eqs.(1), (7), and (8).

A calculated example of loss increase due to sheath shrinkage for a 40-fiber slotted-core cable (to be described later) is shown in Fig.18. The transfer coefficient of this cable was obtained by measuring the ratio of the coated fiber displacement to the sheath displacement in a cable core by pulling it from the sheath. The upper line of Fig.18 shows the relation between the sheath thickness and the friction force. This must be known to suppress the loss increase, due to the sheath shrinkage, to less than 0.05 dB.

The same figure also shows (as the lower line), the area where the sheath does not break down. The area within the two lines gives the appropriate design area of the sheath.

2. Design considering moisture permeation

Moisture permeates through a nonmetallic sheath easily, compared with a conventional LAP sheath. Here, the accumulated amount of moisture which permeates through the sheath is estimated, and the sheath design is shown.

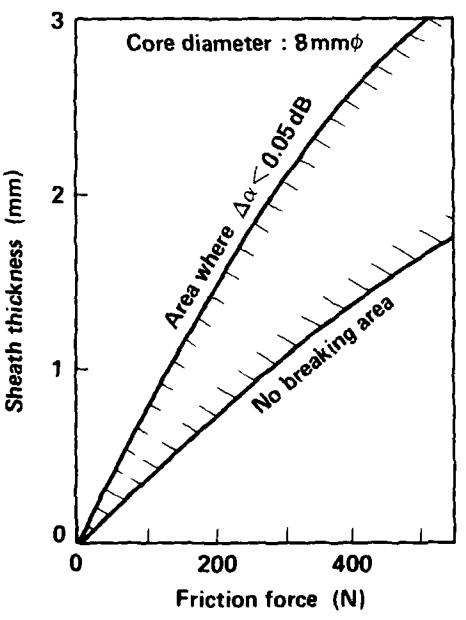


Fig.18 Calculated sheath design parameters in consideration of sheath shrinkage

2.1 The amount of moisture permeation

The permeability of a plastic cylinder is given by the following equation:

$$G = P \cdot \frac{2\pi}{\ln(b/a)} \quad , \quad (9)$$

where P is the permeability of sheath, and a and b are the cable diameter and cable core diameter, respectively.

The amount of moisture which permeates is shown by the following equation, assuming that the cable space is always dry:

$$W = \frac{18}{22400} \int^{t} HGdt \quad , \quad (10)$$

where H is the saturated steam pressure at temperature TC.

The calculated amount of moisture accumulation for one year is shown in Fig.19. The accumulation of moisture increases steeply for thin sheaths.

On the other hand, the materials which compose the cable absorb the permeated moisture. For example, for the 40-fiber slotted-core cable (to be described later), the component materials containing absorbent polymer can absorb more than 10 g. Therefore, to have a service life of more than 10 years with this cable, the moisture accumulation per year should be less than 1 g. For this condition, Figure 19 indicates that a sheath thickness of more than 1 mm is necessary.

The adequate sheath thickness and the adequate friction between the sheath and the cable core can be designed in consideration of the area shown in Fig.18 and the minimum sheath thickness given from Fig.19.

5. Nonmetallic strength member application design

The material for the strength member should satisfy the following conditions.

(1) High breaking strength,
(2) High Young's modulus,
(3) Low linear expansion coefficient, and
(4) High reliability under the actual operating circumstances of the cable.

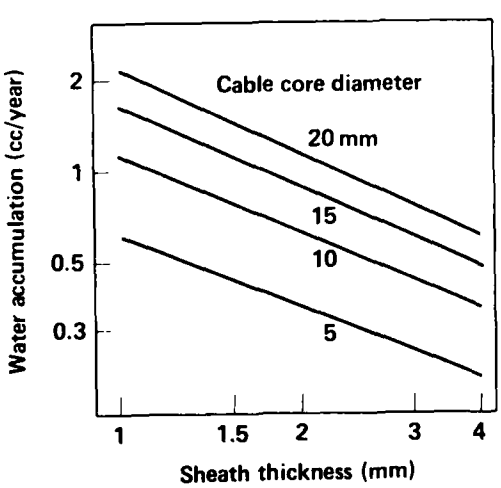


Fig.19 Calculated sheath design parameters in consideration of moisture permeation .

For these conditions, Fiber Reinforced Plastic (FRP), Aramid yarn, Polyoxy Methylene (POM), and Liquid Crystal Polymer (LCP) can be considered for application. To develop the cable, FRP using glass yarn as the high modulus yarn was adopted, considering its heat resisting property, bending strength, and resistance against the shrinkage of plastic materials.

1. Mechanical characteristics of the FRP

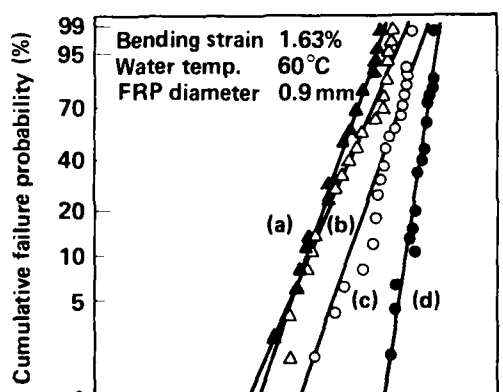
A comparison of the mechanical characteristics of FRP with conventional steel wire shows that its inferior characteristics are its bending strength and resistance to lateral pressure. However, for practical use, the lateral pressure characteristics of FRP are sufficient, but the most serious practical problem is its bending strength. Therefore, a design considering the bending fatigue characteristics is necessary.

2. Relation between material composition and bending fatigue characteristics

The FRP was bent at a certain curvature radius, and fixed. The samples were set under various circumstances, and the time until the FRP broke was measured.

The results for FRP samples composed of different glass materials, resin, and resin catalyst are shown in Fig.20. The results indicate that the bending fatigue characteristics depend mainly on the glass material, and that T-glass FRP can much improve the characteristics of E-glass FRP.

To clarify the cause of this, the dipping liquid for the sample was analyzed with Ion Coupled Plasma (ICP). The analyses showed that the amount of eluted alkaline-metals from the E-glass



(a) Conventional E-glass FRP
(b) E-glass FRP composed by resin catalyst as a parameter
(c) E-glass FRP composed by resin as a parameter
(d) T-glass FRP

Fig.20 Cumulative failure probability as a function of time, using material composition as a parameter

FRP were much more than that from the T-glass FRP. This suggests that the alkaline-metal elution caused surface cracks in the glass, and degradation of the fiber strength.

3. Allowable bending radius design in application

Bent E-glass FRP and T-glass FRP were dipped in 60℃ water, which is considered to be the most severe practical condition, and the mean failure time was measured. The results are shown in Fig.21. It is clear that the T-glass FRP can be bent to a smaller curvature radius than can the E-glass FRP.

If the failure probability of FRP is assumed to be the same as that of a coated fiber, the required mean failure time can be determined from the hatched area in Fig.21. Bending strain in this hatched area is allowable, and the allowable bending radius in application can be determined according to the diameter of the FRP rod.

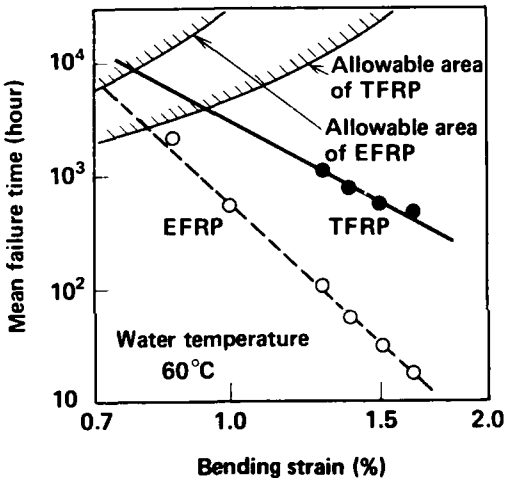


Fig.21 Mean failure time as a function of bending strain

6. Nonmetallic water penetration sensor

Cable joints have a high probability of being damaged, or of having pin-holes, due to miss-operation. When water penetrates through these damaged parts or pin-holes, troubles such as loss increase due to freezing can occur. Therefore, it is desirable to detect the water penetration into the joints as soon as possible. However, no nonmetallic water penetration sensors have been developed. Here, a novel, nonmetallic, water-penetration sensor is proposed. It can detect water penetration quickly, and can also locate the points where the penetration occurred.

1. Structure and mechanism of sensor

Figure 22 shows the structure and mechanism of the sensor. The sensor can be constructed easily by holding a monitoring fiber in grooves on two hinged plates. A shrinkable thread is hung over the monitoring fiber. When water penetration occurs, the thread shrinks, and the fiber bends sharply. This causes an increase in transmission loss. Thus, the penetration can be detected by

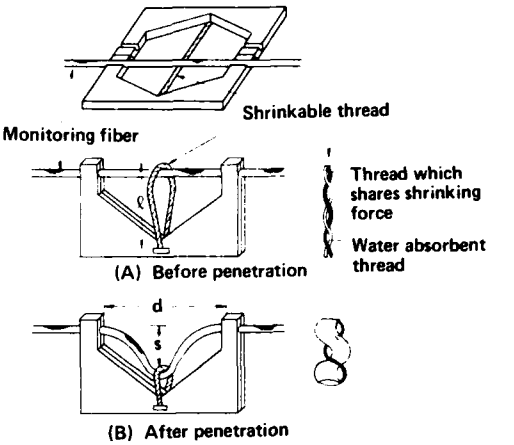


Fig.22 Structure and mechanism of nonmetallic water penetration sensor

monitoring the transmission loss change with an Optical-Power-Meter (OPM). Also the penetration points can be located using an Optical-Time-Domain-Reflectometer (OTDR). The sensors can be set anywhere along the monitoring fiber without causing any degradation in the transmission characteristics of the fiber.

2. Characteristics of sensor

The shrinking force of the thread was approximately 200g at the maximum, and this force decreased exponentially as the shrinkage continued. The shrinking speed was so high that the maximum shrinkage was attained in about 10 seconds. The loss increase of the monitoring fiber due to thread shrinkage was measured, and the results are shown in Fig.23. Bending loss increased sharply for small changes in the shrinking length, s, and a large loss increase was easily obtained.

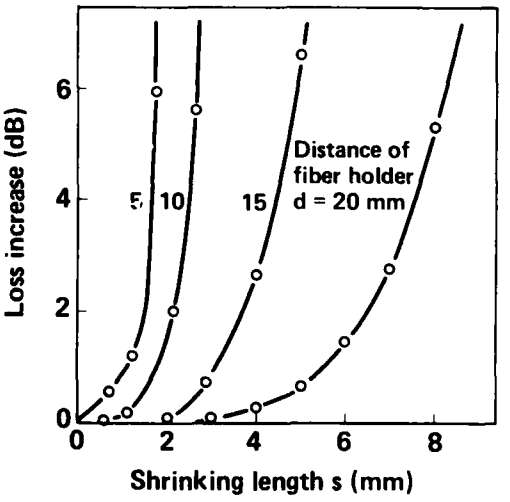
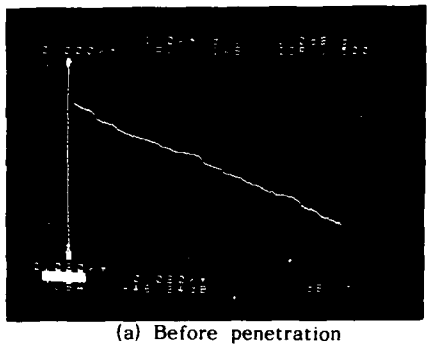


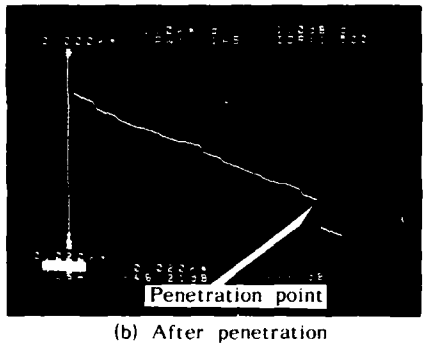
Fig.23 Loss increase as a function of shrinkage length of the shrinkable thread

3. Applications

The proposed sensors are applied to monitor water penetration into joints of optical cable lines. The sensors are set at every cable joint on a monitoring fiber. Water penetration point can be detect from the fiber end in a telephone office. A measured OTDR scan, when the sensor is set at 7.2 km from the office, is shown in Fig.24. A loss increase of 1 dB can be clearly observed at the penetration point. The applicable limit for the distance depends on the sensitivity of the OTDR, but in this study, a length of more than 10 km was achieved.



(a) Before penetration



(b) After penetration

Fig.24 OTDR scan of optical fiber cable line (1 km/div.; 1 dB/div.; pulse width=1 us)

7. Characteristics of the manufactured cable

A waterproof, nonmetallic, optical-fiber cable was manufactured taking into account the aforesaid designs, and the cable performance was evaluated. Here, the 40-fiber sigle-mode cable structure and its characteristics are discussed.

1. Structure of the manufactured cable

To minimize the cable core size, a cable structure consisting of a slotted core, with piled-up fiber ribbons, was selected. The relationship between the cable core size and the number of slots is shown in Fig.25. For the 40-fiber cable, 6 is an adequate number of slots. The structure of the manufactured 40-fiber slotted-core cable is shown in Fig.26, and its appearance is shown in Fig.27. To make the structure nonmetallic, FRP rod was used for the strength member instead of steel wire, and a PE sheath was used instead of an LAP sheath. As for the waterproofing materials,

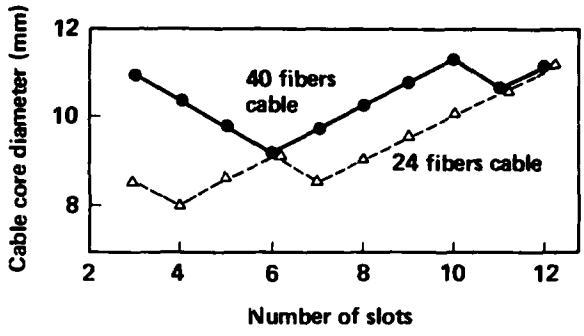


Fig.25 Relationship between cable core diameter and number of slots

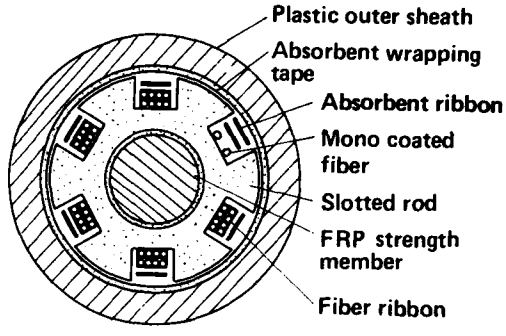


Fig.26 Cross-sectional structure of 40-fiber, nonmetallic, waterproof, optical fiber cable

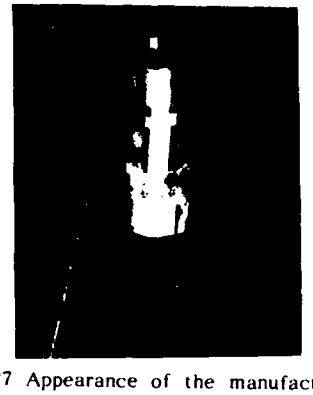


Fig.27 Appearance of the manufactured cable

absorbent ribbons were assembled in slots, together with fiber ribbons, and absorbent wrapping tapes were used around the slotted core.

Poly-acrylic-acid was used as the absorbent material. A normalized filling density of 18, and a wetted perimeter ratio of 20%, respectively, were chosen to suppress the initial penetration length to within 50 cm. This value was determined by setting the total allowable penetration length to 100 cm, and the long-term penetration length elongation to 50 cm.

2. Evaluation results

2.1 Waterproofing characteristics

Water containing ions was applied to the cross-section of the cable at a pressure of 0.1 atm, and the penetration length was measured after 24 hours. The results are shown in Table 1. The values are in good agreement with the designed initial penetration length of 50 cm.

2.2 Mechanical characteristics

The cable was subjected to external forces, such as lateral load, bending force, and tensile force, and the loss changes were measured. The results are shown in Table 2. The performance characteristics for the cable were essentially the same as those for conventional air-core cables.

2.3 Heat-cycle test results

The sheath shrinkage was examined in the temperature range of -20℃ to +60 ℃. The sheath displacement and shrinking force at the cable end are shown in Fig.28. The maximum sheath displacement was 10 mm, and the maximum shrinking force was 12 kg. The transmission loss change was less than 0.02 dB. These values are sufficiently small for practical applications.

2.4 Field trials

To confirm the efficiency of installation and jointing, and long-term reliability, this cable was installed in the field and evaluated. The installation length was 42.5 km in total, and the number of cable joints was 31. Some photographs of the installation configuration are shown in Fig.29.

The trial results showed that this cable yielded high efficiency for both installation and jointing.

Table 1. Waterproof test results

Penetrated part	Penetration length	
	Designed	Measured (mean S.D.)
Wrapping tape	50	42.5 12.3
Slot	50	44.0 10.0

(unit:cm)

Table 2. Mechanical characteristics

Items	Test conditions	Execess loss
Tensile test	T = 0 - 200 kg	< 0.01 dB
Bending test	R = 30 - 100 mm	< 0.01 dB (R > 65mm)
Lateral load test	W = 0 - 10 kg/mm	< 0.01 dB (W<9kg/mm)
Dynamic bend-tension test	T = 0 - 200 kg R = 250 mm L = 50 m	< 0.01 dB

T: Tension L: Cable length
R: Bending radius W: Lateral load

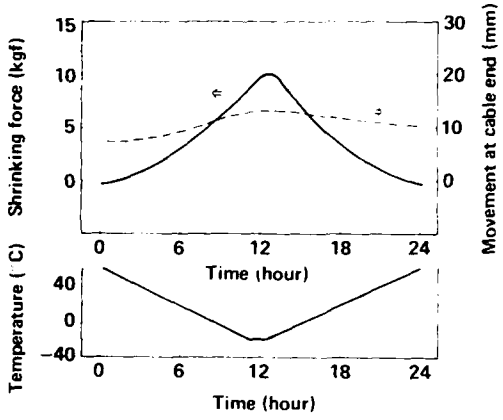
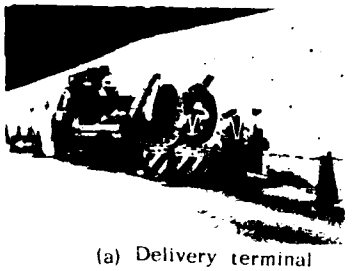


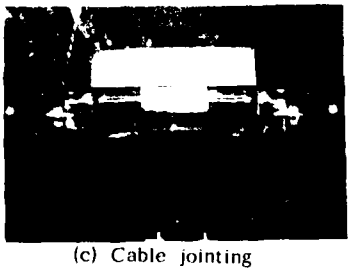
Fig.28 Movement at cable and shrinking force of sheath during heat cycle test



(a) Delivery terminal



(b) Pulling terminal



(c) Cable jointing

Fig.29 Photographs of the field trial installation configuration

8. Conclusion

A nonmetallic optical fiber cable waterproofed with absorbent polymer, was developed. To identify an effective waterproofing technique, a method for evaluating the reliability of the absorbent polymer, as well as the waterproofing design, were investigated. For the nonmetallic technique, a nonmetallic sheath, a nonmetallic strength member, and a nonmetallic water penetration sensor design were discussed. The following main points were made.

A. Waterproofing technique

(1) Poly-acrylic-acid, which is a synthetic polymer, is suitable for use as a waterproofing material.
(2) The optical fiber loss of water-penetrated cables increases due to freezing. The allowable penetration length of waterproof cables can be determined so as to suppress this loss increase.
(3) Penetration length increases according to two modes. One is an initial penetration mode, which is determined by the water pressure level and the absorbent polymer filling conditions in the cable. The other is a long-term penetration mode, which is determined by the diffusion of water in the absorbent polymer.

B. Nonmetallic technique

(1) The design of a nonmetallic sheath can be determined from two factors. One is to suppress the sheath shrinkage in relation to the friction force between the sheath and the cable core. The other is to suppress the moisture permeation.
(2) The reliability of the FRP depends mainly on the glass material. The FRP with a T-glass fiber has high reliability, compared with the conventional E-glass fiber. The allowable bending radius can be set.
(3) A nonmetallic water-penetration sensor can be composed by fiber and shrinkable thread, and it can detect water penetration at point of 10 km apart from the telephone office.

Cables manufactured on the basis of the results from the investigation described above were shown to perform satisfactorily for practical applications.

Acknowledgments

The authors wish to thank Nobuya Kojima, Dr. Naoya Uchida and Dr. Masamitsu Tokuda for their support and encouragement throughout the course of this work. They also wish to thank Tsuneo Kuwabara for his helpful comments and discussions.

References

1. T.K.McManus and R.Beveridge: 'A new generation of filled core cable', IWCS, 26, 1977
2. T.S.Hope, R.J.Williams and K.Abe: 'Developments in slotted core optical fiber cables', IWCS, 30, 1981
3. D.J.Dekker, J.Bruining and G.A.C.Schuring: 'Compartmentalized longitudinal waterproof cables', IWCS, 28, 1979
4. Sugawara et al.: 'Attenuation increase mechanism of jacketed and cabled fibers at low temperature', IECE, J62-C, 12, 1979 (in Japanese)
5. S.Oiwake,H.Saito,H.Inada and I.Tokura: 'Study on dimensionless criterion of fracture of closed pipe due to freezing of water',Wärm und stoffübertragung, 20, pp.323-328, 1986
6. Y.Miyajima et al.: 'Fiber strength assurance for deep-submarine optical-fiber cable using the proof-testing method', J. Lightwave Technol., LT-3, 2, pp.248-255, 1985
7. N.Honma: private communication.



Shigezou Kukita

NTT Transmission
Systems Laboratories
Tokai, Ibaraki, Japan

Shigezou Kukita received the B. E. degree in electrical engineering from Shizuoka University in 1973. Since joining NTT Electrical Communications Laboratories in 1973, he has been engaged mainly in the development of the optical fiber cable for subscriber loops. His present interests are in waterproof optical fiber cables. He is a member of the Institute of Electronics, Information and Communication Engineers of Japan.



Akira Hayashi

NTT Transmission
Systems Laboratories
Tokai, Ibaraki, Japan

Akira Hayashi received the B. E. and M. E.degrees in Mechanical engineering from Keio University in 1982 and 1984, respectively. He joined NTT Electrical Communications Laboratories in 1984, where he has investigated the mechanical characteristics of metal-free optical fiber cables. His current interests include the mechanism of metal cable decay. He is a member of the Institute of Electronics, Information and Communication Engineers of Japan.



Takashi Nakai

NTT Transmission
Systems Laboratories
Tokai, Ibaraki, Japan

Takashi Nakai graduated from Kamioka technical high school in 1973. He joined NTT corporation in 1973 and engaged in the construction and maintenance of transmission lines. In 1986, he joined NTT Electrical Communications Laboratories, where he has been engaged in the development of waterproof optical fiber cable. His present interests include the reliability of absorbent polymers.



Hiroaki Koga

NTT Transmission
Systems Laboratories
Tokai, Ibaraki, Japan

Mr. Koga's early work dealt with cable designs for subscriber loops, and the protection and maintenance techniques for telecommunication lines against lightning surges. Since 1979, he has been engaged in the development of optical fiber cables. He received his M. E. degree in electrical engineering from Kagoshima University in 1970.

A Study of Multi Channel Optical Rotary Joint with Ring-Shaped Photo Diode

K. NEMOTO M. INOUE

Ocean Cable Co., Ltd. (OCC)
Detamachi 1, Kanagawa-ku, Yokohama 221, Japan

Summary

This paper relates to an evaluation of the characteristics of the optical rotary joint developed by extending the concept of the slip ring to an optical system using ring-shaped photo diode. We carried out a characteristics evaluation test and as a result obtained a good rotation variance characteristic (below 1 dB), frequency characteristic (cut-off frequency: 50 MHz), and inter-ring crosstalk characteristic (isolation ratio of 60 dB at 4.2 MHz), and further we carried out the base band analog color video signal transmission by making a level difference of 7 dB between the E/O converter and the ring-shaped photo diode and obtained a SN ratio of 47 dB and also obtained a favorable result of digital signal transmission.

1. Introduction

The superiority of optical fiber in light weight, wide band, inductive-proof, and so on attracts attention to the applicability of optical fiber to such ocean engineering systems containing rotary mechanism as vuoy system and winch system, and the development of a highly reliable multi-channel optical rotary joint has become an important subject in the field of marine technology.

In the conventional ocean engineering system using metallic cable, the jointing mechanism, as can be seen in the joint section between marine cable and the terminal device, the jointing section between marine cable and the winch on board, or the like, uses slip rings, whereby multi-channel rotary joint could be implemented relatively easily.

On the other hand, as for the rotary joint mechanism for optical fiber cable, single-channel optical rotary connector by facing each ends of fiber has been already developed, but this method is limited in use, that is, it can apply to only single-core optical fiber cable. Although a number of types of multi-channel rotary joint mechanism have been developed so far using prism, spherical mirror, or the like, they all have as much joint loss as a few decibels and a rotation variance of greater than one decibel, which the authors consider there still remains the necessity of further examining characteristics.

The requirements that the optical fiber rotary joint must meet are considered as follows.

(1) No signal deterioration is caused by rotation.
(2) Frequency band width is wide enough.
(3) Insertion loss is small.
(4) Mechanical reliability is high.

Under the situation stated so far, as a means of implementing a multi-channel optical rotary joint that meets these requirements we proposed the ring-shaped photo diode devised by extending the concept of the slip ring for an optical system, developed the 4-channel optical rotary connector using the photo diode consisting of quadruple ring-shaped Si-PIN-PD, and carried out an evaluation experiment.

The ring-shaped PD is the photo diode consisting of a plural number of rings which are arranged concentrically and which have a uniform photo receiving sensitivity, and it is characterized by having an extremely small rotation variance of signal output.

In this paper, the authors will describe the result of the evaluation test done for the rotation variance characteristic, frequency characteristic, and inter-ring crosstalk characteristic of the 4-channel optical rotary connector constituted by mounting this ring-shaped PD to the bearing rotary mechanism and the case provided with 4 receptacles for connecting optical fiber and the result of the experiment of base band analog color video signal transmission and that of digital signal transmission.

2. An Outline of the Quadruple Ring-Shaped Si-PIN-PD

2.1 Structure

Fig. 1 shows the structure of the quadruple ring-shaped Si-PIN-PD. Outer diameters of the innermost ring and outermost ring are 10 mm, 25 mm, respectively, and their widths are all 1 m.m. The outer diameter and thickness of the package where this element is enclosed are 50 mm and 5 mm, respectively. The photo receiving surface is protected by the metallic coated glass in order to shadow disturbance light.

2.2 Principal characteristics

As the PIN-PD has a high quantum efficiency and small dark current and is operated at low voltage, it can be easily dealt with. Table 1 shows principal characteristics of the ring-shaped PD prepared for the experiment.

Briefly explaining the meaning of each item, the quantum efficiency in item 1 defines the photoelectric conversion efficiency, where η = (No. of carriers which affects the production of photoelectric current) / (No. of incident photos) = $(I/e) / (P/h\nu)$. (I: Anode current, e: elementary charge quantity, P: Light power, h: Planck's

constant, ν: Light frequency). Photo receiving sensitivity in item 2 is the ratio of electric signal to photo signal $S = I/P = (\eta e)/(h\nu)$. Cut-off frequency in item 3 is the frequency obtained when the output level drops by 3 dB by connecting a 50Ω load resistance to receive a sine wave signal. Dark current in item 4 is the electric current that flows when no incident light is applied to the PD. The capacitance between the terminals in item 5 is the capacitance between the anode and the cathode and is the parameter that determines the cut-off frequency. Crosstalk in item 6 indicates the degree of separation between rings and is defined by an isolation ratio.

To measure these characteristics, we mounted the ring-shaped PD to the bearing rotary mechanism and to the case provided with 4 receptacles for connecting the optical fiber cables to prepare the 4-channel optical rotary connector.

3. Rotation Variance Characteristic

3.1 Surface sensitivity distribution characteristic

Fig. 2 shows a schematic diagram of the quadruple ring-shaped photo receiving surface. It proves that the section where the bonding wire connected to the anode of each ring passes over the ring photo receiving surface is present at one place in ring #2, at two places in ring #3, and at three places in ring #4. Therefore, it can be predicted that when the end of optical fiber passes above the bonding wire, a very small variance occurs.

In the measurement system shown in Fig. 3, we measured the variance which occurs due primarily to bonding wire when rotating the 4-channel optical rotary connector by one turn.

The result of the measurement is shown in Fig. 4, from which we could ensure that no level variation due to rotation is observed in the place other than the place where the bonding wire passes above the photo receiving surface and that the level variation due to rotation occurring even in the place through which the bonding wire passes is as small as only 0.5 dB which is practically a negligibly small value.

3.2 Connection efficiency between optical fiber and ring-shaped PD

The area Af of a spot on the detected surface distant by ℓ from the outgoing end of optical fiber having a radius of r and numerical aperture NA is represented with the equation (1) below assuming that the optical fiber has perfect roundness.

$$Af = \pi \cdot (\ell \cdot NA + r)^2 \qquad (1)$$

If the spot area is greater than the detected area, the connection loss takes place. Let the detected area be Aa, the connection loss α_c is represented with equation (2) below.

$$\alpha_c = 10 \cdot \log (Aa/Af) \ [dB] \quad Aa < Af \qquad (2)$$

Fig. 5 shows the result of the numerically calculated relationship between the connection loss and the connection efficiency relative to the distance between the outgoing end of fiber and the photo receiving surface by taking the numerical aperture NA as a parameter. The calculation result proves that when the NA is set at 0.2, 0.25, and 0.3 the maximum distance which eliminates the connection loss are 2.36, 1.88, and 1.56 mm, respectively. In other words, it indicates that if the place where there is no bonding wire is within these distances, the connection efficiency can be considered nearly 100%.

On the other hand, if expanding the spot diameter to the ring width in the place where bonding wire passes across and above the photo receiving surface, the influence of bonding wire can be minimized. For example, if a bonding wire with an external diameter of 25 μm is located at the center of the spot under this condition, its connection loss is calculated as shown in Fig. 6. That is, this diagram proves that under the ideal condition, the connection loss can be reduced down to 0.15 dB. Therefore, the above consideration is desired for practical design.

4. Frequency Characteristic

4.1 An equivalent circuit of the PD

An equivalent circuit of the PD can be represented as shown in Fig. 7, where the PD absorbs light in the depletion layer so as to play a role of the current generating source and has the internal resistance Ri and junction capacitance Cj. Internal resistance Ri determines dark current and junction capacitance Cj is proportional to PN junction area. The output signal is detected by connecting load resistance $R\ell$.

When the light modulated by sine wave enters the PD, the photoelectric current i(t) is generated in response to the light entered, and the voltage v(t) generated at both ends of load resistance $R\ell$ is represented with equation (3) below assuming that photoelectric current i(t) is a sine wave having an amplitude of i.

$$v(t) = i \cdot e^{j\omega t} \cdot R\ell / \sqrt{1 + (\omega Cj R\ell)^2} \qquad (3)$$

In equation (3), letting the frequency that reduces the voltage to $1/\sqrt{2}$, that is, the power to half (3 dB down) be the cut-off frequency fc, it can be represented with equation (4) below.

$$fc = 1/(2\pi Cj R\ell) \qquad (4)$$

On the other hand, Cj is in inverse proportion to the width of the depletion layer and the width of the depletion layer increases in proportion to 1/2 power of the inverse voltage (bias voltage Vr), that is, the following relation is satisfied.

$$Cj \propto 1/\sqrt{Vr} \qquad (5)$$

4.2 Frequency band width measurement using the bias voltage as parameter

The measurement system having the same constitution as that used for the surface sensitivity distribution (Fig. 3) was used to measure the frequency at which the normalized modulation output level drops by 3 dB and we made the measured frequency represent the frequency band width. The measurement was executed for the two ring PDs having the same structure and we obtained the same measurement result. The measurement result of the band width for the bias voltage of ring PD No. 1 is shown in Fig. 8 as a characteristic example. Here, ring PD #1 indicates the innermost ring, and ring PD #4 the outermost ring.

This result indicates that the band width increases nearly linearly until the bias voltage reaches the neighborhood of 20 V and in the range of voltage exceeding 20 V the band width ascends moderately with a saturation tendency. Characteristically speaking, the innermost ring #1 having the least photo receiving area indicates the best band as 80 MHz at a bias voltage of 50 V and even the outermost ring #4 having the largest photo receiving area holds a band of 50 MHz.

Fig. 9 shows the relationship between the photo receiving area of each ring and its capacitance between terminals when holding the bias voltage at 30 V, where the broken lines are drawn taking ring #4 as reference with the assumption that both the photo receiving area and the junction capacity are linear. As is obvious from Fig. 9 as a ring is situated at an inner side the difference between the solid line and the broken line tends to increase in steps of about 10 pF. The reason for such tendency resulting in the diagram in Fig. 9 would be that when considering the distance between each ring and the output terminal for the bonding wire connected to the ring the number of contact points existing between adjacent rings via insulator in between is 3 for ring #1, 2 for ring #2, and 1 for ring #3, respectively, and that every contact point causes a capacity of 10 pF to be added. Pertaining to this, an attempt to reduce the capacitance to be added is under examination.

5. Crosstalk Characteristic

5.1 An equivalent circuits for crosstalk

In this paragraph, we will explain the crosstalk characteristic which is an important transmission characteristic of the multi-channel optical rotary connector. To simplify the problem, here, we used an equivalent circuit for two rings to try to analyze the crosstalk.

The equivalent circuit, taken in this analysis here, is the one for the cathode common double-ring PD. We now assume that there is incident light toward each of two rings, respectively, whereby two current sources $i_1(t)$ and $i_2(t)$ exist. Then, the equivalent circuit can be represented as shown in Fig. 10(a), where Cj1 and Cj2 are terminal capacities between the anodes and cathodes of the rings, and Rℓ1 and Rℓ2 the load resistances, respectively. We consider that although in such ideal equivalent circuit no crosstalk can occur, a slight amount of capacity component must be actually present between rings (A1 - A2 between anodes). Therefore, when there is present only one incident light toward either one ring, its equivalent circuit becomes as shown in Fig. 10(b), where symbol Cc represents the capacity component existing between the rings or between anodes (A1 - A2). How much percent of the signal that occurred in ring #1 leaks to the output of ring #2 is represented with an isolation ratio, and the frequency at which the isolation ratio exceeds 40 dB is subjected to evaluation.

When #1 ring PD receives the photoelectric signal modulated by sine wave in this equivalent circuit, the signal voltage $v_2(t)$ applied to both ends of the load resistance for #2 ring PD is represented with equation (6) below, and isolation ratio I with equation (7), respectively.

$$v_2(t) = \frac{j\omega C_c R_\ell}{1 + j\omega R_\ell (C_j + C_c)} v_1(t) \qquad (6)$$

($R_{\ell 1} = R_{\ell 2} = R_\ell$ is assumed.)

$$I = 10 \log \left\{ (1 + C_j/C_c)^2 + (1/\omega C_c R_\ell)^2 \right\} \text{ [dB]} \qquad (7)$$

Fig. 11 shows numerically calculated result of crosstalk characteristic using the ratio Cc/Cj of the inter-ring capacity Cc to the inter-terminal capacity Cj as parameter. This result is the calculation done assuming that the inter-terminal capacitance be 50 pF, where the frequencies at which the isolation ratio becomes 40 dB are 6.4, 12, 18.5, 26, 34 and 70 MHz for Cc/Cj = 1/10, 1/20, 1/30, 1/40, 1/50, and 1/100, respectively. Namely, this result indicates the tendency that as the inter-terminal capacitance Cj decreases and the ratio Cc/Cj decreases, the crosstalk characteristic gets better.

5.2 A measurement result of crosstalk characteristic between rings

The same measurement system as that (Fig. 3) for surface sensitivity distribution was used to measure the frequency at which the level difference between rings reaches 40 dB. As a characteristic example, Fig. 12 shows the measurement result of crosstalk characteristic between rings #1 and #2 of ring PD No. 1 obtained when holding the bias voltage at 30 V. This result indicates that the frequencies at which the level difference between rings reaches 40 dB are 9.8 MHz between #1 - #2 and 11 MHz between #2 - #1, and that at frequency of 4.2 MHz which is the band width for the NTSC color system a level difference can be obtained 60 dB. Table 2 shows the measurement result of crosstalk characteristic between all the rings of No. 1 and No. 2 ring PDs obtained when holding the bias voltage at 30 V. Table 2 proves that the crosstalk characteristic in the direction from an inner ring to an outer ring is worse than that in the reverse direction. We think that this is due to the difference in capacitance between terminals of each ring which is further due to the difference between photo receiving areas of rings, whereby crosstalk more easily leaks from an inner ring having a small capacitance to an outer ring having a large capacitance while crosstalk leak in the opposite direction becomes hard.

6. The Experiment of Transmitting the Base Band Analog Color Video Signal

We installed a video amplifier at the stage following each ring PD of rings #1 through #4 and measured the SN ratio obtained when receiving a base band analog color video signal. As a result, we confirmed that a SN ratio of 47 dB was obtained for all the ring PDs when a level difference of 7 dB was prepared in terms of light output between the transmission and reception lines, and even when a level difference of 10 dB was prepared between the transmission and reception lines a SN ratio of greater than 40 dB was obtained.

It is generally said that the SN ratio at which one can be released from a bothersome picture noise is around 40 dB, and we made sure that since the measuring value we have obtained this time exceeds 40 dB, the picture quality can be obtained which has actually no problem.

7. The Experiment of Transmitting the Digital/Analog Signal

We executed an experiment of receiving both a rectangular wave signal and a sine wave signal concurrently by rings #3 and #4.

The result is as shown in Photos 1 through 3, where Photo 1 shows the result of receiving a 2 MHz sine wave signal and a 1.4 MHz rectangular wave signal at a time with the use of 220 Ω load resistor and indicates that signal reproduction is properly made without any interference and Photo 2 shows the result of receiving a 6 MHz sine wave signal and a 3.3 MHz rectangular wave signal at a time with the use of 100 Ω and it indicates that signal reproduction is properly made without any interference.

In this connection, Photo 3 shows the waveform obtained when receiving a 100 KHz rectangular wave signal.

8. Conclusion

As a result of the various characteristic tests executed on the optical fiber rotary joint using the quadruple ring Si-PIN-PD, good rotation variance characteristic (below 1 dB), frequency characteristic (cut-off frequency: 50 MHz), and inter-ring cross talk characteristic (isolation ration of 60 dB at a frequency of 4.2 MHz) could be obtained, and further as a result of transmitting the base band analog color video signal a SN ratio of 47 dB could be obtained and a good result was also acquired from the transmission of a digital signal.

References

(1) K. NEMOTO, M. INOUE: Record of National Convention, IEICE, Japan 240. P. 2-58 (1986)

(2) Ammon Yariv: Introduction to Optical Electronics Holt Rinehart and Wiston, Inc., 1971

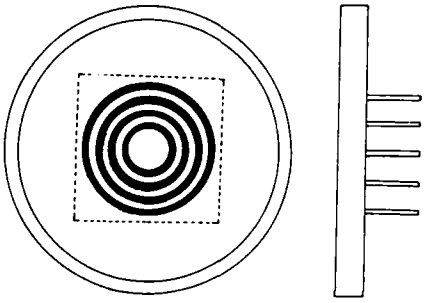


Fig.1 Structure of the quadruple ring shaped Si PIN PD

Table 1. Principal characterristics of ring shaped PD

No.	Items	Symbols	Conditions	Units	Values
1	Quantum Efficiency	η	λ 0.85 μm, Vr 10 V	%	80
2	Photo Sensitivity	S	λ 0.85 μm, Vr 10 V	A/W	0.6
3	Cut off Frequency	f_c	R_g 50 Ω, 3dB Down	MHz	50
4	Dark Current	Id	Vr 10 V	nA	3
5	Capaci tance	Cj	Vr 10 V, f 1 MHz	pF	50
6	Cross talk	T	Vr 10 V, f 4.2MHz	dB	60

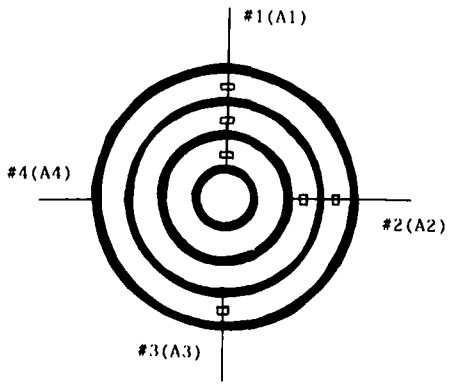


Fig.2 Schematic diagram of the quadrpule ring shaped photo receiving surface

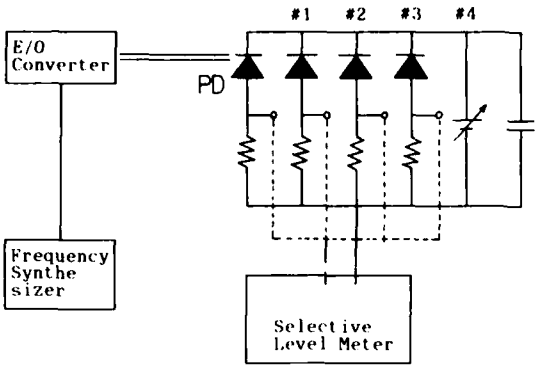


Fig.3 Measurement system

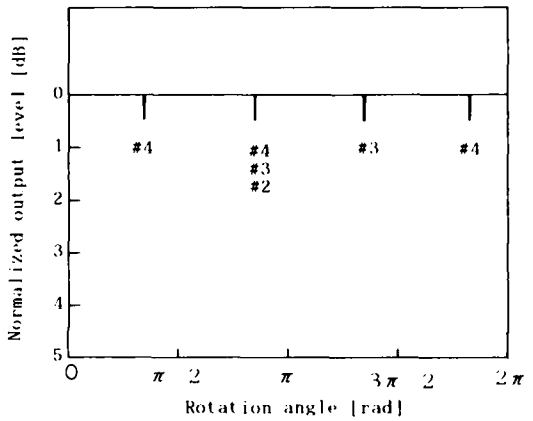


Fig.4 Sensitivity distribution characteristic of ring shaped PD

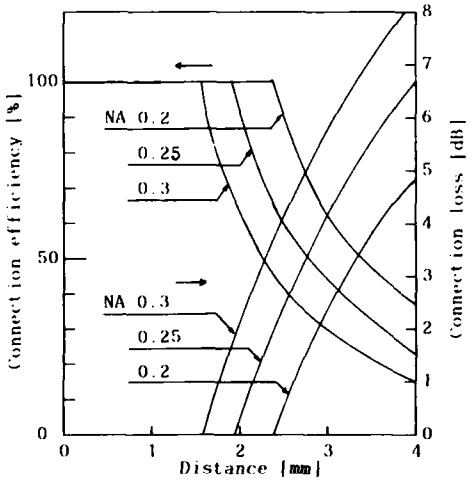


Fig.5 Connection loss and conection efficiency relative to the distance between the end of fiber and the photo receiving surface by taking the numerical apertures NA as parameter

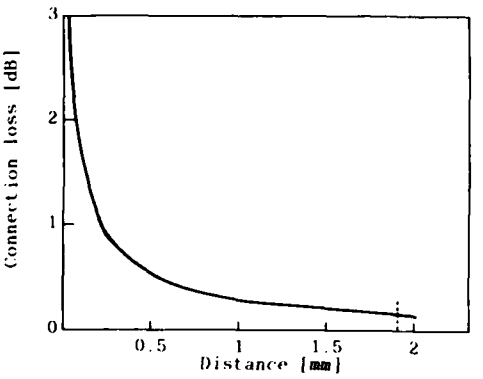
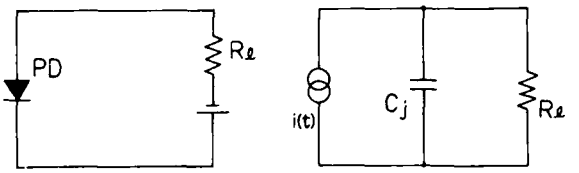


Fig.6 Connection loss when a bonding wire located at the center of spot (NA 0.25)



(a) Physical circuit (b) Equivalent circuit

Fig.7 An equivalent circuit of the PD

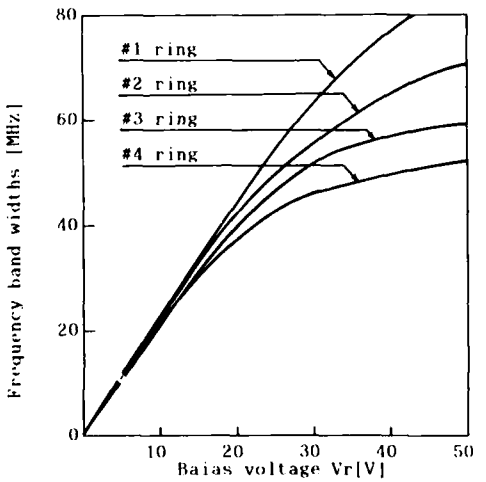


Fig.8 Frequency band widths for bias voltage

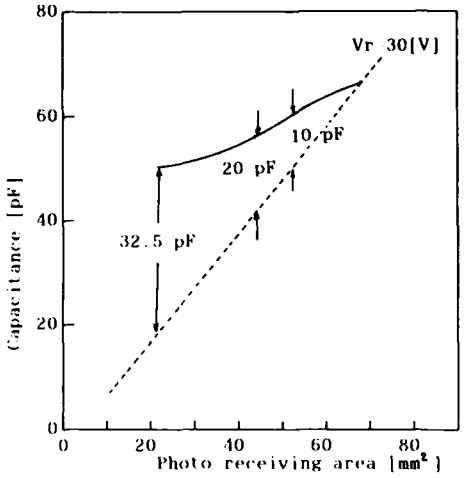


Fig.9 Relationship between the photo receiving area of each ring and its capacitnce between terminals

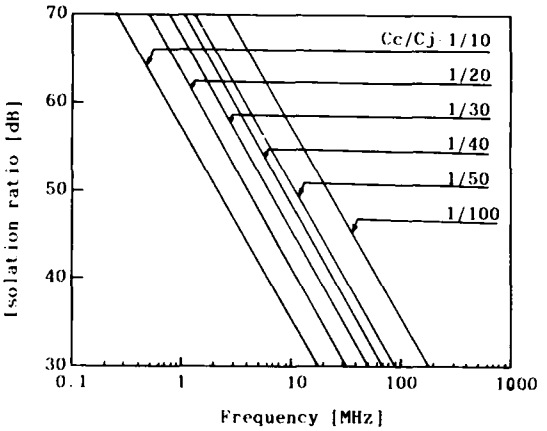


Fig.11 Numerically calculated result of crosstalk characteristic using ratio Cc/Cj as a parameter

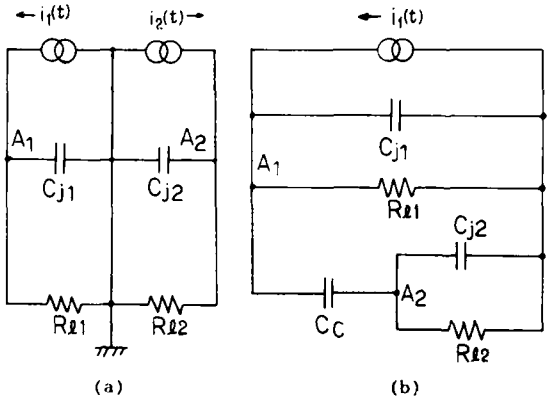


Fig.10 Equivalent circuits for crosstalk

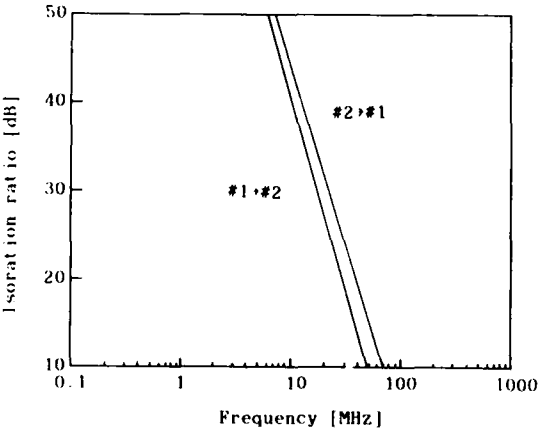


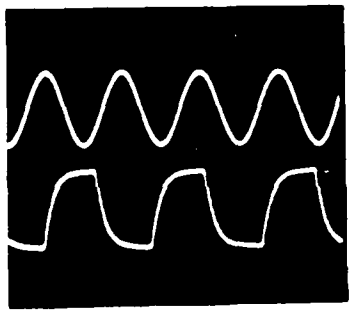
Fig.12 Measurment result of crosstalk characteristic using ratio Cc/Cj as a parameter

Table 2. Crosstalk characteristics

Test Positions / Photo Receiving Rings	# 1	# 2	# 3	# 4
# 1		9.8 10.0	9.2 9.0	9.0 8.2
# 2	11.0 12.0		8.6 8.6	8.6 9.0
# 3	12.0 12.0	9.6 9.4		8.4 7.8
# 4	12.0 13.0	10.5 11.0	8.8 9.0	

Over (No.1)
Under(No.2)

Units : MHz
Vr 30 V

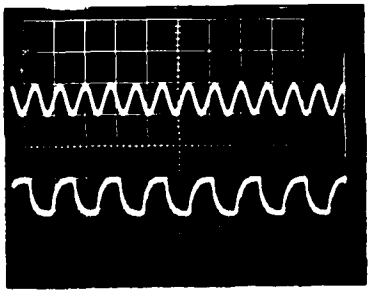


2 [MHz]

R_ℓ 220 [Ω]

1.4 [MHz]

Photo 1

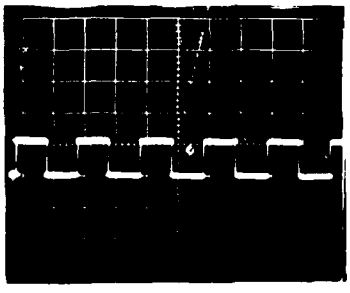


6 MHz]

R_ℓ 100 [Ω]

3.3 [MHz]

Photo 2



R_ℓ 100 [Ω]

100 [KHz]

Photo 3



Kazumasa Nemoto received the B.S degree in electrical communication engineering and the M.S degree in electronic engi neering from Tokyo Denki University in 1976 and 1979, respectively. He joined Ocean Cable Co,Ltd.,where he has been engaged in R&D of undersea observational eqiupments.



Masami Inoue received the B.S degree from Tokyo metoroporitan University in 1971, then he joined Ocean Cable Co.,Ltd. Now, he has been engaged in R&D of undersea observational equipments and cables.

Design and Performance of the New Single-Mode Fiber Connector with MP-Ferrule in Subscriber Network

K. Kashihara, M. Fukuma, T. Kakii, S. Suzuki

Sumitomo Electric Industries, Ltd.
1, Taya-cho, Sakae-ku, Yokohama, 244, Japan

Abstract

Small-size connectors for both jacketed fibers (SJ) and pre-connectorized cables (SP) have been developed using the same composite metal-plastic ferrules(MP). The SJ single-mode fiber connector with MP-ferrule may be mounted on connecting board at intervals of 6 mm using a push-on connecting mechanism. The average insertion loss was found to be 0.14 dB with physical contact condition; the return loss of the MP-ferrules polished by elastic polishing sheet was more than 35 dB without index matching oil.

As for the SP connector, by clamping the MP-ferrule flange portion directly with the spring clip, the outer dimension is reduced to only 4 mm. The average insertion loss was 0.13 dB using index matching oil.

1. Introduction

Optical fiber cables have been used in various applications. Therefore, various kinds of connectors are in demand.

As the application for high density cables in subscriber network increases, the miniaturization of a connecting portion is needed.

Types of connectors are divided into jacketed fibers and coated fibers. The connector for jacketed fiber has Kevlar fixing structure, and is mainly used in case of frequent reconnection of connectors. Therefore, the mechanism for easy reconnection is fit to the structure of the connector for jacketed fiber. The push-on type connector which has the mechanism for easy reconnection has already been developed [1][2]. The connector for coated fiber is used for connecting cable to cable to construct optical transmission line and mainly applies to pre-connectorized cables. Pre-connectorized cables have come into use to facilitate field connecting operations which are being substituted for fusion splicing. Therefore, to mount the high density cables, miniaturization of the connector and simplification of the structure are needed. The small-size connector with precision plastic-molded ferrule has already been developed [3][4].

This paper describes the design and performance of the new single-mode fiber connector with MP-ferrule in subscriber network.

2. Connector Design

(1) MP-ferrule

Optical fiber connector ferrule is a very important part for performance of optical fiber connector. Metal-type, ceramic-type and plastic-type ferrules have been developed. Metal-type and ceramic-type ferrules have the advantage of high performance and high reliability, but a disadvantage in production costs. Plastic-type ferrule has the opposite inherent characteristics to those mentioned above. Therefore, to achieve both advantageous characteristics in a ferrule, composite metal-plastic ferrule (MP) have been developed [6], and applied to the new single-mode fiber connectors.

The structure of the MP-ferrule, illustrated in Figure 1, consists of a molded plastic body partially surrounded by a stainless steel sleeve. Part of the outer metal sleeve is embedded in the flange of the ferrule to increase the ferrule's bending strength. To facilitate the polishing of the endface of the ferrule, the molded plastic portion projects out from the end of the metal sleeve. The MP-ferrule's physical contact portion with a low Young's modulus is more effective in eliminating the Fresnel reflection loss compared with metal-type and ceramic-type ferrules in terms of Hertz contact theory. Experimental result using MP-ferrule is shown in Figure 2.

(2) SJ connector with MP-ferrule

The connector for jacketed fiber requires the mechanism for easy reconnection and miniaturization of the connecting portion. To facilifate the reconnection of connectors which are mounted on connecting board in high density, a push-on connecting mechanism [1][2] is applied. The push-on connecting mechanism has the characteristics that pushing the plug into the adaptor is only needed for connection, and only pulling the plug

out for disconnection.

The SJ connector with the push-on connecting mechanism is shown in Figure 3. To mount the connecting boad in high density, the side of the ejector and the side of the adaptor are cut at widths of 5.9 mm and 6 mm respectively. Therefore, the SJ connector may be mounted at intervals of 6 mm.

(3) SP connector with MP- ferrule

The connector for coated fiber is applies to pre-connectorized cables. The miniaturization of the connector to mount the high density cables and the simplification of the structure of the connector to facilitate connecting operations are in demand. Furthermore, the connector for coated fiber is needed to reduce the connector weight.

The SP connector is shown in Figure 4, and consists of the plug, adaptor and spring clip. As a result of simplifying the structure of the connector and reducing the connector weight, the plug consists of only MP-ferrule. Consequently, only fixing the MP-ferrule to the coated fibers is sufficient for mounting to the cables. The SJ connector is connected by the spring clip. By clamping the MP-ferrule flange portion directly using the spring clip, the outer dimension is reduced to only 4 mm.

3. MP-Ferrule Production and Connector Assembly

(1) MP-ferrule

Using the metal sleeve insert molding technique, MP-ferrule can be produced in the same manner as plastic-type ferrule [5] (Figure 5). Metal sleeve is inserted into the cavity, and then, epoxy resin is transfermolded with low pressure into the cavity. After curing the epoxy resin, the mold pin is removed from the MP-ferrule to form the optical fiber guide hole.

(2) SJ connector with MP-ferrule

The SJ connector is assembled using the following 4 steps:

1) The jacketed fiber is inserted through the five parts which will compose the plug. The outer jacket and the buffer jacket are removed by stripper.

2) The stripped jacketed fiber is inserted into the MP-ferrule filled with epoxy resin. The epoxy resin is cured using the heating machine.

3) After curing the epoxy resin, the MP-ferrule's endface is polished by the polishing machine. The polishing procedure is shown in Table 1. Using elastic polishing sheet, the MP-ferrule's endface made of plastic can be easily polished to a spherical surface. Spherical polishing method is illustrated in Figure 6, the spherical surface radius polished by this method was $\sim$ 20 mm.

4) The last part is fixed and the finally assembled plug is inserted into the adaptor.

(3) SP connector with MP-ferrule

The SP connector is assembled using the following 4 steps:

1) The buffer jacket is removed by stripper.

2) The stripped coated fiber is inserted into the MP-ferrule filled with epoxy resin. The epoxy resin is cured using the heating machine.

3) After curing the epoxy resin, the MP-ferrule's endface is polished by the polishing machine. The polishing procedure is shown in Table 2.

4) The polished MP-ferrule is inserted into the adaptor, and clamped by spring clip.

4. MP-Ferrule Characteristics and Connector Performance

(1) MP-ferrule

MP-ferrule characteristics are shown in Table 3. Using the metal sleeve, the outer circumference portion is completed in high precision. This metal sleeve was embedded in the flange of the ferrule and the MP-ferrule's bending and tensile strength were more than 8 kg and 15 kg, respectively.

(2) SJ connector with MP-ferrule

The insertion loss of the SJ connector with MP-ferrules applied to single-mode fibers is shown in Figure 7. The average insertion loss was 0.14 dB with physical contact; the return loss of the MP-ferrules polished by elastic polishing sheet was found to be more than 35 dB. Figure 8 shows the result of reconnection endurance test. Variation in the insertion loss during 500 insertion and removal was within $\pm$0.1 dB with the connection endface being cleaned after every 25 insertions. Vibration test was made at the frequency of 20 Hz and the amplitude of 0.75 mm for 2 hours. Variation in the insertion loss was less than 0.05 dB.

Furthermore, the temperature cycling test was performed at a temperature from -30 °C to 60 °C for 30 cycles, as shown in Figure 9. The measured

variation in the insertion loss was within ±0.1 dB.

(3) SP connector with MP-ferrule

Figure 10 shows the insertion loss of the SP connector with the MP-ferrule. The average insertion loss was 0.13 dB using index matching oil. To confirm the reliability of this connector, various environmental tests were conducted as follows:

1) Vibration test was made at the frequency of 20 Hz and the amplitude of 0.75 mm for 2 hours. Variation in the insertion loss was less than 0.02 dB.

2) Temperature cycling test was performed at a temperature from -30 °C to 60 °C for 30 cycles, as shown in Figure 11. Variation in the insertion loss was within ±0.1 dB.

3) High humidity test was conducted under the condition of 80 °C and 95 % RH for 180 hours. Variation in the insertion loss was less than 0.04 dB, as shown in Figure 12.

5. Conclusions

Composite metal-plastic ferrules (MP) have been developed with both advantageous characteristics of conventional metal-type and plastic-type ferrules. New single-mode fiber connectors (SJ and SP) have been developed using the same MP-ferrules. As a result of miniaturization of the connectors, the SJ connectors and the SP connectors may be mounted at intervals of 6 mm and 4 mm respectively. The average insertion loss of the SJ connectors applied to single-mode fibers was 0.14 dB with physical contact. The average insertion loss of the SP connectors applied to single-mode fibers was 0.13 dB using index matching oil. Various environmental tests were conducted to confirm the reliability of the SJ and SP connectors. The results show that the both connectors can be used in the subscriber network.

References

[1] S. Nagasawa, T. Satake, I. Sankawa and R. Arioka, "Optical-fiber fanout connector for 10-fiber ribbon cable termination", IEEE J. Lightwave Technol., Vol.LT-4, 8, pp. 1243 ∿ 1247, 1986.

[2] S. Nagasawa, I. Sankawa, T. Satake and N. Kashima, "Small-size push-on type optical fiber connector", Trans. IEICE Japan, Vol.E70, 5, pp. 451 ∿ 454, 1987.

[3] I. Sankawa, S. Nagasawa, T. Satake, M. Ishida and R. Arioka, "Low-loss small-size optical-fiber connector with a precision plastic-molded ferrule", IEEE J. Lightwave Technol., Vol.LT-4, 8, pp. 1237 ∿ 1242, 1986.

[4] I. Sankawa, S. Nagasawa, M. Ishida, and R. Arioka, "Design and performance of small-size optical fiber connector", IECE Technical Report, CS 85 ∿ 129, 1985.

[5] T. Satake, I. Sankawa, S. Nagasawa and F. Ashiya, "Design and characteristics of direct molded optical fiber connector for subscriber optical line system", IECE Technical Report, CS 84 ∿ 127, 1984.

[6] T. Kakii, K. Kashihara, Y. Asano and S. Suzuki, "Composite metal-plastic ferrule for single-mode fiber connector", in Tech. Dig. OFC/IOOC, TUF5, 1987.

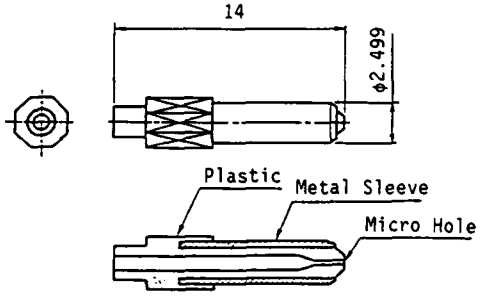


Figure 1 MP-Ferrule

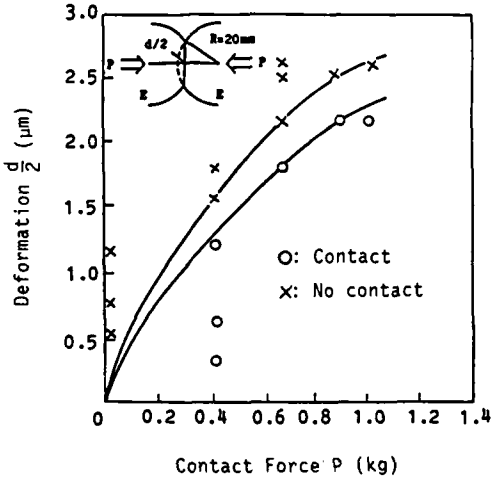


Figure 2 MP-Ferrule Contact Characteristic

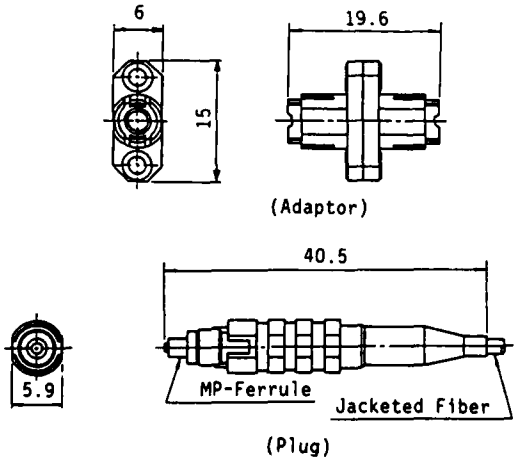


Figure 3 SJ Connector with MP-Ferrule

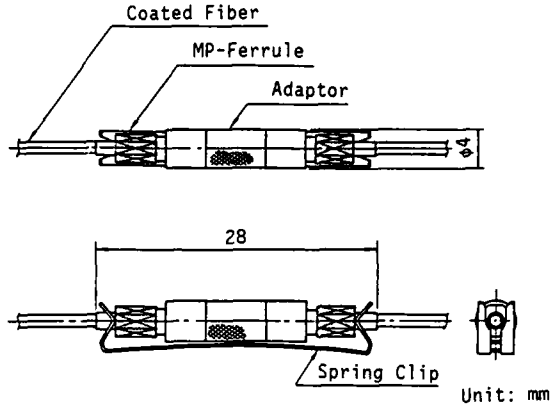


Figure 4 SP Connector with MP-Ferrule

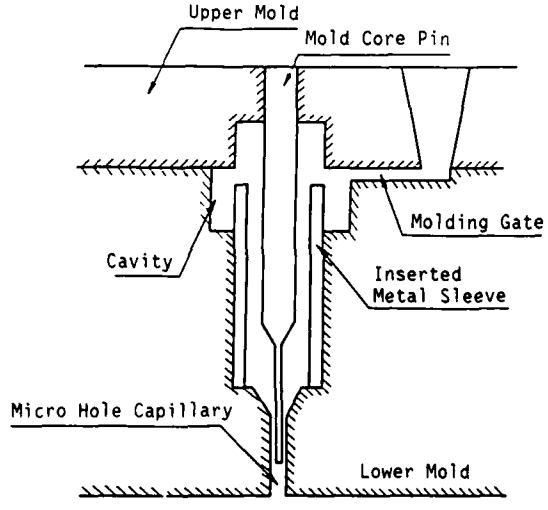
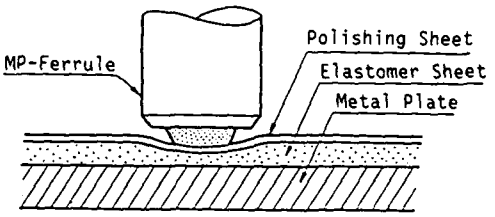
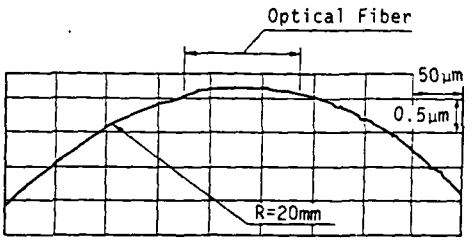


Figure 5 Metal Sleeve Insertion Molding for MP-Ferrule Production

Table 1 Polishing Procedure of SJ Connector

	Polishing Sheet	Time
Step 1	6 μm	1 sec
Step 2	1 μm	30 sec
Step 3	0.5 μm + Elastomer Sheet	50 sec





Shape of PC
Polished Endface

Figure 6 Physical Contact Polishing of MP-Ferrule

Table 2 Polishing Procedure of SP Connector

	Polishing Sheet	Time
Step 1	6 μm	1 sec
Step 2	1 μm	30 sec
Step 3	0.3 μm	30 sec

Table 3 MP-Ferrule Characteristics

Item	Result
Diameter	2.499 ± 0.0005 mm
Eccentricity	< 0.5 μm
Roundness	< 0.5 μm
Surface Roughness	< 0.1 μm Ra
Bending Strength	> 8 kg
Tensile Strength	> 15 kg

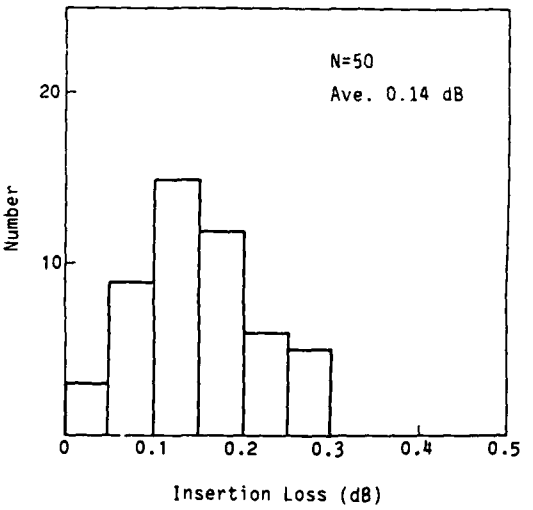


Figure 7 Insertion Loss of SJ Connector for Single-Mode Fibers

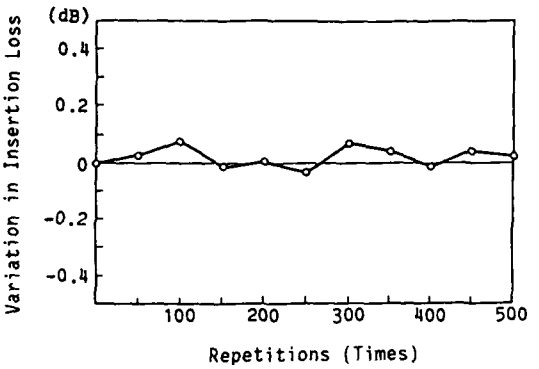


Figure 8 Reconnection Endurance Test of SJ Connector

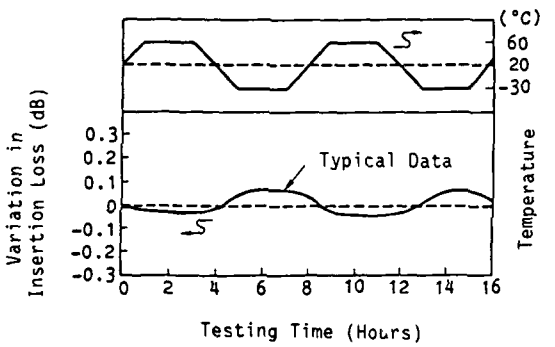


Figure 9 Temperature Cycling Test of SJ Connector

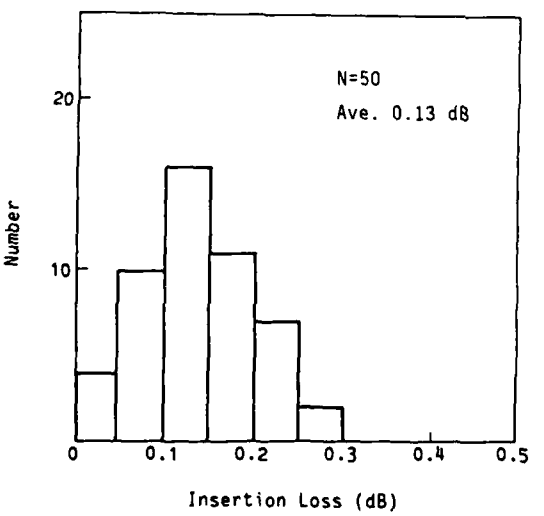


Figure 10 Insertion Loss of SP Connector for Single-Mode Fibers

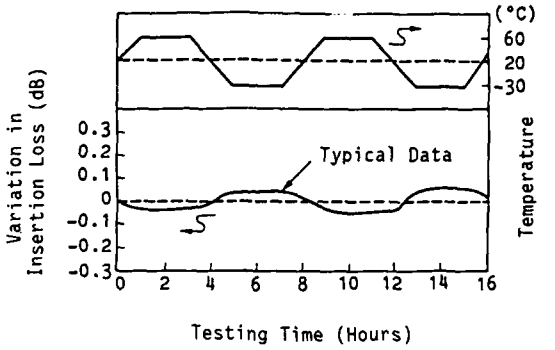


Figure 11 Temperature Cycling Test of SP Connector

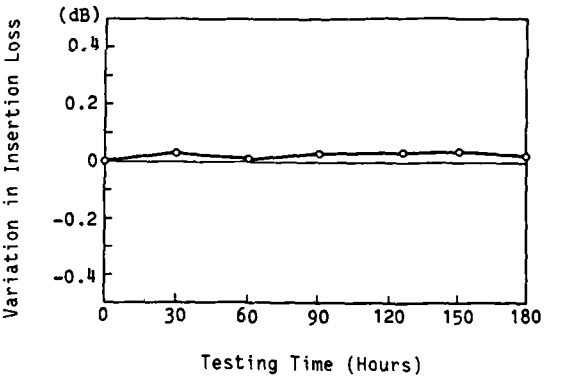


Figure 12 High Humidity Test of SP Connector



Koji Kashihara

Sumitomo Electric
Industries, Ltd.

1, Taya-cho, Sakae-ku,
Yokohama, Japan

Koji Kashihara received his B.S. degree in mechanical engineering from Science University of Tokyo in 1985. He then joined Sumitomo Electric Industries and has been engaged in research and development of optical fiber jointing technologies. Mr. Kashihara is a member of Communication R & D Department in Yokohama Research Laboratories, and a member of the Institute of Electronics and Communication Engineers of Japan.



Toshiaki Kakii

Sumitomo Electric
Industries, Ltd.

1, Taya-cho, Sakae-ku,
Yokohama, Japan

Toshiaki Kakii was born in 1955 and received a M.E. degree from Keio University in 1980. He joined Sumitomo Electric Industries, Ltd. in 1980 and has been engaged in research and development of optical fiber jointing technologies. He is a member of the Institute of Electronics and Communication Engineers of Japan.



Masumi Fukuma

Sumitomo Electric
Industries, Ltd.

1, Taya-cho, Sakae-ku
Yokohama, Japan

Masumi Fukuma received a M.S. degree in Electrical and Electronic Engineering from Toyohashi University of Technology in 1985. He joined Sumitomo Electric Industries, Ltd. in 1985, and has been engaged in research and development of optical fiber and cables. Mr. Fukuma is a member of Communication R & D Department in Yokohama Research Laboratories.



Shuzo Suzuki

Sumitomo Electric
Industies, Ltd.

1, Taya-cho, Sakae-ku
Yokohama, Japan

Shuzo Suzuki received a M.S. in 1972 from Tokyo University. He joined Sumitomo Electric Industries, Ltd. in 1972, and has been engaged in research and development of optical fiber, cable and jointing technologies. He is a member of the Institute of Electronics and Communication Engineers of Japan.

Single-Mode Optical Fiber Ribbon Splicer

Yasuyuki Kato*, Akihiko Ishikura*, Teruyuki Sano**, and Seiji Takashima**

* NTT Laboratories.
Tokai, Ibaraki-ken, 319-11, Japan

** NTT Network Systems Development Center.
1-2-1 Uchisaiwai, Chiyoda-ku, Tokyo, 100, Japan.

SUMMARY

A new stuffing-pulling fusion technique for mass fusion splicing of single-mode fibers is presented. The fiber spliced-region is pulled after the fiber end faces are fused and stuffed to each other. The characteristic feature of this technique is that the stuffing and pulling strokes are varied, based on observation of the fiber end face gaps for every splice. This technique can reduce splice loss to approximately 50 percent of that realized by the conventional method, and can eliminate splice failure due to end face gap variance. A mass fusion splice machine based on this method is newly developed, and it is confirmed that an average splice loss of 0.024 dB and fusion splice time of one minute per ribbon unit are attained for mass fusion splicing of single-mode fibers.

1. INTRODUCTION

Recently, the application area of single-mode fibers has been rapidly expanding. Further introduction of single-mode fibers for subscriber systems is expected in the near future. For this purpose, a mass splicing technique that can splice a large number of fibers with low-loss and minimal working-time is indispensable.[1] [4]

In this paper, the problem of mass fusion splicing for single-mode fibers is discussed with regard to splice loss and splice failure probability. The methods presented are two new stuffing-pulling fusion techniques (Constant Stuffing and Pulling: CSP and Variable Stuffing and Pulling: VSP methods), where the fiber spliced-region is pulled after end faces are fused and stuffed to each other. In addition, a mass fusion splice machine based on the present method is newly developed, and its performance with respect to splice loss and splice time is investigated. Finally, efficiency and utility of the present methods are confirmed theoretically and experimentally.

2. PROBLEM WITH MASS FUSION SPLICE

2.1 END FACE GAP VARIANCE

Ribbon fiber end faces are prepared by bending pulling stress, after the ribbon fibers are scratched perpendicularly to the fiber axis and straight by a cemented carbide blade.[5] Fiber end face variance is caused by bending-pulling stress. Because the fiber jacket coat is designed so that fiber is virtually mobile in the jacket coat. This feature is vital for removing the jacket coat at fiber end face preparation.

Thus, a ribbon fiber holder[6] is used to reduce end face variance for the end face preparation. However, this is difficult to achieve. A schematic view of the prepared ribbon fibers at the splice point is shown in Fig.1. Fiber end face gaps are varied as $D_1 \sim D_N$. Figure 2 shows the distribution of fiber end face gaps D_n when ribbon fiber end faces are butted with each other on V-grooves of a splice machine using the ribbon fiber holder. The fiber ribbon unit to be spliced consists of ten fibers. The horizontal axis D_n denotes the values obtained by subtracting the minimum end face gap D_{MIN} in each ribbon unit from actual values D_n of end face gaps for individual fibers, and expressed as

$$D_n = D_n - D_{MIN} \qquad (1 \leq n \leq 10). \tag{1}$$

It can be determine from this figure that average and maximum end face gap values are 11 μm and 50 μm, respectively. With such a large variance, the stuffing stroke[7] of fiber end face should be increased to minimize splice failure ratio. The solid curve in the figure shows the end face gap distribution calculated by the least-squares method. The probability density function P_D is represented as

$$P_D = C_1 (D_n + 1) \exp \{ - (D_n + 1) / C_2 \} . \tag{2}$$

where coefficients C_1 and C_2 are evaluated as 0.025 (μm^{-1}) and 6.4 (μm), respectively.

2.2 SPLICE LOSS AND SPLICE FAILURE RATIO

The influence of the end face gap variance on splice loss is investigated in this section. Fiber end faces to be spliced are separated a specific distance D_0 prior to fusion. Then, the end faces are fused and stuffed into each other by continuous heating. In our experiment, this pre-fusion technique[8] is also used. Thus, fiber end faces are over stuffed when the end face gap is narrow, while, fiber end faces can not be fused because of wide end face gaps. In the latter case, splicing is unsuccessful. Fiber end face gap variance also causes stuffing stroke variance. The relationship between splice loss α_s and stuffing stroke S is shown in Fig.3. and expressed as

$$\alpha_s = C_3 S + C_4 \qquad \text{(dB)}. \tag{3}$$

where coefficients C_3 and C_4 are evaluated to be 1.23 (dB/μm) and 0.016 (dB), respectively. Vertical segments represent scattering of data for 10 splices. Structural parameters of fibers used in the experiment are listed in Table 1. Discharge duration time is 5 sec. Here, if we let the stuffing stroke of the splice machine be S_0; actual stuffing stroke of fiber end face is (S_0+D_0), stuffing stroke S_n of fiber n in a ribbon unit is given by

$$S_n = S_0 - D_n. \tag{4}$$

Therefore, α_s can be expressed from Eqs.(3) and (4) as

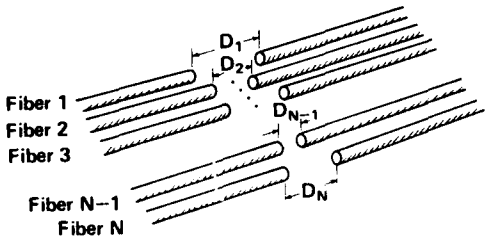


Fig.1 Schematic view of fiber end face gap deviation for mass fusion splice.

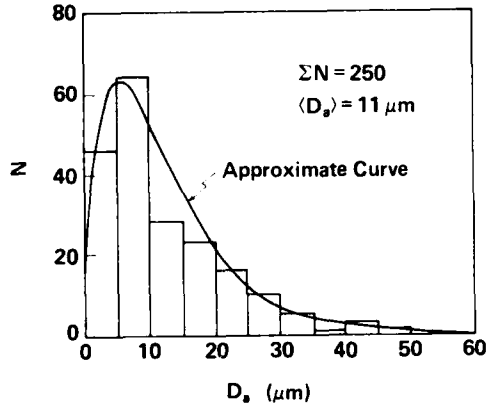


Fig.2 Distribution of fiber end face gap.

$$\alpha_s = C_3 (S_o - D_s) + C_4 \quad (dB). \tag{5}$$

Here, the splice is successful for $S_n > 0$, and fails for $S_n < 0$. Furthermore, distribution of α_s is derived using Eqs.(2) and (5). The distribution function Q_S of α_s is obtained as

$$Q_S = P_D / (d\alpha_s / dD_s) \tag{6}$$

$$= C_1(C_C - \alpha_s)\exp\{(C_C - \alpha_s)/C_2C_3\} / C_3^2,$$

$$C_C = C_3 + C_4 + C_3S_o.$$

Splice failure ratio R_f can be also derived on the condition that the splice is unsuccessful unless all fibers in the ribbon unit are fused together.

$$R_f = 1 - \left[\int_0^{S_o} P_D \, dD_s\right]^N. \tag{7}$$

Average splice loss $\langle \alpha_s \rangle$ is given by Eq.(6) as

$$\langle \alpha_s \rangle = \int_{C_4}^{\alpha_{so}} \alpha_s Q_S \, d\alpha_s \Big/ \int_{C_4}^{\alpha_{so}} Q_S \, d\alpha_s, \tag{8}$$

$$\alpha_{so} = C_3S_o + C_4.$$

Figure 4 shows the dependence of average splice loss $\langle \alpha_s \rangle$ and the splice failure ratio R_f on the stuffing stroke S of fiber end face. It is found that splice failure probability decreases dramatically by increasing the stuffing stroke. However, this results in increased splice loss. This is the most significant problem in mass fusion splicing.

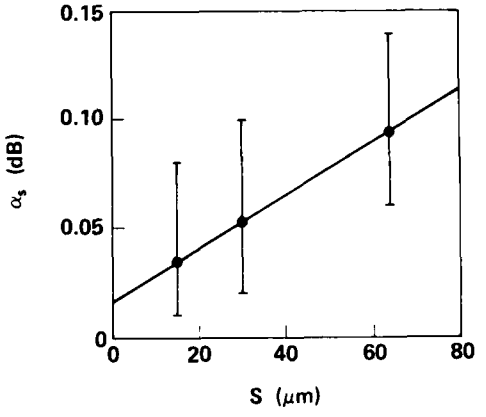


Fig.3 Relationship between splice loss and stuffing stroke of fiber end face.

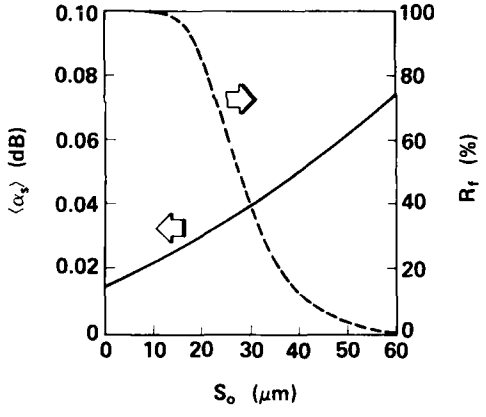


Fig.4 Dependence of average splice loss and splice failure ratio on stuffing stroke of fiber end face.

3. LOSS REDUCTION IN MASS FUSION SPLICING

In this section, a new stuffing-pulling fusion technique, in which the fiber spliced-region is pulled after the fiber end faces are fused and stuffed into each other, is presented for reducing splice loss.

3.1 TREATMENT OF SPLICE POINT AND SPLICE LOSS

It has been confirmed in our various experiments that excess loss due to the core metamorphosis caused by over stuffing the fiber end face was alleviated by pulling the spliced-region after the fiber end faces were fused and stuffed into each other. The stuffing-pulling technique is based on this effect, and its splice process is schematically shown in Fig.5.

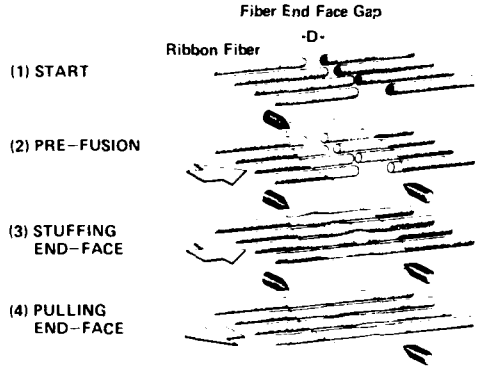


Fig.5 Fusion splicing process for the present method.

The measured relationship between splice loss α_s and pulling stroke L as a function of stuffing stroke S_o is shown in Fig.6. Measured points in the figure indicate mean values for ten splices. Fibers used in the experiment are the same as shown Table 1. The curves in the figure represent the best-fit curves obtained by the least squares method. Splice loss decreases gradually in the $0 \leq L \leq S_o$ range, which corresponds to the dissolution of core metamorphosis. For further pulling ($L > S_o$), splice loss increases gradually again due to the formation of steep taper[9] at the splice point. As a result, the optimum value of the pulling stroke appears to be near $L = S_o$. Furthermore, the minimum value of the splice loss at $L \leq S_o$ increases as the stuffing stroke increases. It is clear from these measurements that a stuffing-pulling fusion technique effectively reduces splice loss. Splice loss α_s after the pulling process is approximated as follows:

$$\alpha_s \quad G_A(S)L^2 + G_B(S)L + G_C(S) \quad \text{(dB)}, \qquad (9)$$

$$G_A(S) \quad C_6S + C_8, \quad G_B(S) \quad C_7S + C_9, \quad G_C(S) \quad C_3S + C_4,$$

where coefficients C_6, C_8, C_7, and C_9 are evaluated as 4×10^{-8} (dB/μm^3), 4.6×10^{-6} (dB/μm^2), 1.3×10^{-5} (dB/μm^2), and -6.5×10^{-5} (dB/μm), respectively. In Eq.(9), when $L = 0$, α_s corresponds to Eq.(3).

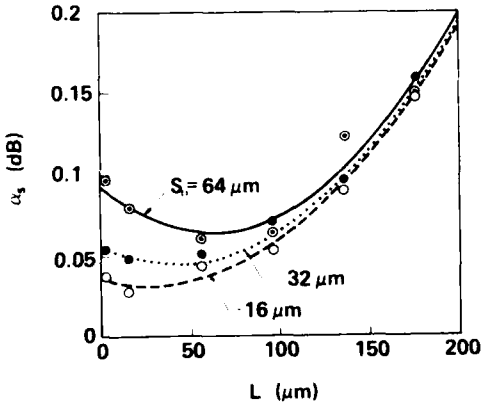


Fig.6 Dependence of splice loss on pulling stroke of fiber end face.

3.2 OPTIMUM PULLING STROKE

As previously mentioned, stuffing stroke varies depending on end face gap variance. Therefore, the optimum pulling stroke L_o which minimizes average splice loss is considered to exist. The optimum pulling stroke is derived from the distribution of splice loss. Splice loss distribution Q_L introduced the pulling process is given by Eqs.(2), (3), (4), and (9).

$$Q_L = P_D / \left(d\alpha_s / dD_a \right) \qquad (10)$$

$$= -C_1(D_L + 1) \exp\left\{ -(D_L + 1)/C_2 \right\} / F,$$

where

$$D_L = (E - \alpha_s)/F, \qquad B_A = C_6S_o + C_8,$$
$$E = B_AL^2 + B_BL + B_C, \qquad B_B = C_7S_o + C_9,$$
$$F = C_6L^2 + C_7L + C_3, \qquad B_C = C_3S_o + C_4.$$

Average splice loss $<\alpha_s>$ introduced in the pulling process is given by

$$<\alpha_s> = \int_H^E \alpha_s Q_L \, d\alpha_s \Big/ \int_H^E Q_L \, d\alpha_s. \qquad (11)$$

$$H \quad C_6L^2 + C_8L + C_4.$$

Optimum pulling stroke L_o with respect to a certain stuffing stroke S_o of the splice machine exists, and can be obtained by $d<\alpha_s>/dL_o = 0$. As this results in a very complex equation, we choose to omit it, and show the calculated result in Fig.7. This figure shows the dependence of the optimum pulling stroke on the stuffing stroke. Figure 8 shows relationship between the average splice loss $<\alpha_s>$ and the stuffing stroke S_o. The dashed and solid curves in the figure indicate $L=0$ and $L=L_o$ cases, respectively. It is found that splice loss increase can be mitigated by choosing the optimum pulling stroke. For instance, average splice loss is reduced from 0.06 dB to 0.05 dB when $S_o=50$ μm. We call the technique CSP-method (Constant Stuffing and Pulling end face method), since the pulling stroke is chosen, and fixed based on the stuffing stroke.

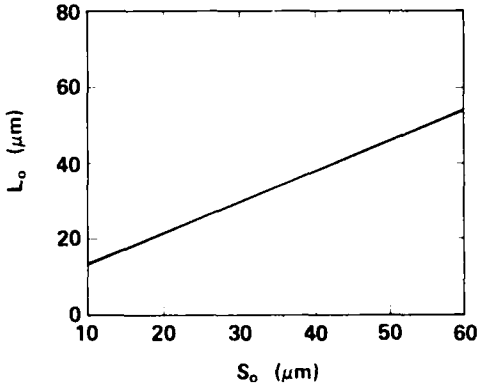


Fig.7 Relationship between the optimum pulling stroke and stuffing stroke of fiber end face.

3.3 VSP SPLICE METHOD

If the stuffing stroke is chosen so that a pair of fibers with the maximum end face gap are fused with each other for ribbon unit splicing, it is possible to eliminate splice failure due to end face gap variance. That is, when

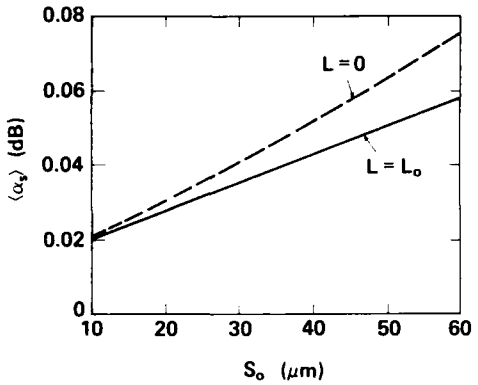


Fig.8 Comparison between conventional and CSP methods as a function of stuffing stroke.

the maximum and minimum end face gaps in a ribbon unit are D_{MAX} and D_{MIN}, the splice machine stuffing stroke is determined as

$$S_o = D_{MAX} - D_{MIN}. \quad (12)$$

For this purpose, all end face gaps in ribbon units should be measured before fusion splicing. It is possible to use image processing with microscopic observation[10]. A schematic view of the end face gaps observation system is shown in Fig.9. In this figure, the fiber end faces fixed in V-grooves are magnified by an objective lens, and focused on a CCD-image sensor. Then, the end face gaps are measured using image processing.

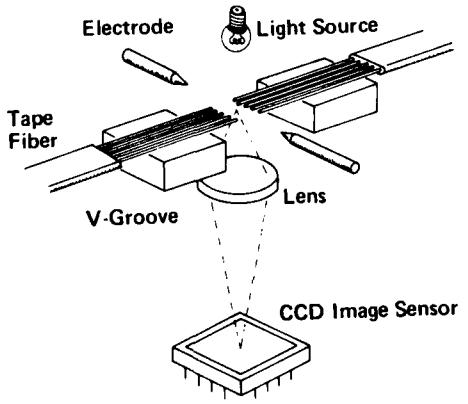


Fig.9 Measurement method of fiber end face gap.

In this method, the stuffing stroke of number n fiber in the ribbon unit can be represented by using measured end face gaps $D_1 \sim D_N$ as

$$S_n = D_{MAX} - D_n, \quad (1 \leq n \leq N) \quad (13)$$

where N denotes the total number of fibers in a ribbon unit. Splice loss for this fiber α_{sn} is derived from Eqs.(9) and (13).

TABLE 1. Structural Parameters of Single-Mode Fibers

Fiber Diameter (μm)	Core Diameter (μm)	Cutoff Wavelength (μm)	Spot Size (μm)	Core Eccentricity (μm)
125 ± 1	10 ± 0.5	1.2 ± 0.1	5 ± 0.2	0 ~ 0.2

$$\alpha_{sn} = G_A(S_n)L^2 + G_B(S_n)L + G_C(S_n) \quad (dB). \quad (14)$$

Then, the average splice loss $\langle \alpha_s \rangle$ is expressed as

$$\langle \alpha_s \rangle = \Sigma\, \alpha_{sn} / N. \quad (1 \leq n \leq N) \quad (15)$$

Consequently, the optimum pulling stroke L_o to minimize average splice loss is obtained as the next equation:

$$L_o = -\, \Sigma\, G_B(S_n) / \Sigma\, G_A(S_n), \quad (1 \leq n \leq N) \quad (16)$$

This method has the special feature that the stuffing and pulling strokes are controlled by a microprocesser to minimize average splice loss. This is based on the observation of fiber end face gaps for each splice. We call the technique VSP-method (Variable Stuffing and Pulling end face method).

3.4 CALCULATED SPLICE LOSS

The calculated cumulative probabilities of splice loss for the CSP- and VSP-methods, along with the results for the conventional method[4] are shown in Fig.10. Probabilities were estimated by a numerical calculation using the end face gap data in Fig.1. Average splice losses of 0.06 dB, 0.05 dB, and 0.03 dB are obtained for the conventional, CSP-, and VSP-methods, respectively. Furthermore, it is found that splice failure probabilities of 5%, 5%, and 0% are obtained for these methods, respectively. A comparison of these results with respect to average splice loss, splice failure ratio, stuffing stroke, and pulling stroke is shown in Table 2. It is confirmed from these results that the VSP splice method reduces splice loss to approximately 50 percent of that realized by the conventional method, thus, it is suitable for mass fusion splicing of single-mode fibers.

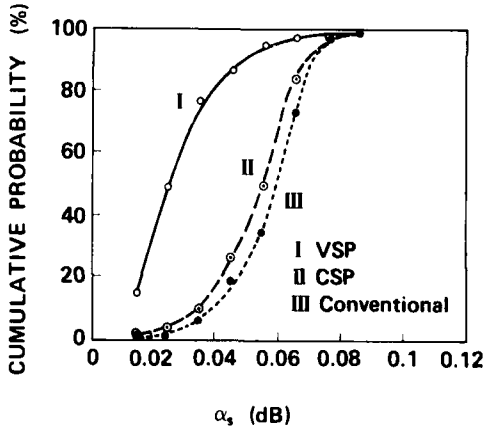


Fig.10 Cumulative probability of splice loss for VSP, CSP, and conventional methods.

TABLE 2. Comparison of the conventional, CSP, and VSP splice methods.

Method	α_m	R_f	S_o	L_o
Conventional	0.06 dB	5 %	50 μm	0
CSP	0.05 dB	5 %	50 μm	46 μm
VSP	0.03 dB	0 %	variable	variable

4. PERFORMANCE OF MANUFACTURED MASS FUSION SPLICE MACHINE

A photograph of a manufactured mass fusion splice machine, constructed to perform the VSP splice process is shown Fig.11. The front panel of the machine is simplified. The machine has only two switches to be manipulated for fiber setting resetting and discharge start. It also has a micro-monitor for displaying splice loss, machine status, and warning messages.

Figure 12 shows a splice loss histogram obtained by the machine. Ribbon fiber used in the experiment is the same as shown in Table 1. It is found from the figure that an average splice loss of 0.024 dB for 80 splices is successfully attained. This result approximates the calculated result of the VSP method in Sec.3.4, and suggests that the VSP method is quite useful. A fusion splice time of one minute per ribbon unit on average is achieved. This time includes inspections of end face irregularities and fiber axis misalignment.

The cumulative probability of estimation error with respect to splice loss for the machine is shown in Fig.13. High level splice losses are intentionally generated to obtain the various splice losses in the experiment. Misalignment in the direction perpendicular to the CCD sensor plane is measured using the focus depth. Although, splice loss is roughly estimated by using misalignment, the average estimation error of 0.039 dB is obtained, and is considered to be sufficiently realistic.

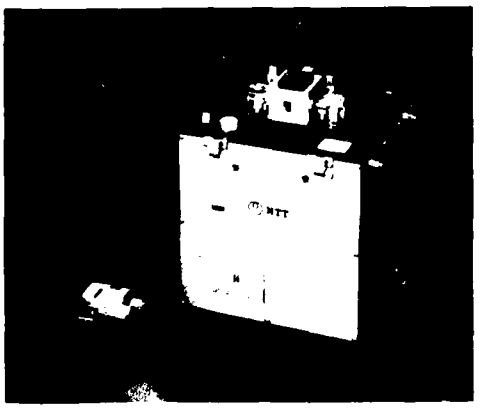


Fig.11 Manufactured mass fusion splice machine.

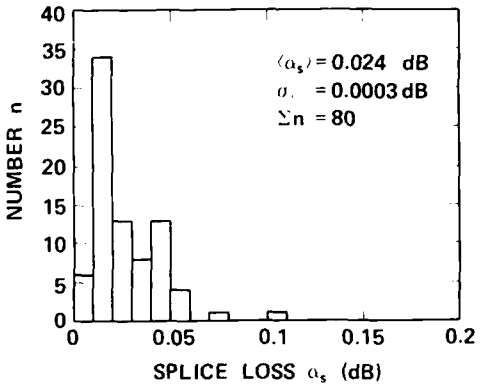


Fig.12 Splice loss histogram obtained by the manufactured splice machine.

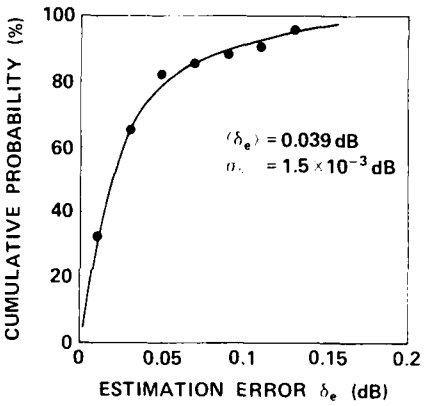


Fig.13 Cumulative probability of estimation error.

5. CONCLUSION

A mass fusion splicing technique for single-mode fibers has been investigated in detail with respect to splice loss and splice failure probability. A new stuffing-pulling fusion technique, where the fiber spliced region is pulled after the fiber end faces are fused and stuffed to each other, is proposed. The technique involves a new version in which the stuffing and pulling strokes are varied based on the observation of fiber end face gaps for every splice. Computer simulation reveals that this technique reduces splice loss by 50 percent in dB unit in comparison with the conventional method. Furthermore, it is possible to eliminate splice failure due to end face gap variance. A new mass fusion splice machine manufactured based on the present method has also been developed and evaluated. As a result, it was confirmed that an average splice loss of 0.024 dB and fusion splice time of one minute per ribbon unit were successfully attained for mass fusion splicing of single-mode fibers.

The authors wish to express their sincere thanks to K.Ishihara, M.Miyauch, Y.Murakami, T.Ooyanagi, and K.Uema for their helpful discussions, and to N.Kojima and A.Sakamoto, for their encouragement.

REFERENCES

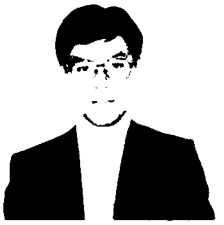
(1) J.W.Olson and A.J.Schepis: "Subscriber loop and trunking systems", OFC'84, New Orleans, 1984.
(2) J.R.Stern: "Optical wideband subscriber loops and local area networks in the UK", ICC'84, Amsterdam, 29.2, 1984.
(3) S.Seikai, K.Kitayama, N.Uesugi, and Y.Kato, "Design consideration on single-mode fibers suitable for subscriber cables", IEEE/OSA J. Lightwave Technol., LT-4, pp.1005-1009, 1986.
(4) M.Tachikura and N.Kashima, "Fusion mass splicing for optical fibers using high-frequency discharge", IEEE/OSA J. Lightwave Technol., LT-2, pp.25-31, 1984.
(5) T.Haibara, M.Mastumoto, and M.Miyauchi, "Design and development of an automatic cutting for optical fibers", IEEE/OSA J. Lightwave Technol., LT-4, pp.1434-1439, 1986.
(6) T.Haibara, M.Mastumoto, M.Miyauchi, and M.Shirai, "Design of fiber-holder for optical fiber ribbon splice", IEICE J70-C, pp.1164-1172, 1987.
(7) Y.Kato, S.Seikai, and M.Tateda, "Arc-fusion splicing of single-mode fibers 1: Optimum splice conditions", Appl. Opt., 21, pp.1332-1336, 1982.
(8) M.Hirai and N.Uchida, "Melt splice of multimode optical fiber with an electric arc", Electron. Lett., 13, pp.123-125, 1977.
(9) A.Ishikura, Y.Kato and M.Miyauchi, "Taper splice method for single-mode fibers", Appl. Opt., 25, pp.3460-3465, 1986.
(10) O.Kawata, K.Hoshino, Y.Miyajima, M.Ohnishi, and K.Ishihara, "A splicing and inspection technique for single-mode fibers using direct core monitoring", IEEE/OSA J. Lightwave Technol., LT-2, pp.185-191, 1984.



Yasuyuki Kato is a research engineer in NTT Transmission Systems Laboratories, Tokai, Ibaraki-ken, Japan. He was born in Yamagata, Japan, on July 20, 1954. He received the B.S. degree in electrical engineering Yamagata University, in 1977, and Ph.D. from Osaka University in 1987. In 1977, he joined the NTT Laboratories, Tokai, Ibaraki, Japan, where he was engaged in research work on transmission characteristics for designing single-mode optical-fiber cables until 1981. Since 1982, He has been engaged in development study on discharge fusion splice for low-order-mode optical fibers. Dr. Kato received the 1982 Paper Award, the 1983 Young Engineer Award from IEICE of Japan, and the 1986 President Award from NTT.



Akihiko Ishikura is a engineer in NTT Transmission Systems Laboratories, Ibaraki-ken Japan. He was born in Kyoto, Japan, on Nov. 5, 1958. He recieved his B.E. degree in 1982 and M.E. degree in 1984 from Osaka University. He has been engaged in resarch and development of low loss splice method for single-mode optical fibers. He is a member of the Institute of Electronics, Information and Communication Engineers of Japan.



Teruyuki Sano received his B.S. degree in electrical engineering from Tohoku University in 1983. He joind NTT in 1983 and has been engaged in development of trunk optical fiber cable systems. He is a member of Institute of Electronics, Information and Communication Engineers of Japan.



Seiji Takashima is a General Manager, both Fiber Optics Local Network Systems Project Group and Telecommunication Cable Systems & Outside Plant Project in Network Systems Development Center of NTT. He received his B.S. and M.S. degrees in electrical engineering from Waseda University in Japan in 1967 and 1969, respectivery. He also received M.S. in Management from Massachusetts Institute of Technology in 1983.

He joined NTT in 1969 and has been engaged in development both of subscriver optical fiber network systems, and whole range of copper telecommunication cable systems and outside plant technologies. He is a member of Institute of Electrical and Electronics Engineers, and Institute of Electronics, Information and Communication Engineers of Japan.

STUDY ON ARC-FUSION SPLICING Ge-DOPED SILICA SINGLE-MODE FIBERS MANUFACTURED BY OUTSIDE AND INSIDE VAPOR DEPOSITION PROCESSES

E. Matti Hopiavuori
James E. Matthews III
Corning Glass Works
Corning, New York

Anthony DeVito
BellSouth Services
Birmingham, Alabama

ABSTRACT

Over the past few years single-mode fiber has proven in for long-haul and subscriber loop telecommunication applications. The majority of single-mode fibers are manufactured by either the Outside Vapor Deposition (OVD) or the Inside Vapor Deposition (IVD) process. Arc-fusion splicing is widely accepted for permanent, stable, reliable, and low-loss interconnection of optical fibers from within the same manufacturing process[1,2]. This study examines fusion splicing single-mode fibers from multiple vendors and processes to ensure maximum flexibility for operating companies, installers, and system designers in responding to industry and technology trends as well as in extending existing routes.

Four commercially available matched clad (MC) and depressed clad (DC) single-mode fibers manufactured by OVD and IVD processes were spliced using both laboratory and field fusion splicers and cleavers. Evaluation included fibers with nominal and extreme mode field diameters. Homogeneous and heterogeneous splice losses and tensile strengths are reported. Additionally, effects of a particular heat shrink sleeve on the splice loss under temperature cycling were studied.

This study demonstrates that under typical field splice conditions single-mode fibers from OVD and IVD manufacturing processes and of different profile designs can be consistently spliced with $\leq$ 0.2 dB average splice loss and $\geq$ 50 kpsi (0.35 GN/m^2) average tensile strength. This performance meets the requirements of most telecommunication installations.

INTRODUCTION

Single-mode fibers were arc-fusion spliced using two different splicers and cleavers. Fibers A, B, and C were manufactured using the IVD process and fiber D using the OVD process. Splicer #1 and cleaver X represented commercially available laboratory equipment; splicer #2 and cleaver Y were typical field equipment. As expected, the laboratory equipment provided the best splice performance for any fiber combination. Therefore, these data were used as the baseline for optimizing the field fusion splicer settings.

The experiment consisted of three phases with mode-field diameter and end angle being the key controlled parameters:

Phase I investigated the feasibility of arc-fusion splicing IVD and OVD fibers with approximately nominal mode-field diameters using a field arc-fusion splicer (#2) and cleaver (Y) with end angles held less than or equal to one degree. Splices were acceptable if the average loss was $\leq$ 0.1 dB and average tensile strength $\geq$ 50 kpsi (0.35 GN/m^2).

In Phase II, fibers with more extreme mode-field diameters were arc-fusion spliced. Phase II splices were acceptable if the average splice loss was $\leq$ 0.2 dB and tensile strength $\geq$ 50 kpsi. The increased splice loss was allowed due to the larger mode field diameter mismatch and larger allowed fiber end angles of one to two degrees with 10% of the end angles being less than one degree.

In Phase III, a few Phase II heterogeneous splice combinations were remade, a heat shrink sleeve applied on the splice section to simulate actual field conditions, and then mounted in two different commercially available splice trays of 50 mm and 75 mm bend diameter. End angles were between one and two degrees. Splice losses were monitored as a function of temperature to determine any long term attenuation increases.

SPLICING PROCEDURE

In all cases, the fiber coating was removed mechanically using an optical fiber stripping tool designed to minimize mechanical damage to the glass surface. Fiber ends were cleaved a short distance from the point of coating termination minimizing the amount of glass exposed to airborne contaminants. Additionally, this reduced the probability of contact between the exposed glass and the clamping surfaces of the splicer and, therefore, maintains the splice tensile strength[1].

The effect of fiber end angle on the splice loss was studied by varying the end angle requirements for each phase as stated above. The end angles

were measured using the end angle reflection technique[3] which has ± ¼° accuracy and is less prone to variation in operator interpretation. This study further verified earlier results that fiber end angle and face condition have a significant effect on the splice loss and geometry[2]. For large end angles, distortion of the core during arc fusion, due to the flow of core glass in a direction away from the point of contact, can contribute 0.2 dB or more to the splice loss. This effect can be substantially reduced by limiting fiber end angles to one degree or less.

Residual coating particles and other contaminants on fiber ends were removed by careful cleaning just prior to arc-fusion splicing. Maintenance of a clean surface is necessary to obtain low extrinsic splice loss and high tensile strength. In Phase I, fiber ends were immersed in an ultrasonic bath of clean isopropyl alcohol. In Phases II and III the bath was replaced with an alcohol wipe.

Fiber cores were aligned in the three axes to minimize attenuation measured on an OTDR incorporating a high resolution real-time display. The automatic control of the longitudinal (z) axis of one or both chucks drives the fiber ends together during the fusion cycle. Optimum arc voltage, current, and duration settings on the field fusion splicer were determined, whereby various OVD and IVD single-mode fibers could be spliced with consistently low splice loss and high tensile strength. Once the optimum splicer settings were obtained, those "universal settings" were used throughout the remainder of the experiment.

The splice loss was measured using an OTDR. Due to the directionality of the backscattering of two spliced fibers, splice loss was determined as a bidirectional average[4,5]. Using the bidirectional average eliminates the OTDR measurement artifact of apparent gain in one direction and loss in the opposite direction.

To determine the splice tensile strength, the uncoated spliced fiber sections were progressively loaded up to failure on a Rotating Capstan Fiber Tester (RCFT), and the fracture stress was recorded.

THEORETICAL BACKGROUND

The splice loss is determined by two factors; loss due to intrinsic fiber properties, and loss due to extrinsic factors. The major intrinsic contributor to a single-mode fiber splice loss is the mode-field diameter mismatch between the spliced fibers[2,6]. For step-index single-mode fibers, mode-field diameter, rather than core diameter, is the functional parameter since the mode power distribution is not exclusively confined to the core region of the fiber. A major extrinsic factor contributing to the fusion splice loss in the field can be the fiber end angle. Lateral offset and glass geometry are other factors affecting the splice loss although current splicing techniques, which use active core alignment, can somewhat reduce their impact on splice loss.

MODE-FIELD DIAMETER MISMATCH

The splice loss in dB due to the mode-field diameter mismatch of two fibers as given by Marcuse[7] is in equation (1):

$$\text{MFD MISMATCH LOSS} = 20 \log \tfrac{1}{2}\left[\frac{MFD_1}{MFD_2} + \frac{MFD_2}{MFD_1}\right] \text{dB} \quad (1)$$

where MFD_1 and MFD_2 are mode-field diameters of the spliced fibers, respectively.

FIBER END ANGLE

The major extrinsic factor is the end angle of the cleaved fiber. The correlation between the extrinsic splice loss and the end angle is presented in Figure 1. Experience has shown that end angles of one degree or less must be maintained to obtain a low loss splice.

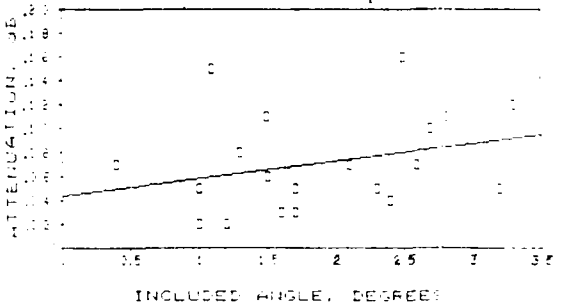


Figure 1: Extrinsic splice loss versus end angle

LATERAL OFFSET

For fusion splicing, lateral offset between the fiber cores is generally considered a contributor to the extrinsic splice loss. Based on Gambling et al[6,8], the lateral offset loss can be approximated using equation (4):

$$\text{Loss} = 4.34(\delta/W_{avg})^2 \quad (2)$$

where:

- δ : is the radial distance between the core centers of the two fibers
- W_{avg} : is the average mode-field radius of the two fibers

Current splicing techniques with active fiber alignment have reduced the impact of lateral offset on the splice loss. The referenced theoretical studies[6] discuss the effects of lateral offset in more detail. Experimental data, however, indicate that the contribution of a 2 μm lateral offset on the splice loss is negligible i.e. ≤ 0.01 dB[2].

MULTI-VENDOR SPLICE LOSS

BASELINE

A set of each manufacturers' fibers were homogeneously spliced using the laboratory splice equipment (splicer #1, cleaver X) to determine the extrinsic losses i.e. losses attributable to the splicing procedure only. This became the baseline for further experimental work. Table 1 summarizes the measured mode-field diameter, and intrinsic tensile strength for fibers used in determining the baseline and in Phase I. The tensile strength of each vendors' coated fiber was determined from ten (one meter gage length) tests utilizing the RCFT apparatus. The obtained intrinsic strengths were essentially equivalent.

TABLE 1

BASIC FIBER PARAMETERS - BASE LINE AND PHASE I

FIBER ID	MFD [μm]	MEAN STRENGTH [kpsi]
A	9.22	672
B	10.07	650
C	9.33	603
D	10.17	668

The splice losses at 1300 nm were measured with both a source/detector test set and an OTDR using bidirectional averaging. The data shown in Table 2 are typical for homogeneous single-mode fiber splices. Since the difference between the OTDR and the source/detector test set was $\leq$ 0.02 dB, an OTDR was used in all subsequent measurements.

TABLE 2

HOMOGENEOUS SPLICE LOSS @ 1300 nm [dB]

FIBER ID	SOURCE & DETECTOR	OTDR	Δ(OTDR-S&D)
A	0.05	0.07	0.02
B	0.05	0.06	0.01
C	0.06	0.07	0.01
D	0.04	0.04	0.00

The tensile strength data for the homogeneous splices are shown in Table 3. The splice strength results are typical under well controlled laboratory conditions and exceed the field performance criteria. For reference, Table 3 also contains the above intrinsic (unspliced) tensile strengths observed for each manufacturer's fiber.

TABLE 3

MEAN TENSILE STRENGTH [kpsi]

FIBER ID	UNSPLICED	SPLICED
A	672	130
B	650	110
C	603	60[1]
D	668	150

[1] No apparent reason existed for the lower tensile strength for this particular fiber

PHASE I

After determining the homogeneous splice losses and splice strengths for each vendors' fibers, the baseline performance of the heterogeneous splicing, i.e. splicing fibers from different manufacturers, was determined utilizing the laboratory fusion splicer (#1) and cleaver (X). The fibers were heterogeneously spliced using the same universal splicer settings as in the base line case. The splice loss and strength results are in Table 4:

TABLE 4

HETEROGENEOUS SPLICING - LABORATORY EQUIPMENT

FIBER COMBINATION	MEAN 1300 nm LOSS [dB]	MEAN TENSILE STRENGTH [kpsi]
A-B	0.04	90
A-C	0.03	70
A-D	0.07	115
B-C	0.07	70
B-D	0.08	110
C-D	0.08	70

The obtained splice losses and tensile strengths easily met the acceptance criteria established for Phase I. However, as the above results were obtained using the laboratory equipment and splicing procedure, the next logical step was to try and obtain the same excellent results using the field equipment. The actual technology transfer included optimizing the field fusion splicer settings. The field splicer settings were optimized through several phases. First, another baseline ("laboratory cleaver") was established by homogeneously splicing fiber D using the field splicer and laboratory cleaver (Table 5; trial #1). The obtained splice loss compares favorable with those reported in Tables 1 and 2, however one would expect these results due to the very small end angles of less than 0.5 degrees achieved with the laboratory cleaver.

Secondly, the laboratory cleaver was replaced with the field cleaver in trial #2. The data in Table 5 (trial #2) as expected reflect the use of a field cleaver with somewhat larger end-angles. The splice losses increased slightly and the strength decreased slightly indicating that optimization of the arc voltage, current, and duration of the field splicer was necessary. The post optimization data are shown in Table 5 as trial #3. Evidently the "optimized" field splicer settings compensated for the higher allowed end-angles of $\leq$ 1.0 degree.

TABLE 5

TECHNOLOGY TRANSFER (FROM FACTORY TO FIELD SPLICER)

HOMOGENEOUS SPLICE; FIBER D

TRIAL #	ICE [dB]	MEAN TENSILE STRENGTH [kpsi]	NOTE
1	0.04	100	'Laboratory cleaver'
2	0.08	92	'field cleaver'
3	0.06	102	'optimized'

The subsequent objective of the study was to duplicate the encouraging results obtained splicing fiber D for heterogeneous splices using the optimized field splicer and cleaver. Table 6 summarizes the obtained, excellent heterogeneous splice performance. For five out of six fiber combinations the splice loss using the optimized field splicer was equal or less than the losses obtained using the laboratory equipment (refer to Table 4). Slight differences noted in the obtained tensile strengths using the laboratory versus the optimized field splicer (Table 4 versus Table 6) were in the order of eight percent. All splices easily met the established acceptance criteria of $\leq$ 0.1 dB splice loss and $\geq$ 50 kpsi tensile strength.

TABLE 6

HETEROGENEOUS SPLICING - "OPTIMIZED" FIELD EQUIPMENT

FIBER COMBINATION	MEAN SPLICE LOSS [dB]	MEAN TENSILE STRENGTH (kpsi)
A-B	0.05	80
A-C	0.03	75
A-D	0.06	85
B-C	0.04	65
B-D	0.04	105
C-D	0.03	75

Theoretically, the mode-field diameter mismatches between these fibers were expected to cause somewhat (0.02-0.03 dB) higher heterogeneous splice losses than experienced (Figures 2a, 2b and 3).

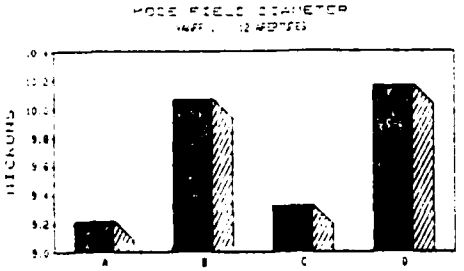


Figure 2a: Mode-field diameters of the experiment fibers

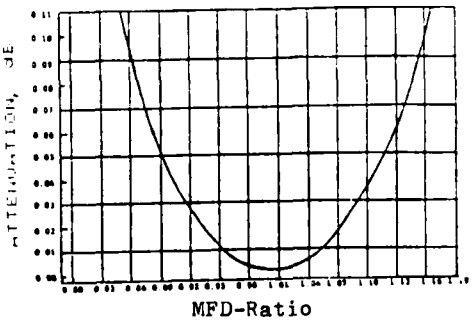


Figure 2b: Theoretical splice loss due to mode-field diameter mismatch

The theoretical splice losses due to the mode-field diameter mismatch were calculated in Phase I for each fiber combination, then algebraically summed with the anticipated extrinsic loss of 0.04 dB. The comparison between the experimental and the expected theoretical splice losses is presented in Figure 3. The measured splice losses were very encouraging; note from Figure 3 that the measured (observed) losses were slightly lower than the calculated (theoretical + extrinsic) losses in all cases.

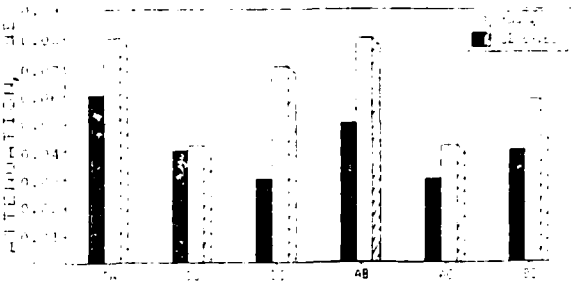


Figure 3: Theoretical versus experimental splice loss for Phase I multi-vendor splicing

PHASE I CONCLUSIONS

Phase I results concluded that multiple manufacturers' Germania doped Silica single-mode fibers designed for 1300 nm operation and manufactured by either LVD or OVD processes can be arc fusion spliced using the optimized field splicer and cleaver. Combination of proper end preparation, cleanliness, end angles of one degree or less, and a single optimized splicer settings yielded fusion splices that met the established criteria of $\leq$ 0.1 dB splice loss and $\geq$ 50 kpsi tensile strength.

PHASE-II

Phase I showed that multiple manufacturers' single-mode fibers could be arc fusion spliced using the optimized field equipment. The heterogeneous splices of the evaluated fibers having approximately nominal mode-field diameters met the established performance criteria. However, to fully examine the feasibility of multi-vendor splicing, further investigations with fibers from the extremes of each manufacturers' process were pursued. In Phase II, the approximate extremes of manufacturers' A, B, C, and D single-mode fibers with respect to the mode-field diameter were arc fusion spliced. The mode-field diameters and intrinsic tensile strengths measured using a two-meter gauge length for the fibers used in both Phase-II and subsequent Phase-III are shown in Table 7.

TABLE 7

FIBER PROPERTIES FOR PHASES II AND III

FIBER ID	MFD [μm]	MEAN STRENGTH [kpsi]
A-L	8.67	692
A-H	9.01	685
B-L	8.79	671
B-H	9.34	350[1]
C-L	9.60	654
C-H	10.08	663
D-L	9.76	677
D-H	10.26	673

Where "L" and "H" refer to low and high mode-field diameter, respectively

[1] No apparent reason existed for the lower tensile strength for this particular fiber.

Each manufacturer's high and low mode-field diameter fibers were spliced with the other three manufacturer's high and low mode-field diameter fibers. Phase-II consisted of a total of 24 splice combinations each repeated five (5) times. The total number of splices was 120. The splice losses were measured at 1300 nm with an OTDR using bidirectional averaging.

The average splice losses at 1300 nm and tensile strengths for each vendor combination are presented in Tables 8 and 9, respectively.

TABLE 8

HETEROGENEOUS SPLICE; MFD EXTREMES
AVERAGE SPLICE LOSS [dB] AT 1300 nm

FIBER ID	B-L	B-H	C-L	C-H	D-L	D-H
A-L	.058	.180	.175	.115	.105	.125
A-H	.030	.278	.110	.143	.090	.058
B-L	NA	NA	.101	.120	.125	.088
B-H	NA	NA	.163	.165	.115	.170
C-L			NA	NA	.128	.088
C-H			NA	NA	.135	.100

The above data indicates that the mode field diameter mismatch is not always the major contributor to the splice loss.

TABLE 9

HETEROGENEOUS SPLICE; MFD EXTREMES
AVERAGE SPLICE STRENGTH [kpsi]

FIBER ID	B-L	B-H	C-L	C-H	D-L	D-H
A-L	64	76	75	69	69	63
A-H	72	52	61	51	77	76
B-L	NA	NA	68	61	70	82
B-H	NA	NA	69	60	68	77
C-L			NA	NA	69	74
C-H			NA	NA	60	60

Table 10 summarizes the average values and pooled standard deviation for splice loss at 1300 nm and tensile strength. Table 10 values include all splice combinations with high and low mode-field diameter fibers for each vendor combination.

TABLE 10

HETEROGENEOUS SPLICE; MFD EXTREMES

FIBER COMBINATION	LOSS @ 1300 nm [dB] AVG.	LOSS @ 1300 nm [dB] STD. DEV.	TENSILE STRENGTH [kpsi] AVG.	TENSILE STRENGTH [kpsi] STD. DEV.
A-B	.14	.08	66	11.8
A-C	.14	.05	64	13.7
A-D	.10	.03	71	15.0
B-C	.14	.07	65	10.5
B-D	.13	.06	74	14.8
C-D	.11	.04	66	8.7

PHASE II CONCLUSIONS

Using the optimized fusion splicer and cleaver, different manufacturers' single-mode fibers with more extreme mode-field diameter mismatches were consistently spliced yielding average splice losses $\leq$ 0.2 dB at 1300 nm and average tensile strengths $\geq$ 50 kpsi. Only one combination failed to meet the $\leq$ 0.2 dB average splice loss criteria; the actual average splice loss being 0.278 dB. The splice loss is surprisingly high considering that the mode-field diameter mismatch for this particular fiber combination was only 0.33 μm. The major contributors to the higher splice losses compared to Phase I were larger alloved end angles, larger mode-field diameter mismatch, and replacing of the ultrasonic bath end cleaning with isopropyl alcohol soak and wipe.

PHASE-III

Phases I and II demonstrated that single-mode fibers from different manufacturers and processes can be fusion spliced meeting the performance criteria of most telecommunication installations. However, the possible environmental effects on the splice performance were yet to be determined.

Phase III was implemented by remaking two splices of the combinations listed below; installing heat shrink sleeves on the splice sections; inserting them on a splice tray; and placing the whole assembly inside a temperature chamber. Repetitive temperature cycling between room temperature (RT), +70°C, and -40°C was used to determine if any temperature induced attenuation increases of the splices occurred. The bidirectional splice losses at 1300 nm were measured with an OTDR and recorded at selected times during the temperature cycling.

In Phase-III, all end angles were maintained between one and two degrees to simulate less optimistic field conditions.

Spliced fiber sections were placed in either a 50 mm or a 75 mm diameter splice tray maximizing the

bend diameter. Each fiber was preconnectorized for ease of measurement. The connector ends were periodically cleaned with alcohol. Ten Phase III fiber combinations were distributed in the two splice trays as follows:

	50 mm Diameter	75 mm Diameter
* Batch one	D-H to D-L	A-H to C-H
	D-H to B-H	C-L to B-L
	D-L to A-L	
* Batch two	D-H to A-H	D-L to B-L
	D-H to C-H	D-L to C-L
	B-H to A-L	

The following temperature cycle was used:

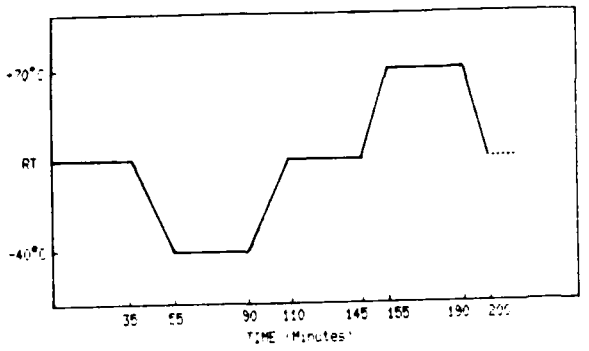


Table 11 presents the average change in splice loss at 1300 nm for each fiber combination after ten temperature cycles. The splice losses before adding the heat shrink sleeves were used as reference. Splice losses at room temperature and +70°C for each combination were measured only for cycles # 1, 2, and 10. As the splice losses for cycles 1 and 2 were constant, the splice losses were measured for each cycle only at -40°C since bending effects are most likely at cold temperatures. As expected, there were no significant deviations in the data. The fluctuations in the 1300 nm splice loss data were less than 0.02 dB, falling well within the repeatability of the measurement.

TABLE 11

INITIAL SPLICE LOSS AND AVERAGE CHANGE IN SPLICE LOSS [dB] AT 1300 DUE TO TEMPERATURE CYCLING

FIBER COMBINATION	INITIAL LOSS	AVG. CHANGE IN LOSS @ 1300 @ RT	@ -40°C	@ +70°C
A-L to B-H	.15	.007	.011	.018
A-L to D-L	.19	-.007	.004	-.001
A-H to C-H	.12	-.004	-.001	.005
A-H to D-H	.07	.014	.014	.006
B-L to C-L	.06	-.007	.009	-.001
B-L to D-L	.02	.004	.007	.000
B-H to D-H	.13	-.016	-.007	-.017
C-L to D-L	.06	.002	.003	.010
C-H to D-H	.07	-.006	-.002	-.007
D-H to D-L	.13	.006	.014	.011

PHASE III CONCLUSIONS

Based on the reported data, the effects of the evaluated splice protection sleeve on the heterogeneous splice loss after ten temperature cycles from room temperature to -40°C and to +70°C are negligible. All attenuation increases at 1300 nm were $\leq$ 0.02 dB.

CONCLUSIONS

The limits previously imposed on single-mode fiber users to differentiate fiber manufacturers within cables and point-to-point systems were demonstrated to have no technical merit. This study successfully demonstrated that multiple vendors' 1300 nm optimized, Germania doped Silica, single-mode fibers manufactured by IVD or OVD processes can be arc-fusion spliced using a single universal splicer setting achieved by optimizing the field splicing equipment. OVD and IVD single-mode fibers with mode-field diameters approaching the limits of their specified range were spliced meeting the established requirements of $\leq$ 0.2 dB average splice loss and $\geq$ 50 kpsi (.35 GN/m^2) average tensile strength. It should be noted that the necessary fusion splicer adjustments are minor.

Proper fiber end preparation procedures combined with optimized field arc-fusion splicer settings can yield splices that approach the intrinsic loss limit.

Data indicated that the two previously reported parameters affecting arc-fusion splice loss, mode-field diameter and lateral offset of the cores, contribute less to the splice loss than the included end angle. End angles must be maintained less than one degree. Good cleaving tool performance is a critical contributor to the success of the optimized field arc-fusion splicer for low losses when splicing single-mode fibers from different manufacturers and processes.

The tested heat shrink sleeve had negligible effect on the actual splice losses of the evaluated fiber combinations under described temperature cycling. The changes in the splice losses were in the order of the measurement accuracy.

ACKNOWLEDGMENTS

The authors gratefully acknowledge Mr. Alan R. Minthorn and Mr. Stephen Wemple for their contributions to these experiments.

REFERENCES

1. D.H. Taylor and S.L. Saikkonen; "Factory Splicing of Optical Waveguide Fiber", TR-9, November 1983, Corning Glass Works

2. S.L. Saikkonen and M.J. Hackert; "An Update on Practical Fusion Splicing of Multimode and Single-Mode Fibers", TR-18, November 1985, Corning Glass Works

3. P. Reitz; "Fiber End Preparation and Inspection Techniques", TR 2, April 1980, Corning Glass Works

4. F. Kapron, C. Kozikowski, R. Crotts; "Mode Field Diameter Effects on OTDR Splice Measurements", NBS Special Publication 720, Technical Digest Symposium on Optical Fiber Measurements, September 1986, Boulder, Colorado

5. John Lindh; "Splice Loss, How Measurements Can Mislead", Lightwave, June 1986, p. 43

6. L.M. Hevey, S.L. Saikkonen, and D.H. Taylor; "Theoretical Splice Loss Study of Single-Mode Fiber", Proceedings of SPIE, Vol. 479, May 1984

7. D. Marcuse; "Loss Analysis of Single Mode Fiber Splices", Bell Systems Technical Journal, Vol. 56, May - June 1977

8. W.A. Gambling, H. Matsumura and C.M. Ragsdale; "Joint Loss in Single-Mode Fibers", Electronic Letters, p. 14, No 15 (July 1978)



Mr. Matthews is currently the Supervisor of Corning's End Customer Applications Engineering Group. He has been with Corning since 1981 and has previously served in both Applications Engineering as well as product Engineering and measurement development positions for Corning's Telecommunications Products Division. Prior to joining Corning, he worked for the Georgia Tech Research Institute as a research engineer performing applied development on radar and antenna systems.

Mr. Matthews is a graduate of Georgia Institute of Technology (GA Tech) with a Master's of Science in Electrical Engineering and a Bachelor's of Science in Electrical Engineering.



Mr. Matti Hopiavuori is a Senior Applications Engineer with the End Customer Applications Engineering Group of Corning Glass Works. After joining Corning in 1984 he has been engaged in cabler and end customer technical support. Prior to joining Corning, Mr. Hopiavuori worked with The Finnish Naval Headquarters as a radio communication system planning engineer and with Nokia Cable Machinery as control system designer.

Mr. Hopiavuori received his M.S.E.E. degree from the Tampere University of Technology, Finland, in 1981 and is currently enrolled in Syracuse University for his M.B.A. degree.



ANTHONY DE VITO
STAFF MANAGER-TRANSMISSION
PRODUCT EVALUATION

BELLSOUTH SERVICES

Mr. DeVito started his career in the Outside Plant Construction Department with the New York Telephone Company in March, 1971. He remained there until accepting a transfer to the Southern Bell Telephone and Telegraph Company in Miami, Florida in May, 1978. While in Miami he supervised construction crews and in 1982 accepted the responsibility of constructing south Florida's first major fiber optic project. This project was the first to carry optical fibers from a central office to a heavy concentration of large customers in a metropolitan environment. In December, 1983 Mr. DeVito accepted a transfer to his current position on the BellSouth Services Transmission Product Evaluation Staff. His responsibilities include the evaluation of fiber optic splicing and testing equipment.

WHAT IS SUPERCONDUCTIVITY? FUNDAMENTALS AND STATE OF THE ART

P.H. HOR

DEPARTMENT OF PHYSICS, UNIVERSITY OF HOUSTON
HOUSTON, TX. 77004

Abstract

A brief account of the history and properties of superconductivity is presented. The development of oxide superconductors has been reviewed and current status of higher temperature superconductivity discussed.

Introduction

Superconductivity is a physical phenomenon in which the electrical resistivity of a specimen, when cooled below a critical temperature T_c, drops suddenly to zero and all the magnetic flux is expelled from the interior of the specimen. Superconductivity was first discovered in 1911 by Kamerlingh Onnes.[1] It occured in mercury at a temperature around 4.2 Kelvin. By 1986, the temperature at which superconductivity could be achieved had been slowly increased to 23 Kelvin by the discovery of new high T_c metallic oxides. (see finure 1).

Basic Properties of a Superconductor

It is well known that two most basic signatures of superconductivity are: 1) zero resistivity and 2) Meissner effect. At the beginning, when Kamerlingh Onnes first observed superconductivity in mercury, no upper limit of resistivity was determined. Subsequent experiment by Quinn and Ittner[2] placed the upper limit of resistivity of a superconducting thin film tube to 10^{-23} ohm-cm. It is extremely small compared to the resistivity of 10^{-9} ohm-cm for the purest copper at low temperature. Therefore, there is little doubt that a superconducting state is a genuine zero-resistance state.

Only a zero-resistance state is not sufficient to characterize superconductor. Experiment shows that below a critical value H_c, an externally applied magnetic field will be expelled from the superconductor, except for a very thin temperature-dependent layer at the surface, having a thickness (penetration depth) $\lambda_L \sim 10^{-5}$cm. This Meissner effect, first observed by Meissner and Ochsenfeld[3], separates a superconductor from a perfect conductor and finally leads to the full thermodynamical treament of superconductivity as a phase transition by Gorter and Casimir.[4] Above the critical field H_c, superconducting behavior is quenched and normal conductivity restored.

A simple short introduction of other fundamental characteristics as well as theoretical treaments of a superconductor can be found in "Superconductivity" by E.A. Lynton.

Oxide Superconductors

Based on the BCS theory, it is clear that a high density of states with strong electron-phonon coupling will yield a high transition temperature. Oxidation is known to degrade, in general, the matallic and, in particular, the superconducting characteristics of matter. However, superconductivity has been observed in some highly oxidized perovskite and related compounds such as $SrTiO_{3-x}$, Na_xWO_3, $Li_{1+x}Ti_{2-x}O_4$ and $BaPb_{1-x}Bi_xO_3$,

with a T_c exceeding 13K for the last two oxides. Such a high T_c is especially unusual for $BaPb_{1-x}Bi_xO_3$, which consists of no transition metal elements and displays no large electron density of states, both being essential for conventional high T_c intermetallic compounds.

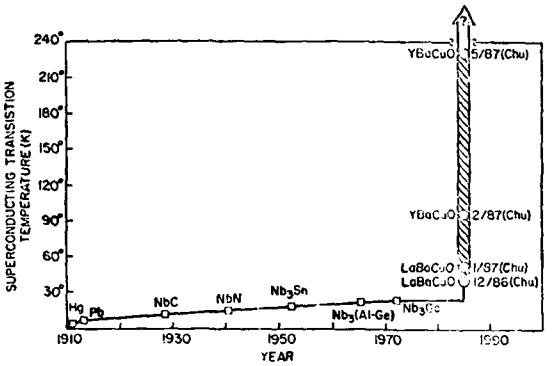


Fig. 1. Evolution of the superconducting transition temperature

It is thirteen years after the observation of superconductivity at 23K in Nb_3Ge, the record temperature was broken last year[5] following the observation of superconductivity in the mixed La-Ba-Cu-O (LaBCO) compound system in the 30K-range. Later the observation was confirmed[6,7] and the superconductivity phase was identified to be with the single layered K_2NiF_4 structure.[8] A second break through of superconducting transition temperature in mixed phased Y-Ba-Cu-O has finally push T_c to above liquid Nitrogen temperature with T_c 93K. The superconductivity above 90K was subsequently attributed to the $YBa_2Cu_3O_{6+x}$ phase[10] with CuO_2-BaO_2-CuO_{2-y}-BaO_2-CuO_2 layer assemblies sandwiched between two Y- layers.

A New Class of 90K-Superconductors

To investigate the role of Y in superconducting $YBa_2Cu_3O_{6+x}$ above 90K, experiments showed that the complete replacement of Y even with the most magnetic Gd does not affect the T_c of these compounds. A new class of superconductors, $ABa_2Cu_3O_{6+x}$ with A=Y, La, Nd, Sm, En, Gd, Ho, Er, and Ln, with T_c above 90K was therefore discovered.[11] The results show[12] that the "A" elements are used only to stablize the so-called three-layer structure to sustain the 90K superconductivity between the Y-layers and that superconductivity must be confined to the three Cu-O layer assembly sandwiched between the Y-layers.

Higher Temperature Superconductivity

T_c at 155K[13], 225K[14], and 285K[15] have been reported. Indications of superconductivity at 240K and higher have been detected[16,17] as sharp drops in resistance without truly achieving the zero-resistance state. Such resistance drops were too unstable and too difficult to reproduce in a systematic fashion for diagnosis. However, strong evidence of superconductivity, the appearance of the reverse Josephson effect, has been reported by the Wayne State group[18] below 240K.

If one accepts all reports of superconductivity substantially higher than 100K, the immediate question is: what is the location of superconductivity in the samples? It cannot be associated with a random distribution of superconducting dispersions because a zero resistance path would have required a minimum of 16% of the volume fraction to be superconducting which is substantially large than the magnetic anomaly observed. It must be filamentary and located in the grain boundaries or in the twin phase boundaries due to the tetragonal-to-orthohombic trantition at ~750 °C. The superconducting filaments may then be extremely fragile physically due to difference in thermal expansions between them and the surroundings, or unstable chemically due to their strong interaction with the surrounding. Thermal cycling can also perturb the oxygen content at the grain boundaries and in turn cause a change in chemistry.

Conclusions

Great progress has been made in raising the transition temperature and the understanding of the high T_c compounds. Evidence of superconductivity, although strong but hindered by poor stability and poor reproducibility, has been reported at various high temperatures. More work is required to clarify the whole situation.

References

1. H. Kamerlingh Onnes, Akad. van Wetenschappen (Amsterdam)14, 113, 818 (1911).
2. D.J. Quinn III, and W.B. Ittner III, J. Appl. Phys. 33, 748 (1962).
3. W. Meissner and R. Ochsenfeld, Naturwiss, 21, 787 (1933).
4. C.J. Gorter and H.B.G. Casimir, Physica 1, 306 (1934).
5. J.G. Bednoz and K.A. Muller, Z. Phys. B64, 189 (1986).
6. S. Uchida, et al., Jpn. J. Appl. Phys. 26, 21 (1987).
7. C.W. Chu, et al., Phys. Rev. Lett. 58, 405 (1987); Science 235, 567 (1987).
8. H. Takagi, et al., Jpn J. Appl. Phys. Lett. 36 (1987).
9. M.K. Wu, J.R. Ashburn, C.J. Torng, P.H. Hor, R.L. Meng, L. Gao, Z.J. Huang, Y.Q. Wang and C.W. Chu, Phys. Rev. Lett. 58, 908 (1987).
10. R.M. Hazen, et al., Phys. Rev. B35, 7238 (1987)
11. P.H. Hor, R.L. Meng, Y.Q. Wang, L. Gao, Z.J. Huang, J. Bechtold, K. Forster and C.W. Chu, Phys. Rev. Lett. 58, 1891 (1987).
12. C.W. Chu, to appear in Proc. Natl. Acad. Sci. (USA) (1987).
13. S.R. Ovshinsky, R.T. Yound, D.D. Allred, G. DeMaggio, and G.A. Van der Leeden, Phys. Rev. B. 58, 2579 (1987).
14. C.Y. Huang, L. Dries, R.L. Meng, P.H. Hor, C.W. Chu and R. Frankel, to appear in Nature.
15. A Zettl and M. Cohen, private communication through C.W. Chu.
16. L.C. Bourne, M.L. Cohen, W.N. Creager, M.F. Crommie, A.M. Stacy and A. Zettl, Phys. Lett. A120, 494 (1987).
17. C.W. Chu, et al., NSF News Release, February 16, 1987.
18. J.T. Chen, L.E. Wenger, C.J. McEwan and E.M. Logothetis, Phys. Rev. Lett. 58, 1972 (1987).



Peiherng Hor received his Ph.D. in Physics from the University of Houston in 1987, and joined the Physics Department as a faculty member. Currently he is working on the high temperature superconducting oxides.

PROCESSING OF SUPERCONDUCTIVE MATERIALS AND HIGH FREQUENCY

James L. Smith

Los Alamos National Laboratory
Los Alamos, New Mexico 87545

Abstract

We do not know yet if superconductivity will become useful without refrigeration. Now the superconductors are so different from copper that it is difficult to imagine replacing copper with such a brittle material. Superconductors conduct dc with no loss, ac with small losses, and microwaves in co-axial lines with almost no loss and with no dispersion from dc to the highest frequencies. They will probably allow us to close the gap between radio frequency and infra red optical transmission. Clearly your industry should know some things about where superconductivity may lead us and must consider whether the greater risk is to develop them or to let others try it. There are no easy answers yet.

Introduction

There are now materials that become superconducting at a critical temperature T_c of just under 100 K (-173°C), which the previous speaker, P. H. Hor, helped to discover. This discovery just made this year, is now one of the most widely confirmed discoveries ever made. At this temperature, cooling with liquid nitrogen or refrigerators is far more economical than for previously known superconductors. Nonetheless, except for rather high tech devices, these new materials may not have great impact because cooling remains necessary. We continue to read in the popular press about T_c's as high as room temperature. It is fair to say that most laboratories have seen evidence of these higher temperatures, which disappear in hours or days. Either we will find out what rather unstable, trace chemical compound in our samples is the room temperature superconductor or we will convince ourselves that these are only indications of our difficulty in making measurements on a ceramic. If room temperature superconductivity (actually it is best to work at or below 3/4 of T_c) is achieved, the technology will so enter our daily lives as to genuinely change society.

To the wire and cable industry, the course of action is not obvious. The research is moving at a record pace, but the refrigeration still required limits widespread applications. It seems clear that the electronics industry will be using these superconductors for yet another revolution. This could fundamentally alter the way information is transmitted. It seems appropriate to mention that after the transistor was invented, its use to replace vacuum tubes was considered a great breakthrough. What has since come from the transistor was not forseen. We must now determine, and to some extent bet our resources, on whether we are in this situation again.

Materials

These superconducting compounds are made of a stoichiometric mix of (1) an alkaline earth, say barium, (2) a rare earth or mixture of them, say yttrium, europium, gadolinium, and (3) copper that is partially oxidized. These elements are not particularly expensive or hard to find, and they are not toxic or hazardous. This mix is usually obtained by grinding together oxides and carbonates or by precipitating water soluble forms. This is followed by one or more sequences of grinding, compacting, firing in air or oxygen at about 950°C, and slow cooling. This basic preparation can now be performed by an overwhelming array of specific processes. It thus seems clear that different applications will each use the most optimal process. All of this is necessary to make what will replace copper in many applications and the next speaker will expand on this.

The resulting superconductor will break if you drop it on a hard surface. Various cladding procedures or use of fine fibers (like optical fibers) can improve on this. But remember that like the transistor, we may not need a direct replacement for plain old copper wire. For example, quite likely, coils could be manufactured as monolithic ceramics where firing is the final step.

Overall the progress on producing these materials has proceeded at an unprecedented rate because of the large number of workers around the world. I will give a few examples of perceived problems that are being solved. In general, this is why I present no list of problems. The high temperature firing is a difficult production step, and any semiconductors that are to be married to the superconductor would not survive. Recently Bell Communications Research has reported that a treatment in an oxygen plasma at room temperature can replace the firing. Although this currently takes many hours, it is an impressive step

forward. It is difficult to make a connection between the superconductor and a conventional conductor. On the other hand a transformer with a copper primary and a superconducting secondary will work fine if the bandwidth is adequate. Also the fabrication of more components from ceramics can eliminate this problem.

The biggest limitation on the present materials that may be fundamental, that is not fixable, is the current carrying capacity. If room temperature superconductors are found it seems likely that they will have this same limitation. Near the T_c, currents roughly of the capacity of copper wire destroy the superconductivity. The older, lower T_c materials can easily carry a thousand times the current that copper can. While higher currents are being vigorously sought, it is important to note that for communications, the present ratings are more than adequate.

High Frequency

If you set resistance equal to zero in your transmission equations, you find that dispersion vanishes. If you make the gap narrow in a co-axial line you find that a superconducting delay line can be 20 times shorter. At high frequencies, the fact that the present materials are superconducting grains connected by poorer conductors is solved by capacitive coupling. Superconducting switching circuits have always been much faster than semiconductors (and are orders of magnitude less sensitive to radiation damage). Shielding made of superconductors works down to dc. The word bandwidth can be forgotten.

Superconductors really are super for high frequencies. There must be small scale applications where the refrigeration is worth the price. Preliminary measurements by Los Alamos and the University of Wuppertal in West Germany on materials in superconducting cavities suggest that the higher T_c superconductors are even less lossy than the now common lower T_c materials. We speculate that this is because there are actually fewer non-superconducting electrons present to cause residual losses. This may also provide clues as to why the T_c's are so high and as how to make them higher.

Conclusion

People who work in the field of superconductivity cannot tell if the public is being oversold on the promise of applications for the new superconductors. Indeed no one can see the future, but we can feel the excitement of the potential of these new materials. Turn your thinking loose on how to use these new specifications.

Acknowledgement

Work performed under the auspices of the US Department of Energy.



James L. Smith received his B.S. in Physics in 1965 from Wayne State University in Detroit, MI and his Ph.D. in physics in 1974 from Brown University in Providence, RI. Since 1973 he has held various positions at the Los Alamos National Laboratory. He has published over a hundred papers on superconductivity.

HIGH-T_C SUPERCONDUCTING WIRE FABRICATION AND TESTING

D. W. Capone II, J. T. Dusek, and K. C. Goretta

Argonne National Laboratory, Argonne IL 60439

Abstract

This paper describes the fabrication of ceramic fibers of the high-T_c superconductor $YBa_2Cu_3O_7$ and the testing procedures used to characterize these materials. The major factors important to the fabrication of these fibers are described in general terms including some of the issues relating to the strength and flexibility of the wires. Measurements of the three parameters which most easily characterize the superconducting properties of the fibers, T_c, H_{c2}, and J_c, are described, particularly the critical current density, J_c.

Introduction

The discovery of the high-T_c superconductor $YBa_2Cu_3O_7$[1] has stimulated a tremendous interest in superconductivity in recent months. One important reason for this excitement is the fact that a new class of materials, namely oxides, has been found to posess superconducting transition temperatures far above those achieved with conventional metallic superconductors, such as the A-15's. This means that whole new avenues of research into which materials can attain superconductivity have been opened. More importantly for applications, a brand new discipline has been focused onto superconductivity, namely ceramic science and engineering, bringing with it new processing routes which have not been previously considered for the fabrication of superconducting wires. However, with this new infusion of researchers into superconductivity one must be cogniscent of the fact that superconductivity applications has existed as a matured field of research for more than 25 years. Issues involving conductor design, stabilization, and engineering,[2] all of which are beyond the scope of this paper, have long been optimized for specific applications, such as high-field solenoids, accelerators, r.f. cavities, etc.. While liquid nitrogen temperatures introduce potential simplifications to the design of conductors it is not the miracle cure, so to speak, that the press might make one believe. It is therefore crucially important to take advantage of the storehouse of information which already exists both in technical journals[3] and in the research and industrial groups[4] which have a long history of research in superconductivity applications.

In this paper we present a general description of the fabrication of superconducting wires using ceramic fiber processing routes. In addition, we give a brief overview of some of the testing procedures which are used to characterize the superconducting properties of these materials.

Fabrication of High-T_c Superconducting Wires

Ceramics can be manufactured into wires by a number of techniques. Depending on the specific material, some or all of the following can be used to produce a filament: drawing from a melt; zone melting; spinning; chemical vapor deposition; and extrusion.

Drawing from a melt is limited in general to crystalline ceramics which melt congruently or to glasses. This method of wire fabrication has been used to make short sections of high T_c wires. Densities of 98% of theoretical have been produced. The resulting wire is initially inhomogeneous owing to peritectic melting, and is nonsuperconducting. Subsequent heat treatment in oxygen reduces much of the inhomogeneity and converts the nonsupercon-

ducting tetragonal phase to the superconducting orthorhombic phase. This approach has been used to make short sections of high T_c wires with critical current densities of hundreds of A/cm^2 in zero field at 77K [5].

Zone melting relies on the same set of solidification properties as drawing does. A molten pool is cooled to form a solid of the desired composition. Melting can occur through the entire wire; or a central core of another material, which does not melt, can be used as a substrate. Superconducting wires similar in properties to melt-drawn wires have been produced by this process [5].

Spinning of wires can be accomplished in one of two ways. Either a melt of the material or a solution containing the material can be spun. Melt spinning is in principle capable of producing long, continuous wires. The process is, however, difficult to control, and lengths obtained are generally short. Spinning of a solution which contains the desired ceramic constituents makes use of technology used in textile production. Two main types of solutions are currently spun into ceramic wires: powders of the desired composition suspended in a fluid; and polymers which yield ceramics when fired to high temperatures. Neither technique has as yet been used to make high-T_c superconductors. The former technique has been successfully applied to production of continuous lengths of oxides such as Al_2O_3. The resulting wires are, once heat treated, nearly fully dense, of uniform cross section, with diameters of about 20 μm [6]. A problem exists in that the filaments do not appear to be fully crystalline; a glassy phase may coat grain boundaries [7]. Spinning of polymers has been used to make non-oxide ceramics such as SiC into filaments hundreds of meters in length [8]. It is difficult to envision development of polymeric precursors which will yield $YBa_2Cu_3O_{7-\delta}$ when fired, but the possibility can't be ignored.

Chemical vapor deposition onto a graphite core has been used to make SiC filaments about 140 μm in diameter. The filaments are very flexible owing to their high strengths and relatively small diameters [9]. Gradients in carbon and silicon exist through the SiC layer, however [10]. For this type of process to be effective for superconductor fabrication, the superconducting layer would need to be much more homogeneous than in the current SiC. High-T_c superconductors contain three metallic elements rather than just one, and achievement of a uniform distribution of all elements will be extremely difficult. No attempts of chemical vapor deposition of high-T_c superconductors have been reported, thus far.

Extrusion can yield ceramic wires of any length desired. Several different approaches to extruding high- T_c wires have been attempted. Powders have been extruded hot to form short lengths [11]. Scaling up to useful lengths has not been accomplished. Composite wires of superconductors with sheaths of various metals have been extruded, but problems have been reported. Silver has been found to be compatible with the superconductor, and incorporation of AgO can prevent degradation of the superconductor during hot processing [12]. Silver is, however, expensive and there is evidence that metals tougher than Ag may be needed to impart the stress needed to deform the superconductor during processing [13].

Another method for extrusion of ceramic wires employs a plastic mix of ceramic powders and various organics. The basic mix consists of 1-2-3 powder of fine particle size (generally less than 5 μm to promote sintering) , a binder and plasticizer to impart green strength and plasticity to the extruded wire prior to sintering, a deflocculent to insure optimal mixing, and a solvent which is compatible with all of the constituents. Certain mixes may require a lubricant to achieve uniformity in the green extrusion. The plastic mix is generally ball milled to insure homogeneity and then partially dried to create a consistency suitable for extrusion--about like that of modeling clay. The plastic mix is pressed through a die and wound onto a spindle. Die design and extrusion pressures are determined by the character of the particular mix. Once extruded, the mix is heated very slowly to a few hundred degrees C in order to drive off the organics, and is then heated rapidly to temperatures between 900 and 1000 °C to sinter the powder and increase the density of the mass. Controlled cooling in dry oxygen results in a superconducting wire. This method is now in use at Argonne National Laboratory and has produced 90% dense wires less than 100 μm in diameter. Critical current densities of hundreds of A/cm^2 in zero field and 77K have been obtained. The small diameter and reasonable strength allows for substantial flexiblity in the resulting wire, even though the material itself

is not ductile. Incorporation of these ceramic fibers into a metallic matrix may be accomplished using a technique similar to that used for making Al/C composites in the aerospace industry.

Testing Procedures

Three main parameters, the superconducting transition temperature, T_c, the upper critical field, H_{c2}, and the critical current density, J_c, are important for characterizing the parameter space within which one can potentially operate a superconducting device. All three of these parameters can be measured using a standard four-terminal dc resistance measurement. For our dense ceramic samples contacts can be made, using indium solder, which have low enough contact resistances to carry about a 10 A dc current without contact heating. While a detailed description of the testing procedures used to determine these parameters is outside the scope of this paper, a brief general description of each is given along with some references where one can find more detailed information.

Transition Temperature

One standard technique for measuring the superconducting transition temperature is to use a relatively small constant current density ($\leq 20 A/cm^2$) and measure the voltage drop across the sample as a function of temperature. Care must be taken to ensure that the sample and the thermometer used are in thermal equilibrium with each other. In particular, interfaces between the thermometer and the sample can cause substantial measurement errors if equilibrium is not maintained. This can be especially difficult if one is using one of the more simple testing rigs, such as a dipping rig, where temperature is varied by adjusting the height of a sample above a suitable cryogenic liquid, for example liquid nitrogen. A simple test of the accuracy of the temperature measurement is to check for agreement between data taken during warming and cooling the sample. Another difficulty, commonly encountered, occurs when trying to measure samples with large normal state resistances. In this case one can exceed the output impedence of the constant current supply as the temperature decreases. This can cause the current to drop to zero, and hence, the voltage to drop to zero as well. This can be misinterpreted as a superconducting transition to the zero-resistance state when, in fact, the actual sample resistance is several MΩ. It is therefore important to monitor the output current in order to be sure that the voltage being measured corresponds to the sample resistance. This seems like simple common sense, however the reports of room temperature superconductivity by many groups have all been in mixed-phase systems where samples exhibit semiconducting behavior with large normal state resistances.

Upper Critical Fields

Measurements of the upper critical field involve the measurement of T_c as a function of increasing applied magnetic fields. This measurement can be done in two equivalent ways distinguished by the logistical considerations of the situation. Firstly, a constant magnetic field is applied to the sample and the transition temperature is measured as described above. Secondly, the temperature is fixed, using a suitable controller, and the magnetic field is swept. Care must be taken to avoid magnetoresistive sample heating caused by sweeping the magnetic fields too quickly. In addition, most commercially available thermometers cannot be used in the presence of large magnetic fields because of the large magnetoresistive calibration changes which occur. Carbon-glass thermometers are about the only suitable thermometers which can be used in large magnetic fields and these need to be corrected in fields above 6-8 Tesla.[14]. In either case the data are plotted as T_c vs. H and the upper critical field is the T_c=0 intercept. In cases where the upper critical field is larger than the available magnetic field, the H_{c2} of the superconductor can be estimated using the WHH approximation [15]. Operationally, this involves the determination of the critical field slope, that is the slope of the T_c vs. H curve near the H=0 intercept. In the dirty limit, the H_{c2} of the superconductor is given by :

$$H_{c2}=0.692 \cdot T_c \cdot \text{critical field slope.}$$

However, this is a grossly oversimplified explanation of how critical fields are determined and should not be arbitrarily used without obtaining some understanding of the background associated with these issues.

Critical Current Density

Accurate measurements of the critical current density in superconductors are crucially important in characterizing the utility of practical superconducting materials[16]. As such it is probably the most important superconducting parameter to measure. Unfortunately, in most cases, it is also the most difficult to measure. The basic information from which the critical current density (J_c) is determined is a plot of voltage as a function of applied current. Other parameters, such as the applied magnetic field and temperature or uniaxial strain, are held constant during the measurement. However, unlike the measurement of T_c, the voltage sensitivity must be better than ~10nV if one expects to determine the J_c with any degree of accuracy. Basically one looks very carefully for the onset of resistance in the sample as the applied current is slowly increased from zero. The current which first produces resistance in the sample is the critical current, I_c, which is converted to J_c by dividing by the cross-sectional area of the sample. J_c is usually quoted in A/cm^2 although A/m^2 is more appropriate in the MKS system of units. Since the determination of zero resistance in a sample involves, at best, the setting of an upper limit for the resistance, J_c is usually specified using an electric field or a resistivity criterion. For example, that current which produces a measured resistivity of 10^{-12} Ω-m is commonly used to define the critical current of a sample. This criterion requires a very sensitive measurement of the voltage of a sample. A less sensitive but more commonly used criterion is to specify a voltage per unit length along the sample. A typical criterion is 1μV/cm; how- ever, 0.1μV/cm is much better if one has the voltage sensitivity available.

There are two major sample geometries used for the measurement of J_c. Firstly, the short sample measurement involves placing a short sample of superconductor transverse to the applied magnetic field. Current contacts are made at the ends of the sample and voltage contacts placed in the middle far enough from the current contacts to avoid transfer voltages [17]. This geometry suffers from an inability to obtain sensitive voltage measurements because of the shortness of the samples, however, when comparing large numbers of samples this technique is most commonly used. Secondly, the barrel geometry involves winding a small single layer coil from the sample onto a coil form for testing. This technique has the advantage of allowing long samples to be measured, which greatly increases the accuracy with which one can determine J_c. The coil is placed in an applied magnetic field so that the field is parallel to the coil axis. It is a good idea, and for materials sensitive to strain a necessity, to have the direction of current flow such that the Lorentz force, produced by the interaction of the current with the magnetic field, be radially inward.

Critical Currents in $YBa_2Cu_3O_7$

The critical currents in these high-T_c superconductors are dominated by the presence of weak-links separating grains of the "123" material and preventing large currents from flowing between grains. These weak-links are most likely a result of the anisotropic nature of the superconductor itself. That is, current flowing along the high-J_c direction in one grain must Josephson tunnel into the next misaligned grain. The result of these weak-links is that, even though the J_c of these materials is already quite low at 77K in zero magnetic field (≤1000 A/cm^2), in small applied magnetic fields (as low as 10-50 Gauss) the J_c at 77K decreases by another two orders of magnitude. In order to produce bulk ceramic conductors capable of supporting large currents the microstructure of the fired material must be textured so that the c-axis of the "123" grains are aligned transverse to the direction of current transport. This has been accomplished by several groups using thin-film deposition techniques resulting in films with large J_c's at 77K (≥$1x10^5$ A/cm^2)[18]. A complete review of weak links and their effects in these materials can be found in the paper by Ekin et. al.[19].

Summary

In this paper we have given a brief overview of the issues involving the processing of ceramic fibers of the "123" high-T_c materials. In addition some of the testing procedures used to characterize the superconducting behavior have been briefly described. The references given are not meant to be a comprehensive review of the field, but simply as a starting point for interested readers. The work at Argonne is supported by the U. S. Department of Energy- Basic Energy Sciences under contract #W-31- 109-ENG- 38.

References

1. M. K. Wu, J. R. Ashburn, C. J. Torng, P. H. Hor, R. L. Meng, L. Gao, Z. J. Huang, Y. Q. Wang, and C. W. Chu, Phys. Rev. Lett. 58, 908 (1987).

2. see for example, "Applied Superconductivity, Metallurgy and Physics of Titanium Alloys", Vol. 1 and 2, E. W. Collings, Plenum Press, New York (1986).

3. see for example the journal "Cryogenics".

4. for example; Supercon,Inc, 830 Boston Turnpike Rd. Shrewsbury, Ma 01545, with over 25 years pro-ducing superconducting composites.

5. S. Jin, T. H. Tiefel, R. C. Sherwood, G. W. Kammlott and S. M. Zahurak, Appl. Phys. Lett., in press.

6. A. K. Dhingra, Trans. R. Soc. Lond. A **294**, 411 (1980).

7. D. J. Pysher, K. C. Goretta, R. S. Hodder, Jr. and R. E. Tressler, *Adv. Cer. Mat., submitted.*

8. K. Okamura, Composites **18** [2] 107 (1987).

9. AVCO Specialty Materials Division, Lowell, MA.

10. J. A. DiCarlo, J. Mat. Sci. **21**, 217 (1986).

11. I.-W. Chen, X. Wu, S. Keating, C. Y. Keating, P. Johnson and T. Y. Tien, J. Am. Cer. Soc., *in press.*

12. S. Jin, R. C. Sherwood, R. B. van Dover, T. H. Tiefel and D. W. Johnson, Jr., Appl. Phys. Lett. **51** [29] 203 (1987).

13. R. McCallum, Ames National Laboratory, unpublished work.

14. H. H. Sample, B. L. Brandt, and L. Rubin, Rev. Sci. Inst. 53 , 1129 (1982).

15. N. R. Werthamer, E. Helfand, and P. C. Hohenberg, Phys Rev. 147, 295 (1966).

16. For an excellent review of the issues involving the measurement of J_c see: L. F. Goodrich and F. R. Fickett, Cryogenics May , 225-241 (1982).

17. J. W. Ekin, J. Appl. Phys. 49 , 3406 (1978).

18. P. Chaudhari, R. H. Koch, R. B. Laibowitz, R. R. McGuire, and R. J. Gambino, Phys. Rev. Lett. 58, 2684 (1987).

19. J. W. Ekin, A. I. Braginski, A. J. Panson, M. Janocko, D. W. Capone II, N. J. Zaluzec, B. Flandermeyer, O. F. de Lima, M. Hong, J. Kwo, S. H. Liou, Jour. Appl. Phys. 62, (1987) in press.



Dr. Donald W. Capone II
Materials Science Division
223-A113
Argonne National Laboratory
Argonne, IL 60439

Dr. Donald W. Capone II recieved his Ph.D. from Tufts University, Medford, Ma. in 1984. The research for his thesis was done at the Francis Bitter National Magnet Laboratory at MIT. After a two year post- doctoral appointment at Argonne National Laboratory, where he was one of the principal investigators on a NbN superconductor development program, he was promoted to the permanent staff at Argonne to continue that work in addition to work on Chevrel-phase superconductors. In Dec. 1986, he, along with three other staff members, initiated the Argonne program to investigate the properties of the new oxide superconductors. Subsequently, a conductor development program has been funded as a joint program between Argonne, Ames, and Brookhaven National Laboratories.

Josepf T. Dusek has worked in the field of ceramic processing and product development for nearly 50 years, the past 25 of which have been spent at Argonne National Laboratory. Prior to joining Argonne he held positions at the Armour Research Foundation and the IIT Research Institute.

Dr. Kenneth C. Goretta is an Assistant Ceramist in the Materials and Components Technology Division at Argonne National Laboratory. His research has focussed on the mechanical properties and fabrication of oxide ceramics. He recieved a B. S. in Metallurgical Engineering from the University of Illinois at Urbana and a Ph.D. in Metallurgical Engineering from the Illinois Institute of Technology.

TRANSMISSION PARAMETERS ON SUPERCONDUCTIVE COMMUNICATION CABLES

by

P.P. Kish

Northern Telecom Canada Limited
Montreal, Quebec

ABSTRACT

Remarkable progress has been achieved in just over a year by researchers in different countries who have discovered new classes of materials which are superconducting at liquid nitrogen temperatures or higher. It is conceivable that such materials can be processed in the form of wires or composite tapes and might lead to the development of a new generation of superconductive transmission lines.

It is the intent of this paper to present the theory of superconductivity as applied to the transmission of high frequency communication signals. Previous development work on superconducting communication cables operating at the temperature of liquid helium is reviewed. Theoretical results are derived for miniature coaxial lines constructed from metallic superconductors such as lead or niobium. These results provide an insight into the improved transmission performance that can be expected compared with conventional copper-based media.

INTRODUCTION

Recent discoveries of superconductive materials at temperatures higher than the boiling point of liquid nitrogen (77 K) have stimulated much interest in the scientific community. The glamour of these discoveries has been widely publicized in the media and has inspired images of levitating trains and superfast computers. Although there is the promise that these discoveries could lead to a major technological revolution, the prospects for realization of practical superconducting communication systems will depend on the economic factors and on the progress in the solution of the many engineering problems involved.

The intent of this paper is to present an overview of the transmission parameters of superconductive communication cables. First, the author would like to draw your attention to other published results in the literature (see references) most of which predate the advent of fiber optics in the mid-seventies. Experiments were then undertaken by researchers in the USA, USSR and Japan among others on coaxial cables manufactured with conductors of elemental niobium and lead which are superconducting at temperatures of liquid helium (4.2 K). Some of the cable constructions were evaluated for specialized applications such as nuclear test instrumentation which required very fast rise-time and low signal distortion characteristics. Other studies in Japan and the USSR focused on the design and performance of superconductive coaxial cables for large capacity communications media. At the time, the economics of cryogenic cable systems were dubious because of the high cost of refrigeration equipment and associated transport systems and the relative scarcity of liquid helium. Given the fast pace of recent developments with materials exhibiting superconductive properties approaching room temperature, the suitability of some of these materials for communication applications deserves further investigation.

Very little quantitative data is commonly available on the properties of the new superconductive materials except perhaps to those scientists intimately involved in current research efforts. Some of the most recent information will be presented by the invited authors at this session of the International Wire and Cable Symposium. Consequently, the main focus of this paper will be to present the theory of superconductive transmission lines with a view towards facilitating an understanding of the underlying concepts. The theory is based on the classical two-fluid model first proposed by Gorter and Casimir in 1934. The validity of this model has been subsequently confirmed for a wide range of traditional superconducting materials and operating conditions. This model will be used to calculate the transmission parameters of superconductive coaxial lines compared with the characteristics of normally conducting communication cables. Coaxial transmission lines have been considered because of the simplified mathematical relationships involved which help to illustrate the concepts.

THEORY OF SUPERCONDUCTORS

The DC resistance of superconductors is effectively zero below a critical temperature (T_c) which depends on the properties of the material. By comparison, the AC resistance of superconductors has a finite value, albeit small, which is both frequency- and temperature-dependent. The phenomenon of superconductivity can best be visualized with reference to the macroscopic two-fluid model and some of the more modern concepts embodied in microscopic BCS theory.[4] At a temperature below the critical temperature, some of the electrons in a superconductive material bind together in pairs (Cooper pairs) and occupy a lower energy state than the normal conduction electrons. The particular nature of the paired electron state makes it impossible for the coupled pair to lose kinetic energy in interactions with the atoms of the lattice. Hence the material exhibits zero resistance to the flow of direct current. When an applied magnetic field is increased above a critical value (H_c) or when the temperature of the material is increased above (T_c), the superconducting electron pair can acquire sufficient kinetic energy to "split apart" and the material reverts to its normal state.

The two-fluid model assumes that both normal and super electrons are present in the superconductive state ($T<T_c, H<H_c$). The fraction of the available super electrons and normal electrons are given by the following relation based on the thermal properties of superconductors.

$$N_s = N\left(1-(T/T_c)^4\right) \tag{1}$$

$$N_n = N-N_s \tag{2}$$

N = Total number of conduction electrons

Only the super electrons can contribute to the flow of direct current (DC) since according to Ohm's law ($J=\sigma E$), for DC, the electric field in the material is effectively zero and there is no energy transfer to the normal electrons. For alternating current (AC), the accelerating motion of the super electrons, by virtue of their inertial mass, introduces a reactive impedance which gives rise to an electric field in the material. The presence of an electric field unmasks the normal electrons which can now contribute to the current flow. The normal component of current flow depends on the number of available electrons (N_n= function of temperature and material properties) and the magnitude of the electric field in the material (E = function of frequency).

The relation between super current density and the applied electric field is given by London's equation:

$$\frac{dJ_s}{dt} = E/\mu\lambda^2 \tag{3}$$

where, μ = permeability constant
$\lambda^2 = m/\mu N_s e^2$
m = mass of an electron
e = charge of an electron

The parameter (λ) has the dimensions of distance and is termed the London penetration depth. As will be seen later, this term has an analogous meaning to the classical skin depth of normal conductive materials. The magnitude of (λ) is typically in the order of 200-2000 Angstroms for traditional superconducting materials.

The combined current density in the material is determined by using Maxwell's and London's equations and is equal to the normal current, the super current and the displacement current densities as follows:

$$\begin{aligned} J_{total} &= J_n + J_s + \frac{dE}{dt} \\ &= \frac{N_n}{N}\sigma_n - j/\omega\mu\lambda^2 + j\omega \end{aligned} \tag{4}$$

where, d/dt = $j\omega$ for sinusoids

The displacement current density term ($j\omega$) can be neglected compared to the other terms for a good conductor i.e., $\sigma \gg \omega$. Equation (4) thus reduces into an Ohm's Law relationship $J_{total}=\sigma E$) if we introduce the notion of a complex conductivity. [1]

$$\sigma = Re[\sigma] - jIm[\sigma] = \left(\frac{N_n}{N}\sigma_n\right) - j\left(1/\omega\mu\lambda^2\right) \tag{5}$$

The above equations summarize in a nutshell the theoretical relationships for the classical (local) model of superconductivity. The expression for the complex conductivity can now be plugged into the traditional transmission line equations for coaxial pairs as will be seen in the next section. Before applying the theory in a practical example, the author will briefly review the conditions that determine the applicability of the model.

The local condition of the two-fluid model refers to the expression for Ohm's Law ($J = \sigma E$) where it is assumed that the current density at a point in the material is determined by the electric field at that point by a local J(E) relationship. This will hold true in a normal metal where the electric field does not change appreciably over the mean free path (ℓ)

which is defined as the distance a normal electron can travel without being scattered. Such metals exhibit the classical skin effect ($\delta \gg \ell$) where δ is the skin depth. In other moderately pure metals at very high frequencies, the skin depth can be much less than the mean free path ($\delta \ll \ell$) and the electric field changes rapidly over very short distances. In such materials, the current density at a point is determined by a non-local J(E) relationship involving an integral of the electric field at distances up to the mean free path from the point. The materials under these conditions exhibit what is referred to as the anomalous skin effect.

Similar limiting conditions have been developed for the superconducting state.[5] In this case the penetration depth (λ) is compared with the coherence distance of electron pairs (ξ) where the coherence distance is defined as the extent of coupling between bound electron pairs. The local case applies when ($\lambda \gg \xi$) and is called the "London limit". Estimates for the ratio of (λ/ξ) are given in reference 37 from which it is concluded that the London condition applies in most cases. The theoretical relationships for the non-local model are somewhat different and are applicable when ($\lambda \ll \xi$). The limiting condition is called The "Pippard limit". In a paper by McCaa and Nahman,[16] the measured values of attenuation and step response for a Pb-Nb coaxial line at 4.24 K have been presented. Their results show that the measurements are bounded between the values calculated using the classical and anomalous models. In this case, the classical model predicts the worst case characteristics.

SUPERCONDUCTIVE COAXIAL LINE MODEL

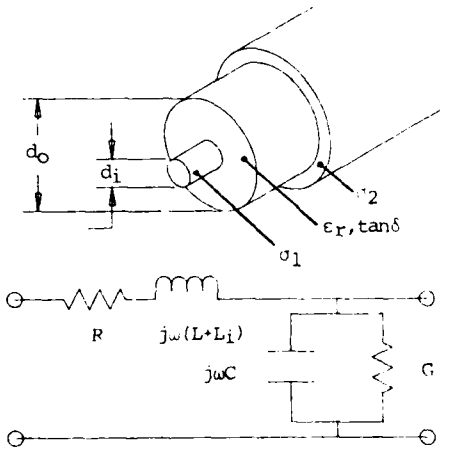


Fig. 1 - Cross-sectional View of a Coaxial Pair and Corresponding Equivalent Circuit

Fig. 1 shows a cross-sectional view of a coaxial pair and its equivalent circuit. The transmission parameters are determined from the primary constants, namely the distributed resistance, inductance, capacitance and conductance per unit length. The primary constants are obtained from a theoretical analysis of the field equations for a cylindrical coordinate system. The well known relationships for L, C and G of a coaxial pair due to the external field in the dielectric material are given by:

$$L = \frac{\mu_o}{2\pi} \ln(d_o/d_i) \qquad (6)$$

$$C = \varepsilon_r \varepsilon_o 2\pi / \ln(d_o/d_i) \qquad (7)$$

$$G = \omega C \tan\delta \qquad (8)$$

where $\omega = 2\pi f$

An additional expression is needed for the resistance and internal inductance of the conductor material. The classical method involves finding a solution for the current density distribution in the conductor which for the case of round or tubular conductors is given by the following differential equation:

$$\frac{\partial^2}{\partial r^2} J_z(r) + \frac{1}{r} \frac{\partial}{\partial r} J_z(r) - j\omega\mu\sigma J_z(r) = 0 \qquad (9)$$

Equation (9) is a modified form of Bessel's equation of order zero for which solutions have been determined in the literature in terms of the argument $k = \sqrt{-j\omega\mu\sigma}$. It is noted that the equation is in a convenient form whereby the expression for the complex conductivity given in (5) can be directly substituted for the superconductive state. It is beyond the scope of this paper to present a rigorous mathematical treatment for the general case. A simple solution is given for the special case at high frequencies where the current flow in a coaxial pair is concentrated at the outer surface of the inner conductor and the inner surface of the outer conductor.

The surface impedance of a good conductor at high frequencies is given by:

$$Z_s = (j\omega\mu/\sigma)^{\frac{1}{2}} \qquad (10)$$

From which,

$$Z_s = R_s + j\omega L_s \qquad (11)$$

$R_s = 1/\sigma\delta_n$ in ohms per square

$L_s = R_s/\omega$

and, $\delta_n = (2/\omega\mu\sigma)^{\frac{1}{2}}$ (12)

where,

δ_n is called the skin depth which is the depth where the current density has decayed to 1/e of its surface value.

For normal conducting materials, the total resistance and the internal inductance of the inner and outer conductors are obtained from (11):

$$R = R_{s1}/\pi d_i + R_{s2}/\pi d_o \quad (13)$$

$$L_i = R/\omega \quad (14)$$

where,

R_{s1} and R_{s2} is the surface resistivity in ohms per square of the inner and outer conductors respectively.

For superconducting materials, the expression for complex conductivity of equation (9) is substituted in (10) and gives approximately:

$$R_{ss} = Re\left[Z_s\right] \cdot \frac{2}{\pi d_i} \cdot \frac{3}{2} \frac{N_n}{2N} \delta_n \quad (15)$$

$$L_{ss} = Im\left[Z_s\right] \cdot \frac{1}{\omega}$$

Equation (15) can be further simplified in terms of the normal conductive parameters by taking out the ω as a factor:

$$R_{ss} = 2R_s^2 \left(\frac{\delta_n}{\lambda}\right)^3 \frac{N_n}{N} \quad (16)$$

$$L_{ss} = 2R_s^2 \left(\frac{\delta_n}{\lambda}\right)^3 \cdot$$

From equation (15) it is noted that the AC resistance of superconductors varies as the square of the frequency compared with the square root relationship for normal conductors. From equation (16), the magnitude of the superconducting AC resistance varies as the cube of the penetration depth ratio (δ_n/λ) and directly with the available number of normal electrons in the material. The London penetration depth (λ) is invariant with frequency and depends only on temperature, the applied field and material properties. Consequently, it is inferred from equation (16) that at very high frequencies the AC resistance of superconductors approaches the normal resistance when the skin depth (δ_n) approaches the London penetration depth (λ).

In order to complete the model, the secondary transmission line parameters are derived from the primary constants using the following well known transmission line equations:

Attenuation:	α	$= 8.686 Re\left[\sqrt{ZY}\right]$ (dB length)	(17)
Phase Angle:	β	$= Im\left[\sqrt{ZY}\right]$ (rad/length)	(18)
Characteristic Impedance:	Z_o	$= \sqrt{Z/Y}$ (ohms)	(19)
Phase Delay:	T	$= \beta/\omega$ (sec/length)	(20)
Impedance:	Z	$= R + j\omega(L + L_i)$ (ohms/length)	(21)
Admittance:	Y	$= G + j\omega C$ (mhos length)	22)

[illegible]

[illegible] [illegible] [illegible] [

DESIGN PARAMETERS				
Name		Value		SI
		SCCX	CCX	Units
Inner condr dia.	d_i	0.275	2.60	mm
Outer condr dia.	d_o	0.85	3.60	mm
Relative permittivity	e_r	2.10	1.10	-
Loss angle	tanδ	1.0×10^{-6}	1.0×10^{-4}	-
Inductance	L	0.226	0.261	µH/m
Capacitance	C	103.5	46.8	pF/m
Characteristic Impedance	Z_o	46.7	74.7	Ω
Phase delay	T	4.83	3.50	ns/m

TABLE I

Table I presents the design parameters for a typical superconductive coaxial line[36] compared with a conventional coaxial cable. The conventional cable is constructed of copper inner and outer conductors with a semi-air dielectric.

PHYSICAL CONSTANTS			
Name		Value	SI Units
Permeability of free space	μ_o	1.26×10^{-6}	H/m
Permittivity of free space	e_o	8.85×10^{-12}	F/m
Electron charge magnitude	e	1.60×10^{-19}	C
Electron rest mass	m	9.11×10^{-31}	kg
Conductivity of copper @ 20°C	σ_{cu}	5.80×10^{7}	1/(Ω·m)
Boiling point of helium	T_{he}	4.24	K

PROPERTIES OF NIOBIUM AND LEAD				
Property		Value		SI
		Niobium	Lead	Units
London penetration depth	λ	5.50×10^{-8}	8.35×10^{-8}	m
Density of paired electrons	N_s	9.34×10^{27}	4.05×10^{27}	1/m^3
Density of normal electrons	N_n	4.37×10^{26}	5.33×10^{26}	1/m^3
Density of total electrons	N	9.77×10^{27}	4.58×10^{27}	1/m^3
Conductivity of 4.2K($H>>H_c$)	σ	6.67×10^{7}	4.35×10^{9}	1/(Ω·m)
Critical temperature	T_c	9.22	7.26	K
Critical magnetic field strength	H_c	1.64×10^{5}	6.40×10^{4}	A/m

TABLE II

The key results are presented in Fig.2 through Fig.5 inclusive. They are calculated for the example given in Table I using the two-fluid model and the physical constants given in Table II. The physical constants were obtained from published data.[37,41]

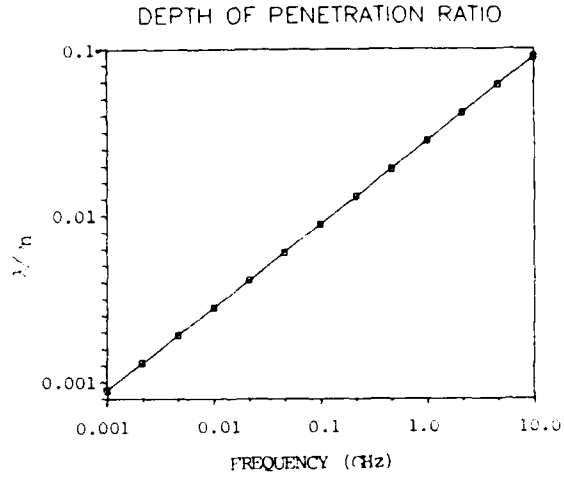


Fig. 2 - Ratio of Penetration Depths for Superconductive vs. Normal State of Niobium @ 4.2 K

At high frequencies, the current flow is concentrated in a thin layer at the outer surface of the inner conductor and the inner surface of the outer conductor. The layer thickness is given by the London penetration depth (λ) for the superconductive state and by the skin depth (δ_n) for the normal state. The ratio of the penetration depth to the skin depth as a function of frequency is illustrated in Fig. 2 for niobium at a temperature of 4.2 K. From Fig. 2, it is seen that the penetration depth for the superconductive state is much less than the normal skin depth.

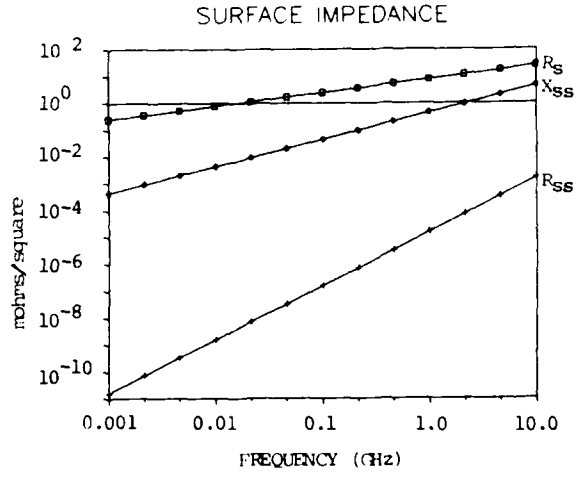


Fig. 3 - Surface Impedance of Niobium Conductor @ 4.2 K for the Superconductive and the Normal State

The surface impedance calculated from equations (11) and (15) is shown in Fig. 3 for the case of niobium at a temperature of 4.2 K. For the superconductive state, it is seen that the resistive component is very small compared with the reactive component of surface impedance. Also, it is seen that there is a dramatic increase in the surface resistivity when the material undergoes a transition from the superconductive to the normal state (bottom curve to the top curve).

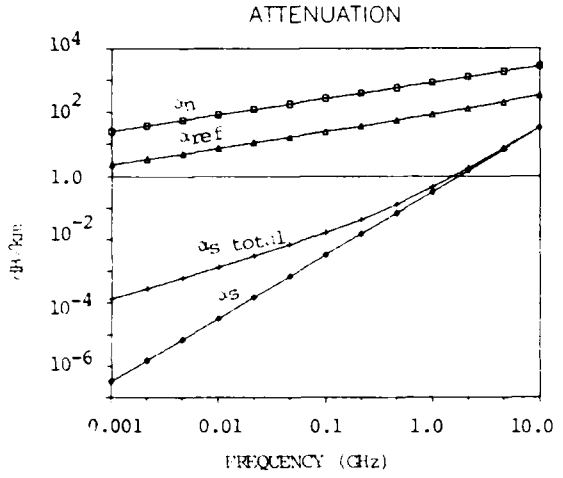


Fig. 4 - Attenuation Frequency Characteristics for the Normal and Superconductive State compared with a Reference Coaxial Line

The attenuation characteristics are presented in Fig. 4 over the frequency range between 1 MHz and 10 GHz. The attenuation values are given at a temperature of 4.2 K for the superconductive coaxial line and at 295 K for the reference cable. Despite its smaller size, the total attenuation including dielectric losses of the superconductive cable (second curve from the bottom) is at least two orders of magnitude lower than the reference cable (second curve from the top). The calculated attenuation at 1 GHz is 0.5 dB/km. Also, it is seen that there is a dramatic increase in attenuation (top curve) when the superconductive cable reverts to its normal state.

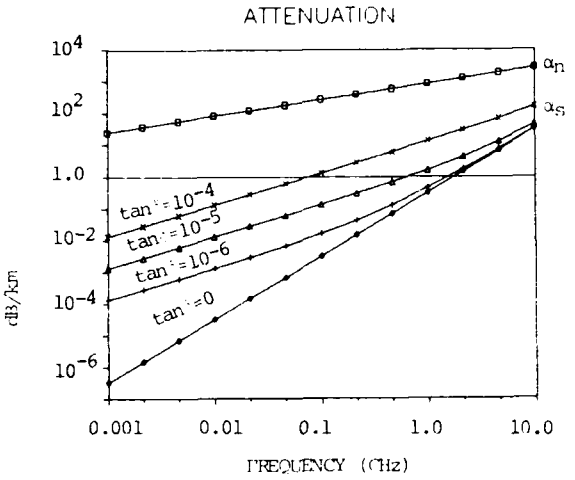


Fig. 5 - Attenuation Frequency Characteristics as a Function of the Dielectric Losses in the Insulation

Fig. 5 illustrates the effect of dielectric losses on the total attenuation for the superconductive cable given in Table I. At lower frequencies, it is noted that the dielectric loss is the dominant component of attenuation. A change in the dielectric loss from $\tan\delta = 10^{-6}$ which is typical of fluoropolymers at cryogenic temperatures to $\tan\delta = 10^{-4}$ which is typical of polyolefins at room temperature results in a significant increase in attenuation.

DISCUSSION

The theoretical results presented in this paper have been derived from previous studies and experiments with superconductive coaxial cables. These cables were constructed with metallic conductors such as niobium and lead which become superconductive at critical temperatures close to the temperature of liquid helium (4.2 K). These results are intended to illustrate the magnitude of the improvement that can be expected in the transmission parameters of superconducting vs. normally conducting communications cables at high frequencies. Similar results might be obtained for the new class of ceramic compounds that have been found to exhibit superconducting properties at temperatures much higher than the temperature of liquid nitrogen (77 K). The properties of one such material are given in reference.[2] However, it still remains to be determined to what extent the two-fluid model can be used to predict the high frequency characteristics for these materials. Consequently, the author has refrained from presenting any theoretical results for these materials at this time.

There are a number of other practical considerations that need to be addressed in the design and manufacture of superconductive communication cable. One important consideration is the dimensional uniformity and the homogeneity of the insulation along the length of the coaxial pair. Previous studies in Japan[28,40] have shown that periodic dimensional variations can give rise to significant ripples in the attenuation frequency characteristics. Another major consideration relates to the physical properties of the new materials which are intrinsically brittle. Can flexible wires or coatings be made from such ceramics? What is the environmental stability of these materials? To what extent are the superconducting properties affected by mechanical stresses? The answers to these questions will bring more challenges and it will be some time yet before all the technical hurdles can be overcome.

The critical current density and the critical magnetic field parameters of the new superconducting materials will need to be evaluated for the transmission line application. For communication signals, only small magnetic fields are generated and the critical field has not been identified as a limiting factor. The current density on the other hand can be quite large in view of the fact that the current flow is concentrated in a thin layer at the surface of the conductor. There are indications that the new materials have low critical current densities (1000 a cm^2 or lower for the bulk material). Such low values are of concern and can be an overriding criterion for this application. It is believed that the orientation of the crystals is responsible for the low values of critical current densities that have been reported. The question is being studied at this time by scientists in the field.

Initially, it is likely that the new materials and their derivatives will find a home in specialized electronic circuits and computer applications.[45] The practical implementation of a superconductive communication cable presents a more difficult technical and economic challenge. First, it is not known whether the new materials can be adapted to accommodate the mechanical stresses involved during cable manufacture and installation. Second, in order to be commercially viable, such cables would have to compete directly with the already established fibre optics and copper based media.

In theory, the new superconducting materials offer exciting opportunities for the future along with a new set of challenges. It is too early to tell what technical breakthrough still lies ahead and what can be realized in practice. Given the fast pace of current research efforts a flexible, low cost, room temperature superconductor may be just around the corner.

ACKNOWLEDGEMENTS

The author would like to acknowledge the valuable assistance of Mr. Philip McGettigan and Dr. J. Walling in reseaching the information for this paper and in the technical consultations that were provided. The author wishes to thank his wife Susan for her patience, support and encouragement.

REFERENCES

1. Principles of Superconducting Devices and Circuits, Chapter 3, T. Van Duzer and C.W. Turner, Elsevier, New York, Oxford.

2. Electronics of Solids, Chapter 6, Walter R. Beam, McGraw-Hill Book Company.

3. The Electromagnetic Equations of the Supraconductor F. and H. London, Proc. Roy Soc. (London) 1935, A149, pp. 71-88.

4. Theory of Superconductivity, J. Bardeen, L.N. Cooper and J.R. Shrieffer, Phys. Rev. vol. 108, Dec. 1957, pp. 1175-1204.

5. Theory of the Anomalous Skin Effect in Normal and Superconducting Metals, D.C. Mattis and J. Bardeen, Phys. Rev. vol. 111, July 1958, pp. 412-417.

6. Surface Impedance of Superconductors, P.B. Miller, Phys. Rev. vol. 118, May 1960, pp. 928-934.

7. Nanosecond Response and Attenuation Characteristics of a Superconductive Coaxial Line N.S. Nahman and G.M. Gooch, Proc. IRE, vol. 48, Nov. 1960, pp. 1852-1856.

8. Field Solution for a Thin Film Superconducting Strip Transmission Line, J.C. Swihart, J. Appl. Phys. vol. 32, Mar. 1961, pp. 461-469.

9. Superconducting Co-axial Delay Line, P.K. Shizume and E.O. Vaher, IRE Intern. Conv. Rec. 1962, Pt 3.

10. Analysis and Performance of Superconductor Coaxial Transmission Line, R.J. Allen and N.S. Nahman, Proc. IEEE, vol. 52, Oct. 1964, pp. 1147-1154.

11. Microwave Properties of Superconductors, J.I.Gittleman and B. Rosenblum, Proc. IEEE, vol. 52, Oct. 1964, pp. 1138-1147.

12. Superconducting High Voltage Delay Line, A.J. Cummings and H. Kuettner, 14th IWCS, 1965.

13. High-Voltage Pulse Characteristics of Superconducting Transmission Lines, A.J. Cummings and A.P. Wilson, J. Appl. Phys., vol. 47, July 1966, pp. 3297-3300.

14. Dielectric Properties of Some Insulating Materials over the Temperature Range 4.2-300 K, M.J. Chant, Cryogenics, vol. 8, Dec. 1967, pp. 351-354.

15. Dielectric Losses in Solids at Cryogenic Temperatures, R.N. Allen and E. Kuffel, Proc. IEE (London), vol. 115, Mar. 1968, pp. 432-440.

16. Frequency and Time-Domain Analysis of a Superconductive Coaxial Line using the Two-Fluid Model, W.D. McCaa and N.S. Nahman, J. Appl. Phys. vol. 39, April 1968, pp. 2591-2596.

17. Measurement of the Surface Resistance of Superconducting Lead at 2.866 GHz, H. Hahn, H.J. Halama and E.H. Foster, J. Appl. Phys. 39, May 1968, pp. 2606-2609.

18. Nuclear Test Instrumentation with Miniature Superconductive Cables, P.K. Rathbun and H.J. Jensen, IEEE Spectrum, vol. 5, Sept. 1968, pp. 91-99.

19. Frequency Dependence of the Skin Depth in Superconducting Tin, J. Matisso, J. Appl. Phys. vol. 40, April 1969, pp. 2091-2097.

20. Frequency and Time Domain Analysis of a Superconductive Coaxial Line using the BCS Theory, W.D. McCaa and N.S. Nahman, J. Appl. Phys. vol. 40, April 1969, pp. 2098-2100.

21. Comparison between Measured and Calculated RF Losses in the Superconducting State, J. Halbritter, Z. Physik, vol. 238, 1970, pp. 466-476.

22. The Measured Time and Frequency Response of a Miniature Superconducting Coaxial Line, M.P. Ekstrom, W.D. McCaa and N.S. Nahman, IEEE Trans. Nuclear Sci., vol. NS-18, Oct. 1971, pp. 18-25.

23. Miniature Superconductive Coaxial Transmission Lines, N.S. Nahman, Proc. IEEE, vol. 61, Jan. 1973, pp. 76-79.

24. Frequency Characteristics of Superconducting Coaxial Lines, N. Chiba, Y. Kashewaymagi and K. Mikoshiba, Proc. IEEE, Jan. 1973, pp. 124-125.

25. On surface Resistance of Superconductors, J. Halbritter, Z. Physik, vol. 266, 1974, pp. 209-217.

26. Superconducting Communication Cables, I.I. Grodnev, K.G. Levinov and D. Ya Gal'perovich, Telecomm. Radio Engng., Part 1, vol. 28, Feb. 1974, pp. 1-6.

27. Superconductive Communication Transmission, Y. Hoshiko, Proc. 5th Intern. Cryog. Eng. Conf., Kyoto, Japan, May 1974, pp. 282-286.

28. Superconducting Coaxial Cable as a Large Capacity Transmission Medium for Communications, K. Mikoshiba, Y. Shimohori, N. Ohmori and F. Sone, Proc. 5th Intern. Cryog. Eng. Conf., Kyoto, Japan, May 1974, pp. 289-292.

29. High Frequency Study of a Short Niobium/Lead Alloy Line, J. Mazuer and J. Gilchrist, Proc. 5th Intern. Cryog. Eng. Conf., Kyoto, Japan, May 1974, pp. 293-295.

30. Superconducting cable for Telecommunications, Cryogenic News, Cryogenics, Sept. 1974, p.536.

31. The Theory and Electrical Design of Superconducting Coaxial Cables, I.I. Grodnev, and D. Ya. Gal'pervoich, Telecom Radio Engng, Part 1, vol. 29, May 1975, pp. 1-5.

32. Aspects of the Development of Guided Systems for Intercity Communications, I.I. Grodnev and V.M. Dmitrachenko, Telecom Radio Engng, Part 1, vol. 30, Feb. 1976, pp. 1-9.

33. Dielectric Properties of Polymeric Materials at Low Temperatures and High Frequencies, W. Meyer, Proc. 6th Intern. Cryog. Eng. Conf. Grenoble, France, May 1976, pp. 367-371.

34. Low Temperature Mechanical Properties of Insulating Materials, J. Thoris and J.C. Bobo, Proc. 6th Intern. Cryog. Eng. Conf. Grenoble, France, May 1976, pp. 353-357.

35. Superconductive Coaxial Cable as a Communication Medium with Enormous Capacity, K. Mikoshiba, F. Sone, Y. Shimohori and S. Kuma, IEEE Trans. on Comm, vol. 24, Aug. 1976, pp. 874-880.

36. Studies of Vacuum Sealed Cryocables for Superconductive Line using Absorbents, K. Funaki, Rev. Electr Commun. Lab., vol. 24, Nov.-Dec. 1976, pp. 1016-1025.

37. Penetration Depth Measurements on Type II Superconducting Films, W.H. Henkels and C.J. Kercher, IEEE Trans. on Magnetics, Jan. 1977, Vol. Mag-13.

38. Attenuation in Superconducting Coaxial Cables in the Frequency Range up to 17 GHz, D. Ya. Gal'perovich and I.I. Grodnev, Telecom. Radio Engng, July 1977, pp. 10-15.

39. Superconducting Telecommunication Cable Studies in Japan, H. Yoshikiyo, S. Yoshikiyo and K. Noda, Cryogenics, Sept. 1977, pp. 521-527.

40. Improvement of Transmission Characteristics of Superconducting Coaxial Cable: Spectral Analysis of Dimensional Irregularity of Raw Materials of Coaxial Cable, H. Kajioka and F. Sone, IEEE Trans on Comm., vol. Com. 25, Oct. 1977, pp. 1155-1163.

41. Influence of Direct Current on Performance of Niobium Conductor for Miniature Coaxial Line, J. Mazuer and J. Gilchrist, Cryogenics, Oct. 1977, pp. 39-45.

42. Superconducting Coaxial High Frequency Miniature Lines, D. Ya. Gal'perovich, T.V. Korzhakova, A.A. Laptev, B.V. Mal'kov, A.A. Pavlov, L.F. Sukharakova and N.N. Krenkov, Telecomm. Radio Eng., vol. 32, Dec. 1977, pp. 31-36.

43. Miniature Superconducting High Frequency Coaxial Lines, J. Mazuer, Cryogenics, Jan. 1978, pp. 39-45.

44. New Materials for Superconductive Communication Cables, W. Meyer, IEEE Trans. on Comm. vol. Com. 26, April 1978, pp. 449-456.

45. The Superconducting Computer, J. Matisso, Scientific American, May 1980, pp. 50-65.

46. Effect of Inhomogeneities on the Characteristics of Superconductive Coaxial Cable, V.A. Bystrov, M. Dmitriyev, I.A. Lyulicheva, V.A. Pavlyuk and A.L. Solovyev, Proc. Intern. Cryog. Eng. Conf., Geneva, June 1980, pp. 471-475.

47. Long Term High-Vacuum Maintenance in the Cryogenic Envelope for Superconducting Telecommunication Cables, M. Hikita and H. Yoshikiyo, Rev. Elect. Commun. Lab, vol. 29, May-June 1981, pp. 612-626.

48. Characteristics of Superconducting Coaxial Line in the Millimeter-Wave Band, D. Ya. Gal'perovich, A.A. Laptev and N.N. Krenkov, Telecomm. Radio Eng., vol. 37, June 1982, pp. 50-55.

49. Experimental Studies of Superconducting Communication Lines: A Survey, D. Ya. Gal'perovich, Telecomm. Radio Eng., Nov. 1983, pp. 12-16.

50. Spectral Estimate of the Irregularity in Superconducting Coaxial Line, D. Ya. Gal'perovich, A.A. Laptev, A. Yu. Podshivalav, Sov. Electr. Eng., Vol. 55 No. 9, 1984, pp. 89-92.

51. Superconductors, E.T. Smith, J.E. Davis, E. Clark, J.W. Wilson and O. Port, Business Week Cover Story, April 6, 1987.

52. Bulk Superconductivity at 91 K in Single-Phase Oxygen-Deficient Perovskite $Ba_2YCu_3O_{9-\delta}$, R.J. Cava, B. Batlogg, R.B. van Dover, D.W. Murphy, S. Sunshine, T. Siegrist, J.P. Remeika, E.A. Rietman S. Zahurak and G.P. Espinosa, Phys. Rev. Let., Vol. 58 No. 16, April 1987, pp. 1676-1679.

53. Do-it-yourself Superconductors, P. Brant, New Scientist, July 1987.

54. Superconductivity, Hype vs. Reality, G. Maranto, Discover, Aug. 1987.



P. Kish received his B.A.Sc. (1971) and M.A. Sc. (1972) degrees in Electrical Engineering from the University of Waterloo in Ontario, Canada. He joined Bell-Northern Research and later Northern Telecom Canada Ltd. as a member of Cable Research and Development Staff. He has worked on the design and development of paired communication cables for digital transmission systems. In 1978 he was appointed as Manager of the Communication Cable Laboratory and in 1980 as the Manager of Cable Design at Northern's Lachine Cable plant. Since 1985, as Manager of Cable Development, he has overall responsibility for both groups.

FIGURE-8 FIBER OPTIC CABLE

P. Stephen Keith*, Eric L. Buckland**, Stanley K. Hovis*

* Sumitomo Electric Fiber Optic Corp.
** Sumitomo Electric Research Triangle, Inc.

Abstract

The adaptation of the Figure-8 cable concept to fiber optics is presented. Aerial installation phenomena, including sag and tension analysis and wind-induced cable motion, are reviewed as criteria for the subsequent test plan. Prototype cables in both tight buffer and loose tube design were manufactured using a stranded steel messenger. Subsequently, an all-dielectric option was developed, featuring an FRP messenger bonded to the jacket. All were evaluated in tests developed to simulate aerial service.

I. Introduction

Aerial telecommunication cable can offer the operating company advantages in installation convenience and costs, particularly in cases where support structures already exist. Among aerial designs, those which self-contain the necessary strength elements will obviate the need for a separate messenger-stringing/lashing operation, lowering installation costs still further. Of these self-supporting types, the integral messenger (or "Figure-8") design offers the advantage of a strength member external to the signal-carrying core. This messenger can therefore be subjected to jacket stripping, dead-ending, and suspending, often rugged procedures, without undue concern for the integrity of the core. This paper reports on the adaptation of this traditional cable configuration to the field of fiber optics.

II. Aerial Installation Phenomena

The development of a Figure-8 fiber optic cable begins with analysis of classical aerial installation phenomena into which have been incorporated the special considerations associated with Figure-8 cross sections and optical transmission. Dividing such phenomena into static and dynamic, let us first consider the static situation, that of sag and tension.

A. Sag and Tension

Sag and tension investigation seeks to answer the following questions:

1. For a given span between poles, will a tension member of known area and modulus support a cable of known weight?
2. Once installed at a selected initial sag and tension, how will tension and sag subsequently vary under different conditions of wind and ice loading?

Classically, a cable hanging between two supports would have to be described according to the "catenary curve":

$$y = \frac{T \cos\theta}{w} \cosh\left(\frac{xW}{T \cos\theta} - 1\right) \qquad (1)$$

where x, y are horizontal and vertical components of location

W = cable weight, effective
T = tension at any point of the cable
θ = angle relative to the horizontal

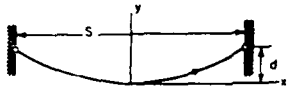


Figure 1. Uniform cable loaded by its own weight.

By setting y = d (sag) at x = S/2 where S = span, Equation 1 becomes:

$$d = \frac{T \cos\theta}{W} \cosh\left(\frac{WS}{2T \cos\theta} - 1\right) \qquad (2)$$

To avoid hyperbolic functions, it is acceptable to assume that a parabolic function applies in cases of actual cable stringing, where sag is small compared to span. Even where sag equals so much as 5 percent of span, the error in assuming a parabolic relationship is less than 0.3 percent and the following equation applies:

$$T = \frac{WS^2}{8d} \qquad (3)$$

Effective cable weight, W, is a vector resultant of three primary forces: actual cable weight, W_o, ice load, and the effect of wind loading. The equation has the general form of a vector resultant:

$$W = [(W_o + \text{Ice Load})^2 + (\text{Wind Load})^2]^{\frac{1}{2}}$$

Applying specifics, this equation becomes:

$$[W_o + \underbrace{[(OD + 2I)^2 - (OD)^2](\pi/4 \times K \times 10^{-3})}_{\text{ice load}}]^2 + [(OD + 2I) \times Z \times 10^{-3}]^2]^{\frac{1}{2}} + C \qquad (4)$$

(OD + 2I): Effective Cable Diameter

where I = ice thickness, mm
K = density of ice (usually .92)[13]
Z = wind load (kg/sq. meter)
C = constant to be added (per National Electrical Safety Code)[12]

Next, cable strain, ε, is addressed[3] and is the summation of elongations due to tension T and thermal expansion at temperature t,

$$\varepsilon = \alpha(t - t_m) + T/EA \qquad (5)$$

where t_m = cable manufacturing temperature
E = Young's modulus of the tension member
A = area of the tension member
α = coefficient of linear expansion of the tension member.

At this point, the actual total strain maximums are introduced. For long-term service, ε must be less than ε_o, the allowable system strain. (For example, ε_o could equal .002 for tight buffer and equal .005 for loose tube, but these parameters can be adjusted for state-of-the-art.)[4,15] From this prerequisite comes the requirement that

$$\frac{WS^2}{8EA} \leq [\varepsilon_o - \alpha(t - t_m)]d \qquad (6)$$

Now the variable sag, d, is also related to temperatures at time of installation, t_i, and the variable temperature, t, as well as initial sag at installation, d_o, so that the preceding requirement can be expanded to

$$EA \geq \frac{WS^2}{8p\ 3/8(qS^2) + d_o^2} \qquad (7)$$

where $p = \varepsilon_o - (t - t_m)$
$q = \varepsilon_o - (t_i - t_m)$

This our first working equation. If the relationship of Equation 7 holds true, the choice of strength member variables E and A are adequate for the desired span S under the other related conditions. If EA exceeds the right-hand side of the equation, the installation is valid. If EA is less than the right side, the variables must be modified (usually by shortening the span). In this way, the answer to the first question posed in sag and tension is arrived at.

The second question, of defining sag and tension after loading, is dealt with, by the following equation, based on the parabolic:[3]

$$\frac{8d^2}{3S} - \frac{8d_o^2}{3S} = (t - t_i)\,S\,(1 + \frac{8d_o^2}{3S}) + \frac{(T - T_o)}{EA}\,S\,\frac{(1 + 8d_o^2)}{3S} \qquad (8)$$

where $T = \frac{WS^2}{8d}$ and $T_o = \frac{W_o S^2}{8d_o}$

Because $d_o \ll S$, then the assumption that $1 + 8d_o/(3S) \approx 1$ can be made. This simplifies Equation 8 to

$$d^3 + \frac{3}{8}S^2\left[\frac{T_o}{EA} - (t - t_i)\right] - d_o^2 = \frac{3WS^4}{64EA} \qquad (9)$$

Equation 9 is our second working equation.

The output values in sag and tension calculations are initial sag, maximum span, and service sag (usually under worse-case conditions). In the course of this work an extensive analysis was made of thirteen sag and tension input variables ranging from ice density theory to empirical calculation of the actual Young's modulus of a stranded messenger. Inclusion of material would unduly burden the present paper, but it is hoped that separate publication can be made soon.

B. Vibratory

Vibratory motion in aerial cable installations is of two types: the low-frequency/high amplitude movement known as "galloping" or "dancing" and the high frequency/low amplitude motion of aeolian vibration.

1. Galloping. Any consideration of Figure-8 cable service must address this form of movement. When wind blows against a cable showing a smooth, circular shape the result is a drag force which pushes the cable in the direction of the wind. When the cable shape is asymmetrical, however, there is a lift component of wind force as well as drag. As this upward force is acted against by gravity in the downward direction, the result is a vibration of often powerful energy. The frequency of this wave may be on the order of 1 to 4 Hz and of an amplitude dependent on stringing variables such as initial tension, span length, and initial sag.

Classical work in this area was done by J. P. Den Hartog in 1932[5] and has been more recently reviewed as well.[6,7] Examples of asymmetrical shapes include lashed messenger cable, overhead conductors which have undergone icing, and the Figure-8 design.

Tendency to gallop can be minimized by selection of the stringing variables mentioned. Higher messenger tension, lower sag, and limited span length all act to alleviate this phenomenon. Thus, even though prototype Figure-8 optical cables performed extremely well in severe galloping tests described later, our company has recommended that these cables be limited to spans of about 150 meters or less as conservative practice, if for no other reason than to lessen wear on installation hardware.

An alternate or supplementary approach to galloping can be taken at installation. By alternating the relative orientation of core to messenger by rotating the cable in an oscillation between spans, the asymmetry presented to the wind can be randomized and the high-amplitude vibration neutralized. This theory is incorporated in the commercially-available plastic helical galloping suppression devices which can be wrapped on existing spans to accomplish the same purpose.[7,8]

2. Aeolian. For all the consideration directed toward high-amplitude vibration, the other mode of wind-induced movement, the low-amplitude aeolian motion, is essentially absent in this type of cable. Theory would predict that a uniform shape (in contrast to Figure-8) is needed to provide the vortex shedding phenomenon responsible for initiation of aeolian vibration.[14,16] This expectation has been confirmed empirically in asymmetrical cable shapes by other investigators.[9]

III. Developmental Cables

A. Prototype Cables

Two sets of prototype cables have been designed and produced at the Research Triangle facility. A set consisted of a loose tube and a tight buffer design, while sets differed by the type of messenger employed, as illustated in Figures 2 and 3:

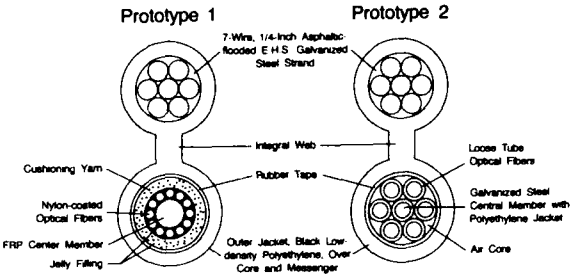


Figure 2: Metallic messenger designs.

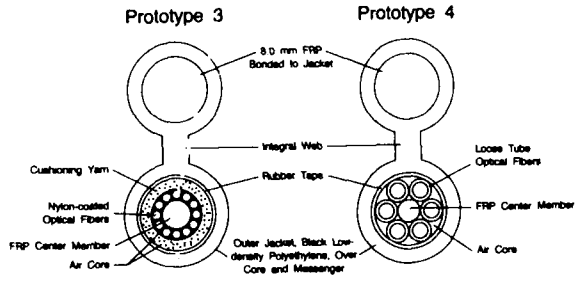


Figure 3: All-dielectric designs.

As there are several variables which may be specified regarding not only fiber buffer but central member and filling option, an attempt was made to incorporate all of these features within the prototypes:

Messenger	Fiber Buffer	Central Member	Filling Option
Steel	Tight Buffer	FRP	Filled Core
Steel	Loose Tube	Steel	Air Core
FRP	Tight Buffer	FRP	Air Core
FRP	Loose Tube	FRP	Air Core

Table 1.

B. Design and Manufacturing Philosophy

1. Core. Although most optical cable activity in this country is of the loose tube design, there is no reason not to consider tight buffer for evaluation in these designs.[10] In fact, in the present work, the tight buffer cable was designed first as a result of specific customer interest. A hypothetical advantage of loose tube cable is that with the excess fiber of this design the allowable system strain is usually greater. Referring back to our sag and tension discussions we can see that greater spans could be expected in theory; however, if we agree to limit span length in order to minimize high-amplitude wind motion, this potential advantage is of little importance.

The central member serves as an anti-buckling device for the fibers and does not provide design strength, this function being allocated to the messenger exclusively. Thus the choice of central member material relates to the preference for dielectric or non-dielectric core rather than a load-bearing decision. The influence upon cable weight and total cost, however, may be ancillary considerations in material choice.

The core wrap in these prototypes was chosen with the objective of coupling the movement of the cabled fibers in the core to that of the outer jacket. Due to temperature changes and load variations in the cantenary, length changes of a few tenths of a percent in the messenger-jacket system will be inevitable in actual service. Due to the cabling helix factor, however, this change will not necessarily directly translate into fiber strain. What can occur when the core-to-jacket relative motion is high is a possibility of fiber bend at the splice closure location over a few millimeters radius of curvature, resulting in transmission loss. This phenomenon was documented by Ishihata, et al., in 1984.[11] These researchers found an improvement in optical field performance in aerial cable when the friction force between the sheath and the core was increased. Our approach in this vein was to use a core wrap consisting of a nylon weave base covered on both sides with neoprene rubber. Although already vulcanized prior to cable processing, the neoprene wrap in the unfilled cable bonded to itself at the helical overlap areas, thus forming a sealed tube. Among advantages which may result from this feature is the fact that there is no tendency for the tape overlap to either gap or to rub against the fibers or tubes during any sheath strain. Due to jelly seepage at the overlap in the filled version, this feature is more difficult to achieve in the filled design.

This brings us to the choice between filled and unfilled core, a decision which may be determined by the user's total system. If splice and termination points can be adequately secured against water ingress, our preference would go to an unfilled core. Historical avoidance of filled cable in aerial plant can be understood given the unpredictability of temperature extremes and the handicap of additional weight in the span. Additionally, friction between core and sheath, an advantage discussed previously, is enhanced by the absence of filling compound.

2. Messenger -- Metallic Design. The messenger selected for this design will be familiar to users of twisted pair Figure-8 cable in the various telephone systems in the U.S. This member is a 7-wire, 1/4-inch extra high strength grade galvanized steel strand conforming to ASTM A 640. The strand is fully flooded with an asphaltic flooding compound which has long been accepted by the industry as being compatible with polyethylene jackets.

The 1/4-inch messenger size was chosen because of its availability as a "standard" material and the familiarity it would enjoy to those users already experienced in placing Figure-8 cable. In some installations, the size could be said to exceed the need for supporting a cable which weighs only 0.3 kg/m, almost three-fifths of which is the messenger itself. Theoretical spans of many hundreds of meters are possible under some loading conditions, although lesser spans will probably be chosen as a precaution relative to vibration. A definite advantage of the high-strength messenger is that it permits a large initial stringing tension that acts to dampen wind-induced motion and to lessen storm-related sag.

3. Messenger -- All-Dielectric Design. There is growing interest in aerial fiber optic cable which can be strung without concern for grounding or induced voltages in metallic components. Heretofore, a drawback

of utilizing an FRP strength element was the inability to couple the tension applied to the FRP to the polyethylene jacket surrounding the messenger. Without such a couple, jacket slippage or even tearing could be expected. As part of this cable project, a method of obtaining a thermo-chemical bond between an FRP messenger and its protective jacket was developed. It has been determined that the full rated breaking strength and Young's modulus of the FRP can be obtained when clamps are applied over a P.E. jacket bonded in this manner to the underlying rod. For a first design an 8.0 mm FRP messenger was chosen, permitting spans in excess of 150 meters in heavy loading districts. A future design will offer a smaller diameter rod for less severe installations.

4. Jacket. The long-standing material for twisted pair Figure-8 cable jacket is conventional telecommunications grade low-density polyethylene. This material should perform equally well in fiber optics applications. For our trials, however, we utilized linear low-density P.E. as the sheath material. We recognized the growing interest in LLDPE as jacket in more cable applications, and we wished to evaluate our extrusion tooling on what is the more challenging compound from a process viewpoint. It is known that compared to conventional low-density P.E., linear low reacts more adversely to extrusion in a high-shear situation. Process through the complex dual-land tip and die of the Figure-8 extrusion tooling presented such a potential situation. The core is covered in a tube-extrusion of low draw-down ratio, optimizing a balance between minimal residual stress in the jacket over the core and avoiding jacket pressure on the fibers. In the same die, the integral messenger is coated by pressure extrusion which forces the jacket tightly into the interstices of the steel strand to form a gripping action between messenger and jacket which is considerable. The quality of the jacket over core and messenger was excellent, confirming that either type of low-density P.E. is feasible for this design.

The nominal jacket wall thickness over both core and messenger is 1.3 mm (0.051 inch). Heavier walls are avoided in this design; the resultant larger diameters would not only be non-functional, but would present a greater surface for ice and wind loading as well as add to basic cable weight.

Web dimensions were chosen with the height slightly greater than the width to permit comfortable passage of a web slitting tool.

IV. Test Results

Based on the foregoing design philosophy, prototype cables were manufactured in 2 km lengths and subjected to the evaluation described below. A series of three tests was designed to simulate the field performance of each cable design.

A. Galloping -- Metallic Messenger

In order to simulate galloping, 150-foot spans of cable were strung at 343 lb. tension, supported in the center by a three bolt clamp rigging. Each end of the cable was terminated by a helical dead end grip secured around the messenger. The messenger was separated from the core and stripped of the P.E. jacket. Sufficient extra core length was provided to allow tension-free connection to the optical measurement equipment. Forced oscillation was induced near one end of a span and tuned closely to the natural frequency of the span. Oscillation was monitored and controlled only in this first span due to imperfect transmission through the node forced at the three bolt clamp. The resultant galloping conditions for each cable are outlined in Table 2.

Design	Frequency	Amplitude	1/2 Wavelength	# Cycles
T.B.	1.9 Hz	36in ± 3	75'	73,326
L.T.	2.0 Hz	36in ± 3	75'	100,000

Table 2.

Both designs exhibited no measurable loss increase at 1.3μm through six concatenated fibers throughout the stated number of cycles. In addition, the tight buffered fiber design was measured also at 1.5μm, where again no loss increase was observed. Note that this test was stopped prematurely. This is due to failure of the messenger wire, which testifies to the extreme severity of the test.

1. All-Dielectric Design. The same apparatus was used to force galloping in the all-dielectric design. Tensioning parameters were identical. This test was run subsequent to the metallic cables and it had been decided that, since the core designs themselves had proven stable under galloping, only one of the newer cables (it happened to be the loose tube) would be tested, basically to evaluate the durability of the bonded FRP messenger.

One of the purposes of this testing program was to gain the knowledge for potential cable users regarding the best way to treat the FRP messenger at termination and suspension points, particularly whether the jacket should be stripped and hardware applied to the rod or if the hardware could be applied over the

jacket. Therefore, the tests were varied in the following manner:

Test Period (cycles)	Application of Suspension Clamp	Application of Dead-Ends
1-50,000	Over jacket	Over jacket
50,001-75,000	Over jacket	On bare rod (strip jacket)
75,001-100,000	On bare rod (strip jacket)	On bare rod

The messenger rod showed no evidence of wear at any span point, independent of whether hardware was applied over the jacket or directly to the rod. With continuous monitoring at 1.3 and 1.5 μm, there was no measurable attenuation change during the 14-hour galloping period.

B. Cyclic Tension

The effects of wind and ice loading were simulated through a cyclic tension test. A 9.5m cable sample was supported horizontally and terminated with helical dead-ends. Load was applied as shown in Figure 4.

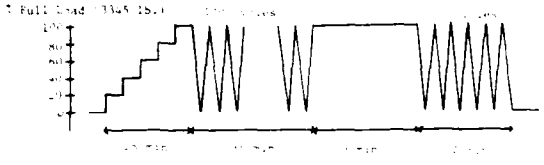


Figure 4. Representation of the Cyclic Tension test.

Attenuation as a function of load was monitored at 1.3 μm and 1.5 μm to a maximum 3345-pound load. The comparative relevance of this load for the two messengers is:

3345-Pound Applied Load

Messenger Type	% of Rated Break Strength (RBS)	Resultant Cable Strain, %
1/4" E.H.S. Steel	50	0.46
8.0mm FRP	22	0.69

The load was then oscillated at approximately 3 cycles/minute for 35 minutes between 0 and 3345 pounds. No attenuation increase was observed in any cable sample through four concatenated fibers. To further test the cable performance, the tension was held at 3345 pounds for 30 additional minutes and the cable then subjected to five final cycles. No loss increase was observed. The jacket over the steel messenger was stripped to accommodate the dead-ends in accordance with common practice. The jacket over the messenger in the tight buffer FRP design was stripped for the dead-end while the helical grip was placed over the jacket in the loose tube FRP design, seeking out any disadvantage to either method of terminating. Differences in load maintenance and messenger durability could not be distinguished.

C. Temperature Dependence of Attenuation

As a final optical test, the temperature dependence of attenuation for all Figure-8 designs was measured through the range of -40°C to +70°C. There was no measurable attenuation change at 1.3 μm or 1.55 μm through links of six concatenated fibers in either cable.

V. Conclusions

Figure-8 fiber optic cables were evaluated in a simulated extreme-case aerial scenario. No attenuation increase was detected even in tests which destroyed state-of-the-art installations. The results of this work are very encouraging for the future of this new concept in fiber optic cable design.

VI. References

1. I. H. Shames, Engineering Mechanics, Vol. 1, pp. 236-242, Prentice-Hall, Inc., 1980.

2. P. Forte, "Cable Stringing Calculations by Computer," International Electrical, Electronics Conference and Exposition, IEEE, 1981.

3. Sumitomo Electric Industries, Ltd., "Technical Report and Design Criteria of Self-Supporting Optical Cable," TR-82124, 1982.

4. U. Oestreich, "Fiber Optic Aerial Cables," Fiber and Integrated Optics, Vol. 4, No. 1, 1982.

5. J. P. Den Hartog, "Transmission Line Vibration Due to Sleet," AIEE Transactions, Vol. 51, 1932.

6. M. Iwazaki, et al., "Theoretical Analysis and Reluctional Countermeasure of Dancing Phenomena on Self-Supporting Cable," 29th International Wire and Cable Symposium, 1980.

7. R. Whapham and S. Abbott, "Spoiling Device Controls Dancing on Overhead Cables," Outside Plant (periodical), Vol. 4, No. 1, January, 1986.

8. J. O'Donnell and R. Whapham, "Galloping Control Device is Evaluated," Transmission Distribution (periodical), March, 1984.

9. E. Hayasaka, et al., "The Clarification of Movement of Non-Metallic Self-Supporting Optical Cable Caused by Wind and the Design of Its Installation at Steel Pylons," 33rd International Wire and Cable Symposium, 1984.

10. A. Portinari and G. Grasso, "Metal Free, Fully Filled Optical Cable for Telecommucations Use," 30th International Wire and Cable Symposium, 1981.

11. Y. Ishihata, et al., "Improvement in Fiber Reliability in Splice Enclosures Resulting in Reduction in Relative Movement between Cable Core and Sheath," 33rd International Wire and Cable Symposium, 1984.

12. Institute of Electrical and Electronics Engineers, National Electrical Safety Code, 1984 edition, IEEE, publishers.

13. E. K. Hall, "Ice and Wind Loading Analysis of Bonneville Power Administration's Transmission Lines and Test Spans," IEEE Power Engineering Society Summer Meeting, July, 1977.

14. D. S. Sunkle, Preformed Line Products Company, Cleveland, Ohio, October 31, 1986, private communication.

15. F. Oestreich, et al., "Fiber Optic Cable for Aerial Application," 29th International Wire and Cable Symposium, 1980.

16. Electric Power Research Institute (EPRI), Transmission Line Reference Book: Wind-Induced Conductor Motion, EPRI, Palo Alto, CA, 1979.



P. Stephen Keith
Sumitomo Electric
Fiber Optics Corp.
78 Alexander Drive
Research Triangle Park,
North Carolina, 27709

P. Stephen Keith graduated from Georgia Institute of Technology in 1968 with a B.S. degree in Physics and later did graduate work in Metallurgy at the same institution. His career has been in the cable industry, previously being involved in materials development and the design and manufacturing of multi-conductor telephone and instrumentation cable. Prior to joining the Design Department of Sumitomo Electric Fiber Optics Corp. in 1986, Mr. Keith was associated with Superior Cable Corp. and National Wire and Cable Corp. He is presently Senior Process Engineer at Sumitomo Electric.



Eric L. Buckland
Sumitomo Electric
Research Triangle, Inc.
78 Alexander Drive
Research Triangle Park,
North Carolina, 27709

Eric L. Buckland was born in 1961. He received the B.S. Degree in Physics from North Carolina State University in 1985. He joined Sumitomo Electric Research Triangle, Inc., in 1985, where he has been engaged in the research and development of optical fibers and cables. Mr. Buckland is a member of the Optical Society of America.



Stanley K. Hovis
Sumitomo Electric
Fiber Optics Corp.
78 Alexander Drive
Research Triangle Park,
North Carolina, 27709

Stanley K. Hovis is a Design-Applications Engineer for Sumitomo Electric Research Triangle, Inc. He graduated from North Carolina State University with a B.S. and M.S. in Materials Engineering in 1983 and 1985, respectively. He has been involved in developing fiber optic cables since joining Sumitomo in 1985.

PRACTICAL EXPERIENCE WITH METAL-FREE SELF-SUPPORTING AERIAL OPTICAL FIBRE CABLE IN HIGH VOLTAGE NETWORKS

A T M Grooten
E J Bresser
A G W M Berkers

NKF KABEL B V
Telecommunication Cable Systems
Waddinxveen
The Netherlands

ABSTRACT

The process of optimizing the construction of a metal-free self-supporting aerial optical fibre cable is described. This is mainly based upon study of requirements and monitoring field installations. Starting with the theory of cable elongation, practical cables are designed. Materials are selected based upon practical experience. Several important production processes of the cable are highlighted.

Results of laboratory tests are presented dealing with mechanical behaviour and electrical stress mechanisms. The cable installation is described and results of 6 years of monitoring field installations are presented. Finally all results are discussed and conclusions on the product application are drawn.

1. INTRODUCTION

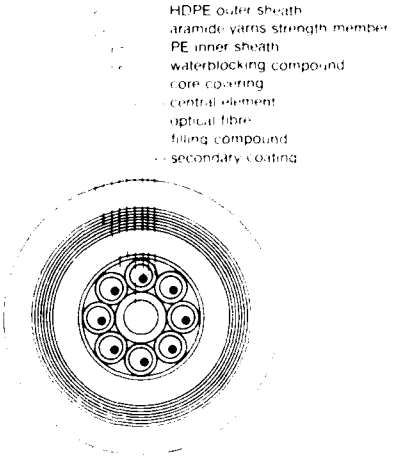
The application of metal-free self-supporting aerial optical fibre cable in high voltage networks has increased substantially during the last few years.
Several cable designs have been developed, utilizing different materials and constructions. This paper describes our theoretical and practical experience to obtain an optimized cable construction with long-term reliability.

In the process of optimizing the cable construction a continuous quality improvement loop was followed:

- Study of theoretical and practical requirements
- Establishment of cable design including the selection of materials
- Production of the cable under stringent process control
- Cable verification tests on laboratory scale
- Monitoring of field installations to gather practical data
- Evaluation of this information which may lead to alterations in the requirements and/or improvements of the cable design.

The cable consists of stranded loose tubes, protected by an inner-sheath, high modulus (HM) aramide yarns as strenght members and a protective high density polyethylene (HDPE) outer-sheath (figure 1).

Metalfree aerial optical fibre cable with 8 fibres



2. CABLE DESIGN

2.1 Theory of cable elongation

During the full life-time of an aerial cable a tensile force will be present in the cable. This tensile force causes a certain cable elongation.
The main feature in the design of optical aerial cables is to control this inevitable cable elongation.

For a given optical aerial cable the actual elongation is the sum of:

1. a constant elongation which depends on the span, the sag, the weight and the mechanical strength of the cable.
2. a variable elongation which depends on the environmental conditions such as wind velocity, ice load and temperature variations.
3. Creep of the strength members, caused by the tensile force in the cable.

The constant elongation (ϵ_C) is derived from the pulling force (F_C) in an aerial cable which can be calculated from:

$$F_C = \frac{L^2 * W_O}{8 * S} \quad (1)$$

This formula is valid only if the sag (S) is very small compared to the span (L) and in the case of equal pole heights. W_O is the weight of the cable per unit of length.
The cable elongation (ϵ_C) follows from:

$$\epsilon_C = \frac{F_C}{AE} = \frac{L^2 * W_O}{AE * 8 * S} \quad (2)$$

The product AE represents the mechanical strength of the aerial cable and is composed of the cross-sectional area (A) and the modulus of elasticity (E) of the strength members of the cable.

Temperature variations (ΔT) change the unloaded cable length with a factor ($\alpha_C \Delta T + 1$). The sag changes and thus the mechanical strain ϵ_C changes to ϵ_T. The resulting strain will be:

$$\epsilon_T = \epsilon_C + \alpha_C \Delta T \quad (3)$$

in which α_C is the thermal coefficient of expansion of the cable. This depends upon the coefficient of expansion and mechanical strength of the various construction elements.

Wind and ice load cause an effective weight-increase of the cable. Ice increases the weight of a cable by:

$$W_i = M_i * g \quad (4)$$

in which W_i = weight of ice per unit of length
M_i = mass of ice per unit of length
g = acceleration of gravity (9.81 m/s²)

Wind causes a transverse pressure (P_W) which can be calculated from the wind velocity (v):

$$P_W = C_W * 0.5 * \rho_a * v^2 \quad (5)$$

ρ_a = specific mass of air (1.23 kg/m³)
C_W = shape factor (= 1.1 for a round cable at common wind velocities)

The wind force per unit of length (F_W) is:

$$F_W = P_W * A_p \quad (6)$$

A_p = the surface area per unit of length

Requirements for both the radial thickness of ice (d_i) and the wind pressure (P_W) are standardised in national and international specifications.
Following the United States standard NESC we have the demands for heavy loading conditions:

d_i = 12.5 mm (0.5 inch)
P_W = 190 N/m² (4 lbs/ft²)

Additionally NESC describes extreme wind loading of tall structures exceeding 18 m (60 ft) up to 1400 N/m² (30 lbs/ft²).

The total resulting force F_t follows from:

$$F_t = \sqrt{F_W^2 + (W_O + W_i)^2} \quad (7)$$

and replaces W_O in formula (1) to calculate the resulting tensile force (F_C) and the total cable elongation ϵ_C taking into account that the sag will increase due to wind pressure or ice loading.

To restrict the cable elongation to an acceptable level we have to apply strength members with a high modulus of elasticity in combination with a low specific mass to keep the cable weight low (formula 2). Nevertheless elongation of aerial cable is inevitable.

One of our basic criteria is, however, to avoid any axial fibre strain for all loading conditions of the cable. This condition will limit the mechanical fibre stress and prevents micro bending caused by physical contact between the fibre and other cable parts. This is especially important when using certain types of single mode fibres with their optimal specification in the 1550 nm region (no cabling).
No axial fibre strain implies that there has to be a free length of fibre in a certain cable elongation window. This length must always be greater than the cable elongation window.

One of the well known possibilities to realize a free cable elongation of ϵ_f is by stranding loose tubes helically with a certain pitch.
The amount of excess fibre length in the tubes, ϵ_R, is another important factor which determines the allowable free cable elongation. This is mainly regulated during the extrusion process of the loose tubes.
Combining these two factors we obtain the expression:

$$\epsilon_f = \epsilon_R - \frac{2\pi}{p} * (r_{nom} - r_{min}) \quad (8)$$

in which r_{nom} and r_{min} are the radius of the fibre spiral in nominal position and when the fibre has reached the inner wall of the tube respectively. By reducing the pitch p we enlarge the maximum allowable cable elongation.
The fibre bending radius present due to the spiral form of the fibre will, however, decrease by reducing the pitch.

This fibre bending radius has to be choosen within bounderies set by both mechanical (bending the fibre induces stress) and optical properties (bending the fibre can cause macro-bending in the 1550 nm region).
The optical aerial cable design is always a harmony of the minimum amount of strength member which determines the maximum practical cable elongation and a minimum bending radius for the fibre which determines the maximum free cable elongation.

2.2 Practical cable design

Based upon the formulae given above a dedicated computer program has been developed to calculate very accurately the number of strength members necessary to meet all the requirements. This enables an optimised cable design to suit the customers demands.

Customer demands may include:
- Maximum cable span
- Maximum sag after installation (normally 2-4%) including a certain minimum clearance
- Maximum wind and ice load according to NESC or other (international) standards
- The number of optical fibres resulting in a certain design for the cable core
- Maximum allowable cable tension. To protect tower constructions against overloading a maximum allowable cable tension may be specified. Limiting the cable tension implies or allowing more sag limiting the cable span to certain values.

Some other data required to perform the calculations are:
- Cable mass. This figure is influenced by the number of aramide yarns itself but is mainly determined by the mass of the cable core including the inner-sheath and the outer-sheath.
- Material properties
- Maximum allowable cable elongation to prevent axial fibre elongation. This results (for a given cable design) in a maximum operating tensile force.

The cable core is standardised at 6, 8 or 12 tubes which each contain 1 or more optical fibres. Either singlemode or multimode fibres can be included in the cable.
The pitch of the lay-up of the loose tubes is choosen depending on the demand for free cable elongation and maximum allowable bending radius of the fibre.

A completely custom-made cable can be designed according to the mechanical demands and the optical characteristics of the customers favourite fibre.

As an example table 1 summarises some important data of three different cable types with 6, 8 and 24 fibres respectively.

Table 1

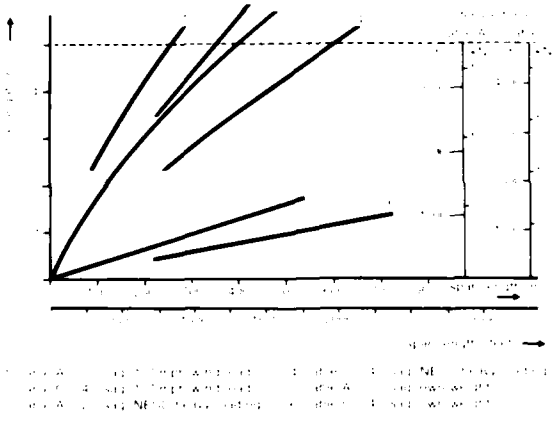
Calculated data for three types of metal-free aerial optical cables

Cable type	A	B	C
Fibre type	MM	MM	SM
Number of fibres	6	8	24
Number of loose tubes	6	8	12
Attenuation at 1300 nm (dB/km)	0.6	0.5	0.4
at 1550 nm (dB/km)	-	-	0.3
Overall cable diameter (mm)	15.0	15.4	17.6
Cable mass (kg/km)	175	191	265
Effective cross section of aramide yarns (mm²)	35	35	45
Span (m/ft)	250/820	450/1500	160/525
Nominal sag (%)	2.5	2	2
Maximum wind pressure (N/m²)	700	500	2340
Every Day Stress (EDS) nominal load (kN)	2.2	4.1	4.4
Maximum Operating Stress (MOS) (kN)	9.5	14.5	20.4
Maximum Allowable Stress (MAS) (kN)	15.0	14.5	20.4
Ultimate Tensile Stress (UTS) breaking load (kN)	62.6	58	60
Cable elongation at maximum operating stress (%)	1.5	0.5	0.45
Axial fibre strain at maximum operating stress (%)	none	none	none

The difference between the free cable elongation and the cable elongation at maximum load has to be at least 0.2%, taking into account the long-term creep of the aramide yarns, the variation in excess fibre length in the loose tube and the initial cable elongation.

Figure 2 gives the cable elongation and cable tension as a function of span and sag for two types of aerial cable. Depending upon the sag spans upto 600 m (2000 ft) can be reached for these particular cables.

Example of tensile force diagram as a function of cable span and cable sag



3. MATERIAL SELECTION

The selection of materials has been performed on the basis of two main criteria:

a. Technical performance

b. Long term stability and aging resistance

3.1 Technical performance of materials

3.2.1 Choise of strength members

The effective elasticity modulus of high strength glass filaments bonded in hot curing resins (FRP) is about 50 kN/mm². The specific mass is about 2000 kg/m³. The stiffness and the complete lack of relaxation of such elements permanently maintains bending and torsion stresses and makes this material sensitive to fatigue. Depending upon the type of glass filaments (E-, R-and S-glass) these materials are varyingly sensitive to attack by acid rain.

For aramide yarn filaments the elasticity modulus is 100 kN/mm² and the specific mass is only 1450 kg/m³.
Compared with the FRP strength member, the cable elongation, weight and diameter will be reduced by using aramide yarns. We only have to compress and pre-stress the aramide yarns to obtain a flexible load bearing element combining highest possible strength with smallest possible fatigue and resitance to acid rain.

3.1.2 Behaviour of materials at high and low temperatures

Aerial cables are exposed to much more extreme temperature variations than any other cable type.
Looking at the direct influence of temperature variations to the materials characteristics we summarize as follows:

element	-45 °C (-49 °F)	+85 °C (+185 °F)
1 fibre	·	·
2 central element	·	·
3 aquagel tube filling	·	·
4 tube material	·	·
5 core filling	· ·	· ·
6 inner-sheath PE	·	·
7 aramide yarns	·	·
8 outer-sheath HDPE	·	·

Ad 1: Attenuation increase of the bare fibre (independent of cable design) at -45 °C: 0.05 dB/km at 1300 nm.

Ad 3: Commonly used gel has a too high viscosity below -30 °C. Below this temperature other (known) compounds are used.

Ad 5: This material has a drop-point of up to 120 °C (250 °F).

3.1.3 Temperature variations and cable expansion/contraction

An installed aerial optical cable encounters temperature variations of about 100 °C. Thanks to the low thermal coefficient of expansion of aramide yarns in combination with the high modulus of elasticity (table 2) the cable expansion will be dominated by the aramide and thus be very low.
A completely different situation exists during low temperature storage on drum. The aramide yarns cannot absorb any axial compression forces. The fibre reinforced plastic (FRP) central strength member acts as thermal splint.

Table 2

Thermal coefficient of expansion (α_t) and modulus of elasticity (ϵ_t) of cable elements

cable element	material	thermal coefficient of expansion (10^{-6} K^{-1})	modulus of elasticity (kN/mm²)
central strength member	FRP	5.0	50 (25 at compression)
stranded tubes	Polyester	80	1.4
inner sheath	PE	150	0.45
strength members	aramide yarns	-2.0	100
outer-sheath	HDPE	150	0.6

We can calculate the thermal coefficient of expansion of the cable (α_c) from

$$\alpha_c = \frac{\sum \alpha_i E_i A_i}{\sum E_i A_i} \qquad (9)$$

Every cable type has a different thermal coefficient of expansion because the surface areas are different
For cable type A (table 1) we get

in the case of installed cable (tension on aramide yarns)
α_c 0.68 * 10^{-6} K^{-1} (high and low temperature after installation)

in the case of cable stored on drum

α_c 62 * 10^{-6} K^{-1} (low temperature storage)

After installation the cable elongation and contraction due to temperature variations from -30° C to -70° C will be 0.007%
During storage on drum cooling down to -40° C will give 0.37% contraction

Formula (9) is valid only if the differences in the thermal coefficient of expansion of the cable and the components will not result in any shifting between the layers. The static coefficient of friction within a length of cable has to be larger than the force arising from the differences in expansion.

During storage on drum and cooling from 20° C to -40° C the minimum friction stress between the loose tubes and the central element (calculated for a 10 m cable length) has to be at least 8.6 * 10^{-3} N/mm^2 to prevent shifting
Practical values are in the order of 50 * 10^{-3} N/mm^2.

After cable installation the minimum friction stress between the aramide yarns and the outer-sheath for a 10 m length has to be 3.0 * 10^{-3} N/mm^2. This is much lower than the practical values for this friction stress.

3.2 Long term stability of materials

3.2.1 Determination of the maximum allowable fibre stress level

The life-time of an optical fibre is determined by the stress level in the fibre and the amount of moisture (relative humidity) present at the surface of the fibre (fig. 3).
Obviously the metal-free aerial cable does not contain a metallic moisture barrier.

Life-time of optical fibres as a function of the mechanical load and the relative humidity (R.H.)

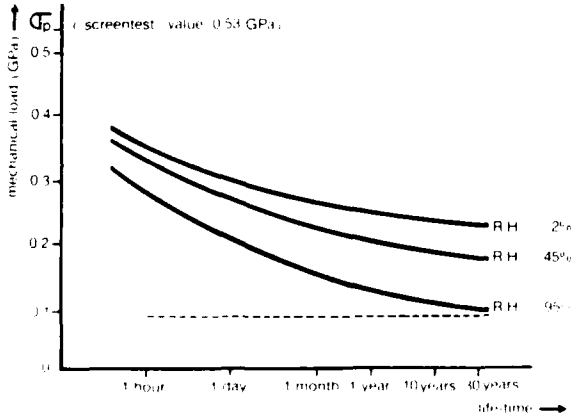


Fig. 3

Therefore we assume that a relative humidity of about 95% can occur in the cable core although the HDPE outer-sheath has a very low water permeability and the loose tubes and the interstices are completely filled with jelly compound.
Thus in order to ensure a long working life-time measures must be taken to minimize fibre stress.
This is achieved with stranded loose tubes which results in a certain free cable elongation (cable elongation without fibre elongation). By stranding the loosely buffered fibres, the fibre is bent with a certain radius which does stress the fibre surface.

To prevent inadmissible stresses the bending radius of the optical fibre has to be never less than 58 mm.

With this criterion fibre stress is limited to 0.077 GPa.
This is the limit necessary to obtain a 30 year life expactancy of the fibre.
Due to optical requirements in the 1550 nm region this bending radius will be larger in most practical applications.

3.2.2 Long term mechanical properties of twisted aramide yarns

Creep properties
From literature (7,8) it is known that the maximum creep strain of HM aramide yarns at a constant loading of 50% of the ultimate tensile strength (UTS) is 0.11% during a life-time of 30 years. Practical values of the every day stress (EDS) are only about 5% of UTS.

Time to failure
The time to breakage of aramide yarns depends upon loading. By keeping the static loading below 50% of UTS a life expectancy of about 100 years can be reached. In aerial optical cables the loading will always be dynamic, for which reason a value below 1.3 of UTS, below 1.3 of elongation at breakage is chosen as the maximum working stress.

UV aging
The high strength and weather resistant HDPE outer-sheath protects the aramide yarns from direct sunlight, specifically from UV-radiation.

3.2.3 Outer-sheath material

The outer-sheath material has to be resistant against wheathering, UV radiation, acid rain and the influence of electric fields. We have selected a black weather resistant HDPE compound according to ASTM D 1248 Grade W8 combining important features:

- High mechanical strength (tensile strength about 20 N/mm^2 (2800 psi)). Spirals used for installation purposes are clamped directly over the outer-sheath and transfer all the cable tension. The high strength of the sheath guarantees excellent performance of the cable when exposed to extreme loading conditions.
- Very low water permeability.
- Carbon black content to protect against material aging caused by UV radiation.
- High thermal stress cracking resistance to protect against thermo-oxidative attack.
- Resistance against corona and tracking.

Other outer-sheath materials like some specially developed compounds with lower surface resistance to increase the tracking prevention were not selected, as they do not satisfy the requirements of ASTM D 1248 Grade W8 concerning the mechanical strength (the tensile strength of these compounds is about 10 N/mm^2 (1500 psi)).

4. CABLE PRODUCTION

To reach good mechanical and optical characteristics all production processes must be controlled very carefully. The main processes are:

- Extrusion of the loose tube with controlled fibre excess length mainly to achieve the desired free cable elongation (formula 8) and to prevent undesirable microbending phenomena in the 1550 nm region.

- Stranding the tubes with an accurately designed pitch. To prevent macrobending the tubes must be stranded in accordance with the limitations of the fibre design (matched cladding type or depressed cladding type).

- Filling the interstices with a high drop-point jelly compound to obtain longitudinal watertightness.
This requires specialized equipment in which the pressure of the jelly compound can be controlled.

- Extrusion of the inner-sheath to protect the cable core.

- Stranding of the aramide yarns with accurate tension control, thus reducing the initial elongation of the cable. No pre-stressing during cable installation is necessary.

- Extrusion of the HDPE outer-sheath with an accurate and continuous diameter control to properly fit the dead-end spirals.

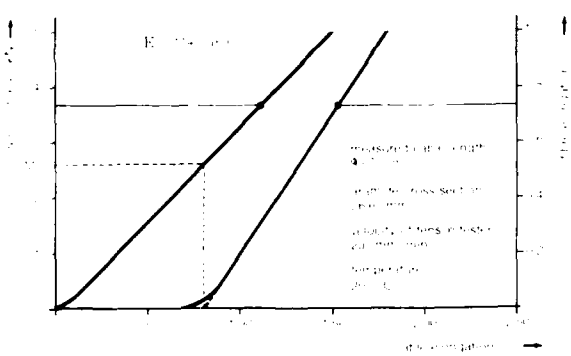
5. MECHANICAL LABORATORY TESTS

In addition to tests for the transmission characteristics of the optical fibre the metal-free self supporting optical fibre cable is subjected to a number of mechanical tests according to IEC 794-1. Tests are performed on cable B (table 1).

5.1 Tensile performance (IEC 794-1-E1)

The cable is fixed by means of the same dead end spirals used for field installation. The maximum tensile force applied to the cable was 50 kN. No cable break occured at this force.
Fig. 4 shows the stress strain curve of the cable. The initial elongation is very low because the aramide yarns are pre-stressed during production.

Tensile test (cable B)



The modulus of elasticity of the cable is defined as

$$E_{cable} = \frac{\sum E_i A_i}{A_{aramide}} \qquad (10)$$

E_i and A_i being the modulus of elasticity and the cross sectional area respectively of a cable element.
$A_{aramide}$ is the cross section of the aramide yarns.
The modulus of elasticity of the cable amounts to 115 kN mm^{-2} giving a safety margin of the aramide yarns (100 kN mm^{-2}) as used during cable design.

An optical propagation time measurement is used to determine the fibre elongation as a function of the cable elongation. The tensile force at the beginning of fibre elongation is the MAS (Maximum Allowable Stress) and amounts to 25 kN.
The Ultimate Tensile Strength (UTS) was determined in a separate experiment. The cable breaking load is 62.6 kN.
The spirals used to apply tension to the cable prevented any significant cable shifting up to the cable breakage which did occur in the middle of the cable sample between the two spirals (photo 1).

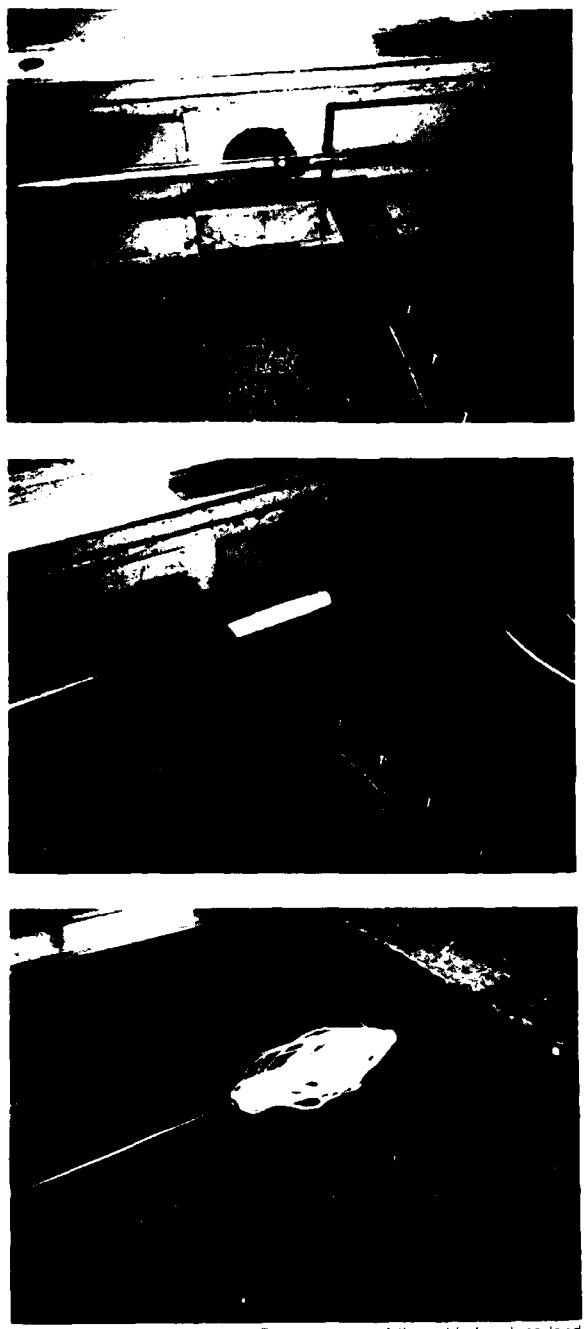
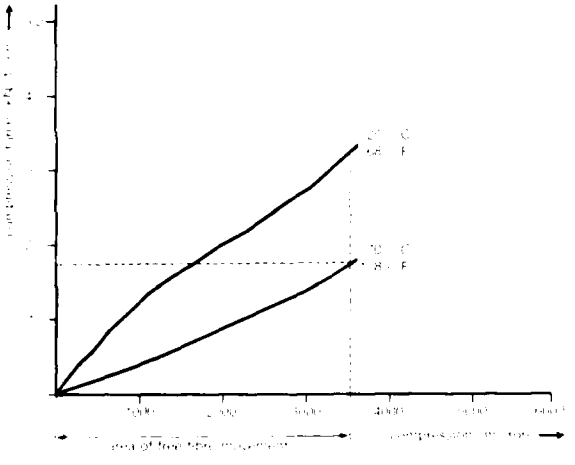


photo 1 Determination of the cable breaking load

5.2 Crush resistance (IEC 794-1-E 3)

Fig. 5 shows the compression force as a function of the cable compression measured at 20 °C (70 °C) and 70 °C (160 °F) (not specified by IEC). The cable compression at which the fibres no longer can move freely amounts to 3.5 mm. Even at 70 °C a compression force of 18 kN/m can be sustained before reaching this point.

Compression force as a function of the cable compression



5.3 Impact resistance (IEC 794-1-E4)

E[illegible] impacts at -55 °C (-67 °F) with a impact momentum of 21 Nm cause no damage to cable nor to individual fibres. The radius at the point of the hammer is 1.5 mm (0.059 inch).

5.4 Bending (IEC 794-1-E6)

After 250 repeated bends with a bending radius of 10 x D (D = cable diameter) no defects on any cable element including the optical fibres [illegible]

5.5 Temperature cycling (IEC 794-1-E6)

To simulate practical conditions a temperature cycle test was performed on a 12 m sample loaded in the tensile test machine with a constant 1 kN force. The fibres are spliced together to make a single loop and the ends are fitted to an optical power meter. With the aid of a double walled tube surrounding the cable, measurements are performed at [illegible] (-40 °F) hot water (+55 °C / 22 °F) a mixture of ethanol and [illegible]

The results of the measurements [illegible]

$\Delta\alpha$ [illegible] °C [illegible] dB/km
$\Delta\alpha$ [illegible] °C [illegible] dB/km

5.6 Water penetration (IEC 794-1-F5)

After pre-stressing the complete cable with a tensile force of 12.5 kN during 5 minutes the sample is tested without stress during 90 hours according to the "sheath gap" method. A head of water of 1 meter (3 ft) is applied to a circumferential sheath gap of 25 mm (1 inch) (less than 5 cm (2 inch) except close water penetration in the cable was observed.

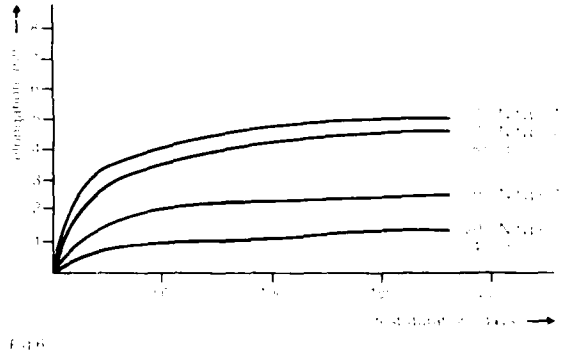
5.7 Cable creep after installation

In a specially developed test equipment (photo 2) creep was measured with hours after installation of the cable with dead-end spirals. Two nominal stress levels were examined and two types of dead-end spirals. Test duration was 200 days. Results (fig. 6) show that the worst case creep is very limited (about 5 mm) and can be neglected with respect to an installation span of several hundreds of meters.



photo 2: Creep test equipment

Initial elongation after installation with dead-end spirals as a function of cable tension and type of dead-end spiral

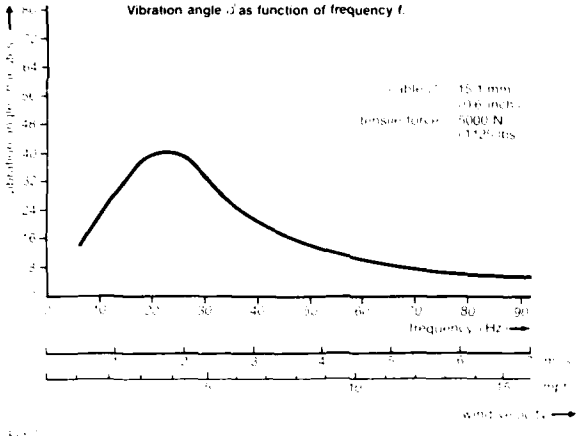


5.8 Vibration characteristics

Two important features of the [illegible] are best measured in specialized laboratories.

Self-damping of the cable

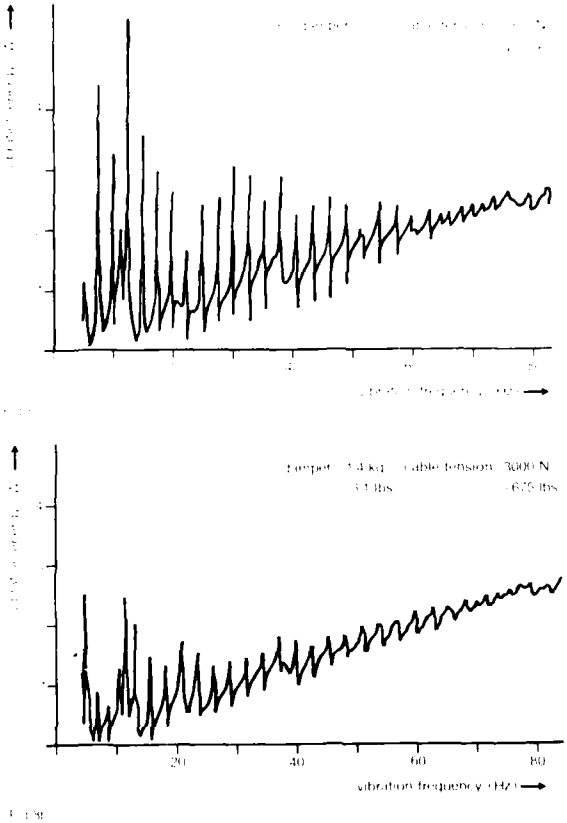
These measurements are carried out according to the CIGRE / IEEE Guide on conductor self-damping measurement at different tensile forces and frequencies. At a tensile force of 5000 N the vibration angle β (see section 8.2) reaches a maximum value of 40 minutes at a frequency of 20 Hz (fig. 7). This will in no way damage the cable. The good self-damping properties of the cable in almost the entire frequency range are caused by the internal friction of the flexible aramide yarns damping most of the friction energy very quickly.



Damping of the cable with the use of dampers

The remaining vibration amplitudes in the low frequency range (10- 30 Hz) can be damped further by the application of dampers with a weight of 1.5 - 3 kg (fig. 8).

Cable vibration energy as a function of frequency, with and without damping



5.9 *Resistance to shot-gun damage*

Damage of aerial cables caused by shot-guns is unfortunately in some areas a frequently occurring phenomenon.

A series of tests have been performed with different diameters of pellet of shot from various distances.
The several layers of aramide yarns designed to control heavy loading conditions also protect the cable against penetration of shot to the cable core. As well known, aramide yarns are often used in bullet-proof vests.

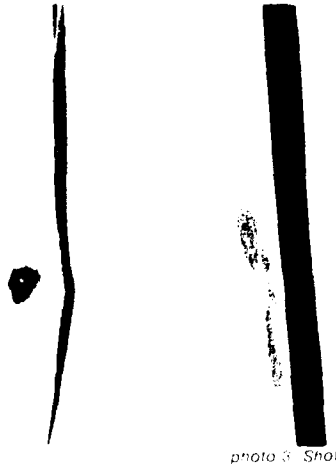


photo 3: Shot-gun damage

Test details	
Type of gun	Beaumont shot-gun, caliber 16
Pellet diameter	shot 5: 3.00 mm lead (0.118 inch) shot 6: 2.75 mm lead (0.108 inch) shot 7: 2.50 mm lead (0.0098 inch)
Firing range	15, 20 and 25 m (50, 65 and 80 feet)
Results	At *short range, shot of all diameters will pierce* the outer-sheath, but will not get through the inner-sheath (photo 3). It leaves only an impression on the inner-sheath. The aramide yarns catch the shot without breakage. The tensile performance of the cable did not change. Tests revealed that water penetration in the layer of aramide yarns between inner-sheath and outer-sheath through the holes in the outer-sheath is very limited due to the hydrophobic nature of the aramide yarns.

6. ELECTRICAL STRESS MECHANISMS

6.1 Theory

Electrical stress mechanisms (ref. 6) contribute to the aging of the outer-sheath of the optical fibre cable. The two contributing mechanisms are:

- corona: partial discharges in a non-uniform electric field, often luminous and audible
- tracking: the process that produces more or less conducting paths of localized deterioration as a result of the action of electric discharges on or close to the insulation surface.

The cable is grounded at the suspension towers. In the middle of the span the cable is charged by capacitive coupling.
Because of the charging, the cable will have a potential that depends on the phase voltage and the position of the cable between the phase-lines and earth. Since the electrical resistivity of the cable is high, the capacitively coupled voltage will also be present near the spiral ends at the towers. The resulting electric field strength at the spiral ends can cause corona. When the cable is polluted and wet, a current will flow from the middle of the span to the tower. At a point of higher current

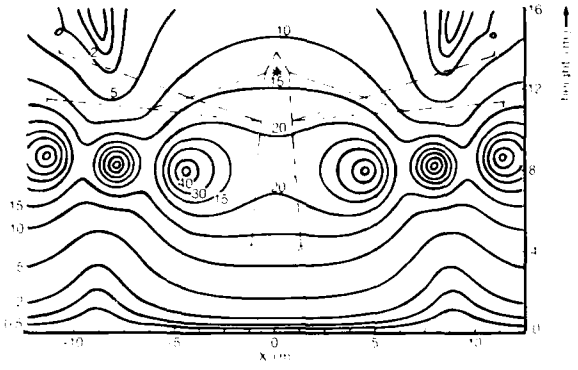
density the moisture will avaporate and cause a discharge This happens because almost the entire capacitively coupled voltage is now across the gap in the conducting (moisture) layer
This process can be continuous in some weather conditions and causes tracking Both mechanisms, tracking and corona, are strongly influenced by the electric field configuration

6.2 Calculations

A computer model bas been developed to calculate the radial and axial electric field strengths From this model it is possible to determine the optimum suspension position of the cable

The influence of cable parameters on the axial field (along the cable surface) is analysed The results show that when no special measures are taken, considerable voltage jumps may occur across interruptions of the (semi-conductive) cable surface that results from pollution and wetting
Figure 9 shows the potential distribution in the field of a 150 kV network between two towers The cable is suspended in the position marked with an asterisk (*) The figure shows that the cable potential is about 13% of the phase ground voltage i e 11 kV

Equipotential lines indicated as a percentage of the phase-ground voltage



U = 150 kV 86.6 kV phase-ground
$D_{phase\ wire}$ = 36.1 mm (1.42 inch)
$D_{ground\text{-}wire}$ = 11.7 mm (0.46 inch)

phase distribution C B A A B C

Fig. 9

6.3 Measurements

The longitudinal resistivity of the cable is the most important cable parameter Calculations show an optimal resistivity of about $10^{7} - 10^{8}$ Ω m
Material property measurements were performed on HDPE and on an Al(OH)$_3$ filled copolymer A surface resistivity of 4×10^{13} Ω for HDPE and 1×10^{9} Ω for the filled copolymer was measured
Tracking resistance was measured according to IEC 112 Both materials withstood the test three times at the maximum level of 600V (Qualification CTI 600 M) The filled copolymer does however not fulfil the requirements of ASTM D 1248 grade W8 for outdoor cable-sheath materials regarding tensile strength and elongation at break For that reason, and because the resistivity is not low enough, the material was rejected and HDPE was chosen as outer-sheath material

A laboratory set up was built in a specialized laboratory to simulate the electrical conditions in a HV circuit In this set up corona was observed using partial discharge detection techniques at a dry and clean cable *The corona activity was eliminated by shielding the suspension spirals* with toroids With corona eliminated, tracking was observed when the cable was wet with a salty solution
No damage of the sheath material was noticed at any experiment

6.4 Results

Potential plots and experiments show that the choice of an optimum suspension *position results in a considerable* decrease of corona and tracking activity Corona may be eliminated by shielding the suspension spiral ends The amount of tracking may be reduced by using a cable sheath with higher conductivity Usually this results in a lower tracking resistance
It is important that alternative cable sheath constructions have to fulfil the mechanical requirements Insulated suspension is also advantageous with regard to corona and tracking reduction but problems may arise when the cable runs through the tower body

6.5 Electrical failure mechanisms

Electrical failure mechanisms also may have an influence on the cable
1 When the cable is non-conducting (dry) and touches a phase wire the resulting current is very small and therefore harmless A wet (conducting) cable touching a phase wire carries in the first instance a high current which evaporates the moisture quickly resulting in a moment of high tracking activity

2 Impulse voltages on the earth and phase wires (originating from lightning or short circuits) contain components of higher frequencies which lead to a somewhet stronger capacitive coupling between wires and cable

7. INSTALLATION

7.1 Engineering

The installation techniques and the applied equipment for metal-free aerial cables correspond to the generally employed methods for overhead lines
Since the cable is self-supporting, the cable must be positioned in such a way that 'free space' within the tower configuration is guaranteed for all loading conditions
Because of its low eight (generally 175 - 200 kg/km 625 - 700 lbs/mile) the cable shows a tendency to drift with the wind
The preferred cable position to achieve ease of installation is underneath the phase conductors This position is, however, very often in conflict with the requirements for minimum ground clearance
Esthetics within the power line configuration require often an equal sag for all conductors
In practice the cable is strung between or above the phase conductors depending on the power profile
The proper 'free space' is assured by adjustment of the sag (not necessarily completely equal to the conductor sag)
Proper establishment of the cable sag is a prime concern of the customer
By adjusting of the sag, different loading for the towers can be obtained In general the additional load to the tower construction is a small percentage (less than 5%) of the basic load
Computer calculations of the temperature dependent sag and tension values for each span result in a proper positioning of the cable

7.2 Armatures

Fittings commonly in use with the electric power utilities will have the preference above other newly developed hardware For that reason we adopted suspension and dead-end spirals for installation purposes (photo 4) Slippage of the sheath through the spirals is undesirable therefore the spirals must be carefully dimensioned in agreement with the cable diameter
Standard spirals have been adapted and tested to take up all cable tensions without slippage up till cable breakage (UTS) Suitable equipment is available on the market



photo 4 Spirals for installation purpose

7.3 Installation of the cable

Once having established the mounting positions for the cable, all towers and yokes must be provided with the necessary mounting arrangements



photo 5 Cable installation

These arrangements include mounting points for supporting spirals and dead-end spirals in the towers, installation of pulleys and provisions in sub-stations for dead-ending the cable.
Next, the cable installation can take place with or without a pulling rope (photo 5). There is no need to pre-stress the cable. For a cable lenght of 4.2 km (2.6 miles) a winch handles the pulling forces which will not exceed the 4400 N (1000 lbs) level. Shorter cable lengths of 2.1 km (1.3 miles) have been installed using manpower only by walking with the cable from tower to tower.
Installation times of 1.5 km (1 mile) per day (all preparations included) have been achieved easily with a crew of 3 to 4 men.
De-energizing the power system to install the MFSS cable is not necessary. Especially for spurroutes where outages can be critical MFSS cable offers advantages.

7.4 Splicing

Fibre splicing has to be carried out after a cable has been terminated at an end tower. To avoid break-neck activities with expensive equipment the cable is brought downwards to splice the fibres at ground-level. Afterwards the splice housing is fixed within the tower at an appropriate level.

Normally, terminating towards an equipment room often leads to the implementation of short lengths of direct buried cable types, implicating extra joint boxes, extra cable stock and extra system attenuation. However, the metal free cable can also be used as a directly through-going cable and eliminates these disadvantages.
Local diggers and omnipresent gnawing rodents can be dealt with by pulling the cable into a protective metal or plastic pipe.

8. FIELD EXPERIENCE

8.1 General

Laboratory research on the metal-free aerial cable with aramide yarns as a strength member started in 1979. The first field trial was installed in 1981 (lit. 1) in a 150 kV network near the North Sea mainly to test the influence of wind loading, salt deposit and electrical aging. After inspection in January 1987 which revealed no sign of any attack, the cable was shifted to the 380 kV network. To test ice loading and galloping a special test sample was installed in 1983 in the northern part of the Netherlands, which survived an extreme ice loading of 23 mm (0.9 inch) without any damage in march 1987.

In 1985 a cable section of about 9 km was installed in the 150 kV network in the southern part of the Netherlands (Cable type A from table 1). In this trial section information is being gathered regarding telecommunication by the electric power utility and by monitoring cable behaviour. Commercial projects are being carried out both in the Netherlands and in the USA. A large electric power company in the USA is installing after a previous successful field trial a commercial 24 fibre connection of 2.5 km in the 345 kV network (Cable type C from table 1).

8.2 Wind excited vibrations

Wind excited transversal periodic cable movements can be divided into three types:

a. Vibrations in a part of the span with a typical frequency of 1 - 3 Hz generated by parallel cables where aerodynamic coupling takes place.

b. Galloping is a high amplitude but low frequency (up to 11 Hz) phenomenon. The energy content is low, so generally no damage due to fatigue is expected. Parallel cables, however, can touch each other.

c. Resonance vibrations or aeolian vibrations with smaller wavelengths and typical frequency 5 - 150 Hz. Wind velocities which evoke this kind of vibrations are in the range of 0.5 - 10 m/s when air flow is still laminar. This type of vibration can be dangerous because of the high energy content and the frequent occurrence. All our measurements are related to this type of vibrations.

The frequency of vibration (f_W) can be calculated from the wind velocity (V_W) and the cable diameter (D) according to Strouhals formula

$$f_W = 0.2 * V_W / D \qquad (11)$$

D = 15.1 mm, V_W = 10 m/s, so f_W = 133 Hz

The resonant frequency f_n and the wave speed C_W have been calculated. For the monitoring section (cable A) we find

T = 1900 N
m = 0.175 kg/m
L = 250 m
C_W = 104 m/s

leading to: $f_n = n * 0.21$ Hz

At almost every wind speed a vibration can be caused. In practice a limited frequency range will occur due to self-damping of the cable as was proven by laboratory experiments and anti-damping. The wavelength λ can be calculated from:

$$\lambda = 2 * L / n \qquad (12)$$

The vibration angle $\beta = 2\pi y_0 / \lambda$ in which y_0 is the amplitude of the vibration.
The allowable vibration angle for an aluminium/steel conductor lies in the order of magnitude of 10 minutes. For metal free aerial cables there are no practical limits to β. To prevent secondary damage to towers and additional hardware the same limit for β has been taken during the evaluation of field vibration measurements.

Field vibration measurements

Vibrations were measured with accelerometer test equipment together with wind speed and wind direction monitors to check if Strouhals formula would hold under field conditions.
Vibrations were measured in the frequency range of 1 to 150 Hz with very small amplitudes (several tenths of a millimeter). The measured frequency values and the calculated values from wind speeds (above about 10 m/s) concur very well.
In another experiment the frequency and amplitude of the cable vibrations were measured without physical contact using a camera with telescopic lens. Vibrations were measured in the frequency range 10 - 35 Hz with amplitudes of several centimeters. The wind speed was only 3.4 - 5.2 m/s. The vibration angle was below the limit of 10 (fig. 10). Nevertheless the use of dampers will limit the amplitudes further to prevent possible secondary damage to towers, constructions and associated hardware like the suspension grips.

Diagram with amplitudes of vibration as a function of frequency

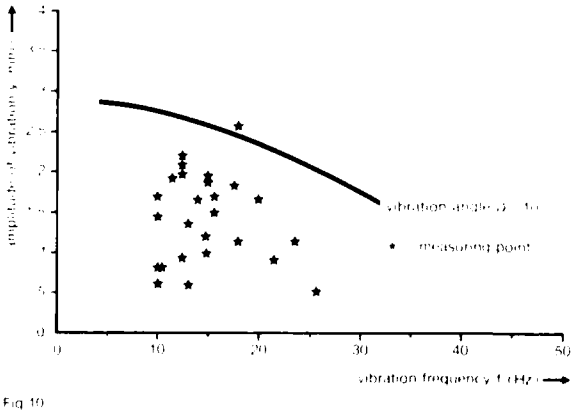
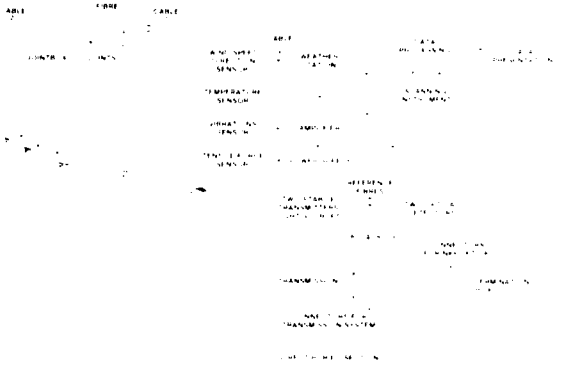


Fig. 10

8.3 Field monitoring

Fig. 11 gives an overview of the installed systems over the optical cable section (cable A).
A 2 Mbit/s optical transmission system has been connected as no. two fibres (indicated with 1 and 2). Six out of the thirty available channels are used for communication (voice, data and telemetry). The four other fibres are spliced two by two, half way in the section, thus creating a loop. The changes in the optical attenuation of the original two circuits are continuously measured with highly stable multi-port power meters.

Measuring set-up optical fibre aerial cable link



In the control tower recording instruments are installed to measure cable tension, vibrations, temperature, wind velocity and direction. All measured data are fed into a microcomputer which processes and stores this data.

The acquired monitoring experience covers a period of 2 years. No change of attenuation as a function of cable tension occurred during this period. To check the results of the monitoring, power meters for the evaluation of the total section (94.7 km) were mounted, both at the insertion loss method directly after installation and after 12 months. No significant changes were noticed.

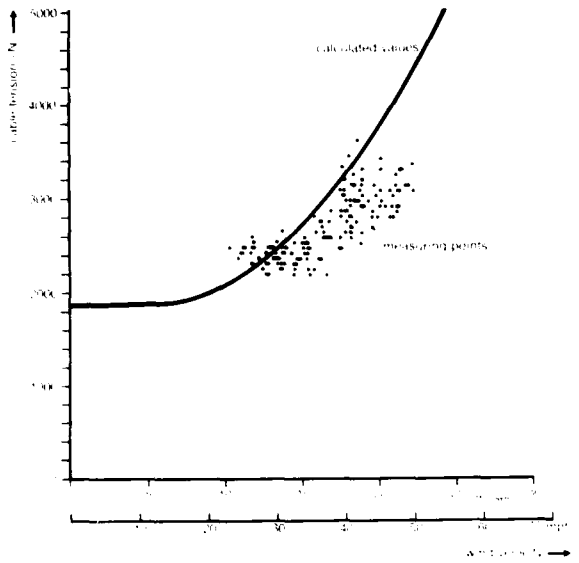
Table 3. Attenuation of total fibre section at various measuring times

measuring time	$(\alpha_{1300}$ dB) average of fibres 1 and 2
directly after installation	6.37
after 12 months	6.29

As expected, the cable tension increased with increasing wind velocity (fig. 12). The nominal tension is 1900 N, the maximum tension during this period was 5 kN. The points in the figure are measurement points of the cable tension and the corresponding component of the wind velocity perpendicular to the cable span.

The plotted line gives the calculated values of the cable tension as a function of wind velocity according to formula (9). Nearly all measurements give lower values for the cable tension than the calculated values, mainly because wind velocities will not be constant for the full cable span. This implies that an extra safety margin between theoretical design and practical application exists.
Cable tension monitoring during these 2 years showed no measurable alteration in the EDS value of the cable. This implies that no creep of the cable sheath, dead-end spiral combination occurred.

Diagram with cable tension as a function of wind velocity



8.4 Practical experiences with electrical aging mechanisms.

In September 1981 a test cable was installed in a 380 kV circuit (operated at 150 kV) in which the cable potential is about 11 kV. The circuit is situated in a coastal environment. The cable sheath was examined in January 1987. There were no signs of deterioration.

Cable A (table 1) was installed August 1985 in a 150 kV circuit resulting in a cable potential of 11 kV and checked in November 1986. Also on the sheath of this cable no signs of deterioration were found.

CONCLUSIONS

Excellent experience with the metal-free aerial optical cable is gathered during the last 8 years.
With the aid of a dedicated computer programme completely custom made cables can be designed which contain the minimum amount of aramide yarn strength member. Depending upon the sag, spans of 600 m (2000 ft) and more can be reached. Single mode fibres (with an optical specification in the 1550 nm region) as well as multimode fibres can be included in the cable.
Selection of materials has been performed on the basis of technical performance and long-term stability leading to the application of HM aramide yarns as strength member and HDPE as outer-sheath material.

Laboratory measurements showed that cable characteristics are at least equal to the values used during cable design, provided that the cable production is controlled very carefully.
Electrical stress mechanisms like corona and tracking do not influence the life-expectancy of the cable.
Installation techniques guarantee easy and quick cable installation without de-energizing the power system if necessary.
Monitoring of field installations since 1981 shows no changes of any cable property. This applies to both the optical and the mechanical cable characteristics as well to the material properties. Long-span metal-free aerial optical cables have proven there practical reliability completely.

Acknowledgements

The authors wish to acknowledge the support of many people and organisations.
Electric power utilities and material suppliers gave their permission to publish practical data and co-operated at the realization of pilot projects. Many persons in our own organization contributed to the accomplishment of this paper.

REFERENCES

1 O R Bresser. Experiences with a metal-free aerial cable design for long span application. Global Telecom Conf. '85. San Diego USA 1983.

2 E J Bresser. Metal-free fibre optic cable in power supply networks. FODC 85. Ljubljana Yugoslavia.

3 O R Bresser et al. 'On the predicted life-time of optical fibre telecommunication cables'. Trends in Telecommunications Volume 2 No 1. 1986.

4 J Th van Eck. Metal-free Fibre Optic Cable in Power Supply Networks. Int. seminar on telecom and electronics. Jakarta Indonesia. 1986.

5 J Th van Eck. Optische kabelsystemen. Elektrotechniek **65** (1987) 4.

6 A G W M Berkers. Electrical stresses on a self-supporting metal-free optical fibre cable in high voltage networks. Eindhoven University of Technology. april 1987.

7 'Creep and stress-rupture of kevlar ropes'. Technical Documentation kevlar 29 - kevlar 49 aramid fibres.

8 Twaron - Technical documentation engineering with fibres. Enka Industrial fibres. 1985.



Albert T M Grooten was born in 1952 He holds a Materials Engineering degree of Delft University of Technology (The Netherlands) He joined NKF Kabel B V in 1978 worked in the Research and Development department and is currently Marketing engineer for optical fibre cable applications He is a member of the CCITT Study Group VI



Erik J Bresser graduated from Eindhoven University of Technology (The Netherlands) with a degree in High Voltage Engineering He joined NKF Kabel B V in 1983 as marketing engineer for fibre optic cables and is currently account manager for (Electricity Power) Utilities



Arnie G W M Berkers was born in 1960 in the Netherlands He obtained a degree in Electrical Engineering of Eindhoven University of Technology and joined NKF Kabel B V in 1987 He is a member of the cable development group His main concern is the development of optical fibre cables for high voltage networks

PRE-STRANDED SELF SUPPORTING AERIAL CABLE DESIGN

David Wong and Sandy Lyons

Siecor Corporation
489 Siecor Park
Hickory, NC

Abstract

The replacement of the traditional lashing of fiber optic cable to steel wire messengers has been studied. The suggested alternative is to utilize a self-supporting cable that incorporates light weight Aramid rovings. Siecor, in conjuction with United Ropeworks, Inc. has evaluated a system that combines a dielectric fiber optic cable with a 100% Kevlar messenger for aerial span applications.

Background

As the need for a low cost self-supporting aerial cables is becoming more evident, a study is being conducted to evaluate the feasibility of designs other than the self-supporting figure-8 or self-supporting concentric design.

Fiber optic self-supporting aerial cable designs are not new. In fact two basic designs have been available for several years. Those designs are the figure-8 and the concentric. The figure-8 consists of a fiber optic cable bonded or clipped to a messenger. Most concentric cable designs are basically standard aerial cable constructions with higher tensile strength ratings. Each of these designs is capable of satisfying a few of the requirements demanded of a self-supporting cable but neither the figure-8 nor the concentric design satisfies the compilation of technical and commercial needs inherent in an aerial application.

The primary requirements that must be satisfied by a self-supporting aerial cable are as follows:

1. Flexibility of fiber counts up to 192 fibers.
2. Loose tube cable design.
3. Fully specified for -40 to +70 C operation as well as worst case ice and wind loading.
4. All dielectric.
5. Maintain optical integrity in a strain-free state throughout specified operating conditions.
6. Allow for a simplified and more economical method of installation.

With a figure-8 cable, the fiber cable is bonded or clipped to the messenger and strain may be coupled from the messenger to the cabled fibers during manufacturing, installation, or under load. The standard fiberglass reinforced plastic messenger material makes for a stiff cable that is difficult to work with.

In regard to concentric cables, the standard design consists of multiple buffer tubes stranded around a central member with an increased cross-sectional tensile rating. When hardware is applied to a concentric, it must wrap around the cable and may create compressive problems with the fibers. If compression is not uniform, the buffer tubes may shift. Another concern with a concentric design is vibration. These cables are subject to both galloping and aeolian vibration.

In order to overcome the shortcomings of these designs and meet the primary requirements of a self-supporting aerial cable, Siecor and United Ropeworks have developed a pre-stranded self-supporting aerial cable. The pre-stranded design eliminates the negative aspects of previous designs while providing the desired benefits. The cable is constructed by helically wrapping a fiber optic cable around a polyethylene jacketed Kevlar messenger. There is no physical bonding between the two as with the figure-8 and it is a torque balanced system. The system is designed so that the messenger takes the tensioning during installation as well as under worst case loadings. Thus, the fibers remain in a virtually strain-free state throughout operation. Also, the helical design makes the cable very aerodynamically stable. It is self-dampening, reducing galloping and aeolian vibration. The hardware is designed to attach to the messenger without putting compressive forces on the fiber optic cable. The system is capable of containing up to 192 fibers, is loose tube, is all-dielectric, is fully specified for operation over the required temperature range, and simple and economic to install.

Construction & Tensile Test

The Siecor cable was stranded around a Phillystran messenger in a production facility and tested for messenger strain, fiber strain, attenuation and messenger loading. A 100 meter tensile test bed was utilized. The loose tube fiber optic cable was stranded around a similarly sized Phillystran messenger. The excess length of cable to messenger was pre-determined. The degree of excess length is a function of the sag and tension requirements of the end user.

The purpose of the long length tensile test was to determine the optical and mechanical performance of the pre-stranded system while being subjected to loading conditions approaching the rated breaking strength of the messenger. (See figure 1.)

Test Installation

The purpose of this test is to determine the long term optical and mechanical performance of the pre-stranded Phillystran messenger while being subjected to extreme loading conditions indicative of an actual installation.

A long term test was set up at United Ropework's facility in Montogomeryville, PA. The test equipment at this facility monitors wind speed, wind direction, temperature and messenger loading. Attenuation is monitored during peak loading conditions. The 15400 pound Phillystran messenger was installed on a 650 foot test span with relative ease. The cable payoff and sheave wheel handling characteristics were identical to that of a standard aerial cable. The 15400 pound Phillystran messenger was installed at 1375 pounds which resulted in an installation sag of approximately 1 meter. When subjected to NESC Class 1 heavy loading conditions, the cable tension will increase to approximately 3500 pounds with a resultant sag of 4 meters.

Conclusions

The current specifications require a maximum service load of no greater than 25% of the rated breaking strength of the messenger, equivalent to 3850 pounds. At this load no fiber strain or change in attenuation was evident. The test was terminated at 75% RBS since the ram travel had been maximized. The maximum messenger strain was approximately 1.5% at the 75% RBS loading level.

The installed Pre-Stranded Optical System (P-SOS) exhibited virtually no aeolian vibration or galloping when subjected to either calm or turbulent wind conditions. The HV conductors in the background exhibited more movement than the pre-stranded cable. The pre-stranded design minimizes vibration due to the counteracting resonant frequencies of the fiber optic cable and messenger.

Commercial/Installation Considerations

To be of value, it is not enough for the pre-stranded system to be technically superior to previous designs. It must also be economic and simple to install when compared to the traditional lashing methods. In some cases, it may be a moot point do to the inability of steel to meet the requirements. An example would be installations with span lengths in excess of 2,000 feet. In most cases, however, direct comparisons are necessary.

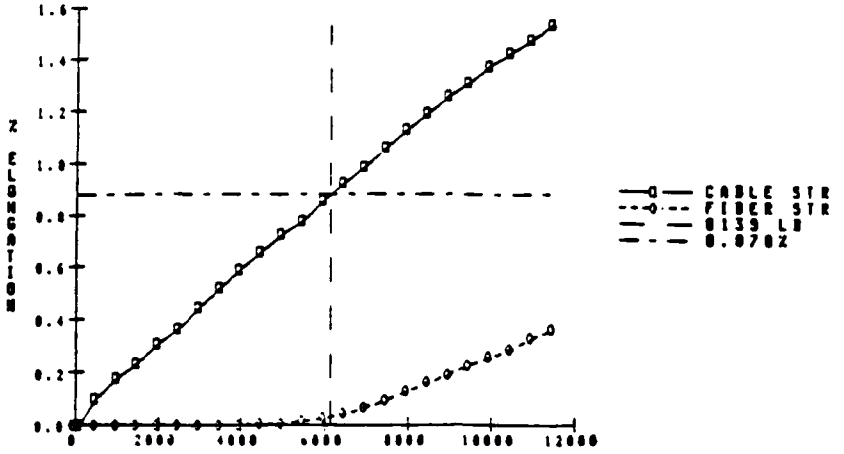
The raw material cost of the pre-stranded system will usually be greater than the cost of a steel messenger, a fiber optic cable, and the lashing wire. This is driven by the higher cost of kevlar vice steel. The labor cost of installing the pre-stranded system will be less than lashing a cable to a dedicated messenger. It takes approximately the same amount of time to completely install the self-supporting system as it does to install the messenger in a lashing process. Becuase of this, actual installation cost estimates for the pre-stranded system have typically been 35 to 50% less than lashing. This savings more than compensates for the higher product cost.

During a recent installation of the pre-stranded system, the user pulled in a 4.1km reel of the product in 1/2 hours. It was estimated that all things being equal, a lashing operation would have taken a minimum of 2 days.

Summary

Siecor, in conjuction with United Ropeworks has developed a pre-stranded aerial cable which can be utilized for virtually all aerial span applications. Vibration problems are minimized due to the pre-stranded design and the all dielectric construction is ideal for HV applications. A variable messenger tensile rating allows the cable to be tailored to the customers exact requirements while fiber counts up to 192 are readily available for both single mode and multimode fiber types. The pre-stranded cable is complemented by specially designed dead end and suspension hardware which will not alter the optical or mechanical integrity of the cable under specified loading conditions. Typically, a 35-50% savings on installation costs can be expected when compared to an equivalent performance dedicated steel messenger installation.

SIECOR LASHED CABLE



0 TENSION LBS	1 PHASE ANGLE	2 SCALE A	3 SCALE B	4 CABLE STRAIN	5 FIBER STRAIN
1 0	0.0	0.00	0.00	0.000	0.000000
2 100	0.0	0.00	0.00	0.000	0.000000
3 500	0.1	0.70	0.20	0.100	-0.000103
4 1000	0.1	1.20	0.30	0.100	-0.000103
5 1500	0.1	1.60	0.42	0.230	-0.000103
6 2000	0.1	2.10	0.55	0.310	-0.000103
7 2500	0.1	2.55	0.70	0.370	-0.000103
8 3000	0.0	3.00	0.75	0.450	0.000000
9 3500	0.0	3.50	0.89	0.522	0.000000
10 4000	0.0	3.95	1.00	0.590	0.000000
11 4500	-0.3	4.40	1.12	0.658	0.003319
12 5000	-0.8	4.85	1.23	0.724	0.008020
13 5500	-1.2	5.30	1.40	0.780	0.012410
14 6000	-2.4	5.75	1.45	0.860	0.024402
15 6500	-4.2	6.20	1.58	0.924	0.043430
16 7000	-5.6	6.65	1.70	0.990	0.060825
17 7500	-9.3	7.10	1.78	1.084	0.098110
18 8000	-12.4	7.55	1.91	1.128	0.128240
19 8500	-15.8	8.00	2.02	1.198	0.161340
20 9000	-18.5	8.40	2.12	1.258	0.191330
21 9500	-22.0	8.80	2.25	1.318	0.227530
22 10000	-25.0	9.20	2.35	1.378	0.258550
23 10500	-28.0	9.60	2.50	1.420	0.289580
24 11000	-32.0	9.95	2.60	1.470	0.330950
25 11500	-35.5	10.35	2.70	1.530	0.367150

FIGURE 1



David P. Wong
Senior Applications Engineer
Siecor Corporation
489 Siecor Park
Hickory, NC 28603
(704) 327-5884

David Peter Wong graduated from Georgia Institute of Technology with a Bachelor's degree in Mechanical Engineering in 1983. He joined Siecor Corporation in 1985 as an Applications Engineer and has been engaged in the product identification, cable design, cable qualification and production testing for specialized and conventional cable products. He is a member of the IEEE and ASME.



Santord D. Lyons
Sales Engineer
Siecor Coporation
Hickory, NC 28603
(704) 327-5806

Sanford David Lyons graduated from the United States Military Academy with a Bachelor's Degree in Mechanical Engineering. He joined Siecor Corporation in 1985. Mr. Lyons is responsible for Siecor's Sales and Marketing efforts to the Utility Industry. He is a member of the IEEE and has spoken both nationally and internationally regarding fiber optics and utilities.

WITHSTANDING HIGH-VOLTAGE CHARACTERISTICS OF NON-METALLIC SELF-SUPPORTING OPTICAL CABLE

H. TAKEHARA*, Y. ISHIHATA*, K. SAITO*, K. NIIKURA**, H. HORIMA**

A. KUROSAWA***, T. TAKEDA***, T. OHMORI***

*TOHOKU ELECTRIC POWER CO., INC. 3-7-1, ICHIBANCHO, SENDAI 980, JAPAN
**SUMITOMO ELECTRIC INDUSTRIES, LTD. 1, TAYA, SAKAE-KU, YOKOHAMA 244, JAPAN
***KITANIHON ELECTRIC CABLE CO., LTD. 1-2-1, KORIYAMA, SENDAI 982, JAPAN

Abstract

The authors have previously reported on the development of non-metallic self-supporting optical cable for use as optical transmission line on steel pylons.

When installing non-metallic self-supporting optical cable [illegible] with high voltage [illegible] it is necessary to [illegible] characteristics of this cable [illegible] the power line [illegible] [illegible]

Therefore, a series of [illegible] were [illegible] [illegible]

[illegible] [illegible] [illegible]

1. Introduction

[illegible] [illegible] [illegible] [

Study of the impact of electricity on optical cable installed in conjunction with a power transmission line.

[illegible] the most important reasons for [illegible] self-supporting [illegible] cable in which fiber reinforced plastic (FRP) is used as a light-weight material to support and protect the optical cable is stringing a power transmission line and could cause the electrical impact of power transmission [illegible].

[illegible] will be considered to be electrical phenomena or impact sustained by optical cable installed on power transmission steel poles.

[illegible] impact of grounding and short [illegible] power transmission line due [illegible] as the result of a short [illegible] the pole and the power transmission line.

[illegible] potential impact [illegible] conductor [illegible] installation [illegible] with a current flowing between [illegible] cable sheath or [illegible] insulator will [illegible] the optical [illegible] power [illegible].

[illegible]

[illegible]

[illegible]

A schematic of the test equipment is shown in Fig. 3, and the test site is shown in Fig. 4.

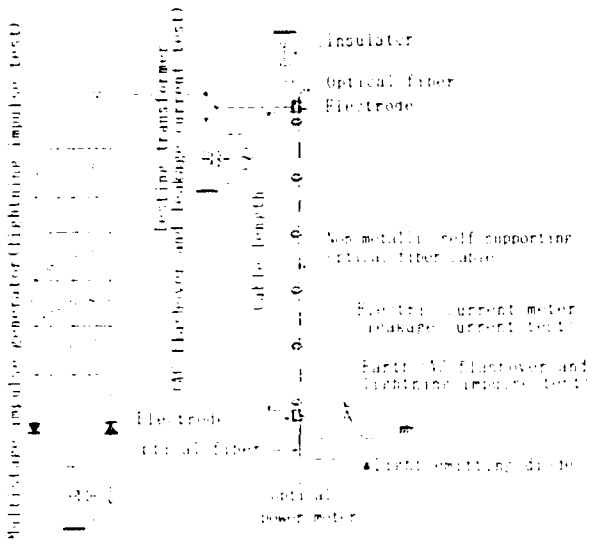


Fig. 3 Schematic of test equipment



Fig. 4 Test site

(a) Flashover voltage test

Voltage of commercial frequency was imposed between the electrodes and raised gradually. Measurements of the voltage that commenced flashover and the variance of optical transmission loss were recorded. Test items are shown in Table 1, and test results are shown in Table 2 and Fig. 5.

The level of voltage which commenced flashover was highest for dry conditions, lower when the cable was sprayed with tap water, and yet lower under saltwater conditions. During the tests, the variance of optical transmission loss was observed.

Table 1. Condition of flashover test and items measured

Test piece surface condition \ Cable length	1 m	3 m	7 m
dry (cable surface is dry)	voltage commencing flashover	voltage commencing flashover and variance of transmission loss	voltage commencing flashover
wet (tap water on cable surface)	same as above	same as above	same as above
wet (salt water on cable surface)	same as above	same as above	same as above

Table 2. Optical loss variance at the time of flashover

Condition of surface \ Items	Optical loss variance	Flashover voltage	Number of test pieces
dry	no variance	420-660kV	5
wet (tap water)	no variance	240-410kV	5
wet (salt water)	no variance	180-220kV	5

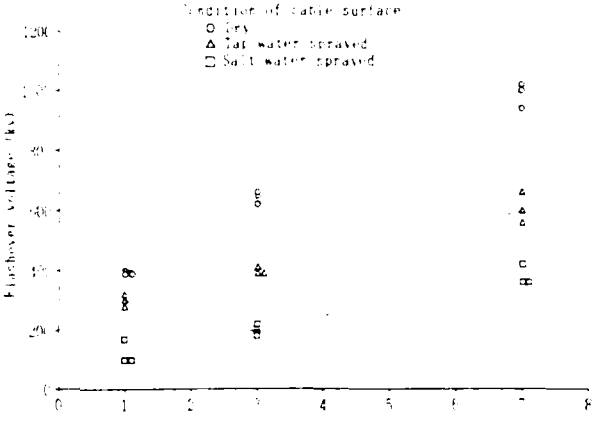


Fig. 5 Relationship between cable length and flashover voltage

(b) Leakage current test

Voltage of commercial frequency (60 Hz) was imposed between electrodes. This voltage was then gradually raised and leakage current was measured. Test results are shown in Fig. 6. At a constant level of imposed voltage, leakage current was greatest under salt water conditions, less when the cable was sprayed with tap water, and least under dry conditions.

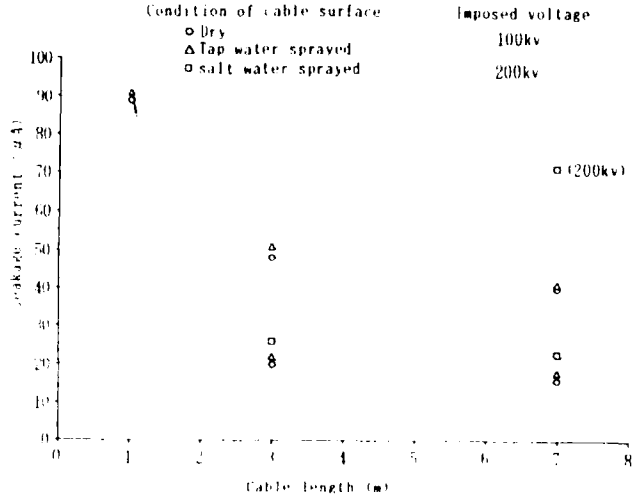


Fig. 6 Relationship between cable length and leakage current

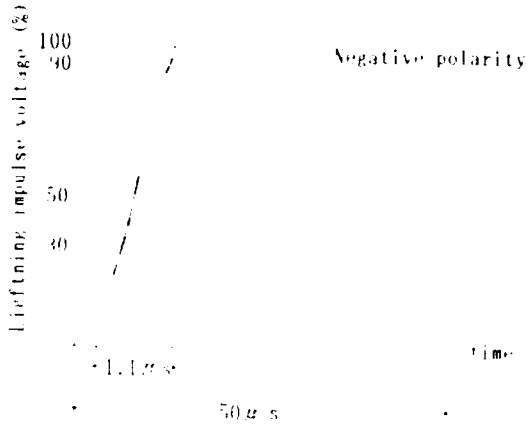


Fig. 7 Lightning impulse waveform

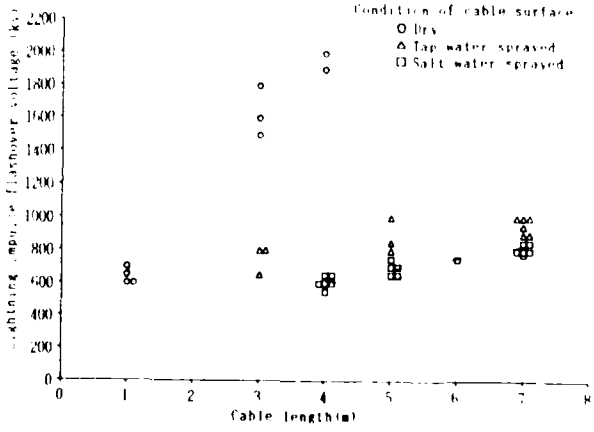


Fig. 8 Relationship between cable length and lightning impulse flashover voltage

Installation of optical cable

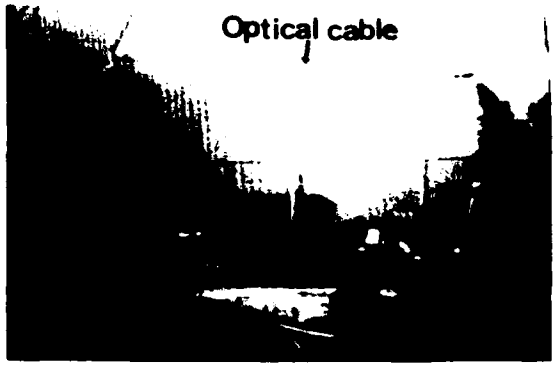


Fig. 9 Photograph of the flashover

of salt water if the distance "d" from the anchored part is more than about 2.5 m as shown in Fig. 5. This is because the effective value between a line and the ground is about 100 kV, for example in 275 kV power transmission.

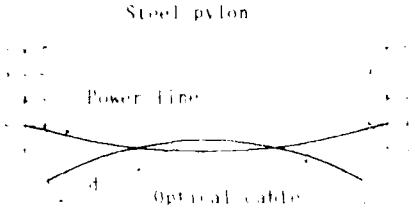


Fig. 10 Example assuming contact between power line and optical cable (1)

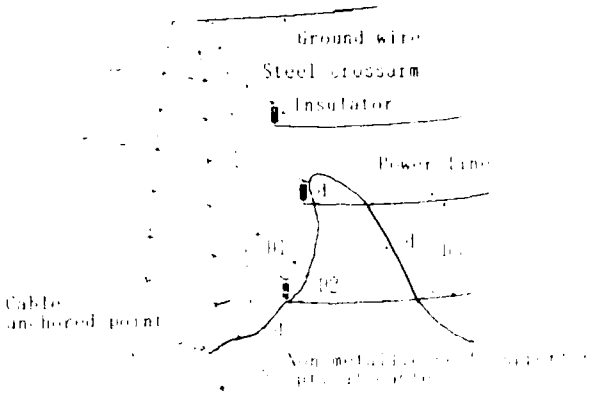


Fig. 11 Example assuming contact between power line and optical cable (2)

Table 5 Comparison between maximum [illegible] of optical cable in salt water and the [illegible]

Items	Between power line and ground: Distance of maximum optical cable length for flash-over	Between power line and ground: [illegible]	Between power line and ground: [illegible]	[illegible]
[illegible] power transmission line				
500kV between lines / 275kV between one line and ground	about [illegible] m	about [illegible] m	about [illegible] m	[illegible]
275kV between lines / 154kV between one line and ground	about [illegible] m	about [illegible] m	about [illegible] m	[illegible]
154kV between [illegible] / 66kV between one line and ground	about [illegible] m	about [illegible] m	about [illegible] m	[illegible]

This indicates that the value poses no problem when compared to 0.5mA [4] which is the threshold value that does not have impact on the human body. Also, since optical cable is anchored to steel pylon and is grounded, there seems to be no impact on an installation.

(2) Cable entering the communication installation

The configuration of optical cable entering a telecommunication installation located in a substation near a steel pylon is shown in Fig. 12.

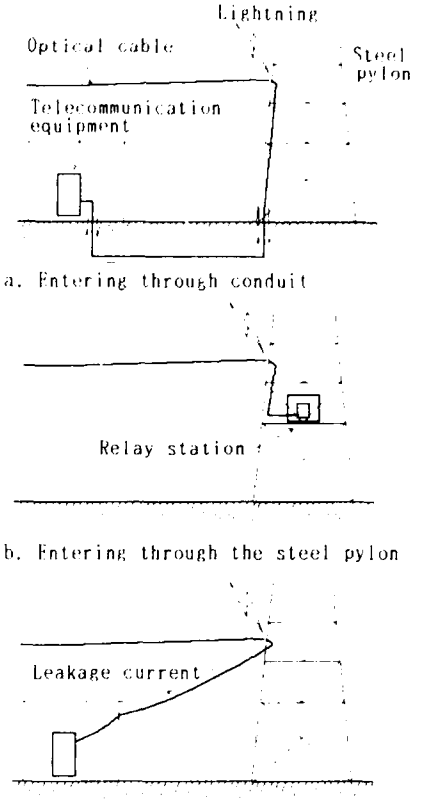
If the ground wire shield should fail when lightning directly strikes the location where the optical cable is anchored resulting in a flashover to the optical cable, it can be assumed that the lightning will directly affect the telecommunication installation.
In case the incoming cable passes through an underground conduit and/or duct or when the optical cable that approaches the relay station is connected to the steel pylon and repeater housing as shown in "a" and "b" of Fig. 12, since the optical cable is grounded, the lightning is not directly transmitted to the equipment.

In case the optical cable enters the power station aerially as shown in "c" of Fig. 12, since flashover caused by an impulse of 800 kv occurs for optical cables 7 m in length when sprayed with salt water (see Fig. 8), it can be predicted that electricity from a bolt of lightning would pass through the optical cable to the station housing. It is desirable to avoid such a contingency if at all possible, and therefore, the configuration shown in "c" of Fig. 12 should not be employed.

5. Conclusion

Assuming the impact of high voltage on optical cable installed in conjunction with power transmission lines, a variety of simulation tests were conducted.

With regards to proximity and contact between a power transmission line and optical cable under normal stringing conditions, insulation was confirmed to be sufficient. Therefore, it is expected that the application of non-metallic optical cable in conjuction with high voltage class power transmission line will [illegible].



a. Entering through conduit

b. Entering through the steel pylon

c. Entering from overhead

Fig. 12 Configuration of optical cable entering an installation housing

References

(1) F. Hayasaka, F. Ohtsuka, M. Monma, S. Ohira, H. Horima, K. Yamashita, M. Dosei and N. Abe, Non-metallic optical cable with optical fiber catenary for long span aerial application, IWCS, 1983.

(2) F. Hayasaka, Y. Ishihata, H. Horima, S. Hisano, T. Shishido and T. Ohmori, The clarification of movement of non-metallic self-supporting optical cable caused by wind and the design of its installation at steel pylon, IWCS, 1984.

(3) Electric Collaboration Research of Japan, The value of adherence of salt in the vicinity of seacoast, ECR Report 20-NO. 2, 1964.

(4) C.F. Dalziel, Threshold 60-cycle fibrillating currents, AIEE Paper 60-40.



Hidetomi Takehara
Tohoku Electric
Power Co., Inc.
7-1, 3-chome
Ichibancho
Sendai 980, Japan

Hidetomi Takehara received his B.E. degree from Hokkaido University in 1980. He then joined Tohoku Electric Power Co., Inc., where he has been engaged in telecommunications and electronics engineering. He is now an engineer for the Integrated Communication Network Development Office and a member of the Institute of Electronics and Communication Engineers of Japan.



Yoshinori Ishihata
Tohoku Electric
Power Co, Inc.
7-1, 3-chome
Ichibancho
Sendai 980, Japan

Yoshinori Ishihata received his M.S. degree from Tohoku University in 1979. He then joined Tohoku Electric Power Co., Inc., where he has been engaged in telecommunications and electronics engineering. He now serves as an engineer for the Integrated Communication Network Development Office and a member of the Institute of Electronics and Communication Engineers of Japan.



Kazunori Saito
Tohoku Electric
Power Co., Inc.
7-1, 3-chome
Ichibancho
Sendai 980, Japan

Kazunori Saito graduated from Fukushima Technical School in 1975. He then joined Tohoku Electric Power Co., Inc. and has been engaged in communications and electronics engineering. He is now an engineer for the Integrated Communication Network Development Office.



Koji Niikura
Sumitomo Electric
Industries, Ltd.
1, Taya-cho
Sakae-ku
Yokohama 244, Japan

Koji Niikura received his B.S. degree in engineering from Waseda University in 1984 and joined Sumitomo Electric Industries, Ltd. He has been engaged in the development and design of optical fiber cables in the Fiber Optics Division.



Hiroaki Horima
Sumitomo Electric
Industries, Ltd.
1, Taya-cho
Sakae-ku
Yokohama 244, Japan

Hiroaki Horima received his M.S. degree in engineering from Osaka University in 1972. He then joined Sumitomo Electric Industries, Ltd. and worked on the development of CATV coaxial cables, multi-pair PEF-insulated junction cables and low loss unbalanced type cables. Thereafter, he concentrated on the development of optical fiber cables. He is now Section Manager of the Fiber Optics Division at Sumitomo Electric Industries, Ltd. He is a member of the Institute of Electronics and Communication Engineers of Japan.



Akira Kurosawa
Kitanihon Electric
Cable Co., Ltd.
1-2-1, Koriyama
Sendai 982, Japan

Akira Kurosawa received his B.E. degree from Tohoku University in 1970. At Kitanihon Electric Cable Company, Ltd., he has been engaged in the design and development of communication cables. He is a member of the Institute of Electronics and Communication Engineers of Japan.



Tsuyoshi Takeda
Kitanihon Electric
Cable Co., Ltd.
1-2-1, Koriyama
Sendai 982, Japan

Tsuyoshi Takeda received his B.E. degree from Tohoku University in 1968. At Kitanihon Electric Cable Co., Ltd., he has been engaged in research and development of communication cables and power cables. He is now a deputy manager of the Engineering Division. He is a member of the Institute of Electrical Engineers of Japan.



Toshiyuki Ohmori
Kitanihon Electric
Cable Co., Ltd.
1-2-1, Koriyama
Sendai 982, Japan

Toshiyuki Ohmori received his B.E. degree from Tohoku Gakuin University in 1966. At Kitanihon Electric Cable Co., Ltd., he has been engaged in research and development of communication cables, power cables and accessories for these cables. He is now a deputy manager of the Engineering Division. He is a member of the Institute of Electronics and Communication Engineers of Japan and the Institute of Electrical Engineers of Japan.

THE DEVELOPMENT OF A METAL-FREE, SELF-SUPPORTING OPTICAL CABLE FOR USE ON LONG SPAN, HIGH VOLTAGE OVERHEAD POWER LINES

S.M. Rowland*, K. Craddock**, C.N. Carter+, I. Houghton++, D. Delme-Jones++

* STC Technology Ltd, Harlow, UK. **STC Telecoms, Basildon, UK.
+ CERL, Leatherhead, UK. ++ STC Telecoms, Newport, UK.

ABSTRACT

The requirements of a self supporting cable for high voltage, overhead power line application are discussed. The novel design of one such optical communication system which can be installed on live systems is presented. Developments of this metal-free, self supporting cable and associated jointing and splicing techniques are described together with installation procedures. Optical and mechanical performance details of the complete transmission system are outlined

The key problems of the product development are considered and the reasons for the design choices are discussed. The cable consists of a specially shaped pultruded rod strength member containing optical fibres in ribbon form. A track resistant material is used to sheath the cable. Results of calculations of electrical fields to be endured in service and clearance to phase conductors under a range of environmental loadings are presented.

1. INTRODUCTION

Since the advent of optical fibres, the advantages of interference free operation have encouraged the installation of optical telecommunications on power lines. The high voltage power transmission and distribution system, a network reaching every population centre and industrial area, can now offer alternative telecommunication routes for the electrical utilities or for common carriers. The development of products, designed to meet the demanding conditions of aerial installation on power lines, have made power based telecommunication networks a practical and economical proposition.

It is unlikely that an electrical utility would require more than six fibres for its own use but the use of power lines for long haul, wide band telecommunications is becoming quite common. The ability to choose any number of fibres up to say, twenty four, should accommodate a wide range of requirements. The electrical utility may itself become a carrier, may enter joint use agreements or may offer the wayleave to an established carrier. Such a cable could be used for a wide variety of communications which may vary from a very basic four channel power system protection signalling scheme on one pair of fibres up to twelve fully equipped 565 Mb/s systems.

There are existing methods for installing optical cables on power lines. One well documented solution is the use of a composite overhead line conductor which contains optical fibre. In general, however, it is too expensive to use except during reconductoring or on new lines. Attaching optical cables to the outside of existing power line conductors can be economic in some cases but their mechanical vulnerability and inability to be separated from the power system operation can be problematic.

Self-supporting, metal-free cables are totally independent of the power function of the network and can be installed more cheaply and with less disruption than composite conductors. The recent development of one such cable gives an economic solution for communications on existing high-voltage lines. This paper describes the key requirements of such an optical cable and a unique design which meets them. This cable, together with its installation accessories and equipment, is now fully developed.

2. DESIGN CRITERIA

The following is a list of criteria which this self-supporting cable was designed to meet:

- To operate singlemode, 1300 nm with an installed attenuation of less than 0.5 dB/km in any expected service conditions;
- To have a potential 1550 nm capability;
- To contain any number of fibres up to 24;
- To have a predicted life in excess of 25 years;
- To be manufactured in lengths of up to 4 km;
- To minimise costs of materials, manufacture and installation;

- To use materials already commercially available and technically proven;

- To permit rapid installation using lightweight equipment and near standard overhead line techniques;

- To be non-metallic so as to maintain phase isolation from earth and ease route installation without power disruption;

- To be used on spans up to 540 m with either simultaneous loadings of 380 N/m² wind and 12.5 mm ice radial or with 960 N/m² wind only;

- To be installed low on the structure with small sags so that ground clearance regulations can be met and to minimise the possibility of clashing with conductors;

- To minimise cable diameter so as to reduce tower loadings and avoid tower reinforcement;

- To be smooth and circular to avoid aerodynamic instability;

- To be non-deformable so as to maintain physical isolation of fibres from clamping forces and protect from handling damage;

- To provide easy fibre access for jointing in the field;

- To be fully filled so as to prevent water condensation and electrical degradation within the sheath;

- To withstand the electrical environment seen in service;

- To show negligible creep so as to maintain sags and tension;

- To be torsionally stable to simplify installation.

3. DESIGN IMPLEMENTATION

The cable construction is illustrated in Figure 1. The strength member consists of a single pultruded glass reinforced plastic (grp) rod. A slot in the rod provides the location for the optical fibres. A rod with an outside diameter of 10 mm has been found to be optimum for the United Kingdom, giving sufficient strength without being too stiff.

A high fibre packing density has been achieved by using a ribbon element. A ribbon consists of up to twelve fibres and two such ribbons may be accommodated within the slot in the strength member. Each fibre of the ribbon is individually inked for identification. During cable manufacture the fibre ribbons are fed into the slot in such a way that each is 0.52% longer than the strength member. This is accommodated by the ribbons forming a smooth sine wave along the slot. This has the effect that at normal working tensions the optical fibres are completely free from strain. At maximum working tension the fibres see a maximum strain of 0.25%. This is around a third of the fibre proof strain and is quite compatible with a cable life in excess of 25 years. The cable is constructed in such a way that the application of a 0.25% longitudinal fibre strain does not increase the fibre attenuation. This has been confirmed during type approval testing.

A soft hydrophobic compound is used to fill the slot volume. This compound allows ribbons to move up and down and thus use the excess fibre when the cable is tensioned and to recover when tensions are released. A continuous cap seals the ribbons and filling compounds in the slot and protects the fibres when the sheath is cut away for termination. The cap is held in position with a binder yarn.

The sheath material chosen has the physical properties required to enable clamping using spiral preforms that do not stress-concentrate and so avoid fatigue damage or crush damage (4.3). The sheath is also stable to U.V. radiation and resistant to damage caused by the cable's electrical environment.

The cable is of a density and diameter which allow the use of low cost spiral vibration dampers. These have proved fully effective in preventing aeolian vibration.

Tables 1 and 2 present the principal characteristics of the cable.

Table 1. Cable Technical Data

Cable Weight	220 kg/km
Outer Diameter	13.0 mm
Typical Minimum Bend Radius	500 mm
Storage Bend Radius	700 mm
Maximum Working Tension	22.5 kN
Minimum Ultimate Tensile Strength	65 kN
Minimum Tension Without Sheath Slippage	45 kN
Minimum Strength Member Tensile Modulus	47.5 kN/mm²
Thermal Coefficient of Exp nsion	$5.2 \times 10^{-6}/^{o}C$
Minimum Excess Fibre Length	0.45%
Maximum Fibre Strain at Maximum Working Tension	0.25%
Operating Temperature Range	$-40^{o}C$ to $70^{o}C$
Maximum Number of Fibres	24

Table 2. Cable Characteristics

In temperate climates
(12.5 mm radial ice + 88 km/h wind)

Span (m)	300	400	500	550+	720*
Minimum Normal Working Sag (m)	1.5	4.2	12.2	16.0	42.4
Ice loaded Sag (m)	6.6	12.9	21.7	27.0	50.0

In tropical climates (no ice + 135 km/h wind)

Span (m)	400	500	600	700	800+	1000*
Min. Normal Working Sag (m)	2.3	4.3	8.1	15.0	25.0	50.9

+ Maximum span likely on normal pylon
* Maximum span likely on canyon or river crossings

3.1 Optical Characteristics

Comprehensive testing of the cable's optical performance has been satisfactorily carried out under a wide range of conditions. The most important of these are temperature cycling and mechanical load cycling. Figure 2 shows a schematic of measured strain against load for a cable sample up to 22500 N. The associated fibre strain which peaked at 0.23% is also shown. In this particular test the optical loss increased but remained below the target level of 0.5 dB/km. On mechanical relaxation the loss returned to its original value. The effect of temperature cycling on the optical loss of the cable on its storage drum has been measured between -40°C and 80°C. A target of loss remaining below 0.5 dB/km has been set. This target has sometimes been exceeded. However, with new production techniques this should soon be guaranteed on all such cables.

To gain confidence in the all-weather optical performance a prototype cable sample has been installed on a CEGB overhead test line in southern England which has been used for 800 kV development work. This has a central span of 366 m and corresponding half spans at either end terminated by tension stub towers. The sample has been strung using materials and techniques described in section 4 and has been monitored for attenuation variation and mechanical behaviour for just over a year. Wind speed and direction, temperature, humidity and cable tension have also been continuously monitored. Attenuation has shown minimal dependence on weather conditions and performance has exceeded expectations.

3.2 The Strength Member

A pultruded glass reinforced plastic was selected as the all dielectric strength member for a number of reasons. It has a high modulus, both longitudinal and lateral and, unlike DuPont's aromatic polyamide fibre, Kevlar, can withstand high clamping forces. It is also less prone to creep than other dielectric strength members. Conventional pultrusion technology also allows any cross sectional geometry to be chosen. Other advantages include low coefficient of thermal expansion and inherent torque balance.

A wide range of manufacturers' products has been tested in the extensive technical and quality programmes carried out. In particular, the long term reliability of the strength member is of concern to users. Some work has already been carried out on glass/resin systems.[1,2] In addition to this, a substantial programme of work has been performed at University College, Cardiff on candidate materials. The effects of long term ageing in both wet, dry and cycled environments on ultimate tensile strength and minimum bend radius have been assessed. This data has been used to estimate product lifetime and to choose the best sources for high quality rod. It has also been used to define rigorous quality assurance procedures for use under production conditions.

3.3 Ageing by Electrical Processes

By the nature of its application the cable has to survive in a high voltage environment. Potential gradients exist in the regions between each of the phase conductors which result in a field gradient along the length of the cable near to the towers. If suitable precautions are not taken, capacitively induced currents on the surface of a wet or dirty cable can cause sheath damage [3,4] and ultimately cable failure. Induced currents within the cable are prevented by using only quality pultruded rod with no detectable voids and complete filling of the fibre slot during manufacture.

Results of calculations on the worst case longitudinal field seen by a cable hung mid-way between the bottom four phase conductors of a typical 400 kV double circuit UK tower construction are presented in Figure 3. Also shown is the greater field resulting when only one of the circuits is energised. The cable is hung in this position to gain the maximum benefit from phase cancellation (Section 4.1). The maximum magnitude of the transverse field has also been calculated as 5 kV m^{-1} which is insufficient to damage the cable.

Calculations suggest that currents of the order of 10 mA would be capacitively induced on a metal free cable with a wet or dirty (conducting) surface. A current of this magnitude is sufficient to cause surface tracking and presents a severe threat to a poorly designed cable[3]. Two solutions to this problem have been considered. Firstly attempts can be made to reduce the current. Techniques such as isolation of cable clamps from earth,

forms of shedding and local protection by smearing silicone grease over the cable fall into this category. The drawbacks of these schemes include added expense, maintenance requirements and the possibility of incorrect installation. Secondly choose a sheath material which will resist degradation by the surface currents. Such a sheath may be semiconducting, so that surface currents are dispersed in its bulk. This avoids the damaging high local current densities associated with dry band arcing and tracking. Alternatively select an insulating material resistant to damage by surface currents. It is this latter option that has been adopted for this cable.

Standard tracking tests such at IEC 112, comparative tracking index, and ASTM D2303, inclined plane test, have been found useful for roughly ordering the performance of materials. However such tests do not model service conditions closely enough to give data suitable for evaluating long term product performance[5]. Larger scale laboratory tests have been developed to compare materials performance on extruded cable samples. A schematic of the apparatus used is shown in Figure 4. In these experiments a voltage is applied to electrodes on the cable surface. The cable is then regularly sprayed with electrolyte. Both the nature of the electrolyte and electrodes is found to be important in promoting damage. In most cases to reduce the time taken for degradation to begin, graphite electrodes and a high conductivity solution are used. These facilities have also enabled investigations into the effects of various types of foreign matter on the cable surface. These effects have also been found to be dependent on the sheath material. In this manner a number of possible sheathing materials has been identified.

To reinforce knowledge gained from laboratory tests an outdoor 275 kV facility at Brighton Insulator Test Centre on the south coast of England has been used to age some samples in an environment more closely related to service conditions. 16 m lengths of cable have been hung parallel to a 10 m long conductor maintained at 160 kV to ground, 50 Hz at a distance of 1 m. Cables were suspended using the clamps described in Section 4.3. Calculations show that the greatest field gradient experienced by this cable is approximately five times greater than that seen on a 400 kV tower. Extrapolating to a working stress from accelerated tests to define a minimum product life time is a formidable task[6]. However, intense testing has given great confidence in the performance of the sheath material currently being used for the product.

4. INSTALLATION

4.1 Tower Fixing

There is a number of requirements which have a bearing on where to fix the cable on towers which were originally designed exclusively for supporting high voltage metallic phase conductors and an earth conductor.

First, minimum ground clearance must be maintained on each span under worst case conditions. In the UK, statutory requirements are contained within the Electricity (Overhead Lines) Regulations 1970. These require, for new lines, a minimum clearance for cables of 5.8 m over any road accessible to vehicular traffic. This is less than the minimum height for line conductors (which varies from 6.7 m at 132 kV to 7.3 m at 400 kV) which permits the possibility of fixings on towers slightly lower than the fixing levels of the lowest phase conductor for equal worst case sags of the optical cable and the phase conductor.

Second, tower loadings must be minimised. The maximum working tension is 22.5 kN under worst case environmental loading (Table 1). Normal working tensions are in the range 6 kN - 10 kN. Whilst these loadings are low in comparison with those of the phase conductors, their effect will be minimised by locating the cable as low as practicable within the main body of the tower. Individual tower steel work configuration around the lower cross arm level, and the possible need to strengthen an individual member, will influence the precise location of the cable attachment.

Third, the possibility of the cable being blown out to touch any of the phase conductors must be negligible. A computer programme has been developed to assess this situation and shows that for the various high voltage towers employed in the UK, this requirement can be met even for the longest spans and worst weather conditions.

Finally, the installation must be possible under live working conditions. In the most demanding case when working with both circuits live, this implies working below the level of the bottom cross arm and within the tower body symmetrically spaced between each circuit.

Figure 5 shows the preferred location on two tower types employed widely in the UK.

4.2 Cable Sag and Tension

The physical characteristics of the g.r.p strength member and a typical metallic phase conductor are different. They therefore respond differently to variations of temperature, ice loading and wind. The maximum cable sag, for example for a phase conductor is at high temperatures whereas for the optical cable it is

just below freezing point with full ice loading.

When considering a particular span, a knowledge of the maximum allowable cable sag enables the installation tension to be calculated over a small range of possible installation temperatures. For long spans, a further check is then made, using a specially developed programme, to ensure that no clashing will occur between the cable and the phase conductors when subject to high winds (with and without ice loading) and a wide range of temperatures.

4.3 Suspension Arrangements

The terminal clamp is a galvanised steel preformed spiral design about 1.2 m long as used within the electricity industry. Preformed spiral reinforcing rods are employed beneath the clamp to distribute the compressive load over an adequate cable length. The clamp holds the cable without slipping up to a tensile load of at least 45 kN. The requirements of BS 3288 have been met in this respect. This clamp is employed at all tension towers.

The suspension clamp, made of aluminium alloy, is also a preformed spiral design fitted over reinforcing rods about 1.8 m long. It is used at all intermediate suspension towers. The central pick-up bracket has neoprene inserts to provide further cushioning to the cable. The clamp provides a limited slip facility to prevent cable damage in the event of significant differential loading on each side of the clamp due, for example, to unequal ice loadings or tower movement.

Aeolian vibration, induced by wind blowing transversely across the tensioned cable, could give rise to cable fatigue at the interface with the clamp. This is countered by the application of a proprietary light weight helical damper made of high impact track resistant material. One or two dampers, depending on the span length, are fitted at each end of the span, adjacent to the clamp.

4.4 Stringing

Continuous tension stringing, a technique used for conductor installation, has been adopted to pull in up to 4 km of the cable. This ensures that the cable does not come into contact with the ground or any potentially damaging obstacle during the pulling in process.

The necessary back tension is effected by hydraulically controlled torque arms operating on the flanges of the cable pay off drum. Up to 6 kN back tension can be applied.

The winch is a double bull wheel capstan hydraulically controlled to provide up to 20 kN bond tension. Tension monitoring and automatic cut out facilities are provided. A total of 4 km of low stretch rope bond is carried on two drums.

Running out blocks are first positioned at or near the clamp position on each tower in the cable section to be strung. These are 600 mm diameter aluminium alloy low friction sheave blocks with neoprene lined grooves. Approximately 500 m lengths of small diameter polyester pilot rope are walked into position along the route and connected together over the blocks. One end is connected to the main bond on the winch and the other to an empty pilot reel fitted to an auxiliary drive on the tensioner, which now operates as a reel winder pulling in both the pilot rope and the main bond.

The main bond is connected to the cable via a secure clamp and swivel and the winch pulls the main bond and cable into position.

One cable section may contain a number of tension sections comprising one or more spans between tension towers. These are progressively tensioned and clamped off, starting at the section remote from the winch end. Conventional optical sighting techniques are used to measure the sag on a selected span within each tension section. As the creep of the cable is very low, no compensation has to be made for this effect, as is necessary for the metallic phase conductors.

Safety is a prime concern during the stringing, particularly when one or both circuits are live. A detailed written Code of Practice must be agreed between the Contractor and the Authority prior to commencement of any on-site work.

4.5 Cable Jointing

Joint housings are required at splices between either successive lengths of aerial cable at intermediate angle towers or aerial cable and the non-metallic underground cable (normally used for building entry) at terminal towers.

In the first case, lengths of up to 4 km both minimise the total number of joints required on a given route and provide greater flexibility in selecting the most accessible intermediate angle tower for locating the joint.

In both cases, cable jointing and fibre splicing are performed at ground level. The joint housing is then positioned on a tower leg well above the climbing guard. Shotgun protection is provided by locating the housing within a galvanised steel tube fixed to the tower leg (Figure 6).

The housing itself comprises a hard plastic cylindrical shell closed at one end. The other end heat shrinks down over the two entry cables. Up to 24 splices can be accommodated within the overall shell dimension of 540 mm x 100 mm diameter.

In the unlikely event of splice failure, the housing can be re entered. Access for repair work is facilitated as each spliced fibre is coiled within its own plastic envelope and suitably designated.

4.6 Splicing and Testing

Fibre splicing is required at external joint housings and termination (splitter) boxes within the building where the Optical Line Terminating Equipment is installed. At both locations arc fusion welding is employed to ensure maximum long term splice stability.

An Optical Time Domain Reflectometer (OTDR) is used to evaluate each splice in a joint housing before the housing is closed. Fibre end to fibre end (or connector to connector) losses are measured conventionally with a stabilised light source and power meter to complete the optical testing.

5. CONCLUSIONS

A need has been identified for a self-supporting optical cable which can be installed economically on existing high voltage power lines.

The requirements of such a cable have been identified: it must have good optical performance; it must cope with long spans and maintain clearances to phase conductors and ground during ice and wind loading without compromising the support structures; it must be compatible with its environments including high electric fields.

These requirements have been met by the development of a 13 mm diameter cable consisting of a pultruded grp strength member, slotted to house ribbons of optical fibre, all sheathed in a track resistant material. Up to 24 fibres can be contained in one cable. A comprehensive range of qualification testing has been completed.

An installation procedure has been devised which permits stringing without circuit interruption. For completeness, a full range of terminal and suspension clamps, vibration dampers, joint housings and other ancillary equipment has been developed and tested.

REFERENCES

1. S.J. Harris, B. Nobel and M.J. Owen, 'Metallographic Investigation of the Damage Caused to GRP by the Combined Action of Electrical, Mechanical and Chemical Environments', J. Mat. Sci. 19 (1984) 1596-1604.

2. J.N. Price and D. Hull, 'Propagation of Stress Corrosion Cracks in Aligned Glass Fibre Composite Materials', J. Mat. Sci. 18 (1983) 2798-2810.

3. M.J. Billings and K.W. Humphreys, 'An Outdoor Tracking and Erosion Test of Some Epoxide Resins', IEEE Trans EI-3 (1968) 62-70.

4. D.J. Parr and R.M. Scarisbrick, 'Performance of Synthetic Insulating Materials under Polluted Conditions', Proc IEE 112 (1965) 1625-1632.

5. A.W. Stannett and D.A. Swift, 'Some Comments on the Value of Tests on Materials in the Design of Plastics Insulators', 5th BEAMA Int. Elec. Ins. Conf. (1986) 160-165.

6. G.C. Stone, 'Application of Statistical Methods to the Design of Solid Insulation Systems', CEIDP (1985) 234-249.

ACKNOWLEDGEMENTS

The authors wish to thank the directors of STC Technology, STC Telecommunications and the Central Electricity Generating Board for permission to publish this paper.

Figure 1. **Cable Cross Section**

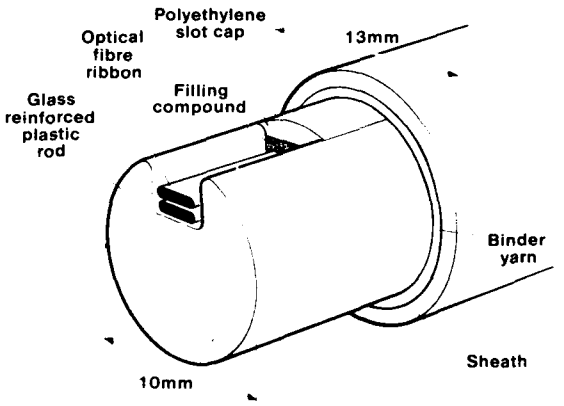


Figure 2.

Load-Strain Plot for Cable and Associated Strain for Fibres

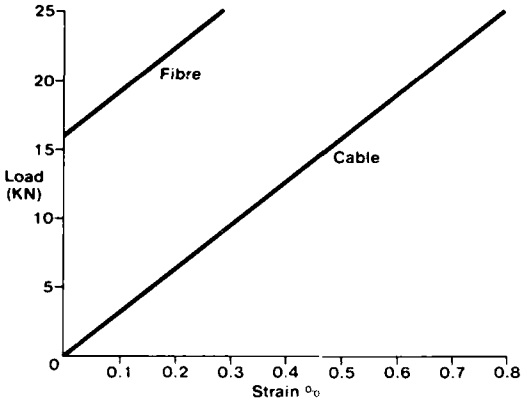


Figure 3.

Field Gradients Along Cable Away From Clamp

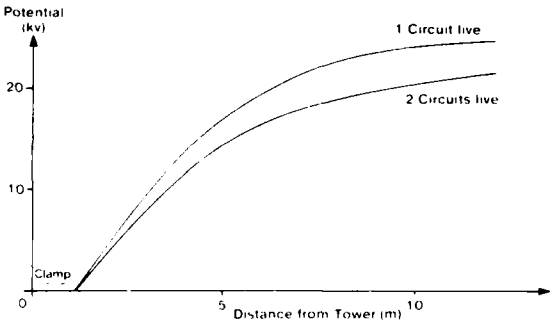


Figure 4.

Laboratory Electrical Degradation Test Rig. Example Values of Applied Voltage and Electrode Separation are given

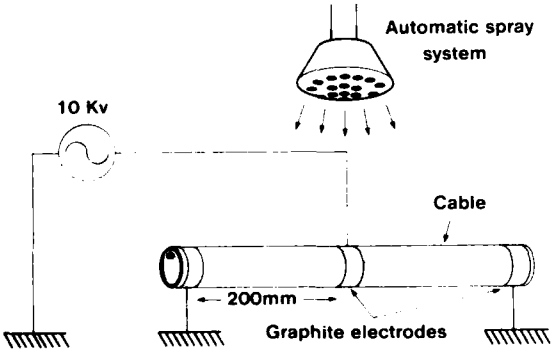


Figure 5.

Location of Self Supporting Cable on Towers

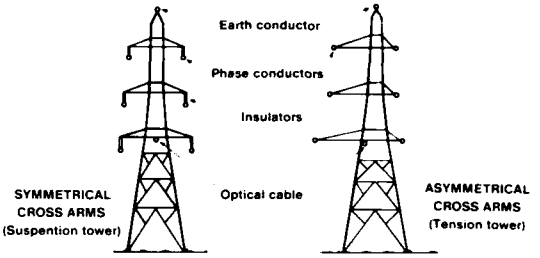
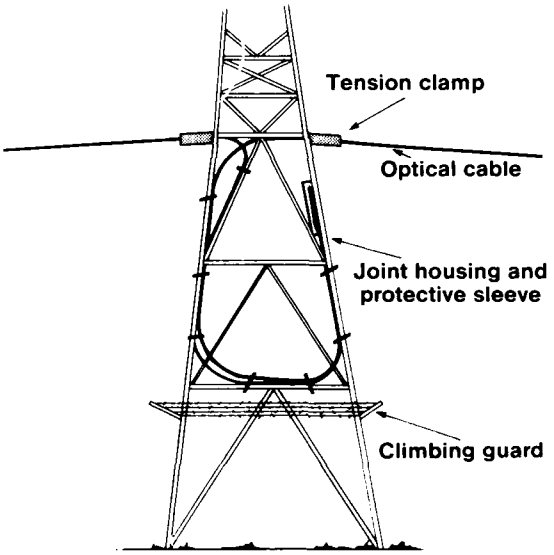


Figure 6.

Joint Housing Location





Simon M. Rowland,
STC Technology Ltd,
London Road,
HARLOW,
Essex,
CM17 9NA
UK

Simon Rowland was born in London, England. He received a B.Sc from the University of East Anglia and a Ph.D from Chelsea College, University of London. Since joining STC Technology Ltd he has worked in the Polymer Technology Department concentrating on problems of electrical insulation degradation.



Keith Craddock,
STC Telecommunications,
Chester Hall Lane,
BASILDON,
Essex,
SS14 3BW,
UK

Keith Craddock was born in Northumberland, England. He joined the Marconi Company after graduating from Durham University in 1956 with a B.Sc. (Eng). He joined STC in 1969 as a microwave systems engineer and has subsequently been involved in many civil and military telecommunications projects, with recent emphasis on installation engineering and field testing of optical transmission systems.



Chris N. Carter,
Central Electricity
Research Laboratories,
Kelvin Avenue,
LEATHERHEAD,
Surrey
KT22 7SE,
UK

Chris Carter graduated from the University of London with a B.Sc. Honours degree in Mathematics and Physics in 1963. He has since carried out research work for the CEGB on magnetohydrodynamic power generation, superconducting magnet design, ac loss measurements in superconductors, failure mechanisms in power cable stop joints and, since 1979, on the development of optical communications on power lines.

Ian Houghton,
STC Telecommunications,
Cable Products Division,
Wednesbury Street,
NEWPORT,
Gwent,
NP9 OWS,
UK

Ian Houghton was born in London, England. He received a B.Sc. in Chemical Physics from the University of Sheffield in 1981. After graduation he worked as a polymer technologist for Metal Box Research and Development Division in Oxfordshire, until 1984. He then joined the Cable Products Division of STC in Newport, South Wales, as senior development engineer, Optical Cables. He originated the self-supporting cable design presented in this paper, and has been extensively involved with the cable's development.



David Delme Jones,
STC Telecommunications,
Cable Products Division,
Wednesbury Street,
NEWPORT,
Gwent,
NP9 OWS,
UK

David Delme Jones was born in Wales. He gained a HNC in Applied Physics and Mathematics from Watford College of Technology and a B.Sc. from North East London Polytechnic. He is a member of the British Computer Society and also a member of the British Institute of Management. He was responsible for setting up the first Optical Cable Manufacturing Plant in STC and he is currently Manager of Optical Projects.

DEVELOPMENT OF OPTICAL GROUND WIRE FOR 1.55 μm WAVELENGTH

B. Lin Y. Kitayama, Y. Masuda

Sumitomo Electric Industries, Ltd.
1, Taya-cho, Sakae-ku, Yokohama, 244, Japan

Abstract

An OPGW (Optical Ground Wire) for 1.55 μm wavelength operation using cut-off shifted pure silica core single-mode fibers has been developed. It has very low and stable transmission loss and good long-term reliability at 1.55 μm wavelength. This work solved the problems concerning the microbending loss at high temperature and loss increase due to hydrogen generation.

1. Introduction

The demand to make repeater spacing as long as possible is strong in many OPGW transmission systems, since the distance between two substations is often very long and repeaters have to be equipped at locations difficult for installation and maintenance. The 1.55 μm wavelength application seems to be suitable for that purpose, but two problems have been forseen when OPGW is used at 1.55 μm wavelength. They are fiber microbending loss at high temperature and loss increase due to hydrogen generation (1). These problems may arise more easily in OPGW than in other types of optical cable because the fiber in OPGW is confined in a small space inside an aluminum tube and subjected to high temperatures. Therefore, development of an OPGW having very low and stable transmission characteristics at 1.55 μm wavelength is greatly needed. Previously we presented about the low loss OPGW with pure silica core single-mode fiber whose design in optimized for 1.3 μm wavelength operation (2). In this paper, we propose an OPGW with newly designed cut-off shifted pure silica core single-mode fibers, which performs best in 1.55 μm wavelength operation.

2. Fiber Design

The conventional pure silica core single-mode fiber parameters are summarized in Table 1. The cut-off wavelength is around 1.2 μm, which enable us to use the fiber at 1.3 μm wavelength and possibly at 1.55 μm wavelength. But when only the 1.55 μm wavelength operation is considered, it is beneficial to shift the cut-off wavelength to a longer one from the viewpoint of bending resistance. There are two ways to shift the cut-off wavelength to a longer one. One is to make the refractive index difference Δn larger, the other is to make the core diameter, or mode field diameter (MFD), larger. The relationship among effective cut-off wavelength λce, Δn, MFD and bending loss (3) is shown in Figure 1. By using this figure, λce and MFD were chosen as 1.35 μm ≤ λce ≤ 1.60 μm, 10.0 μm ≤ MFD ≤ 12.0 μm, taking the following requirements into consideration:

1) Single-mode operation shall be secured at 1.55 μm wavelength.

2) Dispersion shall be less than 21 ps/km/nm.

3) Bending loss shall be equivalent or smaller than that of 1.3 μm optimized fiber at 1.55 μm wavelength.

4) MFD shall be equivalent to that of 1.3 μm optimized fiber at 1.55 μm wavelength from the viewpoint of splicing compatibility.

Table 1 Fiber Parameters of Pure Silica Core Single-Mode Fiber for 1.3 μm Use

Core diam. 2a	8.1 μm
Outer diam. D	125 μm
Δ	0.3 %
LP_{11} Cut-off wavelength	1.20μm
Mode field diam.	9.50μm

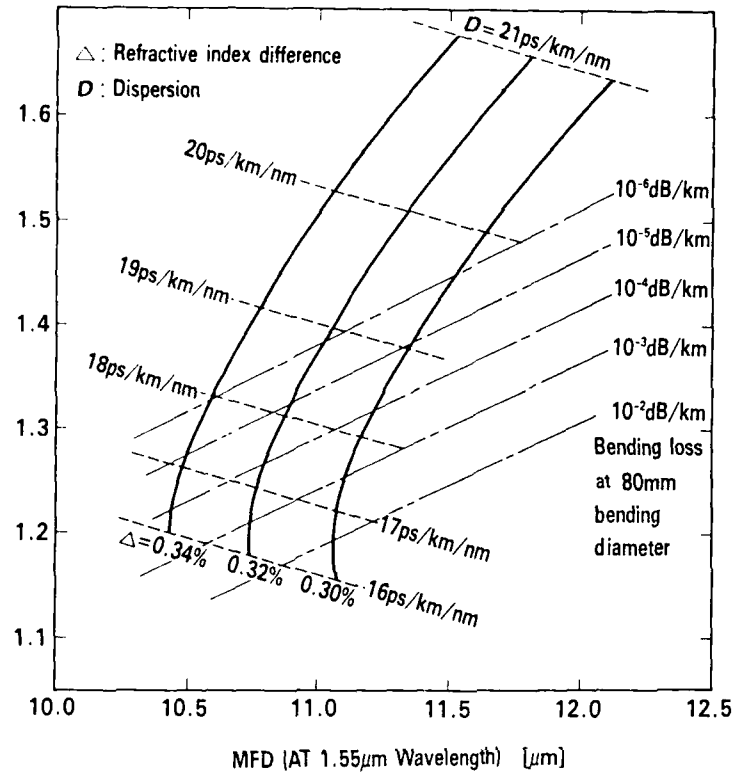


Figure 1 The Relationship among Refractive Index Difference, Cut-Off Wavelength, Mold Field Diameter, Bending Loss and Dispersion

3. Cable Construction

A trial OPGW was made to compare the performances of the three types of single-mode fibers. Figure 2 shows the construction of the trial OPGW. It had the conventional aluminum spacer construction and contains three six-fiber units (4) with three different types of fibers. The No.1 unit was composed of single-mode fibers with cut-off shifted pure silica core, the No.2 unit was composed of 1.3 μm optimized single-mode fibers with pure silica core and the No.3 unit contains 1.3 μm optimized single-mode fibers with a conventional germanium added core. Table 2 shows the typical fiber parameters. The cut-off shifted pure silica core single-mode fibers had a fluorine added cladding with a negative index difference Δ = 0.34 %, the effective cut-off wavelength λ_{ce} = 1.46 μm, the mode-field diameter MFD = 10.52 μm at 1.55 μm wavelength, and the diameter d = 125 μm. It was fabricated by the VAD method and the average transmission loss at 1.55 μm wavelength was 0.19 dB/km.

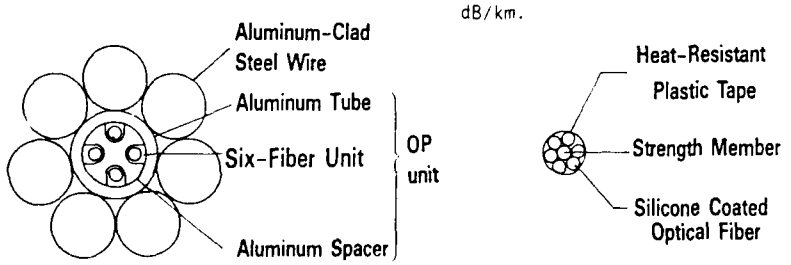


Figure 2 Construction of Trial OPGW and Six-Fiber Units

Table 2 Typical Fiber Parameters of Trial Cable

Unit No.	Transmission loss (dB/km)		Cut-off wavelength (μm)	Mode-field diameter (μm) at 1.55μm	Zero dispersion wavelength (μm)
	1.3μm	1.55μm			
1	——	0.19	1.46	10.52	1.28
2	0.34	0.19	1.27	9.87	1.29
3	0.37	0.25	1.20	10.23	1.32

Six single-mode optical fibers surround on FRP (Fiber Reinforced Plastic) strength member, and then are wrapped by a thin heat-resistant plastic tape. The outer diameter of this six-fiber unit was 1.25 mm. The six-fiber units were housed in helically grooved slots of aluminum spacer, which was then covered with an aluminum tube, this central portion is called an OP unit here. The OP unit was surrounded by aluminum-clad steel wires to form an OPGW.

4. Cabling

Throughout the cabling process, no transmission loss deterioration was observed for any one of the three different types of fibers. Figure 3 shows an example of transmission loss increase at 1.0 μm ~ 1.8 μm wavelength before and after the cabling process.

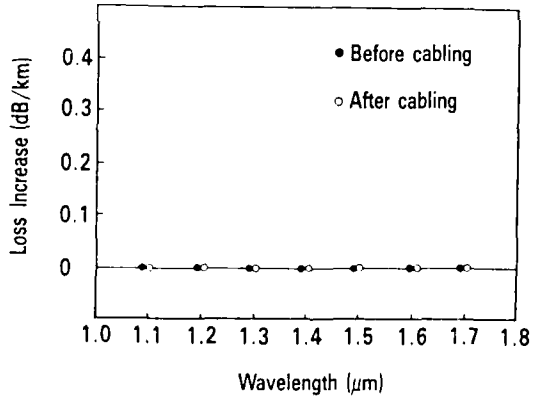


Figure 3 Transmission Loss Change during Cabling

5. Cable Performance

5-1 Fiber Unit Performance

(1) Bending Test

Each six-fiber [illegible]
around a mandrel [illegible]
[illegible]

fiber (No.3 unit).

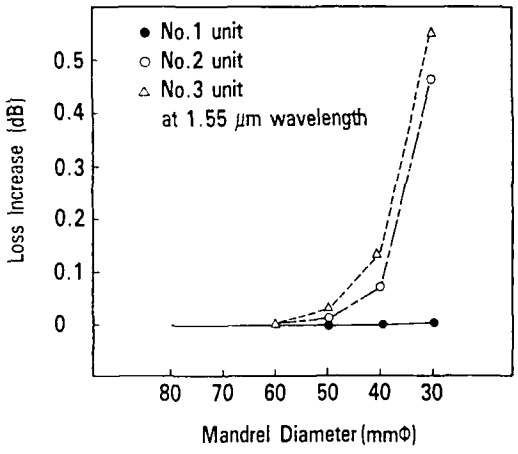
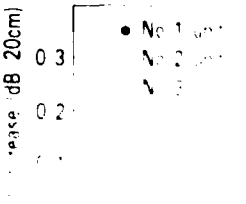


Figure 4 Bending Loss of Six-Fiber [illegible]

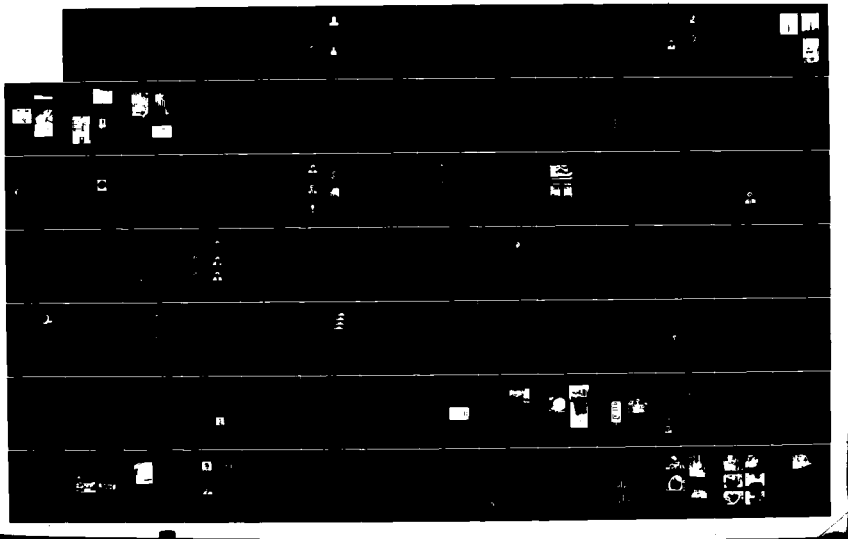
(2) Lateral Pressure Test

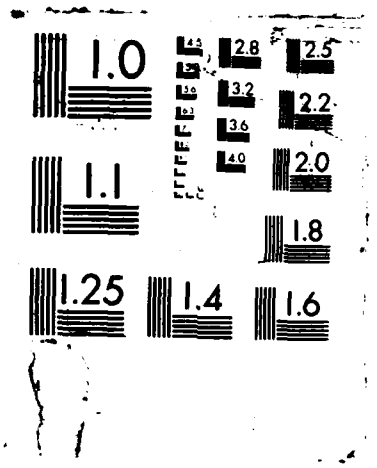
A lateral load was applied [illegible]
fiber unit by use of two [illegible]
shows transmission loss [illegible]
length against lateral [illegible]
six-fiber unit. It was [illegible]
shifted pure silica [illegible]
was the best.



AD-A189 610 PROCEEDINGS OF THE INTERNATIONAL WIRE AND CABLE SYMPOSIUM (36TH) HELD IN..(U) ARMY COMMUNICATIONS-ELECTRONICS COMMAND FORT MONMOUTH NJ 6/9

UNCLASSIFIED 19 NOV 87 F/G 9/1 NL




1.0
1.1
1.25
1.4
1.6
1.8
2.0
2.2
2.5
2.8
3.2
3.6
4.0

(3) Heat Shock Test

Figure 6 shows the transmission loss change at 1.55 μm wavelength of each six-fiber unit versus heat shock. The deterioration of transmission loss of cut-off shift pure silica fiber unit (No.1 unit) was the smallest and less than 0.05 dB/km up to 300 °C heat shock. The loss increase of 1.3 μm wavelength optimized pure silica core fiber unit (No.2 unit) was smaller than 1.3 μm optimized germanium added core fiber unit (No.3 unit).

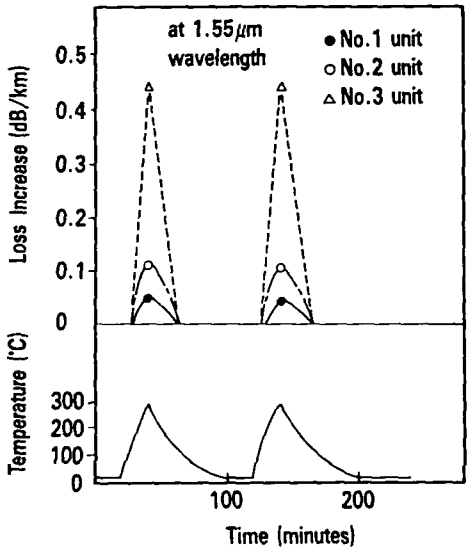


Figure 6 Transmission Loss Change of Six-Fiber Unit as a Result of Heat Shock (L=500m)

(4) Temperature Cycle Test

Figure 7 shows the maximum transmission loss change at 1.55 μm wavelength of each six-fiber unit for cyclic temperature. The temperature range was from -40 °C to 150 °C. The maximum deterioration of transmission loss of cut-off shifted pure silica core fiber was less than 0.05 dB/km over the temperature range from -40 °C to 150 °C.

(5) Continuous 150 °C Temperature Test

The transmission loss change of each six-fiber unit under long term high temperature condition was measured at 1.55 μm wavelength by the cut-back method. The 500 m six-fiber unit in bundle condition was placed in an oven.

Figure 8 shows the transmission loss change at 1.55 μm wavelength under continuous 150 °C temperature conditions. The maximum transmission loss change of the cut-off shift pure silica core fiber unit (No.1 unit) was less than 0.02 dB/km, which was almost within the range of the measurement error. No residual losses were observed for all fiber units when the temperature was returned to room temperature.

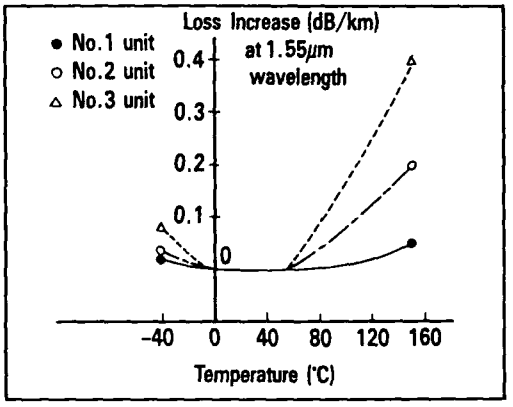


Figure 7 Temperature Dependence of Transmission Loss Change (L=500m)

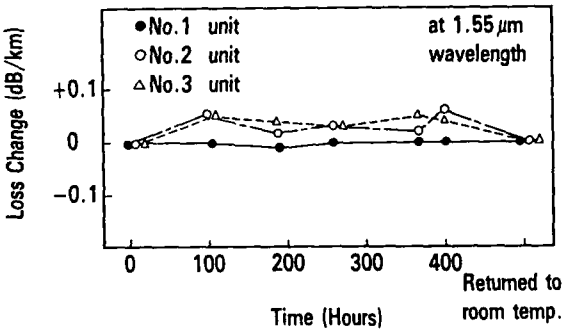


Figure 8 Transmission Loss Change of Six-Fiber Units under a Continuous High Temperature (150 °C)

From these investigations above, we confirmed that the cut-off shifted pure silica core fiber unit has the best mechanical and temperature characteristics for 1.55 μm wavelength operation. The 1.3 μm wavelength optimized pure silica core fiber unit is not as good but still usable at 1.55 μm wavelength.

5.2 Hydrogen Characteristics

To estimate the infre-red loss increase due to chemical reaction of hydrogen in the fiber, an OP unit shown in Figure 2(a) was exposed to a temperature of 200 °C for 170 hours. Figure 9 shows the loss change at 1.55 μm wavelength obtained by the heat treatment at 200 °C after 170 hours. No loss increase was observed for pure silica core fibers while 2.8 dB/km at 1.55 μm loss increase was observed for single-mode fiber with germanium added core. Pure silica core fibers have an advantage in terms of transmission loss stability as well.

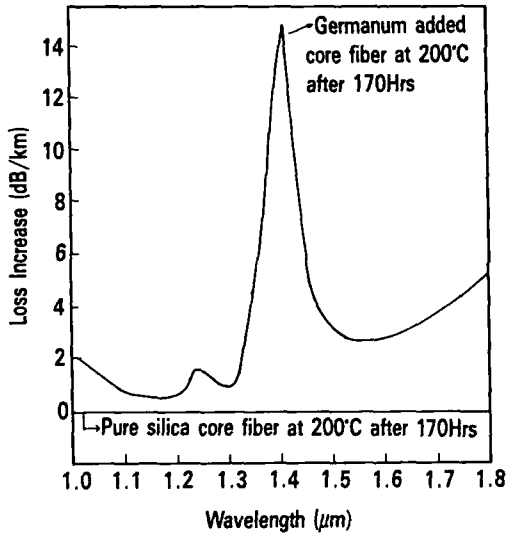


Figure 9 Heat Treatment Test of OP Unit

Even if germanium added core fibers are used, the hydrogen problem is not serious in 1.3 μm which are most popular now in OPGW network, because the effects of loss increase at 1.3 μm due to hydrogen is estimated to be very small (5). However, in the future 1.55 μm systems, the hydrogen problem is more important than in the 1.3 μm system, since the sensitivity of loss increase is several times larger at the 1.55 μm region.

If the cut-off shifted single-mode fiber is made up of germanium added core, the mechanical and temperature characteristics at 1.55 μm wavelength of this fiber may be as good as the cut-off shifted single-mode fiber with pure silica core, but the hydrogen-induced attenuation increase may be a problem in some circumstances. Therefore, the cut-off shifted fiber with a pure silica core is most suitable for OPGW for 1.55 μm wavelength use.

5.3 Test on OPGW

Various tests on the OPGW with cut-off shifted pure silica single-mdoe fibers for practical use were carried out such as a short-circuit test, an arc-discharge test, a crushing force test, a heat cycle test, a tensile load test, a vibration test, a twist test, a minimum bend test, a freezing test and a squeezing test. Table 3 shows these test results. It was confirmed the OPGW with cut-off shifted oure silica core single-mode fibers has as good characteristics at 1.55 μm wavelength as those of conventional OPGW at 1.3 μm wavelength.

6. Conclusion

An OPGW for 1.55 μm operation using cut-off shifted single-mode fiber has been developed, which has a very low and stable transmission loss and has excellent long term reliability. This will contribute to making the repeater span very long. The applicability of 1.3 μm optimized fiber at 1.55 μm operation was also investigated and the application may cause problems in long term reliability at 1.55 μm wavelength.

Table 3 Various Test of the OPGW for Practical Use

Test item	Test conditions OPGW: 80 mm²	Evaluation results (Loss increase at 1.55 μm)		
		No.1 unit	No.2 unit	No.3 unit
Short-circuit	Sample length: 8 m Fusion splicing: 2 fibers Alternating current: 14.8 KA Time: 0.34 second Stringing tension: 15 % UTS (1460 kg) OP unit temperature: 500 °C	0.00 dB	0.00 dB	0.00dB
Arc-discharge	Sample length: 4 m Fusion splicing: 2 fibers Discharge current: 5.9 KA to 9.5 KA Time: 115 ms Stringing tension: 15 % UTS (1460 kg)	0.00 dB	0.00 dB	0.00 dB
Crushing force	Plate width: 50 mm Fusion splicing: 2 fibers Crushing force: 1000 kg	0.00 dB	0.00 dB	0.00 dB
Heat cycle	Sample length: 20 m Fusion splicing: 2 fibers Stringing tension: 15 % UTS (1460 kg) Temperature range: From temperature to 150 °C x 100 cycles Holding time: 1 hour	0.00 dB	0.01 dB	0.03 dB
Tensile load	Sample length: 5 m Fusion splicing: 2 fibers Tensile load: until 100 % UTS (9770 kg)	0.00 dB	0.00 dB	0.00 dB
Vibration	Sample length: 30 m Fusion splicing: 2 fibers Stringing tension: 20 % UTS (1950 kg) Cycle: 40 Hz Amplitude: 10 mm Number of times: 10^7 times	0.01 dB	0.03 dB	0.05 dB
Twist	Sample length: 10 m Fusion splicing: 2 fibers Stringing tension: 20 % UTS (1950 kg) until 1 rotation/1m	0.01 dB	0.03 dB	0.04 dB
Minimum bend (OP unit)	Bending diameter (D): 40, 50, 100, 200, 300 mm Fusion splicing: 2 fibers Bending angle: 180°	0.00 dB until 40 mm	0.02 dB at 40 mm	0.03 dB at 40 mm
Freezing	Sample length: 10 m Fusion splicing: 2 fibers Flood time: 1 hour Freezing temperature: -24.3 °C Freezing times: 2 hours Sample is after squeezing	0.00 dB	0.00 dB	0.00 dB
Squeezing	Sample length: 10 m Fusion splicing: 2 fibers Stringing tension: 20 % UTS (1950 kg) Bending angle: 60° Pulley: 450 mm Round-Trip cycle: 20 cycles	0.00 dB	0.00 dB	0.00 dB

Measurement accuracy: ±0.01 dB

References

(1) K. Noguchi, N. Shibata, N. Uesugi and Y. Negishi, "Loss Increase for Optical Fibers Exposed to Hydrogen Atomosphere", J. Lightwave Technol., Vol.LT-3, pp. 236 ∿ 243, Apr. 1985.

(2) Y. Saito, M. Ishikawa, S. Kawabata and Y. Kitayama, "Improved Composite Fiber-Optic Overhead Ground Wire", Proc. of 33th I.W.C.S., 1984.

(3) Y. Suetsugu, H. Kanamori, K. Shimoda, S. Tanaka and S. Suzuki, "Design Consideration on Cut-off Wavelength Shifted Pure Silica Core Single Mode Fiber in 1.5 μm Wavelength Region", National Convention Record, 1987, IEICE of Japan, pp. 4 ∿ 266.

(4) K. Nakagaki, Y. Masuda, M. Ishikawa, Y. Kimura, I. Matsubara, Y. Kitayama and A. Ona, "Development of High-Performance Composite Fiber-Optic Overhead Ground Wire", Proc. of 35th I.W.C.S. 1986.

(5) H. Kanamori, H. Yokota, G. Tanaka, M. Watanabe Y. Ishiguro, I. Yoshida, T. Kakii, S. Itoh, Y. Asano and S. Tanaka, "Transmission Characteristics and Reliability of Pure-Silica-Core Single-Mode Fibers", J. Lightwave Technol., Vol.LT-4, pp. 1144 ∿ 1150, Aug. 1986.



Yoshinobu Kitayama

Sumitomo Electric Industries, Ltd.

1, Taya-cho, Sakae-ku, Yokohama, Japan

Yoshiyuki Kitayama received his M.S. degree in Electrical Engineering from Kyoto Univ. in 1982. He then joined Sumitomo Electric Industries and has been engaged in research and development of optical fiber and cables. Mr. Kitayama is a member of Communication R & D Department in Yokohama Research Laboratories, and a member of the Institute of Electronics & Communication Engineers of Japan.



Bang Lin

Sumitomo Electric Industries, Ltd.

1, Taya-cho, Sakae-ku, Yokohama, Japan

Bang Lin was born in Shanghai, China on August 21, 1958. He received his B.S. degree in Electrical Engineering from Chiba Univ. in 1986. He then joined Sumitomo Electric Industries and has been engaged in research and development of optical fiber and cables. Mr. Lin is a member of Communication R & D Department in Yokohama Research Laboratories, and a member of the Institute of Electronics & Communication Engineers of Japan.



Yuichi Masuda

Sumitomo Electric Industries, Ltd.

1, Taya-cho, Sakae-ku, Yokohama, Japan

Yuichi Masuda received his M.S. degree in Electrical Engineering from Kyoto Univ. in 1970. He then joined Sumitomo Electric Industries and has been engaged in development and sales of optical fiber and cables. Mr. Masuda is now a chief research associate of Yokohama Research laboratories, and a member of the Institute of Electronics & Communication Engineers of Japan.

OPTICAL FIBER GROUND WIRE

G. Bianchi and D. Rota
Societa Cavi Pirelli, Milan, Italy

M. Rahman
Pirelli Cable Corp., Lexington, S.C.

1. SUMMARY

Overhead Ground Wire containing optical fibres (OPGW) has recently experimented a rapid growth all around the world. This paper describes the design criteria, development, accessories, installation methods and various specific tests applied to OPGW.

2. INTRODUCTION

Optical fibre cables are now used on a large scale in telecommunication networks. Because of their high information capability, optical fibres can meet present and future Power Utilities telecommunication needs. OPGW is a transmission media that many Utilities around the world have already adopted or taken into serious consideration.
The reason for this choice is based on the following factors:

- High transmission capability, complete immunity to electromagnetic phenomena and longer lengths between repeaters
- Utilization of existing structures (power lines) and right of ways, therefore reducing the installation costs
- Supply other users (i.e. Telecommunication Companies) with an economical cable laying alternative in areas of difficult ground conditions (i.e. mountains)

3. DESIGN CRITERIA

Presently, there are no international standards for OPGW, however Working Groups of IEEE and ASTM are addressing the matter. The OPGW design depends on the requirements of each specific installation the Utility is planning.
It is however important for the OPGW, to have mechanical and electrical characteristics equivalent to those of a standard ground wire, but the design constraints may be tougher if the cable is to be placed on existing towers than if it is a completely new line.

Such characteristics are related to:

- tensile strength
- stiffness (EA), which influences sag and tension conditions
- conductivity to carry the short circuit current, without exceeding the maximum temperatures admissible for the materials.

The correct design of OPGW is achieved by balancing the mechanical and electrical characteristics within the limits imposed by diameter and weight. The optical fibre incorporated in the ground wire must maintain its own transmission characteristics under all service conditions.

3.1 Optical core

The optical core is designed with the aim of having high reliability through the service life which is required to be the same as standard ground wire. This aim is best achieved by using the loose type construction. This type allows the fibre to move radially inside a tube or a groove to compensate any change of length of the OPGW. Therefore the fibres are never stressed even for the maximum OPGW elongation which occurs for the worst overload or during short circuit. The absence of mechanical stresses on the fibre is an outstanding characteristic of the loose structure which makes it particularly suitable for the application in question.
This characteristic is not shared by the tight construction, where the optical fibres are continuously under mechanical stress.
The core generally consists of four plastic tubes stranded around a dielectric central strength member. The tube diameter and thickness depend on the number of fibres to be allocated. Each tube generally contains 1 to 6 fibres. Design with higher fibre count, e.g. 50, is feasible.
The number and the type of fibre depends on:

- the transmission capacity required (e.g. number of channels)
- the distance between the repeaters.

Fibres used in the telecommunication field are multimode or singlemode. The singlemode fibre is used when a long repeater distance and high capacity is required. This is achieved through intrinsic performance of the fibre which in practice has no limitation of bandwidth and has very low attenuation. For particular transmission needs (short distances and low number of channels) the use of multimode fibre may be economically advantageous due to the lower cost of electronic equipment.
Table 1 shows data related to the type of fibre.
Table 2 represents typical system length between repeaters.

The optical core being completely dielectric, is immune to the effects of overvoltage due to lightning and short circuit. The core is also completely filled with a special grease to protect against moisture and hydrogen contamination.

3.2 Aluminum tube and metallic wires

The seamless aluminum sheath, obtained by extrusion, provides an absolutely hermetic and mechanically strong protection for the optical core and necessary support for the surrounding wires. It also heavily contributes to the electrical conductivity of the OPGW. The surrounding wires, depending on the required mechanical and electrical characteristics, can be stranded in one or two layers. The materials of the wires are the same as the conductor material used on the standard ground wire (aluminum alloy, galvanized steel, aluminum clad steel) and are in compliance with the same specifications.

4. EFFECTS OF HYDROGEN

The effects of hydrogen on the fibre optical characteristics is now fairly well known and need to be controlled (1) (2).

The effects are related to:

- Light absorption by the hydrogen molecule diffused in the fibre. This phenomenon is reversible and it is a function of the temperature and relative pressure. It is present both at 1300 nm and more accentuated at 1550 nm.
- Formation of hydroxide (OH). This phenomenon is irreversible. The chemical elements of the fibre (for example the presence of P2O5) are responsible for this effect. Generally, the singlemode fibre is less affected than the multimode fibers, because of different dopant content.
- Center of color. This interferes with the entire frequency spectrum in which the fibre operates and is heavily affected by temperature. It is essentially due to the hydrogen interaction with the glass causing irregularity on the structure.

The hydrogen which is present in the cable, either dissolved in constituent materials and released over the time or generated by chemical reaction during manufacture or service life, will build up partial pressures affecting the optical transmission. OPGW, which is subjected to higher temperature than typical direct burial cables used for telecommunication, is particular sensitive to the hydrogen effects.
Consequently, it is necessary to:

- use an optical fibre with low sensitivity to hydrogen attack
- choose materials with low hydrogen content
- use an extruded or soldered sheath that eliminates the humidity responsible for superficial oxidation phenomenon.

However, none of the above elements will protect the fibres against hydrogen in the long run. A complete immunity can be obtained by applying a special filling compound (Hydroget) that acts as an irreversible chemical absorbant to hydrogen. The absorption capacity of this type of material is independent of temperature and relative pressure. Figure 2 shows the attenuation spectrum of optical fiber cable with and without the hydrogen absorber filling compound during the accelerated ageing test at 70 C for 10 days.

5. SPECIFIC TESTS ON OPGW

The OPGW is tested in laboratory with the aim of establishing its characteristics and performances under the conditions it will be subjected both during installation and service. The main tests are the following:

5.1 Tensile Test
The test is carried out:

a) to determine the stress/strain characteristic of the composite cable;
b) to measure the attenuation and the elongation of the fibre.

The test is carried out by using a cable sample of about 60 m. The optical core is restricted to move along the aluminum tube by means of suitable clamp connecting the tube and the central strength member of the optical core. This connection is always used for all the different tests which are performed on the OPGW when a tension is applied and optical performance on fibres is measured.
The tensile test is generally performed using the same dead ends that will be utilized in the field (Fig. 3).
To obtain a longer fibre sample, the fibres are spliced together by fusion technique. As tension is applied to the cable sample, the fibre elongation and attenuation are monitored to detect changes, if any.
Figure 4 shows a typical stress/strain relationship of OPGW. Tests did not show any increase in attenuation nor a significant fiber elongation.

5.2 Breaking Load Test

This test is carried out on a cable sample of 5 to 10 meters, according to the normal procedure used for the standard conductors without optical fibres.

5.3 Creep Test

The objective of this test is to determine the increment on the sample length vs. time by applying a constant tension and temperature. The increment on the length and consequently the increase in sag will be taken into account for sagging. The test is carried out according to the procedure stated for the standard conductor (3) with a test temperature between 21 C and 27 C for a duration of 1000 hours.

5.4 Lightning Simulation Test

This test is to determine the effect caused by lightning on the OPGW. The test is carried out on a sample under the required stress (Fig. 5). An electric arc is generated between the conductor and a graphite electrode placed at a distance of approx. 10 mm. The optical fibres, spliced in series, are monitored continuously for any variation in transmitted power.
The impulse current wave normally used for this test is similar to the test on "Heavy Duty Surge Arresters" (4): 100 kA for 4-6/10-15 microseconds.
Oscillating current has also been applied with a peak value of about 200 kA with a duration of about 1250 micro seconds (Fig. 6) which simulates a much higher electric discharge.
The test shows that the discharge on the OPGW has no influence on attenuation of the fiber nor the mechanical integrity of the OPGW (Fig. 7).

5.5 Short Circuit Simulation Test

This test is to verify the behaviour of the OPGW, especially the optical core, during the short circuit between phase and earth.
In this situation the cable will carry a high current for a short time which main effect is the sudden heating of OPGW.
The test is carried out using approx. 30-50 m sample (Fig. 8). The sample is under stress at all times during the test, in particular during the application of the short circuit current, by means of a pulley-load system.
The optical fibres, spliced in series, are monitored constantly for any variation in transmitted power. Some thermocouples are inserted between the wires of the cable in order to compare the temperature rise with the theoretical results. Figure 9 shows the test results obtained on the OPGW.

5.6 Vibration Test

One of the main effects of the wind on an aerial cable is the vibration resulting from vortex shedding. The test simulating this effect serves two objectives:

a) to determine the self-damping coefficient

b) to verify the capacity of all cable components to resist the fatigue.

By knowing the self-damping coefficient, the level of deformation caused by the wind can be calculated by using mathematical models. The methodology is the same as for the standard conductor test. The OPGW is tested under tension corresponding to "every day stress" and it is placed in resonance by an electro-dynamic vibrator (Fig. 10). The measurement of self-damping coefficient is done by varying both the frequency and the amplitude of vibration (5). The fatigue test, at constant frequency, is carried out imposing a deformation at the maximum stress point. At the beginning, during and at the end of the test, the attenuation of the fiber

is measured. The result obtained shows that both the self-damping coefficient and the fatigue resistance are equivalent to similar standard conductor (6). Regarding the fatigue resistance test, two types of OPGW, one with a single wire layer and the other with a double wire layer, were tested. Each OPGW were subjected to 10 million cycles with 300 microstrain (peak to peak) of deformation plus 20 million cycles with 600 microstrain (peak to peak). The cable components did not show any defect nor changes of fibre attenuation.

Repeated bending test on suspension

This test is to verify that OPGW resists the repeated flexures occurring on the suspension as a consequence of daily thermal cycles. The OPGW sample is tensioned on the suspension at the every day stress. The change of the bending angle is given at a frequency of 5 ÷ 10 cycles per minute. Samples of both single and double layers OPGW have been tested with different types of suspensions.
Tests carried out up to ten times the number of cycles expected during the OPGW life and angle change of 2 ÷ 3 degrees have not shown any defect both on the metallic components and on the optical core.

6. ACCESSORIES

6.1 Hardware

The hardware for the OPGW are designed to guarantee the same mechanical performance as for the standard conductor and to ensure a perfect functioning of the optical core. The hardware performance is verified with the same procedures already established for the standard conductors. The effect of the hardware on the cable optical performance is also verified. In addition to the bolted type hardware described below, the "preformed" type is also currently used.

a) Bolted Type Strain Clamp (Dead End)

The clamp is designed to attain a "slip" strength greater than 90% of the rated breaking strength of the OPGW. The main parameters to obtain the required performance are a particular manufacturing process of the body, a suitable clamp length and the use of different materials from the ones used for standard clamps.

b) Bolted Type Suspension

The form and the performance are the same as for the standard application; normally, a slip strength of 20% of the nominal rated breaking strength of the OPGW is required. Figure 11 shows a recent development of a suspension clamp that is inserted at the pole top. The central part of this clamp is rectilinear and it is the same as the strain clamp except for the length.

c) Damper

The conventional stockbridge damper is used with the clamp adapted to the OPGW size. The characteristics, position and number are established utilizing the same mathematical model used for the standard conductors (7).

d) Holding Clamps

The clamps for holding the OPGW to the tower as it descends to the splicing box are made to be attached to the tower without any need to make holes in it. The clamps used are suitable for a wide range of tower angle dimensions. The OPGW can be fixed either internally or externally to the tower.

6.2 Optical Splicing Box

The box contains the spliced fibres and the necessary extra length of optical fiber (Fig. 12). The box is waterproof: a perfect seal for the incoming OPGW is made by using a rubber gasket applied over the aluminum tube. The box is supported on a frame that is fixed to the tower angle by means of clamps without any need to make holes in the tower.

7. INSTALLATION

7.1 Stringing

The equipment and the method used for stringing the OPGW are the same as for standard conductors. In the laboratory, the stringing test is carried out by simulating the stress, such as passing through the tensioner and a pulley using the set up shown in Fig. 13. Tests carried out so far confirm field experience. The diameter of the tensioner is in the 1200 - 1500 mm range and pulleys of 600 - 800 mm diameter are suitable to meet any combination of main stringing parameters (i.e. pulling tension, number of passages and bending angle on pulleys).

"Self-gripping come along clamp" with changeable liners may be adopted by using suitable materials and shape for the liners.

A special device is used for stringing the single layer type OPGW to avoid twisting. This device (Fig. 14) is made by a counterweight dimensioned to pass through the pulleys.
Normally it is preferred to pull a length at a time because it is easier to handle the surplus of OPGW needed for the drop along the tower down to the splice box but, if necessary, two or more lengths of OPGW may be pulled in series.

7.2 Splicing

Splices are always made at a tower, normally near its base, so it is possible to carry out the splicing of the OPGW independently from the other works on the overhead line therefore reducing installation time.
The distance between two consecutive splices can usually go up to 4 km.
The splicing operation can be carried out basically in two ways:

1) by performing it at the ground level, on a van situated at the tower base. The splicing box is then raised and fixed to its final position

2) by performing it at the box final height (3 to 8 meters above ground), using a platform protected against environmental hazards. The platform can be supported by a tubular structure, raised externally by a lift or raised and supported internally by rope and tackle hooked to the tower (Fig. 15).

The splicing of the fiber is carried out by means of fusion. Each splice is protected by means of a heat shrinkable sleeve which is inserted in a groove of the organizer. The attenuation of each splice is measured before closing the splice box to verify its required performance. At the end of the installation, the attenuation measurement is carried out by means of cut back method on the complete length.

8. INSTALLATIONS CARRIED OUT

Five years ago Pirelli supplied its first OPGW links to ENEL (Italian State Power Board) in connection with the TESEO Project (Italian acrostic for Telstransmission of Electro - Optical Signals via Electrical Line) (8) (9) (10) (11).

Since then Pirelli has supplied several hundred kilometers of OPGW in Brazil, the Middle East, North America (12), Spain and Italy.

9. CONCLUSION

The concept of combining the power transmission line with a very high capacity telecommunication line is having considerable success all around the world. This has been made possible because of the development of ground wire containing optical fibers. Optimized mechanical and optical properties, the flexibility and expandibility of the system have allowed the OPGW to be part of many Power Utilities projects and open the door to new ventures between Power and Telecommunication Utilities.

Thanks

The authors thank Società Cavi Pirelli for giving permission to publish this paper.

Thanks are also due to ENEL, CESI, SERVOCAVI, SALVI, for allowing publication of the photos related to installation and accessories.

Bibliography

1. P. Anelli et alii
Overcoming the hydrogen problem in optical fibers
I.W.C.S. Cherry Hills - 1985

2. P. Anelli et alii
Investigation on hydrogen induced effects on optical cables and possible countermeasures
ECOC - 1985

3. The aluminium association - A method of stress-strain - Testing of aluminium conductor and ASCR and a test method for determining the long tim tensile creep of aluminium conductors in overhead lines

4. IEEE C 62.1 - 1984
Revision of ANSI/IEEE C 62.1 - 1981
IEEE standard for surge arresters for AC power circuits

5. CIGRE, Study Committee No. 22
Guide on conductor self damping measurements (Electra No. 62, 1979)

6. CIGRE, Comité d'Etudes 22-GT04
Recommendations pour l'évaluation de la longevité des conducteurs de lignes de transport aeriennes (Electra No. 63, Mars 1979)

7. G. Diana et alii:
A method to define the efficiency of damping devices for single and bundled conductors of EHV and UHV lines
IEEE/PES 1986 Winter Meeting

8. Fibres optiques, technologie et applications pour les compagnies d'electricite (Electra No. 107, 1986)

9. G. Bianchi et alii:
Cavi ottici contenuti entro la fune di guardia delle linee per trasporto di energia elettrica
AEI Cagliari 1983 - B.20

10. G. Bianchi et alii:
Composite optical earthwire cables for power overhead line
Copimera - Buenos Aires - 1983

11. G. Bianchi et alii:
Technical and economic analysis of various solutions for optical fibre telecommunications systems on EHV power lines
CIGRE Meeting - Munich - 1985

12. M.W. Conroy et alii:
Integration of SCADA and line protection for 138 kV transmission line using a fibre optic network
IEEE/PES - Anaheim - 1986



Giuseppe Bianchi graduated from Bologna University in 1967 with a degree in Electrical Engineering. He joined the Applied Mathematics Section of the Societa Cavi Pirelli's R&D labs in 1970. Since 1974 he was in charge of the Applied Mathematics Sections. In addition, from 1978 to 1982 he was responsible for the Mechanical Section, devoting his activity mainly to mechanical tests on submarine power cables and relevant accessories. From 1982 to 1985 he was in charge of the Mathematical, Physical and Chemical Centre. Presently his activity is devoted to research and development of optical ground wires.



Dimenico Rota was born in Turin in 1949. He graduated in Electrical Engineering at Politecnico of Turin in 1973. He joined Alfacavi (cable firm now belonging to Pirelli Group) in 1976 where he was involved in the Power and Telephone Design Department. He joined Societa Cavi Pirelli in 1983 where he has been involved in Telecommunication Design activity with particular reference to the field of optical telecommunication cables. At present he is OPGW Product Manger for Pirelli Group worldwide.



Mujib M. Rahman received his Bachelor of Engineering from Bangledesh and Dipl.-Ing. from West Germany. He has worked in West Germany, Austria, Canada and the U.S.A. since 1968 in power, telecommunications and fiber optic cable R, D & E. At present he is responsible for all communications cables R, D & E for Pirelli Cable in U.S.A. and Canada.

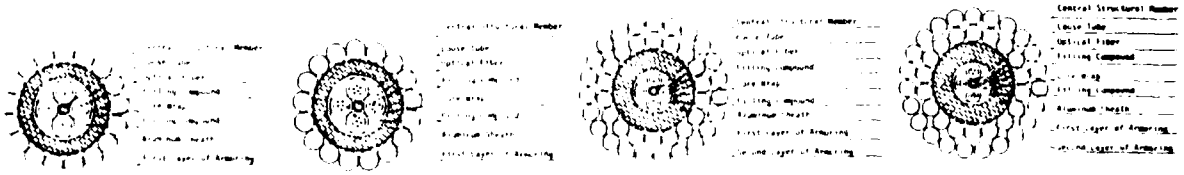
TABLE 1
OPTICAL FIBER CHARACTERISTICS

	ATTENUATION AT 850nm dB/km	ATTEN. AT 1300nm dB/km	ATTEN. AT 1550nm dB/km	NUMERICAL APERTURE	BANDWIDTH AT 1300nm MHz.km	DISPERSION AT 1300nm ps/(nm.km)
Multimode 50/125 micron	2.6	0.7	---	0.2	1000/1200	6
Single Mode 10/125 micron	---	0.4	0.25	---	---	3.5

TABLE 2
BIT RATE VS. REPEATER LENGTH

TYPE OF FIBER	Mbit/s	NO. OF TELEPHONE LINES	REPEATER LENGTH (km)
Multimode	2	30	40
Multimode	8	120	30
Single Mode	2/8	30/120	60
Single Mode	34	480	55
Single Mode	140	1920	45

TABLE 3
CHARACTERISTICS OF COMMONLY USED OPGW



Type A | Type B | Type C | Type D

TYPE OF OPGW		A	B	C	D
Outside Diameter	mm	13.8	14.7	17.9	21.6
No. of Fiber		4	24	4	12
Protection for F.O. Core					
- Material		AL	AL	AL	AL
- Thickness	mm	1.6	1.5	2	2.8
Armoring					
- I layer of wires	no x mm	15x2.34 ACS	17x2.25 ACS	18x2 ac.zin	18x2.45 ACS
- II layer of wires	no x mm	---	---	23x2 legaAL	23x2.45 ACS
Weight	kg/m	0.57	0.6	0.83	1.56
Breaking Load	kN	79	83	107	233
Modulus of elasticity	kN/mm2	104	104	85	113
Stiffness	kN	10730	11250	15420	30850
Coefficient of thermal expansion	1/ C	$14.8.10^{-6}$	$14.8.10^{-6}$	$16.7.10^{-6}$	$14.2.10^{-6}$
Electrical Resistance in c.c. at 20 C	ohm/km	0.5	0.5	0.3	0.2
Max. current for a					
- duration of 0.5 sec	kA	11	11	19.8	31.6
- equivalent I^2t	$kA^2.sec$	60	60	196	500

ACS = Aluminum Clad Steel

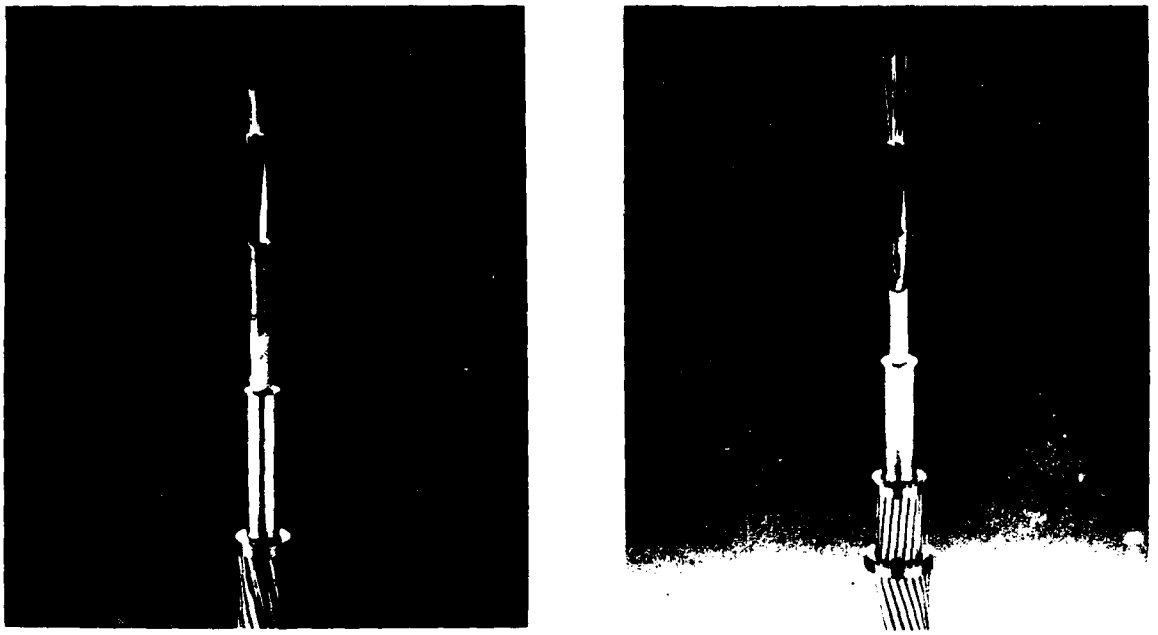


Fig. 1
Optical Overhead Ground Wire
Single and Double Layer 4 to 12 Fiber

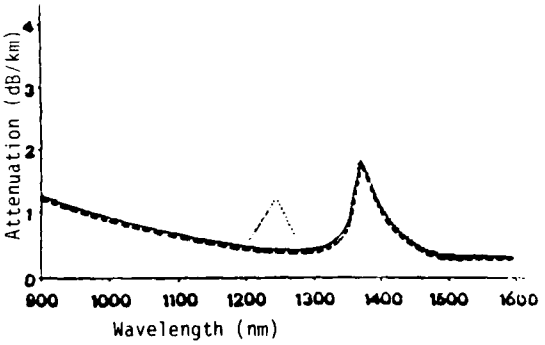


Fig. 2
Spectral Attenuation Single Mode Fiber
With (——) & Without (...) Chemical Absorption
of Hydrogen
Dashed line represents initial value.



Fig. 3
Tensile Load Machine

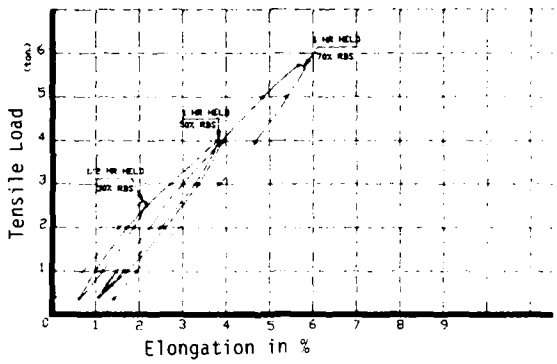


Fig. 4
Tensile Load vs Elongation for
OPGW, O.D. = 13.8mm



Fig. 7
Effect of Lightning Simulation With
Oscillating Wave Form
I = 210KA, F = 16.5KHz at 1250 micro seconds



Fig. 5
Lightning Simulation Test in
CESI Laboratory in Milan

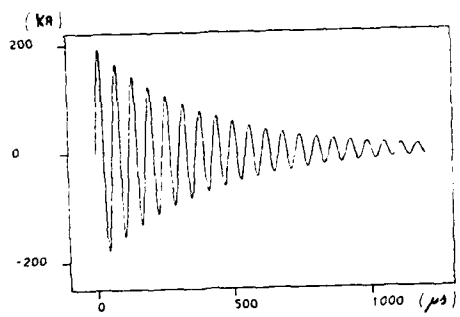


Fig. 6
Oscillating Wave Form for
Lightning Simulation Test.

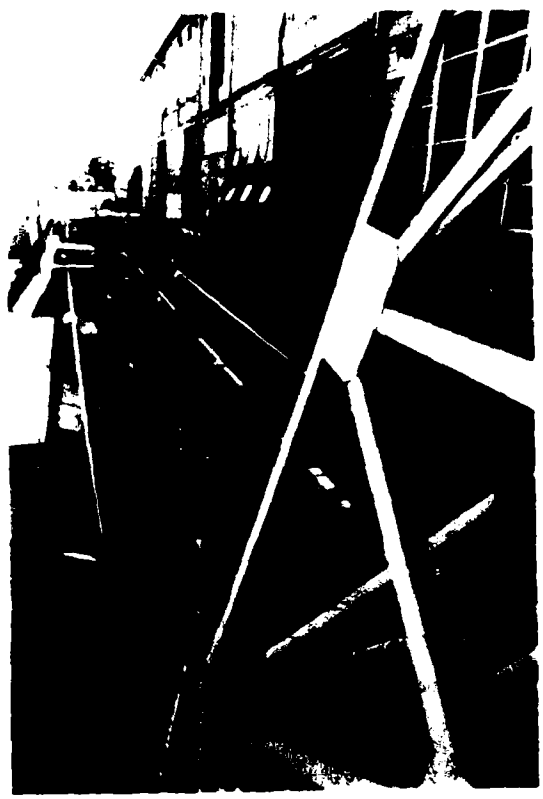


Fig. 8
Short Circuit Test in
CESI Laboratory in Milan

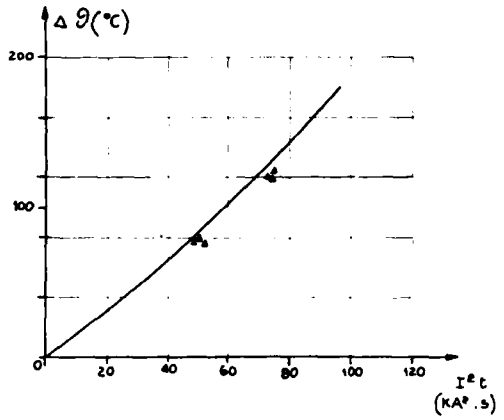


Fig. 9
Increase in temperature on 13.8mm OPGW as short circuit current is applied and comparison with calculated values.



Fig. 11
Suspension Clamp

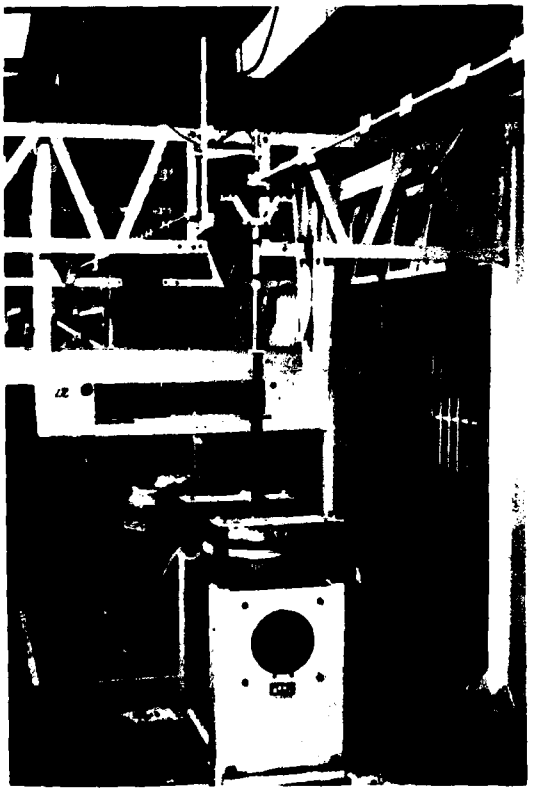


Fig. 10
Detail of Vibration Test Set-Up

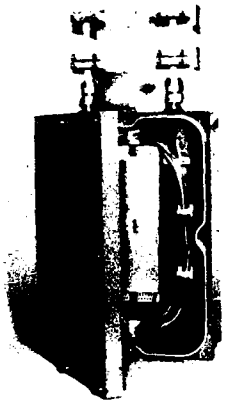


Fig. 12
Optical Fiber Joint Box



Fig. 13
Simulation of Installation Stress
in the Laboratory

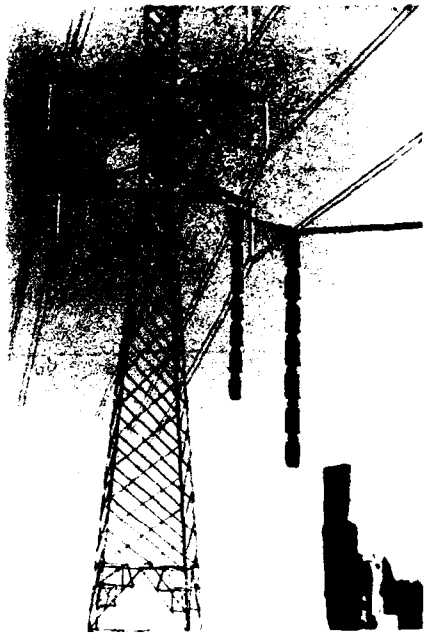


Fig. 14
Anti-torsional device for
single layer armored OPGW

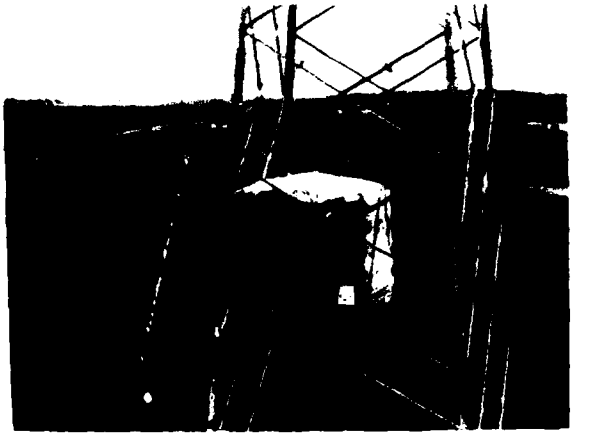


Fig. 15
Su , ended Platform
for J inting Operations

A Global Test Method for Long Term Stability of Solid and Foam Skin Insulation

Lawrence E. Davis

Superior Cable Corporation

Abstract

The stability of polyethylene insulation has traditionally been evaluated by test methods which primarily determine oxidative resistance at elevated temperatures which exceed material transition ranges. Additional degradation processes can cause polyethylene to fail in field applications. A test method has been developed which simulates worse case installation of filled cable and addresses failure for polyethylene insulation without exceeding material transition temperature.

Foam skin insulation, when evaluated with the new procedure, has been found to crack from mechanisms other than oxidation and to have a life prediction as short as ten years in the hotter regions of the country. The predicted failures have been substantiated by field reports of foam skin failure.

The new test method evaluated material for oxidative stability, thermal embrittlement, environmental stress cracking (due to the presence of filling compound), and extraction of antioxidants by filling compound. This procedure can be used to screen new materials, for obtaining improved performance of foam skin insulation and for quality control.

Introduction

High-density polyethylene may be degraded by several mechanisms: thermal embrittlement, oxidation, environmental stress cracking, solvent cracking, electromechanical stress cracking, and ultraviolet light exposure. Present methods of determining long term stability of high-density polyethylene concentrate on oxidative degradation. However, foam skin insulation, due to the expanded form, is more susceptible to additional modes than solid insulation. A test method for evaluation of cellular insulation which, including all of the major failure paths, has been developed and is presented below. The new procedure successfully predicts foam skin field failures and may be employed to screen new materials which may be used to improve life expectancy of cellular insulation in communications cables.

Failure Mechanisms

Crack initiation and propagation in polyethylene is a complex process which is often misinterpreted. There are several mechanisms by which crack growth can occur and it is necessary to understand the cause of each failure mode so that the data obtained can be properly interpreted. Each of the failure mechanisms may occur alone or in combination, further complicating the analysis of polyethylene failure without careful review of the material's properties, test conditions, and failure data. Also to determine the test conditions required to evaluate potential failure paths, it is necessary to understand the failure mechanisms involved in polyethylene process.

Thermal Embrittlement

Thermal embrittlement is a mechanism in which an applied strain results in an elastic dislocation of crystallites from their lower energy spherelitic arrangement into an adjacent higher energy arrangement. The elastic forces of restoration overcome the viscous drag component leaving points of inherent weakness in the growth structure leading to eventual brittle failure. This mechanism is a temperature/time dependent reaction which is purely thermal in nature. Because thermal embrittlement involves only the arrangement of the molecules within a part, it can be reversed by appropriate heat treating. The rearrangement of the molecular structure in the crystal orientation will occur at the same rate regardless of the presence of oxygen or various flow rates of air past the sample. The effect of thermal embrittlement is to reduce the strength of the materials and to decrease elongation properties. Crack growth resulting from thermal embrittlement is initiated within the body of the material. The crack flow path through and around spherelites depends on which route offers least resistance. Thermal embrittlement will occur without applied stress in the material, but the presence of stress will promote thermal stress crack growth.

Oxidation

Oxidation is the chemical interaction of oxygen with the polyethylene, resulting in chain scission and gellation, which leads to brittle failure. The oxidation process is a rate reaction which is temperature dependent and may also be affected by air movement about the sample. The chemical structure of the polymer is altered, leading to reduced strength, lower elongation, and brittle failure. The presence of applied stress is not required in order to induce oxidative crack failure.

Environmantal Stress Crack

Environmental stress cracking is highly dependent upon the physical state of the polymer and requires a contact medium. In an environmental stress crack condition, there appears to be an alteration of the intermolecular forces in the polyethylene as a result of contact with the stress crack medium. This allows the molecules to seperate where the stress crack medium is in contact with the polyethylene. As a result, crack propagation is initiated at the surface of the sample. The flow of the stress crack agent into flaws on the surface concentrates the applied stress in the flaw resulting in destructive cracking. This type of crack growth does not alter the physical properties of the material except in the vicinity of the crack. The tensile and elongation properties of the insulation therefore are not affected. Microscopically, the crack surface would appear as a brittle fracture. Under

a higher magnification some localized yielding may be evident. The presence of polyaxial stress in the polymer results in a greater susceptibility of polyethylene to environmental stress cracking. Since surface flaws may provide the initiation sites for crack growth, heat polishing of the surface reduces the susceptibility of the material to environmental stress cracking. No physical changes other than crack propagation will be evident in environmental stress crack failure.

Solvent Cracking

Solvent cracking is closely associated with environmental stress cracking. Unlike environmental stress cracking however, solvent cracking agents will affect other physical properties of the material such as swelling of the insulation or plasticizing of the material. Due to the plasticizing action of the solvent, the fractured surfaces will be ductile in nature and will, therefore, exhibit fibral formation along the crack surface. Solvent cracks initiated in the polymer will start at the surface of the material. The presence of polyaxial stress in the sample is not required for solvent cracking to occur; however, the presence of polyaxial stress does promote the formation of solvent cracks in polyethylene.

Electromechanical Stress Cracking

Electromechanical stress cracking is a specialized type of oxidative stress cracking in the insulation of electrical conductors operating under mechanical as well as electrical stress in high voltage alternating fields. Both mechanical stress and corona conditions are essential to initiate failure through this mechanism. Ozone formed by the electrical discharge produces rapid oxidative failure of the stressed but not the unstressed polyethylene. Since high voltage applications are not present in communications cable, this mechanism can be ruled out as a contributing factor in the cracking of the foam skin insulation.

Ultraviolet light Exposure

Polyethylene, when exposed to ultraviolet light (UV), absorbs the energy of the light, exciting the bonds between the atoms. If this energy is not rapidly dissipated, it will break chemical bonds in the polymer's molecular chains. The rupture of chemical bonds fragment the chains, thus reducing the molecular weight and creating free radicals which further attack the remaining chains. As a result, the polymer loses its physical properties and becomes brittle and discolored. The rate of UV degradation is accelerated by increasing exposure time to UV, increasing UV intensity, and increasing the temperature of the polymer.

Insulated wire is protected by the cable sheath or protective closure (pedestal, ready-access closure, splice case, etc.) and therefore should not be significantly affected by UV. Since exposure of the insulated conductor to light is limited, degradation caused by UV should not be of general concern.

Test Design

Current cable specification procedures primarily evaluate stability to insure life expectancy. Present tests include oxidative induction time (thermal oxidative stability quality control tests), weight change during aging, and heat aging in pedestals (thermal oxidative stability qualification tests) as a measure of oxidative stability. The narrow scope of these procedures are valid since the insulated conductors are exposed to the environment in pedestals. Due to consumption of antioxidants during the foaming process and leaching of antioxidants by filling compounds, any cellular insulation will be susceptible to oxidative deterioration. The new test method must include exposure of the foam skin insulation to air at elevated temperatures to insure proper protection relative to this failure mode. See companion paper "Performance of High Density Polyethylene Insulation Antioxidant in Filled Telephone Cable Applications".

The foam manufacturing process also incorporates stresses into cellular insulation which are not present in solid insulation. Material is expanded radially as well as longitudinally and thus will be more susceptible to environmental stress cracking since it contains polyaxial stresses not found in solid extruded material. Therefore, a procedure for evaluating cellular insulation found in contact with filling compounds should investigate the possibility of environmental stress cracking. To accomplish this, insulated conductors can be wrapped around themselves (formed into "pigtails") after exposure to filling compound. The filling compound would remain, to some degree, in contact with the insulated wire.

The higher stress levels in cellular polyethylene will cause the material to be more susceptible to thermal embrittlement than the same polyethylene compound utilized in solid insulation. Therefore a method of investigating thermal embrittlement needs to be incorporated into any new evaluation method. In addition, thermal embrittlement incorporates changes in the molecular structure over time increasing the susceptibility of the insulation to stress crack failure. The insulation must be investigated for thermal embrittlement after some initial exposure to elevated temperature. This time frame should be consistent with the possible need to rework splices or pedestal connections which would occur in the field.

The ability of commercially available filling compounds to extract stabilizers, plasticize polyethylene, and cause swelling of the material suggests the need to include a method for observing solvent cracking into a long-term stability test program for foam skin material. This can be accomplished by exposing the foam skin cables to elevated temperatures prior to removing the insulation test samples from the cable. Foam skin is primarily used underground, and once installed, would tend to maintain a relatively constant and moderate temperature. The exposure time therefore should be consistent with possible exposure of the filled cable to elevated temperatures prior to installation.

Temperatures selected for evaluation of any insulating material should be maintained at levels which would not alter the molecular structure or properties of the material. If test temperatures are selected which exceed transitional levels which would not be encountered in the field, the test data becomes very suspect as to the primary field failure modes. Such results would be quite difficult to correlate to field conditions since the rate of deterioration of any given mechanism could be altered.

The construction of foam skin insulation contains higher stress levels, polyaxial stresses, and less mass of material in contact with the solvating agent (filling compound). It is potentially degraded to a greater extent than solid insulation by failure modes other than oxidation. In addition, the four potential failure mechanisms may act with synergistic effects to accelerate failure faster than would otherwise be encountered by a single mechanism.

Selection of Test Parameters

Determination of compatibility of the cellular insulation with filling compound should be accomplished by exposure in a completed cable. This ensures that the relative amount of absorption of oils into the polyethylene and extraction of stabilizers from the polyethylene into the filling

compound will be consistent with the actual exposure and not altered by gross amounts of either material relative to the other. Aging in the final cable most closely simulates the aging which would actually occur in application, including the filling process and subsequent migration of components between the cellular insulation and filling compound. The amount of oil absorption into polyethylene can have an effect on the rate of thermal embrittlement since the oil may act as an internal lubricant to facilitate molecular rearrangement. The ratio of filling compound to insulation could also affect the rate of extraction of stabilizers by altering potential equilibrium concentrations between the two materials.

The time and temperature for preaging the foam skin insulation in the filling compound must be consistent with field exposure. Finished cables may routinely be exposed to the environment for several months before installation even when cables are manufactured to order and for longer periods if the product is placed in stock against future orders. Simulated aging of cable held in a reel yard over the summer months would be a reasonable time frame for the cable constructed to order. Average daily temperature in the deep south and the west for the summer months is approximately 30° C. The maximum accelerated aging temperature of 70° C was chosen to ensure that a filling compound (80° C drip) remains below its crystalline component melt range. A time frame of 4 weeks at 70° C was chosen to simulate four to five months of summer time exposure of the foam skin cable before installation as a preaged compatibility exposure.

Following installation of the cable, the insulated conductors may be exposed to the environment in pedestals with some filling compound removed due to handling. To provide consistent exposure to air for the test sample, the insulated conductor should be removed from the cable and wiped with a clean cloth or tissue to remove most of the filling compound. Removal of the filling compound from the wire will also extract any stabilizers which have leached from the polyethylene during the preaging exposure. Filling compound absorbed into the insulation will, during additional testing, migrate to the surface and maintain contact with the skin to act as a stress cracking agent. Stress concentration to simulate wire bends in the pedestal is formed by wrapping the insulated wire around itself to form pigtails.

Aging of the sample, to be realistic, must be conducted below polymer transition temperatures. Differential scanning calorimetry studies show that high-density polyethylene begins to undergo melt phase transitions at temperatures between 80° C and 90° C. Therefore, a maximum aging temperature of 80° C should be set for test conditions to establish accelerated aging rate factors. Since deterioration of insulation varies with the type of degradation as well as material variation and process variation, at least 25 samples or pigtails should be evaluated for each test condition to provide a statistical basis for analysis of test results.

The susceptability of polyethylene to stress cracking may change as the insulation ages. To investigate alteration in molecular structure with time, additional pigtails should be formed in the test samples after aging of the initial pigtails is underway. Following exposure to heat aging of exposed pigtail samples for 6 weeks, the sample should be removed from the oven and a second set of pigtails formed in the insulated wire. This simulates bending of the wire in pedestals following initial installation.

To aid in distinguishing between environmental stress cracking and oxidative or thermal embrittlement failure, additional pigtails should be formed after 50% of the initial samples have failed and at the completion of the test (100% failure of first pigtails). The samples should be monitored every two weeks and the failure rate indicated by cracking of the pigtails, recorded for both first and second pigtails.

Evaluation of Test Procedures

A number of questions relative to the assumptions in devising the new test method must be answered to determined if the new test method can be used to differentiate between products and establish the credibility of the procedure. The following questions are included: Does preaging of the cable affect subsequent aging characteristics of insulation for both foam skin and solid insulation? If preaging affects performance of insulation in subsequent exposure to elevated temperature, what period of preaging is required? Does preaging correlate to any extent of actual field exposure? Do second pigtails age differently relative to the initial pigtails? Do third and fourth pigtails give any indication of thermal embrittlement activity? Is there any indication of environmental stress cracking? Do PE-PJ and ETPR type filling compounds have similar effects on foam skin insulation? Do failure modes other than oxidative deterioration significantly alter life time expectancy of foam skin insulation? Can the test method be accurately employed to predict field failures?

The answers to the above questions have been obtained. 24 gauge foam skin and solid insulation were evaluated using the new procedure, along with control samples which were not exposed to preaging. An experimental cable of insulated conductors from a single primary machine was constructed to evaluate aging properties of foam skin insulation following controlled exposure to filling compound. Cable filler exposure levels included: no exposure, exposure to cable filling process, four weeks preaging at 70°C, and eight weeks preaging at 70°C. This data was compared to insulation removed from a cable that had remained in a cable plant reel yard for 2 years.

The data presented in Table 1 clearly shows that preaging of cable at 70°C for four weeks caused faster failure rate for stressed polyolefin insulation as compared to material which was not subjected to preaging. This tendency is the same for solid insulation and foam skin insulation with various polyolefin materials and filling compound variations.

The acceleration factor for a 10°C rise in temperature for the preaged foam skin cable ranges between 1.3 and 3.25 with an average of 2.35 using 50% failure as reference point. Crack failure of pigtail samples tends to have a normal-type distribution when the failures are plotted as a function of time. As a general rule, the first and last samples to crack will be separated in time from the bulk of the failures. Additional data presented in the companion paper "Evaluation of Materials for Improved Life Expectancy" exhibits the same type of distribution failure between cables. Considering the number of factors affecting the aging characteristics of polyethylene, a spread of this size is expected. A partial list of variables that can alter aging rate of insulated wire include: molecular weight, molecular weight distribution, degree of long and short chain branching, antioxidant content and distribution, addition of processing aids, crystallinity, extrusion profile, cooling rate, line speed, degree of mechanical stress applied during cable production, effects of grease filling and cable jacketing (which varies with cable size, line speed and filling compound temperature), variations in filling compound composition, as well as variations of sample preparation and artificial aging test conditions.

The second pigtails formed in the evaluation samples crack before or at about the same time as the original pigtails even though they were formed six weeks after the initial pigtails. Molecular reorientation has taken place in the insulation as a result of aging at elevated temperature. Thermal embrittlement may be contributing to the overall deterioration of the foam skin insulation. The inconsistency of the data presented in Table 2 indicates differences in the rate of thermal embrittlement; this may or may not be the primary failure mechanism for the initial pigtail formed in the insulation. The presence of thermal embrittlement suggests that the stressing of previously installed foam skin material in the pedestals contributes to early crack failure of the insulation. The extent to which reworking of pedestals in the field would promote insulation failure would be dependent on the length of time the cable has been in service prior to the addition of bend stresses and the avergae temperature of the pedestal.

Graphs 1 and 2 provide stress crack failure data for material removed from the same cable as a function of time along with tensile and elongation data for a straight section of insulation removed from the stress crack sample at the time of failure for material preaged in the cable for four and eight weeks. The sample population in each preaged test group consisted of three wires of each of the ten colors. There is no indication of color dependency in time to failure. The tensile and elongation values obtained are within the range of normal variation for values obtained from insulation removed from the cable prior to preaging. Insulation which cracks due to thermal embrittlement or oxidative deterioration is brittle and does not retain plasticity. Therefore, the primary failure mechanism for preaged insulation pigtail samples is environmental stress cracking or solvent cracking. The need to address these failure modes has been clearly demonstrated.

Graph 3 illustrates the effect of filling compound exposure to foam skin insulation relative to accelerated aging of pigtail samples. A, B, C, and D test groups used insulation from the same cable. Test group D was obtained from the cable core prior to grease filling and jacketing. Test group E consists of material removed from a cable stored in a cable plant reel yard for two years.

There is a dramatic increase in the failure rate of foam skin insulation when it is artificially aged in filled cable. Four weeks preaging at 70°C would appear to be reasonable as a method of artificially aging cable when the data from the 2 year old cable is compared to the preaged cable material. The data presented in Table 3 shows that the material which was not preaged in the cable before oven aging and solid preaged wire failed as a result of oxidative or thermal embrittlement. By the time the initial pigtails cracked, the insulation had lost its plasticity so that the polyethylene cracked when the wire was bent. In contrast, foam skin material which had been preaged retained plasticity after failure of the initial pigtails, indicating failure was due to environmental stress cracking or solvent cracking. By constructing additional pigtails at the time of failure of the initial samples, information can be obtained as to the primary mechanism causing cracking of the insulation.

Estimation of Life Expectancy for Stress Cracking of Foam Skin Insulation

Assumption 1

Reel storage (3-4 months) in the South and Southwest at the manufacturers' and customers' reel yard, in the sun, will be equivalent to four weeks preconditioning at 70°C.

For a four month period, the average daily temperature in the Southwest for the summer months is over 26°C as measured in the shade. The average reel temperature stored in direct sunlight will be higher.

Reels sitting in truck trailers could see temperatures of 60°C for short periods.

The preaging effect may not adhere to the general thermodynamic or chemical reaction rate increase of 2 to the x power, where x is the number of 10°C incremental increases in temperature, since the 25% failure rate for samples of foam skin preaged for four weeks was 20 weeks vs. 17 weeks for samples preaged for eight weeks in the original data. The preaging effect is probably controlled by diffusion rate not chemical reaction rate.

Assumption 2

Failure rate in a pedestal can be accelerated in oven aging tests.

Environmental stress crack does have a temperature coefficient and will increase at some constant to the x power rate. Also, synergistic effects of thermal embrittlement and oxidation will be controlled by temperature. In addition, oxidation will be affected by air movement in the pedestal relative to oven air velocity (greater flow in oven). The insulation in the pedestal will see additional stress due to temperature cycling and humidity that will not occur in the oven.

Assumption 3

The first failure will occur in the South and Southwest due to higher average temperatures. The following are 30 year averages of daily temperatures as measured at night and during the day (in the shade).

Birmingham, AL	20°C
Galveston, TX	21.1°C
Houston, TX	20.6°C
Jacksonville, FL	20°C
Miami, FL	23.9°C
New Orleans, LA	20°C
Phoenix, AZ	21.1°C
San Antonio, TX	20.6°C
Tampa, FL	22.2°C
Average	21°C

NOTE: Average temperature data from World Almanac.

Life expectancy calculations based on seven commercially produced cables (five different manufacturers) preaged for four weeks at 70°C and then oven aged at 70°C yields an average 25% failure at 17.8 week intervals for oven aged samples. A temperature acceleration rate factor of 2.35 was obtained by comparing failure times for samples aged at 70°C and 80°C.

Based on assumptions 1 through 3, foam skin cable may have a life expectancy of 24.6 years. Foam skin was installed in quantity in the United States starting approximately 10 years ago.

Assumption 4

Assume an increase in average temperature in a pedestal installation due to direct sunlight and insulation effect at night of 10°C. A ten degree rise in average temperature in pedestals would decrease foam skin life expectancy to 10.4 years.

Estimation of temperature increase may be high , but in "Polymer Engineering and Science 1971" the mean effective temperature for air core, worst case was reported to be 43°C. Maximum temperature in pedestals in the high seventies have been reported.

In using the above life time calculations, it must be remembered that not all cable will be subjected to storage under summer time conditions and that the average summer temperatures and average pedestal temperatures vary with location.

Assumption 1 can be substantiated by the cable data. A section of foam skin cable, produced April 1982 and removed from the Brownwood reel yard and evaluated in April 1984, exhibits rapid stress crack failure simular to cables which were preaged artificially in 70°C ovens.

Field failures for foam skin installed 10 years ago may show evidence of cracking in the warmer regions of the country. Reports of field failures of foam skin have been reported in the Southwest. Failures in pedastals in this region of the country were predicted several years before they occurred providing credibility for the test method.

Conclusion

An enhanced or global test procedure is needed for foam skin insulation which evaluates degradation modes which are not currently addressed in cable specifications. A procedure for detecting solvent cracking, environmental stress cracking, thermal embrittlement, as well as oxidative deterioration has been developed and demonstrated. The procedure described in this paper should replace current specification tests for insuring adequate cable lifetime expectancy.

Preaging of cable is required to obtain accelerated test data in a reasonable time frame at test temperatures below polyethylene's transition range and to simulate cable reel storage of filled cable.

Foam and foam skin cables installed in the early seventies in the South and Southwest may begin to show cracking in pedestals.

References

1. J.H. Huss and V.L. Langa. "The Thermal Embrittlement of Stressed Polyethylene", Annual Convention of the Wire Association in Atlantic City, December 14, 1958.

2. John B. Howard, " A Review of Stress Cracking in Polyethyene", SPE Journal, May 1959.

3. M.E.R. Shanahan and J. Schultz, "A Kinetic Effect in the Environmental Stress Cracking of Polyethylene Due to Liquid Viscosity", Journal of Polymer Science, Polymer Physics Edition, Vol. 14, pp. 1567-1573 (1976).

4. M.E.R. Shanahan and J. Shultz, "Environmental Stress Cracking of Polyethylene: Criteria for Liquid Efficiency", Journal of Polymer Science; Polmer Physics Edition, Vol. 17, pp. 705-710 (1979).

5. S. Bandyapadhyay, "Studies of Environmental Stress Crack in Low-Density Polyethylene", Journal of Polymer Science; Polymer Physics Edition, Vol. 19, pp. 749-761 (1981).

6. P.L. Soni and P.H. Gail, "Enivironmental Stress Cracking of Polyethylene: Temperature Effect", Journal of Applied Polymer Science; Vol. 23, pp. 1167-1179 (1979).

7. W.L. Hawkins, M.G. Chan and C.L. Lenp, "Factors Influencing the Thermal Oxidation of Polyethylene", Polymer Engineering and Science, September, 1971, Vol. 11, No. 5.

8. H.M. Gilroy, "Polyolefin Longevity for Telephone Service", ANTEC, 1985.

9. M.E.R. Shanahan and J. Shultz, "Influence of Wetting Properties of the Liquid on Environmental Stress Cracking of Polyethelene of High Stress", Journal of Polymer Science; Polymer Physics Edition, Vol. 16, pp. 803-812 (1978).

10. M.E.R. Shanahan and J. Shultz, "Correlation Between Environmental Stress Cracking and Liquid Absorption for Low-Swelling Liquids", Journal of Polymer Science; Polymer Physics Edition, Vol. 18, pp. 19-26 (1980).

11. Glenn E. Fulmer, "Time - Temperature Strain and Molecular Weight Effects in the Environmental Stress Cracking of 0.95 Density Polyethylene", Transactions of the Society of Realogy, 10:2, pp. 502-512 (1966).

12. Glenn E. Fulmer, "Time, Temperture and Molecular Weight Effects in Environmental Stress Cracking", Transactions of the Society of Rhealogy, 9:2, pp. 121-133 (1965).

13. John B. Howard, "Stabilization Problems with Low-Density Polyethylene Insulation", 21st International Wire and Cable Symposium, pp. 329-341 (1972).

14. B.D. Gesner, J.W. Shea and F.R. Wright, "Establishing Longevity Criteria for Thermo-Oxidative Cracking Measurements on Polyolefin Insulation", 22nd International Wire and Cable Symposium, p. 7-10 (1973).

15. Louis Ance and Joseph P. McCann, "System Evaluation and Protection of Conductor Insulation for Outside Plant", 23rd International Wire and Cable Symposium, pp. 82-90 (1974).

16. D.A. O'Rell and A. Patel, "Oxidative Stability Studies on Cellular High-Density Polyethylene Insulation for Communications Wire", 24th International Wire and Cable Symposium, pp. 231-236 (1975).

17. G.A. Schmidt, "Life Prediction of Insulation for Filled Cables in Pedestal Terminals", 26th International Wire and Cable Symposium, pp. 161-181 (1979).

Table I

Comparison of number of weeks to aged pigtail failure of foam skin and solid insulation after pre-aging at 70° C for four weeks and no pre-aging.

24 Gauge Sample	Filling Compound Type	Pigtails aged at 80° C						Pigtails aged at 70° C					
		No Pre-aging			Pre-aged			No Pre-aging			Pre-aged		
		Initial	50%	100%	Initial	50%	100%	Initial	50%	100%	Initial	50%	100%
HDPE Solid	PE - PJ	53	86	>127	40	49	54	--	--	--	--	--	--
HDPE Foam Skin	ETPR	39	56	>100	7	8	11	31	59	106	19	26	36
HDPE Foam Skin	PE - PJ	18	24	29	9	13	17	25	52	74	12	17	25
HDPE Foam PP Skin	PE - PJ	22	27	29	9	10	12	44	66	85	18	23	28

Table II

Comparison of number of weeks to failure of second pigtails formed after aging at 80° C for 8 weeks, for wire not exposed to pre-aging and second pigtails formed after 6 weeks aging at 80° C for wire exposed to pre-aging at 70° C for 4 weeks.

24 Gauge Sample	Filling Compound Type	No Pre-aging 50% Failure Rate		Pre-age 50% Failure Rate	
		1st Pigtail	2nd Pigtail[1]	1st Pigtail	2nd Pigtail[1]
HDPE Solid	PE - PJ	86	55	49	35
HDPE Foam Skin	ETPR	56	48	8	11
HDPE Foam Skin	PE - PJ	24	18	13	11
HDPE Foam PP Skin	PE - PJ	27	26	10	10

(1) Weeks to failure for second pigtails include the time in the 80° C oven before the second pigtails were constructed.

Table III

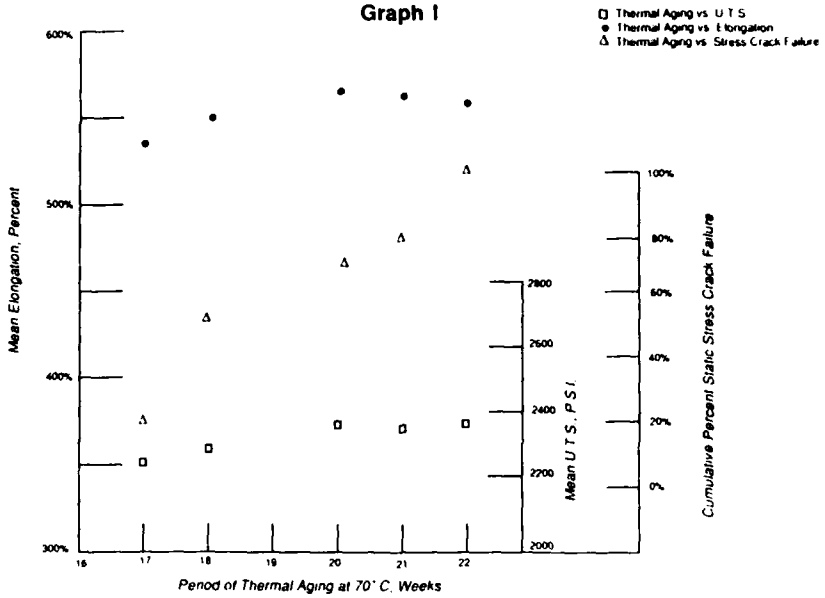
Percentage Formation of Third and Fourth Pigtails without cracks

24 Gauge Sample	Filling Compound Type	Pigtails aged at 80° C			
		No Pre-aging		Pre-aged	
		3rd	4th	3rd	4th
HDPE Solid	PE - PJ	0	0	0	0
HDPE Foam Skin	ETPR	0	0	100	100
HDPE Foam Skin	PE - PJ	0	0	85	90
HDPE Foam PP Skin	PE - PJ	0	0	100	100

* 3rd pigtails made at 50% stress crack failure of first pigtail

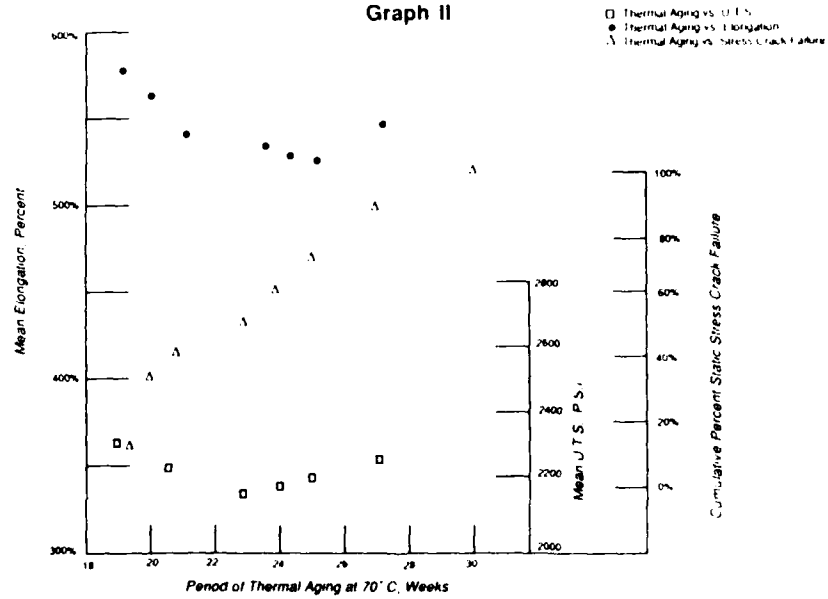
* 4th pigtails made at 100% stress crack failure of first pigtail

Graph I



Foam Skin Insulation Static Stress Crack Failure Samples
Pre-Conditioning - 8 weeks @ 70° C

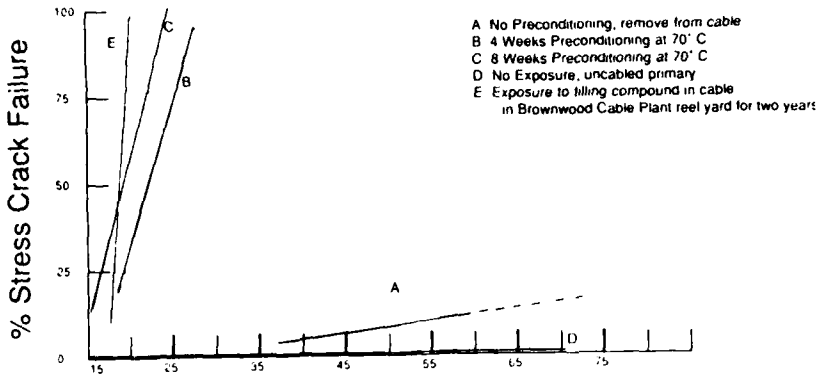
Graph II



Foam Skin Insulation Static Stress Crack Failure Samples
Pre-Conditioning - 4 weeks @ 70° C

Graph III

Pigtail Stress Crack Failure Rate as a Function
of Exposure to Filling Compound
(22 AWG Foam Skin Insulation)



Weeks Thermal Aging @ 70°C



Lawrence E. Davis is the Senior Engineer for Materials / Processing for Superior Cable Corporation. He received his B.S. degree in physics from the Appalachian State University in 1969 and graduated with a Master's degree in physics from the University of Wisconsin, Milwaukee in 1974. Prior to joining Superior Cable, Mr. Davis was the Materials Engineering Manager for Technical Staff, Siecor Corporation and was formerly a Materials Engineer for Continental Telephone Laboratories.

High Speed Coaxial Cables for Electronic Computers

K. SAKAMOTO S. YAMAMOTO T. KATO K. NEGISHI and K. AKIMOTO

THE FURUKAWA ELECTRIC CO., LTD.

CHIBA, JAPAN

Summary

Highly expanded Fluorocarbon resin insulated core (so we call "H-TEF") and highly expanded cross-linked polyethylene insulated core (so we call "H-XLPEF") have been developed as miniature highly expanded insulation used in a coaxial cable for the wiring of a general purpose computer capable of high speed propagation.

(1) H-TEF: Development of a fluorocarbon resin insulated core of 0.4 mm thickness of insulation and 70% expansion ratio has been achieved by employing a special designed screw and introducing a constant flow injection system.

(2) H-XLPEF: Development of a polyethylene insulated core of 0.2 mm thickness of insulation and 70% expansion ratio has been achieved by arranging large cells near around a conductor and small cells near the surface of insulation by employing several kinds of gas having different diffusion coefficients together with thermally decomposable blowing chemical agent.

1. Introduction

Shorting of cable length in circuits (intensification in density) and increasing of velocity of propagation are being carried out for the purpose of expediting operation processing in general purpose computers capable of high speed propagation and testing devices of evaluating the characteristics of LSI. In the presently used general purpose computers, a coaxial cable of less than 2.0 mm OD and of a velocity of propagation of 87% or more of air is required.

Until now, highly expanded PTFE tape wrapped core has been used for this kind of insulation. However, it is high in material expenses and its productivity is poor. Therefore, H-TEF and H-XLPEF have been developed by extrusion as alternates of highly expanded PTFE.

H-TEF produced by extrusion is characterized in stabilized electrical properties because of smaller fluctuation of its outer diameter and capacitance, excellent features in mechanical strength as heat deformation property. Besides, it pocesses excellent heat resitance property. Besides, it pocesses excellent heat resistance property and flame retardance property. On the other hand, although H-XLPEF is inferior to H-TEF in its mechanical strength, heat resistance property and flame retardance property, it is equivalent in its electrical property, it is equivalent in its electrical properties and also can present superiority in view of cost.

Use of these kinds of insulation are properly selected depending upon the natures of circuit design or method of end treatment so that some merits concerning the price levels can be expected and these insulations have just started those practicability in place of the highly expanded PTFE.

2. Necessary electric properties and structure

2.1. Electrical properties

In any cable used in a computer, the most important electrical properties are characteristic impedance and propagation delay time. These properties in the case of presently used general purpose computers are follows:

Characteristic impedance: 50 - 90 Ω
Velocity of propagation: 87% of air

From view of cable manufacturing techniques, a low impedance with high velocity of propagation is nothing but the demand on a structure with miniature and highly expanded insulation.

The ratio of a velocity of propagation of air (K) is generally given by the following formula.

$$K = \frac{1}{\sqrt{\varepsilon_s}} \times 100 \ (\%)$$

There is, ε_s = Effective relative dielectrics constant of insulation

Namely, condition $\varepsilon_s \leq 1.32$ is required so that $K \geq 87$ be satisfied. In addition, there is a relation give the next formula between ε_s and expansion ratio.

$$\frac{\varepsilon_i - \varepsilon_s}{\varepsilon_i - \varepsilon_a} = \frac{F}{100} \times \frac{3\varepsilon_s}{2\varepsilon_s + \varepsilon_a} \quad \text{(A.S. Windeler's Formula)}$$

There is, ε_i = Relative dielectric constant proper to insulation material
polyethylene = 2.3
fluorocarbon resin (PTFE, PFA, FEP) = 2.1

ε_a = Relative dielectric constant of air = 1.0

Namely, in order to satisfy the above-mentioned conditions, miniature highly expanded insulation of more than 65% expansion ratio and less than 1.0 mm thickness of insulation is required.

2.2. Structure

For the purpose of deciding the cable structure, wiring spaces, configurations of connectors and end treatment feasibility must be taken into account together besides the above-mentioned propagation properties.

2.2.1 Structure of outer conductor

Material and structures for outer conductor of coaxial cable are decided by taking not only electrical properties but also the flexibility of cable as well as the end treatment feasibility therefore into consideration. Principally employed structures are braiding and wrap shielding using copper wire, and tape wrapping or longitudinal wrapping using aluminium-polyester laminated (Al-PET) tape.

2.2.2 Structure of cable

The structure of a coaxial cable consisting of multiple coaxial cores can be roughly classified into a round type cable and a flat type cable.

The flat type cable is principally used for internal wiring and the dimension of cable is designed to meet the structure of connector (for example, connector contact pitch = 2.54 mm, 1.27 mm etc.). In addition, a multi-flat type cable, hvaing stuck portion subjected to connector attachment and having the intermediate portion separated for easy wiring, has been also used very often recently.

3. Manufacturing techniques for H-TEF

In manufacturing of miniature H-TEF, factors for exerting significant influence on the state of expansion and the surface of insulation are those items stated below.

(1) Uniform diffusion of gas (forming agent)
(2) Resin temperature, quantity of added gas.
(3) Resin pressure.

3.1 Uniform diffusion of gas

Requirements for the gas used as a forming agent are, to be not decomposed under molding temperature and pressure, to make no reaction with resin, to be well diffused in molten resin and so on. Fluorinated hydrocarbon, which is both thermally and chemically stabilized, is considered to be applicable to expansion of fluorocarbon resin.

With regard to this kind of techniques there has been a report[1] on an example which evidences that an expansion ratio in the range from 50% to 60% can be obtained with 1 mm or more thickness of insulation, by means of a constant pressure injection system in which a vent type screw is used, as shown in Table 1, for maintaining the pressure on the gas injection section at about 0 kg/cm^2 so as to supply gas at a constant pressure. However, if this constant pressure injection system is applied to set up 60% expansion ratio with less than 1 mm thickness of insulation, soluble amount of gas is fluctuated on account of delicate pressure fluctuation on the injection section, duly causing fluctuation in capacitance and outer diameter of expanded insulation to get in difficulty of manufacturing stabilized products. Individual factors shown in Table 2 have been investigated so far as the points of improvement on troubles. Those points are;

(1) Establishment of constant flow gas injection techniques.
(2) Fine control of extrusion rate, temperature and line speed etc. for the purpose of restricting the pressure on each part of extruder within a defined range.
(3) Application of a special screw

and these items shall be outlined next.

Table 1 Known Techniques of Manufacturing of Expanded Fluorocarbon Resin

Material	
Base Resin	FEP,PFA
Nuclear Agent	Boron Nitride
Forming Agent	Fluorinated Hydrocarbon
Limited Shear Rate of Resin	
Design of Tip & Die	
Extrusion Rate	
Line Speed	
Special Designed Vent Type Screw	
Gas : 0 $Kg/_{Cm}{}^2$ Const. press. Injection	
$> 1mm^t$	Expansion Ratio 50-60%
$< 1mm^t$	Not Information

Table 2 Obstructive Factors & Improvements in the Manufacturing of Miniature H-TEF

Factors	Improvements
1. Fluctuation of Temp.	Subtle Temp. Control
2. Fluctuation of Screw rotations	Control of Screw Motor
3. Fluctuation of Take-up	Control of Take-up Equipment
4. Fluctuation of Gas Injection by Const. Press. System	Const. Flow System by Precision Pump
5. Screw Design	Accurate Design & Precise Manufacturing
6. Tip & Die Design	Accurate Design & Precise Manufacturing

3.1.1 Constant flow gas injection techniques

A constant flow gas injection techniques has been developed, whereby highly expanded insulation with stabilized electrical properties can be produced by injecting a minute quantity of liquefied gas into high pressure molten resin at a constant flow rate, and the techniques are dependent upon a precision pump provided with a driving device requiring only small expense for installation but built up through such processes

as an injection inlet for liquefied gas being provided in the intermediate portion of the barrel of an extruder, multiple piston pump being, mutually connected in series between the above-mentioned injection inlet and liquefied gas supply source, and phases of respective pump being shifted by equal intervals to be put in reciprocating motion. The outline of this device is shown in Fig. 1. Meanwhile, is also shown in Fig. 2 relationship between inhalation and exhalation of each piston in the case of three pistons pump. solid lines A, B, C show the inhalation quantities and exhalation quantities of respective pistons pump and dotted lines D, E show the synthetic inhalation quantity and exhalation quantity for the total pump devices.

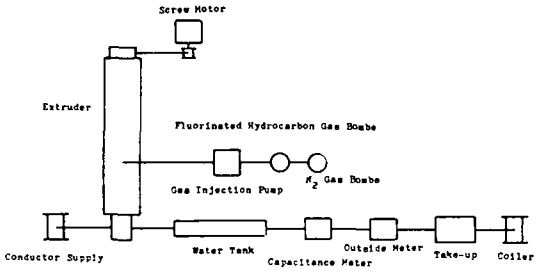


Fig.1 Extrusion Layout of H-TEF

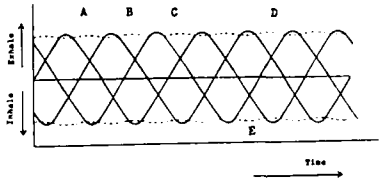
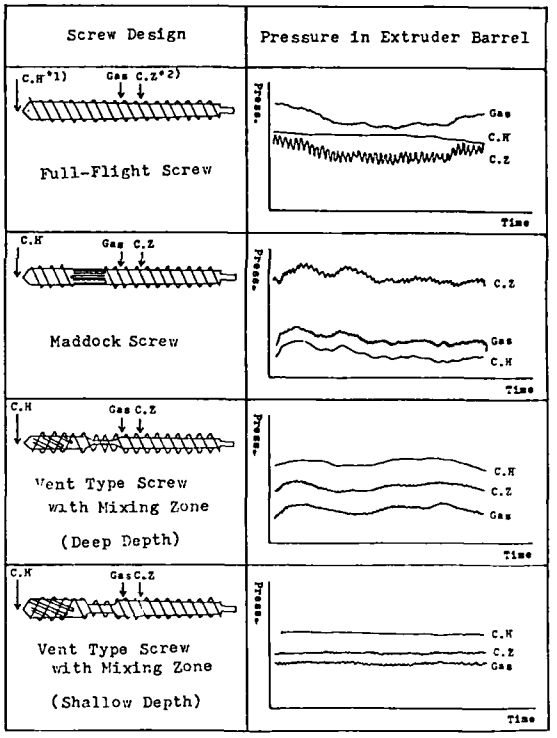


Fig.2 Inhale & Exhale of Three Pistons Pump

3.1.2. Screw design

When miniature H-TEF is manufactured by extrusion, a point of screw design is to suppress any pressure fluctuation on a gas injection section as small as possible. Fig. 3 shows the configuration of a screw and fluctuation of the pressure inside the barrel of the extruder due to lapse of time, thereby it is also shown that in the case of a full-flight screw or a Maddock screw provided with no vent zone (injection section is a compression zone in the case of full-flight screw and Maddock zone in the case of Maddock screw, as shown in Fig. 3) , pressure fluctuation is large on the gas injection section, duly causing a large fluctuation in the capacitance and outer diameter of insulation. On the contrary the pressure fluctuation is suppressed low in the case of a screw provided with a vent zone at intermediate portion of a compression zone and with a mixing zone on its tip area, because back pressure occured in the mixing zone and cross-head is dwindled in the vent zone, so the pressure fluctuation at the injection section where is rear of the vent zone as shown in fig. 3 becomes small. Furthermore, the pressure fluctuation smaller in a shallow depth type than in a deep depth type, because in the case of a small depth type it is more difficult for the back pressure to turn back to the gas injection section. However, caution must be used in this case, because an excessively large load may be applied to the screw unless the channel dpeth in the vent zone is properly balanced with the channel depth of compression zone with shallow depth in front and rear of the vent zone.

Fig.3 Relations between Screw Design & Pressure in Extruder



*1) C.H : Cross-head *2) C.Z : Compression Zone

3.2. Resin temperature, quantity of added gas

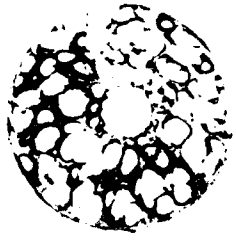
The state of expansion (size and number of cells) , adhesion to a conductor and the appearance of insulation are significantly influenced by resin temperature and quantity of added gas.

Firstly, with regard to the size and number

of cells, the more the quantity of added gas is, the smaller and the more the size and the number of cells are respectively, provided that various conditions such as the screw rotations and diameter of tip and die etc. beside the resin temperature are all kept constant as shown in Fig. 4. In the case of miniature highly expansion, the cells must be limited to a small size in order to be rendered "miniature", but cells of excessively small size can not maintain necessary expansion ratio. Therefore, it is preferable to arrange a large number of cells with the allowable maximum size. Photo 1, 2 show examples of both cases of small cells and large cells respectively, as photo 1 presents the case of 59% expansion ratio, while photo 2 presents the case of 67% expansion ratio which is characterized in existence of a number of rather large-sized cells in indefinite shapes.



Photo 1.



Phot 2.

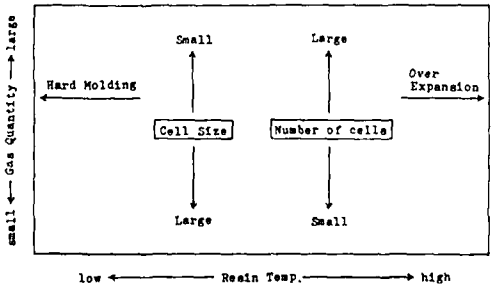


Fig.4 Relations between Resin Temperature, Gas Quantity & State of Cells

Next, with regard to the influence on adhesion to a conductor, the higher the resin temperature is and the more the quantity of added gas is, the worse the state of adhesion is rendered, as shown in Fig. 5.

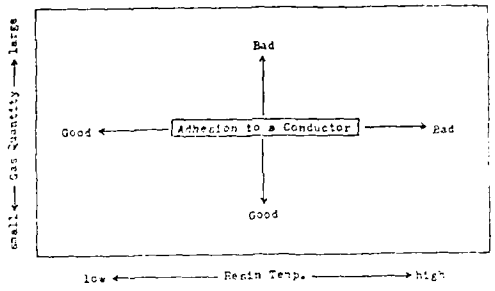


Fig.5 Relations between Resin Temperature, Gas Quantity & State of Adhesion to a Conductor

Lastly, with regard to the influence on the surface of insulation, the more the quantity of added gas is, and the lower the resin temperature is, the worse the surface of insulation is rendered, as shown in Fig. 6. However, the surface of insulation becomes worse if the resin temperature is excessively high because the gas can easily escape outside the insulation.

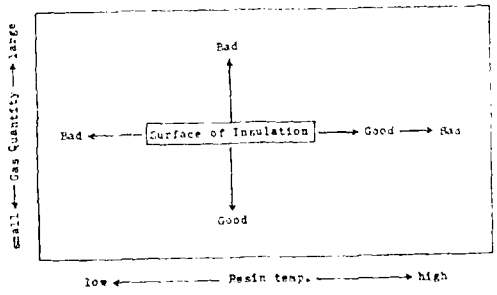


Fig.6 Relations between Resin Temperature, Gas Quantity & state of Surface of Insulation

3.3. Resin pressure

It has been well known that the surface of insulation etc. may be remarkably influenced by shear rate of resin when fluorocarbon resin is molded in extrusion, but mutual influence has been confirmed to take place between the shear rate of resin and resin temperature in case of expansion. Fig. 7 shows the results of selecting both a cross-head pressure and a die set temperature as one each scale of shear rate of resin and resin temperature respectively so as to show the relations between those date and expansion ratio. As shown in this figure, the expansion ratio increases, as the cross-head pressure rises, until it reaches its peak value and rather decreases across the peak value accompanied by a worsened surface of insulation. In addition, since it has been also found out that die set temperature also has a peak, both the cross-head pressure and die set temperature must be kept in a definite range so as to set up an expansion ratio of more than the required 65%. Then, the design of a tip, a die and a screw, temperature control and selection of material viscosity etc. are considered significant for the above-mentioned purpose.

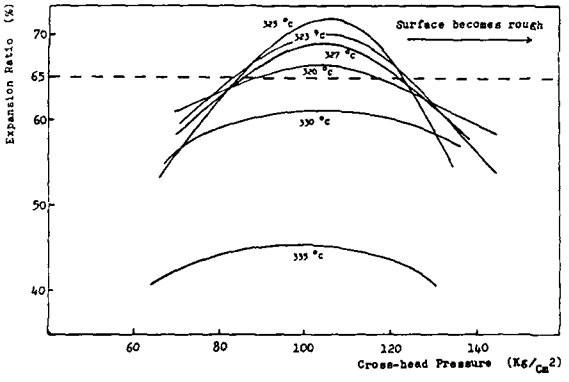


Fig.7 Relations between Cross-head Pressure & Expansion Ratio

4. Manufacturing techniques for H-XLPEF

There has been a report[2] on an example which represent a miniature highly expanded polyethylene insulated core techniques effected by double layer insulation by common-head extrusion, so far as the conventional manufacturing techniques concern, but a single layer insulation considered to be limited to expansion ratio 60% also to have such a shortcoming as low mechanical strength. Processes for improving this problem have been put in successful result by means of a below-mentioned method, in form of development of a miniature H-XLPEF with high mechanical strength. The points of developmen. of H-XLPEF are as follows.

1 To employ several kinds of gas different in each diffusion coefficient together with a thermally decomposable blowing chemical agent so as to arrange large cells near around a conductor and small cells near the surface of insulation.

2 To select a polyethylene of high mechanical strength and enhance this strength by means of cross-linking by irradiation of electron beam.

A section of H-XLPEF is shown in Photo 3.

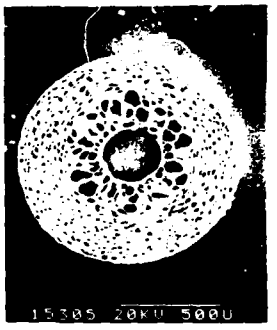


Photo 3. Section of highly expanded cross-linked polyethylene

5. Properties

Results of evaluation for both highly expanded fluorocarbon resin insulated core and highly expanded cross-linked polyethylene insulated core are reported herein. The structure of the presently evaluated insulated core is as follows.

Conductor	:	7/0.08 mm annealed copper wire (32AWG)
Expansion ratio	:	70%
Outer diameter	:	1.15 mm

Meanwhile, the evaluation was carried out in comparison with a highly expanded PTFE.

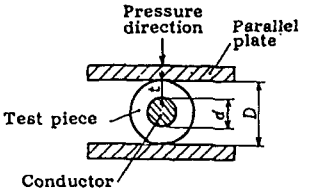
5.1. Heat resistance properties

A tensile test after heating in UL method and a heat bend test in the same heating condition as the above have been carried out for evaluating the heat resistance property. Meanwhile, the method of the heat bend test is that insulated core shall be wrapped 6 times around a mandrel of a diameter of insulated core after heating, and no generation of crack is assigned to a satisfactory grade.

Table 3 includes the results of tests which imply such heat resistance properties as applicable to UL 250℃ rating for H-TEF and to UL 105°C rating for H-XLPEF.

Table 3 Heat Resistance Properties

Item	UL Rating	Heating Condition	UL Standard	Highly Expanded Cross-linked Polyethylene	Highly Expanded Fluorocarbon Resin	(Comparison) Highly Expanded PTFE
Residual Tensile Strength after Heating (%)	80 °C	113 °C x 7days	> 70	122	——	——
	90 °C	121 °C x 7days	> 70	106	——	——
	105 °C	136 °C x 7days	> 70	94	——	——
	125 °C	158 °C x 7days	> 70	76	——	——
	250 °C	287 °C x 7days	> 85	——	117	110
Residual Elongation after Heating (%)	80 °C	113 °C x 7days	> 70	142	——	——
	90 °C	121 °C x 7days	> 70	133	——	——
	105 °C	136 °C x 7days	> 70	80	——	——
	125 °C	158 °C x 7days	> 70	38	——	——
	250 °C	287 °C x 7days	> 85	——	100	100
Heat Bend	——	113 °C x 7days	——	Passed	——	——
	——	121 °C x 7days	——	Passed	——	——
	——	136 °C x 7days	——	Passed	——	——
	——	158 °C x 7days	——	Failed	——	——
	——	287 °C x 7days	——	——	Passed	Passed



t = thickness of insulation

d = diameter of conductor

D = outer diameter of insulation

$$t = \frac{D - d}{2}$$

Fig.8 Method of Heat Deformation

5.2. Shrinkage ratio after heat cycle

Any material insulated on a conductor possesses such unfavorable properties as occurrence of shrinkage due to the ambient temperature subject to presence of redidual strain or poor adhesion to the conductor. When the shrinkage occurs, practically serious problems may take place because the conductor is exposed. Hereat the shrinkage ratio of an insulation was measured after the about 1000 mm long insulation provided with a conductor thereon had been subjected to a cycle test 10 times, wherein the insulation is left at -20°C for 30 minutes immediately after it has been left at 60°C for 30 minutes. The obtained results are shown in Table 4 in which it has been confirmed that both H-TEF and H-XLPEF can make hardly any shrinkage.

Table 4 Shrinkage Ratio after Heat Cycle

Insulation Material	Shrinkage Ratio (%)
Highly Expanded Fluorocarbon Resin	0.1
Highly Expanded Cross-linked Polyethylene	0.1
(Comparison) Highly Expanded PTFE	0.4

60 °C X 30 min. — -20 °C X 30 min. 10 cycles

5.3. Heat deformation properties

When expanded material is utilized as insulation its deformation responding to an external stress points out problems. Hereat the heat deformation properties against a temperature were obtained through a test method JIS C 3005 as shown in Fig. 8, thereby the used weight is 250 gr. Meanwhile, a deformation ratio is found out from the following formula.

$$\text{Deformation ratio (\%)} = \frac{\text{(Thickness of insulation before heating)} - \text{(Thickness of insulation after heating)}}{\text{(Thickness of insulation before heating)}} \times 100$$

The results are shown in Fig. 9, in which it is known that the deformation ratio is small such as less than 3% at ordinary temperature (20°C) being at quite a normal level where no trouble may occur in a practical work. Further, the deformation ratio is less than 10% even in a high ambient temperature, up to 80°C, and both H-TEF and H-XLPEF proved to be superior to a highly expanded PTFE.

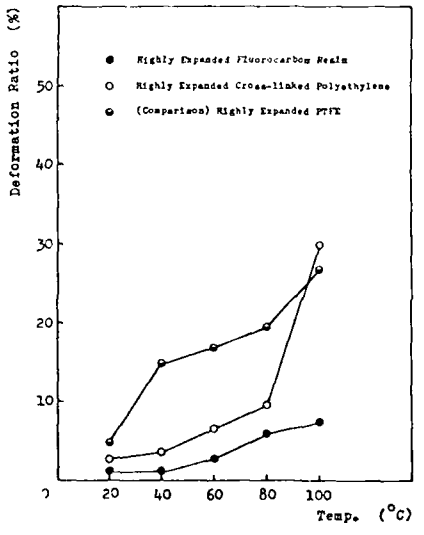


Fig.9 Heat Deformation Properties

5.4. Cut through properties

The cut through test prescribed in UL sub. 758 is an effective means for evaluating the strength of insulation. A weight is placed on the insulated core via a V-edge of 3 mil blade tip as shown in Fig. 10 and the amount of weight is measured just when the insulation breaks to bring the metal blade tip in contact with a conductor to set up electric continuity. Hearat, the tests have been applied to both a solid fluorocarbon resin insulated core and a solid cross-linked polyethylene insulated core in the same structure for the purpose of comparison, besides the above-mentioned highly expanded PTFE.

Table 5 shows the results of a cut through test at ordinary temperature, wherein any remarkable deterioration of properties can be observed in neither H-TEF nor H-XLPEF in comparison with those of a slid resin insulated core.

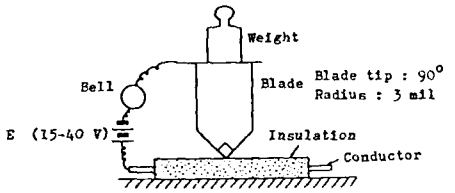


Fig.10 Cut Through Test

Table 5 Cut Through Properties

Insulation Material	Weight (Kg)
Highly Expanded Fluorocarbon Resin	2.6
Highly Expanded Cross-linked Polyethylene	1.6
(Comparison) Highly Expanded PTFE	1.7
(Comparison) Solid Fluorocarbon Resin	3.1
(Comparison) Solid Cross-linked Polyethylene	2.0

5.5. Flexibility

The flexibility has been evaluated by having a weight hung on a circular sample with 300 mm diameter and measuring the diminution length of the diameter in the central portion of the sample as shown in Fig. 11. The diminution length is found out from the following formula.

Diminution length (mm)
= (Diameter of central portion before weight loading (=300mm))
- (Diameter of central portion after weight loading (=Xmm))

Fig. 12 shows the relations between a weight and diminution length, wherein, the highly expanded insulations prove to have much more excellent property than that of solid insulations.

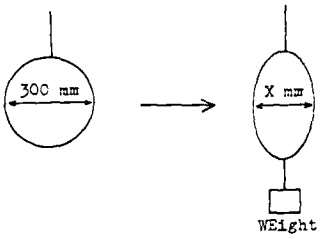


Fig.11 Method of Flexibility Test

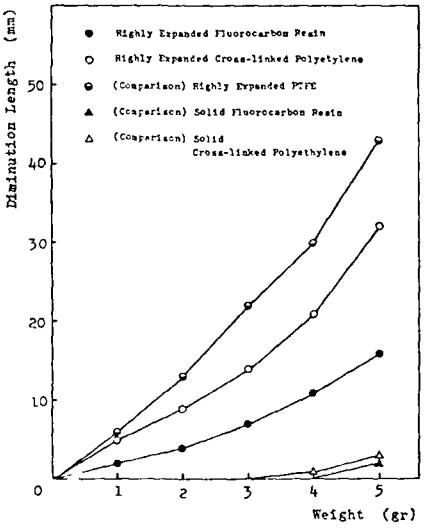


Fig.12 Flexibility

5.6. Electrical properties

Table 6 shows the typical values of capacitance, propagation delay time, and characteristic impedance of coaxial cores consisted of a highly expanded insulation which has been presently developed. Meanwhile, the propagation delay time and the characteristic impedance were measured by means of TDR (Time Domain Reflectometry) method.

Table 6 Electrical Properties

Item \ Insulation Material	Highly Expanded Fluorocarbon Resin	Highly Expanded Cross-linked Polyethylene
Expansion Ratio (%)	70	71
Capacitance (PF/m)	43	44
Effective Relative Dielectric Constant (-)	1.28	1.29
Propagation Delay Time (nsec/m)	3.8	3.8
Characteristic Impedance (Ω)	91	90

6. Application to other kinds of cable

Apparatuses presently requiring a velocity of propagation of 87% of air are principally general purpose computers, but furthermore, characteristic evaluating tester as LSI or the like and medical apparatuses belong to this categoly. On the other hand, miniature highly expansion techniques may become indispensable for miniaturization of cables required in accordance with further progress of thin thickness, light weight and compactness of apparatuses in future. A cable insisted of highly expanded insulation is required in OA apparatuses or Audio/Video implements in view of more "miniature" than "high speed propagation" and particularly, highly expanded polyethylene of a low cost can be expected to be widely employed in these engineering fields.

7. Conclusion

As the result of developing H-TEF and H-XLPEF to obtain a miniature highly expanded insulation used for a miniature coaxial cable having a velocity of 87% or more of air applicable to the wirings of a general purpose computer capable of high speed propagation,

(1) it has been successful to develop a fluorocarbon resin insulated core having 0.4 mm thickness of insulation and 70% expansion ratio as the result of employing a special screw for suppressing pressure fluctuation of molten polymer in a extruder, introducing a gas constant flow injection system, and further finely controlling a temperature, a gas quantity and a cross-head pressure. By means of the above-mentioned insulation, we have been able to provide such a coaxial cable as being excellent in its flame retardance property, heat resistance property and mechanical strength besides its electrical property presenting a velocity of propagation of 87% or more of air and characteristic impedance of 85 to 90Ω, and

(2) it has been successful to develop a polyethylene insulated core having 0.2 mm thickness of insulation and 70% expansion ratio, as the result of employing several kinds of gas having different diffusion coefficients together with thermally decomposable blowing chemical agent. By means of the above-mentioned insulation, we have been able to provide such a coaxial cable of a low cost as being excellent in its heat resistance property and mechanical strength owing to cross-linking by irradiation of electron beam, besides its electrical property presenting a velocity of propagation of 87% or more of air and characteristic impedance of 52 to 90Ω.

8. References

1) S.K. Randa, M.S. Carlson, D.P. Reifschneider
32nd IWCS proceedings, pp. 1983.

2) F. Suzuki, T. Komura, A. Mori
33rd IWCS proceedings, pp. 1984



KAZUHIDE SAKAMOTO
The Furukawa Electric Co., Ltd.
6-Yawata-kaigandori,
Ichihara, Chiba
Japan

Mr. Sakamoto graduated from Waseda University with a master of engineering degree majoring in organic chemistry in 1982. Then he joined The Furukawa Electric Co., Ltd. and has been engaged in research and development of plastics insulation material.

He is now a member of Chiba Research Laboratories of Research and Development Division.



SHOJI YAMAMOTO
The Furukawa electric Co., Ltd.
6-Yawata-kaigandori,
Ichihara, Chiba
Japan

Mr. yamamoto graduated from Hakodate Technical College majoring in industrial chemistry in 1972. Then he joined The Furukawa electric Co., Ltd. and has been engaged in research and development of flame retardant plastics and manufacturing methods for foamed plastics insulation.

He is now an assistant manager of Electronic Appliance Wire Production Section of Electronic Appliance Division.



TATSUZO KATO
The Furukawa electric Co., Ltd.
6-Yawata-kaigandori,
Ichihara, Chiba
Japan

Mr. Kato graduated from The University of Electro-communications majoring in a B. Sc. in communication engineering in 1972. Then he joined The Furukawa Electric Co., Ltd. and has been engaged in research and development of transmission lines.

He is now an assistant manager of Electronic Appliance Wire Production Section of Electronic Appliance Division.



KUNIO NEGISHI
The Furukawa electric Co., Ltd.
6-1, Marunouchi
2-chome, Chiyoda-ku,
Tokyo., Japan

Mr. Negishi graduated from Sophia University majoring in electronics engineering in 1972. Then he joined The Furukawa Electric Co., Ltd. and has been engaged in new cable design and developing.

He is now a chief engineer of Electronic Appliance Wire and Products Division.



KOICHI AKIMOTO
The Furukawa Electric Co., Ltd.
6-Yawata-kaigandori,
Ichihara, Chiba,
Japan.

Mr. Akimoto graduated from Tokyo Aeronautics College majoring in mechanical engineering in 1975. Then he joined The Furukawa Electric Co., Ltd. and has been engaged in quality assurance of communication cable, afterward in development and manufacturing of electric wires.

He is now a member of Electronic Appliance Wire Production Section of Electronic Appliance Division.

A Compact Cable for Within Building 1.544 Mb/s Digital Transmission

M. L. Fuller

AT&T Bell Laboratories
2000 N.E. Expressway
Norcross, Georgia 30071

A new spatially efficient 26 gauge cable has been developed to relieve the cable congestion that is often encountered in telephone company central offices. The new cable is intended to replace the traditional 22 gauge cables used to interconnect 1.544 Mb/s (DS1) equipment to a standard interface called a Digital Signal Cross-connect (DSX) frame. With one-half the cross-sectional area of the current 22 gauge cable, the new cable will help relieve the growing cable congestion problems created by the increased use of ever smaller digital equipment.

The new cable has improved impedance and attenuation uniformity, better crosstalk isolation between pairs, reduced pulse distortion, lower mutual capacitance, higher impedance, and higher attenuation. The higher impedance and attenuation limit the maximum cabling distance to 450', down from 655' for the current 22 gauge cables. However, the 450' limit is adequate for over 99% of the applications.

This paper will describe the physical, electrical and systems characteristics of the new cable by comparing it with the traditional 22 gauge cable it is intended to replace.

1. Background

Telephone company central offices have a rapidly increasing concentration of digital equipment and associated cabling. Of particular interest in this paper is the twisted pair copper cabling between equipment transmitting 1.544 Mb/s (or DS1 rate) and a standard interface called a Digital Signal Cross-connect frame, or DSX.[1] Traditionally, the central office cabling between DS1 equipment and the DSX has been via 22 gauge, corrugated aluminum shielded cables, often called ABAM.[2] In more recent years, ABAM cable has been upgraded to a foil shielded version, called 600C cable.

DS1 signals already widely used for inter-office trunks and loop carriers, are now economically multiplexed to higher bit rates and transmitted for long distances over single-mode lightguide fibers. This, combined with VLSI technology making the equipment smaller and smaller, has led to ever larger volumes of cable being required to interconnect digital equipment with DSX frames. The additional cable is causing severe cable congestion. To help alleviate these cable congestion problems a new 26 gauge foil shielded cable has been designed.

The remainder of this paper will describe the new cable by comparing first the physical characteristics, then the electrical characteristics between the new 26 gauge cable and the existing 22 gauge cable. Overall system limitations will also be discussed. For simplicity, I will use the AT&T cable codes, "600C" for the traditional 22 gauge cable, and "1249" for the new 26 gauge cable.

2. Comparison of Physical Characteristics

The 600C cable uses 22 gauge tinned copper conductors insulated with solid polyethylene (PE) with a polyvinylchloride (PVC) skin, a dual aluminum foil shield with drain wire, and a PVC jacket. The 1249 cables use 26 gauge tinned copper conductors insulated with **expanded** polyethylene (XPE) with a PVC skin, an inner PVC jacket over the pairs, a dual aluminum foil shield with drain wire over the inner jacket, and an outer PVC jacket. Figure 1 depicts the cable components.

Table 1 compares the physical components of the two cables. The effects of each of the physical differences is discussed in the following sections.

TABLE 1. Cable Construction Comparison - 1249 vs. 600C

Component	600C	1249
Conductor Gauge	22	26
Insulation Materials	PE/PVC	XPE/PVC
Insulation Thickness	.0105"/.0015"	.0065"/.0015"
DOD*	.049"	.032"
Twist Lengths	2"- 5"	0.5"- 1"
Color Code	Dual	Solid
Shield Material	Alum. Foils	Alum. Foils
PVC Jacket	Outer Only	Inner & Outer

* Diameter Over Dielectric (DOD).

2.1 Insulated Conductors

Tinning is added to the copper conductors in both cables to ensure a low resistance long life termination when used with insulation displacement contact elements or wire-wrap pins. The insulation material used on the conductors in 1249 cable is 0.0065" of XPE and 0.0015" of PVC. The 600C conductors are insulated with 0.0105" of PE and 0.0015" of PVC. The XPE/PVC insulation is softer than PE/PVC. However, initial field trials have shown that the softness does not create installation problems.

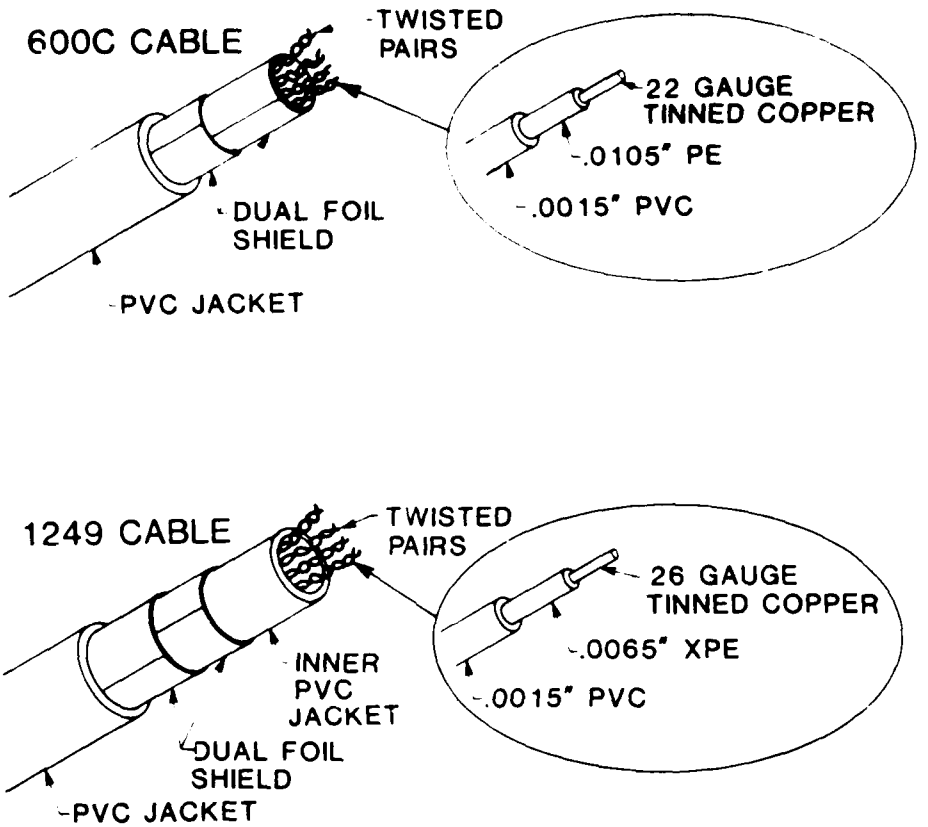


FIGURE 1. CABLE CONSTRUCTION COMPARISON 1249 vs. 600C

2.2 Twisted Pairs

Both cables use the standard telephony color code (blue, orange, green, brown and slate as primary colors, and white, red, black, yellow and violet as secondary colors[3]) to identify the pairs. In 600C cable each **lead** is *uniquely* identified. For example, pair one has a blue lead with white dots and a white lead with blue dots. In 1249 cable each **pair** *is uniquely identified*. For example, pair one has a solid blue lead and a solid white lead. Short twist lengths used in 1249 cable (less than one inch) ensure the leads of each pair do not come untwisted when the sheath is removed and pairs are handled for termination. The longer twist lengths used in 600C cable (2" to 5") may come untwisted when the sheath is removed. The short twists on 1249 cable not only guarantee the identification of each pair, but also reduce the chance of picking up extraneous interference, as discussed later.

2.3 Shield

The shield used on both cables is the same. It consists of two aluminum foil tapes applied longitudinally. Each tapes has .001" of aluminum with .002" mylar backing for mechanical stability. The tapes are applied with the aluminum surfaces facing each other, and a common drain wire between the two foils. To ground the shield, the drain wire can be wire-wrapped or soldered to the equipment ground system.

2.4 Cable Dimensions

Both cables come in a variety of pair counts. Table 2 shows the diameter and cross-sectional area of both cables. The combination of reduced conductor size and improved insulation material used on 1249 cable yields cross-sectional areas one-half that of the 600C cables. This reduced cross-section will result in one-half the cable pile-up in cable racks in central offices.

Figure 2 shows the congestion difference between the two cables in actual central office installations.

TABLE 2. Diameter and Cross-section vs. Pair Size - 1249 vs 600C

Pair Count	Diameter (inches)		Cross-section (sq. in.)	
	600C	1249	600C	1249
6	.39	.29	.15	.08
12	.48	.32	.23	.10
16	.54	.36	.29	.13
20	-	.39	-	.15
25	.64	.43	.41	.18
30	.69	-	.48	-
32	-	.47	-	.22
50	-	.60	-	.36

3. Comparison of Electrical Characteristics

Table 3 compares the nominal electrical parameters of the cables. Sections following the table relate the physical and electrical parameters to the performance of the cable.

TABLE 3. Typical Electrical Parameters - 1249 and 600C Cables

Parameter		600C	1249
Capacitance (nF/mi)		83	63
Impedance Ω at 772kHz		100	120
Attenuation dB per 1000'	772 kHz	4.6	5.9
	1.6 MHz	6.6	8.2
Crosstalk Improvement		-	5-15 dB
Meets DSX Template? - maximum length		yes 655'	yes 450'

3.1 Attenuation Comparison

As G. H. Webster shows,[4] 26 gauge pairs with 63 nF/mi mutual capacitance yield a cable of minimum cross-section for carrier frequency applications. Using expanded polyethylene (dielectric constant, ϵ = 1.6 nominal) as an insulation material for 1249 cable, instead of the solid polyethylene (ϵ = 2.3 nominal) used in 600C cable, along with choosing the appropriate insulation thickness yields a low capacitance, spatially efficient cable. The following equation is an excellent approximation for the high frequency attenuation (α) in terms of resistance (R), mutual capacitance (C), and inductance (L)[5] for pairs insulated with low loss dielectric materials like PE, PVC or XPE/PVC.

$$\alpha = \frac{R}{2}\sqrt{\frac{C}{L}}$$

Equation 1. High Frequency Attenuation

As Equation 1 shows, reduced mutual capacitance translates into reduced attenuation if all other parameters are constant. Therefore, as Webster suggests, by reducing the mutual capacitance of the 26 gauge cable to 63 nF/mi, we have lowered its attenuation by approximately 15%, when compared to a 26 gauge cable with 83 nF/mi capacitance. Due to the increased resistance of the 26 gauge conductors, the 1249 cable has approximately 30% higher attenuation than 600C cable. Figure 3 graphically

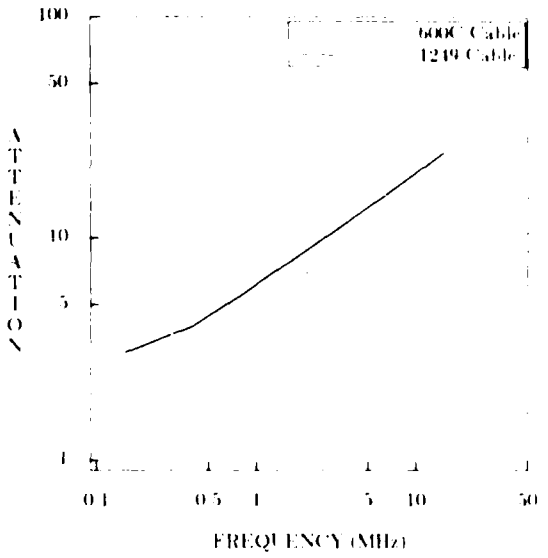


Figure 3. Attenuation (dB per 1000') vs. Frequency (MHz)

depicts the attenuation of both cables. While both cables have loss that is approximately proportional to the square root of frequency, it is interesting to compare the ratio of losses at 1.0 MHz and 0.1 MHz. This ratio is 2.8 for the 600C cable and is 2.2 for the 1249 cable. As will be shown below, the 1249 cable has less pulse distortion.

3.2 Impedance Comparison

Reducing the capacitance also raises the impedance (Z_0) as Equation 2 shows.[5]

$$Z_0 = \sqrt{\frac{L}{C}}$$

Equation 2. High Frequency Impedance

The impedance difference between 1249 and 600C cable may create a signal reflection at the DSX when equipment cabled with one type cable is connected to equipment cabled with the other type cable. Experiments have shown that these reflections are less than 0.4 dB, with very few reflections greater than 0.2 dB. Figure 4 shows the test set-up used to measure the reflections. The system implications of this reflection is discussed later.

3.3 Crosstalk and Immunity to Interference

The short twists improve the crosstalk between pairs within the 1249 cable. As Figure 5 shows, the short twists force the pairs to remain more spatially separated, while the longer twists used on 600C cable allow the pairs to nest together. The additional spatial separation is a major contributor to the improved crosstalk between pairs in the 1249 cable. Figure 6 graphically depicts the crosstalk differences between the two cables.

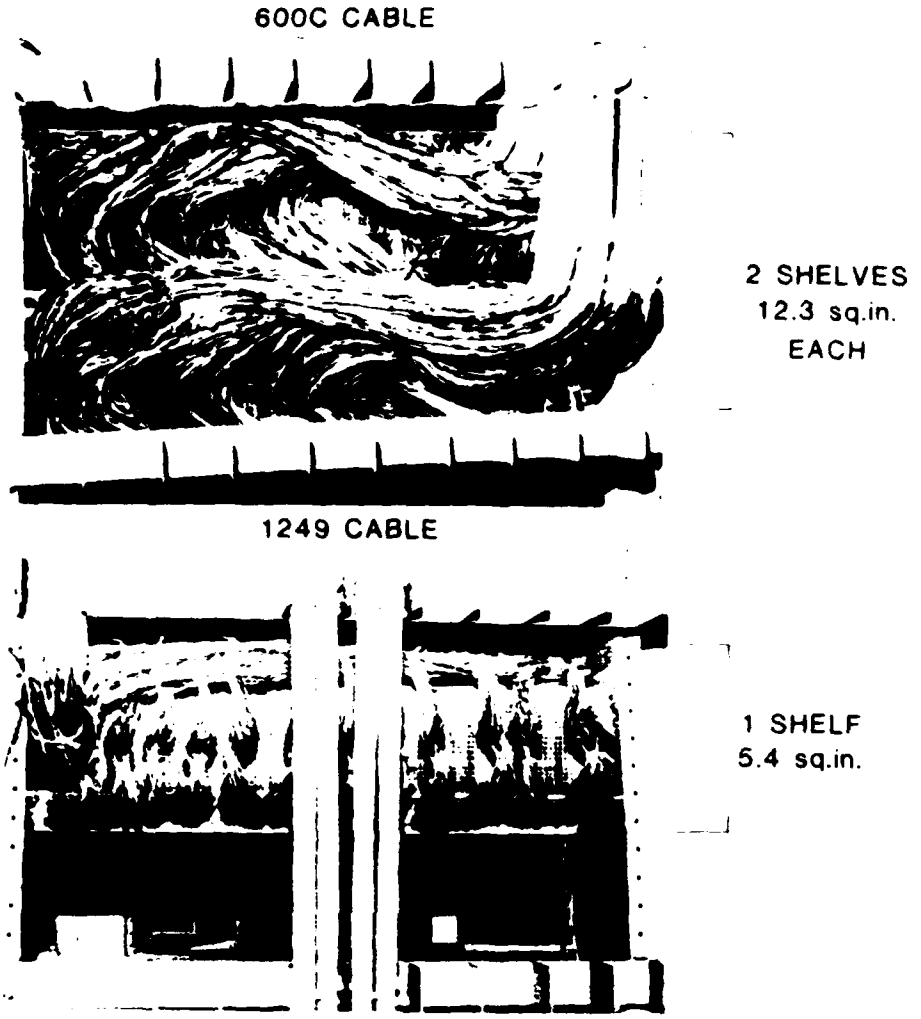


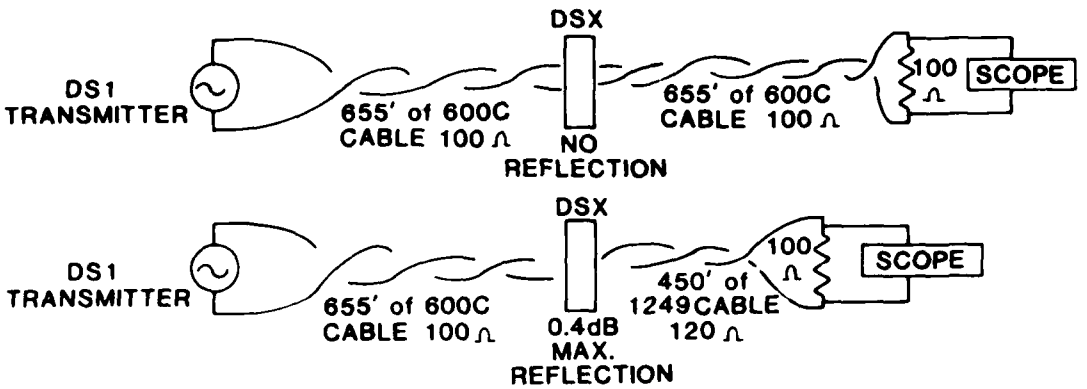
FIGURE 2. INSTALLATION COMPARISON

To terminate the cable leads on equipment, the sheath including the shield, must be removed from up to thirty six inches of cable. When the shield is removed, the pairs of both cables are more susceptible to EMI from outside interferers. The pairs of 600C cable, with their longer twists, often become untwisted when the sheath is removed, making them even more susceptible to EMI. The short twists used in the 1249 cable do not come untwisted when the sheath is removed. Therefore 1249 cables are more immune to central office interferers than 600C cables. This difference is difficult to quantify due to the variation in installation methods for these cables.

3.4 Inner Jacket Effect

The inner jacket on the 1249 cable spatially separates the insulated conductors from the foil shields. This separation reduces the high frequency resistance and capacitance while increasing the inductance. All of these changes as shown by Equation 1 reduce the attenuation for those pairs near the shield.

We gain another benefit from the inner jacket - improved impedance and attenuation **uniformity** between pairs within a cable and between different pair size cables. For example, at 1 MHz, the typical standard deviation for impedance is 1.0 Ω for 1249 cable and 2.3 Ω for 600C, and



METHOD :

1. MEASURE LOSS THROUGH TWO 655' PIECES OF 600C CABLE (6.0 dB)
2. MEASURE LOSS THROUGH 655' of 600C and 450' of 1249

655'	600C	= 3.0 dB
450'	1249	= 2.6 dB
REFLECTION		= 0.4 dB MAX.
TOTAL LOSS		6.0 dB MAX.

FIGURE 4. IMPEDANCE MISMATCH REFLECTION MEASUREMENTS

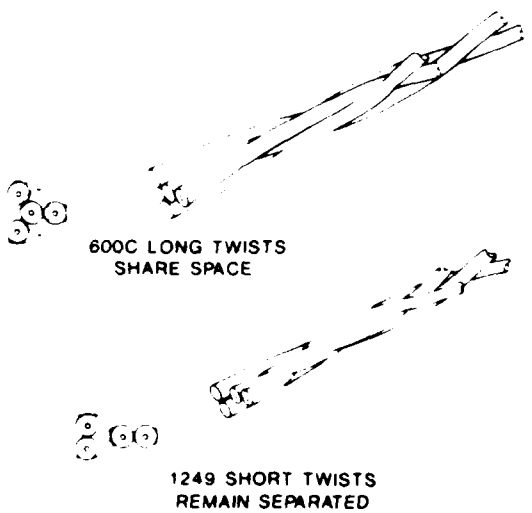
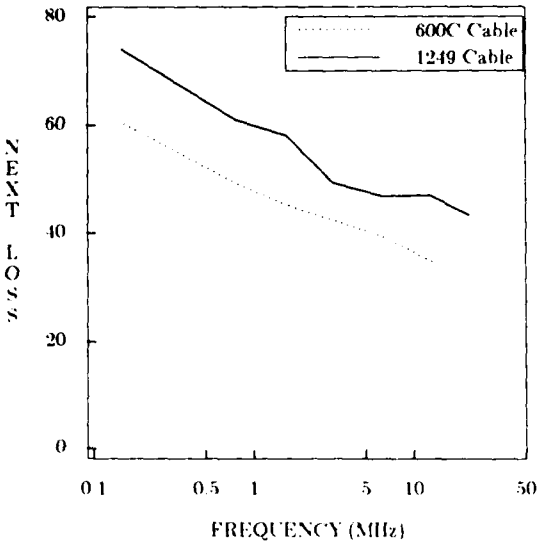


FIGURE 5. EFFECT OF TWIST LENGTH ON SPATIAL SEPARATION

the typical standard deviation for attenuation is 0.4 dB for 1249 cable and 0.7 dB for 600C cable. This means the transmission properties of each pair will be closer to the stated values for the 1249 cable than for the 600C.

4. DSX Standards

The DSX is a manual cross-connect point to interconnect the DS1 signals in a central office. It is a centralized location for testing, maintenance, and circuit rearrangement for these DS1 signals. In order to administer these functions, the DSX has become a well documented and standardized interface. The requirements stipulate that all signals on the DSX must meet the DSX pulse template, as shown in Figure 7. Therefore, the transmission properties of both the 600C and 1249 cables are designed to deliver the output of the DS1 equipment to the DSX so that the signal meets the DSX pulse template. Figure 8 depicts how the DSX pulse template measurements were performed. In all test cases (various types of equipment over various lengths of both cables), the pulse delivered to the DSX met the template. Figure 9 shows typical pulse shapes measured at the DSX for both cables. Additional information regarding the DSX, its uses, and test methods can be found in References 1 and 2.



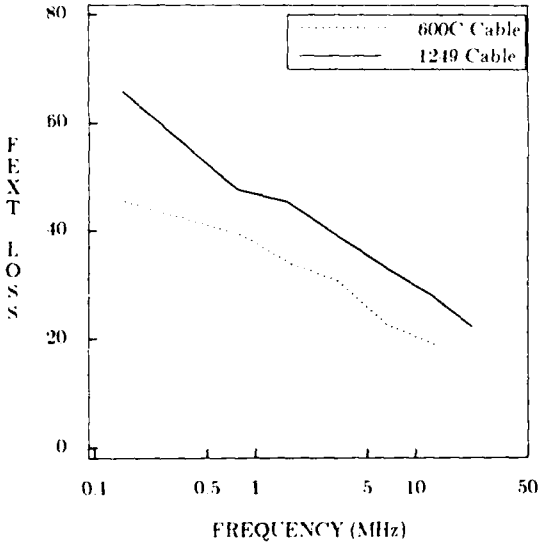


Figure 6. Near End Crosstalk (NEXT) and Far End Crosstalk (FEXT) vs Frequency (MHz)

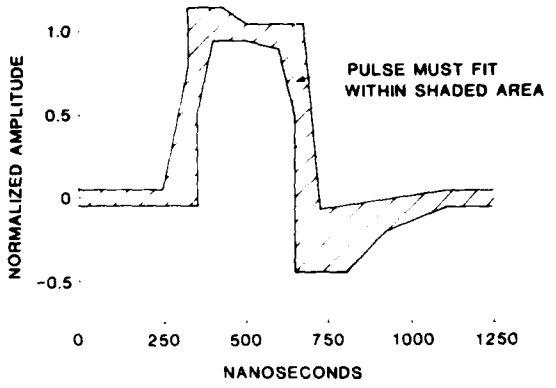


FIGURE 7. DSX PULSE TEMPLATE



FIGURE 8. DSX PULSE TEMPLATE TEST SET-UP

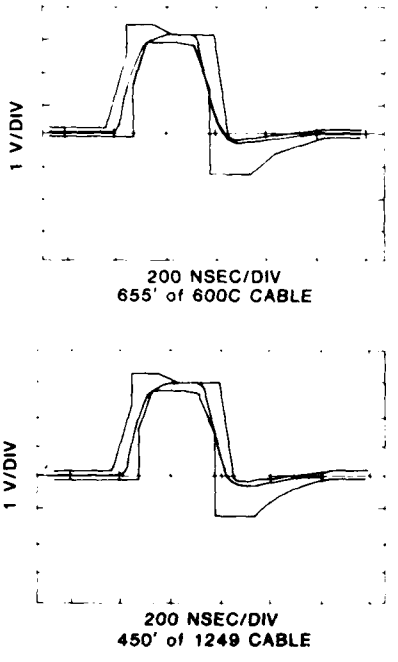


FIGURE 9. DSX PULSE TEMPLATE COMPARISON

As one would expect, there is a maximum cabling distance from the equipment to the DSX over which the pulse will meet the template. For 600C cables, this maximum distance is 655', or 3 dB of loss at 772 kHz. To account for the maximum possible reflection loss of 0.4 dB at the interface between equipment cabled with different cables, this maximum distance for 1249 cable is 450', or 2.6 dB of loss at 772 kHz.

At first glance, the length limitation for 1249 cable appears severe. However, a study of the 1985 central office cabling shows that over 99% of the cable runs are under 450', and in fact, over 96% are under 250'. Figure 10 shows the distribution of cable lengths. For those few cases where cable runs do exceed 450', the 600C cable should be used.

Several initial applications have been installed using 1249 cable between DS1 equipment and the DSX. All systems have performed without problems.

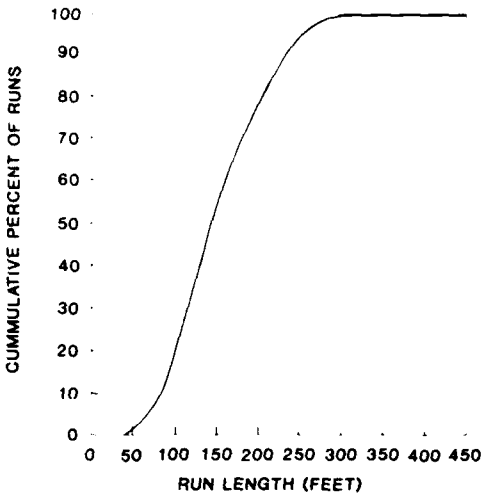


FIGURE 10. EQUIPMENT TO DSX CABLE LENGTH DISTRIBUTION

5. Summary

Laboratory tests and field experience show that the 26 gauge 1249 cable may be used in place of the 22 gauge 600C cable from DS1 equipment to the DSX when cable lengths are less than 450'. The reduced size of the 1249 cable helps relieves the cabling congestion problems in DS1 equipment and the DSX.

6. Acknowledgments

I would like to that the following people for their help in developing the cable, performing test, and editing this paper - Mr. H. W. Friesen, Mr. J. C. Hyder, Mr. E. L. Johnson, Mr. D. A. Lane, and Mr. W. G. Nutt, all of AT&T Bell Laboratories.

REFERENCES

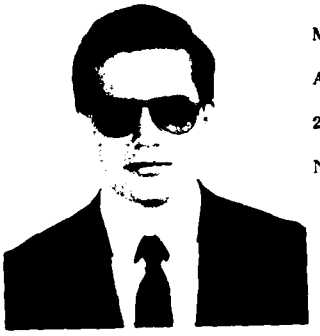
1. Bell Communication Research Technical Advisory TA-NPL-000320, "Fundamental Generic Requirements and Design Considerations for Metallic Digital Signal Cross-connect Systems DSX1, -1C, -2, -3," Issue 2, September 1986.

2. AT&T Compatibility Bulletin No. 119, "Interconnection Specification for Digital Cross-Connects," Issue 3, October, 1979.

3. "Standard PE-PVC Terminating Cable, Specification L-780491", Issue 1, AT&T Bell Laboratories, July 15, 1985.

4. Webster, G. H., "Material Savings by Design in Exchange and Trunk Telephone Cable", 1974 International Wire and Cable Symposium Proceedings, pp. 222-225.

5. Walter C. Johnson, *Transmission Lines and Networks* (New York: McGraw-Hill, 1950).



M. L. Fuller

AT&T Bell Laboratories

2000 Northeast Expressway

Norcross, Georgia 30071

Michael L. Fuller joined AT&T Bell Laboratories in Whippany, New Jersey in 1981 as a Member of Technical Staff. His responsibilities included physical design and systems design of copper interconnection equipment. In 1986 he moved to his current position in Atlanta where his responsibilities have included electronic wire and cable design. Before joining AT&T Bell Laboratories he received his BS and MS in Engineering Mechanics from Georgia Institute of Technology in 1980 and 1981 respectively.

HIGH SPEED MINIATURE COAXIAL RIBBON CABLE (RECTANGULAR JACKET TYPE)

Kazushi Kadoya, Akinori Mori, Toshiro Komura, Toshiyuki Abe and Kenichi Tanaka

Sumitomo Electric Industries, Ltd.
Tochigi, Japan

Summary

The advanced technology of highly expanded polyolefine, which comes from Sumitomo's original techniques for highly expanded insulation and irradiation is applied to develop high speed transmission cable of miniature size. We developed an advanced data transmission flat cable with high speed transmission, high density cabling and ease of assembly with a special profile rectangular jacket.

Highly expanded irradiated polyolefine insulation, which enables high speed transmission and miniature construction, and has a double-layer construction, the inner layer being foamed polyolefine with an expantion ratio of more than 80% and the outer layer being a solid skin layer. This construction was developed for the purpose of obtaining a higher expansion ratio, increasing the mechanical strength and maintaining good heat resistance.

Rectangular profile jacket construction (two signal conductors and two ground conductors laid longitudinally parallel) enables development of flat cable which has high density cabling, accuracy of conductor pitch and stability of conductor's horizontal positions.

We developed these electrical properties:
- dielectric constant of insulation is 1.25.
- propagation delay time is 1.1 nsec/ft.

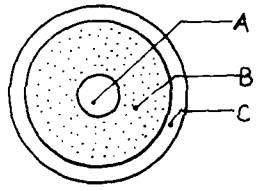
1. Introduction

Modern computers require coaxial cables in their main frames to achieve ultimate speeds. As the data processing capacity of these computers increases with reduced signal levels, hardware engineers want coaxial cables which have higher speed, higher density and better noise immunity, for use in their computers. To meet these needs, we have completed a high-speed, high-density coaxial flat cable using our unique expanded polyolefine extrusion technique, and irradiation techniques. The cable has an unusually low dielectric constant with high integration density, which can not be achieved by conventional high speed cables. This report introduces the production process to and performance parameters of the completed high speed miniature coaxial flat cable.

2. Construction

2-1. Insulation

While fluoric resin has a low dielectric constant and good stability as an insulation material, it is very expensive. Our interest was therefore turned to the inexpensive polyolefine. Conventional expanded polyolefine has an expansion ratio of around 60%. If the expansion ratio is increased to more than 80%, a dielectric constant 1.25 can be achieved. To increase the mechanical strength and to maintain good heat resistance, we employed a double layer construction, the inner layer being expanded polyolefine and outer layer being solid (Ref. Fig. 1), with both layers being irradiated.



A: center conductar
B: inner layer — expanded polyolefine
C: outer layer — solid polyolefine

Fig. 1 Construction of double-layer insulation

2-2. shielding

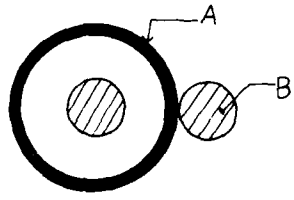
To facilitate outer shield conductor treatment at the ends of the cable, we employed an aluminum-polyester bonded tape. In order to improve the reliability of contact between shielding material and the drain wire, the aluminum surface of the tape was coated with evaporated copper.

During the jacket process, to prevent the change of the drain wire horizontal position by revolution of insulated conductor, we employed this construction. Drain wire was laid along the insulated conductor which was wrapped by shielding tape, to obtain electrical contact. The evaporated copper coated side was positioned outside. To adhere to the jacket, copper surface was partially coated with adhesive. (Ref. Fig. 2 and Fig. 3)



A: Adhesive
B: Evaporated copper
C: Aluminum
D: Polyester

Fig. 2 construction of shielding tape



A: shielding tape
B: drain wire

Fig. 3 position of drain wire

- - Jacket

To facilitate the treatment at the ends of the flattened cable and to prevent change of the drain wires position, we employed rectangler construction, and after the jacket process to prevent revolution, we employed a construction which is one unit with two conductors and two drain wires.

Ref. Fig. 4

For the jacket material, we employed PVC (polyvinyl chloride due to its superior flexibility.

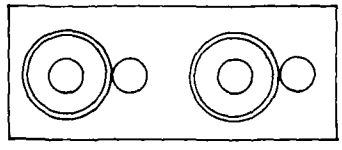


Fig. 4 one unit of rectangular construction

: Lamination

Fig. 5 shows the construction of flat cable. Both ends are laminated by special polyester tape with a coated adhesive. This adhesive adheres at low temperature and prevents electrical properties from decreasing. This tape facilitates the treatment at both ends of the cable.



Fig. 5 flat cable construction

Production process

Fig. 6 shows the production process.

extrusion of insulation

irradiation

shield tape wrapping

extrusion of jacket with drain

lamination

Fig. 6 production process

Properties of High Speed miniature coaxial flat cable

Table 1 shows the construction parameters of the high-speed miniature coaxial flat cable with an impedance characteristic of 75 ohm.

Table 1 construction of 75Ω high speed miniature coaxial flat cable

Item		Detail	
center conductor	material	silver coated copper alloy	
	size	AWG 32 / 0.18 mm φ	
insulation	inner layer	material	expanded polyolefine
		size	0.165 mm t
	outer layer	material	solid polyolefine
		size	0.07 mm t
drain wire	material	silver coated copper alloy	
	size	AWG 32 / 0.203 mm φ	
shielding tape	material	copper coated alumi polyester tape	
	size	0.015 mm t	
jacket	material	PVC	
	size	0.18 mm t	
laminated tape	material	polyester	
	size	0.05 mm t	

The following describes the characteristics of this cable.

: Dimensions

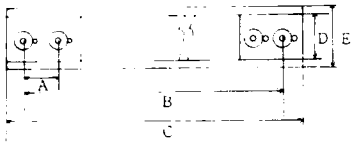
Table 2 shows the specification and measurement results of the cable.

- Electrical properties

The method of testing the electrical properties and their respective test results are shown in table 3, and the frequency dependence of attenuation is plotted in Fig. 7.

Table 2 specification and measurment results

construction



UNIT: inch

Item		Specification	Measurement results
number of unit		24	same
number of center conductor		48	same
number of drain wire		48	same
conductor pitch	(A)	0.05±0.006	0.0439～0.0552
total pitch	(B)	2.35±.002	2.348～2.369
cable width	(C)	2.48±.002	2.398～2.417
cable thickness	(D)	0.045±0.004	0.0428～0.0453
cable thickness	(E)	max. 0.05	0.0419～0.0440

Table 3 Electrical properties

Item	Test method	Test results
Conductor resistance of center conductor	Equipment: milliohmmeter at 20°C	N 5 Ω/km × 7066 3σ 107.1
Conductor resistance of drain wire	Equipment: milliohmmeter at 20°C	N 5 Ω/km × 674.2 3σ 7.47
Contact resistance of shielding tape and drain wire	Equipment: milliohmmeter method	N 5 (mΩ/m) × 13.06 3σ 21.9
insulation resistance	Equipment: Method 302, MIL STD-202E Test Voltage: DC 1000V	N 5 MΩ·km × $4.8 \cdot 10^{4}$ 3σ $1.2 \cdot 10^{4}$
static capacity	Equipment: LCR meter Test frequency: 1KHz	N 5 pF/m × 56.8 3σ 0.39
characteristic impedance (Zo)	Equipment: time domain reflectmeter sample length: 2m	N 20 Ω × 75.3 3σ 2.88
propagation delay (Td)		(nsec/m) N 20 × 3.83 3σ 0.05

$Zo = \frac{V \cdot V}{Vi - V} \cdot 50\ \Omega$

$Td = \frac{h \times \text{nsec/div}}{1 \times 2}$ (nsec/m)

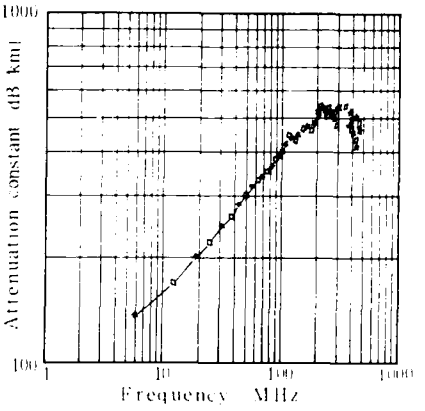


Fig. 7 The frequency dependence of attenuation

In order to achieve a high installation density in computers, intra bay cables may often be folded many times. We carried out the following flexibility test with actual installation situations in mind, and measured propagation delay. Ref Table 4

Table 4 Change of propagation delay after flexibility test

Item	Test method	N	Test results before test	during test	after test
Wind around a cylindorical 1.8inch rod	sample length: 1 meter 1.8 inch rod	1	383	383	383
		2	383	383	383
		3	381	381	381
		4	383	383	383
		5	383	383	383
Twist of cable (5 turn)	sample length: 1 meter	1	383	383	383
		2	381	381	381
		×	384	384	384
		4	383	383	383
		5	381	381	381
folding	sample length 1 meter 1kg weight 1turn	1	384	384	384
		2	383	383	383
		×	384	384	384
		4	383	383	383
		5	381	382	382

Table 4 shows that there was almost no change in propagation delay after the cable was subjected to various flexibility test. The tests results proved that the cable would easily endure the physical conditions in computer main frames.

(Ref. Table 5.) Table 5 shows that there was almost no change in characteristic impedance after environmental tests.

Table 5 Change of characteristic impedance after environmental test.

Item	Test method	N	Test result before test	Test result after test
Thermal shock test	temperature: 40℃ ~ +80℃ 5 cycle method: MIL-STD-202	1	76.9	76.9
		2	76.3	76.0
		3	75.7	76.1
		4	76.0	76.2
		5	75.8	75.8
Humidity test	Humidity: 90~95%, 40℃ 96 Hr method MIL-STD-202	1	74.2	74.2
		2	74.3	74.3
		3	75.8	75.8
		4	73.8	73.8
		5	75.2	75.2
Aging test	temperature: 12~℃ 168 Hr	1	77.~	75.1
		2	73.~	74.~
		3	74.8	74.8
		4	76.2	76.2
		5	75.~	75.~

4.3 Physical properties

The method of testing the physical properties and their respective results are shown in table 5.

Table 5 Physical properties

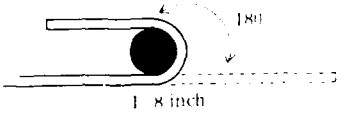
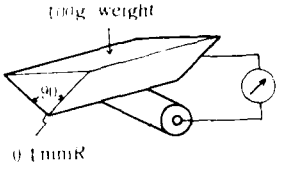
Item	test method	test results
Tensile strength	equipment: tensilon peeling speed: 50 mm/min when center conductor is broken, we measured tensile strength	(kg) N 5 x̄ 60.2 3σ 12.2
Bending test		(times) N 5 x̄ 1094 3σ 276
Friction life	movement rate of 0.5 mm φ rod is 60 times/min 	(times) N 5 x̄ 1515 3σ 156.9
Cut through of insulation	We measured the weight required to obtain a short between the cutting edge and the conductor or shielding tape	(kg) N 5 MIN. 1.0
Cut through of jacket		(kg) N 5 MIN. 3.0
	we measured insulation shrink back.	(mm)
soldering		N 5 x̄ 0.249 3σ 0.15
	Temperature of solder: 270 ℃	
Flamability	Vertical flame test UL 1581	N 5 all sample pass

Table 5 shows that the present cable has no problem with any of the physical tests described above.

5 Cable assembly

This flat cable usually connects to a connector or printed circuit board. Fig 8 shows an example of cable assembly.

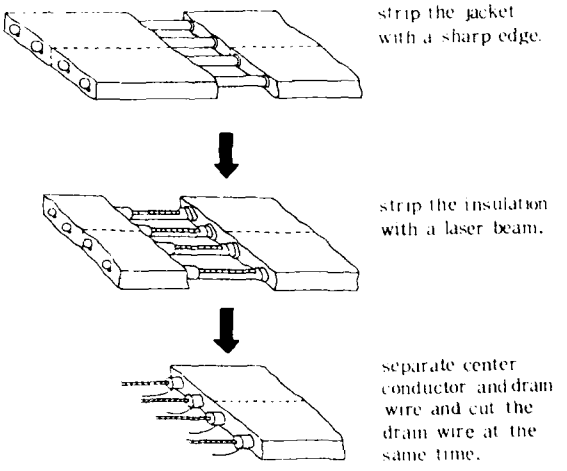


Fig 8 One example of cable assembly

Shielding tape did not appear at the cut section, because it adhered to the jacket. And because the center conductor and drain wire lay parallel equally spaced apart, it was very easy to assemble this cable.

6 Conclusion

A high-quality, high speed, miniature coaxial flat cable has been achieved using our unique expanded polyolefine extrusion technique, and electron radiation and lamination techniques. Its steady supply to the market has been assured. The cable satisfies all customer requirements, and provides extremely high cost effectiveness due to improved machinability.



Toshiro Komura

Sumitomo Electric Industries, Ltd. , Satsuki-cho, Kanuma-city, Tochigi prefecture Japan

Toshiro Komura received his B.S. degree in applied chemical engineering from Kyushu University in 1981. He then joined Sumitomo Electric Industries, Ltd., and engaged in manufacturing of plastic cables. Mr. Komura is now a member of Electronics Wire Division.



Kazushi Kadoya

Sumitomo Electric Industries, Ltd , Satsuki-cho, Kanuma-city, Tochigi prefecture Japan

Kazushi Kadoya received his B.S. degree in applied chemical engineering from Hokkaido University in 1976. He then joined Sumitomo Electric Industries, Ltd., and engaged in development and design of flat cables. Mr. Kadoya is now manager, Flat Components Section, Electronics Wire Division.



Toshiyuki Abe

Sumitomo Electric Industries, Ltd. , Satsuki-cho, Kanuma-city, Japan.

Toshiyuki Abe received his B.S. degree in applied chemistry from Hokkaido University in 1979. He then joined Sumitomo Electric Industries, Ltd., and engaged in development and design of plastic cables. Mr. Abe is now a member of Electronics Wire Division.



Akinori Mori

Sumitomo Electric Industries, Ltd. , Satsuki-cho, Kanuma-city, Tochigi prefecture Japan

Akinori Mori received his B.S. degree in mechanical engineering from Kyushu University in 1970. He then joined Sumitomo Electric Industries, Ltd., and engaged in development and design of plastic cables. Mr. Mori is now manager, Industrial Electronics Wire Section, Electronics Wire Division.



Kenichi Tanaka

Sumitomo Electric Industries, Ltd. , Satsuki-cho, Kanuma-city, Japan

Kenichi Tanaka received his B.S. degree in applied chemical engineering from Tohoku University in 1983. He then joined Sumitomo Electric Industries, Ltd., and engaged in development and design of flat cables. Mr. Tanaka is now a member of Electronics Wire Division.

ERROR CORRECTION OF CHARACTERISTIC IMPEDANCE MEASUREMENT OF TWISTED PAIR CABLES

Roland Hoffmann and Erich Stremme

Philips Kommunikations Industrie AG
D-5000 Köln 80, West Germany

ABSTRACT

Measuring the characteristic impedance of a twisted pair in a larger frequency range, its magnitude shows remarkable oscillating behaviour in the frequency region where the length of the cable is a whole number multiple of a quarter of the wavelength. Obviously, there will be a larger error in the results, measured at a single frequency in this region. This experimentally found effect has been explained by the occurence of an additional error current. Based on experimental and theoretical results a procedure has been developed and implemented on a computer controlled measurement system which gives error corrected values for the characteristic impedance for arbitrary frequencies.

1. INTRODUCTION

For carrier frequency application of twisted pair cables it is important to take impedance matching into account. To be able to do this it is necessary to know the relevant characteristic impedance. Since twisted pair cables are normally driven in the balanced mode, the odd-mode (or signal mode) characteristic impedance has to be measured. This will usually be done by measuring the input-impedances of the cable with open and short circuit end and calculating the value of the wanted characteristic impedance. Modern impedance measuring devices with an autobalancing bridge allow high precision impedance measurement and offer the possibilitiy of computer controlled systems. Carrying out a single measurement at a fixed frequency no problems are to be seen, while in a larger frequency range the magnitude of the characteristic impedance shows strong oscillatory behaviour periodic with frequency. This indicates that a large error will be obtained in the critical frequency range. To overcome this problem the behaviour will be analysed and a procedure given which allows to calculate error corrected values Z_O for arbitrary frequencies.

2. MEASURING PRINCIPLE AND RESULTS

In a two wire system symmetrical to ground two modes can propagate independently, the odd or signal mode and the even mode[1]. The characteristic impedances relate the voltages and the currents of each mode. They are in general different for each mode of propagation. As symmetrical cables are generally driven in the balanced mode we are interested in the odd-mode characteristic impedance.

Providing a symmetrical cable the input impedance will be symmetrical, too, for any symmetrical load. Thus, connecting the two wires to the test port of an impedance meter, without connecting the shield of the cable to ground will ensure the only excitation of the odd mode, independent of the voltages of the test port to ground. With the cable terminated with open and short circuits two input

impedances Z_{short} and Z_{open} will be obtained, and the characteristic impedance Z_o may be calculated by

$$Z_o = \sqrt{Z_{short} \cdot Z_{open}} \quad (1)$$

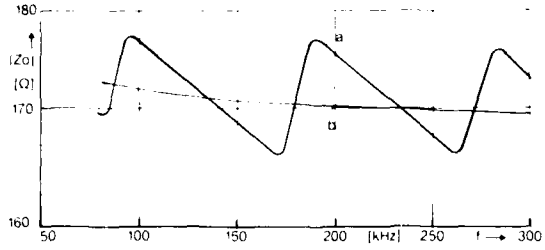


Fig. 1. Characteristic impedance of a twisted pair, l = 520 m,
a) measured values
b) error corrected values according to chapter 4.

Plotting the magnitude of the characteristic impedance over a large frequency range, an oscillatory behaviour will be observed, which occures periodic in frequency, Fig. 1. Taking additionally the curves of Z_{short} and Z_{open} into account, which are given in Fig. 2 for the frequency range of the first oscillation of Fig. 1 the following conclusions can be drawn:

1. The oscillations occur in the frequency range where the length of the cable is an integer multiple of a quarter of the wavelength, i.e.

$$l / \lambda = n/4, \quad n=1,2,3,....$$

Thus, this frequency range depends on cable parameters as well as on length and can not be predicted in advance.

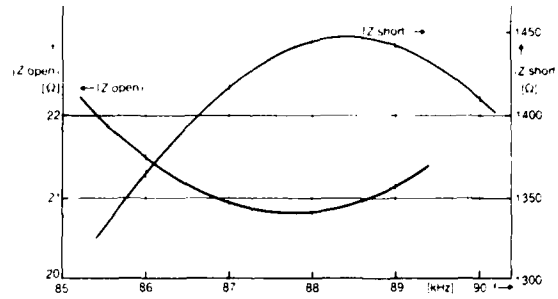


Fig. 2. Input impedances for the cable of Fig. 1, with short circuit (Z_{short}) and open circuit end (Z_{open}).

2. The maximum of Z_{short} and the minimum of Z_{open} occur at considerable different frequencies, while from theory they are expected to be at almost the same frequency (shifting some Hz).

3. ANALYSIS

To analyse the reason for this measuring result described above, we have to look more closely to the measuring principle and the environment of the device under test (DUT). The principle of the bridge measurement, Fig. 3 demands, that the test signal current I_1 is exactly equal at all points in the closed loop measuring circuit. If the DUT has no return path to ground, this condition will be met. In case of a cable as measuring object its shield has to be isolated from the measuring circuit. Doing this, the only excitation of the wanted odd mode will be ensured.

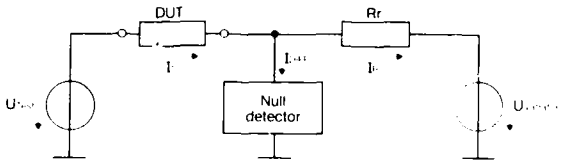


Fig. 3. Bridge measurement principle.

Due to the large extension of a reeled up cable, there will be a remarkable coupling to the surrounding environment. It has been found experimentally, that the optained measurement results depend on the grounding condition corresponding to the location, which may for instance be a stone or a steel floor in the factory. Increasing the coupling to ground weakly by a connection of the cable shield and ground with a resistor of some kOhm showed additionally that high values of the input impedance changed while low values remained unaffected.

The conductive and capacitive connection to ground will cause a small excitation of the even mode in the cable, which results in different currents in the conductors of the pair and an additional leakage current flowing from the cable shield to the measurement ground. Thus, the above mentioned condition for correct measurement is violated.

For a further analysis let us consider the following basical theoretical model. We assume, that the distributed effect of leakage current will finally result in a small error current dI superposed on the correct current in the near end of the cable. The input impedance for the open ending line can then be written as

$$\frac{i_n}{i_0} = \frac{\cosh(\gamma l)}{\frac{1}{Z_0}\cdot Z_{open}\cdot\sinh(\gamma l) + dI} \qquad (2)$$

and transformed into

$$Z_{open} = \frac{Z_0\cosh(\gamma l)}{\sinh(\gamma l) + i} \qquad (3)$$

where i indicates the resulting normalized error current, γ is the propagation constant and l the length of the cable. In a similar way we obtain the expression

$$Z_{short} = \frac{Z_0\sinh(\gamma l)}{\cosh(\gamma l) + i} \qquad (4)$$

for the line with short circuit end.

Fig. 4 shows the calculated results of the input impedances for realistic cable parameters, assuming a small error current effect. It is to be seen that the minimum and maximum of the input impedances are shifted, in agreement with experiments, (see Fig. 2). Furthermore, the error current only influences high values of the input impedance, while it lets low values unaffected, as described for the experimental behaviour above.

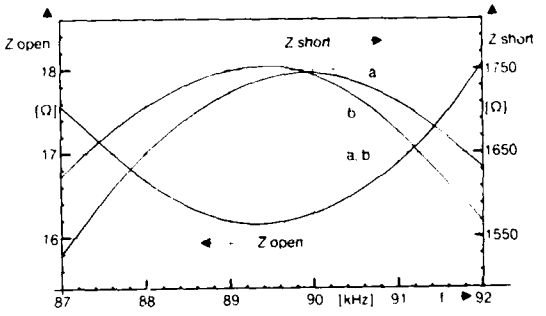


Fig. 4. Calculated input impedances for short circuit and open circuit cable, with (curve a) and without (curve b) error current (i_{max} = 0,012). Cable parameters
R′ = 55 Ohm/km, L′ = 0,9 mH/km,
C′ = 32 nF/km, G′ = 0,1 µS/km.
l = 520 m.

Calculating the characteristic impedance by eq. (1) from these input impedances, finally gives the curve in Fig. 5 showing the oscillating behaviour.

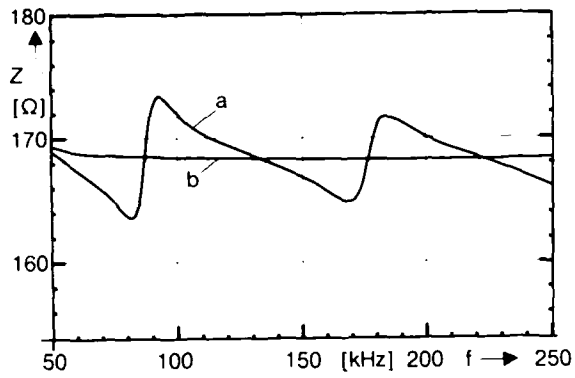


Fig. 5 Calculated characteristic impedance, with (a) and without (b) error current. (Same parameters as Fig. 4).

4. ERROR CORRECTION PROCEDUR

To correct the measurement error, it is necessary to obtain a curve corresponding to curve b in Fig. 5 from the measured results.

From Fig. 5 it is to be seen, that the measured curve and the correct one coincide in certain points. Measuring at these frequencies, the values will be correct. Comparing with the theoretical results for the input impedances, it turns out that the above mentioned points of coincidence occur for frequencies, where

$$|\quad| = |\quad| \qquad (5)$$

holds.

With the above obtained results, error correction will proceed as follows

1. Measuring the input impedances for cable open and short circuited in a certain frequency range with small frequency steps.

2. From these measured values calculating the frequencies fc where the condition eq. (5) holds.

3. Calculating the characteristic impedances by eq. (1) for the frequencies fc.

4. With the results of point 3. calculating the parameters A and B of the function

$$\quad A \frac{1}{\sqrt{\quad}} + \quad \qquad (6)$$

which approximates the correct behaviour of the magnitude of Z_0 by the method of least squares. Having abtained A and B of eq. (6) it is possible to calculate the characteristic impedance for any desired frequency within the measured frequency range.

A computer controlled measurement system has been used to implement the measurement procedure described above. The system consists of an automatic impedance meter, a computer and a printer. A user oriented program has been written that carries out all the measurements and calculations automatically and gives the characteristic impedance for the desired frequency.

Fig. 1 shows a plot of measured raw values (curve a) and error corrected values (curve b), while the user may choose, to print out only the numerical values for the desired frequencies.

CONCLUSION

When measuring the characteristic impedance with an impedance meter directly, wrong values will be obtained in periodic frequency ranges. These errors have been found to be caused by additional currents from cabel shield to ground, which violate the bridge measurement condition. An error correction procedure based on experimental and theoretical results has been implemented on a computer controlled measurement system.

REFERENCE

1 Marx, K.D., Propagation Modes, equivilent circuits, and characteristic terminations for multiconductor transmission lines with inhomogeneous dielectric, IEEE Transact. Microwave Theory Tech., MTT-21, pp. 450 - 457, July 1973.



Roland Hoffmann studied at the University of Bochum, West Germany, and received the Diplom degree in 1975 and the Dr.-Ing. degree in 1982 both in Electrical Engineering. From 1976 to 1985 he was a Research and Teaching Assistent at the Institut of High Frequency in Bochum where he worked on microwave theory and measuring technique. Since 1985 he has been with Philips Kommunikations Industrie AG in Cologne, where he is engaged in the development of cable measuring equipment.

Erich Stremme studied at the TH Aachen and received the Diplom degree in Electrical Engineering. Since 1965 he is with Felten & Guilleaume (F & G) which is now Philips Kommunikations Industrie AG (PKI), where he was head of the high-frequency cable production. Since 1976 he is engaged in the quality control of copper cables and optical fiber cables.

ULTRAFINE COAXIAL CABLE FOR HIGH SPEED TRANSMISSION

K.Yokoi , S.Satoh and A.Mori

Sumitomo Electric Industries , Ltd.
Tochigi , Japan

Summary

This paper describes the properties and features of ultrafine high speed coaxial cable developed for use in digital signal transmission. Recently,according to office automation through the introduction of LAN, complicated and large-scale networks have been emerging. As a result,maintaining space for wiring and the appearance of the cables can be serious problems.

To solve these problems,we have developed ultrafine coaxial cable with a velocity propagation of approximately 85% of air and a compact SMB connector, which have greatly improved the space factor and external appearance. Also,to design this new product, we have introduced waveform analysis by computer simulation. We believe this simulation will be very useful for the design of other transmission lines.

1 Introduction

Coaxial cable is widely used in digital signal transmission lines. The applications of this cable have increased in recent years as the pace of office automation has accelerated through the inroduction of LAN. With these developments,attention has been focused on such problems as the space required for wiring and the effect on office appearance. To solve these problems,it has become necessary to develop cable with greatly reduced size. Firstly,to develop this cable,it was necessary to clearly identify the requirements of the cable. Because coaxial cable was originally designed for use in analog transmission,this task was not a simple one. Thus,with the objective of analyzing the responsiveness of the cable in digital signal transmission,we developed and introduced a computer simulation for waveform analysis. To reduce the size of the cable,we first considered all of the wiring components,and then reduced the size which maintaining the balance between the cable and the connectors. For the cable,we used the highly expanded irradiated polyolefin insulation,and combined this with new SMB connectors. As a result,we were able to develop miniature coaxial cables for high speed signal transmission with a external diameter of approximately 50% and an overall space factor of approximately 30% of the previous product. We named this new product "Interface Coaxial Series" and have started marketing it.

2. Conventional coaxial cable and its design policy

2-1 Types and properties of coaxial cable

Conventional coaxial cables used for industrial wiring are usually devided into three types according to characteristic impedance,which is the most important electrical properties. Between computers and surrounding equipment such as display terminals,RG-62A/U coaxial cable with 93Ω characteristic impedance and air space dielectric for low copacitance is most widely used.

Recently,50Ω and 75Ω cables have been required for increased signal rates, and it is expected that the demand for these cables will steadily grow in the future. We initially selected representative conventional eables from each impedance category and started developing new miniature high speed coaxial cables that retained the other important properties of existing products. Construction and properties of conventional cables are shown in Table1. These cable can be defined as intermediate cables from a viewpoint of external diameter. For these cables,it is common to use BNC type connectors with a diameter of approximately 15mm ; Photo.1 shows its appearance. For reference,the ratio of connector diameter to cable diameter is about 2.4~3.0 and the overall appearance of the cable and the connector is poor.

Table1 Construction and properties of representative conventional cables

	Characteristic Impedance		93Ω	50Ω	75Ω
	Item \ Name		RG-62A/U	RG-58C/U	RG-59B/U
Construction	Inner Conductor	Material	Copper clad steel wire	Tinned annealed copper wire	Copper clad steel wire
		Nom.O.D.	0.643	0.900	0.584
	Insulation	Material	PE string + PE	PE	FE
		Nom.O.D.	3.71	2.87	3.67
	Outer Conductor	Material	Annealed copper wire single Braid	Tinned annealed copper wire single Braid	Annealed copper wire single Braid
		Nom.O.D.	4.51	3.51	4.47
	Sheath	Material		P.V.C.(Black)	
		Nom.O.D.	6.15	4.95	6.15
	Weight (Kg/Km)		52.65	37.66	55.75
Electrical properties	Conductor Resistance (Ω/loop·Km)		Nom. 146	Nom. 60	Nom. 176
	Dielectric Strength(ACV/1min)		3000	5000	7000
	Characteristic Impedance (Ω)		95 ± 5	50 ± 2	75 ± 3
	Velocity of Propagation (%)		Min 82	Min 64	Min 64
	Attenuation Constant (dB/Km) (at 400MHz)		Nom. 190	Nom. 340	Nom. 250
	Capacitance (pF/m)		Nom. 44.3	Nom. 93.5	Nom. 68.9
	Crosstalk (at 20MHz) (dB)		—	—	—
Connector	Connector		BNC	BNC	BNC
	Connector diameter /cable diameter		2.44	3.03	2.44

※ PE : Polyethylene



Photo.1

External appearance of conventional cable

2-2 Design considerations

Our main objective was to reduce cable diameter,but extreme miniaturization was not practical because the reduced mechanical strength of the cable would probably result in damage during installation. Moreover total balance of cable and connector size is an important factor for office appearance.

From these viewpoints,we finally decided to develop new miniature coaxial cable with an external diameter of approximately 50% of conventional products.

3. Design of miniature high speed coaxial cables

Conventional coaxial cables were originally developed for high frequency analog transmission. Through understanding of the frequency characteristic of the carrier wave, it is relatively easy to predict their output waveform. Because, in analog transmission, several signals are generally put on one carrier wave. However, it is very complicated to predict the output waveform of digital signal due to its mixed signal of various sinusoidal waves. Very little work has been done in the field of digital transmission analysis. Usually practical estimations are performed to confirm the properties of transmission lines. The estimation for one cable can't be applied to any other case, so the whole procedure has been extremely inefficient. This paper describes an analytical system for digital signal transmission by computer simulation.

3-1 Transmission line and model waveform

A cable circuit can be defined as a linear and time constant system. The transfer mechanism in a transmission line is simply described as shown in Fig.1. Provided that the digital input f(t) is a periodic wave, its output g(t) can be described by

$$g(t) = \sum_{n=-\infty}^{\infty} Cn \cdot H(n\omega_0) e^{jn\omega_0 t} \quad \cdots (1)$$

$$f(t) = \sum_{n=-\infty}^{\infty} Cn \cdot e^{jn\omega_0 t}$$

where ω_0 =fundamental angular frequency

Cn =complex fourier coefficient

Cn and $H(n\omega_0)$ as expressed in the above equations are both complex and can be devided as follows:

$$Cn = Cnr + jCni \quad \cdots (2)$$

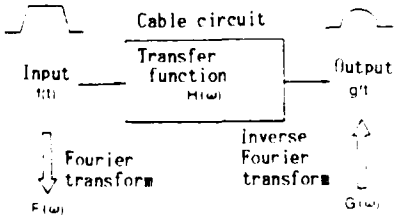
$$H(\omega) = R(\omega) + jX(\omega)$$

Cnr : real part of Cn

Cni : imaginary part of Cn

$R(\omega)$: real part of $H(\omega)$

$X(\omega)$: imaginary part of $H(\omega)$



$$H(\omega) = G(\omega) \cdot F(\omega)$$

Fig.1 Transfer mechanism of cable circuit

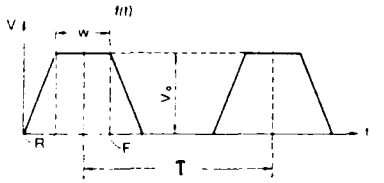
Any transmission line is a passive circuit because the primary constants (R,L,C,G) are all represented by real numbers. For this reason, Cr and $R(\omega)$ become even an function and Ci and $X(\omega)$ become an odd function. Therefore, equation(1) can be transformed as follow.

$$g(t) = CorR(0) + 2\sum_{n=1}^{\infty} Cnr\, R(n\omega_0)\cos(n\omega_0 t) - X(n\omega_0)\sin(n\omega_0 t) - 2\sum_{n=1}^{\infty} Cni\, R(n\omega_0)\sin(n\omega_0 t) + X(n\omega_0)\cos(n\omega_0 t) \quad \cdots (3)$$

we can actually calculate g(t) from equation(3)

3-2 Simulation procedure

The digital signal f(t) can be approximately described by a trapezoidal waveform as shown in Fig.2.



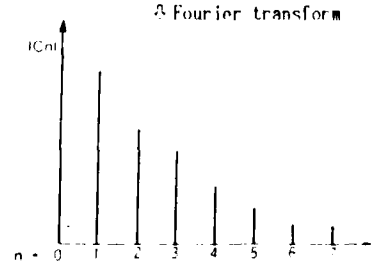
T : period

R : rise time (0~100%)

F : fall time (0~100%)

W : pulse width (upper width)

② Fourier transform



$$\left(\omega_0 = \frac{2\pi}{T} = 2\pi f_0\right)$$

$$Cn = \frac{Vo}{T(n\omega_0)^2}\left\{\frac{1}{R}(e^{-jn\omega_0 R} - 1) + \frac{1}{F}(e^{-jn\omega_0(R+W)} - e^{-jn\omega_0(R+W+F)})\right\}$$

Fig.2 Pulse waveform

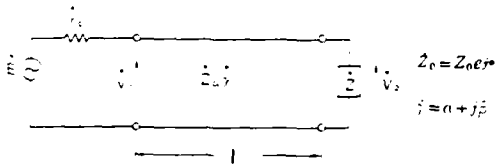
The equivalent circuit of a transmission line is shown in Fig.3 and the transfer function is defined as follow.

$$\dot{H}(\omega)=\dot{V}_2(\omega)/\dot{V}_1(\omega)\cdots(4)$$

From equation (4) and Fig.3, we can introduce the next equation.

$$\dot{H}(\omega)=\frac{2\dot{Z}_L(\omega)}{\dot{Z}_0(\omega)+\dot{Z}_L(\omega)}\,e^{\dot{\gamma}\omega l}\,\frac{1}{1+\dot{e}(\omega)e^{-2\dot{\gamma}(\omega)l}}\quad\cdots(5)$$

$$\text{Where } \dot{e}(\omega)=\frac{\dot{Z}_L(\omega)-\dot{Z}_0(\omega)}{\dot{Z}_L(\omega)+\dot{Z}_0(\omega)}\quad\text{(reflection cofficient)}$$



Where

Z_0 = absolute value of $\dot{Z}_0$ (Characteristic Impedance)
ϕ = angle of $\dot{Z}_0$
$\dot{\gamma}$ = propagation constant (per unit length)
α = attenuation constant
β = phase constant
$\dot{Z}_L$ = lord impedance
$\dot{r}$ = source impedance
l = cable length
$\dot{V}_1$ = input voltage
$\dot{V}_2$ = output voltage

Fig.3 Equivalent circuit of transmission line

To obtain the output wave g(t) from the input wave f(t), following processes are necessary.

(1) calculation of $\dot{C}_n$ from f(t) by Fourier Transform.
(2) calculation of $\dot{H}(\omega)$ from transfer properties ($\dot{Z}_0$, $\dot{\gamma}$, l) and external circuit parameters.
(3) multiplication of $\dot{C}_n$ and $\dot{H}(\omega)$
(4) calculation of g(t) by inverse FFT (Fast Fourier Transform)

These processes are schematically described in Fig.4. As shown in Fig.4, our simulation program can be devided into several important blocks and the main feature of this simulation is that the precision of the calculation logic can be verified in each block.

Actual and simulated waveform are shown in Fig.5 and Fig.6. Values of actual measurement and computer simulation are described in Table2. Regarding Vp-p (peak to peak of the voltage) and Tr (rise time) of the output wave, errors between their evaluations are about 5%. We can say that this simulation is accurate enough for most applications.

Table2 Comparision between actual measurement and computer simulation

Item	Sample		Interface coaxial cable 502111
Td	actual	ns	15.51
	simulation	ns	15.52
	difference	%	0.06
Vp-p	actual	ns	550.0
	simulation	ns	572.0
	difference	%	4.0

3-3 Other design considerations

In addition to the previous considerations, shilding effectiveness is expected to become more important in the future. Even though several method for estimating shielding effectiveness have already been announced, a conclusive one has not been found yet. In this case, we selected crosstalk and surfase transfer impedance for the evaluation of shielding effectiveness.

4. The properties of new products

Construction and properties of representative of our "interface coaxial cable" are shown in Table3. Photo.2 shows external appearance of these new products. Characteristic impedance (Zo), attenuation constant(α) and phase constant(β) of component No.502101 are shown in Fig.7. By selecting highly expanded irradiated polyolefin insulation, we have achieved the desired reduction of the external diameter.

As a result, we were able to develop new coaxial cables with an external diameter of 56~70% and a space factor of 32~49% of conventional cables. However the outer conductor described in Table3 is a double shielded construction composed of aluminized polyester tape and tinned annealed copper wire braid, we can produce a cable with a shield composed of annealed copper wire braid. Customers can selected the preferable one by considering use conditions. Differences between the single and double shielded constructions are shown in Fig.8 and Fig. 9. When we decided the cable constructions, we paid much attention to the size and the properties of a connector.

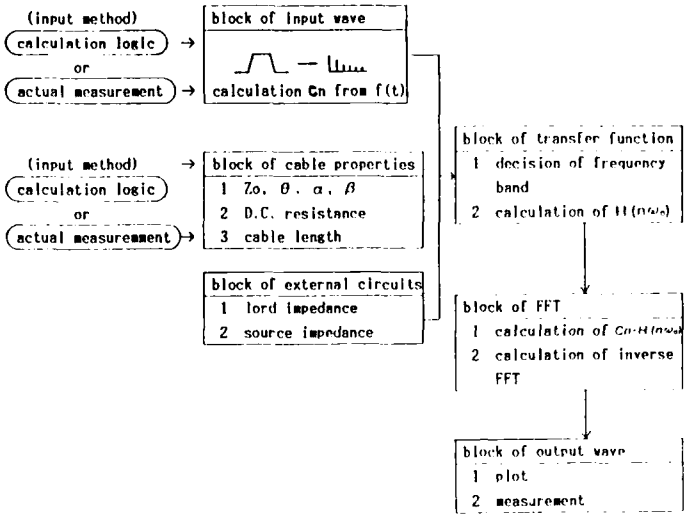
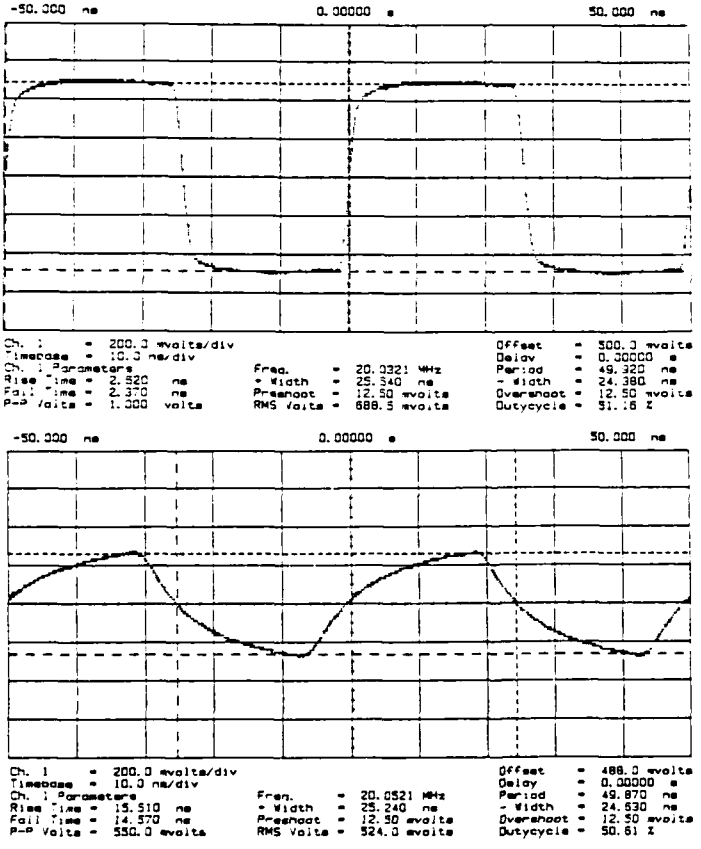


Fig.4 Block chart for simulation



input waveform

output waveform after driving of 100m cable

Fig.5 Actual pulse waveform

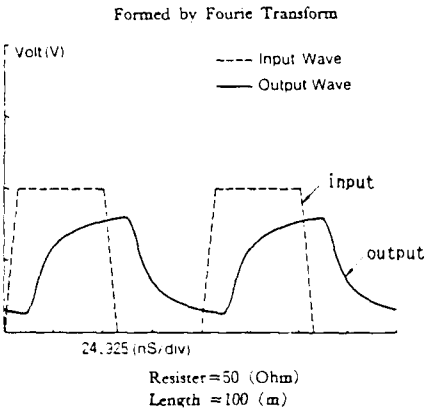


Fig.6 Pulse waveform by computer simulation



Photo.2
Interface coaxial cable and connectors

Table3 Construction and properties of interface coaxial cables

	Item		93Ω	50Ω	75Ω
	Characteristic Impedance / Component No.		932601	502101	752201
Construction	Inner Conductor	Material	Tinned annealed copper wire	Annealed copper wire	Annealed copper wire
		Nom.O.D.	0.404	0.900	0.600
	Insulation	Material	Highly expanded irradiated polyolefin	Highly expanded polyolefin	Highly expanded polyolefin
		Nom.O.D.	2.25	2.25	2.60
	Outer Conductor	Material	Alminized polyester tape and single Braid of 0.1 ~ 0.12 + tinned annealed copper wire		
		Nom.O.D.	2.85	2.80	3.30
	Sheath	Material	P.V.C.(Black·Gray)		
		Nom.O.D.	3.45	3.45	4.20
	Weight (Kg/Km)		12.78	18.45	23.08
	Conductor Resistance (Ω/loop·Km)		Nom. 166	Nom. 74	Nom. 79
Electrical properties	Dielectric Strength(ACV/1min)			1000	
	Characteristic Impedance (Ω)		93 ± 5	50 ± 2	75 ± 3
	Velocity of propagation (%)		Min. 87	Min. 80	Min. 80
	Attenuation Constant (dB/Km) (at 400MHz)		Nom. 260	Nom. 340	Nom. 250
	Capacitance (pF/m)		Nom. 44.3	Nom. 93.5	Nom. 68.9
	Crosstalk (at 20MHz) (dB)			Max −70	
Connector	Connector		SMB	SMB	SMB
	Connector diameter /cable diameter		1.74	1.74	1.43
Comparision with conventional products	Weigtht		0.24	0.49	0.43
	Ratio of external diameter		0.56	0.70	0.68
	Space Factor		0.32	0.49	0.47
	Conventional cable		RG-62A/U	RG-58C/U	RG-59B/U

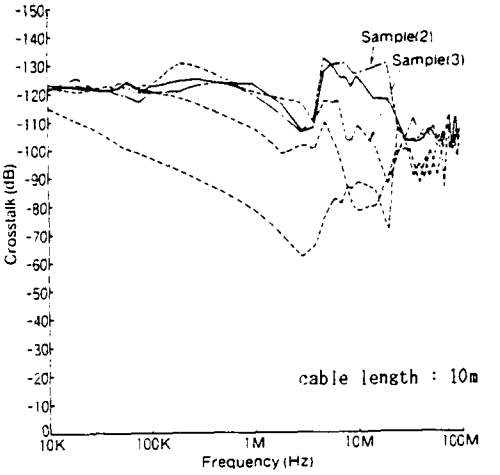
We finally selected a compact SMB connector because its external diameter is less than 50% of conventional BNC connectors. Also,it has a good appearance with the interface coaxial cable and it is easily handled as a "push-on" type.

This interface coaxial cable is most appropriate for use as a digital signal transmission line,which the length is less than 100m and the signaling rate is less than 50Mbps. In addition to above use,this cable may be used as a patch cable for measuring equipment and communication products where the benefit of small size and light weight are important.

5. Conclusion

Previous approaches to reduce the size of wiring systems have considered only the cable or the connector. By designing the cable and the connector as a total system,we have developed components that are totally compatible and that can be mated with existing equipment.

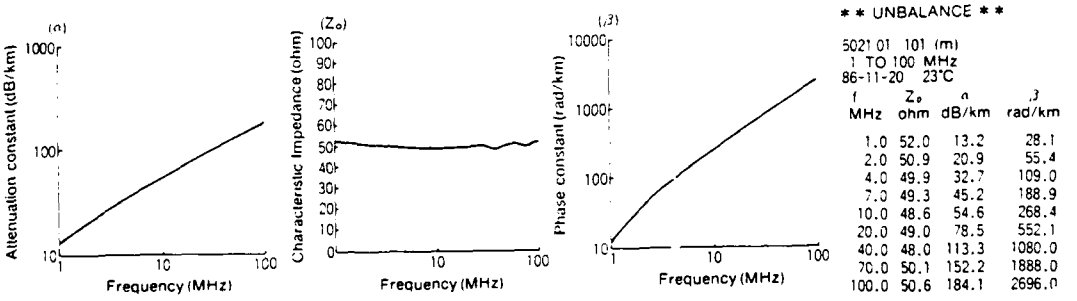
Finally,there were few examples of evaluation of digital signal transmission because of inadequate measuring equipment. Our simulation system has reached the level of practical use. Now,we are proceeding to develop this simulation for application for more complex circuits. We will be able to recommend most suitable design for cable as a wiring component of large-scale network systems.



	Name	N/F
Sample(2)	932601 (Double shielded)	NEXT
Sample(3)	932211 (Single shielded)	NEXT

Freq (MHz)	Sample(2) Val.	Sample(3) Val.	Freq. (MHz)	Sample(2) Val.	Sample(3) Val.
.0100	-121.4	-122.5	4.0000	-110.8	-108.8
.0200	-125.7	-120.6	5.0000	-132.3	-117.1
.0400	-121.2	-119.9	6.0000	-129.5	-116.3
.0700	-118.2	-120.1	7.0000	-130.1	-117.1
.1000	-120.3	-122.3	8.0000	-130.5	-102.9
.2000	-120.5	-130.7	9.0000	-126.6	-102.1
.3000	-122.9	-129.2	10.0000	-126.3	-108.3
.4000	-123.3	-127.6	20.0000	-130.2	-86.1
.5000	-123.7	-125.3	30.0000	-101.5	-104.3
.6000	-123.7	-124.7	40.0000	-105.2	-86.4
.7000	-122.3	-122.9	50.0000	-105.3	-89.1
.8000	-122.1	-121.9	60.0000	-102.3	-89.7
.9000	-120.3	-121.2	70.0000	-103.1	-84.0
1.0000	-119.3	-120.7	80.0000	-102.6	-104.8
2.0000	-112.0	-118.1	90.0000	-101.4	-107.5
3.0000	-105.8	-116.3	100.0000	-106.0	-101.2

Fig.8 Crosstalk characteristic of interface coaxial cable



f MHz	Z_o ohm	α dB/km	β rad/km
1.0	52.0	13.2	28.1
2.0	50.9	20.9	55.4
4.0	49.9	32.7	109.0
7.0	49.3	45.2	188.9
10.0	48.6	54.6	268.4
20.0	49.0	78.5	552.1
40.0	48.0	113.3	1080.0
70.0	50.1	152.2	1888.0
100.0	50.6	184.1	2696.0

Fig.7 Properties of interface coaxial cable

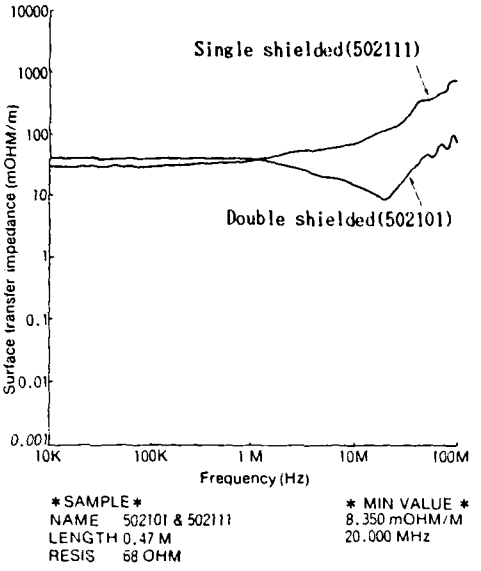


Fig.9 Surface transfer impedance of interface coaxial cable



Kiyonori Yokoi

Sumitomo Electric Industries,Ltd.
3-3,Satsuki-cho,
Kanuma-city,
Tochigi-prefecture
Japan

Kiyonori Yokoi received his B.S. degree in electric engineering from Keio university in 1985. He then joined Sumitomo Electric Industries,LTd.,and engaged in development and design of plastic cables. Mr.Yokoi is now a member of Engineering Section,Electronics Wire Division.



Shizuyoshi Satoh

Sumitomo Electric Industries,Ltd.
3-3,Satsuki-cho,
Kanuma-city,
Tochigi-prefecture
Japan

Shizuyoshi Satoh finished the electric engineering course of Tsuyama Technical College in 1968. He then joined Sumitomo Electric Industries,LTd.,and engaged in development and design of plastic cables. Mr.satoh is now Senior Engineer,Engineering section, Electronics Wire Division.



Akinori Mori

Sumitomo Electric Industries,Ltd.
3-3,Satsuki-cho,
Kanuma-city,
Tochigi-prefecture
Japan

Akinori Mori received his B.S. degree in Mechanical engineering from kyusyu University in 1970. He then joined Sumitomo Electric Industries,LTd.,and engaged in development and design of plastic cables. Mr.Mori is now Manager,Engineering Section,Electronics Wire Division.

CROSSTALK AND SHIELD PERFORMANCE SPECIFICATIONS FOR ALUMINUM FOIL SHIELDED TWISTED PAIR CABLE (MIL-C-49285)

James A. Krabec

Belden Technical Research Center
Geneva, IL

ABSTRACT

Statistical results for balanced mode near-end and far-end crosstalk measurements are presented for individually aluminum foil shielded twisted pair cables. Results are shown to demonstrate an inherent wide variation in performance from pair to pair. These results are compared to measurements on common axis (parallel) pairs. Data is presented to support higher frequency (above 1 MHz) test requirements for shielded pair crosstalk specifications. Measurements for shielding effectiveness of these cable designs are presented using the SEED® fixture test method proposed for MIL-C-49285. The method is discussed and results are interpreted in terms of the shield transfer impedance.

* SEED is a registered trademark of Cooper Industries.

INTRODUCTION

Aluminum foil shielded twisted pair cables have enjoyed wide acceptance in both U.S. military and industrial applications for over 20 years. This high degree of acceptance has been possible because there has essentially been a single supplier of this cable type. U.S. patent protection of the design and high quality cable manufacturing practices have ensured a steady supply of cable for U.S. military usage without the need for costly Mil Spec paperwork and QPL procedures. In a post-patent protection era, however, purchase documents and Mil Specs are required to ensure a reliable supply of cable product from the cable industry.

This paper reports on the work undertaken to develop new shielding and crosstalk specifications for aluminum foil shielded twisted pair cables. The specifications are currently embodied in a U.S. government purchase document CR-CS-0099-000 (CR-CS), and will appear in MIL-C-49285 in the near future. These are important parameters for the evaluation of cable performance and quality, but they can be difficult to measure and specify. During the past two years, crosstalk and shielding measurements have been conducted on these types of cable designs to assist in the development of the government specifications. The emphasis in these evaluations is placed on the test methods and requirements that were specified in the then newly released CR-CS document (1984). Therefore the data presented in this paper is focused on results from these test methods.

The CR-CS crosstalk test is conducted on adjacent cable pairs in a balanced configuration using a sample length of 150 feet. The requirement currently gives only worst case limits for near-end and far-end crosstalk at 40 KHz, 70 KHz, 100 KHz, and 1000 KHz. These crosstalk measurements were made on more than twenty cable constructions. The results show a large pair to pair variation, similar to those found for unshielded telephone cables, making the assignment of minimum values difficult.

The shielding requirement in CR-CS calls for a SEED test with minimum limits for nine frequencies between 0.1 MHz to 30 MHz plus one limit at 100 MHz. During the study, this test was conducted on samples that had defects intentionally introduced in the shield to see if performance changes were observable. These results are shown along with results of a similar evaluation using an absorbing clamp test method. More than thirty cable constructions were evaluated using the SEED test method. Above 20 MHz, a data range of more than 20 dB is found for different shielded pair designs and an explanation is provided through consideration of the shield transfer impedance.

CROSSTALK

Cable Designs

The cable types subjected to crosstalk are described in Table 1. Each pair has a foil wrap consisting of a lamination of 0.00033 inch aluminum and 0.0005 inch polyester. The wrap is applied with the edges folded to isolate the two laminated layers. Cable types A through E consist of standard twisted shielded pairs which are wrapped with the foil facing inward. In these constructions, the pairs are cabled in layers with each layer having the same lay length; thus the position of a pair is maintained along the cable. Cable types A, B, and C comprise a family of different pair count constructions as shown. The last two cables described in Table 1, types F and G, are common

TABLE 1 - Description of Multipair Cables

TYPE	WIRE AWG	INSULATION TYPE, THICKNESS (inches)	DRAIN AWG	NO. OF PAIRS	PAIR LAY (inches)	CR-CS DESIGNATION
A	22(1)	PVC, .013	22(1)	3,6,9, 11,15	1.75	015, 018, 003 006, 017
B	22(7)	PP, .010	22(7)	3,6,9,11, 12,15,19,27	1.75	012,004,[illegible],009, 022,002,005,015
C	24(7)	Foam PE, .023	24(16)	3,6,9, 15,19,27	1.75	035,038,037 036,034,033
D	18(16)	PP, .016	20(26)	9	2.0	006
E	20(10)	PP, .013	22(16)	15	1.75	025
F	22(7)	PP, .008	22(16)	2	1.5	013
G	22(7)	PP, .008	24(7)	2	1.25	020

axis designs. Here the pairs are twisted around a common center, but are not twisted around each other. In type F, the foil is facing outward and a common drain wire is used. The type G design has the foil facing inward with individual drain wires for each pair. (These designs are detailed in CR-CS and the appropriate slash sheet code is shown in the table.)

Test Method

Both near-end and far-end crosstalk tests were performed; the near-end test set-up is diagrammed in Figure 1.

According to the CR-CS method, a voltage signal is applied to one cable pair and the induced voltage on an adjacent pair is monitored. The crosstalk value is then expressed as the ratio of the induced to the applied voltage, in dB. The other pair shields within the cable are grounded at the input end during the test. A Hewlett-Packard 3577A Network Analyzer was used to generate the input signal and to detect the coupled signal on the adjacent pair. Center-tapped transformers - baluns - provided the balanced load for the cable pairs. This was chosen to be 100 ohms for the type C cable constructions and 50 ohms for all the others, to best match the characteristic impedance of the shielded pair. The crosstalk data was stored on computer files for later statistical evaluations.

Measurements

Many different adjacent pair crosstalk values can be measured on multipair cables. A fifteen pair (11 @ 4) cable design has 23 such combinations of driven and receptor pairs. Our testing was structured to evaluate all possible combinations on three cable samples taken from a single manufacturing lot. Following this, a second manufacturing lot was tested in the same way.

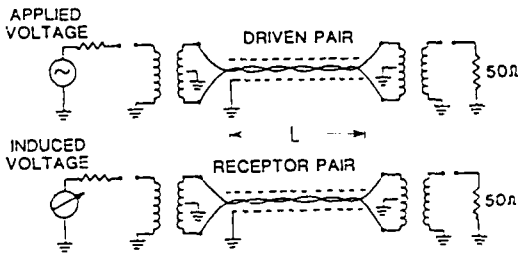


Figure 1 - Test configuration for near-end crosstalk measurement.

Table 2 presents the mean crosstalk values and standard deviations for the 19 pair type C cable. Two hundred sixteen pairs were measured at 40 KHz, 70 KHz, 100 KHz, and 1000 KHz, for both near-end (NEXT) and far-end crosstalk (FEXT). The measurements are seen to have a standard deviation of 8 dB to 10 dB at all frequencies. Also notice that the NE and FE values are essentially equivalent for the first three frequencies tested. This is expected at frequency measurements where $L < \lambda/10$. At 1000 KHz, $L \sim \lambda/5$ for this shielded pair design and a small difference in the two crosstalk values is observed here.

Table 2 - Crosstalk data for 19 pair Type C Cable - 216 Pairs Tested
m = mean value
s = std. dev.

Freq. (KHz)	NEXT(dB) m	NEXT(dB) s	FEXT(dB) m	FEXT(dB) s
40	96.1	9.4	96.2	9.6
70	91.5	9.4	91.4	9.4
100	88.8	9.3	88.9	9.4
1000	83.6	8.0	86.1	10.2

Figure 2 shows histograms corresponding to the NEXT data given in Table 2, so that the data distributions can be seen clearly. The values are broadly dispersed with a shape that resembles a normal probability distribution.

Table 3 shows the same NEXT data, at 100 MHz, broken down into pair groups within the 12 @ 6 @ 1 cable design and the two production lots. The crosstalk values and standard deviations are reasonably consistent from group to group and lot to lot.

Table 3 - Statistical Data for NEXT @ 100 MHz
19 Pair type C Cable

Pair Groups	Lot 1		Lot 2		Both Lots	
	m	s	m	s	m	s
Outer	86.1	8.1	85.4	9.7	85.7	8.9
Middle	92.8	13.2	88.0	7.3	90.4	10.8
Outer Middle	92.4	9.5	89.3	6.6	90.8	8.3
Middle Inner	89.0	6.9	89.8	9.5	89.4	9.1
All Groups	89.8	10.0	87.9	8.5	88.8	9.3

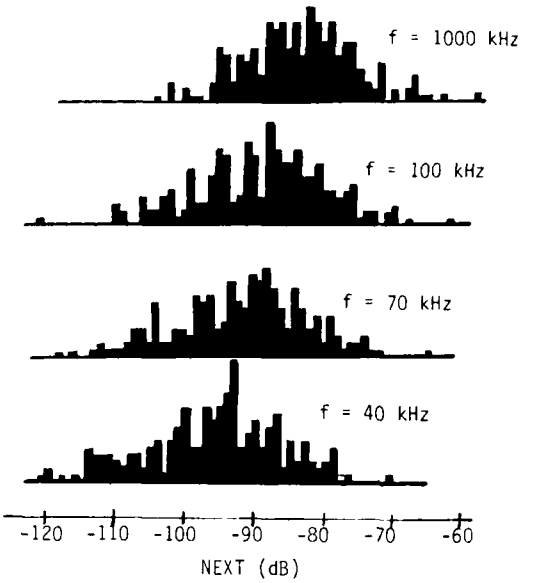


Figure 2 - Data distributions for 216 NEXT measurements on 19 pair type C cable.

Table 4 - Crosstalk Data For Foil Shielded Twisted Pair Cable Designs

Type	No. of Pairs	Pairs Tested	NEXT (dB)/Std. Dev. (dB) @ 40 KHz	@ 70 KHz	@ 100 KHz	@ 1000 KHz	FEXT (dB)/Std. Dev. (dB) @ 40 KHz	@ 70 KHz	@ 100 KHz	@ 1000 KHz
A	3	18	87.7/8.2	82.2/ 7.3	79.8/7.5	74.6/5.4	88.1/8.9	82.8/8.1	80.6/7.9	76.6/7.0
A	6	27	85.4/7.1	81.2/6.6	79.1/6.5	75.2/6.4	85.5/7.1	81.2/6.5	79.1/6.5	75.2/6.4
A	9	63	84.2/9.8	80.1/9.3	77.6/8.8	74.0/5.6	84.8/9.8	80.8/9.4	78.0/8.8	75.0/6.0
A	11	147	86.7/9.3	82.2/8.8	80.6/8.5	77.8/8.1	86.8/9.6	82.9/9.5	81.1/9.1	78.8/8.5
A	15	135	84.5/9.1	80.1/8.6	78.1/8.6	77.0/7.5	84.4/8.9	80.2/8.4	78.1/8.3	77.1/7.4
(All "A")		411	85.6/9.2	81.3/8.7	79.2/8.5	76.6/7.4	85.7/9.3	81.4/8.9	79.4/8.6	76.7/7.5
B	3	18	81.0/9.4	76.4/8.9	73.9/8.7	77.4/5.9	80.8/9.2	76.2/8.7	73.8/8.4	76.4/7.4
B	6	36	85.7/8.7	80.9/8.0	78.5/7.6	76.3/6.1	85.5/8.4	80.7/7.7	78.1/7.4	76.3/6.4
B	9	60	87.7/8.1	83.0/7.8	80.6/6.3	80.7/7.4	87.6/8.0	83.0/7.5	80.5/7.2	80.7/7.4
B	11	99	82.4/7.4	78.0/7.1	75.8/7.1	74.5/5.1	82.6/7.8	78.2/7.6	76.0/7.5	74.8/7.0
B	12	75	80.4/7.7	75.7/8.2	73.4/7.8	72.7/6.6	80.5/7.1	76.1/8.2	73.8/8.4	72.8/6.6
B	15	138	86.3/10.3	81.5/10.1	79.2/10.0	77.9/9.1	86.3/10.1	81.4/9.8	78.9/9.7	77.9/9.1
B	19	216	87.9/10.2	83.1/10.0	80.6/10.0	79.0/9.4	88.0/10.6	83.3/10.4	80.9/10.5	79.0/9.4
B	27	270	86.3/9.0	81.5/8.5	79.0/8.3	76.6/6.8	86.5/9.3	81.7/8.9	79.3/8.7	76.6/6.8
(All "B")		843	85.8/9.6	81.1/9.2	78.7/9.1	77.2/8.1	85.9/9.8	81.2/9.5	78.8/9.4	77.2/8.1
C	3	18	94.8/10.9	89.2/10.9	86.8/11.1	85.3/11.3	94.3/11.2	89.8/11.3	87.4/11.4	84.4/11.1
C	6	27	94.4/7.9	90.1/8.8	87.6/9.2	82.3/5.9	94.2/7.1	89.6/7.1	86.9/7.0	82.3/5.9
C	9	60	94.1/10.8	89.3/10.9	86.8/11.1	79.3/10.0	94.4/11.0	87.8/14.6	86.2/10.2	81.7/10.3
C	15	138	95.1/11.6	90.0/11.5	87.1/11.9	80.3/10.0	94.8/11.5	89.5/11.5	87.0/11.8	83.0/10.2
C	19	216	96.1/9.4	91.5/9.4	88.8/9.3	83.6/8.0	96.2/9.6	91.4/9.4	88.9/9.4	84.2/8.2
C	27	306	89.8/8.4	85.2/8.1	82.7/7.7	80.1/7.4	89.9/8.7	85.1/8.1	82.9/8.1	81.2/8.2
(All "C")		765	93.1/10.0	88.4/9.8	85.8/9.8	81.2/8.5	93.2/10.1	88.3/10.2	85.9/9.8	82.2/8.5
D	9	96	85.8/10.5	81.2/9.9	78.7/9.6	76.4/7.8	85.6/10.1	81.0/9.8	78.7/9.8	76.4/8.0
E	15	138	85.8/9.6	80.6/9.6	77.5/11.1	75.8/11.1	85.2/9.3	80.5/9.2	77.7/9.1	75.6/10.3
F	2	24	39.8/2.9	36.2/3.3	34.5/3.5	41.3/3.3	39.8/2.9	36.2/3.3	34.4/3.3	41.3/3.2
G	2	12	40.9/2.3	37.6/3.0	37.1/2.9	47.3/5.8	40.9/2.1	37.7/2.9	36.1/3.1	40.7/5.9

Table 4 presents the mean crosstalk values and standard deviations for the rest of the cables in the study. Among the standard twisted pair designs, the results for types D and E along with the composite values for types A and B are very similar. These are all 50 ohm cable designs. The composite result for the type C cable, which is a 100 ohm design, shows a 5 to 8 dB improvement in crosstalk values. Individual results for cables within the type B and C families show an approximate 7 dB range in crosstalk values over the frequencies tested, while the type A family had a narrower 4 dB range. Whether this is caused by statistical chance or relates to the cable design is difficult to determine because of the large standard deviations. However, no consistency is noticeable between pair count and relative performance among all three family groups. Standard deviations are seen to generally fall in the 8 to 10 dB range noted above. (For the composite type A, B, and C data plus the data for D and E, the maximum standard deviation measured was 11.1 and the minimum was 7.4). Data histograms and pair group breakdowns for these standard twisted pair designs were reviewed, and behaved quite similar to those already presented.

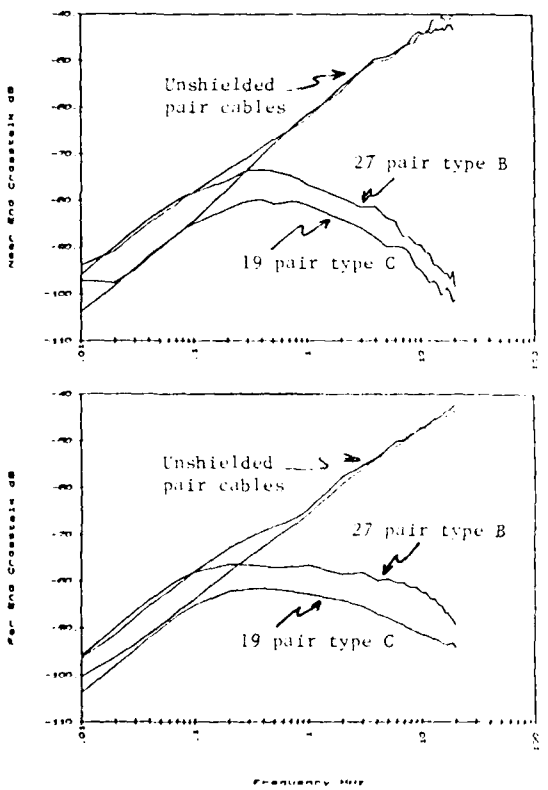


Figure 3 - Mean values of NEXT (top) and FEXT (bottom) for unshielded pair cables and shielded pair cables.

The common axis designs, types F and G, have a much poorer mean crosstalk performance than the standard twisted pair cables. Specifically, the crosstalk values are from 35 dB to 50 dB worse. The increase in crosstalk illustrates the significance of using twisted pairs to reduce inductive coupling. For these designs, the standard deviations are measured to be about 2 to 3 times smaller than those discussed above.

Discussion

Given the data in Table 4, how should the crosstalk performance be specified for these cable designs? It seems that the mean values and standard deviations can be defined, within limits, when a reasonable sample size is measured. However, it is the minimum crosstalk value that is required in the CR-CS document. To estimate this minimum value, the statistical distribution curve that describes the data must be known. This requires an extensive data base. With only limited measurements available for the CR-CS designs, the mean and standard deviation crosstalk results might be better suited for specificati values.

In addition to describing performance, a specification value is used in monitoring the quality of a manufactured product. Figure 3 shows average NEXT and FEXT values for two unshielded and two shielded pair cables over a .01 KHz to 20 MHz frequency range. Above 100 KHz, a substantial difference in performance is observed between the two types of designs. If an additional higher frequency requirement was added to the specification, it would increase the probability that manufacturing defects in the shield would be detected. In Figure 4, note that the magnitude of the standard deviation does not change at higher frequency, so the problem of specifying a value remains.

SHIELDING

Cable Designs

The cables tested for shielding effectiveness included designs previously tested for crosstalk (Table I) plus eleven single pair foil shielded cables. Details of these single pair cables are given in Table 5. The foil wraps are the same type as those used on the multipair designs, but they are applied with the foils facing outward.

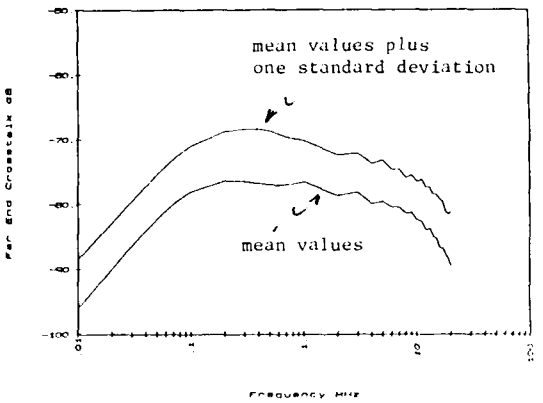


Figure 4 - Statistical results for FEXT data, 27 pair type B cable.

Test Method

The method cited in the CR-CS specification is based on measurements using a SEED fixture. This is a quadraxial test method for measuring shield performance. A schematic diagram of the test is shown in Figure 5.

The test sample is obtained by removing a shielded pair from the original cable. This pair is cut to a 38 inch length. The two conductors are then shorted at both ends, BNC connectors are applied, and a 50 ohm load is attached at the far end. After forming this coaxial configuration, the sample is inserted into the fixture. The test is conducted by applying a signal to the sample and measuring the signal that is coupled to the fixture. The voltage ratio of the fixture signal to the input signal, in dB, represents the shield performance. Further details are available in [1] and [2]. Again, two manufacturing lots were tested in the cable evaluations.

Defects such as gaps in the tape cause a degradation in the shield performance. From transfer impedance analysis, the defects increase the magnitude of the inductive coupling which affects the higher frequency performance. Since the requirements are set primarily in the .1 MHz to 30 MHz frequency range, tests were conducted on the SEED fixture to examine if changes in measurements could be observed after introducing known defects into the shield. For comparison, similar measurements were made at higher frequencies using an absorbing clamp method.[5] These results will be discussed shortly.

Before presenting the results, several observations must be made about the CR-CS SEED method. First, the test involves measuring multipair cables that must be disassembled to retrieve an unprotected foil shielded pair. The pair is then further handled in terminating and testing. During these processes, the potential for unpredictable variations is high.

Second, the terminations are part of the system being tested along with the shielded pair. These are not conventional terminations and careful preparation and hand assembly is required. During the evaluations, termination problems were discovered only after careful review of the resulting data. Finally, the result of the SEED measurement must be distinguished from the actual performance of the shield construction being tested. Figure 6 shows a typical measurement obtained with the SEED test. The measured values degrade approximately 40 dB across the frequency span 0.1 MHz to 10 MHz. However, the transfer impedance characteristic across the same span is known to be approximately flat. Thus transfer impedance indicates little change in performance while the CR-CS SEED test shows a 40 dB reduction. These results make sense when it is realized that the shield under test is the resistive element of an

Table 3 - Description of Single Pair Cables

CR-CS	Wire AWG	Insulation Type, Thickness (inches)	Drain AWG	Pair Lay (inches)
001	18(16)	PE, .018	20(7)	1.5
007	22(1)	PP, .006	22(1)	1.75
010	22(7)	PP, .008	22(7)	1.75
011	22(7)	PE, .016	22(7)	1.5
014	20(7)	PE, .016	20(7)	1.5
019	20(7)	PVC, .015	22(16)	1.75
026	18(19)	PE, .032	18(16)	1.5
027	24(7)	PE, .016	24(7)	1.5
030	20(7)	PVC, .013	22(7)	1.5
031	22(7)	PVC, .016	22(7)	1.25
032	24(19)	PP, .008	24(19)	1.5

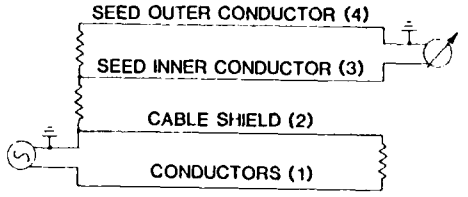


Figure 5 - Schematic diagram of CR-CS SEED test.

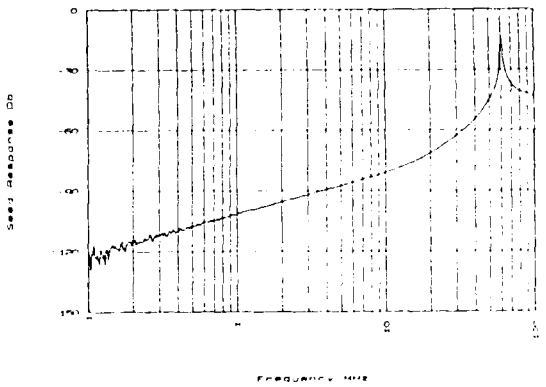


Figure 6 - SEED measurement of the 030 cable in Table 5.

open circuited stub which is excited to resonance as the frequency increases. The true shielding performance is obscured by this inherent fixture resonance, thus the measured values should be regarded as relative numbers only.

The tests for sensitivity to defects were conducted on the 010 cable listed in Table 5. In the tests, radial slots - 1/16 inch x 360° - were made in the foil shield and samples were tested after each increment of damage. Distinctive changes are seen for both test methods, as shown in Table 6. The absorbing clamp data, measured on a 10 ft. cable length, changed about 3 dB after one slot was introduced. After one slot, frequency dependent changes from 2 to 9 dB occurred in the SEED test. Both tests had larger changes as the number of defects increased. This behavior indicates that the SEED test is sensitive to the intentional shield degradation over the tested frequency range.

Table 6 - Data Measured After Introducing Slot Defects into the Foil Shield (values in dB)

	CR-CS SEED TEST					MDS ABSORBING CLAMP TEST			
	No. of Slots					No. of Slots			
f(MHZ)	0	1	3	5	f(MHz)	0	1	3	5
.5	106	104	103	101	100	43	41	36	33
1	100	97	96	93	200	40	36	32	29
5	85	82	80	78	300	41	37	32	30
10	79	76	74	71	400	40	37	30	28
15	75	72	70	67					
20	72	69	66	63					
25	69	65	62	59					
30	67	62	58	57					
100	52	43	39	34					

Table 7 - CR-CS SEED Test Results, Mean Values of Measurements (dB)

Type	No. of Samples	Frequency (MHz) .1	.5	1	5	10	15	20	25	30	100
001	12	122.8	107.8	101.7	86.9	79.0	73.9	68.0	63.2	59.2	38.2
007	22	119.2	107.4	100.8	87.5	82.9	80.5	78.9	77.0	74.6	54.2
010	12	119.2	106.7	100.4	85.9	80.2	76.9	74.4	71.8	69.4	52.6
011	12	121.7	105.7	99.4	84.7	78.2	73.6	69.2	65.4	61.7	44.1
014	24	119.7	108.6	102.4	88.8	81.8	75.9	70.8	65.8	61.8	41.4
019	24	120.0	107.0	100.6	86.0	79.7	75.2	71.1	67.0	63.1	45.3
026	12	188.8	105.9	99.7	80.5	69.3	61.9	56.7	51.8	48.0	30.0
027	12	118.8	106.0	99.5	85.9	80.2	76.2	72.7	68.8	63.6	44.9
030	12	121.2	107.0	101.0	86.9	80.7	76.0	71.9	67.4	63.3	42.5
031	20	117.8	104.5	97.9	82.1	75.0	69.9	65.2	60.9	57.1	39.9
032	12	120.2	104.9	98.7	83.3	75.3	68.8	63.7	58.9	54.7	38.3
All"A"	62	120.6	109.5	103.4	91.2	85.7	79.9	74.4	69.6	65.3	44.5
(Std. deviations, dB)			(1.4)	(1.4)	(1.9)	(2.4)	(2.1)	(1.8)	(1.6)	(1.6)	(1.1)
All"B"	95	120.0	110.0	104.0	92.0	87.8	83.3	78.1	73.3	69.1	48.3
(Std. deviations, dB)			(1.0)	(1.1)	(1.6)	(2.2)	(2.3)	(2.0)	(1.7)	(1.6)	(1.3)
All"C"	76	119.4	107.9	102.0	88.5	81.5	75.8	70.7	66.1	61.2	43.9
(Std. deviations, dB)			(1.4)	(1.3)	(1.5)	(1.9)	(2.1)	(2.1)	(2.0)	(2.0)	(2.1)

Measurements

Table 7 gives results of the shield performance measurements. Note that the mean values for the foil shielded pair cables have a performance range extending over 20 dB at the highest frequencies measured. Standard deviations were generally between 1 to 2 dB. Values for the standard deviations are shown in Table 7 for tests among the multipair cable families.

Work done by Simons[3] is helpful in understanding the data behavior. He presented an equivalent circuit of the SEED fixture analyzed in terms of the transfer impedance (Zt) and capacitive coupling impedance (Zf) of the shield under test. From this circuit, Zt can be calculated from SEED test data assuming that $Zt \gg Zf$ which should be reasonable for this design. This is shown in Figure 7. Converting the data to Zt aided in evaluating the quality of the SEED results as they were being accumulated.

Based upon known behavior of the transfer impedance of the shield designs, an explanation can be provided for the larger range in the high frequency results noted above. All of the foils on the shielded pair samples tested are spirally applied. Although other factors contribute, the tape wrap angle of a spirally applied shield is usually the dominant factor controlling the transfer impedance value above 10 MHz. A larger wrap angle results in a higher (therefore poorer) transfer impedance value. In Figure 8, SEED results at 30 MHz and 100 MHz are plotted as a function of tape wrap angle used in the cable design. The data show a good correlation to the known dependence of shielding on tape angle.

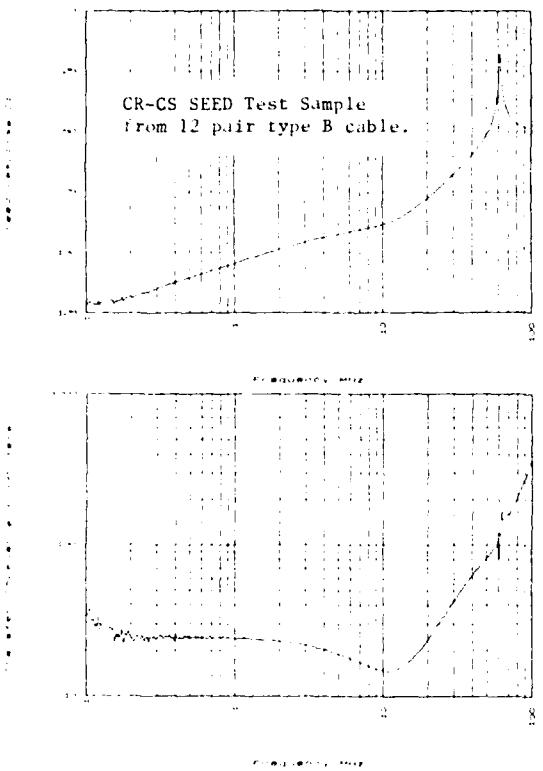


Figure 7 - Transfer impedance curve (bottom) calculated from measured SEED values (top).

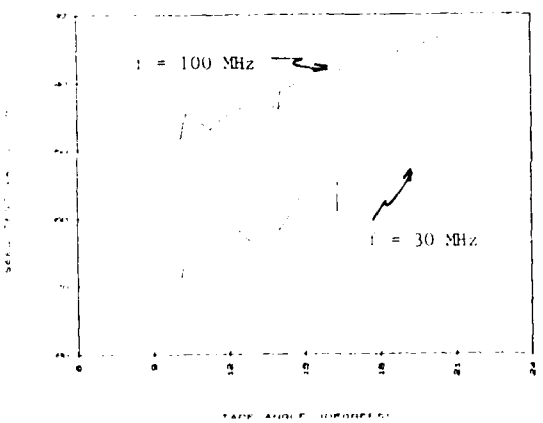


Figure 8 - Correlation of shield test results to wrap angle of tape.

Discussion

For these shield designs, the data show that the SEED fixture test provides performance comparisons that measure a relative shield effectiveness. In addition, the data range which represents variances for both the test method and the cable itself, is reasonable for random sample testing. Therefore meaningful limit values using this test can be assigned in a cable specification, as long as they are determined in accordance with the specific design of the cable shield.

Regarding the observations about this test method discussed above, problems in terminating cables for the test can be controlled and the specification itself should qualify the limit values as relative numbers only. The concern about dissecting multipair cables and handling unjacketed pairs is still valid however. It seems that alternative methods, such as absorbing clamp or antenna tests, could be developed to test individually shielded multipair cables with their jackets intact.

CONCLUSION

Test methods and requirements for shielding and crosstalk measurements are difficult criteria to specify. A minimum value crosstalk requirement for these designs, as it currently appears in the CR-CS purchase specification, is not a well defined number from available data. The shield test method using the SEED fixture, does not give a true indication of the shield effectiveness performance. However, it can be used as a relative determination of the shield integrity. It is hoped that this paper stimulates more work on characterizing foil shielded pair cable in these areas.

ACKNOWLEDGEMENTS

The author expresses his appreciation of the efforts by co-workers in making this paper possible. A special recognition must be given to Nuri Anter and Ric Wagner for excellent assistance in these evaluations.

REFERENCES

1. CR-CS-0099-000 Purchase Specification, "Cables, Special Purpose Electrical, Aluminum Foil Shielded Pairs".

2. M. R. Lombardo, "Aluminum Foil Shield Effectiveness for Electronic Cables", International Wire and Cable Symposium Proceeding 1983, pp 17-23.

3. NEMA, Shielding Measurement Standards Task Force, Tech. Comm. 7-WE, minutes of Jan. 23-24, 1974.

4. S. H. Lin, "Statistical Behavior of Multi-pair Crosstalk", Bell System Tech. Journal, Vol. 59, No. 6, pp 955-974.

5. International Electrotechnical Commission, Subcommittee 46A, amendment to Appendix of IEC Publication 96-1.

6. C. R. Paul, M. B. Jolly, "Sensitivity of Crosstalk in Twisted-Pair Circuits to Line Twist", IEEE Trans. on EMC, Vol. EMC-24, No. 3, pp 359-364.



Jim Krabec received his BS and MS degrees in Physics from the University of Illinois in 1966 and 1968, respectively. He joined Belden in 1978 as a Product Development Engineer at the Belden Technical Research Center. Prior to joining Belden, Jim was involved in the design and application of electronic and CATV cables.

OPERATING HISTORY OF LIGHTWAVE SYSTEMS IN THE REA TELEPHONE PROGRAM

WILLIAM O. GRANT

Rural Electrification Administration
U.S. Department of Agriculture

To date, eighty (80) individual lightwave transmission systems have been constructed under the Rural Electrification Administration (REA) Telephone Program. Collecting and analyzing operational data on this experience may improve the technical performance, reliability, transmission capacity, or cost effectiveness of future lightwave projects.

With this objective, REA generated a questionnaire and circulated it throughout REA systems which had lightwave facilities in operation.

This paper reports on this activity and presents the data collected, along with some conclusions drawn from the general experience with lightwave technology.

The Program

The lightwave study program was intended to identify, if possible, patterns of system failure or deficiencies in individual system elements. It was not designed to grade or evaluate particular system designs, nor does it address the cost effectiveness of individual installations.

One objective, for example, was to determine if optical fibers evidenced a higher probability of failure than opto-electronic terminal units, such as transmitters or receivers. Given information of this nature, it may be possible to reexamine system configurations as well as individual equipment and materials, and perhaps improve system reliability or performance, or reduce system costs.

The basic unit for reporting purposes was denoted a "system", which was defined as any complete facility that provides electrical transmission capability between two discrete terminals. A system includes digital multiplexers, opto-electronic terminal equipments such as transmitters and receivers, and the interconnecting optical fibers.

Under this definition, a system may include intermediate regenerative repeaters, and an individual REA operating company may report on more than one lightave system.

General Discussion

The survey mechanism utilized REA field personnel, and recognized the additional work load that would be imposed on both these people, and the already overburdened operating company staffs. To minimize the intrusion, the questionnaire was designed to maximize check-off type responses. Simplification in this manner did encourage participation in the program, but it also reduced the sophistication of the responses.

The deficiencies of the questionnaire are evidenced in the number of written-in comments received, and in the fact that some of the responses were difficult to reconcile. Of course, if the questions had been less specific, the result may have been even more ambiguous responses. It is important that the limitations of the program be recognized.

First, this is not a very broad data base.

Second, many of these systems have been in place for three years and more. Some of these earlier installations employed embryonic materials and equipment. It is reasonable to assume that later generations of equipment would exhibit a higher level of reliability. A case in point could certainly be made for laser light sources.

Third, there is the subtle factor of experience. Many of the construction and testing techniques have been improved since some of these systems were built. For most of the operating companies involved, these installations could be classified as pilot programs, and subsequent efforts would undoubtedly be accomplished more efficiently and effectively. A case in point here might be in fiber splicing operations.

The data is presented as actually reported without adjustment. Although it does have some value in identifying those elements of a lightwave system which are most susceptible to failure, it may have questionable merit as a basis for statistical analysis or prediction.

Report Structure

Any lightwave system can logically be divided into three basic elements which are the digital multiplex terminal equipment, the opto-electronic terminal equipment, and the inter-connecting optical fibers themselves. This distinction was maintained throughout the study and in this report.

The report is presented in four parts.

1. Equipment and Cable Failure Analysis
2. System Failure Analysis
3. Service Protection Analysis
4. Reported Data

Anomalous Reported Data

Several systems with higher transmission data rates were identified as not equipped with protection switching. Some of these were 135 Mb/s installations, and inquiry revealed that these systems utilized alternate cable routes as a protective mechanism.

One system reported six (6) single fiber failures correlated with six (6) apparently related service interruptions. Inquiry identified the root cause to be one (1) optical fiber connector which, after being initially identified as faulty, was reinstalled five (5) more times.

Twelve (12) protection switch operations reported by one system did not correlate with other reported failures in this system. Inquiry revealed that a single circuit board in the protection switching sensing and control unit had been identified as faulty. Due to a lack of maintenance spares, this faulty unit was simply reinstalled a number of times, resulting in a multiplicity of anomalous switch operations.

An apparent discrepancy was noted in one report which showed more service interruptions than protection switch operations. This may be possible, but appears somewhat improbable.

There were a number of reports that were difficult to accept or reconcile, and several logical subjects for further investigation were identified. Unfortunately, the limited manpower and resources at our disposal, do not permit a thorough follow up on all of these. We did initiate further inquiries on the more obvious cases, and this effort is continuing.

Although the limitations of our resources for this effort are readily apparent, perhaps this report may present a point of departure for further studies by others. We would be happy to cooperate with anyone undertaking such an activity.

Evaluating the Reported Data

The study program was intended to examine the reliability of lightwave transmission facilities. The questionnaire does report on the operating experience with a wide variety of equipment, but it also reflects, perhaps unavoidably, the inexperience of the system operators as well.

A good example was the case of six (6) reports of optical fiber connector failure that were eventually traced to a single connector, which had been reinstalled five (5) times, even after being initially identified to be faulty. Accepting the original data without question might lead to the conclusion that all optical connectors are much less reliable than they actually have been demonstrated to be by the total operating experience, and the probability of drawing an erroneous conclusion is increased when the data base is limited. In this particular instance, one could certainly argue that only one connector failure is statistically significant.

Ideally, the data should be reviewed for unusual or irrational items, and each such case should be individually investigated. An informed judgement could then be made qualifying the actual data that is applied in analysis or statistical development, but introducing any element of judgement could be taken as invalidating the data itself.

In this program, the process of evaluating the reported data presented only a limited number of options, none of which was entirely satisfactory.

1. All data can accepted as reported without qualification.

2. Data could be qualified by adjusting irrational reports on the basis of explainable anomalies.

3. Widely variant reports could be discarded entirely, at the same time discarding an equal number of trouble free reports.

In the balance of this report, all data is as reported, and presentations are developed using unadjusted data. In some instances, however, some analysis is presented even though it may, in our judgement, have questionable value. All such cases are identified, and they have been included primarily to suggest a methodology for a more meaningful analysis of more authoritative data, should such become available at a later date, from another program.

With this in mind, we offer separate discussion of each of the three major elements of the report: Equipment and Cable Failure Analysis, System Failure Analysis, and Service Protection Analysis.

Equipment and Cable Failure Analysis

Total Number of Systems Reporting	79
Total Number of Working Optical Cables	79
Number of Total Cable Failures	18
Percent of Working Cables Experiencing Total Failure	22.8%
Total Number of Optical Cable Miles	1,182
Number of Total Cable Failures	18
Average Cable Miles per Total Cable Failure	65.7
Total Number of Working Optical Fibers	284
Number of Single Fiber Failures (incl. splices)	14
Percent of Working Fibers Experiencing Failure	4.9%
Total Number of Optical Terminal Units (TX and RX)	568
Number of Optical Terminal Unit Failures	45
Percent of Optical Units Experiencing Failure	7.9%
Total Number of Digital MUX Units	284
Number of Digital MUX Unit Failures	14
Percent of Digital MUX Experiencing Failure	4.9%

Equipment Failures Correlated to Data Rate

Optical Units	Number Working	Number Failed	Percent Failed
under 45 Mb/s	28	13	46%
45 Mb/s	360	23	6.4%
90 Mb/s	36	8	22%
135 Mb/s	144	1	.7%
Digital Units	**Number Working**	**Number Failed**	**Percent Failed**
under 45 Mb/s	8	6	75%
45 Mb/s	176	5	2.8%
90 Mb/s	36	2	5.6%
135 Mb/s	64	1	1.6%

Although we have presented the reported data correlated to transmission data rate, we strongly discount the value of this correlation. It would appear from the correlation, that both optical terminal units and digital multiplex equipments which are operating at lower data rates, are substantially less reliable than the same types of equipment operating at higher data rates.

Note the fact, however, that there were only four low data rate systems reported on. A data base this small is easily distorted, and two of these low data rate systems were clearly identified as presenting misleading information. In addition, one system that reported 5 optical unit failures, had been in service for 5 years. This may well have been an example of infant mortality in optical equipment, since some of these units must have been early product developments.

Although we do not endorse any treatment or qualification of the reported data, it might be useful to demonstrate the impact of any such alterations. If we adjusted the reported data from the one system which had 6 single fiber failures reported due to only one faulty fiber connector, to show only one single fiber failure, then the analysis would be corrected as follows:

	Original	Adjusted
Total # of Working Opt. Fibers	284	284
# of Single Fiber Failures	14	9
% of Fibers Experiencing Failure	4.9%	3.2%

This change, which is arguably permissable, makes a significant difference in the review of the study results.

Whether or not the data is adjusted in some manner, the analysis of Equipment and Cable Failures clearly shows a significantly higher failure probability for optical terminal units than for either digital multiplexers, or the optical fibers themselves.

Note the reported number of total cable failures. This data references disruptions that resulted in complete loss of continuity of all optical fibers. This would be a cable inadvertantly cut by excavations, aerial cables destroyed by fire, etc. In such catastrophic failures, protection switched system configurations offer no improvement in service relaibility at all if the redundant fibers are located under the same cable sheat as the working fibers they are intended to protect.

System Failure Analysis

Total Number of Systems Reporting	79 systems
Total Miles of Working Optical Cable	1,182 miles
Average Cable Miles per Reporting System	14.95 miles
Total In-Service Operating Time Reported	1,302 months
Average In-Service Time per Reporting System	16.5 months

Transmission Data Rate Distribution

Data Rate	Number of Systems	Percent of Total Systems
under 45 Mb/s	4	5.01%
45 Mb/s	50	63.29%
90 Mb/s	9	11.39%
135 Mb/s	16	20.25%

Total Number of Systems Protection Switched Equipped	63
Percent of Total Systems Protection Equipped	79.74%
Total Number of Protection Switch Operations Experienced	76
Number of Systems Experiencing Protection Switching	27
Percent of Protected Systems Experiencing Switching	42.86%
Total Number of Traffic Interruptions Experienced	48
Number of Systems Experiencing Interruption	21
Percent of Systems Experiencing Interruption	26.58%
Total Number of Optical Unit Failures (TX or RX)	45
Number of Systems Experiencing Optical Failure	21
Percent of Total Systems Experiencing Optical Failure	26.58%
Total Number of Digital MUX Unit Failures	15
Number of Systems Experiencing MUX Failure	9
Percent of Total Systems Experiencing MUX Failure	11.39%
Total Number of Single Optical Fiber Failures	14
Number of Systems Experiencing Single Fiber Failure	9
Percent of Total Systems Experiencing Fiber Failure	11.39%
Total Number of Total Cable Failures Experienced	18
Number of Systems Experiencing Total Cable Failure	14
Percent of Total Systems Experiencing Cable Failure	17.72%

Although the distribution of reporting systems is presented correlated to transmission data rate, we did not attemp to relate individual system failures to data rate, for the reasons discussed earlier in our comments on the Equipment and Cable Failure Analysis portion of the report.

It is reasonable to expect that protection switch operations would be initiated primarily by only five conditions, and these are:

Initiating Event	# of Operations	% of Operations
1. Opt. Unit Fail.	34	45%
2. Digital Unit Fail.	15	20%
3. Single Fiber Fail.	7	9%
4. Total Cable Fail.	14	18%
5. Prot. Switch Fail.	6	8%

There were a total of 76 switch operations reported, and 70 may be accounted for in the first four items above. The remaining 6 are explained by the report discussed earlier, where a circuit card, known to be faulty, was reinstalled several times.

The distribution of Service Interruptions showed one system reporting 9 interruptions, and two other systems reporting 6 each. Thus 21 of the total 48 events (44 percent) were incurred in only three (4 percent) of the total systems reporting.

The ratio of optical unit failures to the failures experienced in both single fibers, and in digital multiplex units, reinforces the earlier evidence that optical units present a significantly lower level of reliability then the other two system elements.

Note that 18 percent of the systems experienced a total cable failure, and these appear to be randomly distributed also, with only one system reporting 3 events.

Service Protection Analysis

	Service Protected	Not Protected
Total Number of Systems Reporting.....	63	16
Total Number of Service Interruptions.....	26	22
Number of Total Cable Failures.....	14	4
Number of Systems in Service.....	63	16
Number Experiencing Interruption.....	16	7
Percent Experiencing Interruption.....	25%	43%
Number of Systems in Service.....	63	16
Number Experiencing Total Cable Failure.....	12	2
Percent Experiencing Total Cable Failure....	19%	13%

Although one objective of the program was to compare protection switched system reliability directly with unprotected facilities, the results are by no means conclusive. One might have expected, for example, that in protection switched systems, very few service interruptions would occur unless total cable failures were experienced. The protection configuration provides redundant fibers and terminal equipments specifically to avoid outages due to single element failures, and the probability of concurrent element failures seems remote.

Examination of the data, however, shows 17 service interruptions in protected facilities in the complete absence of any total cable failure at all. This is surprising, and suggests a possible flaw either in the questions asked, or in the responses made.

Another deficiency of the study is evident in the Service Protection Analysis sheet. The data indicates that in a total of 16 unprotected systems, 7 systems experienced a service interruption, which is 43 percent of the total unprotected installations. Note, however, that a total of 10 of these events (Service Interruptions) were incurred in only 5 of the systems.

Investigation revealed that these 5 systems all utilized alternative cable routed transmission links as a service protecting facility. What is unclear from the data is just how these paralleling facilities were configured at the terminal ends. It is quite possible that service interruptions have been reported for these individual transmission links, when no actual disruption of traffic continuity through the protecting (paralleling) alternate cable was introduced at all. If this were so, the analysis should have produced the following:

	Original	Corrected
# of Sys. in Service	16	11
# Experiencing Ser. Inter.	7	2
% Experiencing Ser. Inter.	43%	18%

The operational history of these installations would still be included in the earlier Equipment and Systems Failure Analysis sheets, and no correction is necessary in those presentations, but certainly the discrepancy we note would have a significant impact on any conclusions that might be drawn from this analysis.

Note that the very small number of systems that were constructed without service protection switching presents too small a base for any meaningful analysis.

Although considerable expense was incurred for redundant facilities and equipment in the 63 protected installations, total cable failures completely negated any protection in 12 (19 percent) of these same systems, and 42 of them (67 percent) experienced no service interruptions. Of the 63 protected systems, 38 (57 percent) experienced no protection switch operation at all.

Summary

The limited size of the data base, as well as the ambiguities in some responses, suggest caution in drawing firm conclusions from this report. Nevertheless, there is some usable data to be extracted, and some general conclusions that are supported.

There is evidence of significantly lower reliability in opto-electronic units than in either of the other two system elements. The study does suggest that the three system elements do not, in fact, evidence the same probability of failure.

Regarding the lower reliability of the opto-electronic units, we initially considered trying to identify the light sources by type, that is, as LED or laser units, so that we might compare service life, but there were too few LED's in service in the test systems to provide a meaningful data base.

Conventional service protection configurations provide backup for all three system elements (fibers, digital equipment, and optical terminals) equally, without regard for their individual probability of failure. This design approach is almost universally applied regardless of the traffic density, service priority, or revenue potentials of the application involved.

There are practical technical alternatives, however, such as parallel independent systems with traffic divided equally across both. Perhaps we ought to reexamine the entire question of service protection, particularly in lower traffic density, shorter length systems.

One significant fact brought out by the study is the high incidence of complete failure of the interconnecting optical cables. Failures of this type far exceeded any other single contributing cause of system disruption.

This suggests that an effort be made at analyzing all reported total cable failures. If any pattern could be identified, say a higher percentage of problems near road crossings, just for example, then perhaps special protective measures could be discriminately taken to improve mechanical cable protection in those areas. It might even be possible to provide alternate cable routing for short, selected portions of a cable run, if those short portions could be identified as presenting higher exposure to failure.

We are pursuing this further, but our experience with conventional cable plant in the rural environment suggests that cable disruptions are naturally random in nature, and we are not optimistic that any useful patterns can actually be identified.

Perhaps the report serves best simply as a presentation of the worst case performance to be expected from systems constructed with state of the art equipment and techniques available today. It seems reasonable to assume that new systems will perform up to these levels at a minimum, and may well present a higher degree of operating reliability than the questionnaire responses indicate.

Overall, lightwave systems have evidenced a remarkably high level of operating reliability, while requiring a minimum of maintenance. This in itself presents a unique problem that the study program exposed. One question that was asked of all participants was if they had a scheduled program to exercise protection switching capabilities, when systems were so equipped. It was suspected that few system operators actually did exercise this feature on a regular basis, and this suspicion verified by the responses received.

In general, REA experience with this technology has been excellent. Although most of the operating companies within the REA program are relatively small and limited in staff size, we know of none that have had any serious difficulty in constructing optical systems or in maintaining them. The problems we are focusing on now are not really technical at all, but are primarily directed at implementing more cost effective designs.

The questionnaire responses have been included in this paper so that interested readers may make their own analysis, and draw their own conclusions. We invite discussion on the subject, and would be most interested in any similar studies done by others.



William O. Grant is a Communications Specialist in the Transmission Branch, Telecommunications Staff Division, of the Rural Electrification Administration, United States Department of Agriculture, in Washington, D.C.

REPORTED DATA

The REA Questionnaire

Question 1: How many months has the system been in regular service?

Question 2: What is the transmission data rate in Mb/s?

Question 3: How many regenerative repeaters are there in the system?

Question 4: Is the system equipped for service protection switching?

Question 5: How many protection switch operations have occurred?

Question 6: How many times has traffic been interrupted?

Question 7: How many opto-electronic units (TX or RX) have failed?

Question 8: How many digital MUX units have failed?

Question 9: How many single fiber disruptions have occurred?

Question 10: How many total cable disruptions have occurred?

Sys. No.	Cable Miles	Questions #1	#2	#3	#4	#5	#6	#7	#8	#9	#10
1	19	6	45	0	N	0	0	0	0	0	0
2	15	24	90	0	N	0	1	1	0	0	0
3	29	6	45	0	Y	0	1	0	0	0	0
4	8	18	45	0	Y	0	0	0	0	0	0
5	15	12	45	0	Y	1	1	0	1	0	0
6	10	18	45	0	Y	0	0	0	0	0	0
7	13	18	45	0	Y	1	1	3	0	0	1
8	13	30	12	0	Y	6	9	6	6	0	0
9	16	6	45	0	Y	0	0	0	0	0	0
10	21	12	45	0	Y	0	0	0	0	1	0
11	17	12	45	0	Y	0	0	0	0	0	0
12	16	12	45	0	Y	0	0	0	0	0	0
13	26	12	45	0	Y	0	0	1	0	0	0
14	14	18	45	0	Y	0	0	1	0	0	0
15	22	18	45	0	Y	0	0	0	0	0	0
16	15	18	45	0	Y	0	0	1	0	0	0
17	11	30	45	0	Y	1	0	1	0	0	0
18	3	30	6	0	Y	2	0	2	0	0	0
19	4	6	90	0	Y	0	0	0	0	0	0
20	1	60	1.5	0	Y	5	0	5	0	0	0
21	17	6	90	0	Y	0	0	0	0	0	0
22	12	6	90	0	Y	1	0	0	0	0	0
23	10	6	90	0	Y	0	0	0	0	0	0
24	5	6	45	0	Y	1	1	1	0	0	1
25	26	60	45	0	N	0	6	3	0	0	3
26	17	18	45	0	Y	1	2	1	0	0	0
27	11	36	16	0	N	0	6	0	0	6	0
28	7	12	45	0	Y	0	0	0	0	0	0
29	14	30	135	0	Y	0	0	0	0	0	0
30	19	36	90	1	Y	12	2	0	1	1	2
31	7	54	45	1	Y	4	0	3	0	0	0
32	20	6	135	0	Y	0	0	0	0	0	0
33	6	12	45	0	Y	0	0	0	0	0	0
34	8	12	45	0	Y	0	0	0	0	0	0
35	8	12	45	0	Y	1	0	0	0	0	0
36	7	24	45	0	Y	2	0	0	0	0	0
37	19	18	135	0	Y	3	1	0	0	0	0
38	29	30	135	0	Y	3	1	0	0	1	0
39	18	6	45	0	Y	3	1	1	1	0	1
40	21	6	135	0	Y	1	0	0	0	0	0

REPORTED DATA

Sys. No.	Cable Miles	Questions #1	#2	#3	#4	#5	#6	#7	#8	#9	#10
41	10	30	45	0	Y	5	0	2	0	1	2
42	11	30	45	0	Y	4	0	1	1	0	1
43	21	24	135	0	Y	5	3	1	1	1	1
44	15	24	45	0	Y	2	1	0	0	1	0
45	6	24	45	0	Y	1	0	0	0	0	0
46	3	24	45	0	Y	2	0	0	0	0	0
47	4	6	45	0	Y	3	1	1	0	0	1
48	7	24	45	0	Y	4	0	2	2	0	0
49	13	6	45	0	Y	0	0	0	0	0	0
50	6	6	45	0	Y	0	1	0	0	0	0
51	11	6	45	0	Y	0	0	0	0	0	0
52	17	6	90	0	Y	0	0	0	1	0	0
53	6	12	135	0	Y	0	0	0	0	0	0
54	60	12	135	0	Y	0	0	0	0	0	0
55	23	12	135	0	Y	0	0	0	0	0	0
56	11	6	135	0	Y	0	0	0	0	0	0
57	11	18	45	0	Y	1	0	0	1	0	0
58	10	30	45	0	Y	0	0	0	0	1	1
59	10	30	90	0	Y	0	0	0	0	0	1
60	11	18	45	0	Y	0	0	0	0	0	1
61	12	6	45	0	Y	0	0	0	0	0	0
62	19	6	45	0	N	0	0	0	0	0	0
63	7	6	45	0	N	0	0	0	0	0	0
64	10	6	45	0	N	0	0	0	0	0	0
65	7	6	45	0	N	0	0	0	0	0	0
66	11	6	45	0	N	0	0	0	0	0	0
67	14	6	45	0	N	0	0	0	0	0	0
68	18	6	45	0	N	0	0	0	0	0	0
69	29	12	135	0	Y	0	0	0	0	0	0
70	15	18	135	0	Y	1	0	0	0	0	1
71	22	18	135	0	Y	0	0	0	0	0	0
72	18	6	45	0	Y	0	0	1	0	0	0
73	29	6	45	0	Y	0	0	0	0	0	0
74	13	6	45	0	N	0	0	0	0	0	0
75	5	6	45	0	Y	0	0	0	0	0	0
76	36	24	90	0	N	0	3	7	0	0	0
77	33	18	135	0	N	0	2	0	0	1	1
78	26	18	135	0	N	0	2	0	0	0	0
79	23	12	135	0	N	0	2	0	0	0	0
Totals	.	.	.	2	16 N	76	48	45	15	14	18
	1,182 miles	.	.		63 Y						
		1,302 months	.								

4 - under 45 Mb/s
50 - 45 Mb/s
9 - 90 Mb/s
16 - 135 Mb/s

FIBER OPTIC SUBSCRIBER NETWORKS USING 85/125 FIBERS

J.P. BOINET* - M. de VECCHIS* - J.P. BONICEL** - J.P. BREGEON ***

*LES CABLES DE LYON - BP 309 - 92111 CLICHY CEDEX - FRANCE
**LES CABLES DE LYON - BP 7153 - 69344 LYON CEDEX 07 - FRANCE
***DIRECTION GENERALE DES TELECOMMUNICATIONS - RUE DE LA GALERA 34035 MONTPELLIER - FRANCE

ABSTRACT

The installation of large subscriber networks is now in progress is various French cities.
They correspond to a large program of introduction of optical fiber networks, mainly offering cable TV services. Orders received today are for 420.000 subscribers, corresponding to a total amount of about 100.000 km of fibres. Due to system considerations, the 85/125 fiber is used. The influence on the cable design is discussed, considering mainly the microbending sensitivity of the fiber. Cable structure has been adapted to the particular characteristics of urban distribution French networks : short lengths of cable are laid in small ducts. A reverse helix slotted core structure has been selected with a modularity of 5 or 10 fibers depending on the fiber count comprised between 5 and 210. The accessories used with these cables and adapted to their structure are described : termination frames, splice boxes including description of splicing procedure, drop terminals.
Installation procedures are also described : It is very important to minimize wastes of cable during laying and to optimize the configuration of the cable network.A computer aided design system has been developped for that purpose. It gives the exact total need for each type of cable which is used for production planning.

1. INTRODUCTION

The installation of large subscriber networks using optical fibers is now in progress in various French cities and some networks are now installed and operated for cable TV services distribution. A joint venture has been established between Alcatel CIT and Les Câbles de Lyon to deliver turn-key systems and has received to day orders for 420 000 subscribers corresponding to a total amount of more than 100.000 km of fibers. The system installed is a star network using 85/125 fibers to improve light injection and in order to use LED as light sources for a maximum length of 1.1 km.

2. CONFIGURATION OF THE DISTRIBUTION NETWORK

The figure 1 shows a typical configuration of the distribution network. A distribution center can serve 960 subscribers. Cables coming out of the distribution center are generally high count fiber cables. They are fanned out into smaller and smaller capacities down to a 5 fiber cable ended by a drop terminal. The subscribers are connected by single fiber drop cables to the drop terminal.

In a first step of installation, 5 subscribers are connected to the 5 fibers on the drop terminal. In a second step it is possible to connect 5 more subscribers by inserting frequency demultiplexers. 10 subscribers are then connected to a drop terminal and each fiber is shared by 2 subscribers : one uses the 850 nm window and the second uses the 1300 nm window. The complete range of services (including future extensions) delivered to one subscriber is carried on one wavelength window of a fiber, that determines the band width of the fiber.

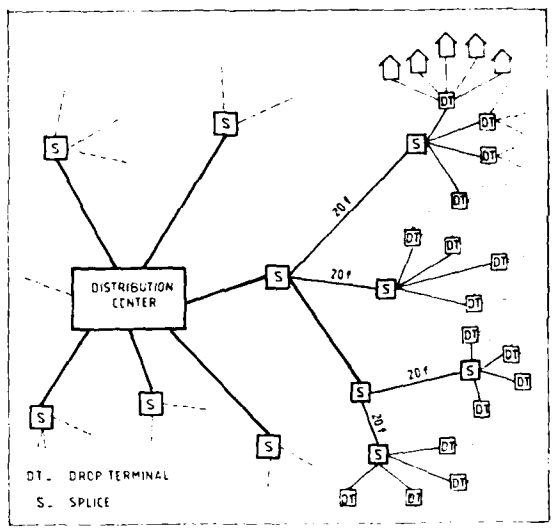


Figure 1

3. FIBER

As it has been said above, the fiber used is a 85/125 one. The selection of fiber parameters comes from a system analysis to meet the power budget and band width requirements. The main characteristics of the fiber are :

Core diameter 85 ± 5 µm
Cladding diameter 125 ± 3 µm
Primary coating diameter 250 ± 15 µm
Core non circularity < 6 µm
Cladding non circularity < 2 µm
Core/cladding non concentricity < 6 µm
Cladding/Prim. coating non concentricity < 10 µm
Numerical aperture 0.26 ± 0.02

Attenuation at	850 nm	< 4 dB/km
	1300 nm	< 2 dB/km
Bandwidth at	850 nm	> 200 MHz.km
	1300 nm	> 200 MHz.km

4. CABLES

Distribution cables have been designed to match the particular characteristics of urban distribution French networks : they use a large amount of small diameter plastic ducts (Ø 28 - 33 or 45 mm).

Furthermore, the distance between distribution center and drop terminal is short (average 400 m, maximum 1100 m) and the cables are usually laid by short lengths. Consequently some parameters become predominant for these cables : diameter, bending capability and flexibility in particular.

The use of 85/125 fiber adds some specificity to the cable design : the fiber is basically more microbending sensitive compared to a standard 50/125 fiber. It is therefore important to use a structure and a cabling process that insure a minimum level of microbending on the cabled fibers.

Finally, the importance of cable splicing due to the laying by short lengths and the great number of splicing points has been considered during the selection of the cable structure : an easy access to fibers and a simple identification are important parameters. Structures with more than one fiber per cavity (tube or groove) have been rejected for that reason.

A reverse helix slotted core structure is used (1) : the basic unit has 5 or 10 grooves and one fiber by groove. The 5 fibers unit is used only on single unit cables whilst 10 fiber units are stranded to obtain cables from 20 to 210 fibers.

The range of standard cables is : 20 - 30 - 50 - 70 - 90 -120 - 150 and 210 fibers. The figure 2 shows cross sections of the central part of these cables.

These cables and the single unit 5 fiber cables are protected by a laminated aluminium and polyethylene sheath. This outer sheath is made of high density polyethylene.

Due to the variety of locations of drop terminal, 5 fiber cables can be used not only in ducts but also as aerial or wall-mounted cables. For that purpose a special version has been developped, distinguished by a filling of the optical core and a single polyethylene sheath.

The figure 3 shows the complete range of distribution cables.

Two types of drop cables have been developped : an in door cable and a multipurpose cable that can be used as aerial, wall mounted or buried cable. In both cases the cable uses a U stucture with 2 metallic strength members (figure 4). The multipurpose cable is distinguished by a jelly filling and by kevlar strength members included in the sheath.

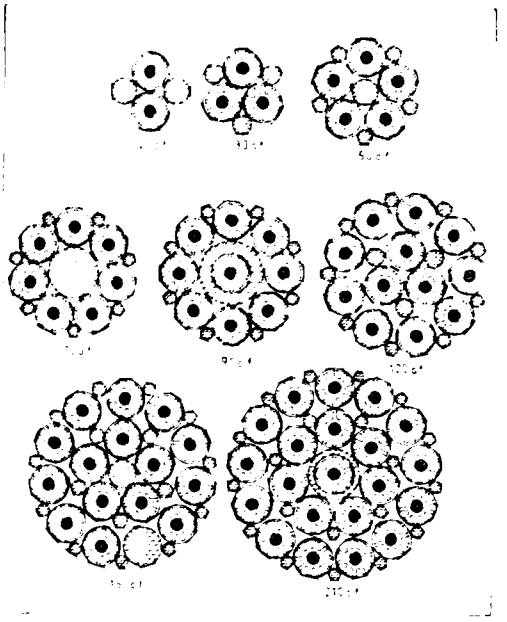


Figure 2

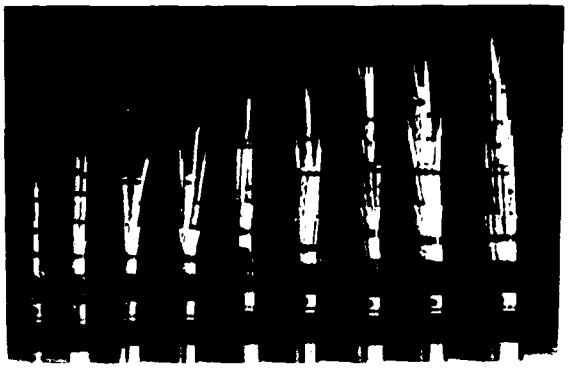


Figure 3

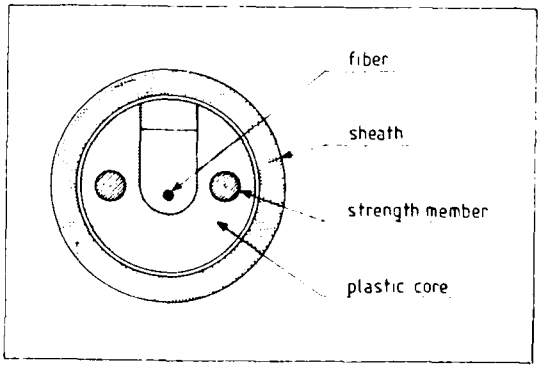


Figure 4

5. CABLES ACCESSORIES

Cables accessories have been developped in parallel with the cable structures in order to obtain the best fitting all along the line.

During the design of cable accessories a great attention has been paid to the reduction of installation times and simplification of operational procedures.

5 A Splices

The splicing method has been selected on the basis of the following requirements :

- quality of the splice in terms of attenuation, reliability, stability versus environmental (thermal and mechanical) conditions,
- easy field installation, including short time to perform the splice and a low number of defects,
- simple and low cost tool-kit and materials,
- short training time for the operators.

We have selected the ATI Placoptic System (2). It uses a bonding technique with a UV curable adhesive. Fibers are aligned by an elastomeric V grooved centering device and bonded on a glass plate. The splice is protected by a stainless steel cradle. Average splice loss on 85/125 fibers is 0.15 db at 850 nm.

This method has been preferred to fusion splicing as it gives similar results in terms of attenuation and environmental behaviour with advantages regarding the cost and safety : the investment for the tool-kit is much lower than for a fusion splicer and there is no electric arc or flame in order to minimize potential hazards under severe conditions.

The cost of consumable products and the time needed to perform the splice are comparable to those of a fusion splice.

5 B Semi permanent splices

These devices are intermediate between a permanent splice and a reusable connector. They can be used in the distribution center for connecting a subscriber to a distribution line in a drop terminal. They meet the same basic requirements as the permanent splices and moreover they offer some possibility of reintervention.

They are made of (3) :

- a mounting block with a buffer retention mechanism at each end,
- an alignement block with a V groove to align the fiber and clamping mechanisms,
- a cover for mechanical protection.

The figure 5 shows the termination of a 10 fiber unit in a distribution center : the 10 fibers are ended in a termination frame by 10 semi permanent splices (on the left) and ready to be connected to 10 single fiber cords.

This organization is matched to the 10 fiber modularity of the cables and offers a great adaptativity : the 210 fibers of a high count cable can be distributed very easily in 21 different points.



5 C Splice housing

The basic component in the splice housing system is the cassette splice organizer. It has been designed especially for the use in distribution networks where it is sometime impossible to work in the vicinity of the final splice location .
Therefore it is necessary to accommodate some extra length of cable unit. This is done by the external part of the cassette acting like a drum on which the required extra lengths of cable units are wound (figure 6).

This operation can be done very safely as the 10 fibers are protected by a slotted core unit which has a good mechanical strength. It is the reason why we have preferred a low fiber count modularity instead of using a structure with several fibers by groove or by tube. If so, in order to keep the easiness of division of high count cables it shouldbe likely to match the number of fibers in a groove and the number of fibers connected in a cassette. But in that case, the group of fibers, even protected by a tube, has not the same mechanical strength as the slotted core unit and the work out of the hole followed by the winding of the extra length of fibers can't be done with the same level of safety.

The central part of the cassette houses the 10 splices corresponding to the 10 fibers cable units. These cable units are clamped at the periphery of the central part and a plastic organizer holds the 10 single fiber splices. Plastic walls are integral parts of the organizer to avoid any sharp bending of the fibers.

A plastic cover closes the central part in order to protect the splices and the fibers.

By rotating the cassette the extra lengths of cable units are wound on the external part : Up to 6 feet of each cable unit can be easily stored. The cassette in then placed within the housing in a plastic holder and a plastic cover is used to close the cassette and to protect the cable units.



Figure 6

Accesses to splice housing exhibit cylinders calibrated at the outer diameter of various cables used. Thermoshrinkable sleeves are applied to protect against water penetration.
Two types of housing have been developped, PFL 30 and PFL 90 respectively for a maximum of 30 and 90 splices (i.e. holding 3 or 9 cassettes).

If necessary (for example with high count cables) several housings can be cascaded to obtain the required capacity.

Splice housing is waterproof, can be pressurized and can insure the grounding of cable sheaths. It can be easily reopened for future intervention and can be adapted for the use of other types of permanent splices if required

The figure 7 shows a PFL 30 mounted in a wall and the figure 8 shows a PFL 90 installed in a hand hole.

5.0 Drop terminal

The drop terminal realizes the fanning out of distribution cables.It corresponds to the point where single fiber drop cables coming from the subscriber's premices are connected to the distribution network.



Figure 7



Figure 8

According to the system's requirements two subscribers can share a single fiber, one using the 850 nm, the second using the 1300 nm window. Optical accesses of a drop terminal are constituted by :

- one 5 fiber cable
- ten single fiber drop cables.

In that case the drop terminal houses :

- the fanning out system of the 5 fiber cable that provides a 1,2 m excess length of fibers and enables at least 12 reinterventions on fibers (4)

  New low cost connecting devices are presently developped. They will facilitate future interventions by providing an easy connection or disconnection.

- 5 demultiplexers connected to the 5 distribution fibers.

- 10 connecting points between demultiplexers outputs and single fiber cables.

Figure 9 shows a drop terminal mounted in a wall and its internal organization including the 5 demultiplexers

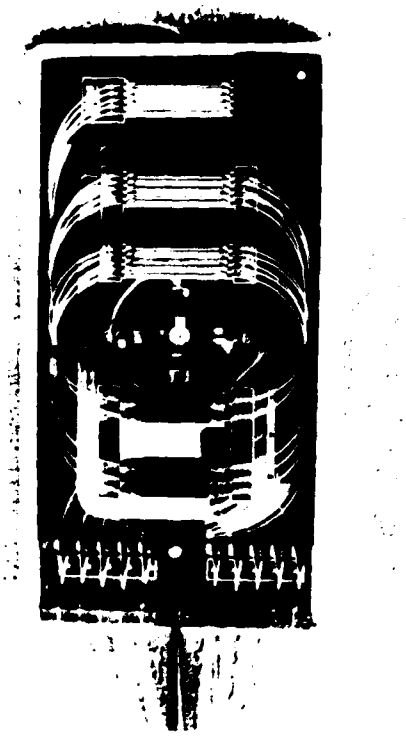


Figure 9

6. Network engineering

As it has been said previously, the average laying length of cables is small. Considering the production costs, it is impossible to produce lengths of cable at request. Cables are manufactured by long lengths (typically 2 400 m) and cut at the real length in the field. Especially for high fiber count cables it is very important to minimize wastes of cable in terms of overall cost of the system.

Furthermore, it is necessary to optimize the cable network considering the existing duct network : a computer aided design system has been developped. It takes into account the existing duct network and locations of distribution center and potential subscribers and gives an optimized cable network with location of drop terminals and splices. Included in this output are new works to be done before the cable installation (i.e. creation of new ducts) and the detail of lengths of cable necessary given for every fiber count. Figure 10 shows the equipment used and figure 11 represents a part of results obtained giving the necessary lengths and types of cable for a part of the area covered by a distribution center. Other outputs of the system are maps with location of ducts, splices and drop terminals and all the lists of materials and works to perform necessary for the area covered by the considered distribution center.



Figure 10

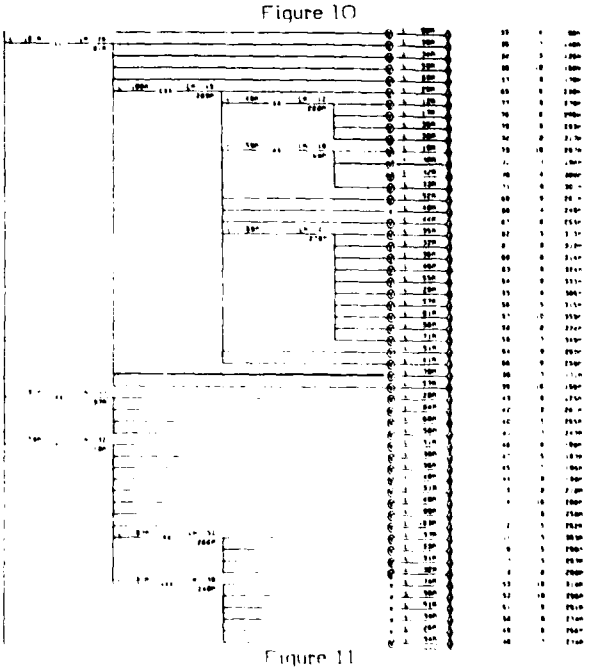


Figure 11

7 CONCLUSIONS

A complete line of products has been developped for the installation of new optical subscriber networks. The installation is started in a very large scale : when this paper was written several networks, corresponding to more than 100 000 subscribers, were already installed using these products, and a large experience has been gained in actual field conditions that proves the efficiency of the selected solutions.

REFERENCES :

(1) M. de VECCHIS - JP HULIN : Overview of the cylindrical grooved structure.
Globecom 83 - Nov. 28 - Déc 1. 1983 - SAN DIEGO PP 34.3.1. - 34.3.5.

(2) Y. RUELLO - F.L. MALAVIEILLE : A New multimode optical fiber splicing technique IWCS, Nov. 1986, Reno pp. 95-99

(3) M.C. SOSTER - J.L. MALINGE : Low loss splices and special tool kit for multimode optical fibers.
Proceedings of SPIE Vol 722 SEPT 86 Cambridge (MA) pp. 153-159.

(4) A. BOUVARD - JP. HULIN - M. de VECCHIS - W. POULSON Termination of cylindrical grooved optical cables. IWCS, Nov. 1983 - Cherry Hill pp. 49-53.



Jean Pierre BOINET was born in 1944. He is graduated from Ecole Nationale Superieure des Arts et Métiers (1967). He joined LTT in 1969 and has been involved in the construction of the French Interurban Network.
He has been in charge of the development of installation procedures for optical cables. Since the merging of LTT cable activities with Les Câbles de Lyon he is Project Manager for Videocommunications activities in the Installation and Engineering Branch.



Jean Pierre BONICEL was born in 1952. He received his engineer degree from the Institut des Sciences de l'Ingénieur de Montpellier (ISIM) in 1976. He joined Les Câbles de Lyon in 1977 where he was in charge of material and mechanical problems for telecommunication cables. Now he is the head of telecommunication cables laboratory.

J.P. BREGEON was born in 1949. He received his engineer degree from Ecole Centrale de LYON in 1973. Since 1981 he is in charge of technical engineering for brodband networks at the Direction générale des Telecommunications.



Michel de VECCHIS was born in 1946. He is graduated from Ecole Nationale Supérieure des Télécommunications (1969). He joined LTT in 1970 where he worked on microwave components. He started to work on fiber optics in 1974 and has been Technical Director of the cable Division until the merging of LTT cable activities with Les Cables de Lyon in 1986. He his now Director of Technical International Marketing at Les Cables de Lyon Telecommunications Branch.

PROVISION OF WIDEBAND OPTICAL FIBRE CABLE NETWORKS FOR CENTRAL BUSINESS DISTRICTS

I de Valle W I Harry M McKiterick

TELECOM AUSTRALIA
MELBOURNE AUSTRALIA

SUMMARY

Telecom Australia has installed a wideband network using optical fibre cable technology to serve major business customers in the central business district of the city of Melbourne.

The main objective of the network was to provide Telecom with experience in serving the wideband market place. The installation was used as a test bed for the development of engineering knowledge and work practices for use in providing wideband optical fibre networks in other concentrated business locations.

This paper provides details of the cable reticulation adopted for the Melbourne network together with the cable designs employed. It also describes the practices used for placing, splicing, terminating and testing of the cable.

BACK GROUND

Early in 1983 a working group was established to examine feasible network configurations and the available technology for establishing a wideband network which would provide access for up to 50 selected Melbourne CBD buildings. Various analogue and digital wideband services were considered including video, data and LAN services together with wideband and optical switching applications. Economic evaluation was also carried out to determine the most appropriate transmission medium. The choice narrowed to the two alternatives of optical fibre cable and CATV type coaxial cable.

The assumed development trend was an initial 30 services increasing to 1000 services over a 10 year period. It was considered that the cost of optical fibre technology would reduce dramatically over this period whereas coaxial cable costs would at least remain constant or could possibly increase.

Cost comparisons showed that in the first year an optical fibre network was clearly more expensive than coaxial cable but over 10 years the overall costs were approximately the same. This was considered to give sufficient indication that in the longer term optical fibre would be the preferred transmission medium. This choice avoids the need for active coaxial transmission elements in the external network and concentrates training and operational support needs to a developing new technological area. Also the high transmission capabilities of optical fibre would enable Telecom to expand its technological profile and competitive status in the telecommunications industry. It is now expected that growth will be more rapid and will reach a substantially higher level than the originally assumed trend.

NETWORK STRUCTURE

The Melbourne network consists of a ring of optical fibre cables linking 4 city telephone exchanges and a system of loop and spur distribution cables emanating from these exchanges. These cables pass in the vicinity of approximately 50 identified major business houses including buildings occupied by staff of Telecom Australia. Ring and loop topology was chosen for this network as overseas experience had indicated that customers requiring services with high data rates often desired two space diverse cables from their buildings for security. The arrangement adopted allows customers to be provided with space diverse fibres from their buildings to the local exchange as well as having space diversity in traversing the CBD inter exchange network. (See Fig 1)

In the distribution loops nominated fibres are cut at predetermined locations and the ends extended to customer buildings so that they can be manually patched to provide circuits in both directions. Similar patching arrangements are also provided in the 4 exchanges to inter connect fibres in the ring and distribution cables.

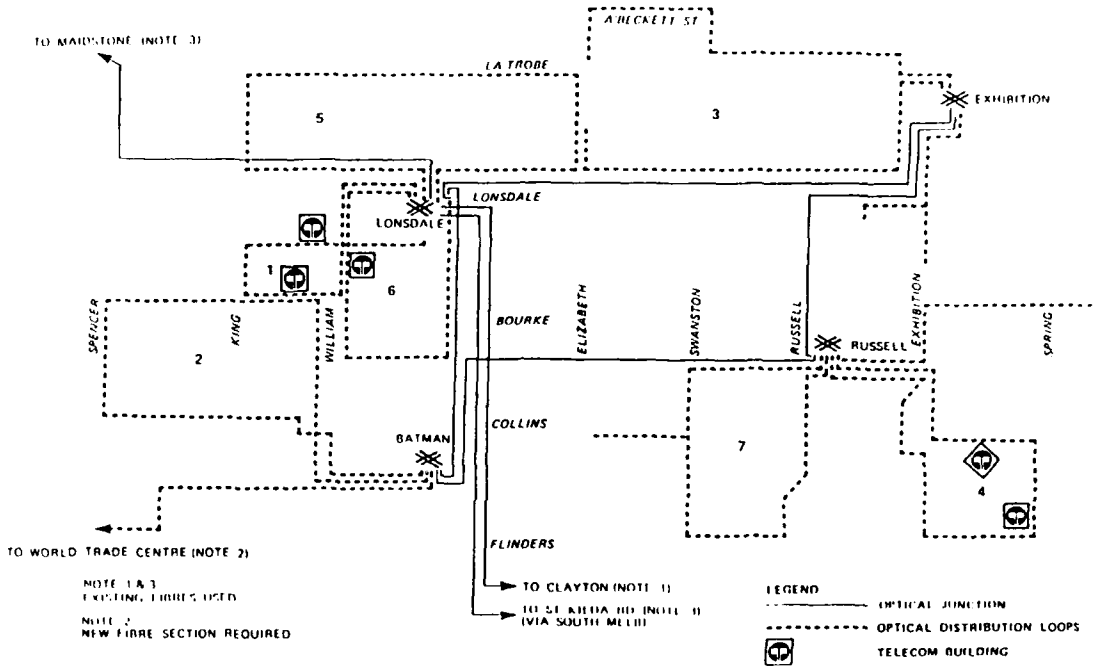


Fig. 1 Melbourne Optical Fibre Ring and Distribution Plan

A small number of spur routes were provided in the CBD where looped distribution could not be feasibly achieved without costly augmentation of the duct system. In addition optical fibre cable spurs were provided from the CBD to a number of Telecom establishments in suburban suburbs.

EXTERNAL CABLE DESIGN

General

External cables used in the inter exchange and distribution part of the network contained 30 fibres while 12 fibre cables were employed as lead in to customer buildings. Further details are provided below (See also Fig 2)

Optical Fibre Characteristics

Multimode 50/125 um core/cladding
1.8 dB/km maximum attenuation
600 MHz km minimum bandwidth
Second window (1300 nm) operation
Protective coating 0.4 mm O.D. UV acrylate

Cable Construction and Mechanical Characteristics

Fibre reinforced plastic strength member
Six slotted polyethylene core
Jelly filling compound
Plastic core wrapping tape
Low Density polyethylene inner sheath
Flame retardant PVC outer sheath
Cable outer diameter 12.9 mm
Cable mass (30 fibre) 151 kg/km (approx)
(12 fibre) 149 kg/km (approx)
Minimum bend radius
190 mm (no load)
600 mm (at 1344 N)
Tensile strength 1344 Newtons
Strength Mass (Newton kg/km)
8.9.1 (30 fibre)
9.0.1 (12 fibre)

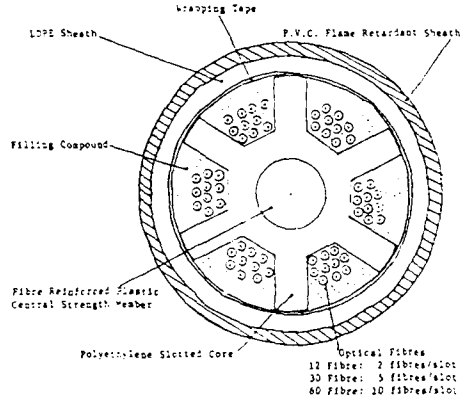


Fig. 2 External Cable Construction

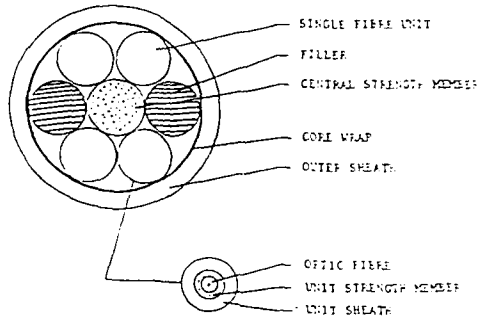


Fig. 3 Internal Cable Construction

INTERNAL CABLE DESIGN

General

These provide the connection between distribution frames in customer buildings at which lead in cables terminate and the terminal equipment. The cable contains four single fibre cords, each cord consisting of a nylon jacketted fibre strengthened peripherally with aramid yarns and enclosed in a PVC sheath. The four cords together with two fillers are tightly stranded around a central strength member to form the final cable. Further details are provided below (See also fig 3)

Optical Fibre Characteristics

Multimode - 50/125 um core/cladding
1.3 dB/km maximum attenuation
600 MHz km minimum bandwidth
Second window (1300 nm) operation
Protective coating - 0.9 mm O.D. nylon

Cable Construction and Mechanical Characteristics

GRP rod central strength member
Polyester core wrap
Cord and Cable sheath - flame retardant PVC
Cable mass - 120 kg/km (approx)
Minimum bend radius:
175 mm (no load)
440 mm (1000 N)
Cable strength - 1000 Newtons
Strength Mass (Newtons - kg/km)
8 x 1

INSTALLATION ASPECTS

Cable Placement

The ring of cables linking the four telephone exchanges were installed in the existing tunnel system. The practice used was to feed the cable from a cable drum trailer positioned at street level into the tunnel 8 metres below. It was hauled along the tunnel floor and then lifted by hand on to 150 mm wide trays on which it was permanently supported.

The distribution cables emanating from the city exchanges were hauled into one of three 35 mm polyethylene pipes which had previously been installed in a vacant 100 mm PVC conduit forming part of an existing duct route located under the city footpaths. The provision of these sub ducts allows the 100 mm conduit to be utilized for future optical cable installations without incurring possible damage to cables in situ. The conduit selected to house the distribution cable was located where possible beneath the top layer of the duct route and as close as practicable to the building alignment. With this arrangement the upper and outer ducts of the route would afford some protection in the event of mechanical damage occurring.

The main challenge of the installation was to haul the ring and loop cables in one continuous length between terminating points in the exchange buildings. This required a careful placement of the hauling winches so that work would progress satisfactorally without exceeding maxium permissible cable tensions. All cable hauling work was performed at night to avoid disrupting day time vehicular and pedestrian traffic.

The winch trucks used were locally designed and were mounted on a 1.5 tonne cab chassis. An aluminium tray fitted to the chassis supported the 1.1 metre diameter aluminium capstan wheel which could be angled to suit the direction of haul. A power take off from a hydraulic pump provided the drive to the capstan. A control panel with safety surround is situated between the cab and winch. (See fig 4). The cable was hauled at speeds of 30-45 metres per minute with hauling lengths varying between 1 to 2.5 Km. At pre designated manholes a 20-30 metre loop was left in distribution cables to facilitate connection to customers.

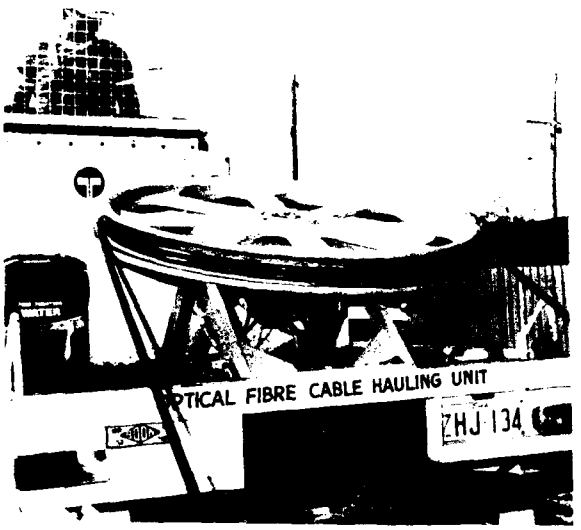


Fig. 4 Hauling Optical Fibre Cable

At these loops openable type joints are being installed which enable up to four 12 fibre lead-in cables to be run from each location. When a customer is to be connected to the network the nearest openable joint on the distribution cable serving the building is accessed and a lead in cable is provided from the joint to the building. In many instances an openable joint will not be located opposite the desired building in which case the lead in cable will follow the distribtuion cable in a separate sub duct for some distance before branching off into the building.

Cable Jointing and Terminating

The principle initially adopted for the openable joints was that all distribution fibres would be jointed through except those required for immediate use which would be spliced to the lead in fibres. Subsequently it has been decided to install an alternative jointing technique involving a 24 fibre terminating and patching panel. In this system flexible pigtails are spliced to the desired distribution and lead-in fibres to facilitate manual cross connection of up to a maximum of 24 fibres via the through connectors in the connector frame (See fig 5). This enables a range of jointing and fibre allocation arrangements to be developed to provide flexibility in the connection and re-arrangement of services. Splicing of fibres in the openable joints was performed using the fusion technique and the operation was conducted in specially designed air conditioned vehicles to provide a controlled environment free from dust and dirt.

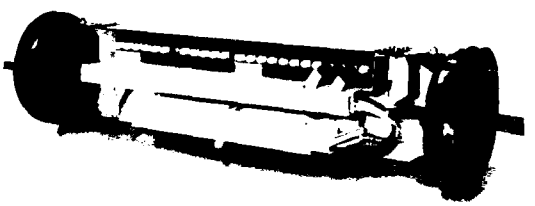


Fig. 5 Connectorised Optical Fibre Joint

In the four exchanges and at customer buildings each cable end is terminated at the optical fibre distribution frame via 10 metre pigtails fusion spliced to the street fibres. The pigtails connect to 48 fibre capacity termination and patching modules which are capable of accepting up to 48 D4 through connectors. The module is also designed to house the organizer trays used for storing the fusion splices and excess fibre pigtail (See fig 6). The internal cable connecting to the termination and patching modules were provided with D4 field fittable connectors.

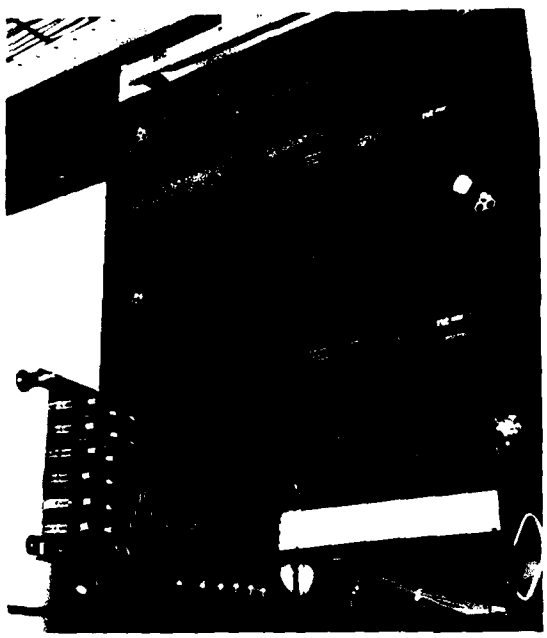


Fig. 6 Optical Fibre Distribution Frame

Cable Testing

Cable testing was performed to ensure splice continuity and integrity and to provide valuable feedback to the jointers as part of their training programme. Measurements of insertion loss and splice loss where taken on each jointed fibre. An Optical Time Domain Reflectometer was used to provide the splice loss, the distance to a splice and the loss of the fibre up to and beyond the splice. Prints of the OTDR traces were recorded for future maintenance purposes.

OPTICAL FIBRE CABLE RECORDING

With the establishment of the Melbourne wideband network and the prospect of similar networks in other locations an agreed national fibre numbering scheme has been developed which will form the basis of a plant recording system. It is expected that the complexity of loop connections generated by customer access and security requirements will necessitate field staff involved in providing and maintaining the service to have direct access to computerised records. One system under consideration is to provide portable personal computers and a set of updateable disk records in field vehicles.

CONCLUSIONS

This article has described the establishment of an optical fibre cable network in the Melbourne CBD to provide the means to link selected buildings with high capacity digital services. The network has been designed to transport these services over diverse routes to give an enhanced level of security and reliability.

The techniques to be used in subsequent CBD networks will largely evolve from the experience gained with the Melbourne CBD installation. For example, the use of looped fibre distribution and the recording methods developed for its effective management will be universally implemented. The complexity possible with customer fibre interconnections highlights the need for a computerised recording system which is currently receiving attention.

A CBD network employing single mode optical fibre cable is to be installed in the city of Sydney during 1987/88 and further such networks will be established in the remaining capital cities and the larger regional centres. All of these networks will eventually have access to O/F trunk and junction cables so that in due course all major business areas in Australia will be able to be linked via high performance O/F bearers.

ACKNOWLEDGEMENT

The permission of the Chief General Manager, Telecom Australia, to publish this paper is hereby acknowledged.

L de Valle
Trunk and Data Network
Engineering Branch
Telecom Australia
11/31 Spring Street
MELBOURNE VIC 3000
AUSTRALIA



Laurie de Valle graduated with a Fellowship Diploma in Communication Engineering from the Royal Melbourne Institute of Technology in 1958. He joined Telecom Australia in the same year and was principally involved in providing engineering support for the provision and maintenance of telephone services in a country district. Since 1980, he has been working on the planning, resourcing and implementation of transmission and data facility projects. During this time he assumed the role as the project manager for the Melbourne CBD optical fibre installation.

M J McKiterick
Optical Installation &
Maintenance Section
Telecom Australia
29/570 Bourke Street
MELBOURNE VIC 3000
AUSTRALIA



Michael McKiterick graduated in 1970 from the Royal Melbourne Institute of Technology in Civil Engineering and joined Telecom Australia in 1974. Currently, he has national oversight for the development of external plant practices associated with optical fibre cable installation and jointing.

W I Harry
External Plant
Construction Section
Telecom Australia
3/60 Albert Road
SOUTH MELBOURNE VIC 3205
AUSTRALIA



Ian Harry joined Telecom Australia in 1958 and since that year he has worked on a wide range of external plant activities. In recent times he has headed a section responsible for the installation of all optical fibre cables in the State of Victoria. This included a major trunk cable of about 1100 Km between the cities of Melbourne and Sydney.

PRODUCTION AND INSTALLATION OF SINGLE-MODE OPTICAL CABLE ON A 39 KM ROUTE WITHOUT REPETEARS UNDER EMI CONDITIONS AT MEXICO CITY AREA.

Gerardo Chávez Díaz, Juan Carlos Salazar Cerda, Eduardo Goddard Moore

Condumex, Telecommunications Division

ABSTRACT

The Mexican Telephone Administration TELMEX after analyzing different alternatives to solve communications growing demand in some areas of the country, has chosen an Optical Fiber System to cover the route between México City and a industrial city, "Cuautitlán", that is 39 Km away. As an important remark, the network has had several problems in the past because of high Electro-Magnetic Interference causing severe damages on Central Office equipment. This implied that 2 types of structures were proposed as a solution for the link : One metalic and the other all-dielectric. It uses single mode fiber with 0.5 dB/Km maximum attenuation operating in the 1300 nm wavelength range. The 140Mb/s system installed operates without repeaters taking full advantage of dynamic range for the whole system and giveing this alternative good competitivity and cost effectiveness.

INTRODUCTION

As a result of the increasing demand for high performance digital capability in the long-haul trunk networks within the country, and because of severe EMI problems occurred previously on the link from México City (Telephone main exchange "San Juan") to a city in the suburbs area called "Cuautitlán" (a 39-Km route), the Mexican Telephone Administration, Teléfonos de México (TELMEX) decided to establish an Optical Fiber System for protection and warranty on communication performance between both cities.

Route

The 39 km route runs from México City downtown to the northern part of the city suburbs with 2 Km - length cables installed on ducts. This route was covered using 31.5 Km of armored optical cable to protect against rodent attack at the metropolitan area. 7.5 km of dielectric cable were used on the last part of the route prior to arrival at "Cuautitlán" Central Office, because the vicinity of a 230-KV Electrical substation could cause considerable inductions if an armored cable was istalled there with the risk of damage of digital equipment. In general the environmental conditions were stable but the temperatures could rise up to 30 Celsius degrees in strong sunlight. The route has no gentle contours as we can expect on a high density telephone area and required an adequate planning to fully control and handle the installation with proper test procedures. Figure 1 shows the cable route.

CABLE DESIGN AND MANUFACTURE

Single mode fiber specification

The single mode optical fiber used in this link has the following characteristics:

1) Maximum fiber attenuation: 0.4 dB/km at 1300 nm.
2) Cut-off wavelength: 1200 +/- 70 nm (Transmission method)
3) Mode Field Diameter at 1300 nm: 10 +/- 1.0 microns.
4) Maximum total dispersion between 1285-1330 nm: $\leq$ 3.5 ps/nm. Km
5) Core-Clad concentricity error: $\leq$ 1 micron
6) Cladding diameter: 125 +/- 3 microns

These fiber were coated with a two layer UV acrylate corposite. The inner layer is a "low modulus" material to provide microbend resistance, whereas the outer layer is a "high modulus" material to resist abrasion and provide strength retention. The outer diameter of the coating was nominally 250 microns.

Single mode fiber characterization

The fiber was measured, prior to packaging to determine:

1) Attenuation at 1300 nm. Measured using the cut-back reference technique, and verified by OTDR read out.
2) Cutoff Wavelength and Mode Field Diameter at 1300 nm.
3) Core concentricity and cladding diameter. Measured using a microscope system employing an image shearing technique.

The average values for these parameters measured on single mode fibers for the link were:

Attenuation at 1300 nm: 0.35 dB/Km
Cutoff Wavelength: 1200 nm.
Mode Field Diameter at 1300 nm.: 10 microns
Core/clad concentricity: 1 micron
Cladding diameter: 125 +/- 1 micron

Cable Specification

Single mode optical cables are specified to meet an operating temperature range from -10 Celsius degrees to + 50°C under normal conditions with a maximum compression load af 3000 Kgf over 15 cm of cable, and must be fully filled to avoid water or moisture penetration on the cable.

Cable Construction

The cable design is based on a filled loose tube stranded configuration comprising 10 single mode fibers; the fibers are color-coded (black and white) for easy identification. Two fibers are packaged pertube. One filler is used to conform properly the structure. The tubes and filler are stranded around a bare tensile steel strength member or a fiberglass epoxy member according to the type of cable.

This last material offers advantages because it has a similar coefficient of thermal expansion to the optical fibers. On the same process an interstitial filling compound is applied to protect the cable against moisture migration. In general these jellies permit a stress free placement of the fiber and a longitudinal water tightness on the structure. This optical cable is them lapped with a longitudinal polypropylene tape and over this an inner PE jacket is extruded to bring the first mechanical and evironmental protection on the core. After this process, a longitudinal corrugated steel tape is applied in tandem with the outer jacket to conform the finished armored cable. On the other hand, two layers of aramid varns are applied helically to reinforce and support strength member on the dielectric cable, under installation conditions.

This material was chosen primarily because it is dielectric, but also it exhibits a high strength-to- weight ratio, and low elongation. The lay length has been calculated to ensure that when the cable is subjected to a tensile load, the aramid yarns takes this load instead of the fibers'.

The strength member limits cable elongation to less than 1 % when the cables is subjected to a tensile of 200 Kg. Finally an outer PE jacket is extruded to finish the cable. The nominal overall diameter in both cases is 15 mm. The armored cable has a weight of 205 Kg/Km and the dielectric type has only 145 Kg/Km. A cross section of the two cables is shown in Figure 2.

Cable Manufacturing

Special techniques and process systems were employed to manufacture these cables,considering that is very important to handle the proper amount of excess fiber relative to buffer tube and the whole cable, to mantain this relationship adecuate because the cable is strained by tensile or contraction forces mainly caused by temperature variations all day along the route. A range of lay length was chosen to establish a reasonable level of stress which the fiber would be allowed to suffer. This is because shorter lays would induce too much bending stress due to stranding.

Also the inside diameter of the buffer tube, outside diameter of the fiber, the radius of the cable core and the manufacturing conditions during process must be considered to control the total percentage of excess fiber length on the cable. During cabling, a polypropylene tape was longitudinally wraped around the cable core to hold the stranded buffer tubes in place for the inner jacketing operation. The tape also prevents flowing of PE jacket in the cable interstices that would make fiber access difficult on the field, and works as a thermal/moisture barrier to protect buffer tubes along the process and during operation. As was mentioned earlier a proper stranding of the aramid varns must be considered to do an effective work on the installation of the dielectric structure. In the case of the armored cable, an adequate relationship of corrugations/inch on the steel tape must be determined , so it guarrantees the flexibility and the elongation-contraction forces performance suffered by the cable during its life time.

On these cables polyethylene jackets were used because of their good crush and stress - cracking resistance properties and their proven record for long term cable protection. For this project a standard 2 Km - length on production cables was handled.

Cable Test Results

Several tests were performed on single mode optical cables. Optical attenuation and OTDR tests were performed 100% at each manufacturing stage. With the Spectral Attenuation System available we were also capable of measuring the Cut-off Wavelength and the Mode Field Diameter. Some mechanical and environmental properties were verified by initial design qualification and by sampling of production cables. These tests of sample cables have confirmed their ability to perform in their intended environment. Figure 3 summarizes the various tests applied.

During manufacture of the cable no tendency for microbending edge to appear as a result of the process utilised was experimented.The average attenuation obtained for black single mode fibers on finished cable was 0.355 dB/Km at 1300 nm with a standard deviation of 0.027. In the case of the white fibers the average attenuation at 1300 nm was 0.351 dB/Km with a standard deviation of 0.02. The complete data of both single mode fibers is summarized in Figure 4.

CABLE INSTALLATION PROCEDURES AND SPLICING TECHNIQUE UTILIZED

Installation Planning

Field experiences to handle an underground cable installation are well documented[4,5]. On this basis, the first step was the inspection of all the route to check in detail any variations on direction or angles that would submit the cable to critical tensile loads. Also this inspection allowed to consider the adequate excess length of cable to leave on each manhole, the proper location for the splice enclosures, and in the particular area of high Electro-Magnetic Interference, special considerations for cable protection against rodents attack (see Figures 5 and 6).

Manholes Preparation and Innerducts Accomodation

The manholes selected must be cleaned and prepared for placement of plastic innerducts, cables and enclosures inside them. Although not necessary to protect the cable, the use of 25 mm inner diameter plastic subducts into 100 mm normal telephone ducts has become a common practice in order to have maximum duct utilization. In our case 3 innerducts were installed using only one of them for this project along the route. To avoid any obstructions on the ducts steel brushes were used to clean all of them before the installation of the subducts and plastic cap ends.

The cap ends fix the position of the innerducts along the route, avoiding mistakes during the guide of cable or possible damages because of twisting on any of them. Installation of subducts were done manually, and by the use of cable pulling machines. In the last case, special precautions were considered to avoid any critical tensile loads that could collapse the innerducts. Both ends were could cut sharply and well cleaned from any excess a material that cause excessive frictions on cables during their pulling. Finally the cap ends were placed on the ducts, and both ends of the subducts were rounded to ease the guiding and penetration. No special lubricant was required for low friction of the cable along the route (see Figure 7, 8 and 9).

Cable Installation

After the proper identification of the innerduct to be used each monhole the cable reel was placed at an intermediate point and the cable pulled into the duct. After one kilometer length was introduced, the remainder of the cable was then removed from the reel and "Figure eighting" was applied. Finally the other end was pulled into the other duct. That was important to reduce the load necesary for installation because parts of the route had several changes of direction and could alter the final performance of the cable. This method also reduced crew size and the amount of equipment required (see Figure 10).

Because a Pulling Eye is readily attached to the strength elements of the optical cable, the use of a Pulling Rope, which will not stretch during the pull was suggested (see Figure 11). Some precautions were taken to avoid internal cuts in subducts with these ropes. Mechanical Fuses were fixed to the Pulling Eyes of about 100-150 Kg and also a Detorsion Device to protect the cable along the route. In the interior of each manhole several plastic fasten belts were fixed to the wall to properly accomodate the cable.

The operation was controlled by using some "walkie-talkies" where the reel was located and at different points of the route inside the manholes.

Mainly, the placement of the cable was done manually, but in parts of the route winches were utilised to accelerate its placing. When the installation of a cable was finished, both ends were covered with thermal shrinkage caps to eliminate moisture migration previous to splicing. In the particular case of dielectric cables special "LEAD SLEEVES" were used to protect cable ends between the output of the innerducts and the input of each splice enclosure from the attack of rodents.

After installation of the cable the average attenuation on black fibers was 0.369 dB/Km at 1300 nm with a standard deviation of 0.028, and in the case of white fibers it was 0.379 dB/Km at 1300 nm with a standard deviation of 0.032.

Testing and Splicing

All the cables installed were tested for attenuation by OTDR, to check if any fiber had suffered damages on handling (see Figure 12). After this, both cables ends were prepared for jointing.

The fibers were spliced using an Electric - Arc Fusion Splicing Machine and LID technique. All the splices were done on a Special-Conditioned Van for quality assurance of the process, and were verified to obtain lower loss values before termination at the Splicing Trays. All the Splice Enclosures were a double entry cap-ended type with cable entry at one end. These enclosures were fixed to the inner wall in the manhole in a particular area to ease identification (see Figure 13). At the Central Office the terminal Splice Enclosures were prepared to join cable with pigtails that arrive to the Fiber-Optic Line Terminal, working at 140 Mb/s. Here the same technique described above was used except for fixing the Splice Enclosure on a special area assigned to avoid any abstruction inside the Transmission Line Equipment Room (see Figure 14). The average loss obtained on black fibers was 0.123 dB with a standard deviation of 0.053; for white fibers an average loss of 0.108 dB with a atandard deviation of 0.044 was obtained. The distribution of the single mode fusion splices for this project is shown in Figure 15.

FINAL TEST PROCEDURES

All splices were concluded along the route and at the Central Offices several Acceptance Test of the link were required prior to start-up the equipment. These tests consisted on monitoring Total Loss of the link with OTDR and by the use of a 1300 nm Laser source on one end and an Optical Power Meter on the other to measure the existing Total Loss. Both methods brought us accurate values to define the Dynamic Range available on the route (see Figure 16). Considering a Reference Input Power of -21 dBm, an average Received Power of -47.5 dBm was obtained; this gave average difference of -26.5 dBm that covered successfully Dynamic Range and Bit Error Rate expected figures.

CONCLUSIONS

The experience gained from manufacture and installation of a fiber optic cable on a 39 Km. route gave us successful results in demonstrating the technical viability and economic advantages of the technology used to satisfy actual and near future demands on services for this City area. The excellent installed Single Mode Cable attenuation at 1300 nm wavelength shows the posibility of using armored and dielectric optical cables for underground applications to solve any EMI problems without exposing the last structure to rodents attacks that could interrupt communications between both cities. The optical system design applied on this project allows maximum repetears spacing incurring on important savings costs for the total Digital Network installed.

ACKNOWLEDGMENTS

The important support of all personnel at TELMEX and in the Fiber Optics Group of the Telecommunication Division at Condumex has made this project possible. Their work is sincerely appreciated. Acknowledgment are also made to the Director of the Telecommunications Division and to the Technical Director of our Electromanufaruring Sector for permission to publish this paper.

REFERENCES

1.- Young, Jr., D. "ENVIRONMENTAL EFFECTS ON ACRYLATE COATED OPTICAL WAVEGUIDE FIBERS" Corning Glass Works Technical Report, August 1981, pp. 1-7

2.- Johansen, E., Faulks, deBoer, B., "Installation, Evaluation and future design of Optical

fiber [illegible] routes in Australia", 35th International wire and cable Symposium, USA, 1986, [illegible].

[illegible] Sarkar, P. Dobson, P. Burwitz D., Aggarwal [illegible], "Design,fabrication and testing of a [illegible] Fiber Optic Cable", 32nd International wire and cable Symposium, USA, 1983, pp. [illegible].

[illegible] Root, [illegible], Masterson, [illegible], "Installation Experience with Optical Fiber Cable", Telephone engineer & Management Magazine, May 1981, pp. [illegible].

[illegible] Sforzini, G., "Single Mode Cable Technology, Installation, Splicing, Testing and Maintenance", Siecor Technical Bulletin 1984, pp. 1-25.



Gerardo Chávez Díaz
Condumex Telecommunications Division
P. O. Box 100
San Juan del Río, Qro.
México 76800
Tel. 52 (467) 2 31- 05

Gerardo Chávez is a Production Chief Engineer in the Optoelectronics Department at Condumex Telecommunications Division. He is responsible of the Production and Planning for Optical Cables and Optoelectronic Systems. He joined Condumex in 1984. He worked previously at the Mexican Electrical Research Institute in the Communications Deparment on a special Project for Fiber Optic applications in Electrical Utilities. He received his B.S. in Electronic Engineering from Universidad Iberoamericana at México City. He is a Member of IEEE and SPIE.



Juan Carlos Salazar Cerda
Condumex Telecommunications Division
P. O. Box 100
San Juan del Río, Qro.
México 76800
Tel. 52 (467) 2 31- 05

Juan Carlos Salazar holds the position of Installation Manager in the Optoelectronics Department at Condumex Telecommunications Division. He is responsible of the installation for Optical Cables and Optoelectronics Systems. He has worked for Condumex since 1976, first as Production Chief Engineer in the Telecommunications Division and since june 1985 in his current position. He received his B.S. in Electrical Engineering.

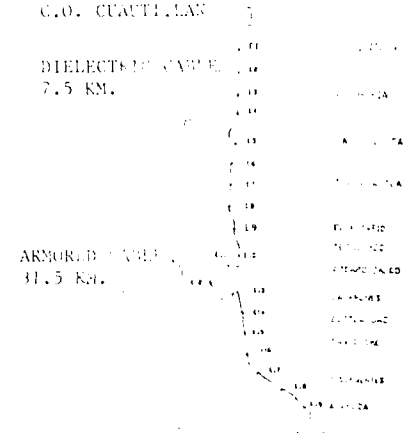


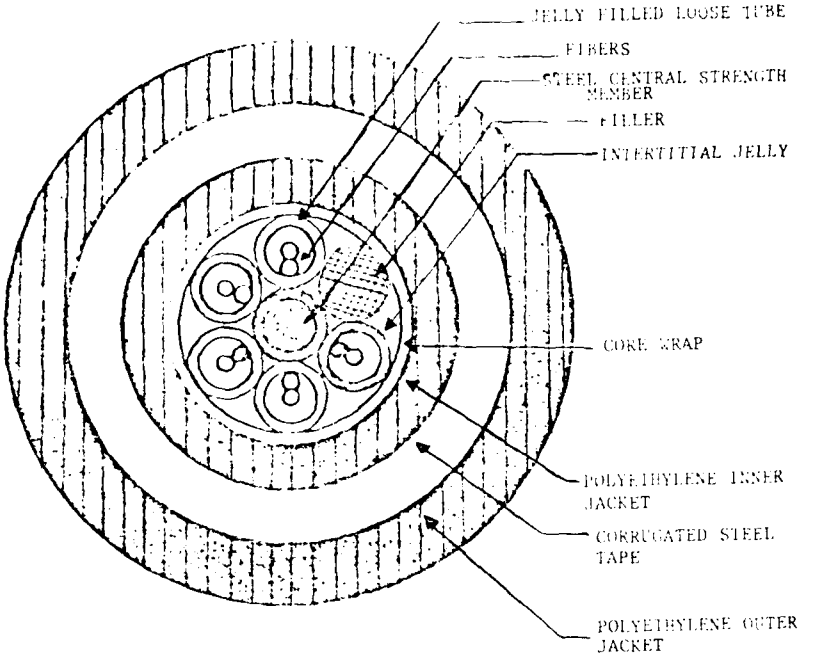
Eduardo Goddard Moore
Condumex Telecommunications Division
P.O. Box 100
San Juan Río, Qro.
México 76800
Tel. 52 (467) 2 31-05

Eduardo Goddard holds the position of Manager Optoelectronics Operations at Condumex Telecommunications Division. He is responsible for the Optoelectronics Group Operations which include Production and Installation of Livhtguide Systems. He has worked for Condumex since 1985 first as Sales and Marketing Manager and since march 1987 in his current position. He holds a B.S. in Electronics and an M.B.A. in Marketing.

SAN JUAN - CUAUTITLAN

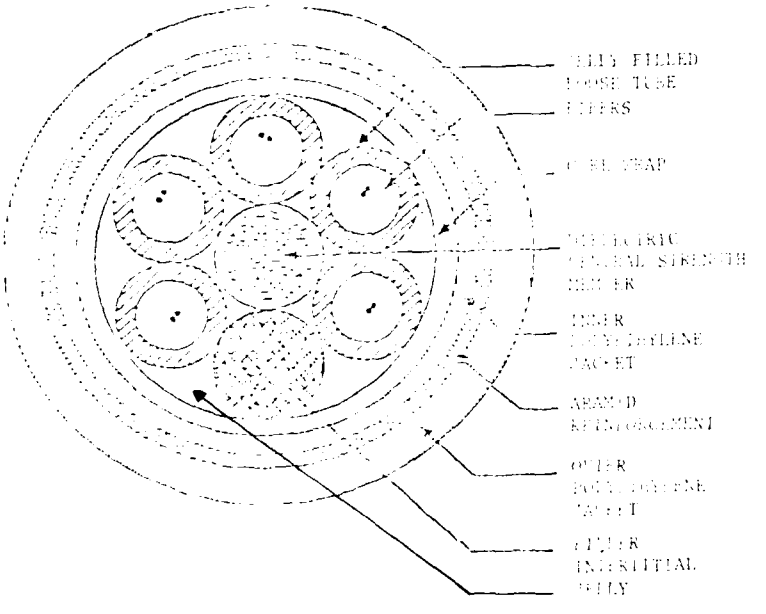
FIBER OPTIC LINK





(A)

ARMORED OPTICAL CABLE



(B)

DIELECTRIC OPTICAL CABLE

FIGURE 2

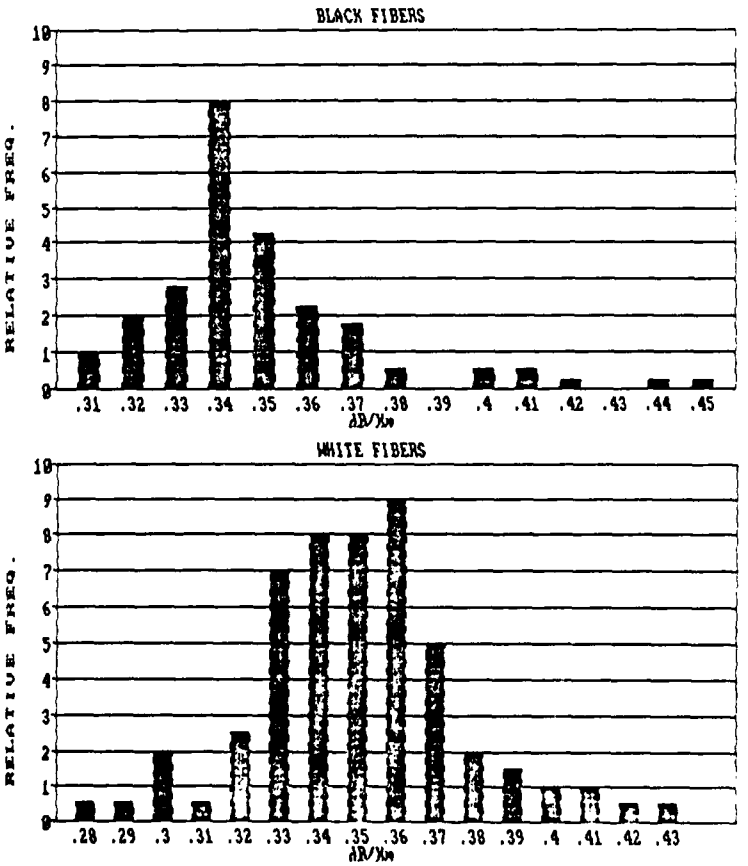
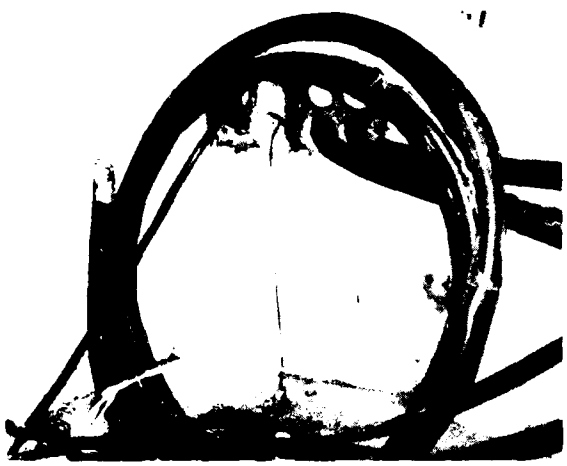

BLACK FIBERS
RELATIVE FREQ.
0
1
2
3
4
5
6
7
8
9
10
.31 .32 .33 .34 .35 .36 .37 .38 .39 .4 .41 .42 .43 .44 .45
dB/Km
WHITE FIBERS
RELATIVE FREQ.
0
1
2
3
4
5
6
7
8
9
10
.28 .29 .3 .31 .32 .33 .34 .35 .36 .37 .38 .39 .4 .41 .42 .43
dB/Km

FIGURE 4



FIGURE 5

INSPECTION OF VARIOUS MANHOLES TO DETERMINE CONDITIONS ON DUCTS TO BE USED FOR THE ROUTE.



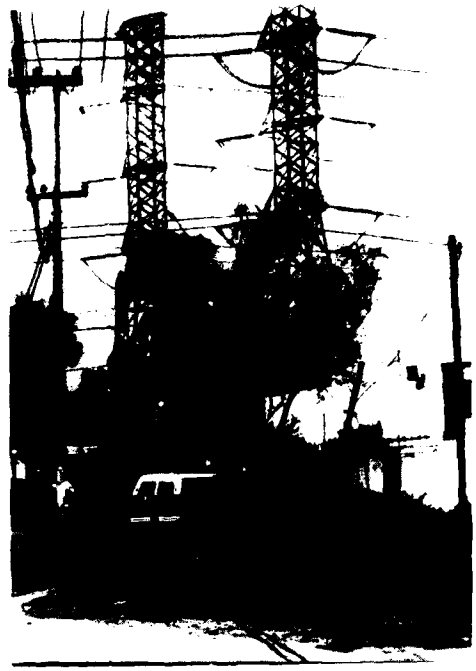


FIGURE 6

VIEW OF THE 230-KV TRANSMISSION LINES THAT ARE CROSSING PART OF THE ROUTE

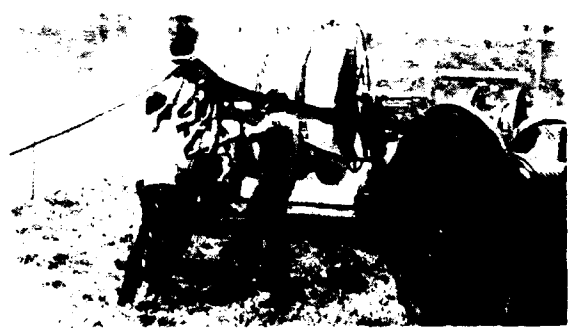


FIGURE 7

PREPARATION OF PLASTIC SUBDUCTS TO BE PLACED ON THE MANHOLES PRIOR THE INSTALLATION OF THE OPTICAL CABLE



FIGURE 8

CUT AND FIXING OF SUBDUCTS IN THE INTERIOR OF A MANHOLE

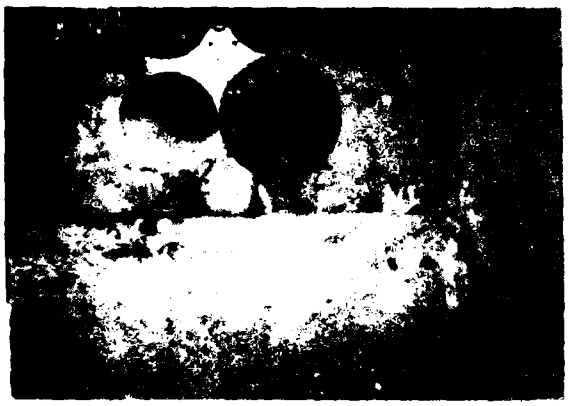


FIGURE 9

3- WAY DUCT FINISHED AT THE MANHOLE

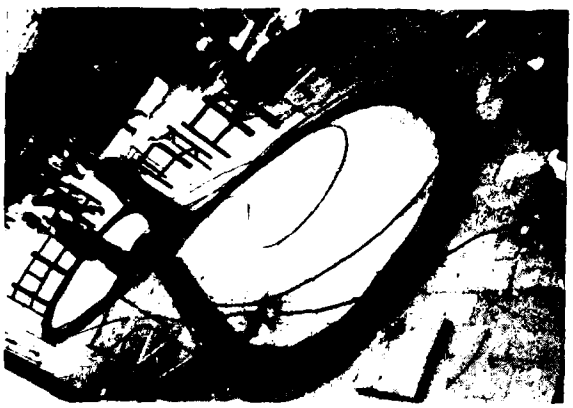


FIGURE 10

"FIGURE - EIGHTING" OF OPTICAL CABLE PRIOR TO INSTALLATION ON PART OF THE ROUTE.



FIGURE 11

PULLING EYE ON THE CABLE AND THE PULLING ROPE TO EASE THE INSTALLATION

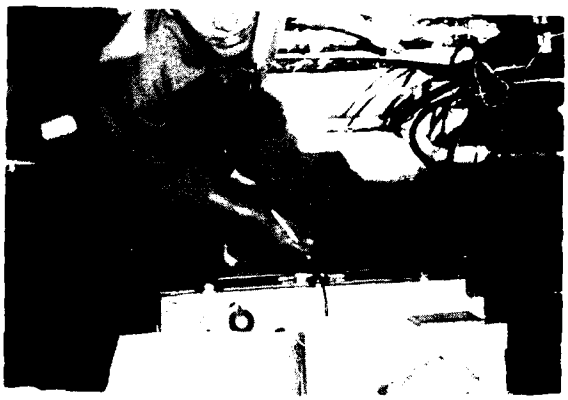


FIGURE 12

INSPECTING ATTENUATION BY OTDR AFTER THE CABLE WAS INSTALLED.

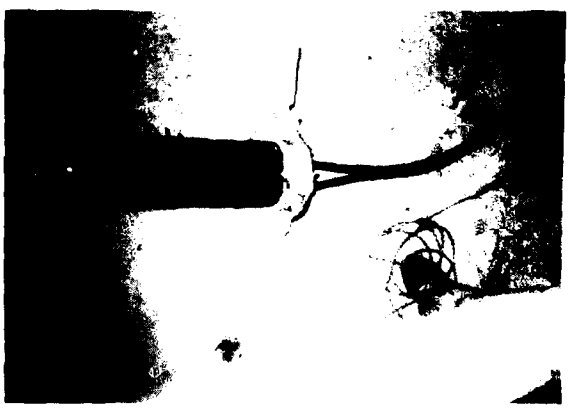


FIGURE 13

FIXING THE SPLICE ENCLOSURE CAP-ENDED TYPE TO THE INNER WALL OF THE MANHOLE.

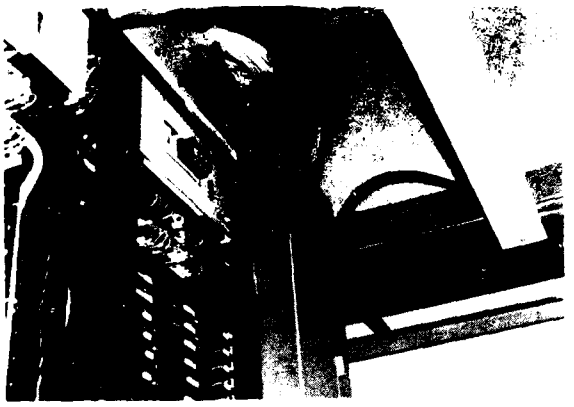


FIGURE 14

FIXING THE TERMINAL SPLICE ENCLOSURE IN THE INTERIOR OF THE TRANSMISSION LINE EQUIPMENT ROOM

DISTRIBUTION OF SINGLE MODE FUSION SPLICES FOR THE "SAN JUAN - CUAUTITLAN" PROJECT.

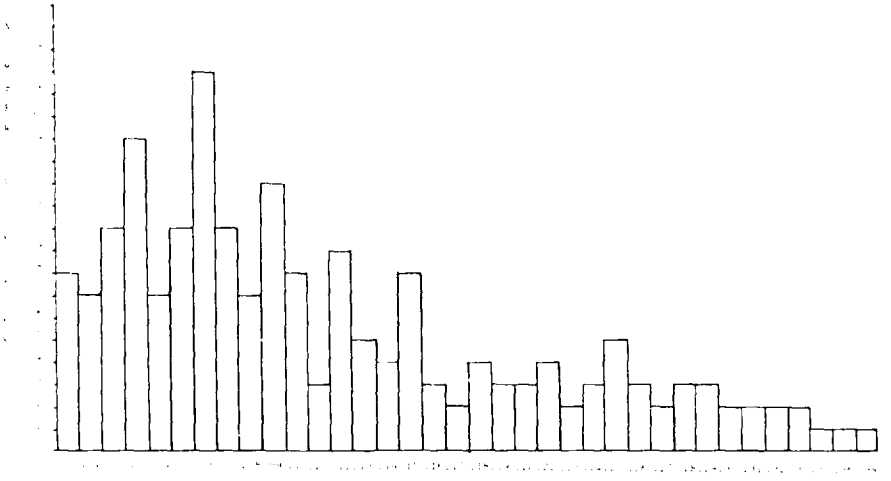
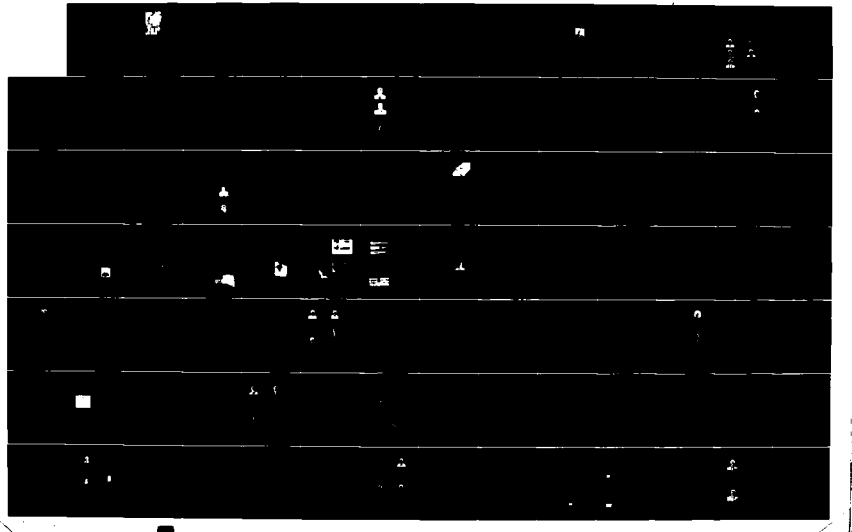


FIGURE 15 SPLICE LOSS (dB)

AD-A189 610 PROCEEDINGS OF THE INTERNATIONAL WIRE AND CABLE SYMPOSIUM (36TH) HELD IN..(U) ARMY COMMUNICATIONS-ELECTRONICS COMMAND FORT MONMOUTH NJ 19 NOV 87 7/9

UNCLASSIFIED F/G 9/1 NL



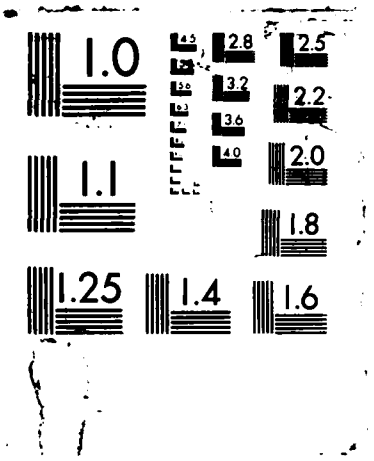

1.0
1.1
1.25
1.4
1.6
1.8
2.0
2.2
2.5
2.8
3.2
3.6
4.0
4.5
5.0
5.6



FIGURE 16

ACCEPTANCE TESTS AT THE CENTRAL OFFICE

Procedure for the Experimental Determination of Friction Coefficient Between a Cable and Duct

Howard M. Kemp

AT&T Bell Laboratories
Whippany, New Jersey 07981

ABSTRACT

The tension required to install a fiber optic cable in underground plant depends on the cable route geometry and the friction coefficient between the cable and duct liner. Installation tension can be reduced (permissible cable length can be increased) by reducing the friction through proper choice of duct liner and cable lubricant. This paper describes a test procedure that is used to evaluate cable lubricants and duct liners in a realistic cable placing environment. The method has also been used to study the effects of cable pulling speed and clearance between a cable and duct liner. In the procedure, cable tension is repeatedly and simultaneously measured at both the entrance and exit of a conduit run using an instrumented sheave and yoke arrangement in the pull and feed manholes. Data acquisition and analysis are automated by using a digital voltmeter and a desktop computer. Since the conduit between the entrance and exit of the test section is occupied only by cable, the moving interface between the cable and winch line is eliminated along with the attendant computational complications. One value of friction coefficient is computed from each corresponding pair of tension measurements. Because of the stepwise nature of tension calculations, a closed form solution for friction coefficient is generally not available; therefore, friction coefficients are computed numerically using the Newton-Raphson method. Proper application of test results will enable better predictions of cable installation tensions in underground plant.

BACKGROUND

A successful fiber optic cable installation in underground plant requires proper selection of splice locations and cable installation techniques. In general, the cable length between splices is selected to be as long as possible to reduce splice loss between regenerator locations. At the same time, the splice locations must be chosen so that the cable installation tension does not exceed recommended maximum load (tensile load rating of the cable).

Cable installation tension depends on the conduit geometry and the friction coefficient between the cable and duct. Given a fixed conduit geometry, permissible cable lengths can be increased by reducing the friction coefficient through appropriate choice of cable lubricant and duct liner.[1] Selection of cable lubricant and duct liner, as well as accurate prediction of cable installation tension, requires testing to determine the friction coefficient. The most reliable method of determining the friction coefficient is by tension measurement of cable pulls in conduit runs of known geometry.

TEST PROCEDURE

Set-Up

To emulate a realistic cable placing environment, the cable is installed in an underground conduit system in a manner similar to that used by a telephone line crew. The conduit system, shown in Figure 1, is a 141-foot-long U-shaped section of four-inch nominal-diameter PVC pipe. The conduit geometry, including elevation changes, was carefully surveyed and recorded during construction. The U-shaped conduit geometry provides a convenient tension multiplier in a short conduit test section because cable tension is exponentially related to the total angle of bend in the conduit section. Manholes at each end of the test section provide access to the conduit system. Various duct liners of interest are installed into the four-inch duct, and fiber optic cable is subsequently pulled into the duct liner. Cable lubricant is applied to the cable in a typical fashion.

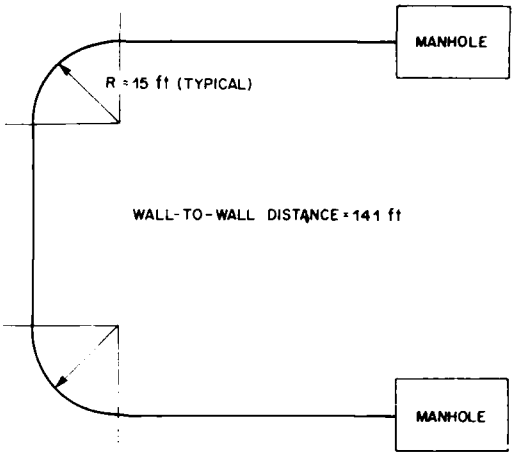


Figure 1. Plan view of conduit system used for cable installation tests. This particular conduit run is divided into fourteen sections: two horizontal straight sections, six grades, two horizontal bends, and four vertical-plane bends.

A sketch of a typical test set-up is shown in Figure 2. The cable reel is mounted on a reel carrier and is positioned at the feed manhole. The winch is positioned about fifty feet away from the pull manhole. The winch line is connected to the end of the cable, and the cable is pulled through the duct liner to the pull manhole. Tension measurement does not begin until the leading end of the cable is out of the pull manhole and has passed over the manhole sheaves. At this point, the cable is pulled towards the winch truck and measurements begin. Cable tension is measured simultaneously at both the feed and pull manholes during the 50-foot pull. An example plot of tension data is shown in Figure 3. Because the duct liner is occupied only by cable during these measurements, the computational and measurement difficulties that arise when a duct liner is occupied by both cable and winch line are eliminated.

1. The term *duct liner* is a generic expression that describes small diameter pipe or tubing placed inside conventional underground ducts. Several duct liners can be placed inside one conventional duct, and fiber optic cables are subsequently placed inside the duct liners.

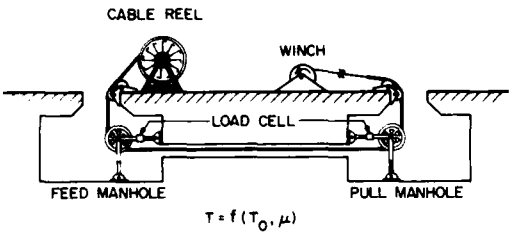


Figure 2. Set-up used for the cable installation test.

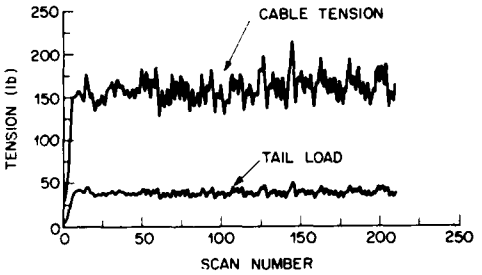


Figure 3. Plot of cable tension and tail load vs. scan number.

Tension Measurement and Data Acquisition

Simultaneous measurements of cable tensions at the feed and pull manholes are required to determine the friction coefficient. A sketch of the tension measurement set-up is shown in Figure 4. The yoke of the cable sheave is attached to telescopic tubing, which in turn is pinned to the wall and floor of the manhole. The telescopic tubing allows accurate horizontal and vertical positioning of the cable sheave within the manhole. A load cell is placed in the horizontal strut to measure the reaction on the strut. Assuming the cable behaves like a flexible string, and bearing friction in the cable sheave is negligible, then the measured force in the strut is equal to cable tension.

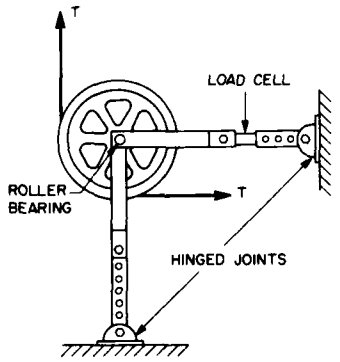


Figure 4. Sketch of tension measurement set-up.

Data acquisition is automated by use of a digital voltmeter and a desktop computer. A diagram of the data acquisition system is shown in Figure 5. Cable tension at the feed and pull manholes is measured simultaneously at a sampling interval of 500 milliseconds. Tension

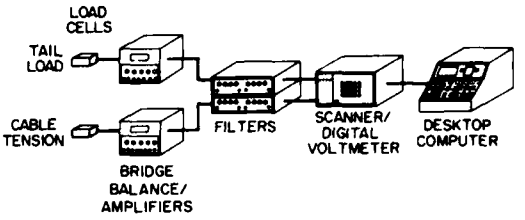


Figure 5. Data acquisition system.

measurements are recorded on diskette and are subsequently used in the numerical determination of friction coefficient.

DATA ANALYSIS

In general, the tension, T, required to pull a particular cable into a particular duct run is a function of two variables, namely, the friction coefficient, μ, and the hold-back force or tail load, T_0, at the feed manhole:

$$T = f(T_0, \mu). \tag{1}$$

The objective of the cable installation test is to determine μ from Equation 1 using the measured values of T and T_0. Except in trivial geometries consisting only of a single bend or a succession of straight sections and grades, a closed form solution for μ does not exist. Instead, μ is determined numerically using the Newton-Raphson method. The Newton-Raphson method finds the value of μ, the root, that satisfies Equation 1 expressed in the form

$$f(T_0, \mu) - T = 0. \tag{2}$$

The analysis begins with a guess at the root, e.g., $\mu = \mu_{i\,(i=0)}$, and the left-hand side of Equation 2 is evaluated using the measured values of T_0 and T. If the first guess at the root is in error by more than a specified amount, a truncated Taylor series expansion is used to predict a new value, μ_{i+1}. In general, each new value is determined by

$$\mu_{i+1} = \mu_i - \frac{f(T_0, \mu_i) - T}{f'(T_0, \mu_i)}. \tag{3}$$

where $f'(T_0,\mu_i)$ denotes $df(T_0,\mu)/d\mu|_{\mu=\mu_i}$. Successive approximations for μ are calculated until Equation 2 is satisfied within specified limits.

In practice, $f(T_0,\mu)$ and $f'(T_0,\mu)$ are computed in stepwise fashion by proceeding section by section through the entire duct run (feed manhole to pull manhole). The geometry of the conduit can be divided into four different section types: horizontal straight sections, grades, horizontal bends, and vertical-plane bends. Each section type has a closed form solution for cable tension at the exit, T_{j+1}, in terms of the cable tension at the entrance, T_j:

$$T_{j+1} = f_k(T_j, \mu), \tag{4}$$

where the subscript $k = 1,2,3,4$ refers to the section type, $j = 0,1,...n$ designates the point at one end of such a conduit section (numbered from the duct entrance in the feed manhole), and n is the number of sections making up the entire duct run. For use in Equation 3, both f_k and its total derivative with respect to μ are needed for each section type k. The equations governing cable tension and their derivatives are shown in the following sections.

Tension Equations and Derivatives

Horizontal straight sections. The tension required to pull cable through a horizontal straight section[1] is given by

$$T_{j+1} = T_j + w/\mu \tag{5}$$

where w is the unit weight of the cable and l is the length of the straight duct section. Differentiating with respect to μ gives

$$\frac{dT_{j+1}}{d\mu} = \frac{dT_j}{d\mu} + wl. \tag{6}$$

Grades. For grades, cable tension is

$$T_{j+1} = T_j + w(x\mu + h) \tag{7}$$

where h is the increase in elevation within the section and x is the horizontal projection of the section length l as shown in Figure 6a.

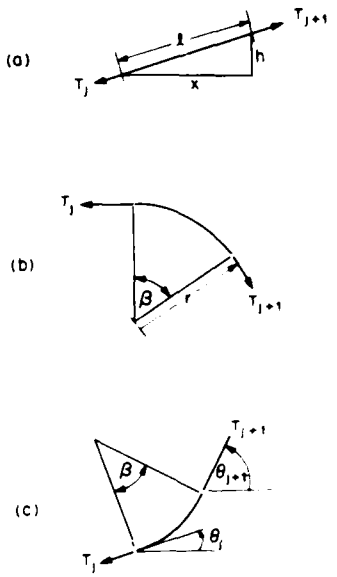


Figure 6. Geometry definitions for (a) grades, (b) horizontal bends, and (c) vertical-plane bends. In case (c), θ_j and θ_{j+1} are measured from the forward horizontal. As drawn in (c), both θ_j and θ_{j+1} are positive.

The derivative is given by

$$\frac{dT_{j+1}}{d\mu} = \frac{dT_j}{d\mu} + wx. \tag{8}$$

Horizontal plane bends. Cable tension for the horizontal bend[1] is expressed as

$$T_{j+1} = wr \sinh\left[\sinh^{-1}\frac{T_j}{wr} + \mu\beta\right] \tag{9}$$

where r is the radius of curvature and β is the angle of bend in radians as shown in Figure 6b. The derivative of Equation 9 is evaluated using the chain rule. In general,

$$\frac{df_k(T_j, \mu)}{d\mu} = \frac{\partial f_k}{\partial T_j} \cdot \frac{dT_j}{d\mu} + \frac{\partial f_k}{\partial \mu} \cdot \frac{d\mu}{d\mu}. \tag{10}$$

The identity

$$\cosh U = \sqrt{\sinh^2 U + 1}, \tag{11}$$

can be used to simplify the partial derivatives as follows:

$$\frac{\partial f_3}{\partial T_j} = \frac{\sqrt{(T_{j+1}/wr)^2 + 1}}{\sqrt{(T_j/wr)^2 + 1}}. \tag{12}$$

and

$$\frac{\partial f_3}{\partial \mu} = wr\beta\sqrt{(T_{j+1}/wr)^2 + 1}. \tag{13}$$

After substitution in the chain rule, the total derivative of Equation 9 is given by

$$\frac{dT_{j+1}}{d\mu} = \sqrt{T_{j+1}^2 + (wr)^2}\left[\frac{dT_j/d\mu}{\sqrt{T_j^2 + (wr)^2}} + \beta\right]. \tag{14}$$

Vertical plane bends. An expression for cable tension in a vertical-plane bend has been developed by A. L. Hale[2],

$$T_{j+1} = \left\{T_j + wr\cos(\theta_j - 2\psi \operatorname{sgn} r)\right\}e^{\mu|\beta|} - wr\cos(\theta_{j+1} - 2\psi \operatorname{sgn} r) \tag{15}$$

where θ_j is the entrance angle and θ_{j+1} is the exit angle of the bend measured from the horizontal (see Figure 6c), $\beta = \theta_{j+1} - \theta_j$, $\psi = \tan^{-1}\mu$, and $\operatorname{sgn} r = \pm 1$ (+1 for upward bends, −1 for downward bends). This equation is valid only when the cable remains in contact with the inside wall of the bend, i.e. when $T > wr\cos\theta$ everywhere within the bend. In the test facility, the maximum radius of vertical-plane bends is 15 feet, and the maximum cable weight is 0.4 pounds/foot. Since $\cos\theta \leq 1$, $wr\cos\theta \leq 6$ pounds. During testing, a high tail load is placed on the cable at the pull manhole; therefore, the assumption that $T > 6$ pounds everywhere in the bend can safely be made and Equation 15 can be used to evaluate cable tension.

The partial derivatives of Equation 15 are evaluated as

$$\frac{\partial f_4}{\partial T_j} = e^{\mu|\beta|}, \tag{16}$$

and after some lengthy mathematics,

$$\frac{\partial f_4}{\partial \mu} = e^{\mu|\beta|}\left[\left\{T_j + wr\cos(\theta_j - 2\psi \operatorname{sgn} r)\right\}|\beta| + \left\{\frac{2wr \operatorname{sgn} r}{1+\mu^2}\sin(\theta_j - 2\psi \operatorname{sgn} r)\right\}\right] - \frac{2wr \operatorname{sgn} r}{1+\mu^2}\sin(\theta_{j+1} - 2\psi \operatorname{sgn} r). \tag{17}$$

Substitution of the partial derivatives into the chain rule gives

$$\frac{dT_{j+1}}{d\mu} = e^{\mu|\beta|}\left[\frac{dT_j}{d\mu} + \left\{T_j + wr\cos(\theta_j - 2\psi \operatorname{sgn} r)\right\}|\beta| + \left\{\frac{2wr \operatorname{sgn} r}{1+\mu^2}\sin(\theta_j - 2\psi \operatorname{sgn} r)\right\}\right] - \left\{\frac{2wr \operatorname{sgn} r}{1+\mu^2}\sin(\theta_{j+1} - 2\psi \operatorname{sgn} r)\right\}. \tag{18}$$

The above expressions are used in the data analysis program to evaluate Equation 3. The program is written in BASIC for a desktop computer system. A flow chart showing the program logic is given in Figure 7. Two data files are required by the program. The first data file contains a description of the conduit run by segment type (straight, grade, or horizontal or vertical bend) and the associated physical parameters (length, slope, angle of bend, entrance and exit angles, and bend radius). The second data file contains measured values of T_0 and T_n collected during the test. Cable weight is entered into the program, then data analysis proceeds automatically.

The program assumes $\mu = 0.200$ as the first guess of the root for the first pair of tensions. The program uses this value stepping through each segment of the conduit geometry, calculating T_{j+1} and $dT_{j+1}/d\mu$ for each segment, until the final cable tension and its derivative are determined. If the final calculated value of $f(T_0, \mu)$ does not satisfy Equation 2 within specified limits, a new approximation for μ is calculated using Equation 3, and the process repeats. After a few iterations in this loop, Equation 2 will be satisfied, and the root (μ) is saved. The program then retrieves the next pair of measured data, and calculates a corresponding value of μ starting with the previous root as the first guess. Finally, after the tension data file is exhausted, the average and standard deviation of μ are reported, and a data plot of μ vs. scan number is generated. An example plot is shown in Figure 8 for a test that was conducted without lubricant using a polyethylene-sheath cable and a smooth-wall polyethylene duct liner.

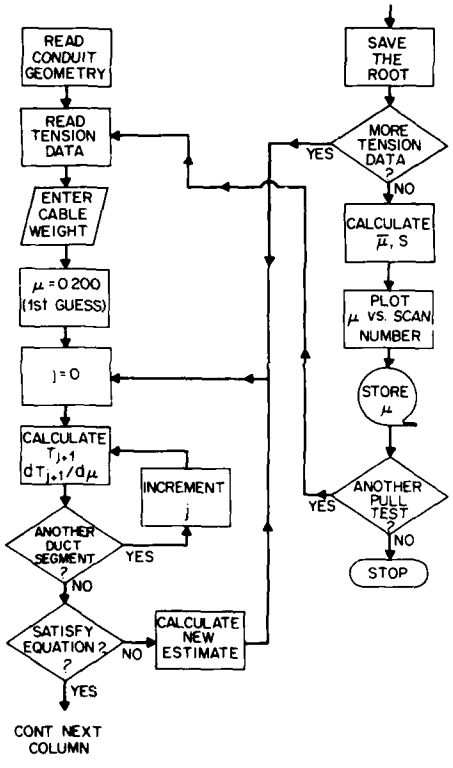


Figure 7. Flowchart for data analysis program.

The Effect of Cable Dynamics on the Calculated Values of Friction Coefficient

Ideally, μ is expected to remain constant during cable placement. Figure 8, however, shows that regular fluctuations in the computed values of μ were sometimes observed. These fluctuations result from the dynamic motion of the cable during installation. The following section analyzes the cable motion and its effect on the calculated values of μ.

Cable motion can be characterized as an undamped forced vibration where the forcing condition is due to Coulomb friction. A spring-mass system is shown in Figure 9a. The winch line between the pull manhole and the winch is the dominant spring having a spring constant k. The cable is considered inextensible and is represented by the mass m. The analysis is simplified by considering motion relative to the winch end of the winch line, so the spring is fixed at the winch, and the surface is moving to the right at velocity V. From the free body diagram in Figure 9b, the equation of motion is written as

$$m\ddot{x} + kx = F_f \quad (\dot{x} < V) \tag{19}$$

where x is the displacement, $\dot{x}$ the velocity, and $\ddot{x}$ the acceleration of the mass, F_f is the magnitude of the frictional force, and V is the velocity of the moving surface.

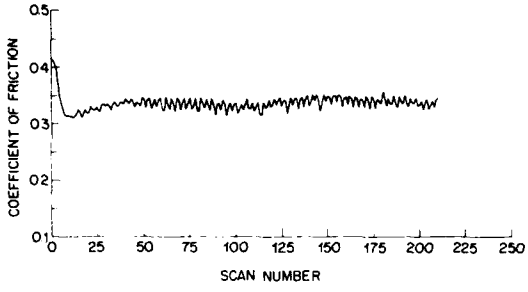


Figure 8. Plot of friction coefficient vs. scan number.

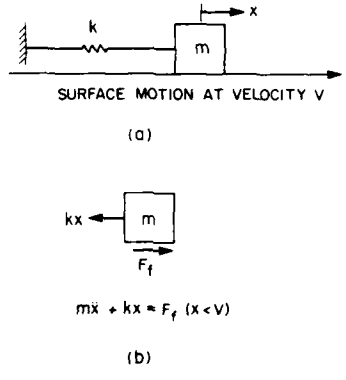


Figure 9. (a) Spring-mass system (b) free body diagram.

In this case, it is assumed that the kinetic frictional force, F_k, is constant (the Coulomb idealization). For the constant friction force, the response of the mass is given by Vierck[3]

$$x = \frac{\dot{x}_o}{\omega_n}\sin\omega_n t + x_o\cos\omega_n t + \frac{F_k}{k}(1-\cos\omega_n t) \tag{20}$$

where x_o and $\dot{x}_o$ are the initial displacement and velocity of the mass, ω_n is the natural frequency $\sqrt{k/m}$, and t is time. The velocity and acceleration of the mass are determined from Equation 20.

$$\dot{x} = \frac{dx}{dt} = \dot{x}_o\cos\omega_n t - x_o\omega_n\sin\omega_n t + \frac{F_k\omega_n}{k}\sin\omega_n t \tag{21}$$

$$\ddot{x} = \frac{d^2x}{dt^2} = -\dot{x}_o\omega_n\sin\omega_n t - x_o\omega_n^2\cos\omega_n t + \frac{F_k\omega_n^2}{k}\cos\omega_n t \tag{22}$$

For now, it is assumed that the maximum static frictional force, F_s, and the kinetic frictional force, F_k, are equal. It is also assumed that the mass is initially at rest relative to the surface ($\dot{x}_o = V$). As the

surface moves to the right, the spring force kx increases linearly. The mass begins to slide when the spring force $kx = F_s = F_k$. The initial conditions at the beginning of slippage are $x_o = F_k/k$ and $\dot{x}_o = V$. Plots of displacement, velocity, and acceleration corresponding to these conditions are shown in Figures 10a-c, where time is measured

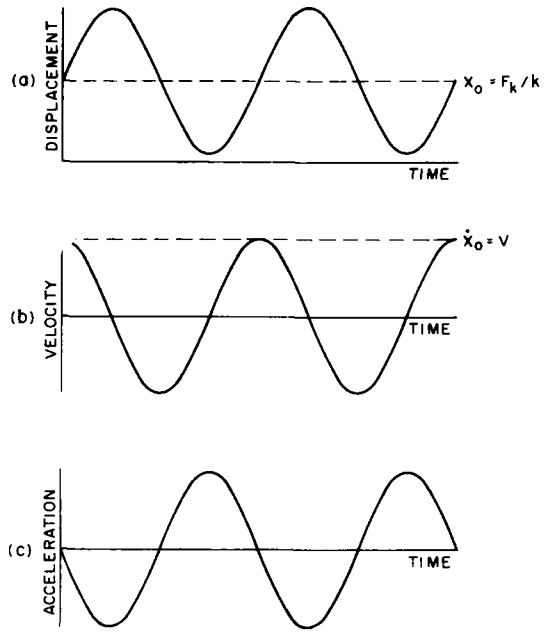


Figure 10. Plots of displacement, velocity, and acceleration for the case $F_s = F_k$.

from the instant when slippage starts. The constant velocity of the moving surface is also shown in Figure 10b. Note that the velocity of the mass never exceeds the velocity of the surface; therefore, the condition that $\dot{x} < V$ in Equation 19 is always satisfied.[2]

During data analysis, μ is determined from measured values of cable tension in the pull manhole. In practice, this tension corresponds to the spring force kx in the model. Equation 19, however, shows that the frictional force is equal to the sum of the spring force and the acceleration term. Since the acceleration term is neglected, the calculated values of μ will be in error by an amount proportional to the acceleration force. Note, however, the symmetric behavior of the acceleration curve in Figure 10c. Since the *average* value of acceleration is zero, the *average* contribution of the acceleration term to the frictional force is zero. Consequently, the average value of μ for the cable pull will be an accurate measure of the kinetic friction coefficient.

Stick-slip cable motion. Occasionally, stick-slip cable motion was experienced during the cable installation test. Since the equations used to determine μ are valid only when the cable is moving, the effect of stick-slip motion on the test results is of interest. As in the previous case, it is assumed that the kinetic friction force is constant when the cable is sliding; however, it is now assumed that the maximum static frictional force F_s exceeds the kinetic friction force, i.e., $F_s > F_k$. Whenever the mass is at rest relative to the surface it is in equilibrium, so that $\ddot{x} = 0$, $\dot{x} = V$, and the (varying) friction force $F_f = kx \leq F_s$. When F_f reaches its maximum value ($F_f = F_s$), the mass begins to slide. The initial conditions at the beginning of slippage are $x_o = F_s/k$ and $\dot{x}_o = V$. During the interval of slippage, $F_f = F_k$ = constant; hence, Equations 20-22 can again be used to determine the response of the mass.

Plots of displacement, velocity, and acceleration are shown in Figures 11a-c. Again, it is assumed that the mass is initially at rest relative to the surface (the cable is sticking). As the surface moves to the right, the spring force increases linearly. At $t = t_1$, $kx = F_f = F_s$ and the mass begins to slide. Displacement and velocity are continuous, but F_f drops abruptly to the kinetic frictional force, F_k, causing a discontinuity in $\ddot{x}$. Throughout the slippage interval F_f remains constant at F_k. As in the previous case, displacement, velocity, and acceleration vary sinusoidally during the slippage interval. At $t = t_2$, the velocity of the mass has again become equal to the velocity of the moving surface. The mass cannot acquire a velocity greater than that of the surface because the resulting reversal of friction force and acceleration would instantly reverse the slope of the velocity curve, and thus the velocity would decrease rather than exceed that of the surface. Consequently the mass sticks to the surface and equilibrium is resumed. A repetition of the cycle begins when the spring force is again high enough to overcome static friction.

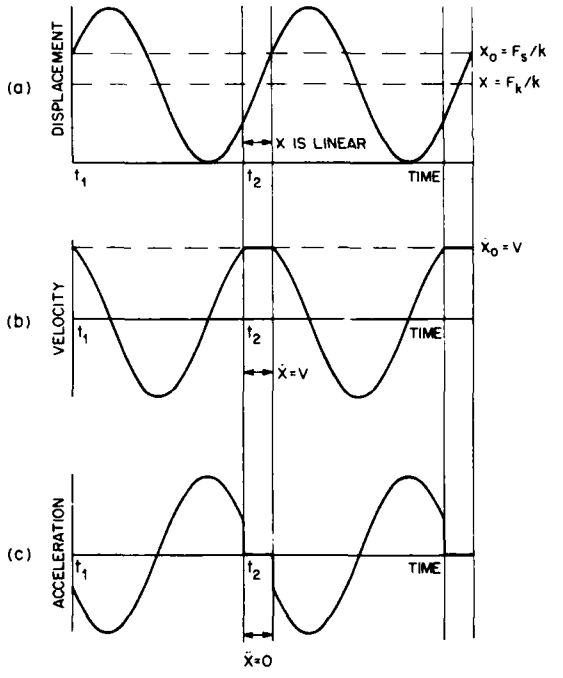


Figure 11. Plots of displacement, velocity, and acceleration for the case $F_s > F_k$.

As previously mentioned, the equations used to determine μ (the *kinetic* friction coefficient corresponding to the friction force F_k in the model) are valid only when the cable is moving. During the "stick" interval, Figure 11a shows that the displacement is symmetric about $x = F_k/k$, and therefore, the spring force kx is symmetric about F_k.

2. Actually, $\dot{x} \leq V$ where equality holds only at isolated instants at the peaks of the sinusoidal motion.

As a result of this symmetric behavior of kx, the *average* value of kx during the stick interval is F_k. Consequently, the average value of μ during the stick interval is an accurate measure of the *kinetic* friction coefficient even though the cable has stopped.

The Effect of Cable Bending Stiffness on Calculated Values of Friction Coefficient

A reel brake was used on the cable reel at the feed manhole to apply a high tail load during the cable pull. Figure 12 is a plot of μ

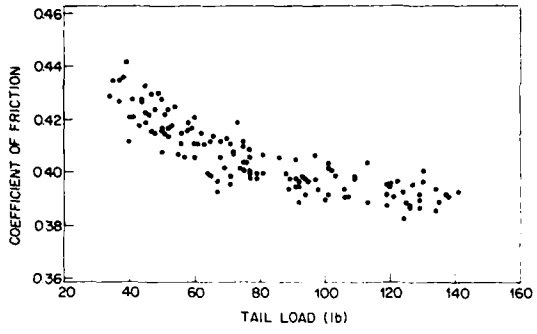


Figure 12. Plot showing the effect of tail load on the calculated values of friction coefficient.

versus T_0 for a cable pull where T_0 was intentionally increased during the pull. As can be seen, μ decreases as T_0 increases. The cause of this trend is not fully understood. Cable bending stiffness, however, can be used to suggest two hypotheses.

Measurement error. During the previous discussion on tension measurement, it was presumed that the cable behaves like a string. This assumption implies that the cable adjacent to the dynamometer sheave is straight as shown in Figure 4, and that the measured reaction in the horizontal strut is equal to cable tension. For a real cable, however, the cable will have a finite curvature that depends both on cable bending stiffness and on cable tension, and this departure from the ideal case will induce some error in the tension measurement scheme.

The direction and magnitude of measurement error depends on the shape of the cable curvature between the two sheaves in the feed manhole (see Figure 2). In the present case, the diameters of the upper and lower cable sheaves are not equal; hence the shape of the cable curvature between the two sheaves is asymmetric and unknown, and the direction and magnitude of measurement error are indeterminate. Cable curvature will be reduced, however, by higher cable tension. Therefore, it is reasonable to expect the calculated value of μ to approach a limit as cable tension (tail load) increases.

This type of measurement error can be avoided if cable curvature is symmetric between the two cable sheaves. For symmetry, the diameters of the two sheaves must be equal, and cable tension must be high enough to keep the cable in conformance with the radius of the sheaves. In this case, free body analysis shows that the measured reaction is equal to the cable tension. In future testing, equal-diameter sheaves should be used.

Duct liner undulations. Experimental studies have shown that duct liners may not lie flat in the main conduit, but may have undulations between the feed and pull manholes.[4] As cable is pulled through the undulating duct liner, it may either conform to the undulations, force the duct liner to lie flat, or some combination thereof. A detailed discussion of these interactions is beyond the scope of this paper. Their effect, however, is to create localized areas of high normal force at the regions of contact between the cable and duct liner. The effect on apparent[3] friction coefficient is expected to diminish at higher cable tension. Therefore, as cable tension (tail load) increases, friction coefficient asymptotically approaches a constant value as shown in Figure 12.

APPLICATIONS

The testing method reported herein can be employed in a multitude of applications of which two of the more obvious are evaluation of cable lubricants and duct liners. Comparisons of various cable lubricants and duct liners can be made to determine the most favorable combination with regard to friction coefficient. In addition, this procedure has also been used to determine the effect of pulling speed on friction coefficient, and the effect of clearance between a cable and duct liner on apparent friction coefficient. For example, Figure 13 shows boxplots[5] that compare the results of three

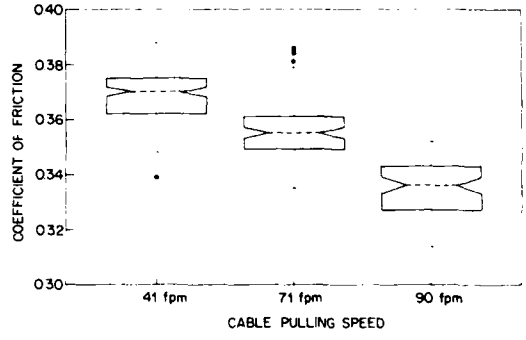


Figure 13. Boxplots comparing experimental values of friction coefficients for three cable pulls at different speeds.

consecutive cable pulls that were identical except for pulling speed. These particular tests were conducted without lubricant using a ¾-inch polyethylene-sheath cable and a 1¼-inch smooth-wall polyethylene duct liner. Reported values of pulling speed are average values determined from the time it took to pull a known length of cable. As can be seen, μ decreases with increasing pulling speed. Note that this effect is significant and it must be accounted for during data analysis, otherwise, it may erroneously be attributed to some other test variable of interest. Therefore, pulling speed should be measured and maintained at a value that is similar to that expected in the intended application.

Figure 14 shows the effect of clearance between a cable and duct liner on friction coefficient. In this test, the ¾-inch polyethylene-sheath cable was installed into 1-, 1¼-, and 1½-inch nominal-diameter smooth-wall polyethylene duct liners. As can be seen, apparent friction coefficient decreases with increasing clearance. As a rule of thumb, cable diameter should not exceed two-thirds of the inside-diameter of the duct liner.

3. The friction coefficient is computed on the basis of measured friction and *nominal* normal-force distributions that do not reflect increases due to the effects of cable bending stiffness, therefore, the term *apparent* friction coefficient is used in conjunction with bending stiffness effects.

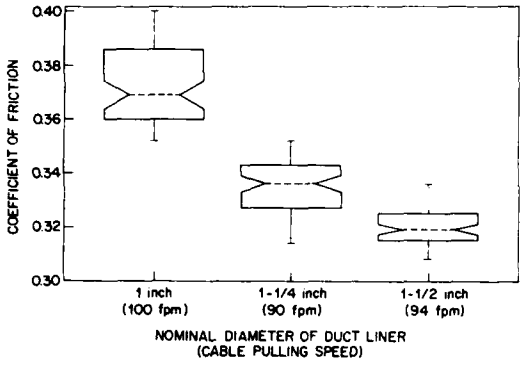


Figure 14. Boxplots showing the effect of clearance on the friction coefficient for a ¾-inch cable and various duct liners.

SUMMARY AND CONCLUSION

A method for the experimental determination of the kinetic friction coefficient between a cable and duct has been presented. Friction coefficients are determined numerically from tension data measured simultaneously in pull and feed manholes during cable pulls in conduit of known geometry. The test procedure provides a means for quantitative comparisons of cable lubricants and duct liners. Because of the nature of the tests, results are directly applicable for prediction of cable installation tension in underground plant. Appropriate selection of cable lubricant and duct liner, along with more accurate predictions of cable installation tensions will help prevent costly installation delays and reduce the potential for cable damage in the field.

ACKNOWLEDGEMENTS

I would like to thank A. L. Hale and D. L. Pope for their discussions and critical review of the manuscript. Also, thanks to L. A. Shallop and L. A. Keggan for their assistance in the final preparation of the manuscript.

REFERENCES

1. R. C. Rifenburg, "Pipe-Line Design for Pipe-Type Feeders", *Trans. AIEE*, December, 1953, pp. 1275-88.
2. A. L. Hale, AT&T Bell Laboratories, personal communication.
3. R. K. Vierck, *Vibration Analysis*, Second Edition (New York: Harper & Row, 1979), p. 162.
4. W. F. Danielczyk, AT&T Bell Laboratories, personal communication.
5. R. McGill, J. W. Tukey, and W. A. Larsen, "Variations of Box Plots", *The American Statistician*, February 1978, Vol. 32, No. 1.



The author received an Associate degree in EET from The Pennsylvania State University in 1978, a BSME from Fairleigh Dickinson University in 1985, and completed the requirements for his MS in Materials and Metallurgical Engineering at Stevens Institute of Technology in 1987. He began work at AT&T Bell Laboratories in 1978 where he is a member of a group that is responsible for cable installation methods.

DEVELOPMENT OF THE PIPE CAMERA FOR TELEPHONE CABLE INSTALLATION AND PIPING MAINTENANCE

M. NAKANO Y. KAJIO H. HINO M. WAKAGI※ T. SHIMIZU※

NIPPON TELEGRAPH AND TELEPHONE CORPORATION
IBARAKI, JAPAN

※THE FURUKAWA ELECTRIC CO., LTD.
TOKYO, JAPAN

ABSTRACT

When the wiring pipe lines for telephone cables which are going to be used for the new construction of networks are quite aged since installed, it is required to do any type of inside inspection before cable installation works.

We succeeded in the development of the camera system which consists of the black/white tube camera with optical fiber signal transmission lines in the form of rigid rod coil from the head of the controller to realize the longer video signal transmission and easier insertion of the camera head deeply into the small sized long pipe line.

The newly developed color camera system covering 50m long is also reported.

REQUIREMENTS

When the wiring pipe lines for telephone cables are installed under the ground particularly in the city area, it is very common that the more lines than required at that moment are installed and then will be used afterwords when necessary for the network expansion.

The demand for development of any proper tool to realize the inside inspection of such long pipes as 250m between manholes and to reduce the installation cost of the new cable by shortening the working time had been very strong in Japan.

The requirements for the pipe camera system for such uses are the followings :

- The high resolution for good cognition of the inside surface condition of the pipes
- The smaller head diameter less than 45mm for the small sized pipes such as 80mm dia.
- The 150m reach of camera head at shortest
- Easier insertion and manipulation

DEVELOPMENT OF PIPE CAMERA

The camera type, the transmission signal line and the structure of camera cable were studied to meet the requirements as mentioned above.

The black/white tube camera with high resolution of 600 TV lines was chosen among three types of camera.

The tested cameras and their capability checked for inside condition of pipes by means of the camera view are as follows.

◇ Types of cameras tested

a Black/white tube camera with resolution of 600 TV lines

b Black/white CCD camera with high resolution of 240 TV lines

c Color tube camera with resolution of 240 TV lines

◇ Check points of inside surface of pipes

- breakage
- out of joint
- irregularity
- bending

- sharp bending
- foreign material
- corrosion
- through hole
- crack

The optical fibers and O/E & E/O links for video signal transmission between the camera head and its controller located at the manipulation site were used, which made it possible to realize the high resolutional image transmission for the distance of longer than 180m.

The special structure of cable with FRP claddings and PE sheath which enables to be inserted into the long distance inside the pipe was newly developed (see Fig.1) and tested for the pipe of several materials actually in the field. (see Fig.2)

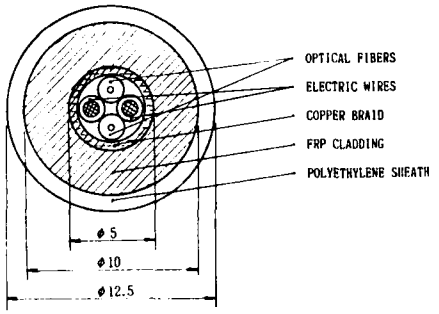


Fig.1 Cross-sectional structure of camera cable

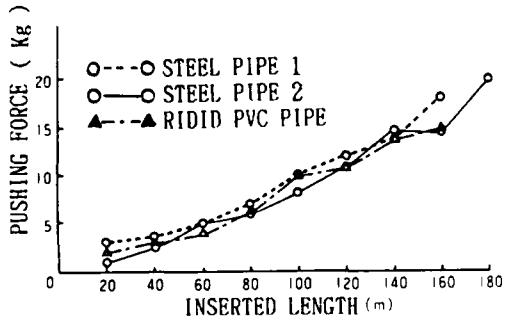


Fig.2 Force for pushing the cable obtained by field test

In addition to the black/white camera system described so far, the color CCD camera system for 50m long inspection which can be used for such a small piping as 50mm dia. with one point of 90° elbow bending was developed, being devised for the good RGB signal transmission and the camera head structure.

The total inspection system for pipe lines actually used in the field is also equipped with the high-pressurized water jet system developed for cleaning the foreign material out of the pipes.

Conclusion

The specification of two types of camera system developed for telephone pipe inspection is described on the table 1.

The systems have been frequently used for recent expansion works of network construction in Japan and highly evaluated by contractors for their effects.

The systems can be applicable for inspection of pipe lines for other utilities such as steams, gas, electrical power line and sewage.

Table 1. The specification of two types of camera system

I T E M	BLACK/WHITE TUBE CAMERA	COLOR CCD CAMERA
CAMERA HEAD · Type · Dimensions · Resolution · Viewing angle	 Black/White tube camera 45mm dia. and 500mm length 600 TV lines 70 degrees	 Color CCD camera 34mm dia. and 520mm length 240 TV lines 70 degrees
CABLE · Signal transmittion · Dimensions	 Optical fiber with analog O/E & E/O links Diameter:12.5mm Length :190m Weight :230kg/km	 Coaxial cable Diameter:19.0mm Length : 50m Weight :392kg/km
CONTROLLER · TV-Monitor · VTR · Video Typewriter	 12 inch-Black/White TV-Monitor β or VHS Method Characters are superimposed on the picture	 9 inch-Color TV-Monitor β or VHS Method Characters are superimposed on the picture



*

MASAHIRO NAKANO joined Nippon Telegraph and Telephone Corporation, Japan in 1972.
He was ago engaged in development on inspecting and repairing technologies for underground conduit and is now engaged in development on seismic measures for outside facilities.



*

YUGO KAJIO joined Nippon Telegraph and Telephone Corporation, Japan in 1975.
He is now engaged in development on inspecting and repairing technologies for conduit under the ground and installed on a bridge.



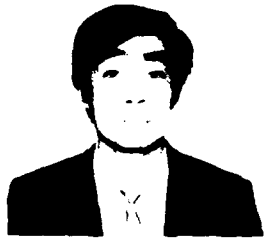
*

HIDENORI HINO joined Nippon Telegraph and Telephone Corporation, Japan in 1980.
He was ago engaged in development on inspecting and repairing technologies for underground conduit and is now engaged in development on maintenance system for outside facilities.



**

MASAAKI WAKAGI joined the ministry of P&T, Japan in 1948 and transfered to The Furukawa Electric Co.,Ltd., Tokyo, Japan in 1969.
He has been engaged in sale's engineering servic of telecommunication cable and devices.



**

TAKEO SHIMIZU joined The Furukawa Electric Co.,Ltd., Tokyo, Japan in 1981.
He has been engaged in developing fiber optical devices.

* : NTT Tukuba Engineering Center, Nippon Telegraph and Telephone Corporation, 1-7-1, Hanabatake, Oho-machi, Tsukuba-gun, Ibaraki, Japan

** : The Furukawa Electric Co., Ltd., Fiber Optics & Telecommunications division, 5-1-9, Higashiyawata, Hiratsuka, 254, Japan

Fiber/Metallic Distribution Plant Concept

F. J. Mullin
W. C. Reed
AT&T Bell Laboratories
2000 Northeast Expressway
Norcross, Georgia 30071

C. Scholly
AT&T Technologies
2000 Northeast Expressway
Norcross, Georgia 30071

Abstract

The Fiber/Metallic Concept (FMC) for design of local buried distribution plant is a fiber complementary alternative to the Serving Area Concept. By this concept, a group of customer service cables are linked to a distribution cable at a group termination point thereby avoiding buried splices and cut-dead ahead media.

The Fiber Ready Plant employs an FMC architecture to be positioned to expand its capabilities with fiber in a few years. Fiber is placed as part of the new Fiber/Metallic Distribution Service Cable, but initial service is provided over copper. This architecture permits major fiber costs to be deferred while the fiber plant is extended and prepares for a graceful transition from copper to fiber service.

The concept may be advantageously applied to a fiber-only distribution plant. Array splicing may be used as a cost effective means of splicing the grouped service cables to distribution cables. Since any combination of a service cable fiber and a distribution cable fiber is a path to a customer, the fibers may be randomly spliced and the customer may then be identified by an automatic number identifier at the home.

Introduction

A local distribution plant or loop plant connects each telephone customer to a central office. In a typical loop plant, feeder networks fan out from an office into serving areas of 200-900 homes. A network of distribution cables distributes telephone services in a serving area. Each customer premise is connected to the nearest distribution cable through a service cable.

The loop plant for copper has evolved to provide conductor pairs to meet customer demands for service (See Appendix A). The demands progressed from party line to private line to enhanced services in a relatively short time. Older generations of plant were churned to meet each new generation of demands causing assignment problems and high maintenance and operating costs. Churning related troubles were eliminated by the Serving Area Concept (SAC) type plant which interfaces a stable feeder network with a stable distribution network through an assignment flexibility point, the Serving Area Interface (SAI).

Need For A New Concept

The design of local fiber distribution plant will be more strongly influenced by construction and maintenance costs than by customer demand for service. The wideband capability of one or two single-mode fibers permanently assigned to each subscriber will permit service upgrades to be done electronically without disturbing the plant.

Unfortunately, an all-fiber loop plant awaits the arrival of the fiber network and the general availability of end point electronics. Fiber can only be deployed today if initial service is provided over copper pairs. Nevertheless, deployment must start now to position fiber for forthcoming wideband services, to avoid the high costs of overlaying fiber on existing copper plant in established neighborhoods and to prevent delays awaiting recovery of copper plant investment.

The Serving Area Concept is a strong candidate for the design of the local fiber distribution plant. It has been successfully employed for many years for copper plant and recently for fiber plant in a few showcase communities.

However, the Serving Area Concept does impose some cost penalties. It obviously includes a number of splice points, each of which entails substantial labor and material costs for fiber splicing and which historically have been trouble

points. Also, as the distribution network branches downward in fiber count, fibers are cut-dead ahead of many of these splice points causing about a third of the fiber footage to be unused.

An alternate concept is required to avoid the SAC cost penalties, to encourage early placement of fiber to the home with initial service over copper pairs, and to design all fiber plant.

Fiber/Metallic Concept

The Fiber/Metallic Concept (FMC) is now proposed for local buried distribution plant (See Figure 1). The concept may be applied to serving areas which typically have 200-900 homes (same as SAC) served through a centrally located remote terminal (RT) or serving area interface (SAI). Along a centerline or backbone of the area are placed distribution cables to connect the RT/SAI to group termination cabinets (GTCs). Each GTC serves a cluster of homes in residential blocks or along a street. A Network Interface Unit (NIU) for each home connects to its respective GTC through a separate distribution service cable placed in a common trench with other distribution service cables along a front lot or rear lot easement. Except for plant architecture, implementation follows operating companies' engineering, assignment, construction and maintenance procedures.

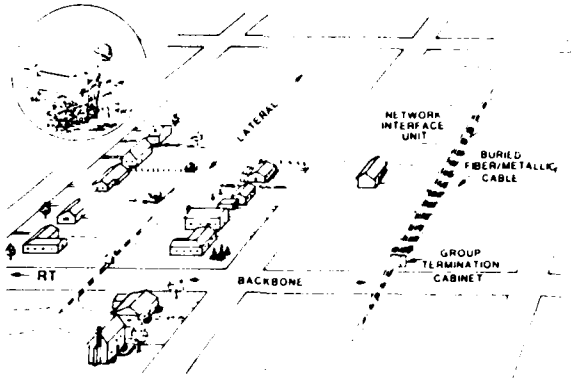


FIGURE 1. PERSPECTIVE VIEW OF A FMC FIBER READY PLANT

The concept may be used to design copper-only, copper/fiber or fiber-only buried distribution plant and hence is named the Fiber/Metallic Concept. It is not applicable to aerial plant because of the undesirable aesthetics of grouping multiple aerial cables in a GTC. It is advantageous to the introduction of fiber into the copper plant of today and to the design of the all fiber plant of the future.

FMC For Fiber Ready Plant

Description

A FMC plant that is ready to expand its capabilities with fiber is a Fiber Ready Plant (See Figure 1). Each customer is served by the new Fiber/Metallic Distribution Service Cable[1] that combines fibers with twisted pairs in a single package. Initial service is over the copper pairs while future wideband services over fiber awaits the arrival of the fiber network and the general availability of associated hardware and electronics.

The copper circuits of Fiber Ready Plant are completed between the RT/SAI and the NIU of each home during initial construction. Pair assignments are made at the RT/SAI by cross connection of a traditional copper distribution cable serving a GTC to a traditional copper feeder cable. The distribution cable pairs are connected to the composite distribution service cable pairs on binding posts in the GTC which permit maintenance access only since assignments are made at the RT/SAI. Each service cable pair terminates on a NIU protector.

The fiber circuits of Fiber Ready Plant are not completed until fiber service is activated. Fiber to each home is positioned as a component of a composite distribution service cable and the fiber ends are stored in trays in the NIU of the home and the GTC. A conduit is placed between the RT/SAI and each GTC to allow conventional fiber optic distribution cable to be placed and connected at a later date. This allows fiber cable, connector, and splicing costs to be deferred until required for fiber service. To facilitate completion of the fiber circuit, the GTC is an above-ground cabinet.

Installed First Cost Comparisons

Installed first costs for local buried distribution plant are a function of a large number of variables which include design concept, material and labor costs, local operating company practices, plant topography, soil conditions and plant designer preferences. To obtain an indication of the cost advantage of one plant over another, a simple distribution plant model was employed (See Appendix B).

Installed first cost comparisons were made of Fiber Ready Plant to SAC type plant with copper-only, copper buried jointly with fiber during initial construction, and fiber overlaid on previously installed copper. To minimize variables all metallic circuits to customer premises consist of five copper pairs (5 P) and all fiber circuits consist of one single mode

fiber (1 F). The results are presented in Table A as average relative costs referenced to copper plant for front lot and rear lot feeds.

TABLE A. Average Installed First Cost Comparisons (Front Lot and Rear Lot Feed)*

Type	Plant	Relative Cost
SAC	Copper (5 P)	1.0
SAC	Fiber (1 F) joint with Copper (5 P).	2.1
SAC	Fiber (1 F) overlay on Copper (5 P), best case.	2.7
FMC	Fiber Ready (1 F and 5 P), fiber costs deferred.	1.4
FMC	Fiber Ready (1 F and 5 P), fiber connected.	1.9

*NOTE: The actual cost for rear lot feed is about 80% the actual cost for front lot feed.

These tabulated results clearly indicate that fiber cannot be economically positioned in the local distribution plant by jointly burying copper and fiber SAC distribution networks or overlaying a copper network with a fiber network at a later date. Indeed, the overlay results assume the best conditions where the original copper plant is not damaged during overlay construction and none of the obstacles to direct burial of plant, usually found in established neighborhoods, are encountered.

The results show that Fiber Ready Plant is a promising vehicle for positioning fiber to customer premises. In addition, the copper pair count to each home for Fiber Ready Plant can be reduced to the lowest practical count without significantly affecting the ultimate capabilities of the Plant thus effecting further savings. Table B tabulates the effect of pair count on relative costs for front lot feed and rear lot feed, respectively.

Table B. Average Installed First Cost Comparisons (Front and Rear Lot Feed)* vs. Fiber Ready Pair Count

Type	Plant	Relative Cost
SAC	Copper (5 P)	1.0
FMC	Fiber Ready (1 F and 5 P) fiber costs deferred.	1.4
FMC	Fiber Ready (1 F and 2 P),fiber costs deferred.	1.2
FMC	Fiber Ready (1 F and 5 P), fiber connected.	1.9
FMC	Fiber Ready (1 F and 2 P), fiber connected.	1.6

*NOTE: The actual cost for rear lot feed is about 80% the actual cost for fron tlot feed.

Operating Company Concerns With Fiber Ready Plant

Operating company personnel have expressed concerns over the placement of the bundle of distribution service cables in a common trench, the susceptibility of the bundled cables to damage and the restoration of damaged distribution service cables.

The distribution service cables may be individually placed in an open common trench with each end tagged for identification. However, a factory prepared distribution service harness promises to be a cost effective means of placing these cables and will further lower the costs for Fiber Ready Plant.

The bundled cables are susceptible to digup damage like all buried structures. However, the bundled portion is placed along an engineered utility easement which lowers the possibility of damage. Historically, most digup damage occurs in the cable run from the property line to the house. The bundle has the additional advantages that it does not look like a root and is more difficult to cut than a single large cable. When damage does occur, some but probably not all, the cables will be affected.

Restoration of a damaged distribution

cable is accomplished with a buried repair closure which accommodates both copper and fiber splices. If a number of cables are cut, the segments are identified and tagged using existing copper plant test sets and identification methods. The pairs and fiber(s) of each segment are then spliced according to their respective color codes.

FMC For Fiber-Only Plant

Description

The Fiber/Metallic Concept may be applied to the fiber-only distribution plant of the near future. Since fiber is the only media serving each home, service over fiber must be activated initially. The media needs of a home can be served by one single mode fiber, but a second fiber may be required to accommodate the end point electronics or by the operating company as a spare.

Installed First Cost Comparison

An installed first cost comparison was made of FMC type fiber-only distribution plant against SAC type plant. The FMC type plant employed GTC's housing individual fiber splices. The SAC type plant was also built with individual fiber splices. The results are presented as relative costs referenced to SAC type plant in Table C for both front and rear lot feeds.

Table C. Average Installed First Cost Comparisons (Front and Rear Lot Feed)*

Type	Plant	Relative Cost
SAC	Fiber (1 F)	1.0
FMC	Fiber (1 F)	0.9

*Note: The actual cost for rear lot feed is about 80% the actual cost for front lot feed.

Further Advantages

A fiber-only FMC type plant has additional advantages which result from the small numbers of fiber required to each home and the need to activate the fiber circuits initially. The fibers from each home may be grouped in array connectors at the GTC and array spliced to the fiber backbone distribution cables. The GTC may be a below ground closure housed in a hand hole to permit access for maintenance.

Fiber systems of the future will probably require an automatic number identifier (ANI) capability at each home for customer identification to facilitate services which include billing, banking, meter reading, and mailing. These ANI's will probably be sensed and identified by electronics in the RT and the information relayed to data collection centers.

The combination of ANIs and FMC plant could eliminate the need for fiber identification for construction or maintenance splicing. Any fiber coming from the home could be randomly spliced to any fiber going to the RT and be properly served if the RT switching function was directed to find and memorize the position of each ANI.

Summary

The Fiber/Metallic Concept (FMC) has been presented for local buried distribution plant employing fiber or copper/fiber media. By this concept, groups of living units are linked to distribution cables at a group termination thereby avoiding buried splices and "cut dead ahead" fiber or copper.

Incorporation of the new composite cable in a FMC Fiber Ready Plant encourages early placement of fiber to customer premises. It provides initial service over copper and permits major fiber costs to be deferred while new technology is developed and fiber plant extended.

The FMC fiber-only plant of the future may be constructed with array connectors. Fibers may be randomly spliced in the connectors if remote terminal switching can be directed to seek an automatic number identifier at each customer premises.

Reference

1. E. R. Campbell, F. J. Mullin and W. C. Reed, "Fiber/Metallic Service and Distribution Media," 36th International Wire and Cable Proceedings, November 1987.

APPENDIX A. EVOLUTION OF LOCAL COPPER DISTRIBUTION PLANT

A. Multiple Fixed Count Concept

The multiple fixed count concept was formulated to employ pulp insulated, lead sheathed cable in the local distribution plant and to meet customer demand for service. The cable was lashed to steel support strands suspended between poles. Splices were made by twisting and sleeving mating conductors and were enclosed in wiped lead sleeves. Cable pairs were available for service at binding posts housed in pole-mounted cable terminals served through a lead sheathed cable stub which was spliced to selected cable pairs. Cable pairs appeared at several locations to provide both private and party line service. This type plant met the needs of the nation through the late 1950's when 1/2 the U.S. households had private lines, 1/4 had party lines and 1/4 had no service at all.

B. Ready Access Concept

The Ready Access Concept followed in the early 1960's to employ polyethylene insulated, aluminum/polyethylene sheathed cable and to meet the increased demand for telephone service. Cables were lashed or self-supported in aerial plant or buried directly. Splices were made with individual conductor connectors and were protected in plastic or metal closures. All cable pairs were exposed and available for assignment in pole mounted terminals or above ground pedestals.

This type plant was easy to build and assign initial service. However, the increasing demands for telephone service, the inward/outward movement of service and the ease in changing pair assignments led to a cable pair administration problem. This in turn greatly increased operating and maintenance costs.

C. Dedicated Outside Plant Concept

The dedicated outside plant concept was intended to avoid the assignment problems of ready access plant by dedicating a cable pair from the central office to each living unit. The cable pair was assigned and never disconnected except by heat coil or protector removal at the central office main frame. The assignments were recorded in ink instead of pencil as used earlier.

The almost complete lack of flexibility in cable pair movement became a problem in meeting a growing and changing demand for second line services. Craftpersons were forced to take trouble causing steps to move cable pairs to provide this service.

D. Serving Area Concept

The serving area concept (SAC) is presently used to design copper residential distribution plant. An area defined by natural boundaries is served through one flexibility point, known as the serving area interface (SAI), to provide at least two copper pairs to each customer living unit.

In a typical SAC plant, feeder cable pairs from the central office (CO) terminate at the SAI. From there, distribution backbone or subfeeder cables are extended along an area centerline or backbone to connect front or rear lot distribution lateral cables extending toward customers premises. The backbone cables step downward in size away from the SAI to minimize waste due to cut-dead ahead pairs. Once a backbone pair is cut and spliced to a lateral pair, the remainder of that backbone pair to the end of the cable ahead of the splice point is unused. Also, in each lateral the pairs beyond successive service cable splice points are unused. The service splice points are protected in a buried splice closure or above-ground pedestals.

Generally 1.2 to 1.5 feeder pairs from the CO are terminated in the SAI to serve the 2 dedicated pairs to each living unit thus minimizing feeder plant investment. First line services are established and never disconnected. Second lines are connected to designated feeder pairs as subscribers demands change. Changes of residences generate a great deal of second line activity since one in five households in the U.S. moves each year.

APPENDIX B. First Cost Comparison - SAC vs FMC

A. Distribution Plant Model

A simple distribution plant model was developed to compare installed first costs of FMC plant against SAC plant from the RT or SAI connections to the customer NIU. It permits examination of copper-only, fiber-only, joint copper and fiber (copper and fiber cable in a common trench) or composite copper/fiber plant (copper pairs and fiber in a common cable).

The model serving area resembles a region of middle to high income family homes and consists of 600 living units on 200' x 200' lots along streets with 60' right-of-ways and 28' wide pavement. The lots are arranged in 20 lot blocks. The serving RT or SAI is centered in the area.

The various plans to be examined fall into two categories, the traditional SAC type (see Figure B1) and the new FMC type (see Figure B2). Both types may be imple-

mented as either front lot (FL) or rear lot (RL) feed as shown in the figures.

To facilitate comparison of installed first cost and features, the number of variables between various plans is minimized. All metallic circuits to subscriber premises consist of five copper pairs and all fiber consist of one single mode fiber. All fiber and connections are made with rotary connectors. All copper and fiber circuits entering a customer service closure, group termination cabinet, SAI or RT are terminated except for the instance where installation of fiber cable and connection of fiber is delayed to defer costs. All lightguide cables are Lightpack® cables. All splices are buried.

B. Material and Labor Cost Items

The material and labor cost items include prices, contractor charges and operating company labor costs. Together they yield the installed first cost to the operating company for installing a particular type of distribution plant. The items and their associated unit costs are explained below.

- Trenching and Placing One Sheath FMC.SAC)- Contractor charges for service trenches (typically 4" wide x 24" deep), lateral and backbone trenches (typically 6" to 8" wide x 36" deep), and the placement of one sheath, e.g., one cable, in each trench.

- Splice Pits (SAC)- Contractor changes for digging and filling in splice pits for service closures (typically 2' x 4' x 3' deep) and backbone closures (typically 4' x 4' x 3' deep).

- Copper (SAC) - Prices for nongopher service wire (0.100 μF/mi) and ASP type distribution cable for laterals and backbone; contractor charges for placing additional cable in a trench containing one cable; labor and material costs for service termination splices (2 service wire/splice for FL or 4 service wires/spice for RL) and backbone splices (4 laterals/ splice) including connectors and closures; and labor costs for terminating the distribution cables in the SAI and the service wires in the customer service closure to a protector or network interface unit.

- Fiber Only (SAC) - Prices for buried fiber service cable and Lightpack® lateral and backbone cables; contractor charges for placing additional cables in a trench containing one cable; labor and material costs for service termination splices (2 fiber service cables/splice for FL and 4 fiber service cables/splice for RL) and backbone splices (4 laterals/ splice) including rotary connectors and closures; and material and labor costs for terminating the distribution cables in the RT and the fiber service cable in customer network interface units with rotary connectors.

- Copper Joint With Fiber (SAC) - Costs for placing additional sheath resulting from the joint burial of the fiber network with the copper network.

- Fiber Only (FMC) - Prices for buried fiber service cable and Lightpack® backbone cable; contractor charges for placing additional sheath; estimated installed cost for group termination cabinet and material and labor costs for terminating fiber in the RT, group termination cabinets, and customer network interface units.

- Fiber Ready (FMC) - Prices for nongopher, composite distribution service cable, ASP copper distribution cable and Lightpack® cable; contractor charges for placing additional sheath; estimated installed cost for group termination cabinet; and labor and material costs for terminating copper and fiber in the RT/SAI, group termination cabinets and customer network interface units using rotary connectors.

- Fiber Ready (FMC), Deferred Cost Items - Material and labor charges for installing 1" conduit to permit later installation of backbone fiber cable; price for Lightpack® backbone cable (deferred); and material labor costs for terminating the fiber in the RT, group termination cabinets, and customer network interface units using rotary connectors (all deferred).

®Registered trademark of AT&T

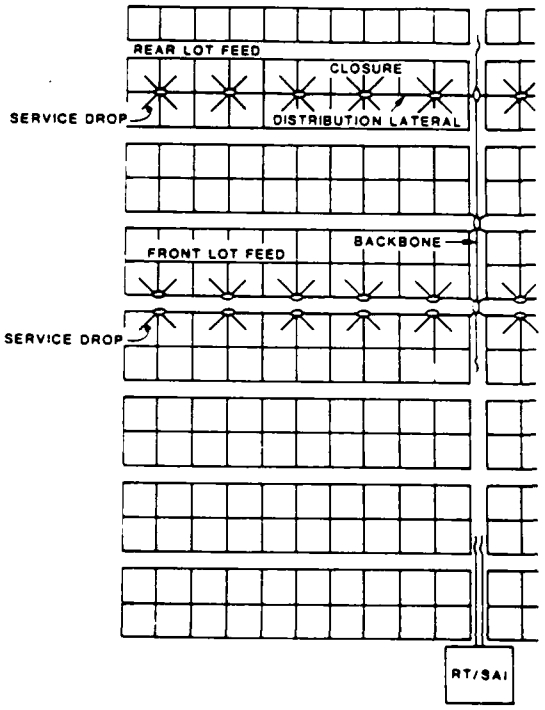


FIGURE B1. SAC DISTRIBUTION PLAN

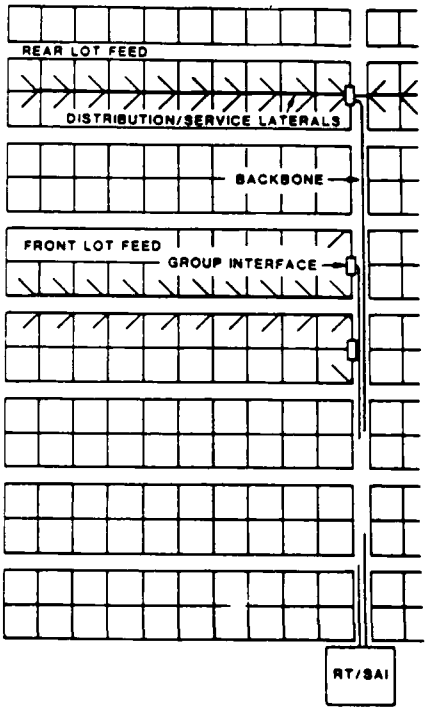


FIGURE B2. FMC DISTRIBUTION PLAN



F. J. Mullin is a member of the Transmission Media Laboratory, AT&T Bell Laboratories, Norcross, Georgia. He attended John Hopkins University and joined AT&T Bell Laboratories in 1955. During this time he has worked in the outside plant area developing mainframe protection; aerial, buried and building cable terminals, closures and connectors; color coded key closets; Buried Waterproof System; SAI concept and customer trouble report reduction. His present responsibilities include outside plant, copper and fiber transmission media.



William C. Reed is a member of the Transmission Media Laboratory, AT&T Bell Laboratories, Norcross Georgia. He received a BA in mathematics and physics from Wittenberg University in 1959 and an MA in physics from Wake Forest University in 1969. He joined AT&T Bell Laboratories in 1970 and has worked on the design and development of military power equipment, maintenance test sets and test methods, copper and fiber splicing equipment, buried wire, and encapsulated closures. His present responsibilities include outside plant, copper and fiber transmission media.



Christian Scholly is an Engineering Manager at the Atlanta Works, supervising Development Engineering for Lightguide Connectorization and Measurement. Born and raised in The Netherlands, Mr. Scholly attended engineering school in West Germany where he received the equivalent of a Bachelor of Science Degree in mechanical engineering at Aachen (West Germany) in 1953. Subsequently, he had the responsibility for cathode ray tube development at NV Phillips Eindhoven. Mr. Scholly joined Western Electric at the Baltimore Works in 1956, joined Bell Laboratories at Baltimore in 1961 and returned to Western Electric in 1969 at the Product Engineering Control Center for Wire and Cable at Cockeysville, Maryland, where he was assigned to development engineering for loop transmission apparatus. In 1978, Mr. Scholly formed an organization to develop manufacturing methods and techniques for Lightguide Connectors, Distribution and Terminating Apparatus and Attenuators. He has been involved in analyzing the application of the above components and assemblies in local area networks utilizing both copper and lightguide technologies. He holds six patents.

METHODS OF DIFFERENTIATING AMONG PTFE FINE POWDER RESINS

John Bednarczyk and Pankaj Mehta

E.I. du Pont de Nemours & Co. (Inc.)

Summary

Wire insulated with polytetrafluoroethylene (PTFE) resins are used in aerospace, computer, military and industrial electronics and other demanding applications. PTFE resins are well suited for these applications due to their unique balance of electrical, thermal and chemical properties. However, distinct differences among PTFE resins do affect processing characteristics and end-use performance. In some cases for example, PTFE insulation has cracked during service due to improper manufacturing conditions or improper resin selection. The combination of processing technique and resin properties will ultimately determine the quality of the finished wire insulation. This presentation will discuss the various methods available to differentiate among PTFE resins. Two new methods, which directly relate to the stress-crack performance of the material, are presented. In addition, these tests allow for improved sensitivity over current methods. These new methods can improve the resin selection criteria to meet demanding end-use requirements.

Discussion

Today, many types of PTFE resins are available. A number of physical and electrical properties of PTFE resins are generally similar. These properties include outstanding chemical resistance, high-temperature resistance, low-flame and low-smoke properties, excellent dielectric properties, outstanding resistance to weather, anti-stick characteristics and high purity. However, there are distinct differences among the resins that will affect their processing and end-use performance characteristics. The remainder of this paper will focus on resin selection criteria to optimize both processing and performance.

Methods of Differentiation

There are several ways to differentiate among PTFE fine powder resins. ASTM D 1457-83 is an excellent reference on this subject. This specification covers six types of PTFE resins generally used for compression molding ram extrusion or paste extrusion with a volatile processing aid. The following discussion is about resins described as Type III in ASTM D 1457-83.

Type III resins are divided into four grades by characteristics such as: average particle size, melting peak temperature, extrusion pressure, standard specific gravity (SSG), tensile strength and elongation. Additional procedures are provided in the appendix of ASTM D 1457-83 for further characterization of the resins. These methods include: dimensional changes during molding (shrinkage and growth); size and distribution of size of particles or agglomerates; yield behavior and tangent modulus at rupture; heats of fusion and crystallization; electrical properties; and tensile creep.[1]

Each grade is further divided into three classes to indicate performance in the test for extrusion pressure. The extrusion pressure ranges are listed in Table I.

Table I

Class	Extrusion Pressure (psi)	Reduction Ratio*
A	1,410 ±610	100:1
B	3,500 ±1,500	400:1
C	8,000 ±3,000	1,600:1

*Reduction ratio is the ratio of the cross-sectional area of the preform to the cross-sectional area of the die.

Choosing the proper PTFE resin is an important consideration for manufacturers of insulated wire. This choice is governed by the available processing equipment, the wire construction to be produced and the specific end-use requirements. The resin with the optimum balance of properties will provide the wire processor with efficiency of operation while maintaining the highest quality insulated wire.

It has been shown that processing efficiencies can be derived from resins that exhibit better lube acceptance, broader reduction-ratio capabilities, lower extrusion pressure at high reduction ratio, narrower extrusion pressure ranges and/or faster sintering capabilities. Resins with better lubricant acceptance will require less aging time before processing. Broader reduction ratio capabilities will allow the use of a resin in a wider variety of wire constructions. Resins with lower extrusion pressures at high-reduction ratios may allow the use of larger diameter extrusion barrels, which will yield longer runs and reduced scrap. Resins that sinter faster will allow higher line speeds with a given setup for improved productivity. These can result in reduced fine powder inventory requirements.

Along with processing efficiencies, a PTFE resin must also provide a finished insulation that meets the end-use performance criteria. Resin properties already identified as being important to end-use characteristics, such as resistance to cracking, include molecular weight, crystallinity and thermal stability. Crystallinity and thermal stability can be measured using test methods specified in ASTM D 1457-83.

Standard specific gravity is a measure of resin crystallinity. ASTM D 1457-83 separates Type III resins into four different grades with varying ranges for SSG. Grades and SSG ranges are listed in Table II.

Table II

Grade	Specific Gravity
1	2.19 - 2.24
2	2.14 - 2.20
3	2.17 - 2.23
4	2.14 - 2.23

The results of MIT flex testing illustrate the dramatic relationship of SSG to mechanical properties. This test measures the folding endurance of a 5-mil film sample.[2] The commercial resins available for wire and cable span a wide range in crystallinity (SSG 2.14 to 2.24). The low end of this range would have a flex life two orders of magnitude greater than the high end.

Thermal instability index (TII) is a measure of molecular weight stability at elevated temperatures. A resin with higher TII will show a higher degree of molecular weight degradation at elevated temperatures. The decrease in molecular weight is reflected by an increase in crystallinity. TII measures this change in resin crystallinity due to thermal exposure.

The TII test procedure is described in ASTM D 1457. SSG and Extended Specific Gravity (ESG) must be determined. ESG specimens are sintered similar to SSG specimens except that the hold time at 380°C is 360 minutes versus 30 minutes for SSG specimens. The thermal instability index is calculated as follows:

TII = (ESG - SSG) x 1000

TII is not used to differentiate among PTFE resins in the present ASTM specification. ASTM D 1457-83 specifies a maximum TII of 50 for all PTFE fine powders. A number of PTFE resins have a TII that is much lower than 50. These resins are more thermally stable. This stability can provide an important benefit for the wire manufacturer and end user alike. Often, PTFE insulated wire will encounter additional thermal exposure during secondary manufacturing operations, such as printing and stripping. Resin with a lower TII (higher thermal stability) will experience less molecular weight degradation due to the additional heat history. This will provide a wire insulation that maintains a higher level of integrity.

The new fine powder specification, which will replace ASTM D 1457-83, contains proposals for new classes and grades submitted by resin manufacturers that list TII maxima of 15 to 50. This change will enhance resin differentiation through the use of TII.

New Methods of Differentiation

Improved understanding of polymer fracture mechanics has provided additional techniques to differentiate further among PTFE fine powder resins. The Crack Susceptibility Index (CSI) technique was

presented in a technical paper to the 35th International Wire and Cable Symposium. CSI measures the tendency of a PTFE resin to form voids when stressed in tension. Void formation has been suggested as a mechanism in the stress cracking of different polymers.[3,4,5,6,7,8,9,10] Based on this mechanism, there are two stages to crack formation: initiation and propagation. Once a critical crack size has formed, propagation is very rapid. Therefore, the crack formation time is controlled by crack initiation. One of the factors affecting crack initiation is the tendency of a resin to form voids. Mechanical stresses over a long period of time can result in voids in some polymers and these voids can eventually lead to cracks.

The CSI technique was described in the technical paper entitled "PTFE Resin Selection for High Performance Wire and Cable."[11] By stretching test specimens at high strain rates, microvoids are nucleated throughout the specimen. Specimens of compression molded resin are stretched to break on a tensile testing machine. The change in specific gravity between the unstrained and the strained specimen is a measure of the void formation in the resin. Percent voids is calculated as follows:

$$\% \text{ Voids} = \frac{(\text{unstrained SG} - \text{strained SG})}{\text{unstrained SG} \times 100}$$

The difference between unstrained and strained specific gravity is multiplied by 1000, as in the TII test, to yield a measure we termed the Crack Susceptibility Index (CSI). The equation is as follows:

$$\text{CSI} = (\text{unstrained SG} - \text{strained SG}) \times 1000$$

Increasing CSI denotes an increased tendency for void formation.

CSI has been renamed Stretching Void Index (SVI) by the ASTM subcommittee that is responsible for revising ASTM D 1457-83 to better reflect what is actually being measured in the test. Additional resin classifications have been submitted with maximum SVI levels to improve further resin differentiation in the new PTFE fine powder specification that will replace ASTM D 1457-83.

The SVI test offers a much wider scale for comparing different PTFE resins than SSG or TII techniques. The SSG range (2.13 to 2.24) covered by ASTM D 1457-83 is only 110 units (Specific Gravity Units x 1000) wide. The TII scale presently has an upper limit of 50 for all classifications. SVI offers a scale of more than 400 units. The Stretching Void Index was measured for a number of PTFE fine powder resins to illustrate the broad scale of differentiation offered by this test. Twelve resins made by five different manufacturers were compared. All of these resins were Type III as defined by ASTM D 1457-83. The specific gravity (SG), SG at break, SVI and percent voids are listed in Table III.

Table III

Resin	SG	SG at Break	SVI	% Voids
A	2.151	2.140	11	0.5
B	2.148	2.079	69	3.2
C	2.168	2.087	81	3.7
D	2.178	2.072	106	4.9
E	2.184	2.064	120	5.5
F	2.178	2.031	147	6.7
G	2.163	1.957	205	9.5
H	2.158	1.952	206	9.5
I	2.182	1.947	235	10.8
J	2.177	1.921	256	11.8
K	2.194	1.923	271	12.3
L	2.200	1.808	393	17.8

Additional refinements to the SVI test were explored to further improve its ability to differentiate among PTFE fine powders. The original SVI test only included a mechanical stress component to differentiate among resins. To combine thermal stability and mechnical stress, the SVI test was performed in combination with the TII test. We have called this new technique the Thermal Stretching Void Index (TSVI) test. It was found that TSVI offers an even larger scale for comparison of PTFE fine powder resins.

Specimens for SVI measurement are sintered using an SSG temperature cycle described in ASTM D 1457-83. The hold time in the SSG cycle is 30 minutes at 380°C. By using the longer TII temperature cycle (hold time of 360 minutes at 380°C), the thermal stress on the TSVI test specimens is significantly increased.

TSVI specimens are stretched to break on a tensile testing machine as in the original SVI test. The change in specific gravity between the unstrained and the

strained specimen is a measure of the void formation in the resin. Percent voids is calculated as in the SVI test. The equation is listed below:

$$\% \text{ Voids} = \frac{(\text{unstrained SG} - \text{strained SG})}{\text{unstrained SG} \times 100}$$

The difference between unstrained and strained specific gravity is multiplied by 1000, as in the TII and SVI tests, to yield the measure we termed the Thermal Stretching Void Index (TSVI). The equation is as follows:

TSVI* = (unstrained SG - strained SG) x 1000

* Specimens are prepared using the TII temperature cycle. The test procedure is listed in the Appendix.

The TSVI of specimens prepared in this manner is considerably higher than the SVI. The range of values obtained by the TSVI test is approximately twice as large as that of the SVI test.

Table IV shows SVI results for several more fine powder resins. Specific Gravity (SG), strained SG (SG @ Break) and percent voids are also listed.

Table IV

Resin	SSG	SG at Break	SVI	% Voids
A	2.152	2.141	11	0.5
B	2.156	2.110	46	2.1
C	2.177	2.035	142	6.5
D	2.175	2.088	87	4.0
E	2.184	2.044	140	6.4
F	2.177	1.919	258	11.8
G	2.213	1.813	400	18.1

TSVI test results are shown in Table V for these same resins. The SG of the TII chip, strained SG (SG @ Break) and percent voids are also listed. As can be seen, the TSVI range of values is approximately twice as large as that of the SVI range.

Table VI contains the SSG, TII, SVI and TSVI results for the resins shown in Tables IV and V. The higher TSVI indices are a result of the higher crystallinity of the specimen on extended thermal treatment. Resins that degrade the most have higher crystallinity and, consequently, a larger increase in the TSVI test. This can be seen by comparing the SVI, TII and TSVI. Resin C with an SSG of 2.177 has an SVI comparable to Resin E. However, the higher TII of resin E is reflected in its much higher TSVI compared with Resin C.

Table V

Resin	SG (TII chip)	SG at Break (TII chip)	TSVI	% Voids
A	2.156	2.134	22	1.0
B	2.171	2.098	73	3.4
C	2.188	1.992	196	8.9
D	2.191	1.983	208	9.5
E	2.226	1.582	644	28.9
F	2.229	1.682	547	24.5
G	2.246	1.322	924	41.1

Table VI

Resin	SSG	TII	SVI	TSVI
A	2.152	4	11	22
B	2.156	15	46	73
C	2.177	11	142	196
D	2.175	16	87	208
E	2.184	42	140	644
F	2.177	52	258	547
G	2.213	33	400	924

Results in the SVI and TSVI tests demonstrate the expanded scales these techniques offer for comparing different PTFE resins. The TSVI test offers a scale greater than 900 units.

Conclusion

Better methods for differentiating among PTFE resins will help wire manufacturers and end users select resins that are best suited to their particular needs. PTFE resins with lower TII can withstand temperature extremes with less molecular weight degradation. Resins with low SVI will experience less void formation when stressed. A low TSVI index indicates that a resin offers a combination of thermal stability and higher resistance to void formation. These types of resins should be better suited for applications where mechanical and/or thermal stresses on wire insulations are of greater concern. The TSVI measurement combines TII and SVI techniques to effectively differentiate among PTFE fine powder resins.

References

1. American Society for Testing and Materials Volume 8.01 Plastics (I): (D 1457).

2. "A Contribution Toward Improved Quality and Consistency of PTFE Insulated Wire," Conference Proceedings, Third SAE AE-8D Aerospace Electrical Interconnect System Conference, September 18, 1985 St. Louis, Missouri, Dr.-Ing. Horst Kuettner, P.E.

3. Williams, J.G., Fracture Mechanics of Polymers, Ellis Horwood Ltd. (Publishers), 1984, p. 123.

4. Kramer, E.J., "Microscopic and Molecular Fundamentals of Crazing," Advances in Polymer Science 52/53, Springer Verlag, (1983).

5. Kinloch, A.J. and Young, R.J., "Fracture Behaviour of Polymers," Applied Science Publishers, (1983).

6. Kausch, H.H., "Polymer Fracture," Springer Verlag, p. 282 (1978).

7. Wendorff, J.H., Polymer 21(5), 553-8, (1980).

8. Argon, A.S., Pure and Applied Chem., 43, 247, (1975).

9. Wellinghof, S. and Baer, E.J., Macromol. Sci., B4(3), 1195, (1977).

10. Rabinowitz, S. and Beardmore, P., CRC Reviews in Macromol. Sci., 1, 1, (1972).

11. "PTFE Resin Selection for High Performance Wire and Cable," Conference Proceedings, 35th International Wire and Cable Symposium, November 18, 1986 Reno, Nevada, Baillie, R.L., Bednarczyk, J.J., Mehta, P.M.

Appendix

Test

Determination of Thermal Stretching Void Index (TSVI)

Apparatus

1. Hydraulic Press
2. Temperature Programmed Oven
3. Tensile Testing Machine

Procedure

1. The die shown in Figure 1 of ASTM D 1457 shall be used for the molding of test specimens. Place flat aluminum disks, 0.08- to 0.38-mm (3- to 15-mils) thick and 76 mm (3 in.) in diameter, on both sides of the resin. The test resin should be near ambient temperature prior to molding.

2. Screen 29 grams of PTFE resin through a No. 10 sieve into the die. Adjust the lower plug so that the resin can be leveled by drawing a straightedge in contact with and across the top of the die cavity. Insert the die in a suitable hydraulic press and apply pressure gradually (500 psi/min) until a pressure of 6.9 MPa (1000 psi) is attained. Hold this pressure for 2 min., then increase the pressure to 13.8 MPa (2000 psi) and hold for an additional 2 min. Remove the disk from the die.

3. Sinter the compression molded disk in a temperature programmed oven according to the TII temperature cycle stated in ASTM D 1457-83, Procedure F, Table III.

4. Remove all flash from those portions of these specimens that will be used for determination of specific gravities so that no air bubbles will cling to their edges when the specimens are immersed in liquid during these tests.

5. Determine the specific gravity of the samples prepared above as per ASTM D 792. This is the unstrained specific gravity of the sample.

6. Cut tensile specimens from the sintered disk using the microtensile die shown in Figure 14 of ASTM D 1457-83.

7. Clamp the specimen in a tensile testing machine, with essential equal lengths in each jaw. The initial jaw separation shall be 12.7 ±0.13 mm (0.5 ±0.005 in.).

8. Strain the specimen at a constant rate of 5.08 mm (0.2 in.) per min. until it breaks. This strain rate and initial jaw separation yield a strain rate of 40%/min., based on the original gauge length of the specimen. If elongation at break is less than 500%, discard the result and repeat this step.

9. Cut off a portion of the stretched part of the specimen. Determine, according to ASTM D 792, the specific gravity of this strained specimen (Strained SG or SG at Break). Care should be exercised to avoid air bubbles on the surface when measuring weights in water.

10. Calculate percent voids as follows:

$$\% \text{ voids} = \frac{(\text{unstrained SG} - \text{SG at break})}{\text{unstrained SG} \times 100}$$

11. Calculate the Thermal Stretching Void Index (TSVI) as follows:

$$\text{TSVI} = (\text{unstrained SG} - \text{SG at break}) \times 1000$$



John Bednarczyk received his B.S. in Chemical Engineering from Rutgers University in 1981. He joined Du Pont in 1981 and worked in the Photographic and Electronic Products Department. In 1984 he joined the Polymer Products Department, Specialty Polymers Division where he is responsible for technical support for fluoropolymers used in the wire and cable industry.



Pankaj Mehta received his Bachelor's Degree in Chemical Engineering from the University of Bombay in 1981. He received a Masters in Chemical Engineering from the University of Delaware in 1983. He joined Du Pont in 1983 as a visiting scientist at the Company's Experimental Station. He joined the Polymer Products Department in 1984 where he has concentrated his efforts on basic fluoropolymer research.

CHARACTERIZATION OF POLYOLEFIN MATERIALS USED AS TELECOMMUNICATION CABLE JACKETS BASED ON THEIR TOUGHNESS RELATED PROPERTIES

VIENEY B. MASCARENPAS WILLIAM H. ENGLEHART

INSULATED CABLE ENGINEERS ASSOCIATION, P.O. BOX P, SOUTH YARMOUTH, MASS. 02664

ABSTRACT

The prime interest was to arrive at a relationship between material's physical properties, the cable jacket thickness, and the ability of the cable jacket to survive the hazards of installation. The first step was to characterize various polyethylene jacket materials by varying degrees of density and types, to be followed by evaluation of cable jacket performance and the recommendations of appropriate thickness dependent on material properties.

During the first stage of the study twelve different materials were evaluated and characterized using the following parameters: density, melt flow index, tensile strength at yield (at three temperatures), yield elongation (at three different temperatures), tensile at break, elongation at break, modulus of elasticity (at three different temperatures), thermal analysis (peak melt, crystallinity, heat of melting, heat at crystallization), abrasion resistance, notched low temperature brittleness and compression cut-through resistance.

The material properties were analyzed by grouping them by density and by type. Then each group and type were characterized by their respective performance in each testing parameter. This was done in spread sheet form so that quick comparison between groups and types could be done. Additionally, the results were graphically assembled to enhance the comparison capability. These techniques allow for easy determination of trends within each group and type depending on which physical parameter is being evaluated. The conclusion drawn from these analysis were compared to existing explanations of material performance. Where discrepancies existed, attempts were made to clarify the measured performance. Results are presented with recommendations for rating the different materials for further performance studies.

All of the information presented is the product of the activity under Working Group 592 and their point of view. It does not represent an official ICEA position on any aspects of this study.

INTRODUCTION

The first line of protection to any outside plant communications cable is its jacket. Once penetrated, the inner components are exposed to conditions that can deteriorate the electrical and physical performance of the cable. Preservation of the jacket integrity is a prime concern in the development of a cable design. This concern is evident in the various physical performance requirements placed on the cable to insure that the jacket will remain intact throughout the cable's installation and service life. Cable bend, low temperature fracture and impact testing are just a few examples of these requirements imposed to insure acceptable performance.

Two factors that contribute to these performance requirements are the material and thickness of the jacket. Because of this the industry has also adopted certain jacket thickness requirements. In addition they have established minimum material performance requirements. With the development of various materials over the past ten years the criteria used to establish material and thickness requirements may no longer be appropriate. Most material suppliers have published data on their polyolefin materials suitable for jacketing, but this is relative to their own product lines. Example of these type of studies are given in references 1 through 5. Performance of some materials has also been studied by some users (references 6, 7, 8). In 1982 the Communications Section of the Insulated Cable Engineers Association (ICEA) decided to evaluate various polyethylene jacket materials. The objective of this evaluation was to characterize these materials by several physical parameters that could be related to installation or environmental hazards. This characterization was necessary because existing data from the material suppliers are limited to typical properties used for quality control purposes.

Therefore the first order of activity was to determine what physical tests could be used that would relate to field performance. In terms of installation practices, several concerns are evident. These are:

1. Tearing or splitting of the jacket during

pulling or bending of the cable.
2. Tearing or wearing of the jacket due to rubbing across coarse surfaces or sharp objects.
3. Splitting or puncture of the jacket due to impact.
4. Deformation of the jacket due to heat and pressure.

A number of, then active, manufacturers of black polyethylene compounds were contacted for samples to cover most commercially available materials.

These materials were obtained and identified by a letter code and are listed in Table 1.

All samples were collected by one of the participating laboratories, coded, and distributed to the other laboratories. After due consideration, the Working Group decided on seven tests (as shown in Table 2). Taking into consideration the time required and the expense of doing all tests by each participating laboratory, the Working Group agreed to split the testing between laboratories in a manner that each test was done by three laboratories (as shown in Table 2). A brief description of each test is provided here. A more detailed write-up of the non standard test methods can be obtained by written request to the authors.

Density - This was the controlling property used to group the 12 materials evaluated relative to the above characteristics. Testing was done per ASTM D 1505.

Melt Flow Rate - This testing was done per ASTM D 1238. It does not directly relate to performance but was included to further categorize the various materials used.

Stress/Strain Properties

1. Tensile Strength at Yield and Break - All testing was done per ASTM D-638. These properties were measured at three temperatures, 23°C, 43°C and 63°C. The use of elevated temperatures was for the purpose of determining loss of strength due to heat exposure. Because of test equipment limitations only tensile strength at yield could be measured at the elevated temperature.

2. Elongation at Yield and Break - This parallels the tensile properties and is measured during the same test. It, along with tensile, can be used to determine toughness. It is also a good indicator of flexibility or brittleness. Because it is part of the tensile test the yield was also measured at the same three temperatures.

3. Modulus of Elasticity - This property is more commonly referred to as tangent modulus since most plastics do not have a true elastic modulus. Again this property was measured at 23°C, 43°C, and 63°C per ASTM D-638 with the dual purpose of determining retention of stiffness and changes in toughness.

Thermal Characteristics - The jacket materials were thermally characterized by Differential Scanning Calorimetry (DSC) where their peak melt, crystallization, heat of melting, heat of crystallization, crystallize onset, and melt onset temperatures were determined dynamically at the programmed rate of 10°C/minute from the thermograms.

A sample of jacket material 5 to 8 milligrams was weighed on an electronic microbalance and sealed in a standard aluminum pan. The sample was heated in a DSC cell under a nitrogen atmosphere to 175°C to remove prior heat history and then subsequently cooled and reheated at a programmed rate of 10°C per minute. This procedure was chosen for its simplicity and to provide the necessary thermal transition temperatures of the jacket materials. A relative degree of crystallinity can be obtained from the heat of crystallization; however, an individual isothermal procedure would be necessary for each jacket material for quantitative results.

Notched Brittleness - This testing was done per ASTM D 746 with the samples notched to a depth of 0.02 inches using a notching jig. The notch was necessary because most of the materials tested would not fail impact at the lowest temperature of the equipment in an unnotched condition. As documented by Yanizeski, et al[6], the effects on impact results due to the notch geometry can be dramatic. There was also concern about the influence on results due to notch sensitivity. However, this test method does provide relative magnitude of impact resistance and does provide an indication of cold temperature performance.

Abrasion Resistance - The testing was done per ASTM D 3389 except that the abrasive wheels were CS-17 and the load was 1000 grams. There were two, 500 revolutions cycles with a wheel cleaning between each cycle. The only other standard test method for abrasion resistance on solid plastic material is ASTM D 1242. This was not considered because of its complexity and lack of available equipment. The method used did yield results that gave some indication of the resistance to wear against coarse surfaces.

Compression Cut-Through - This was a special test developed by the Working Group. It involves a curved sample on a wooden dowel being compressed by a 0.015" thick blade. Contact between the blade and a copper strip located under the sample indicate total penetration. The force required to cause penetration is a good indication of the material ability to withstand compressive loads by sharp objects.

RESULTS

In general the study reaffirmed existing concepts of polyethylene published in various literature and supplier data. As the density of the polyethylene increases so does its tensile strength, modulus, melt characteristics and cut through resistance. On the other hand elongation tends

to decrease with increasing in density. There were several non classic responses that required further analysis. The most noticeable were the behavior of the two linear low density materials, the various medium density materials, and the response to the cold impact testing.

One of the two linear low density polyethylene exhibited performance along the lines of the standard low densities (Material E). The other linear low (Material D) had properties that, for the most part, approached the medium density range. The two medium density blends show properties that, although similar to the non blended medium densities, were distinctly lower in performance. However in terms of their performances relative to their densities they do follow the expected path.

All of the data was organized by looking at each material per a given property and the three laboratories doing the test. Table 3 is a complete representation of the data used in the analysis process. In addition to the tabulation, graphs were constructed comparing the results of a given property versus the various materials tested. Accuracy and agreement between laboratories was good on most tests based on ASTM guidelines. The special tests not covered by ASTM procedures gave the most variability. The following are the working group's interpretation of the results and their significance to performance.

Melt Flow Rate - The data clearly demonstrates that this property is not a function of density alone. It is also obvious that this property can not be used to judge the relative physical performance of material. This holds true whether the materials are of the same density or of different density ranges. All that can be said for this property was that it was the only one in which all three testing labs had good agreement on all materials.

Tensile Strength at Break - Allowing for some significant variation in results, the behavior of the various types of materials was as expected. The LLDPE showed improved strength over the LDPE. The MDPE were even stronger. Surprising, was the drop in strength of one of the HDPE (Material M). This same material was the only one whose yield strength was found to be higher than its break strength. It was noted that this material exhibited delamination which could result in premature breaks and deceptively low values. Figure 1 is an example of this type of fracture.

Tensile Strength at Yield - This test showed good response in terms of increasing yield strength with increased density. The LLDPE do not show as much of an improved strength over LDPE as was the case with strength at break. A significant fact was the near uniform reduction in yield strength with increased temperature for all materials. A 20°C rise in temperature results in a 24% to 40% drop in yield strength. A 40°C rise results in a 45% to 61% drop. Figure 2 contains the graphs at all three temperatures and clearly illustrates this condition. This is in agreement with results reported by Lawler, Rossi and Virkes,[7] in their work on medium density jacket materials. At least from the study, if there is a need for high yield strength at elevated temperature, one needs to start with a proportionally higher strength material at room temperature.

Elongation at Break - This was one of those tests that resulted in considerable scatter of data between testing labs. There appears to be two levels of performance. The LDPE materials along with one LLDPE fall in a range between 600% and 730%. The other LLDPE, the MDPE and HDPE materials are in the second group between 750% and 950%. The behavior of the various materials relative to each other is very similar to the tensile strength at break. Again material M showed lower than expected values due to the delamination effect.

Elongation at Yield - This follows classic material behavior for materials of similar chemistry. As the tensile values increase the corresponding elongation decreases. The high density polyethylenes with their higher tensile yield values have a correspondingly lower elongation at yield as compared to the low density materials. What did not follow classic behavior was the response to elevated temperatures. A 20°C rise in temperature caused the low and linear low density materials to increase in elongation between 350% and 425%. However the medium and high density materials increased at a much lower percentage, running between 35% and 80%. On the other hand a 40°C increase in temperature invokes a slightly different response. The elongation at yield of the low density materials increases between 415 and 540%. The linear low between 410% and 450% and the medium blend between 310% and 370%. This time the straight medium density and the high density only increase between 75% and 100%. It is possible that the low and linear low density polyethylene, having a low degree of crystallinity, react to the higher temperature by intermolecular slippage. Increasing the temperature further does not result in as dramatic an increase in elongation because the mechanism is the same. The high density and straight medium density polyethylenes, with their higher order of crystallinity, tend to maintain their rigidity at the elevated temperatures. Apparently even the 63°C test temperature was not sufficient to overcome the crystallization forces so that intermolecular slippage could occur. The medium density blends, being part low and part high density showed resistance to the 43°C temperature but reverted to the low density behavior at 63°C. This is probably due to the limited influence of the high density crystalline structure above 43°C.

Modulus of Elasticity - The modulus results tracked fairly close to the tensile yield values. As expected the higher the density the stiffer the material. Again one of the linear low density materials showed higher rigidity than the other one. The response to increase in tempera-

ture was significant but not unusual. At a 20°C increase the modulus values dropped between 30% and 60%. At a 40°C increase they dropped between 65% and 80%. Figure 3 shows the graphs at the three temperatures.

Thermal Characteristics - The correlation of the thermal transition temperatures and caloric information for the jacket compounds between the three laboratories conducting the tests was not very good; however, within the same laboratory the relative distinction of the four polyethylene types is evident. The discrepancies of the actual transition temperature is probably due to variations of calibration, instrument design and temperature control variables.

In general, the DSC thermal transitions determined within a laboratory can group the jacket materials into the four polymer types. The data shown in Table 4 from Laboratory 3 lists the heat of crystallization cal/gm, polymer type and a relative degree of crystallinity. The crystallization onset temperature shown in Table 5 categorizes the polymer types and also correlates with the average yield strength within each polymer type. As the onset temperature increases so does the yield strength. This also appears to be the case with heat of crystallization and degree of crystallinity. The DSC thermograms of the jacket compounds are quite distinctive and can provide valuable information to categorize the polymer type and to identify the jacket compound. This study shows that a simple computerized DSC system provides sufficient information to thermally categorize a polyethylene jacket compound. It further shows that relative physical performance can be predicted based on the thermal transition temperatures and caloric information. A representative group of DSC curves, one for each type of material, are included in the appendix to help illustrate the methodology. Each figure has two graphs. The one on the left is developed from cooling the material down past its crystallinity point. The graph on the right occurs during reheating past the melt point. Figure 4 covers material A which is a low density polyethylene. Figure 5 is material D which is a linear low density polyethylene. Figure 6 represents material H which is a medium density blend. Figure 7 is material J which is a straight medium density polyethylene. Figure 8 covers material M which is a high density polyethylene.

Notched Brittleness - The original intent was to mold in the notch to insure uniformity. Due to the unavailability of the dies and timing it was decided to notch the samples with a notching jig. This may have exaggerated the discrepancy between labs. Even with the large difference in results between labs, the trend between materials was somewhat consistent at each lab. It would normally be expected that the lower strength, lower modulus, higher elongation materials would have better impact characteristics. Based on the results of all three labs the opposite took place. Brittleness temperature depends on several other factors, of which the degree of crystallinity and thus density are important indicators. Differences in crystallite nucleation during quenching can also affect the brittleness temperature. The blending of copolymers can affect these conditions and enhance nominally brittle polymers to a higher level of impact resistance.

Abrasion Resistance - From the scatter of data within and between labs it was obvious that this test method needs considerable refinement. However it did yield comparative results indicating a relationship to density. The higher the density the more resistant to this type of abrasion. Another property that would probably correlate well with abrasion would be hardness. Since hardness is dependent on the degree of crystallinity and hence density, the degree of hardness should parallel the degree of abrasion resistance.

Compression Cut Through - Based on the data this is clearly a function of density. The ability to penetrate the material is going to depend on its hardness and how easily it yields under stress. Therefore the higher density, stiffer materials will resist cut through more than lower density flexible materials.

With all of this information on physical performance the question arises as to what all of this data has to do with jacket thickness. It is possible that materials, of higher strength, better heat resistance and equal flexibility at room and cold temperatures, can be used as reduced thickness without sacrifice in performance. In fact it is normal practice in other industries to down-gauge when higher strength materials are utilized. The concern that exists is how well these "better properties" translate into finished cable performance.

SUMMARY

This study provided a good understanding of various properties of polyethylene jacket materials. It also provided an understanding of the relationship of density and crystallinity to strength and stiffness. Other properties such as abrasion and impact are not as clear cut but they too are better quantified from this study.

In addition to confirming that strength and stiffness increase with density it was also demonstrated that low temperature brittleness is not necessarily an offsetting penalty. One area that was not addressed was the effect of cold temperature on strength and stiffness. There is concern that the higher density materials may become too stiff at lower temperatures. Such stiffness could impair installation or result in fractures at normal bending conditions.

As with any study on material properties the proof is in the performance in an intended application. That is the next step in our work and one we hope to address in the near future. What is desired is to construct several different cables using the various materials of this study. Within each cable type and material, varying

jacket thickness would be used. All of these cables would be subjected to a variety of laboratory tests and installation conditions to determine actual performance. Hopefully this information could then be correlated to the results of this initial study. From that correlation would come a standard showing recommended jacket thicknesses based on certain material properties.

ACKNOWLEDGEMENTS

We would like to take this opportunity to thank all the material suppliers who complied with our request for samples:

Dow Chemical, USA
DuPont Canada, Inc.
E.I. DuPont de Nemours Company (Inc.)
National Petrochemical Company
Phillips Petroleum
Union Carbide Canada Limited
Union Carbide Corporation, USA

We also wish to thank the members of ICEA Working Group 592 participating in the Round Robin testing and their companies for their support for this study:

W.H. Englehart	:	Essex Group, Inc.
W.A. Fallon	:	The Okonite Company
L.M. Hore, J. Fech	:	General Cable Corporation
B.W.Tyrell, P.F.Kish	:	Northern Telecom
V.B. Mascarenhas	:	Canada Wire and Cable Ltd.
T. McLaughlin	:	Celwave Technologies
H.M. McNeil	:	Siecor Corporation
F.D. Metcalf	:	BRintec Corporation
S.A. Mills	:	Ericsson, Inc.
G.A. Straniero	:	Triangle PWC, Inc.

REFERENCES:

1. S. Kottle and R.B. McAda, Dow Chemical, U.S.A., "Improved Telephone Jacket Compounds", Proceedings of 24th International Wire and Cable Symposium, 1975, pp. 225-230.

2. J. Fisher, Union Carbide Corporation, "Trends in Polyethylene Materials for Wire and Cable", Conference Proceedings, 52nd Annual Convention of Wire Association International, Pittsburgh, Oct. 1982, pp. 91-103.

3. A.J. Houston, H.A.B. Monro and E.T. O'Brien, DuPont Canada Limited, "Intermediate and Low Density Low-Pressure Polyethylenes - Their Properties and Applications in the Wire and Cable Industry", Proceedings of 12th International Wire and Cable Symposium, 1963.

4. R. McAda, Dow Chemical, USA, "Notched Tensile Low Temperature Brittleness Test for Cable Jacketing Polyethylene", Conference Proceedings, 52nd Annual Convention of Wire Association International, Pittsburgh, Oct. 1982, pp. 104-109.

5. R.H. Handwerk, R. Bostwick, Dr. B.K. Hwang, Dr. J.C. Miller, "New Process Technology for Linear Low Density Black Jacketing Compounds", Union Carbide Corporation, Bonnal Brook, N.N., 1983 Wire Association International.

6. G.M. Yanizeski, E.D. Nelson and C.J. Aloisio, "Predicting Fracture, Creep, and Stiffness Characteristics of Cable Jackets from Material Properties", Proceedings of 25th International Wire and Cable Symposium, 1976, pp. 272-280.

7. J.D. Lawler, R. Rossi, K.G. Virkus, "More Rigorous Sheathing for Outside Plant Cables", Proceedings of 27th International Wire and Cable Symposium, 1978, pp. 84-90.

8. G.M. Yanizeski, E.C. Johnson, R.G. Schneider, "Cable Sheath Buckling Studies and the Development of a Bonded Stalpeth Sheath", Proceedings of 29th International Wire and Cable Symposium, 1980, pp. 48-58.

Vieney B. Mascarenhas received his MSc degree in Chemistry from the University of Bombay (India) in 1960. He worked for a total of nine years in cable manufacturing plants in India. He joined Canada Wire and Cable Limited, Toronto, Ontario, Canada, as a member of Corporate Materials Development Laboratory in 1969 and is currently Supervisor of the Laboratory. He is first Vice-President of Communications Section of the Insulated Cable Engineers Association (ICEA).



William H. Englehart received his B.S. in Chemical Engineering from Indiana Institute of Technology in 1969. He worked for 13 years at International Harvester's Truck Engineering Group as a Materials Engineer responsible for non-metallic components. He joined Essex Group, Inc. in 1982 and currently holds the position of Materials Engineering Manager. He is second Vice President of the Communication Section of the Insulated Cable Engineers Association (ICEA).



TABLE 1

LIST OF BLACK[7] POLYETHYLENE JACKET COMPOUND SAMPLES[8]

MATERIAL CODE	MATERIAL[1] TYPE	DENSITY g/cm³[5]	MELT FLOW INDEX g/10 min[6]
A	LDPE	0.922	0.274
B	LDPE	0.933	0.294
C	LDPE	0.934	0.235
D	LLDPE	0.937	0.629
E	LLDPE	0.932	0.560
G	MDPE (2)	0.943	0.352
H	MDPE (3)	0.941	0.134
I	MDPE (4)	0.950	0.630
J	MDPE (4)	0.949	0.525
K	MDPE (4)	0.949	0.505
L	HDPE	0.960	0.249
M	HDPE	0.958	0.262

NOTES: (1) LD = Low Density, High pressure process,
LLD = Linear Low Density, low pressure process,
MD = Medium Density, HD = High Density

(2) Blend of LLDPE and HDPE (3) Blend of LDPE and HDPE

(4) Single component material (low pressure reactor).

(5) Average of test results from three participating laboratories (ASTM D 1505).

(6) Average of test results from three participating laboratories (ASTM D 1238).

(7) All materials were Type C (ASTM D 1248), containing 2.5% carbon black (nominal).

(8) For melt flow index, pellet samples were used, for density and all other tests, 0.070" thick plaque samples were used. Plaques were prepared as per procedure specified in ASTM D 1248 (ASTM D 1928, Procedure C).

TABLE 2

TESTS AND APPLICATION TO WORKING CABLE NUMBER COMPANY LABORATORY

PROPERTY	TEST METHOD[1]	APPLICATION TO CABLE[2]
(ABSOL.)		
1. Density	ASTM D 1505	6, 8, 9
2. Melt Flow Rate	ASTM D 1238	6, 7, 10
3. Stress/Strain Properties	ASTM D 638	1, 3, 4
at 73°F (23°C)		
at 110°F (43°C)		
at 145°F (63°C)		
4. Thermal Characteristics by DSC	Special	3, 5, 11
5. Notched Brittleness Impact (1/50)	ASTM D 256A (Modified)	2, 7, 12
6. Abrasion Resistance at 73°F (23°C)	ASTM D 3389 (Modified)	2, 7, 12
7. Compression Cut Through with Wedge at 73°F (23°C)	Special	6, 11, 13

[1] Figures or test methods given in text, complete methods available upon request.

[2] One of the participating laboratories was unable to complete the tests illustrated. This was then used by the other two participating laboratories.

TABLE 3

MATERIALS

PROPERTY		A	B	C	D	E	G	H	I	J	K	L	M
DENSITY	LAB-4	0.933	0.935	0.934	0.938	0.932	0.944	0.935	0.949	0.949	0.948	0.960	0.959
	LAB-6	0.930	0.931	0.933	0.934	0.930	0.941	0.942	0.949	0.948	0.949	0.958	0.952
	LAB-7	0.934	0.934	0.935	0.938	0.934	0.944	0.947	0.952	0.950	0.950	0.963	0.958
	AVG.	0.932	0.933	0.934	0.937	0.932	0.943	0.941	0.950	0.949	0.949	0.960	0.956
MELT FLOW (g/10 min)	LAB-4	0.2670	0.2730	0.2250	0.6250	0.5510	0.3670	0.1500	0.6120	0.5170	0.5890	0.2610	0.2750
	LAB-7	0.2829	0.2923	0.2360	0.6084	0.5445	0.3356	0.1209	0.6271	0.5229	0.5880	0.2650	0.2464
	LAB-10	0.2722	0.2856	0.2452	0.6217	0.5832	0.3522	0.1307	0.6519	0.5342	0.5955	0.2649	0.2633
	AVG.	0.2740	0.2836	0.2354	0.6184	0.5596	0.3516	0.1339	0.6303	0.5247	0.5908	0.2636	0.2616
TEN. STR. @ BREAK 23C (PSI)	LAB-1	2628	2657	2157	3457	2914	3571	3628	3685	4257	----	----	2743
	LAB-3	2565	2533	2342	3301	2672	3438	3440	2757	4261	2000	4355	3125
	LAB-5	2572	2488	2219	3221	2635	3263	3775	2965	3920	4686	3835	2173
	AVG.	2588	2559	2239	3326	2740	3424	3614	3325	4146	3343	4095	2680
ULTIMATE ELONGATION (%)	LAB-1	720	760	580	900	770	960	870	950	890	----	----	650
	LAB-3	656	714	624	832	686	832	750	750	816	670	1000	750
	LAB-5	706	689	610	875	731	930	850	830	870	1001	932	870
	AVG.	694	721	605	869	729	907	823	890	859	836	966	753
TEN. STR. @ YIELD 23C (PSI)	LAB-1	1338	1391	1300	1614	1397	2085	2271	2771	2600	----	----	3182
	LAB-3	1279	1365	1258	1592	1442	2077	2286	2849	2722	2613	3460	3146
	LAB-5	1345	1383	1284	1706	1323	2016	2445	2572	2675	3492	3436	3182
	AVG.	1321	1380	1261	1637	1387	2059	2334	2731	2666	3152	3448	3170
TEN. STR. @ YIELD 63C (PSI)	LAB-1	946	966	933	1088	986	1428	1571	2028	1928	----	----	2285
	LAB-3	988	993	977	1205	1039	1509	1652	2056	2204	1852	2480	2615
	LAB-5	899	926	894	1158	1028	1471	1779	1873	1930	1904	2581	2227
	AVG.	944	962	935	1150	1018	1469	1667	1986	2021	1878	2531	2376
TEN. STR. @ YIELD 63C (PSI)	LAB-1	695	694	661	743	710	941	1051	1327	1264	----	----	1528
	LAB-3	423	517	557	780	732	959	1104	1383	1305	1232	1743	1606
	LAB-5	712	681	677	774	863	975	1218	1362	1322	1207	1683	1663
	AVG.	669	631	632	766	768	958	1124	1357	1297	1220	1713	1599
YIELD ELONGATION 23C (%)	LAB-1	----	----	----	----	----	----	----	----	----	----	----	----
	LAB-3	10.8	11.0	11.8	8.4	10.6	8.0	8.4	7.4	7.4	8.5	7.2	7.7
	LAB-5	10.5	14.0	10.6	11.0	10.8	8.2	8.7	8.0	7.7	9.6	9.7	8.1
	AVG.	10.7	12.5	11.2	9.7	10.7	8.1	8.6	7.7	7.6	9.1	8.5	7.9
YIELD ELONGATION 43C (%)	LAB-1	----	----	----	----	----	----	----	----	----	----	----	----
	LAB-3	45.0	48.4	46.0	30.0	43.7	13.0	14.0	13.3	13.0	11.7	10.3	13.0
	LAB-5	65.2	65.3	71.3	29.1	59.0	13.3	13.9	13.0	13.7	14.4	12.6	13.3
	AVG.	55.1	56.9	58.6	29.6	51.4	13.2	13.9	13.7	13.4	13.1	11.4	13.2
YIELD ELONGATION 63C (%)	LAB-1	----	----	----	----	----	----	----	----	----	----	----	----
	LAB-3	53.2	55.0	62.4	43.1	54.1	31.4	36.6	14.6	14.7	15.0	13.0	12.4
	LAB-5	71.8	74.0	80.5	55.5	62.5	35.4	43.6	15.2	15.4	19.4	16.4	14.9
	AVG.	62.5	64.5	71.4	49.3	58.3	33.4	40.1	14.9	15.1	17.2	14.7	13.7

TABLE 3 (CONT)

PROPERTY		MATERIALS A	B	C	D	E	G	H	I	J	K	L	M
MODULUS OF ELASTICITY 23C (PSI)	LAB-1	40200	37700	30800	57250	37475	76450	80525	104150	99425	96525	142385	124875
	LAB-3	30425	41693	28750	50000	43891	69910	81625	100727	102103	108307	141026	118250
	LAB-5	32515	39778	29083	56412	34803	59606	78241	98666	104586	118416	181959	113428
	AVG.	34380	39724	29544	54554	38723	68655	80130	101181	102038	107749	155123	118851
MODULUS OF ELASTICITY 43C (PSI)	LAB-1	20750	21085	20095	32575	22930	47940	52115	73865	70540	58860	95335	89285
	LAB-3	12385	14263	17172	29946	15686	45487	52371	41928	58654	40493	58670	76305
	LAB-5	14625	14434	13050	23902	17268	28836	35604	52421	49957	49617	73272	73824
	AVG.	15920	16594	16772	28808	18628	40754	46697	56071	59717	49657	75759	79805
MODULUS OF ELASTICITY 63C (PSI)	LAB-1	10870	10535	8990	16385	13840	24810	28825	44200	38970	32615	52730	48475
	LAB-3	7043	7341	6786	9418	7044	16534	16097	25290	15860	20279	27089	27952
	LAB-5	8481	7103	6318	12501	9734	23269	30070	34115	30819	23794	38663	52575
	AVG.	8798	8326	7365	12768	10206	21538	24997	34535	28550	25563	39494	43001
PEAK MELT TEMPERATURE (C)	LAB-3	108	109	108	110,119	108,119	125	110,124	127	125	124	127	128
	LAB-5	100	107	110	115,125	112,125	130	130	130	125	128	135	130
	LAB-11	101	101	100	99,111	100,113	117	102,117	120	118	117	121	120
	AVG.	103	106	106	113	113	124	117	126	123	123	123	123
CRYSTALLINITY ONSET (C)	LAB-3	102	103	101	109	110	114	113	116	115	114	117	116
	LAB-5	108	115	100	133	115,125	120	124	135	118	123	124	120
	LAB-11	101	105	98	107	112	113	114	116	114	114	117	114
	AVG.	104	108	100	116	116	116	117	122	116	117	119	117
Hm (cal/g)	LAB-3	21.0	20.0	19.0	21.0	25.0	26.0	29.0	37.0	37.0	26.0	37.0	37
	LAB-5	22.0	28.0	32.0	31.0	22.0	35.0	55.0	40.0	48.0	----	----	31
	LAB-11	25.0	25.1	23.0	27.0	25.8	33.0	35.0	37.6	39.0	40.6	45.3	43
	AVG.	22.7	24.4	24.7	26.3	24.3	31.3	39.7	38.2	41.3	33.3	41.1	37.0
H-crys. (cal/g)	LAB-3	26.5	27.2	26.5	31.6	27.7	36.5	38.3	41.1	39.4	34.0	48.3	44.2
	LAB-5	18.0	19.0	29.0	21.0	36.0	29.0	28.0	40.0	39.0	----	----	28.0
	LAB-11	19.1	19.0	17.6	20.8	18.9	25.5	28.1	33.4	31.4	34.0	40.0	37.2
	AVG.	21.2	21.7	24.4	24.5	27.5	30.3	31.5	38.2	36.6	34.0	44.1	36.5
ABRASION RESISTANCE (mg/rev)	LAB-2	0.0703	0.0819	0.0924	0.0404	0.0766	0.0384	0.0334	0.0348	0.0290	0.0620	0.0620	0.0378
	LAB-2	0.0869	0.0828	0.0935	0.0495	0.0867	0.0441	0.0561	0.0464	0.0408	0.0478	0.0499	0.0467
	LAB-11	0.0119	0.0136	0.0159	0.0059	0.0103	0.0067	0.0105	0.0110	0.0058	0.0047	0.0061	0.0020
	AVG.	0.0564	0.0594	0.0673	0.0319	0.0579	0.0297	0.0333	0.0307	0.0252	0.0382	0.0393	0.0288
NOTCHED BRITTLEMESS (Deg.C)	LAB-2	-30	-24	-24	-59	-43	-49	-36	-76	-69	-63	-64	-76
	LAB-7	-33	-28	-23	-49	-43	-52	-53	-55	-54	-55	-55	-55
	LAB-11	-12	-12	-9	-30	-27	-27	-12	-24	-27	-17	-62	-27
	AVG.	-25	-21	-19	-46	-38	-43	-34	-52	-50	-45	-60	-53
COMPRESSION CUT-THROUGH (lbs.f./mil)	LAB-6	8.4	9.9	6.6	10.1	9.8	14.7	11.2	12.3	15.9	8.9	11.6	13.8
	LAB-11	8.8	8.6	8.1	10.2	8.9	12.4	10.9	13.7	13.3	11.7	12.9	13.5
	LAB-11	10.0	10.1	9.2	14.1	8.5	12.5	11.8	12.4	13.3	10.5	12.8	12.6
	AVG.	9.1	9.5	8.0	11.5	9.1	13.2	11.3	12.8	14.2	10.4	12.4	13.3

TABLE 4

Compound	Polymer Type	Avg. Crystallization Value *	Percent Relative Degree of Crystallinity at [illegible]
J	MDPE	[illegible]	[illegible]
M	HDPE	[illegible]	[illegible]
[illegible]	MDPE	[illegible]	[illegible]
[illegible]	MDPE	[illegible]	[illegible]
[illegible]	MDPE [illegible] MDPE	[illegible]	[illegible]
[illegible]	MDPE [illegible] MDPE	[illegible]	[illegible]
K	MDPE	[illegible]	
[illegible]	[illegible]	[illegible]	[illegible]
[illegible]	[illegible]	[illegible]	[illegible]
[illegible]	[illegible]	[illegible]	[illegible]
[illegible]	[illegible]	[illegible]	[illegible]
[illegible]	[illegible]	[illegible]	[illegible]

* [illegible]

TABLE 5

Polymer Type	Compound	Tan Delta Peak Temperature °C	Avg. Yield Strength (Reported by Compound) 23°C	43°C	71°C
HDPE	J	117	L	L	L
HDPE	M	114	M	M	M
MDPE	I	116	K	I	I
MDPE	[illegible]	117	I	I	
MDPE	K	114	[illegible]	K	K
MDPE [illegible]	G	114	H	H	H
MDPE [illegible]	H	113	G	G	
[illegible]	[illegible]	116	D	D	[illegible]
[illegible]	I	109	E	E	[illegible]
[illegible]	B	103	[illegible]	B	C
[illegible]	A	102	A	A	B
[illegible]	C	101	C	C	[illegible]



FIGURE 1

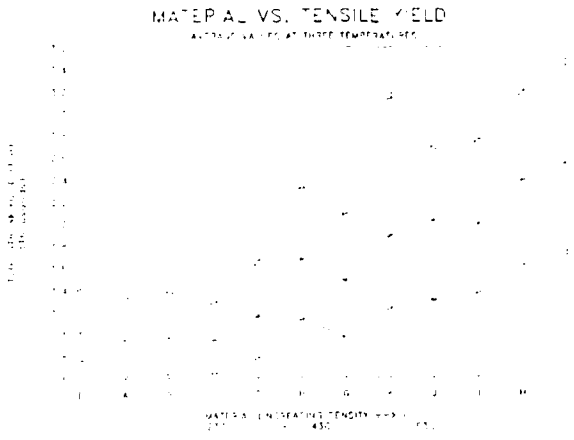


FIGURE 2

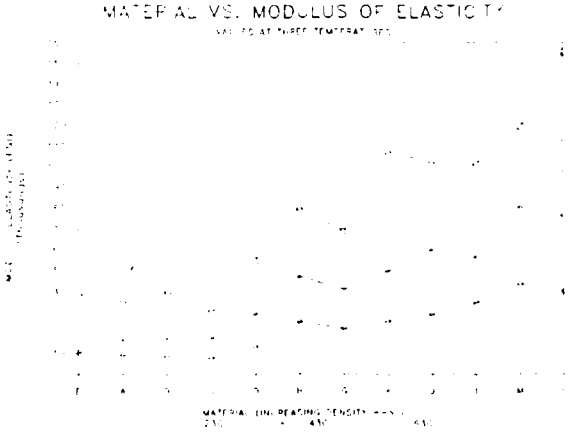


FIGURE 3

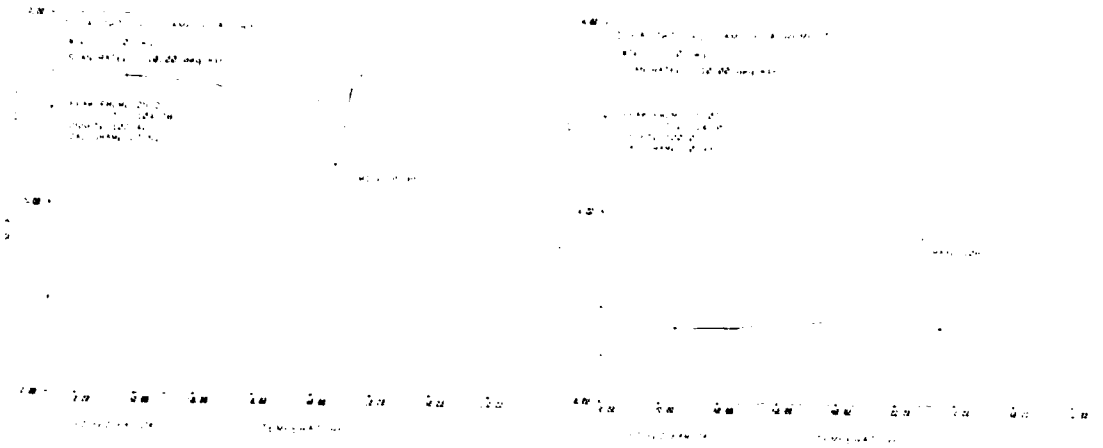


FIGURE 4

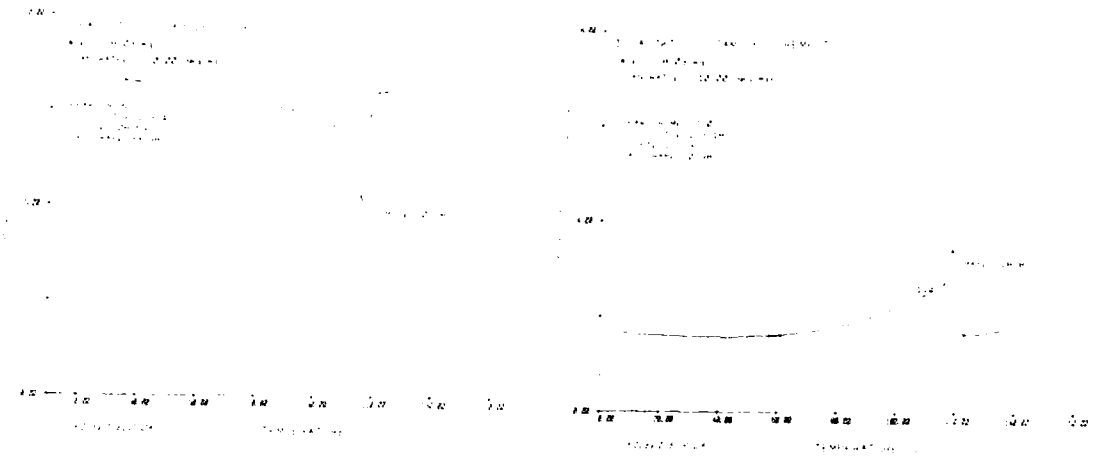


FIGURE 5

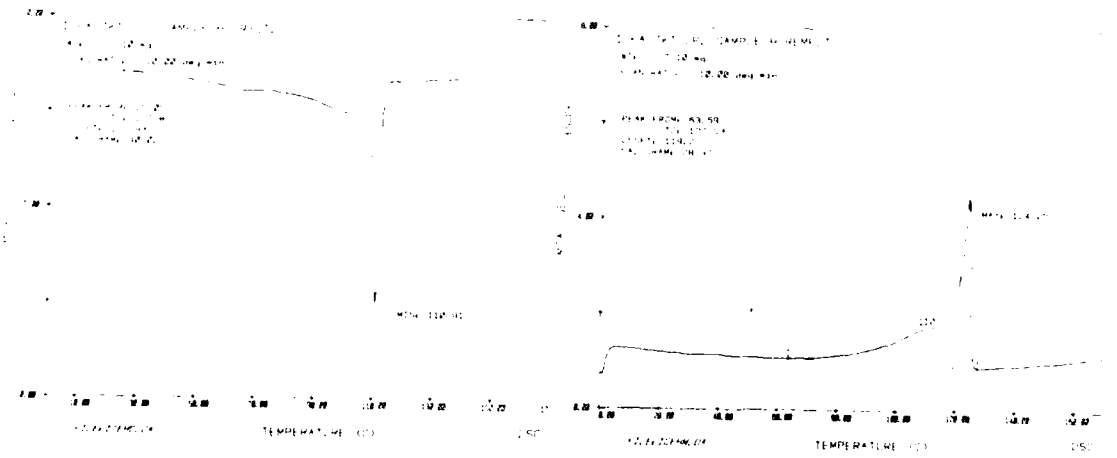


FIGURE 6



FIGURE 7



FIGURE 8

REDUCED EMISSIONS PLENUM CABLE TELEPHONE JACKET COMPOUNDS

M. J. Keogh

Union Carbide Corporation
Somerset, New Jersey

ABSTRACT

A new [illegible] polyolefin-based cable jacket compound with significantly reduced [illegible] (RE-PJC) was developed for application on type "MI" plenum cable [illegible]. This is the first [illegible] twenty-five pair shielded cable, that can easily pass the vertical "E-84" test for cable in plenum. The jacket material was extensively characterized for a [illegible] important fire safety features [illegible] including those which are [illegible] Underwriters Laboratories (UL), U.S. Navy, [illegible] and New Haven Smoke Chamber. A correlation of these data with various [illegible] jacket materials in the RE-PJC test [illegible] types. Typical physical properties and typical end-use [illegible] are also presented.

INTRODUCTION

In [illegible] the [illegible] Electrical Code (NEC) was changed to permit [illegible] telephone cable in plenum and air-handling spaces. This allowed the use where "adequate fire-retardant and low-smoke properties characteristics" are demonstrated. They [illegible] required because of fire safety problems and through compliance with Underwriters Laboratories (UL)-910, "E-84" is a "Standard for Test Method for Fire and Smoke Characteristics of Cables Used in Air-Handling Spaces." Specifically a cable will meet the requirements of a maximum flame spread of less than 5.0 feet, a maximum optical density (MOD) of less than 0.5 and an average optical density (AOD) of less than 0.15 for the test.

In the almost ten years since the NEC change, a heightened awareness and an increased understanding of the many factors involved in fire safety and hazard assessment have occurred. In 1982, for example, the National Fire Protection Association (NFPA) officially recognized combustion toxicity as an important factor in loss of life from fire.[1] In 1984, following independent assessments on the causative factors for extensive property damage and threat to life resulting from fires in their installations, both NTT in Japan and the U.S. Navy acted with specifications to limit fire and smoke emissions from cable materials.[2,3] Finally in the last three years work has been underway to limit fire hazard cable in subway and transit facilities in Europe and to a lesser extent in the United States.[4]

These and other earlier events, and accelerated efforts in many areas to develop alternatives to fire hazard materials, [illegible] both [illegible] results [illegible] to develop [illegible] polyolefin cable jacket (RE-PJC) [illegible] plenum.

RESULTS

[illegible] "Standard for Test Method for Fire and Smoke Characteristics of Cables Used in Air-Handling Spaces."

UL-910 characterizes cables for fire safety in a limited manner. Cables are evaluated for flame spread and the degree of light attenuation by smoke particles. An allowance of 5.0 feet maximum in flame spread and a maximum optical density (MOD) and average optical density (AOD) of 0.50 and 0.15, respectively, is set. No other fire safety factors are measured.

Figures 1 and 2 present the results of the UL-910 investigative study carried out on RE-POCJ. The flame spread maximum given in Figure 1, 3.6 feet, is well below the allowed level of 5.0 feet. Figure 2 shows graphically the optical density change over the twenty minutes testing time. Again, compliance with the requirement is easily made and the level of performance is substantially beyond the set point of UL-910.

As a UL-910 control, we tested the twenty-five pair commercial polyethylenechlorotrifluoroethylene (ECTFE) insulation core, used in the RE-POCJ test, jacketed with a commercial polyvinylidienefluoride (PVDF) resin compound. UL-910 results on this construction are presented in Figures 3 and 4. As expected, compliance with UL-910 is found. The overall performance level averages to about that for the experimental cable. Flame spread was reduced in the control to 2.3 feet but the average optical density was at twice the value obtained for the experimental cable. The latter observation suggests that the total amount of visible smoke emitted from the RE-POCJ construction will be reduced relative to certain commercial constructions.

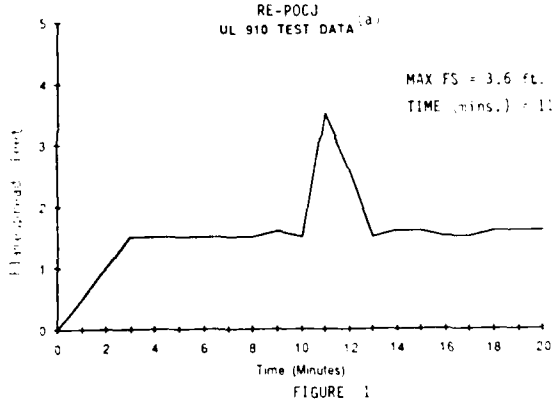


FIGURE 1

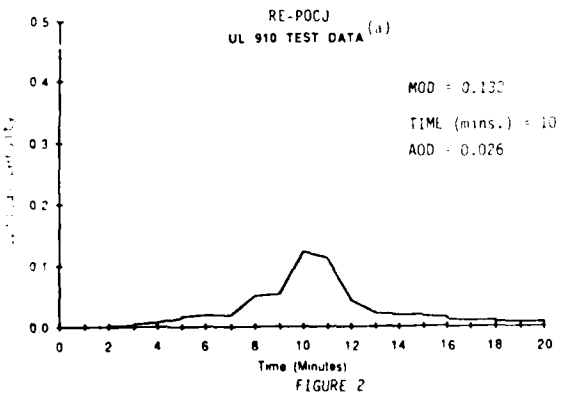


FIGURE 2

(a) 15 mil. RE-POCJ over 25 pair Poly (ECTFE), 5.5 mil over 24 AWG Copper Core

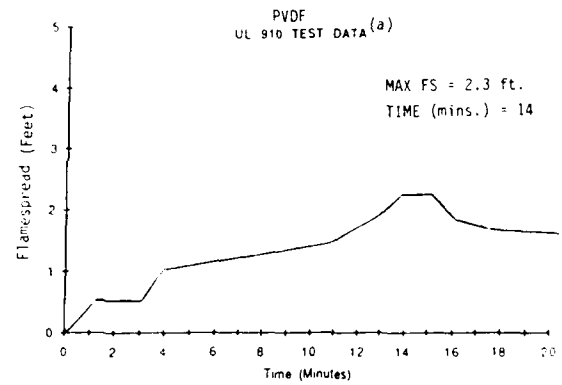


Figure 3

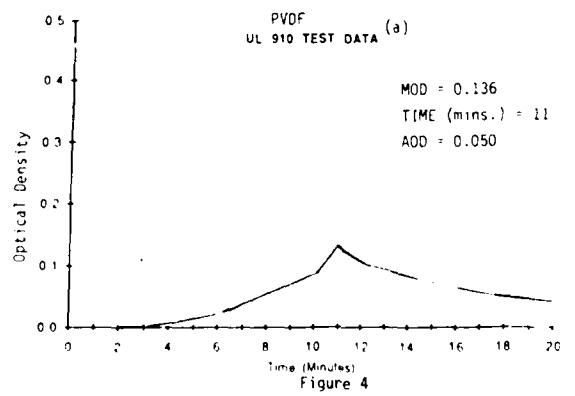


Figure 4

(a) 14 mil PVDF jacket over 25 pair Poly (ECTFE), 5.5 mil over 24 AWG Copper Core

Further Characterization of RE-POCJ Material for Visible Smoke

The UL-910 results on visible smoke contain a component from the insulation core used in the test. This variable was not a part of our laboratory development study. In our development work two established test methodologies were used. We evaluated performance using ASTM-E-662-83 (National Bureau of Standards Smoke Chamber) procedure[6] and the Smoke Index value obtained in Mil-C-24643. The NBS method was chosen for its ubiquity in the fire hazard assessment community and the existing data bank on materials. The Smoke Index (SI) was studied because it deals directly with wire and cable application into an area not far removed from plenum cable, namely shipboard cable. Additionally, the SI heavily weights smoke produced from materials in the early stages of a fire, hence it places a premium on allowing "time for escape."

The data set forth in Table I are the results from testing a typical RE-POCJ material following the standard procedures for the methods. For comparison smoke values determined under the same conditions are reported for typical non-smoke suppressed halogen-antimony flame retarded polyolefin and flame retarded polyvinylchloride jacket compounds. Clearly a substantial improvement in lowering visible smoke generation is accomplished with the RE-POCJ material. Particularly noteworthy is the very low Smoke Index for RE-POCJ material.

TABLE I

SMOKE DATA

	RE-POCJ	FR-PE	FR-PVC	Allowed
NBS E-662 (0.125 in.)				
D_m Flaming	190	688	801	
Non-Flaming	160	527	582	
D_S (1.5 min.) F	4.0	15	161	
N-F	1.4	2	6	
D_S (4 min.) F	105	532	606	
N-F	19	8	143	
Smoke Index (Mil-C-24643)	10		150	25

Thus far, the discussion has focused on visible smoke. If this type were the only concern then, for example, a sightless person would be exposed to no smoke related hazard in a fire. We know this not to be the case. The American Society for Testing and Materials (ASTM) defines smoke as a complex mixture of "the airborne solid and liquid particulates and gases evolved when a material undergoes pyrolysis or decomposition."[7] With this in mind, we studied RE-POCJ materials for their smoke toxicity and smoke corrosivity characteristics.

RE-POCJ Material - Smoke Toxicity

The most controversial component of fire safety, smoke (combustion) toxicity, was officially recognized for its importance by the National Fire Prevention Association (NFPA) in 1982. As mentioned earlier, the UL-910 testing procedure used for cable in plenum does not address this aspect of smoke.

Recently for shipboard wires and cables the U.S. Navy introduced, through Mil-C-24643, a toxicity component expressed as an index. In addition the State of New York, with the issuance of Article 15,[8] will begin to measure and compile a data bank on fire gas toxicity for wire and cable materials. To put perspective on the RE-POCJ development, we evaluated its performance using these established procedures.

Table II reports the smoke toxicity data obtained on RE-POCJ compound from the tests in Mil-C-24643 and N.Y.S. Article 15. Relative to existing data on other materials used as wire and cable jackets the RE-POCJ material exhibits outstanding performance. In both tests RE-POCJ ranks among the best polymerics for which data exist.

TABLE II

COMBUSTION TOXICITY RE-POCJ

Toxicity Index	Method	Value	Value Allowed
U.S. Navy	Mil-C-24643	0.76	5.0
N.Y.State Art. 15	U.of Pitt.	77.1	N.A.

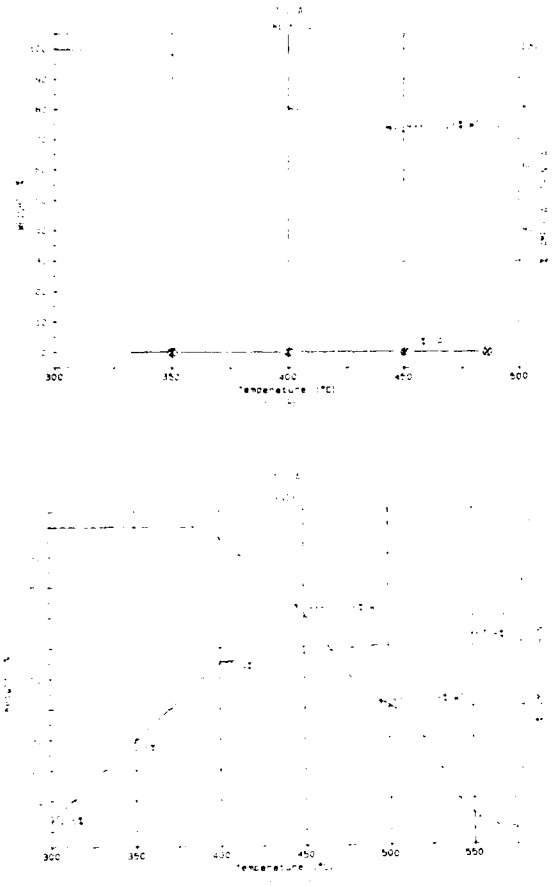
RE-POCJ Material - Smoke Corrosivity

While smoke toxicity is the most important life safety aspect of a fire event, smoke corrosivity ranks high as the cause of property loss. Depending on the type equipment in the fire environment it can easily be the largest contributing factor to property loss. The elements contained in conventional fire resistant polymerics contributing most to corrosivity are acid gas releasing, generally halogen containing additives and resins. On pyrolysis and/or combustion the acidic fire gases produced, particularly in combination with water, continue their corrosive action long after the fire is extinguished. During the fire event corrosive gases present a real hazard to circuit integrity of the fire control systems, including alarms.

Examples exist today where following extensive corrosive gas fire damage direct action has been taken to limit future losses. In Japan, Nippon Telegraph & Telephone (NTT) following the Setagaya, Tokyo telecommunications network fire in 1984, acted with the issuance of directives for the development of non-halogen fire retardant materials for telecommunications application. In a similar vain, following their analysis of the damage from shipboard fires, first the U.K Royal Navy and then the U.S. Navy acted to limit halogen and other strong acid gas producing elements from the materials of construction in wires and cables. In these instances the actions cited were taken even though suitable commercial substitute materials did not yet exist.

A common argument advanced to support the application of highly halogenated materials is their well recognized resistance to ignition. From a corrosivity and toxicity viewpoint, particularly in the case of halogenated hydrocarbons, ignitability and/or oxidative combustibility may not be the only issue. More often than not, the only requirement for the release of copious corrosive and toxic smoke is radiant energy. Recognize radiant energy as a familiar product of fire.

RE-POCJ material was evaluated for its thermal behavior and strong acid gas release using thermogravimetric analysis (TGA) and the acid gas determination procedure contained in Mil-C-24643. A similar analysis was carried out on the commercial PVTF jacket compound used as the study control in our MIL-W-16 qualification testing. Figures 5 and 6 graphically summarize the results obtained from this evaluation.



The thermograms for RR-P30J and PVDF materials show an equivalent weight loss of 1.0% at 441°C. Beyond this temperature, the PVDF pyrolysis, dehydrofluorination and char formation again until at about 5[illegible] temperature. On the other hand, the measurements for RR-P30J and PVDF during pyrolysis at the temperature indicated.

For PVDF at [illegible] weight equivalent of the original acid is released from the sample, while at [illegible] minutes 6.4% of the weight of the sample is released as nitric acid. Based on structure, TGA and the acid gas data PVDF is assumed to undergo [illegible] mechanism. The first of the two possible dehydrofluorination reactions per monomer unit initiates at a measurable level below 300°C and accelerates rapidly above this temperature. From the thermogram this first stage is completed at about 475-495°C. On the other hand, the RR-P30J material, although decomposing thermally in a manner similar to the fluorohydrocarbon, produces no strong acid in the pyrosylate.

It is significant that the omission of corrosive smoke does not require ignition and oxidative decomposition (burning); only radiant energy. RR-P30J pyrolysis is not a corrosive smoke hazard. PVDF as a jacket material represents a substantial corrosive smoke hazard.

RR-P30J Materials - Physical Properties

Physical and mechanical properties for a typical RR-P30J formulation are listed in Table III. In general, the properties meet or exceed jacket specifications where flame retardant polyolefins find commercial wire and cable application as, for example, shipboard cable (Mil-C-24643).

TABLE III

TYPICAL PROPERTIES[a]

Property	Method	Unit	Test Typical Value
Density	D1505	g/cm^3	1.60-1.70
Melt Index	D1238	g/10 min	3.13
Flow Index	D1238	g/10 min	51.7
Tens. Str.	D638	psi	1100-1300
Elongation	D638		250-350
Oxygen Index After 7 Days @ 121°C			
Retained Tens. Str.	D638		102
Retained Elong.	D638		95
Tensile Impact Str.	D1822	ft-lb in^{-2}	45
Flame Retardancy	UL94	per 125 mil specimen	5VA
Water Absorption	D570	%	<1

(a) Physical properties are determined on extruded 16 pair cable with a 35 mil (0.89mm) thick jacket except where noted.

Processing Characteristics

Materials developed can be processed on a wide range of extrusion equipment. They show an ease of processability unique for a heavily filled polyolefin compound. No corrosive strong acid gases are formed in the extrusion processing. With proper screw and tooling selection, commercial extrusion rates are expected. Predrying of the material is recommended to insure smooth melt-free extrusion.

Below are recommendations for equipment selection and a typical extrusion profile.

EXTRUDER TYPE

Screw L:D	20:1 to 24:1
Screw Type	PE Metering
Compression Ratio	2.5:1 to 3.5:1
Screen Pack	20-40-60-20 Mesh

TEMPERATURE PROFILE

Feed Zone	150°F
Center Zones	430°F
Metering Zone	350°F
Head	250°F
Die	250°F
Melt Temperature	370°F

CONCLUSIONS

Reduced emissions telecommunication cable jacket compound based on a polyolefin resin represents an attractive alternative material for plenum installations where a lower fire hazard potential is a key objective.

ACKNOWLEDGEMENTS

The experimental work of Messrs. D. L. McDaniel and A. Adamczyk is greatly appreciated. The extrusion expertise and efforts of Mr. G.D. Brown is acknowledged.

REFERENCES

(1) UL-910, Standard for Test Method for Fire and Smoke Characteristics of Cables Used in Air-Handling Spaces, Underwriters Laboratories, Inc., Melville, New York, 1981.

(2) National Fire Protection Association, Board of Directors, December 3, 1982.

(3) H., Nishizawa, "Recent Development of Non-Halogen Flame Retardant Materials in Japan," Proceedings FRCA, March 1987, pp. 29-44.

(4) U.S. Navy Military Specification Mil-C-24640 and Mil-C-24643, September 28, 1994.

(5) Massachusetts Bay Transportation Authority, Specification P-1200, October 1978.

(6) ASTM E662-83, "Standard Test Method for Specific Optical Density of Smoke Generated by Solid Materials."

(7) ASTM E176-82, "Standard Terminology Relating to Fire Standards," American Society for Testing and Materials, Philadelphia, Pennsylvania.

(8) New York State Uniform Fire Prevention and Building Code, Article 15, Part 1120, Subchapter B Safety Rules, 1987.

BIOGRAPHY



Michael J. Keogh is a Research Associate in the Polyolefins Specialties Division of Union Carbide Corporation. He received a B.S. in Chemistry from Manhattan College and a Ph.D. in Organic Chemistry from Purdue University. He has been involved in research and product development for wire and cable application for thirteen years. He holds over forty U.S. patents in this and related areas.

REDUCTION OF FIRE HAZARDS DUE TO CABLES FITTED TO WARSHIPS

MR J A POWNALL HEAD OF CABLE SECTION

MINISTRY OF DEFENCE (NAVY) UK

Abstract

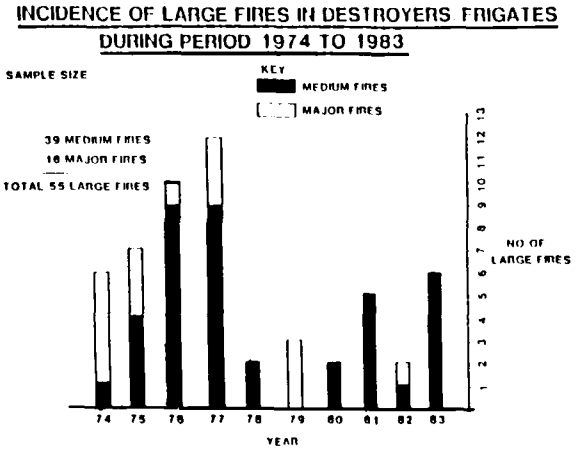
The incentives leading to a change in the fire characteristic requirements of cables to UK warships is briefly reviewed. How these reductions in fire hazards associated with cables was defined in a new set of performance specification is outlined. The adoption of the generic term Limited Fire Hazard (LFH) type cable is explained The technical assessments that led to the adoption of the stated performance limits is surveyed and the cable constructions that comply with these (LFH) limits are given. The ongoing problems being experienced with this new cable construction during manufacture, warship construction, equipment design and in-service are illustrated in some detail. The corrective measures modification and development of special tools that have proved necessary in order to incorporate these cables into a reliable power and/or communication network on a warship are discussed, and future development tasks predicted. The cost of procurement of these cables is compared with earlier types, and the conclusion drawn that the enhanced safety of a warship during and after a fire justifies the higher cost.

SUMMARY

1. The hazards involved in a fire on a warship are well documented in history. The singeing of the King of Spain's beard when Drake set fire to Spain's Armada in Cadiz, and more recently in the Falklands when HMS SHEFFIELD was lost due to uncontrollable fires. Certain measures have always existed to reduce fire hazards, but the allocation of materials and resources has always needed a political or dramatic incentive. The Falklands gave that incentive and the UK are introducing cables of a type known as Limited Fire Hazard (LFH) on all new construction warships. But to alter the materials used in the construction of a cable is not a sufficient quantum change to justify the cost. The whole cable system as part of a power and communication network has to be subject to scrutiny for fire risk. There is little virtue in reducing the fire hazards caused by polymers if thereby the connectors and terminal blocks overheat and increase the risk of an electrical fault initiating a fire.

FIG 1

Incidence of large fires in Destroyers/Frigates during period 1974 to 1983



FIRE HAZARDS

2. These can be briefly summarised as:

a. Heat.

b. Smoke and fumes.

The intensity of these hazards depends upon:

(i) Volume and weight of the combustibles.

(ii) Calorific value of combustibles.

(iii) Materials of the combustibles.

(iv) Availability of air or oxygen to support combustion.

FIG 2

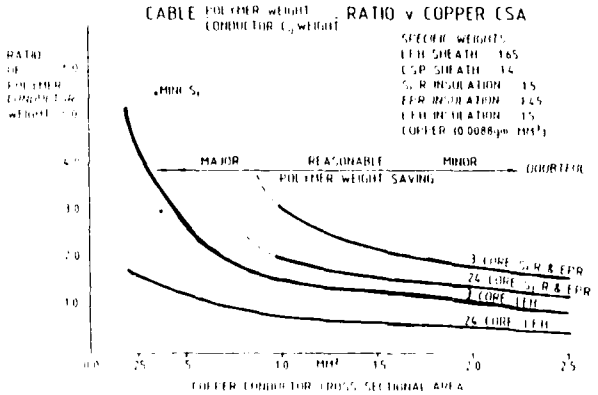
Weights of Polymers on cables of similar copper cross sectional area.

WEIGHTS OF POLYMERS ON CABLES

CABLE NSN	TYPE	NO OF CORES	OD CORE mm	OD SHEATH mm	SG OF SHEATH	SG OF INSUL'N	POLYMER wt g/M
743-0503	LFH NES525	7	1.65	9.25	1.65	1.4	82
521-6879	SIR DGS211	7	2.6	12.8	1.4	1.5	157
521-8431	EPR DGS212	7	2.7	12.4	1.4	0.86	145

FIG 3

Reduction of polymer weight of two LFH type cables compared with similar type cables of earlier construction over range 0 to 2.5mm (U.K./U.S.A.



NEW CABLE TYPE

The new cable type termed Limited Fire Hazard (LFH) has contributed to a reduction in all these aspects. The term "limited" is adopted because the limits quoted in the Naval Engineering Standards (NES's) are under constant review.

3.1 Volume and Weight

Some 70 to 80% of cables fitted to a modern warship have cores less than 2.5mm (0.004in) copper cross section. The ratio of insulation area in proportion to the copper area is also high, thus a reduction in insulation weight and volume on these small cables makes a considerable improvement in the combustibles in any warship compartment. These wires are specified in performance terms in the Defence Standard 61-12 Part 18.

The reduction in core size enables the cable diameter to be proportionally reduced making a further saving in the combustible sheath (jacket in USA terminology) materials installed in a warship.

FIG 4

Analysis of wire copper cross sectional area (csa) fitted to a typical Frigate.

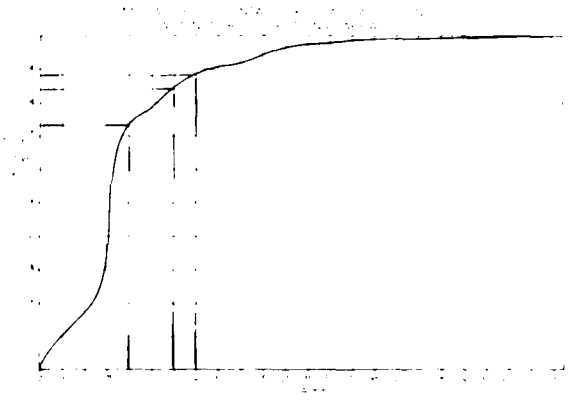


FIG 5

Space saved by the adoption of LFH cable compared with earlier type.



3.2 Calorific Value

This has not been specified in any detail in the applicable performance specifications, since the release of heat is so vastly dependent upon the availability of oxygen. The oxygen index, and the temperature index of materials are checked for the sheath in accordance with specifications Naval Engineering Specification 714, /15 . How these tests on small samples relate to the performance in an actual fire is at the moment a matter of conjecture .

3.3 Materials

A comparison between the LFH materials and those used on earlier types of cables is difficult because the cables were procured to a materials specification for example BS 6234 which limited the performance data to the tensile strength of the jacket and the maximum operating temperature of the polymer. The Limited Fire Hazard cables list performance limits in considerable detail. Only a few manufacturers have been able to meet these limits over the whole cable range.

TABLE 1

Comparison of fire hazard characteristics of three types of cable jacket sheath.

FEATURE	SHEATH MATERIAL			APPLICABLE SPECIFICATION
	CSP	PVC	LFH	
SMOKE	450	92	20 MAX	NES 711
TOXICITY	>5	>10	5 MAX	NES 713
TEMPERATURE INDEX *	250	NA	250 MIN	NES 715
OXYGEN INDEX *	29	NA	29 MIN	NES 714
PROPAGATION *	NK	NK	1hr MAX	(NES 790) BS4066 Pt 3
WEIGHT OF POLYMER PER METER (1)	c150	c150	c60	743-0503 521-6879 521-8431
H Cl RELEASE	29 L. Kgm	75 L. Kgm	0	

* ALL FIRE PROPOGATION FACTORS

3.4 Air Supply

Included in air will be smoke, and it was this factor which was so emotionally highlighted in the Falklands conflict. A fire that can be seen is no longer a fire in a warship, given that the fire fighting teams equipment is functioning. In the past, this is one of the aspects of cable design that has received little detailed attention. Smoke under the influence of air pressure differences can easily penetrate poorly designed cable seals. Therefore the circular profile of a cable is specified in order that the multiple leakage paths apparent in every bulkhead will not allow smoke or fire to promulgate along them. Despite this close tolerancing of the cable circularity, only about two types of glands are smoke, fire, and water-tight before and after a fire. Tests have proved that glands that purport in the commercial world to be water-tight will not perform satisfactorily under warship environmental conditions. Gland sealing materials fail to adhere to the various LFH sheath polymers and it is suspected that some of the volatiles in the polymers react adversely with the cable seal polymers of adjacent cables. This sealing around the cable sheaths becomes even more important in preventing corrosion of the exposed braids of a cable as occurs in the design of an Electrical Magnetic Pulse proof deck gland.

FIG 1

Gland leakage round multiple transit type glands packed with non-approved commercial compounds.



CABLE SYSTEM

4. With the introduction of LFH there has developed a requirement for a cable to be considered as part of a secure, reliable communication and or power transmission system. Previously some cables connecting two pieces of equipment had to use the space that was left after the equipment pipes and ventilation trunking had been installed. Greater importance is now allocated to reducing mutual electromagnetic interference between cable runs and earlier consideration is therefore being given to the definition of cables and cable functions in the design of a warship compartment.

4.1 Cable Wire Installation

A section through the new thin wall insulated type wires shows that a dual wall construction is used by some manufacturers. Thus it is possible to remove an outer coating but not the inner. The insulation is also tougher and not so easy to bend or strip without damaging the conductor strands. The cost of tools and documentation has to be initially funded in order to ensure that a reliable system is installed on a warship. The training video and NES 727 gives guidance to fitters on the proper handling of LFH wires and cables. This is essential if the benefits of space and weight saving are not to be negated by a decrease in the reliability caused typically by cable strands breaking due to nicks being inflicted when fitting terminals or crimps. Similarly, crimping a terminal to these thin wall insulation wires requires a degree of adaptation to new tools when crimping and also a loss of support between the wire insulation and the terminal. Tests have proved that properly installed, the reliability of a connection is equal to that of the earlier types. These precise tests for susceptibility to vibration were initiated after complaints that the survival of LFH thin wall insulated wires was suspect when used on a diesel engine which inherently has a high level of vibration.

FIG 9

Typical damage inflicted on strands of a conductor by incorrect method of stripping insulation.



FIG 10

LFH type termination giving support back to insulation.

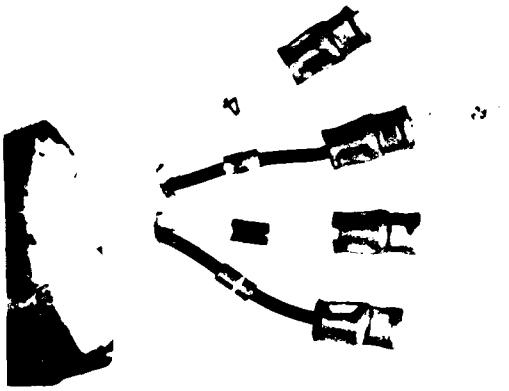


FIG 11

Special tool needed to efficiently strip the insulation from a LFH insulated wire.



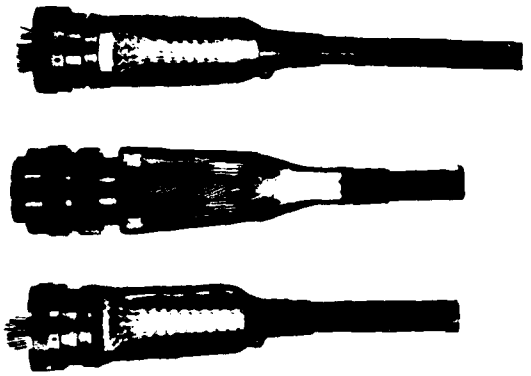
THIN WALL INSULATED WIRE SPECIAL STRIPPING TOOL

4.2 Connectors

Multipin circuit UK warship communication cables are often terminated in circular connectors. Typically at the back of some equipments there may be tens of these all fulfilling an essential weapon control function. The hermatic seal ensuring that humidity does not penetrate the cable has to be a tight tolerance fit over the insulation of every strand. These hermatic seals have had to be redesigned to accommodate the thin wall insulation conductor types.

FIG 11

Circular connector with LFH cable and Heat Shrink back-end.

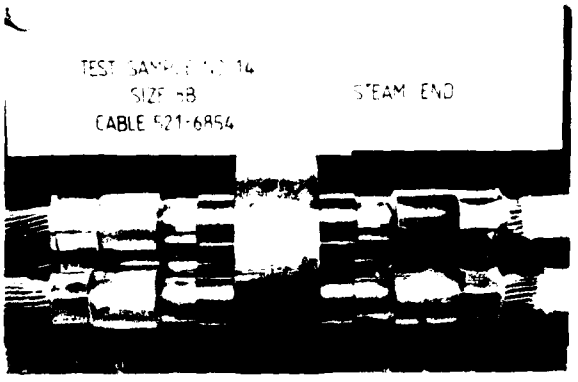


4.3 Submarine Bulkhead Penetrations

The integrity of submarine bulkheads must not be compromised even under the worst conditions of fire, flood and mechanical damage. This is achieved by terminating cables at a bulkhead in a sintered glass seal arrangement. Proving that the new LFH cables would survive the shock, fitting and production rigours passed by the earlier CSP type cables was another on-cost that had to be funded when the limited fire hazard type cables were introduced to a submarine.

FIG 12

Penetrator Sintered Glass insert showing connection to cable.



4.4 Commercial Aspects

Cores, cables, terminal strips, terminations, glands all forming part of the cable system on a warship or a submarine have to be comprehended and the development costs funded when a new cable type is introduced into a warship. The UK has still not developed a complete range of LFH cables (the elimination of smoke from polythene used for the co-axial type cables is a difficult problem). Private venture funding of developments is the preferred option, but this is only possible when the cable company can envisage an expanding and continuous market in which it can recover the development costs. Development of special cables or terminations has to be funded by the Ministry and then the production offered for competitive tender. This process can be lengthy, and resource limited. Hence a UK warship fully compliant with the policy of fitting reduced fire hazard type cables throughout has yet to be launched.

FIG 13

Table showing reduction of LFH cable cost since introduction of competition, compared with similar non-LFH cables.

COST COMPARISONS £'s PER KILOMETRE

CABLE TYPE	YEAR OF PURCHASE			
	1978	1981	1984	1986
0561 521 6840 3 Core 1mm² CSA EPR INSULATED & CSP SHEATHED Specification DGS 212	£ 216	£ 445	£ 493	£ 612
0561 521 8286 3 Core 1mm² CSA SR RUBBER INSULATED CSP SHEATHED Specification DGS 211	NA	£ 1163	£ 1282	£ 1870
0561 743 0476 3 Core 1mm² CSA LIMITED FIRE HAZARD MATERIAL INSULATED & SHEATHED Specifications NES 525,518,526	NA	NA	£ 1600	£ 920

The additional purchase cost of the LFH type cables can be justified by professional assessment of the reduction in hazards and savings in space and weight. The policy of the Ministry is to ultimately fit LFH type cables throughout all new construction warships. This policy is defined in a Defence Council Instruction.

5. My thanks are extended to colleagues in the Ministry and in the cable industry for technical assistance and loan of slide material. My formal thanks are extended to the Ministry of Defence Procurement Executive for giving me access to the resources that have enabled me to write and illustrate this talk.

NOTE

This Document has been approved for public release or sale; its distribution is unlimited.

21 July 1987 - In Draft form

REFERENCES

1. YARD report No 2970 "Report on the review of Fire Incident Records (CONF)".

2. CB.8362(2) "Operation Corporate Ship Damage Reports - Detailed Reports". (SECRET)

3. Defence Standard 61-12 Pt 18 "Wires, Cords and Cables. Equipment Wires Low Toxicity".

4. NES 518 - Requirements for Limited Fire Hazard Sheathing for Electric Cables.

5. NES 525 - Requirements for Electric Cables Thin Wall Insulated - Limited Fire Hazard.

6. NES 711 - Determination of the Smoke Index of the Products of Combustion for small specimens of materials.

7. NES 713 - Determination of the Toxicity Index of the Products of Combustion for small specimens of materials.

8. NES 714 - Determination of the Oxygen Index of small samples of materials.

9. NES 715 - Determination of the Temperature Index of small specimens of materials.

10. NES 502 - Requirements for Electrical Installations.

11. NES 503 - Requirements for Electrical Installation cabling Diagrams and Associated Data.

12. NES 523 - Guide to the Installation of Thin-Wall Insulated Limited Fire Hazard Equipment Wire and Electrical Cable.

13. British Standard 4066 - Flame Retardent Characteristics of Electrical Cables.

14. VSEL Report "An Investigation into the Vibration Performance of LFH Cables.

15. BR4569 - Pattern 608 Connectors.

16. ERA Report 86-0135 "Tests to Determine Current Carrying Capacities for NES 525 in Multilayer Groups".

17. ERA Report 86-0057 "Tests to Determine the Current Carrying Capacities of LFH Cables Installed in Free Air".

18. ERA Report 86-0136 "Procedure for Selecting Cable Sizes in Multi-layer Groups".

19. NES 526 "Requirements for Cables Electric, Rubber Insulated, Limited Fire Hazard Sheathed for General Services".

20. VSEL Report "Electrical tests on submarine Bulkhead penetrations (sintered glass type) at Falcon Testing Laboratories" Ref S/EL/DES405/ 1987.



J A Pownall after graduation joined Industry and was responsible for the 1.5 MW turbo-generator designs for the early nuclear submarines. Subsequently, he designed the 1.25 KVA generators coupled to various diesels for the DLG, T42, Nuclear support ships along with commercial designs. After a short spell designing power station generators up to 900 MW he returned to the Marine environment by joining the MOD where he has variously been employed as a specialist in switchgear, documenting support, submarine battery and more recently cable and termination expert as head of that section. He will shortly retire and devote all his time to raising bees and house DIY activities to the general chagrin of his long suffering wife.

J A Pownall is Head of ME313, Room 102, B Block, Foxhill, BATH BA1 5AB, ENGLAND.

OPTICAL FIBERS IRRADIATED WITH 3800 RADS X- OR GAMMA-RAYS SHOW LARGE ATTENUATION DIFFERENCES

B. H. W. S. de Jong

Corning Glass Works, Corning, NY, 14831

^{60}Co gamma-ray and x-ray irradiated optical fibers show very different degrees of attenuation at equivalent total dosage. The reason for this lies in two different, uncoupled, mechanisms of energy absorption by fibers exposed to these two types of irradiation. Fibers irradiated with gamma-rays show primarily a linear increase in 1300 nm attenuation affecting the vibrational states of the fiber. The principal contributors to this type of attenuation are Compton and Rayleigh scattering. X-ray irradiated fibers show the same phenomenon, but in addition, a strong coupling to the fiber material resulting in substantial generation of E' centers. The principal contributor to this type of attenuation is photoelectric absorption. The generation of E' centers shows a strong dependence on dose rate. Both energy absorption mechanisms are a function of temperature.

Introduction

The effect of adverse environments on the transmission characteristics of optical fibers is an area of active study (e.g. Friebele and Griscom, 1986). Such studies address the effects on fibers of natural environments with low levels of radiation as well as nuclear environments with very high radiation levels.

The characteristic tests for radiation hardness, i.e. the resistance to attenuation variation as a function of radiation, are commonly carried out using high-dose-rate ^{60}Co gamma-ray radiation. It is tacitly assumed that testing fibers with such high energy radiation will give a conservative estimate of their radiation resistance relative to other forms of radiation, e.g. Siegel, 1984.

We shall show in this paper that the assumption that ^{60}Co gamma-ray radiation is the most severe test of fibers for radiation resistance is incorrect and that intermediate energy x-rays are substantially more damaging at equivalent total dosage. We shall show in addition that there is a pronounced dose rate dependence on the observed attenuation in fibers irradiated with x-rays. Finally we shall address issues related to why x-rays are more damaging vis a vis gamma-rays, and what the nature of the defects sites is in irradiated fibers.

Experimental

Two hundred meters of high NA, multimode, 62.5/125 fiber was wound into either 3 or 8 inch diameter coils and put on an aluminum tray in a GE industrial x-ray cabinet with maximum settings of 225 kV, 10 ma. The irradiated coil of fiber was attached to a longer reel of fiber, kept outside the x-ray cabinet, and used as a reference standard. The x-ray source was calibrated using a Victoreen rate meter with probes capable of sampling 25 to 2,500 Roentgen. A Laser Precision Corporation TD-9950 OTDR was used to measure fiber attenuation at 1300 and 1550 nm. Calibration of this instrument against a spectral attenuation bench showed readout differences on the order of 0.01 dB. Higher temperature experiments were carried out using a standard hot plate, the sidewalls of the aluminum tray being insulated by cotton and the top covered with a sheet of mylar.

Results

The results of our experiments are collected in Figures 1, 2, 3, and 4. Figure 1 shows the reproducibility of our experiments on four 62.5/125 fibers from different productions, after exposure to 3,800 Rads at a rate of 70 Rads/minute for 8 inch or 3 inch diameter coils at room temperature, 1300 nm. In Figure 2 the differences in attenuation are shown between 62.5/125 fiber exposed to 3,800 Rads with dose rates varying between 1 and 467 Rads/minute, together with gamma-ray data, whereas in Figure 3 the attenuation spectra after high x-ray total dose are illustrated. Finally in Figure 4, vari-

ation in attenuation as a function of temperature is shown.

Discussion

We shall start the discussion asking why gamma-rays and x-rays show such a large difference in damage. We shall question if these differences can be explained in terms of variations in mass absorption coefficients or if some other mechanism plays a role. Next we shall discuss the effect of irradiation rate on attenuation and show that the radiation response curves for ^{60}Co and x-ray radiation are similar in shape and can be approximated by a first order rate law for a defect species and a linear contribution. Next we shall show that differences in ^{60}Co gamma-ray dose rate do not seem to have a significant influence on attenuation. Finally, we shall suggest an alternative explanation for the geometry of an E' center using ab initio Hartree Fock calculations on the $H_6Si_2O_7$ molecule.

X-ray Versus Gamma-ray Attenuation

X-rays and ^{60}Co gamma-rays differ in that the latter is monochromatic and has a substantially smaller wavelength. The characteristic intensity as a function of wavelength for a copper x-ray source is shown in Figure 5. Here the sharp peaks associated with CuK_α and CuK_β are superimposed upon the background radiation, the bremsstrahlung. This background radiation accounts for about 30 percent of the total emitted intensity and spans a wavelength range, depending on the acceleration voltage used, between 1.6 and 0.05 Angstrom with a maximum around 0.5 Angstrom. The ^{60}Co gamma-ray radiation wavelength on the other hand is 0.01 Angstrom.

Absorption of radiant energy by materials hinges on two main effects, true or photoelectric absorption, incoherent or Compton, and coherent or Rayleigh scattering. Photoelectric absorption predominates in the long and intermediate x-ray wavelength range, whereas Compton and Rayleigh scattering predominate in the small, less than 0.04 Angstrom, wavelength range.

The absorption of beam intensity passing through matter depends on the amount of matter and its chemical composition. Radiation transmission is expressed in terms of the mass absorption coefficient, μ, which is equal to the total linear absorption coefficient divided by the density of the absorber, the material thickness, t, the emergent, I, and incident, beam I_0, by the following relation:

$$I = I_0 \exp(-\mu t)$$

Mass absorption coefficients, which are a function of wavelength, are illustrated in Figure 6 for germanium, silicon, and oxygen (Jenkins and de Vries, 1972). This figure shows that beams with relatively large wavelength will adsorb substantial amounts of radiation whereas beams with wavelength at or below 0.1 Angstrom are almost not attenuated at all. In order to illustrate this more clearly we have calculated the mass absorption coefficients for a 62.5/125 multimode graded-index fiber with a peak concentration of 38 weight% GeO_2 at different wavelengths. The results of this calculation are shown in Figure 7. Thus, in the x-ray regime maximum mass absorption coefficients vary between 64 and 0.2 cm^2/gram. In the gamma-ray regime on the other hand the mass absorption coefficients are below 0.1 cm^2/gram. Thus, in such fiber, x-rays will be absorbed at peak value exp(-64t) times more than gamma-rays.

Another consideration is that the value of the mass absorption coefficients differ, as a function of wavelength, for the three elements considered in this study. These differences are large for the x-ray regime especially at 1.1 Angstrom where germanium has an absorption edge and, as illustrated in Figure 6, tend to become insignificant at very small wavelength. Thus it can be inferred that though x-rays may show enhanced damage due to the presence of germania in a fiber, the same is not necessarily true for gamma-rays.

The transparency of optical fibers for gamma-rays would suggest that no attenuation would be observed in fibers exposed to very high radiation doses. Given the enormous difference in mass absorption, it is surprising that the attenuation difference between x-rays and gamma-rays is relatively small. We, therefore, looked for an alternative explanation to account for the observed differences in attenuation between x-rays and gamma-rays.

In radiation, the unit of adsorbed dose is the rad. This unit is defined as the absorption of 100 ergs of energy per gram of target material. In our x-ray experiments, with maximum dose rate of 505 Rads/minute, the maximum amount of energy per minute impinging upon a fiber is 50,500 ergs or .021 Joule (minute.gram). Whereas, in gamma-ray experiments typically ten times as much energy is impinging upon the target. With the room temperature heat capacity of amorphous GeO_2 and SiO_2 of 44.38 and 37.94 Joule (mole.K)$^{-1}$ respectively (Robie et al., 1979); an average core chemical composition of the fiber of 18 mole% GeO_2 and 82 mole% SiO_2; and a total mass of fiber/km of 27 grams, one can calculate the degree of heating of the fiber. Carrying out this calculation for 37 meter (about 1 gram of glass) of fiber

indicates that 0.57 Joules are needed to raise the fiber one degree in temperature. Thus irradiating 37 meter of fiber for 2 minutes at a dose rate of 5,000 Rads/minute would increase the temperature by one degree. This heating effect is not likely to affect the gamma-ray experiments discussed here markedly because of the short, less than 9 minute, exposure to gamma-ray radiation.

To test heating effects on attenuation, we decided to warm a 62.5/125 fiber on a hotplate and determine at what temperature the fiber attenuation due to x-ray irradiation would become comparable to that due to room-temperature gamma-ray irradiation. The dose rate used was 70 Rads/minute and the total dosage 3,800 Rads. The results in Figure 4 indicate that the attenuation after exposure to 3,800 Rads of x-rays at a temperature of 60°C is about 3.6 dB/km, about 2 dB lower than that found for fibers exposed to ^{60}Co gamma-rays for the same total dose. Linear extrapolation of our x-ray data to 6 dB loss suggests that if one heats a fiber between 30° and 40°C; and irradiates the fiber with a dose rate of 70 Rads/minute at a total dosage of 3,800 Rads one will get an attenuation comparable to that of gamma irradiated fibers with variable dose rate at the same total dosage.

Attenuation Processes in Fibers Exposed to Gamma and X-rays

The difference between gamma-ray and x-ray experiments are most clearly seen in Figure 2. The attenuation versus total dose curves in this fiber can be broken down into two contributions, one of which has a linear dose dependence and the other a higher-order dependence.

Inspection of Figure 2 shows that the x-ray attenuation as a function of total dose approaches a straight line at low dose rates. In addition, at higher doses such linear dependence persists with an increasingly greater slope. Surprisingly, the single gamma-ray experiment for which we have attenuation data as a function of time during irradiation also shows a straight line which nearly coincides with the limiting line of the x-ray experiments. We postulate that this linear dependence reflects the scattering contribution to the overall absorption of radiant energy, whereas the non-linear part indicates the "true" or photoelectric absorption. This assignment of the non-linear contribution to photoelectric absorption is based on the known predominance of this type of absorption for intermediate wavelength x-rays, and the observed attenuation curves in Figure 2 for x-ray irradiated fibers.

Supporting evidence for these two types of absorption comes from comparing the attenuation of fibers before and after irradiation as illustrated in Figure 8. In this figure the ratio of the attenuation before and after irradiation is shown as a function of wavelength. Rather than showing a straight horizontal line, i.e. a homogeneous decrease in transmission of the fiber upon irradiation, this figure shows a wavelength region around 1100 nm where this ratio is smallest. At the smaller wavelength side, as well as the longer wavelength side, damage due to irradiation increases. For comparison, a straight horizontal line is drawn in Figure 8 depicting homogeneous complete recovery after irradiation. The increase of loss in the short wavelength region is, as is well known, due to the formation of color centers affecting the UV edge of the spectrum. This non-linear part reflects the generation of E' centers and follows a first order rate law of 1-exp(-t). For the longer wavelength side, this result is surprising. It indicates that vibrational states are affected by radiation. Comparing this with the ^{60}Co attenuation curve in Figure 2 shows that these vibrational states are predominantly affected by gamma rays. As the three ^{60}Co gamma-ray attenuation results in Figure 2 show, these states are dependent on total dosage but not on irradiation rate.

Additional evidence for these two types of absorption mechanisms comes from comparing attenuation at 1300 and 1550 nm as illustrated in Figure 9. Here we show, that at a high x-ray dose rate, the attenuation at 1300 nm is higher than at 1550 nm, up to a total dose of 3,800 Rads. However at a low dose rate, the attenuation at 1550 nm increases more rapidly than that at 1300 nm. The attenuation crosses over after exposure to 2,100 Rads (3.7 Rads/minute) and 120 Rads (1 Rad/minute). We infer from these results that, at low x-ray dose rates, Compton and Rayleigh scattering become more prominent vis a vis photoelectric absorption.

A consequence of the differences in attenuation mechanism between fibers irradiated with gamma-rays and x-rays might be that recovery rates are different. However this turns out not to be the case as Figure 10 illustrates. In this figure recovery rates are illustrated for gamma and x-ray irradiated fibers. The recovery rates of the gamma-ray irradiated fibers are similar to one another and to those observed for the x-ray irradiated fibers. This reflects a similarity in time dependence of the relaxation process.

The Nature of the E' Center

As discussed above, x-ray attenuation depends on dose rate, exhibits primarily

photoelectric absorption, and is the primary agent for the generation of E' centers. In order to get some better insight into the nature of these defects, we carried out some Hartree-Fock calculations on a $H_6Si_2O_7$ molecule.

The current model regarding E' defect centers in silicas entails the removal of a bridging oxygen atom from Si-O-Si or Si-O-Ge linkages. Concomitant with this removal of an oxygen atom, one of the silicon atoms moves into the plane of the three remaining oxygen atoms becoming trigonally coordinated. The other silicon atom remains approximately in its tetrahedral position. The unpaired electron resides on the latter atom (Griscom, 1986). As we have shown previously (de Jong and Brown, 1980), bending of Si-O-Si linkages actually decreases repulsion between silicon atoms resulting in metal-metal bond formation. In order to test this hypothesis, we carried out some ab initio Gaussian 82 molecular orbital calculations on the closed shell $H_6Si_2O_7$ and $H_6Si_2O_6$+2 molecules [silicon-oxygen bond distance, d(Si-O)=1.62 Angstrom, Si-O-Si angle: 140 degrees] using a minimum basis set. Some preliminary results of these calculations are reported here.

The highest occupied state in a $H_6Si_2O_7$ molecule is calculated to be at -8.19 eV, reasonably close to that observed for vitreous silica (10.5 eV, Greaves, 1978). The total bandgap is on the order of 18.58 eV. As is well known the top of the valence band in SiO_2 consists solely of non-bonding electron density which resides on the oxygen atom. Removal of an oxygen atom, keeping the Si-Si distance, d(Si-Si), fixed at 3.22 Angstrom, leads to a lowering of the top of the valence band to -9.23 eV and the creation of a defect level consisting of antibonding Si 3s, and 3p orbitals at -5.7908 eV. This would suggest that the E' center occurs at 3.44 eV above the UV edge, an estimate which is certainly too low. Reducing the d(Si-Si) to 2.88 Angstrom has two effects. First, it raises the total energy, indicating that a silicon-silicon approach would not energetically be favorable. Second, the top of the valence band now moves to -10.82 eV, with a defect level occuring at -5.91 eV. Thus, in this case, the calculations suggest a defect level at 4.91 eV above the UV edge, substantially closer to the observed E' energy of 5.8 eV (Griscom, 1978). The results of this calculation seem to suggest that approaching silicon atoms give defect states fairly close to those observed. Thus suggesting the possibility of defect sites involving Si-Si metal bonding. More detailed calculations have to be carried out to find the specific minimum in total energy as a function of d(Si-Si) in order to confirm this conclusion.

Summary and Conclusions

Attenuation of optical fibers upon irradiation is caused by photoelectric absorption and Compton and Rayleigh scattering. Photoelectric absorption, primarily associated with x-ray irradiation, causes substantial attenuation upon irradiation, and is strongly dose rate dependent. Compton and Rayleigh scattering increase linearly with total dosage and are primarily associated with ^{60}Co gamma irradiation. Recovery curves show that gamma-ray irradiated fiber and x-ray irradiated fiber recover at similar rates. It is also possible that E' centers may be generated by formation of metal-metal bonding between silicon or germanium atoms. More calculations need to be carried out to confirm this conclusion.

Acknowledgements

Lauren Cornelius and Andrea Sadd carried out the attenuation measurements. Milt Adams provided advice on measurement technique and helped in setting up experiments in the initial stages of this project. Pete Oberlander calibrated the x-ray source.

References

de Jong, B. H. W. S. and G. E. Brown (1980) Geochim. Cosmochim. Acta 44, p. 491.

Friebele, E. J. and D. L. Griscom (1986) Mat. Res. Symp. Proc. 61, p. 319.

Graeves, G. N. (1978) In: The physics of SiO_2 and its interfaces, S. T. Pantelides ed., p. 268.

Griscom, D. L. (1978) In: The physics of SiO_2 and its interfaces, S. T. Pantelides ed., p. 232.

Griscom, D. L. (1986) Mat. Res. Symp. Proc. 61, p. 213.

Jenkins, R. and J. C. de Vries (1972) Worked examples in x-ray analysis, Springer, NY, p. 129.

Robie, R. A., B. S. Hemingway, and J. R. Fisher (1979) Thermodynamic properties of minerals and related substances at 298.15 K and 1 bar (10^5 Pascals) and at higher temperatures. U.S. Geological Survey Bull 1452, p. 456.

Siegel, G. H. (1984) Testing and Characterization of optical fibers in adverse environments. SPIE Tutorial T16, 28th Annual International Technical Symposium.

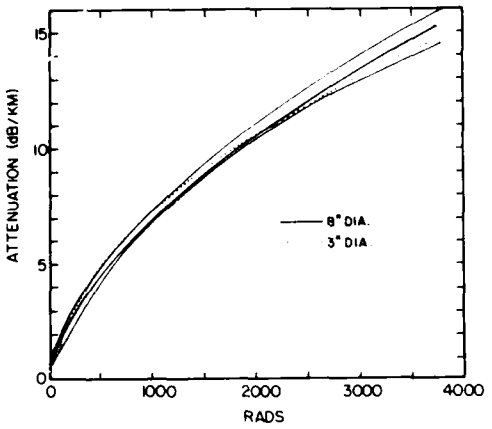


Figure 1. Attenuation at 1300 nm of multimode, high NA, 62.5/125 fiber irradiated at room temperature with 70 Rads/min x-rays for a total dose of 3,800 Rads. Three of the fibers were wound in an 8 inch coil, one in a three inch coil.

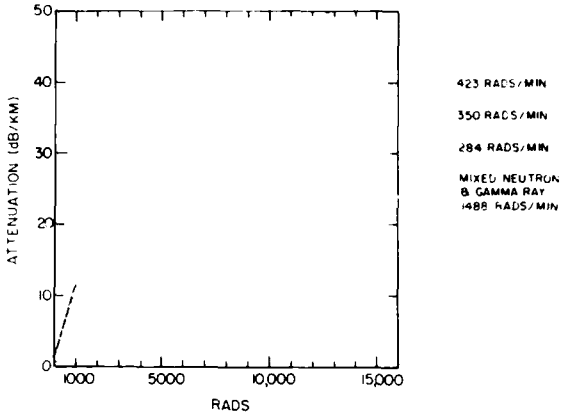


Figure 3. Attenuation at 1300 nm of multimode, high NA, 62.5/125 fiber irradiated at room temperature with varying dose rates and varying total dose.

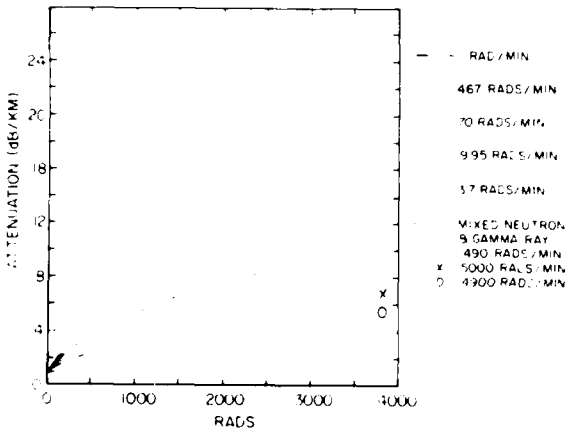


Figure 2. Attenuation at 1300 nm of multimode, high NA, 62.5/125 fiber irradiated at room temperature with varying dose rates for a total dose of 3,800 Rads. The neutron flux for the mixed neutron and gamma-ray experiment is 7×10^{12} neutrons/cm^2.sec.

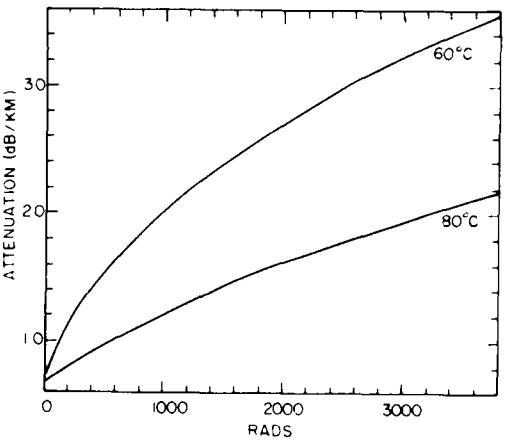


Figure 4. Attenuation at 1300 nm of multimode, high NA, 62.5/125 fiber irradiated at different temperatures with 70 Rads/min x-rays for a total dose of 3,800 Rads.

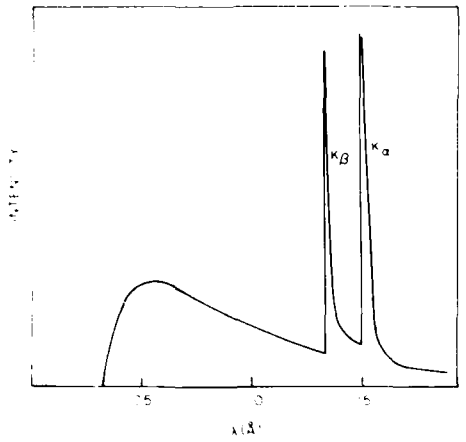


Figure 5. X-ray spectrum of Copper at 35 Kv. The shaded area represents the bremsstrahlung.

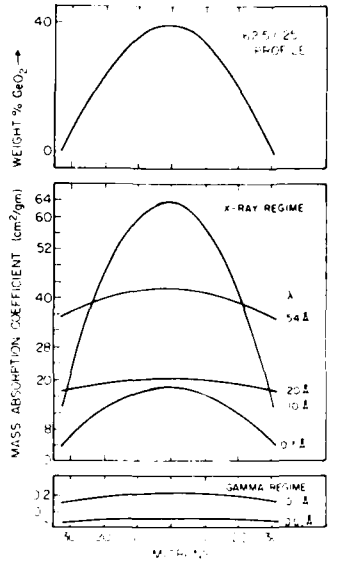


Figure 7. Mass absorption of a graded index, multimode, high NA 62.5/125 fiber as a function of radius and wavelength.

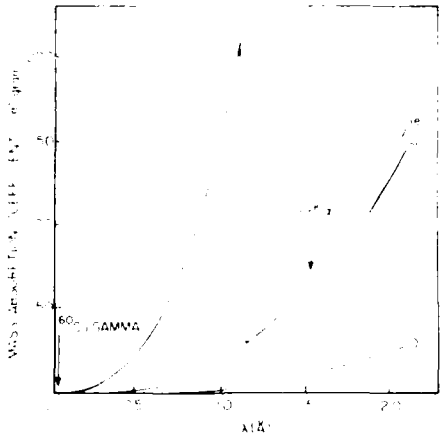


Figure 6. Mass absorption coefficients for germanium, silicon, and oxygen as a function of wavelength.

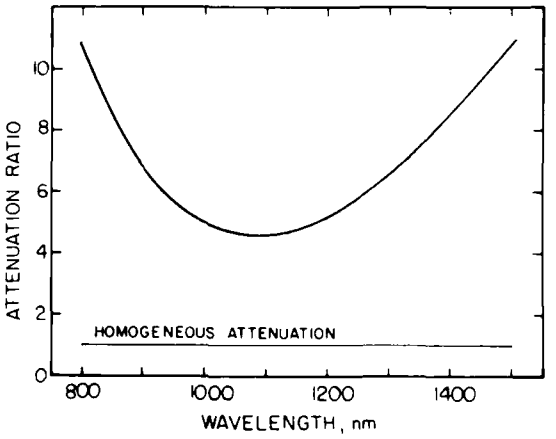


Figure 8. Attenuation ratio for fiber before and after x-ray irradiation as a function of wavelength. Horizontal straight lines indicate homogeneous attenuation over the whole wavelength range. The particular line drawn here at a ratio of 1 depicts complete, homogeneous recovery after irradiation.

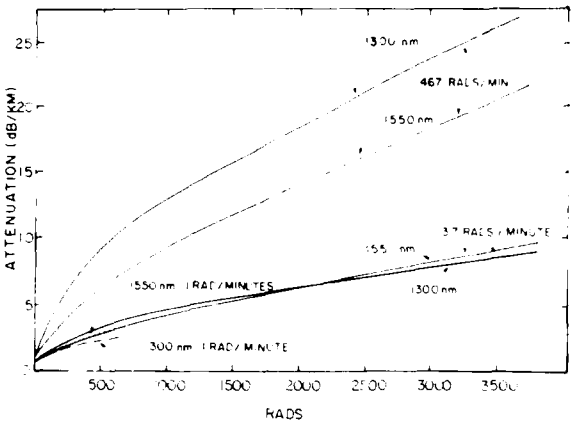


Figure 9. Attenuation at 1300 and 1500 nm of multimode, high NA, 62.5/125 fiber irradiated with different dose rates.

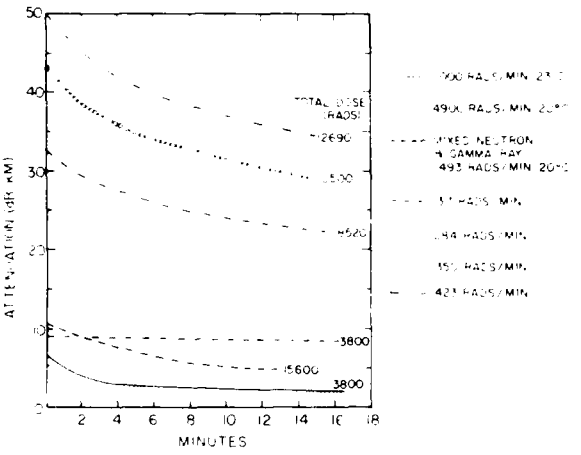


Figure 10. Recovery of multimode, high NA, 62.5/125 fiber after irradiation at different total dose with x-rays, gamma-rays, and mixed neutron-gamma rays.

Biography



Bernard de Jong
Corning Glass Works
Corning, NY 14831

Attended the University of Utrecht, The Netherlands, Iowa State University, Princeton University, the summer school of Uppsala, Sweden, and Stanford University. With a Drs. degree in Geology, a M.Sc. in physical chemistry, and a Ph.D. in mineralogy. Worked as Senior Research Chemist at Occidental Oil Company in Irvine, CA; as manager of Research and Process Technology at Smitweld, The Netherlands, and since 1.5 years as Research Associate in Applied Physics at Corning Glass Works. Principal interest is aluminosilicate chemistry. Author of about 40 papers dealing with MASNMR, emission and photoelectron spectroscopy, and molecular orbital calculations of silicate glasses and solutions.

RADIATION RESISTANT OPTICAL GI CABLES

Akira IINO, Masayuki NIIJIMA, Hirotaka HAYASHI, Hideharu YOSHINO, and Shintaro SENTSUI

THE FURUKAWA ELECTRIC CO., LTD., Ichihara, Chiba, 290 Japan

Summary

Germanium-doped optical fibers free from metal impurities such as phosphorus or alkalies were found to have good resistivity to γ -ray exposure. The induced-losses were dependent on the dose rate, and a similar behaviour to those of multi-mode fibers with pure silica cores. The germanium-doped graded-index optical fibers having high radiation resistivity and bandwidth could be easily fabricated by VAD process, which allowed obtaining radiation resistant cables used for transmission systems with large information capacity in reasonable cost. In practice the graded-index fibers were put into a optical cable which possessed the resistance to heating test of 121°C, 168 hours, and the minimized bend-loss increases were investigated.

1. Introduction

Recently transmission systems with optical fibers have been applied to process control in nuclear power plants.[1] In the optical fibers employed for the systems, the multi-mode step-index design having pure silica glass core was preferred for the reasons of high radiation resistivity and enough bandwidth to transmit the informations in local area. Future optical fiber systems used for the radiation environments, however, will require larger information capacity than those employing conventional step-index optical fibers with pure silica cores. For the increase of information capacity, the radiation resistivity of germanium-doped graded-index fibers is significantly improved in the present paper since those fibers having much higher bandwidth than that in multi-mode step-index fibers can be easily fabricated by VAD process. The optical cable employing the radiation-resistant graded-index fibers with germanium-doped cores is also described.

2. Experimental

A schematic diagram of the apparatus for the measurements of γ -ray induced-loss is shown in Fig.1. The growth of the induced-loss at 0.85 μm was measured "in situ" during ^{60}Co irradiation at 20 ~ 25°C. The light intensity put in the fibers was 3 nW at 0.85 μm.

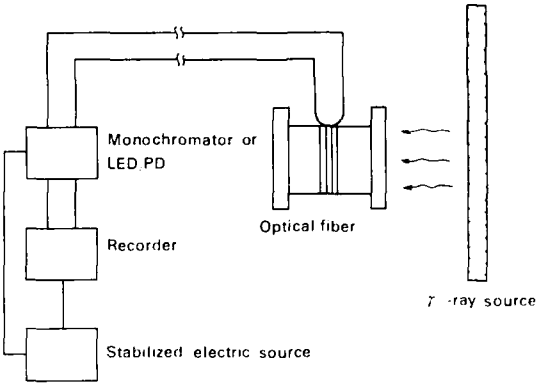


Fig.1 Schematic diagram of the apparatus for the measurement of the γ -ray induced-loss

3. Results and Discussion

3.1 Radiation-resistant graded-index fibers

Multi-mode step-index fibers in which core and cladding composition were pure silica and boron, fluorine co-doped silica respectively had the highest resistivity against γ-ray in silica fibers. Increase of the γ -ray induced-loss was dependent on dose rate, and very small even under the high dose exposure in the step-index fibers as shown in Fig.2. But the bandwidth (~ 30 MHz·km) in the step-index fibers was much smaller than that (~ 1.5 GHz·km) in graded-index fibers.

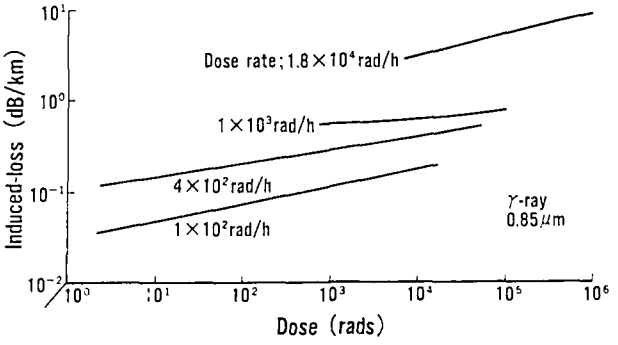


Fig.2 Increase of the γ -ray induced-loss of the step-index (multi-mode) fiber with pure silica core

Although conventional graded-index fibers with germanium-doped cores showed low loss and high bandwidth at 0.85 and 1.3μm, the radiation resistivity of those fibers had been reported to be much lower than that of the step-index fibers with pure silica cores. To improve the characteristics, three kinds of germanium-doped graded-index fibers (core and cladding diameter; 50 and 125μm respectively, $^{+}$ 1.0%) were fabricated, and irradiated by γ-ray. First graded-index fiber with germanium and phosphorus co-doped core fabricated by MCVD process showed the induced-loss-increases in proportion to dose, which were independent on the dose rate as shown in Fig.3. The induced-losses in second graded-index fiber, which consists of germanium doped core part fabricated by VAD process and cladding part of jacketed natural silica tube, are shown in Fig.3. They are also approximately proportional to dose and slightly dependent on dose rate. While third graded-index fiber with the same germanium doped core part fabricated by VAD process and jacketed with synthetic silica tube as cladding part showed γ-ray induced-loss-increases which were non-proportion to dose and dependent on the dose rate as shown in Fig.4.

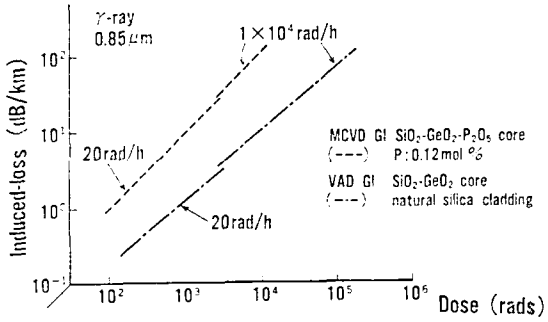


Fig.3 Increase of the γ-ray induced-loss of the graded-index fibers fabricated by (----) MCVD and (---·-) VAD process

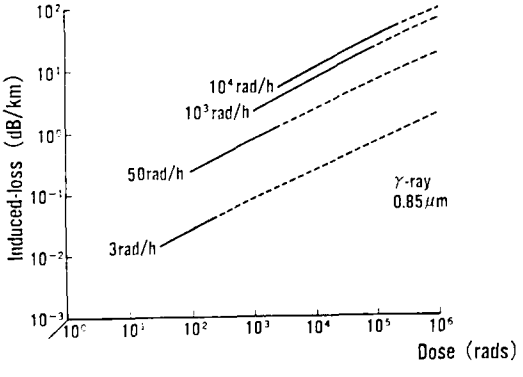


Fig.4 Increase of the γ-ray induced-loss of the graded index fibers with germanium-doped silica core fabricated by VAD process and synthetic silica cladding. The dashed curves represent the increases extrapolated.

The characteristics of γ-ray induced-loss in first graded-index fiber was found to result in the structural change of SiO_2-GeO_2 core glass due to the presence of phosphorus, that deteriorated the resistivity against γ-ray, with electron spin resonance.[2,3] The induced-losses in second graded-index fiber with germanium-doped core part and natural silica cladding part were a similar behavior to that of first graded-index fiber although no phosphorus was contained in second fibers. Some impurities which played a role similar to phosphorus were therefore assumed to exist in the germanium-doped core part of second fiber with natural silica cladding. Impurities in natural and synthetic silica tubes were determined by activation analysis and atomic absorption spectrometry as summarized in Table 1. Concentration of metal impurities such as sodium, potassium, and aluminium in the former was much higher than that in the latter. Additionally the migration of impurities from the jacketed natural silica tube to synthesized core part was investigated by secondary ion mass spectrometry.[3] Sub ppm of sodium and potassium was found in the core part of second graded-index fiber jacketed with natural silica tube while not detected in that of third graded-index fiber jacketed with synthetic silica tube.[3] The impurities were presumed to have migrated by heating during the drawing process. The presence of alkali elements in SiO_2-GeO_2 core glass would also cause the structural change to lower the radiation resistivity.

Table 1 Concentration of impurities in natural and synthetic silica tubes

Type	Impurities (ppm)							
	Al	Ti	Fe	Co	Cr	Na	K	Cl
Natural silica	25	5	0.20	<0.02	<0.10	3.5	1.0	3
Synthetic silica	<0.04	<1	0.15	<0.02	<0.10	0.04	0.001	1000

Na, Cl ; activation analysis
Other elements ; atomic absorption spectrometry

Whereas third graded-index fiber with cladding part of jacketed synthetic silica tube free from the impurities showed γ-ray induced-loss increases which were dependent on the dose rate and a similar behavior to those of pure silica core fibers as shown in Fig.2 and 4. This seemed to be resulted from the same valency of silicon and germanium atom in glass network.

From the above results, the germanium-doped graded-index fiber free from the impurities which had low loss (2.3 and 0.45 dB/km at 0.85 and 1.3μm respectively) and high bandwidth (1.2 GHz·km) was

found to show good resistivity against γ-ray. The dependence of γ-ray induced-loss at 0.85 μm after 10^4 rad of the irradiation on the dose rate are shown Fig.5 in third graded-index fiber. By the extrapolated curve, negligible loss increases at 0.85 μm are expected even after 10^4 rad of γ-ray irradiation in the radiation environments of dose rate of less than 1rad/hour. In addition the loss spectra after 2×10^3 rad of γ-ray irradiation are shown in Fig.6. The γ-ray induced-loss at 1.3 μm was decreased about one order of magnitude compared to that at 0.85 μm in third graded-index fiber. The use of 1.3 μm band is therefore of greater advantage than that of 0.85 μm in optical transmission systems for the radiation environments of high dose rate of more than 10^2 rad/hour.

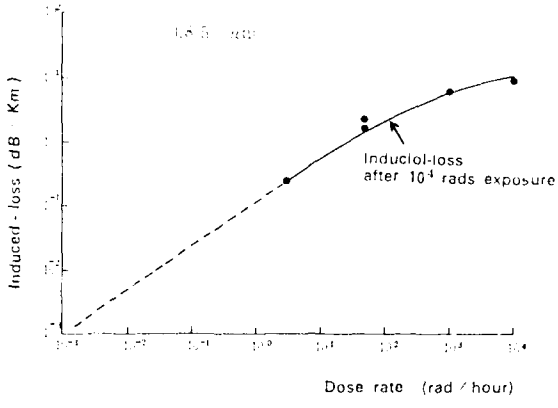


Fig.5 Dependence of the induced-losses after 10^4 rads exposure on the dose rate. The dashed curve represents the induced-loss extrapolated.

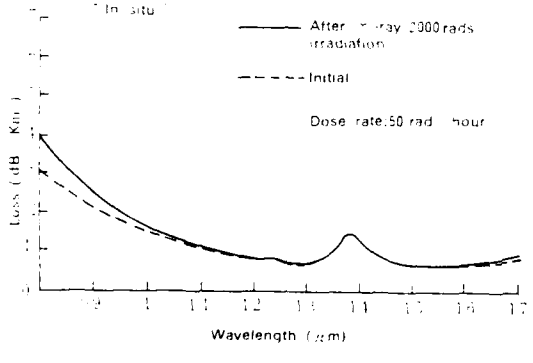


Fig.6 Loss spectra of the graded-index fibers with synthetic SiO_2-GeO_2 core and SiO_2 cladding

3.2 Performance of radiation-resistant optical cable

A non-metalic type cable in which the radiation resistant graded-index fibers were put has been experimentally manufactured. Cross sectional views of this cable is shown in Fig.7. All cable materials were flame retardant. 6 nylon coated fibers and spacers were stranded together around a 2.5 mm diameter FRP on which flame retardant non-corrosive PVC was sheathed. Outer diameter of cable was 11 mm and the weight was 100 kg/cm.

Transmission loss change during cable manufacturing process was negligible small as shown in Fig.8.

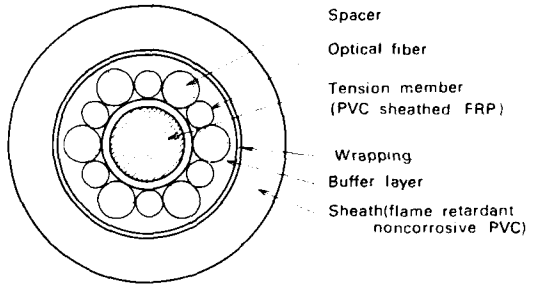


Fig.7 Cross sectional views of experimentally manufactured cables

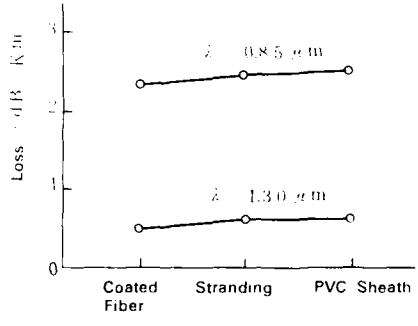


Fig.8 Transmission loss change during cable manufacturing process

In case of applying optical fiber cables to radiation environments, some other characteristics were needed except for the initial transmission and radiation characteristics. Heating, flame retardant, and mechanical tests were carried out in the radiation resistant optical cable.

(1) Heating test; the cable sample of 300 m in length was heated at 121°C for 168 hours. The accelerated deterioration conditions correspond to the life time of a common nuclear power plant. The obtained results are shown in Table 2. The bend-loss increases were less than 0.07 dB/km at 0.85 μm.

Table 2 Loss increases after the heating test

Loop [1] NO.	loss increase at 0.85 μm
1	0.07 dB / Km
2	0.03 dB / Km

1) a piece of three fibers

(ii) Vertical tray flame test; the cable sample of 2.4 m in length was mounted on the vertical tray flame test apparatus as shown in Fig.9. The method employed was in accordance with IEEE383-1974. The cable was impaired to 0.7~0.9 m in length above the torch after the flame was set on. The flame with the optical cable, however, did not reach the upper end of it and disappeared itself when propane gas introduced in the torch was turned off. The obtained results satisfied the above standard.

(iii) Mechanical tests[4] ; such as tensile, vibration bending, twisting, compression, impact, and pulling on pulley were carried out in the optical cable. No loss increases was found after the mechanical tests.

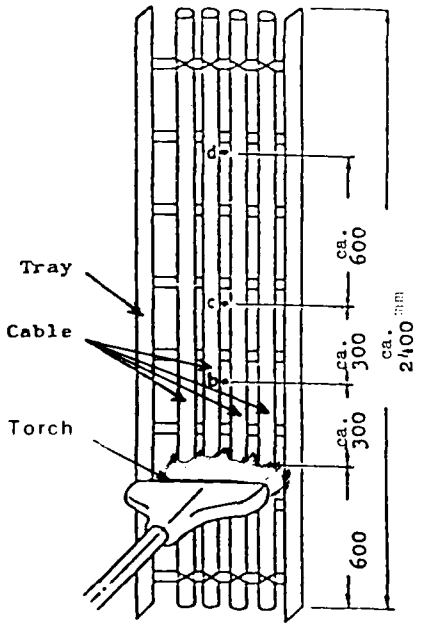


Fig.9 Vertical tray flame test apparatus

4. Conclusions

The present study has shown that γ-ray induced-losses in germanium-doped graded-index fibers free from metal impurities were dependent on the dose rate. The loss increases at 0.85 μm were estimated to be negligibly small even after 10^4 rad of the irradiation if the germanium-doped fibers were exposed to γ-ray of dose rate of less than 1rad/hour. When the graded-index fibers having high bandwidth and radiation resistivity were put into the optical cable and subjected to the heating test of 121°C, 168 hours, the maximum bend-loss increase was less than 0.07 dB/km at 0.85 μm. The optical cables would allow design of transmission systems with large information capacity in radiation environments.

References

1) K. Yahagi (Ed.), "Fiber optics and their applications in nuclear power plants" (Japanese), J. At. Energy Soc. Japan vol. , pp.768-803, 1985.

2) A. Iino, J. Tamura, K. Orimo, K. Kamiya, and M. Ogai, "Defect studies in MCVD fibers", IOOC-ECOC'85 Technical Digest Volume I, p.527.

3) A. Iino, J. Tamura, "Radiation resistivity in silica optical fibers", J. Lightwave Technol., to be published.

4) K. Shibuya, S. Ohashi, Y. Kumazawa, F. Nakane, and T. Kojima, "Environmental characteristics of optical fiber cable for use in nuclear power plants", IWCS'84 Proceedings p.251.



Akira IINO

The Furukawa Electric Co., Ltd.
6 Yawata-Kaigandori,
Ichihara, Chiba, Japan

Akira Iino graduated from Yokohama National University, Yokohama, Japan, where he received in the B.S. and M.S. degrees in 1972 and 1974, respectively. He received the Ph.D. degree in analytical chemistry from Nagoya University, Japan, in 1981.

He joined Furukawa Electric Co., Ltd., Chiba, Japan, in 1981, and has been engaged in research on fabrication and characterization of optical fibers. He is presently a Senior Staff Engineer in Chiba Research Laboratory, Furukawa Electric Co., Ltd.

Dr. Iino is a member of the Insitute of Electronics, Information, and Communication Engineers of Japan.



Masayuki NIIJIMA

The Furukawa Electric Co., Ltd.
6 Yawata-Kaigandori,
Ichihara, Chiba, 290
Japan

Mr. Niijima graduated from Waseda Univ. 1985 with a B.Sc. in electrical engineering. Then he joined The Furukawa Electric Co., Ltd. and has been engaged in development of optical fiber cables.

Mr. Niijima is now a staff engineer of Optical Fiber Transmission Group, Chiba Research Laboratory and Development Division at the Furukawa Electric Co., Ltd. and a member of Institute of Electronics, Information, and Communication Engineers of Japan.



Hirotaka HAYASHI

The Furukawa Electric Co., Ltd.
6 Yawata-Kaigandori,
Ichihara, Chiba, 290
Japan

Mr. Hayashi graduated from Chiba Institute of Technology 1985 with a B.Sc. in precision mechanical engineering. Then he joined The Furukawa Electric Co., Ltd. and has been engaged in development of optical fibers.

Mr. Hayashi is now a production engineer of Optical Fiber Priform, Fiber Telecommunication Division at The Furukawa Electric Co., Ltd.



Hideharu YOSHINO

The Furukawa Electric Co., Ltd.
6-1, Marunouchi 2-chome,
Chiyodaku, Tokyo, Japan

Mr. Yoshino received the B.Sc. and M.Sc. degrees in engineering physics from University of Electro-Communications in 1973 and 1975, respectively. Then he joined The Furukawa Electric Co., Ltd. and engaged in research and development on optical fiber cables.

Mr. Yoshino is now a assistant manager of System Engineering Section of Information and Communication Division at The Furukawa Electric Co., Ltd. He is a member of the Institute of Electronics, Information,and Communication Engineers of Japan, the Japan Society of Applied Physics and the Physical Society of Japan.

Sintaro SENTSUI
The Furukawa Electric Co., Ltd.
6 Yawata-Kaigandori,
Ichihara , Chiba , Japan
His photograph and biography not available at time of submittion

EVALUATION OF HYDROGEN GENERATION FROM OPTICAL FIBER CABLE

Irene Plitz and Paul C. Warren

Bell Communications Research, Inc.
Red Bank, N. J.

ABSTRACT

Hydrogen contamination of optical fiber can cause increased transmission loss due to enhanced H_2 and/or -OH absorptions. It might originate inside a cable from either electrochemical reactions of metals of from degradation of organic compounds. This work is confined to the latter pathway, which could have long term implications on fiber reliability, particularly in harsh loop environments. Hydrogen outgassing was determined by gas chromatography with a lower limit of detectability of 2×10^{-3} ul. Cable components such as UV-cured acrylate protective coatings and waterproofing filling compounds emitted small but variable amounts of hydrogen when heated in air. We believe that the primary mechanism of degradation is thermal oxidation, and suggest that hydrogen is the product of a little-known intramolecular reaction of peroxides to split out the gas *in moderate* yield. We conclude that organic materials that are well stabilized against thermal oxidation might be protected against hydrogen outgassing as well.

INTRODUCTION

It has been established that internal components of optical fiber cables can generate hydrogen gas, either from electrochemical corrosion of metals or thermal deterioration of organic materials.[1-3] The latter pathway is of particular concern because few of the chemical details have been worked out. Since it is known that hydrogen can diffuse into glass, a phenomenon known to increase transmission loss[4-7], the long term reliability of installed optical fiber could be affected. There are two distinct types of hydrogen-related absorption losses[8], namely, (1) those resulting from molecular hydrogen trapped at interstitial sites in the silica network and (2) those due to chemical reaction of hydrogen with oxygen atoms to form -OH groups. Although the first mechanism is reversible, the second is permanent and becomes significantly more pronounced at higher temperatures. The operating telephone companies are currently installing optical cable along major trunk routes and eventually will extend it to the local loop. Long distance and trunk installations are usually protected from the weather, but aerial, pedestal and direct buried plant might be more exposed to the outside environment. Therefore, the issue of long term stability of cable components with regard to hydrogen generation in the local loop is likely to be of great importance to those planning such installations in the future.

Although there are scattered references to hydrogen generation by organic materials within optical cables[9-12], the experimental conditions, results and conclusions vary widely and consequently are confusing. For instance, some investigators have measured hydrogen on cast films rather than actual coated fiber[10,11], while others have determined the gas at temperatures that do not even closely simulate actual cable environments. Since the reported measurements of hydrogen evolution range over several orders of magnitude, it is difficult to decide whether or not significant accumulations will occur over the life of installed cable. On the other hand, several research groups have exposed glass fiber to hydrogen-containing atmospheres and carefully measured transmission losses as a function of time and partial pressure of the gas.[6,7,13,14] Rush[13], et al., for example, have determined that a lower limit of 0.1 atmosphere of hydrogen would be required for any long term increase in attenuation of a single mode optical fiber. Accordingly, we wanted to determine whether that minimum would be approached or surpassed by any cable constructions currently on, or destined for, the market.

In most cases the emphasis on possible hydrogen sources has focused on the organic protective coating over the glass fiber itself, probably because the problem first surfaced with certain silicone coatings. We were more concerned, however, with all organic materials within typical optical cables, including not just the UV-cured acrylate coatings but also the waterproof filling compounds, buffer tube materials and other plastic supports, substrates, and core wraps. To what extent do they participate in filling the cable with small amounts of hydrogen over long lengths of time? Do any of these polymers show induction times, where larger amounts of the gas might arise sometime later rather than those encountered in short term, high temperature screening tests? What is the mechanism of hydrogen formation and can ways be devised to minimize it? For all these reasons, we have examined optical cables from various manufacturers, as well as several random polymeric materials, in order to decide whether long term hydrogen contamination might be a potential field problem.

EXPERIMENTAL

Samples

Coated glass fibers and filling compounds were obtained from a variety of manufacturers, generally in the form of optical cable. Samples were removed from the cable for testing unless otherwise noted. While most of the samples examined are commercially available, they may or may not represent actual products used in the current market. A random selection of polymers and long chain alkanes was also examined. All cable components tested are listed in Table 1.

TABLE 1
Identification of Samples Analyzed for H_2 Generation

	Sample	Type	Source
Optical Fiber			
1.	A	cable	Field installed
2.	B	cable	uninstalled
3.	C	cable	"
4.	D	cable	"
5.	E	cable	"
6.	F	cable	"
7.	G	cable	"
8.	H	cable	"
9.	I	fiber sample	"
10.	J	fiber sample	"
11.	K	fiber sample	"
Filling Compounds			
1.	A	petrolatum (silicate filled)	
2.	B	oil extended TPR	
3.	C	oil extended TPR	
4.	D	silicone oil based	
5.	E	low molecular weight polyisobutene	
6.	F	petrolatum (silicate filled)	

Hydrogen Analysis

Hydrogen generation was monitored by withdrawing 500 microliters via syringe from the headspace of 300-500 mg samples contained in 2, 5, or 50 ml vials. The vials were sealed by crimping with polytetrafluoroethylene-lined silicone septa. Empty vials as well as those containing an equivalent amount of bare glass fiber were sampled concurrently with vials containing coated fiber samples to serve as controls. The syringe full of gas was injected into a Shimadzu GC 9A gas chromatograph equipped with a thermal conductivity detector (TCD). The analysis was performed under the following conditions: column, 6 feet by 1/8 inch SS packed with 5A molecular sieves or 80/100 mesh Carbosphere at 35° C and an Argon carrier gas flow rate of 30 ml/min; detector, 125° C; injection port, 125° C. Hydrogen was identified by comparison of its retention time with that obtained from samples of pure H_2 (Alltech Associates Calibration Gas; 100% H_2, 1000ppm H_2 in N_2, and 100ppm H_2 in N_2). The peak was further confirmed by changing the carrier gas from argon to helium to look for changes in the relative thermal conductivity of the hydrogen peak. A sample of optical fiber and one of filling compound were analyzed by mass spectrometry. The technique consisted of placing a weighed amount of each sample in a quartz chamber, evacuating the system to better than 10^{-6} mm, and heating to 100° C for ten minutes. The evolved gases were collected and analyzed. Sampling continued until a constant hydrogen level was reached or no more H_2 could be detected.

The effect of oxygen on the rate of hydrogen evolution from fiber C and filling compound F, which generate relatively substantial amounts of H_2 over a short period of time, was monitored. Samples were placed in standard head space vials and one set of samples was kept in a N_2 environment and another in O_2. At the beginning of the test period, each vial contained at least 95% of the desired gas as determined by GC.

RESULTS AND DISCUSSION

Hydrogen Analysis

A typical chromatogram of the headspace above a coated fiber which had been aged for three weeks at 100°C is shown in Figure 1. It shows the presence of two sharp peaks with retention times separated by only 0.15 minutes. Peak 1 was tentatively identified as helium. Published chromatograms[11] of fiber coatings aged in He also showed two peaks separated by that same retention time. The chromatograms from the control samples which contained air or bare fiber exhibited a similar peak. Even an injection of 500 ul of laboratory air yielded a peak with a comparable retention time, accounting for 0.04% of the total area. In a few cases, the He area fraction was as high as 0.3%, although there is no obvious explanation why this number should differ from the above control samples. In fact, one would not expect to see this peak at all since He only occupies 0.0005% of total air volume. This apparently anomalous finding is not understood by us at present.

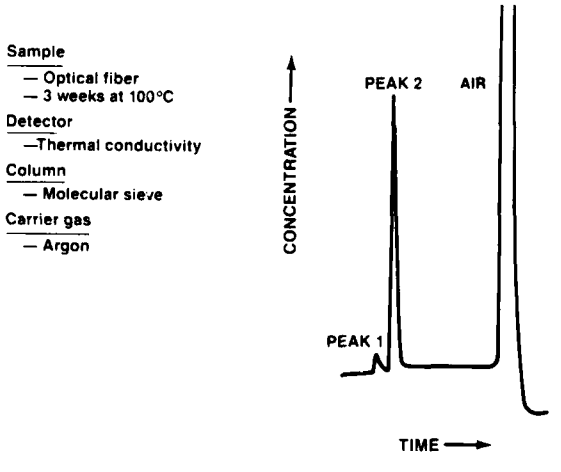


FIGURE 1

Peak 2 was ascribed to hydrogen by comparison with the retention time of of a known sample. The minimum detectable amount was determined to be 2 x 10^{-3} ul. To further verify the assignment, a change of carrier gas from argon to helium resulted in the expected diminution of the area of Peak 2 and reversal in its direction. An independent mass spectrometer analysis also confirmed that the headspace sample contained hydrogen, although it was quantitatively ambiguous because the method itself generated background hydrogen.

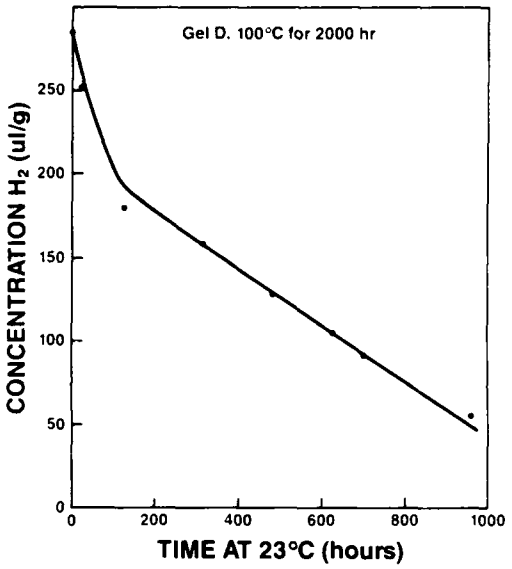


FIGURE 2

Hydrogen Outgassing from Organic Materials

Figure 2 illustrates a problem that was never fully solved, namely, the slow escape of hydrogen from the septum-sealed glass containers. Accordingly, our reported amounts of the gas are probably understated from those that were actually evolved. The volumes of gas generated from optical fiber coatings were varied but small, depending on the cable manufacturer, design and vintage. Table 2 shows that as little as no (<0.01 ul/g) to as much as several hundred ul/g were measured for coated fibers aged at 100° C for time periods up to about one month. In a few cases, hydrogen was generated initially but subsequently ceased evolution. In others, an induction time was necessary before the gas was detected. The table also lists the quantities of hydrogen produced by several waterproof filling compounds. They were all based on either petrolatum, thermoplastic rubber or silicone oil, and three of the five did not give off any detectable hydrogen. One of the other two, however, evolved close to 1 ml/g, which, when combined with the fact that relatively large amounts of this ingredient are incorporated into the cable, could represent a serious source of the contaminant.

TABLE 2

Amount (ul/g) of H_2 Evolved from Optical Fiber Coatings or Waterproof Filling Compound after Aging at 100°C

	Sample	Days at 100° C					
		3	7	15	23	31	38
COATINGS							
	A	0.4	0.9	136	...	...	...
	C	18	75	204	334	466	399
	E	<3	3.4	8.9	...	...	...
	G	73	...	0.2	...	...	...
	I	0.3	0.2	0.2	5	7	...
	J	ND	ND	ND	ND	ND	ND
FILLING COMPOUNDS							
	A	ND	ND	ND	ND	ND	ND
	B	ND	ND	ND	ND	ND	ND
	C	ND	ND	ND	ND	ND	ND
	F	0.4	0.6	11	49	137	70
	Yellowed F	0.3	110	331	728	478	473

ND = Not Detected (< 2×10^{-3} ul)

Table 3 compares the results of this work with others in the literature. The most noteworthy conclusion is the great variability in numbers. For example, the data published by Aoki[10], et al. were much larger than the others (eg., 730 vs. 0-56 ul/g), while those from Okagawa[11], et al. seem markedly smaller. Presumably these differences result from dissimilarities in experimental conditions, materials, cable geometries and analytic techniques. Especially interesting is the large difference in the amounts of hydrogen generated from cured films on glass slides relative to those from analogous materials on coated fiber. While there is no apparent reason for this discrepancy, it illustrates that meaningful data need to be collected from "real world" samples.

Randomly selected plastics and low molecular weight hydrocarbons were also aged at 100 °C and their evolution of hydrogen with time was monitored. As shown in Table 4, very small or undetectable amounts were evolved in most cases, but in two of them the opposite was true. A C_{24} straight chain hydrocarbon and polyisobutylene both showed significant hydrogen evolution. We conclude that the potential for hydrogen evolution is highly dependent on the chemical structure of the organic material.

TABLE 3

Amount (ul/g) of H_2 Evolved by Fiber Coatings and Filling Compounds as Reported in the Literature

	Aging Conditions									
Temperature	80°C		100°C					200°C		
Time	17h	1000h	4h			100h	320h	4h		
Atmosphere	air	air	air	O_2	N_2	air	air	O_2	N_2	air
Fibers										
Aoki[10]	-	-	730	-	-	36	-	-	-	-
Okagawa[11]	-	-	-	-	-	-	-	-	-	4.1
A	2.4	-	-	-	-	-	-	-	-	-
G	ND	<1	56	-	-	2	2	-	-	-
B	-	-	<3	-	-	4	136	-	-	-
E			<3	-	-	<3	9	-	-	-
C	ND	ND	9	0.1	.04	30	204	-	-	-
Filling Compounds										
Okagawa 1	-	-	-	-	-	-	-	03	< 002	-
Okagawa 2	-	-	-	-	-	-	-	02	< 002	-
Barnes[9]	-	6.9	-	-	-	-	-	-	-	-
Yellow F	-	-	2	-	124	320	-	-	-	-
F	-	-	<1	ND	ND	<1	11	-	-	-
D	-	-	< 03	-	-	ND	<2	-	-	-
Films										
Aoki	-	-	2.2	-	-	-	-	-	-	-
Okagawa	-	-	0026	0003	-	-	-	-	-	-

Partial Pressure of Hydrogen within Optical Cables

Hydrogen evolution in units of ul of gas/g of polymer had to be converted to partial pressure within a cable to predict whether the accumulation would ultimately affect transmission. In order to make a simple conversion we made the following two assumptions: (1) Since many cables are sheathed with metal, any accumulated hydrogen would be retained within the cable, and (2) other plastic cable components such as polyethylene, polyester, filling compound, etc. would not significantly impede diffusion of the small hydrogen molecule. Table 5 lists the results of calculations of partial pressure of hydrogen in several optical cables, where the worst cases of hydrogen evolution from coatings and filling compounds were utilized from Table 3. In all cases, the coating contribution was well below the minimum 0.1 atmosphere hydrogen concentration. However, the filling compound contribution accounted for

TABLE 4

Amount (ul g) H_2 Evolved from Miscellaneous Compounds

COMPOUND	ul g H_2 2H	24H	48H	144H	240H
C_{24}	ND	.54	2.09	17.45	-
LDPE	ND	.22	.47	.75	.99
HDPE	ND	.58	.42	.53	ND
Nylon 6	ND	.50	.49	.47	.66
PMMA	ND	.14	.56	-	ND
Polyisobutylene	.88	19.78	14.55	20.38	14.70
Epoxybutane	ND	.13	.38	ND	ND

TABLE 5

Calculated Partial Pressure (atm) of H_2 Found in a Worst Case Analysis of an Optical Fiber Cable

	Partial Pressure (atm)		
Sample	Coating	Filling Compound	Cable Total
A	002	04- 09	042- 092
C	009	ND	009
E	< 001	0 49	0 49
G	006	ND	006

ND - Not Detected

possible concentrations of 0.5 atmosphere, well above this minimum. While we do not believe that half of the cable volume would ever be filled with this contaminant, the order of magnitude of accumulation is clearly similar to the threshold value. Since most current optical cable constructions contain such waterproof filling compounds, it is essential to understand the reasons for hydrogen evolution from these materials.

Mechanism of Hydrogen Formation

Several studies[9,10] have shown that hydrogen generation is greater in an oxygen atmosphere than that in an inert environment. Our results, summarized in Table 6, are in agreement with those findings. Samples of waterproof compounds aged in oxygen or air atmospheres generated substantially more hydrogen than those under nitrogen. Often an induction time was evident before hydrogen was observed; this was especially true for filling compounds. Both coatings and filling compounds always seemed to turn color to yellow or amber before hydrogen was observed; such discoloration is typical of oxidation products such as quinones and other conjugated systems. In one instance we extracted a filling compound with methanol and reduced the induction time from >3 months to 48 hours. All of these observations suggest that hydrogen formation correlates with oxidation. The implication is that materials that are well-stabilized against thermal oxidation will also be protected from outgassing of hydrogen.

TABLE 6

Amount (ul/g) H_2 Evolved from Coating or Filling Compound Exposed to O_2 or N_2 Environments

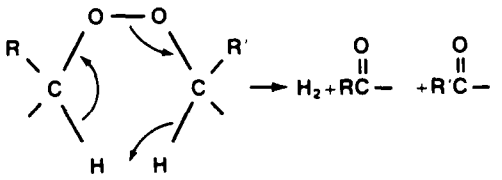
	Days at 100°C											
	3		7		15		23		31		38	
Sample	N_2	O_2	N_2	O_2	N_2	O_2	N_2	O_2	N_2	O_2	N_2	O_2
Fiber C	1	24	2	50	3	75	--	110	6	138	9	142
Compound F	ND	ND	2	1	3	44	24	63	3	44	24	63

ND = Not Detected

There are relatively few references in the literature to reactions of organic materials which yield hydrogen. As mentioned earlier, some silicone polymer coatings produced hydrogen but they degraded by a unique mechanism that does not apply in this case[3]. Hydrogen often appears as a by-product of gamma or electron beam irradiation of polymers because of formation of H· radicals, but this intermediate appears unlikely in our low energy, thermal experiments. Nevertheless, Barnes[9], et al. have proposed such a mechanism as the source for the contaminant:

$$H\bullet + RH \longrightarrow H_2 + R\bullet$$

It is not obvious how this mechanism explains the observed sensitivity to oxidation. We therefore suggest that hydrogen in this instance is a product of peroxides, which are known to yield the gas via an intramolecular cyclic transition state.[16] Liquid sec-butyl peroxide, for example, is reported to give hydrogen in 30% yield when aged at 100 °C:



Organic peroxides are known to be termination products of oxidation that arise from the coupling of peroxy and alkyl radicals. If the amount of hydrogen measured over some time period were, say, 250 ul/g, and the reaction yield were 30%, then the accumulated concentration of peroxide precursor would have to be at least 0.04 mmoles/g, too small an amount to detect.

Temperature Dependence of Hydrogen Formation

Recently published work[12] has revealed that at elevated temperatures (>25 °C), permanent transmission loss rapidly becomes more significant with irreversible formation of -OH groups in the silica network. This is of concern because many of the optical fiber installations in the loop will be aerial, and temperatures of 50 °C or higher are regularly encountered in this configuration. While much of our laboratory work was conducted at 100°C, recent experiments at 80 °C have shown that hydrogen is produced at this temperature as well, albeit much more slowly.

CONCLUSIONS

1. A reliable method has been found to analyze optical cable components for the evolution of hydrogen, with a minimum sensitivity of 2×10^{-3} ul.

2. The amounts of hydrogen generated from optical

fiber cable components varied over a wide range depending on cable materials, design and vintage. In no case was the amount evolved from protective coatings on fiber sufficient to cause long term transmission loss. On the other hand, some waterproof filling compounds produced significant amounts of the contaminant after long term aging, which, in one case, demonstrated that increased attenuation might be a real possibility.

3. The mechanism for hydrogen formation is thought to be related to thermal oxidation of alkyl hydrocarbon chains in the coatings and waterproofing gels. A mechanism based on the thermal decomposition of di-secbutyl peroxide, which splits out hydrogen in 30% yield, was proposed as a precedent for the source of optical fiber hydrogen contamination.

4. It is clear that optical cables can be manufactured with components that give off virtually no hydrogen, and it is equally clear that the opposite is also true.

ACKNOWLEDGMENTS

Contributions of samples from W.T. Anderson and M.A. Saifi are gratefully acknowledged. Thanks are also due to D.L. Allara for helpful discussions concerning peroxide decompositions.

REFERENCES

[1] P. L. Philen and C. H. Gartside, III, *IWCS*, 1984, 33, 415.

[2] K. Noguchi, N. Uesugi, and K. Ishihara, *Electron. Lett.*, 1984, 20, 897.

[3] W. E. Dennis, D. A. Sierawski, and D. N. Ingebrigtson, *IWCS*, 1984, 33, 401.

[4] K. Mochizuki, Y. Namihira, and H. Yamamoto *Electron. Lett.*, 1983, 19, 743.

[5] K. J. Beales, D. M. Cooper, J. D. Rush, *Electron. Lett.*, 1983, 19, 917.

[6] N. J. Pitt, A. Marshall, et.al., *Proceedings of 10th European Conference on Optical Communications*, Stuttgart, 1984, 308.

[7] P. J. Lemaire and A. Tomita, *Proceedings of 10th European Conference on Optical Communications*, Stuttgart, 1984, 307.

[8] K. Abe, R. Lowe, and E. Thomson, *IWCS*, 1984, 33, 424.

[9] S. R. Barnes, S. P. Riley, et.al., *Fourth International Conference on Plastics in Telecommunications*, London, 1986, 24/1.

[10] T. Aoki, H. Sano, F. Suzuki, *ibid.*, 23/1.

[11] S. Okagawa, M. Nishimura, et.al., *ibid.*, 22/1.

[12] G. McKay, W. Cousineau, et.al., *IWCS*, 1986, 35, 307.

[13] J.D. Rush, K.J. Beales, et.al., *10th European Conference on Optical Comm.*, Stuttgart, 1984.

[14] N.J. Pitt, A. Marshall, *Electron. Lett.*, 1984, 20, 512.

[15] S.R.Barnes, S.P.Riley and S.V.Wolfe, *Electron. Lett.*, 1985, 21, 897.

[16] R. Hiatt and S. Szilagyi, *Can J. Chem.*, 1970, 48, 615 and references cited therein.



Irene Plitz is a Member of Technical Staff in the Polymer Chemistry and Engineering Research District of Bell Communications Research, Inc. She received her B.S. in Chemistry from Morgan State University in 1970 and then directly joined Bell Laboratories. Since transferring to Bellcore in 1984 her interests have centered on the chemical and structural analysis of degraded organic materials.



Paul C. Warren is Manager of the Polymer Chemistry and Engineering Research District in Bell Communications Research, Inc. at Red Bank, N.J. After receiving a Ph.D. in organic chemistry from Cornell University in 1969, he joined Bell Laboratories where he pursued research in polymer flammability, test methods and PVC technology. He attained his present position in January, 1984 and his interests now center on the use and reliability of polymeric materials in telecommunications products.

MODAL NOISE DUE TO SECOND MODE INTERFERENCE IN SINGLEMODE FIBER SYSTEMS

Max Brandtner
Dieter Schicketanz
Chris Eoll

Siecor Corporation
489 Siecor Park (RD)
Hickory, NC 28603-0489

SUMMARY

In a singlemode fiber system, the second mode - LP11 - is generated either at a transmitter with overfilled launch conditions, or at an imperfect connection. If the LP11 mode is coupled back into the fundamental mode at a subsequent connection, interference may occur and noise may result. To avoid Modal Noise problems, the LP11 mode must be sufficiently attenuated before it reaches the next connection. With a matched clad fiber, a bend of short length does the job. For a depressed clad fiber, a significant fiber length is required to achieve sufficient attenuation of the LP11 mode.

1. INTRODUCTION

In a singlemode fiber system, the second mode LP11 is generated either at a transmitter with overfilled launch conditions or at an imperfect connection with coupling between the fundamental mode and the LP11 mode. If the LP11 mode is coupled back into the fundamental mode at a subsequent connection, interference occurs if the difference in optical path length of the two modes is less than the coherence length of the light. Slight variations in laser wavelength vary the phase difference between the interfering waves, and Modal Noise results. However, no Modal Noise is induced in the system at a perfect subsequent connection where no power is transferred from one mode to the other /1/.

2. LP11 MODE AND CUTOFF WAVELENGTH

At lower wavelengths, singlemode fibers behave like multimode step-index fibers, and more than one mode can be excited. To find an estimate of the lowest possible wavelength for singlemode transmission - the cutoff wavelength - procedures with two spectral scans using two different bend diameters (d1 = 280 mm / d2 = 60 mm) or a single bend (d = 280 mm) and a multimode reference are standard (EIA draft FOTP-80).

At this cutoff wavelength, λc, that is associated with one loop having an (arbitrary) diameter of 280 mm, the LP11 mode has a defined attenuation of ≈20 dB /8/. At shorter wavelengths the attenuation of this mode is lower; at longer wavelengths this mode will see a higher attenuation.

Due to the bending loss characteristics of matched clad fibers, the attenuation of the LP11 mode depends on bend diameter: the larger the diameter, the longer the effective cutoff wavelength. By reducing the diameter of a single loop from 280 mm to 80 mm, measurements on several fibers have shown shifts in the effective cutoff around 80 nm. In contrast, the LP11 mode attenuation for depressed clad fibers is approximately constant over a broad range of diameters.

The different bending loss characteristics of the two fiber designs can be explained by considering how bending stress affects the refractive index profiles and the effective indices of refraction of the LP01 and the LP11 modes. Figure 1 shows the refractive index profile of a matched clad singlemode fiber and the effective indices of refraction of the LP01 and LP11 modes below cutoff wavelength without fiber bending.



Fig. 1 Profile of a Matched Clad Fiber along with Effective Indices of Refraction of the LP01 and LP11 Modes ($\lambda<\lambda c$)

The index of refraction of the cladding goes down on the outside of a bend. The local effective index of either mode also decreases by an amount that is proportional to the distance from the fiber axis; however, the change in the effective index is larger than the change in the cladding index. Leakage of power from either mode will occur where the cladding index exceeds the local effective index of refraction /10/, and the closer the crossover to the fiber axis, the greater the leakage. The net effects of these changes in index are shown schematically in Fig. 2, where, for simplicity, the effective indices are shown as horizontal lines.

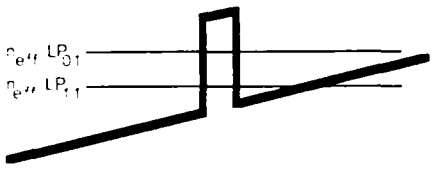


Fig. 2 Profile of a Matched Clad Fiber with Bending Stress (Outside of bend is to the right)

The sharper the bend, the higher the leakage of power, the higher the attenuation for the LP11 mode and the shorter the effective cutoff wavelength.

A different behavior is observed for singlemode fibers with depressed cladding. Without bending stress, the refractive index profile and the effective indices of refraction for the LP01 and LP11 modes are shown below:

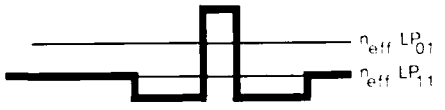


Fig. 3 Profile of a Depressed Clad Fiber with Effective Indices of Refraction of the LP01 and LP11 Modes ($\lambda<\lambda c$)

As in the case of matched clad fibers, the refractive index of the cladding on the outside of a bend decreases under bending stress (Fig. 4). But the local effective index of each mode decreases even more, and leakage of power will occur where the cladding index exceeds the local effective index of refraction for a given mode.

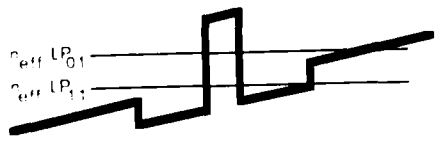


Fig. 4 Profile of a Depressed Clad Fiber with Bending Stress (Outside of bend is to the right)

At the upward step on the right-hand side of Fig. 4, the local effective index of refraction of the LP11 mode crosses the profile at the same radius for a certain range of bend diameters. Thus the attenuation of the LP11 mode is approximately constant within this range and the effective cutoff wavelength is approximately independent of bend diameter. Cutoff measurements using single loops in 2 m of fiber have shown that bend diameters from 280 mm to 60 mm lead to effective cutoff wavelengths that range within $\pm$10 nm. (Fig. 5) /3/.

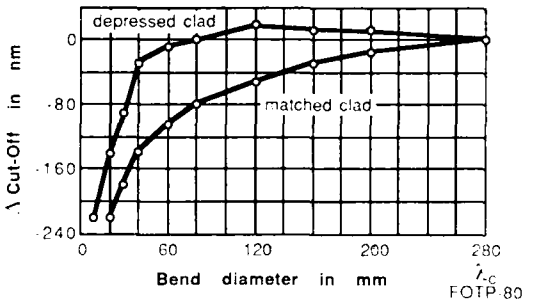


Fig. 5 Shift of Effective Cutoff Wavelength for a Single Loop in 2m of Fiber ($\Delta n \approx 0.35\%$)

Even though the measurements shown in Fig. 5 were made on fibers with a delta of about 0.35%, the character of the curves is the same for other typical fibers.

3. SIMULATED REPAIR SECTION

The following set-up was used to simulate a repair section and to determine the power penalty caused by Modal Noise (Fig. 6). Bit-Error-Rate (BER) measurements using this set-up are described in the next section.

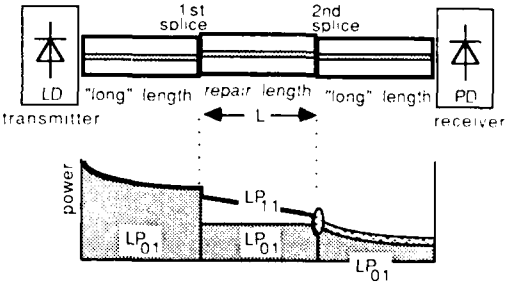


Fig. 6 Simulation of a Repair Section

A short repair length L (matched clad or depressed clad fiber) is connected using splices of high transmission loss between two lengths of matched clad fiber. To simulate long lengths, bends with 25 mm diameter attenuate the LP11 mode in the first and third fiber lengths. Therefore, only the fundamental mode can reach the first splice and the receiver. The loss at the second splice was 3 dB in every case.

Due to the misalignment at the first splice, the LP11 mode is generated; then, because of the misalignment at the second splice, the LP11 mode is coupled back into the fundamental mode. If the length of the fiber between the splices is short enough for the difference in optical path length of the two modes in that section to be less than the coherence length of the light, interference is generated at the second splice.

A short length of straight matched clad fiber or a sufficiently short length of depressed clad fiber does not significantly attenuate the LP11 mode, so most of its power reaches the second splice where part of the power is coupled back into the fundamental mode. Due to small changes of the laser wavelength, the relative phase of the two modes and the interference at the second splice varies, and Modal Noise is induced (see Appendix). If the LP11 mode was somehow attenuated, only the fundamental mode would reach the second splice; no constructive or destructive interference could occur and no additional noise would be added to the system.

Measurements on matched and depressed clad fibers have shown different slopes for the attenuation of the LP11 mode vs. wavelength /2,3,4,9/. "Slopes" of ≈24 nm/decade[dB] and ≈68 nm/decade[dB] were measured here and elsewhere for matched clad fibers and depressed clad fibers, respectively /4,8,9/.

Once the cutoff wavelength is known, the attenuation of the LP11 mode can be calculated for any other wavelength as follows:

$$\alpha_{11}(\lambda) = \alpha_{11}(\lambda_c) \cdot 10^{\left(\frac{\lambda - \lambda_c}{\text{slope}}\right)}$$

where λ and λ_c are the operating and cutoff wavelengths in nm, respectively, "slope" is in nm/decade[dB], $\alpha 11(\lambda)$ is the attenuation of the LP11 mode in dB/m and $\alpha 11(\lambda_c)$ is the attenuation of the LP11 mode at its cutoff wavelength as measured under standard condition i.e. an attenuation of approximately 20 dB divided by the length of fiber under bend ($\pi \times 0.280$ m here) for matched clad fibers, or by the total fiber length (2 m here) for depressed clad fibers.

4. BIT-ERROR-RATE MEASUREMENTS

Measurements were made using the set-up described in the previous section. The matched clad and depressed clad fibers used as repair lengths had cutoff wavelengths of 1304 nm and 1302 nm, respectively. Bit-Error-Rate (BER) was measured as a function of offset at the first splice, bend diameter in the repair length, and distance between the splices, all at a wavelength of λ = 1275 nm. The computerized set-up consisted of a Northern Telecom laser source, a Lasertron receiver and a Tautron BER analyzer.

4.1 Distance between the Splices

Measuring interesting BER values as function of distance between the splices requires the use of light with a coherence length that is longer than the difference in optical path length of the two modes for the distances involved. The laser transmitter available for this study allowed lengths up to approximately 0.7 m only. By cutting back a fiber, no Modal Noise could be measured until the fiber length was <0.8 m.

4.2 Offset at First Splice

Using precise stepping motors, the fiber offset at the first splice was adjusted in 1-µm steps within a range of ±3 µm. Transmission and attenuation with these offsets are shown in the figure below for the matched clad case using a half loop of 280 mm bend diameter, so that the effective cutoff wavelength in the repair section was 1310 nm. (This is, of course, an unrealistically large diameter for applications in the field.)

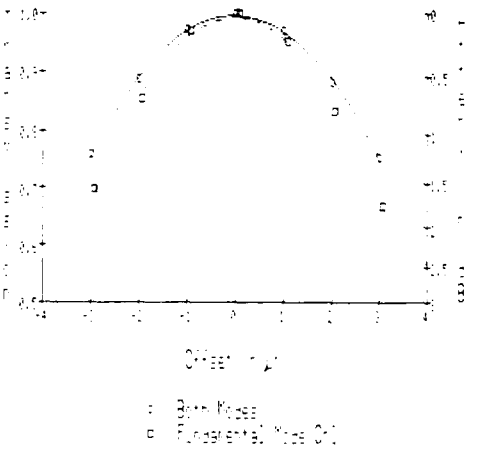


Fig. 7 Splice Loss Due to Fiber Offset
Matched Clad Fiber
1275 nm Laser Wavelength

	Both modes	Fundamental mode only
Bend Diameter (mm)	280	60
Effective Cutoff (nm)	1310	1200

When the matched clad fiber between the splices was more severely bent (d = 60 mm, one loop), the LP11 mode no longer reached the second connection (Fig. 7, fundamental mode only). No such transmission loss measurements were made using the depressed clad fiber because the LP11 mode in that fiber has about the same attenuation for the two bend diameters used.

When the fiber ends at the first splice are aligned perfectly, no additional noise can be seen at the receiver output (Fig. 8, center trace). After misaligning the fiber ends in either direction, additional noise can be observed in the '1' states. Because of the 100% laser modulation, no such noise is seen in the '0' states (Fig. 8, upper and lower traces).

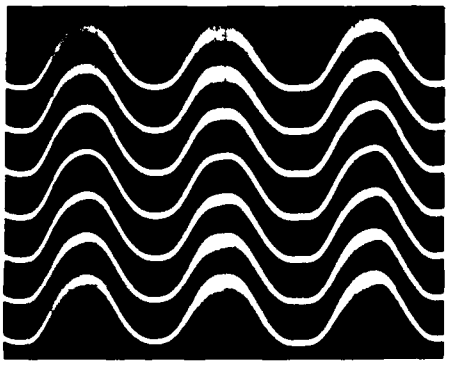


Fig. 8 Modal Noise as Function of Fiber Offset in µm (top to bottom):
+3, +2, +1, 0, -1, -2, -3
Matched Clad Fiber
1310 nm Effective Cutoff Wavelength
1275 nm Laser Wavelength
280 mm Bend Diameter, half Loop

For each fiber type, BER as a function of offset and receiver power level was measured with the automated set-up described above, and lines were fitted through the measured points by the computer. To obtain an effective cutoff wavelength slightly above 1300 nm for the matched clad fiber, an unrealistic bending condition within the repair section of a half loop of 280 mm diameter had to be used. As shown in Fig. 9, for low BER (10^{-9}) the curves spread out and high power penalties are measured. Equivalently, as also expected from theory /6/, the BER cannot be improved by higher input power at the receiver if the power of the LP11 mode at the second splice is too high.

Similar curves were obtained for the depressed clad fiber when the length of that fiber was chosen so that its effective cutoff wavelength was also slightly above 1300 nm.

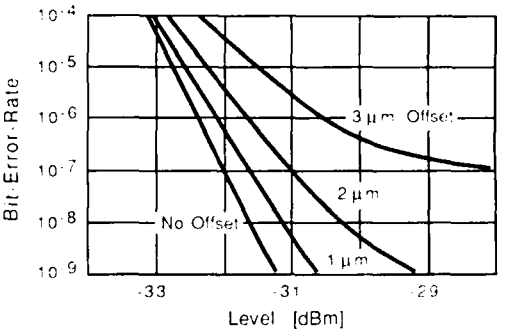


Fig.9 Bit-Error-Rate as Function of Offset at the First Splice, Second Splice 3 dB
Matched Clad Fiber
1310 nm Effective Cutoff Wavelength
1275 nm Laser Wavelength
280 mm Bend Diameter, half Loop

The next section will look into results for realistic bending conditions within a repair section.

4.3 Power Penalty vs. Bend Diameter in Repair Length

The fiber between the splices (0.7 m for each fiber design; see section 4.1) was bent in single loops with different diameters, and BER as a function of bend diameter was measured. The different behavior of matched clad and depressed clad fibers can be seen clearly in Fig. 10 which shows power penalty as a function of bend diameter. For realistic bending conditions within repair lengths (bend diameters of, for example, 60 mm to 100 mm), the Modal Noise power penalty for the matched clad design was zero. This is in sharp contrast to the results for the depressed clad design. The traces correspond well to the shift in cutoff wavelength as a function of bend diameter as shown for each fiber type in Fig. 5.

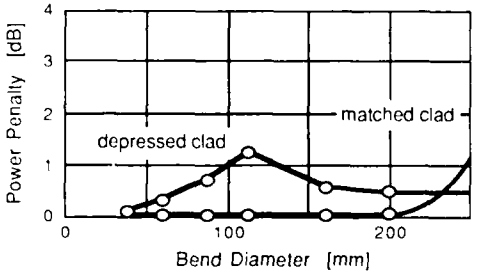


Fig.10 Power Penalty as Function of Bend Diameter
BER = 10^{-7}
3 µm Offset
Cutoff Wavelength: 1302 nm Depressed Clad
1304 nm Matched Clad
Laser Wavelength: 1275 nm
Fiber Length: 0.7 m

5. CONCLUSION

To prevent Modal Noise in singlemode fiber systems, the LP11 mode must be attenuated before it reaches the second connection of a repair section or the connection to a pigtail that is attached to a transmitter using overfilled launch conditions.

A sufficient attenuation can be achieved:

- in matched clad fibers by moderate bends over short lengths;
- in depressed clad fibers by significant fiber length only, over a wide range of bend diameters.

REFERENCES

1. S. Heckmann
'Modal Noise in Singlemode Fibers operated slightly above Cut-Off'
Electronic Letters, vol. 17, no. 14, page 499, July 1981

2. K.A.H. van Leeuwen, H.T. Nijhuis
'Measurement of higher-order mode attenuation in singlemode fibers: effective Cut-Off wavelength'
Optic Letters, vol. 9, no. 6, June 1984

3. K.A.H. van Leeuwen, H.T. Nijhuis
'Length and curvature dependence of effective Cut-Off wavelength and LP11-mode attenuation in singlemode fibers'
Technical Digest, Symposium on Optical Fiber Measurements 1984, Boulder, page 11

V.S. Shah
'Effective Cut-Off wavelength for singlemode fibers. The combined effect of curvature and index profile'
Technical Digest, Symposium on Optical Fiber Measurements 1984, Boulder, page 7

4. L. Wei, C. Saravanos, R.S. Lowe
'Practical upper limits to Cut-Off wavelength for different singlemode fiber designs'
Technical Digest, Symposium on Optical Fiber Measurements 1986, Boulder, page 121

5. D.G. Duff, F.T. Stone
'Measurements of modal noise in siglemode lightwave systems'
OFC '85, TU 01, page 52, 1985

6. K. Ogawa, R.S. Vodhanel
'Measurements of mode partition noise of laser diodes'
IEEE Journal, QE-18, page 1090-1093, 1982

7. F.M. Sears, I.A.White, S.P. Gentry
'Cable Cut-Off wavelength and attenuation of the LP11-mode'
OFC '86, TUL 19, page 66, 1986

8. W.T. Anderson, T.A. Lenahan
'Length dependence of the effective Cut-Off wavelength in 'singlemode fibers'
Journal of Lightwave Technology, vol. LT-2, no. 3, June 1984

9. A. Tomita, L.G. Cohen
'Leaky-mode loss of the second propagating mode in single-mode fibers with index well profiles'
Applied Optics, vol. 24, no. 11, June 1985

10. L.G. Cohen, D. Marcuse, W.L. Mammel
'Radiating leaky-mode losses in singlemode lightguides with depressed index claddings'
IEEE Journal of Quantum Electronics, vol. QE-18, no. 10, Oct. 1982

Appendix

Heckmann /1/ was the first to describe Modal Noise at splices in singlemode fiber systems. Prior work related to multimode fibers where it is difficult to quantify this issue. Heckmann assumed that a first splice would generate an LP11 mode that would interfere with the LP01 mode at a second splice and generate Modal Noise if system parameters changed (Fig. 6). While slow changes such as in temperature or in cable position are absorbed by a receiver's automatic gain control circuit, fast changes like mode partitioning of the laser /6/ degrade system performance. In /6/ a so-called k-factor for mode partitioning was introduced. Its value is zero for perfect lasers and a maximum of 1 for "bad" lasers. This factor usually increases with bit rate, so, even with improved lasers, the use of higher bit rates will probably keep the value of k in the range from 0.2 to 0.5.

Because the type of laser to be used in a system is not usually known ahead of time, worst case Modal Noise should be assumed; the LP11 mode should be attenuated sufficiently to handle the worst case situation. Heckmann /1/ assumed no attenuation for the second mode. This is not realistic. Including LP11 attenuation in his theory, the following overall transmission efficiency for the LP01 mode for the system presented in Fig. 6 can be calculated:

$$\eta_T = \eta_{011}\eta_{012} + \eta_{111}\eta_{112}\, 10^{-\frac{\alpha_{11} L}{10}} + 2\sqrt{\eta_{011}\eta_{012}\eta_{111}\eta_{112}}\; 10^{-\frac{\alpha_{11} L}{20}} \cos(\Phi) \qquad \text{(A1)}$$

η_{011} Power Transmission Efficiency of LP_{01} Mode at Splice 1

η_{012} Power Transmission Efficiency of LP_{01} Mode at Splice 2

η_{111} Power Coupling Efficiency from LP_{01} to LP_{11} at Splice 1

η_{112} Power Coupling Efficiency from LP_{11} to LP_{01} at Splice 2

α_{11} Attenuation of the LP_{11} Mode in dB/m
(Attenuation of the LP_{01} Mode is assumed negligible)

L Length of Repair Section in m

$\Phi = (\beta_{01} - \beta_{11})L$ Phase Difference of LP_{01} and LP_{11} Modes

Let us assume that, for splices with less than 2 dB of loss, most of the power lost by the first mode is transferred to the second mode. Let us also assume that, at splice 2, the coupling efficiency from LP01 to LP11 is at least approximately equal to that from LP11 to LP01. Then Eq. (A1) can be rewritten as (cf./5/)

$$\eta_T = \eta_1\eta_2 + (1-\eta_1)(1-\eta_2)\ 10^{-\frac{\alpha_{11}L}{10}} + 2\sqrt{\eta_1\eta_2(1-\eta_1)(1-\eta_2)}\ 10^{-\frac{\alpha_{11}L}{20}}\cos(\Phi) \qquad (A2)$$

where, $\eta_1(\eta_2)$ is the transmission efficiency of the LP01 mode at splice 1(2). The last term is the time varying term that generates the so-called Modal Noise.

The worst case S/N-ratio can be calculated as in /1/ using Eq. (A2):

for $\eta_{1,2} > 0.5$ or $\alpha_{11}L > 10$ dB

$$S/N = \sqrt{\frac{\eta_1\eta_2}{2(1-\eta_1)(1-\eta_2)}}\ 10^{\frac{+\alpha_{11}L}{20}} \qquad (A3)$$

Correspondingly,

$$\alpha_{11}L = 20\log_{10}\left(\frac{S/N}{\sqrt{\frac{\eta_1\eta_2}{2(1-\eta_1)(1-\eta_2)}}}\right) \qquad (A4)$$

A S/N-ratio of about 15 dB will lead to a system power penalty of only 0.02 dB, while 11 dB will add 1 dB of penalty /4,5,7/ . One could multiply these S/N-ratios by the k factor /5/, but in general it is safer not to do so.

Splice losses up to 1 dB (η>0.8) and a Modal Noise S/N-ratio of 15 dB imply that the second mode must be attenuated by about 20 dB. At a wavelength equal to the effective cutoff wavelength of the repair section, the second mode is attenuated by 19.3 dB; therefore, the Modal Noise penalty will be negligible as long as the laser wavelength is approximately equal to or greater than that effective cutoff wavelength.

To simulate an overfilled jumper, one may take the splice transmission efficiency of the first "splice" to be 0.33; this implies that the second mode contains twice as much power as the first. Thus, if the connector on a laser pigtail has a loss of 1.5 dB, the LP11 mode in the pigtail must be attenuated by 27 dB to overcome the overfilling [Eq. (A3)]. This implies that the effective cutoff should be lower than the operating wavelength. For a matched clad fiber, a loop of 60 mm in diameter in the transmitter pigtail would provide plenty of margin in a system operating at 1250 nm and using a fiber with a measured λc of 1330 nm (per FOTP-80).

For depressed clad fibers, a special fiber with a low λc ($\lambda c \approx 1200$ nm) is commonly used to reduce Modal Noise where the pigtail length is less than one meter.



M.J. Brandtner

Siecor Corporation
489 Siecor Park
Hickory, NC 28603
U.S.A.

Max Brandtner was born in Munich, West Germany in 1955. He received his M.S. degree in Electrical Engineering from the Fachhochschule in Munich in 1979. For two years he was employed in the Sales Department of the Communication Cable Division of Siemens Corporation as a Sales Engineer. Beginning in 1981, he worked for five years at the Development Department for fiber optic cables where he was particularly involved in the design and implementation of fiber optic test equipment.

Mr. Brandtner has been working for Siecor Corporation since 1986 and is currently Supervisor, Measurement Systems.



C.K. Eoll

Siecor Corporation
489 Siecor Park
Hickory, NC 28603
U.S.A.

Christopher K. Eoll was born in Thunder Bay, Ont., Canada in 1940. He received a B.Sc. degree in physics and an M.Sc. degree in theoretical physics from Queen's University, Kingston, Ont., Canada in 1962 and 1964, respectively. Then in 1967 he was granted a Ph.D. degree in mathematical physics by the University of Toronto, Ont., Canada. Subsequently, he spent two years as a Postdoctoral Fellow at the University of Sussex, Brighton, England and the International Centre for Theoretical Physics, Trieste, Italy.

From 1968 to 1977 he was employed by Canada Wire and Cable Ltd., where his final position was Product Development Manager for the Communication Products Div. He joined Superior Cable Corp. in 1977 as Technical Director. At present, he is Manager, Scientific Staff for Siecor Corporation.



D.W. Schicketanz

Siecor Corporation
489 Siecor Park
Hickory, NC 28603
U.S.A.

Dieter Schicketanz was born in Puerto Montt, Chile in 1943. He received an Ingeniero Civil in Electrical Engineering from the University of Chile, Santiago, Chile in 1968, and a Ph.D. in Physics from the University of Graz, Austria in 1974. In 1970 he joined Siemens Research Laboratory in Munich where he worked in several different areas of optical communications.

Dr. Schicketanz worked for Siecor Corporation from 1984 to 1987, most recently as Manager, Computers, Systems & Measurements. Currently, he is again with Siemens AG in Munich. He has written many papers on subjects related to optical communications.

LOSS SPREAD IN SINGLE-MODE FIBERS DUE TO OH-ION CONCENTRATION AND TRANSMITER-WAVELENGTH FLUCTUATIONS

R. Díaz de la Iglesia, D.J. Lao Soriano,
E. Tobías Azpitarte, J. Rueda García

TELEFONICA. Subdirección General de Tecnología
3, Beatriz de Bobadilla. 28040-Madrid (SPAIN)

ABSTRACT

The influence of hydroxyl (OH) on the attenuation average (X) and std. deviation (S) of GeO_2-doped fused silica single-mode fibres are evaluated by a Monte-Carlo sampling proccess. The results take also into account: (1) the laser source wavelength distribution, and (2) the allowed intervals for the optical source wavelength. As the main results it has been found that absorption peaks of 2 dB/Km, and even more, at the 1.39 microms hydroxyl band could be beneficial for decreasing the fibre attenuation spread. In addition, a practical criterium is proposed to quantify the maximum acceptable OH contents in fused silica fibres.

Introduction

The optical attenuation of fibre paths between repeaters suffers fluctuations due to the changes in the source lasing wavelength and the non-flat performance of spectral fibre attenuation. Wavelength variations of most presently available laser sources fall within 60 to 80 nanometers, resulting in wavelength related power and loss measurement errors (see Figure 1).

Both, source wavelength and fibre attenuation variations lead to an uncertainly (Fig. 2) in optical paths attenuation which have practical implications from a number of viewpoints, including: power budget desing; acceptance tests during optical cable deployment and system installation; and, later on, in measurements performed for maintenance. As a result, the desing, installation and maintenance phases may be impacted.

Most of the extrinsic reasons, introduced during fibre manufac-turing, influencing the spectral fibre attenuation have been reduced as low as to get them undetectable except for the OH ion absortion[1-4]. Under manufacturing conditions OH fibre contents in the range from 10 to 70 ppb are achievable, leading to a median attenuation figure around 0.35 dB/Km ($\simeq$ 1.3 μm) in single-mode silica based fibres[5].

Contrary to the general line of thinking which dictates that the lower the OH contents the better fibre performance, in this paper it is hypothesized that a limited amount of OH content is not detrimental but beneficial from a practical viewpoint.

This paper investigates both: a) the influence of OH ion content in reducing the attenuation fluctuation due to source wavelength variations; and, b) the influence of OH fibre contents in the discrepancies araising when fibre attenuation is described by using either a statisticall (i.e., average and std. deviation) or a worst-case value within a wavelength operating window.

For testing that hypotesis we limit our scope to silica based GeO_2-doped single-mode fibres operating at the 1.3 μm region. Using a Monte-Carlo technique the fibre attenuation is statistically described (in terms of averge and std. deviation) and related to three independent variables: the OH fibre content; the source lasing wavelength distribution, and, the wavelength operating window. We have made some assumptions: the OH contents is in the range between 10 to 70 ppb; the average laser wavelength is between 1300 to 1310 nm, showing a standard deviation between 3.3 to 13.3 nm. Finally, the wavelength operating regions considered was 1285-1330 and 1280-1340 nm.

As main results we have found:

1) some quantity of OH - ion content leading to 1-2 dB/Km (or even larger values, depending upon the nature of source wavelength variations) absortion at 1.38 μm is beneficial for decreasing the attenuation uncertainly (see figs. 6-8).

2) the maximum acceptable OH content should be that at which the attenuation at the upper-side of the wavelength operating region (i.e. 1330 or 1340 nm) aquals that at the lower-side (i.e. 1285 or 1280 nm). Otherwise, discrepancies as large as 10% and even larger may arise between a statistical or a worst-case description of the fibre attenuation within the wavelength operating window.

The following sections describe the purpose and the study method, the results, and some final

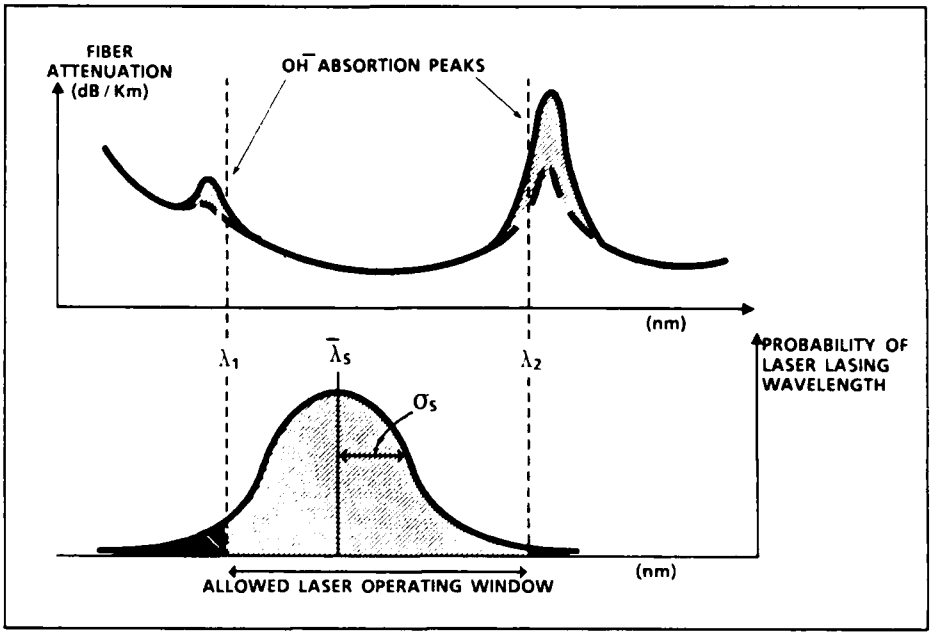


Figure 1 - Variations in the lasing wavelength of lasers and in the spectral attenuation of silica fibres.

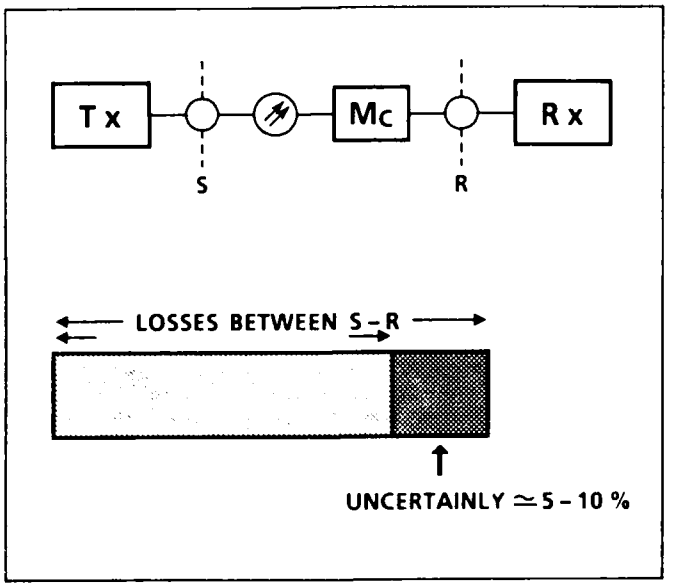


Figure 2 - Uncertainly of fibre attenuation between repeaters.

remarks. Under the later section is given a recomendation to quantify the maximum acceptable OH quantity in fused silica fibres for telecomunication.

Purpose and study method

Objetive and scope

In this paper it is hypothesized that a limited quantity of hydroxyl (OH) impurity is beneficial for reducing the attenuation fluctuations due to the optical source lasing wavelength variations. In addition, we will explore to what extent the quantity of OH impurity impact on discrepancies which may arise when fibre attenuation is described either statistically or by employing a worst-case approach (worts value within a given wavelength operating region).

We have limited our scope to silica based GeO_2-doped single-mode fibres operating at wavelength windows around 1.3. μm.

Study method

For testing the above hypothesis, the attenuation average (X) and the std. deviation (S) was determined as a function of the hydroxyl (OH) quantity in GeO_2-doped silica based fibres. Such statistical parameters (X and S) were determined employing a Monte-Carlo sampling process[7]. The OH quantity has been taken as an independent variable. The study considers two additional independent variables: the statistical distribution of the source lasing wavelength, and the allowed operating wavelength window (see fig. 3).

Some assumptions have been made. The range of hydroxyl quantity explored has been limited up to the one which produces an absortion of 2.5 dB/Km at the 1.38 μm band. That is reasonable because in current fibre plants hydroxyl quantity of fibres is well under 70 to 100 ppb.

Dealing with the source lasing wavelength, we assume a population average in the range from 1300 to 1310 nm. For lasers available from stock, most manufacturers offer products made from VPE or LPE showing a nominal lasing wavelength of 1300 nm. More recently, a number of manufacturers are producing lasers showing a wavelength average more closely located to the nominal zero-dispersion wavelength of fibres. Being zero-dispersion generally specified with a nominal value near to 1310 nm.

The source lasing wavelength may change due to a number of reasons, including: manufacturing, ageing and temperature. Ageing variations have been reported[8] to be of some few nanometers, in addition in most situations the lasers operate under controlled temperature environment. Therefore, the more significant cause of changes in lasing wavelength is due to the manufacturing processes. Employing a LPE grow process, a wavelength distribution of $\pm$ 3.2 nm within a wafer has been recently reported[8]. However, from wafer to wafer the variations may be one order of magnitude larger. For the purpose of our study we assume the lasing wavelength distribution to be in the range from $\pm$ 10 nm to $\pm$ 40 nm ($\pm$ 3 x σ_S) interval). In addition, we assume the distributions show a Gaussian shape as proposed by Sears et al.[9] (see last paragraph under discussion heading).

Finally, we consider two particular wavelength windows around 1.3 μm: one from 1285 to 1330 nm and other from 1280 to 1340 nm. This is because such windows are receiving particular attention wthin some large national and international standarization bodies, engaged with works on fibre optic digital line systems, such as the EIA or the CCITT-COM XV.

Model of the wavelength dependance of fibre attenuation

An acurate equation which would describe the wavelength dependance of fibre attenuation is required to perform the Monte-Carlo simulation. In the following lines it is indicated the nature of those factors which influence the spectrum of fibre attenuation and, then, a specific aquation is proposed for describing the total loss of high silica fibres. Emphasis is given to the hydroxyl (OH) impurity absortion.

Impurity Hydroxyl (OH) absortion. Both, transition metals and Hydroxyl (OH) ions may rise to strong absortion peaks. In the first stage of developing low-loss fibres, the transition metal ions were major loss origings. However, by using the "soot process", it is no longer a serious problem to reduce the transition metal impurities. In recent low-loss glasses, the absortion due to these ions can not be detected. The major reason of the success is that halides of S_i, and dopants, are used as the raw materials of glass: the halides of transition metal are easily removed from the raw materials of glass by a single destilation.

The hydroxyl (OH) ion in silica glass gives rise to strong absortion[10] at 2.72 μm, which is assigned to fundamental stretching vibrational mode. The overtones and the combinations tones with S_i - O - S_i bending vibration mode were observed[10,11], including those at 1.38 and 1.24 μm which may influence the fibre performance when operating at the 1.3 microms wavelength region. The nature and magnitude of OH formation appeared to depend in a very conplicated way of the particular type of silica, its past history, and the conditions of an eventual treatment with H_2. Analysis of the spectral shape of the OH Raman and IR absortion bands in pure silica[12,13], indicated that the bands consisted of

several unresolved components that could be associeted with different types of sites for OH formation within the glass.

The absortion peaks shift sligtly by doping the pure silica with other oxides. Measurements of OH formation in doped-silica showed a OH absortion spectrum which includes an additional overtone absortion peak centered at 1.41 μm in GeO_2 doped silica[13,14]. More recently, the absortion peak at 2.86 μm of GeO_2 glass has been reported, as well as a peak shifting to longer wavelength (from the 2.72 μm peak in pure silica) when increasing the GeO_2 doping content[15].

In addition, when OH is formed by H_2 treatment of fibers, it is found that the Ge (OH) increases more rapidly than the S_i (OH). Furthermore, the amount of OH formed depends on the phosphorous concentration[16].

Intrinsic absortion factors. Under this paragraph it will be considered the multiphonon and the ultraviolet absortions, and the Rayleigh scattering loss as well.

The phonon and multiphonon absortion processes increase fibre attenuation in S_iO_2 based fibres. The multiphonon absortion coefficient of pure silica shows strong absortion bands at 9.1 μm, 12.5 μm and 21 μm. At shorter wavelength the absortion coefficient is given [17].

$$A_{MP} = 7.81 \times 10^{11} \exp(-48.48/\lambda) \quad (dB/Km) \qquad (1)$$

where λ is the wavelength.

In GeO_2-doped fused silica, the multiphonon absortion spectrum is not a simple superposition of that of S_iO_2 and GeO_2, but broader and more diffuse. However, the spectrum of 10 wt% GeO_2--doped fused silica is almost the same as that of nondoped silica except for a slight shift of the absortion peaks to longer wavelength. In P_2O_5 and B_2O_3-doped silica the absortion spectrum shifts to shorter wavelength as compared to the pure silica[18].

Another wavelength-dependant intrinsic absortion fenomena deals with the ultraviolet region. Four strong absortion bands were observed in silica[19] attributed to excitonic transition and to the conduction band. The absortion tails of doped silica glass are changed by the dopping element and the quantity. The absortion tail of GeO_2-doped silica shifts toward longer wavelength region, and its absortion coefficient has been expressed[20] by

$$A_{UV} = 1542\,\Delta/(446\,\Delta + 6000) \times 10^{-2} \times \exp(4.63/\lambda) \quad (dB/Km) \qquad (2)$$

where Δ is the refractive-index difference of doped silica and pure silica.

Rayleigh scattering loss is the major intrinsic source of loss in the range of 0.6 -1.6 μm. The scatering intensity is strongly affected by the doping element and the quantity because the fictive temperature decreases with doping, therefore, the density fluctuation will decrease.

Using the data reported by[15] for GeO_2-doped silica, the Rayleigh scattering loss, A_{RS}, as a function of wavelength and refractive index difference has been expressed[21] by

$$A_{RS} = (0.51\,\Delta + 0.76)/\lambda^4 \quad (dB/Km) \qquad (3)$$

Total loss model of high silica fibres. Summing up above descriptions, the spectral attenuation of GeO_2-doped silica single-mode fibres may be described in the 1.3 μm region by

$$A_T = A_{RS} + A_{UV} + A_{OH} \qquad (4)$$

Multiphonon absortion coefficient is not relevant (cfr eq. (1)) when fibres operate at 1.3 μm region. A_{RS} is given by eq. (3). In the A_{UV} contribution we assume that fibres show a refractive-index differende about 0.3%. Therefore, from eq. (2) the A_{UV} shows a roughly constant performance equal to 0.025 dB/Km at the 1.3 microns region.

For modeling the A_{OH} contribution we employ the representation proposed by Walker[22] which, in spite of their complexity, is to our knowledge the most accurate model proposed to date. In particular, the 1.24 and the 1.38 μm OH absortion bands are described by

$$A_{OH} = \sum_{i}^{6} C_i \times \exp(-(\lambda - \lambda_i)^2/2\sigma_i^2) \qquad (5)$$

being the 1.38 μm absortion band represented by a quadruple Gaussian equation, and the 1.24 μm absortion band by a double Gaussian equation. Coefficients λ_i and σ_i are given in table 1. Coefficients C_i depend on the hydroxyl (OH) quantity. Figure 4 shows the C_i coefficients when eq. (5) is fitted to measured results of a fibre showing some 0.56 dB/Km OH absortion at 1.38 μm. Figure 5 shows the total spectral attenuation measured at 10 nm intervals. Note that these values include both ultraviolet absortion and Rayleigh scattering loss contributions. For larger A_{OH} (1.38) absortions, we assume in the calculations that the C_i coefficients are proportional to those indicated in Figure 4 (which correspond to a A_{OH} (1.38) equal to 0.56 dB/Km).

Results

The influence of hydroxyl (OH) on the attenuation average (X) and std. deviation (S) of GeO_2-doped fused silica single-mode fibres were computed by a Monte-Carlo sampling process. The results take also into account: (1) the lasing source wavelength distribution, and (2) the allowed intervals of the optical source wavelength.

Figures 6 to 8 show the influence of hydroxyl (OH) contents in the spread of fibre attenuation. Such spread is measured by the $\Delta S/X$ (%) ratio. Figures 6 to 8 deal with a $\Delta\lambda_s$ value of 40, 30 and 10 nm respectively.

Figures 6 to 8 also show the influence, in the fibre attenuation spread, of the lasing average wavelength (1300 to 1310 nm) as well as theimpacts of limiting the operating wavelength to within the 1285-1330 or to the 1280-1340 nm windows.

Divergences which arise due to OH content, when fibre attenuation is described either by a statistical value (X + K.S dB/Km) or by the worst-case spectral value, within the allowed operating wavelength interval, are shown in figures 9 and 10.

Figure 9 deals with the wavelength interval from 1285 to 1330 nm, and figure 10 considers the 1280 to 1340 nm window. In both figures, the statistical (X + 2.05 S dB/Km) and the worst-case spectral attenuation are compared. The OH absorption overtone A_{OH} (1.38) covers a range from 0 to 2.5 dB/Km.

Final remarks

Discussion

Much attention has been paid to reduce the OH-ion impurity quantity in fused silica fibres. However, figures 6 to 8 show that a significan hydroxyl (OH quantity is admisible: in particular, up to 2.0 or 2.5 dB/Km absorption peak at 1.38 μm band (and even more, depending upon the laser-source) may be beneficial for reducing both: the attenuation spread and the attenuation average as well, over a wavelength operating region around 1.3 microns. That situation could be understood as a "flattening" effect in the fibre spectral-attenuation caused by the tolerances in the laser-source lasing wavelength. In other words, existing manufacturing tolerances of multilongitudinal mode lasers leads a loss-compensation effect of the hydroxyl absorption bands in the 1.3 μm region.

Figures 9 and 10 suggest a very interesting consideration dealing which what could be a practical guide for limiting the admisible hydroxyl absorption. If the worst-case spectral attenuation (within a given wavelength window, let say 1285-1330 or 1280-1340 nm) relies on the Rayleigh absorption tail, the hydroxyl absorption impacts by some 3% (or even less, see fig. 9) in terms of the divergence between the worst-case value and the statistical value of fibre attenuation. However, if the maximum value of the fibre spectral-attenuation relies on the tail of the 1.38 μm absorption band, that divergence may be quite significant (that situation is shown in fig. 10 for a A_{OH} (1.38) larger than 2.0 dB/Km).

Concerning the equation for modeling the fibre spectral attenuation, we have noticed that a very precise model is required to get an accurate statistical description of fibres attenuation. In spite of its complexity, the equation we have employed shows a larger potential accuracy than the equations previously proposed by Cohen[23] and by Ishida et al.[24] . Furthermore, those analytical expresion proposed by Cohen (a double Gaussian function) and Ishida (Lorentzian functions) were really empirical and had litle definite physical basis. However, equation (5) relies on a physically justificable structure for OH absortion peaks as has shown Stone and Walrafe[12,13] using Raman and IR spectra . Their preference for Gaussian over Lorentzian functions is based on the response of decoupled OH oscillators to the random structural distorsions present in amorphous fused silica.

Dealing with the source lasing wavelength, it is recognized that improved manufacturing processes such as the MOCVD may produce lasers with a very narrow lasing wavelength distribution which, in addition, may shows a shape far from Gaussian. However, based upon preliminary calculations, we have tentatively concluded that the narrower the lasing wavelength distribution the lesser relevant (from the viewpoint of this study) how the actual distribution shape should looks like.

Recomendation

Based upon results given in figures 9 and 10 and also considering above discussion, we suggest that a practical guide for limiting the acceptable hydroxyl contents in fused Geo2-doped silica fibres could be: That (OH quantity) at which the attenuation at the upper-side of the wavelength operating window (i.e., 1330 or 1340) equals that at the lower-side (i.e. 1285 or 1280 nm).

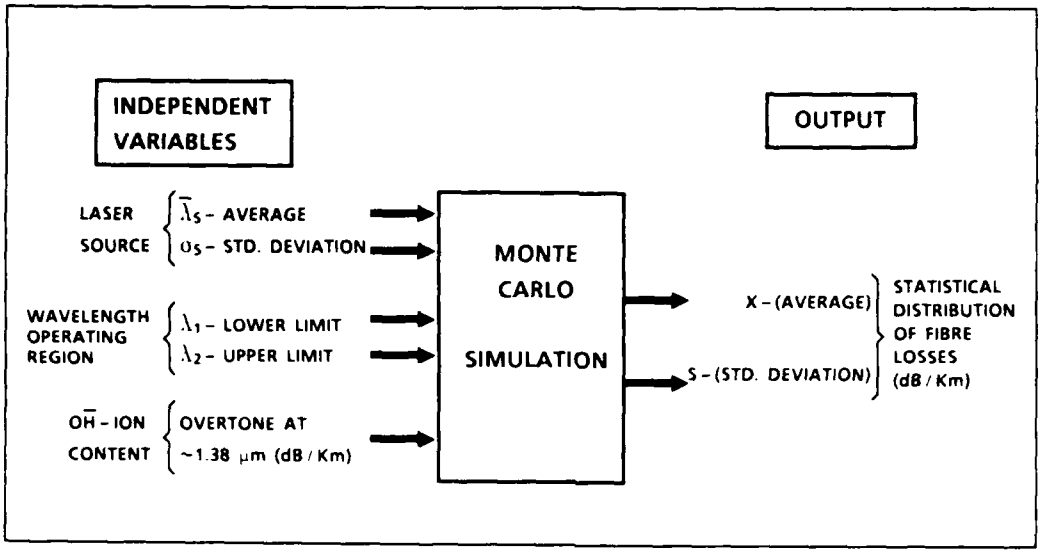


Figure 3 - Statistical quantification method about the influence of hydroxyl (OH) absorption peaks in the attenuation of silica fibres.

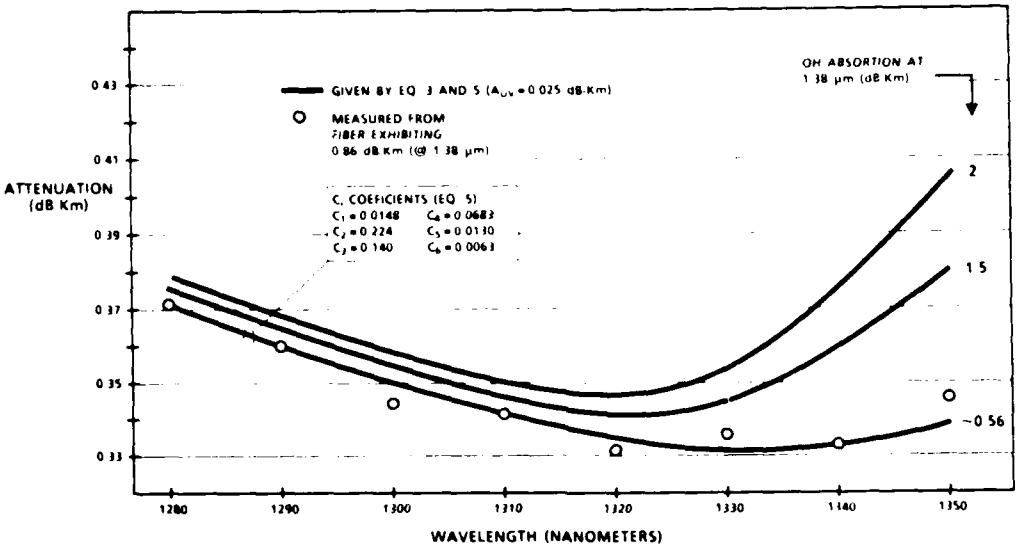


Figure 4 - Spectral attenuation: measured results and fitted curves (given by equations (3) and (5), being A_{UV} = 0.025 dB/Km).

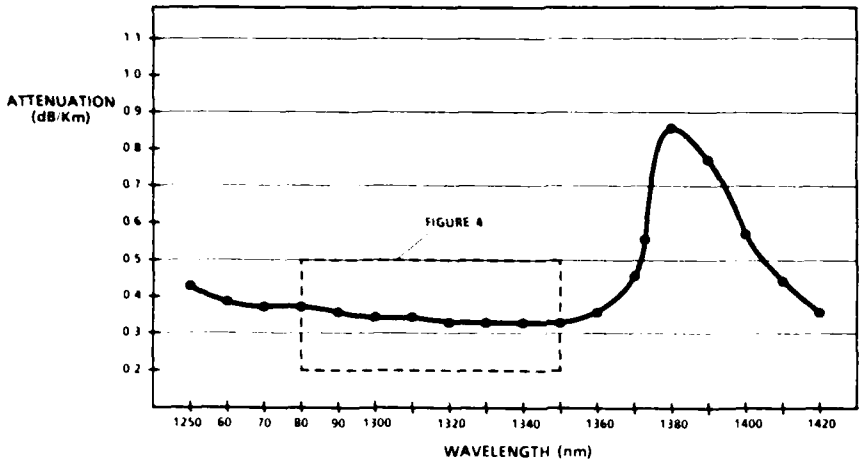


Figure 5 - Example of spectral attenuation of a GeO_2-doped silica single-mode fibre. Measurements were done each 10 nm from 1250 to 1420 nm.

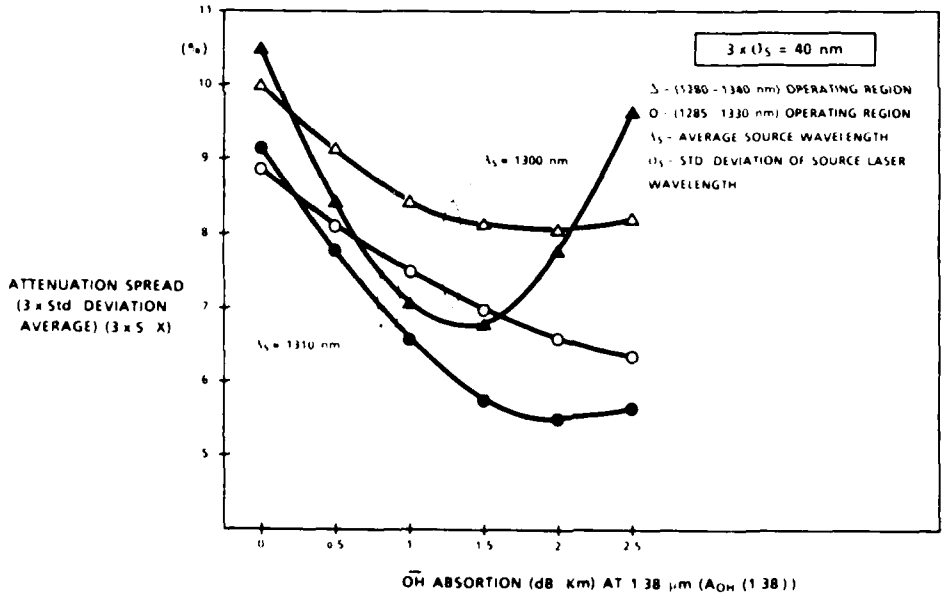


Figure 6 - Influence of hydroxyl (OH) impurity in the attenuation spread of GeO_2-doped single-mode fibres operating in the 1285-1330 nm and in the 1280-1340 nm windows. The standard deviation in the source lasing wavelength is assumed to be 13.33 nm.

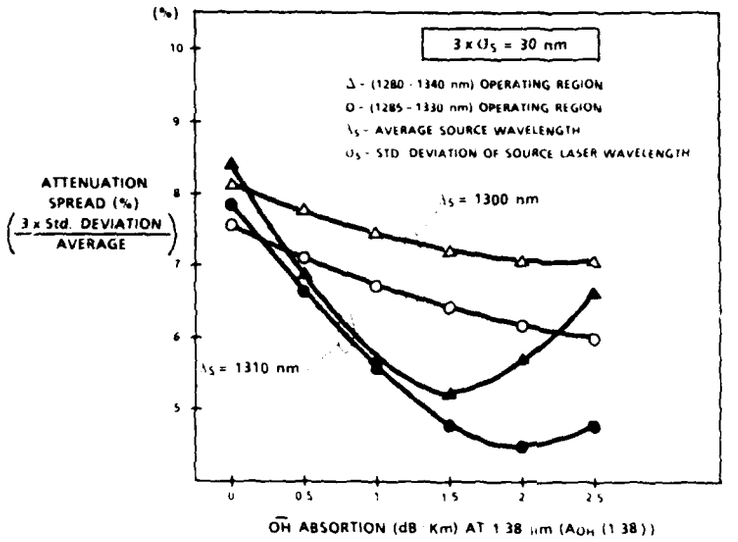


Figure 7 - Influence of hydroxyl (OH) impurity in the attenuation spread of GeO_2-doped single-mode fibres operating in the 1285-1330 nm and in the 1280-1340 nm windows. The standard deviation in the source lasing wavelength is assumed to be 10 nm.

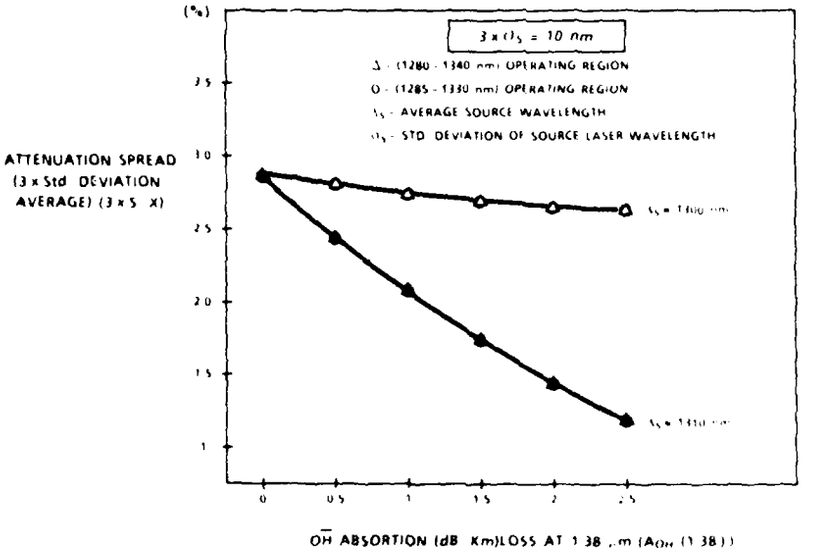


Figure 8 - Influence of hydroxyl (OH) impurity in the attenuation spread of GeO_2-doped single-mode fibres operating in the 1285-1330 nm and in the 1280-1340 nm windows. The standard deviation in the source lasing wavelength is assumed to be 3.33 nm.

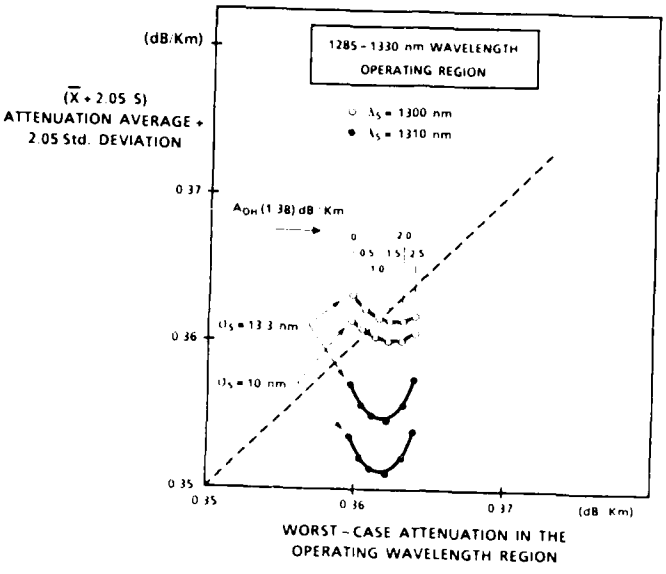


Figure 9 - Statistiscal vs. worst-case fibre attenuation in the 1285--1340 nm window, for GeO_2-doped silica based single-mode fibres.

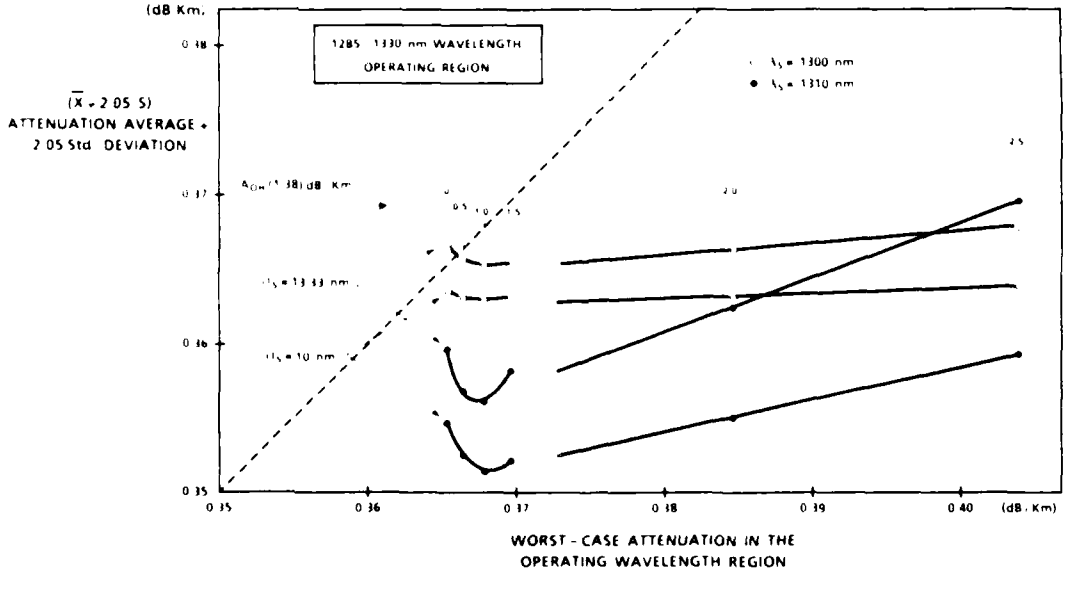


Figure 10 - Statistiscal vs. worst-case fibre attenuation in the 1285--1340 nm window, for GeO_2-doped silica based single-mode fibres.

i	λ_i (nm)	σ_i (nm)
1	1347.3	13.9
2	1378.9	7.0
3	1390.0	11.7
4	1401.6	27.7
5	1242.6	8.5
6	1256.2	13.6

Table 1 - Coefficients of A_{OH} (1.38) in equation (5).

References

1| D.P. JABLONOWSKI, "Fiber Manufacture at AT&T with the MCDV Process", Journal of Lightwave Technology, Vol. LT-4, pp. 1016-1019, 1986.

2| R.V. VANDEWOESTINE and A.J. MORROW, "Developments in Optical Waveguide Fabrication by the Outside Vapour Deposition Process", Ibid., pp. 1020-1015.

3| HIROSHI MURATA, "Recent Developments in Vapour Axial Deposition", Ibid., pp.1026-1033.

4| HANS LYDTIN, "PCVD: A Technique Suitable for Large-Scale Fabrication of Optical Fibers", Ibid., pp. 1034-1038.

5| T.LI, Optical Fiber Communications, Vol. 1. New York: Academic Press, 1985.

6| M.H. KALOS and P.A. WHITLOCK, Monte-Carlo Methods, Vol. 1, chap. III, New York: John Wiley, 1986.

7| M. MIZUGUCHI, T. OGAWA and K. KAMEO, "405 Mbit/s Single-Mode Optical Fiber Transmission System", Fujitsu Sci. Tech.J., Vol. 21, 1, pp. 50-66, 1985.

8| S.TSUJI et al., "Low Threshold Operation of 1.5 μm DFB Laser Diodes", Journal of Lightwave Technology, Vol. LT-5, pp. 822-826, 1987

9| F.M. SEARS, et al., "Probability of Modal Noise in Single-Mode lightguide Systems", Journal of lightwave Technology, Vol. LT-4, pp. 652-655, 1986.

10| P.KAISER et al., "Spectral losses of unclad vitreous silica and soda-line-silicate fibres", Journal of the Optical Society of America, Vol. 63, 9, pp. 1141-1148, 1973.

11| F.P. KAPRON, R.D. MAURER, P.C. SHULTZ, " On the Ultimate limit of Attenuation in Glass Optical Waveguides", Appl. Phys. Letters, , , pp. 307-309, 1973.

12| G.E. WALRAFEN, and S.R. SAMANTA, "Infrared Absorvance Spectra and Interactions Involving OH Groups in Fused Silica", J. Chem. Phys., Vol. 69, pp. 493-495, 1978.

13| J. STONE and G.E. WALRAFEN, "Overtone Vibrations of OH Groups in Fused Silica Optical Fibers", J. Chem. Phys., Vol. 76, pp. 1712-1722, 1982.

14| A.V. BELOV, E.M. DIANOV, and P.N. LEBEDEV, "OH Absortion in GeO_2 - doped Fused Silica Fibers", Electron Lett., Vol. 18, pp. 836--837, 1982.

15| N. SHIBATA, "Optical Characteristics of High Silica Glass Fibers for Communications" (in Japanese), Ph. D. Thesis, Nagoya Univ, 1983.

16| J. STONE, "Interactions of Hydrogen and Deuterium with Silica Optical Fibres: A Review", Journal of Lightwave Technology, LT-5, pp. 712--733, 1987.

17| T. MIYA, "Low-Loss and Low-dispersion Single-Mode Fibers for Long Wavelengt Region" (in Japanese). Ph. D. Thesis, Tohoku, Univ., 1983.

18| H. OSANAI et al., "Effect of Dopants on the transmission loss of Low-OH-Content Optical Fibers", Electron. lett., Vol. 12, p. 549, 1976.

19| H.R. PHILIP, "Optical Transmition in Crystaline and Fused Quartz", Solid State Communications, Vol. 4 p. 73, 1966.

20| T. IZAWA and S. SUDO, Optical Fibers: Materials and Fabrication, Tokyo: KTK Scientific Publishers, p. 31, 1987

21| Ibid., p. 35

22| S.S. WALKER, "Rapid Modeling and Stimation of Total Spectral loss in Optical Fibers", Journal of Lightwave Technology, Vol. LT-4 pp 11251131, 1986.

23| COHEN, and S. LUMISH, "Effects of Water Absortion Peaks on Transmission Characteristics of LED-Based Lightwave Systems Operating Near 1.3 μm Wavelength", IEEE Journal of Quantum Electronics, Vol. QE-17 pp. 1270-1276, 1981.

24| Y. ISHIDA et. al., "Transmission characteristics of a Single-Mode Fiber in the 1.3. μm Wavelength Region", Journal of light. Technology, Vol. LT-2, pp. 322-327, 1984.

R. Díaz de la Iglesia
TELEFONICA
S. G. de Tecnología
Madrid - Spain



Raimundo Díaz de la Iglesia, was born in Madrid, on March 10, 1954. He received the M. S. degree in telecomunication engineering from the Politechnica University, Madrid, Spain, in 1976.

In 1978 he joined Telefónica. He was engaged in high-capacity line-systems standarization. Since 1980, he has been engaged in reseach and studies on fiber-optic communications. From 1986 he also serves as chairman of the spanish section of the IEC-86 (Fiber Optic) group. He has written more than 30 papers in the area of fiber optics, and is the author of the book "Comunicaciones por fibra óptica: Manual de ingeniería", Marcombo, Barcelona, 1985. Mr. Díaz is a member of FITCE, IEEE, SPIE and OSA.

Diego J. Lao Soriano
TELEFONICA
S. G. de Tecnología
Madrid - Spain



Diego-Jesús Lao Soriano, was born in Almería, Spain, on December, 1951. He received the B.S. degree (1974) and the M.S. degree (1984) in Telecommunication Engineering from Politechnica University, Madrid, Spain.

In 1976 he joined Telefonica. He was engaged in qualification and standarization of high-capacity analog coaxial systems. Since 1984 he has been engaged in studies on fiber-optic communications.

E. Tobías Azpitarte
TELEFONICA
S. G. de Tecnología
Madrid - Spain

Enrique Tobías Azpitarte, was born in Logroño, Spain, on January 1953. He received the B. S. degree (1974) and the M. S. degree (1980) in Telecommunication Engineering from Politechnica University, Madrid, Spain.

From 1980 is a lecturer on electronic technology of high school level. He joined Telefonica in 1983, since then has been engaged in research and studies on fiber-optic communications orientad to television networks.

Fco.J. Rueda García
TELEFONICA
S. G. de Tecnología
Madrid - Spain



Fco. Javier Rueda García, was born in Madrid, Spain, on April, 1958. He received the M.S. degree (1982) in Telecommunication Engineering from Politechnica University, Madrid, Spain.

He joined Standard Electrica, S.A., ITT spanish subsidiare, in 1983. He was engaged in research and development of high-capacity optical fiber systems. In 1986 he moved to Telefonica, being engaged in fiber optic communications studies.

A NOVEL EVALUATION TECHNIQUE AND REFRACTIVE INDEX PROFILE CONTROL IN THE VAD METHOD.

S. OKUBO W. NAKAGAWA S. ASARI

TATSUTA ELECTRIC WIRE & CABLE Co., Ltd.

ABSTRACT

The GI optical fiber stabilizes the group delay between modes by controlling the refractive index profile which provides a wide bandwidth for data transmission. A mismatch of refractive index may degrade the 6dB bandwidth or harm the baseband frequency response.

The refractive index profile of a GI fiber made by the VAD process is formed over the whole core simultaneously in soot preform synthesis. This effect has often provided the fiber with a smooth distribution of the refractive index but the refractive index profile in the peripheral area of the core has tended to assume the shape of a Gaussian distribution.

By adopting a new method to estimate the refractive index profile, the authors have determined the requirements for GI optical fiber. By improving the technology for controlling the refractive index profile, we have also developed a fabrication technique for GI optical fiber preforms with the optimum distribution of refractive index over the core.

1. INTRODUCTION

The GI optical fiber has low losses and a wide bandwidth, and offers easy connection for short and middle-distance communications.

The refractive index profile of a GI fiber made by the VAD process is formed over the whole core simultaneously in soot preform synthesis. This effect provides the fiber with a smooth distribution of refractive index and has the advantage of reducing the refractive index dip at the center of the core - this improves the transmission bandwidth.

But some optical fibers made by the VAD method degrade the baseband frequency response, which may make the performance unstable when it is processed for cabling.

The authors have determined how to estimate the distribution of the refractive index and have found that fluctuation of baseband frequency response can be attributed to an uneven distribution of refractive index outside the core. On this basis, it has been possible to form a refractive index profile that is ideal for GI optical fiber. The transmission characteristics of an optical fiber made by this method are excellent.

2. Problems with the conventional way of estimating the refractive index profile

In the GI optical fiber, a suitable refractive index profile is used to make the group delay between modes suitable. Figure 1, for a wavelength of 1.3 μm, shows the relation between the profile parameter (α) of the refractive index distribution and the 6 dB bandwidth (α is calculated by the least squares method). The refractive index, determined in the process of transparent preform, varies from 20 to 80% of the maximum refractive index in the core.

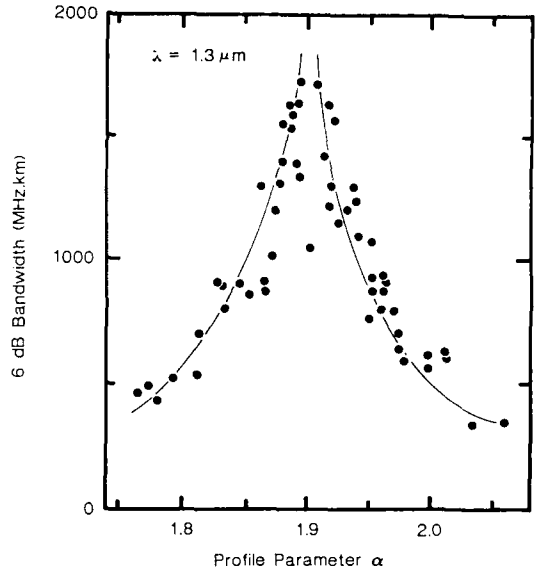


Fig. 1 Relation between profile parameter α and 6 dB bandwidth

Aware of these relations, the authors have examined a method to control the distribution of the refractive index during the process of manufacturing soot preforms, and have estimated the 6 dB bandwidth after fiber drawing. Although estimating the 6 dB bandwidth after fiber drawing is easy for transparent preforms, this method is not accurate enough nor does it allow us to predict whether the baseband frequency response will deteriorate.

The authors have examined a new method for estimating the distribution of the refractive index, based on the assumption that the problem is caused by deviation of the actual distribution from the calculated α.

3. Improved method for estimating the refractive index profile

The conventional method of estimating the refractive index profile determines α in the range of 20 to 80% of the maximum variation in the refractive index of the core. This method has the following problems which are yet to be resolved:

(1) A mismatch of refractive index profile outside the range used to determine α cannot be estimated.

(2) The estimated bandwidth, based on the data on its statistical relativities, does not allow the baseband frequency response to be estimated from an actual refractive index profile.

Because of this, we have examined a new method to improve the estimation of a refractive index profile.

3.1 Improving the conventional method.

Making an estimate near the outside of an optical fiber core (part equal to or less than 20% of the difference in maximum refractive index), where many modes are set up outside the range used to determine (and which is not estimated in the conventional method), is done as follows:

$K(n) = [D(n)-I(n)]/I(n) \times 100$

Where, at a refractive index difference of n%,

K(n): Deviation from the calculated refractive index profile (α curve)

D(n): Diameter of actual distribution of the refractive index

I(n): Diameter of the calculated refractive index profile (α curve)

A coefficient of correlation (R) given by the least squares method is used to determine matching of the calculated α curve and the actual distribution of the refractive index between 20% and 80%.

Figure 2 shows an example of refractive index profile of a preform for a conventional VAD optical fiber, K(n), and R.

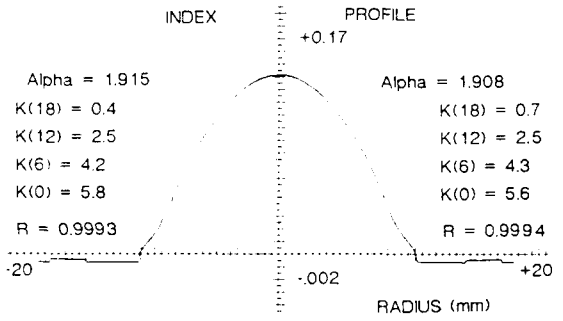


Fig. 2 Example of Refractive Index Profile

Figure 3 shows the relations between K(12) and R of a transparent preform whose α is from 1.90 to 1.95. These results show us that K(12) is related to R in a primary correlation and that, when K(12) is greater than 2.5, the baseband frequency response begins to deteriorate and deviate. When R is equal to or less than 0.9990, the 6 dB bandwidth value is degraded.

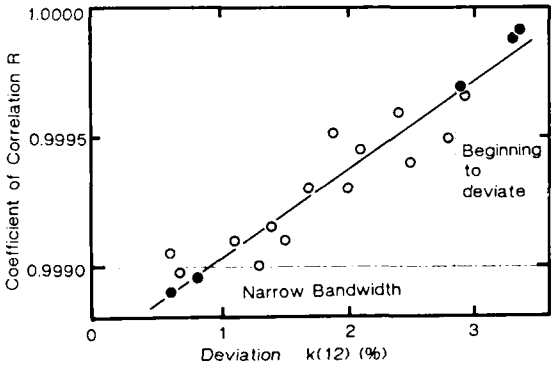


Fig. 3 Relation between Deviation k(12) and Coefficient of Correlation

3.2 Examining the method for estimating the baseband frequency response.

The authors have used the given refractive index profile of a transparent preform to develop a method for estimating the baseband frequency response.

Figure 4 is a flow chart indicating this method. The distribution of the refractive index is first divided into layers at determined intervals of refractive index, then the light path length and the average refractive index are determined consecutively from the lower modes to the higher ones using a light-tracking method. Next, a signal frequency is introduced to each mode and the baseband frequency response is calculated at the end of light emission.

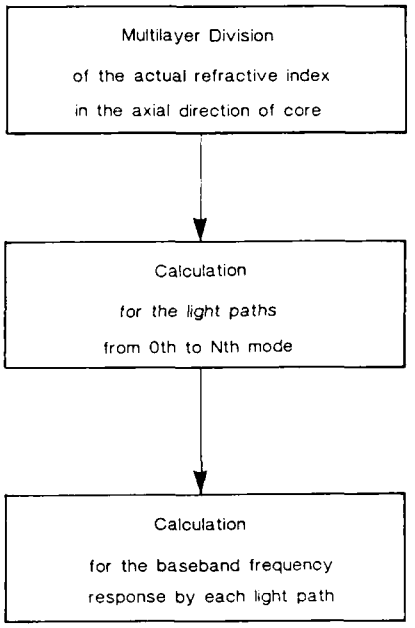


Fig. 4 Flow Chart

Figure 5 shows that baseband frequency response estimated in this way correspond well to the actual ones. This method also shows that the deformation of baseband frequency response waveform increases as the mismatch around a core, K(12), increases.

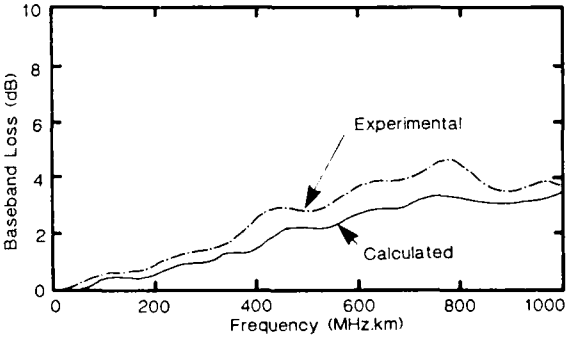


Fig. 5 Baseband frequency response

4. Improving the refractive index profile

To manufacture a GI optical fiber with good baseband frequency response at 1.3 μm, three requirements must be satisfied:
(1) The value of α must be between 1.85 and 1.95.
(2) Mismatch around the core must be small ($0 < K(12) < 2.5$).
(3) The refractive index profile must be well matched ($R > 0.9990$).

Obviously, these requirements can be satisfied only under a small range of conditions.

Next, the authors decided to improve the technology for controlling the refractive index profile. In examining the distribution mechanism of GeO_2 used for this procedure, we have taken into consideration the following points:

(a) Reducing the unevenness in the refractive index distribution (VAD process)
(b) Correcting the refractive index profile around the core (consolidation process)

4.1 Reducing the unevenness in the refractive index profile in the VAD process

Figure 6 outlines the VAD process. The reaction in the VAD process can be expressed by equations (1) and (2); the distribution of the refractive index formed by this reaction can be controlled by temperature distribution on the soot growing surface, the set point of the burner, and the mixing rate of the raw material and gas. The mismatched distribution of refractive index around a core depends largely on the mixing rate of the materials of first layers ($SiCl_4$ + $GeCl_4$) and of second layers ($SiCl_4$) supplied to flame burner.

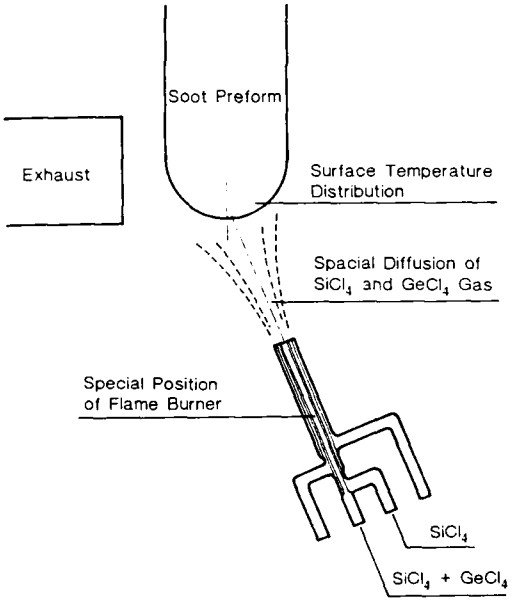


Fig. 6 VAD process

$$SiCl_4 + O_2 \longrightarrow SiO_2 + 2Cl_2 \quad (1)$$
$$GeCl_4 + O_2 \longrightarrow GeO_2 + 2Cl_2 \quad (2)$$

Equation of reactions

Figure 7 shows the relations between the mixing rate of the material and the deviation K(0). From this figure, we can say that adequate mixing of materials minimizes the values of K(0). The VAD process, which does not allow K(0) and K(12) to be minimized at the same time, first minimizes K(0) before correcting the remaining mismatch around the core in the consolidation process

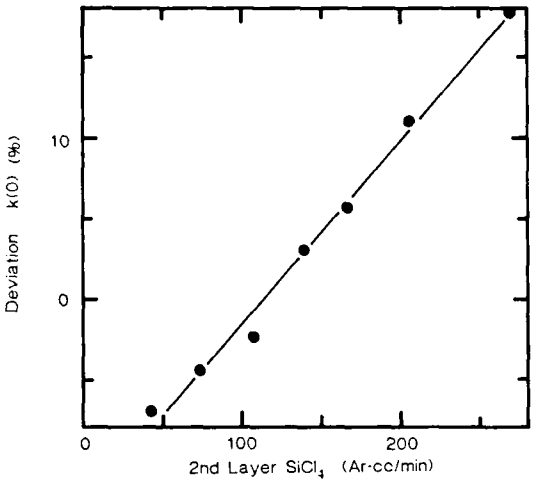


Fig. 7 Relation between mixing rate of the material and Deviation k(0)

4.2 Correcting the refractive index profile around a core in the consolidation process

The consolidation process obtains a transparent preform from the soot preform and removes hydroxide from it at the same time. The conventional method uses a desiccant such as $C1_2$ for the soot preform but adding $C1_2$ accelerates this dehydration and reverse the reaction (See Equation (2)). These effects change the refractive index profile formed in the VAD process.

Figure 8 shows two refractive index profiles that can be obtained by adding O_2 (a) and Cl_2 (b) to the consolidation atmosphere. As these two distributions show, the Cl_2 affects the entire soot preform and changes the refractive index profile throughout the core.

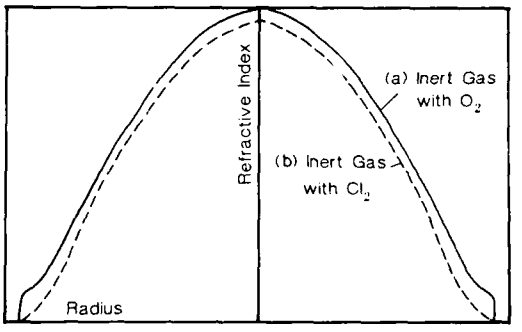


Fig. 8 Refractive index profile obtained by consolidation Atmosphere

Only the outside of the core can be corrected for faulty refractive index profile as Figure 7(a), so the authors think that, if a Ge-removing agent with high reactivity to GeO_2 can be found , Ge can be reduced strongly from the outside of a core, and any mismatched refractive index profile around the core will be corrected effectively.

Equation (3) represents a Ge reduction eaction using thionyl chloride, where the Gibbs energy at 1000°C is calculated to be -77kcal/mol. This value is extremely low compared to the Gibbs energy -6kcal/mol of reversing the reaction as shown in equation (2), and allows us to estimate how far the reaction goes.

$$GeO_2 + 2SOCl_2 \longrightarrow GeCl_4 + 2SO_2 \quad (3)$$

Equation of reactions

Figure 9 shows the relation between the amount of thionyl chloride added to the consolidation process atmosphere and K(12). In this case, where the K(0) of the soot preform in the VAD process is set to 0%, a transparent preform with an optimum profile can be obtained by adding enough thionyl chloride to make K(12) = 0%.

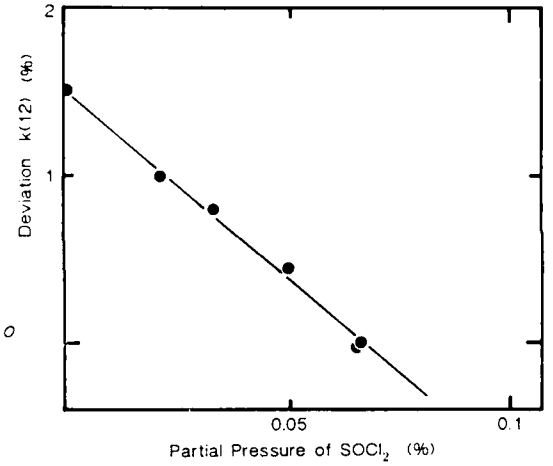


Fig. 9 Relation between reductant ratio and Deviation k(12)

Figure 10 represents a preform obtained in this way, with an ideal refractive index profile throughout the core. K(12) and R in the refractive index profile are nearly 0% and more than 0.9995 respectively. The authors' examination of these results indicated that the improvement of refractive index profile is effective.

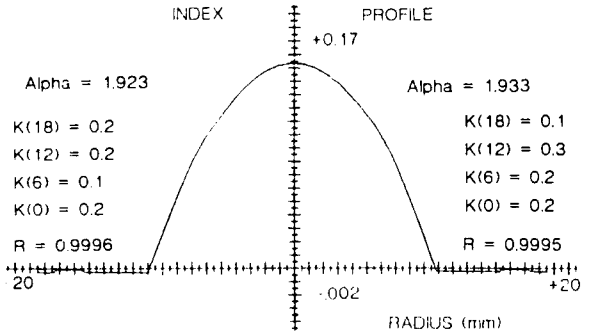


Fig. 10 Optimum Refractive Index Profile

5. Characteristics of the optical fiber

We used transparent preform as shown in Figure 10 to make optical fibers for testing. We made a cable to estimate its fiber preformance. The fiber are coated with a silicon resin and jacketted with nyion resin. Six of these fibers are wound tightly around a steel wire to make a six fiber unit. These units are wound with interstitial material before being covered with a water-resistant laminated aluminium-polyethylene sheath. The finished cable is shown in Figure 11.

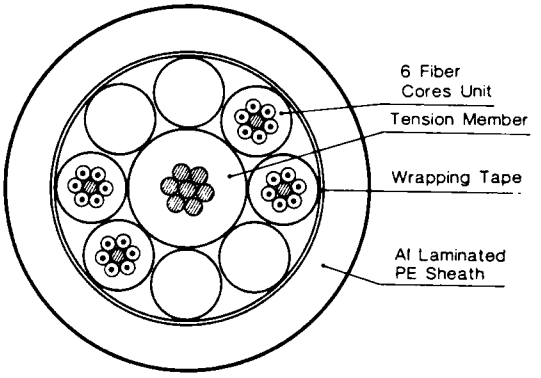


Fig. 11 Construction of 24 Fiber Cores Cable

The fiber parameters and transmission characteristics of this cable are all satisfactory, as indicated in Table 1. The bandwidth characteristics, which are particularly important, are very stable at all stages as shown in Figure 12.

Table 1 CHARACTERISTICS OF FINISHED OPTICAL FIBER CABLE

	ITEM		DATA (AVE)
FIBER PARAMETER	CORE DIAMETER	(μm)	50.2
	CLADDING DIAMETER	(μm)	125.2
	CORE CONCENTRICITY	(%)	2.3
	CORE NON-CIRCULARITY	(%)	1.2
	REFRACTIVE INDEX DIFFERENCE		0.0153
TRANSMISSION CHARACTERISTICS (1.3 μm)	OPTICAL LOSS	(dB/km)	0.49
	6 dB BAND WIDTH	(MHz.km)	> 1000

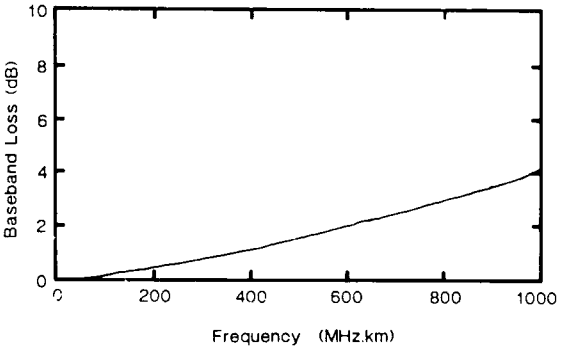


Fig. 12 Baseband frequency response

6. Conclusion

The method described in this report for determining the refractive index distribution specifies the conditions under which a GI optical fiber has good baseband frequency response.

To meet these conditions, further investigation was made into the manufacturing conditions of the preform. The resulting preform achieved the ideal refractive index profile over the whole core.

The optical fiber characteristics of the preform obtained by this method provide better baseband frequency response than those available by conventional methods.

References

[I] T. Izawa, S. Sudo, and F. Hanawa "Continuous Fabrication Process for High-Silica Fiber Preforms," Trans. IECE Jap., VOl E62. NOVEMBER 1979.

[II] T. Izawa, and N. Inagaki "Materials and Processes for Fiber Preform Fabrication-Vapor-Phase Axial Deposition, "Proc. of THE IEEE, VOL 68 No. ID 1980.

Saburo Asari
Tatsuta Electric Wire
and Cable Co., Ltd.
2-3-1 Iwata-Cho,
Higashi-Osaka City,
Osaka, 578 Japan



Mr. Asari graduated from Osaka prefecture Univ. in 1966 with B.E. in Electric engineering, then joined Tatsuta Electric Wire & Cable Co., Ltd. and has been engaged in development of the telecommunication cables and Optical fiber cables.
Mr. Asari now belongs to Optical fiber Division and is a member of the Institute of Electronics, Information and Communication Engineers of Japan.

Syuichi Okubo
Tatsuta Electric Wire
and Cable Co., Ltd.
2-3-1 Iwata-Cho,
Higashi-Osaka City,
Osaka, 578 Japan



Mr. Syuichi Okubo received the B.E. and M.E. degrees in metallagical engineering from Hokkaido University in 1979 and 1981, respectively, then joined Tatsuta Electric Wire & Cable Co., Ltd. where he has been engaged in R&D work on fabrication of GI optical fiber preforms. Mr. Okubo is a member of the Institute of Electronics, Information and Communication Engineers of Japan.

Wataru Nakagawa
Tatsuta Electric Wire
and Cable Co., Ltd.
2-3-1 Iwata-Cho,
Higashi-Osaka City,
Osaka, 578 Japan



Mr. Nakagawa graduated from Osaka Univ. in 1972 with a B.E. in material science, then joined Tatsuta Electric Wire & Cable Co., Ltd. and has been engaged in development of the optical fiber cables since 1980.
Mr. Nakagawa now belongs to R & D Division and is a member of the Institute of Electronics, Information and Communication Engineers of Japan.

Fiber/Metallic Service and Distribution Media

E. R. Campbell
F. J. Mullin
W. C. Reed

AT&T Bell Laboratories
2000 Northeast Expressway
Norcross, Georgia 30071

Abstract

Fiber/metallic service and distribution media are being developed for use in subscriber loop distribution systems. Combining copper and lightguide in common structures permits the early placement of fiber to customer premises, provides initial service over copper and prepares for the implementation of wideband service over fiber.

These products are existing multipair copper structures with one pair (or more) replaced by a reinforced buffered single-mode fiber unit. Dual media versions of gopher and non-gopher buried wire and aerial wire are planned.

Introduction

Lightwave transmission systems are widely deployed in high-capacity long-haul, interoffice and subscriber loop feeder applications. The system architectures combine low loss fiber and reliable high-performance devices to provide enormous information carrying capacity at relatively low cost.[1,2]

Single-mode technology has become the first choice for these systems and is preferred for future local distribution systems.[1,3] Single-mode fiber exhibits lower loss and has a bandwidth potential of about 25,000 gigahertz.

Lightwave subscriber loop distribution systems, now being developed to provide fiber to the home, face challenges not encountered in the deployed long-range systems. Distribution cables branch downward in fiber count to supply one or two fibers to each home causing a corresponding increase in cable sheath, placement, and splicing costs per fiber. Fiber termination at the home requires a dedicated end-point electronic device which is not easily shared. Utilization of distribution system capacity depends upon the arrival of the optical network, development of end-point electronic devices and generation of new services.

Nevertheless, the benefit of an all fiber communication network will cause these challenges to be met.[1,2,4] Digital transmission over fiber will allow full realization of an Integrated Services Digital Network.[1,2] Service upgrades will be accomplished electronically thus avoiding premature plant obsolescence. Service possibilities will be limited by man's imagination rather than system bandwidth.

The subscriber loop distribution plant can be prepared for fiber now as copper facilities are installed by serving each home over a Fiber/Metallic Distribution Service Cable. These composite cables are the subject of this paper. The Fiber/Metallic concept for economically introducing fiber into the local buried distribution plant by employing composite media is described in a companion paper.[5]

Potential For Fiber/Metallic Media

Fiber/Metallic Distribution Service Cables are existing 22 AWG multipair, aerial or buried copper wires with one or more twisted pairs replaced with a reinforced buffered single-mode fiber unit. The fiber units and twisted pairs have exchange cable transmission characteristics. The resulting transmission range of seven miles permits its use in a variety of plant applications and architectures.

Composite cables are primarily an economical means for placing fiber to residences while installing copper service facilities today. The early placement of fiber in aerial or buried service cable will facilitate the later transition from a metallic to an optical operating system. Obviously, the first cost for installing fiber to customer premises is minimized by this approach. Initial service is over the copper pairs while future wideband service over fiber awaits the arrival of the fiber network and development of associated hardware and electronics.

With the Fiber/Metallic Distribution Service Cable in place, service will

evolve from the copper pairs to the optical fibers. Plain-Old-Telephone-Service can begin immediately over a copper pair. Other copper pairs may serve as second lines or alarm circuits.

At a later date, more sophisticated offerings requiring more bandwidth and customer interaction such as electronic newspapers and mail, catalogs and shopping, banking and business activities, data and computer functions and cable television may be served over fiber through a remote terminal. For this application, copper pairs may provide power to on-premise electronics or serve as control circuits. Still later, all offerings may be provided over the optical fiber with on-premise electronics powered by the power or telephone operating company. The copper pairs are also useful for circuit maintenance.

Fiber Unit Design Criteria

The Fiber/Metallic Distribution Service Cables can be manufactured on copper cabling facilities by combining the reinforced buffered fiber unit with the host copper wire. The fiber unit must survive the cabling process without special handling. The unit must be sized to replace a single pair of insulated 22 AWG distribution wire conductors to permit a variety of fiber unit and pair combinations for each cable sheath. The unit must not degrade the performance of the host structure.

Such composite cables will be handled and placed by the same methods and installation personnel as their all-copper counter parts. Accordingly, the fiber unit must be robust enough to withstand plowing and trenching or aerial stringing of the host structure and be capable of survival outside the host structure in a separate run to a fiber storage or termination point.

A tensile load capability of approximately 100 pounds (445N) is required for the fiber unit to survive in a buried distribution wire structure. Buried wires have minimum breaking strengths of 150 pounds (668N) with onset of damage occurring near 100 pounds (445N). Loads near 100 pounds (445N) may develop on rare occasions during wire plowing and are localized to a relatively short section of wire. The high tensile stiffness strength members of the unit, which are required to protect the fiber, will accept most of the cable tensile loads. In self supported aerial wire structures, the unit will be slightly undulated causing the wire strength members to accept the full load.

A minimum bend radius of 1 inch (25 mm) is needed to match that required for successful plowing of buried wire. This is a supported bend for the unit inside the wire structure. The unit may experience bending to the minimum radius during termination but installation radii will be greater than 1 1/2 inches (38 mm).

Even though the unit must bend, some stiffness is required so that the fiber unit does not follow the twists and turns of neighboring twisted pairs. The fiber should remain as straight as possible to minimize bend losses.

The unit must also withstand compressive loads which develop in the cable manufacturing process and during cable installation. The highest load is 150 pounds per inch (263 N/cm) which is the static load equivalent of repeated impacts by vehicles on structures laid across roadways during installation.

An outer diameter of approximately 0.120 inches (3 mm) is desired to permit the unit to replace a single twisted pair. This is approximately the diameter of the circular space needed for the twisted pair of buried distribution wire conductors which are insulated to a diameter-over-dielectric of 0.059 inches (1.5 mm). Matching the sizes of these media elements permits a variety of unit and pair combinations within a given sheath.

The unit must be water resistant to prevent fiber damage due to water induced crack propagation or freezing and to maintain the water resistance of the host structure. Water blockage is accomplished by employing a solid jacket, a solid buffered fiber, impregnated fiber glass strength members and filling compound in the remaining space. The filling compound is selected for proper viscosity and shear strength to maintain the optical fiber in a relatively low state of stress.

The unit should accommodate either single-mode or multimode fiber, but single-mode fiber is preferred. Single-mode fiber has a large bandwidth, permitting upgrades of subscriber offerings without plant replacement or reinforcement. It decreases the number of fibers required throughout the distribution plant for each subscriber. The single-mode fiber unit should meet the maximum individual fiber loss requirements for exchange cable, 0.70 dB/km at 1310 nm and 0.50 dB/km at 1550 nm.

The unit must be materially compatible with the host structure. The presence of the unit must not affect the flame retardance of the completed cable which contacts customers premises. The unit must not be adversely affected by the flame

retardant wire filling compound. The unit must not degrade the transmission performance of the copper pairs. The materials of the units and host structure must not evolve or support galvanic action to produce hydrogen in quantities that will affect fiber loss.

The completed structure must operate properly over the range -40°F to +158°F (-40°C to +60°C). For buried wire, at a depth of about 2 feet (0.6m), the typical range is 55 ± 20°F (13 ± 11°C), reaching 95°F (37°C) under pavement. However, buried cable laid on top of the ground for emergency repair or later burial and aerial cable may experience the full temperature range.

Fiber Unit Design

A design for a reinforced buffered fiber unit which meets the above criteria is shown in Figure 1. This design consists of buffered single-mode fiber in the center of a triangular shaped cavity formed by stranding three flat strength members about the buffered fiber. Filling compound is flooded into the cavity containing the buffered fiber and over the assembled triangular core. The flooded core is enclosed with a nylon jacket.

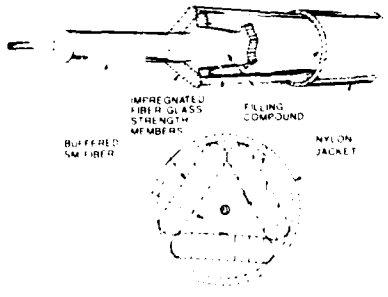


FIGURE 1 REINFORCED BUFFERED FIBER UNIT

The fiber buffer is a polyester elastomer which is compatible with the filling compound and affords excellent impact protection to the fiber. The buffer diameter is 0.035 inch (0.86 mm), the same diameter as building cable buffered fibers, to permit a wide selection of fiber connectors.

The strength members are impregnated fiber glass rovings.[6] Impregnation protects the fiber glass filaments from abrasion induced flaws by neighboring filaments, causes filament flaws to be bridged, distributes tensile loads evenly over all filaments and blocks water.

The filling compound is a colloidal particle-filled grease selected to effectively block entry of water into the core while minimizing the added loss to the unit. The grease does not adversely affect the properties of the unit over the operating temperature range and is relatively free of syneresis over this same range. The material has a relatively low shear modulus to maintain the optical fiber in a relatively low state of stress and minimize microbending loss.

The unit jacket is a selected nylon. This nylon has a relatively high modulus which contributes to impact and compression resistance yet allows the unit to be flexible. It has relatively low shrinkage and low moisture absorption which provide dimensional stability for good loss performance.

The capability of this fiber unit design to meet the above design criteria was verified in a series of tests. A partial list of the tests and representative test results are given in Appendix A.

Buried Fiber/Metwllic Cable - Nongopher

Buried Fiber/Metallic Distribution Service Cable for use in nongopher areas has been manufactured and is shown in Figure 2. The cable is available in sheath sizes which accommodate three, four or five transmission media elements. The fiber elements are the reinforced buffered fiber units. The copper elements are twisted pairs of individually insulated 22 AWG copper conductors. A water and flame retardant thermoplastic filling compound encapsulates the pairs and units after which they are enclosed by a polyester core wrap. The outer surface of the wrapped core is covered by a second application of filling compound. A corrugated bronze shield is formed over the wrapped core. The outer surface of the shield is flooded with a flame retardant flooding compound. A black vinyl jacket is applied directly over the flooded shield and a jacket slitting cord to complete the structure.

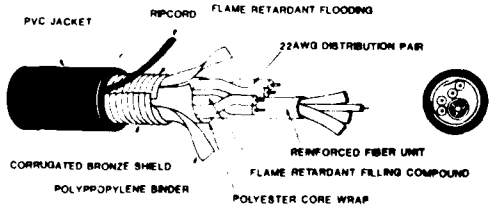


FIGURE 2 BURIED FIBER/METALLIC CABLE (NON-GOPHER)

Buried Fiber/Metallic Cable - Gopher

Buried fiber/metallic distribution service cable for use in gopher areas is being developed and is shown in Figure 3. The cable sheath sizes will accommodate three, four or five media elements. The media elements and an inner jacket slitting cord are encapsulated in the flame retardant filling compound inside a polyethylene jacket. Copper clad stainless steel armor is helically wrapped over the jacketed core. A black vinyl jacket is applied over the armored core and a jacket slitting cord to complete the structure.

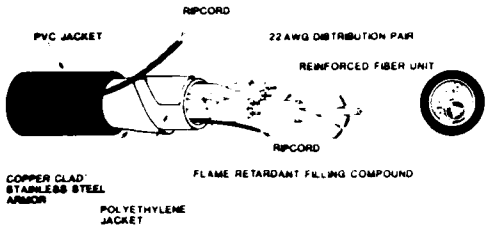


FIGURE 3. BURIED FIBER/METALLIC CABLE (GOPHER)

Aerial Fiber/Metallic Cable

Aerial fiber/metallic distribution service cable is also being developed and is shown in Figure 4. The cable is a "Figure 8" design with a steel strength member in the smaller loop of the "8" and the cable core in the larger loop. The core will accommodate three, four or five media elements. The copper elements are dual insulated with polyvinyl chloride over polyethylene. This insulation combination allows the wire to meet transmission, weatherability, flammability and fusing requirements. The core is wrapped with a polyester core wrap. A jacket slitting cord is laid along the wrapped core to facilitate jacket stripping. A black vinyl jacket forms the "Figure 8" construction.

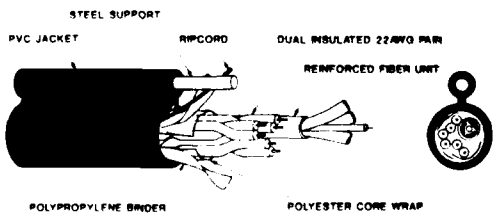


FIGURE 4 AERIAL FIBER/METALLIC CABLE

Costs of Fiber/Metallic Cable

The true value of these composite cables cannot be ascertained in a comparison of a copper to a copper/fiber structure. The true value is revealed in a comparison of fiber deployment schemes in local distribution plant following various design concepts.

Such a comparison is made for buried distribution plant in a companion paper.[1] The comparison shows cost avoidance opportunities which should encourage installation of fiber to the home by use of composite cables.

Summary

Fiber/Metallic Distribution Service Cables are being developed to position fiber to the home as copper service facilities are installed. The combination of copper and fiber in a common structure allows initial services over copper until wideband service can be provided over fiber. A buried non-gopher cable has been manufactured and a buried gopher and an aerial cable are being developed.

Acknowledgement

The Fiber/Metallic Service and Distribution Media are being developed by the joint efforts of AT&T Bell Laboratories and AT&T Technologies - Network Systems.

References

1. Russell P. De Witt, "Evolution of Fiber Optics in Rural Telephone Networks," Fiber Optics Magazine, May/June, 1987.

2. Thomas J. Herr, "The Impact of Technology, Investiture and Deregulation," International Wire and Cable Symposium opening session "The Impact of Technology, Investiture and Deregulation on our Industry", November 18, 1986.

3. David Kalish and Leonard G. Cohen, "Single Mode Fiber: From Research and Development to Manufacturing," AT&T Technical Journal, January/February 1987.

4. Tingye Li, "Advances in Lightwave Systems Research," AT&T Technical Journal, January/February 1987.

5. E. J. Mullin, W. C. Reed and C. Scholly, "Fiber/Metallic Distribution Plant Concept," 36th International Wire and Cable Symposium Proceedings, November 1987.

6. Mikhail M. Girgis and Marshall G. Decker, "Impregnated Fiber Glass Yarn for Reinforcing Fiber Optic Cables," 35th International Wire and Cable Symposium Proceedings, November 1986.

Appendix A. FIBER UNIT PERFORMANCE

The capability of the reinforced buffered fiber unit to meet each of the design criteria was verified in a series of tests. Following is a partial list of the tests along with representative results.

a. EIA FOTP-33 Fiber Optic Cable Tensile Loading and Bending Test

Units subjected to a 100 pound (445N) tensile load exhibited no added loss at 1310 and 1550 nm and no strength member or fiber breaks at loads of 400 pounds (1780N).

b. Cold Wrap Test

Units conditioned for four hours at -10°F (-23°C) displayed no jacket cracks or fiber breaks in five complete wraps around a 1 inch (25 mm) diameter mandrel which had been similarly conditioned.

c. EIA FOTP-104 Fiber Optic Cable Cyclic Flexing Test

Units subjected to 2000 cycles of 180 degree bends around a 1 inch (25 mm) radius mandrel had added losses of less than 0.03 dB at 1310 and 1550 nm and displayed no visible damage.

d. EIA FOTP-25 Impact of Fiber Optic Cables and Cable Assemblies

Units impacted 200 times at a 1.00 ft-lb (1.36 N-m) energy level displayed no added loss at 1550 nm.

e. EIA FOTP-41 Compressive Loading of Fiber Optic Cables

Units compressed by 600 pounds (2667N) applied over 4 inches (102 mm) of length showed no added loss at 1550 nm after 5 minutes under load and a return to the original loss after the load was removed.

f. EIA FOTP-82 Fluid Penetration Test for Filled Fiber Optic Cable

One meter lengths of unit with a one meter waterhead applied at one end continues to block water flow after over six months.

g. EIA FOTP-81 Compound Flow (Drip) Test for Filled Fiber Optic Cable

No material accumulated below 12 inch (305 mm) unit samples which had been suspended vertically in a chamber at 158°F (70°C) for 24 hours.

h. Temperature Cycling Test

The added losses at extreme operational temperatures are not greater than 0.2 dB/km at 1310 and 1550 nm for cables cycled from 72°F (22°C), the reference temperature, to -40°F (-40°C), the low extreme, to 158°F (70°C), the high extreme.

i. Optical Transmission Tests

The absolute loss for the unit in a composite cable was typically less than 0.5 dB/km at both 1310 nm and 1550 nm.



Eric R. Campbell is a member of the Transmission Media Laboratory, AT&T Bell Laboratories, Norcross, Georgia. After receiving a B.S. in Engineering from the University of Massachusetts/Amherst, he received an M.S. in Mechanical Engineering from Northeastern University (Boston, MA) in 1984. Since joining AT&T Bell Laboratories in 1984, he has worked on the design and development of waterproof encapsulated closures, lightguide premise/LAN cables, and composite (fiber/copper) media.



F. J. Mullin is a member of the Transmission Media Laboratory, AT&T Bell Laboratories, Norcross, Georgia. He attended Johns Hopkins University and joined AT&T Bell Laboratories in 1959. During this time he has worked in the outside plant area developing mainframe protection; aerial, buried and building cable terminals, closures and connectors; color coded key closets; buried waterproof system; SAI concept and customer trouble report reduction. His present responsibilities include outside plant, copper and fiber transmission media.



William C. Reed is a member of the Transmission Media Laboratory, AT&T Bell Laboratories, Norcross Georgia. He received a BA in mathematics and physics from Wittenberg University in 1959 and an MA in physics from Wake Forest University in 1969. He joined AT&T Bell Laboratories in 1970 and has worked on the design and development of military power equipment, maintenance test sets and test methods, copper and fiber splicing equipment, buried wire, and encapsulated closures. His present responsibilities include outside plant, copper and fiber transmission media.

A STUDY ON THE DESIGN OF COMPOSITE CABLE CONTAINING OPTICAL FIBER AND MULTI PAIRS

S.Hisano S.Shirada Y.Tokuraru Y.Amano

Sumitomo Electric Industries, Ltd.
1, Taya-cho, Sakae-ku, Yokohama, 244, Japan

Abstract

Recently demands for composite cable containing optical fibers and multi copper pairs have been increasing for the saving of duct spaces and the reduction of installation costs. We have studied the suitable design of the composite cable which satisfies various requirements, and have developed two kinds of composite cable. The transmission loss changes of the cables during each manufacturing process were not observe, mechanical characteristics were very stable, because optical fibers were protected by the grooved plastic spacer. We also confirmed that the tension was loaded on not only the center strength member but also pairs of copper conductor. On the composite cable jointing, it was possible to use the conventional closure.

1. Introduction

In Japan the use of the optical fiber cable has spread more and more. In a part of them, demands for the composite cable containing optical fibers and multi copper pairs have been increasing for the saving of duct spaces and the reduction of installation costs. The combination of the number of optical fibers and copper pairs is decided according to the demand [illegible] so the most suitable construction [illegible] varies case by case. On the other hand, the condition of the installation and the jointing method must be also considered to design the composite cable.

Lately we have developed two kinds of composite cable which satisfied different requirements of the system. In this paper, we will discuss the detail of the design, the characteristic and the jointing of their composite cables.

2. Cable Construction

2.1 Requirements of composite cable

The requirements of the composite cable containing optical fibers and multi copper pairs are as follows.

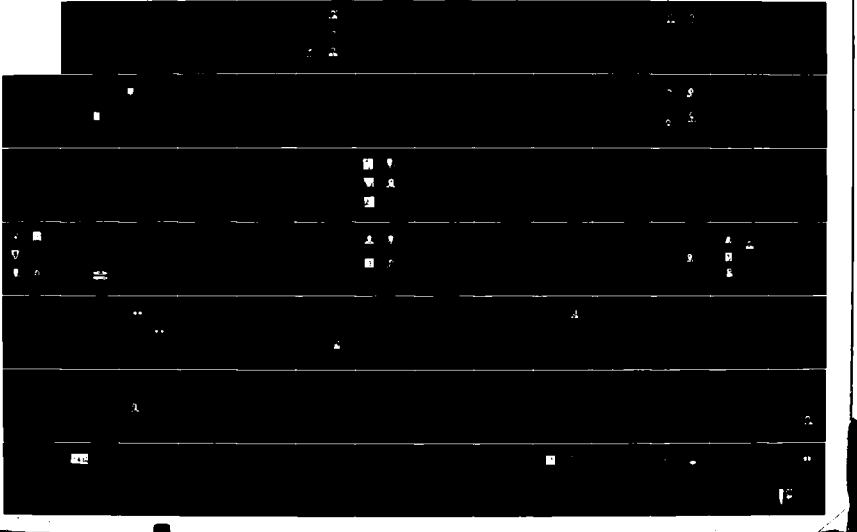
(1) The overall diameter of the composite cable is smaller, and its weight lighter.

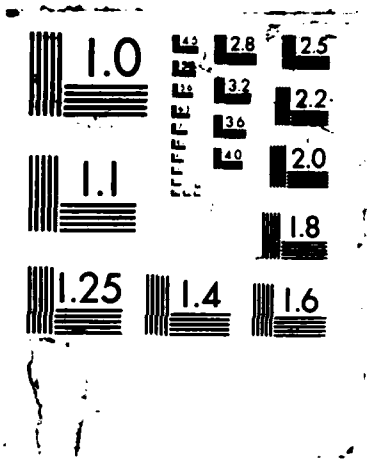
(2) During manufacturing process, degradation of transmission characteristics does not occur.

(3) The [illegible]

AD-A189 610 PROCEEDINGS OF THE INTERNATIONAL WIRE AND CABLE SYMPOSIUM (36TH) HELD IN..(U) ARMY COMMUNICATIONS-ELECTRONICS COMMAND FORT MONMOUTH NJ 8/9

UNCLASSIFIED 19 NOV 87 F/G 9/1 NL



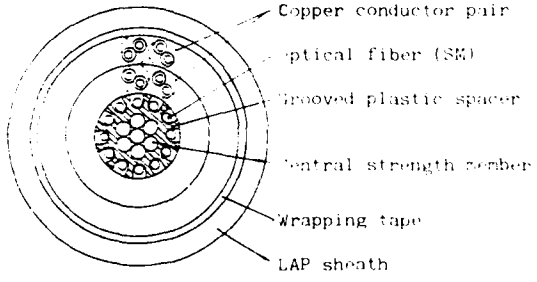

1.0
1.1
1.25
1.4
1.6
1.8
2.0
2.2
2.5
2.8
3.2
3.6
4.0

2.2 Cable construction

The constructions of two kinds of the composite cable are shown in Fig.1 and Fig.2.

Type 1. 12 SM fibers and 0.9mm×30pairs

This cable is installed over 200m without jointing. So to make the cable diameter smaller for the saving of duct spaces, the grooved plastic spacer which accommodates 12 single mode fibers is placed in the center of this cable. The fiber is 0.9 mm diameter and has the tight buffer coating. 30 pairs of 0.9mm copper conductor are stranded around the central spacer. The cable core is covered with the LAP (Laminated Alminium Polyethylene) sheath of 2.0mm thickness.

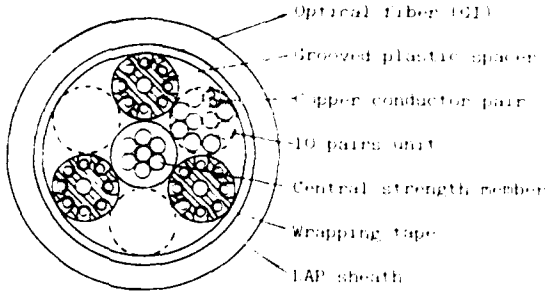


Diameter : 31mm
Weight : 870kg/km

Fig.1 Type 1 cable structure
(12 SM fibers and 0.9mm X 30 pairs)

Type 2. 24 GI fibers and 0.65mm ×30pairs

This cable is used in the system of 2km distance, and jointed together in the center of 2km length. 24 graded index optical fibers are placed in the slots of 3 grooved plastic spacers. 10 pairs of 0.65mm copper conductor are stranded into a unit. Considering the jointing, 3 grooved plastic spacers and three 10-pair units are stranded around the central strength member. The cable core is covered with the LAP sheath of 2.0mm thickness.



Diameter : 31mm
Weight : 880kg/km

Fig.2 Type 2 cable structure
(24 GI fibers and 0.65mm X 30 pairs)

Type 1 cable is designed that the optical grooved spacer is placed in the center of this cable, so the overall diameter is smaller. On the other hand, Type 2 cable is designed that the optical grooved spacers are placed in the outer layer, so the optical jointing is easily. It is possible to select Type 1 or Type 2 composite cable, according to the demand of every system.

3. Transmission loss in manufacturing processes

The transmission loss changes of two kinds of the composite cable during each manufacturing process were measured. The results of measured are shown in Fig.3. These changes are kept within measurement error range, because optical fibers are protected by the grooved spacer from lateral pressure of copper conductors.

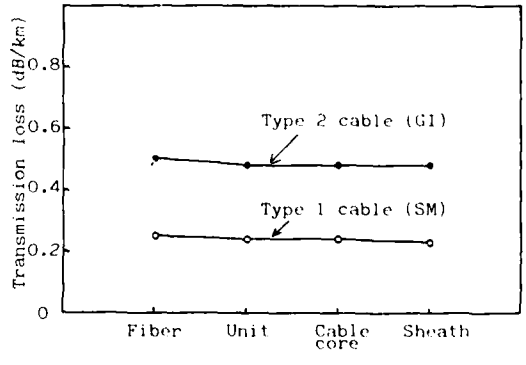


Fig.3 Transmission loss in manufacturing process

4. Mechanical characteristics of composite cable

4.1 Tensile Test

The length of sample cable was 5 meter, both ends of the cable were secured. While the cable was tensed up to 1500kg, the change of the transmission loss and the elongation was measured. The results shows that the transmission loss of two composite cables doesn't change up to the load of 1500kg. The results of the elongation of Type 2 cable are shown in Fig.4.

The dashed line in Fig.4 shows the calculated values. (however, without regard to the stress distribution of copper conductors). The difference between two lines in Fig.4 is considered to be due to the stress distribution of copper conductors. Young's modulus of copper conductors is given by

$$E(Cu) = \frac{T1 - T2}{S} \cdot \frac{\ell}{\Delta\ell}$$

E(Cu) : Young's modulus (kg/ mm²)
T1 : Tension of composite cable at $\Delta\ell$ (kg)
T2 : Tension of composite cable without copper conductor at $\Delta\ell$ (kg)
S : Cross section copper conductor (mm²)
ℓ : Cable length (mm)
$\Delta\ell$: Elongation (mm)

The calculated value of Young's modulus of copper conductors using above formula is 6.5 x 10 kg/m m². So in case of the composite cable, the allowed tensile strength can be designed to deliberate both Young's modulus of the strength member and copper conductors. However, Young's modulus of copper conductors is considered to change with the stranding pitch and the insulation thickness.

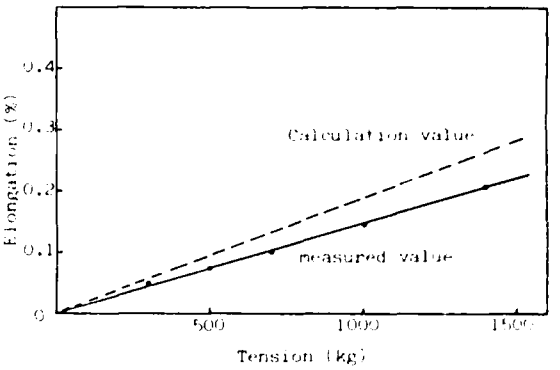


Fig.4 Tension-elongation characteristic

4.2 Bending Test

The sample cable was bended around the mandrel whose radius was 6 times and 10 times as large as the outer diameter of the cable. The test was repeated for 10 times. The results shows that the transmission loss didn't increased at 6 and 10 times mandrel. The bent area of the cable didn't show visible evidence of the fracture.

4.3 Torsion Test

The length of sample cable was 1m, and both ends of the cable were secured. While the cable was weighted 50kg and the lower was twisted left and right 180 ° .the change of optical loss was measured. When composite cables were twisted to the right, optical fibers were elongated. The results shows that the optical loss does not increase when the cable is twisted to the left and right.

4.4 Squeezing Test

As shown in Fig.5, both ends of cable were secured under loads of 250kg and 500kg, the cable were bended in a 90° at a radius of 250mm. We measured the change of the optical loss and the insulation resistance of copper conductors. If the cable is squeezed, the insulations of copper conductors may be damaged by grooved plastic spacers. The results shows that the optical loss and insulation resistance are not changed. After this test, the sample cable was dismantled, and we checked each component of the cable. However, there weren't damages on the surfaces of optical fibers and insulations.

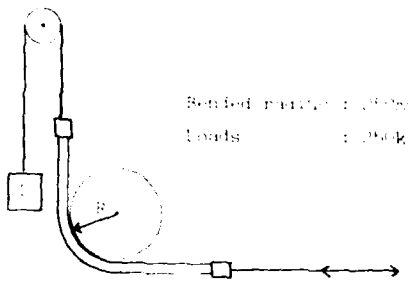


Fig.5 Squeezing test method

5. Jointing of composite cable

We examined the jointing of two kinds of composite cable. Type 1 composite cable has optical grooved speacer in the center, so two jointing methods were considered.

Case 1 After optical fibers were spliced and accommodated, copper conductors were jointed around them.

Case 2 After optical fibers were taken out, copper conductors were jointed, and optical fibers were spliced and accommodated beside copper jointing.

Case 1 method has the problem that the closer is larger. So, on case 2 method, optical fibers must be protected from lateral pressure of copper conductors when these were take out from the copper jointing. And also the jointing operation is difficult and it will take a long time.

On the other hand, in the case of Type 2 cable, as the optical grooved spacers are stranded around the central strength member together with the copper units, optical fibers taken out can be easily. It is possible that optical fibers are spliced and accommodated beside the copper jointing. So, it was able to use the conventional closure as shown in Fig.6.

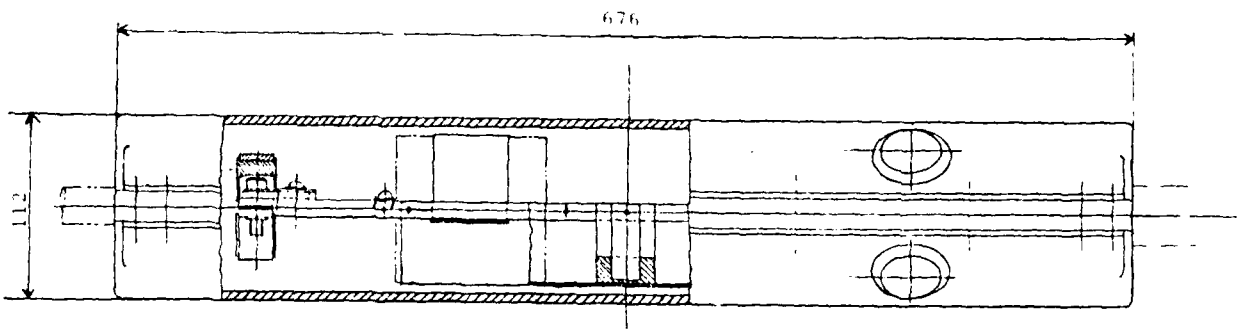


Fig. 6. Closure structure

6. Conclusions

We have developed two kinds of the composite cable containing optical fibers and multi copper pairs. We confirmed that the composite cable can be manufactured stably and have satisfactory mechanical characteristics. Now the composite cables developed was inslalled, and used in each system.

References

(1) T.Matsuo et al., " Composite Submarine Cable Containing Optical Fibers And Pilot Pairs ". 35th IWCS, 1986.

(2) S.Shimada et al., " Characteristics of Optical/ Copper Composite Cable ". IECE Japan, NO.1814 National Convention 1982.

(3) S.Takaoka et al., " Design and Electrical Characteristics of High Quality Communication Pairs in optical/copper Pairs Composite Cable " IEICE Japan, NO.2040 National Convention 1987.



Shin Shimada
Sumitomo Electric Industries, Ltd.
1, Taya-cho,
Sakae-ku, Yokohama
Japan

Shin Shimada received his B.S. and M.S. degrees both in telecommunication engineering from Waseda University in 1970 and 1972, respectively. He then joined Sumitomo Electric Industries, Ltd. and has been engaged in development and design of communication cable and optical fiber cable. Mr. Shimada is now a assustant manager of fiber optics division, and also a member of the IEEE and the Institute of Electronics, Information and Communication Engineers of Japan.



Yuzo Tokumaru
Sumitomo Electric Industries, Ltd.
1, Taya-cho,
Sakae-ku, Yokohama
Japan

Yuzo Tokumaru graduated from Oita Technical College 1970 in mechanical engineering. He then joined Sumitomo Electric Industries, Ltd. and has been engaged in development and design of accessories for communication cable and optical fiber cable. He is now an senior engineer of Communication cable Accessories Engineering Section.



Satoshi Hisano
Sumitomo Electric Industries, Ltd.
1, Taya-cho,
Sakae-ku, Yokohama
Japan

Satoshi Hisano received the B.E.degree from Sizuoka University in 1983. He joined Sumitomo Electric Industries, Ltd. in 1983, and has been engaged in development and design of optical fiber cable and communication cable. He is a member of the Institute of Electronics, Information and Communication Engineers of Japan.



Yoshikazu Amano
Sumitomo Electric Industries, Ltd.
1, Taya-cho,
Sakae-ku, Yokohama
Japan

Yoshikazu Amano received a B.S. degree in electrical engineering from Osaka University in 1968. He joined Sumitomo Electric Industries, Ltd. in 1968, and has been engaged in development and design of communication cable and optical fiber cable. He is a manager of cable Engineering Section of Communication Division and is a member of the institute of Electronics, Information and Communication Engineers of Japan.

DESIGNING COMPRESSION RESISTANCE in LOOSE TUBE CABLES

Paul E. Neveux, Jr. and William H. Hatton

Sumitomo Electric Research Triangle, Inc., Research Triangle Park, North Carolina, 27709

ABSTRACT

The relative contribution of each component in the cable to resist compression was determined from the results of compression experiments. An equation which relates the dimensions and material composition of the element in the cable to compression performance is described. The intrinsic compressive resistance of several materials were determined from this equation. Also discussed is how the stranding pitch and other cable parameters affect compression resistance.

I. INTRODUCTION

One of the primary functions of a loose tube cable is to resist compressive forces which may cause attenuation losses or worse permanent fiber damage. These compressive forces can either by those externally applied or, more insidiously, the forces exerted by the central strength member against the loose tubes during installation. In order to protect the fiber, a cable design must have the right material in the right configuration to oppose these forces. In addition, it is important to be able to predict what changes will occur in a cable's ability to resist compression when materials or component dimensions change. To our knowledge these issues have not been previously addressed in manner which might allow prediction of a trend in the cable performance.

II. EXPERIMENTAL

A. Theory

The general equation for an external circumferential pressure is

$$P = \frac{f\pi l}{3} * \frac{(od - id)^3}{(od + id)^3} \qquad \text{Equation (1)}$$

where f = material constant, l = the length of the tube in cm, id = the internal diameter, od = the external diameter. The term containing the outer and inner diameters is dimensionless and will be considered, for discussion purposes, as the geometric factor,

$$GF = \frac{(od - id)^3}{(od + id)^3} \qquad \text{Equation (2)}$$

The parameter, f, can be found by experimentally determining, P, the yield point of the material in a stress-strain curve. The first step in the process is to determine the dependence of *P* on the *length, l, keeping the size of the* tube , and hence, GF, constant. By plotting P vs. l the slope of the line is equivalent to the remaining terms in the equation:

$$m(1) = \frac{f\pi}{3} * \frac{(od - id)^3}{(od + id)^3} \qquad \text{Equation (3)}$$

The next step in the analysis is to plot the slopes of this equation from various sizes of tubes of the same material vs. their geometric factor, GF. The slope of this curve is proportional to the following:

$$m(2) = \frac{f\pi}{3} \qquad \text{Equation (4)}$$

Therefore, by multiplying the slope, m(2), by $3/\pi$, the material constant, f, can be derived:

$$f = \frac{m(2) * 3}{\pi} \qquad \text{Equation (5)}$$

B. Methodology

All samples were tested using an Instron with a 5 kN load cell and a 10 cm by 10 cm compression pad. The results were plotted an a chart recorder. The internal and external diameters of

the tubes were determined with a Nikon V-12 Optical Comparator.

C. Materials

The three materials tested were commercially available linear low-density polyethylene used in the cable sheath, and polybutylene terepthalate and nylon 12, used in the loose tubes.

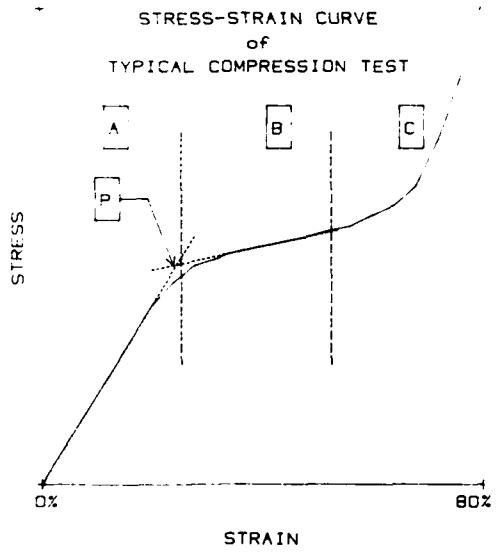
III. RESULTS and DISCUSSION

A. Factors Affecting Compression Resistance in Loose Tube Cables.

1. General Considerations

P is obtained from the stress-strain curve of tubes placed between the compression pads of a standard Instron. A typical curve with the characteristic regions are shown in Figure 1. In region A, the stress rises quickly until the yield point, P is reached. Here, in region B, the tube

FIGURE 1.



begins to deform. In region C, the top and the bottom inner wall have contacted and the stress is seen to rise quickly. Typically, the Yield Point was used for the value, P, and was determined by taking the intersection of the slopes of regions A and B. In some cases, as will be explained below, this was not possible.

In an effort to identify the most critical component in resisting compression a typical loose tube cable was carefully taken apart and the components tested for their compression resistance. Shown in Table 1 are the results of this investigation.

Table 1. Compression Resistance of Various Loose Tube Components

Component	Compression Resistance (N/cm)
Full Sheath (steel armor)	122
Outer PE Sheath + Steel Armor	58
Inner PE Sheath	33
PBT Loose Tube	162

As can be seen from the table, the loose tube itself contributes over approximately one half of the compression resistance of the cable. Because of the nature of the dependence of geometry on compression resistance small changes in the dimension of the much smaller loose tube affect the compression resistance greater than small changes in the dimensionally larger sheath. For this reason the discussion will now focus on the loose tube which plays a major role in both external and internal compressive resistance.

2. Material.

In order to determine the parameter, f, in Equation (1) various tube sizes of PBT were made. First, the compression resistance for a particular tube size was plotted against the length of the tube. The results for the different tube sizes are shown in Figure 2. By taking the slope of these curves and plotting against the geometric factor, the length dependence is removed, and the material constant, f, is obtained. The graph, shown in Figure 3, yields an f-value of 2558 N/cm. Shown in Figure 4 is a comparison of nylon and PBT tubes whose sizes are essentially the same. As can be seen the compression resistance of nylon is nearly half that of PBT.

FIGURE 2.

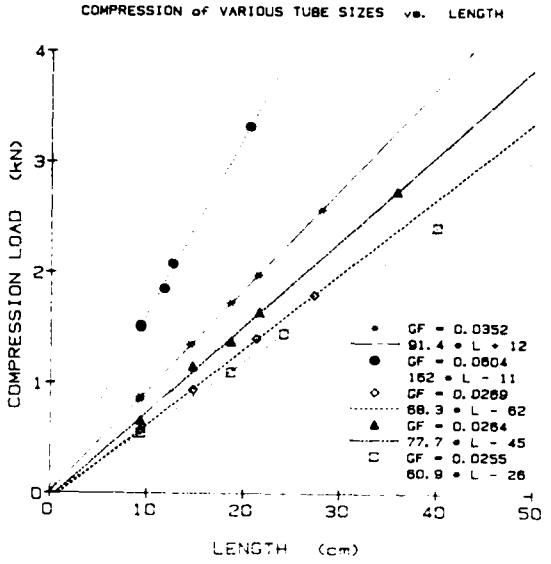
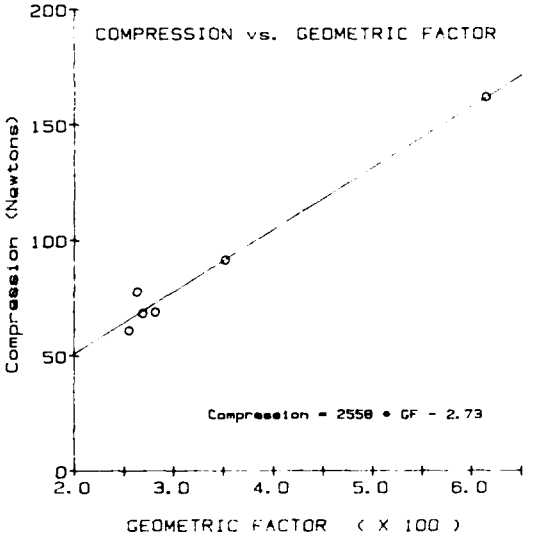
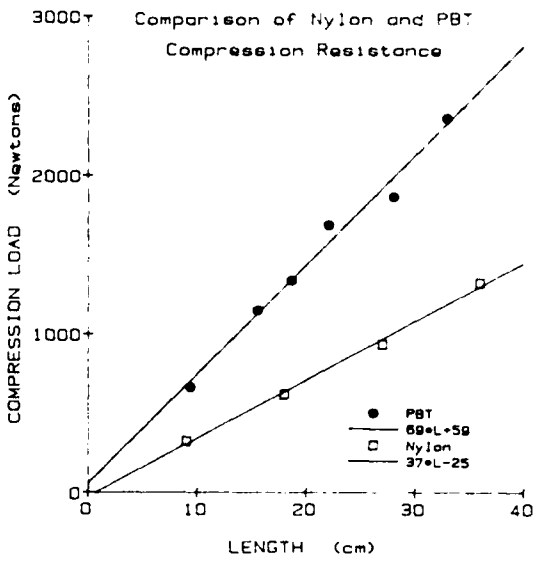


FIGURE 3.



Intuitively, the common mechanical characteristic which would contribute the most to compression resistance would be flexural modulus. If the f value for the two materials are compared with their respective flexural moduli, a definite correlation is apparent: the f values for PBT and nylon are 2558 N/cm and 1404 N/cm, respectively, while the flexural moduli for the materials are 2600 N/mm² and 1170 N/mm², respectively.

FIGURE 4.

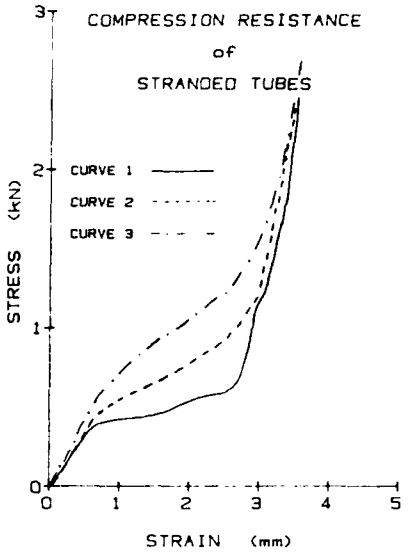


3. 'Adjacent Tube Support'

An experiment was performed utilizing six loose tubes around a central strength member. The stranding pitch was set at 135 mm with the tubes tightly held in place with hose clamps. Three different stress-strain curves were obtained as shown in Figure 5. The first curve was obtained with the hose clamps at least 20 cm from the 10 cm² testing area. The second had hose clamps adjacent the compression pads. The hose clamps helped prevent the tubes from slipping off the central strength member. In the third curve, the area to be tested was tightly wrapped with tape. As can be seen from the figure, the more the tubes were prevented from being displaced from their normal position, the more they aided the tube supporting most of the compression force. In this way the compression force was dissipated by adjacent tubes, in addition to the central strength member.

Note from the figure that the yield point becomes progressively obscure as the amount of adjacent tube support increases. In this case it might be better to use the slope in region 'B' to describe the change in the cores' ability to withstand compression.

FIGURE 5.



The reliance on adjacent tube support cannot be understated. Although a full mathematical treatment is necessary to fully explain the dynamics involved, it is clear that a tightly designed cable will be able to withstand greater compression than a cable where there is significant clearance between tubes.

4. Stranding Pitch.

In order to determine the effect of stranding pitch on the compression resistance, it was not possible to simply test various cable cores with different stranding pitches due to the interaction of the tubes in the core, i.e., adjacent tube support. Instead parallel rows of PBT tubes were arranged approximately one cm apart on the compression pad. On top of these tubes, a 2.7 mm steel central strength member was placed at 90° to the tubes for the first test and at a 45° angle in the second test. The 0° angle was accomplished by simply placing a tube by itself on the compression pad. The compression results, shown in Figure 5, were normalized to the unit length, cm.

Since degrees are not normally used to express stranding pitch, the conversion is as follows:

$$\text{Pitch} = \frac{\pi * D}{\tan \alpha} \qquad \text{Equation (5)}$$

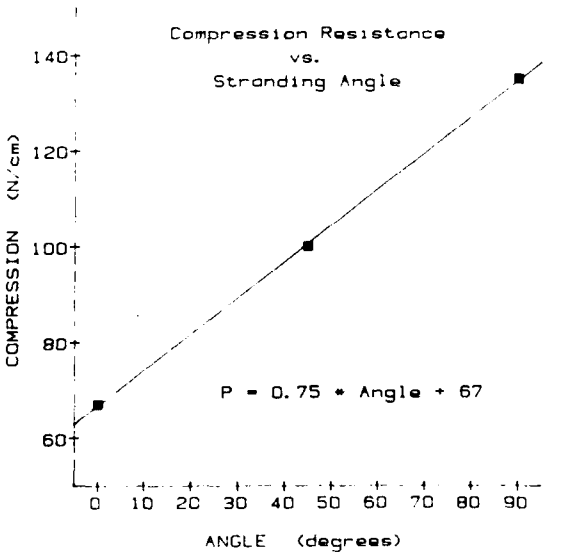
where D = the stranding diameter (tube o.d. + c.s.m. o.d.) and α = the angle of the tube with respect to the central strength member. In Table 2 below the various stranding angles and their corresponding pitches are given using a typical value of πD.

Table 2. Correlation Between Stranding Angle and Stranding Pitch.

Angle, α (degrees)	Stranding Pitch (mm)
0°	∞
5°	183
10°	91
15°	60
25°	34
45°	16
85°	1.4
90°	0

As a consequence of this relationship, a 90° angle yields a 0 mm pitch - a manufacturing impossibility - and a 0° angle yields an infinite pitch - an undesirable manufacturing possibility. Despite these practical questions, the experiment displayed a trend which might not otherwise have been assumed.

FIGURE 6.



The results of the experiment show that compression resistance increases slightly with decreasing pitch. This result was substantiated in actual cables where the pitches were 100 mm and 85 mm: the cable with the smaller pitch displayed improved compression resistance. It must also be remembered that, all other parameters being constant, the space between the tubes decrease with decreasing pitch. So that while pitch alone may help compression resistance, the close packing of the tubes probably plays a more significant role.

As mentioned above this test was performed using PBT tubes. It is not known what, if any, affect on the curve would be if another material, e.g. nylon, was used.

B. Designing for Compression Resistance in Loose Tube Cables.

As the results indicate above increasing the tube wall thickness, decreasing the pitch, using a material with a high flexural modulus, and placing the tubes in a core tightly next to each other, would all improve the compression resistance of the cable. Changes in these parameters obviously cannot be made indiscriminantly and must be made with other design and performance considerations. Increasing the flexural modulus of the tube, for example, would make for a sturdier tube, but the likelihood of problems, such as the tube kinking in the splice box would increase.

The results from 'Adjacent Tube Support' point to the important concept of force distribution in enhancing compression resistance: the more the force applied to one tube is distributed along its circumference, the more force the tube is able to withstand. Taking this idea to its logical conclusion, having a matrix with a higher modulus than the typical flooding compound around the tubes would impart significant compression resistance.

In addition to the parameters discussed above, there are a number of other factors which have not been taken into account, e.g. the steel armor, or the type of polyethylene. Given these other factors, it would be difficult to give an accurate relationship which describes the mechanical characteristics of the individual elements of the cable and a predicted value of compression resistance based solely on the items discussed in this paper.

CONCLUSIONS

The factors which contribute to compression resistance have been identified and discussed. The most important factor in resisting compression appears to be the loose tube itself. Although the overall cable design limits the dimensional improvement of the loose tube, the use of new polymer materials show promise in improving the compression performance by nearly 50% without compromising flexibility.

A mathematical model which describes the interaction of all the components is now under investigation.





Paul E. Neveux, Jr. obtained his double B.S. in Chemistry and Biology in 1979 from Antioch College, Yellow Springs, Ohio. After completing his Doctorate in Chemistry at the University of North Carolina in Chapel Hill, he held post-doctoral fellowship investigating conducting liquid crystal polymers under the direction of Dr. William Erigbaum. He joined Sumitomo Electric Research Triangle, Inc. in 1986. Recently, he has been consultant to Sumitomo Electric Fiber Optic Corp. as a materials and process development engineer. Dr. Neveux is a member of the American Chemical Society and the New York Academy of Sciences.

William Hatton received the B.S. and M.S. degrees in Electrical Engineering from North Carolina State University in 1981 and 1983, respectively. He joined Sumitomo Electric Research Triangle, Inc., in 1984 and has been engaged in the research and development of fiber optics cables and components. Mr. Hatton is a member of the Optical Society of America.

AN ANALYSIS OF LOOSE TUBE CABLE DESIGN THEORY, COMPATIBLE WITH PHYSICAL MEASUREMENT

I. Houghton, A. Summers, S. R. Barnes

STC Telecommunications, Newport, Gwent, UK.

ABSTRACT

The performance of loose tube cables is generally governed by two criteria: The ability of the cable to withstand the mechanical rigours of installation and service, and the ability of the cable to perform over a wide temperature range.

A model has been developed by STC to predict the performance of a loose tube cable under strain and at low temperatures.

1. INTRODUCTION

Design analyses of loose tube constructions have not previously considered the relationship between manufacturing processes, measurements, and theory. This has meant that the treatments have been of little practical use to optical cable makers. This is because most theoretical treatments have assumed that the mean position of the fibres in the tube is known at some stage of manufacture. However, in practice the position of fibres present in excess will vary along the tube, and experimental determination of the mean position is impractical. This has meant that the theories can only be used to determine cable performance with some prior knowledge of the performance of a cable using identical tubes. Similarly there is no theory to assist the cable designer to tailor the excess in the tubes to a specific requirement.

These limitations can be overcome by a theoretical treatment in which all the variables used can be determined on the cable and components experimentally. By relating this to the lay-up tensions of tubes, and given a knowledge of the stress-strain response of the tube material, the amount of excess fibre in the cable can then be determined. It is now possible to use the excess fibre data in the design analysis, rather than make an assumption for fibre position.

The theory of stranded loose tube cable design can now be advanced using excess fibre at tube manufacture as a variable. An expression is obtained that contains no indeterminate variables.

The expression can be used in three ways. Firstly, the fibre strains for given cable strains can be analysed for existing cable designs to determine fibre life. Secondly, when designing new cables, this expression can be used to define the minimum excess fibre level - the maximum excess level is determined by microbending at the environmental extremes. The expression therefore defines the lower limit of the fibre excess window. Finally, the expression can be used to determine how variation of materials and process conditions is likely to affect cable performance, particularly the environmental response.

2. THEORY

2.1 Overlength Of Fibre

The overlength of fibre (excess) in the cable is given by the ratio Y of unstrained fibre length to the cable length at stranding.

$$\text{Therefore } Y = UX, \qquad (1)$$

where U is the ratio of tube length at stranding against the cable length at stranding (see Fig. 1), given by:

$$U = \frac{\sqrt{(\pi(C+D))^2 + L^2}}{L}, \qquad (2)$$

where C = diameter of built up centre member
D = loose tube outer diameter
L = lay length at stranding

$$\text{and} \quad X = \frac{W(H+1)}{(I+1)}, \qquad (3)$$

where W = ratio of unstrained fibre length at measurement to strained tube length at measurement
H = tube strain at measurement
I = tube strain at stranding

2.2 Tensile Performance

The maximum allowable working tension T is calculated from the increase in lay length until the fibres reach their maximum permissible strain (see Fig. 2), and is given by.

$$T = EA\left[\frac{M(1+J)}{L} - 1\right], \quad (4)$$

where E is the tensile modulus of the strength member
A is the area of the strength member
J is the cable strain at stranding

M, the lay length at maximum working tension is given by:

$$M = \sqrt{(2YL)^2 - K^2}, \quad (5)$$

where Z is the maximum allowed fibre strain
K is the circumference of the strained outer fibre helix
and Y is the overlength of fibre given in equation (1)

2.3 Environmental Performance

Part 1

The environmental performance of the cable is largely determined by the radius of curvature of the fibres. By considering the fibres on a drum in an environmental chamber to be in a helix on a helix (see Fig. 3), the radius of curvature R can be calculated from the fibre excess using the equation.

$$R = \frac{2B^3}{2\pi Q - P} \quad (6)$$

$$\text{where } B = \sqrt{(s+r\sin\phi)^2 + r^2Q^2 + m^2 - 2rmQ\sin\phi}\ ; \quad (7)$$

$$Q = \sqrt{(s+r\sin\phi)^2 + r^2Q^4 + 2r^2Q^2(1+\cos^2\phi) + 2rsQ^2\sin\phi}\ ; \quad (8)$$

$$P = 2rQ(s+r\sin\phi)\cos\phi - 2rmQ^2\cos\phi\ ; \quad (9)$$

$$f = \frac{N}{2\pi}, \quad (10)$$

and ϕ is the point on the helix at which the curvature is measured
N is the laylength on the drum at the test temperature
r is the radius of the helix of the fibres within the tube
s is the supporting helix radius

Q is the number of helixes per lay, where Q is related to the length of fibre l in one lay at the test temperature by the integral:

$$l = \int_0^{2\pi} \sqrt{r^2\sin^2 Q\theta + F\sin Q\theta + G}\, d\theta, \quad (11)$$

where $F = 2rs - 2rsfQ$ (12)

$G = s^2 + r^2Q^2 + f^2$ (13)

and $l = YL(1+\sigma t)$ (14)

where σ is the fibre coefficient of thermal expansion
t is the difference between the stranding temperature and test temperature
Y is the overlength of fibre given in equation (1)

Part 2

When the cable is environmentally cycled, the fibre radius of curvature decreases. Because of the predominantly macrobending effects, the loss increment will eventually become critical at a radius Rc. The design of the fibre is defined by three critical parameters:

ω_c = spot size

λ_c = cut-off wavelength

λ_o = zero dispersion wavelength

These in turn define the tolerances on refractive index difference δn and core radius a. Typical ranges are:

n = n-m = 0.0045 to 0.0055

a = 4.0 to 4.5 microns

where n = core refractive index
m = cladding refractive index

The tolerances on refractive index difference and core radius uniquely define the propagation velocity constant V of a specified wavelength (see Fig. 4) by the equation:

$$V = \frac{2\pi a\sqrt{n^2-m^2}}{\lambda}. \quad (15)$$

The attenuation increment γ due to macrobending is given by:

$$\gamma = \frac{\pi}{2a}\left(\frac{a}{R}\right)^{\frac{1}{2}}\left(\frac{V^2w^2}{u^2}\right)^{\frac{1}{2}} \exp - \left[\frac{4Rw^3(n-m)}{3aV^2}\right], \quad (16)$$

where R = radius of curvature of fibre
u,w = scalar mode parameters

The propagation velocity constant can be shown to be proportional to bend performance (see Fig. 5). The highest increment due to bending is produced with the lowest V value [1]. The ranges of refractive index difference and core radii produce values of V in the range 1.8557 to 2.3083, which from Fig. 5 produces a dramatic change in bend performance. The critical bend radii Rc, to ensure a maximum increment of 0.2 dB at 1550 nm for the two extremes of V, are:

V	Rc
1.8557	21.5 mm
2.3083	10.6 mm

3. CONCLUSIONS

A theoretical model has been developed by STC which allows an optimisation of the critical parameters for both fibre and cable. This in turn gives the designer of loose tube optical cables the ability and freedom to select from

the range of input material and processing conditions which may be combined to produce high performance, tensile, and environmentally insensitive cables.

The benefits of such an approach to cable design are realised by viewing both optical fibre and optical cable manufacture as an integrated operation. High performance product may then be optimised with maximum manufacturing yields, leading to total cost-effective manufacture.

GLOSSARY OF TERMS

A = Area of strength member
B = Intermediate used in calculation
C = Diameter of built up centre member
D = Loose tube outer diameter
E = Tensile modulus of strength member
F = Intermediate used in calculation
G = Intermediate used in calculation
H = Tube strain at measurement
I = Tube strain at stranding
J = Cable strain at stranding
K = Circumference of stranded tube/fibre helix
L = Lay length at stranding
M = Lay length at maximum working tension
N = Lay length at room/test temperature
O = Intermediate used in calculation
P = Intermediate used in calculation
Q = Number of helixes per lay
R = Radius of curvature
T = Maximum allowable working tension
U = Ratio of tube length at stranding against the cable length at stranding
V = Propagation velocity constant
W = Ratio of unstrained fibre length at measurement against strained fibre length at measurement
X = Ratio of unstrained fibre length at measurement against strained tube length at stranding
Y = Ratio of unstrained fibre length against cable length at stranding
Z = Maximum allowed fibre strain
a = Fibre core radius
f = Intermediate used in calculation
l = Length of fibre in one lay at the test temperature
m = Cladding refractive index
n = Core refractive index
r = Radius of helix of fibre within tube
s = Supporting helix radius
t = Difference between stranding temperature and test temperature
u = Scalar mode parameter
w = Scalar mode parameter
ϕ = Point on helix at which curvature is measured
α = Fibre coefficient of thermal expansion
ω = Spot size
λ_c = Cut off wavelength
λ_o = Zero dispersion wavelength
δn = Refractive index difference
λ = Wavelength
γ = Attenuation increment

REFERENCES

[1] OPTICAL WAVEGUIDE THEORY
Snyder A. W., Love D. J.
Pub. Chapman & Hall 19[illegible]
ISBN 0 412 [illegible]

ACKNOWLEDGEMENT

The authors wish to thank Dr. J. P. Dakin et Mr. M. H. Ramsay for their comments and helpful assistance, and the Director of STC Submarine Systems Ltd for their permission to publish this paper.

DIAGRAMS

Fig. 1

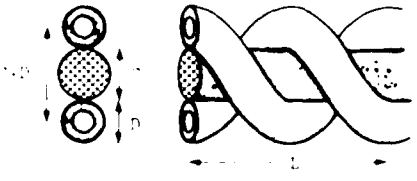


Fig. 2

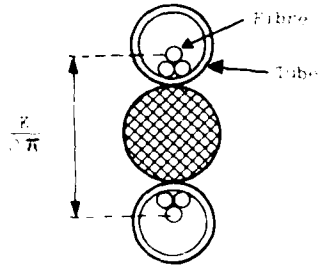


FIG. 3

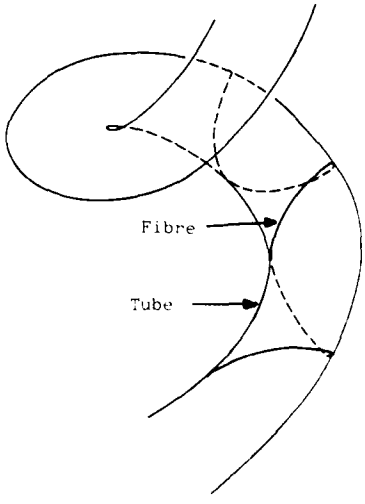


FIG. 4

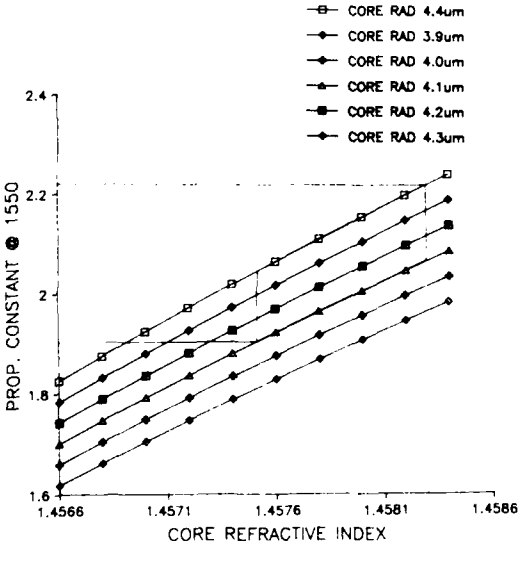
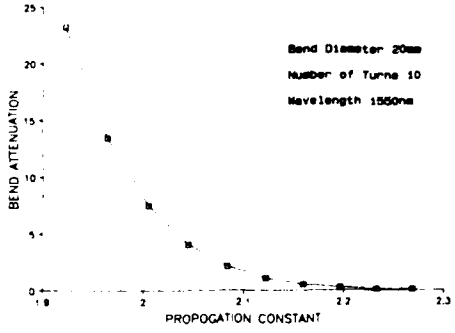


FIG. 5

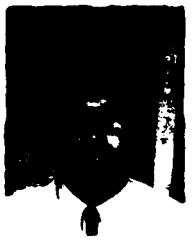


AUTHORS



Ian Houghton,
STC Telecommunications,
Cable Products Division,
Wednesbury Street,
Newport,
Gwent,
NP9 0WS,
UK.

Ian Houghton was born in London, England. He received a B.Sc. in Chemical Physics from the University of Sheffield in 1981. After graduation he worked as a polymer technologist for Metal Box Research and Development Division in Oxfordshire, until 1984. He then joined STC as Senior Development Engineer, Optical Cables. He has since been involved with equipment design for slotted core cables, design and manufacture of optical fibre ribbons, material studies and testing of composite, tube materials and filling compounds, aerial cable design and development, and development of loose tube cabling theory.



Andy Summers,
STC Telecommunications,
Cable Products Division,
Wednesbury Street,
Newport,
Gwent,
NP9 OWS,
UK.

Andy Summers was born in Haverfordwest, England, in 1961. He graduated from Aston University in 1984 with a B.Sc. in Electrical and Electronic Engineering. After this he joined STC as Measurements Engineer, to develop production and reference test methods for optical cable manufacture. In 1986 he became Quality Manager for the Optical Fibre and Cable Manufacturing Units, from where he became Development Manager for optical cables, based at Newport.



Dr. S, R. Barnes,
STC Telecommunications,
Cable Products Division,
Wednesbury Street,
Newport,
Gwent,
NP9 OWS,
UK.

Dr. S. R. Barnes was born in Worksop, England, and received a B.SC.(Eng.) and Ph.D from Queen Mary College, University of London. After this he joined STL where he was involved in many aspects of cable design and development; in particular, cables for submarine applications. Later he concentrated on all aspects of the manufacture of optical fibre cables. Currently he is Technical Manager of STC Cable Products Division, Newport.

PERFORMANCE CHARACTERISTICS OF ENHANCED BUFFER TUBE CABLE

R.J. WILLIAMS
NORTHERN TELECOM
OPTICAL CABLE DIV.
SASKATOON,
SASKATCHEWAN

J.A. ROWE
NORTHERN TELECOM
OPTICAL CABLE DIV.
SASKATOON,
SASKATCHEWAN

B.P. HURTIG
BELL CANADA
CORPORATE ENG.
TORONTO,
ONTARIO

M. PLOUFFE
BELL CANADA
CORPORATE ENG.
MONTREAL,
QUEBEC

ABSTRACT

This paper presents the design and performance characteristics of a tube in slot cable construction from the point of view of lightning withstand capability and the effect of water entering the cable due to lightning induced damage with subsequent freeze thaw conditions prevailing.

The optical performance and logitudinal water propagation within the cable is evaluated.

A new test method for evaluation of cable freeze thaw testing is proposed.

INTRODUCTION

Lightning strikes to ground in the vicinity of buried optical fiber cable can cause sheath holing and fiber attenuation/breakage. It is hypothesised that a lightning strike can damage a cable by crushing, thermal effects or arcing between metallic components of the cable. As reported previously (1), some of the effects of lightning strikes can be averted by increasing the dielectric strength of the cable and by increasing the mechanical cushioning to the fibers using a plastic layer next to the fibers. In the cable design where the fibers are placed in tubes and the tubes arranged in the slots of a slotted core, the tubes provide additional protection to the fibers.

Should cables become damaged by lightning or some other mechanical means, it is clear that in some cases the optical integrity of the cable will initially not be compromised. This damage may not easily be detected unless a definite fault such as a fiber break or OTDR point discontinuity exists at the damage location.

When a puncture in the cable sheath exposes optical fibers the potential exists for water to enter the cable. In certain areas there will be the possibility of water freezing inside the cable and for this reason it is important to evaluate this type of cable damage for short and long term cable performance effects.

Two areas are of major concern in cable freeze thaw cycling,

i) Expansion of ice within the cable may cause microbending which will affect the optical performance of the fibers,

ii) When a punctured cable sheath is exposed to a water head that alternately freezes and thaws, there may be a 'pumping' action which could force cable filling gel longitudinally down the cable. If this damage is close to a splice enclosure this pumping action could force the gel out of the tubes eventually allowing water to enter the closure.

It is necessary to evaluate cable characteristics to determine the effects of a cyclic freezing head of water on fiber microbending and also to determine the minimum length of cable which will effectively block any flow of gel/water due to a freeze thaw pumping action.

LIGHTNING WITHSTAND CAPABILITY OF OPTICAL CABLE CONSTRUCTIONS

Various constructions of tube in slot cable were selected for evaluation of their lightning withstand capability using the simulated lightning surge test method (as outlined in Bellcore

TR-TSY000020 (2)) The test set up is shown in Fig. 1.

Representitive values of the energy or I^2t are plotted against the test Lightning current in Fig. 2 for this configuration.

The cable samples were stressed with the simulated lightning stroke. All the fibers in the stressed samples were tested for optical continuity and the cable samples were opened to visually inspect for broken fibers. A probabilistic statistical approach was used to estimate and compare the test results for various cable designs.

The test current range was 60 to 160 KA. The current at which the 0.5% cumulative failure rate occurred is shown for comparison in Table 1. Estimates for the 95% confidence intervals are also provided. It should be noted that some uncertainty does exist, since it is not practical to keep all the test parameters absolutely constant.

To put these results in perspective it is emphasized that the probability of occurance for lightning strikes of the higher current magnitudes is low. This is illustrated in Fig. 3 (3).

It is important that the whole installed cable be capable of withstanding the lightning surge. Hence, the bond clamp assembly, at splice locations must be able to withstand the same lightning surge current as the cable. Proper bonding and grounding is thus essential for the installed cable. Maintaining shield continuity and providing grounds at repeaters and central offices are of the utmost importance from the electrical protection viewpoint

CABLE FREEZE THAW TESTING

The cable design chosen for evaluation was the tube in slot construction as shown in Fig. 4.

The cable contained three, four fiber tubes and two fillers in a 5-slot core with a dielectric strength member. The core was protected by a triple sheath consisting of a polysteelpeth jacket with rodent protective layer (ie. core/polyethylene/steel/ polyethylene/steel/polyethylene). Swellable tape was used as the water blocking agent under the middle and outer sheaths while gel was used in and around the tubes in the core.

SAMPLE PREPARATION

A 550 m sample of cable was hand coiled into an environmental chamber in oval shaped coils approximately 2 x 3 m in size. The ends of the cable were brought into the laboratory. Two fibers from each of the three tubes were spliced together to form two loops of fiber 3300 m long. (Fig. 5) One loop was monitored for attenuation change at 1.3 um the other for changes at 1.55 um.

A 6.4 mm hole was manually drilled with an end mill through the three sheaths and into one of the fiber tubes (Fig. 6) at a point 50 m from one end of the sample.

Attenuations on the two fiber loops were monitored during this drilling process to ensure that the fibers in the tube penetrated by the hole were not damaged. A 1 m head was applied via a 19 mm copper standpipe with a tee at one end. The tee was slipped over the cable until the sheath hole was aligned under the standpipe. The tee was then sealed to the cable sheath with heat shrink tube. A solution of red dyed water was used to aid in the detection of water paths in the cable at the conclusion of the test.

TEMPERATURE CYCLING

The cable was subjected to 54 cycles of minus 10 degrees C to plus 10 degrees C with a four hour soak at each temperature extreme. Cable temperature was monitored by removing one of the fiber tubes from a 0.5 m sample of cable and inserting a thermocouple in its place. This short length of cable was then placed into the middle of the test cable coils to provide an indication of the average core temperature. A second thermocouple was used to monitor chamber air temperature at the level of the cable coils. Output from both thermocouples was recorded continuously with a chart recorder.

TEST EQUIPMENT

Cable attenuations were monitored with the equipment arrangement shown in Fig. 5. A splitter was used to direct part

of the output of each laser directly to a detector. This was done to provide a reference signal for correction of laser drift. The outputs of the four detectors were read by a computer and stored on floppy disk at 2 minute intervals during the test. To help minimize equipment drift, the lasers, splitters and the four detectors were all contained in a small environmental chamber where the temperature was kept within the limits of 21 degrees C plus or minus 1 degree C.

ATTENUATION RESULTS

The changes in attenuation with time are shown graphically in Figs. 7 and 8 for the two fiber loops. Change in attenuation was calculated using the following formula.

$$A = 10 \times \log (P1/P2) - A1$$

where A = Attenuation change from start of test
A1 = Reference attenuation at start of test
P1 = Reference power level
P2 = Power level on monitored fiber loop

Essentially no significant change in attenuation was observed at either wavelength.

OTDR RESULTS

The two fiber loops were examined before and after temperature cycling with a 1.3 um OTDR and at the temperature extremes of the final cycle with a 1.55 nm OTDR. Results are shown in Fig. 9-18. The steps on the traces are located at the points where fibers were spliced together to form the loops.

The attenuations measured with the OTDR are summarized in Table 2.

The 1.3 um OTDR traces show no measurable effect from the temperature cycling on either fiber loop. The 1.55 um OTDR traces show no difference in fiber attenuation between the temperature extremes of the test. These results confirm the attenuation results gathered by the laser based test equipment during the 19 day test period.

The exact location of the hole was confirmed at the conclusion of the test by removing the water head standpipe and microbending the fibers. This is shown in the OTDR trace Fig. 19. Note that there is no evidence of any microbending induced attenuation losses due to frozen water in the punctured (ie. green) fiber tube in any of the OTDR traces when the cable is at minus 10 degrees C.

PHYSICAL EXAMINATION

There was no sign of physical degradation of the cable sheath in the vicinity of the puncture at the conclusion of the test (ie. no cracking or bulging). The sheaths were stripped and water ingress was measured. Results are summarized in Table 3.

WATER PENETRATION TEST

To determine the resistance of a cable to the pumping action of a freezing/thawing water head, the following test was undertaken.

Two samples of cable were each prepared with a 6.5 mm hole drilled through the three sheaths and into one of the fiber tubes. The first sample was 15 m long and had the hole drilled at the 5 m point. The second sample was 35 m long and had the hole drilled at the 15 m point. In this way cable lengths of 5, 10, 15 and 20 m were effectively tested.

A 1 m water head was applied via a 19 mm standpipe over the puncture and sealed to the cable as outlined previously.

Both samples were placed into the environmental chamber with the 550 m attenuation test sample. Excess length was coiled around the floor of the chamber in oval-shaped coils approximately 2 x 3 m in size.

The samples were cycled at the same rate as the 550 m attenuation sample (ie. 54 cycles of minus 10 degrees C to plus 10 degrees C with a four hour soak at each temperature extreme).

RESULTS

At the conclusion of the temperature cycling, the samples were stripped and water ingress through various paths was measured. Results are summarized in Table 3.

There was no evidence of gel being forced from the ends of any of the tubes in any sample during the test.

CONCLUSION

It is possible to design an optical cable with a lightning withstand capability in excess of 160 KA with respect to optical continuity. This is achieved by utilization of the tube in slot cable construction and a multiple sheath combination.

When a tube in slot cable sheath is punctured some ingress of water may take place which has no significant effect on attenuation at either 1.3 um or 1.55 um on this cable construction should subsequent freeze thaw conditions occur.

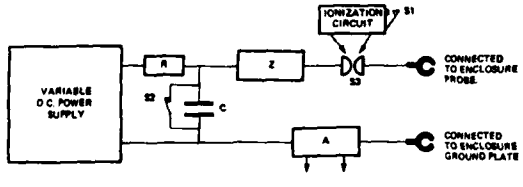
The pumping action of a 1 m freezing/thawing water head on this type of cable construction is not sufficiently strong to force gel from the end of a 5 m or longer cable sample.

REFERENCES

(1) G. McKay, W. Cousineau, B. Braham and J. Rowe, "Qualification Procedure for Fiber Optic Cable Design", International Wire and Cable Symposium Proceedings 1986 pp 307-314.

(2) Bell Communications Research, "Generic Requirements for Optical Fiber and Optical Fiber Cable", TR-TSY-000020, Issue 2, December 1986.

(3) E.D. Sunde, Earth Conduction Effects in Transmission Systems, D. Van Nostrand Company Inc., 1949.



S1 DISCHARGING SWITCH
S2 SAFETY SWITCH
S3 SPARK GAP
Z CURRENT LIMITING IMPEDANCE (L and R)
A CURRENT SENSING DETECTOR
C CAPACITORS
R CHARGING IMPEDANCE

FIG. 1 STIMULATED LIGHTNING SURGE TEST SET-UP

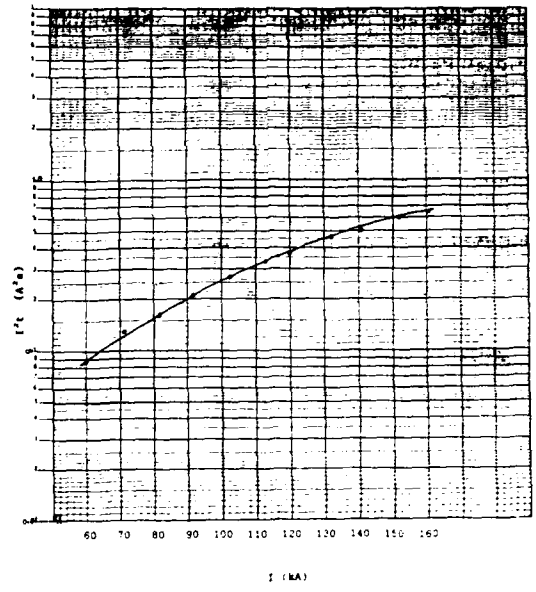


FIG. 2 REPRESENTATIVE VALUES OF I^2t Vs I FOR SIMULATED LIGHTNING TESTS

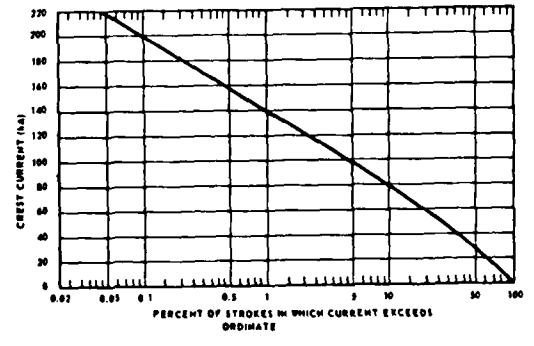


FIG. 3 CUMULATIVE PROBABILITY DISTRIBUTION OF LIGHTNING STROKE CREST CURRENTS TO BURIED METALLIC OBJECTS

TABLE 1: SIMULATED LIGHTNING SURGE WITHSTAND CAPABILITY OF TUBE IN SLOT OPTICAL FIBER CABLES

TYPE DESIGN	CABLE SECTION	SIMULATED LIGHTNING CURRENT AMPLITUDE WITHSTAND RATING RATE WITH NO DETECTABLE INTERNAL FIBER DAMAGE
	8 Dielectric with 864 Fiber Count	kA
	8 Dielectric with Steel Member	kA
All STEEL CORE WITH TUBES	Stranded with Jkt	kA
	Stranded	kA
	Stranded with Jkt No Fiber Slot	kA

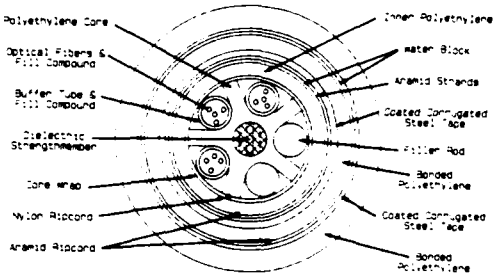


Fig. 4 TUBE IN SLOT CABLE CONSTRUCTION

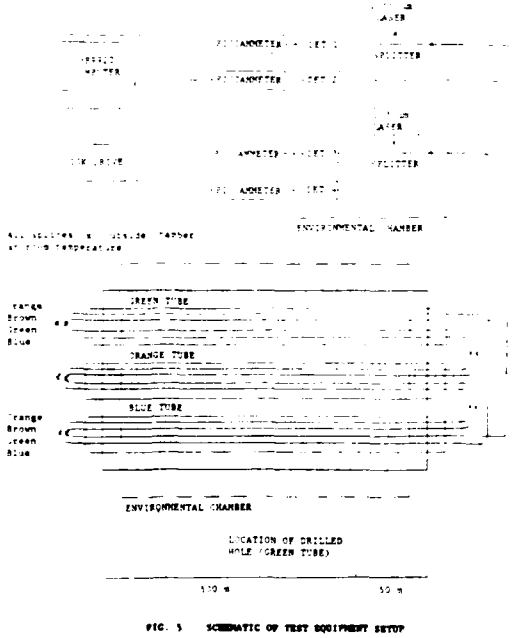


FIG. 5 SCHEMATIC OF TEST EQUIPMENT SETUP

6.4 mm

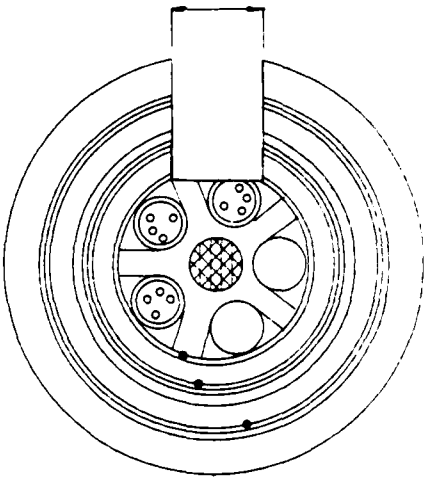
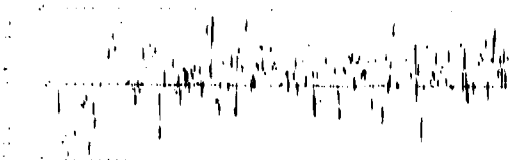
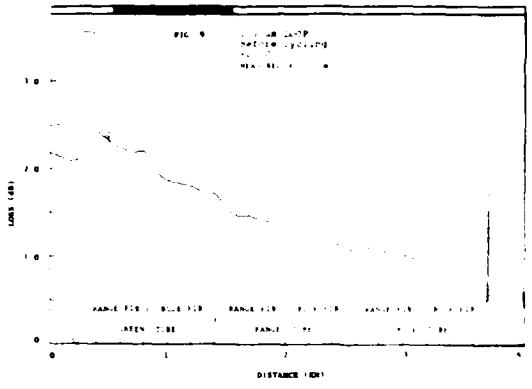
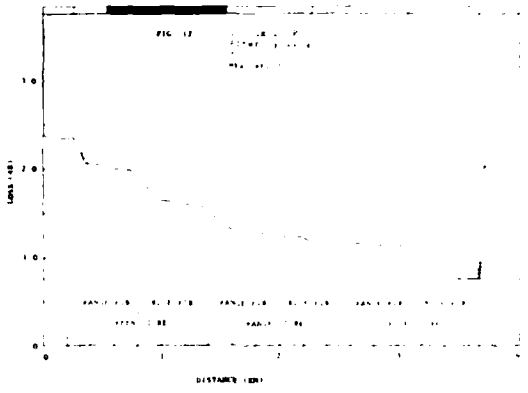


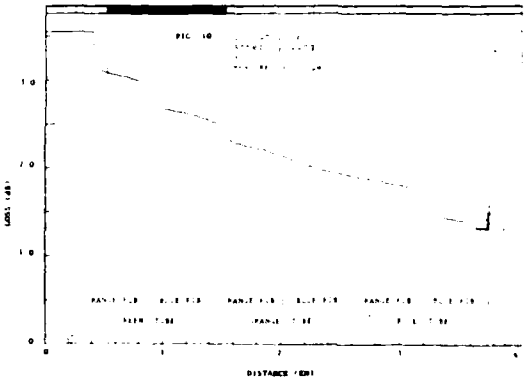
FIG. 6 6.4 mm HOLE DRILLED INTO CABLE

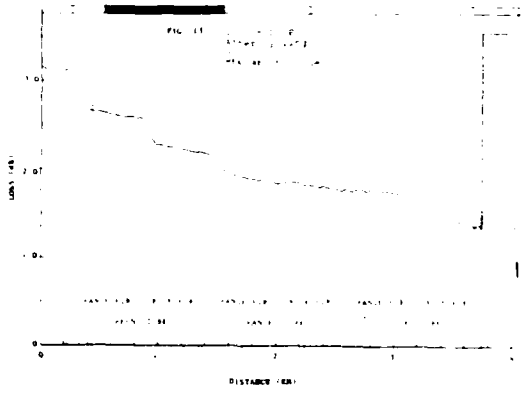


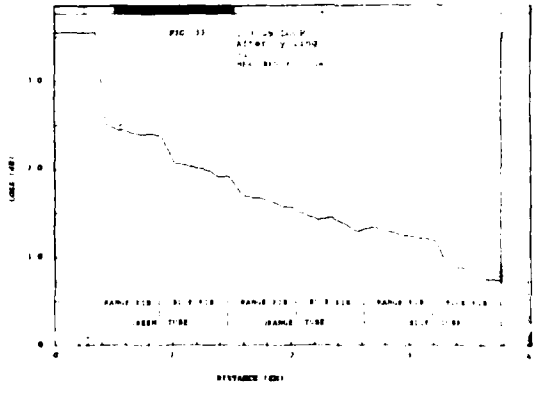


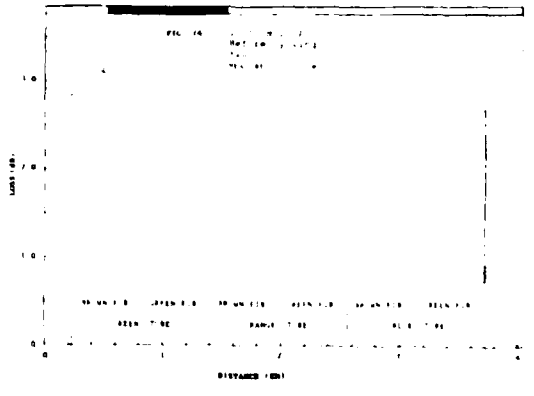


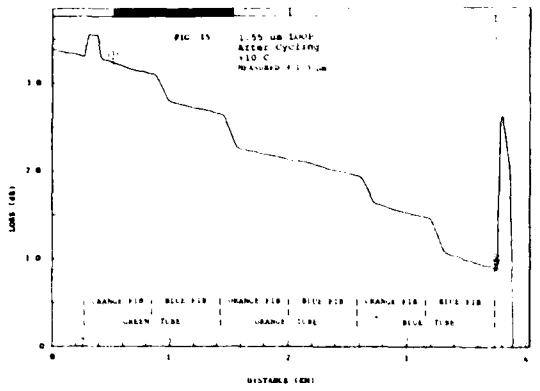


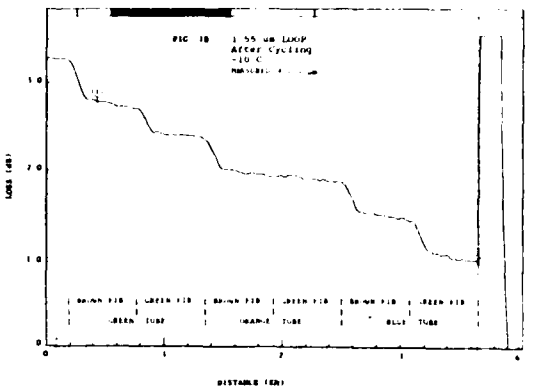












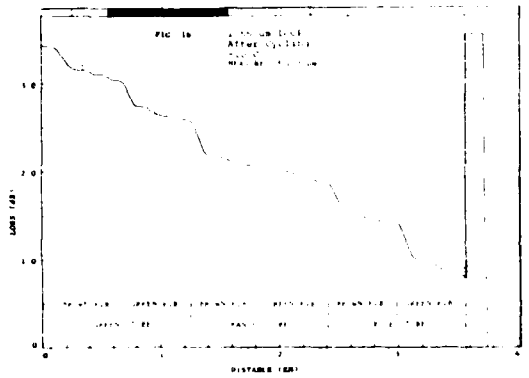
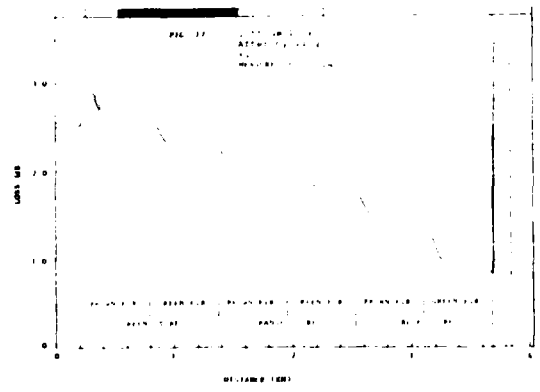


TABLE 2 SUMMARY OF ATTENUATION RESULTS FROM OTDR TRACES

	1.3 um LOOP (Blue/Orange Fibers)			1.55 um LOOP (Green/Brown Fibers)		
	dB/km	dB	km	dB/km	dB	km
1.3 um OTDR						
BEFORE CYCLING + 20 C	0.56	1.81	3.219	0.73	2.35	3.219
AFTER CYCLING +10 C	0.54	1.75	3.219	0.73	2.34	3.219
AFTER CYCLING -10 C	0.53	1.71	3.215	0.73	2.35	3.215
1.55 um OTDR						
AFTER CYCLING +10 C	0.39	1.29	3.313	0.56	1.86	3.313
AFTER CYCLING -10 C	0.40	1.31	3.311	0.56	1.81	3.219



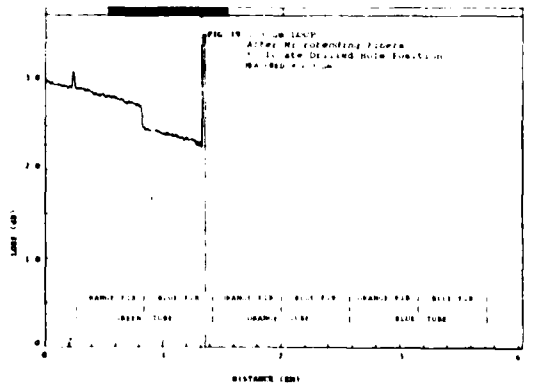


TABLE 3 DISTANCE (IN METERS) OF WATER PENETRATION AT CONCLUSION OF TEMPERATURE CYCLING TEST

TUBE 'COLOUR' IDENTIFIES THE TUBE PENETRATED BY THE DRILLED HOLE

PATH	SAMPLE #1		SAMPLE #2		SAMPLE #3	
	5 m	10 m	15 m	20 m	50 m	500 m
UNDER RODENT PROTECTIVE SHEATH	.11	.09	.05	.36	.46	.54
UNDER 2ND SHEATH	0	.08	.40	.39	.84	.93
UNDER 1ST SHEATH *ALONG RIPCORD	1.48	1.50	.36	.52	.46	.75
TUBE	GREEN		BLUE		GREEN	
PENETRATION	2.00	1.50	.28	.30	1.90	2.25



Robert John Williams was born and educated in Wales. While employed by Standard Telephones and Cables in Newport-Gwent, UK, he attained a Diploma in Engineering at the Gwent College of Technology. From 1973 to 1976, he worked on the production of submarine telephone cables at the Southampton, UK plant of S.T.C. In 1976, he emigrated to Canada and joined Northern Telecom at the Lachine Cable Plant in Quebec. He worked in the R&D laboratories, where he was primarily involved in environmental testing and the production of PVC formulations for wire and cable use. In 1980 he joined the Optical Cable Division of Northern Telecom where he has held a number of positions in the manufacture and development of optical cable. His most recent assignment being manager of Optical Cable Research and Development.



John A. Rowe Received a B.Sc. in Mechanical Engineering from the University of Saskatchewan in 1983 and joined the Northern Telecom, Optical Systems Division in Saskatoon, Saskatchewan the same year. He is currently a member of the Research and Development group responsible for the design and characterization of new fiber optic cable types.



Bannu P. Hurtig received a BASc in Electrical Engineering from the University of Waterloo and a MASc, also in Electrical Engineering from the University of Toronto. In 1985, she joined Bell Canada in the Network Transmission and Protection Standards group of Corporate Engineering. She is currently involved with the research necessary to develop the electrical protection standards for the optical fiber cable.



Michel Plouffe graduated in 1979 from Ecole Ploytechnique in Montreal, as an Industrial Engineer. He joined Bell Canada the same year and worked in Outside Plant Engineering and in Outside Plant Methods and Support. Since December 1984, he has been responsible to introduce Fiber Cable Design in Bell Canada, he is presently Section Manager Technology Development in charge of the Research and the Standardization of both copper and fiber cable design for Bell Canada.

A Novel Non-Polyurethane Re-enterable Encapsulant Compatible with Both Filled Cable and Polycarbonate Connectors

T.S. Croft, H.A. Haugen, S.P. Hays, T.I. Chen and G.J. Swampillai

TelComm Products Division Laboratory/3M
Austin, Texas

Abstract

Cable splices are widely protected from moisture penetration by splice closures filled with a re-enterable encapsulant in order to maintain the cable integrity. The present encapsulants are two part, extended polyurethane gels based on isocyanate compounds. This paper describes the development of a novel re-enterable encapsulant which is not based on isocyanate compounds. A theory is proposed which can explain and predict an encapsulant's ability to absorb cable filling materials and its compatibility with the polycarbonate connectors commonly used in cable splices. Data are presented relating the filling compound compatibility and polycarbonate compatibility, as seen in accelerated aging tests, to the approximate total solubility parameter of a polyester gel encapsulant system. The result is a new non-polyurethane encapsulant which offers compatibility both with the cable filling materials and with polycarbonate connectors.

Introduction

The development of filled cable, using a grease-like composition such as Flexgel[a] around the individual conductors, has greatly contributed to a reliable, low maintenance outside telephone plant. Recent work[1,2] has shown that oily interfaces can develop around these coated conductors when in contact with certain encapsulants and can potentially lead to water ingress. New second generation encapsulants absorb the filling compounds in the cable, allowing the encapsulant to seal around the wires removing a potential water pathway. This absorption capacity is measured by a coated conductor pullout test[3] and a filling compound compatibility test.[4]

An encapsulant has been developed using polyester chemistry which absorbs the cable filling material yet passes accelerated aging tests for polycarbonate compatibility under which polyurethane encapsulants have been reported to affect polycarbonate.[5] The compatibility testing on polycarbonate connectors with encapsulants reported in this paper was carried out with accelerated aging tests at 50°C and 60°C, similar to the test outlined in a recent technical paper.[5] Polycarbonate compatibility was monitored in one test following a flexure test outlined in ASTM D-790 in which connector modules were subjected to an Instron tensile testing machine to obtain a flexure force to failure (breaking) of the module.

The data obtained on the compatibility of an encapsulant with the filling compounds and with the polycarbonate connectors was related to the approximate total solubility parameter of the encapsulant system. This allowed a practical understanding of the relationship between the two to be obtained. It should be emphasized that this is a simplified correlation which does not utilize more sophisticated theories.[6]

Solubility Parameter

The solubility parameter concept is an attempt to quantify the old adage "like dissolves like". The solubility parameter values (represented by δ) are a measure of the intermolecular forces between the molecules in a material and are normally given without units. However, the values have the units $(\text{cal/per CC})^{\frac{1}{2}}$. Every compound or chemical system is characterized by a specific solubility parameter value and materials having similar solubility parameters tend to be miscible or dissolve. Solubility parameters can be obtained by experimentation or by calculation as reviewed by Barton.[6] Many of the values used in this paper have been estimated by summation of the effects contributed by the groups of molecular structure, using available group molar attraction constants developed by Hoy[7], not only for the individual components but also for the polymer itself.

For a plasticized crosslinked polymer system, the total solubility parameter would be the weighted arithmetic mean of the value of each component.

$$\delta_T = \delta_a \Phi_a + \delta_b \Phi_b + \delta_c \Phi_c \cdots$$

Where Φ a, Φ b and Φ c are the fractions of A,B, and C in the system, and δ a, δ b, and δ c are the solubility parameter of the individual components.

Compatibility with Cable Filling Compounds

Buried telecommunication cables may be filled with a hydrophobic filling material to help protect the cable core from water entry. The most common cable filler is Flexgel[1] which contains a styrene-ethylene/butylene-styrene block copolymer dissolved in a paraffinic or naphthenic oil, with

[a]Registered trademark of AT&T

polyethylene added for consistency. Other cables may have petroleum jelly (PJ) or polyethylene modified petroleum jelly (PEPJ). Both petroleum jelly grease and Flexgel filled cables have shown oily interfaces when in contact with encapsulants in cable splices which can potentially lead to water ingress and subsequent failure of the closure.[1,2] An encapsulant which is compatible with the filling compound in the cable and which absorbs the filling compounds allows the encapsulant to close or seal around the wire, thus obtaining the adhesion to filled cable conductors.

The encapsulant development work at 3M did not involve isocyanates. Instead, the base polymer utilized is a polyester derived from polybutadiene. The solubility parameter of polybutadiene has been reported to be about 8.2[8] based on calculations with Hoy's method[7]. Similar calculations for the polyester derived from polybutadiene resulted in a value of 8.3 which was then used for further calculation of the total solubility parameter of the candidate encapsulants (plasticized polymer encapsulant system).

A series of encapsulants were prepared with the base polymer extended with hydrocarbon extender oils (see Table I). The absorption of the filling

Table I - Extender Oils

Name	Aniline Point °F	Calc. Sol. Par. Extender Oil[a]
Flexon 766	223	7.6
Tufflo 500	192	7.67
Tufflo 300	188	7.7
Calumet 200	175	7.7
Calumet 6100	160	7.7
Flexon 391	129	7.76
Telura 171	117	7.9
Sundex 750T	121	7.94

[a]The following equation was used to determine the solubility parameter for the hydrocarbon extender oils[9].

$$\delta = 6.9 + 0.02 \text{ Kauri-butanol value}$$

The Kauri-butanol value was calculated using the following equation[10].

$$KB = 21.5 + 0.206 (\% \text{ wt. naphthenes}) + 0.723 (\% \text{ wt. aromatics})$$

compounds was measured by a coated conductor pullout test. Uncleaned conductors from filled cable were placed in the uncured encapsulant and the force necessary to pull the conductors after the encapsulant had cured was measured[3]. Table II details the results of the coated conductor pullout test using conductors from PEPJ and Flexgel filled General Cables and the calculated total solubility parameter for each oil plasticized polymer encapsulant system. The data

Table II - Oil Plasticized Polymer Encapsulant System[a]

Extender Oil Used	Calc. Total Sol. Par (δ_T)[b] for Oil Plasticized Polymer Encap. System	Coated Conductor[c] Pullout Force (lbs) PEPJ	Flexgel
Flexon 766	7.8	0.2	0.4
Tufflo 500	7.86	0.1	0.6
Calumet 200	7.9	0.2	1.5
Tufflo 300	7.9	0.2	2.8
Calumet 6100	7.9	0.8	2.1
Flexon 391	7.92	2.3	6.7
Telura 171	8.0	4.2	6.2
Sundex 750T	8.03	4.6	5.7

[a]Formulation - 35% polyester derived from polybutadiene, 64.7-64.8% extender oil, 0.2-0.3% catalyst.

[b]The following equation was used to determine the total solubility parameter of the oil plasticized polymer encapsulant system.

$$\delta_T = \delta_a \Phi_a + \delta_b \Phi_b$$

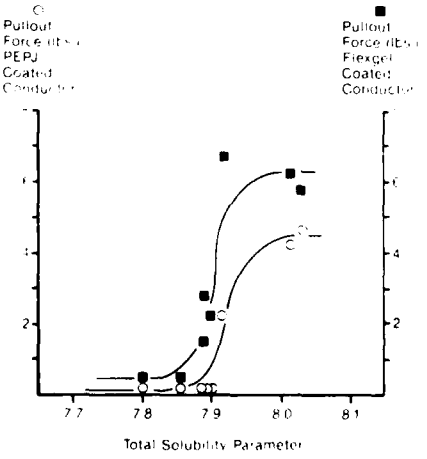
Where Φ_a and Φ_b were the weight fractions of the polymer and extender oil, respectively and δ_a and δ_b the solubility parameter of the polymer and extender oil respectively.

[c]General Cable.

are plotted in Figure 1, and show little absorption of filling material if the total solubility parameter was below 7.9. A threshold value of about 8.0 must be reached to achieve adhesion to both the PEPJ and Flexgel cable

Figure 1

Correlation of the pullout force of coated conductors to the calculated total solubility parameter of oil plasticized polymer encapsulant system



filling compounds, thus establishing the lower limit of the encapsulants solubility parameter for compatibility with the filling compounds.

Another method used to quantify the solvating power of the hydrocarbon extender oil was also included in Table I. The aniline point (defined as the minimum temperature for a complete mixing of aniline and a petroleum product) is utilized to indicate the aromatic content of hydrocarbon extender oils. A high number indicates a low aromatic content whereas a lower number signifies a higher aromatic content. Although not plotted, a distinct correlation can be seen between the aniline point of the extender oil used in the oil extended polymer encapsulant and the coated conductor pullout force data (see Tables I and II). Adhesion to grease coated conductors with the cured encapsulant increased dramatically with aromatic type extender oils (low aniline point). However, it is well known in the industry that extender oils high in aromatic content cause stress cracking of polycarbonate splicing connectors[11].

Therefore, data was collected utilizing ester plasticizers to prepare an additional series of encapsulants with the base polymer. A series of ester plasticizers containing at least two ester groups were chosen with steadily increasing solubility parameters. Table III indicates the solubility parameters for this series of ester plasticizers. The results of the pullout force of uncleaned PEPJ and Flexgel coated conductors from each ester plastisized polymer encapsulant system are presented in Table IV, as is the calculated total solubility parameter for each.

Table III - Ester Plasticizers

Name (structure)	Solubility Parameter
Emery 2900 [di(2-ethylhexyl dimerate]	7.8[a]
Kodaflex TXIB [2,2,4-trimethyl-1,3-pentanediol diisobutyrate]	8.2[a]
Soybean Oil	8.3[11]
Plasthall DTDA [Ditridecyl adipate]	8.5[a]
Flexricn P-6 [butyl acetyl ricinoleate]	8.6[a]
Nuoplaz 6959 [tris (2-ethyl hexyl)trimellitate]	8.9[a]
Hatco DOP [dioctyl phthalate]	9.0[a]
Hatco DBP [dibutyl phthalate]	9.6[a]
Benzoflex 9-88 [dipropylene glycol dibenzoate]	9.8[a]

[a]Calculated by method of Hoy[7]

Table IV - Ester Plasticized Polymer Encapsulant System[a]

Extender Oil Used	Calc. Total Sol. Par. (δ)[b] for Ester Plasticized Polymer Encap. System	Coated Conductor[c] Pullout Force (lbs) PEPJ	Flexgel
Emery 2900	8.0	2.9	3.8
Kodaflex TXIB	8.2	4.7	5.7
Soybean Oil	8.3	4.4	5.5
Plasthall DTDA	8.4	4.5	5.8
Flexricin P-6	8.5	4.1	6.0
Nuoplaz 6959	8.6	3.9	5.3
Hatco DOP	8.7	4.6	6.1
Hatco DBP	9.1	4.6	4.1
Benzoflex 9-88	9.2	2.2	1.8

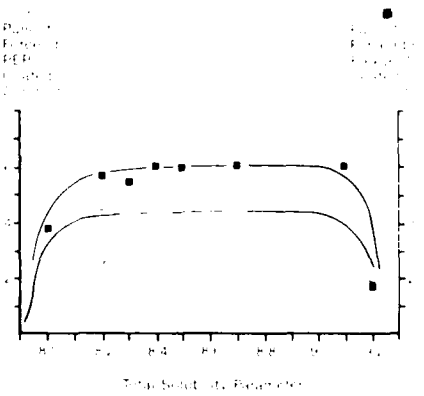
[a]Formulation - 40% polyester derived from polybutadiene, 59% ester plastisizer, 1.0% catalyst.

[b]The total solubility parameter determined as the weighted arithmetic mean of the value of each component (see Table II for method).

[c]General Cable

The data from Table IV was plotted in Figure 2 to indicate the correlation of the pullout force from the coated conductor pullout test to the calculated total solubility parameter of each ester plasticized polymer encapsulant system. A

Figure 2



generally constant absorption of both PEPJ and Flexgel occurred over a solubility range from about 8.0 to 9.0 with the adhesion of the cured

encapsulant to PEPJ coated conductors of about 4.2 lbs/conductor and to Flexgel coated conductors of about 6.0 lbs/conductor.

The absorption by this series of ester plasticized polymer encapsulant systems of PJ, PEPJ, and Flexgel has also been measured following the filling compound compatibility test of the Bellcore reenterable encapsulant specification[4]. This test consists of determining the percent weight change of a specified amount of encapsulant in contact with a similar amount of filling compound at 70°F for seven days. Only the room temperature test was run due to the volatility of some of the ester plasticizers. The percent weight changes with the filling compounds to the encapsulants are summarized in Table V and the

Table V - Filling Compound Compatibility at 70°F of Ester Plasticized Polymer Encapsulant System[a]

Ester Plasticizer	Calc Total Sol Par. (δ)[b] for Ester Plasticized Polymer Encap. System	Percent Change with Filling Compound[c] Flexgel	PEPJ	PJ
Emery 2900	8.0	7.1	1.0	1.3
Kodaflex TXIB	8.2	9.4	3.2	3.2
Soybean Oil	8.3	6.7	1.9	2.1
Plasthall DTDA	8.4	6.1	2.6	3.4
Flexricin P-6	8.5	10.8	5.9	2.8
Nuoplaz 6959	8.6	5.0	2.5	2.2
Hatco DOP	8.7	7.2	4.0	2.2
Hatco DBP	9.1	9.5	5.1	1.0
Benzoflex 9-88	9.2	3.1	3.5	-0.6

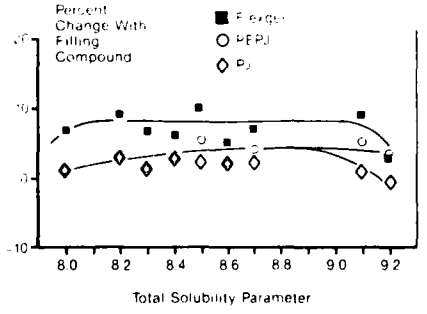
[a]Formulation - 40% polyester derived from polybutadiene, 59% ester plasticizer, 1% catalyst.

[b]The total solubility parameter determined as the weighted arithmetic mean of the value of each component (see Table II for method).

[c]Flexgel from Witco
PEPJ, GCI from Witco
PJ, Penreco Cable Filler Base Code 4576

Figure 3

Correlation of the filling compound compatibility at 70°F to the calculated total solubility parameter of ester plasticized polymer encapsulant system



data plotted in Figure 3. A general constant absorption of Flexgel was noted over a total solubility parameter range of about 8.0 to 9.0. A similar absorption range was exhibited with both PEPJ and PJ although at a lower level. The fact that encapsulants have higher compatibility with Flexgel than petroleum jelly has also been noted previously[1,2,5].

Why are the cable filling materials absorbed in this solubility parameter region? We postulate that the answer lies in the fact that "like dissolves like" and the plastisized polymer encapsulant system is substantially compatible with major constituents of the Flexgel, PEPJ or PJ filling material. For example, each block in the styrene-ethylene/ butylene-stryene block copolymer in Flexgel exhibits its own characteristic solubility parameter value and can then be individually dissolved by a suitable system. Table VI indicates the solubility parameters of major constituents in the PJ, PEPJ and Flexgel cable filling compounds and an encapsulant with a total solubility parameter in this region should interact in some fashion.

Table VI - Solubility Parameters (δ)

	(δ)
Flexgel	
Kraton 1650[12]	
Polyethylene/ Butylene Block	7.9
Polystyrene Block	9.1
Polyethylene[13]	7.8-8.3
Grease	
Petrolatum[a]	7.8
Polyethylene[13]	8.1
Polycarbonate[13]	9.3-10.3

[a]Calculated as C_{16} alkane but solubility parameter should be broadened since petrolatum is a mixture.

Polycarbonate Connector Compatibility

Compatibility with polycarbonate has the opposite meaning to that of the previous section. Since absorption of the cable filling materials into the encapsulant was necessary to obtain adhesion to the coated conductors, the total solubility parameter of the encapsulant was adjusted to dissolve some portion of the filling material. An encapsulant should be as far as possible, in total solubility parameter, from that of polycarbonate to prevent stress cracking, crazing or weakening of the polycarbonate connectors. A solubility parameter of 9.3 to 10.3 has been reported for polycarbonate[13] (see Table VI).

Two methods were utilized to test for compatibility with polycarbonate. The first method was to immerse polycarbonate bars in the

ester plasticized polymer encapsulant systems. The total solubility parameter for each encapsulant, presented in Table IV, is repeated in Tables VII and VIII. After 21 days at 122°F (50°C), the bars were removed from the encapsulants, conditioned at 23°C for 24 hours, and tested for tensile strength at a cross head speed of 0.5 mm/sec using an Instron Model 1123 tensile machine. This data is collected in Table VII and plotted in Figure 4. The second method utilized 3M MS²™ Super Mate™ 4005-DPM module splicing connectors spliced with the maximum wire gauge recommended (22 gauge) emmersed in the encapsulants for 9 weeks at 50°C. During and following the test, the modules were subjected to the Instron tensile machine to obtain a flexure force to break the modules (flexure force to failure) following the procedure outlined in ASTM D790. This data is collected in Table VIII and is plotted in Figure 5. See Attachment A and B for method descriptions.

Table VII - Ester Plasticized Polymer Encapsulant System[a] Compatibility to Polycarbonate Bar After 21 Days at 50°C

Ester Plasticizer Used	Calc Total Sol. Par. (δ)[b] For Ester Plasticized Polymer Encap. System	Tensile Strength[c] (N/Cm²)	Tensile Strength as Percent of Control[d]
Control	-----	6510	100
Emery 2900	8.0	6020	92
Soybean Oil	8.3	6330	97
Plasthall DTDA	8.4	5800	89
Flexricin P-6	8.5	5420	83
Nuoplaz 6959	8.6	5750	88
Hatco DOP	8.7	5060	78
Hatco DBP	9.1	4440	68
Benzoflex 9-88	9.2	4280	66

[a]Formulation - 40% Polyester derived from polybutadiene, 59% ester plasticizer, 1% catalyst.

[b]The total solubility parameter determined as the weighed arithmetic mean of the value of each component (see Table II for method).

[c]Average of three samples.

[d]Tensile Strength of Encapsulated Bar After Test / Tensile strength of non-encapsulated bar control. x100

Table VIII - Ester Plasticized Polymer Encapsulant System[a] Compatibility to 3M 4005 DPM Polycarbonate Module After 63 Days at 50°C

Ester Plasticizer Used	Calc Total Sol. Par. (δ)[b] For Ester Plasticized Polymer Encap. System	Breaking Force (lbs)[c]	Breaking Force as Percent of Control[d]
Control	----	121	100
Emery 2900	8.0	128	106
Soybean Oil	8.3	123	102
Plasthall DTDA	8.4	116	96
Nuoplaz 6959	8.6	108	89
Hatco DOP	8.7	37	31
Hatco DBP	9.1	26	21
Benzoflex 9-88	9.2	27	22

[a]Formulation - 40% polyester derived from polybutadiene - 58-59.7% plasticizer, 0.3-1% catalyst.

[b]The total solubility parameter determined as the weighed arithmetic mean of the value of each component (see Table II for method).

[c]Average of three samples.

[d]Breaking Force of Encapsulated Module After Test / Breaking force of non-encapsulant module control x 100.

Figure 4

Correlation of polycarbonate bar compatibility after 21 days at 50°C to calculated total solubility parameter of ester plasticized polymer encapsulant system.

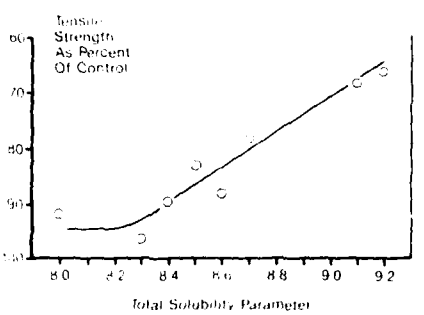
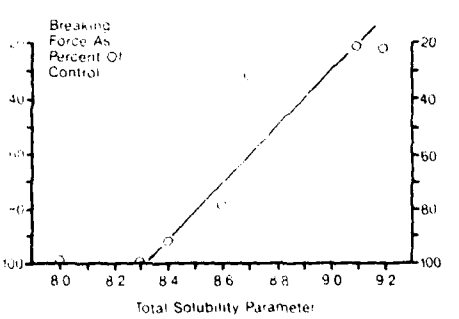


Figure 5

Correlation of polycarbonate module compatibility after 63 days at 50°C to calculated total solubility parameter of ester plasticized polymer encapsulant system.



An examination of both Figures 4 and 5 revealed that to be fully compatible, i.e. non-weakening or non-stress cracking, the total solubility parameter of the encapsulant system should be below about 8.3. This would be about one solubility parameter unit from the 9.3 lower limit reported to be the solubility parameter of polycarbonate (see Table VI). This falls midway in the region reported in the literature[14] to be the crazing region for polycarbonate and well below the region of solubility parameter range of 9.0 to 10.7 which is the cracking region for polycarbonate.

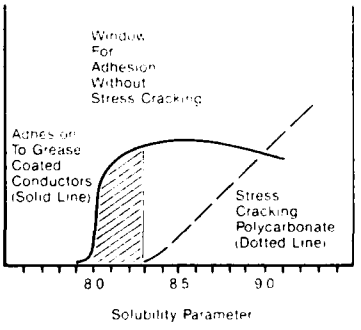
Solubility Parameter Theory Applied to Re-enterable Encapsulant

The previous sections indicated that a threshold solubility parameter value of about 7.9 was the lower limit to achieve absorption of cable filler and obtain adhesion to the coated conductors. In addition, a generally constant absorption of the cable filling materials occurred if the total solubility parameter of the encapsulant had a range of about 8.0 to 9.0. Finally, the accelerated aging test data were interpreted to indicate that the total solubility parameter of the encapsulant should be below about 8.3 to avoid weakening or stress cracking the polycarbonate connectors. Therefore, there is a window in which the total solubility parameter of an encapsulant can be situated where adhesion can be obtained without stress cracking the polycarbonate.

Figure 6 is an idealized representation of the relationship between adhesion to grease coated conductors from filled cables and the stress cracking of polycarbonate. Absorption of the cable filling materials occurred in the range of about 8.0 to 9.0 where the encapsulant was substantially compatible with the major constituents in the cable filling compounds. Stress cracking of the polycarbonate connecting devices steadily increases as the total solubility parameter of the encapsulant goes above 8.3 and increases toward the solubility parameter of polycarbonate at 9.3 to 10.3.

Figure 6

Relationship of solubility parameter of encapsulant to adhesion to grease coated conductors and stress cracking of polycarbonate



3M Brand 4442 High Gel Re-enterable Encapsulant

The total solubility parameter of 3M Brand 4442 High Gel[a] encapsulant has been adjusted to fall within the window discussed in the last section.

When accelerated aging at 60°C was carried out with fully spliced 3M 4005 DPM connecting modules encapsulated with 4442 High Gel, no change was observed in the breaking force to failure data after 63 days. This would indicate that 4442 High Gel did not weaken the module under these conditions (see Table IX for data). A recent paper[5] presented data from a similar test on 710 SB1-25 modular connectors in D-Encapsulant and D-1000 Encapsulant, both polyurethane encapsulants. These data have been incorporated into Table IX

Table IX - Flexure Force to Failure Data for Encapsulated Splice Modular Connectors at 60°C

	Aging Time, Days	Breaking Force, lbs. 4005 DPM[a]	710-SB1[b]
Control (not encapsulated)	0	128c	136c
	7	130	---
	15	---	130
	21	129	---
	31	---	119
	63	129	---
3M 4442 High Gel	7	130	---
	21	130	---
	63	127	---
D-Encapsulant	15	---	92
	31	---	84
D-1000	15	---	70
	31	---	75

[a]3M MS²™ Super Mate™ 4005-DPM Modules, average of 3 samples.

[b]Data taken from Table IV of reference 5 on AT&T Technologies, 710 SB1-25 modular connector, average of 2 samples.

[c]Initial breaking force at 23°C.

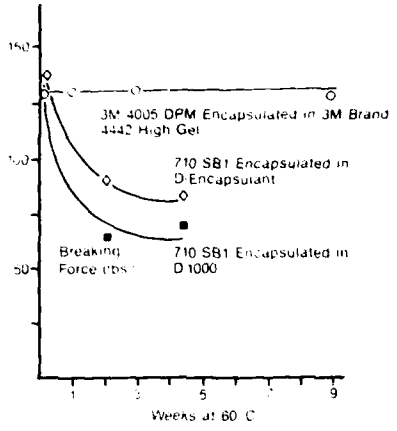
and plotted along with the 3M data on 3M 4442 High Gel in Figure 7. Both the 3M and AT&T tests obtain the breaking force to failure on the encapsulated modules following ASTM D 790 after accelerated aging, although the duration of the 3M test is 63 days compared to 31 days in the AT&T test sequence.

Examination of Table IX and Figure 7 indicated that 3M 4442 High Gel did not stress crack 3M 4005-DPM modules in an accelerated aging test whereas D-Encapsulant and D-1000 affected 710-SB1 modular connectors in a similar test.

[a]Registered trademark of 3M.

Figure 7

Compatibility test of encapsulants on polycarbonate modules at 60°C.



Examination of Table IX and Figure 7 indicated that 3M 4442 High Gel did not stress crack 3M 4005-DPM modules in an accelerated aging test whereas D-Encapsulant and D-1000 affected 710-SB1 modular connectors in a similar test.

Conclusions

The use of the total solubility parameter of an encapsulant provides a practical method for understanding the encapsulants compatibility with both cable filling compounds and polycarbonate connectors. Data were presented which indicated a window in which the total solubility parameter of an encapsulant could be situated to obtain adhesion to filled cable conductors without stress cracking polycarbonate connectors. The result is a new encapsulant based on polyester chemistry which offers the first alternative to polyurethane encapsulants based on isocyanates. This new encapsulant does not stress crack polycarbonate modules in accelerated aging tests and does not exhibit environmental difficulties normally reported for isocyanate based polyurethanes.

Acknowledgements

The authors wish to thank the following people for their contributions to the paper: Michael C. Reese and Karen Staff; and to Doreen Grubicy, A.J. Swiderski, Bonnie LeMere and Sue Lytle for their help in preparing this manuscript.

References

1. Mitchell, D.M. and Sabia, R., Proceedings of the Twenty-Ninth International Wire and Cable Symposium, p. 15, 1980

2. Dawes, K. And McNeal, T.E., Proceedings of the Thirty-Fourth International Wire and Cable Symposium, p. 402, 1985

3. BellSouth Specification CAO 8735-BS dated May 1, 1985 on "Re-enterable Encapsulants".

4. Bellcore Technical Advisory TA-TSY-000354 dated February, 1986 on "Re-enterable Encapsulants".

5. Chapin, J.T. and Sabia, R., Proceedings of the Thirty-Fourth International Wire and Cable Symposium, p. 418, 1985

6. A.F.M. Barton "CRC Handbook of Solubility Parameters and Other Cohesion Parameters", 1983, CRC Press, Boca Ranton, Florida

7. K.L. Hoy, "Tables of Solubility Parameters", Union Carbide Corporation, 1975; J. Paint Technol. 42, 76 (1970)

8. Barton, op. cit., pg. 314

9. W.W. Reynolds and E.C. Larson, Off. Dig. Fed.Soc. Paint Technol. 34, 311 (1962)

10. Shell Chemicals, "Solvent Power", Technical Bulletin ICS (X)/79/2, 1979

11. M. Brauer, W.J. Downey, F.C. Naughton, J.C. Chao U.S. Patent 4,596,743 (1986)

12. Shell Chemical Company Technical Bulletin "Kraton G 1650 Thermoplastic Rubber", SC:38-82

13. Barton, op. cit., pg 280

14. J. Miltz, A.T. DeBenenetto and S. Petric, J. of Materials Science, 13, p. 2037 (1978)

Attachment A

Compatibility Testing of Encapsulant with Polycarbonate Bars

1.1 The polycarbonate bar compatibility with the encapsulant will be tested as follows:

1.11 This evaluation requires polycarbonate bars, 5" x 1/2" x 1/8", from General Electric, Lexan 141-112 (clear).

1.12 Measure the tensile strength in newtons per cm² of three bars following the tensile test method outline in ASTM D638 using an Instron tensile machine at a cross head speed of 0.5 mm. These values will serves as con-

1.13 Lai an aluminum tray as: Control-3 weeks and lace three of the above bars in the tray These modules will not be enca ulated.

1.14 Label each aluminum tray as: Encapsulant 3 weeks. Place three of the above bars in each tray.

1.15 Prepare the encapsulant to be tested and fill each tray, except the control tray, so that all bars are submerged in the encapsulant.

1.16 Allow the encapsulant to cure 24 hours.

1.17 Place all the sample trays in an air circulating oven at 50°C.

1.18 Remove the trays after three weeks and allow to cool to room temperature. Peel away the encapsulant from the bars.

1.19 Measure the tensile strength of the bars as in 1.12 for the control and for each encapsulant-3 weeks tray.

Attachment B

Compatibility Testing of Encapsulant with Polycarbonate Modules

1.1 The module compatibility with the encapsulant will be tested as follows:

1.11 The module evaluation requires thirty telecommunication connector modules. Each module will be crimped with the maximum wire gauge allowed, and the conductor shall be of solid PIC insulation. This step is required to impart maximum stress on each module.

Note: Conductors of the crimped module will be of any length.

1.12 Measure the breaking force in pounds of three modules, following the flexure test outlined in ASTM D790 using an Instron tensile machine at a cross head speed of 0.5 in/min. (support span of 130 mm, radius support cylinder of 0.5 inch, nose radius of 0.75 inch). These values will serve as controls.

1.13 Label three aluminum trays: Control 1 week, Control 3 weeks, and Control 9 weeks. In each tray, place three of the above modules. These modules will not be encapsulated.

1.14 Label three aluminum trays: 1 week, 3 weeks, and 9 weeks. In each tray place six of the above modules.

1.15 Prepare the encapsulant according to the manufacture's instructions, and fill each tray, except the control trays, so that all modules are submerged in the encapsulant.

1.16 As soon as possible and before gelling has occurred, place each aluminum tray, except the control trays, into a pressure pot and apply an external pressure of 20 psi until the encapsulant gels.

1.17 Allow encapsulant to cure 24 hours.

1.18 Place all the sample trays in an air-circulating oven at 50°C.

1.19 Remove the 1-week tray and allow to cool to room temperature. Peel away the encapsulant from the modules.

Measure the breaking force following the flexure test as in 1.12 for three modules.

1.20 Remove the control 1-week tray and allow to cool to room temperature. Measure the breaking force as in 1.12 using three modules.

1.21 Repeat 1.19 and 1.20 at the 3 week and 9 week intervals.



3M Company
TelComm Products Division
2111 West Braker Lane
Austin, Texas 78769-2963

Dr. Thomas S. (Stoney) Croft - Dr. Croft received a B.S. in Chemistry from the University of Florida and a PhD. in Organic Chemistry from the University of Colorado. He has worked at 3M since 1966 and is presently a Senior Research Specialist.



3M Company
TelComm Products Division
2111 West Braker Lane
Austin, Texas 78769-2963

Dr. Tsung I. (Tony) Chen - Dr. Chen is a member of technical staff in TelComm Products Division/3M. He received a M.S. in Chemical Engineering from the University of Virginia and a PhD. in Polymer Science from the University of Akron. He has been active in research and development of polymeric materials for various applications from their structure-property-performance correlations since he joined 3M in 1976.



3M Company
TelComm Products Division
2111 West Braker Lane
Austin, Texas 78769-2963

Steven P. Hays - Mr. Hays graduated from the University of Virginia in 1983 with a B.S. degree in Chemical Engineering. He is employed by 3M TelComm Products Division.



3M Laboratories (Europe)
Electro-Telecommuncations
Georg-Wilhelm-Strasse 183
Postfach 93 0240
2102 Hamburg 93

Dr. Gregory J. Swampillai - Dr. Swampillai obtained his B.S. in Chemical Engineering from Liverpool University, England and his Ph.D. degree in Polymer Science from London University, England. He became working at the University as lecturere. This was followed by work at Paint Research Association in England. Since joining 3M he has been engaged in Polymer development. He is a member of the Institute of Chemical Engineering and the Plastics and Rubber Institute, both in England.



3M Company
TelComm Products Division
2111 West Braker Lane
Austin, Texas 78769-2963

Hartwick A. (Hart) Haugen - Mr. Haugen received a A.A. degree in Mathematics and Science from Waldorf College of Iowa. He joined TelComm Products Division of 3M in 1981. Currently, Hart is attending the University of Texas at Austin.

A NOVEL ADHESIVE CLOSURE SYSTEM FOR HEAT RECOVERABLE SLEEVES

Linwood P. Beltz, Thomas J. Bonk, Tsung I. Chen,
Patricia M. Olson, Jeanine I. Zeller-Pendrey
Douglas E. Weiss

TelComm Products Division Laboratory/3M
Austin, Texas

Abstract

Heat recoverable articles are used extensively in telecommunications over sheath splice bundles, often in directly buried applications. This paper will describe a wraparound heat recoverable sleeve closure mechanism that consists of a high strength, high temperature resistant acrylic pressure sensitive adhesive tape. Central to the performance of this tape is a high adhesion coating which chemically bonds to the adhesive. Several of the problems involved in the development of the pressure sensitive tape were overcome using interesting new test metnods. These accurately predicted some parameters that are now incorporated into the tape. Finding a test method that accurately predicted how these tapes would function in actual applications was central to the success of this project.

Some aspects of the polyethylene backing also affect the tape bond, such as the shrink force and degree of crosslinking. A new way of testing the backing has led to insights into properties such as notch-tear resistance.

Introduction

Heat shrinkable articles for the telecommunications industry have been in widespread use for several years. They include heat recoverable tubes, tapes, end caps, articles, and wrap-around sleeves. The wrap-around sleeve concept is particularly useful for sealing telephone splice joints and repairing damaged cable sheath. These sleeves are generally polyethylene or one of its copolymers that has been crosslinked and stretched at high temperatures, then frozen into the stretched condition by rapid cooling. These products are easily installed and may be re-entered at a later time if, for example, a splice must be re-opened. They are installed by first preparing the splice and cable, fastening the longitudinal edges of the sheet together either mechanically or adhesively to form a tube around the cable, and then heating the sheet to above its softening point, most commonly with a gas torch. Generally a layer of hot melt adhesive is coated onto the inner surface of the polyethylene backing which melts below the softening point of the backing and provides a tight, waterproof seal to the cable at each end of the splice. This is vitally important for the success of the installation. In order to insure that enough heat reaches the hot melt layer to effect adhesive bonding, a thermal sensitive indicator paint is often coated on the exterior of the sleeve. Enough heat has been applied when this paint turns color. After installation the polyethylene sleeve must provide the same sort of mechanical, electrical and chemical protection that the original cable sheath imparted. See Figure 1 for a typical sleeve construction.

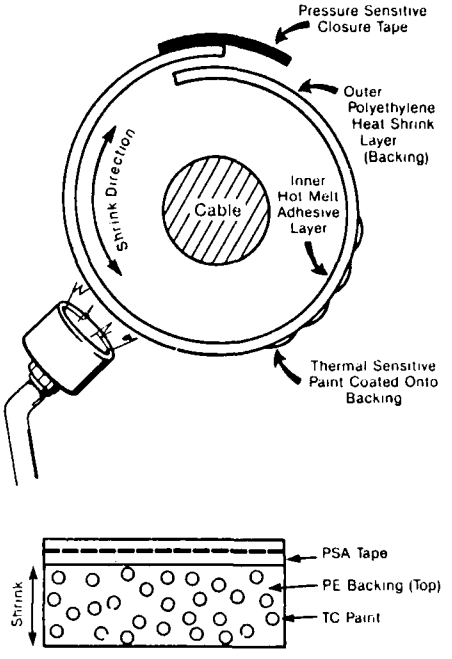


Fig 1 Wraparound sleeve.

It is important that the installation of the sleeve be as simple and trouble-free as possible. Typical problems that can occur are scorching and splitting of the sleeve, splitting of the sleeve due to nicks or cuts in the edge or because of accidentally hitting it with the torch head, difficulty in fastening the edges together, or putting insufficient heat into the material to melt the hot melt adhesive layer. One of the goals in developing a wrap-around sleeve was

to eliminate as many of these problems as possible. This paper will attempt to describe the development of a new closure mechanism using a pressure sensitive adhesive tape and some of the technical problems that were overcome in its development, including a unique test method that relates laboratory testing to actual performance. We will also explore a new way of testing experimental polyethylene sleeve backings that gives insight into their development and manufacture.

Pressure Sensitive Tape Closure

A crucial element in any heat recoverable wrap-around sleeve is the closure mechanism that holds the edges of the sleeve together. It must be convenient to use and reliable in operation. A unique way to fasten two edges of the backing sheet is to use a reinforced pressure sensitive tape. This approach has the advantages of being convenient, allowing repositionability of the closure, allowing changing dimensions because only one edge of the sheet is fixed, being easier to use in close quarters (i.e. in a pit) than a slip-on mechanical closure, following the contour of bends easier because of its flexibility, and allowing reinforcement of specific areas of the sheet.

The requirements, however, for a suitable tape are strict. The tape has to be able to be applied at a broad range of temperatures, has to be resistant to dirt and water contamination, has to have enough initial tack to hold at low application temperatures but not loosen at the high temperatures of the torch, must form a bond that can withstand the shrink forces of the polyethylene backing as it contracts, must have at least a three year shelf life and must be repositionable if initially misapplied.

In order to achieve all this an adhesion promoter was needed on the polyethylene backing to enhance the adhesion of the pressure sensitive tape adhesive. This adhesion promoter is applied in a proprietary process that permanently bonds it to the backing. The pressure sensitive adhesive then cross-links to itself (internally) to withstand the heat of the torch and also bonds to the backing through the adhesion promoter. The resulting bond is well able to hold the forces of the polyethylene shrinking under high temperatures.

Pressure Sensitive Tape Testing

Original attempts to test the pressure sensitive closure tape using conventional shear and peel tests met with mixed results. Data from these types of tests were ambiguous and did not correlate well with actually testing sleeves on splice closures. A new test was needed that could utilize the shrinking forces of the polyethylene backing, could be done at high temperatures to simulate the use of a torch, and could incorporate the adhesion promoter used in the backing to test its efficacy. Such a method was developed and is shown in Figure 2.

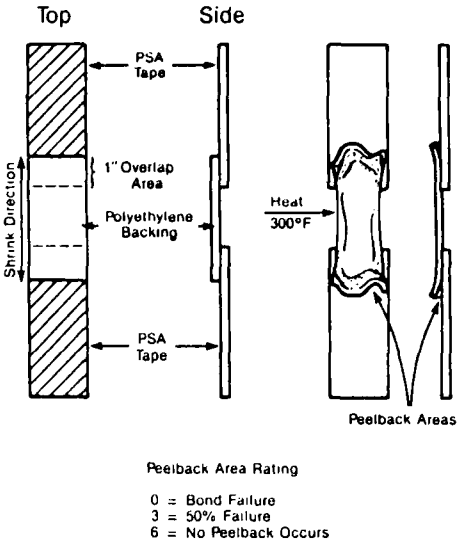


Fig. 2 Test used to measure PSA tape-to-polyethylene backing bond.

The test specimens are made up of one inch by three inch pieces of pressure sensitive tape bonded at each end of a stretched piece of polyethylene backing. The tape ends are clamped in a set of immovable jaws and quickly heated to at least 300°F, which is well above the softening point of the backing. The quality of the bond is determined by how much of the polyethylene is able to peel away from the tape. A rating scale of 0-6 is used, with zero indicating complete release of the tape and six indicating the best bond possible, i.e. complete tape coverage. This test has elements of shear, peel, and cleavage incorporated into the failure mechanism and proved to be closely correlatable to real life testing of full sheets over splice closures.

One of the first uses of this test method was in determining optimum thickness of the closure tape. In studying the geometry of a typical heat shrink application, Figure 3, it appears that

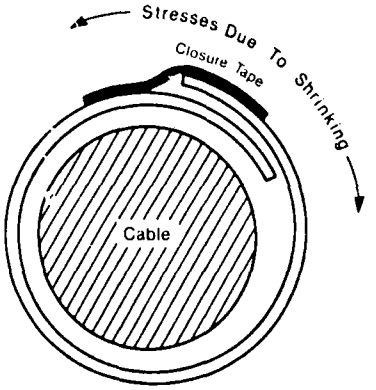


Fig. 3 Geometry of typical sleeve installation

shear stresses would determine the failure mode. Shear testing in the laboratory indicated that thinner tapes (low adhesive caliper) would resist these forces best. This was not borne out in actual attempts to install sleeves, however, where thin tapes gave erratic results. On the other hand, peel testing of the tape from the backing gave no consistent trends at all. Yet we knew by observation that tape caliper was significant to success. However, the new test method which combined these failure modes, gave the best answer, as shown in Figure 4. It turned out that increasing caliper gave better results until an optimum point, after which increased thickness was detrimental. This allowed an accurate prediction of the optimum value of pressure sensitive tape caliper.

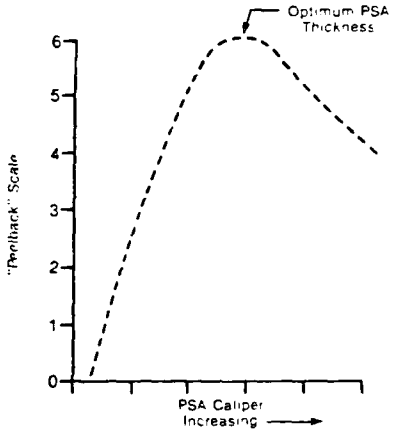


Fig 4 Graph indicating performance of PSA tape versus caliper

Pressure Sensitive Adhesive Formulation

Perhaps the biggest challenge to the program came in trying to balance the properties of the pressure sensitive adhesive used on the tape. This material must cure quickly under the heat of the torch during application, but must maintain a shelf life measured in years at ambient temperatures ranging to 140°F. The initial tape adhesive formulation is shown generically in Figure 5. This was the first material developed that indicated feasibility. It had good initial tack and was repositionable, yet also cross-linked fast enough at high temperatures to hold the shrinking polythylene backing together.

FIGURE 5
Original PSA Adhesive Formulation

	Parts
Acrylate Esters	84
Acidic Monomer	16
MFX*	3.5
Reinforcing Filler	6.5

*Multifunctional thermal crosslinker

Unfortunately this formula had one major problem - it slowly cured at room temperature and became useless, losing all of its pressure sensitive tack properties.

A test method was developed to measure this increased cross-linking with time called the gel swell test, which then gave a basis for further research. The gel swell test gives a swelling index, "Q", by soaking one inch diameter thin discs of the adhesive to be tested in a solvent for twenty four hours, then weighing to give the swollen PSA weight, which is compared to the original weight of the disc before soaking.

The Q is calculated as:

$$\text{Swelling Index} = Q = \frac{Ws - Wo}{Wo},$$

where Wo is the dry weight of the PSA and Ws is the swollen weight. The higher the Q value is, the more solvent is absorbed and the lower the crosslinking of the adhesive. In other words, Q is an inverse measure of the reaction that has occurred in the adhesive. Figure 6 shows the results of running this test on the original adhesive.

FIGURE 6
Gel Swell Test

Conditions	Q Value
Before Aging	4.6
Cured 350°F - 4 minutes	2.4
Aged at 155°F	
1 day	4.4
2 days	3.3
3 days	3.2
4 days	3.2
6 days	3.4
8 days	2.8
Aged at 180°F	
12 hours	3.1
24 hours	2.5

Full cure is considered to be after four minutes at 350°F, and the Q value goes from 4.6 to 2.4 during full cure. Significant curing and loss of tack occurs at 155°F in a matter of a few days, while at higher temperatures the same effects may be measured in hours. At room temperatures this adhesive slowly lost tack until it was useless within a few months.

Testing variations of the original formula gives the results shown in Figure 7. Here the original formulation is compared to materials with no multi-functional cross-linker and with no reinforcing filler. The multi-functional cross-linker was the key to achieving the quick cure needed during torching, yet was a liability to having long shelf life.

FIGURE 7
Formula Variation of Original Formulation

	A	B	C	D
Acrylate Esters	84	84	84	84
Acidic Monomer	16	16	16	16
MFX	3.5	--	3.5	--
Reinforcing Filler	6.5	--	--	6.5

"Q" Results

Original (no aging)	4.9	30.0	34.1	26.8
5 days at 155°F	2.6	34.9	3.3	18.6
10 days at 155°F	2.3	30.7	2.9	16.2

It also was evident from the results of formula D that the reinforcing filler was having a slight curing effect on the adhesive. Neither formula B nor formula D were effective as tapes for holding a heat shrinkable sleeve together during torching. Simply scaling down the amount of MFX (the multi-functional thermal crosslinking agent) used in the formula was tried but did not give the long term results that were needed. Fortunately at this same time research on several new crosslinkers was going on. Figure 8 shows three formulations typical of the experimental materials tried with the new cross-linker, EXP-A which uses a different reaction intermediate than the MFX.

FIGURE 8
Effect of Varying Crosslinking Material

	E	F	G
Acrylate Esters	90	90	90
Acidic Monomer	10	10	10
MFX	2.2	--	0.5
Reinforcing Filler	4	4	4
EXP-A	--	0.1	0.1

Swell Index Q

	E	F	G
Not Aged	Dissolves	13.0	8.0
Cured at 350°F	4.2	12.8	6.2

Formulas E and G were both initially effective in holding the wraparound sleeve during torching. Formula F, with no MFX did not seem to cure fast enough to withstand the heat. All these formulas were aged at 150°F and tested for gel swell (Q) and were also tested on actual sleeves after the 150°F aging. This data is presented in Figure 9.

FIGURE 9
Q Values

Days Aged at 150°F	E	F	G	A
0	Dissolves	13.1	8.0	4.9
5	3.8	11.9	5.3	2.6
10	3.3	12.2	5.5	2.3
17	3.1	11.6	5.4	2.2
35	2.9	12.5	5.6	2.2

Functional Sleeve Evaluation

Days at 150°F	E	F	G	A
1	Holds	Fails	Holds	Holds
5	Holds	Fails	Holds	Fails
10	Holds	Fails	Holds	Fails
35	Fails	Fails	Holds	Fails

along with data from the original tape. Note that only formula G lasts the full 35 days of aging at 150°F in functional sleeve testing. Note also that the Q index for formula G drops to an intermediate level after one day of aging and then stays very steady. This is shown graphically in Figure 10.

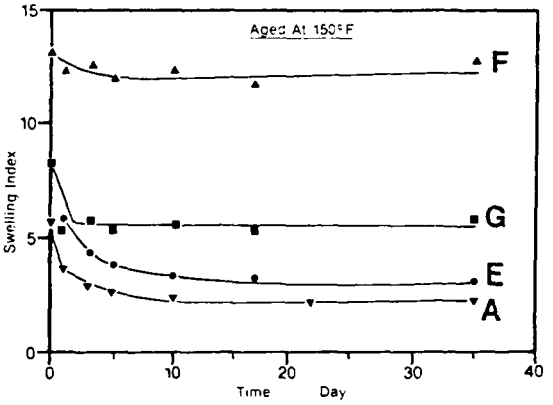


Fig. 10 Swelling results for various formulations

Although this has been recounted and abbreviated in a few paragraphs, in fact the search for the right combination of cross-linkers took many months, with many materials being evaluated and abandoned. The results were well worth it. The finalized tape has an indefinite shelf life at ambient temperatures, good aggressive tack over a wide temperature range, is repositionable, and performs exceptionally well under torching conditions.

These backings may be reinforced at particular areas of the sleeve, for instance where a valve needs to be inserted. This is possible because of the adhesion promoter which acts in concert with the pressure sensitive closure tape. To reinforce around a valve, a hole is cut into a separate piece of the closure tape, which is then bonded to the backing around the valve. See Figure 11. This feature allows new uses for the backing which may not be possible with other types of heat recoverable materials.

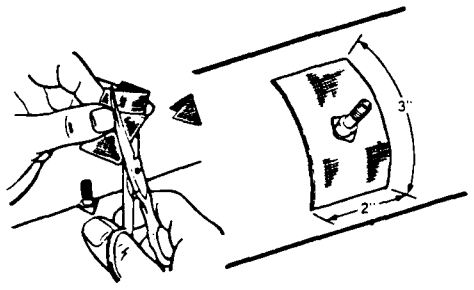


Fig 11 Installation of a valve through a wraparound sleeve

Optimizing the Polyethylene Backing

The manner of fabricating the polyethylene backing, particularly the stretching step, had a large effect on the success of the tape bond. Very large stresses could be induced by not controlling the maximum force created during the shrinking process itself. On the other hand, some minimum internal forces were necessary in order to get a material that shrank efficiently. The "shrink force" for a stretched material is shown in Figure 12 and is typically measured on a tensiometer such as an Instron by grasping both ends of a strip of stretched backing in the machines fixed jaws at a temperature above the softening point of the backing. The forces build to a maximum as the material is quickly heated past its softening point, then tail off as stress relaxation occurs. Obviously the higher this maximum, the more stresses imposed on the adhesive bond during sleeve installation.

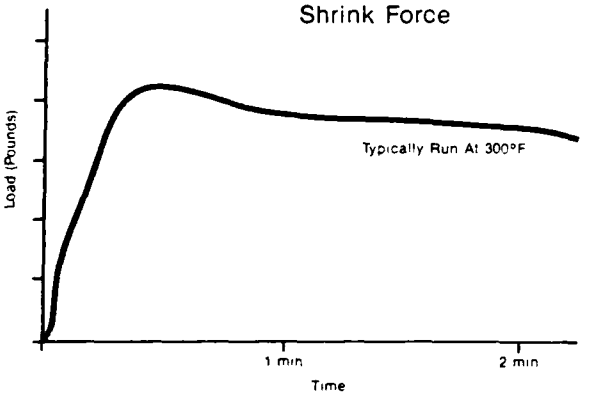


Fig 12 Typical shrink force results on a stretched polyethylene backing

Several factors can influence the amount of shrink force in the stretched sheet. For any given compound formulation, the temperature of stretching, annealing temperature, speed of stretching, amount of crosslinking, and backing thickness all play a part. One of the fundamental questions in the development of the polyethylene backing was how much to crosslink it. Up to a point, the more crosslinked a backing is, the tougher it becomes but at the same time the shrink forces get very high. Some minimal crosslinking is needed to enable the material to hold together during stretching and installation without melting or tearing. The optimum crosslinking level must be chosen to balance toughness against shrink force.

In investigating this a slightly different test method was used that increased our understanding of the process and pointed to some improvements that could be made in this type of product. For simplification we will consider two levels of crosslinking, a medium amount and a high amount of crosslinking as measured by the hot modulus of the material. Using the new test method, instead of starting the force measurements at high temperatures, the material was placed cold into the test jaws and the temperature of the test oven gradually increased to 300°F, then allowed to cool. The graphs of the forces generated are shown in Figures 13 and 14 for the two levels of crosslinking. Some of the points to note on the curves are:

1. There is a well defined softening point for each material (the peak of the curve).

2. The softening point of the high modulus material is slightly elevated.

3. Higher overall stresses or shrink forces are generated with the high modulus material.

4. Stress relief occurs with the medium modulus material above the softening point, but not with the high modulus material. This is shown by the shape of the curve past the softening point. The forces in the high modulus material stay essentially constant above the softening point, while the medium modulus material resolves the stresses as shown by the falling force curve.

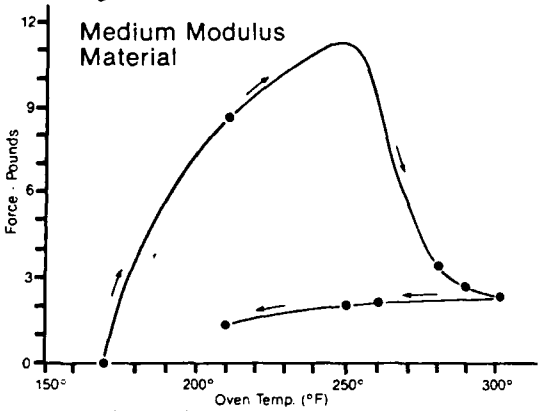


Fig 13 Typical force curve generated for a medium modulus material as temperature is increased to 300°F, then allowed to cool

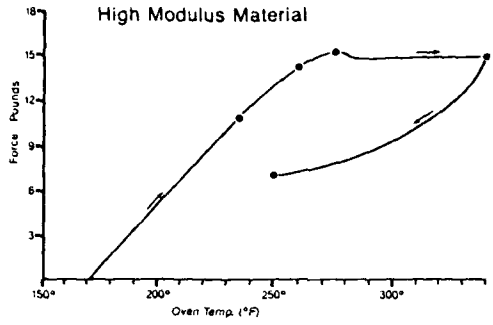


Fig. 14 Typical force curve generated for a high modulus material as temperature is increased to 340°F, then allowed to cool.

To maintain the lowest stresses on the PSA bond the medium modulus materials were investigated because they generated lower stresses.

Fortuitously they were also far superior in a property known as notch tear resistance - that is, the ability to resist propagating a tear during shrinking. This is measured by conducting a test similar to the shrink force test, but with a notched test specimen. This is an extremely important property during the installation of a sleeve, when improper trimming by the craftsmen, or accidentally hitting the hot backing with a torch head, or a protruding edge from a splice bundle, may cause tearing of the backing and an unsuccessful installation. When a notch is deliberately put into the high modulus material immediate failure results, whereas survival of the medium modulus materials can be anywhere from thirty seconds to "infinity" (no failure) depending on the type of notch and other properties of the backing. This is possible because of the stress relaxation that occurs and that is illustrated in Figure 13. It was also discovered that the optimum stretching temperature occurs very near the peak of the graphs, especially for the medium modulus materials. Stretching below this point introduces "cold stretch" forces that are quite high and detrimental to the pressure sensitive tape closure bond. Stretching at temperatures much above this point allows stress relaxation mechanisms to occur in the material, with loss of ability to fully recover to the original dimensions.

The final backing represents an optimized blend of properties. It puts minimal stress on the PSA bond during shrinking, yet is tough, resistant to heat and chemicals, and does what it is designed to do - be a satisfactory replacement for the cable sheath.

Typical Data for Magnashrink™ Heat Recoverable Backings

The following is a compilation of typical performance data for the heat recoverable material.

Test	Reference	Value
Tensile (ultimate)	ASTM D412	3100 psi
Elongation (ultimate)	ASTM D412	600%
Low Temp. Flex	ASTM C509	Below -40°F
Heat Resistance	Bell Labs KS-21766 (4 hrs. @ 150°C	No dripping flowing, or cracking
Heat Resistance	ASTM D2671 (168 hr. at 150°C)	3100 psi 600%
Water Absorption	ASTM D570	0.015%
Volume Resistivity	ASTM D257	10^{17} ohm/cm
Dielectric Strength	ASTM D2671	905 kv/cm
Corrosion Testing	ASTM D2671	Non-corrosive
Stress Cracking	ASTM D1693	No cracking

Chemical Resistance

The MagnashrinkTM HR Sleeve was evaluated for chemical resistance per the criteria below with the following results:

A. Chemical Resistance
Tensile bar samples were aged for 24 hours at 100°F in the environment indicated below and then tested for their physical properties in accordance with ASTM D-412.

Chemical Environments
3% H_2SO_4 (Sulfuric Acid)
0.2N NaOH (Sodium Hydroxide)
10% Igepal CO-630
Gasoline (Room Temperature)

Chemical Resistance Test Results

Environment	Parameter	Magnashrink™ Backing	Percent Change
Initial	Tensile	2936 lbs.	
	Elongation	609%	
	Hardness	56*	
3% H_2SO_4	Tensile	3014 lbs.	2.7
	Elongation	617%	1.3
	Hardness	55.5	-0.89
	Weight Change	0.028	
.2N NaOH	Tensile	3046 lbs.	3.7
	Elongation	616%	1.1
	Hardness	55.3	-1.2
	Weight Change	0.042	
10% IGEPAL CO-630	Tensile	3204 lbs.	9.1
	Elongation	629%	3.3
	Hardness	55	-1.8
	Weight Change	0.008	
Gasoline (Room Temp.)	Tensile	2814 lbs.	-4.2
	Elongation	647%	6.2
	Hardness	55	-1.8
	Weight Change	5.2	

Note: Values in table are based on the average of 3 samples.

*Shore D

Conclusion

All components of the wraparound sleeve must complement each other. The pressure sensitive closure strip and adhesion promoting layer must bond properly under highly varying environmental conditions and must not release at high temperatures. The backing must be formulated and processed to put minimal stress on the adhesive closure bond during application. This system has demonstrated a useful blend of properties with each component optimized to gain the best overall properties.

Acknowledgements

The authors wish to thank the following people for their contributions to the paper: Doreen Grubicy, Sue Lytle, Bonnie LeMere and A.J. Swiderski for their help in preparing this manuscript.

References

1) R. Bradley, "Radiation Technology Handbook", Marcel'Decker, Inc.; New York, New York, 1984

2) J. A. Cornell, "Experiments with Mixtures: Designs, Models and Analysis of Mixture Data", J. Wiley & Sons; New York, New York, 1981

3) P. J. Flory, "Principles of Polymer Chemistry," Cornell University Press; Ithaca, New York, 1969

4) D. Stas (Ed) "Handbook of Pressure Sensitive Adhesive Technology," Van Nostrand, Rheinhold; New York, New York, 1982



3M Company
TelComm Products Division
2111 West Braker Lane
Austin, Texas 78769-2963

Linwood P. (Bud) Beltz - Mr. Beltz received a B.S. degree in Chemistry from Lehigh University in 1966 and an M.S. degree from Northwestern University in Evanston, Illinois, in 1968. He has been employed with 3M for nineteen years studying adhesion and formulating adhesives for industrial uses.



3M Company
TelComm Products Division
2111 West Braker Lane
Austin, Texas 78769-2963

Patricia M. Olson - Ms. Olson received an A.A.S. degree in Animal Health Technology at the University of Minnestoa Technical College at Waseca. She has several years of college level study in chemistry and biology. She joined 3M in 1979 and has worked in the areas of pressure sensitive technology and radiation processing.



3M Company
TelComm Products Division
2111 West Braker Lane
Austin, Texas 78769-2963

Thomas J. Bonk - Mr. Bonk graduated from Loyola University in 1964 with a B.S. degree in Chemistry from the University of Missouri at Rollas in 1966 with an M.S. in Organic Chemistry. He has worked at 3M since 1977 in the areas of polymer and adhesive technologies.

3M Company
Electrical Products Div.
279 Billerica Road
Chelmsford, MA 01824

Dr. Douglas E. Weiss - Dr. Weiss received a B.S. degree from the University of Kansas in 1968 and a Ph.D. degree from the University of Nebraska in 1972. He joined 3M in 1978 and has spent most of his career working in areas related to heat recoverable products. He joined Electrical Products/3M in 1985.



3M Company
TelComm Products Division
2111 West Braker Lane
Austin, Texas 78769-2963

Dr. Tsung I. (Tony) Chen - Dr. Chen received an M.S. in Chemical Engineering from the University of Virginia and a Ph.D. in Polymer Science from the University of Akron. He joined 3M in 1976 and has worked in research and development of polymeric materials.



3M Company
TelComm Products Division
2111 West Braker Lane
Austin, Texas 78769-2963

Jeanine I. Zeller-Pendrey - Ms. Zeller-Pendrey received a B.A. degree in chemistry in 1978 from Macalester College in St. Paul, Minnesota. She has been employed with 3M for ten years working in photo thermographic and telecommunication areas designing materials and products.

[illegible]

[illegible]

[illegible]

[illegible]

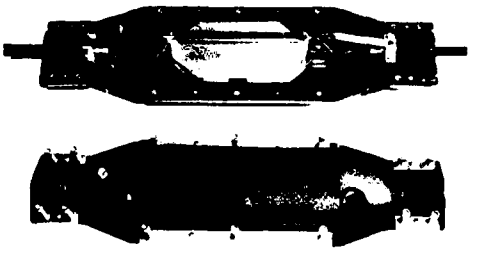
[illegible]

[illegible]

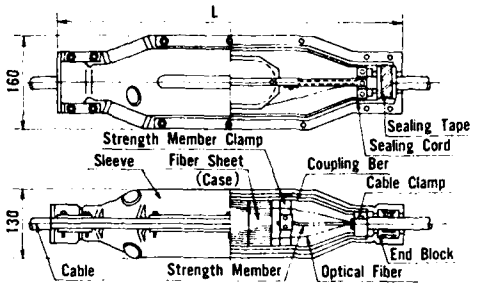
[illegible]

[illegible]

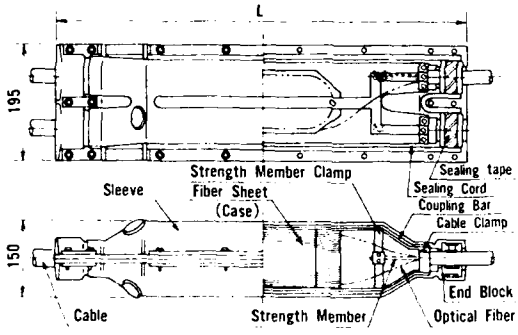
[illegible]



[illegible]



i) For Straight Jointing (Type S, L)



ii) For Branch Jointing (Type B)

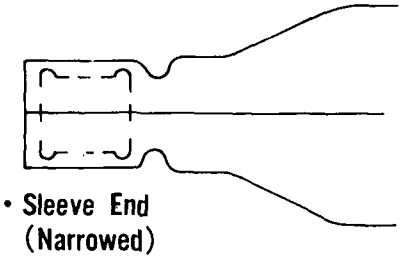
Type	L (mm)	Weight (kg)
S	590	5.3
L	690	7.0
B	690	9.5

Unit : mm

Fig.1 Structure, Dimensions and Weight

Table 1 Aplicable Cable

Type	Number of fibers to be enclosed		Cable outside diameter (mm)	Number of cables to be entered (each side)
	single-fiber	Multi-fiber		
S	30	—	Max. 25	1
L	60	120		
B	100	160		2



• Sleeve End
(Narrowed)

Fig.2 Shape of Sleeve End

3-2 Airtight portion

(1) Structure of airtight portion

Figure 3 shows the structure of the airtight portion of the closure.

The end block uses a rubber material, so that its elasticity always presses the sealing tape.

Further, the end block has a protrusion to prevent the cold-flow of the sealing tape.

The sleeve joint is sealed with a cord-like rubber material to facilitate disassembly and prevent cold-flow. Also, a sealing compound is applied on the rubber surface to ensure the airtightness if the sealed surface of sleeves is damaged to fine scratches.

(2) Materials of airtight portion

A special rubber material specifically excellent in the strain and temperature properties are used to minimize the change of properties caused by pressure drop and temperature change, so that the closure can maintain its airtightness for long-term.

Figure 4 shows the estimated service life of the rubber material.

The sealing tape between the end block and sleeve uses a material that has adhesive power at low temperature and that does not cause cold-flow.

The sealing tape between the end block and sleeve uses a material that has adhesive and elasticity, which facilitates the disassembly.

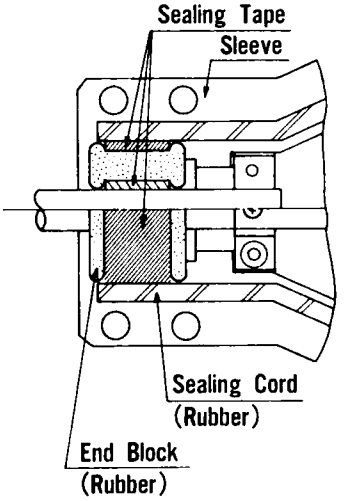


Fig.3 Structure of Airtightness Portion

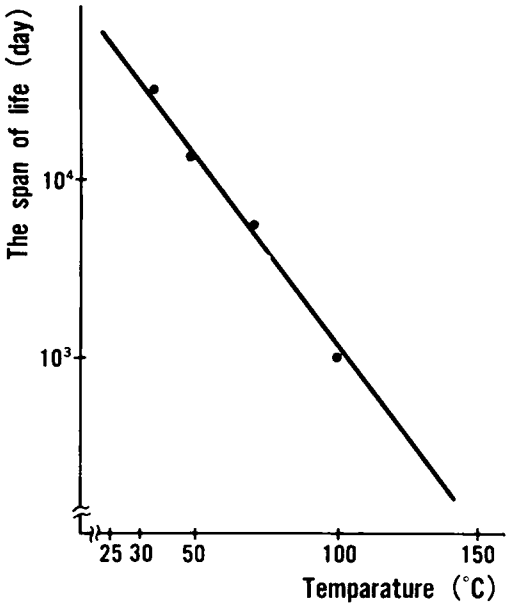


Fig.4 Durability of Rubber Material
(Permanent Compressive Strain)

3-3 Structure of fiber retaining part

Figure 5 shows fiber retaining part.

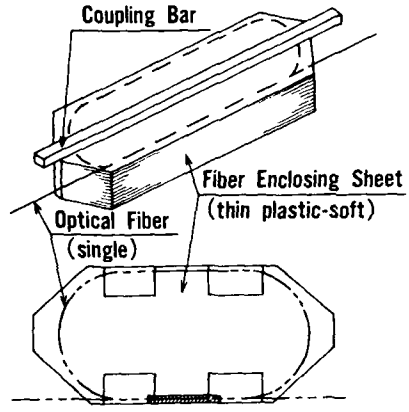
Fixing holes of fiber-fixer to sleeve, in units of one or six fibers, in milk plastic sheets. Plastic sheets can be piled or can be pulled out from sleeve easily whenever necessary.

Space length of multi-fiber joint or single fiber is about 10mm, in case of about 20 fibers, in a drawer-type plastic sheet. Plastic sheet can be piled or can be pulled out from sleeve easily whenever necessary.

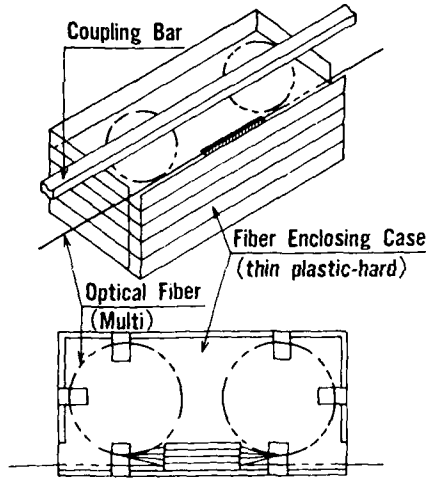
3-4 Structure of each component

By decreased the number of components and simplified the structure to improve the workability.

As a result, the closure can be assembled with no special skill or experience, and anyone can assemble the closure in half an hour.



i) For Single-Fiber (1 or 2 Fiber/sheet)



ii) For Multi-Fiber (5 Fibers/case)

Fig.5 Fiber Enclosing Method

[illegible] performance are [illegible] after the tests.

Table 2 Airtight test results

Item	Test conditions	n	Results
Room temperature	• gas 1.0kgf/cm² filled • After 30days	100	No gas leakage
Temperature cycling	• gas 1.0kgf/cm² filled • 2cycles/day, 100cycles		ditto
	① 0°C to +80°C	20	
	② −20°C to + 60°C	20	
Cable bending	• gas 1.0kgf/cm² filled • Bending radius=6D (D=Cable diameter) • 10reciprocal bend	4	ditto
Vibration	• gas 1.0kgf/cm² filled • 10Hz • Support pitch : 50cm • Single amplitude : 5mm • One million cycles	4	ditto
Hydraulic	• 72hr		No water ingress
	1 • gas 1.0kgf/cm² filled • 30m-water head	5	
	2 20m-water head	4	
Crush	• gas 1.0kgf/cm² filled • 300kgf (load speed 10mm/min)	5	No gas leakage
Impact	• gas 1.0kgf/cm² filled • Temperature −20°C (1hr • A 1.0kgf weight • height of 1m	5	ditto
Tensile	• gas 1.0kgf/cm² filled		ditto
	1 Cable sheath • more than 70% of cable sheath strength	10	
	2 more than 50kgf	10	
Static load	• gas 1.0kgf/cm² filled • A 50kgf weight • outdoor 6 months	2	ditto

Table 3 Loss increase test results

Item	Test conditions	Results
Accomodation of excess length	Loss increase by accomodation of excess length of fiber in the closure	Below 0.02 dB
Temperature cycling	• −20°C to +60°C • 2 cycles/day, 100 cycles • State of accomodation	ditto
Vibration	• 10Hz • Support pitch : 50cm • Single amplitude : 5mm • One million cycles • State of accomodation	ditto

Table 4 Environment test results (rubber)

Item	Environment conditions	Elongation (Residual rate)	
		Initial stage	After test
Weather-O-merer (JIS-D-0202)	• 1 cycle (shower 12 min, sunshine 60 min) • 2000 hr	100	100
Resistance of plastics to Chemical Substances (JIS-K-7114)	• 4 weeks		
	① H_2O	100	100
	② 10% H_2SO_4	100	98
	③ 10% Hcl	100	96
	④ 10% NaOH	100	96
Thermal ageing properties (JIS-K-6301)	• 80°C • 4 weeks	100	91

Table 5 Environment test results (plastic)

Item	Environment conditions	Bending Strength (Residual rate)	
		Initial stage	After test
Weather-O-meter (JIS-D-0202)	• 1 cycle (shpwer 12 min, sunshine 60 min) • 2000 hr	100	93
Resistance of plastics to Chemical Substances (JIS-K-7114)	• 4 weeks		
	① H_2O	100	98
	② 10% H_2SO_4	100	85
	③ 10% Hcl	100	83
	④ 10% NaOH	100	80
Thermal ageing properties (JIS-K-7114)	• 80°C • 4 weeks	100	95

6. Conclusion

We have developed a new insulating material having excellent reliability for electronics. The features are the following characteristics:

(1) Light and thinner in comparison with specially developed for coaxial cables.

(2) [illegible]

(3) [illegible]

(4) Accuracy is easy and [illegible] in half an hour.

(5) Very easy [illegible]

(6) [illegible]

(7) Sturdy structure and good environmental properties allow installation in any places.

(8) High airtightness maintained for a long-term.

7. Acknowledgement

We would like to express our appreciation to Mr. A. Matsui and Mr. M. Murai of Mie Factory of the Furukawa Electric Co., Ltd., for many helpful contribution in manufacturing.

8. References

[1] J. Y. Hsu, et al., "Behavior of [illegible] Cylindrical Vessel under External Pressure" 30th Annual [illegible] Reinforced Plastics/ [illegible] Institute, SPI, 1975.

[2] E. Smith, et al., "[illegible] for Glass Fiber" [illegible], [illegible], 1977.

[3] S. Suzuki, et al., "Estimation of Water Absorption in Resin Sheath of the Coaxial Cable" [illegible] [illegible], 1982.



Shinichiro ITA

The Furukawa Electric Co., Ltd.
6 Yawata-Kaigan-Dori, Ichihara, Chiba, Japan

Mr. Ita graduated from University of Electro-Communications 1983 with a B. Sc. in mechanical engineering. Then he joined the Furukawa Electric Co., Ltd. and has been engaged in research and development of accessories for telecommunication systems.

Mr. Ita is now a staff engineer of Telecommunication Group, Fiber Optics & Telecommunication Division.



Hidehiro MIYAZAWA

The Furukawa Electric Co., Ltd.
6 Yawata-Kaigan-Dori, Ichihara, Chiba, Japan

Mr. Miyazawa graduated from Kyoto Univ. 1971 with a B. Sc. in chemical engineering. Then he joined the Furukawa Electric Co., Ltd. and has been engaged in research and development of outside plant engineering. He is presently engaged in research and development of accessories of optical fiber cable.

Mr. Miyazawa is now a manager of Fiber Optics Apparatus Group, Optical Fiber Laboratory, Research & Development Division.



Yuji TANAKA

The Furukawa Electric Co., Ltd.
6 Yawata-Kaigan-Dori, Ichihara, Chiba, Japan

Mr. Tanaka graduated from Niigata Univ. 1975 with a B. Sc. in mechanical engineering. Then he joined the Furukawa Electric Co., Ltd. and has been engaged in research and development of accessories for telecommunication systems.

Mr. Tanaka is now an assistant manager of Telecommunication Group, Fiber Optics & Telecommunications Division.



Tsuneo [illegible]

The Furukawa Electric Co., Ltd.
6 Yawata-Kaigan-Dori, Ichihara, Chiba, Japan

Mr. [illegible] graduated from [illegible] Univ. 19[illegible] with a B. Sc. in mechanical engineering. [illegible] joined the Furukawa Electric Co., Ltd. and has been engaged in research and development of accessories for telecommunication systems. He is presently engaged in research and development of accessories for telecommunication systems.

Mr. [illegible] is now a manager of Telecommunication Group, Fiber Optics & Telecommunications Division. He is a member of the Institute of Electronics Engineers of Japan.

A NEW UNIVERSAL SPLICE CLOSURE SYSTEM

D. Kunze, J. Rost, E. Bachel - Siemens AG
G. Boscher - RXS L. Mendat - AMP

RXS Schrumpftechnik
D-5800 Hagen 1
West Germany

ABSTRACT

This paper details a new splice closure system developed for use in pressurized/nonpressurized buried, aerial, and underground telecommunication environments. This closure system was designed to specific requirements to achieve desired performance in a wide variety of applications.

Installation of this system requires no external power source and minimal tooling. Ease of installation and reduction of parts are addressed. A permanent reusable sealing system greatly reduces reentry cost, and the cable strain relief system has been integrated into the end cap closing system. The complete product family provides closures of different lengths and diameters to meet industry requirements for cable entry, as well as splice capacity. Laboratory testing simulating outside plant environments has been performed to determine the long-term reliability of the product.

INTRODUCTION

The introduction of plastic sheathed telecommunications cables provided a requirement for new closures to replace the lead-sleeve type closures which had been in application for many years. Worldwide many products were developed which utilized installation techniques such as welding, bonding, and the injection of thermal plastics. At present, heat shrinkable and mechanically sealed closures are most prevalent in the industry.

When compared with other techniques, mechanically sealed closures show advantages, as they can be installed without an outside power source and are reusable. Mechanical closures do, however, present design challenges. Development of a reliable sealing system of plastics or elastomers, as well as a strain relief system which is effective and easily installed, are of great concern, since they are fundamental to the overall performance of the product. The use of high viscosity plastic sealing materials would provide an advantage, as they tend to compensate for rough surfaces or molding deviations in the critical sealing areas. Conversely, elastomeric materials are reusable, which reduces user costs and speeds the reentry process.

Mechanically sealed closures must have a well-designed strain relief system. In heat shrinkable and cast resin closures, the strain relief is inherent to the system. The strain relief system for mechanically sealed closures usually involves several installation steps, as well as components specifically designed for this purpose. These extra components and installation steps must be considered a disadvantage, since misinstallation or omission can significantly reduce the life of the installed closure.

REQUIREMENTS FOR A UNIVERSAL CLOSURE

A. Closures must be easy to install.
   1. Installation must be safe and economical.
   2. No special tools required for reentry
   3. Reusable sealing materials

B. Closures must be suitable for various applications.
   1. Installed on cut or uncut cable
   2. Straight and branch splices
   3. Suitable for direct buried, aerial, and underground installations
   4. Used on various cable types

C. Closures must be pressuretight.

D. Closures must be economical to use.

The demand for easy reentry of the closure leads to the design principle that the sealing of the cable entrance is performed by plastic end caps. The splice is sealed by a longitudinally split plastic tube.

Presently, there are two versions of end caps. These are end caps with precut cable inlets and uncut end caps which are prepared on site according to the cable configuration.

Years of field experience worldwide has shown that on-site end cap preparation is an advantage, as only one end cap is required for a wide variety of applications. It is of no consequence whether one, several, or no cables are introduced to the closure. The need for washers or enlarging the cable with various thicknesses of sealing tape is eliminated. On-site cutting provides the flexibility of installing cables per the particular application. Only this principle completely meets the demands of universal application. Therefore, one of the prerequisites in the development of a

new closure is that the drilled cable inlets in which the cables, which are never completely smooth or circular, are best sealed with an adhesive durable plastic sealing compound. Installation on uncut cables requires that end caps be of a two-piece design. These end caps are secured with connecting bars.

The longitudinally slit plastic tube provides easy installation and reentry of the closure. Compared with two-piece covers, this method is of advantage since there is only one longitudinal seal which can always be brought to the most favorable position of installation. Tapered clamping bars have proven effective in securing the cover. Great importance was placed in the fact that no special tools should be required for installation or removal of the clamping bars. To aid in this process, a reusable elastomer is used to seal the plastic tube.

Criteria for the selection of the closure material are corrosion resistance, durability, elasticity, low temperature crack resistance, and compatibility with cable materials, as well as low permeation.

The shield connection is accomplished via industry standard bonding clips. Sheath continuity is established with a provided grounding wire.

STRAIN RELIEF SYSTEM

The strain relief system serves to relieve external pull, pushing, and torsion forces from affecting the performance of the cable seal and the splice inside the closure. This is usually accomplished by installing jagged metal parts which grip the cable sheath and are secured with screws or hose clamps. These supports must be installed carefully. This procedure is especially difficult when simultaneously introducing multiple cables of varying diameters. The splice capacity is also reduced.

The New Universal Closure provides flexible strain relief disks which are incorporated into each end cap half as shown in Figure 1. Since the new end cap design contains the strain relief system mechanism, custom fitting occurs during the cable entry cutting procedure. During the installation of the end caps the strain relief disks are automatically pressed on the cables irrespective of the number or size of cable installed. As these disks grip the cable, this compression reduces the cavities in the cable, as well as the overall cable diameter providing the necessary strain relief. The increase in pneumatic resistance resulting from this compression is negligible. This system is suitable for use on copper cables, as well as optical waveguides. Measurements show no decrease in insulation resistance nor increase in attenuation.

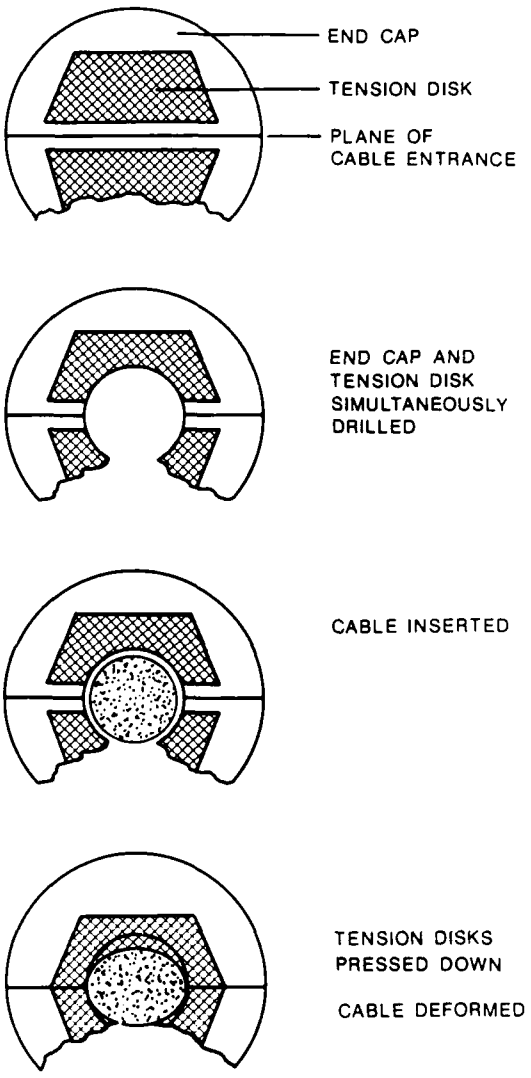


FIGURE 1 STRAIN RELIEF SYSTEM

END CAPS

The two-piece end caps consist of waffles to seal the cable entry ports, the strain relief disks, and the closing system. (See Figure 2.) Each end cap section contains one half of the closing system. After cutting the cable entry ports, applying the thermal plastic sealing tape, and installing the cables, the two halves are bolted together. During this process the strain relief system is automatically pushed into place via the metal frame, reducing the possibility of installation error. Removal is easily accomplished by removing and placing the closing screws in the ports designed for end cap removal.

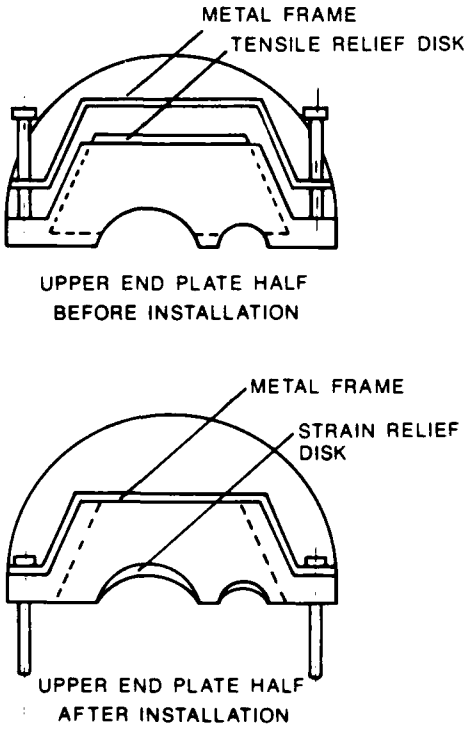


FIGURE 2 END CAP

CLOSURE TUBE

The plastic tube must be thin, light, and inexpensive to manufacture. It must also be capable of withstanding long-term internal pressure, as well as external forces such as waterhead. Minimal effort should be required to install the tube and assure sufficient compression of the elastic seals. Optimal design, wall thickness, and reinforcement of the tube were ascertained by testing and computation.

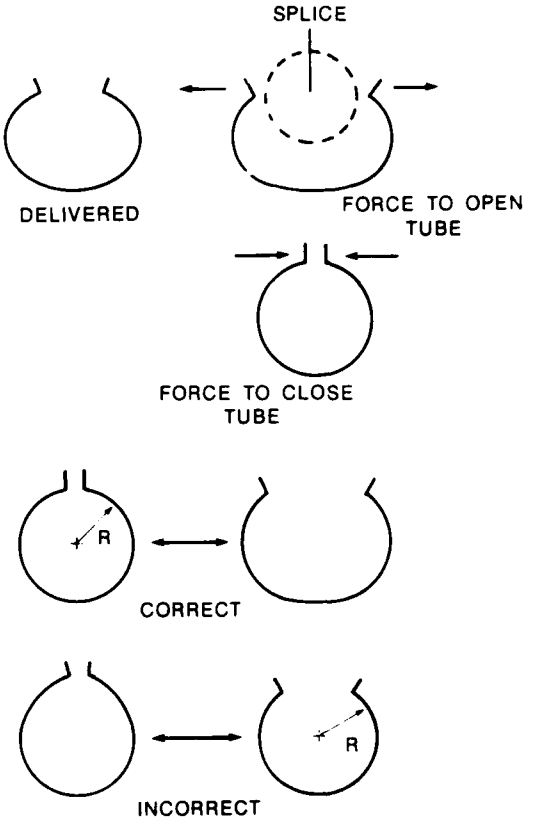


FIGURE 3 CLOSURE TUBE

SEALING

The most difficult problem to overcome is the design of a sealing system, which is further complicated as the system must be applicable to both cut and uncut cable installations. It is of no consequence what principle of construction is chosen. There are always areas in which three components meet at one point or in one line.,e.g. the closure tube, round seal, and longitudinal seal. Subsequently, manufacturing tolerances, thermal expansion, relaxation of the materials, smoothness of the molded parts, and compressibility of the sealing material are important design issues.

FIGURE 5 SPECIFICATION TESTS FOR UCN

TEST	CONDITIONS	TESTED UP TO
FLASH TEST	1.1 Bar, 25°C/1 Hour	16 Hours
STATIC PRESSURE	1 Bar, 25°C/24 Hours	48 Hours
WATERHEAD	5 Meters, 26°C/20 Days	20 Days
STATIC LOAD	1000N, $5cm^2$, 1 Bar, 25°C/10 Minutes	1 Hour
BENDING	$\pm$30°, 1 bar, 25°C/10 Minutes	1 Hour
VIBRATION	5...12 Hz, $\pm$10mm 12...500 Hz, 5g | 10ct/min, 1 Bar/2 Hours	2 Hours
TENSILE STRENGTH	1000 N, 1 Bar/15 Minutes	15 Minutes
IMPACT	14 Nm, -20/+40°C, .7 Bar, 2 Times	-40/+40°C 2 Times
STRESS CRACK	Surface active liquid 50°C, Concentration 10%, 7 Days	
TEMP. CYCLING	-40/+60°C, 8 Hours, .7 Bar, 30 Cycles	50 Cycles
RE-ENTERING	Open and Close, 25°C, 3 Times	5 Times
TORSION	$\pm$90°, max. 50 Nm, 5 Minutes/2 Cycles	5 Cycles

The sealing system must be elastic, as well as compressible. Excellent results have been obtained utilizing expanded elastomers. Upon completion of the seal, high cellular pressure is realized. Due to permeation this pressure has a tendancy to decrease under long-term loads. However, under the given circumstances cellular overpressure corresponds to the internal overpressure of the installed closure, producing almost balanced conditions from the beginning of the load.

CLOSING SYSTEM

Time proven tapered clamping bars are utilized to keep each tube seal pressed together on the installed closure. The use of plastic clamping bars eliminates external nuts and bolts and associated torquing, as well as corrosion concerns. The constructional design and the elastic seal make it possible to install or remove the plastic clamping bars with a few strokes of a hammer.

INSTALLATION PROCEDURE

Installation steps are as follows:

A. Measure the cables with the provided measuring tape and cut end caps according to these measurements.
B. Clean and apply sealing paste and tape to each cable.
C. Apply one layer of sealing tape to each lower end cap segment.
D. Install each end cap over the tape wrap, alternately tightening the bolts.
E. Install connecting bars and internal and external grounding hardware.
F. Install and apply lubricant to all sealing materials.
G. Center the tube over the end caps and install the clamping bars.

CLOSURE CAPACITIES

Figure 4 outlines the closure family with regard to usable internal dimensions and approximate splice capacities.

UCN	INTERNAL DIAMETER(inches)	SHEATH OPENING(inches)	PAIR CAPACITY
6-10	6	10	50-400
6-20	6	20	50-900
8-20	8	20	600-1100
8-24	8	24	1100-1500
8-30	8	30	1100-1800
10-20	10	20	1500-2400
10-30	10	30	2100-3600
10-40	10	40	2700-4200

FIGURE 4

TESTING

The UCN has been tested per the criteria outlined in Figure 5.

SUMMARY

A new closure system has been developed for use in the outside plant telecommunications industry. This system features permanent reusable sealing materials, integrated strain relief, and an all plastic exterior to eliminate corrosion concerns. User friendliness was a key issue in the development effort. This product has been and continues to be tested to industry standards. At present this new UCN closure system is in the field evaluation stage at various operating telephone companies.

ACKNOWLEDGMENT

The authors would like to express their deep appreciation to the many members of Siemens, RXS, and AMP for their untiring efforts leading to the development of the new closure system. Special appreciation is expressed to M. Heier for providing expert advice and guidance throughout this development effort.

AUTHORS



D. Kunze received his Dipl.-Ing. degree in physics from the Technical University of Berlin, Germany in 1965 afterwhich he joined the SIEMENS AG Division for Telecommunication Cables in Berlin. He worked in the "Technology Problems/ Physics" Laboratory and became the manager of this division in 1969. He later became head of a group of laboratories for the construction and testing of cable accessories. He is now lead of the department of outside plant techniques in Munich.



From 1961 to 1978 J. Rost worked as an electrical engineer in the development laboratories for domestic appliances and in the planning department for power cable plants. In 1979 he joined Siemens AG in Munich. In 1985 he became head of the research group for testing cable accessories in the Telecommunication Cables Division of Siemens AG, Munich.



E. Bachel studied electrical engineering in Munich. Since then he has been working as a development engineer in the department for the construction of accessories for telecommunication cables at Siemens AG, Munich.



G. Boscher received his Dipl.-Phys. in physics from the University of Munich, Germany in 1967. He joined Siemens AG in 1967 and worked as a development engineer in the laboratories for mechanical and climatic simulation. In 1970 he became head of a development group responsible for testing accessories in the Telecommunication Cables Division of Siemens AG in Munich. Since 1985 he has been working as a deputy director and head of the Department of Export Sales and Marketing at RXS Schrumpftechnik-Garnituren GmbH, a fully-owned subsiciary of Siemens AG. RXS manufactures and markets accessories for the telecommunication and power industries.



Leonard R. Mendat is Product Market Manager for AMP NETCON Division and heads this AMP, Incorporated subsidiary's Closure Program. After seven years working within the outside plant telephone industry, Mr. Mendat joined AMP in 1976 as an Application Product Specialist. He has been involved in international product marketing for the past five years.

VOLTAGE GRADIENT CONSIDERATIONS IN COMMUNICATION CABLES

J. W. LEVENGOOD

AT&T TECHNOLOGIES, INC.

Abstract

This paper investigates the fields and gradients impressed on the insulated wires during spark testing or dielectric voltage-withstand testing. The ability of a wire or wires to accommodate high voltage levels depends upon the voltage gradient impressed on the insulations in the configuration used.

Assignment of suitable test voltages to insure that the maximum voltage gradient imposed on the product is consistent with raw material capability is also discussed. A failure mechanism (the dendritic growth of failure paths) due to excessive voltage gradients is explored. Data is presented to show that excessive gradients may not produce a failure during the initial test application of voltage but may lead to a failure at a lower voltage in subsequent test or use.

1. INTRODUCTION

The two basic wire configurations used in communication cables are the coaxial and the twisted pair. These configurations are designed to carry analog and digital information generated from telephone, computer and control signals that are generally low level signals (i.e. less than 100 volts). Transient conditions on the lines may raise the voltage level by a factor of two but the signals would still be considered low level. In order to insure that manufactured cables are capable of carrying these signals, the manufacturers use test methods that exercise these cables far above the expected voltage levels.

The test method used to test the wires are:

- spark testing which places a coaxial field around both single and twisted pair wire during manufacturing to check the integrity of the wire, and
- dielectric withstand testing is used on the pair configuration after the wire has been placed into a cable structure.

The selection of the voltage levels used in these tests is critical since these tests are suspected of causing testing induced flaws. The selection process should consider the voltage gradient imposed on the wires and cables to insure that the levels that are selected will:

- be sufficiently high to detect the flaws expected, and
- be sufficiently low to insure that the tests do not induce flaws in the insulation.

This paper addresses the search for proper levels of test voltage considering both single and dual insulation arrangements. Furthermore, the issue of testing induced flaws is investigated experimentally.

2. DISCUSSION

The two configurations of primary interest to manufacturers and users of cables are the coax. and paired configurations. Coaxial voltage distribution is found when testing coaxial cables and when performing spark testing on insulated wires. It also shows up in some paired configuration tests. These configurations have been studied by many authors.

2.1 COAXIAL

The equations for the voltage distribution (V) and voltage gradient (g) are:

- for a single insulation:

$$V = \frac{V_0}{\ln\left(\frac{R_i}{R_0}\right)} \times \ln\left(\frac{r}{R_0}\right)$$

$$g = \frac{V_0}{\ln\left(\frac{R_0}{R_i}\right)} \times \left(\frac{1}{r}\right), \text{ and}$$

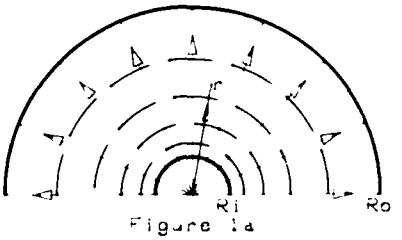
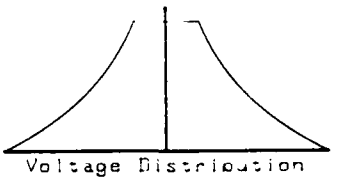
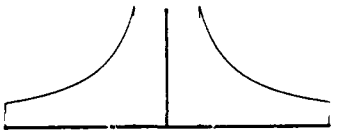


Figure 1a


Voltage Distribution
Figure 1b


Voltage Gradient
Figure 1c

- for two insulations:

$$V_1 = V_0 \frac{\frac{1}{\epsilon_1}\ln\frac{R_2}{r} + \frac{1}{\epsilon_2}\ln\frac{R_3}{R_2}}{\frac{1}{\epsilon_1}\ln\frac{R_2}{R_1} + \frac{1}{\epsilon_2}\ln\frac{R_3}{R_2}}$$

$$V_2 = \frac{\frac{V_0}{\epsilon_2} \times \ln\left(\frac{R_3}{r}\right)}{\frac{1}{\epsilon_1}\ln\frac{R_2}{R_1} + \frac{1}{\epsilon_2}\ln\frac{R_3}{R_2}}$$

$$g_1 = \frac{\frac{V_0}{\epsilon_1} \times \frac{1}{r}}{\frac{1}{\epsilon_1}\ln\frac{R_2}{R_1} + \frac{1}{\epsilon_2}\ln\frac{R_3}{R_2}}$$

$$g_2 = \frac{\frac{V_0}{\epsilon_2} \times \frac{1}{r}}{\frac{1}{\epsilon_1}\ln\frac{R_2}{R_1} + \frac{1}{\epsilon_2}\ln\frac{R_3}{R_2}}$$

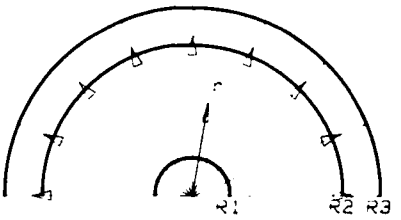
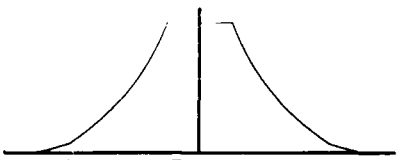
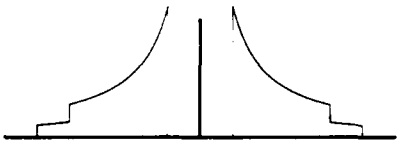


Figure 2a


Voltage Distribution
Figure 2b


Voltage Gradient
Figure 2c

If there is only one insulation involved between the inner and outer conductor, the voltage distribution and hence the voltage gradient is independent of the insulation. However, if there is more than one insulation involved, then the voltage distribution and the voltage gradient will be functions of the position of the insulations.

Figure 1 is a plot of the coaxial field between the inner conductor at a voltage level of Vo volts and the outer conductor at a voltage of zero volts with a single insulation between the two conductors. Figure 2 is a similar plot of the coaxial field with two insulation where the dielectric constant of the outer insulation is greater than the second or inner insulation.

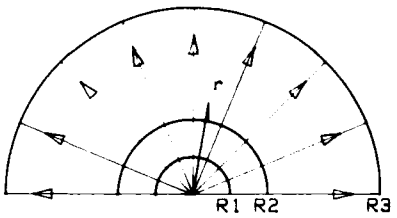


Figure 3a

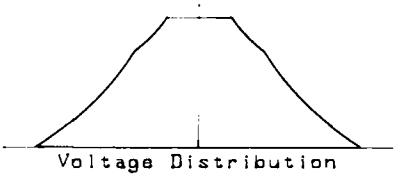


Figure 3b

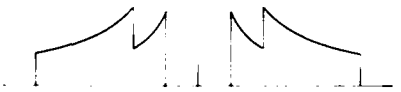


Figure 3c

Figure 3 is a plot of the coaxial field between the inner conductor and the outer conductor with two insulations where the dielectric constant of the inner insulation is greater than that of the outer insulation. Each of these figures has three parts which show:

- a partial end view of the two conductors,
- a plot of the voltage distribution between the two conductors, and
- a plot of the gradient of the voltage distribution.

In the case of the first two configurations the gradient of the voltage is a maximum at the surface of the inner conductor whereas the third example had two peaks in the gradient. This last example is an example of a graded insulation used in power cables. Unfortunately the first two examples are the ones usually used in communication cables since the third example significantly reduces the maximum gradient for a given voltage level between the conductors.

A plot of the maximum gradient (gradient at the inner conductor) for various conductor gauges versus the total insulation thickness is

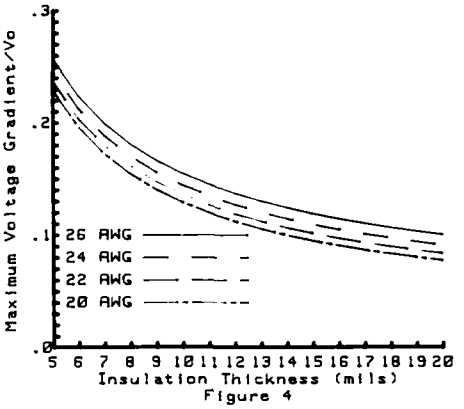


Figure 4

presented in Figure 4. It should be noted that the gradient varies by as much as 18% over gauge size at a given insulation thickness and as much as 160% over the insulation thickness range from 5 to 20 mils. Thus there is an obvious problem when using one voltage level to test all products.

2.2 PAIR

Figure 5 presents a plot of constant voltage surfaces and the field lines about a pair of conductors in space. This is the classical textbook presentation where the entire area outside the conductors is assumed to have one uniform dielectric. The shape of the voltage gradient along the axis of the centers of the pair and the voltage distribution over the center line of the pair is presented in Figure 6. *Peek*[4] developed the equation for the gradient (g) between the conductors:

$$g = \frac{E_n \sqrt{S^2-4r^2}}{[(r+x)(S-2r)-x^2]\ln\left[\frac{S}{2r}+\left\{\left(\frac{S}{2r}\right)^2-1\right\}^{1/2}\right]}$$

where:

E_n = *voltage neutral*
S = *the distance between centers of the conductors*
r = *the radius of the wires*

What would happen if an insulation was placed around the wires? We could first develop the field as we did for the case above and then assess how this field would change at the insulating medium/air interface. Since air would have a dielectric constant less than any solid insulation the curves of constant

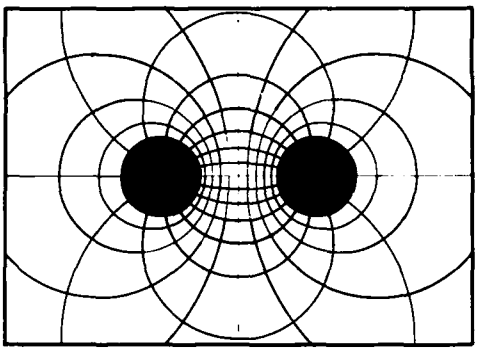
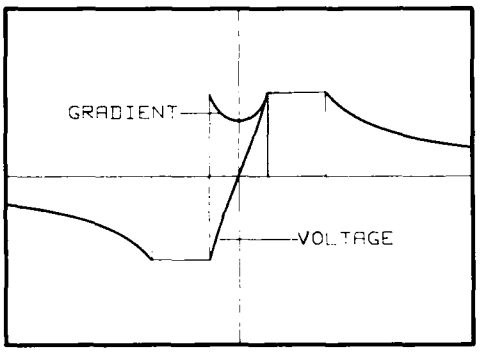


FIGURE 5

voltage would change direction at the interface in such a way that they opened up (i.e. were further apart) and as a consequence the



VOLTAGE AND GRADIENT DISTRIBUTION

FIGURE 6

voltage gradient would be less outside the insulation.

If we had kept the voltage constant between the two conductors then the voltage distribution and the voltage gradient on the line of centers between the two conductors would be similar to the case presented in Figure 6 above. This also happens to be the area of maximum gradient.

What happens when this pair is placed in a cable with other pairs? In general the total field will be changed. However, the maximum gradient will still occur on the line between the centers of the pairs provided that all the other pairs have the same gauge and insulation thickness of the pair under study.

2.3 SHIELDED PAIR

Figure 7 presents a model of a shielded pair. From this representation we can see that on the line between the two conductors the field and voltage distribution will be similar to the presentation for a pair in space whereas the line extending from the conductor to the shield will be similar to the coaxial system. All flux lines will either terminate on the shield or the conductors or emulate from the shield or the conductors. The shield will have induced on it the current or charge distribution sufficient to contain the field within the space inside the shield. The shield being a conductor will become a equipotential surface (neutral) and will deform the field to insure this configuration.

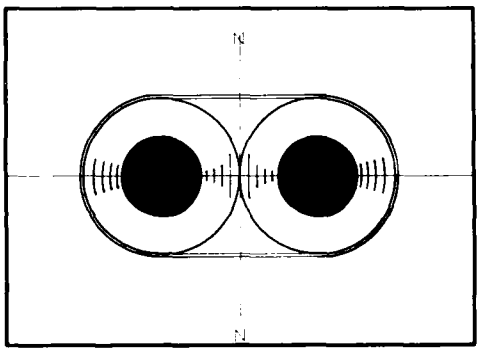


FIGURE 7

In dielectric withstand testing one conductor is shorted to the shield and voltage is applied between one conductor and the other conductor and shield. The voltage on the line between the conductors may still be the same, although probably not. However, the conductor under test and the shield will have the total impressed voltage between them. This will apply the total voltage across one thickness of insulation and will significantly increase the gradient imposed on that insulation.

3. TESTING

3.1 SPARK TESTING

In the manufacturing of cables the individual wires are usually spark tested during the insulating process. The spark test applies a

coaxial voltage distribution around the insulated wire. This is used to test the integrity of the insulated wire and to insure that there are no uninsulated sections of wire.

The desire to assign one voltage value for spark testing all wire configurations, while commendable, does not provide a fair test. If we look at the voltage gradient calculated from the equation for one insulation over the insulation range of 5 mils to 20 mils using 2500 DC volts we obtain the data in the following table.

AWG	Thickness mils	Gradient Volts/mil
20	5	287
	20	193
26	5	645
	20	250

The actual detection of the integrity of the wire is based upon the voltage gradient applied. When we use a single level of test voltage for different thicknesses of insulation, we are testing to different levels of integrity.

Another part of the whole story has to be the capability of the insulation chosen for the wire. Each insulation type has a voltage gradient capability and this must be considered when assigning a test voltage.

For four insulation types, the following table summarizes maximum voltage gradients that have proven to be effective.

Insulation Type	Maximum Gradient Volts/mil
Solid Polyethylene	750
Solid Fluoropolymer	750
Solid Polyvinyl Chloride	500
Expanded (Foam)	250

These limits on voltage gradients protect the insulations from damage during tests while providing sufficient margins to detect flaws in the insulated wire.

3.2 PAIR TESTING

As a final test of the integrity of a cable the dielectric withstand test is applied to each conductor. This test consists of appling a voltage level between one wire in a cable with all other wires and shields (if present) shorted together. This is usually in a pair configuration as is shown in figure 5. We have seen that the field plots of a pair in space will produce a maximum gradient on the axis between the conductors and that the actual maximum gradient occurs at the conductor surface. The same concerns on maximum voltage gradient apply to these tests as applied to spark testing.

3.3 TEST INDUCED FLAWS

Spark testing may be applied at insulate, at twisting and at jacketing operations with pair testing performed as a final test. Thus it is possible to apply high voltage gradients to the same wire several times during manufacturing. There has been considerable evidence that such testing may "set up" insulation to fail. In fact cables thus tested can subsequently fail at a reduced voltage level.

Insulating materials have intrinsic gradient capabilities that if exceeded may cause premature damage to the insulation. It has been previously reported that treeing occurs in various insulations[1] . This is described as microscopic channels extending partly or wholly through a wall of insulation and representing a characteristic form of latent damage.

As the authors indicated in the paper "Treeing in Polyethylene as a Prelude to Breakdown",

> *"A striking example of this was noted 20 years ago in an experiment in which a 2,000 foot length of rubber-insulated wire was subjected to alternating stress. After each breakdown the failure was lifted out*

1. D. W. Kitchen, O. S. Pratt: "*Treeing in Polyethylene as a Prelude to Breakdown*" AIEE Winter General Meeting, New York, New York, February 2-7, 1958

   D. W. Kitchen, O. S. Pratt: "*Treeing Effects in Polyethylene*" AIEE Power Apparatus and Systems, 1958

of water and stress again applied to the remaining length. Without latent damage the successive breakdowns should form an increasing or at least a nondecreasing sequence. ...".

In order to test this hypothesis several lengths of a PVC insulated wire were tested. These tests consisted of placing a wire in a conductive water bath where the voltage was applied between the water and the conductor. The voltage was increased until breakdown occurred. The section of the wire containing the breakdown was located and removed from the water and the test repeated. A sequence of fifteen tests were completed on each wire and the results were plotted versus the test sequence number. If some form of latent damage was not occurring it would be expected that the sequence presented in the plots would be a monotonic nondecreasing function of breakdown voltage gradient versus sequence number. As can be observed, this was not the case on any of the wires. Therefore it must be concluded that some form of latent damage is occurring in the test.

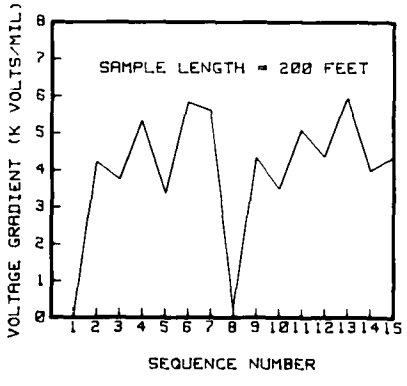


FIGURE 8a

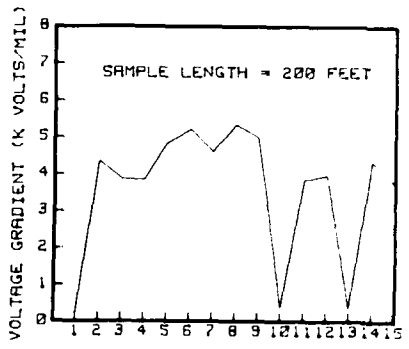


FIGURE 8b

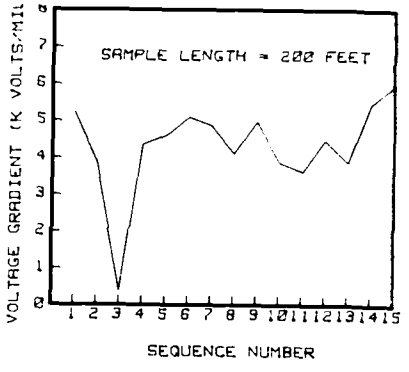


FIGURE 8c

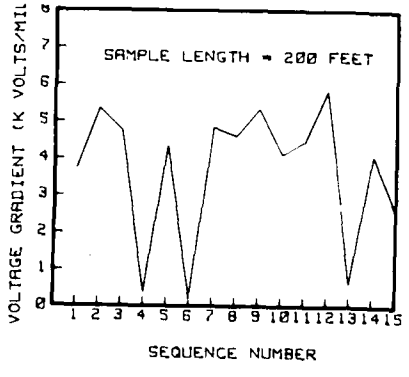


FIGURE 8d

4. SUMMARY

The use of a single voltage level as test a requirement may in some cases overtest a wire or cable configuration while undertesting others. The selection of test voltage level should use the gradient imposed on the configuration as primary consideration for test levels.

The test of the the integrity of the insulating process is not the level of voltage that can be impressed upon the wire or wires in the configuration. Rather it is the gradient of the voltage impressed. The condition that should be maintained for all configurations and insulation types is that the gradient impressed on the configuration be adequate to detect a flaw in the manufacturing process (pin holes, splits, thin insulation, etc.) but not inflict damage to the insulation. It is particularly noted that expanded (foam) insulations should have substantially lower maximum test voltage gradient than solid insulations.

It has been shown that overtesting can induce faults in the insulation that may be discovered at a later time at a lower voltage. Thus high voltage test levels should be set at the lowest level to verify product quality and repeat testing should be minimized.

[1] Attwood, Stephen S., "*Electric and Magnetic Fields*" Dover Publications, INC., New York

[2] Kraus, John D., "*Electromagnetics*", McGraw-Hill Book Company, Inc., New York, 1953

[3] Panofsky, Wolfgang K. H. and Phillips, Melba, "*Classical Electricity and Magnetism*" 2d ed, Addison-Wesley Publishing Company, Inc., Reading, Massachusetts, 1962

[4] Peek, F. W. Jr., *Dielectric Phenomena in High Voltage Engineering*, McGraw-Hill Book Company, Inc., New York, 1929.

[5] Ramo, Simon and Whinnery, John R., "*Fields and Waves in Modern Radio*", John Wiley & Sons, Inc., New York, 1953

[6] Schelkunoff, S. A., "*Electromagnetic Waves*" D. Van Nostrand Company, Inc., New York, 1943

[7] Smythe, William R., "*Static and Dynamic Electricity*" 2d ed, McGraw-Hill Book Company, Inc., New York, 1950

[8] Stratton, J. A., "*Electromagnetic Theory*", McGraw-Hill, 1941



John W. Levengood holds a BSEE degree from University of Florida (1959), and a MSEE degree from the New York University (1961). He joined Bell Laboratories in 1959 and transfered to Western Electric Company in 1970. He presently works for AT&T Technologies, Inc. in the Electronic Wire and Cable Development Department in Atlanta.

COMPARISON OF ONE SECOND AND THREE SECOND DIELECTRIC WITHSTAND TEST

J.A. Isley

AT&T Technologies, Inc.
Omaha, Nebraska

ABSTRACT

This study compares the defect rates from the dielectric withstand test using one-second and three-second dwell times. Six months of test results from four high-voltage test sets were collected and analyzed. Results indicate that the test effectiveness is comparable for the two test configurations.

INTRODUCTION

High-voltage dielectric withstand testing is performed on all cable manufactured at the Omaha Works. The primary objectives of this test are to detect serious mechanical defects and to ensure a minimal dielectric strength in case lightning should enter the core. No inference can be made from the dielectric withstand test with respect to the insulation service life. Tests of this nature are routinely run on high-voltage power cable where dwell times are typically measured in days.

The dielectric withstand test consists of an automatic application of AC or DC high voltage to each conductor with all other conductors and the shield (if any) grounded. The test set operation includes the following steps: 1. Apply high voltage to a conductor, 2. Start a dwell timer upon sensing the appropriate voltage level on the conductor, 3. Enable the fault detect circuit, 4. Disable the fault detect circuit and discharge the high voltage after the dwell timer times out, and 5. Step to the next conductor and repeat steps 1 through 5.

The UL document on communication cable, Subject 444 (1), calls for a three-second application of high voltage during the dielectric withstand test. We contend that a one-second application, which has been our standard dwell time since 1961, does not significantly alter the effectiveness of our fault detection scheme.

A study to compare the difference in test effectiveness of a one-second vs. three-second high-voltage test was conducted for a period of six months. The study, which was authorized by UL, was confined to customer premise cable and central office cable.

TEST PROCEDURES

The cable involved in this study was tested on three AC test sets and one DC test set. Because of the proximity of the DC test set to the small pair size jacketing lines, this test set handled the majority of the small pair size cables.

For this study the dwell timer on AC test set No. 3 was initially set at three seconds and the dwell timers on test sets Nos. 1 and 2 were left at one second. This setup was altered, four months into the study, because of problems with test set No. 3. At that time the dwell timer on No. 2 was set at three seconds and the dwell timer on No. 3 was set back to one second. The dwell timer on the DC test set No. 4 is accessible to the operator, therefore the one-second vs. three-second adjustment was made by the operator alternating between dwell times as each new cable was tested.

No special arrangements were made to direct a specific number of cables or codes to any one test set. It was decided that a large enough sample size could be obtained for both dwell times by allowing a normal flow of products through the test stations. Figure 1 summarizes the product mix obtained.

TEST RESULTS

The test results were entered on the operator's log sheet and turned in daily. The operator's entry included tag number, cable length, cable code, test set number, a check mark for rejection as required, and number of high-voltage breakdowns if any. The operator on test set No. 4 was instructed to include the test time along with the test set number entry. The operator log sheet data was entered into the computer on a weekly basis and a summary report was then generated. This report allowed for verification that an adequate number of cables were being tested at the three-second dwell time.

From the test results of more than 16,000 reels, we deleted those codes which had less than 30 reels tested in either the one-second or three-second category. A comparison of the high-voltage dropout rates for the 24 codes remaining is shown in Figure 2. Nine cable codes show a higher dropout rate at the one-second test and fifteen show a higher dropout rate at the three-second test.

ANALYSIS

As shown in Figure 3, 22 of the 24 codes analyzed have a higher average length per reel for the three second test. This would seem to bias the results toward a higher dropout rate for the three-second test. To confirm this, a correlation analysis was made on one of the high-volume customer premise codes (A10) which had a large difference in average length per reel for the two test categories. Dropout rate is plotted against cable length in Figure 4. The abscissa represents 1K feet cable length cells and the ordinate represents the normalized average dropout rate of those cables tested in the specific length cell.

The scatter plot shows no correlation. However, if the 1K and 2K length cells were discarded, a slight positive correlation can be seen. The regression line with a correlation coefficient of 0.45 is drawn in. This positive correlation would support our contention that the longer cables should have a higher dropout rate. The disparity at the 1K and 2K length cells may be explained by the higher than normal dropout rate for cables which have been cut in the fault locate and repair area and sent back through the high-voltage test stations.

FIGURE 1
REELS TESTED

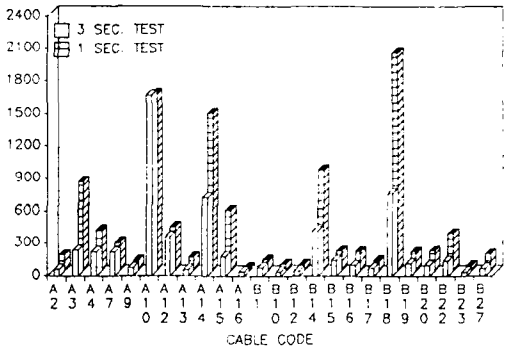


FIGURE 2
HIGH VOLTAGE DROPOUT RATE

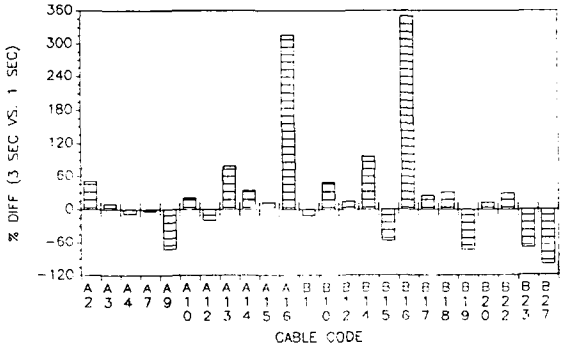
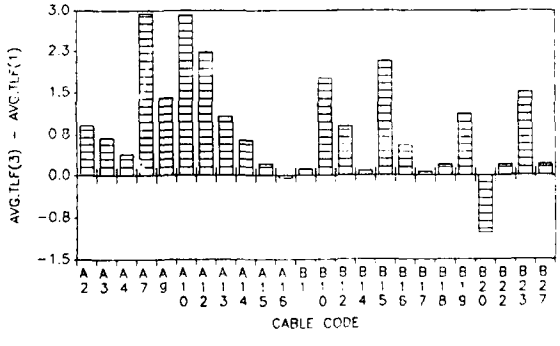
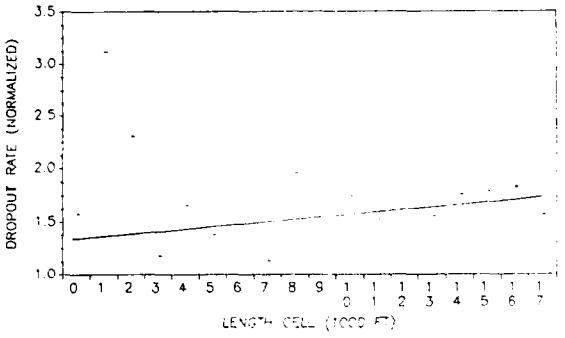
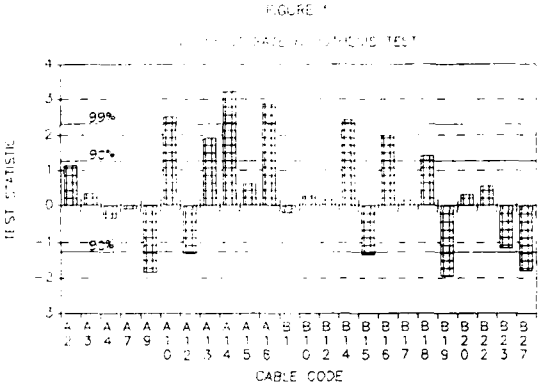


FIGURE 3
DIFFERENCE IN AVERAGE TLF/REEL
FOR 3 SEC VS. 1 SEC TEST







Two other methods of comparing the dropout rates are presented. The first, shown in Figure 5, tests the hypothesis (2)(3) that there is no difference between the two dropout rates. Where independent samples of size $N1$ and $N3$ (> 29) are selected at random from two binomial populations, the statistic for testing the difference between the two proportions is:

$$Z = \frac{R3 - R1}{\sqrt{\bar{R}(1-\bar{R})\,(1/N3)+(1/N1)}}$$

where:

$R1$ = Proportion of failures for the one-second test

$R3$ = Proportion of failures for the three-second test

$\bar{R}$ = Proportion of failures for both tests

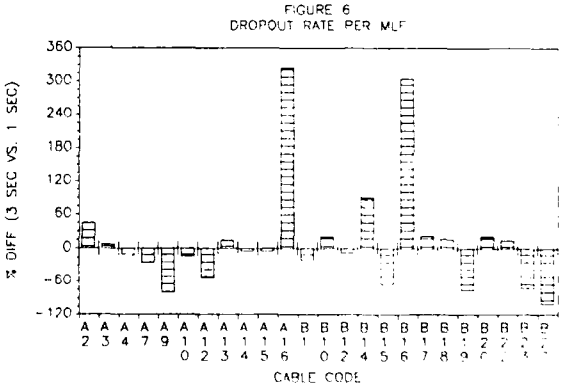
$N1$ = Sample size for the one-second test

$N3$ = Sample size for the three-second test

Our null hypothesis states that the dropout rate at three seconds equals the dropout rate at one second (H0: $R3 = R1$). The alternative to the null hypothesis is that the dropout rate at three seconds is greater than the dropout rate at one second (H1: $R3 > R1$). Using a 99% confidence level we reject the null hypothesis if the test statistic Z is greater than 2.326 ($t_{0.01}$ from t distribution table). From our test results, the null hypothesis H0 can be rejected for only four cable codes. For these codes we would accept the alternative hypothesis H1. The remaining 20 codes show no statistical basis of rejecting the null hypothesis.

If a confidence level of 90% ($t_{0.1} = 1.282$) were chosen instead of 99%, we can conclude from the test results of seven cable codes that the dropout rate is greater for the three-second dwell time. However, from the test results of five different cable codes, we can conclude that the dropout rate is greater for the one-second dwell time.

The last method of comparison removes any bias in dropout rate which may be caused by the difference in cable length tested. As stated previously, there is a significant difference in average length per reel for some cable codes. Figure 6 shows the percent difference of the three-second dropout per million linear feet (MLF) with respect to the one-second dropout per MLF.



Thirteen of the 24 codes show a negative percent difference, indicating a lower dropout rate per MLF for the three second test. Note also that two of the customer premise codes (A10 and A14) which showed a statistical basis of rejecting H0 in the previous analysis have a lower dropout rate per MLF for the three-second test.

Analysis of the dropout rate by the hypothesis test shows conflicting results depending on which cable codes are considered. Analysis of the dropout rate per linear feet removes the reel length variations and shows essentially no difference in the two tests. In conclusion, the effectiveness of the one-second and the three-second dielectric withstand tests are comparable.

ACKNOWLEDGMENTS

The author would like to acknowledge the following people for their contribution to this project: N.J. Cogelia - Bell Labs Atlanta, D.E. Geller - AT&T Atlanta, W.R. Urban and G.J. Alvarez - AT&T Omaha.

REFERENCES

1. Underwriters Laboratories Inc., "Outline of Investigation of Communication Cable, Subject 444", Issue: 1, Dated: July 9, 1987

2. Ronald, E.W. and Raymond, H.M. "Probability and Statistics for Engineers and Scientists" Macmillan Publishing, NY, 1978

3. Graybeal, W.T. and Pooch, U.W. "Simulation Principles and Methods" Little, Brown and Company, Boston, 1980



James A. Isley received his B.S. degree in Electrical Engineering from North Dakota State University and his M.S. degree in Electrical Engineering from the University of Nebraska - Lincoln. He joined AT&T in 1969 and has worked in insulate and jacketing factory engineering and in optical fiber manufacturing. He is currently assigned to final testing of multipair and coaxial cables.

DIGITAL TRANSMISSION ON CUSTOMER PREMISES WIRING

Stephen B. Pierce

Contel Laboratories
Norcross, GA 30092

ABSTRACT

Performance criteria for Integrated Services Digital Network premises wiring are discussed. Although economics dictate that existing wiring be used to the fullest possible extent, error rates on circuits designed for analog transmission may become unacceptable when too high a rate is transmitted over too long a distance.

Digital capacity, defined as the product of bit rate and distance, is limited by crosstalk and intersymbol interference on the premises wiring and by other impairments on the exchange loop. The interface between the network and the premises relies on adaptive echo cancellation to convert between unidirectional and bidirectional transmission. Transmission noise will appear as an uncancellable component at the receiver and could also hinder convergence of the echo canceller.

INTRODUCTION

Factors influencing the suitability of conventional premises wiring for use in the Integrated Services Digital Network (ISDN) are discussed. The ISDN is an end-to-end, repeaterless digital system operating over a conventional twisted-pair exchange loop known as a digital subscriber line (DSL). Signal-to-noise requirements must account for attenuation and noise on the DSL and noise originating on the premises wiring.

The U-DSL interface is critical to the ISDN. Uncancellable noise could cause echo cancellation to fail with resulting breakdown of the system. Crosstalk on premises wiring is expected to be the main source of noise. Digital crosstalk is modeled for the case where mutual induction is negligible. Intersymbol interference due to frequency-dependent attenuation becomes important for pairs that are well-shielded and optimally twisted. Interference can be predicted from formulas derived for the impulse response provided that pulse rise time is much faster than circuit response time.

INTEGRATED SERVICES DIGITAL NETWORK

A digital system has the ability to reconstruct a signal transmitted over a noisy, dispersive medium. A sampled waveform can be reconstructed almost exactly if the sampling rate is twice the bandwidth and the bandwidth includes substantially all the energy in the waveform. Ultimate fidelity depends on bandlimiting and quantization, both of which introduce uncorrectable errors: the first by excluding out-of-band energy, the second by approximating a continuous variable by a discrete set of levels. While one should be aware of them, noise and distortion are usually of far greater importance.

Digital Capacity

The transmission rate of a digital channel carrying signal power P, noise power N, and distortion D, was derived many years ago[1,2]:

$$1/T(b/s) = W \cdot \log_2(1+P/K(PD+N)) \qquad (1)$$

where, W, the equivalent bandwidth, is the area under the amplitude characteristic (the cut-off frequency of an ideal low-pass channel with unit amplitude, for example) and K approaches unity for sufficiently complex coding (K = 8 for PCM). Since transmission distance is implicit in the signal-to-noise ratio, capacity may be stated in terms of the maximum rate over the longest distance for a given error.

A related definition, the "figure of merit", $F = 1^a/T$, is useful where intersymbol interference due to frequency-dependent attenuation is limiting. The figure of merit is the maximum value the product of bit rate and (distance)^a may have for a given error criterion. The exponent is 2 for metallic media and 1 for optical fiber[3].

Digital Subscriber Line

The ISDN is an end-to-end digital system operating between the subscriber terminal and the local exchange switch[4,5]. The exchange network portion is known as a digital subscriber line. The DSL supports bidirectional transmission on the exchange pair between the station side of the

U-DSL interface and the local office. Transmission on the subscriber premises is unidirectional (4-wire) and requires a hybrid interface.

Full-duplex transmission is achieved by adaptive echo cancellation. Figure 1 illustrates the functions of the U-DSL interface. The hybrid transformer converts 4-wire transmission on the premises wiring to 2-wire transmission on the DSL. Imperfect impedance balancing causes the transmitted and received signals to be reflected into each others channels with amplitudes depending on the degree of imbalance. The echo of the received signal, having been attenuated by the DSL, has little effect on transmission, but the echo of the transmitted signal may be at the same level as the received signal. Thus, the received signal is a composite of the desired signal, noise, and reflections at the hybrid and at other points on the DSL.

The DSL is intended to be repeaterless, with a range limited to 18 kft or about 40 dB at the present time[6]. This range restricts the level of interference that can be tolerated if an adequate signal-to-noise ratio and a low error rate are to be achieved.

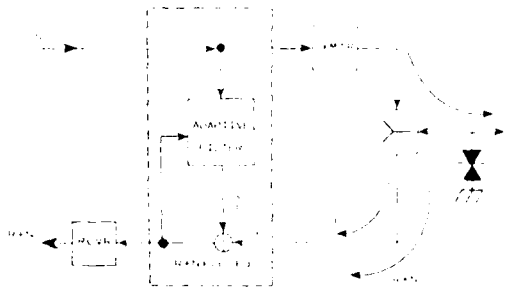


FIGURE 1. U-DSL INTERFACE SHOWING ADAPTIVE ECHO CANCELLER, 2/4 WIRE HYBRID, AND INCIDENTAL. THE RECEIVER OUTPUT CONSISTS OF THE DESIRED SIGNAL PLUS NOISE. PERFECT CANCELLATION OF THE TRANSMITTER ECHO IS ASSUMED OF ETC. THE EFFECT OF THE FAR ECHO OF RATIO IS IGNORED.

Echo Cancellation

The function of the echo canceller is to determine the impulse response of the echo channel, replicate the echo, delay it appropriately, and then subtract it from the received signal. The canceller is adaptive in that it adjusts its impulse response according to the difference signal. An ideal canceller may be envisioned as the inverse of the echo channel in tandem with it. Convergence of the replica to the true response is affected by noise. While the consequences of nonconvergence may be tolerable for speech, data communications are more demanding[7].

Echo cancellation requires the transmitted signal as a reference--the replica is obtained by convolution of the transmitted signal with the echo channel response. However, since transmission noise cannot be referenced, the signal at the receiver contains an uncancellable component. Near-end crosstalk is expected to be the most significant impairment on premises wiring. This is because transmitting and receiving circuits that are not segregated or shielded from each other can interfere effectively along their entire length. Intersymbol interference could become limiting if crosstalk is negligible.

Far-end crosstalk, intersystem crosstalk, and impulse noise are regarded as DSL impairments and will not be discussed at length. FEXT is ordinarily unimportant except for very long lines. However, unequal level far-end crosstalk due to the interference of a station relatively near the office with one relatively remote is similar to NEXT, and the effect is compounded if the interference is between systems operating at different power levels within the same cable. Impulse noise due to switching transients coupled between adjacent lines within the office should also be taken into account.

Error Probability

Transmission errors are due to incorrect decisions at the detector. Hence, error probability is related directly to the signal-to-noise ratio at the decision point. Equivalently, it may be described in terms of the eye diagram showing all possible pulses within the sampled time slot. Figure 2 shows a fully open eye diagram for a bipolar pulse. Pulses above and below the decision crosshairs (CH) are coded as ones, those between the crosshairs as zeroes[8].

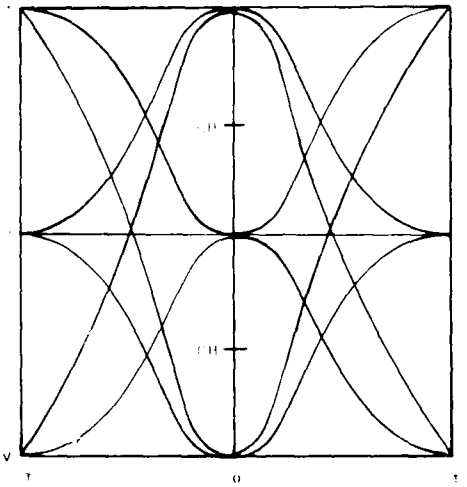


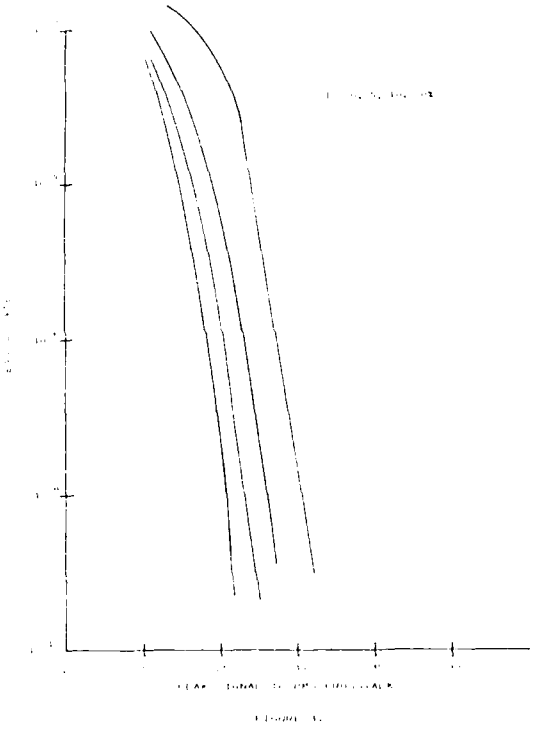
FIGURE 2. EYE DIAGRAM FOR BIPOLAR TRANSMISSION. PULSES BETWEEN THE DECISION CROSSHAIRS ARE CODED AS ZERO, THOSE ABOVE OR BELOW AS ONES. INTERFERENCES CAUSE THE EYE TO CLOSE THEREBY INCREASING THE ERROR PROBABILITY.

Noise and dispersion cause pulse amplitude fluctuations which reduce the vertical eye opening. Timing jitter closes the eye horizontally.

The error probability for a bipolar pulse with random noise is the probability that the noise will exceed one-half the pulse amplitude at the sampling instant:

$$Pr(e) = (2/3)\mathrm{erfc}(V/\sigma(8)^{\frac{1}{2}}) \qquad (2)$$

where erfc is the complimentary error function, V is the pulse peak amplitude, and σ is the rms noise power. Independent interferences are additive. It may be useful to estimate Pr(e) when more than one noise is operative but only one rms value is available. As an example, Figure 3 shows a plot of the error probability versus peak signal-rms crosstalk for four levels of intersymbol interference.



CROSSTALK MODELS

Near-end crosstalk may be modeled as an input signal that propagates on a circuit until it is coupled into an adjacent circuit and then propagates in the opposite direction:

$$N(w) = jw\int_0^{\infty} X\cdot\exp(^{-2\gamma x})dx \qquad (3)$$

The quantity $X=(Z_0C/4+M/Z_0)$ is the crosstalk function, C is capacitance unbalance, M is mutual inductance, and γ is the propagation constant.

Average values are appropriate for parallel pairs. It can be seen that twisting causes positive and negative variations in X, effectively reducing the average value to zero. In this case, X becomes a random variable with zero mean and crosstalk becomes proportional to the mean-squared value of X.

Crosstalk interference depends on the isolation of transmit and receive pairs from each other. Isolation is a function of geometry, shielding, and twisting. Unshielded parallel pairs will have strong capacitive and inductive couplings while shielded pairs with short twist lengths will interfere weakly.

Capacitive Coupling

This model illustrates the role played by pair-to-pair capacitance unbalance[9]. The interference is obtained as the convolution of the impulse response of the crosstalk path between balanced pairs (the virtual coupling circuit) with the voltage on the disturbing pair. The result is an equation for the signal-to-noise ratio on the disturbed pair. The interference voltage is:

$$V(s) = (sC/(s+a))V_0(s) \qquad (4)$$

where $s = jw$, $C = C_c/(C_c+4C_d)$ is a ratio of capacitances, $1/a = R(4C_d+C_c)/4$, and

C_d = direct capacitance between paired conductors

C_c = capacitance unbalance between pairs

R = circuit resistance

The disturbing voltage is modeled as a trapezoidal pulse with equal rise and fall times:

$$V_0(s) = (1/t_r s^2)\ ((1-e^{-str})-e^{-sT}(1-e^{str})) \qquad (5)$$

where 1/T is the pulse repetition rate and t_r is the rise time. This yields the disturbance as a sum of delayed step responses multiplied by a ratio of characteristic times, t_x/t_r, where t_x is the characteristic time for the virtual crosstalk circuit and t_c is the characteristic time for the disturbed circuit:

$$V(t) = t_x/t_r[u(t)(1-e^{t/tc})-u(t-t_r)(1-e^{(t_r-t)/tc})] - t_x/t_r[u(t-T+t_r)(1-e^{(T-t_r-t)/tc})-u(t-T)(1-e^{(T-t)/tc})] \qquad (6)$$

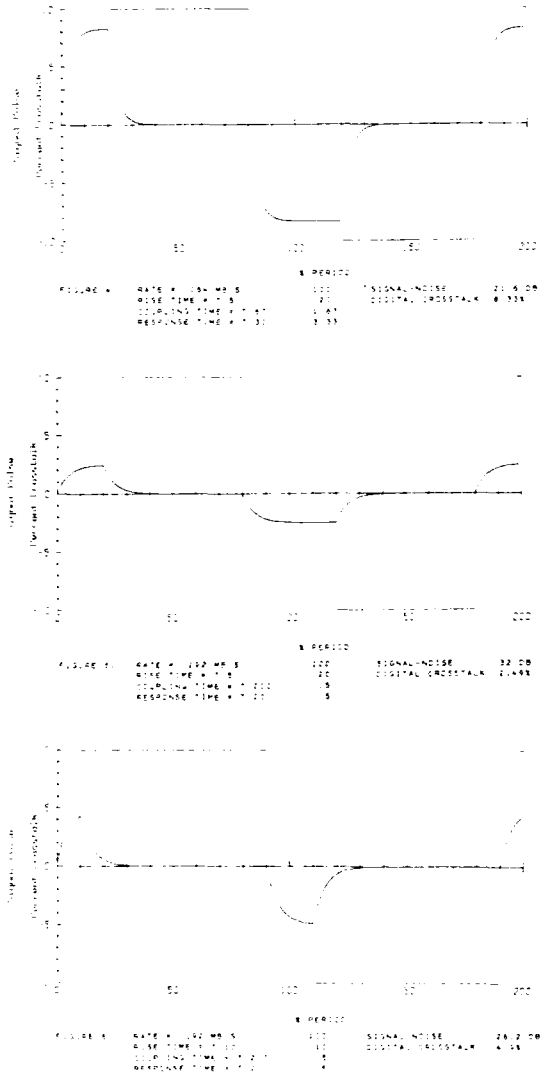
The required signal-to-noise ratio is then $S = 20\log(t_r/t_x U)$.

If there are n interferences, each with the same coupling, the pulse rise time must be longer than $nt_x 10^{S/20}$. With the rise time expressed as a multiple of the pulse rate, $r = T/t_r$, the maximum value of the pulse rate-distance product becomes:

$$1/T = 1/(rnRC_c 10^{S/20}) \qquad (7)$$

Also, if the duty cycle is 100 percent/d, then the maximum rise time is T/2d.

Crosstalk interference is illustrated in Figures 4, 5, and 6. In these figures, the circuit length is 100 feet, mutual capacitance is 25 nF/kft, resistance is 100 ohms, and there are four circuits interfering in phase. Pulse rise is T/5 in Figures 4 and 5 and T/10 in Figure 6. The ratio of characteristic times t_c/t_x is 2 in Figure 4, 10 in Figure 5, and 10 in Figure 6. The signal-to-noise ratio is seen to depend on the ratio of characteristic times. The dependence of crosstalk on pulse rise time and circuit response time is apparent.



This model neglects mutual inductance and tends to understate near-end crosstalk. Inductance may be safely ignored at low frequencies where characteristic impedance is large. Screening pairs from each other can improve isolation at high frequencies where inductance may not be neglected. This might require careful pair selection in some existing premises wiring, especially long runs of flat parallel-wire undercarpet cable.

Magnetic Shielding

Induction may be decreased by enclosing the pair in a shield. The shielding loss consists of absorption and reflection:

$$A+R = 20\log(H/H')dB \qquad (8)$$

where H and H' are the magnetic field intensities (amperes/meter) on the outside and inside of the shield and:

$A = 8.686t(wu/2p)^{\frac{1}{2}}$ dB = 8.686 t/δdB

$\delta = \left(\frac{2p}{wu}\right)^{\frac{1}{2}}$ = skin depth

$R = 20\log(|K+1|^2/|4K|)dB$

$K = d(2j)^{\frac{1}{2}}/\delta$

u = permeability = $4\pi X10^{-7}$(H/m)

p = resistivity = $2.83X10^{-8}$(ohm-m) for aluminum

d = distance of pair from screen

t = screen thickness

f = frequency (Hz)

w = $2\pi f$

For distances in mils and frequency in MHz, $A = 2.63tf^{\frac{1}{2}}$dB and $K = .42d(jf)^{\frac{1}{2}}$

Shielding can offset the increase in near-end crosstalk with frequency. For $df^{\frac{1}{2}} \gg 2$ the requirement is:

$$\Delta(A+R) = 2.63t(f^{\frac{1}{2}}-f_o^{\frac{1}{2}})+10\log(f/f_o)>15\log(f/f_o)$$

or

$$t > 1.9\log(f/fo)/(f^{\frac{1}{2}}-fo^{\frac{1}{2}}) \qquad (9)$$

Calculated screening losses for 4-mil aluminum and a pair-screen distance of 100 mils are tabulated below. Observed increases in crosstalk isolation with frequency may be attributed to screening.

	0.1 MHz	1.0 MHz	10 MHz
K	13.4	42.4	134
A	3.3	10.5	33.3
R	11	20.8	30.4
A + R	14	31	64

Twisting

Coupling between widely separated pairs is largely inductive since intervening pairs screen the electric field responsible for capacitive coupling. Since mutual induction is also more sensitive to twist, crosstalk becomes increasingly twist-sensitive with frequency. The variation of magnetic flux density of a twisted wire pair as a function of twist period may illustrate the effect of twisting on magnetic induction[10].

The tabulation shows $B_z(dB)$, the flux density in the direction of the current, at points off the axis of the pair as a function of twist period. Flux is constant for an intermediate range of twists, a short twist is desirable, and there is a common limiting behavior for long twists. The geometrical factor governing mutual inductance between pairs is the cosine of the difference of pitch angles. Incoherent phase serves to reduce the average inductance. In addition, random manufacturing variations randomize the phase angle so that its mean square value governs the interaction.

	CONDUCTOR SEPARATION					
	.05			.1		
	PAIR SEPARATION			PAIR SEPARATION		
TWIST PERIOD	.1	.2	.4	.2	.4	.8
.5	13	28	54	19	46	92
1	16	26	41	19	33	60
2	18	25	35	22	32	46
4	18	26	33	24	32	42
8	23	29	34	24	31	39
16	27	33	32	27	31	38
32	30	36	35	33	34	38
256	48	48	49	49	50	50

Crosstalk data obtained from available sources is difficult to assess, except for specific lengths and frequencies, because of the different test conditions used. In general, twisting and shielding individual pairs each contributes from 5 to 10 dB at ISDN frequencies and lengths from 50 to 1000 ft. A cable shield has little effect by itself, but a cable shield together with individual pair shields adds tens of decibels at ISDN frequencies. Since the loop loss could be 40 dB, crosstalk loss should be 60 dB to provide a marginal signal-to-noise ratio. This requirement could restrict transmission distance and cable fill for existing premises wiring.

INTERSYMBOL INTERFERENCE

Intersymbol interference becomes a consideration when crosstalk is negligible. A figure of merit, defined as the maximum value of product of rate and (distance)^a, $F = l^a/T(max)$, for a stated error criterion was derived for dispersion due to frequency-dependent attenuation[3]. Metallic media were investigated in the high frequency limit where impedance is dominated by the skin effect. The model was later extended to low frequencies[11].

High Frequency Limit

A normalized impulse response was obtained for coaxial cable at frequencies where impedance is dominated by the skin effect. The figure of merit was then obtained by invoking either pulse overlap or rise time criteria. The normalized impulse response is:

$$h(x) = \pi^{1/2}Ag(x) = x^{-3/2}\exp(-1/x) \qquad (10)$$

where:

$x = t/A$ = normalized time

$A = (lk/4Z_0)^2$

l = circuit length

$Z_0 = (L/C)^{1/2}$ = characteristic impedance

$k = (up)^{1/2}/2r\pi = 2.342\times10^{-8}/r$ for copper

u = permeability = $4\pi\times10^{-7}$ (H/m)

p = resistivity = 1.77×10^{-8} (ohm-m) for copper

r = wire radius

and $h(max) = .41$ at $x = 2/3$.

The figure of merit, $F = l^2/T$, is obtained from the value of x corresponding to the allowable pulse overlap. Using $0.1h(max)$ as a criterion yields $x = 7.715$, $T = 7.715A$, and

$$F = l^2/T(max) = 3.8\times10^{-3}(rZ_0)^2 = 9.5 \text{ (Mb/s-km}^2\text{)}$$

where the final result is for a coaxial cable with inner conductor radius of 1.0 mm and characteristic impedance of 50 ohms. Accordingly, this cable should transmit 9.5 Mb/s over a distance of 1 km with a maximum pulse overlap of 10 percent.

For paired wires, $k^2=(up/(\pi r)^2)/(1-(2r/D)^2)$ where D is pair separation. This yields

$$F = 9.44\times10^{-4}(Z_0r)^2(1-(2r/D)^2)$$
$$= 1.15 \text{ (Mb/s-km}^2\text{)} \qquad (11)$$

and the result uses $Z_0 = (120)\cosh^{-1}(D/2r)$, $D/2r = 2$, and $r = .255$mm(24 gauge). Accordingly, an isolated 24-gauge pair should transmit 1.0 Mb/s over a distance of 1.15 km with an error rate corresponding to a pulse overlap of 10 percent.

Low Frequency Limit

The model was extended to low frequencies by using the low-frequency propagation constant to derive the normalized impulse response[11]. The response was found to have the same form as for the high frequency case:

$$h(y) = B\pi^{\frac{1}{2}}g(y) = y^{-3/2}\exp(-1/y) \qquad (12)$$

where:

$y = t/B$ = normalized time

$B = (1\alpha)^2/2w$

$\alpha = (wRC/2)^{\frac{1}{2}}$ = attenuation

R,C = resistance, capacitance

Z_0 = characteristic impedance = $(R/wC)^{\frac{1}{2}}$

and the other symbols have their previous meanings.

As for the high frequency case, the figure of merit was based on a 10-percent overlap criterion to yield the result:

$$F = 123f/\alpha^2(km^2\text{-}Mb/s) \qquad (13)$$

where $\alpha(f)$ is in dB/km measured at f(MHz).

Unfortunately, there was little correspondence between this result and eye distortion[11]. Measurements using pseudorandom NRZ (non-return to zero) code over a wide range of bit rates indicated that 50-percent overlap ($y = 2$) could be tolerated for 5-percent peak-peak time jitter. Although this did not seem reasonable, it could be rationalized as a rise time phenomenon.

However, similar measurements identified a correspondence between pulse overlap and eye distortion on paired conductors at both high and low frequencies by using the high-frequency paired-wire model[12]. Applying the formula to a 24-gauge cable pair with Z_0 = 110 ohms yields:

$$F = 9.44\times10^{-4}(Z_0r)^2(1-(2r/D)^2)$$
$$= .557(Mb/s\text{-}km^2) \qquad (14)$$

This equation fits the data of Reference 11 quite accurately from 10 kb/s to 60 Mb/s.

The success of the high-frequency model implies that skin effect impedance was dominant over the entire range, which would be so for pulse rise times much faster than the circuit response time. The circuit response time may be estimated as $t_c = (\alpha l)^2/f$ nanoseconds, where αl is the circuit attenuation in dB measured at frequency f MHz. Assuming that $t_r < 0.1\ t_c$ is sufficient, skin impedance should dominate in the case of 24-gauge pairs for pulse rise times less than those tabulated below:

MAXIMUM RISE TIMES (ns)

f(kHz)	10 m	100 m	1 km
8	.17	17	1700
60	.068	6.8	680
100	.047	4.7	470
1000	.031	3.1	310

Bit rate-transmission distance capability may be predicted from high frequency formulae if rise times are shorter than those shown.

CONCLUSION

Digital transmission capability on premises wiring is limited by near-end crosstalk and intersymbol interference. Fast pulses reduce intersymbol interference but increase crosstalk. Pulse characteristics should be optimized for a given system. Crosstalk due to mutual induction at high frequencies may be counteracted by screening. Induction is increasingly twist-sensitive as the frequency increases, and optimized twisting and geometry are desirable.

Intersymbol interference is limiting where crosstalk is negligible. This would be the case for individually shielded, twisted pairs with an overall cable shield. The high-frequency figure of merit predicts peak-peak time jitter over a wide range of frequencies provided pulse rise time is much shorter than circuit response time.

The suitability of existing premises wiring for ISDN service is a question that will require consideration on an individual basis. Circuit design for minimal transmission distance along with pair selection may be necessary to obtain the required signal-to-noise ratio.

ACKNOWLEDGEMENTS

Helpful discussions with R. Gerdes and R. Raman are acknowledged. Contel management graciously granted permission for publication.

REFERENCES

1. C.E. Shannon, Bell System Technical Journal, 27, 379 and 623, 1948.

2. E.D. Sunde, Bell System Technical Journal, 33, 987, 1954.

3. J.A. Hull, A.G. Hanson, and L.R. Bloom, NITA Report 83-121 (5/83), Accession No. PB-83-238345, National Technical Information Service, Springfield, Virginia 22161.

4. CCITT 1984 Series I Recommendations.

5. Integrated Services Digital Network, AT&T Technical Journal, 65, Jan./Feb. 1986.

6. Bellcore TA-TSY-000393, Issue 1, March 1987.

7. J.J. Werner, AT&T Technical Journal, 64, 91, 1985.

8. Transmission Systems for Communications, Bell Telephone Laboratories, Inc., Fifth Edition, 1982.

9. D. Woodard, Proc. 32nd Int. Wire & Cable Symp., p. 24, November 1983.

10. S. Shenfeld, IEEE Trans. on Electromagnetic Comp., EMC-11, 168, 1969.

11. J.W. Kincaid, Jr., and D. Johnson, Proc. 33rd Int. Wire & Cable Symp., p. 228, November 1984.

12. J.A. Hull, Telecommunications, p. 70, February 1984.



Stephen B. Pierce

Contel Laboratories
270 Scientific Drive
Technology Park/Atlanta
Norcross, GA 30092

Stephen Pierce joined Contel Laboratories in 1982. His responsibilities include the evaluation of copper exchange cable. He received a Ph.D. in Physical Chemistry from the University of Wisconsin in 1967.

GEOMETRIC CALCULATION OF LONGITUDINAL WRAPPING TOOLING USED IN TELECOMMUNICATION CABLE MANUFACTURE

Yuan Zhang

Chengdu Cable Plant, Chengdu, Sichuan
P. R. China

Abstract

Longitudinal wrapping technique is in recent years more and more applied to telecommunication cable in regard to conductor, and jacketing forming process, especially to the formation of metal tape. As for all the materials for butt or overlap wrapping, geometric calculation needs to be considered for longitudinal wrapping model and find the optimun parameters of formation curves to obtain good electrical and mechanical performances of the wrapping.

This paper presents the geometric calculation formula of longitudinal wrapping model in a broad sense by an example of the overlap longitudinal wrapping of aluminum tape used as the shield of a bonded integral sheathed telephone cable, in which uniform formation model was verified in practice and yielded satisfied results in the trial production of relative products, thus eliminating pucker edge of aluminum tape in longitudinal wrapping model determined by experience in the past. Meanwhile it can smoothly fulfill overlap longitudinal wrapping far more complicated than butt longitudinal wrapping. Based on the formulas generated in this paper, the required butt or overlap longitudinal wrapping tooling can be designed out.

Main Symbols

l_c - the formation trajectory of a certain point on the tape edge of the wrapping arc section, i.e. formation spacial curve.
ρ - the distance between the projection of a certain point of l_c on X-Y plane and the original point.
R - the curvature radius of formation arc corresponding to formation angle α in wrapping arc section.
d - the diameter of the butt closure of the terminal in wrapping arc section.
d_0 - the diameter of the base circle of the cardioid curve when the projection of l_c on X-Y plane formsinto a cardioid curve.
l_m - the length of wrapping arc section.
Z - the model length from 0 to α relative to the formation angle in wrapping arc section.
S - the spacial curve length from 0 to α relative to formation angle in wrapping arc section.
P - the overlap width of longitudinal wrap tape.
d' - the outer diameter of longitudinal wrap tape with overlap,(the radius expressed by r')
α_0 - the central angle relative to overlap section.
h - the distance between the projection of a certain point of l_c on X-Y plane and X-axis.
Δl_m - the length of overlap section.
Δl_c - the formation trajectory of a certain point on the tape edge in overlap section.
R' - the curvature radius of formation arc relative to formation angle α' in overlap section.
Z' - a model length from 0 to α' relative to formation angle in overlap section.
S' - a spatial curve length from 0 to α' relative to formation angle in overlap section.
d'' - the outer diameter of a half tape when longitudinally wrapped to complete overlap with the outer diameter d' of longitudinal wrap of the other smaller half tape.
ε - the relative elongation of tape edge (%).
w - the distance between the projection of a certain point of l_c on X-Y plane and Y-axis.
(all the lengths expressed in mm)

1. Formation Trajectory of a Certain Point on The Tape Edge in Butt Longitudinal Wrapping

In Fig. 1, one half tape is $\overline{01}$ in width, it becomes a semi-periphery $\widehat{011}$ when formed by circular contraction method. The relative arc lengths $\widehat{02}$, $\widehat{03}$, remain equal and to $\overline{01}$ during formation. The projection of spatial curve l_c on X-Y plane can be characterized by ρ. Combining Fig.3, it gives:

$$R \cdot \sin\alpha = \frac{\rho}{2}$$

and

$$2R \cdot \alpha = \frac{\pi d}{2}$$

$$\therefore \quad \rho = \frac{\pi d}{2} \cdot \sin\alpha = \frac{90d}{\alpha^\circ} \cdot \sin\alpha$$

The formula $\rho \approx \frac{3(d+d_0)\cos\frac{\alpha}{2}}{4 - \cos\frac{\alpha}{2}}$ (derivation omitted)
derived by arc-chord approximate calculation is compared with the formula $\rho = d_0 \cos\alpha + d = d \cdot (1+0.5708\cos\alpha)$ obtained by taking projection curve as cardioid curve.

The errors are shown in Table 1 and the formulas are all applicable in engineering.

For the convenience of following calculation, taking cardioid equation, the projection curve equation of ℓ_c on X-Y plane can be written as:

$$\rho = d_o \cos\alpha + d \tag{1}$$

where,

$d_o = 0.5708d$

If the formation of uniform circular contraction is to be applied, the angle of tape varies uniformly (Another shortest formation is described in Section 6 for reference), Z becomes the linear function of . From the boundary condition we obtain:

$$Z = \frac{2\ell_m}{\pi}\alpha \tag{2}$$

Combining equations (1) and (2), the parametric equation is given for ℓ_c below a cylindrical coordinate as follows:

$$\begin{aligned}\rho &= d_o\cos\alpha + d \\ Z &= \frac{2\ell_m}{\pi}\alpha\end{aligned} \tag{3}$$

As the differential formula of arc length is

$$\begin{aligned}d_s &= \sqrt{dZ^2+d\rho^2+\rho^2 d\alpha^2} \\ &= \sqrt{(\frac{2\ell_m}{\pi})^2+d_o^2+d^2+2d_o d\cos\alpha d\alpha}\end{aligned}$$

assuming

$$k_1 = \sqrt{(\frac{2\ell_m}{\pi})^2+d_o^2+d^2} \tag{4}$$

$$k_2 = \frac{2d_o d}{k_1^2} \tag{5}$$

The integral from 0 to α in equation (4)

$$S(\alpha) = k_1 \int_0^{\alpha}\sqrt{1+k_2\cos\theta}\,d\theta \tag{6}$$

It is an elliptical integral, for which there is no accurate solution, but approximate solution can be found by series expansion.

$$\because \quad k_2 \ll 1$$

$$\therefore \quad \sqrt{1+k_2\cos\theta} \approx 1 + \frac{1}{2}k_2\cos\theta - \frac{1}{8}k_2^2\cos^2\theta$$

Substituted into equation (6), term-by-term integration gives:

$$S(\alpha) = k_1\left[\alpha + \frac{k_2}{2}\sin\alpha - \frac{k_2^2\alpha}{16} - \frac{k_2^2}{32}\sin 2\alpha\right]$$

$$\approx k_1\alpha + \frac{k_1k_2}{2}\sin\alpha \tag{7}$$

$$\ell_c = S(\frac{\pi}{2}) = \frac{\pi}{2}k_1 + \frac{k_1k_2}{2}$$

$$= \frac{\pi}{2}k_1 + \frac{d_o d}{k_1} \tag{8}$$

Equation (8) represents the trajectory length of a certain point on the edge of butt longitudinal wrapping tape in the formation of uniform circular contraction.

2. Butt Longitudinal Wrapping Section Length with Working Elongation Satisfied

In materials science, all metal materials with elongation greater than 5% are plastic materials. They have no evident yielding point. Therefore, the yielding stress of a plastic material when producing 0.2% plastic deformation is its yielding limit, as normally specified in engineering. Thus, in order to avoid the yielding tendancy of a metal material, which produces deformation without increasing its stress, the working elongation of a plastic material is conventionally limited to less than 0.2%. However, some literature also mentions that the pucker caused by too much tension on the edge of an Al foil tape can be eliminated by controlling the elongation of tape within less than 0.25%. Therefore, the average elongation of the deformation curve in full length is confined to less than 0.20%, the maximum elongation of any section not greater than 0.25%.

Thus

$$\frac{\ell_c - \ell_m}{\ell_m} \le 0.002 \tag{9}$$

$$\ell_c \le 1.002\ell_m$$

$$\ell_c^2 \le 1.004\ell_m^2$$

But from equation (8),

$$\ell_c^2 \approx (\frac{\pi k_1}{2})^2 + \pi d_o d + (\frac{d_o d}{k_1})^2$$

$$\approx \frac{\pi^2}{4}k_1^2 + \pi d_o d$$

$$\therefore \quad 1.004\ell_m^2 \ge \ell_m^2 + \frac{\pi^2}{4}(d_o^2 + d^2) + \pi d_o d$$

$$\ell_m \ge \sqrt{\frac{\pi^2(d_o^2+d^2)+4\pi d_o d}{0.016}}$$

$$= d\sqrt{\frac{\pi^2(1+0.5708)^2+4\pi\times 0.5708}{0.016}}$$

$$\approx 35.5855d \tag{10}$$

Equation (10) expresses the necessary length in butt longitudinal wrap section when using circular contraction formation with average working elongation of 0.20%. At this point, the maximum relative elongation of any section on the formation curve is not greater than 0.25%. Their checking calculation and the graph versus Z-axis are shown in Fig. 7.

3. Model Parameter For Implementing Butt Longitudinal Wrap

Butt longitudinal wrap is only applied to wrapping arc section. The longitudinal wrapping formation for laminated Al shield tape is:

$$k_1 = \sqrt{(\frac{2\ell_m}{\pi})^2 + d_o^2 + d^2}$$

$$= d\sqrt{22.6544^2 + 1.3258} \approx 22.6837d$$

$$k_2 = \frac{2d_0 \cdot d}{k_1^2} = \frac{2x0.5708}{514.5485} \approx 0.002219$$

Being substituted into equation (7) leads to

$$S(\alpha) \approx k_1 \alpha + \frac{k_1 k_2}{2} \sin\alpha$$

$$= 22.6837d \cdot \alpha + 0.02516d \cdot \sin\alpha$$

in which, α is radian value. If degree value is to be used, it should be multiplied by $\frac{\pi}{180}$

Thus,

$$S(\alpha) = 0.3959d \cdot \alpha^\circ + 0.02516d \cdot \sin\alpha \qquad (11)$$

From Fig.2, it can be seen

$$R \sin\alpha = \frac{\rho}{2}$$

$$R(\alpha) = \frac{d + \frac{d}{2}(\pi - 2)\cos\alpha}{2\sin\alpha}$$

$$= \frac{d}{2\sin\alpha}\left[1 + \frac{\pi - 2}{2}\cos\alpha\right]$$

$$\therefore \quad R(\alpha) = \frac{d}{2\sin\alpha} + 0.2854d \cdot \cot\alpha \qquad (12)$$

Besides,

$$Z(\alpha) = \frac{2l_m}{\pi} \cdot \alpha = 22.6544d \cdot \alpha$$

$$= \frac{l_m}{90} \cdot \alpha^\circ = \frac{35.5855}{90} d \cdot \alpha^\circ$$

$$\approx 0.3954d \cdot \alpha^\circ (0 \le \alpha \le 90^\circ) \qquad (13)$$

Equations (12) and (13) give the axial length Z (α) from the initial point when wrapping arc section is at a certain formation angle and its corresponding value of the formation radius R(α) respectively.

4. Model Parameter For Overlap Longitudinal Wrap

4.1 Wrapping Arc Section

Butt longitudinal wrapping arc section can be broken up into an overlap section, for which equations (11) - (13) are approximately applied.

Bonded integral sheathed telephone cable requires that the overlap bonded width of laminated shield tape should not be less than 5 mm, the width of overlap being increased with the increment of cable diameter. Design equation (14) is taken as general equation for the relatioship between overlapped width P and outer diameter d' of longitudinal wrap of laminated shield tape:

$$P = \frac{d'}{5} + 4 \text{ mm} \qquad (14)$$

If the overlap section is considered as a truncated cone, the completion of the procedure from butt wrap to overlap should meet:

$$\pi d' + P = \pi d$$

$$d' = \frac{\pi d - (\frac{d'}{5} + 4)}{\pi} = \frac{5\pi d - d' - 20}{5\pi}$$

$$\therefore \quad d = \frac{d'(5\pi + 1) + 20}{5\pi}$$

$$= 1.06366d' + 1.27324 \qquad (15)$$

Thus, equation (11) - (13) used for overlap longitudinal wrapping arc section can be expressed in diameter d' of longitudinally wrapped Al tape so that the die parameters for wrapping arc section can be indicated in equations (16) - (18)

$$S(\alpha) = 0.3959d \cdot \alpha^\circ + 0.02516d \cdot \sin\alpha$$

$$= (0.4211d' + 0.5041) \cdot \alpha^\circ + (0.02677d' + 0.03204)\sin\alpha \qquad (16)$$

$$R(\alpha) = \frac{d}{2\sin\alpha} + 0.2854 \cot\alpha$$

$$= \frac{0.5318d' + 0.6366}{\sin\alpha} + (0.3036d' + 0.3634)\cot\alpha \qquad (17)$$

$$Z(\alpha) = 0.3954d \cdot \alpha^\circ$$

$$= (0.4206d' + 0.5034) \cdot \alpha^\circ \quad (0 \le \alpha \le 90^\circ) \qquad (18)$$

4.2 Overlap Section

Assuming the die length for overlap section be , because

$$\alpha_0 = \frac{P}{r'} = \frac{\frac{2r'}{5} + 4}{r'} = 0.4 + \frac{8}{d'}$$

or

$$\alpha_0 = \frac{360}{2\pi}\left[0.4 + \frac{4}{r'}\right]^\circ$$

$$= \left[22.9183(1 + \frac{20}{d'})\right]^\circ$$

Therefore

$$\frac{\alpha_0^\circ}{4} = \left[5.7296(1 + \frac{20}{d'})\right]^\circ \qquad (19)$$

$$\Delta l_m = \frac{2l_m}{\pi} \cdot \frac{\alpha_0}{4} = \frac{2l_m}{\pi}(0.1 + \frac{2}{d'})$$

$$= \frac{2x35.5855(1.06366d' + 1.27324)}{\pi} x(0.1 + \frac{2}{d'})$$

$$= 2.4097d' + \frac{57.6890}{d'} + 51.0776 \qquad (20)$$

Hence, the overall axial length of the cable on the completion of overlapping is

$$l_m + \Delta l_m = 35.5855(1.06366d' + 1.27324) + \Delta l_m$$

$$= 40.2605d' + \frac{57.6890}{d'} + 96.3865 \qquad (21)$$

Again, assuming formation trajectory length at a certain point on tape edge in overlap section be Δl_c, from Fig.3, formation angle $\alpha_0/4$ is increased between the two spatial curves on the left and

right, both based on $\pi/2$, from equation (16), the total length of each spatial curve is:

$$l_c + \Delta l_c = S(90 + \frac{\alpha_o}{4})^\circ$$

$$= (0.4211d' + 0.5041) \times \left[90 + 5.7296\left(1 + \frac{20}{d'}\right)\right]$$

$$+ (0.02677d' + 0.03204) \times \sin\left[90 + 5.7296\left(1 + \frac{20}{d'}\right)\right]^\circ$$

$$= 40.3125d' + \frac{57.7637}{d'} + 96.5111 + (0.02677d' + 0.0320_4) \times \cos\left[5.7296 + \frac{114.592}{d'}\right]^\circ \quad (22)$$

but,

$$l_c = S(90^\circ) = (0.4211d' + 0.5041) \times 90$$

$$+ (0.2677d' + 0.3204)$$

$$= 37.9265d' + 45.3994$$

$$\therefore \quad \Delta l_c = 2.3860d' + \frac{57.7637}{d'} + 51.118$$

$$+ (0.02677d' + 0.03204)$$

$$\times \cos\left[5.7296 + \frac{114.592}{d'}\right]^\circ \quad (23)$$

As shown in Fig. 4, overlap section being regarded as a truncated cone, the relationship between formation radius $R'(\alpha')$ in this range and the die length $Z'(\alpha')$ in the overlap section from the initial point of butt closure meets following equation

$$\frac{R'(\alpha') - \frac{d'}{2}}{\frac{d}{2} - \frac{d'}{2}} = \frac{\Delta l_m - Z'(\alpha')}{\Delta l_m} \quad (24)$$

Since the tape should be subject to uniform formation in overlap section, similar to equation (2), it generates:

$$Z'(\alpha') = \frac{\Delta l_m}{\frac{\alpha_o}{4}} \cdot \alpha'$$

in which, $0 \leq \alpha' \leq \alpha_o/4$, α' is the formation angle of the overlap section initiated from OY axis in Fig. 2.

But,

$$\Delta l_m = \frac{2\,l_m}{\pi} \cdot \frac{\alpha_o}{4}$$

$$\therefore \quad Z'(\alpha') = \frac{2\,l_m}{\pi} \cdot \alpha'$$

or

$$Z'(\alpha') = \frac{2l_m}{180}(\alpha')^\circ = 0.3954d \cdot (\alpha')^\circ$$

$$= (0.4206d' + 0.5034) \cdot (\alpha')^\circ$$

$$(0 \leq \alpha' \leq \frac{\alpha_o^\circ}{4}) \quad (25)$$

Equation (25) is substituted into equation (24), then

$$R'(\alpha') = \frac{d}{2} - \frac{d - d'}{2} \cdot \frac{Z'(\alpha')}{\Delta l_m}$$

$$= \frac{d}{2} - \frac{d - d'}{2} \cdot \frac{(\alpha')^\circ}{\frac{\alpha_o^\circ}{4}}$$

$$= \frac{d}{2} - \frac{d - d'}{2} \cdot \frac{(\alpha')^\circ}{\left[5.7296 + \frac{114.592}{d'}\right]^\circ}$$

$$= (0.5318d' + 0.6366)$$

$$- \frac{(0.03183d' + 0.6366)d'}{5.7296d' + 114.596} \cdot (\alpha')^\circ$$

$$(0 \leq \alpha' \leq \frac{\alpha_o^\circ}{4}) \quad (26)$$

Additionally, by the same reason of equation (16) it gives:

$$S'(\alpha') = (0.4211d' + 0.5041) \cdot (\alpha')^\circ$$

$$+ (0.02677d' + 0.03204) \sin\alpha'$$

$$(0 \leq \alpha' \leq \frac{\alpha_o^\circ}{4}) \quad (27)$$

Equation (25) -(27) are essential parametric formulas for overlap section when overlap longitudinal wrap is applied.

5. Correction of The Parameters of Overlap Longitudinal Wrap Model

5.1 Transverse Correction

Should the radius of the formation of the left and right half tape be completely symmetric, the tape edges at the closure could not be overlapped due to head-on joint, transverse correction should be carried out for the parameters so as to make the left and right halves different in height when closed. The amount of transverse correction depends on how big a gap is between overlap sections in process. This can be dealt with in the following cases:

5.1.1 Long Tooling for Longitudinal Wrap

It is an integral tooling, good in formation and guiding, applicable to cables of medium or small diameter. It can be seen from Fig.5 that the gap $\Delta 3$ on OY axis in conventional formation design is unequal to that at the terminal of the tape after the completion of overlap, e.g., $\Delta 3'$ on O'Y' axis.

As for the telephone cable normally produced in large quantity, $\alpha_o/4$ is in $_{8}{}^{\circ}{}_{-15}{}^{\circ}$, the central distance $\overline{O_1'O_1''}$ of the final formation circle of the right and left halves of tape merely occupies 1/20-1/50 of d', the only care should be taken of having enough tolerance for gap $\Delta 3$ in order that a laminated shield tape with joints could pass through continuously and smoothly, so could $\Delta 3$. The slight difference in magnitude is negligible.

Brass tape with thickness of $\Delta 1$=0.8 mm can be used as the material of long tooling for logitudinal wrap.

The thickness of a laminated shield tape depends on that of the Al tape and the films heat-bonded on both sides of the tape.

$$\Delta 2 = 0.20 + 2\times0.05 = 0.3 \text{ mm}$$

Gap $\Delta 3$ = 0.9 mm is taken,
Thus,
$$d'' = d' + (0.8 + 0.3 + 0.9) = d' + 2 \text{ mm}$$

5.1.2 Segment Tooling

This tooling permils reduction of friction between tape and tooling, improves tensile formation and makes the device more ingenious, simplifies the range of tooling size and can be considered to apply to the cable of medium size and larger.

From Fig. 6, thickness $\Delta 1$ of overlapped crescent guide finger formed on OY axis should be taken into account as well as thickness $\Delta 2$ of laminated shield tape and gap $\Delta 3$, similar to Fig. 5, the correction amount being their sumtotal. In case it is difficult to make overlap section, a length of long tooling for longitudinal wrap can be used as an auxiliary means for final formation, the correction amount being the same as for the long tooling by estimate.

5.1.3 Forming Roll

The roll is more often used in the butt formation of thicker tape, sometimes also in the formation before butt welding of tapes, and overlap welded edges are further folded into a tube. It can also most possibly be applied to the overlap longitudinal wrapping formation of the shield tape for bigger cables without the problem of $\Delta 1$ and with the above-mentioned correction principle referred. To combine this operation with the last half section of the long tooling for the completion of overlap formation will be a very promising process for cables of large diameter.

To sum up, transverse correction can be concluded as: on the complection of overlap, if the final diameter of one half tape is assumed to be d', then d' + 2 mm can be taken as that of the other half.

5.2 Longitudinal Correction

In making forming toolings, the normal practice is to render the lengths of right and left halves equal, attention is also paid that the half tooling of larger diameter should also have the relative elongation of the tape edge not greater than the working elongation, so longitudinal correction needs to be made for model parameters. It involves following two considerations:

5.2.1 On condition that the right and left half edges of the tape keep relstive elongation equal, the formation angle of right and left half edges is not equal corresponding to any position on model length and keeps a definite proportion, in the meantime, the position for the butt closure of right and left half edges is no longer OY axis in Fig. 5, but will bias by an angle of a certain degree to the larger diameter formed, the magnitude of the bias angle will vary with cable diameter. As it is no good to forming technique and brings more trouble in finding the forming radii at various points, hence not adoptable.

5.2.2 On condition that the half edge of smaller diameter formed has working elongation less than that available for the other half, the shorter half model length can be forced with its wrapping arc and overlap sections respectively extended equal to the corresponding sections of the other half model, the final state remains the same as shown in Fig. 5.

In order that the position of butt closure will not vary with cable diameter, the specific practice is to increase in proportion the formation angle of the half edge of smaller diameter merely in overlap section to eliminate the difference in length between right and left half models, and let $R1(\alpha)$ and $R_1'(\alpha_1')$ of the half model d' not in the same longitudinal position of the model, to which as previously should be corresponded, but let $R_2(\alpha)$ and $R_2'(\alpha_2')$ of the half model d" respectively correspond to $Z_2(\alpha)$ and $Z_2'(\alpha_2')$.

Since the overlap section of either right or left half model is regarded as a truncated cone, the formation radii at the terminals of both wrapping arc and overlap sections being known, two straight lines can be respectively linked on the model diagram without finding the formation radii at other points in overlap section by calculation. It is apparently easier to use this method for longitudinal correction.

5.3 Parameters for Longitudinal Wrap Model

After the above two corrections, the parameters for longitudinal wrap model of uniform circular contraction formation are:

5.3.1 Wrapping Arc Section ($0 \leq \alpha \leq 90^\circ$):

5.3.1.1 The half tape of diameter d'

$$R_1(\alpha) = \frac{0.5318d' + 0.6366}{\sin\alpha} + (0.3036d' + 0.3634)\cot\alpha \qquad (17)$$

$$Z_1(\alpha) = Z_2(\alpha) = \left[0.4206(d' + 2) + 0.5034\right]\cdot\alpha^\circ \qquad (28)$$

5.3.1.2 The half of diameter d"

$$R_2(\alpha) = \frac{\left[0.5318(d' + 2) + 0.6366\right]}{\sin\alpha} + 0.3036(d' + 2) + 0.3634\cot\alpha \qquad (29)$$

$$Z_2(\alpha) = \left[0.4206(d' + 2) + 0.5034\right]\cdot\alpha^\circ \qquad (28)$$

5.3.2 Overlap Section

5.3.2.1 The half tape of diameter d'

$$R_1(\alpha_1') = (0.5318d' + 0.6366) - \frac{(0.03183d' + 0.6366)d'}{5.7296d' + 114.592}(\alpha_1')^\circ \quad (26)$$

$$Z_1(\alpha_1') = Z_2'(\alpha_2') = \left[0.4206(d' + 2) + 0.5034\right] \cdot (\alpha_2')^\circ \quad (30)$$

5.3.2.2 The half of diameter d"

$$R_2'(\alpha_2') = \left[0.5318(d' + 2) + 0.6366\right] - \frac{(0.03183(d'+2)+0.6366(d'+2)}{5.7296(d'+2)+114.592}(\alpha_2')^\circ \quad (31)$$

$$Z_2'(\alpha_2') = \left[0.4206(d'+2)+0.5034\right]\cdot(\alpha_2')^\circ \quad (30)$$

where in the half tape of diameter d'

$$0 \le \alpha_1' \le \frac{\alpha_{01}^\circ}{4} = \left[5.7296\left(1+\frac{20}{d'}\right)\right]^\circ \quad (19)$$

in the half of diameter d"

$$0 \le \alpha_2' \le \frac{\alpha_{02}^\circ}{4} = \left[5.7296\left(1+\frac{20}{d'+2}\right)\right]^\circ \quad (32)$$

The corresponding relationship of both $R_1'(\alpha_1') \sim Z_2'(\alpha_2')$ and $R_2'(\alpha_2') \sim Z_2'(\alpha_2')$ depends on boundary condition by means of straight-line schematic method.

6. The Shortest Circular Contraction Formation Model

When a tape undergoes circular contraction, formation angle is not in a linear relationship with the model length. Assuming the spatial curve be a straight line and keeping $l_c \le 1.002$ then, the model length would be the shortest. The advantage is that the relative elongation of any section of the tape edge is entirely equal so that material characteristics can be brought into full play to make forming tooling the shortest while the formation angle will not uniformly vary with tooling length. But the results would preferrable be verified by tests.

For the shortest circular contraction formation, there is:

$$\begin{cases} x = \frac{\pi d}{2} - \frac{\frac{\pi d}{2}}{l_m} \cdot Z = \frac{\pi d}{2}\left(1 - \frac{Z}{l_m}\right) \\ y = \frac{d}{l_m} Z \end{cases} \quad (33)$$

$$\therefore \operatorname{tg}\alpha = \frac{y}{x} = \frac{2Z}{\pi(l_m - Z)}$$

hereby

$$Z = \frac{\pi \cdot l_m \cdot \operatorname{tg}\alpha}{\pi \operatorname{tg}\alpha + 2} \quad (34)$$

Equation (34) shows the relationship between and Z in the shortest formation, corresponding to equation (2). From equation (34)is listed Table 2 to compare the variation of the formation angle in the shortest and uniform formations.
In addition,

$$dS = \sqrt{(dx)^2 + (dy)^2 + (dz)^2} = \sqrt{\left(\frac{\pi d}{2l_m}\right)^2 + \left(\frac{d}{l_m}\right)^2 + 1}\cdot Z$$

$$S(Z) = \sqrt{\frac{\pi d}{2} + d^2 + l_m} \cdot \frac{Z}{l_m} \quad (35)$$

$$l_c = \sqrt{l_m^2 + \left(\frac{\pi d}{2}\right)^2 + d^2}$$

As $l_c \le 1.002$, the solution gives:

$$l_m \ge \sqrt{\frac{(\pi^2+1)d^2}{0.016}} \approx 29.4423d \quad (36)$$

Accordingly, the major parameters for the overlap longitudinal wrap model in the shortest formation are as follows:

6.1 The correction in process not involved:

6.1.1 Wrapping arc section $(0 \le \alpha \le 90^\circ)$

$$R(\alpha) = \frac{0.5318d' + 0.6366}{\sin\alpha} + (0.3036d' + 0.3634)\cot\alpha \quad (17)$$

$$Z(\alpha) = \frac{(98.3840d' + 117.7693)\operatorname{tg}\alpha}{\pi \operatorname{tg}\alpha + 2} \quad (37)$$

6.1.2 Overlap section $\left(0 \le \alpha' \le \frac{\alpha_0^\circ}{4}\right)$

$$R'(\alpha') = (0.5318d' + 0.6366) - \frac{(0.03183d' + 0.6366)d'}{5.7296d' + 114.592}(\alpha')^\circ \quad (26)$$

$$Z'(\alpha') = \frac{\pi l_m \operatorname{tg}(90^\circ+\alpha')}{\pi \operatorname{tg}(90^\circ+\alpha')+2} - l_m = \frac{l_m}{\frac{\pi}{2}\cot\alpha' - 1} = \frac{31.3166d' + 37.4871}{\frac{\pi}{2}\cot\alpha' - 1} \quad (38)$$

6.2 Both transverse and longitudinal corrections taken into comprehensive account

6.2.1 Wrapping arc section $(0 \le \alpha \le 90^\circ)$

6.2.1.1 The half tape of diameter d'

$$R_1(\alpha) = \frac{0.5318d' + 0.6366}{\sin\alpha} + (0.3036d' + 0.3634)\cot\alpha \quad (17)$$

$$Z_1(\alpha) = Z_2(\alpha) = \frac{\left[98.3840(d'+2)+117.7693\right]\operatorname{tg}\alpha}{\pi \operatorname{tg}\alpha + 2} \quad (39)$$

6.2.1.2 The half of diameter d"

$$R_2(\alpha) = \frac{[0.5318(d' + 2) + 0.6366]}{\sin\alpha} + [0.3036(d' + 2) + 0.3634]\cot\alpha \quad (29)$$

$$Z_2(\alpha) = \frac{[98.3840(d' + 2) + 117.7693]\ tg\alpha}{\pi\ tg\alpha + 2} \quad (39)$$

6.2.2 Overlap Section

(In the half tape of diameter d', $0 \le \alpha_1' \le \frac{\alpha_{01}^\circ}{4}$, $\frac{\alpha_{01}^\circ}{4}$ is defined by equation (19) while in the half of diameter d", $0 \le \alpha_2' \le \frac{\alpha_{02}^\circ}{4}$, $\frac{\alpha_{02}^\circ}{4}$ by equation (32))

6.2.2.1 The half tape of diameter d"

$$R_1'(\alpha_1') = (0.5318d' + 0.6366) - \frac{(0.03183d' + 0.6366)d'}{5.7296d' + 114.592}(\alpha_1')^\circ \quad (26)$$

$$Z_1'(\alpha_1') = Z_2'(\alpha_2') = \frac{31.3166(d' + 2) + 374871}{\frac{\pi}{2}\cot\alpha_2' - 1} \quad (40)$$

6.2.2.2 The half of diameter d"

$$R_2'(\alpha_2') = 0.5318(d' + 2) + 0.6366 - \frac{[0.03183(d' + 2) + 0.6366](d' + 2)}{5.7296(d' + 2) + 114.592}(\alpha_2') \quad (31)$$

$$Z_2'(\alpha_2') = \frac{31.3166(d' + 2) + 37.4871}{\frac{\pi}{2}\cot\alpha_2' - 1} \quad (40)$$

So the comparison data for longitudinal wrap model length in both the shortest and uniform circular formations are shown in Table 3.

Relative elongation

$$\varepsilon = \frac{\Delta l}{l}$$

In the shortest deformation

$$\varepsilon = \varepsilon_{max} = 0.20\% = \text{constant}$$

In uniform formation, substituting the formula characterized by radian gives

$$S(\alpha) = 22.6837d\cdot\alpha + 0.0216\sin\alpha$$

$$Z(\alpha) = 22.6544d\cdot\alpha$$

$$\therefore \varepsilon = \frac{0.0293}{22.6544} + \frac{0.02516}{22.6544}\cdot\frac{\sin\alpha}{\alpha} = 0.0012933 + 0.0011106\cdot\frac{\sin\alpha}{\alpha} = 0.0012933 + 0.06363\frac{\sin\alpha}{\alpha^\circ}$$

In overlap longitudinal wrap, whole formation angle is in the range of $0 \sim \frac{\pi}{2} + \frac{\alpha_0}{4}$ as shown in Fig.2, practically, $0 \sim 110^\circ$.

Since first-order derivative of function $\frac{\sin\alpha}{\alpha}$ is zero at $\alpha = 0$ by Roberta Law.

$$\lim_{\alpha\to 0}\frac{d}{d\alpha}\left(\frac{\sin\alpha}{\alpha}\right) = \lim_{\alpha\to 0}\frac{\alpha\cos\alpha - \sin\alpha}{\alpha^2} = \lim_{\alpha\to 0}\left(\frac{\sin\alpha}{2}\right) = 0$$

Also, second-order derivative of function $\frac{\sin\alpha}{\alpha}$ is negative by Roberta Law

$$\lim_{\alpha\to 0}\frac{d^2}{d\alpha^2}\left(\frac{\sin\alpha}{\alpha}\right) = \lim_{\alpha\to 0}\frac{-\alpha^3\sin\alpha - 2\alpha^2\cos\alpha + 2\alpha\sin\alpha}{\alpha^4} = \lim_{\alpha\to 0}\frac{-\alpha^2\sin\alpha - 2\alpha\cos\alpha + 2\sin\alpha}{\alpha^3} = \lim_{\alpha\to 0}\frac{-2\alpha\sin\alpha - \alpha^2\cos\alpha + 2\alpha\sin\alpha}{3\alpha^2} = \lim_{\alpha\to 0}\left(\frac{-\cos\alpha}{3}\right) = -\frac{1}{3}$$

So function $\frac{\sin\alpha}{\alpha}$ yields maximum value at $\alpha = 0$.

$$\varepsilon_{max} = 0.0012933 + 0.0011106\lim_{\alpha\to 0}\frac{\sin\alpha}{\alpha} = 0.0012933 + 0.0011106 = 0.0024039 \approx 0.2404\%$$

The relative elongations of various points in formation section with angle range 0 - 110° in uniform formation are listed in Table 4.

In uniform and shortest formations the corresponding relationship between the relative elongation of tape edge against tape center in width and various formation angles along the length of longitudinal wrapping tooling is shown in Fig.7. The two curves in the graph are also respectively applicable to the corresponding relationship between relative elongation and tooling length in the two different formations.

7. Miscellaneous

7.1 Base Line of Longitudinal Wrap Model

The base line of longitudinal wrap model can be designed as a curve that accords with the rule of gradually contracting formation circle, or as a straight line. As long as the terminal center of longitudinal wrap model is ensured to be coincident with cable center, it is not quite necessary for the formation circle center of tape to be in coincidence with the axial line of cable core. As a result, the base line of longitudinal wrap model coincides with Z axis so as to simplify the design of longitudinal wrap tooling.

7.2 Tape Width Required for Longitudinal Wrap

7.2.1 Butt Longitudinal Wrap

When butt longitudinal wrap is applied, the tape is rolled up into a complete circle. Assuming tape thickness be $\Delta 2$, it generates:

$$b = \pi(d' - \Delta 2) \tag{41}$$

7.2.2 Overlap Longitudinal Wrap

Taking long tooling for longitudinal wrap as an example, one half tape will pass through the gap in overlap of the tooling. As previously described, the outer diameter of laminated shield tape after longitudinally wrapped is d' while that of the other half model during overlap longitudinal wrap is d' + 2, considering the gap of tape will be eliminated by bonding, sizing and rolling upon the completion of longitudinal wrap, the intermediate status, therefore, should be selected in effect for the gap of tape in longitudinal wrap, that is:

$$b = \frac{\pi(d' - \Delta 2)}{2} + \frac{\pi[(d' - \Delta 2)+1}{2} + P$$

$$= \pi d' - \pi\Delta 2 + \frac{\pi}{2} + \left(\frac{d' - \Delta 2}{5} + 4\right)$$

$$\approx 3.34d' + 4.57 \text{ mm} \tag{42}$$

Where the thickness of Al - plastic laminated shield tape $\Delta 2$=0.3 mm

7.3 Material Width of Long Tooling for Longitudinal Wrap

The terminal inner diameter D' of long tooling for longitudinal wrap can be a little larger than the outer diameter d' of longitudinally wrapped tape. When d' $\leq$ 15 mm, taking D' = d' = 0.5 mm, after that, the increment of d' by 5 mm increases D' by 0.1 mm, the material thickness of long tooling $\Delta 1$ = 0.8 mm being known, the inside bore diameter of one half tooling is

$$D' = d' + 0.5 + \frac{d' - 15}{5} \times 0.1$$

$$= 1.02d' + 0.2 \text{ mm} \tag{43}$$

and that of the other half is

$$D'' = D' + 2 \text{ mm} \tag{44}$$

hereby the material width of long tooling is

$$B = \frac{\pi(D' + \Delta 1)}{2} + \frac{\pi(D' + \Delta 1) + 2}{2} + \left[\frac{(D' + \Delta 1) + 1}{5} + 4\right]$$

$$= 3.41d' + 10 \text{ mm} \tag{45}$$

7.4 Relationship in The Positions of Cable Axial Line, Laminated Shield Tape and Long Tooling for Longitudinal Wrap

In order to avoid twisting of laminated shield tape during longitudinal wrapping to guarantee the quality of heat-sealing and roll-sizing, it should be noted that the top view projection of cable axial line should be coincident with the base line of long tooling and laminated shield tape. Since there is difference in diameters of the left and right halves of the latter two after longitudinally wrapped, the base lines should be plotted at the point of $\pi/2$ mm, away from the geometric central line of tape width, biasing towards the half tape of smaller diameter with longitudinal wrap.

7.5 Design of Long Tooling for Longitudinal Wrap (in the case of uniform formation)

Besides the fore-mentioned related formulas to be used, some other minor parameters need to be found so that a complete drawing of a long tooling for longitudinal wrap can be provided. Here, special attention should be paid to that what the geometric model of longitudinal wrap expresses is the neutral line position of tape.

7.5.1 Front View

7.5.1.1 Finding the lengths of toolings corresponding to various formation angles

From Fig. 1, according to equations (28), (43) and (44) it gives:

$$Z_2(\alpha) = [0.4206(D' + 2 + \Delta 1) + 0.5034] \cdot \alpha^\circ$$

$$= [0.4206(1.02d' + 3) + 0.5034] \cdot \alpha^\circ \tag{46}$$

Find each corresponding Z, when $\alpha^\circ = 0^\circ, 5^\circ, 10^\circ \ldots 90^\circ, \left(90^\circ + \frac{\alpha^\circ_{02}}{4}\right)$

From equations (31) and (44),

$$\frac{\alpha^\circ_{02}}{4} = 5.7296\left[1 + \frac{20}{1.02d'+3}\right]^\circ \tag{47}$$

7.5.1.2 Finding the height of the neutral line on tooling edge at crimple circle from neutral base

From Fig. 3, based on equations (17), (43) and (29) (44) it gives:

$$R_1(\alpha) = \frac{0.5318(1.02d' + 1) + 0.6366}{\sin\alpha} + [0.3036\ (1.02d' + 1) + 0.3634]\cot\alpha \tag{48}$$

$$R_2(\alpha) = \frac{0.5318(1.02d' + 3) + 0.6366}{\sin\alpha} + [0.3036\ (1.02d' + 3) + 0.3634]\cot\alpha \tag{49}$$

Again, from

$$h_1 = 2R_1(\alpha) \cdot \sin^2\alpha \tag{50}$$

$$h_2 = 2R_2(\alpha) \cdot \sin^2\alpha \tag{51}$$

find the corresponding h_1 and h_2 when $\alpha^\circ = 0^\circ$, 5°, 10°, ... 90° in wrapping arc section.

From Fig. 4, based on equations (26), (43) and (31) (44), it leads to:

$$R_1'(\alpha_1') = [0.5318(1.02d' + 1) + 0.6366]$$
$$[0.03183(1.02d' + 1)$$
$$- \frac{+ 0.6366](1.02d' + 1)}{5.7296(1.02d' + 1)+114.592} (\alpha_1')^\circ \quad (52)$$

in which,

$$0 \leq (\alpha_1')^\circ \leq \frac{\alpha_{01}^\circ}{4} = 5.7296\left[1+ \frac{2}{1.02d'+1}\right]^\circ \quad (53)$$

$$R_2'(\alpha_2') = [0.5318(1.02d' + 3)+ 0.6366]$$
$$[0.03183(1.02d' + 3)$$
$$- \frac{+ 0.6366](1.02d' + 3)}{5.7296(1.02d' + 3)+114.592}(\alpha_2')^\circ \quad (54)$$

where, $0 \leq (\alpha_2')^\circ \leq \frac{\alpha_{02}^\circ}{4}$, $\frac{\alpha_{02}^\circ}{4}$ is determined by equation (47).

Again from

$$h_1' = 2R_1'(\alpha_1') \quad (55)$$

$$h_2' = 2R_2'(\alpha_2') \quad (56)$$

find h_1' and h_2' corresponding to beginning and end locations in wrapping arc section. In practice, h_1' and h_2' at the beginning location of overlap section are respectively equal to h_1' and h_2' at the end location of wrapping arc section.

7.5.2 Top View

7.5.2.1 Finding the distance from the neutral line on both edges of the tooling at crimping circle to vertical axis plane.

From Fig. 3, based on equation (1), (43) and (1), (44), it yields:

$$W_1 = \rho_1 \cos\alpha$$
$$\approx (1.02d' + 1)(1+ 0.5708 \cos\alpha) \cdot \cos\alpha \quad (57)$$

$$W_2 = \rho_2 \cos\alpha$$
$$\approx (1.02d' + 3)(1 + 0.5708 \cos\alpha) \cdot \cos\alpha \quad (58)$$

Because the butt closure of left and right half tooling is implemented as $\alpha = 90^\circ$, we can find the corresponding W_1 and W_2 when $\alpha = 0^\circ, 5^\circ, 10^\circ, \ldots 90^\circ$, $W_1 + W_2$ is the width B of tooling when not crimped.

7.5.2.2 Finding the distance from the profile of tooling bounded by the neutral line of the edge to vertical axis plane of tooling.

Use formulas

$$M_1 = R_1(\alpha)$$

$$M_2 = R_2(\alpha)$$

to find out corresponding M_1 and M_2 when $\alpha = 45^\circ$, 50°, 55°, ...90°

Use formulas

$$M_1' = R_1'(\alpha_1')$$

$$M_2' = R_2'(\alpha_2')$$

to find out M_1' and M_2' corresponding to the beginning and end locations of overlap section. M_1' and M_2' at the beginning location of overlap section are in fact respectively equal to the M_1' and M_2' at the end locations of wrapping arc section.

7.5.2.3 Find the distance from the neutral point of the two edges of tooling with the terminals overlapped to the vertical axis plane of the tooling to determine the final overlap position. From Fig. 2, according to equation (59) and (60), it gives:

$$T_1 = (D' + \Delta 1) \sin\frac{\alpha_{01}^\circ}{4} \cdot \cos\frac{\alpha_{01}^\circ}{4}$$
$$= \frac{(1.02d' + 1)}{2} \sin(2\times\frac{\alpha_{01}^\circ}{4}) \quad (59)$$

$$T_2 = (D' + \Delta 1 + 2)\sin\frac{\alpha_{02}^\circ}{4}\cos\frac{\alpha_{02}^\circ}{4}$$
$$= \frac{(1.02d' + 3)}{2} \sin(2\times\frac{\alpha_{02}^\circ}{4}) \quad (60)$$

7.5.3 Left View

It can be plotted out from the front and vertical views. And plot the formation trajectory of two cardioid curves located on the right and left sides of OY axis based on the neutral layer of tooling tape. In case of need mark $\frac{\alpha_{01}^\circ}{4}$ and $\frac{\alpha_{02}^\circ}{4}$ at the final overlap location and the thickness of tooling tape.

7.5.4 Sectional View

Plot the cross sectional view at various corresponding tooling lengths when $\alpha = 0^\circ$, 5°, 10°, ... $90^\circ + \frac{\alpha_{02}^\circ}{4}$ and mark on the view R_1, R_2, h_1, h_2, W_1, W_2, of right and left half tooling in the course of formation, and also the thickness Δ_1 of the tooling tape, if necessary. After long tooling for longitudinal wrap is drawn on the scale of 1:1, notes should be added to illustrate that the graph sizes are calculated on the basis of the neutral layer of tooling tape so as to draw special attention when a tooling model is made in accordance with the sectional view.

Acknowledgement

The author would like to thank Mr. Xu Nai Ying, senoir engineer, deputy chief engineer of No. 5 Research Institute of the Posts and Telecommunications Ministry for his check of the paper and Mr. Hong Fu Ming, professor of Chengdu Telecommunication Engineering Institute for his review. Two of them are my former schoolmate of Jiao Tong University.

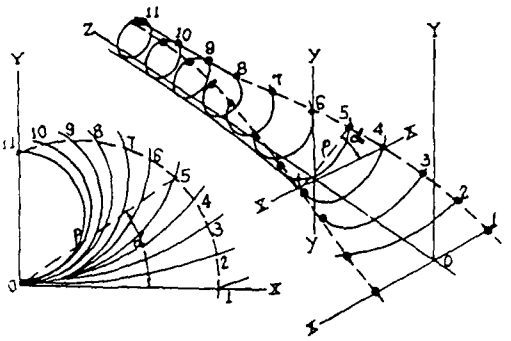


Fig. 1

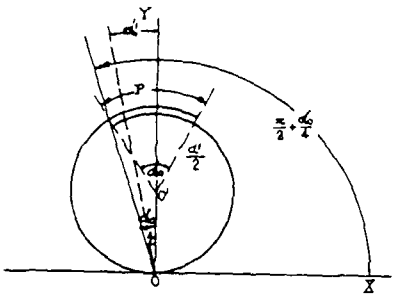


Fig. 2

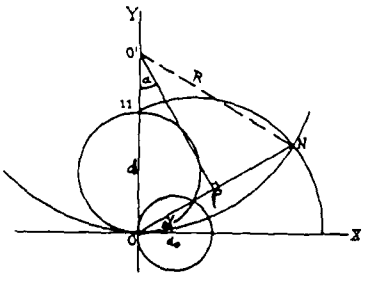


Fig. 3

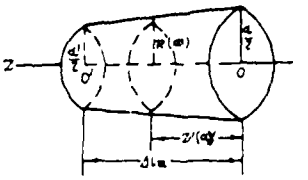


Fig. 4

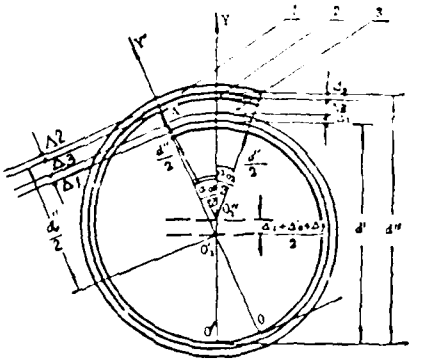


Fig. 5
1. Long Tooling, thickness Δ_1.
2. Laminated Shield, Thickness Δ_2.
3. Gap Δ_3.

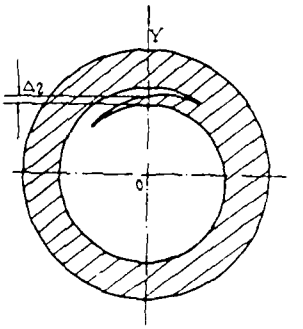


Fig. 6

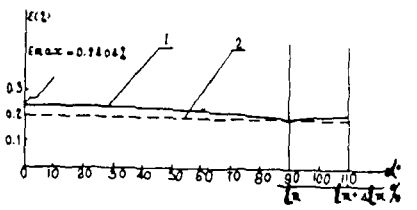


Fig. 7
1. Uniform Formation
2. Shortest Formation

Table 1

α	$\rho=\frac{\pi d}{2\pi}\sin\alpha$	$\rho\approx d(1+0.5708\cos\alpha)$	$\rho\approx\frac{3(d+d_0)\cos\frac{\alpha}{2}}{4-\cos\frac{\alpha}{2}}$
0°	1.5708 d	1.5708 d	1.5708 d
5°	1.5696 d	1.5686 d	1.5687 d
10°	1.5624 d	1.5621 d	1.5626 d
15°	1.5528 d	1.5513 d	1.5528 d
20°	1.5390 d	1.5364 d	1.5391 d
25°	1.5214 d	1.5173 d	1.5215 d
30°	1.5000 d	1.4943 d	1.5000 d
35°	1.4750 d	1.4676 d	1.4753 d
40°	1.4462 d	1.4372 d	1.4470 d
45°	1.4142 d	1.4036 d	1.4154 d
50°	1.3788 d	1.3669 d	1.3805 d
55°	1.3405 d	1.3274 d	1.3432 d
60°	1.2990 d	1.2854 d	1.3020 d
65°	1.2549 d	1.2412 d	1.2591 d
70°	1.2082 d	1.1952 d	1.2134 d
75°	1.1591 d	1.1477 d	1.1660 d
80°	1.1080 d	1.0991 d	1.1161 d
85°	1.0548 d	1.0498 d	1.0649 d
90°	d	d	1.0117 d

Table 2

Model Length of WAS	Formation Angle α	
	Shortest Form	Uniform Form
0	0°	0°
$0.1l_\pi$	4°3'	5°
$0.2l_\pi$	9°2'	18°
$0.3l_\pi$	15°18'	27°
$0.4l_\pi$	23°0'	36°
$0.5l_\pi$	32°36'	45°
$0.6l_\pi$	43°43'	54°
$0.7l_\pi$	56°02'	63°
$0.8l_\pi$	68°30'	72°
$0.9l_\pi$	80°7'	81°
l_π	90°	90°

Table 3

OD of LW Tape (mm)	LW Model Length in Uniform Form (mm)			LW Model Length in Shortest Form(mm)		
	WAS	OS	Total Length	WAS	OS	Total Length
5	310.28	76.19	386.5	294.19	88.84	383.0
10	499.55	84.81	584.4	413.29	85.33	498.6
20	878.09	104.64	982.7	726.45	93.44	819.9
30	1256.63	130.00	1386.6	1039.62	117.32	1156.9
40	1635.17	153.67	1788.8	1352.78	134.32	1487.1
50	2013.71	177.50	2191.2	1665.95	144.84	1810.8
60	2392.25	201.43	2593.7	1979.11	170.37	2149.5

Table 4

Whole angle α°	Relative Elongation ε(%)	Whole angle α°	Relative Elongation ε(%)
0°	0.2404	60°	0.2222
5°	0.2403		
10°	0.2398	65°	0.2181
15°	0.2391	70°	0.2148
20°	0.2381	75°	0.2113
25°	0.2369	80°	0.2077
30°	0.2354	85°	0.2038
35°	0.2336	90°	0.2000
40°	0.2316	95°	0.2038
45°	0.2293	100°	0.2077
50°	0.2268	105°	0.2113
55°	0.2241	110°	0.2148

Note: WAS = wrapping arc section
LW = Longitudinal wrapping
OS = overlap section

Reference:
C.H.Masters et alii.Special Issue Wire And Cable Manufacture The Western Electric Engineer Vol.15, No.3,PP65-73



Yuan Zhang, cable manufacture engineer, graduated from Electric Machinary Department of Jiao Tong University, Majoring in electrical insulation and cable technology, has been working in the field of design and manufacture process of telecommunication cable in large enterprise, published a few papers on analysis and studies of product structure, once being deputy cheif engineer of Chengdu Cable Plant, after advanced study on enterprise management, then promoted to be plant director.

Evaluation of Materials for Improved Life Expectancy of Foam Skin Insulation

Geoffrey D. Brown

Union Carbide Corporation

Lawrence E. Davis

Superior Cable Corporation

ABSTRACT

Commercial foam/skin insulations exhibit unexpectedly rapid accelerated aging failures when evaluated with a new cable testing procedure. The filled cable is preaged in an air oven prior to removal of the insulated wire for oven aging studies. Two failure modes are observed, with rapid cracking of ductile insulation specimens occuring along with oxidative embrittlement. Thermal embrittlement behavior is also evident. The failure rates are greatly accelerated by the cable preaging and this effect is apparent with all filling compounds and insulation materials evaluated.

Evaluations of commercial and experimental polyethylene insulating materials were conducted to determine if improved foam/skin insulation life expectancy can be obtained. A major improvement is demonstrated via optimization of the cellular product antioxidant system.

INTRODUCTION

Foam/skin insulations have generally provided good performance in the 10 years since commercial introduction. This experience encompasses a broad range of application including the relatively severe environments of installations in the southern and southwestern regions of the United States. A thermal-oxidative history in these severe climates[1] typically corresponds to much longer aging elsewhere. Therefore, experience to date gives confidence that the majority of foam/skin plant in moderate climates will provide good service life. Less certain is the continued good performance of foam/skin insulations in the more severe environments.

Previous studies[2,3,4] have extrapolated accelerated aging data to predict marginal commercial performance of cellular and foam/skin insulations after cable filler exposure. Because of uncertainties regarding Arrhenius extrapolation of the elevated temperature data to application conditions, it is difficult to gauge the extent of future problems (if any?) with current commercial products. In fact, it is known that complex mechanisms such as antioxidant solubility and migration can be highly nonlinear[5] and even modest temperature extrapolation can be erroneous. Nevertheless, accelerated aging studies with minimal temperature extrapolation are generally recognized[1,6] as the best method of predicting long term performance.

The accelerated aging testing methods used in this study were developed to measure the compability of experimental filler compounds with commercial insulations. Emphasis is placed upon aggressive conditioning of cables prior to removal of insulation samples for aging studies. When the study produced unexpectedly rapid failures of numerous commercial foam skin insulation samples, a technical program was initiated to develop improved insulations.

TEST METHOD

The cable aging test is presented in detail in the complementary paper by L.E.Davis, "A Global Test Method for Long Term Stability of Solid and Foam Skin Insulation." The test method is summarized below:

Standard processing conditions and techniques are used to insulate the primaries and to assemble these into filled cables. Insulation samples removed from cable as received or after manufacture are identified as "regular" samples. Additional cable sample is capped and placed into a circulating air oven for 4 week conditioning at 70°C. Insulation samples undergoing this 4 week cable conditioning at 70°C prior to removal are identified as "preaged" samples. After removal from the cable, the insulation samples are thoroughly wiped to remove surface filling compound. For each sample, a set of at least 20 insulation specimens about two feet long is prepared. With each specimen, a first pigtail to place stress on the sample is formed by wrapping the insulator about itself. The insulation specimens are then placed in a vented circulating air oven with accelerated oven aging performed at 70° and 80°C conditions, with the 80° C condition becoming the standard. After six weeks of oven aging a second pigtail is formed in each specimen to simulate stresses associated with periodic reworking of commercial installations. In addition, 3rd and 4th pigtails are respectively formed after 50% and 100% cracking failure of the 1st pigtails to aid in definition of the failure mechanism. Figure 1 illustrates the pigtail formations while Figure 2 shows a testing series deployed in a circulating air oven.

Figure 1

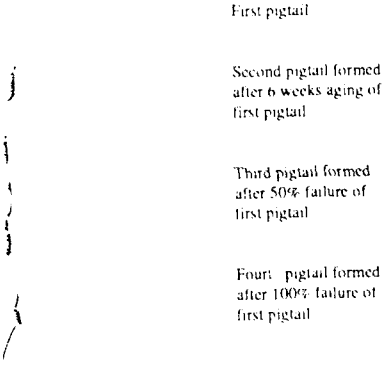
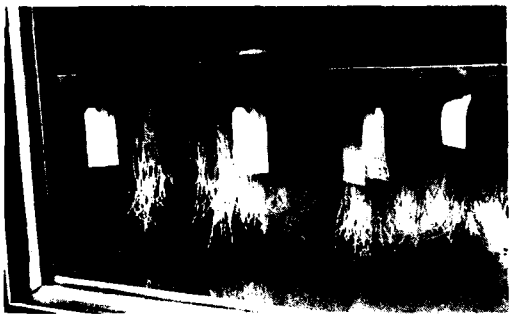


Figure 2



The test has several significant differences as compared to the Bell Thermal Oxidative Stability Performance Test[7] (Bell Pedestal Test) which has become an industry standard for evaluating long term aging performance. Most important is the 70°C four week preaging of cable samples prior to the removal of primaries for oven aging studies. This preaging simulates commercial applications, since cables often experience a substantial time/temperature history prior to exposure of the insulation in a pedestal environment. Utilizing reduced test temperatures of 70° and 80°C while providing quantified performance differentiation within a year is also advantageous in minimizing error from nonlinear temperature effects. The technique of stressing the insulation by forming a pigtail has been used in many studies. For example, "periodic" pigtail stressing and inspection was included in the original Bell Experimental Pedestal Installation Complex (EPIC test) protocol[8]. The use of 1st and 2nd pigtails to investigate thermal aging phenomena is a more novel approach yielding interesting data. Use of a circulating air oven to accelerate air flows provides a desirable safety margin relative to the much longer oxidative aging of commercial pedestals. With the exception of the air flow consideration, these features could be readily incorporated into a Pedestal test methodology.

COMMERCIAL CABLE

Cables from several manufacturers were evaluated to determine variation in test results due to differences in insulation compounds, filling materials, and manufacturing. This test data is presented in Table 1A. Preaged samples failed rapidly compared to regular samples. Third and fourth pigtail data (Table 1B) for the 80°C aging show preaged specimens were typically ductile after 1st pigtail cracking failure, while the regular (no preaging) samples were embrittled. Cables supplied by a single manufacturer show that a wide range of cable performance can be expected. Each manufacturer included produced cables which exhibited early failure.

Variation in insulating compound, filler material, or manufacturing differences between cablers didn't appear to alter the general tendency of the foam/skin insulation to exhibit relatively rapid crack failure. An insulating process correlation wasn't apparent, since insulation from supplier B showing gross process variation (highly elongated cell structure and porosity in the skin layer under microscopic examination) exhibited aging performance equal to insulations with good cell structure.

Significant variation in relative time to failure for first and second pigtails was observed. Second pigtails often failed sooner than the first pigtails. When the six week interval in the oven before forming the second pigtail was subtracted, second pigtails never survive longer then first pigtails. This comparison of 1st and 2nd pigtail data suggests the presence of a thermal embrittlement mechanism.

ALTERNATE COMMERCIAL MATERIALS

Commercial insulation materials from various suppliers were evaluated. Linear low density polyethylene was also included as a skin material. It has been shown[9] that chemical blowing agent residuals subtantially reduce the oxidative stability of cellular insulations. Therefore, a HDPE cellular insulation containing a 50 percent increase in AO-1 (Irganox 1010) primary antioxidant level was also evaluated.

Table 2A summarizes the results obtained from this test cable. The results are similar to those achieved with commercial cable samples. Once again, preaging substantially reduced the time to insulation failure. The increased AO-1 primary antioxidant provided only a slight improvement.

Table 2B summerizes the 3rd and 4th pigtail testing. All of the preaged samples exhibited ductility at 50% (3rd pigtail) and 100% (4th pigtail) failure of the 1st pigtails. With the exception of the cellular only insulation (approximately 30% expansion), all of the regular samples were embrittled before 100% failure of the first pigtails. In general, preaged samples exhibited rapid cracking where good specimen ductility remains. Regular samples typically failed after a longer interval due to thermal-oxidative embrittlement.

Environmental stress cracking was postulated as a mechanism for the rapid failure of preaged samples. It was thought that the absorbtion of cable filling compounds during preaging might introduce a stress cracking agent. It was recognized that classical environmental stress cracking failure is a surface phenomena that doesn't include the filler migration and swelling of polyethylene. Nevertheless, the character of the ductile specimen cracking suggested that improved environmental stress cracking performance should be the priority of the next experimental trials.

EXPERIMENTAL MATERIAL

A number of material combinations to improve environmental stress cracking performance were evaluated. Changes in the HDPE skin included use of ethylene-hexene copolymer in place of ethylene-butene copolymer as the HDPE base resin. In addition, rubber and nucleating agent additives were evaluated in the skin materials. In the cellular product, ethylene-hexene copolymer foam was also tested, both with and without a processing aid additive. The ethylene-hexene foam materials exhibited preblow due to pilot plant equipment limitations, but it was decided to proceed with cable fabrication and testing. To ensure adequate stabilization, these pilot plant cellular compounds were formulated at 50% higher antioxidant concentrations of both the AO-1 and MD-1 components. A control sample of ethylene-butene foam/skin was included and a portion of this insulation was exposed to a 20 megarad electron beam to crosslink the high density polyethylene.

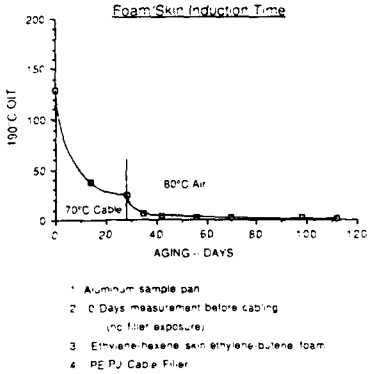
Table 3A summerizes 70°C oven aging results. Once again, the preaged samples failed rapidly compared to regular samples. As before, preaged specimens were ductile after cracking failure, while the regular

samples were embrittled. With the exception of slightly longer time to failure for two of the insulation combinations containing the ethylene-hexene foam compound, no significant trends were noticed in the data. The only significant difference occurred for the ethylene-hexene foam with an ethylene-butene skin which exhibited reduced tensile elongation at the 1st pigtail 50% failure level.

Table 3B contains the 80°C oven aging data for this test cable. The three insulation combinations incorporating ethylene-hexene foam show slightly improved 1st pigtail performance after preaging. In addition the third and fourth pigtail data shows some embrittlement when 1st pigtail failure occurred. This change from ductile to embrittled specimens at failure corresponds to a change to classical thermal-oxidative failure. It was thought that improved cellular product quality might provide additional performance gains.

The need for improved stabilization was confirmed by measurement of 190° C aluminum pan Oxygen Induction Time for the ethylene-hexene skin/ethylene-butene foam insulation in this testing series. As Figure 3 illustrates, there was a dramatic decrease in induction time associated with the 4 week preaging of the cable specimen at 70°C. Additional depletion of antioxidant occurs during the 80°C oven aging with residual OIT induction time well below 5 minutes at the onset of sample cracking.

Figure 3
Foam/Skin Induction Time



1 Aluminum sample pan
2 0 Days measurement before cabling (no filler exposure)
3 Ethylene-hexene skin ethylene-butene foam
4 PE PJ Cable Filler

The dramatic decrease in antioxidant functionality as measured by oxygen induction time during preaging generated a question regarding the compatability of the high density polyethylene antioxidants with cable filler materials. A materials testing method was developed to optimize the antioxidant system for filled cables. This work is summarized in detail in the complementary paper "Performance of HDPE Insulation Antioxidants in Filled Telephone Cable Applications." Among the findings was a poor performance of the AO-1 (Irganox 1010) primary antioxidant after 4 week cable filler conditioning at 70°C. Attempts to define alternative primary antioxidants with substantially improved filler compatability were unsuccessful. However, the study confirmed that the MD-1 (Irganox 1024) metal deactivator currently in use is well suited[10] for filled cable applications. Because this antioxidant also provides primary antioxidant functionality, it assumes the major role for stabilization after extended filler exposure. The bench study demonstrated the ability to increase the MD-1 concentration to provide dramatically improved stabilization after filler immersion.

REPEAT OF HEXENE HIGH DENSITY POLYETHYLENE COPOLYMER

Additional trials were completed with ethylene-hexene copolymer cellular as summarized in Table 4. The ethylene-butene copolymer skin and foam control with the standard antioxidant formulation exhibited the best performance observed to date for this combination. Samples containing hexene copolymer foam with increased antioxidant performed substantially better then the control. In addition, the ethylene-hexene samples showed some embrittlement at failure as indicated by the reduced ability to form 3rd and 4th pigtails. The time to failure of the 2nd pigtail was also increased to the highest level observed for any preaged foam skin insulation aged at 80°C. These results established that improved performance relative to both failure modes could be obtained with the combination of an improved antioxidant system and ethylene-hexene copolymer feedstocks.

WORK IN PROGRESS

As the better aging performance of ethylene-hexene cellulars with improved stabilization became apparent, additional experimental cable was prepared. The focus of this testing series was to better differentiate the performance gain from improved stabilization from the gain achieved through use of an ethylene-hexene base resin.

Four concentrations of the MD-1 antioxidant were evaluated in an ethylene-butene cellulars which were combined with both ethylene-butene and ethylene-hexene skins. Increased MD-1 antioxidant concentrations were also evaluated to a lesser extent in the ethylene-hexene skin. Various combinations of these materials were incorporated into foam/skin insulations as summarized in Table 5.

The preliminary results show that failure rates appear to correspond to the MD-1 antioxidant concentration in the cellular. Overall, the failure rates for all samples including controls appear to be improved over past experimental data. There is a significant trend showing major improvement in oven aging life as the MD-1 concentration in the cellular product is increased. The data trends indicate the ethylene-butene cellulars with improved stabilization most likely provide similar life performance to ethylene-hexene cellulars.

SUMMARY

It is well known that polyethylene insulations can fail at considerable accelerated rates after exposure to cable filling compounds. More novel are testing methods and data showing clear evidence of thermal embrittlement and ductile specimen cracking phenomena. These alternate failure modes were typically present when cable samples were preaged prior to oven aging of the insulations. These failure modes were more rapid then the thermoxidative embrittlement failures observed in prior studies.

The wide variance in performance of preaged versus regular samples, both in oven aging failure times and in failure mechanisms is of great interest. Preaged insulations typically exhibit rapid cracking failure with retained specimen ductility. In some respects, this cracking behavior is characteristic of environmental stress cracking, with good retention of specimen tensile strength, tensile elongation and ductility. However,

attempts to improve aging performance by materials optimization to provide improved environmental stress cracking performance didn't yield a significant improvement. In the course of these studies, poor retention of antioxidant functionality as measured by 190°C Oxygen Induction Time was found to coincide with the cable preaging for 4 weeks at 70°C.

A separate laboratory study was initiated to investigate the performance of the antioxidant system during extended filler contact. This program revealed that the AO-1 primary antioxidant was ineffective after extended filler contact. The bifunctional metal deactivator/hindered phenolic, MD-1, provided much better functionality retention after filler aging. Testing confirmed the capability to substantially improve stabilization by increasing the MD-1 concentration.

The failure mechanisms for preaged insulations apparently include a strong oxidative synergism, since antioxidant system optimization provides a major improvement in life performance. It is interesting that the antioxidant optimization also provides a change in failure mechanism. Samples incorporating cellulars with improved antioxidant show substantially longer life but are more likely to be embrittled at failure. This suggests that further antioxidant system optimization might provide additional gains in aging performance, although the cost/benefit of any such improvement should be carefully evaluated. In addition, it appears that the thermal embrittlement behavior contributing to the faster failure of second pigtails can be minimized by antioxidant optimization. Although these second pigtails continue to fail at slightly faster rates, the relative magnitude and importance of the difference is reduced by the significant increase in insulation life.

Work is continuing to quantify the relative insulation aging performance of ethylene-butene versus ethylene-hexene high density copolymers. Preliminary results indicate that these feedstocks will provide comparable performance if properly stabilized.

This study was pragmatic, with a primary objective being demonstration of commercial methods to substantially improve life performance. A solution was identified by study of polyethylene materials and antioxidant systems. It is known that other variables such as chemical blowing agents and cable fillers materials also exhibit a major influence upon insulation aging performance. The presentation of test methods provides a useful tool to further investigate these variables.

CONCLUSIONS

A cable testing method incorporating features simulating the commercial application was utilized to optimize foam/skin insulations to provide improved long term aging performance. A twofold improvement in the accelerated aging performance was demonstrated via optization of the cellular product antioxidant system. Installed foam/skin insulations have generally performed well for ten years, and this substantial improvement should increase confidence relative to the 40 year service life desired for all applications. All insulation material suppliers and cable producers have the incentive and ability to rapidly implement improved cellular product stabilization as a result of this publication.

ACKNOWLEDGEMENTS:

The support of our coworkers at Superior Cable and Union Carbide in the many phases of this experimental work is gratefully acknowledged. The support and guidance of C. K. Eoll of Siecor Corporation and R. J. Turbett of Union Carbide in the early stages of this program is highly appreciated.

REFERENCES:

1. Howard, J.B., "Stabilization Problems with Low Density Polyethylene Insulations," 21st International Wire and Cable Symposium, 1972, pp. 329-341.

2. Baxter, G.D., Farango, M., and Gouldson, E.J., "Foam-Skin, A Composite Expanded Insulation for Use in Telephone Cables," 21st International Wire and Cable Symposium, 1972, pp. 158-172.

3. Gesner, B.D., Shea, J.W., and Wight, F.R., "Establishing Longevity Criteria From Thermo-Oxidative Cracking Measurements on Polyolefin Insulations," 22nd International Wire and Cable Symposium, 1973, pp. 7-10.

4. Schmidt, G.A., "Methods for Life Prediction of Insulations of Air Core Cables and Filled Cables," 22nd International Wire and Cable Symposium, 1973, pp. 11-22.

5. Kuck, V., "Critical Temperature for Soluability of a Phenolic Antioxidant," Polymer Additives, editor Kresta, J.E., 1984, pp. 103-110.

6. Kokta, E. T., "Comparison of Test Methods for Determination of Stability of Wire and Cable Insulation," 24th International Wire and Cable Symposium, 1975, pp. 220-224.

7. Bell Communications Research, "Generic Requirements for Metallic Telecommunciations Cables," Technical Reference TR-TSY-000421, Issue 1, December 1986, pp B1-B2.

8. Gilroy, H. M., "Thermal Oxidative Cracking of Polyethylene Insulation on Telephone Conductors," 23rd International Wire and Cable Symposium, 1974, pp. 42-45.

9. O'Rell, D.D., and Patel, A., "Oxidative Stability Studies on Cellular High Density Polyolefin Insulation for Communications Wire" 24th International Wire and Cable Symposium, 1975, pp. 231-236.

10. Patel, A., "A Bifunctional Antioxidant/Metal Deactivator for Polyolefin Wire Insulation", 26th International Wire and Cable Symposium, 1977, pp. 83-86.

Table 1A

24 Gauge Foam Skin Commercial Cable (Weeks to 50% Pigtail Failure)

Cable Supplier	70°C		80°C			
	Preaged 1st Pigtail	Regular 1st Pigtail	Preaged 1st Pigtail	Preaged 2nd Pigtail [1]	Regular 1st Pigtail	Regular 2nd Pigtail [1]
A1	60	61	28	27	58	50
A2	26	59	8	11	56	48
B1	27	66	14	13	26	27
B2	26	72	14	12	46	42
C1	26	41	10	10	61	48
C2	17	52	13	11	24	18
D	22	45	9	15	36	38
E1	18	--	7	9	35	41
E2	--	--	28	20	--	--

Note: 1. Time to failure for 2nd pigtail includes aging time in oven before formation of 2nd pigtails

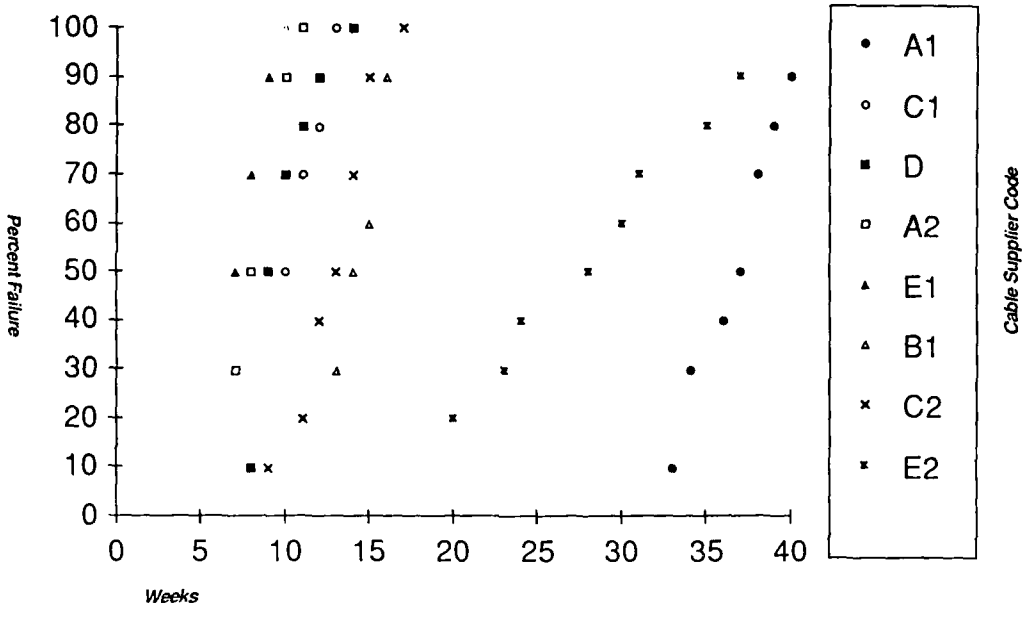
Table 1B

24 Gauge Foam Skin Commercial Cable (Can Make Pigtails without Cracking)

Cable Supplier	80°C			
	Preaged		Regular	
	3rd Pigtail	4th Pigtail	3rd Pigtail	4th Pigtail
A1	yes	yes	no	no
A2	yes	yes	no	no
B1	yes	no	yes	19 / 20
B2	yes	17 / 20	no	no
C1	yes	yes	no	no
C2	17 / 20	18 / 20	no	no
D	yes	yes	yes	no
E1	yes	yes	no	no
E2	yes	no	--	--

Graph 1

Cumulative Failure of Commercial Cable
Preaged at 70°C and Aged at 80°C
(% Failure vs. Weeks)



Graph 2

Cumulative Failure of Commercial Cable
Preaged at 70°C and Aged at 70°C
(% Failure vs. Weeks)

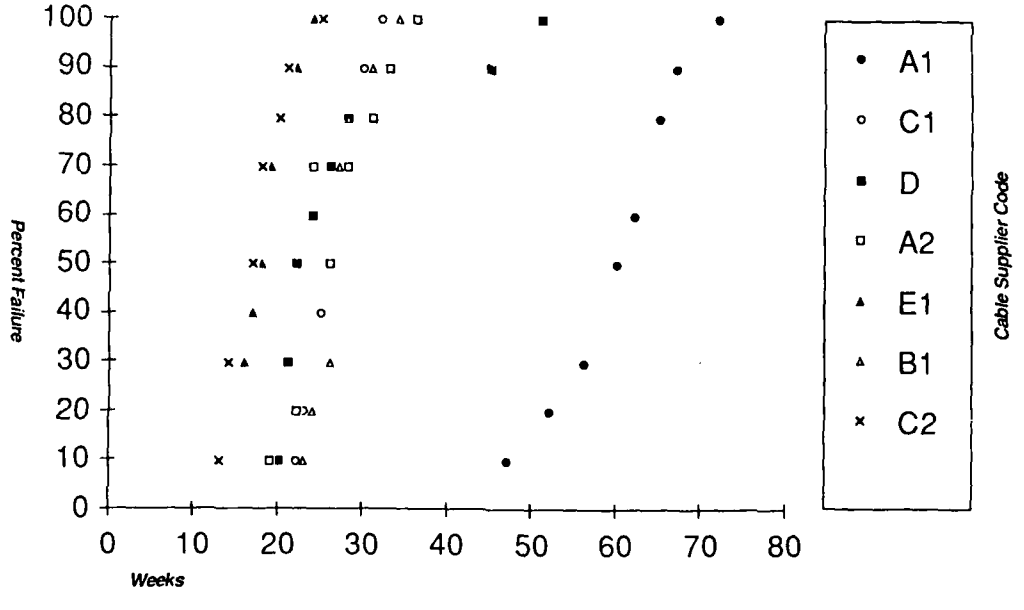


Table 2A

Commercial Materials
(Weeks to 50% Pigtail Failure)

Foam		Skin		70°C		80°C			
Material	Supplier	Material	Supplier	Preaged 1st Pigtail	Regular 1st Pigtail	Preaged 1st Pigtail	Preaged[1] 2nd Pigtail	Regular 1st Pigtail	Regular[1] 2nd Pigtail
HDPE	A	LLDPE	A	27	42	9	8	19	14
HDPE 50% Increase Antioxidant	A	LLDPE	A	29	51	12	12	23	22
HDPE	A	PP	B	23	66	10	10	27	26
HDPE 50% Increase Antioxidant	A	PP	B	26	76	13	11	30	32
HDPE 50% Increase Antioxidant	A	--	--	21	44	10	9	18	20
HDPE 50% Increase Antioxidant	A	HDPE	A	33	53	23	16	35	27
HDPE	A	HDPE	C	30	82	13	12	40	24
HDPE	A	HDPE	D	30	72	12	10	28	16

Note: 1. Time to failure for 2nd pigtail includes aging time in the oven before formation of 2nd pigtail.

Table 2B

Plasticity Measured by Formation of 3rd and 4th Pigtails

Foam		Skin		Preaged		Regular	
Material	Supplier	Material	Supplier	3rd Pigtail Can Make (%)	4th Pigtail Can Make (%)	3rd Pigtail Can Make (%)	4th Pigtail Can Make (%)
HDPE	A	LLDPE	A	100	100	0	0
HDPE 50% Increase Antioxidant	A	LLDPE	A	100	100	95	0
HDPE	A	PP	B	100	100	0	0
HDPE 50% Increase Antioxidant	A	PP	B	100	100	0	0
HDPE 50% Increase Antioxidant	A	--	--	100	100	100	100
HDPE 50% Increase Antioxidant	A	HDPE	A	95	100	0	0
HDPE	A	HDPE	C	100	100	0	0
HDPE	A	HDPE	D	100	100	0	0

Table 3A

Experimental Materials [1]
70°C Aging

Insulation Ethylene Copolymer		Preaged Four Weeks at 70°C			Regular [2]	
Skin HDPE	Foam HDPE	Weeks to 50% Failure 1st Pigtail	Initial Preaged Elongation (%)	Elongation at 50% Failure (%)	Weeks to 50% Failure 1st Pigtail	Elongation at 50% Failure (%)
Butene	Butene	32	460	380	72	< 25
Hexene	Butene	34	490	480	80	< 25
Hexene	Experimental Hexene	44	410	410	> 82	< 25
Hexene with processing aid	Experimental Hexene with processing aid	34	380	390	82	< 25
Butene	Experimental Hexene	46	390	170	80	< 25
Butene with nucleating agent	Butene	30	460	475	74	< 25
Butene and Rubber	Butene	32	380	330	78	< 25

Note: 1. The stabilization package for the Butene materials was 0.1% antioxidant and 0.1% metal deactivator. The Hexene stabilization package 0.15% antioxidant and 0.15% metal deactivator.
2. Wire was brittle when removed from oven.

Table 3 B

Experimental Materials [1]
80°C Aging

Insulation Ethylene Copolymer		Preaged Four Weeks at 70°C				Regular			
		Weeks to 50% Failure		% Pigtails that Could Be Made		Weeks to 50% Failure		% Pigtails that Could Be Made	
Skin HDPE	Foam HDPE	1st Pigtail	2nd Pigtail	3rd Pigtail	4th Pigtail	1st Pigtail	2nd Pigtail	3rd Pigtail	4th Pigtail
Butene	Butene	14	10	100	95	34	20	0	0
Hexene	Butene	18	10	85	100	40	22	0	0
Hexene	Experimental Hexene	22	12	0	0	45	26	0	0
Hexene with processing aid	Experimental Hexene with processing aid	20	12	0	0	36	24	0	0
Butene	Experimental Hexene	20	12	0	0	42	26	0	0
Butene with nucleating agent	Butene	16	10	100	100	40	24	0	0
Butene and Rubber	Butene	12	8	100	100	38	20	0	0
Butene [2] x-linked	Butene [2] x-linked	18	14	100	100	38	> 40	0	--

Note: 1 The stabilization package for the Hexene was 0 15% antioxidant and 0 15% metal deactivator
The stabilization package for the Butene materials was 0 1% antioxidant and 0.1% metal deactivator
2 X-linked by electron beam of 20 mega rad

Table 4

High Density Polyethylene - Hexene Copolymer Repeat
Preaged Four Weeks at 70°C

Material		80°C				70°C			
		Weeks to 50% Failure		Can Make %		Weeks to 50% Failure		Can Make %	
Skin [1]	Foam [2]	1st Pigtail	2nd Pigtail	3rd Pigtail	4th Pigtail	1st Pigtail	2nd Pigtail	3rd Pigtail	4th Pigtail
Butene	Butene	28	< 16	88	52	60	22	92	--
Hexene	Butene	40	16	100	40	64	32	96	92
Hexene	Hexene	48	42	84	0	Note 3	54	--	--
Hexene	Hexene w/ 2% processing agent	52	42	68	4	Note 4	58	--	--

Note: 1. The skin materials contained 0.15% metal deactivator and 0.18% antioxidant.
2. The Butene foam contained 0.1% metal deactivator and 0.1% antioxidant.
The Hexene foam contained 0.15% metal deactivator and 0.18% antioxidant.
3. 36% failure at 68 weeks.
4. 8% failure at 68 weks.

Table 5

Comparison of Stabilization Package at 80°C
After 40 Weeks at 80°C

Hexene Skin		Butene Foam		% Failure	
Antioxidant %	% Metal Deactivator	Antioxidant %	% Metal Deactivator	1st Pigtail	2nd Pigtail
0.18	0.15	0.10	0.10	80	100
0.20	0.15	0.10	0.10	16	76
0.15	0.25	0.10	0.10	16	56
0.20	0.15	0.15	0.15	0	0
0.15	0.25	0.15	0.15	0	0
0.20	0.15	0.15	0.20	0	0
0.20	0.15	0.15	0.25	0	0
0.15	0.25	0.15	0.25	0	0
0.15[1]	0.15[1]	0.10	0.10	72	100
0.15[1]	0.15[1]	0.10	0.10	100	100[2]
0.15[1]	0.15[1]	0.15	0.15	0	0

Note: 1. Butene skin
2. 100% failure in under 16 weeks



Geoff Brown received a MSME degree from Bucknell University in 1977. He joined Union Carbide in 1977 and specialized in polymer melt process development in the Polyolefin Specialities R & D Department. Since 1983, he has been involved in product development for telecommunications.



Lawrence E. Davis is the Senior Engineer for Materials / Processing for Superior Cable Corporation. He received his B.S. degree in physics from the Appalachian State University in 1969 and graduated with a Master's degree in physics from the University of Wisconsin, Milwaukee in 1974. Prior to joining Superior Cable, Mr. Davis was the Materials Engineering Manager for Technical Staff, Siecor Corporation and was formerly a Materials Engineer for Continental Telephone Laboratories.

ACTIVE TRANSCEIVER CABLE FOR LOCAL AREA NETWORKS

H. YOKOSUKA Y. KOBAYASHI K. ARAI K. KARAI O. WATANABE

FUJIKURA LTD. 1440 MUTSUZAKI SAKURA-SHI CHIBA-KEN 285 JAPAN

Summary

A small and light weight active transceiver cable has been developed and introduced into practical use for local area networks. The active transceiver cable was designed to be compatible with the standard IEEE 802.3. It consists of a coaxial cable tap, a transceiver module and a transceiver cable.

The transceiver module, the transceiver cable termination and a female connector of a coaxial tap are mounted on a metal frame and are molded into a body with a plastic resin. The all transceiver circuit is molded into a small chip and mounted on a printed circuit board. The module, the transceiver cable and a coaxial tap are joined on this board.
Since the hybrid IC in the module are very fragile to the molding pressure, many techniques were employed to achieve a successful injection molding.

On the top of the transceiver unit, the coaxial cable tap block is fitted. The tap block consists of two halves: a connection block and a clamping block. The connection block has a signal probe and ground probes on the cable trough . The coaxial cable is gripped with a bolt and the tap block is attached to the transceiver unit with two bolts. The installation can be done in a short time. When this is all assembled it makes a fine configuration suitable for use in any modern office.

Introduction

Recently local area networks have been widely used for office automation, factory automation and laboratory automation in our modern information society. Among several types of these networks, the Ethernet which is standardized as IEEE802.3 is one of the most popular networks because of its simple and easy expansion, inexpensive cost, and high transmitting speed.

The growth of networks brings a need for development of small and fine configuration transceiver units as well as fast and reliable means of tapping cables to add workstations.
Traditional transceiver units are separated into three parts, a big coaxial cable tap, a big transceiver circuit box with a transceiver cable connector and a transceiver cable. When they are assembled and hung from the coaxial cable on the wall, it needs a much space to be installed and it looks bulky. In a contemporary and neat office these kind of a over-size transceiver units are often seen under desks or around the corner of the room.

The newly developed transceiver unit consists of a coaxial cable tap and a transceiver unit which includes a transceiver cable termination. When these two are assembled they are compact and make a fine configuration suitable for a modern office. In this paper the assembled unit of a coaxial cable tap and a transceiver unit with a transceiver cable, is called an active transceiver cable.
The outer dimensions of the active transceiver cable are much smaller than that of the traditional one. In order to realize the new active transceiver cable unit, two important technologies were necessary. They were a small transceiver module and a PVC injection molding technique. In Figure 1 the new transceiver cable and its installation method are shown in comparison with the traditional one.

Transceiver Module

The outside view of the new small transceiver module and its principal dimensions are shown in Figure 2 and Table 1 respectively. All transceiver circuits shown in Figure 3 are packed densely in the module. As standardized by IEEE802.3 and illustrated in figure 3 the module has the following functions.

(1)Transmitting signals to medium
The module receives differential signals from data terminal equipment with the DO± terminals and sends out signals to a coaxial cable by the driver. Among the signals it receives; negative signals having a pulse width less than 7 ns,

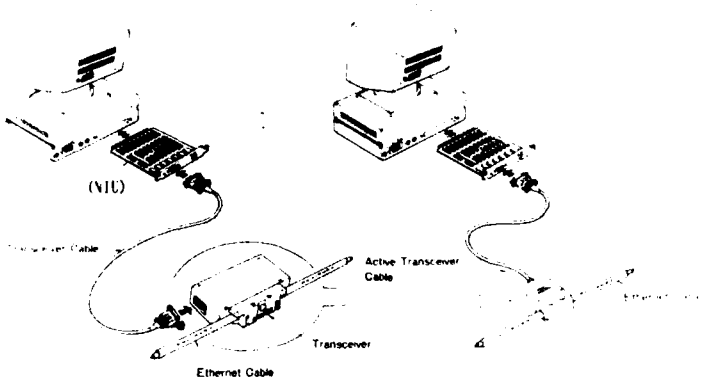


Figure 1. New Active Transceiver Cable and its Installation Method



Figure 2. New Small Transceiver Module

positive pulse signals having a pulse width 160 ns and above, and signals having their peak level less than -175 mV shall be eliminated by a noise filter circuit.

(2)Receiving signals from medium
Signals received from the tap will be transmitted to a differential line driver through an amplifying circuit and a filtering circuit. At this time, the signals are compared with the reference voltage by the carrier detector and only good signals are transmitted to the driver. Then the signals are sent out to data terminal equipment through a pulse transformer from the DI+ terminals.

(3)Collison detection
During transmission the module will detect a collision in the medium when other workstations on the network start transmitting. Signals received are compared with the collision detecting reference level and if they are found below the reference, 10 MHz collision signals will be sent out to a data terminal from the terminal CI+ through a differential line driver and a pulse transformer.

(4)Jabber control
In order to protect the medium from an extraordinarily long message, the jabber time controller monitors the DO+ operation and detects transmitting signal irregurality. It stops transmitting when an active state of the transmitting driver lasts over 26 ms of jabber time.

(5)SQE test
The module makes a signal quality error test at the end of a transmission. At this time, 10 MHz signals will be sent out from the CI+ terminals.

As noted in table 1 the transceiver module is very small. In order to make the smallest module, the following two key techniques played an important role.

Table 1 Principle demension

Discription	Dimension
Outside dimension	Plastic mold: 34x36x13 mm
Number of pins	24 pins
Power supply	10-16 V 150 mA
Dielectric strength	AC 500 V 1 min.
Transmitting output	1.8 V p-p
Receiving differential output	+700 mV
Collision detecting DC level	-1.56 V
SQE test	Possible

(1)A regular DC/DC converter of this capacity has the same volume as the transceiver module. The minimization of the volume was achieved by improving conversion efficiency and by eliminating a noise problem caused by the efficiency improvement.

(2)When all the devices shown in figure 3 are mounted using the existing mounting method, the transceiver module will become more than twice the volume of the new module. A new mounting method was employed to make the small hybrid IC chip.

Active Transceiver Cable

The active transceiver cable has on its one end, a plastic molded transceiver unit which makes a complete shape with the coaxial cable tap block. And it has a D-sub connector with 15 pins at the other end. The whole outside view is shown in

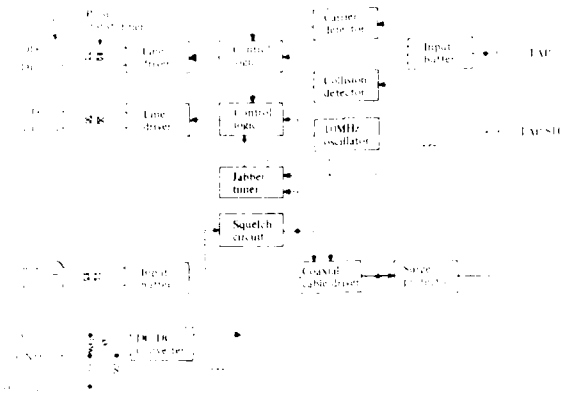


Figure 3. Block Diagram of the Transceiver Circuit

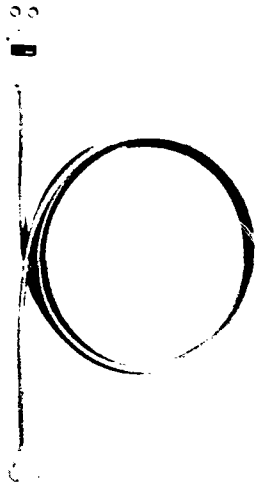


Figure 4. Active Transceiver Cable

figure 4. The transceiver unit including a coaxial cable tap is shown in figure 5 and figure 6.

Designing considerations

In order to realize the small, light-weight and one-body configuration, the following items were taken into designing considerations:
(1)In order to make a fine outside view, all parts are arranged to make the unit as thin as possible.
(2)In order to be stable when installed on the wall or floor, the back of the unit has been kept flat.
(3)In order to make the tap installation simple, the tap block is separated into two parts and the ground probes are bedded into one of the halves.
(4)To keep total capacitance of the tap and active circuitry small, the distance between the female tap connector and the module has been kept to the minimum.

Structure of the transceiver unit

As shown in figure 5, there is a metal common frame in the molded transceiver unit. On the frame there are a transceiver module, a transceiver cable termination and a female connector of a coaxial cable tap. The module is mounted on the printed circuit board and the board is fixed on the frame being electrically isolated. The transceiver cable and the tap connector are connected to the module through this circuit board.

Plastic molding

When the transceiver module, the coaxial cable tap receptacle, the transceiver cable and the power source LED light are fixed on the frame and connected with wires, the next process is an injection molding.

Since the small hybrid IC module is very fragile, the plastic molding pressure must not be loaded on this module. In order to protect the module from the injection molding the following techniques were employed:
(1)Low pressure high melt flow PVC resin was selected.
(2)The mold was designed not to raise the molten PVC pressure at the final stage of the injection. The location of the gate was carefully studied not to load the high pressure directly on the module.
(3)The module is protected againt the pressure and sealed not to allow the high pressure resin flow inside by a box.

Coaxial Cable Tap

The coaxial cable tap is shown in figure 7. It consists of the two halves of the tap block. The center conductor probe and ground probes protruding into the cable gripping hole are attached on one side of the half. The back of the center conductor probe is a male tap connector which is connected to the female one of the transceiver unit.
After checking the cable gripping force and testing the tapping for repeatability, the outer dimensions of the tap block were decided so it would fit in the upper groove of the transceiver unit. The outside surface of the tap block was then covered with a firm insulation coating.

Reliability Test

Various kinds of tests were carried out to confirm long term stability of the transceiver cable. These tests and their

results are listed in table 2. The test conditions are based on the JIS (Japan Industrial Standard) testing method of electronic components.

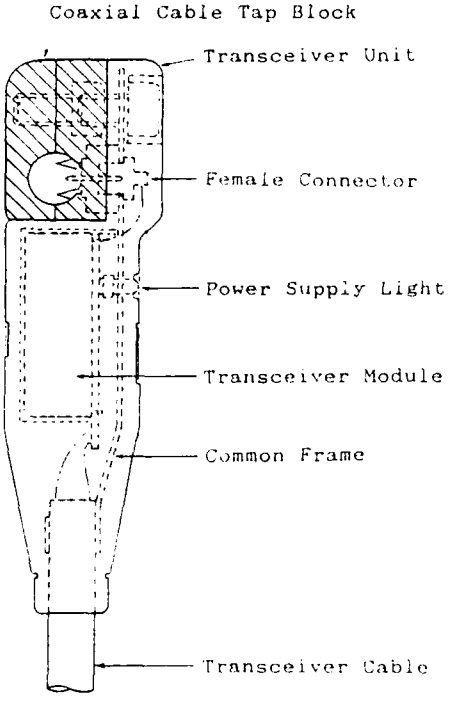


Figure 5. Structure of the Transceiver Unit

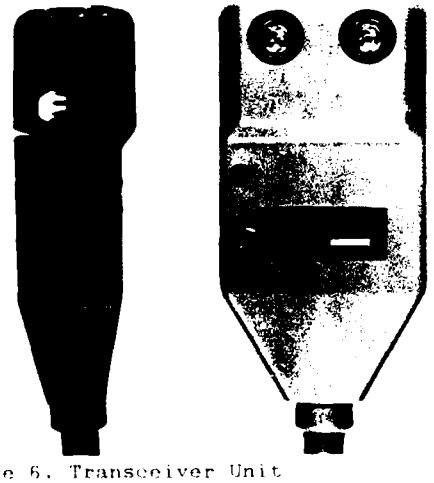


Figure 6. Transceiver Unit

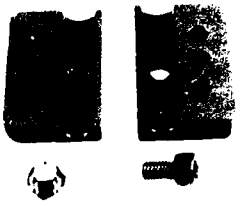


Figure 7. Coaxial Cable Tap Blocks

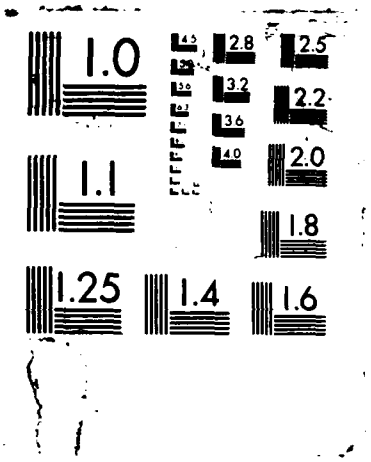
Table 2 Reliability tests

Test Types	Conditions	Results
Thermal Shock Test	JIS C7022 A-3 100°c→0°c,5 cycles	Passed
Thermal Cyclic Test	JIS C7022 A-4 -25°c→25° c→85°c,5 cycles	Passed
Damp Heat Cyclic Test	JIS C7022 A-5 RH95% -10°c~65°c 10 times(2 patterns)	Passed
Mechanical Shock Test	JIS C7022 A-8 3 times 75 cm drop on maple wood	Passed
Vibration Test	JIS C7022 A-10 100~2,000Hz, 10G, 6hrs.(x,y,z)	Passed
Non-stop Endurance Test	JIS C7022 B-1 70°c 1,000 hrs.	Passed
Start-stop Test	JIS C7022 B-2 90 min.on→30 min.off 1,000 hrs	Passed
High Temperature Test	JIS C7022 B-3 80°c 1,000 hrs.	Passed
Low Temperature Test	JIS C7022 B-4 -20°c 1,000hrs.	Passed
Humidity Test	JIS C7022 B-5 40°c,RH90%,1,000hrs.	Passed
Coaxial Cable and Tap Bending Test	±90 degree, 10 times, r=100 mm	Passed
Connection and Disconnection Test	central conductor probe and ground probe, 100 times	Passed

AD-A189 610 PROCEEDINGS OF THE INTERNATIONAL WIRE AND CABLE SYMPOSIUM (36TH) HELD IN..(U) ARMY COMMUNICATIONS-ELECTRONICS COMMAND FORT MONMOUTH NJ 9/9

UNCLASSIFIED 19 NOV 87 F/G 9/1 NL




1.0
1.1
1.25
1.4
1.6
1.8
2.0
2.2
2.5
2.8
3.2
3.6
4.0

Installation Procedure

The installation procedure of the coaxial cable tap is shown in figure 8. The coaxial cable is gripped with a tap block by a bolt and the cable is drilled by the tap block attaching tools. The connector plug is screwed into the tap block and the tap block is fixed to the transceiver unit firmly by two bolts. The whole installation job is finished in just a few minutes.

Conclusion

A new type of transceiver unit for LAN has been introduced and complies with standard IEEE802.3. The new active transceiver cable has a transceiver unit including a coaxial cable tap at one end and a D-sub connector at the other end. The outer dimensions of the transceiver unit including the tap block and the transceiver cable termination are about half of the smallest existing transceiver unit. The transceiver unit has a small and fine configuration. Its convenience makes it very useful in any modern office.

Acknowledgements

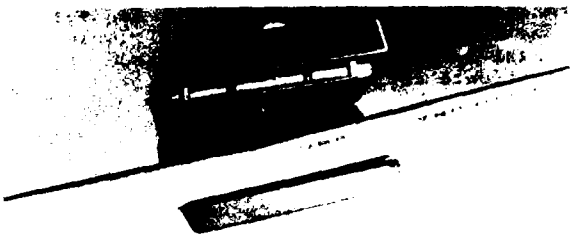
The authors wish to thank Dr. K. Inada for his useful suggestions and colleagues for their cooperation and technical assistance

References

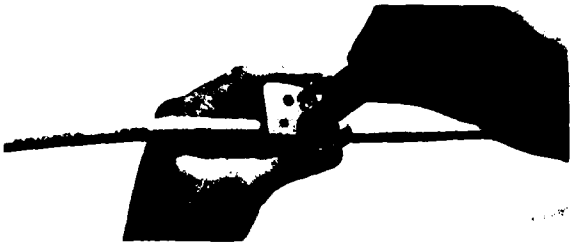
1). ANSI/IEEE Std. 802.3.1985

2). Y. Kobayashi H. Yokosuka
"Active transceiver cable for Ethernet"
1987 Natl. Conv. Rec. IECE Japan

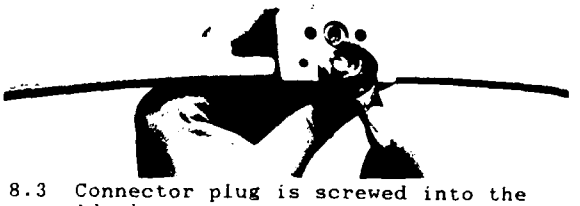
3). K. Karai K. Arai
"Development of Active transceiver cable for Ethernet"
1987 Natl. Conv. Rec. IECE Japan



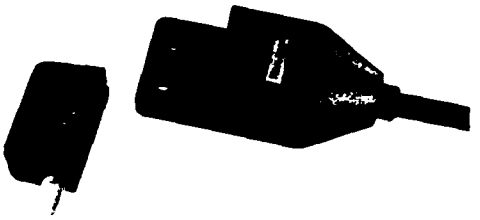
8.1 Tap blocks and coaxial cable



8.2 Drill the coaxial cable



8.3 Connector plug is screwed into the block



8.4 Transceiver unit and tap block



8.5 Tap black is fixed to the transceiver unit

Figure 8. Installation Procedure



Hiroshi Yokosuka joined Fujikura Ltd. in 1967 and has been engaged in research and development of automatic telephone cable splicing machines, joint closures and optical fiber connectors. He is now a chief of the fiber and cable accessory section in Telecommunication Cable R & D Department. He is a member of the Institute of Electronics and Communication Engineers of Japan.



Kenji Karai was born in Okayama, Japan, on January 15, 1959. He received the B.E. degree from University of Electro-Communications, Tokyo, Japan, in 1981. He joined Fujikura Ltd., Sakura, Chiba, Japan, in 1986, and has been engaged in development of Fiber Optic Telecommunication Systems. He is a member of the IECE of Japan.



Yoshio Kobayashi joined Fujikura Ltd. in 1964 and has been engaged in research and development of telephone cable splicing connectors, emergency restoration cable systems, gas dam cables and optical fiber connectors. He is now in the fiber and cable accessory section in Telecommunication Cable R&D Department. He is a member of the IECE of Japan.



Okosu Watanabe was born in 1945. He received the B.E. degree in telecommunication engineering in 1968 from Musashi Institute of Technology. He joined Fujikura Ltd. in 1968 and has been engaged in research and development of automatic telephone cable splicing machines, alarm systems for telephone cable plants, and optical fiber splicing. He is now a Head of the Optical System Section. He is a member of the IECE of Japan.



Katsuyuki Arai was born in Chiba, Japan, on November 20, 1952. He received the B.E. degree from Ibaraki University, Ibaraki, Japan, in 1975. He joined Fujikura Ltd., Sakura, Chiba, Japan, in 1980, and has been engaged in development of Fiber Optic Telecommunication Systems. He is a member of the IECE of Japan.

AUTHORS INDEX

Name	Page
Abe, H.	135
Akagawa, T.	316
Akasaka, N.	350
Akiyama, M.	284
Allfather, W. H.	179
Amano, Y.	651
Amos, L. G.	228
Anderson, W. T.	49
Arai, K.	744
Arroyo, C. J.	344
Artingstall, S.	254
Asari, S.	640
Bachel, E.	699
Baer, N. J.	160
Barker, J. S.	175
Barnes, S. R.	223, 662
Bednarczyk, J. J.	575
Beltz, L. P.	685
Berkers, A. G. W. M.	426
Bianchi, G.	464
Bird, L.	85
Bjerkan, L.	57
Boinet, J. P.	534
Bonesteel, J. E.	276
Bonicel, J. P.	534
Bonk, T. J.	685
Boscher, G.	699
Bowmer, T. N.	5
Brandtner, M. J.	622
Bregeon, J. P.	534
Bresser, E. J.	426
Brinkmeyer, E.	77
Brown, G. D.	337, 734
Buckland, E. L.	419
Buczma, E.	23
Bukowski, R. W.	143
Burkhard, J. D.	322
Campbell, E. R.	645
Carter, C. N.	449
Carter, D. R.	122
Chávez Diaz, G.	546
Chen, T. I.	676, 685
Chien, C. K.	228
Cong Chen, S.	198
Chou, R.	198
Clarke, F. B.	276
Craddock, K.	449
Croft, T. S.	676
Darden, B. V.	108, 193
Davenport, C. M. Conner	49
Davidson, F.	311
Davis, L. E.	734
Day, A. C.	23
de Jong, B. H. W. S.	604
Delme Jones, D.	449
deValle, L.	540
DeVeau, G. F.	202
deVecchis, M.	534
DeVito, A.	392
Diaz de la Iglesia, R.	629
DiPinto, J. G.	276
Dusek, J. T.	404
Eales, B. A.	223
Eccleston, D. J.	228
Eng, T.	39
Englehart, W. H.	581
Eoll, C. K.	622
Fee, J. M.	248
Fidelle, T. P.	245
Fuchs, M.	77
Fukuma, M.	350, 379
Fyrwald, C. R.	14
Gittle, A. L.	209
Glaesemann, G. S.	241
Goretta, K. C.	404
Grant, W. O.	526
Grooten, A. T. M.	426
Haag, H. G.	291
Harry, W. I.	540
Hasemi, A.	316
Hasz, C. H.	169
Hatton, W. H.	656
Haugen, H. A.	676
Hawsegawa, H.	316
Hayashi, A.	357
Hayashi, H.	611
Hays, S. P.	676
Heckmann, S.	77
Hino, H.	564
Hiraiwa, S.	316
Hisano, S.	651
Hög, G.	291
Hopiavuori, M.	392
Hor, P. H.	399
Horima, H.	441
Houghton, I.	449, 662
Hovis, S. K.	419
Hughes, G. J.	148
Hurtig, B.	667
I, Yiang	198
Iino, A.	611
Imamura, K.	217
Inagaki, T.	39
Inoue, M.	372
Ishihata, Y.	441
Ishikura, A.	386
Isley, J. A.	712
Janssens, M.	276
Jenkins, A. C.	344
Judy, A. F.	202
Kajio, Y.	564
Kakii, T.	379
Kakuta, T.	234
Kalomiris, V. E.	108

Name	Page
Kanen, R. M.	49
Kannabiran, R.	228
Kar, G.	228, 241
Karai, K.	744
Kashihara, K.	379
Kathiresan, K.	108
Kato, Y.	386
Keith, P. S.	419
Kemp, H. M.	557
Keogh, M. J.	592
Kilmer, J. P.	49
Kinder, C.	205
Kish, P.	410
Kitayama, Y.	457
Klar, R.	71
Kobayashi, Y.	744
Koga, H.	357
Kojima, O.	284
Kozono, F.	34
Kukita, S.	357
Kunze, D.	699
Kurosawa, A.	441
Kuzushita, H.	217
Laney, R.	311
Lao Soriano, D. J.	629
Lawler, J. D.	205, 209
Levengood, J. W.	705
Lin, B.	457
Lin, S. F.	188
Lowe, R. S.	91
Lu, K. E.	241
Lung Yu, P.	198
Lyons, S.	436
Maguire, C. V.	327
Mascarenhas, V. B.	581
Masuda, Y.	457
Matthews, J. E., III	392
Mayer, H. A.	23
McCallum, W.	311
McDowell, H. R.	265
McKiterick, M.	540
Mean Shiea, L.	198
Mehta, P. M.	575
Mendat, L.	699
Miller, W.	85
Misono, N.	284
Miyazawa, H.	693
Moore, E. Goddard	546
Moses, J.	163
Mullin, F. J.	567, 645
Nakagawa, W.	640
Nakai, T.	357
Nakano, M.	564
Nemoto, K.	372
Neveux, P. E., Jr.	656
Niijima, M.	611
Niikura, K.	441
Niiro, Y.	135
O'Brien, R.	205
Ohlhaber, R. L.	116
Ohmori, T.	441
Okubo, S.	640
Olson, P. M.	685
O'Sullivan, M. S.	91
Ota, S.	693
Packham, S. C.	143
Patel, N. I.	272
Patel, P. D.	344
Peng, H. K.	188
Pierce, S. B.	716
Plitz, I. M.	616
Plouffe, M.	667
Polczynski, C. E.	297
Pownall, J. A.	598
Pyle, A. J.	254
Quist, D. J.	248
Rahman, M.	464
Raman, R.	63
Ramsey, M. M.	223
Randa, S. K.	14
Reed, W. C.	567, 645
Reifschneider, D. P.	14
Roessing, T. J.	322
Rohner, P.	102
Rossi, R.	327
Rost, J.	699
Rota, D.	464
Rowe, J.	667
Rowland, S.	449
Rueda García, J.	629
Rybach, J.	77
Saen, H.	306
Saikkonen, S.	85
Saito, K.	441
Salazar Cerda, J. C.	546
Sano, T.	386
Saravanos, C.	91
Saunders, M. J.	193
Sawano, H.	284
Schicketanz, D. W.	622
Schoenfeld, H.	71
Scholly, C.	567
Sentsui, S.	611
Shimada, S.	651
Shimizu, T.	564
Sigmon, M.	163
Sigmon, M. A.	265
Smith, J. L.	402
Smith, T. R.	122
Spedding, S. T.	94
Stacy, H. W.	144
Stowe, R. W.	212
Stratton, A. W.	322
Sugawara, K.	306
Sugawara, Y.	284
Summers, A.	662
Summers, A. T.	223
Suzuki H.	284

Name	Page
Suzuki, S.	350, 379
Swampillai, G. J.	676
Tachigami, S.	693
Takaesu, F.	34
Takashima, S.	386
Takeda, T.	441
Takehara, H.	441
Tanabe, E.	693
Tanaka, H.	217
Tanaka, K.	34
Tanaka, S.	234
Taylor, J.	254
Taylor, J. E.	94
Tobias Azpitarte, E.	629
Tokumaru, Y.	651
Tsai, F. Y.	188
Tsujita, T.	284
Tzeng, G. T.	188
Ulijasz, T. R.	116
Valentine, R.	276
Vandevelde, P.	276
van Kuijk, H. J.	276
Varachi, J. P.	169
Vyas, M. K. R.	223
Wakagi, M.	564
Warren, P. C.	5, 616
Watanabe, O.	744
Watanabe, T.	217
Williams, R. J.	667
Wong, D.	438
Wood, W. W.	155
Yamamoto, H.	135
Yamazaki, Y.	135
Yano, T.	306
Yasinski, K. M.	202
Yokosuka, H.	744
Yoshino, H.	611
Youngblood, A. V.	179, 183
Zamzow, P. E.	291
Zhang, Yuan	723
Ziemek, G.	102
Zushi, T.	217



International Wire & Cable Symposium

SPONSORED BY U.S. ARMY COMMUNICATIONS-ELECTRONICS COMMAND (CECOM)
FORT MONMOUTH, NEW JERSEY
15, 16 and 17 November 1988
Bally's MGM Grand Hotel, Reno, Nevada

Please provide a 300-500 word abstract (25 copies) of proposed technical paper on such subjects as design, application, materials, and manufacturing of communications and electronics wire and cable of interest to the commercial and military electronics industries. Such offers should be submitted no later than 8 April 1988 to the Headquarters, US Army Communications-Electronics Command, ATTN: AMSEL-RD-C^3-PB, Fort Monmouth, New Jersey 07703-5202.

TITLE:_____

AUTHORS:_____

COMPANY:_____

ADDRESS:_____

AUTHOR(S):_____

CONTACT FOR CORRESPONDENCE:_____

ADDRESS AND TELEPHONE:_____

_____

I. PAPER TITLE:_____

_____

II. BACKGROUND (Why was work undertaken?):

III. PRIMARY CONCLUSION OR RESULT:

IV. DESCRIBE THE NOVELTY AND HOW THIS WORK ADVANCES THEORY OR TECHNOLOGY:

V. 300-500 WORD COMPREHENSIVE SUMMARY, INCLUDING METHODOLOGY IN REACHING CONCLUSION OR RESULT:

Fold here

Stamp

Commander
US Army Communications-Electronics Command
Attn: AMSEL-RD-C^3-PB
Fort Monmouth, NJ 07703-5202

Fold here

IWCS

International Wire & Cable Symposium

SPONSORED BY U.S. ARMY COMMUNICATIONS-ELECTRONICS COMMAND (CECOM)
FORT MONMOUTH, NEW JERSEY
15, 16 and 17 November 1988
Bally's MGM Grand Hotel, Reno, Nevada

Please provide a 300-500 word abstract (25 copies) of proposed technical paper on such subjects as design, application, materials, and manufacturing of communications and electronics wire and cable of interest to the commercial and military electronics industries. Such offers should be submitted no later than 8 April 1988 to the Headquarters, US Army Communications-Electronics Command, ATTN: AMSEL-RD-C^3-PB, Fort Monmouth, New Jersey 07703-5202.

TITLE:_____

AUTHORS:_____

COMPANY:_____

ADDRESS:_____

AUTHOR(S):_____

CONTACT FOR CORRESPONDENCE:_____

ADDRESS AND TELEPHONE:_____

_____

I. PAPER TITLE:_____

_____

II. BACKGROUND (Why was work undertaken?):

III. PRIMARY CONCLUSION OR RESULT:

IV. DESCRIBE THE NOVELTY AND HOW THIS WORK ADVANCES THEORY OR TECHNOLOGY:

V. 300-500 WORD COMPREHENSIVE SUMMARY, INCLUDING METHODOLOGY IN REACHING CONCLUSION OR RESULT:

Fold here

Stamp

Commander
US Army Communications-Electronics Command
Attn: AMSEL-RD-C^3-PB
Fort Monmouth, NJ 07703-5202

Fold here


LMED
8